This is a reproduction of a library book that was digitized by Google as part of an ongoing effort to preserve the information in books and make it universally accessible.

Google™ books

https://books.google.com

C 622,805

PROPERTY OF
University of
Michigan
Libraries
1817
ARTES SCIENTIA VERITAS

OF MICHIGAN
MAR - 5 1964
PHOENIX
LIBRARY

POWER
REACTOR
TECHNOLOGY

A Quarterly Technical Progress Review

Prepared for DIVISION OF TECHNICAL INFORMATION, USAEC, by

W. H. ZINN and J. R. DIETRICH, GENERAL NUCLEAR ENGINEERING CORPORATION

Winter 1963-1964

● **VOLUME 7**

● **NUMBER 1**

TECHNICAL PROGRESS REVIEWS

To meet the needs of industry for concise summaries of current atomic developments, the Atomic Energy Commission is publishing this series, Technical Progress Reviews. Issued quarterly, each of the reviews digests and evaluates the latest findings in a specific area of nuclear technology and science.

The five journals published in this series are:

Isotopes and Radiation Technology, P. S. Baker, A. F. Rupp, and associates, Oak Ridge National Laboratory

Nuclear Safety, Wm. B. Cottrell, W. H. Jordan, and associates, Oak Ridge National Laboratory

Power Reactor Technology, W. H. Zinn and J. R. Dietrich, General Nuclear Engineering Corporation

Reactor Fuel Processing, Stephen Lawroski and associates, Chemical Engineering Division, Argonne National Laboratory

Reactor Materials, R. W. Dayton, E. M. Simons, and associates, Battelle Memorial Institute

Each journal may be purchased from the Superintendent of Documents, U. S. Government Printing Office, Washington, D. C., 20402. *Isotopes and Radiation Technology* at $2.00 per year for subscription or $0.55 for individual issues; the other four journals at $2.50 per year and $0.70 per issue. See back cover for remittance instructions and foreign postage requirements.

The views expressed in this publication do not necessarily represent those of the United States Atomic Energy Commission, its divisions or offices, or of any Commission advisory committee or contractor.

Availability of Reports Cited in This Review

Unclassified AEC reports are available for inspection at AEC depository libraries and are sold by the Office of Technical Services, Department of Commerce, Washington, D. C., 20230. Some of the reports cited are not available owing to their preliminary nature; however, the information contained in them will eventually be made available in formal progress or topical reports.

Unclassified reports issued by other Government agencies or private organizations should be requested from the originator.

Unclassified British and Canadian reports may be inspected at AEC depository libraries. British reports are sold by the British Information Service, 45 Rockefeller Plaza, New York, N. Y.; Canadian reports (AECL series) are sold by the Scientific Document Distribution Office, Atomic Energy of Canada, Ltd., Chalk River, Ontario, Canada.

Classified U. S. and foreign reports identified in this journal as Classified may be purchased by properly cleared Access Permit Holders from the Division of Technical Information Extension, U. S. Atomic Energy Commission, P. O. Box 1001, Oak Ridge, Tenn., 37831. Such reports may be inspected at classified AEC depository libraries.

POWER
REACTOR
TECHNOLOGY

A REVIEW OF RECENT DEVELOPMENTS

Prepared for DIVISION OF TECHNICAL INFORMATION, USAEC,
by W. H. ZINN and J. R. DIETRICH,
GENERAL NUCLEAR ENGINEERING CORPORATION

WINTER 1963–1964

VOLUME 7

NUMBER 1

Foreword

This quarterly review of reactor development has been prepared at the request of the Division of Technical Information of the U. S. Atomic Energy Commission. Its purpose is to assist interested organizations in the task of keeping abreast of new results in reactor technology for civilian application.

Power Reactor Technology contains reviews of selected recently published reports that are judged noteworthy in the fields of power-reactor research and development, power-reactor applications, design practice, and operating experience. It is not meant to be a comprehensive abstract of all material published during the quarter, nor is it meant to be a treatise on any part of the subject. However, related reports from different sources are often treated together to yield reviews having some breadth of scope, and background material may be added to place recent developments in perspective. Occasionally the reviews are written by guest authors. Reviews having unusual breadth or significance are placed at the front of the issue as Feature Articles.

The intention is to cover the various areas of reactor development from the general viewpoint of the reactor designer rather than from the more detailed points of view of specialists in the individual areas. To whatever extent the coverage of *Power Reactor Technology* may occasionally overlap the fields of the other Technical Progress Reviews, the overlaps will be motivated by this objective of viewing current progress through the eyes of the reactor designer.

A degree of critical appraisal and some interpretation of results are often necessary to define the significance of reported work. Any such appraisal or interpretation represents only the opinion of the reviewer and (in the usual case, when the review is written by General Nuclear Engineering Corporation staff) the Editor. When the review is predominantly interpretive, the reviewer is named; unless identified as a guest author, he is a member of the General Nuclear Engineering Corporation staff. Readers are urged to consult the original references to obtain all the background of the work reported and to obtain the interpretation of the results given by the original authors.

For timely coverage, *Power Reactor Technology* must often review fragmentary material. The fixed subject headings listed below have been adopted in the hope of maintaining some continuity and order in the material from one issue to another: all reviews except Feature Articles will be arranged under these headings. A particular issue will not necessarily contain all the headings but only those under which material is reviewed.

Economics, Applications, Programs
Resources and Fuel Cycles
Physics
Fluid and Thermal Technology
Fuel Elements
Materials
Control and Dynamics
Containment, Radiation Control, and Siting
Systems Technology
Components
Design and Construction Practice
Operating Experience
Specific Reactor Types
Specific Applications
Unconventional Approaches

W. H. Zinn, President
J. R. Dietrich, Vice-President and Editor
General Nuclear Engineering Corporation

DEPOSITED BY THE
UNITED STATES OF AMERICA

Contents

Foreword

I ECONOMICS, APPLICATIONS, PROGRAMS 1
Solid-Fuel Gasification 1
References 3

II PHYSICS 4
Critical and Exponential Experiments . . 4
References 12

III FLUID AND THERMAL TECHNOLOGY 14
Burnout Limits for Boiling-Water Reactors 14
References 26

IV FUEL ELEMENTS 27
Programs at GE-APED Sponsored by USAEC and Euratom 27
References 48

V CONTROL AND DYNAMICS 51
Period Meters 51
Transducers 52
Servomechanism Reliability 53
References 53

VI CONTAINMENT, RADIATION CONTROL, AND SITING 54
Low-Pressure Containment Building . . . 54
Moisture Separators and Particulate Filters 55
Iodine Removal 55
References 58

VII COMPONENTS 60
Sodium-Heated Steam Generators 60
Gas-Heated Steam Generators 64
Liquid-Metal Pumps 65
Canned Pump for Organic Service 67
Butterfly-Valve Cavitation Test 68
Fuel-Handling Equipment 68
References 68

VIII DESIGN AND CONSTRUCTION PRACTICE 70
Humboldt Bay and Big Rock Point 70
References 84

IX SPECIFIC REACTOR TYPES 85
Heavy-Water Reactors 85
References 97

X UNCONVENTIONAL APPROACHES . . 99
Design Study of Thermionic Nuclear Plant 99
General Thermionic Considerations . . . 105
Thermoelectric Power Supply 106
References 106

Issued quarterly by the U. S. Atomic Energy Commission. Use of funds for printing this publication approved by the Director of the Bureau of the Budget on October 14, 1963.

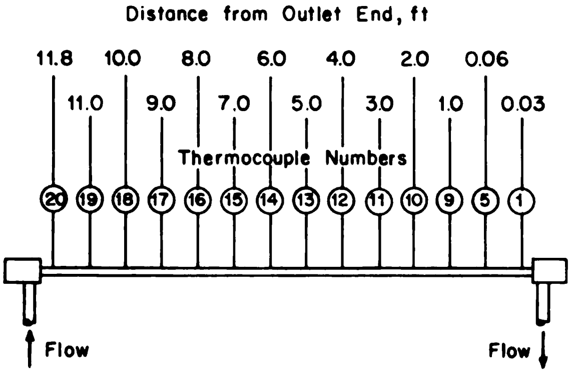

Fig. II-9 Test section thermocouple locations.[16]

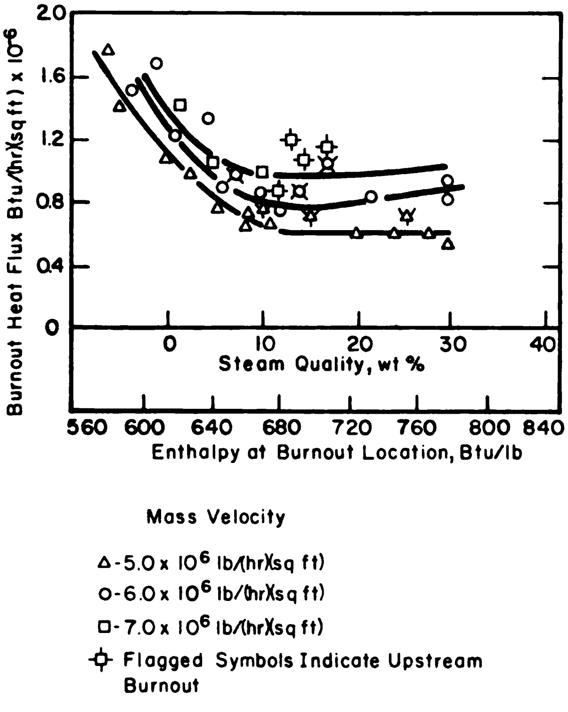

Fig. II-10 Experimental boiling-burnout data.[16]

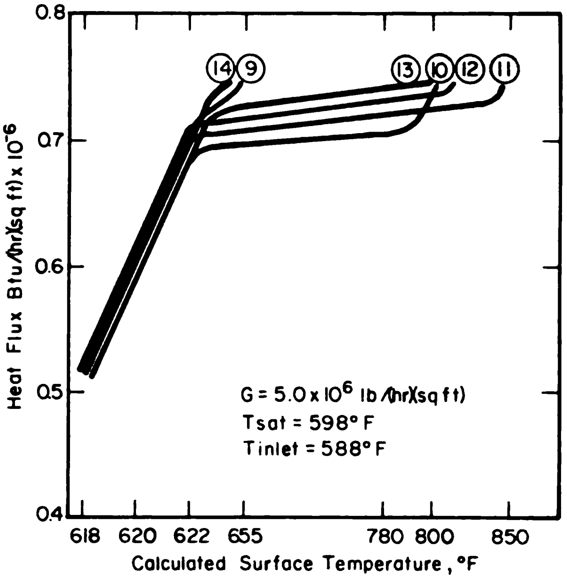

Fig. II-11 Test-section temperatures during a typical upstream burnout run.[16]

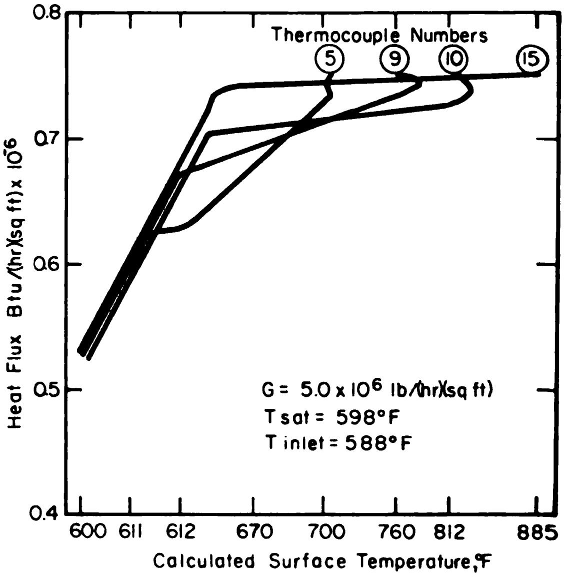

Fig. II-12 Magnitude of temperature excursions during a downstream boiling burnout.[16]

Note: In *Power Reactor Technology*, 6(4): 61, these figures were printed in the wrong order. The correct order is shown here.

67-145A-A-30

Section I

Power Reactor Technology

Economics, Applications, Programs

Solid-Fuel Gasification

A study of the economic feasibility of using nuclear energy to convert coal to synthesis gas for the manufacture of ammonia, methanol, synthetic pipeline gas, and liquid fuels is reported in Ref. 1. The analysis does not consider reactor design but proceeds on the assumption that the nuclear heat is supplied in the form of hot, nonradioactive helium at a pressure of about 435 psig and at temperatures in the 2000 to 2500°F range. The heat consumptions in the installations considered are in the range of 250 to 400 Mw(t). Two plants were evaluated; one produced 90 million standard cubic feet per day of 930 Btu/lb pipeline gas, and the other produced a variety of fuels and chemicals. The investments in the chemical plants considered (exclusive of the nuclear power source) range from $45 million to $133 million; therefore the nuclear plant does not represent the major portion of the total investment.

At present coal gasification, although technically feasible, has not been put into commercial practice in the United States because of cost disadvantages compared to processes utilizing naphtha or natural gas as sources of synthesis gas. A major contributor to the high cost of coal gasification using conventional

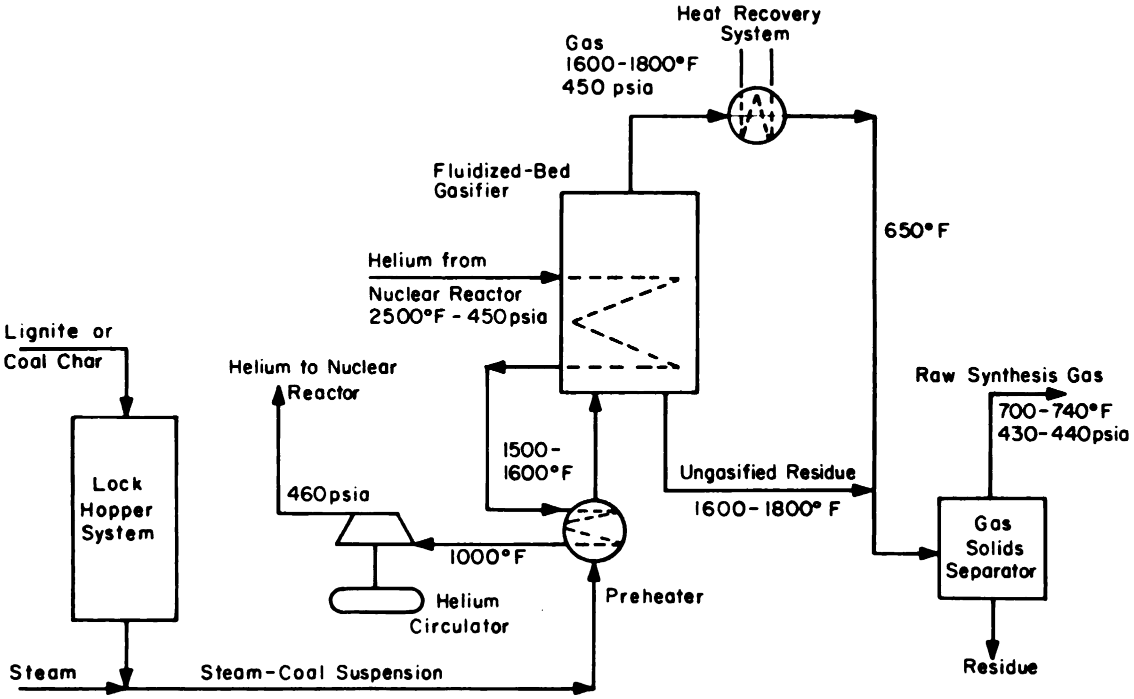

Fig. I-1 Schematic flow diagram of gasification section.[1]

fuels has been the cost of oxygen.[1] The reaction that takes place when coal is gasified is endothermic, and the oxygen is used to burn a portion of the coal to produce the necessary heat. Air cannot be used because the nitrogen thus introduced would end up as a major impurity in the product synthesis gas. The use of a nuclear reactor as a source of heat overcomes the problem of dilution of the product gas by nitrogen and by the CO_2 that is also produced by the combustion of coal. A schematic of the process is shown in Fig. I-1.

The results of the study with respect to the cost of pipeline gas are shown in Table I-1. The selling prices of pipeline gas that is produced from coal gasification by both conventional fuel and nuclear heat are compared in Table I-2.

Although the use of nuclear heat offers substantial cost advantages compared to processes using O_2, the range of $1.32 to $1.51 still is about a factor of 2 higher than natural-gas prices in the eastern portion of the United States.[1]

The lignite processing plant was assumed to be in North Dakota, whereas the bituminous coal processing plant was assumed to be in West Virginia. The reference concludes that the manufacture of pipeline gas with the use of nuclear heat should be studied further if a market could be developed for pipeline gas in North Dakota, since the present market is

Table I-1 EFFECT OF RAW MATERIAL COST, COST OF NUCLEAR HEAT, AND GROSS RETURN ON INVESTMENT ON THE SELLING PRICE OF PIPELINE GAS[1]

Cost of nucleat heat, $/million Btu	Selling price of pipeline gas, $/thousand standard cu ft					
	Lignite			Bituminous coal		
	$1.50/ton	$2.00/ton	$2.50/ton	$4.00/ton	$5.00/ton	$6.00/ton
	Gross Return = 12%					
0.50	0.71	0.75	0.79	1.08	1.13	1.18
0.80	0.78	0.82	0.86	1.19	1.24	1.29
	Gross Return = 20%					
0.50	0.83	0.87	0.91	1.27	1.32	1.37
0.80	0.90	0.94	0.98	1.38	1.43	1.48
	Gross Return = 30%					
0.50	0.98	1.02	1.06	1.51	1.56	1.61
0.80	1.05	1.09	1.13	1.62	1.67	1.72

Table I-2 COMPARISON OF PRICES OF PIPELINE GAS PREPARED BY VARIOUS PROCESSES[1]

Source of information	Process	Gas selling price at 20% gross return, 90% stream efficiency, $5/ton coal, $/thousand standard cu ft
Present study	Fluid-bed gasification, nuclear heat at	
	$0.50/million Btu	1.32
	$0.80/million Btu	1.43
	$1.00/million Btu	1.51
Kellogg[1]	Lurgi steam-oxygen gasification	1.70
	Suspension gasification with steam and oxygen	1.49
Bureau of Mines[2]	Suspension gasification with steam and oxygen	1.55

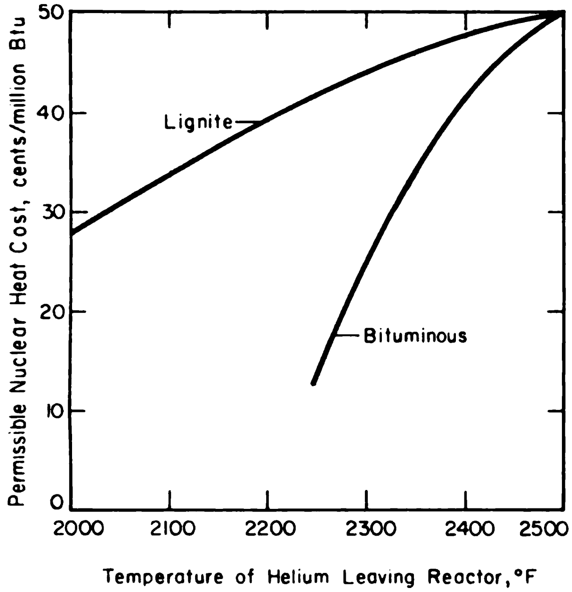

Fig. I-2 Permissible cost of heat to yield same pipeline gas selling price as 2500°F helium at $0.50 per million Btu. Cost of heat includes operating cost of reactor plant, return on investment (20%), and special costs associated with nuclear operation.[1]

limited. It is significant that the effect of the helium temperature is an important one (Fig. I-2). The helium temperature for gasifying bituminous coal[1] should be at least 2500°F, whereas the temperature requirement for gasifying lignite probably would be somewhat lower.

The manufacturing complex for producing a mixture of products consisting of gasoline, ammonia, methanol, hydrogen, and other chemicals from synthesis gas produced with nuclear heat looked unattractive economically. However, the economics of the ammonia and methanol components of the complex appeared quite favorable, and the reference suggests that plants producing these products alone would be fruitful areas for further study. The reference concludes with a general comment on this relation:

> It appears that the best applications for nuclear heat will be found in trying to improve an existing commercial process, not in trying to make a currently uneconomic process look attractive. For example, gasoline and pipeline gas are not produced from synthesis gas in the United States today, and the advent of cheap nuclear heat will not change the picture significantly. On the other hand, ammonia and methanol are manufactured from synthesis gas on a commercial scale, and the use of nuclear heat may furnish a significant cost advantage, whether the raw material used to make the synthesis gas be coal, oil, or natural gas. This would seem to be a fruitful area for further study.

References

1. L. J. Pieroni, R. P. Griffin, and W. H. Heffner, A Technical and Economic Evaluation of Solid-Fuel Gasification Using Nuclear Heat. Production of Pipeline Gas, Liquid Fuels, and Chemicals from Lignite and Bituminous Coal. Period Covered: May to October 1962, USAEC Report NYO-10301, The M. W. Kellogg Company, Nov. 30, 1962.
2. S. Katell, J. H. Faber, P. Wellman, W. C. Morel, and G. B. Taylor, 90 Million Std. Cubic Feet Per Day High-Btu Gas Plant, Report 61-7, U. S. Bureau of Mines, May 31, 1962.

Section
II

Power Reactor Technology

Physics

Critical and Exponential Experiments

A recent paper by Kaplan[1] gives a review of the use of subcritical and critical assemblies for the measurement of reactor parameters. It considers the various methods employing such assemblies from the points of view of their consistency with one another and of their accuracy and usefulness in measuring the basic characteristics of chain-reacting lattices for use in practical reactors. In addition to the conventional critical and exponential assemblies, the review considers three related methods that can utilize much smaller samples of the experimental lattice. These methods are the following:

1. Substitution, or two-region, critical experiments. In these experiments the critical buckling is first measured in a reference lattice; thereafter a central portion of the reference lattice is replaced by the experimental lattice, and the buckling of the experimental lattice is evaluated from the change in critical buckling produced by the substitution. This method has been applied extensively to heavy-water lattices at the Savannah River Laboratory, and it is particularly convenient when liquid moderators are used so that the change in buckling can be evaluated by the change in critical moderator level.

2. The flat-region technique, which has been used at Hanford in the Physical Constants Testing Reactor (PCTR). In this system a reference assembly is first made critical with an empty cavity at its center. The cavity is then filled with the experimental lattice, and some parameter of the experimental lattice is varied uniformly over its volume until the entire assembly is again critical. At this point the gross neutron-flux distribution in the experimental lattice is flat (as it was in the empty cavity), and the infinite multiplication factor (k_∞) for the experimental lattice is unity. Usually the adjustable parameter is an absorbing poison with an absorption cross section that varies with energy in a way that is easily handled by computation.*

3. The miniature-lattice technique. This method utilizes a suitable neutron source, usually a reactor, to irradiate a small assembly of the experimental lattice. No attempt is made to determine reactivity or buckling, but the basic lattice parameters such as thermal utilization and resonance escape probability are measured at points near the center of the assembly.

It is quite evident that a primary concern in any of the small-lattice techniques must be to assure that the quantity measured is characteristic of the neutron spectrum in the experimental lattice and is independent of the spectrum of the lattice that feeds neutrons to the experiment. Basically this involves the use of buffer regions between the two lattices, but the manner in which this technique is applied varies with the general method of the experiment and with the quantities being measured.

The reference[1] examines the mutual consistency of the results that have been obtained in the past by the several methods involving critical or subcritical lattices, with the comparison being organized about the several lattice types that have been subjects of extensive measurement programs: graphite-moderated, heavy-water-moderated, and light-water-moderated lattices. The review emphasizes the limitations of integral experiment techniques for investigating the practical situations such as temperature, voiding, and fission-product poisoning, which occur in practical reactors. However, it necessarily confines its attention to the properties of more or less uniform lattices, since it is only in this area that extensive experimental information exists. Often the reactor designer finds that the major concern is not so much with the basic lattice parameters as with the complexity introduced by such local perturbations as water channels and control rods, the complex power distributions resulting from control-rod installations, temperature and void distributions, and burnup distributions. These questions are sometimes investigated by means of critical experiments of the mockup type. A recent experimental program of this type for a rather complex reactor, the Boiling Nuclear Superheat Reactor (BONUS) is described in Ref. 2.

---

*Recent investigations of this technique, for lattices having important fractions of epithermal fissions, have been carried out at the Babcock & Wilcox laboratory and are reviewed here in later paragraphs (see Fig. II-1).

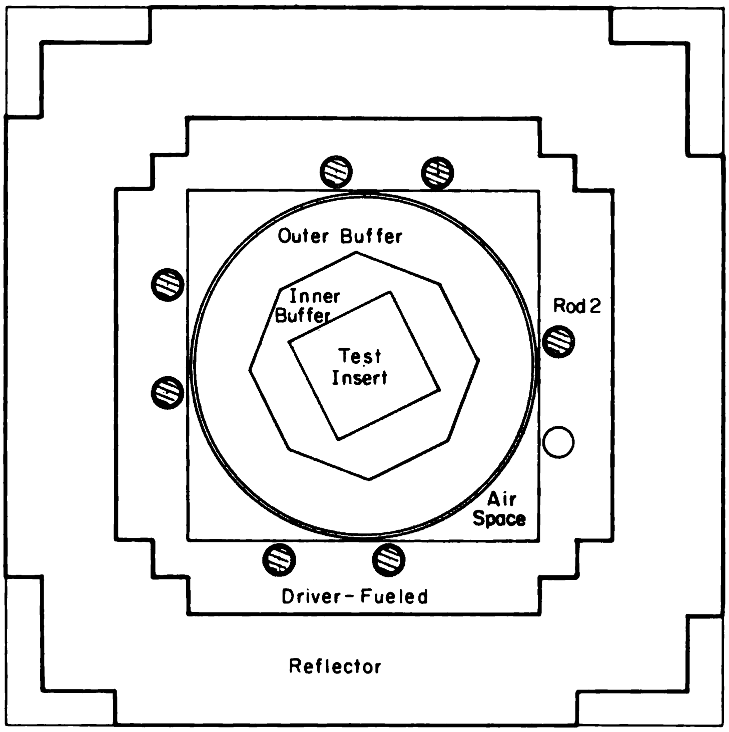

Fig. II-1 Small-lattice assembly plan (top view).[12] The test insert is a removable sublattice of 196 fuel rods. The insert itself is 6 ft long. The central 18 in. of the test insert contains the test region, the region that is poisoned and replaced by a void in the null reactivity measurements. The top and bottom 27-in. lengths form the axial parts of the inner buffer. The outer buffer is ThO_2-UO_2 fuel, and the driver region is graphite blocks containing U^{235} foils. The air space around the tank is not to be confused with the void region which is replaced by the test insert.

Solution Assemblies

Power Reactor Technology, 6(1), contains a description of the Hanford 14-in.-diameter stainless-steel spherical critical assembly and of the experimental technique used there in measuring the worth of various solid reflector materials on critical plutonium nitrate solutions. The measurements covered a range of plutonium concentrations and acid molarities. In a continuation of this program, critical masses were determined[3] as functions of plutonium concentrations (33.5 to 70.4 g/liter) and acid molarities (~2.0 to 6.7) when the sphere was reflected by water and when the sphere was wrapped with a 0.030-in. layer of cadmium and water reflected. In addition, critical mass data were obtained for various thicknesses of the spherical stainless-steel wall to permit an evaluation of wall effects. The following conclusion is drawn by the authors. Results obtained with the cadmium-wrapped vessel are of particular interest in nuclear safety applications where flooding is a possibility since, under the concentration range covered by the experiments, the data show that a vessel wrapped with cadmium would be only nominally reflected (reflector equivalent to 1 in. or less of water). The safe dimension could then be based on the condition of a nominal reflector, rather than on the more restrictive fully reflected condition with its consequent smaller size. After corrections are made for solution volumes and Pu^{240} concentrations, very good agreement is obtained between the present data and data obtained by Kruesi et al.[4] in the Hanford P-11 program.

Criticality measurements on plutonium nitrate solutions contained in an 11.5-in.-diameter stainless-steel sphere with water reflector are reported in Ref. 5. Plutonium concentrations ranged from 51 to 431 g of plutonium per liter. The plutonium contained 4.6 wt.% Pu^{240}. Criticality of the system was studied as a function of nitrate concentration. The results, which consisted of four criticality determinations, indicated a double value (about 150 and 295 g/liter) for the critical plutonium concentration at a nitrate concentration of 303 g/liter. All plutonium concentrations between these two values would be supercritical at the specified nitrate content. This behavior illustrates the sensitivity of the critical mass to neutron-spectrum effects in high-concentration high-leakage plutonium solutions, where the critical value of the thermal utilization is near unity. Analysis of the results indicated that the critical plutonium concentration for zero nitrate content (95.4% Pu^{239}, 4.6% Pu^{240}) would be 65.0 ± 5.0 g/liter for the water-reflected 11.5-in. sphere and 28.3 ± 0.7 g/liter for the water-reflected 14-in. sphere discussed above.

Pulsed neutron-source experiments also were performed along with the critical-mass measurements. The multiplication factor was determined as a function of plutonium concentration and solution volume in the sphere. One of the purposes of these experiments was to examine the feasibility of the pulsed-source technique for k_{eff} measurements on in-plant equipment; it is stated: "Whether k_{eff} measurements can be made on process vessels (which are well subcritical and located in fixed plant areas) with sufficient accuracy to establish nuclear safety limits remains to be demonstrated."[5]

A series of calculations of the critical configurations were performed, using the GAM-I code for fast group parameters and the TEMPEST code for thermal constants. These calculations give k_{eff} to about 0.6%.

Measurements were carried out at the PCTR on the limiting critical concentrations of U^{235} and Pu^{239} in aqueous solutions [*Power Reactor Technology*, 6(1)]; the measured values were 12.94 ± 0.03 g of uranium per liter and 8.4 ± 1.0 g of Pu^{239} per liter, respectively. The relatively large uncertainty in the Pu^{239} value was the result of uncertainties in the corrections for the worth of the stainless-steel containers. Subsequent measurements[6] on the limiting critical concentration of dilute uranyl fluoride in stainless-steel containers have provided more accurate data on the worth of the containers. It was also shown that, for stainless-steel containers, a container filled with helium was less reactive than an evacuated container, the measured reactivity difference being a function of the container wall thickness. Since previous measurements with Pu^{239} solutions used helium-filled containers as a reactivity base for normalization of the data, correction for this effect was necessary. After the corrections were applied, the limiting concentration of uranium (93.15% enriched) was found to be 13.0 ± 0.1 g of uranium per liter. This value is in good agreement with the previously accepted value of 12.94 ± 0.03 g of uranium per liter, which was obtained using aluminum containers. Application of the necessary corrections to the previously measured plutonium data, which also include corrections for the Pu^{240}, Pu^{241}, and nitrate content of the solutions, resulted in a value of 8.1 ± 0.3 g of Pu^{239} per liter as the limiting concentration of a Pu^{239}-water solution. This value is in better agreement with the Monte Carlo calculated value of 7.71 ± 0.46 g of Pu^{239} per liter.

Boiling-Superheating Reactors

The superheater region of the first-generation core for the Pathfinder reactor will contain fully enriched uranium dioxide fuel in stainless-steel cermet, clad with stainless steel, in the form of dual coaxial fuel tubes. An advanced superheater design for the second-generation core contains fuel elements of a seven-pin cluster type which utilize uranium oxide fuel of approximately 4% enrichment. Experiments that are described in Ref. 7 were directed toward obtaining the information necessary for the computation of the thermal utilization and resonance escape probability for this type of fuel. The fuel pins used were 36½ in. long and were made up of 0.214-in. UO_2 pellets which had 95% of the theoretical density and which were in stainless-steel tubes of 0.010-in. wall thickness. The three enrichments studied were 3.5, 4.0, and 7.0% U^{235}, and three lattice spacings were studied for each enrichment. Results are also given for a six-pin cluster (center pin removed) for the 3.5 and 7.0% enrichments. The experiments were performed in the Pathfinder reactor core mockup. This mockup is approximately a right-circular cylinder 6 ft in diameter and 6 ft high, containing a central superheater region approximately 2.5 ft in diameter. The experimental data were taken at the radial geometric center of this superheater region, which was loaded with a sufficient number of the experimental assemblies (at least 25) to yield a typical spectrum at the center. Local flux distributions, disadvantage factors, cadmium ratios, and distributions of U^{238} activation are given for flooded and voided conditions.

A method of measuring the void distribution in an operating boiling reactor was proposed some time ago by S. Untermeyer. The local void content is inferred from the local ratio of epithermal-to-thermal neutron flux, which in turn is indicated by the measured local value of a cadmium ratio. Work on an exponential mockup of the BORAX-V reactor to explore the cadmium-ratio technique and to prepare a calibration curve for use of the technique in BORAX-V is described in Ref. 8. The known voids used in the mockup were made of sealed polyethylene tubes of the appropriate length and number. The void fractions simulated in this manner ranged from 0 to 0.4. The corresponding range of the measured cadmium ratio was 6.1 to 4.6. The radial flux distribution across a BORAX type fuel assembly and the flux details in and around fuel rods were also determined in the program. Nine of the BORAX-V subassemblies were mocked up in the exponential experiment. The neutron source for the experiment was provided by the TREAT reactor.

Heavy-Water Assemblies

A summary of experimental and theoretical results obtained in the Heavy-Water Lattice Project of the Massachusetts Institute of Technology during the period October 1961 to September 1962 is presented in Ref. 9. An initial study has been made in the main subcritical (exponential) assembly with 1-in.-diameter natural-uranium rods in triangular lattices of 4-, 5-, and 7.5-in. pitches. Material bucklings were measured and compared with results measured in both critical and exponential experiments at other laboratories. The ratios of fission rates in U^{238} relative to U^{235}, as well as the epicadmium-to-subcadmium fission ratios in U^{235}, were also measured. Experiments related to resonance capture in U^{238} included measurement of the average U^{238} cadmium ratio, average ratio of the U^{238} capture rate to the U^{235} fission rate, distribution of resonance neutrons in the moderator, and quantities related to the effective resonance integral of U^{238}. Data on intracellular thermal-neutron distribution were measured and compared with the predictions of the one-dimensional THERMOS code. In the relatively tight lattices (those in which the spacing between fuel rods was comparable to or less than the mean free path for thermal neutrons), the one-dimensional cylindrical representation of the unit cell did not predict the correct relative fluxes in the fuel and moderator regions. Two-dimensional THERMOS calculations, which approximated the hexagonal cell boundary more accurately, did provide better agreement with the experimental data. Measurements similar to those described above are being repeated for slightly enriched uranium fuel rods.

Also summarized[9] are the theoretical and experimental results from experiments on slightly enriched fuel rods that were moderated by D_2O and D_2O-H_2O mixtures in the small or miniature lattice studies. These measurements include the axial and radial flux traverses, the cadmium ratio of U^{238}, the U^{238}-to-U^{235} fission ratios, and the intracellular flux traverses with cadmium-covered gold foils.

Calculations reported in Ref. 10 relate to the uniform-lattice critical experiments performed in the ZPR-VII critical assembly with thoria-urania fuel and heavy-water moderator. The fuel consisted of pellets of thorium oxide and highly enriched uranium oxide, with atom ratios of thorium to U^{235} of 25:1 and 15:1. Experiments were carried out with both types of fuel in uniform triangular lattices having pitches of 1.905, 2.8575, 3.81, and 5.715 cm. The results of experiments for both uniform and clustered lattices are given in Ref. 11. Group constants, material bucklings, and reflector savings were calculated for the various lattice pitches employed in the experiments. Analyses were performed, and these included measurements of cadmium ratios of U^{235} and thorium, water-worth experiments, and fuel-substitution experiments.

Spectral Shift

Previous experimental work under the Spectral Shift Control Reactor (SSCR) Basic Physics Program has been reviewed earlier [*Power Reactor Technology,* 5(4): 17; 6(2): 13; and 6(3): 81]. References 12 and 13 contain results of work performed under this program during the ninth and tenth contract quarters. Results from critical experiments with the 2.46%-enriched UO_2 fuel rods at a nonmoderator-to-moderator volume ratio of 0.65 are given. The two moderator compositions studied were 85.5 and 70.0 mole % D_2O (remainder H_2O). For each of these lattices the measurements include critical size, reactivity change with water height, critical buckling, reflector savings, thermal disadvantage factor, cadmium ratio of U^{238}, and the fission cadmium ratio of U^{235}. Also, perturbation experiments were performed at a nonmoderator-to-moderator volume ratio of 1.0 and a moderator composition of 72 mole % D_2O. Local flux distributions and the reactivity worth of various perturbations in the core were studied, including the effect of a boral blade inserted in the uniform lattice, the effect of a moderator gap in the uniform lattice, the effects of boral, cadmium, and aluminum blades, respectively, in a moderator gap, and the effects of boral and aluminum cruciforms, respectively, in a moderator gap.

The results of the first small-lattice experiment are of particular interest. The purpose of this experiment was to demonstrate, for systems having a high percentage of fissions occurring at epithermal energies, the validity of methods used previously for thermal systems in the Physical Constants Testing Reactor at Hanford. Reactor parameters susceptible to measurement by this technique include the infinite multiplication factor and all the intracellular lattice parameters normally measured in a critical experiment. In this first experiment in the SSCR program, a direct comparison of results obtained in the small lattice could be made with a corresponding critical experiment. The critical experiment utilized over 2000 fuel rods that were 6 ft long and 4% enriched, whereas the small test lattice required only about 200 rods which were of the same type but which were 18 in. long.

The source reactor for the small-lattice experiment was a graphite honeycomb mounted on a split-bed assembly (Fig. II-1). Suitable adjustment of graphite bars and highly enriched uranium-aluminum foils gave a critical system. A center cavity approximately 2 ft square houses a 2-ft-diameter aluminum tank that contains the test lattice and buffer regions. In this experiment the buffer region adjacent to the test lattice had the same composition as the test lattice. However, calculations indicate that a substantial part of the buffer might be replaced by dissimilar material without significant increase in the error caused by spectral mismatch. The nonmoderator-to-moderator volume ratio in the test lattice (and buffer region) was unity, and the moderator composition was approximately 70 mole % D_2O.

Table II-1 COMPARISON OF PARAMETER MEASUREMENTS IN THE SMALL-LATTICE AND CRITICAL EXPERIMENTS[12]

Parameter	Small-lattice experiment	Critical experiment
k_∞	1.131 ± 0.008	1.130 ± 0.006
ϕ_m/ϕ_f	1.159 ± 0.007	1.157 ± 0.009
C_{25}*	2.440 ± 0.006	2.434 ± 0.012
C_{28}*	1.086 ± 0.002	1.087 ± 0.004

*Cadmium ratios.

An extensive analysis of the errors introduced by spectral mismatch between the test and buffer region and the nonflatness of the spectral flux across the test region indicated that, at least for this experiment, these errors are small and, in fact, tend to cancel each other. A comparison of the final results obtained from the small-lattice experiment and the corresponding critical experiment is given in Table II-1.

Graphite-Moderated Assemblies

Results of a series of graphite-moderated uranium-metal-fueled critical experiments are given in Ref. 14. The graphite assembly is 8 ft high and 12 ft in diameter. The fuel elements are hollow cylinders that are 1 in. in outside diameter and $^3/_4$ in. in inside diameter, and they contain uranium metal enriched to 2 wt.% U^{235}. The elements are assembled from individual, hollow cylindrical slugs of uranium metal clad with approximately 3 mils of nickel and stacked in 40-mil aluminum tubes to the desired height. The triangular lattice spacings studied ranged from 6.93 to 16.00 in., corresponding to moderator-to-fuel volume ratios from 25 to 140. An effectively infinite reflector was maintained radially for most of the assemblies, but there was no axial reflector.

In addition to critical-size measurements on the various fueled lattices, the thermal-diffusion length of the graphite was measured to determine the effective absorption cross section of the graphite.

The criticality experiments were analyzed by utilizing available IBM-7090 codes, and, in general, good agreement was obtained between calculation and experiment by means of a four-group scheme. The AIM-5 one-dimensional spatial code in four groups was used with fast constants from the FORM Fourier transform slowing-down code and thermal constants from a TEMPEST thermal-spectrum-S_4 spatial scheme. Neutron streaming through the air-filled centers of the fuel elements was accounted for by the method of Behrens. Some two-group calculations were performed, but the fit to experiments was not good. This is attributed to the inadequacy of the epithermal leakage terms and the failure of this scheme to give the proper balance between epithermal absorption and fission. However, the four-group scheme agreed with experiment to better than 1% on k_{eff} for all the lattices. It was also noted that some improvement was obtained in the agreement if the usual assumption of a Maxwell-Boltzmann thermal distribution was replaced by a calculated Wilkins spectrum.

Results of physics work performed under the BICEP program (British Industrial Collaborative Exponential Programme) were originally reported in 21 United Kingdom Atomic Energy Authority reports. A collection of these reports, along with the necessary editorial changes for the collection, is found in Refs. 15 to 17. The program was initiated to provide reactor physics data for the development of gas-cooled graphite-moderated reactor systems. Specifically, physics data were obtained for various fuel-element concepts under development in Britain. Exponential experiments were performed on graphite-moderated assemblies of rods and tubes of natural uranium metal, enriched-uranium metal rods, and clusters of uranium metal and uranium oxide rods. In addition, many fine-structure measurements were made.

The zero-energy reactor ZENITH has been used to measure[18] the temperature coefficients of reactivity of systems fueled with U^{235} and moderated and reflected by graphite. With ZENITH it is possible to investigate the effects of core plus end-reflector temperature up to 800°C and side-reflector temperature up to 400°C. Nitrogen circulates through a heater beneath the core and passes between the fuel elements; in the plenum above the core, the nitrogen may be mixed with cooler gas before passing down through the side reflector. A thermal barrier of lampblack between core and side reflector reduces heat transfer.

Temperature coefficient measurements were made in the fourth loading of ZENITH; this loading contained 7.72 kg of U^{235}, corresponding to a carbon-to-U^{235} atomic ratio of 7788. This core was the most dilute system in the projected experimental program on U^{235} systems. Reactivities were measured by the rod drop method and the critical-balance-point method. In the former method all measurements were made to the same shutdown configuration, whereas in the latter method a fine and a coarse control rod were calibrated by positive period techniques. Temperature coefficients were then evaluated from the change in critical positions of the calibrated rods. The rod oscillator technique was used to evaluate the prompt-neutron lifetime and to provide additional calibration data for the fine control rod. Axial and radial weighting factors for the temperature measurements were evaluated by measuring the worth of copper tubes at various positions in the core.

Core and end-reflector temperature coefficients, as well as side-reflector temperature coefficients, are given[18] for several temperature ranges and control-rod configurations. Apart from a possible insignificant increase in the lowest temperature interval, the temperature coefficient for the core plus end reflectors shows no evidence of temperature dependence. The mean temperature coefficient over the range 147 to 367°C is $-(15.6 \pm 1.6) \times 10^{-5}$ per degree centigrade. The side-reflector coefficient is positive and, as found for previous loadings, decreases as the number of inserted control rods increases. Calculated values of the temperature coefficient, except for the side-reflector values, agree well with experiment. The accuracy of the experimental measurements is somewhat impaired by a nonuniform core-temperature distribution.

In order to test theoretical calculations of buckling and reaction rates in plutonium-graphite assemblies using basic nuclear data, a series of near-homogeneous plutonium–graphite exponential lattices was studied in a program reported in Ref. 19. Measurements were made of the material bucklings, disadvantage factors, and relative fission rates of U^{235}, Pu^{239}, and U^{233}. The carbon-to-plutonium atom ratio covered the range 2420 to 14,520. Relative fission-rate measurements were made in one lattice at 200 and 370°C. One experiment was also performed on an enriched-uranium lattice similar to one of the plutonium experiments. Fuel for the experiments was in the form of plutonium-aluminum spikes that were 28 in. long, 1.2 in. wide, and 0.02 in. thick. Each spike, containing 6.5 g of plutonium, was sheathed in 0.02-in.-thick aluminum. Approximately 2.5 at.% of the plutonium consisted of the isotope Pu^{240}. The graphite was in the form of square prisms, which were 28 in. long and 1.73 in. in the other two dimensions.

STEWPOT, a 43-group slowing-down code for the Mercury computer, was used for theoretical calculations of the experiments. A comparison of the calculations with experiment indicated that for these systems the STEWPOT code will predict the material bucklings to ±3%. Calculations of the U^{233}-to-U^{235} fission ratios show good agreement with experiment. However, the calculated Pu^{239}-to-U^{235} fission ratios are consistently lower than the experiments by almost 6 to 9%. The reference points out that the energy group breakdown in STEWPOT was not intended for plutonium-fueled systems and is not optimum for them.

Measurements of thorium resonance-capture activations relative to those of Au^{197}, which were made in the Peach Bottom (HTGR) critical assembly, are analyzed in Ref. 20 and are compared with thorium resonance activations calculated from the tabulated values of the resonance parameters. Since some of the thorium activation measurements employed thorium oxide dispersed quasi-homogeneously in graphite, resonance captures in thorium were measured by the vanadium-subtraction technique rather than the cadmium-ratio technique. The former method measures the resonance capture rate of an unknown nuclide relative to that of a thin foil of Au^{197}, which is assumed to be known. The vanadium is employed to determine and subtract the $1/v$ cross-section component for the unknown nuclide. To check the technique and assure internal consistency, auxiliary measurements employing U^{238} and Mn^{55} were carried out. The cadmium-ratio technique was employed to obtain measurements of the resonance capture rates of vanadium, Mn^{55}, and Th^{232} foils placed in a void in the HTGR critical assembly. The measurements for the latter two elements were made for comparison with results obtained by the vanadium-subtraction technique.

Included in Ref. 20 is a review of the status of the knowledge of absorption cross sections and resonance parameters for thorium and gold. Two alternative sets of resonance parameters were selected for thorium and were employed in the calculations for comparison with the experimentally measured data on thorium resonance captures. The measurements show that the lowest several resonances of thorium capture less strongly than would be predicted by the listed parameters. This reduced capture is such that the thin-limit, epicadmium, $1/E$ spectrum resonance integral is about 84 barns instead of the 96 barns predicted by listed parameters.

BeO-Moderated Assemblies

The interaction effects of hafnium control rods in a near-homogeneous BeO-moderated oralloy-fueled system were measured[21] for two to five rods by the pulsed-neutron technique. The subcritical assembly used consisted of a matrix of BeO blocks and oralloy foils. One portion of the matrix was stacked on the platform of a hydraulic ram, and the second portion was supported directly above on a 0.019-in.-thick stainless-steel diaphragm. Seven horizontal slots, 1 by $^1/_8$ in., were built into the lower assembly. The delayed critical time constant for a burst of fast neutrons was determined by extrapolation of a curve of prompt decay constant vs. the inverse multiplication of the assembly. Two series of measurements were made with the hafnium control rods. These rods were hafnium strips, 24 by 0.5 by 0.065 in.

for the first series and 24 by 0.5 by 0.0325 in. for the second series. The thinner rods were used to reduce slightly the rod worth and permit the use of more rods. The relative worths of individual rods in the same slot, individual rods in different slots, and combinations of rods are given. Included for comparison purposes are predicted worths assuming no rod interaction. The assumption that the prompt-neutron lifetime remains constant is implicit in the interpretation of the changes of prompt decay constant in terms of reactivity changes. This assumption was validated by measuring the delayed critical decay constant with seven thick hafnium rods in the assembly; it was found to be unchanged within the 2% limit of uncertainty in the measurement of the time constant.

Fast-Neutron Assemblies

The inability to predict the critical masses of three fast dilute assemblies previously examined in the ZPR-III prompted a series of critical studies[22] to obtain data for use in evaluating the adequacy of the sodium and stainless-steel cross sections employed in multigroup calculations. The ZPR-III is a split-bed reactor with each half consisting of a matrix of square stainless-steel tubes. Drawers containing the appropriate materials for each region are inserted into the square tubes. The first assembly (No. 32) was designed for a study of a simple combination of stainless steel and enriched uranium. The second assembly (No. 33) was similar, except that part of the stainless steel in each drawer was replaced by sodium-filled stainless-steel cans. Both assemblies were completely reflected by a natural-uranium blanket. Fission ratios of various fissile materials (U^{233}, U^{234}, U^{236}, U^{238}, Pu^{239}, and Pu^{240}) were measured at the core centers using fission chambers of parallel-plate construction. Average prompt-neutron lifetimes were measured by the Rossi alpha method. The reactivity worths of common reactor materials were measured at the center of each core and, for a few selected materials, near the edge of each core. The latter data were taken for information on the transport properties of the materials. Radial fission rates of various fissile materials were measured with miniature cylindrical fission chambers in each core. A series of bunching experiments was carried out in a wedge section of one-half of core 32. These experiments provided data on the effect of fuel-plate thickness on reactivity. Distributed worths of stainless steel, sodium, and aluminum were determined by substitution of these materials over one octant of the core. A few preliminary measurements were made of the influence of the mass of sodium present on the reactivity worth of sodium and on its variation with radial position. The measurements on these and other ZPR assemblies have been summarized in Ref. 23.

The ZPR-III facility has also been used to study a mockup of the second loading (core B)[24] for the Enrico Fermi fast reactor. The core material for this reactor is UO_2–stainless-steel cermet clad in stainless steel, and the reactor is cooled by sodium. The volumetric composition of the core is 11.5% fully enriched UO_2, 51.8% stainless steel, and 33.2% sodium. The nominal fully loaded volume is 600 liters. The original mockup was too small for criticality, and alterations were necessary. The critical mass was found to be 505.4 kg of U^{235}, corresponding to a core volume of 664.6 liters. The core volume was then reduced to approximately the maximum allowable volume of 600 liters, and criticality was reached by the substitution of a nickel reflector for the radial blanket in an annulus about 2 in. thick adjacent to the core. Measurements of reactivity effects of the most important differences between the mockup and the actual Fermi reactor were necessary in order to establish the critical mass for the actual reactor. Some of these effects are end gaps, UO_2 axial blankets, a central gap, a source that occupies a subassembly at the radial edge of the actual core, and safety-rod and control-rod channels. The distributed reactivity worths of various materials were measured also in order to correct for discrepancies between the mockup and the core. A comparison of the reactivity effects of various radial reflectors was made. These included nickel, nickel oxide, iron oxide, beryllium, and beryllium oxide. Measurements were made of relative reaction rates as functions of both radial and axial position, and fission ratios of the various fissionable isotopes were measured at the center of the core.

Various features related to the dynamic behavior of the reactor were investigated. These included a measurement of the isothermal temperature coefficient, the reactivity effects of axial core expansion, and Rossi alpha measurements at delayed critical. The reactivity effect of heterogeneity of the fuel was estimated by bunching the fuel plates in various arrangements; the final results give reactivity change as a function of effective fuel-plate thickness. This curve extrapolated to zero plate thickness gives the reactivity loss caused by homogenizing the fuel.

References

1. I. Kaplan, Measurements of Reactor Parameters in Subcritical and Critical Assemblies, USAEC Report MITNE-25, Massachusetts Institute of Technology, Aug. 15, 1962.
2. General Nuclear Engineering Corp., BONUS Zero Power Critical Experiments and Application to the Reactor Design, Terminal Report, USAEC Report GNEC-198, Feb. 10, 1962.
3. R. C. Lloyd, E. D. Clayton, and C. R. Richey, Critical Mass Experiments with Plutonium Nitrate Solutions, in Physics Research Quarterly Report, July, August, September 1962, USAEC Report HW-75228, pp. 33-39, Hanford Atomic Products Operation, Oct. 15, 1962.
4. F. E. Kruesi, J. O. Erkman, and D. D. Lanning, Critical Mass Studies of Plutonium Solutions, USAEC Report HW-24514(Del.), Hanford Atomic Products Operation, May 19, 1952.
5. R. C. Lloyd, E. D. Clayton, C. R. Richey, and S. R. Bierman, Critical Experiments with Plutonium Nitrate Solutions, in Physics Research Quarterly Report, January–March 1963, USAEC Report HW-77311, pp. 44-47, Hanford Atomic Products Operation, Apr. 15, 1963.
6. J. D. White, T. J. Powell, and R. H. Masterson, Limiting Critical Concentrations of U^{235} and Pu^{239} in Aqueous Solutions, in Physics Research Quarterly Report, July, August, September 1962, USAEC Report HW-75228, pp. 40-53, Hanford Atomic Products Operation, Oct. 15, 1962.
7. A. Selep, Pathfinder Atomic Power Plant. Clustered Pin Superheater Lattice Experiments, USAEC Report ACNP-63005, Allis-Chalmers Mfg. Co., Feb. 12, 1963.
8. F. S. Kirn and J. I. Hagen, BORAX-V Exponential Experiment, USAEC Report ANL-6707, Argonne National Laboratory, April 1963.
9. I. Kaplan, A. E. Profio, and T. J. Thompson, Heavy Water Lattice Project Annual Report, USAEC Report MITNE-26, Massachusetts Institute of Technology, Sept. 30, 1962.
10. E. M. Pennington, Calculations for ZPR-VII Uniform Lattice Critical Experiments with Thoria-Urania Fuel in Heavy Water, USAEC Report ANL-6661, Argonne National Laboratory, December 1962.
11. W. C. Redman, S. G. Kaufmann, K. E. Plumlee, and Q. L. Baird, Critical Experiments with Thoria-Urania Fuel in Heavy Water, USAEC Report ANL-6378, Argonne National Laboratory, December 1961.
12. The Babcock & Wilcox Co., Spectral Shift Control Reactor Basic Physics Program. Quarterly Technical Report No. 9, USAEC Report BAW-1266, October–December 1962.
13. The Babcock & Wilcox Co., Spectral Shift Control Reactor Basic Physics Program. Quarterly Technical Report No. 10, USAEC Report BAW-1271, January–March 1963.
14. R. W. Campbell, R. J. Doyas, H. C. Field, C. A. Guderjahn, R. L. Guenther, D. F. Hausknecht, M. S. Mayer, and H. A. Morewitz, Critical Experiments on Slightly Enriched Uranium Metal Fuel Elements in Graphite Lattices, USAEC Report NAA-SR-7541, Atomics International, June 30, 1963.
15. British Industries Collaborative Exponential Programme. Volume I. Introduction; Exponential Experiments on Rods and Tubes of Natural Uranium Metal, British Report AEEW-R-235 (Pt. I), March 1963.
16. British Industries Collaborative Exponential Programme. Volume II. Exponential Experiments on Enriched Uranium Metal Rods and on Clusters of Uranium Metal and Uranium Oxide Rods, British Report AEEW-R-235 (Pt. II), March 1963.
17. British Industries Collaborative Exponential Programme. Volume III. Fine Structure Experiments; Miscellaneous Exponential Experiments, British Report AEEW-R-235 (Pt. III), March 1963.
18. R. Caro Manso, R. G. Freemantle, and J. D. Rogers, Temperature Coefficients of Reactivity with Fourth Loading of ZENITH, British Report AEEW-R-208, October 1962.
19. D. H. Carter, W. G. Clarke, C. Hunt, J. Marshall, D. B. McCulloch, J. E. Sanders, and C. R. Symons, Measurements of Buckling and Relative Reaction Rates in Some Plutonium-Graphite Assemblies, British Report AEEW-R-201, January 1963.
20. J. B. Sampson, Analysis of Activation Measurements of Th^{232} Resonance Captures in the Peach Bottom (40-Mw(e) Prototype HTGR) Critical Assembly, USAEC Report GA-3069, General Atomic Division, General Dynamics Corp., Sept. 14, 1962.
21. J. M. Piowaty, J. R. Morton III, and L. L. Gardner, Coupling Effects of Hafnium Control Rods in a Near-Homogeneous, BeO-Moderated, Oralloy-Fueled System, USAEC Report UCRL-7262, University of California, Lawrence Radiation Laboratory, Feb. 27, 1963.
22. P. I. Amundson, W. Gemmell, J. K. Long, and R. L. McVean, Critical Studies of Uranium-Steel and Uranium-Steel-Sodium Fast Reactor Cores (ZPR-III Assemblies 32 and 33), USAEC Report ANL-6690, Argonne National Laboratory, February 1963.
23. J. K. Long, A. R. Baker, W. Gemmell, W. P. Keeney, R. L. McVean, and F. W. Thalgott, Ex-

perimental Results on Large Dilute Fast Critical Systems with Metallic and Ceramic Fuels, in *Physics of Fast and Intermediate Reactors*, Vol. I, International Atomic Energy Agency, Vienna, 1962.

24. T. A. Doyle and A. L. Hess, Critical Studies of Core B for the Enrico Fermi Atomic Power Plant (ZPR-III Assembly No. 35), USAEC Report ANL-6669, Argonne National Laboratory, February 1963.

Section

III

Power Reactor Technology

Fluid and Thermal Technology

Burnout Limits for Boiling-Water Reactors

By John S. Wiley

Heat-transfer burnout is one of the phenomena which determine the power capability of a water-cooled reactor. It is not the only one, nor is it necessarily the controlling one In oxide-fueled reactors the central temperature of the fuel elements often imposes a limitation that is more restrictive than the burnout limitation. Nevertheless, the burnout limitation is a highly important one. Its relative importance is likely to increase as reactor designs become more highly developed and as methods for extracting higher specific powers from oxide fuel elements are proved. Furthermore, rightly or wrongly, the burnout ratio is given serious consideration in safety evaluations of power reactors, and for this reason the question of burnout sometimes proves to be a more restrictive design consideration than might otherwise be supposed.

In recognition of the importance of burnout phenomena to the reactor designer, investigations and analyses related to burnout have been given considerable attention in past issues of *Power Reactor Technology*. Since these investigations are usually described in papers written for the heat-transfer specialist rather than for the reactor designer, it has seemed worthwhile to examine the question briefly from the point of view of the designer's interests. In this article advantage is taken of the opportunity offered by the presentation of two new burnout correlations[1,2] to present such a review. The discussion is limited to burnout under conditions of net boiling, because burnout tends to impose more severe restrictions on boiling reactors than on pressurized-water reactors, and because limitation of the discussion to a single burnout regime simplifies the problem of relating the phenomenon to questions of reactor design and analysis. In the course of the discussion, selected burnout data will be utilized to illustrate various points. Many of these data are taken from the extensive collection that has been assembled in Ref. 3.

To cover the range of practical interest in burnout, one must consider a relatively large number of variables and rather large ranges of these variables. The major variables, in addition to the heat flux, include the size, shape, and degree of interconnection of the coolant channels, the flow velocity of the coolant, its pressure, and the degree to which it is subcooled below the saturation temperature at the entrance to the coolant channel. Large ranges of variables have been covered by the many measurements of burnout which have been made, and the question naturally arises as to how to correlate all these experimental data.

Because the process of burnout is not understood in detail, it has not been possible to arrive at correlations that are based on the fundamental relations among the variables. In such a circumstance it is usually found that no single correlation will meet the needs of all users of the experimental data, and this proves to be the case for burnout. One approach is to attempt to find purely empirical equations that will relate the important variables with acceptable accuracy over the widest possible range. Such correlations are very useful and are widely used as methods of compressing the results of many experiments into a small volume. In arriving at such a correlation, the analyst must sometimes make compromises in the precision with which the correlation will cover the entire range of variables in order to arrive at an expression of reasonable length and complexity. When the

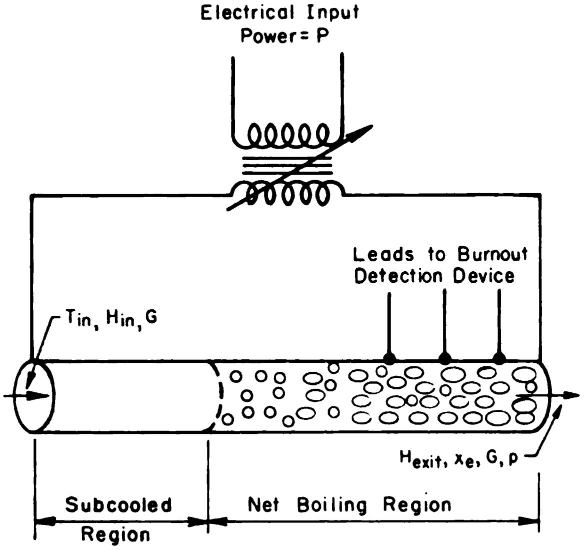

Fig. III-1 Diagram of representative burnout test. T = temperature, °F; H = enthalpy, Btu/lb; x = quality, lb/lb; G = mass flow, lb/(hr)(sq ft); p = pressure, psia.

fundamental relations among the variables are not known, arbitrary groupings and functional dependencies must be assumed. Once this is done the correlation can make no distinction between those deviations from its predictions resulting from true functional dependencies that have been neglected and those resulting from errors of measurement or perhaps from true fluctuations in the phenomenon under consideration. In this respect such a correlation falls short of the needs of the analyst who may desire to infer basic functional relations. Since it seeks to express the entire mass of accumulated data in terms of the fewest possible variables, the variables chosen for correlation are often not the independent variables of reactor design. In this respect the correlation may also fall short of the needs of the designer. It is not usually in a convenient form for illuminating the relations among the design variables.

It is instructive to consider how burnout experiments are run and how the data might be handled in the simple case in which the experimenter is provided with a heat-transfer apparatus of fixed dimensions. It will be assumed that the apparatus consists of a uniform round tube, electrically heated, as is usually the case in such experiments and as indicated in Fig. III-1. If it is assumed that the experimenter has chosen the pressure at which he is to operate (and to simplify later discussion it is here assumed that the pressure specified is that at the tube exit), then he has available only three further variables: the electric power input to the tube, the coolant flow velocity, and the inlet temperature of the coolant. If he fixes the inlet temperature (at, say, some value below the saturation temperature at the ambient pressure), he may choose to run the experiment in one of two ways: either he may fix the coolant flow velocity and gradually increase the power input to the test section until burnout occurs, or he may adjust the coolant flow to some value, fix the power input, and then gradually change the coolant flow until burnout occurs. Presumably, similar results may be obtained by both methods.

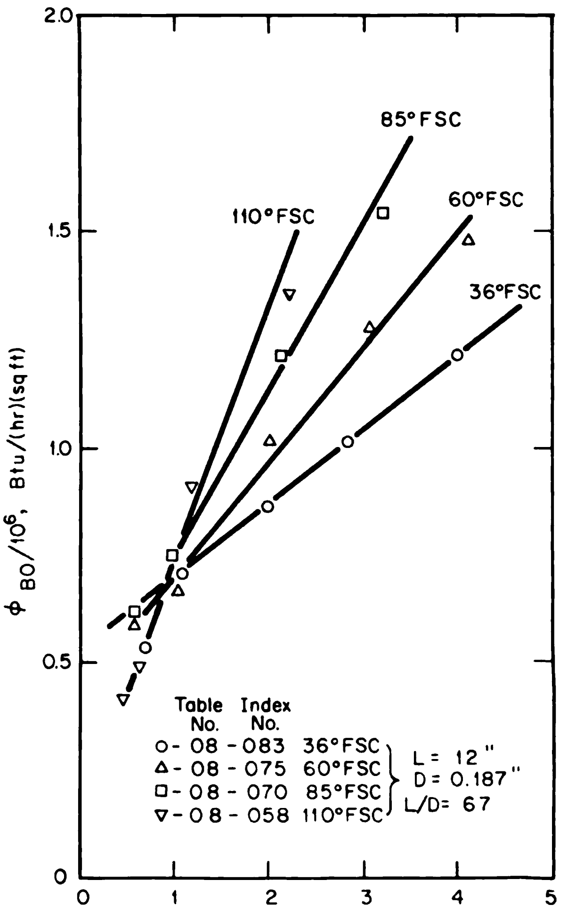

Fig. III-2 Plot of burnout data from Table 8 of Ref. 3. ϕ_{BO} vs. G; pressure = 2000 psia. The "Table No." and "Index No." refer to the method of organizing the data as used in Ref. 3.

If a number of such experiments are run, over a range of coolant flows and power inputs, the experimenter will accumulate a group of data and will be faced with the question of how to present it. A straightforward scheme is to plot the two directly controlled variables, coolant flow and power input (or the more general specification of the power input, the heat flux), against one another. Figure III-2 shows the results of some experimental data of this kind (from Ref. 3), plotted in just such a way. There are four curves shown, each for a different value of inlet subcooling; as might be expected, the heat flux at which burnout occurs increases, for the tube of fixed length-to-diameter ratio, with inlet subcooling.

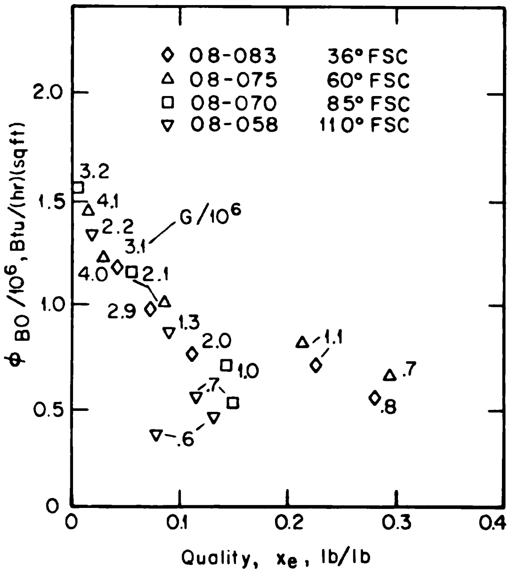

Fig. III-3 Plot of burnout data from Table 8 of Ref. 3. ϕ_{BO} vs. x_e; pressure = 2000 psia.

The question immediately arises as to whether there is some more general way of plotting (correlating) the data which might bring together all the curves for the different degrees of subcooling. This possibility seems particularly reasonable since all the experimental sections are actually observed to burn out at or very near the exit end and since, if burnout is determined purely by the local conditions of the coolant and heat flux (i.e., burnout is not affected by the past history of the coolant at points farther upstream in the tube), the condition of the coolant near the exit end of the tube can thus be completely specified simply by specifying its steam content. The obvious suggestion is to plot the burnout heat flux as a function of the steam quality at the tube exit, x_e. This has been done for the data of Fig. III-2 in Fig. III-3, and it is observed that, although the four sets of data are indeed integrated, there is a disappointing spread in the data points at the higher values of exit quality. This scatter is rather characteristic of burnout data at high exit quality if they are plotted in this way. Figure III-4 shows another set of data taken from the same reference.[3]

In considering the behavior of the data in Figs. III-3 and III-4, it is important to bear in mind that the exit steam quality is not a measured quantity but one that is computed from the measured values of mass flow and heat flux. The exit quality is computed from the heat balance, as follows:

$$4\phi L/D = G(H_{\text{exit}} - H_{\text{in}}) \tag{1}$$

where* ϕ = uniform heat flux, Btu/(hr)(sq ft)
L = total length of test section, ft
D = diameter of test section, ft
H_{exit} = enthalpy of mixture leaving test section, Btu/lb
H_{in} = enthalpy of mixture entering test section, Btu/lb

If the definition of exit quality, x_e, in terms of enthalpy is used, Eq. 1 can be written as

$$\phi = GD/4L(x_e H_{fg} + H_f - H_{\text{in}}) \tag{2}$$

The symbols H_{fg} and H_f have their conventional meanings. Equation 2 has been plotted on Fig. III-5 for two of the points of Fig. III-4 (runs 205 and 206 of Table 10, Ref. 3) where it is called the operating line, again following the nomenclature suggested in Fig. 74 of Ref. 3. The significance of this designation is that, if the burnout experiment was run by the first method described above—by setting the mass flow and the inlet subcooling and gradually increasing the input power until burnout occurred—the exit quality would increase with heat flux during this process in the manner specified by the operating line.

---

*Equation 1 is valid over a range of ϕ from zero power to burnout. At burnout ϕ is termed ϕ_{BO} and the exit enthalpy is termed H_{BO}, following the nomenclature of Ref. 3. Thus the qualities plotted in Figs. III-3 and III-4 could be labeled $x_{e_{BO}}$; the last subscript was dropped, however, for simplicity in nomenclature.

As Eq. 2 shows, the slope of the operating line is proportional to the mass flow, and if, for example, there were in the experiment an uncertainty of ±10% in the mass flow, there would be a corresponding uncertainty in the slope of the operating line. If there were also an uncertainty of ±10% in the heat flux at which burnout occurred, either because of experimental imprecisions or because of real uncertainties in the burnout process, this uncertainty would combine with the uncertainty in mass flow to yield a net uncertainty of approximately ±20% in the value of the exit quality at burnout. These illustrative uncertainty ranges have been indicated for the two burnout points plotted in Fig. III-5. It is clear that the use of the derived exit quality as a plotted variable tends to emphasize whatever uncertainties may exist in the measurements, simply because x_e is given by the ratio of two measured quantities (the heat flux and the mass flow), and consequently its percentage range of uncertainty is approximately the sum of the ranges for the two measured quantities. One must be on the alert for such artificial changes in the apparent uncertainties of experimental determinations when considering the appropriateness and accuracy of correlation procedures.

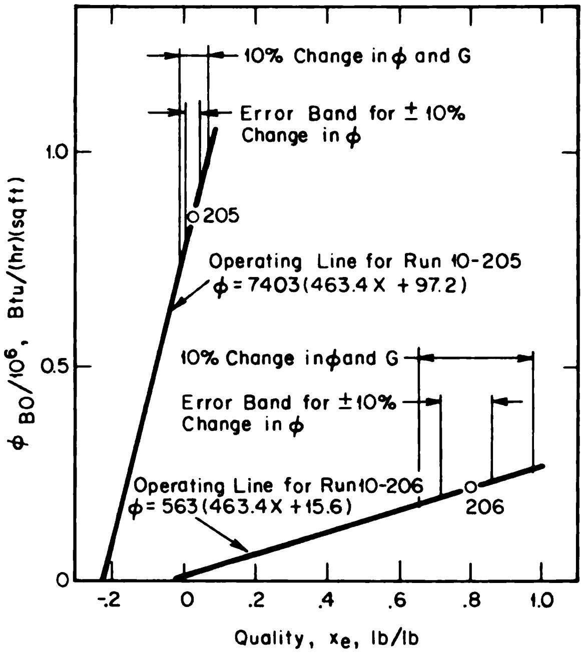

Fig. III-5 Plot of operating lines for runs 10-205 and 10-206 of Ref. 3. ϕ_{BO} vs. x_e; pressure = 2000 psia.

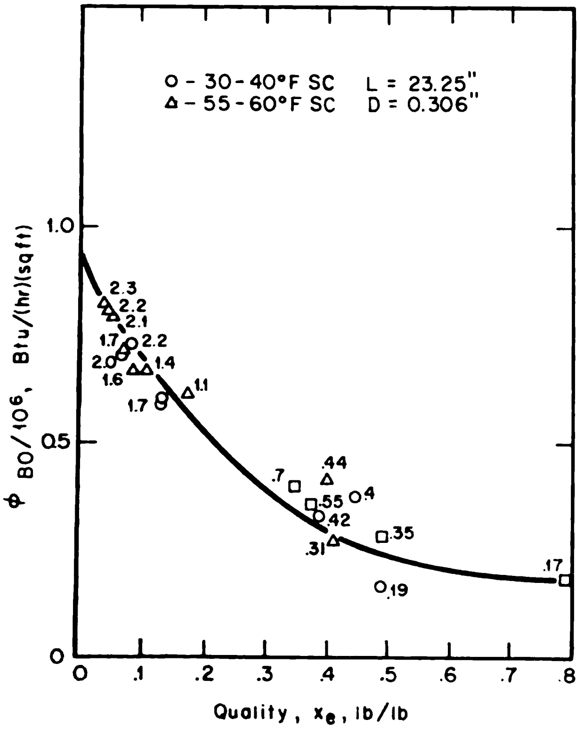

Fig. III-4 Plot of burnout data from Table 10 of Ref. 3. ϕ_{BO} vs. x_e; pressure = 2000 psia.

The plotting of burnout heat flux as a function of exit quality is an elementary correlation arrived at here through an intuitive judgment as to the burnout process, and it is fundamentally useful insofar as it gives some evaluation of that judgment. Although it does bring together data in which the only variables are heat flux, mass flow, and subcooling, it would be surprising if this single parameter alone could correlate the effects of many other variables. The correlations given in Ref. 2, which are discussed in later paragraphs, are expressed primarily in terms of the exit quality variable. They give a good indication of the usefulness of this parameter as a basis for correlation.

For the purposes of boiling reactor design, it is useful to treat the burnout data in a somewhat different manner that amounts to taking the mass flow, G, inside the parentheses in Eq. 2 and using the product Gx_eH_{fg} as the plotted variable

$$\phi = D/4L(Gx_eH_{fg} + GH_f - GH_{in}) \qquad (3)$$

This method of handling the data was first proposed by Levedahl,[4] who gave the name steam-energy flow (SEF) to the quantity Gx_eH_{fg}. When the burnout heat flux is plotted as a function of SEF, the curve presents to the reactor designer the effect of the burnout limit on the two important design quantities that specify the heat-removal characteristics for the boiling reactor core. The significance of the burnout value of the heat flux is well known; the significance of the steam-energy flow at the burnout point is that it tells the designer how much power can be removed, in the form of latent energy of steam, from the unit cross-sectional area of the coolant flow passage.

The data from Figs. III-3 and III-4 (Tables 8 and 10 of Ref. 3) have been replotted on steam-energy plots in Figs. III-6 and III-7. It can be seen that the data no longer fall on single curves but are again, as in Fig. III-2, separated according to mass flow, and each curve consists of two lines of opposite slope arbitrarily called DNB-1 and DNB-2. The scatter of the data about the line appropriate to them is small. In this method of plotting, the effects of compounded uncertainties are not accentuated in the region of low burnout heat flux, as is shown in Fig. III-8. The steam-energy flow plot can hardly be called a correlation, since it does not reduce the number of variables that must be taken into account, but it does have fundamental usefulness in addition to its usefulness to the designer, for it brings some order into the data and it suggests the existence of two quite different processes that may determine burnout (DNB-1 and DNB-2).

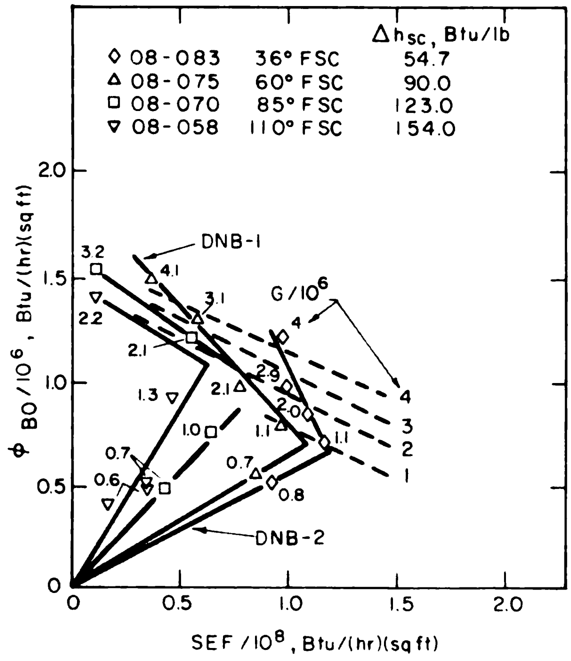

Fig. III-6 SEF plot of Table 8 data of Ref. 3. ϕ_{BO} vs. SEF; pressure = 2000 psia; L = 12.5 in.; D = 0.187 in., L/D = 67; A-nickel.

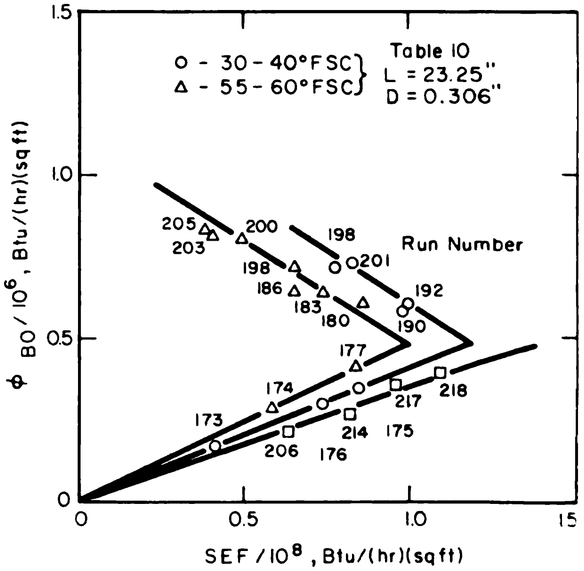

Fig. III-7 SEF plot of Table 10 data of Ref. 3. ϕ_{BO} vs. SEF; pressure = 2000 psia.

In setting the reactor power output, the designer never intentionally approaches near the burnout limit but always leaves a large safety factor that is usually expressed as the burnout ratio. This is the ratio of the burnout heat flux to the actual heat flux at the worst point in the reactor. Since it is the limitation of some specified burnout ratio that sets the permissible power output of the reactor, it is worthwhile to examine just what the ratio means in terms of a safety factor. The steam-energy flow plot is useful for this examination and is employed schematically in Fig. III-9. It shows a hypothetical DNB-1 line and an operating line, $\overline{AC}$, for the worst coolant channel of a hypothetical boiling reactor that has a uniform axial power-generation rate. It is assumed that the channel normally operates at point B, with a heat flux ϕ_1 and a steam-energy flow of SEF$_1$ at the channel exit. The burnout ratio is often defined as

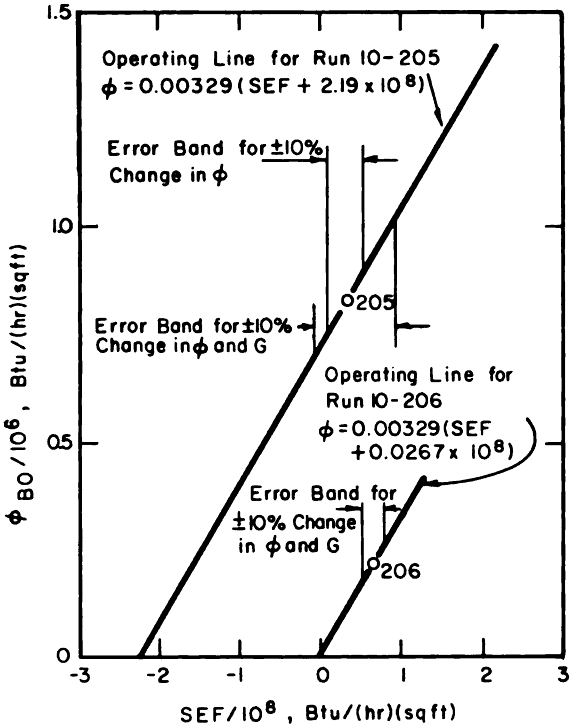

Fig. III-8 Operating lines for runs 10-205 and 10-206 of Ref. 3 on an SEF plot. Pressure = 2000 psia.

the ratio $\phi_3 : \phi_1$, but this ratio has little significance as a safety factor on reactor power, since heat flux and steam-energy flow must vary simultaneously, as specified by the operating line as reactor power is varied. If the reactor power were increased to burnout, the burnout in the coolant channel in question would occur at point *C*, corresponding to a heat flux ϕ_{BO} and a steam-energy flow SEF_{BO}. For normal operation at ϕ_1, the safety factor on reactor power is thus ϕ_{BO}/ϕ_1. These considerations have been pointed out in the past, notably by Ref. 3. In that paper the ratio $\phi_3 : \phi_1$ is called the heat-flux burnout ratio, whereas the ratio $\phi_{BO} : \phi_1$ is called the power burnout ratio. The ratio $\phi_3 : \phi_1$ has a physical significance only if it is postulated that the DNB-1 line is determined entirely by local conditions at the point of burnout. In such a case the ratio $\phi_3 : \phi_1$ in Fig. III-9 is the factor by which the heat flux would have to be increased in a very short section of the coolant channel, near the exit, to cause burnout.

As normally used, however, the burnout ratio is not so much a safety factor on reactor power as it is an uncertainty factor on the burnout prediction. Perhaps it is more precise to say that it is an uncertainty factor on the applicability, to the specific reactor situation in question, of the burnout data or burnout correlation used to predict the burnout limit. In this application it might be argued that the ratio $\phi_3 : \phi_1$ is as good a means of describing the uncertainty as the ratio $\phi_{BO} : \phi_1$. Actually the use of any single number is probably a poor way of expressing a safety factor on burnout, if it is recognized that the burnout correlation (exemplified by the DNB-1 line in Fig. III-9) may have an unexpected shape and that there will be uncertainties in the operating line for the reactor as well as in the burnout correlation. It is perhaps justified only because the burnout ratios actually used in reactor design are large, and because other uncertainties, such as those arising from nonuniform heat generation and complex coolant-channel geometry, may affect the significance of the burnout ratio in a way that is poorly understood in any case.

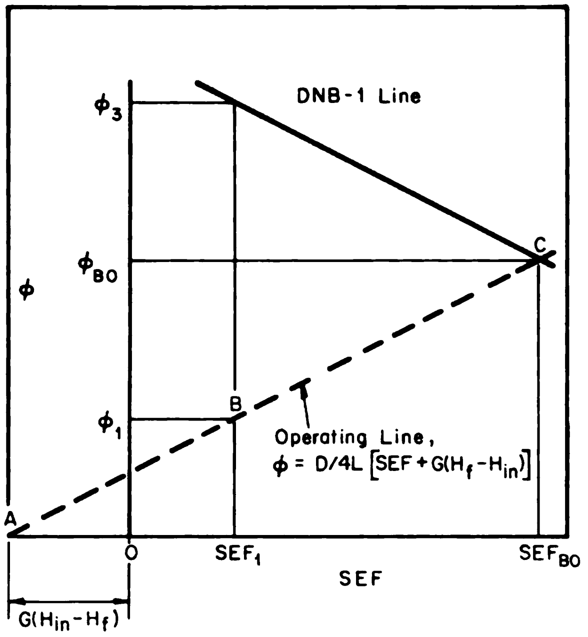

Fig. III-9 Steam-energy flow plot showing hypothetical DNB-1 and operating lines.

The questions raised by axial nonuniformities in heat flux along the coolant channel are particularly significant because axial nonuniformity is the normal situation in reactor applications. This is the key question: Is burnout

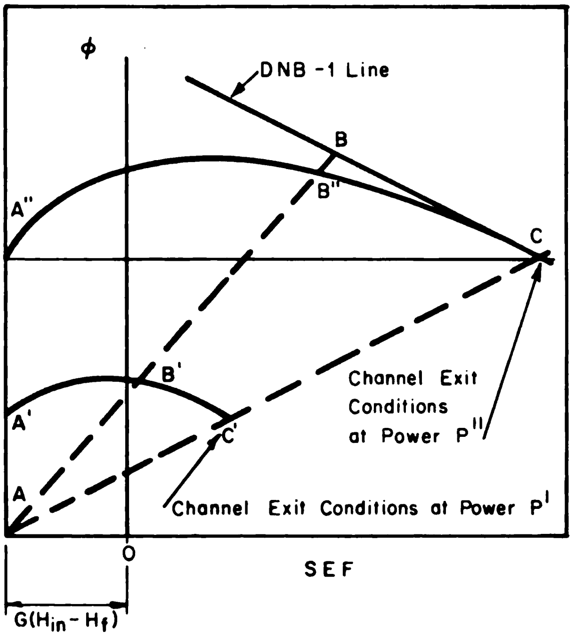
ϕ
DNB -1 Line
B
B''
A''
C
B'
A'
C'
A
Channel Exit Conditions at Power P''
Channel Exit Conditions at Power P'
O
SEF
G(H_in - H_f)

Fig. III-10 Steam-energy flow plot showing hypothetical DNB-1 line and operating lines corresponding to nonuniform axial power production.

determined entirely by the local value of the heat flux and the local time-averaged values of temperature, pressure, mass flow, and quality for the coolant? If the answer is yes, the effects of nonuniform heating should be reasonably predictable from burnout experiments on uniformly heated test sections. Experiments have been made to investigate this question, but they have been inconclusive, at least in the net boiling range. It is well known that in some cases burnout is induced by flow instabilities, and in these cases it would not be anticipated that local conditions will determine burnout.

If it is assumed that burnout is determined by only local factors in the DNB-1 range, the burnout relations along a single coolant channel in a reactor with nonuniform axial power distribution can be discussed in terms of Fig. III-10. In this figure the point values of ϕ and SEF at two powers, P' and P'', are schematically shown. Here there are an infinite number of burnout safety factors given by ratios such as $\overline{AB}:\overline{AB'}$ and $\overline{AC}:\overline{AC'}$. As power is increased (say from P' to P''), one of the ratios becomes unity and burnout ensues. Thus whether burnout occurs at the channel exit or somewhere upstream depends on the detailed shapes and relative positions of curves such as $A'B'C'$, $A''B''C$, and the DNB-1 line. If fairly rapid power transients are considered, the problem is further complicated by the fact that the flow rate may vary during the transient, and this affects the operating line position, as well as possibly the DNB-1 line. As shown in Fig. III-10, some nonuniformly heated test sections will still burn out at their exits. This is illustrated in Fig. III-10 by arbitrarily choosing curve $A''B''C$ so that it intersects the DNB-1 line at point C. A slight increase in the slope of the DNB-1 line could produce upstream burnout.

The preceding discussion is intended as an introduction to the examination of the burnout correlations presented in Refs. 1 and 2. Those presented in Ref. 1 also appear in a Westinghouse topical report[5] that deals with an AEC-sponsored research and development program for a large pressurized-water reactor that is to be built by Westinghouse for Southern California Edison Company. A correction to the material presented in Ref. 1 is contained in a Letter to the Editor published in the July 1963 issue of *Nucleonics*. The present discussion considers only the correlation for the quality region, which is given in Eq. 1 in Ref. 1:

$$\begin{aligned}\Delta H_{\text{DNB}} &= 0.529(H_f - H_{\text{in}}) \\ &\quad + (0.825 + 2.36e^{-204D_e})H_{fg}e^{-1.5G/10^6} \\ &\quad -0.41H_{fg}e^{-0.0048L/D_e} \\ &\quad -1.12H_{fg}\rho_g/\rho_f + 0.548H_{fg} \qquad (4)\end{aligned}$$

where

$$\Delta H_{\text{DNB}} = H_{\text{DNB}} - H_{\text{in}} = 4L_{\text{DNB}}/D_e \times \phi_{\text{BO}}/G \qquad (5)$$

and

D_e = equivalent diameter, ft = 4(cross-sectional area)/heated perimeter)
G = local mass velocity, lb/(hr)(sq ft)
H_{in} = inlet enthalpy, Btu/lb
H_f = saturated liquid enthalpy, Btu/lb
H_{fg} = heat of evaporation, Btu/lb
ΔH_{DNB} = $(H_{\text{DNB}} - H_{\text{in}})$, Btu/lb
L = length of heated channel, ft
ϕ_{BO} = heat flux at DNB, Btu/(hr)(sq ft)
ρ_f = density of saturated liquid, lb/cu ft
ρ_g = density of saturated vapor, lb/cu ft

The parameter ranges of the correlated experimental data are given as follows:[1]

Geometries: circular tube, rectangular channel, and rod bundle

Axial heat-flux distribution: uniform and nonuniform

Mass velocity = 0.2×10^6 to 4.0×10^6 lb/(hr)(sq ft)

Pressure = 800 to 2750 psia

L/D_e = 21 to 656

Inlet subcooling $H_{in} \geq 400$ Btu/lb

Local heat flux = 0.1×10^6 to 1.8×10^6 Btu/(hr)(sq ft)

Exit quality = 0 to 0.90 wt.%

Equivalent diameter = 0.1 to 0.54 in.

Heated-to-wetted perimeter ratio = 0.88 to 1.0

The terms H_{DNB} and L_{DNB} are presumably the enthalpy of the mixture at the point of departure from nucleate boiling and the length of the heated channel from inlet to the point of departure from nucleate boiling. In Ref. 1 ϕ_{BO} is termed q''_{DNB}; for uniformly heated test sections burning out at their exit $L_{DNB} = L$.

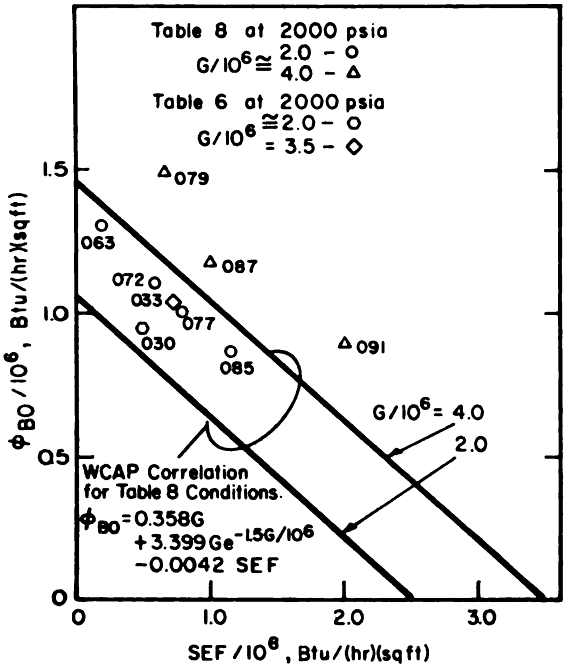

Fig. III-11 Comparison of WCAP correlation at 2000 psia with data from Tables 6 and 8 of Ref. 3.

Equation 4 can be stated in terms of the steam-energy flow if the geometry is fixed, so that the heat input can be specified in terms of the heat flux and the equivalent diameter, as required by the heat balance of Eq.2. The case of circular channels is considered, for which D, the equivalent diameter, is four times the heated perimeter divided by the cross-sectional flow area. Solving Eq. 2 for the quantity $(H_f - H_{in})$ gives

$$\frac{4\phi_{BO}L}{GD} - \frac{\text{SEF}_{BO}}{G} = H_f - H_{in} \tag{6}$$

Substituting Eq. 6 into Eq. 4 yields

$$\begin{aligned} 0.471\,\frac{4\phi_{BO}L}{GD} = {} & -0.529\,\frac{\text{SEF}_{BO}}{G} \\ & +(0.825 + 2.36e^{-204D_e})H_{fg}e^{-1.5\,G/10^6} \\ & -0.41H_{fg}e^{-0.0048L/D_e} \\ & -1.12H_{fg}\rho_g/\rho_f + 0.548H_{\ g} \end{aligned} \tag{7}$$

Figure III-11 shows the Westinghouse Atomic Power Division (WCAP) correlation (in the form given by Eq. 7) as applied to conditions of Table 8, Ref. 3. The four data points of Table 8 for $G/10^6 = 2.0$ fall in a line parallel to the appropriate correlation line, as do the three higher mass-flow data points. The ratio of the experimental burnout heat flux, ϕ_{BO_e}, to the calculated heat flux, ϕ_{BO_c}, however, cannot be obtained directly from the figure. This is true because ϕ and SEF are related by means of the heat balance, and, if the correlation predicts ϕ_{BO}, it also predicts SEF_{BO}. An example will

Table III-1 COMPARISON OF CALCULATED AND EXPERIMENTAL DATA

Run No. (from Table 8 of Ref. 3)	Mass flow, G, lb/(hr)(sq ft) $\times 10^{-6}$	ϕ_{BO_e}, Btu/(hr)(sq ft) $\times 10^{-6}$	ϕ_{BO_c},* Btu/(hr)(sq ft) $\times 10^{-6}$	$\frac{\phi_{BO_e} - \phi_{BO_c}}{\phi_{BO_e}}$	SEF_{BO_e}, Btu/(hr)(sq ft) $\times 10^{-8}$	SEF_{BO_c}, Btu/(hr)(sq ft) $\times 10^{-8}$	$\frac{\text{SEF}_{BO_e} - \text{SEF}_{BO_c}}{\text{SEF}_{BO_e}}$
08-076	1.08	0.75	0.71	5.3	1.08	0.96	11.1
08-077	2.11	0.99	0.86	13.0	0.82	0.48	41.5
08-078	3.14	1.27	1.11	12.6	0.63	0.26	58.5
08-079	4.12	1.48	1.41	4.7	0.36	0.22	38.9

*Calculated from $\phi_{BO} = 0.339G + 1.600Ge^{-1.5G/10^6}$. This is the equation shown on Fig. III-11 after substitution of Eq. 6 for SEF and using $H_{in} = 585.2$ Btu/lb.

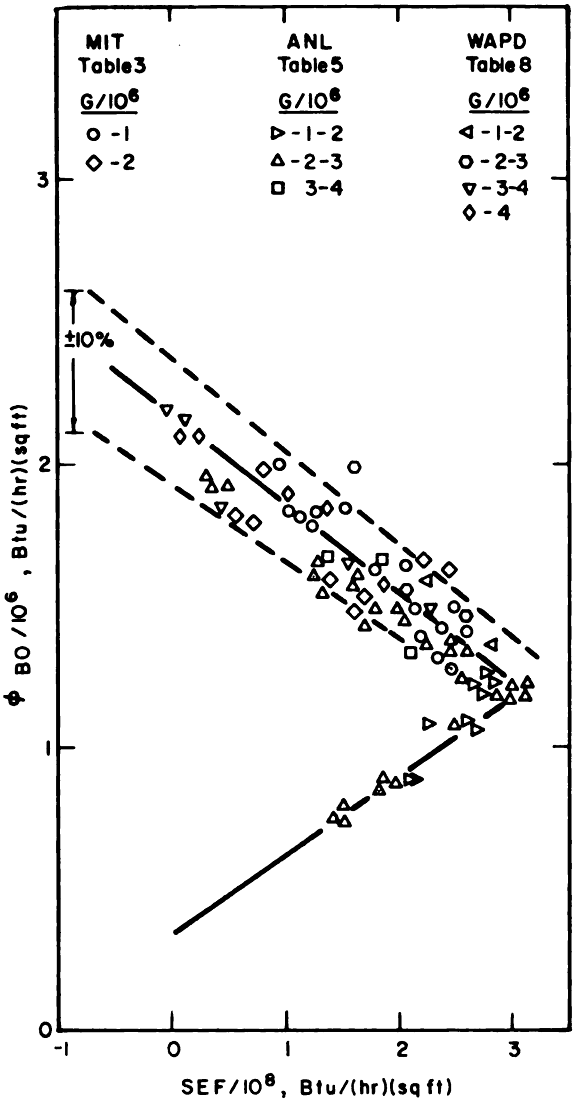

Fig. III-12 Steam-energy flow plot of data appearing in Tables 3, 5, and 8 of Ref. 3. Pressure = 1000 psia.

serve to illustrate the point. Table III-1 lists the experimental and calculated values of ϕ_{BO} and the exit steam-energy flow values at the burnout heat flux, SEF_{BO}, for runs 08-076, -077, -078, and -079. This table shows that the correlation does indeed predict the burnout heat flux within 20%, as stated.[1] The correlation also predicts an exit quality at burnout and the resulting SEF value at burnout; the accuracy of this prediction is quite poor. If nonuniformly heated test sections do burn out as is suggested in Fig. III-10, then the location of the DNB-1 line is important. If a correlation overpredicts ϕ_{BO}, it also overpredicts SEF_{BO}, which has the effect of moving the DNB-1 line both upward and to the right. The burnout safety factor given by the ratio $\overline{AC}:\overline{AC'}$ is thus also overpredicted, since the length of $\overline{AC}$ is given by a correlation and the length $\overline{AC'}$ is set by the designer.

Also plotted on Fig. III-11 are runs 030 and 033 from Table 6 of Ref. 3. This was done to show that there is still some unaccounted-for variable that prevents the Table 6 results from agreeing with the Table 8 results. That they should agree is suggested by the fact that the two test sections used to take the data of Tables 6 and 8 were almost identical in dimensions. This subject has been discussed in Ref. 6.

Figure III-12 contains 1000-psia burnout data contained in Tables 3, 5, and 8 of Ref. 3. Although the data all appear in a Westinghouse publication, they were actually taken at three different laboratories. It can be noted that at this pressure the steam-energy flow plot happens to bring the data for a wide range of mass flows very nearly together into a single curve.

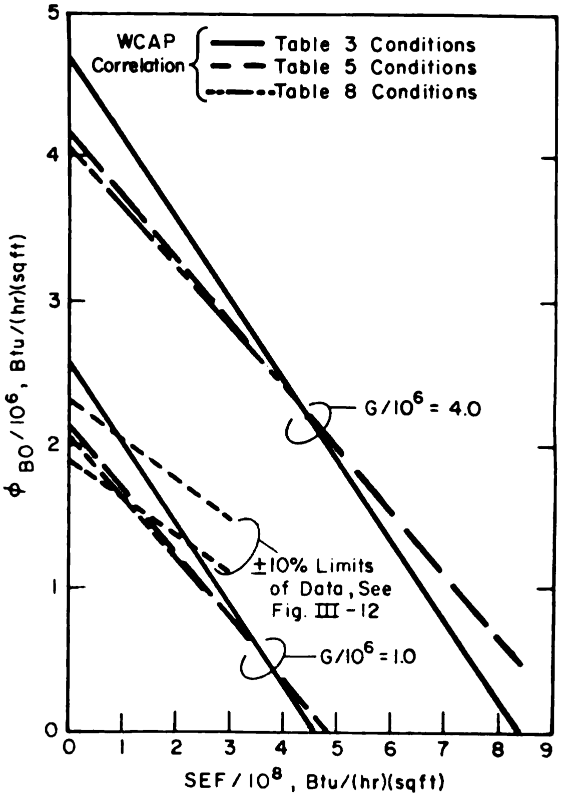

Fig. III-13 Comparison of WCAP correlation with data appearing in Tables 3, 5, and 8 of Ref. 3. Pressure = 1000 psia.

Table III-2 WCAP CORRELATION EQUATIONS PLOTTED ON FIG. III-13

(Pressure = 1000 psia)

Ref. 3 table No. wherein data appear	Test-section parameters		Burnout correlation equation
	Length, in.	Diameter, in.	
3	9.0	0.1805	$\phi_{BO} = 1.17G + 6.464Ge^{-1.5G/10^6} - 0.0056\text{SEF}$
5	11.625	0.180	$\phi_{BO} = 1.029G + 4.994Ge^{-1.5G/10^6} - 0.00435\text{SEF}$
8	12.5	0.187	$\phi_{BO} = 1.01G + 4.763Ge^{-1.5G/10^6} - 0.0042\text{SEF}$

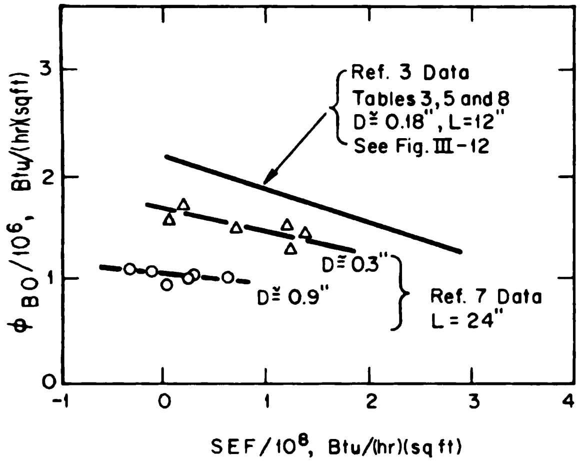

Fig. III-14 Steam-energy flow plot of burnout data from Refs. 7 and 3. Pressure = 1000 psia.

Whatever fundamental significance this may have is not readily apparent, but the practical significance—and possible importance—to the designer operating in this pressure range is obvious. Table 5 contains a few DNB-2 data, and these appear on the figure, although they will not be discussed. Figure III-13 compares the WCAP correlation with the data shown in Fig. III-12. The particular equations plotted are shown in Table III-2. It appears that the correlation does not recognize the insensitivity to mass flow in this pressure range.

An effect of the test-section diameter on ϕ_{BO} is shown in Fig. III-14, which plots data from Ref. 7. The data for $D = 0.3$ in. are replotted in Fig. III-15 along with some additional data from Table 10 of Ref. 3.* Again the data on Fig. III-15 point to a lack of effect of G on ϕ_{BO} on an SEF plot, although the Westinghouse (WCAP) correlation exhibits a rather strong effect.†

It can be noted that the coefficient of the SEF term in the WCAP correlation is pressure-independent, as can be seen from Eq. 7. This is substantiated in Fig. III-16, where data of Table 3 from Ref. 3 are plotted for three pressures. The lines are parallel, as they should be for a constant coefficient of the SEF term in Eq. 7.

The analyses contained in the report[2] by the Atomic Power Equipment Department (APED) of General Electric Company are intended to define lower limits of the burnout flux in practical situations. The analyses are based primarily on data taken at APED and appearing in Ref. 8. The approach can probably best be explained by the following quotation,[2] which explains that the set of burnout limit curves was constructed by:‡

> 1. Defining limit curves based upon extensive critical heat flux data obtained at General Electric Company in an internally heated annulus. The internally heated annulus geometry was selected because it simulates one of the three possible fuel cell geometries shown in [Fig. III-17]. It is not only representative of corner rod conditions, but it also has the highest ratio of unheated to heated surface area. As such, it gives the lowest critical heat flux value of the three possible fuel cells since the "burnout" point has been found to decrease with increased unheated surface area.[9]
>
> 2. Modifying the above limit curves to account for lower trends or special effects reported in some instances by other experimenters. This ensures that differences in test loops and experimental techniques or conditions are included in the recommended curves.

---

*The lines through the data, which were placed by eye, differ between Fig. III-14 and Fig. III-15, because of the modifying effect of the Ref. 3 data. However, the line shown in Fig. III-15 lies within ±10% of all points but three.

†The data in Ref. 7 have been greatly expanded by the appearance of Ref. 10. These latter data extend D to about 1.5 in., L to about 76 in., and $G/10^6$ to about 14 lb/(hr)(sq ft).

‡Figure numbers and reference notations have been changed to conform to the numbering used here.

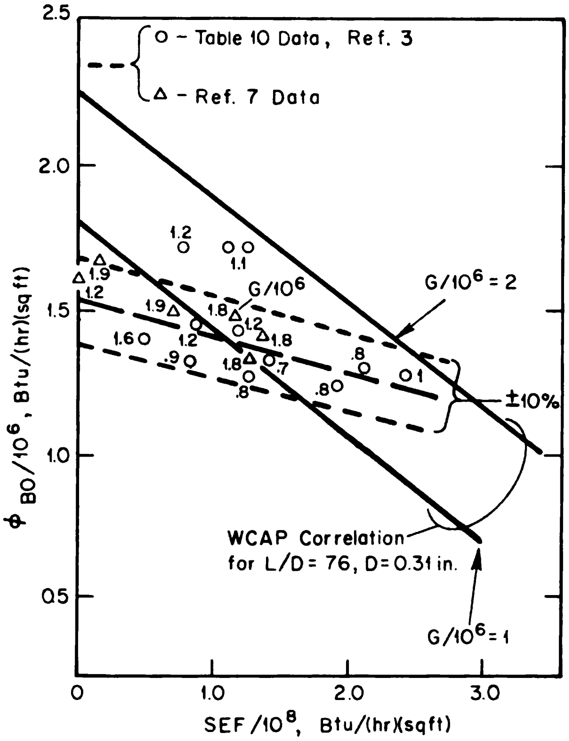

Fig. III-15 Comparison of WCAP correlation with data appearing in Refs. 3 and 7. Pressure = 1000 psia.

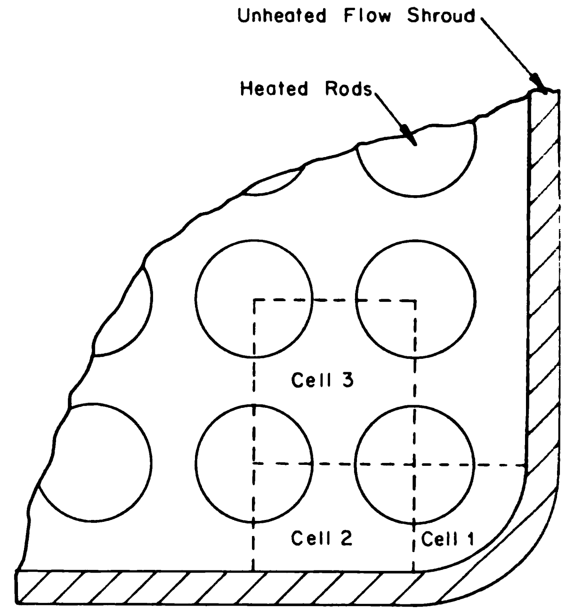

Fig. III-17 Multirod fuel assembly showing various kinds of cells.[2]

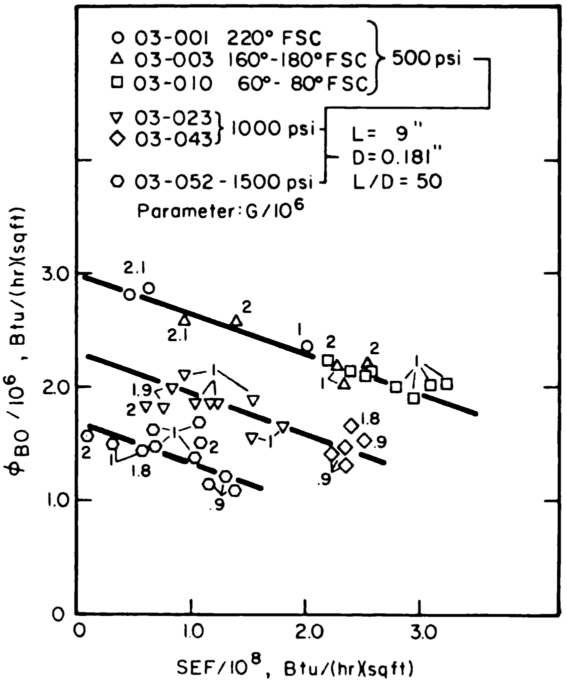

Fig. III-16 SEF plot comparing data at 500, 1000, and 1500 psia (from Table 3 of Ref. 3.)

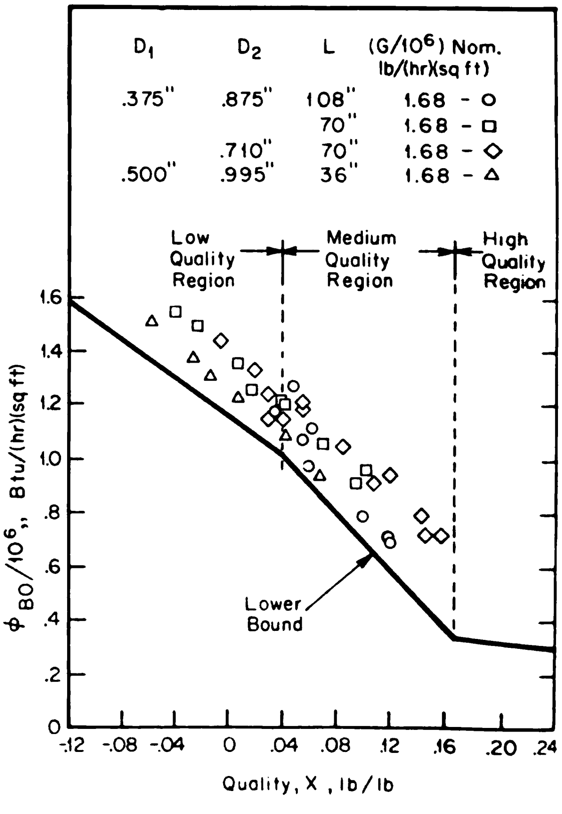

Fig. III-18 APED internally heated annulus data at high flows.[2] Pressure = 1000 psia.

3. Considering data obtained in multirod geometries or annular geometries modified to account for flow redistribution, presence of spacers and rough surface conditions. This step verifies that the limit curves developed for a normal annular geometry can be applied to reactor type multirod systems.
4. Comparing the recommended curves to other available data. This final check gives an overall perspective of how the proposed limit curves fair with respect to other test results.

Figure III-18 is typical of the plots of the APED data appearing in Ref. 2 and covers the high mass-flow range around 1.7×10^6 lb/(hr)(sq ft). Other plots are given which in total cover the mass-flow range from about 0.2 to 6×10^6 lb/(hr)(sq ft). The quality range was arbitrarily divided into three regions, and the burnout limit was described by three connected straight-line segments (see Fig. III-18). The whole range of qualities was not adequately covered by APED data for every value of mass flow. Accordingly, British and Italian data were used to establish the burnout limit curve in the high-quality region, and Ref. 3 data were used to establish the curve in the low-quality and subcooled regions. The complete set of burnout limit curves is shown in Fig. III-19. The reference also presents recipes for conversion of the curves to other pressures and to other hydraulic diameters. The pressure-adjustment recipe is as follows:

$$\phi_{BO_p} = \phi_{BO_{1000}} + 440\,(1000 - p) \qquad (8)$$

where ϕ_{BO_p} is the burnout heat flux at pressure p, Btu/(hr)(sq ft), $\phi_{BO_{1000}}$ is the burnout heat flux at $p = 1000$ psia, Btu/(hr)(sq ft), and p is the pressure, psia.

In conclusion, an attempt will be made to compare the WCAP and APED burnout correlations and recommendations. This is done in Fig. III-20; the APED limit lines shown thereon are merely a replot of the appropriate curves in Fig. III-19 for the middle quality range. The WCAP correlation is for a pressure of 1000 psia, an L/D of 100 and a D of 0.400 in. This comparison is believed to be a valid one, since the authors of both correlations state that their respective correlations are valid for rod bundles.

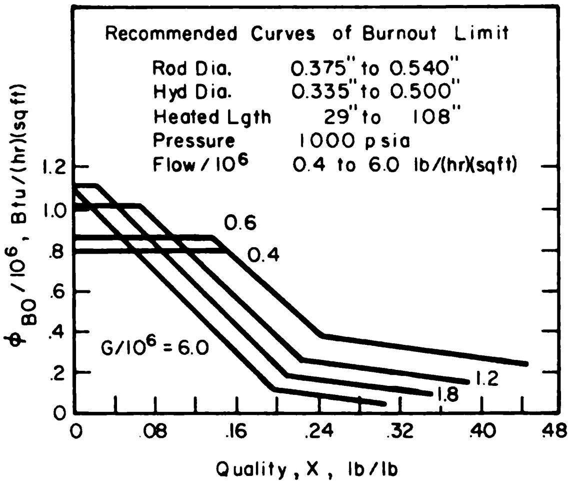

Fig. III-19 Modified burnout limit curve.[2]

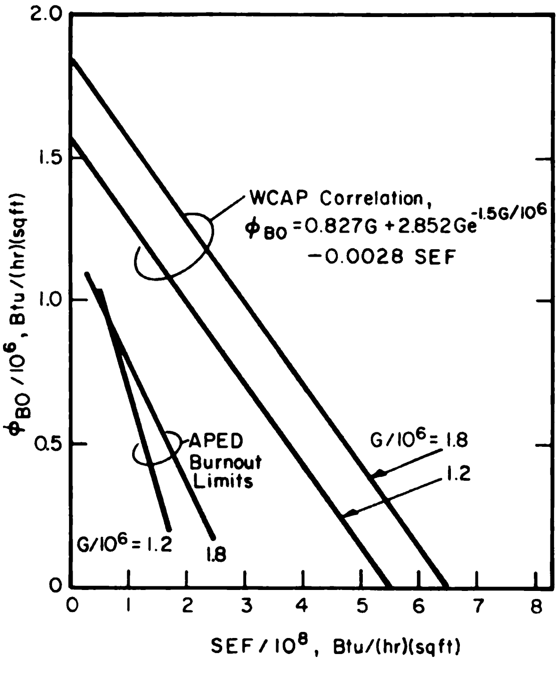

Fig. III-20 Comparison of WCAP correlation with APED burnout limit curves.

It is evident that the two correlations shown in Fig. III-20 are not in agreement. One reason for this is that, although the APED curves were chosen on the low side of the data, the WCAP curves were chosen as best-fit curves. This does not explain the entire difference, however, since the WCAP correlation was stated to be within ±25% of the data. It is believed that the major difference between the WCAP and APED correlations can be explained by geometry. The former correlation was based primarily on circular-tube and rectangular-channel data, whereas the latter correlation considered primarily data taken with internally heated annular-geometry test sections. Collier[11] states: "Burnout heat flux values for tubes and externally heated annuli are always higher than those for internally heated annuli . . . ."

If geometry is the primary reason for the differences shown between the two correlations, then it seems incorrect to state that both correlations will adequately predict the burnout heat flux of a bundle of heated rods such as is found in a power reactor. Further considerations of burnout in multirod clusters will appear in future issues of *Power Reactor Technology*.

References

1. L. S. Tong, H. B. Currin, and A. G. Thorp II, New Correlations Predict DNB Conditions, *Nucleonics*, 21(5): 43-47 (May 1963).
2. E. Janssen and S. Levy, Burnout Limit Curves for Boiling Water Reactors, Report APED-3892, General Electric Company, Atomic Power Equipment Department, Apr. 1, 1962.
3. R. A. DeBortoli, S. J. Green, B. W. LeTourneau, M. Troy, and A. Weiss, Forced-Convection Heat Transfer Burnout Studies for Water in Rectangular Channels and Round Tubes at Pressures Above 500 psia, USAEC Report WAPD-188, Westinghouse Electric Corp., Bettis Plant, October 1958.
4. W. J. Levedahl, Application of Steam Energy Flow to Reactor Design, *Trans. Am. Nucl. Soc.*, 5(1): 149 (June 1962).
5. L. S. Tong, H. B. Currin, and A. G. Thorp II, New DNB (Burnout) Correlations, USAEC Report WCAP-1997(Rev. 2), Westinghouse Electric Corp., Atomic Power Division, May 1963).
6. J. S. Wiley, Additional Comments on Statistical Burnout Correlations, *Nucleonics*, 22(2): (February 1964).
7. R. R. Hood and L. Isakoff (Comps.), Heavy Water Moderated Power Reactors. Progress Report, June 1962, USAEC Report DP-755, E. I. du Pont de Nemours & Co., Inc., July 1962.
8. E. Janssen and J. A. Kervinen, Burnout Conditions for Single Rod in Annular Geometry, Water at 600 to 1400 psia, USAEC Report GEAP-3899, General Electric Company, Atomic Power Equipment Department, February 1963.
9. M. Silvestri, Two-Phase (Steam and Water) Flow and Heat Transfer, Paper 39 in *International Developments in Heat Transfer*, Part II, pp. 341-353, American Society of Mechanical Engineers, 1962.
10. R. R. Hood and L. Isakoff, Heavy Water Moderated Power Reactors Progress Report, May-June 1963, USAEC Report DP-855, E. I. du Pont de Nemours & Co., Inc.
11. J. G. Collier, Heat Transfer and Fluid Dynamic Research As Applied to Fog Cooled Power Reactors, Canadian Report CRARE-1108 (AECL-1631), June 1962.

Section IV

Power Reactor Technology

Fuel Elements

Programs at GE-APED Sponsored by USAEC and Euratom

Three government-sponsored research and development programs that include substantial efforts on oxide fuel elements are under way at the General Electric Atomic Power Equipment Department (APED). Two of these, the Fuel-Cycle Program and the High Power Density Development Project, are sponsored by the U. S. Atomic Energy Commission (AEC); the third, the High-Performance UO_2 Program, is sponsored jointly by AEC and Euratom. A large amount of literature has been produced under these programs in the form of quarterly and topical reports. It is the purpose of this review to summarize the work to date in the area of fuel-element development and to describe the objectives, the experimental approaches, and the existing complement of experimental samples in sufficient detail to form the background for more concise reviews of progress that may appear from time to time in future issues.

Fuel-Cycle Program[1–20]

This program was initiated early in 1959. The purpose of the program is to improve the technological limits of boiling-water reactors in several areas listed below[2] (of these, only Task A-1 is reviewed here):

Task A

1. Extend fuel life information on oxide fuel at high specific power operation and raise the performance limits of oxide fuels.
2. Study power stability and performance characteristics of an oxide fueled core under natural and forced circulation to improve design limits.

Task B

1. Out-of-pile experiments in heat transfer and fluid dynamics in the areas of burnout heat transfer, hydraulic instability, steam void observational studies, and two-phase pressure drop to support in-core work.

Task C

1. Study long-term reactivity characteristics of fuels having lattice characteristics of large power reactors.
2. Measure initial conversion ratio of a number of lattice configurations characteristic of large oxide fueled power reactors.

Task A-1 involves the fabrication of fuel assemblies and evaluation of results of irradiation in the Vallecitos Boiling-Water Reactor (VBWR). A total of 60 assemblies have been irradiated, although all 60 assemblies are not necessarily in the VBWR at the same time. These 60 assemblies are divided into 50 so-called "basic" assemblies and 10 "special" fuel assemblies. The design and fabrication of the basic fuel assemblies are detailed in Ref. 12; two different types were fabricated, one being a control-follower assembly and the other a stationary assembly. The follower assemblies, designated as type H, employ annealed type 304 stainless-steel cladding, whereas the stationary assemblies were fabricated from Zircaloy-2, Zircaloy-4, and cold-worked type 304 stainless-steel cladding. All cladding was designed to be freestanding. Additional details on the assemblies are given in Table IV-1. Figures IV-1 to IV-3 illustrate constructional details of the assemblies and their appearance in the VBWR.

The elements were fabricated in 1960 and 1961, and 25 stainless-steel-clad assemblies were loaded into the VBWR in September 1960. An instrumented stainless-steel assembly was loaded into the VBWR in October 1961, instrumented to provide data on in-core neutron flux,

Table IV-1 CHARACTERISTICS OF THE BASIC FUEL ASSEMBLIES IN THE FUEL-CYCLE PROGRAM[12]

Type of assemblies	H	I	J
Number of assemblies	10	16	24
Rods per assembly*	16	16	16
Removable rods per assembly	0	12	12
Rod center-to-center distance, in.	0.76	0.76	0.76
Cladding material	304 S.S.	304 S.S.	Zircaloy-2†
Nominal cladding thickness, in.	0.020	0.015	0.022
Nominal tube outside diameter, in.	0.420	0.410	0.424
Nominal tube inside diameter, in.	0.380	0.380	0.380
Maximum pellet diameter, in.	0.376	0.376	0.376
Average pellet density, % of theoretical density	95	95	95
UO_2 enrichment, %	2.7	3.2	‡
Water-to-fuel ratio	2.98	4.0	3.9
Active fuel length, in.	30	37	37
Total rod length, in.	$32\frac{5}{8}$	$39\frac{1}{4}$	$40\frac{1}{8}$
Plenum length, in.	$1\frac{7}{8}$	$1\frac{7}{8}$	$1\frac{7}{8}$
Wall thickness of plenum support tube, in.	0.020	0.020	0.020
Coolant-flow area, sq in.	5.25	7.13	6.98
Heat-transfer area, sq ft	4.37	5.28	5.47

*One I and two J assemblies are instrumented and contain only 14 fuel rods.

†One assembly contains three fuel rods clad with Zircaloy-4.

‡Enrichments of the J assemblies are as follows:

No. of assemblies	% enrichment
10	2.76
1	2.76 and 2.98 (8 rods each)
3	2.98
1	2.98 and 3.49 (8 rods each)
3	3.2
5	3.49
1	4.3
1	2.76 + PuO_2 segments

coolant temperature, pressure drop, and flow rates. The Zircaloy-clad assemblies, including two instrumented ones, were placed in the VBWR between June 1961 and January 1962. As of March 1963, the basic fuel assemblies had reached the burnups shown in Table IV-2; this table also illustrates the peak specific power and peak heat flux for the particular assembly operated at the highest power within its group. Table IV-3 compares the thermal performance of these basic fuel assemblies with the Dresden and Big Rock Point reactors.

In May of 1962, during a VBWR outage, four fuel-rod changes were made involving one type I assembly and three type J assemblies.[8] Hot-cell examination revealed that fretting corrosion had occurred on the Zircaloy cladding. Studies of four additional assemblies showed that fretting corrosion had occurred on some rods in each of the Zircaloy-clad assemblies (12J, 25J, and 7L, a special assembly), but not on the stainless-steel-clad assembly (8I). The observations are summarized in Ref. 8:

> The following observations were made . . . : (1) lack of rod support at the upper tie plate caused general fretting corrosion at the middle spacer in the 7L assembly; (2) rods with large clearances at the upper tie plate showed the most penetration, (3) rods with tight support at the upper tie plate suffered comparatively light fretting corrosion even with large clearances at the middle spacer; (4) the corner rods which are rigidly supported at both top and bottom underwent no fretting corrosion.
>
> It appears that wire deformation as a result of fuel handling increases the clearance between the fuel rods and supporting spacer and upper tie plate wires . . . . The clearance subsequently allows the rods to vibrate freely as reeds and fret against the stainless steel wires. It is expected that the fretting corrosion can be reduced or eliminated by spring clips at the upper tie plate which will provide improved rod support. The spring clips can be in-

> stalled on the assemblies in the VBWR storage pool without disassembly of the fuel bundle. Fabrication of trial clips is in progress.

The method of retaining the rods in the assembly is shown in Fig. IV-1. A new, undamaged fuel rod was placed into assembly 12J, and spring clips were fabricated to bear against the rod and damp vibration. This assembly was inserted in the VBWR and operated for about a month until the reactor was shut down because of a leak in the recirculation piping. Subsequent examination revealed no fretting damage to the clipped fuel rod, and spring clips were installed on all but two of the Zircaloy-clad type J assemblies.

No significant cladding deterioration other than fretting was exhibited by the Zircaloy-2- and Zircaloy-4-clad fuel rods. The stainless-steel-clad fuel rods also were sound. An intentionally defected Zircaloy-2-clad rod, an intentionally defected Zircaloy-4-clad rod, and a sound Zircaloy-2-clad rod were sectioned and examined remotely. The defect was a 20-mil hole in the cladding near the peak heat flux region. The results are summarized as follows in Ref. 9:

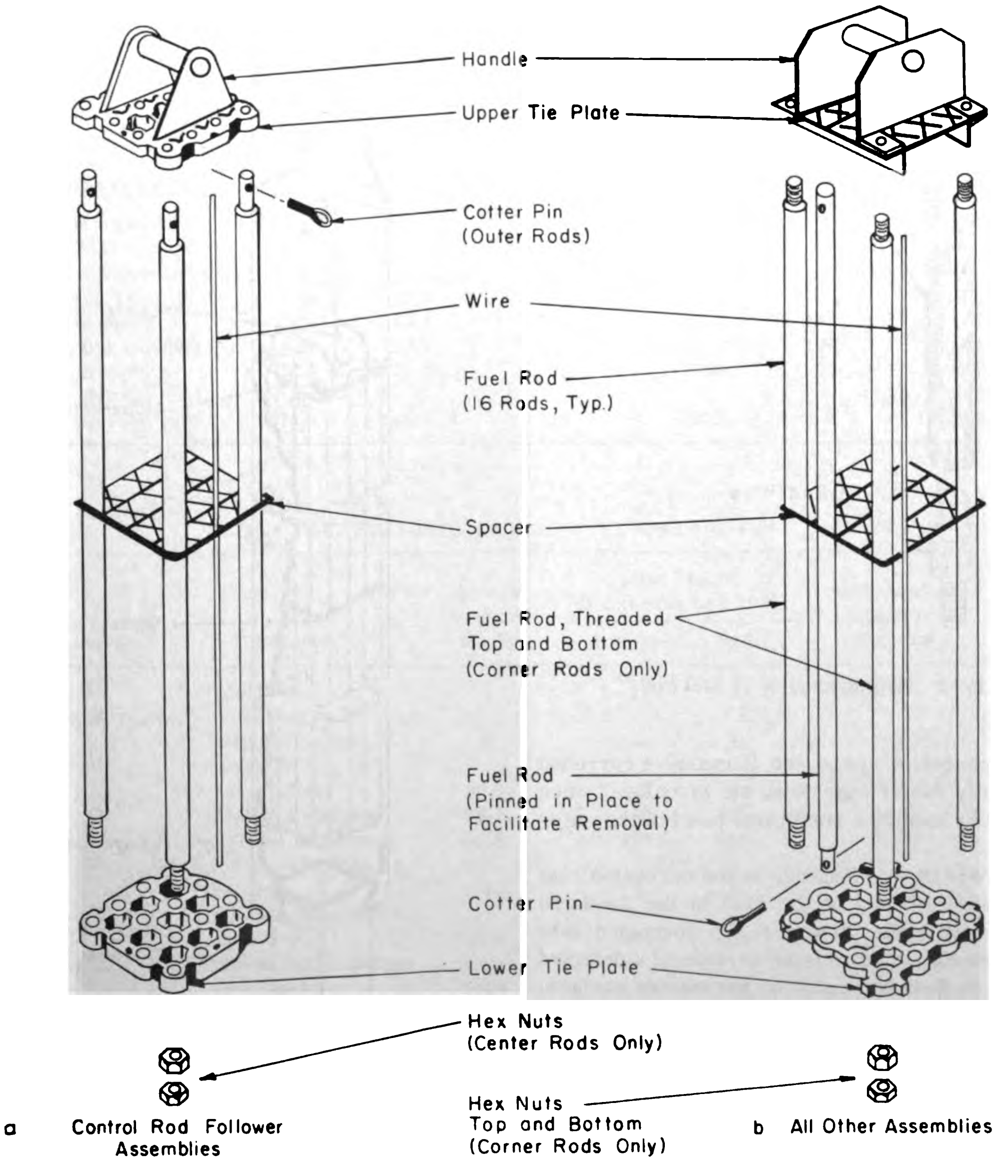
Handle
Upper Tie Plate
Cotter Pin (Outer Rods)
Wire
Fuel Rod (16 Rods, Typ.)
Spacer
Fuel Rod, Threaded Top and Bottom (Corner Rods Only)
Fuel Rod (Pinned in Place to Facilitate Removal)
Cotter Pin
Lower Tie Plate
Hex Nuts (Center Rods Only)
Hex Nuts Top and Bottom (Corner Rods Only)

a Control Rod Follower Assemblies

b All Other Assemblies

Fig. IV-1 Exploded view of fuel assemblies.[12]

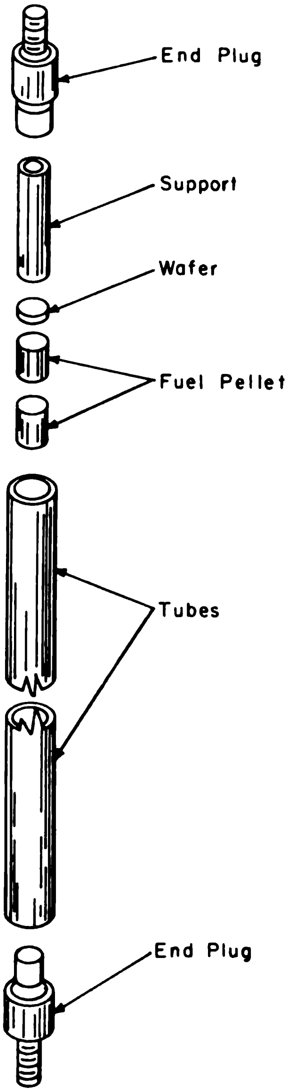

Fig. IV-2 Exploded view of fuel rod.[12]

a. In non-defect areas, the Zircaloy-4 corroded at a slightly faster rate than the Zircaloy-2 when tested under identical conditions in a boiling water reactor.

b. There is little difference in the corrosion rate on the inside surface of the clad in the Zr-2 and Zr-4 defected rods. However, the corrosion rate of both materials on the inside surface of a defected rod is more than twice that on the outside surface.

c. The higher corrosion rate on the inside surface of the defect rods seems consistent with rates expected at inside clad temperatures estimated from heat transfer calculations. Continued operation of intentionally defected Zr rods to evaluate performance at longer exposures may provide information on the effect of other potential factors, such as a reduction in the corrosion resistance of the clad resulting from the impregnation of the clad with fission fragments.

Also included in the VBWR irradiations under the Fuel-Cycle Program are 10 special fuel assemblies, whose status as of March 1963 is summarized in Table IV-4. Assembly 1L was designed to study the lifetime performance of a UO_2 fuel element operated near the melting point of UO_2 at the center line. The maximum heat flux of 1L was 530,000 Btu/(hr)(sq ft) during irradiation, and the assembly contained one purposely defected rod; the cladding of all rods in

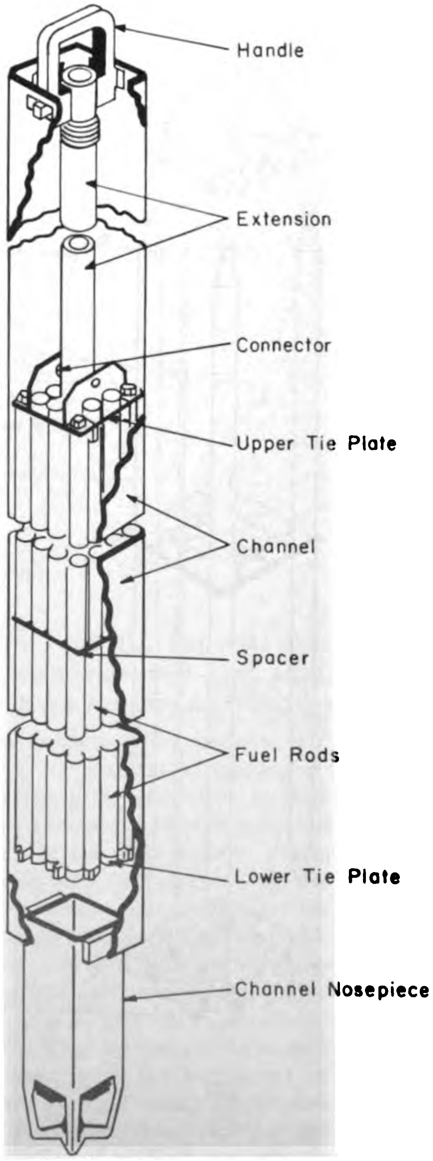

Fig. IV-3 Cutaway view of fuel assembly in VBWR channel.[12]

Table IV-2 STATUS OF THE BASIC FUEL ASSEMBLIES IN THE FUEL-CYCLE PROGRAM[11]

Assembly designation and cladding	Number	Burnup, Mwd/ton*		Peak specific power,‡ kw/kg	Peak heat flux,‡ Btu/(hr)(sq ft)
		Average of group	Average for lead assembly†		
H, annealed S.S. (control-rod follower)	10	5,191	6,231	34.4	367,000
I, cold-worked S.S.	16	4,564	5,803	36.6	405,000
J, Zircaloy	24	3,849	6,176	37.5	382,000

*Burnup that existed at the end of run 155 which was completed on Mar. 24, 1963.

†Peak exposure is about 1.65 times this value.

‡These values were attained in the quarter starting January 1963.

Table IV-3 COMPARISON OF THE BASIC FUEL ASSEMBLIES WITH FUEL CONDITIONS IN OTHER REACTORS[10]

	Average overall fuel			Peak location		
	Specific power, kw/kg	Power density, kw/liter	Heat flux, Btu/(hr)(sq ft) $\times 10^{-3}$	Specific power, kw/kg	Power density, kw/liter	Heat flux, Btu/(hr)(sq ft) $\times 10^{-3}$
Fuel-cycle program (run 153)						
H, S.S.-clad control-rod followers	38.5	53.4	238	78.5	163	377
I, S.S. cladding	30.0	51.4	184	65.0	112	420
J, Zircaloy cladding	31.2	53.1	204	73.7	126	448
Dresden, first core	12.4	31.2	99	35.6	90	285
Big Rock Point, 50 Mw(e), first core	16.5	45.0	110	52.6	144	352

Table IV-4 STATUS OF SPECIAL FUEL ASSEMBLIES[11]

Assembly	Concept	Specific power,* kw/kg	Heat flux,* Btu/(hr)(sq ft) $\times 10^{-3}$		Accumulated† exposure, Mwd/ton
			Average	Peak	
1L	Centermelt	‡	‡	‡	4075
4L	Low-temperature sintered pellets	‡	‡	‡	234
5L	Coextruded UO_2 and S.S. cladding	33.9	223	364	4592
6L	Zircaloy-4 cladding	16.8	145	287	1075
7L	S.S.-lined Zircaloy-2	35.6	224	383	4303
8L	0.005-in. S.S.-clad pellets	‡	‡	‡	2553
9L	Thermal-conductivity improver	30.9	233	385	907
10L	0.005-in. S.S. cladding over powder	19.2	116	211	396
11L	Extruded UO_2	‡	‡	‡	180
12L	Burnable poison	15.4	110	191	307
2L	Undefined§				
3L	Undefined§				

*Peak condition during VBWR run 155.

†Exposures are through VBWR run 155, which was completed on Mar. 24, 1963.

‡Not irradiated during VBWR run 155.

§Held in reserve for future use.

the assembly was stainless steel with an outside diameter of 0.515 in. Destructive examination of one of the rods revealed that center melting of the UO_2 did not occur, and large columnar grains were observed in the region from the center of the pellet to a distance of about one-half the radius. A narrow band of fine grains occurred at midradius and separated the as-sintered structure from the grain-growth region. This was interpreted to mean that recrystallization of the UO_2 occurs prior to grain growth.

Assembly 4L has had a varied history. It originally contained three rods made by hot-gas isostatic pressing of UO_2 in stainless-steel cladding, a specially designed rod known as the "centermelt" calibration test rod and other rods of conventional fabrication.

The gas-pressure-bonding technique was developed in a 2½-year study done at Battelle Memorial Institute and is described in Refs. 13 to 15. Briefly, the process consisted of fabricating UO_2 pellets by cold-pressing the oxide powder and a binder at 50 tsi. The pellets were loaded into type 304L stainless-steel tubing, and end caps were added; the assembly was then heated and cooled, evacuated to 5 μ, and sealed. The rod was then subjected to 10,000 psi for 3 hr at 2100°F, swaged from 0.404 to 0.400 in. in outside diameter, and pressure bonded for 2 hr at 10,000 psi and 2100°F. This produced an average UO_2 density of 96.3% of theoretical. The rods produced in this manner were irradiated to an exposure of 693 Mwd/ton with a peak heat flux at 370,000 Btu/(hr)(sq ft). After irradiation the 4L assembly was damaged, and it was stored in the VBWR pool for about five months. In the process of handling the isostatically pressed rods, all three of them broke into a total of about 15 pieces. The evaluation of the failed isostatically pressed fuel rods is reported on in Ref. 16, and the conclusion is that inadequate removal of the binder from the UO_2 resulted in a very high carbon content of the cladding. In the resulting sigma phase, carbides and ferrite formation at the grain boundaries led to intergranular corrosion and cracking.

The centermelt calibration rod irradiated in assembly 4L was an oxide rod which was 1⅜ in. in outside diameter and which contained 1.235-in.-diameter pellets; the peak heat flux was 535,000 Btu/(hr)(sq ft). The rod was examined remotely after irradiation. The oxide fuel had been molten, and it was established that fuel ran from the upper part of the rod to the lower part. Plastic deformation of the cladding was evident, and it is suggested[7] that this was caused by the relatively greater expansion of the hot UO_2 compared to the cladding. It was also concluded that "... A sintered uranium dioxide body may initially operate with a molten central portion which subsequently totally or partially solidifies during operation because of the increased thermal conductivity due to the growth of columnar grains."[7] This mechanism was discussed in *Power Reactor Technology*, 6(2): 36-37.

After the failure of the isostatically pressed fuel rods, the 4L assembly was rebuilt with three rods containing low-temperature sintered pellets produced by United Nuclear Corporation, three rods (including one intentionally defected) of UO_2 coextruded with the stainless-steel cladding, one intentionally defected rod containing UO_2 pellets clad with stainless-steel-lined Zircaloy-2, and nine standard rods. As indicated in Table IV-4, the assembly had received relatively modest burnups up to March 1963. The low-temperature sintered pellets involve sintering at 1100 to 1300°C, rather than the more customary 1600 to 1700°C. The design and fabrication of the fuel rods containing low-temperature sintered pellets are covered in Ref. 17.

Assembly 5L contains 12 rods fabricated by high-temperature coextrusion. The irradiation cycle for this assembly started in August 1961, whereas irradiation of the three coextruded rods in assembly 4L started in July 1962. The design and fabrication of the coextruded rods are covered in Refs. 18 and 19. The process consists in coextruding UO_2 and type 304 stainless-steel cladding. As of March 1963 assembly 5L had reached a modest burnup and apparently was operating satisfactorily.

Assembly 6L consists of rods containing UO_2 pellets clad with Zircaloy-4. An intentionally defected rod was included in assembly 6L but has been replaced with a sound rod. Assembly 7L contains fuel rods clad with Zircaloy-2 coextruded with approximately a 1-mil stainless-steel lining. This lining is present to prevent corrosion of the Zircaloy-2 by steam that would be formed if any water should leak into the element. Both assemblies are reported to be in satisfactory condition, although fretting corrosion was noticed on assembly 7L, and the rods had to be transferred to another fuel-rod bundle frame owing to damage to the upper tie plate. Spring clips were then added to reduce the possibility of fretting.

Assemblies 8L and 10L test the concept of thin, collapsed cladding. The former assembly contains 0.370-in.-OD UO_2 pellets, whereas the latter assembly contains UO_2 powder compacted by vibratory techniques. Assembly 8L was inserted in the VBWR in November 1961; since the thin cladding prohibits high internal gas pressures, a plenum length of 7.0 in. is provided. To prevent collapse of the gas plenum, it was necessary to provide support to the cladding in the plenum area, and this was done by using an external plenum support with a wall thickness of 0.017 in. on six of the rods and by using an internal plenum support with a wall thickness of 0.016 in. on the remaining six rods. The four corner rods of assembly 8L are constructed of noncollapsed 20-mil cladding and are arranged as shown in part *b* of Fig. IV-1. One collapsed-cladding rod was intentionally defected with a 10-mil hole in the plenum area. The type 304 stainless-steel cladding was cold worked, with a room-temperature yield strength of about 110,000 psi (nonirradiated). The defected rod was installed in the assembly in February 1962, and the activity release from the defected rod was stated to be[7] less than 5 μc/sec. In August 1962 the assembly was transferred to a hot cell for visual examination. Reference 9 states:

> (1) At least two fuel rods were cracked, one in the area of maximum heat flux, the other in a wrinkled plenum area.
>
> (2) Three rods were wrinkled in the plenum area. The wrinkling occurred in rods containing internal plenum supports.

Four of the damaged or failed fuel rods were destructively examined, and the details are given in Ref. 11. The following comments pertain to the fuel rod exhibiting a crack in the peak heat flux region:[11]

> The cause of cracking of this rod is apparently strain cycling fatigue. The differential thermal expansion of the UO_2 and clad during operation of the fuel rod at the peak heat flux condition, about 500,000 Btu/hr-ft^2, would have caused a calculated plastic diametral deformation in the clad of 0.002 inch. When power is reduced after plastic strain of the clad, the contraction of the UO_2 leaves an equivalent gap between the clad and UO_2. If the gap is as large as these calculations indicate, there is high probability that collapse under the 1000-psig coolant pressure would have caused a wrinkle. Repeating cycling of this wrinkle after formation probably led to fatigue cracking. Metallurgical examination of the clad crack supports this conclusion .... The clad in the failure region appears to be slightly harder than the clad in the non-failure region. This increase in hardness may be caused by work hardening during the cycling.

The four rods destructively examined were replaced with four rods that had 5-mil annealed collapsed cladding.

Assembly 10L was placed in-pile in February 1963. The assembly contains rods utilizing both cold-worked and annealed tubing and arc-fused and Dynapak UO_2 powders. The latter process, developed at Hanford Atomic Products Operation (HAPO), involves the densification of the powder by drop forging. Six fuel rods are filled with the Dynapak powder with as-packed densities of about 84%. Ten rods are filled with arc-fused powder with as-packed densities of 84.3 to 84.9%. Additional data on assembly 10L are given in Table IV-5.

Table IV-5 ASSEMBLY 10L DESIGN[7] WITH THIN STAINLESS-STEEL CLADDING OVER UO_2 POWDER

UO_2 enrichment	6% U^{235}
Cladding material	Type 304 S.S.
Cladding thickness, in.	0.005
Number of rods	16
Rod outside diameter, in.	0.385
Rod spacing, in.	0.76, center to center

Irradiation of assembly 9L began in August 1962. The purpose of the irradiation is to evaluate an attempt to improve the thermal conductivity of UO_2 by the dispersion of molybdenum through the oxide. Two methods of dispersion were used to prepare a total of six rods for incorporation in the 9L assembly. One approach was to mix molybdenum fibers with the oxide powder before the pressing of the pellets; in the second approach the individual oxide particles were coated with molybdenum metal prior to pressing. Three rods were fabricated using the fiber process, and three others were fabricated using the coating process. The remaining rods in the assembly are of conventional construction. Whether the molybdenum will improve the thermal conductivity of the fuel is yet to be determined. Table IV-6 gives design data on assembly 9L.

Assembly 11L consists of fuel rods filled with UO_2 extrusions. The extrusions were supplied

Table IV-6 ASSEMBLY 9L DESIGN[7] THAT MAY IMPROVE THERMAL CONDUCTIVITY

Cladding material	Type 304 S.S.
Cladding thickness, in.	0.020
Fuel-rod outside diameter, in.	0.515
Fuel-pellet outside diameter, in.	0.471
Number of rods	8
Two rods contain 6.4% enriched UO_2 pellets (controls)	
Three rods contain 24 in. of 8.0% enriched UO_2 pellets containing 20 vol.% molybdenum fibers and 12 in. of 6.4% enriched UO_2 pellets	
Three rods contain 24 in. of 8.0% enriched molybdenum-coated UO_2 pellets and 12 in. of 6.4% enriched UO_2 pellets	
Rod spacing, in.	1.03, center to center
UO_2 density	95% of theoretical density for UO_2 pellets 95% of theoretical density for UO_2-Mo pellets

by Allis-Chalmers Mfg. Co. and Compagnie Industrielle des Combustibles Atomiques Frittés (CICAF) of France. The extrusions were to be about 6 in. long, although the extrusions prepared by CICAF ranged in length from 0.3 to 6.06 in. One each of the rods containing the two extrusion types was purposely defected by means of a 13-mil hole through the cladding in the plenum region. The assembly has been irradiated for only a short burnup, and little information is available as to the usefulness of the fabrication technique in producing acceptable fuel material. Data on the 11L design are given in Table IV-7.

Assembly 12L, the last special assembly, was inserted in the VBWR in February 1963. The basic purpose of the element is to study the behavior of boron burnable poison when the boron is alloyed into the stainless-steel cladding and when the boron is intimately mixed with the fuel. Table IV-8 illustrates the fabrication details of each rod in assembly 12L. It is evident from Table IV-8 that the assembly also is intended to give information on the relative merits of annealed and cold-worked cladding material. The assembly had received only modest burnup by March 1963.

Table IV-7 ASSEMBLY 11L DESIGN WITH EXTRUDED UO_2

UO_2 enrichment, %	5.5
Cladding material	Type 304 S.S.
Cladding thickness, in.	0.022
Rod outside diameter, in.	0.539
Number of rods	16
Six rods are filled with extrusions from CICAF	
Six rods are filled with extrusions from Allis-Chalmers	
Four rods are filled with pellets	
Fuel outside diameter, in.	0.485 ± 0.002
Fuel density, %	97% of theoretical density

High-Power-Density (HPD) Development Project[20–34,45]

The HPD research and development program was begun in February of 1960 and is a program in support of the Consumers Power Company boiling-water reactor plant at Big Rock Point, Mich. References 20 to 26 are selected quarterly progress reports dealing with the project. The HPD program is divided into four tasks as follows:[21]

1. Task IA—High Power Density Fuel Development. This task will evaluate the feasibility and the performance of a partial reactor core operating in the VBWR at high power density and utilizing fuel elements manufactured from available fabricating processes.
2. Task IB—Fuel Fabrication Development. Design, fabrication, irradiation and examination of high power density fuel elements with potentially low fabrication costs is the objective of this task.
3. Task II—Stability and Heat Transfer Development. This task will evaluate analytically and by

Table IV-8 DESCRIPTION[†] OF BURNABLE-POISON ASSEMBLY 12L

Rod No.	Fuel data	U^{235} enrichment	Cladding data	
Controls (No Poison)				
A-1	Vibratory-compacted arc-fused powder, 85% of theoretical density	5.5%	Type 304 S.S. annealed, ~40,000-psi 2% yield strength, 0.485-in. outside diameter by 0.011-in. wall	
B-1	Pellets, 95% of theoretical density	5.5%		
Borated Cladding but No Poison in Fuel				
C-1	All rods vibratory-compacted arc-fused powder, 85% of theoretical density	6.6%	C-1	Annealed, ~45,000-psi 0.2% yield strength
C-2			C-2	Cold worked, ~70,000-psi 0.2% yield strength
			C-1, C-2	500 ppm B^N + type 304 S.S., 0.485-in. outside diameter by 0.011-in. wall
C-3			C-3	Annealed, ~45,000-psi 0.2% yield strength
C-4			C-4	Cold worked, ~70,000-psi 0.2% yield strength
C-3, C-4			C-3, C-4	750 ppm B^N + type 304 S.S., 0.485-in. outside diameter by 0.011-in. wall
D-1	All rods pellets, 95% of theoretical density	6.6%	D-1	Annealed, ~45,000-psi 0.2% yield strength
D-2			D-2	Cold worked, ~70,000-psi 0.2% yield strength
D-1, D-2			D-1, D-2	500 ppm B^N + type 304 S.S., 0.485-in. outside diameter by 0.011-in. wall
D-3			D-3	Annealed, ~45,000-psi 0.2% yield strength
D-4			D-4	Cold worked, ~70,000-psi 0.2% yield strength
D-3, D-4			D-3, D-4	750 ppm B^N + type 304 S.S., 0.485-in. outside diameter by 0.011-in. wall
Poison in Fuel but No Poison in Cladding				
E-1	Vibratory-compacted arc-fused powder, 85% of theoretical density, poisoned with 50 ppm B^N as BeO-coated ZrB_2 particles	6.6%/5.5%	E-1	Type 304 S.S. annealed, ~40,000-psi yield strength, 0.485 in. by 0.011-in. wall
E-2	Vibratory-compacted and swaged arc-fused powder, 92% of theoretical density, poisoned with 50 ppm B^N as BeO-coated ZrB_2 particles	6.6%/5.5%	E-2	Type 304 S.S. swaged, ~135,000-psi yield strength, 0.485 in. by 0.017-in. wall
Poison in Fuel but No Poison in Cladding				
F-1	Vibratory compacted arc-fused powder, 85% of theoretical density, poisoned with 50 ppm B^N as molybdenum-coated ZrB_2 particles		F-1	Type 304 S.S. annealed, 40,000-psi yield strength, 0.485 in. by 0.011-in. wall
F-2	Vibratory compacted and swaged arc-fused powder, 92% of theoretical density, poisoned with 50 ppm B^N as molybdenum-coated ZrB_2 particles		F-2	Type 304 S.S. swaged, 135,000-psi yield strength, 0.485 in. by 0.017-in. wall
G-1	Vibratory compacted arc-fused powder, 85% of theoretical density, poisoned with 50 ppm B^N as ZrB_2 particles		G-1	Type 304 S.S. annealed, 40,000-psi yield strength, 0.485 in. by 0.017-in. wall
G-2	Vibratory compacted and swaged arc-fused powder, 92% of theoretical density, poisoned with 50 ppm B^N as ZrB_2		G-2	Type 304 S.S. swaged, 135,000-psi yield strength, 0.485 in. by 0.017-in. wall

test the transient behavior and stability characteristics of the HPD reactor, and will determine by test the heat transfer and fluid flow characteristics of the core, using elements simulating core characteristics.

4. Task III — Physics Development. This task involves the physics evaluation of control requirements and hot spot reduction; the physics and engineering conceptual design of a 300 Mwe high power density reactor; and the physics and engineering required to design, procure and put into operation a computer for scheduling control.

5. Task IV — Operational Planning and Test Coordination. The coordination of the R & D program between tasks, with Design Engineering, and with the AEC and Consumers is a major function of this

Table IV-9 DESCRIPTION OF FUEL ASSEMBLIES IN THE HPD PROJECT[27]

Assem-blies	Nominal pellet diameter, in.		Cladding thickness, in.				Cladding condition*		Diametral gap, in. nominal				Enrichment, %			No. of fuel rods†			Swaged	Proto-types	Instru-mented	Single-layer spacer	Proto-type spacer	Requested heat flux, Btu/(hr)(sq ft)
	0.375	0.330	0.020	0.017	0.012	0.014	CW	Ann.	0.005	0.003	0.002	0.000	4.5	3.5	2.7	25	24	16						
1A	X		X					X	X						X			X				X		420,000
2A	X		X					X	X						X			X				X		420,000
1B	X		X					X	X						X			X				X		414,000
2B	X		X					X	X						X			X				X		414,000
1C	X			X				X	X					X		X						X		401,000
2C	X			X			X		X					X		X						X		379,000
3C	‡			X			X			X				X		X			X			X		401,000
4C	X			X			X				X			X		X			X			X		401,000
1D	X				X			X				X		X		X			X			X		409,000
2D	X				X		X					X		X		X			X			X		409,000
3D	X				X			X			X			X		X			X			X		379,000
4D	X				X		X				X			X		X			X			X		401,000
1E to 5E		X				X	X		X				X			X				X			X	422,000
6E		X				X	X		X				X				X				X	X		465,000
1F		X				X	X		X				X			X				X			X	465,000
2F		X				X	X		X				X				X				X	X		422,000
1G		X				X	X					X	X			X			X			X		422,000
2G		X				X		X				X	X			X			X			X		385,000
3G		X				X	X				X		X			X			X			X		395,000
4G		X				X		X			X		X			X			X			X		385,000

*CW - cold worked; Ann. - annealed.

†Fuel length, 37 in.

‡Unground pellets (simulated by grinding in 0.001-in. increments from 0.368 to 0.378 in.).

task, as is the design of tests and the procurement of instrumentation.

This review considers only Tasks IA and IB.

Under the HPD program (Task IA) 24 fuel assemblies have been fabricated and irradiated in the VBWR. These consisted of four 16-rod fuel-follower assemblies and twenty 25-rod test assemblies. The fabrication of these assemblies is detailed in Ref. 27, and the constructional details of the assemblies are given in Table IV-9. Groups A and B assemblies are control-rod follower assemblies. The Group C assemblies duplicate the Consumers Power Company reactor first core fuel assemblies with respect to cladding stress and diametral gap, but a single-layer spacer is used. The spacer designs and the fuel bundle itself are shown in Fig. IV-4. Bundle 3C contains fuel pellets that have been ground to several different diameters to simulate the variability of unground pellets. Group D includes variations in diametral gap, pellet tolerance, cladding thickness (the 12-mil cladding will be collapsed owing to reactor pressure), and the metallurgical condition of the cladding (cold worked or annealed). Group E assemblies are designed to duplicate the first core fuel in the Big Rock Point Reactor as closely as possible; one fuel element is instrumented for inlet and exit coolant flow rates, pressures, and temperatures and contains a flux monitor tube in place of the center fuel rod. Group F assemblies were built of fuel rods having lengths of about 5 ft rather than the normal length of slightly over 3 ft. Group G assemblies incorporated variations in diametral gap and cladding conditions. The fuel rods were swaged to produce a controlled pellet-cladding gap; the process reduced the pellet-cladding gap an average of about 5 mils.

Twenty-two of the 24 fuel assemblies were placed in the VBWR in September of 1960; the remaining two assemblies, the instrumented ones, were placed in the core during June 1961. A difficulty was experienced with the spacers

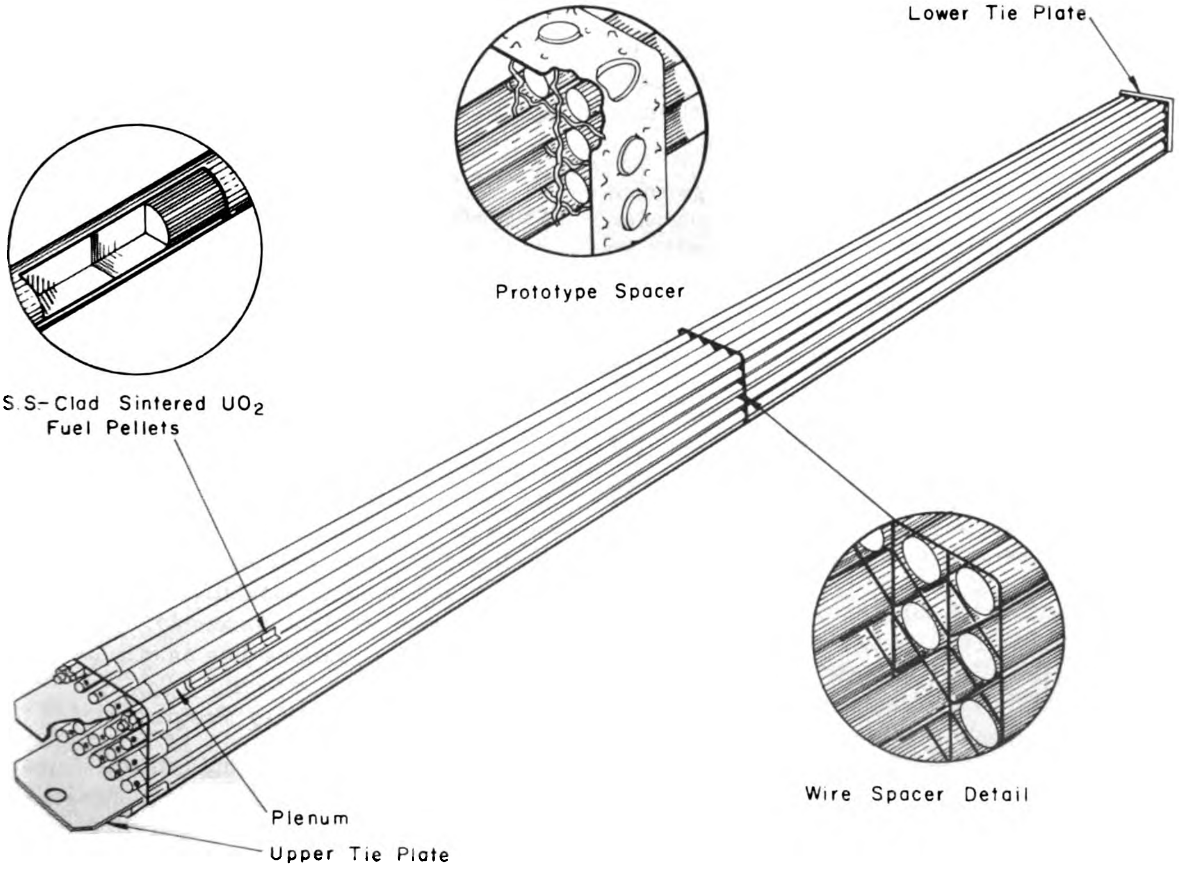

Fig. IV-4 Typical high-power-density VBWR fuel bundle.[27]

on E and F assemblies. The F bundles, with their 5-ft rods, have two spacers between the upper and lower tie plates, whereas the E assemblies, with 3-ft rods, have one spacer. These assemblies employed prototype spacers that were held in position by wires running between the spacers to the upper and lower tie plates. Quoting from Ref. 22: "It appears that the problem of breaking axial tie wires and skidding the spacers on bundles 1E-5E and 1F is one that will plague us through the remaining period of irradiation. Though it is a problem and certainly points to the elimination of this method for axial spacer location, it is not expected that this will affect the performance of the fuel or the information available from it, after irradiation." From the references it is not clear what the difference was between the method of locating the single-layer spacers and the prototype spacers or why the latter method would be giving trouble and the former method would not.

As of June 1963 some of the assemblies had reached peak burnups above 10,000 Mwd/ton. A total of 15 assemblies had been removed from the VBWR because of failed fuel rods. The irradiation exposure data on the sound assemblies are given in Table IV-10, and data on the fuel-rod failures are given in Table IV-11. Preliminary observations are quoted as follows:[26]

> 1. The cracks are predominately intergranular in nature, starting at the fuel rod outer diameter and eventually penetrating the clad thickness.
> 2. No grain boundary precipitates have been observed which may account for the intergranular cracking.
> 3. All of the failed fuel rods were clad with 304 stainless steel tubing purchased with an initial room temperature yield strength of 90–95,000 psi.
> 4. All of the cracks have occurred in the peak heat flux region of the fuel rods.
> 5. All of the cracks occurred in rods which had operated at peak surface heat fluxes in excess of 380,000 Btu/hr-ft^2.

In addition to the HPD project fuel elements listed in Table IV-9, a total of seven special elements (Task IB) have been irradiated in the VBWR. The fabrication details of these elements are given in Table IV-12, and their irradiation exposure data through December 1962 are listed in Table IV-13. The fabrication of these elements comes under Task IB of the HPD project, and it is evident from a consideration of Table IV-12 that the Task has studied a number of advanced methods for the fabrication of fuel rods. These include tandem rolling, electromagnetic vibratory compaction, pneumatic vibratory compaction, swaging employing powder fuel, and swaging employing pelletized fuel. The vibrational compaction of oxide is covered in greater detail in Ref. 28, and Refs. 29 to 31 report on fabrication of fuel elements by swaging.

Also included in Task IB is the preparation of eight developmental fuel assemblies for irradiation in the Consumers reactor. Each assembly contains 121 fuel rods of 6-ft length. The bundle is shown in Fig. IV-5.[22,32] Four of the assemblies contain rods prepared by the swaged-pellet process, whereas the other four assemblies contain swaged powder fuel rods. A functional description of the components shown in Fig. IV-5 is as follows:[22]

Spacer	Laterally positions fuel rods with respect to each other and the channel Adds stiffness to the corner angles and ties them together
Corner angle	Transmits force Positions the spacers axially Provides protection to the fuel rods during insertion and removal from channels by being the outermost part of the fuel bundle
Support	Supports the weight of all fuel rods and transmits this force to the corner angles
Weldment	Provides a handle without obstructing fuel-rod removal Transmits the weight of the fuel bundle from the corner angles to the lifting device
Retainer	Prevents withdrawal of fuel rods Adds stiffness to the weldment

The special assemblies 8S, 9S, and 10S which are being irradiated in the VBWR, as well as assembly 4S, are prototypical of the Consumers development fuel, or they contain mechanical design features representative of the research and development fuel assembly. Table IV-14 lists the Task IB failure data as of June 1963.

High-Performance UO$_2$ Program[35–44,46]

This program is a joint USAEC-Euratom program "... to obtain a better understanding of the maximum achievable operating characteristics of UO$_2$ as a reactor fuel."[35] The program is divided into three major tasks, as follows:

Table IV-10 DESIGN AND OPERATIONAL DATA[46] OF TASK IA

Task IA fuel assembly	Enrichment, %	Nominal rod diameter, in.	No. of rods and cladding thickness, in.	Nominal cladding-to-pellet gap, in.	Initial tubing condition	Fabrication process	Fabricated yield strength, psi	Average bundle exposure,* Mwd/ton of U	Peak bundle exposure, Mwd/ton of U	Peak heat flux, Btu/(hr)(sq ft)	Maximum average power density to date, kw/liter
1A	2.7	0.420	16, 0.020	0.005	Ann.†	Not swaged	40,000	6,330	10,129	361,000	80
2A	2.7	0.420	16, 0.020	0.005	Ann.	Not swaged	40,000	6,350	10,160	358,000	79
1B	2.7	0.420	16, 0.020	0.005	Ann.	Not swaged	40,000	6,464	10,342	333,000	88.9
2B	2.7	0.420	16, 0.020	0.005	Ann.	Not swaged	40,000	6,724	10,758	317,000	92.9
1C	3.5	0.415	25, 0.017	0.005	Ann.	Not swaged	40,000	4,832	7,731	377,000	109.7
2C	3.5	0.415	25, 0.017	0.005	CW‡	Not swaged	90,000	5,517	8,827	400,000	108.2
3C§	3.5	0.415	25, 0.017	0.003	CW	Swaged		4,686	7,498	400,000	103.9
4C	3.5	0.415	25, 0.017	0.002	CW	Swaged		5,308	8,493	393,000	109.3
1D	3.5	0.398	25, 0.012	0	CW	Swaged	100,000	4,948	7,916	400,000	110.4
2D	3.5	0.398	25, 0.012	0	CW	Swaged	100,000	4,030	6,448	399,000	111.3
3D	3.5	0.398	25, 0.012	0.002	CW	Swaged	100,000	4,288	6,860	440,000	109.2
4D	3.5	0.398	25, 0.012	0.002	CW	Swaged	100,000	1,769	2,830	360,000	113.8
1E	4.5	0.360	25, 0.014	0.005	6 Ann. 19 CW	Not swaged	40,000 90,000	6,247	9,995	470,000	116.3
2E	4.5	0.360	25, 0.014	0.005	5 Ann. 20 CW	Not swaged	40,000 90,000	7,920	12,672	470,000	113.9
3E	4.5	0.360	25, 0.014	0.005	2 Ann. 23 CW	Not swaged	40,000 90,000	8,715	13,944	490,000	115.9
4E	4.5	0.360	25, 0.014	0.005	6 Ann. 19 CW	Not swaged	40,000 90,000	8,426	13,482	462,000	109.8
5E	4.5	0.360	25, 0.014	0.005	8 Ann. 17 CW	Not swaged	40,000 90,000	8,039	12,862	450,000	111.6
6E	4.5	0.360	24, 0.014	0.005	2 Ann. 22 CW	Not swaged	40,000 90,000	7,659	12,255	470,000	117.7
1F	4.5	0.360	25, 0.014	0.005	CW	Not swaged	90,000	6,417	10,268	480,000	116.2
2F	4.5	0.360	24, 0.014	0.005	CW	Not swaged	90,000	6,911	11,057	460,000	111.8
1G	4.5	0.358	25, 0.014	0	4 Ann. 21 CW	Swaged	40,000 90,000	5,985	9,576	480,000	118.8
2G	4.5	0.358	25, 0.014	0	8 Ann. 17 CW	Swaged	40,000 90,000	5,625	9,000	480,000	120.7
3G	4.5	0.358	25, 0.014	0.002	6 Ann. 19 CW	Swaged	40,000 90,000	7,252	11,603	500,000	120.5
4G	4.5	0.358	25, 0.014	0.002	2 Ann. 23 CW	Swaged	40,000 90,000	8,084	12,934	480,000	119.8

*Exposures as of June 2, 1963.

†Annealed.

‡Cold worked.

§Unground pellets.

Table IV-11 TASK IA FAILURE DATA[45]

Task IA fuel assembly	Location of failed rod(s)	Type of rod(s) failed	Average exposure, Mwd/ton of U	Exposure in failure location, Mwd/ton of U	Heat flux in failure location, maximum, Btu/(hr)(sq ft)	Type of failure	Remarks
1D	One corner rod	CW	4,948	7,900	400,000	Longitudinal crack	RML metallurgical examination performed
2D	One corner rod	CW	4,030	6,400	399,000	Small longitudinal cracks	RML metallurgical examination performed
3D	One rod next to corner	CW	4,288	6,900	440,000		Previously reported
4D	One corner rod	CW	1,769	2,830	360,000		One corner rod has leaky weld at end plug
1E	One corner rod	CW	6,247	10,000	470,000	Longitudinal cracks	Detailed RML metallurgical examination in progress; see 1E status in text*
2E	One exterior rod O	CW	7,920	12,672	470,000	Longitudinal crack	Crack was not detected by visual observation at VBWR pool; very high sipping signal; RML examination in progress; see Fig. 1*
3E	One rod X adjacent to corner	CW	8,715	13,944	490,000	Large longitudinal crack ~4 in. long	Visual examination at VBWR pool showed crack. RML examination in progress; see Fig. 2*
4E	One exterior rod midway between corners	Ann.	8,426	13,482	462,000	Circumferential cracks	This is the first observation in the HPD program of a crack not in the longitudinal direction. Also it is the first annealed, free-standing rod to fail; see Fig. 3*
5E	?		8,039	12,862	450,000	?	Potential failure by sipping indication, visual examination in VBWR pool showed no crack; RML examining
6E	Corner rod A	CW	7,659	12,255	470,000	Longitudinal cracks	With 4E initial failure detected by in-core sampler
2F	?		6,911	11,057	460,000	?	Visual examination at VBWR pool showed no crack; high sipping signal
1G	One interior rod	CW	5,985	9,600	480,000	Longitudinal cracks	RML metallurgical examination performed; see text* for burst test results on sound rods
2G	Two interior rods	CW	5,625	9,000	480,000	Longitudinal cracks	RML metallurgical examination performed
3G	Three exterior rods on one side, including a corner rod	CW	7,252	11,600	500,000	Longitudinal cracks	RML visual examination performed
4G	One exterior rod adjacent to corner	CW	8,000	13,000	480,000	Longitudinal cracks	Visual examination in VBWR pool

***Refers to material in Ref. 45.**

Table IV-12 DETAILS OF HPD PROJECT SPECIAL FUEL ASSEMBLIES[23]

Assemblies Fabricated by Swaged-over-Pellet Process

Assembly 1S	
Purpose	To irradiation-test marginal quality and good quality 12-mil-thick cladding with as-sintered pellets
Cladding	0.012-in.-thick type 304 stainless steel
Fuel	3.5% sintered UO_2* ground to an as-sintered distribution
Rods	Swaged to zero gap; 12 rods have good quality cladding and pellets with 0.010-in.-diameter range; 12 rods have marginal quality cladding and pellets with 0.006-in.-diameter range; 1 rod has a 0.015-in.-diameter hole through cladding, is three-pass swaged over powder, and has 0.015-in.-thick cladding
End plugs	Current standard machined design
Assembly 4S	
Purpose	To irradiation-test a prototype mechanical design for Consumers fuel that provides for easy removal of fuel rods
Cladding	0.014-in.-thick type 304 stainless steel
Fuel	4.5% sintered UO_2 ground to 0.003-in.-diameter tolerance
Rods	Pellet type fuel
End plugs	Current standard machined design
Assembly 6S	
Purpose	To irradiation-test 8- and 10-mil cladding rods fabricated from commercially available material and utilizing a statistical approach to the relaxation of various manufacturing and design variables
Cladding	0.010- and 0.008-in.-thick type 304 stainless steel
Fuel	3.5% sintered UO_2 ground to simulate as-sintered pellets; 40% of pellets <94% of theoretical density; balance of pellets >94% of theoretical density; pellets to have varying degrees of chips
Rods	Swaged to zero gap; 13 rods to have 10-mil cladding and 12 rods to have 8-mil gap cladding; both cladding sizes to have 9 rods, each containing up to 0.002-in. cladding defects; 4 rods in each cladding size to have X-ray rejectable weld defects
End plugs	Standard machined design
Assembly 3S	
Purpose	To irradiation-test fuel rods fabricated by the Calrod tandem rolling process
Cladding	0.015-in.-thick type 304 stainless steel
Fuel	3.5% fused UO_2 (−6 mesh)
Rods	Rolled to 88.5% ± 1% density
End plugs	Collapsible design

Assemblies Fabricated by the Swaged-over-Powder Process

Assembly 2S	
Purpose	To irradiation-test fuel rods fabricated by three-pass swaged-over-powder process
Cladding	0.015-in.- and 0.010-in.-thick type 304 stainless steel
Fuel	3.5% fused UO_2 (−6 mesh)
Rods	Swaged to 92% ± 1% density using multiple pass techniques; 13 rods to have 15-mil cladding and 12 rods to have 10-mil cladding
End plugs	Collapsible design

Assemblies Fabricated by Swaging and Vibratory-Compaction Process

Assembly 7S	
Purpose	To irradiation-test fuel rods fabricated by vibratory compaction and two-pass swaging
Cladding	0.010-in.-thick type 304 stainless steel (vibratory compacted); 0.016-in.-thick type 304 stainless steel (two-pass swage)
Fuel	3.5% fused UO_2 (−6 mesh, conditioned)
Rods	Vibratory compacted to 86% of theoretical density (12); two-pass swaged to 90% of theoretical density (13)
End plugs	Current standard machine design and drawn cup
Assembly 5S	
Purpose	To irradiation-test two-pass swaged UO_2 rods having 90% of theoretical density and hot-swaged UO_2 rods having 95% of theoretical density

Swage process	Three-pass cold	Hot	Two-pass vibratory compacted
No. of rods	5	10	10
Cladding thickness	0.010	0.016	0.008
UO_2 density	91%	95%	90%

*All UO_2 is 4.0% enriched and arc fused. Supplied by Spencer Chemical Co.

Table IV-13 TASK IB DESIGN AND OPERATIONAL DATA[45]

Task IB fuel assembly	Enrichment, %	Rod diameter, in.	No. of rods and cladding thickness, in.	Type of fuel	Initial tubing condition	Fabrication process	Powder density as fabricated, %	Cladding yield strength as fabricated, psi*	Average bundle exposure,† Mwd/ton of U	Peak bundle exposure, Mwd/ton of U	Peak heat flux, Btu/(hr)(sq ft)	Max. average power density to date, kw/liter
1S	3.5	0.400	25, 0.012	Unground pellets	CW‡	Swaged to 0- to 5-mil gap		105,000	1,800	2,851	380,000	86
1SM	3.5	0.400	21, 0.016	Powder	Ann.§	Tandem rolled	88 to 89	90,000	4,500	7,182	380,000	100
			4, 0.012	Powder	CW	Vibratory compacted	86 to 88	100,000		2,851	380,000	86
2S	3.5	0.400	12, 0.016	Powder	Ann.	Swaged	94	95,000	4,500	7,100	385,000	92.7
			12, 0.010	Powder	Ann.	Swaged	93					
3S	3.5	0.400	4, 0.012	Pellet	CW	Swaged to 0- to 1-mil gap		100,000	4,500	7,182	380,000	100
			21, 0.016	Powder	Ann.	Tandem rolled	88 to 89	90,000				
4S	4.5	0.36	16, 0.014	Pellet	Ann.	Not swaged		40,000	5,734	9,174	492,000	106.1
			9, 0.014	Pellet	CW	~5-mil gap		90,000				
5S	4.0	0.400	5, 0.010	Powder	Ann.	Swaged	90.5	95,000	4,000	6,339	425,000	109.2
			10, 0.008	Powder	Ann.	Swaged	87 to 90	95,000				
			10, 0.016	Powder	Ann.	Hot swaged	95					
6S	3.5	0.400	12, 0.010	Unground pellets	Ann.	Swaged to 1-mil gap		45,000	5,500	8,441	410,000	106.7
			13, 0.008	Unground pellets	Ann.			52,000				
7S	3.5	0.400	12, 0.016	Powder	Ann.	Swaged	90 to 91	95,000	3,800	6,098	460,000	95.2
			13, 0.012	Powder	CW	Vibratory compacted	86 to 88	100,000				
8S	4.0	0.400	16, 0.010	Powder	Ann.	Swaged	91 to 92	95,000	3,600	5,637	527,000	101
9S	4.0	0.400	16, 0.010	Powder	Ann.	Swaged	91 to 92	95,000	3,722	5,956	490,000	120
10S	4.0	0.430	12, 0.010	Powder	Ann.	Swaged	89 to 92	95,000	2,100	3,385	450,000	93
			4, 0.010	Pellet	Ann.	Swaged		50,000				
11S	5.0	0.430	4, 0.010	Pellet	Ann.	Swaged to 3- to 4-mil gap		40,000	0	0	0	
12S¶			12, 0.010	Powder	Ann.	Swaged	89 to 91	95,000				

*Yield strength at 0.2% offset; room temperature.

†Exposure as of June 2, 1963.

‡Cold worked.

§Annealed.

¶Plan to build using annealed rods from failed E assemblies.

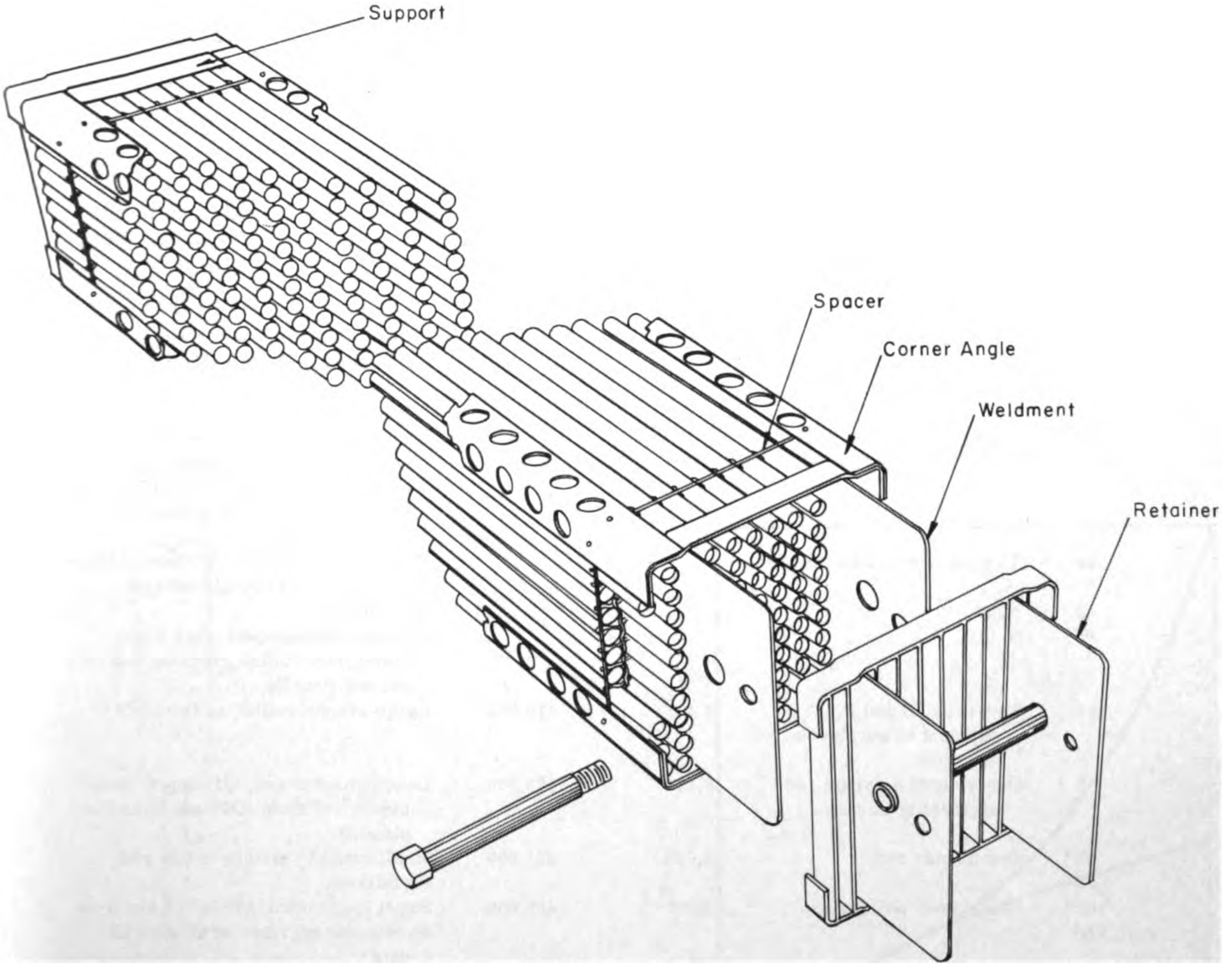

Fig. IV-5 Preliminary development of fuel bundle.[22]

Task I—Measurement of Fission Gas Pressure in Operating Fuel Elements. Objective: Direct measurement of fission gas pressure in UO_2-filled fuel rods, as functions of temperature and fuel configurations. Measurements to be made over an extended period of time during transient and steady-state reactor operation.

Task IIA—Loop Modification. Objective: Design, fabrication and installation of GETR Pressurized Water Loop modifications required by Task IIB experimental program.

Task IIB—Performance of UO_2 Fuel. Objective: Obtain a relationship between the amount of fuel rod central melting and the burn-up that can be attained before fuel-cladding interaction results in rod failure.

A number of progress reports have been issued and are cited as Refs. 35 to 41.

The results obtained under Task I of the UO_2 program are summarized in Ref. 42. The pressure transducer used in the reactor is shown schematically in Fig. IV-6; briefly, the pressure within the fuel rod was measured by increasing the pressure in the tube connected with the source of equalizing pressure until the contacts opened. The fuel elements listed in Table IV-15 were studied. The temperature profiles in the elements were calculated using the UO_2 conductivity data of Bates[43] and some unpublished UO_2 conductivity data of Lyons.[44] For comparison these data are shown in Fig. IV-7. Equivalent gap conductances of 440 and 1762 Btu/(hr)(sq ft)(°F/ft) were assumed. The results are quoted as follows:[42]

> ... These experiments have indicated that fission gas release is negligible from UO_2 operated below the recrystallization temperature. For operation at higher power levels the fractional fission gas release is directly comparable to the volume fraction of fuel operating above the recrystallization temperature.

Table IV-14 TASK IB FAILURE DATA[45]

Task IB fuel assembly	Location of failed rod(s)	Exposure in failure location, Mwd/ton of U	Heat flux in failure location (peak), Btu/(hr)(sq ft)	Remarks
1S	None			No failures; see 1SM
1SM	None			1SM has been reconstituted from fuel rods originally in 3S and 1S, the purpose being to allow irradiation to continue on the tandem-rolled rods
2S	One 0.016-in. rod, one 0.010-in. interior rod	7,100	385,000	Longitudinal crack ~8 to 9 in. long in 0.010-in. cladding; RML ultrasonic examination revealed crack in 0.016-in. cladding
3S	Four corner pellet rods	7,183	380,000	Gross longitudinal cracks varying to very small intergranular and transgranular cracks; RML metallurgical examination performed on one corner rod
3S	Two tandem-rolled rods			Two tandem-rolled rods show indications of cracks by ultrasonics
4S	None			No failures
5S	?			Ultrasonic techniques show many small indications; cracking not observed visually
6S	Two rods, B and D, adjacent to corners on one side	8,441	410,000	Large cracks visible in two rods
7S	One swaged exterior rod adjacent to corner	6,100	460,000	Longitudinal crack, ultrasonic techniques verified; RML examination planned
8S*	One corner rod	5,638	527,000	Small cracks* visible in one rod
9S				No failures
10S*	One corner pellet rod	3,387	458,000	Small longitudinal crack* in one rod
11S				Bundle has not been irradiated to date

*Some difficulty in verification exists among several observers. Ultrasonic examination will be performed.

Table IV-15 FUEL RODS IRRADIATED WITH PRESSURE TRANSDUCERS[42]

	Rod S-1	Rod S-1A	Rod S-2	Rod S-3	Rod P-1	Rod P-2
Enrichment, %	4.0	4.0	7.08	3.84	3.0	6.65
Fuel density ρ/ρ_0, %	98	98	98	93.2	89.4	90.0
Fuel type	Pellet	Pellet	Pellet	Pellet	Powder	Powder
Fuel diameter, in.	0.496	0.496	0.481	0.496	0.500	0.500
Maximum heat flux	348*	334*	532*	348*	223‡	453‡
Maximum burnup,† Mwd/ton	1549	1718	3115	1712	674	1270
Gap, in.	0.004	0.004	0.014	0.004		
Fuel weight, g	957	880.5	897	935	945	946
Fuel length, in.	28.6	26.3	28.3	28.5	28.75	27.5
Void volume, cm^3	5.5	3.5	9.6	4.4	6.3	3.9
Typical oxygen-to-uranium ratios	2.008	2.007				

*Heat flux was 1000 Btu/(hr)(sq ft) in position N-10 at 36 Mw of reactor power.

†At time of removal from reactor.

‡Heat flux was 1000 Btu/(hr)(sq ft) in position O-10 at 40 Mw of reactor power.

These conclusions are based on data taken with rod S-2, since the other rods experienced mechanical difficulties or were of insufficient enrichment to get the maximum temperature above the recrystallization temperature.

The direct measurement experiment was terminated on Sept. 12, 1962. Presumably no further irradiation of the transducer-equipped rods will be made, although the results reported to date indicate that the technique is feasible. It would be of interest to irradiate the powder-filled rods at a higher heat flux, if possible, for comparison to the pellet-filled-rod gas release.

Task IIA is concerned primarily with modification and operation of a pressurized-water loop in the General Electric Test Reactor (GETR). This loop, the PWL loop, is being used to irradiate samples under the High-Performance UO_2 Program (HPP). The loop can accommodate a rod bundle composed of four rods, each with an outside diameter of about $\frac{1}{2}$ in. and an active length of 34 in. Another facility used for the program is the so-called "Trail Cable" facility. This facility, a part of the GETR installation, can accept a single fuel rod of the same geometry as that to be employed in the PWL loop with the exception of length; the Trail Cable capsule has a length of 5 in. The Trail Cable facility was used to obtain calibration data on the UO_2 before the full-length rods were irradiated in

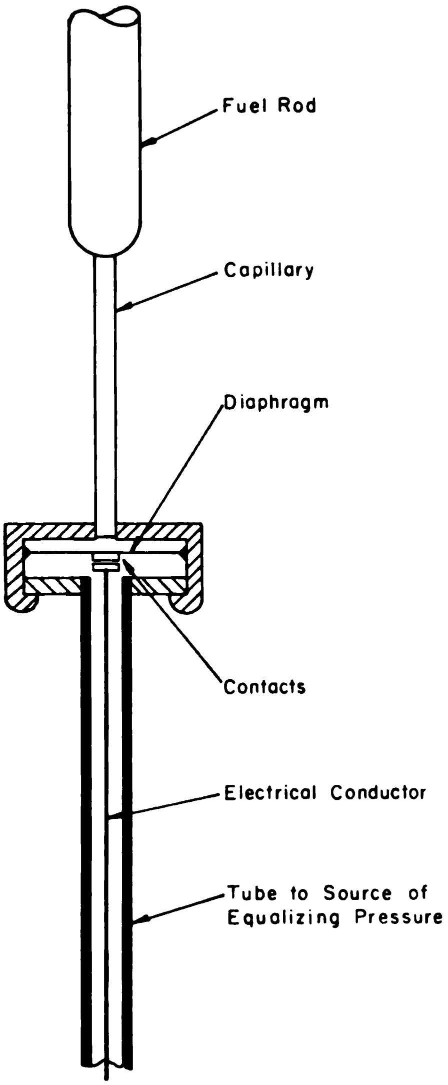

Fig. IV-6 Schematic of transducer.[42]

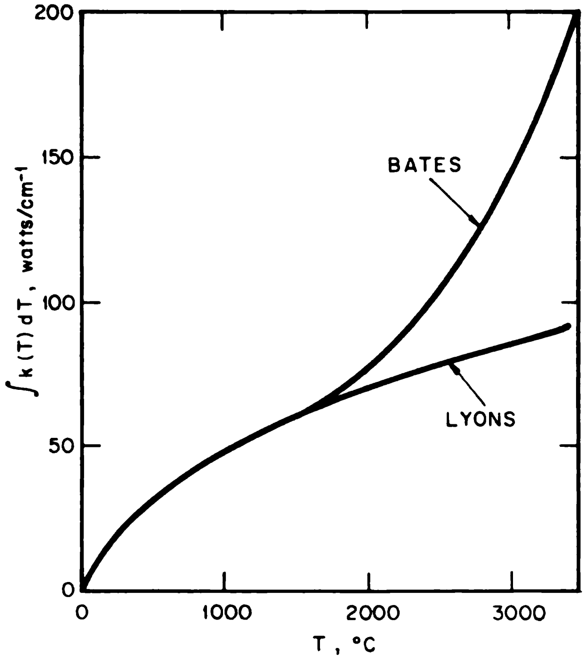

Fig. IV-7 $\int_0^T k(T)\,dT$ vs. T for UO_2 having 95% of theoretical density.[42]

Table IV-16 OPERATING DATA FOR PWL LOOP: HIGH-PERFORMANCE UO_2 PROGRAM

GETR cycle No.	PWL assembly No.	Burnup, Mwd/metric ton	Approximate peak heat flux, Btu/(hr)(sq ft)
33	EPT-6	1180	630,000
34	EPT-8	1442	790,000
35	EPT-10	1182	1,010,000
36 to 39	EPT-COM	1516	1,200,000
40	EPW-6/8	9.8	722,000
40	EPW-6/8A	11.7	800,000
41	EPT-12	2239	1,350,000

the PWL loop. The operation of the Trail Cable facility was coordinated with remote metallurgical examinations of the irradiated capsules to obtain as much information as possible concerning UO_2 temperature distribution and thermal conductivity.

The nomenclature for the assemblies irradiated in the PWL loop is given in Table IV-16, along with other pertinent data. The results of the first three experiments involving EPT-6, -8, and -10 are summarized in Ref. 40. The irradiation conditions are summarized in Table IV-17. The fuel rods contained sintered UO_2 pellets that had 95% of the theoretical density, a diameter of $^1/_2$ in. (nominal), and a total active length of 34 in. The results of the postirradiation examinations indicated increases in the fuel-rod diameter, and the increase in the fuel-rod volume corresponding to the increase in the outside diameter is shown in Fig. IV-8. Reference 40 makes the following comment on the swelling:

> Considered as an entity, all of the different bits of evidence collected in the above post-irradiation examination point to an association between the clad swelling and the UO_2 melting that occurred in the fuel rods. Recent measurements have indicated a fairly large volume increase (~7 percent) in UO_2 upon melting ... which could generate the necessary force to produce clad swelling ....

Surprisingly, similar rods that had been irradiated in the Trail Cable facility had not exhibited dimensional changes after operating at similar thermal performance. This difference has been attributed to the different lengths of the two rods. In the long PWL fuel rod, the molten oxide was contained between two relatively cold, nonplastic sets of fuel pellets, whereas the short Trail Cable rod contained a molten core over essentially its whole length, and the molten oxide expanded into a plenum. Metallographic examination of a transverse section of one of the rods in assembly EPT-10, at the point of maximum swelling, revealed cracks along the outer portion of the cladding surface. Probably some had propagated through the cladding, since puffs of fission gas had been noted during operation of EPT-10.

Table IV-17 PARAMETERS FOR EURATOM PWL FUEL-ASSEMBLY IRRADIATION

Assembly designation	Fuel enrichment, %	Fuel-column length, in.	Fuel-rod peak surface heat flux (average), Btu/(hr)(sq ft)	Assembly thermal power, kw	Average burnup, Mwd/ton	Irradiation period
EPT-6	1.5	34 ± $^1/_4$	645,000	200	1180	4/23/62 to 5/19/62
EPT-8	2.2	34 ± $^1/_4$	895,000	260	1442	6/1/62 to 6/24/62
EPT-10	3.0	31 ± $^1/_4$	1,010,000	310	1182	7/3/62 to 7/19/62

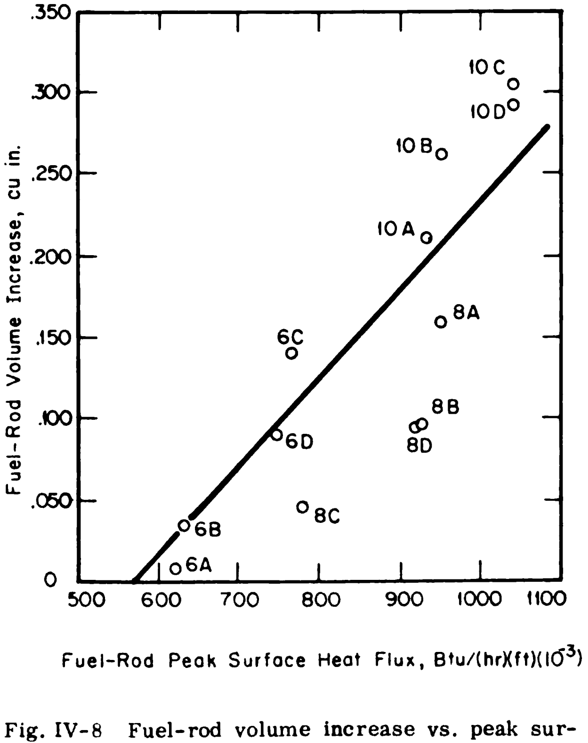

Fig. IV-8 Fuel-rod volume increase vs. peak surface heat flux at startup.[40]

Since expansion of molten UO_2 was responsible for the cladding swelling, the EPT-COM assembly was designed with hollow oxide pellets to accommodate the expanded oxide. The hollow core was an 80- to 90-mil hole drilled in each of the fuel pellets at the center line. Figure IV-9 shows that extensive UO_2 melting and fuel relocation occurred during irradiation. The fuel in all four rods in assembly EPT-COM under-

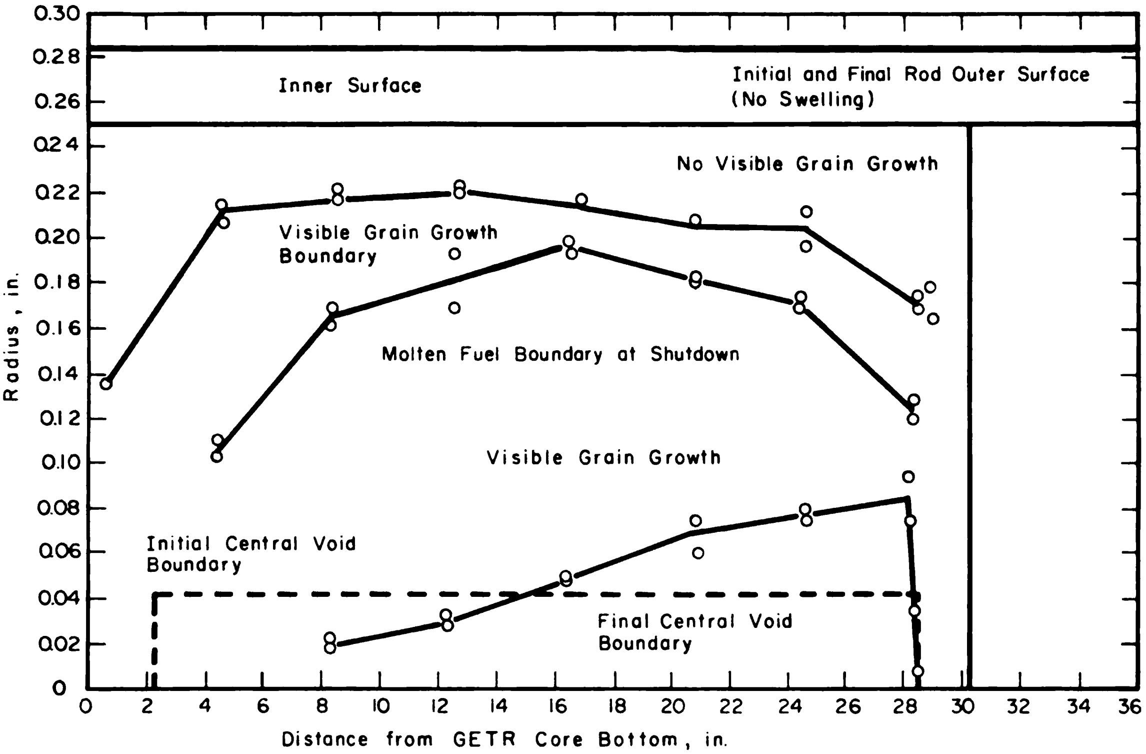

Fig. IV-9 Fuel microstructure boundaries of a rod from assembly EPT-COM.[41]

went some center melting; but of the four, only one rod, the rod in which the heat flux was highest, was swollen. This result was interpreted as an indication that the 80-mil hole was marginal for containing the UO_2 on melting, and assembly EPT-12 was designed with a 140-mil hole. Assembly EPT-12 was still in the GETR PWL loop as of the writing of Ref. 41 and apparently was performing satisfactorily.* The initial startup for the GETR, when the EPT-12 assembly was in place, was programmed to prevent sudden power changes of appreciable magnitude, since it was desired to minimize severe internal volume changes in the fuel rods of EPT-12.

Assemblies EPW-6/8 and -6/8A contained swaged-powder fuel rods. These were prepared from arc-fused powder, denitrided at 1650°C for 4 hr in H_2 before loading. The powder was vibrationally compacted into tubing that was 0.656 in. in outside diameter by 30 mils in wall thickness (Zircaloy-2) and was swaged in two passes to the final outside diameter of 0.565 in. The final oxide density was 90%. Several fuel rods were made by vibrational compaction alone—without swaging—to a final density that was 86% of theoretical. Assembly EPW-6/8, containing all swaged rods, underwent about 10 hr of irradiation in the PWL loop; at that point the reactor scrammed owing to high radiation levels in the loop. Examination of the assembly revealed a longitudinal split in the cladding of the rod in the position of highest relative power for the assembly. Two of the sound rods from the assembly and two rods fabricated by only vibrational methods were reassembled into EPW-6/8A and placed in the PWL loop for GETR cycle 40. Soon after startup, when the power was being increased from 25 to 27 Mw, one of the two swaged rods failed; the failure occurred in the swaged rod having the higher power density. The details of the irradiation and subsequent examination of these assemblies are contained in Refs. 41 and 44. The following quotation illustrates current thinking on the causes of the failures:[41]

> It should be emphasized that the RML investigations of these two failures are incomplete. No firm

---

*A later progress report,[46] however, notes that, during subsequent irradiation, assembly EPT-12 failed with significant release of activity.

conclusion can be made concerning the failure mechanism until the examinations are finished. However, on the basis of the evidence presently available, the failures seem to be basically the result of clad swelling similar to that previously observed in the pellet fuel rods. The magnitude of the clad swelling for a given surface heat flux in the case of the swaged fuel appears to be equal to or greater than that previously experienced with pellet fuel despite its lower fuel density . . . . This may be the result of lower thermal conductivity in the powder fuel with a resultant large degree of fuel melting. The clad swelling coupled with a generally less ductile cladding due to swaging resulted in actual loss of the clad integrity. (The pellet fuel rods experienced significantly larger increases in diameter than the first powder fuel rod failure and did not rupture.)

It is likely that the first powder rod failure was associated with a localized weakness in the cladding. This conclusion is based on the failure being away from the zone of maximum swelling and the circumferentially nonuniform swelling of the UO_2 cross section in the failure zone. The source of the clad weakness has not been identified.

The mechanism for the second powder rod failure appears to have been much more complex. The failure was more severe than the first in terms of the activity release to the loop.

A section of the cladding approximately $\frac{1}{4}$ inch wide by one inch long was lost from the rod and the appearance of the remaining edges of the clad indicates that the clad had melted. The general diameter increase of the rod at the axial location of failure is approximately 80 mils. Two possible mechanisms for the clad melting can be postulated. One is that a heat transfer "burnout" may have occurred at the failure zone as a result of flow starvation from the clad swelling, particularly if the swelling at the failure orientation significantly exceeded the uniform swelling measured at the cross section. A second is that the clad may have fractured, expelling the outer rim of unmelted fuel and permitting molten UO_2 to contact the cladding. The post-irradiation examination has produced some evidence favoring the latter theory. The loss of fuel and cladding makes it difficult to obtain a complete picture of what occurred.

The vibratory compacted fuel rods had approximately four percent lower density than the swaged fuel rods and do not appear to be subject to clad swelling, at least up to a heat flux of approximately 800,000 Btu/hr-ft^2. To confirm this conclusion it is planned to replace the original swaged powder assembly in the irradiation schedule for the program with fuel rods fabricated by vibratory compaction alone. This assembly [was] scheduled for irradiation in the GETR during April 1963. If this irradiation is successful, the remaining higher thermal performance powder fuel rods will also be vibratory compacted.

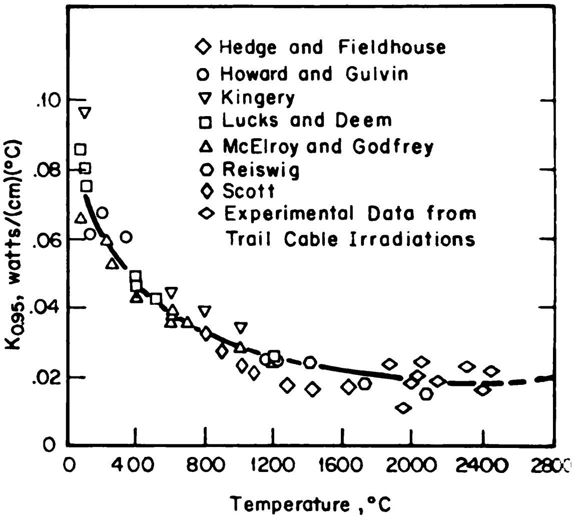

Fig. IV-10 Thermal conductivity vs. temperature for UO_2 having 95% of theoretical density.[41]

Analyses of irradiated pellet-fuel capsules in the Trail Cable facility have resulted in increased knowledge of fuel melting limits and thermal conductivity. Figure IV-10 summarizes the results from various experimenters; the integral of *kdT* from zero to melting temperature has been experimentally determined as 86 ± 3 watts/cm. The Trail Cable data in Fig. IV-10 do not indicate the improvement of UO_2 thermal conductivity at elevated temperatures which has been postulated elsewhere.[43]

References

1. W. H. Cook, Fuel Cycle Program. A Boiling Water Reactor Research and Development Program, First Quarterly Report, August 1960–September 1960, USAEC Report GEAP-3558, General Electric Company, Atomic Power Equipment Department, Oct. 10, 1960.
2. General Electric Company, Atomic Power Equipment Department, Fuel Cycle Program. A Boiling Water Reactor Research and Development Program, Second Quarterly Report (covering the period) October 1960–December 1960, USAEC Report GEAP-3627, July 1961.
3. J. A. Hodde (Comp.), Fuel Cycle Program. A Boiling Water Reactor Research and Development Program, Third Quarterly Report, January 1961–March 1961, USAEC Report GEAP-3709, General Electric Company, Atomic Power Equipment Department, June 1961.

4. J. A. Hodde (Comp.), Fuel Cycle Program. A Boiling Water Reactor Research and Development Program, Fourth Quarterly Report, April 1961–June 1961, USAEC Report GEAP-3781, General Electric Company, Atomic Power Equipment Department, Aug. 1, 1961.
5. J. A. Hodde (Ed.), Fuel Cycle Program. A Boiling Water Reactor Research and Development Program, Fifth Quarterly Report, July 1961–September 1961, USAEC Report GEAP-3835, General Electric Company, Atomic Power Equipment Department, Oct. 10, 1961.
6. J. A. Hodde, General Electric Company, Atomic Power Equipment Department, Jan. 31, 1962. (Unpublished)
7. J. A. Hodde (Comp.), Fuel Cycle Program. A Boiling Water Reactor Research and Development Program, Seventh Quarterly Progress Report, January 1962–March 1962, USAEC Report GEAP-3935, General Electric Company, Atomic Power Equipment Department, Apr. 30, 1962.
8. J. A. Hodde (Comp.), Fuel Cycle Program. A Boiling Water Reactor Research and Development Program, Eighth Quarterly Progress Report, April 1962–June 1962, USAEC Report GEAP-4048, General Electric Company, Atomic Power Equipment Department, July 10, 1962.
9. C. L. Howard (Comp.), Fuel Cycle Program. A Boiling Water Reactor Research and Development Program, Ninth Quarterly Progress Report, July 1962–September 1962, USAEC Report GEAP-4094, General Electric Company, Atomic Power Equipment Department, Oct. 25, 1962.
10. C. L. Howard (Comp.), Fuel Cycle Program. A Boiling Water Reactor Research and Development Program, Tenth Quarterly Progress Report, October–December 1962, USAEC Report GEAP-4159, General Electric Company, Atomic Power Equipment Department, Jan. 14, 1963.
11. C. L. Howard (Comp.), Fuel Cycle Program. A Boiling Water Reactor Research and Development Program, Eleventh Quarterly Progress Report, January–March 1963, USAEC Report GEAP-4215, General Electric Company, Atomic Power Equipment Department, Apr. 5, 1963.
12. C. J. Baroch, J. P. Hoffman, and W. C. Rous, AEC Fuel Cycle Program. Design and Fabrication of the Basic Fuel Assemblies, USAEC Report GEAP-3653, General Electric Company, Atomic Power Equipment Department, Mar. 15, 1963.
13. S. J. Paprocki (Ed.), Progress on the Use of Gas-Pressure Bonding for Fabricating Low-Cost Ceramic, Cermet, and Dispersion Fuels, USAEC Report BMI-1372, Battelle Memorial Institute, Aug. 25, 1959.
14. S. J. Paprocki (Ed.), Progress on the Use of Gas-Pressure Bonding for Fabricating Low-Cost Ceramic, Cermet, and Dispersion Fuels, Phase II Report on AEC Fuel-Cycle Program, USAEC Report BMI-1475, Battelle Memorial Institute, Nov. 7, 1960.
15. S. J. Paprocki (Ed.), Progress on the Use of Gas-Pressure Bonding for Fabricating Low-Cost Ceramic, Cermet, and Dispersion Fuels, USAEC Report BMI-1555, Battelle Memorial Institute, Nov. 24, 1961.
16. C. J. Baroch, C. B. Boyer, and S. N. Porembka, Evaluation of Failed Hot Gas Isostatic Pressed Fuel Rods, USAEC Report GEAP-4206, General Electric Company, Vallecitos Atomic Laboratory, Mar. 20, 1963.
17. C. J. Baroch, Design and Fabrication of Fuel Rods Containing Low Temperature Sintered Pellets, USAEC Report GEAP-4257, General Electric Company, Atomic Power Equipment Department, May 15, 1963.
18. C. J. Baroch, Design and Fabrication of Coextruded Stainless Steel Clad UO_2 Fuel Rods, USAEC Report GEAP-4282, General Electric Company, Atomic Power Equipment Department, June 1963.
19. J. G. Hunt, D. F. Kaufman, and P. Loewenstein, Hot Extrusion of UO_2 Fuel Elements. Fundamental and Applied Research and Development in Metallurgy, Final Report for the Period July 1, 1960 Through June 30, 1961, USAEC Report NMI-1245, Nuclear Metals, Inc., Oct. 31, 1961.
20. L. K. Holland, High Power Density Development Project, First Quarterly Progress Report (covering the period) April–June 1960, USAEC Report GEAP-3543, General Electric Company, Atomic Power Equipment Department, July 1, 1960.
21. L. K. Holland, High Power Density Development Project. Third Quarterly Progress Report, October–December 1960, USAEC Report GEAP-3632, General Electric Company, Atomic Power Equipment Department, Jan. 1, 1961.
22. L. K. Holland, General Electric Company, Atomic Power Equipment Department, July 1, 1961. (Unpublished)
23. L. K. Holland, High Power Density Development Project. Sixth Quarterly Progress Report, July–September 1961, USAEC Report GEAP-3884, General Electric Company, Atomic Power Equipment Department, October 1961.
24. R. L. Holladay, High Power Density Development Project. Seventh Quarterly Progress Report, October–December 1961, USAEC Report GEAP-4001, General Electric Company, Atomic Power Equipment Department, Jan. 1, 1962.
25. R. L. Holladay, High Power Density Development Project. Tenth Quarterly Progress Report, July–September 1962, USAEC Report GEAP-4096, General Electric Company, Atomic Power Equipment Department, Oct. 1, 1962.
26. R. L. Holladay (Comp.), High Power Density Development Project. Eleventh Quarterly Progress Report, October–December 1962, USAEC Report

GEAP-4155, General Electric Company, Atomic Power Equipment Department, Jan. 1, 1963.

27. W. D. Fowler and J. W. Lingafelter, High Power Density Development Project. Design and Fabrication of High Power Density Fuel Assemblies for VBWR Irradiation Testing, USAEC Report GEAP-3609, General Electric Company, Atomic Power Equipment Department, Nov. 1. 1960.
28. W. R. DeHollander, Vibrational Compaction of Uranium Dioxide, USAEC Report GEAP-4032, General Electric Company, Vallecitos Atomic Laboratory, Mar. 1, 1962.
29. E. A. Lees, Fabrication of Fuel Elements by Swaging, USAEC Report GEAP-3918, General Electric Company, Vallecitos Atomic Laboratory, May 21, 1962.
30. C. M. Ryer, Powder Fuel Processing by Two-Pass Swaging. The Effect of Particle Size and Distribution, USAEC Report GEAP-3891, General Electric Company, Vallecitos Atomic Laboratory, Apr. 10, 1962.
31. W. V. Cummings, D. R. Lewis, and R. E. Blood, Examination of 304 Stainless Steel Cladding from Cold-Swaged and Rolled Fuel Rods, USAEC Report GEAP-3997, General Electric Company, Atomic Power Equipment Department, July 1962.
32. W. D. Fowler, General Electric Company, Vallecitos Atomic Laboratory, April 1962. (Unpublished)
33. J. W. Lingafelter, E. A. Lees, and R. J. Seely, Erosion Flow Testing of Purposely Defected Stainless Steel Clad Compacted UO_2 Powder Fuel, USAEC Report GEAP-4020, General Electric Company, Atomic Power Equipment Department, February 1962.
34. T. C. Rowland and J. S. Atkinson, Power Cycling of High Power Density Fuel Specimens Clad with 10-mil Wall Stainless Steel, USAEC Report GEAP-4069, General Electric Company, Atomic Power Equipment Department, October 1962.
35. B. Weidenbaum, High Performance UO_2 Program. Quarterly Progress Report No. 2, July–September 1961, USAEC Report GEAP-3771-2, General Electric Company, Vallecitos Atomic Laboratory, Oct. 1, 1961.
36. B. Weidenbaum, High Performance UO_2 Program. Third Quarterly Progress Report, October–December 1961, USAEC Report GEAP-3771-3, General Electric Company, Vallecitos Atomic Laboratory, Jan. 2, 1962.
37. B. Weidenbaum, High Performance UO_2 Program. Quarterly Progress Report No. 4, January–March 1962, USAEC Report GEAP-3771-4, General Electric Company, Vallecitos Atomic Laboratory, Apr. 1, 1962.
38. B. Weidenbaum, High Performance UO_2 Program. Quarterly Progress Report No. 5, April–June 1962, USAEC Report GEAP-3771-5, General Electric Company, Atomic Power Equipment Department, June 1962.
39. B. Weidenbaum, High Performance UO_2 Program. Quarterly Progress Report No. 6, July–September 1962, USAEC Report GEAP-3771-6, General Electric Company, Atomic Power Equipment Department.
40. B. Weidenbaum, High Performance UO_2 Program. Quarterly Progress Report No. 7, October–December 1962, USAEC Report GEAP-3771-7, General Electric Company, Atomic Power Equipment Department, Apr. 16, 1963.
41. B. Weidenbaum, High Performance UO_2 Program. Quarterly Progress Report No. 8, January-March 1963, USAEC Report GEAP-3771-8, General Electric Company, Atomic Power Equipment Department, Apr. 15, 1963.
42. M. B. Reynolds, The Measurement of Free Fission Gas Pressure in Operating Reactor Fuel Elements, USAEC Report GEAP-4135, General Electric Company, Vallecitos Atomic Laboratory, Jan. 23, 1963.
43. J. Lambert Bates, Thermal Conductivity of UO_2 Improves at High Temperatures, *Nucleonics*, 19(6): 83 (1961).
44. M. F. Lyons, R. C. Nelson, B. Weidenbaum, and T. J. Pashos, UO_2 Swaged Powder Fuel Rod Failures at High Thermal Performance Conditions. Preliminary Results, USAEC Report GEAP-4197, General Electric Company, Atomic Power Equipment Department, Mar. 1, 1963.
45. R. L. Holladay (Comp.), High Power Density Development Project. Thirteenth Quarterly Progress Report, April–June 1963, USAEC Report GEAP-4309, General Electric Company, Atomic Power Equipment Department, July 1, 1963.
46. B. Weidenbaum, High Performance UO_2 Program. Quarterly Progress Report No. 9, April–June 1963, USAEC Report GEAP-3771-9, General Electric Company, Atomic Power Equipment Department, July 15, 1963.

Section

V

Power Reactor Technology

Control and Dynamics

Period Meters

It is well known that the time constants of devices for measuring neutron flux levels are long at low flux levels. For pulse type detectors this is a fundamental result of considerations of signal-to-noise ratio. The instrument must examine a relatively large number of pulses to determine whether an observed change in pulse rate represents a true change in the average flux level or a statistical fluctuation. Current type detectors (ion chambers) are, of course, subject to the same fundamental limitation, but often the time constant is set at some larger value by the practical necessity of producing a voltage signal of useful size across the inherent electrical capacitance of the detector and its connecting cable.

The time constants of instruments used at low flux levels are of particular interest when the instruments provide period information, for it is evident that the instrument cannot assess the true period accurately unless its time constant is short relative to the period; and they are of particular importance because period information is often used to actuate low-level safety circuits. Two recent papers[1,2] illuminate the behavior of period circuits at low flux levels by computing the period meter output as a function of time during a reactor power transient. References 1 and 2 describe digital computer programs for the Ferranti Mercury computer which compute the outputs of period meters during startup transients resulting from specified programs of reactivity addition to the critical or subcritical reactor. The period meter considered in Ref. 1 consists of a mean-level current ionization chamber, a vacuum diode for a logarithmic device, and the usual d-c amplifier, differentiator, and meter. The circuit elements that determine the dynamic response of the meter are shown schematically in Fig. V-1. Reference 2 is similar to Ref. 1, except that it treats a period meter utilizing count rate as input. The detector is a pulse ionization chamber, and several diode pumps are used to give the logarithmic characteristic. The program allows for time delays in the diode pump circuits and in the period meter.

The calculated response of a period meter, with the circuit characteristics listed in Fig. V-1, is shown in Fig. V-2 for a power excursion caused by the addition of reactivity at the rate of 2% per minute to an initially critical reactor. The reactor assumed is graphite moderated, with an effective prompt-neutron lifetime of 1×10^{-3} sec; however, the behavior is not sensitive to neutron lifetime over the range of periods in the figure. Of more significance is the assumed relation between reactor power level and ion chamber output. This is taken as 2×10^{-3} amp per watt of reactor power and in the actual case would be strongly dependent on the ion chamber location.

In addition to the inverse periods, $\bar{\alpha}$, indicated by the period meter when the transient is initiated at various power levels, Fig. V-2 shows plots of the true inverse period, α, of the reactor and the inverse period that would be indicated by the meter if the logarithmic amplifier were perfect, i.e., if the dynamic response of the circuit element shown in part *a* of Fig. V-1 were perfect. The curves for initial powers of 100 kw and higher correspond very closely to this curve. The reference points out that the dynamic response involves both a phase lag, which in Fig. V-2 causes the low-power curves to indicate periods that are much too long for a number of seconds after the beginning of the transient, and an overshoot that at some later time causes each low-power curve to rise above the curve for the perfect logarithmic amplifier, $\bar{\alpha}_1$. Thus, for example, if the period-meter indications were being used to actuate a scram at a period of 2 sec ($\alpha = 0.5$), the scram would occur sooner if the transient started at a power of 100 watts than if it started at one of the higher (or lower) power levels considered. Similarly, if the scram were set for a period of 1.1 sec ($\alpha = 0.9$), the initial power level of 10 watts would provide the earliest scram.

Usually a delay of several seconds in the recognition of a short period at very low power levels need not be interpreted as hazardous, inasmuch as the power must rise many decades before the level becomes dangerous (in Fig. V-2 the power rise is of the order of 10^3 before the period meter begins to show a short period on the 1-watt curve). Curves like those of Fig. V-2 do, however, emphasize the importance of locating period sensors close enough to the reactor core to avoid large attenuation of the neutron flux. They are also useful to the reactor operator for clarifying the observed performances of period meters at low power levels.

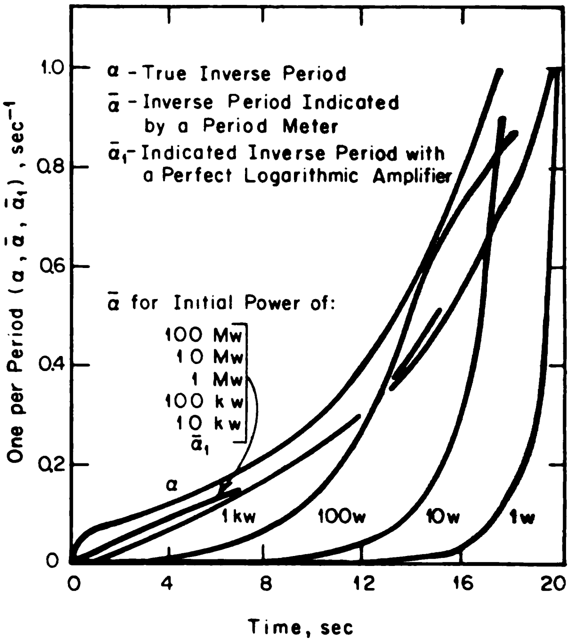

Fig. V-2 Calculated indications of period meter during ramp addition of reactivity to an initially critical reactor.[1] The reactivity addition rate is 2% per minute, and the power levels indicated specify the reactor power at the beginning of the reactivity addition. The mean prompt-neutron lifetime for the reactor is 1×10^{-3} sec, the delayed-neutron characteristics are those of U^{235}, and the ion chamber sensitivity and location are such that the current is 20 μa at the full reactor power of 100 Mw. The characteristics of the period-meter circuit are given in Fig. V-1.

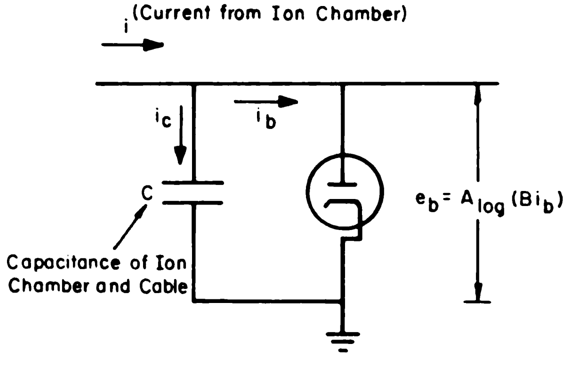

i (Current from Ion Chamber)
i_c
i_b
C
Capacitance of Ion Chamber and Cable
$e_b = A_{log}(Bi_b)$

(a) Logarithmic Circuit

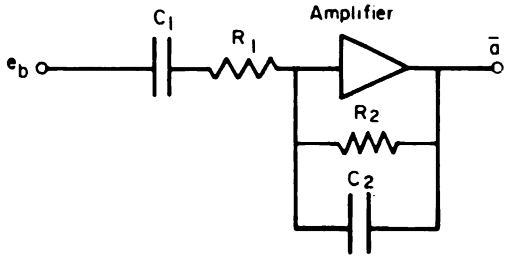

(b) Differentiation Circuit

Fig. V-1 Schematic components of period-meter circuit.[1] For the curves shown in Fig. V-2, the following values were used for the circuit elements: $C = 2000$ picofarads; time constant of $C_1,R_1 = 1.0$ sec; time constant of $C_2,R_2 = 1.0$ sec; gain of logarithmic element = 0.1 volt neper (1 neper = 8.686 db); gain of differentiator = 10 sec.

Transducers

Input transducers are devices that transform a nonelectrical physical quantity into a measurable electrical quantity; transducers of various types are essential parts of nuclear reactor control systems. To incorporate these devices into a reactor system, the designer needs to know temperature and radiation-damage limitations. This important information is supplied by Ref. 3. Tables that give temperature range, measurement range, and fast-neutron and gamma-flux thresholds are presented for displacement, pressure, strain and torque, force, temperature, and radiation transducers. Often the limitations are merely best estimates, since the experimental data on actual transducers and sensing elements are limited. The threshold values quoted were established by contacting users and manufacturers, by extrapolation of irradiation-damage information on the materials of construction, and by relating actual empirical information on irradiated transducers. The limiting components of the transducers for nuclear applications are the organic insulators and dielectrics, the lubricants, and the damping oils. Of considerable interest to the nuclear industry, because of the importance of temperature transducers in reactor instrumentation, is the fact that in thermocouples radiation causes composition changes that change the calibrations. Computer programs have been used to determine the extent of the changes, and the results have been tabulated; chromel was found to undergo very slight transmutation. Temperature transducers may also be subject to other radiation effects such as effects on insulation, connectors, leads, and sealing compounds.

Servomechanism Reliability

Studies and discussions of the reliability of reactor control systems are fairly numerous. Two reviews have appeared in a recent issue of *Nuclear Safety*.[4,5] Reference 6 is a recent British study of the application of redundancy techniques to the automatic control of nuclear reactors to improve reliability. The study considers circuit redundancy, where the circuit is considered to include all components from the instrument sensors to the control-rod drives.

References

1. J. D. Cummins, Period Meter Output During Startup Transients, British Report AEEW-R-231, November 1962.
2. J. D. Cummins, Pulse Counting Period Meter Output During Startup Transients, British Report AEEW-R-245, December 1962.
3. W. E. Chapin, D. J. Hamman, and E. N. Wyler, The Effect of Nuclear Radiation on Transducers, USAEC Report REIC-25, Radiation Effects Information Center, Apr. 19, 1963.
4. E. Siddall, Reliability of Reactor Control Systems, *Nucl. Safety*, 4(4): 1 (June 1963).
5. E. P. Epler, Reliability of Reactor Systems, *Nucl. Safety*, 4(4): 72 (June 1963).
6. L. A. J. Lawrence and R. J. Scotcher, A Study of Servomechanism Reliability in Nuclear Reactor and Plant Control Systems, British Report AEEW-R-220, December 1962.

Section

VI

Power Reactor Technology

Containment, Radiation Control, and Siting

Low-Pressure Containment Building

Two recent reports[1,2] give containment information that is of use in those applications where low leakage rates are required, but where the maximum pressure and permissible leakage limits are not so stringent as to demand the use of a welded-steel containment shell. Reference 1 reports measurements of air leak rates through structural components of concrete and metal-panel buildings. The leak-rate data were used to generate empirical constants for use in analytic expressions that can be used to predict the air flow rates through the building components as a function of size, method of construction, and pressure differential. In addition to the information on walls, information is presented on doors, louvers, butterfly valves, caulking materials, and paints. Also presented are the preferred design methods for reducing leakage, descriptions of procedures for predicting and locating leak paths, and procedures for calculating the expected leakage from a real structure. It is suggested[1] that with improved construction methods the leak rate for a large metal-panel building can be reduced to 1% of the contained volume per day at a pressure of 0.5 psi. Large concrete buildings can be constructed to give a leak rate of 1% of the contained volume per day at a pressure of 5 psi.

A recent leak-rate test of two identical concrete structures shows how important design and inspection during construction will be in order to reduce the leak rate to 1% of the contained volume per day.[2] The tests were done on two reinforced-concrete structures intended to contain nuclear critical experiments at the Argonne National Laboratory. Each structure was in the form of a rectangular box with inside dimensions of 30 by 40 by 30 ft high. Three of the concrete walls and the roof were 4 ft thick, and the remaining wall was 5 ft thick. The wall thicknesses were dictated by biological shielding requirements. The structures were designed to withstand a large pressure loading from a sudden energy release and its subsequent internal pressure, but they were not designed to be leaktight. After construction had been completed, the structures were pressurized to detect areas of gross leakage, and reasonable and practical measures were taken to eliminate or minimize these leaks. For instance, at the surface joints of opening frames the concrete was routed out to form a groove that was filled with the high-temperature mastic. This was also done around all nozzles, pipes, and conduits. When leaks persisted past door frames, epoxy resin was pumped through tapped holes in the door frame to fill the void between the steel and concrete. Also, where leakage was detected through large areas of concrete, about 4 in. of concrete were chipped out back to the reinforcing bars, and expanding grout was troweled into the void created by the removed concrete. All form ties were carefully grouted. Even after all these efforts to plug known leaks and suspected areas, one cell showed a loss of approximately 23% of its contained air per day, whereas the other cell showed a loss of approximately 10% at an internal pressure of 10 psig. To further reduce the leakage, the interior surfaces of the concrete were painted with Carboline 305 that reduced the leakage rates to 8 and 6% per day. From this it can be concluded that concrete placed in the conventional manner, even in 4- and 5-ft thicknesses, is pervious to air.

Structural pressure tests were run on one of the concrete cells. The purpose of the tests was to observe and compare experimental with analytical strains and stresses in the reinforcing steel in the concrete walls. Forty-four strain gauges were placed on the reinforcing steel on both the interior and exterior walls by removing the covering concrete. The cell was treated analytically by homogenizing the steel and concrete into a composite. The steel cross-sectional area was transformed into equivalent concrete area. The moments, shears, stresses, and strains were calculated, using the moment distribution method for longitudinal frame bent, traverse frame bent, and a rectangular box frame, which represented hypothetical 1-ft-wide sections cut vertically or horizontally through the walls and ceiling. A sample calculation is shown in the report. The analytical results and the experimental results were compared at internal pressures of 2, 4, 6, 8, and 10 psig, giving like results at all locations except at reentrant corners. The calculated results were brought into agreement at the reentrant corners by applying the proper stress-concentration factors. The stress-concentration factors produced agreement with measured results at all locations except at the corner of one of the cell entrances. The calculational procedure predicted a compressive strain when, in fact, a tensile strain was measured.

Moisture Separators and Particulate Filters

A recent review in *Power Reactor Technology*, 6(3): 20-21, described an activated-carbon filter that in combination with a particulate filter would constitute the ventilation-air exhaust filter system for the Savannah River Plant (SRP) reactor buildings.[3] These buildings are not pressure-containment buildings; therefore in the event of an accident the released fission products would be carried by the ventilating air through the exhaust filter system where the fission products would be removed. Since the reactors are cooled and moderated by water, a power-surge accident might be expected to introduce entrained water or fog into the ventilation air which could interfere with the particulate system. A report that describes a satisfactory particulate filter and moisture separator to complete the above filter system has been issued.[4]

The filtration system was designed to remove 99+% of the particles of sizes 0.3 μ and larger from the exhaust stream. The exhaust stream that would be expected after a power-surge accident would consist of wet steam for 30 sec at 7000 scfm per filter, followed by 1 lb of water per minute entrained in the exhaust air for a period of 10 days. The rated filter flow is 1000 scfm. Furthermore, the filter system has to work after accumulating dust over a three-month exposure to normal exhaust air.

Preliminary tests on commercially available particulate filters with an air-water fog indicated flooding, with some of the filters rupturing. The amount of water incident on the filters was reduced through the use of moisture separators upstream of the filters. Although the moisture separator removed sufficient water to keep the particulate filter from plugging, it still allowed enough moisture to be incident on the filter to eventually saturate the filter medium. Therefore the filter medium has to have good water-repelling characteristics, good wet strength, and permeability for air in order to continue to function over the length of the accident. The filter must also retain these characteristics when exposed to 90°C air-water fog conditions that are expected following the accident. The details of the tests and the results are presented in the report.

The moisture separator that will be used in the SRP reactor building is 2 ft by 2 ft by 2 in. thick and is rated for 1600 scfm of air at 0.95 in. of water. Each separator is made of several mats of Teflon yarn wrapped over stainless-steel reinforcing wire. The particulate filters, rated at 1000 scfm of air at 0.94 in. of water, consist of 230 sq ft of glass-asbestos fiber medium about 0.02 in. thick with aluminum corrugations separating the folds on both sides. The specifications for both units are given in the appendixes of the report.

Iodine Removal

This is the third in a series of review articles on iodine removal from the atmosphere. The series began in *Power Reactor Technology*, 5(4): 29-33, and continued in *Power Reactor Technology*, 6(3): 20-21. So far these reviews have covered several papers on the behavior of radioactive iodine released in containment buildings and methods of removing this iodine from the building atmosphere to minimize the amount escaping from the building. Several more reports from the United Kingdom Atomic Energy Authority on the removal of iodine from gas streams and containment buildings have been issued.[5–8]

Reference 5 investigates the performance of the scrubber that was originally installed in the cooling system of the British Experimental Pile O to remove iodine from the shutdown flow of air in the event of an accidental release of fission products. Although the caustic soda scrubbers have since been replaced by the more efficient activated-charcoal beds, the test results may be of interest. The scrubbers consisted of four columns with a total cross-sectional area of 26 sq ft, with each column containing a 6.25-ft height of 1-in. mild-steel Raschig rings. The recommended air flow was 3000 cfm with a liquid throughput of 325 gal/min. The scrubber liquor was a 5% caustic soda solution containing some carbonate. The four columns are mounted on a 700-gal horizontal sump tank from which the scrubber liquor is circulated around the scrubber system by a pump that delivers the liquor from the base of the sump tank to each column via a header and feed lines. The air passes countercurrent to the scrubber liquor, entering the bottom of the column and leaving from the top.

Six tests were run to measure the iodine decontamination factor (DF) of the scrubber system. The iodine used in the tests contained a trace amount of radioactive I^{131} that was counted to determine the DF. The first, third, and fifth tests consisted of introducing iodine vapor, by heating sodium iodide, into the air stream just before its entrance into the scrubber. In the second test the iodine vapor was passed over a hot (900 to 1000°C) tungsten wire and then into a glass aspirator where the submicron particles of tungsten and iodine would mix, thus encouraging the iodine to adsorb on the particles. In this way the efficiency of the scrubber for the removal of particulates could be measured. Test 6 was similar except that lead fumes were used to form the submicron nuclei. In test 4 nothing was introduced into the air stream. The measured results in test 4 came from the iodine deposited on the surfaces from previous experiments and absorbed back into the air stream. In test 5 the liquor was changed from caustic soda to sodium carbonate. The test results are shown in Table VI-1.

If test 1 is disregarded, the scrubber appears to give a DF of about 30 for iodine vapor and does not appear to be sensitive to the change in liquor; but tests 2 and 6 show that the DF is reduced by the introduction of particulate nuclei on which the iodine can be adsorbed and pass through the scrubber. In the case of a fuel-element meltdown, presumably many particulate nuclei would be released along with the iodine, thus reducing the effectiveness of the scrubber.

Table VI-1 IODINE DECONTAMINATION FACTOR FOR LIQUID SCRUBBER[5]

Test No.	1	2	3	4	5	6
DF	250	10.5	32	33	29	1.4

Reference 6 discusses the removal of iodine from the atmosphere by sprays; it is primarily a theoretical treatment of the effect of sprays in removing molecular iodine and iodine-containing particles. The molecular iodine is removed from the atmosphere by a water spray primarily by absorption in the water, and the iodine adsorbed on condensation nuclei is removed primarily by the spray by impaction. The two modes of removal require different analytical treatments.

The molecular iodine is assumed to be absorbed by water drops by a diffusion process. It is assumed further that the equilibrium concentration or partition of iodine between air and water follows Henry's law. So that the most efficient use of a water spray can be obtained, each drop should contain an equilibrium concentration of iodine when it reaches the building floor. The analysis shows that equilibrium concentration in the water drop is a function of the water-drop size and the height through which the drop falls. This relation for the attainment of 99% saturation with iodine, for 20 and 100°C water temperatures, is shown in Fig. VI-1. For example, in a containment building that is 10 m in height, the water drops would have to be $<1000\ \mu$ in diameter. The percentage of iodine removed by the water as a function of temperature for several different air-to-water volume ratios is shown in Table VI-2.

It can be seen that for reasonable quantities of water in the spray, very little iodine is actually removed by the spray because of the equilibrium vapor pressure between air and water. The ways suggested for increasing the amount of iodine removed by the spray are (1) continuous removal of the water from the floor of the containment building and (2) combining the iodine chemically in the water.

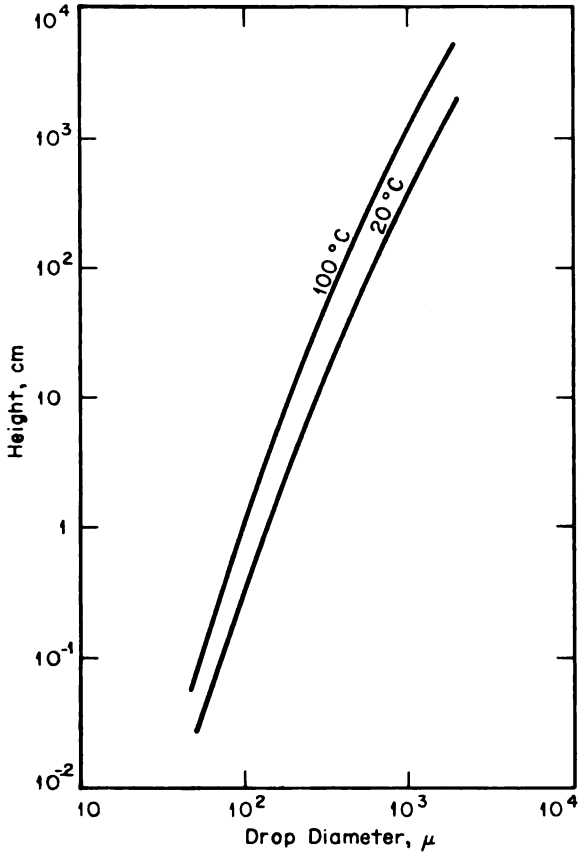

Fig. VI-1 Height in which a falling water drop reaches 99% saturation with iodine.[6]

The iodine and other fission products that are adsorbed on particulate matter in the atmosphere or are released from the fuel in particulate form are removed from the atmosphere mainly by three processes, all of which depend on the size and density of the particles. These processes are (1) diffusion to solid and liquid surfaces, (2) fallout under gravity, and (3) impaction on solid or liquid surfaces. Diffusion is a slow process, and fallout is rapid only for large particles, >10 μ. Sprays can be used to increase the impaction surfaces. Analysis shows that particles of sufficient size and density (>1 μ in diameter and 10 g/cm^3) can be efficiently removed from the atmosphere with drops traversing the atmosphere and impacting with the particles. The calculated removal rates, λ, for 1-, 2-, and 5-μ particles for a water flow rate of 10 g/sec per square meter of floor area for water drops of 100, 200, 500, and 1000 μ, are shown in Table VI-3. The optimum diameter of the water drops in the spray is about 500 μ. If the flow rate is increased to 100 g/(sec)(m^2) the removal rates in Table VI-3 increase by a factor of 10. A flow rate of about 100 g/(sec)(m^2) for 15 min will reduce the air concentration of >1-μ particles to 0.1% of the original concentration.

Table VI-2 IODINE REMOVAL BY WATER AT VARIOUS AIR-TO-WATER VOLUME RATIOS[6]

Air-to-water volume ratio	Iodine removal, %, at the indicated temperature	
	20°C	100°C
1	99	91
10	92	52.5
100	54	9.9
1000	10.5	1.1

Table VI-3 REMOVAL RATES OF PARTICLES BY WATER DROPS[6]

[Water Flow Rate Is 10 g/(sec)(m^2)]

Water-drop diameter, μ	Removal rates (λ), sec^{-1}, at the indicated particle size		
	1 μ	2 μ	5 μ
100	4.5×10^{-5}	1.35×10^{-3}	3×10^{-3}
200	5.2×10^{-4}	4.5×10^{-3}	9×10^{-3}
500	9×10^{-4}	7.2×10^{-3}	1.4×10^{-2}
1000	6×10^{-4}	5.5×10^{-3}	1.0×10^{-2}

Sprays seem to be reasonably efficient in removing molecular iodine and particles of diameter greater than 1 μ but are extremely inefficient in removing the biologically important particles of submicron size. The type of reactor and the method of release seem to have a great deal to do with the chemical nature and the size of particulate iodine released.[9,10] More research on particulate size released from the various types of reactors is required before the effectiveness of sprays can be determined.

A recent British report on the behavior of iodine in low concentrations has been issued.[7] These iodine-release experiments were done in a laboratory with a volume of 1500 m^3. The tests included a measurement of the iodine lost to the laboratory surfaces as a function of time after release, as well as several tests in which absorbers and filters were used to remove iodine from the air.

The iodine loss from the air was assumed to be principally by deposition on the laboratory surfaces and not from leakage or removal by the absorbers and filters that were in operation during the deposition measurements. This assumption is reasonable, since the laboratory was fairly leaktight and of such a size that at least 1000 min would be required to pump all the air in the room through the systems under test. The principal surfaces present in the laboratory are shown in Table VI-4. The reproducibility of the concentration of iodine in the air as a function of time was poor. Several runs with an initial iodine concentration of 5 $\mu g/m^3$ gave air concentrations that differed by a factor of 30 early in the run with the difference decreasing to a factor of 10 at 200 min after the iodine release. An explanation for the discrepancy early in the run was that the rate of mixing in the air was quite slow, giving large variations at the sampling position. No explanation was given for the variation at later times. So that the effect of changing the initial iodine concentration could be explored, tests were run in which the initial concentration was varied from 0.5 to 500 $\mu g/m^3$. The resulting ratios of air concentration to initial concentration as functions of time all fell within the spread of the 5 $\mu g/m^3$ results, thus showing no measurable effect of initial concentration. Condensation nuclei from dusty air, as well as nuclei produced by Bunsen burner flames and by burning magnesium, were used to investigate the effects on deposition rate, but again no significant changes were detected. In all tests the prominent feature was the rapid disappearance of the iodine from the air in the room. At the end of the first hour about 98% of the released iodine was no longer airborne, and at the end of 3 hr about 99.7% was no longer airborne. The exact deposition mechanism is not completely understood, but an additional experiment was done to determine if gravitational settling did occur; although the results were not conclusive, they did show that no more than 10% of the total deposition could be accounted for by this mechanism.

Table VI-4 PRINCIPAL SURFACE MATERIALS AND AREAS IN THE LABORATORY[7]

Type of surface	Area, sq ft
Linoleum (floor)	2,500
Glass	2,500
Asbestos board (walls)	3,500
Painted	13,000
Total	21,500

Several iodine absorber and filter systems were tested to determine their efficiency in removing low-concentration iodine from air. The types of systems tested were activated carbon, gas coke, magnesite, copper mesh, silver mesh, scrubbers, absolute filters, and combinations of absorbers and filters. The activated-carbon system was most effective. In combination with a good particulate filter, a 2-in.-deep activated-carbon bed was better than any other single system. The filter removes the particulates carrying iodine that pass through the carbon bed, whereas the elemental iodine is removed by the carbon bed.

Reference 8 is a review of the work done on the behavior of iodine by the aerosol group of the Atomic Energy Research Establishment since 1959. The following tests are reviewed and summarized:

1. The behavior of iodine in large containers
2. The behavior of iodine at very low concentrations in air and CO_2
3. Adsorption of iodine on surfaces
4. Adsorption of iodine on particulate matter
5. Adsorption of iodine on charcoal
6. Chemistry of iodine at low concentrations

Also included in the report is a review of the work being done presently and a discussion of work that needs to be done before a complete solution of the problem can be expected.

References

1. R. L. Koontz, C. T. Nelson, L. Baurmash, S. E. Becker, and C. V. Di Pol, Low-Pressure Containment Buildings. Component Tests and Design Data, USAEC Report NAA-SR-7234, Atomics International, Mar. 15, 1963.
2. S. H. Fistedis, A. H. Heineman, and M. J. Janicke, Testing of Containment Capabilities of Reinforced Concrete-Shielded Enclosures, USAEC Report ANL-6664, Argonne National Laboratory, March 1963.
3. G. H. Prigge, Application of Activated Carbon in Reactor Containment, USAEC Report DP-778, Savannah River Laboratory, September 1962.
4. A. H. Peters, Application of Moisture Separators and Particulate Filters in Reactor Containment,

USAEC Report DP-812, Savannah River Laboratory, December 1962.

5. F. G. May and J. B. Morris, Performance of the BEPO Scrubber for Iodine Removal, British Report AERE-M-1163, February 1963.
6. V. Griffiths, The Removal of Iodine from the Atmosphere by Sprays, British Report AHSB(S)R-45, Dec. 3, 1962.
7. J. B. Morris and C. H. Rumary, Tests on Absorbers for Iodine at Low Concentrations, British Report AERE-R-4219, February 1963.
8. A. C. Chamberlain, A. E. J. Eggleton, W. J. Megaw, and J. B. Morris, Physical Chemistry of Iodine and Removal of Iodine from Gas Streams, to be published in *J. Nucl. Energy*.
9. G. W. Parker, G. E. Creek, and W. J. Martin, Fuel Element Decomposition Products, paper presented at Seventh AEC Air Cleaning Conference, October 10–12, 1961, Held at Brookhaven National Laboratory, Upton, N. Y., USAEC Report TID-7627, pp. 263-283.
10. W. J. Megaw, R. C. Chadwick, A. C. Wells, and J. E. Bridges, The Oxidation and Release of Iodine-131 from Uranium Slugs Oxidizing in Air and Carbon Dioxide, *J. Nucl. Energy: Pts. A and B*, 15(4): 176-184 (December 1961).

Section VII

Power Reactor Technology

Components

Sodium-Heated Steam Generators

A summary report[1] has been compiled on the current state of the art of sodium-heated steam generators. The report contains information on six plant-size units and several model-size units. A general design description, operating experience, and bibliography are given for each unit. A summary of the performance of the plant-size units is given in Table VII-1.

The steam generator for the Experimental Breeder Reactor I (EBR-I) consists of 31 single-tube heat exchangers, each about 10 ft long. Nine exchangers serve as economizers, 18 as evaporators, and four as superheaters. A typical cross section is shown in Fig. VII-1, illustrated as an evaporator. The economizers and evaporators are mounted vertically, and the superheaters are horizontal. The inner tube is of triple-wall construction that consists of two layers of nickel with a copper core. The three individual tubes were assembled, drawn together, and bonded by thermal diffusion to obtain good heat transfer. The water (or steam)

Table VII-1 PERFORMANCE SUMMARY OF PLANT-SIZE STEAM-GENERATOR UNITS[1]

	EBR-I	SRE natural circulation	SRE once through	EFAPP	EBR-II	HNPF
Full-load heat transferred per unit, Mw(t)	3.92	20	20	143	62.5	85 (reentrant)
Type of unit	Falling film	Recirculating pancake tube	Once-through double-wall tube	Once-through single-wall tube	Recirculating duplex tube	Recirculating double-wall tube
Number of units per plant	1	1	1	3	1	3
Steam temperature, °F	529	654	825	780	840	833
Steam pressure, psig	393	600	605	900	1250	825
Feedwater temparature, °F	214	425	311	380	550	304
Feedwater flow per unit, lb/hr	3630	51,500	88,800	476,000	268,000*	251,000
Liquid-metal temperature						
In, °F	583	850	900	820	866	875
Out, °F	419	580	440	520	588	559
Liquid-metal flow, lb/hr	124,700	546,000	718,000	5,300,000	2,500,000	2,820,000
Manufacturer	Argonne National Laboratory	Combustion Engineering, Inc.	Babcock & Wilcox Co.	Griscom-Russell Co.	Argonne National Laboratory	Griscom-Russell Co.

*Blowdown of 20,000 lb/hr.

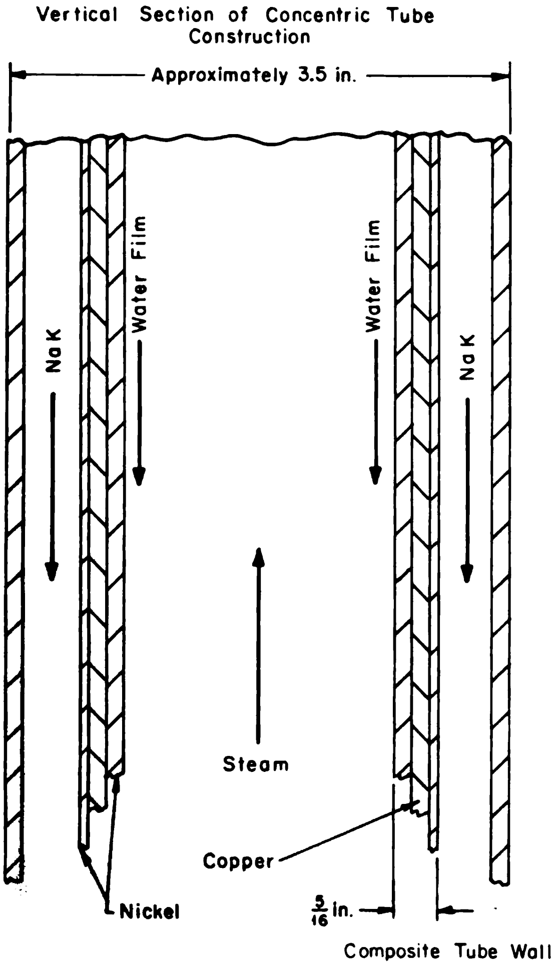

Fig. VII-1 Detail of single-tube evaporator for the Experimental Breeder Reactor I.

flows through the tube, and the NaK flows (countercurrently) through the annulus. Leak detection to the copper core zone is provided at each end of the tubes.

The natural-circulation unit (steam generator) for the Sodium Reactor Experiment (SRE) is made up of two evaporators, one steam drum, and one superheater. The evaporators and superheater are vertical shells filled with many pancake coils stacked on top of each other. A horizontal section of an evaporator, showing a single coil, is illustrated in Fig. VII-2. The evaporator shells are about 5 ft in diameter and about 8 ft high, each containing 48 coils. The coils are of double-wall construction with mercury in the annulus. In the evaporator the inner tube is type 347 stainless steel, and the outer tube is carbon steel. The sodium flows inside the coils, and the steam is generated on the shell side. Water enters at the bottom of the shell, and saturated steam passes out the top to the steam drum and then flows to the superheater. The superheater construction is similar, except that the steam flows inside the tubes and the sodium is on the shell side. Both inner and outer tubes of the coil are type 347 stainless steel. This steam-generation system has been operated up to approximately two-thirds power without significant difficulties.

In the once-through unit (steam generator) for the SRE, the water enters subcooled at one end and emerges as superheated steam at the other end. The unit is a U-shaped shell-and-tube heat exchanger. Sodium flows inside the shell from one end to the other, and the water or steam flows inside the tubes in counterflow. Figure VII-3 shows the general arrangement of the shell and the nozzles and also shows a section view of the tube-sheet design. Double-wall tubes are used with mercury in the annulus. The outside diameter of the outer tube is $^{11}/_{16}$ in. The shell has a diameter of 19 in. and a developed length of 80 ft. Both inner and outer tubes are type 304

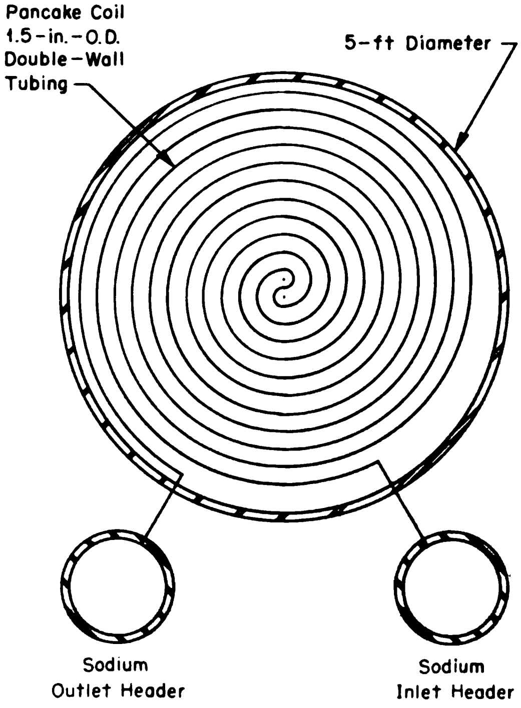

Fig. VII-2 Natural-circulation evaporator for the Sodium Reactor Experiment.

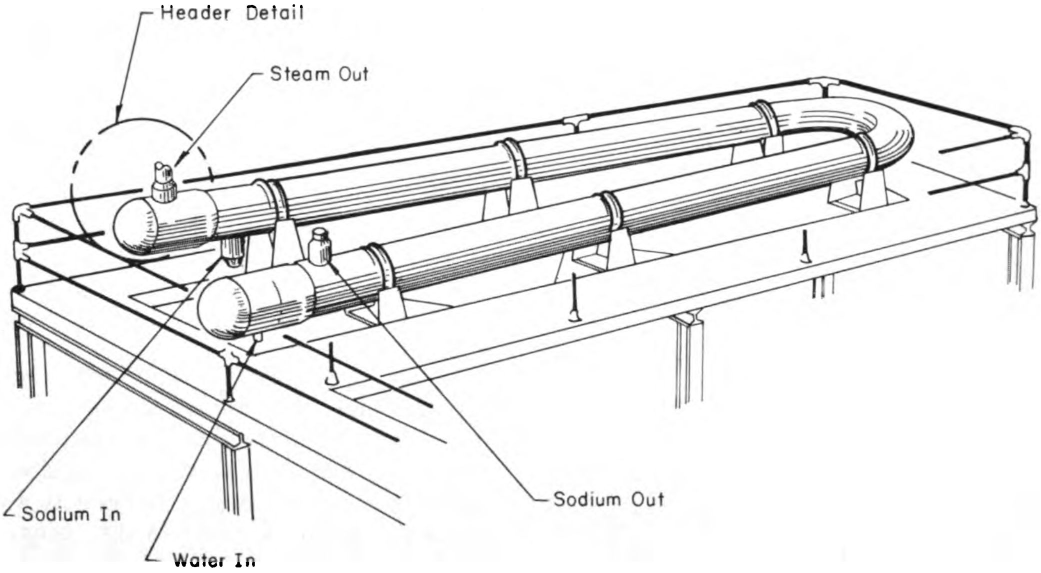

General Arrangement

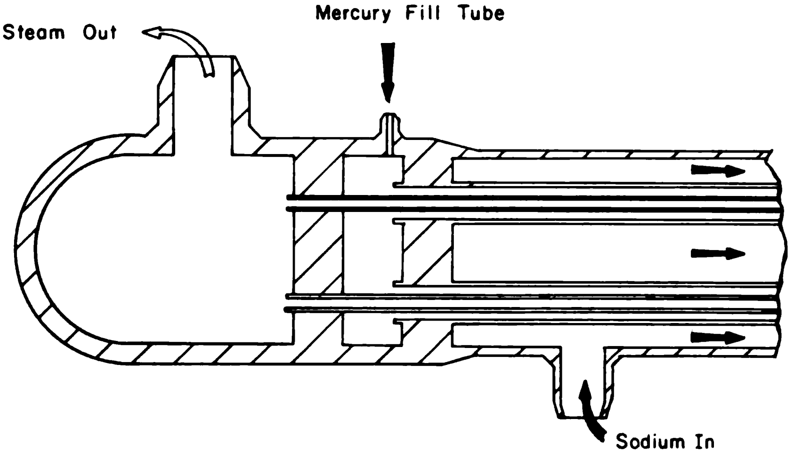

Header Detail

Fig. VII-3 U-tube once-through steam generator for the Sodium Reactor Experiment.[1]

stainless steel, and the shell is the same material.

The unit has operated about 16,000 hr, and for about half of this time the power levels approached 20 Mw(t). During a recent shutdown an inspection was made of the steam-side internals, which disclosed no observable deposits or corrosion. One significant operating phenomenon is the stratification of sodium on the shell side. There are no shell-side baffles (other than eggcrate tube supports), and the denser sodium sinks to the bottom. This adversely affects the uniformity of the outlet steam temperature. The difficulty might be avoided by mounting the U shell vertically.

The Enrico Fermi Atomic Power Plant (EFAPP) has three identical steam generators, one in each coolant loop. The steam generator, schematically shown in Fig. VII-4, is a once-through type unit, with the fluids in counter-

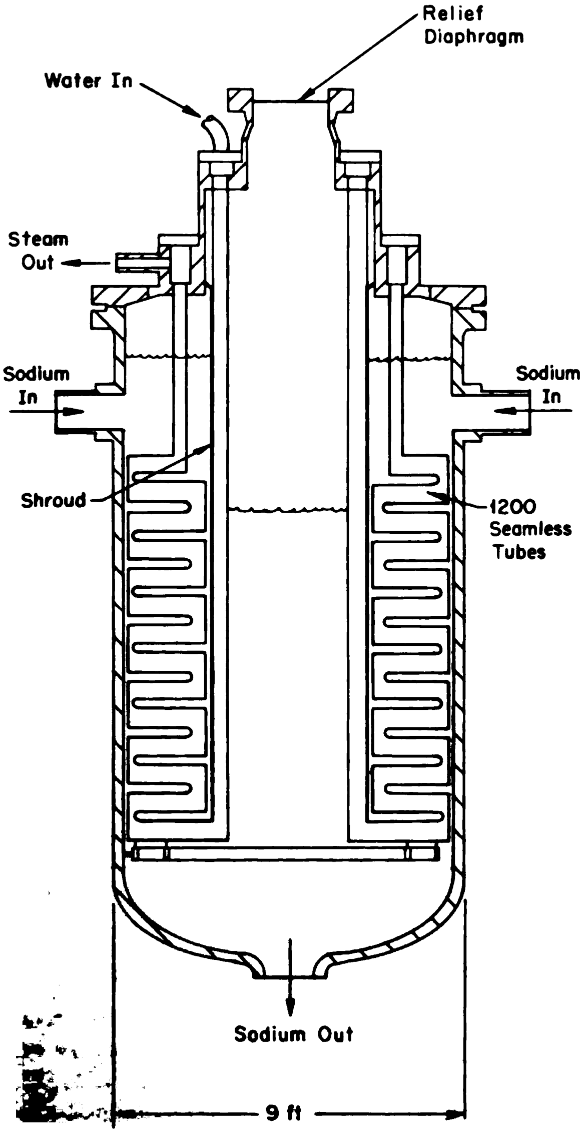

Fig. VII-4 Steam generator for Enrico Fermi Atomic Power Plant.[1]

flow. The sodium enters the shell near the top, flows downward over the tubes, and leaves the shell at the bottom. Each unit has 1200 seamless single-wall tubes that are $^5/_8$ in. in diameter and 0.042 in. thick; the tube material is 2.25% chromium–1.0% molybdenum alloy steel. The tubes are installed in the form of serpentine involutes, trombone nested in banks of eight. The feedwater enters the tubes at the top center and flows down the straight tubing in the central region of the unit. The water then enters the involutes at the bottom, flows upward, and leaves as superheated steam. Before operation it was discovered that some of the tubes were cracked as a result of stress corrosion. The defective tubes were replaced and stress relieved. The plant has only recently started operation, and no operating experience has been reported.

Banks of shell-and-tube heat exchangers comprise the steam generator for the EBR-II (Fig. VII-5). Eight identical units arranged in parallel form the natural-circulation evaporating section. The saturated steam collects in a steam drum and then flows through two superheater units. The original design specified four superheater units, which were never completed be-

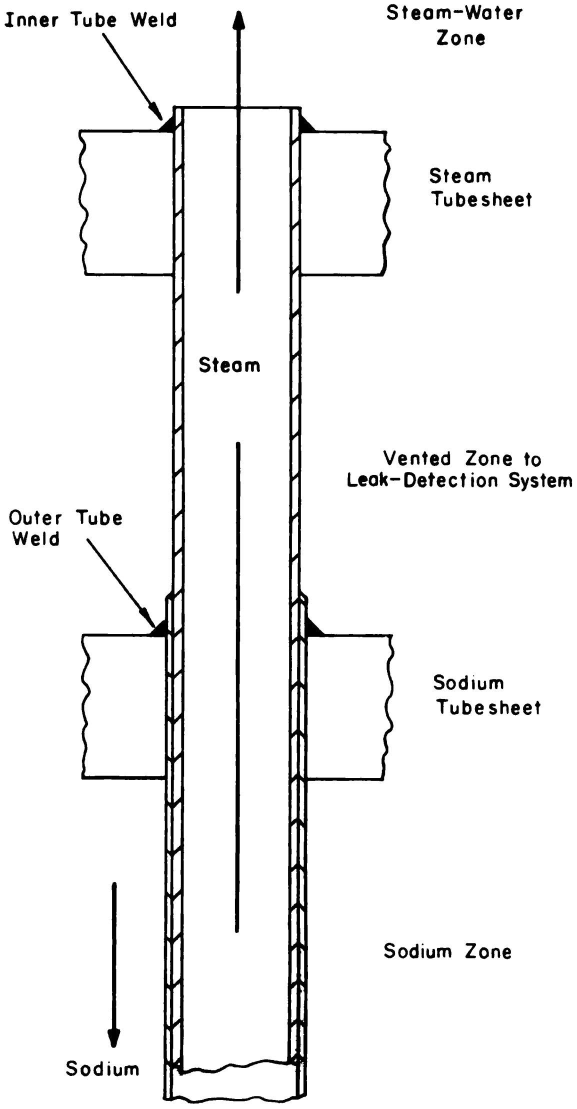

Fig. VII-5 Header detail at top of evaporator for the Experimental Breeder Reactor II.

cause of a tube-sheet welding problem. As a substitute measure two evaporative type units, slightly modified, were fabricated for superheater service. The shells are 20 in. in diameter, 30 ft long, and stand vertically. Sodium, on the shell side, enters at the top and leaves at the bottom. Water flows in at the bottom, and saturated steam flows out at the top. There are 73 double-wall tubes (1.438 in. in diameter) per shell made from 2.25% chromium and 1.0% molybdenum steel. The shell is made of the same material.

Some of the duplex tubes were metallurgically bonded, and some were bonded only mechanically. Figure VII-5 shows the details of assembly of the duplex tubes into the tube sheets. The design specification required that the weld of the outer tube to the sodium tube sheet have a penetration less than the thickness of the outer tube; i.e., there was to be no weld between the outer tube and inner tube in making this joint. This outer-tube weld was successful in the evaporator units with tubes having a wall thickness of approximately 0.10 in. and an outside diameter of 1.438 in. However, a successful weld was never achieved in the superheater units with smaller, thinner tubes (0.052 in. in wall thickness and 0.596 in. in outside diameter).

The design of the evaporators and superheaters incorporated fixed tube sheets. Cold springing of the tubes to satisfy the differential expansion was accomplished by elongating the shell (probably by thermal expansion) about $^1/_8$ in. during the process of welding the tubes to the tube sheets. Upon completion of that process, the shell returned to its original length, compressing (or springing) the tubes. No operating experience has yet been accumulated with the EBR-II steam generators.

The Hallam Nuclear Power Facility (HNPF) has three steam generators, one in each coolant loop. They feature bayonet type tubes, as shown schematically in Fig. VII-6. The outside diameter of the bayonet is 1.33 in. Tubes of this type are mounted horizontally in two different shells to form the separate evaporator and superheater units of a complete steam generator. A review of these steam generators was presented in *Power Reactor Technology*, 5(3): 46-47. The double-wall-tube material is 2.25% chromium – 1.0% molybdenum alloy steel in the evaporators and 5.0% chromium – 0.5% molybdenum alloy steel in the superheaters. There is no operating experience reported at this time. It is reported[1] that the double-wall construction and leak-monitoring system approximately triple the cost of the HNPF steam generators.

Of the six plant-size steam generators discussed in the report,[1] only one features a single-wall separation between the water and the liquid metal. The other five generators use double-wall construction. Two of these use mercury to create a good thermal bond, and three depend on mechanical and metallurgical bonding to achieve good thermal continuity.

Gas-Heated Steam Generators

In a gas-cooled nuclear power plant, the steam generator is one of the most expensive components, and its design has a strong influ-

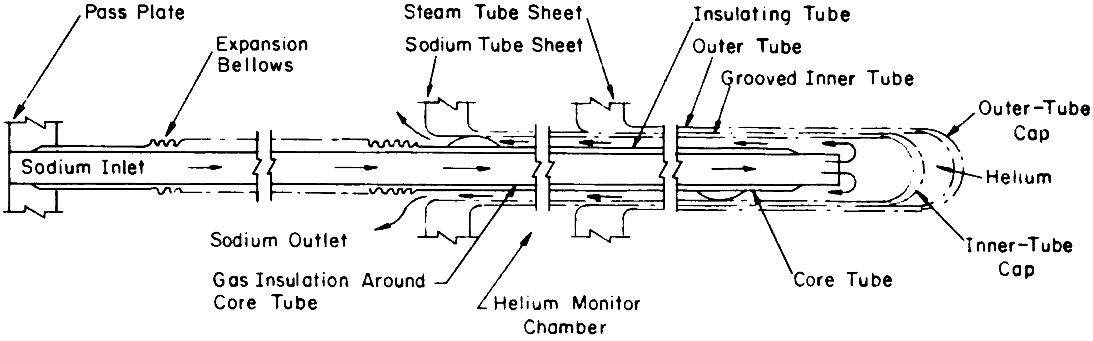

Fig. VII-6 Bayonet tube of the Hallam Nuclear Power Facility steam generator.[8]

ence on the overall plant layout. A parameter study on steam generators for high-temperature gas-cooled reactors has been carried out at Oak Ridge National Laboratory and is reported in Ref. 2. The objective of the study was to provide a sound basis for the optimization of steam-generator design and for the evaluation of the relative merits of major design features. The quantitative study was limited to once-through designs, inasmuch as it was decided that previous design studies had clearly shown the advantages of the once-through type for high-temperature gas-cooled reactor applications. The major parameters of the study were:

1. Axial-flow and cross-flow arrangements
2. Coolant gas (helium, carbon dioxide, nitrogen)
3. Coolant-gas pressure
4. Coolant-gas temperature
5. Steam pressure
6. Steam temperature
7. Tube diameter

The report[2] presents charts to facilitate the design of both axial-flow and cross-flow generators. In addition, it lists 10 important design implications revealed by the study, which may be summarized as follows:

1. When the gas pressure and the mean temperature difference are sufficiently high to give an average heat flux above 30,000 Btu/(hr)(sq ft), the smallest and least expensive steam-generator design employs axial gas flow over bare tubes.

2. Conversely, when the gas pressure and mean-temperature difference give an average heat flux of less than 30,000 Btu/(hr)(sq ft), the smallest and least expensive design employs cross flow of the gas over finned tubes.

3. In axial-flow units the best inside tube diameter is 0.4 to 0.6 in. In cross-flow units there is a tube support problem for tubes smaller than 1.0 in.

4. Croloy tubes should be usable, in suitable designs, for gas temperatures up to 1150 to 1250°F. There is little economic incentive to go to higher gas temperatures that would require refractory alloys, since the higher material cost would offset the thermal advantage.

5. For plants designed to produce steam at pressures of the order of 2500 psi, the reactor inlet gas temperature should be at least 650°F.

6. Important reductions in size and cost in axial-flow units are obtained by increases in gas pressure up to about 500 psi. Above this pressure the benefits of further pressure increases are small.

7. For axial-flow steam generators, the pumping-power-to-heat-removal ratio in the generator should be about 0.5% for minimum cost.

8. The extra cost and complication of a reheater is more than justified by the reductions in fuel-cycle costs and reactor-system capital costs resulting from higher efficiency.

9. A configuration that offers many practical advantages is one using U tubes so arranged that the legs straddle an annular baffle. The hot gas rises up the center and returns downward through the outer annulus, in counterflow to the steam-water.

10. Control considerations indicate that the hot gas temperature entering the steam generator should not be more than 100 to 150°F above the superheated-steam outlet temperature.

In summary:[2] "The results indicate that the least expensive and most promising unit for high-temperature high-pressure gas-cooled reactor plants employs axial-gas flow over 0.5-in.-diameter bare U-tubes arranged with their axes parallel to that of the shell. The proposed design is readily adaptable to the installation of a reheater and is suited to conventional fabrication techniques."

Liquid-Metal Pumps

An electromagnetic pump of unique design has been fabricated and tested at Atomics International.[3] The pump features a rotating magnetic field produced by a mechanically rotating armature, whereas a conventional electromagnetic pump has no moving parts. A schematic cross section of the pump is shown in Fig. VII-7. The liquid flows in an annulus that surrounds the armature, or rotor, and is separated from the rotor and the surrounding magnetic circuit by stainless-steel walls; the rotor thus operates in a normal air environment. The rotor is made of laminated steel plates and is wound helically with field coils, having an appearance similar to the rotor of a d-c motor. The rotor windings are energized by d-c current, and the rotating field induces eddy currents into the liquid metal in the annulus (part *a* of Fig. VII-8). The path of the flux

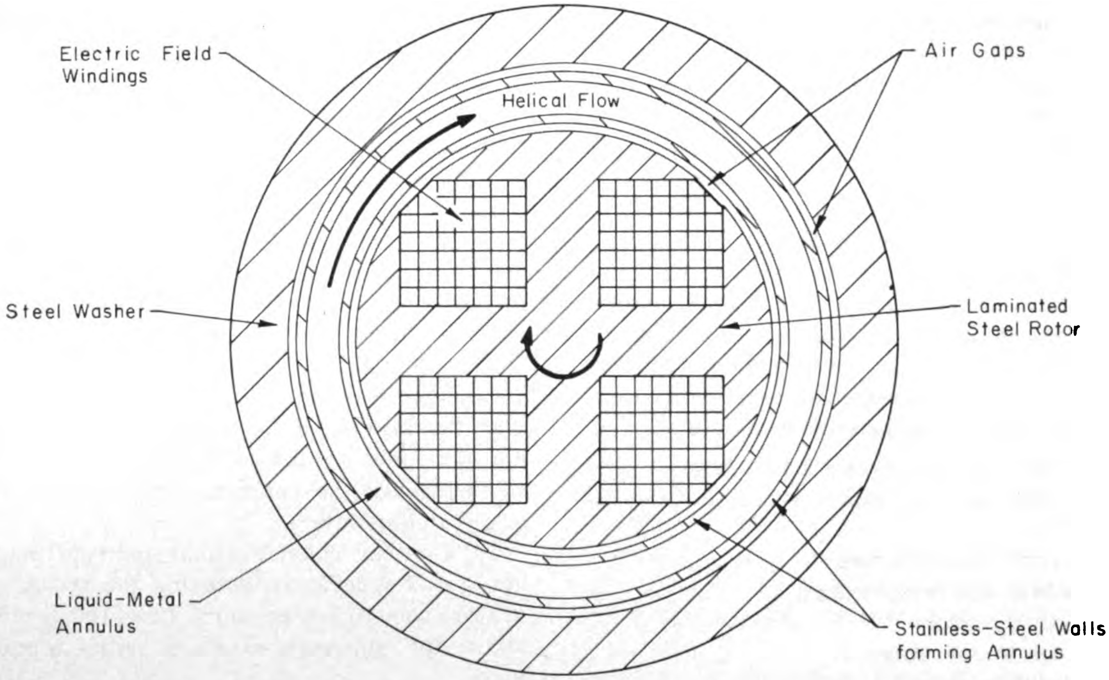

Fig. VII-7 Schematic cross section of helical-rotor electromagnetic pump.

extends radially from the poles through the liquid-metal annulus and connects circumferentially in the outer ring of steel washers (part *b* of Fig. VII-8). The reaction between the moving flux field and the induced current in the liquid metal produces a force on the liquid metal (part *c* of Fig. VII-8), moving it in a helical path, from intake to discharge. With the rotor having a helical configuration, the report[3] indicates that guide vanes are not essential to direct the flow. The helical-rotor electromagnetic pump avoids the necessity for a high-current low-voltage power supply that is characteristic of d-c electromagnetic pumps of conventional types. In addition, it is said to be more efficient than conventional electromagnetic pumps, because the direction of liquid-metal flow is at every point parallel to the driving force. Figure VII-9 shows an exploded view of a typical pump of the helical-rotor type.

A full-size prototype pump has been designed, fabricated, and evaluated in a test loop. The pump delivers 2200 gal of sodium per minute (at 600°F), with a pressure rise of 34 psi and with an efficiency of 26%. The pump completed 1000 hr of testing without loss of performance. The drive motor is rated at 200 hp at 1740 rpm, and the shaft speed is geared down to 374 rpm for the magnetic rotor, which draws 25 amp of direct current at 175 volts.

The report[3] states that the helical-rotor pump can be designed for many applications, ranging from low flows to over 50,000 gal/min, with liquid-metal temperatures up to 2200°F or higher.

Another interesting liquid-metal pump, under development for mobile nuclear plants, is reported in Ref. 4. The application requires high pumping efficiency, small size, low weight, and high reliability. The pump package consists of a shaft-sealed centrifugal pump directly driven by an air turbine. The shaft is vertical, with a single-stage axial-flow air turbine on top and a single-stage unshrouded impeller on the bottom. The shaft is supported with ball and roller bearings that are lubricated and cooled with oil under forced feed. An important feature of the pump is the dynamic shaft seal, in which a liquid-metal-to-inert-gas interface is achieved in a high centrifugal force field.

All the major components have been individually evaluated, and a 3000 gal/min pump has been fabricated and tested using NaK at temperatures up to 1300°F. The report[4] states that the testing has verified the soundness of the

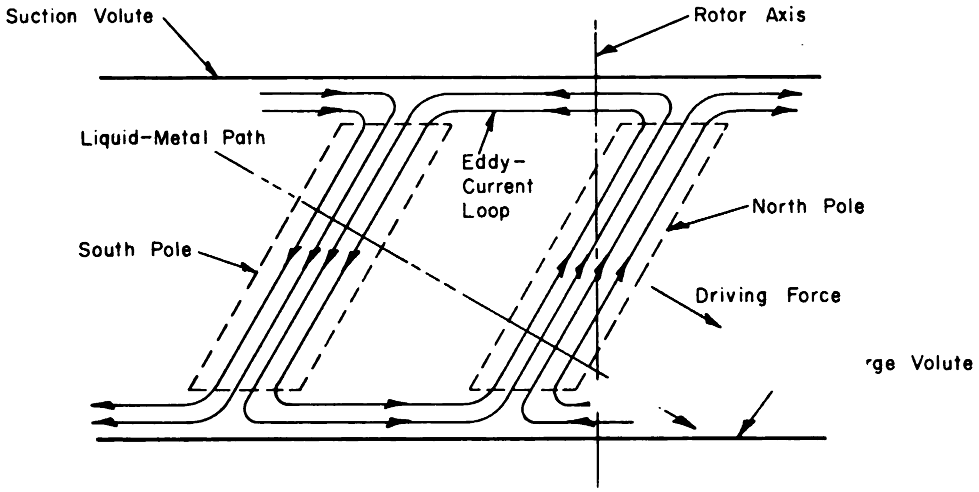

(a) Top View Showing Eddy-Current Paths in Liquid Metal.

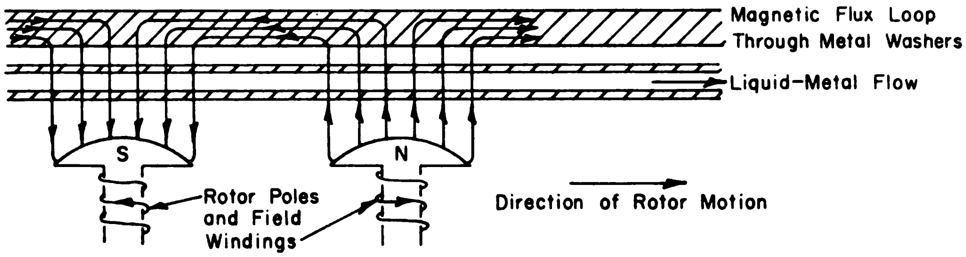
Magnetic Flux Loop Through Metal Washers
Liquid-Metal Flow
S
N
Rotor Poles and Field Windings
Direction of Rotor Motion

(b) End View Showing Magnetic Flux Paths.

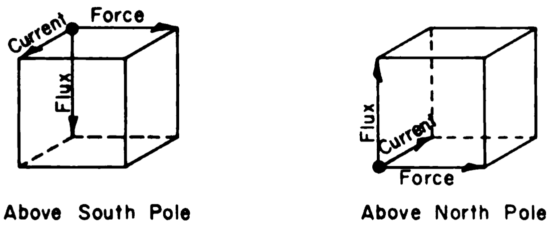

(c) Vector Description of Driving Force on Liquid Metal.

Fig. VII-8 Schematic design of pumping principle.

design philosophy. The air turbine and pump impeller are basically somewhat mismatched (i.e., the turbine should operate at a higher speed and the impeller at a lower speed); however, the simplicity, compactness, and mechanical reliability attained with a single shaft are considered more important than the slight reduction in maximum efficiency due to the mismatch. The dynamic shaft seal proved to operate satisfactorily.

Canned Pump for Organic Service

The development of a canned pump for high-temperature organic service (up to 850°F in Santowax) was completed in the Experimental Organic-Cooled Reactor program (EOCR) before the program was terminated. A description of the pump and its testing program is

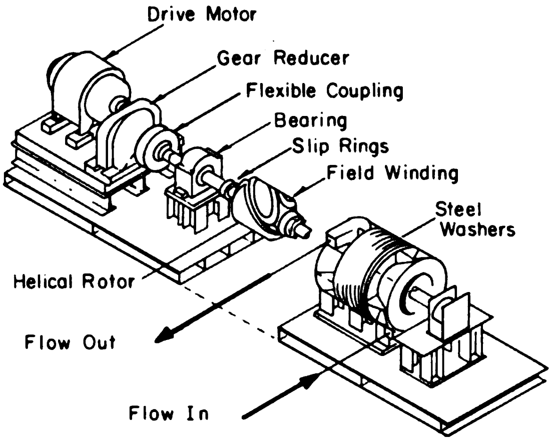

Fig. VII-9 Exploded view of helical-rotor electromagnetic pump.[9]

reported in Ref. 5. Actually two pumps were developed, one having a single pumping stage and the other having two stages; otherwise the pumps were similar. The design flows were 5 and 15 gal/min, respectively. The pump has one moving part, a rotor-impeller assembly completely immersed in Santowax. The pump casing is designed to minimize the intermixing of the fluid between the pump chamber and the rotor cavity; the rotor-cavity fluid is independently circulated through a heat exchanger to remove the bearing and rotor heat. Although the poor lubricating properties of Santowax posed a design problem, the fluid bearings operated satisfactorily during the testing period. The tests have indicated a tendency for gases to build up in the rotor cavity and for overheating to result. This problem has been solved by the installation of a self-venting system. Life tests of the pumps had been planned, but they were not completed because of the termination of the EOCR program.

Butterfly-Valve Cavitation Test

An experimental test program on cavitation in a butterfly valve is reported in Ref. 6. Although critical values for cavitation can be theoretically computed, disagreements were found in the existing calculational and experimental information, and tests were performed to ensure that the throttling valves (butterfly type) in the Pathfinder atomic power plant will always operate in the cavitation-free range. The Pathfinder is a boiling-water reactor with integral superheating. The cooling-moderating water for the core is recirculated through three loops, each having a constant-speed pump, and the amount of recirculation flow is controlled with a 20.5-in.-diameter butterfly valve in each pump discharge line. A similar, but smaller (8-in.-diameter), butterfly valve was tested. The experimentally determined values of the cavitation number were then used to determine the cavitation-free control range of the reactor system valves.

Fuel-Handling Equipment

New equipment for fuel handling has been designed, fabricated, and put into service in the SRE.[7] Although the original fuel-handling machine was well proved with more than 1000 fuel-transfer manipulations, the experience indicated certain areas of weakness in the design which were not only troublesome but which could lead to future difficulties. The new fuel-handling machine will have the following improvements in characteristics and capabilities:

1. Ability to handle deformed or damaged elements
2. Improved cask maintenance and decontamination
3. Decreased cask leakage
4. Improved ability to recover from equipment failure at critical times
5. Ability to inspect cask contents
6. Ability to determine the cask grapple load weight

References

1. Atomic Power Development Associates, Inc., Sodium Heated Steam Generator Summary, USAEC Report TID-18072, Sept. 19, 1962.
2. A. P. Fraas and M. N. Ozisik, Steam Generators for High-Temperature Gas-Cooled Reactors, USAEC Report ORNL-3208, Oak Ridge National Laboratory, Apr. 23, 1963.
3. R. S. Baker, Theory, Design, and Performance of Helical-Rotor, Electromagnetic Pump, USAEC Report NAA-SR-7455, Atomics International, May 31, 1963.
4. R. W. Kelly, G. M. Wood, and H. V. Marman, Development of a High Temperature Liquid Metal Turbopump, *J. Eng. Power*, 85A(2): 99 (April 1963).
5. R. G. Young, Chempump Performance for High

Temperature Organic service, USAEC Report IDO-16844, Phillips Petroleum Company, Mar. 15, 1963.

6. N. P. Grimm, Pathfinder Atomic Power Plant. Butterfly Valve Cavitation Test, USAEC Report ACNP-62004, Allis-Chalmers Mfg. Co., Mar. 20, 1963.
7. E. O. Dryer, E. L. Brown, and W. J. Freede, SRE Reactor Fuel Handling Equipment, USAEC Report NAA-SR-5599, Atomics International, Feb. 1, 1963.
8. Atomics International, Final Summary Safeguards Report for the Hallam Nuclear Power Facility, USAEC Report NAA-SR-5700, Apr. 15, 1961.
9. Electromagnetic Pump, *Mech. Eng.*, 85(5): 70 (May 1963).

Section

VIII

Power Reactor Technology

Design and Construction Practice

Humboldt Bay and Big Rock Point

By Walter Mitchell III

In September 1962 the Big Rock Point Nuclear Power Plant, owned by Consumers Power Company, reached criticality. Five months later unit No. 3 (the nuclear unit) of the Humboldt Bay Power Plant, owned by the Pacific Gas & Electric Company, went into operation. The plants, which were designed and built by the same contractors during roughly the same period, provide an unusual opportunity for comparison, since they have equal ratings and employ variations of the basic boiling-water reactor type. Both plants were built by the Bechtel Corporation as prime contractor to the owners, and the General Electric Company furnished the reactors, turbine-generators, and other electrical apparatus. Each installation consists of a direct-cycle boiling-water reactor, a power-extraction system, and associated service facilities. The reactors are thermal, heterogeneous light-water-cooled and -moderated units that are fueled by slightly enriched UO_2 clad in stainless steel. In both cases bottom-entering control rods are used. The most obvious differences in the plants lie in or result from the methods of coolant recirculation and steam separation: the Big Rock Point reactor[1] is a forced-circulation external-steam-drum unit that is housed in a conventional, spherical steel containment vessel; the Humboldt Bay reactor is a natural-circulation design with internal separation that utilizes the pressure-suppression containment concept. Both plants are designed for an ultimate generating capacity that is about half again as great as the initial capacity of 50 Mw(e), but the values given in the following tables, figures, and discussions pertain to the 50-Mw plants.

	Big Rock Point	Humboldt Bay
Location	Charlevoix, Mich.	Eureka, Calif.
Start of construction	June 1960	November 1960
Date critical	September 1962	February 1963
Thermal power, Mw	157	165
Gross electrical output, Mw	>50	>50
Gross thermal efficiency, %	>31.8	>30.3
Net electrical output, Mw	>47.9	>48.5
Net efficiency, %	>30.5	>29.4
Reactor pressure, psia	1050	1035
Coolant saturation temperature at operating pressure, °F	550.6	549
Turbine pressure, psia	1015	1015

General Mechanical and Hydraulic Characteristics

A comparison of the sizes and arrangements of the reactors and recirculation systems of the two plants is given in Fig. VIII-1, which shows schematic elevations of the nuclear steam-supply systems. The major components are drawn to the same scale to give a size comparison between the nuclear steam-supply system of the external separation forced-circulation reactor and the internal natural-circulation reactor.

The general coolant-flow paths in the two reactors and the numbers of major components in the coolant systems are indicated in Fig. VIII-1. In the Big Rock system, an open bypass connection between the suctions of the two recirculating pumps permits some circulation of water through the two downcomers connected to a pump that is shut down, thus preventing insertion of cold water into the reactor when the pump that has been shut down is started. If both pumps are inoperative but free to rotate, the elevation of the steam drum provides sufficient natural-circulation driving head to permit operation of the Big Rock Point reactor at about 50% load.

The cores of both reactors consist of vertical fuel bundles that are laterally spaced to provide vertical slots for the passage of cruciform control rods. In the Big Rock Point plant, the fuel bundles are unshrouded and fit within flow channels that are semipermanent components of the core structure. The Humboldt Bay bundles have integral shrouds and are held at the top and at the bottom by the permanent core support structure. Thus in principle the Big Rock Point bundles are placed within already formed flow channels, whereas the Humboldt Bay bundles form their own channels. Figure VIII-2 gives horizontal cross sections of the reactor pressure vessels and illustrates the arrangement of the major components of the cores.

Each core flow channel in the Big Rock Point reactor is attached to the top of a support tube. The channel-and-support-tube assemblies, which by virtue of their lateral

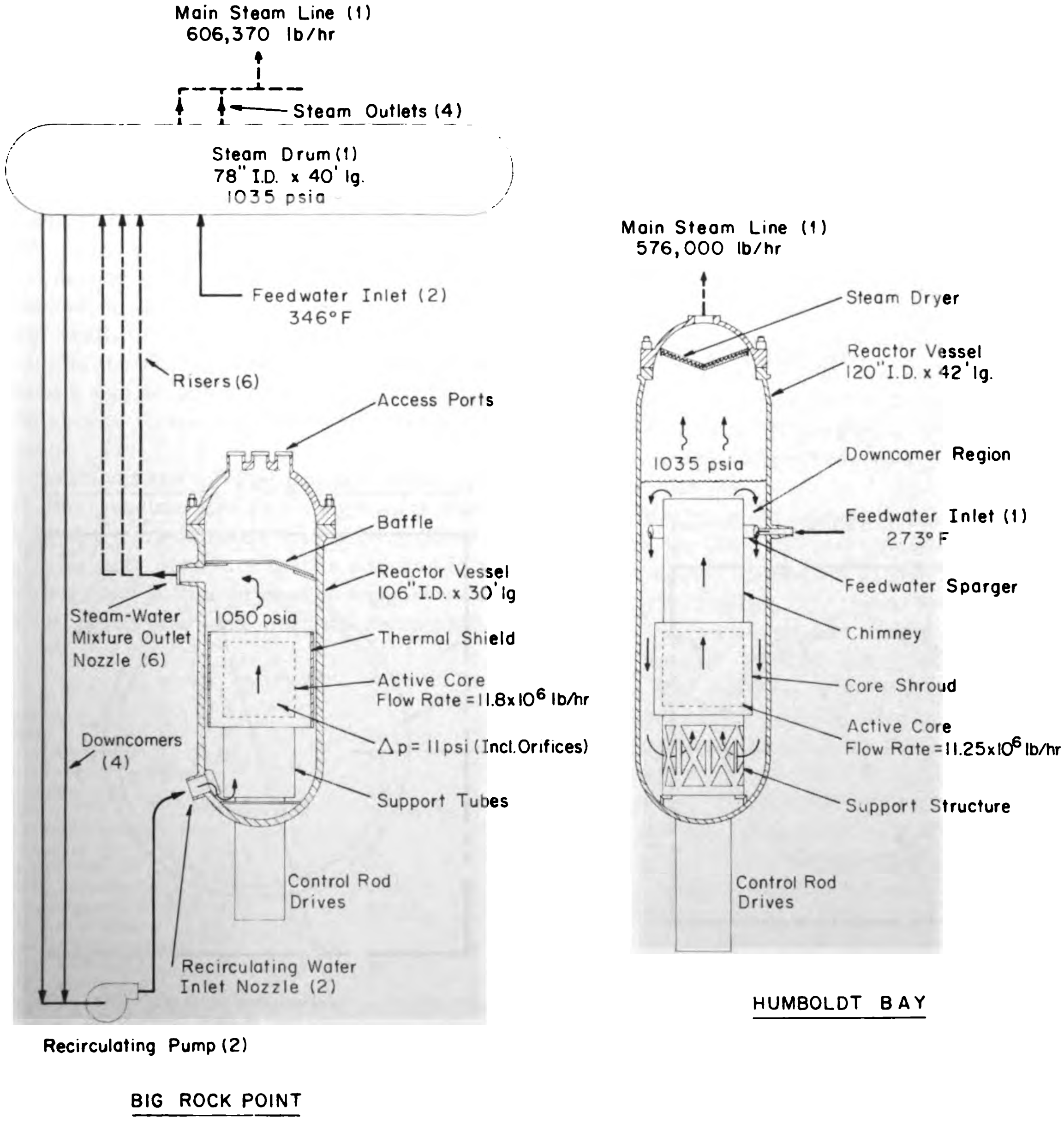

BIG ROCK POINT

HUMBOLDT BAY

Fig. VIII-1 Schematic elevations of nuclear steam supply systems.

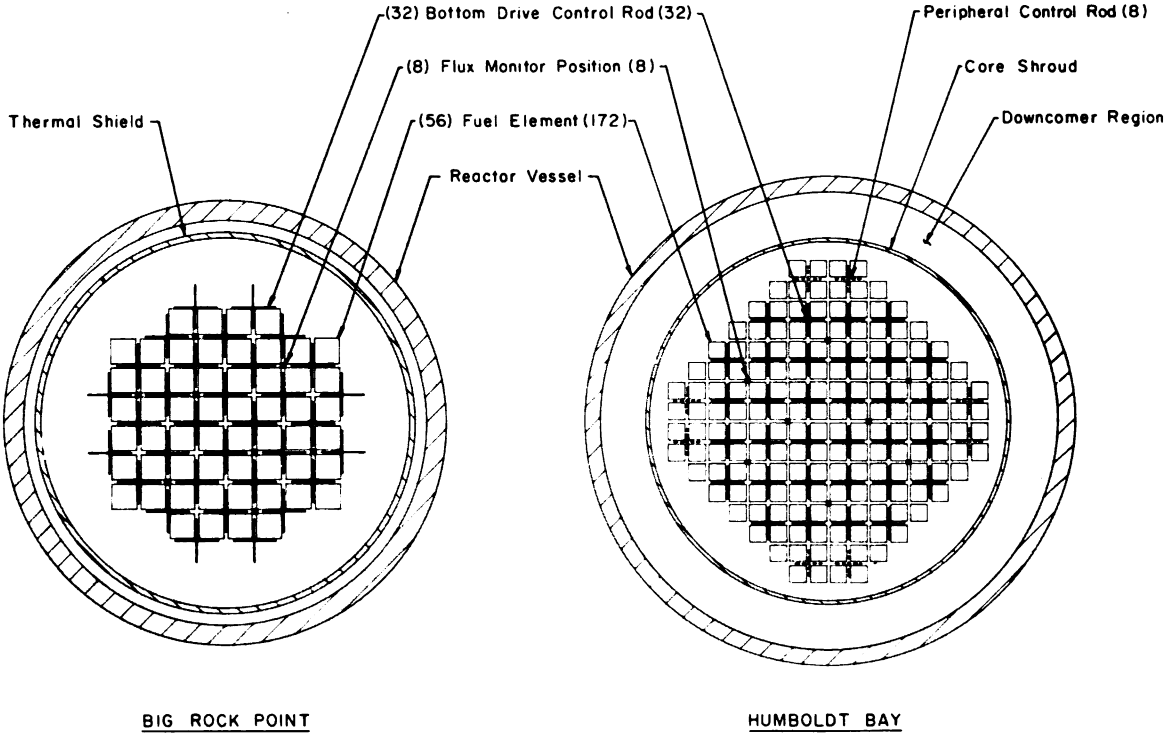

Fig. VIII-2 Horizontal cross sections through reactor vessels.

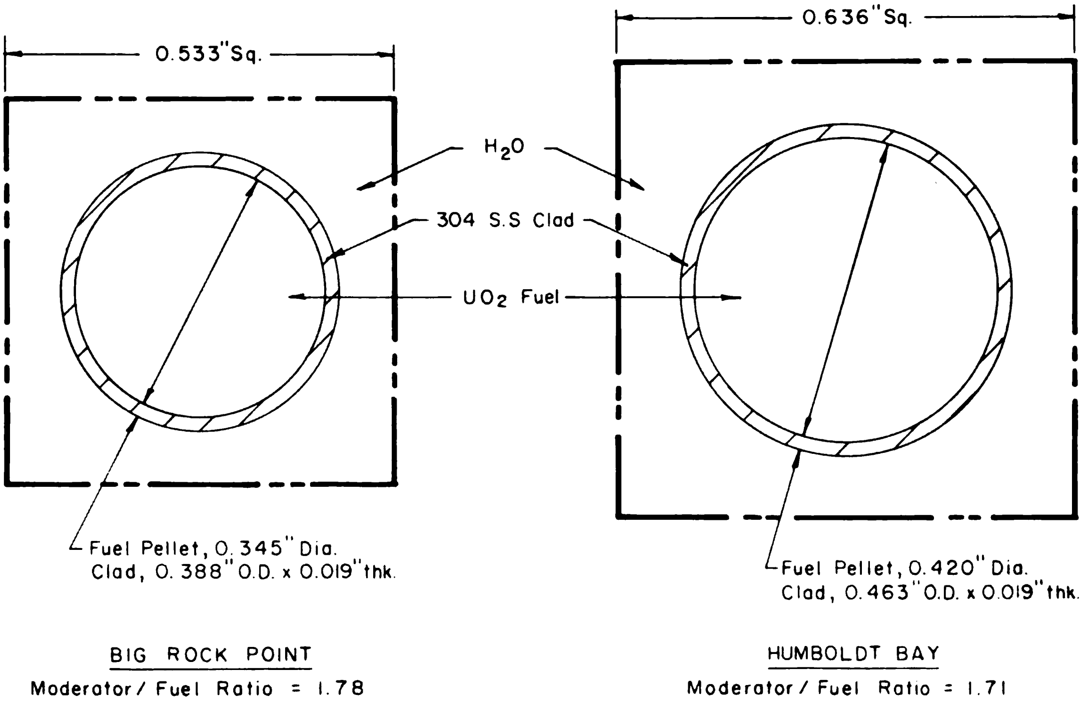
0.533" Sq.
0.636" Sq.
H₂O
304 S.S Clad
UO₂ Fuel
Fuel Pellet, 0.345" Dia.
Clad, 0.388" O.D. x 0.019" thk.
Fuel Pellet, 0.420" Dia.
Clad, 0.463" O.D. x 0.019" thk.
BIG ROCK POINT
Moderator/ Fuel Ratio = 1.78
HUMBOLDT BAY
Moderator/ Fuel Ratio = 1.71

Fig. VIII-3 Cross sections through fuel-rod cells.

spacing provide guidance for the control rods, are positioned by a core support at the bottom and by a guide assembly at the top. The core support is a circular plate that rests on brackets in the reactor vessel near its bottom. The brackets position the core support plate relative to the control-rod-drive penetrations in the vessel bottom head. Support-tube adapters, which align the bases of the channel-and-support-tube assemblies with the control-rod penetrations, are bolted to the support plate. Coolant for each fuel channel enters the bottom of the support tube, which is held clear of the support plate by the adapter. The upper ends of the channel-and-support-tube assemblies are radially supported and are aligned by a top guide assembly that is attached to a thermal shield. The top guide assembly consists of a grid of movable beams that serve as hold-downs for the channel-and-support-tube assemblies but which permit removal of the assemblies through the top of the vessel. The annular steel thermal shield supports the guide assembly and is itself supported by brackets attached to the reactor vessel wall. The baffle plate above the outlet nozzles of the reactor vessel is segmented. The segments can be unlocked and swung upward to allow access to the core from the vessel head nozzles.

At their bottoms the fuel bundles of the Humboldt Bay reactor plug into a core plate that is held by the core shroud. The shroud itself is atop a support structure that is attached to the reactor vessel bottom head. The support structure is perforated and permits recirculation flow from the downcomer region to enter the central part of the vessel, where flow is reversed and the coolant enters the bottom of the active core region. Cruciform guide tubes for the control rods extend from the nozzles in the vessel bottom head to the core plate and furnish additional support. At its top the core shroud supports and positions the chimney structure, which provides radial positioning for the top ends of the fuel bundles. The ring type feedwater sparger located near the top of the chimney structure is supported by brackets attached to the vessel wall.

	Big Rock Point	Humboldt Bay
Reactor vessel		
Height, ft	30	42
Inside diameter, in.	106	120
Wall thickness, excluding cladding, in.	$5\frac{1}{4}$	$4\frac{5}{16}$
Material	Carbon steel	Carbon steel
Cladding thickness, minimum, in.	$\frac{5}{32}$	$\frac{1}{4}$
Cladding material	S.S.	S.S.
Design pressure, psia	1715	1265
Design temperature, °F	650	650
Approximate initial nil ductility transition temperature, °F	10	10
Safety valves, number and location	6, on steam drum	4, on vessel head
Steam drum		
Length, ft	40	
Inside diameter, in.	78	
Wall thickness, excluding cladding, in.	$4\frac{3}{8}$	
Material	Carbon steel	
Cladding thickness, minimum, in.	$\frac{5}{32}$	
Cladding material	S.S.	

Core Details

The basic fuel units in both reactors are rod type elements, made up of stainless-steel tubes containing stacks of cylindrical UO_2 pellets. Figure VIII-3 shows a cross section of a typical rod-moderator cell for each reactor and gives dimensions and moderator-to-fuel ratios of the cells. Most of the fuel rods in both reactors are of full core length. Pellets of UO_2 are placed in the jacket tube in an uninterrupted stack, and a plenum is provided at the top of the stack to accommodate expansion and released fission gases. A coil spring and wafer in each plenum keep the stack of UO_2 pellets in the proper position, and welded plugs are used to seal the fuel rods at each end.

The fuel rods are arranged in a square array to form the fuel bundles shown in Fig. VIII-4. The rods are positioned at the top and at the bottom by fittings that form the handles and bases of the bundles, and wire spacers provide radial spacing at three axial locations in each bundle. The spacers, each of which consists of a double layer of crimped wire grids and a surrounding band, are positioned axially by special, segmented fuel rods that fit through sleeves in the spacers. The Big Rock Point bundle has four of these segmented rods, one at each corner, whereas the Humboldt Bay bundle uses a single segmented rod at its center. Construction of the segmented rods is similar to that of the full-length rods but with correspondingly shorter fuel and plenum lengths. The Big Rock Point bundle is held together axially by 32 fuel rods with special, threaded end plugs which screw into the base of the bundle and which are attached to the bundle handle with safety-wired nuts. In the Humboldt Bay bundle, eight rods are used in a similar manner, and the integral flow shroud adds stiffness to the assembly. In both bundles the rods not used for axial restraint have unthreaded end plugs that slide into holes in the top and bottom fittings. Springs are installed between all rods and the top fitting to accommodate thermal expansion. The Big Rock Point bundle, which has no integral flow liner but fits into a fixed flow channel in the reactor core, is equipped with pad type external spacers on each of the three axial spacer assemblies. Each Big Rock Point bundle has 12 special fuel rods, three in each corner of the bundle, which are smaller in diameter and have thicker jackets

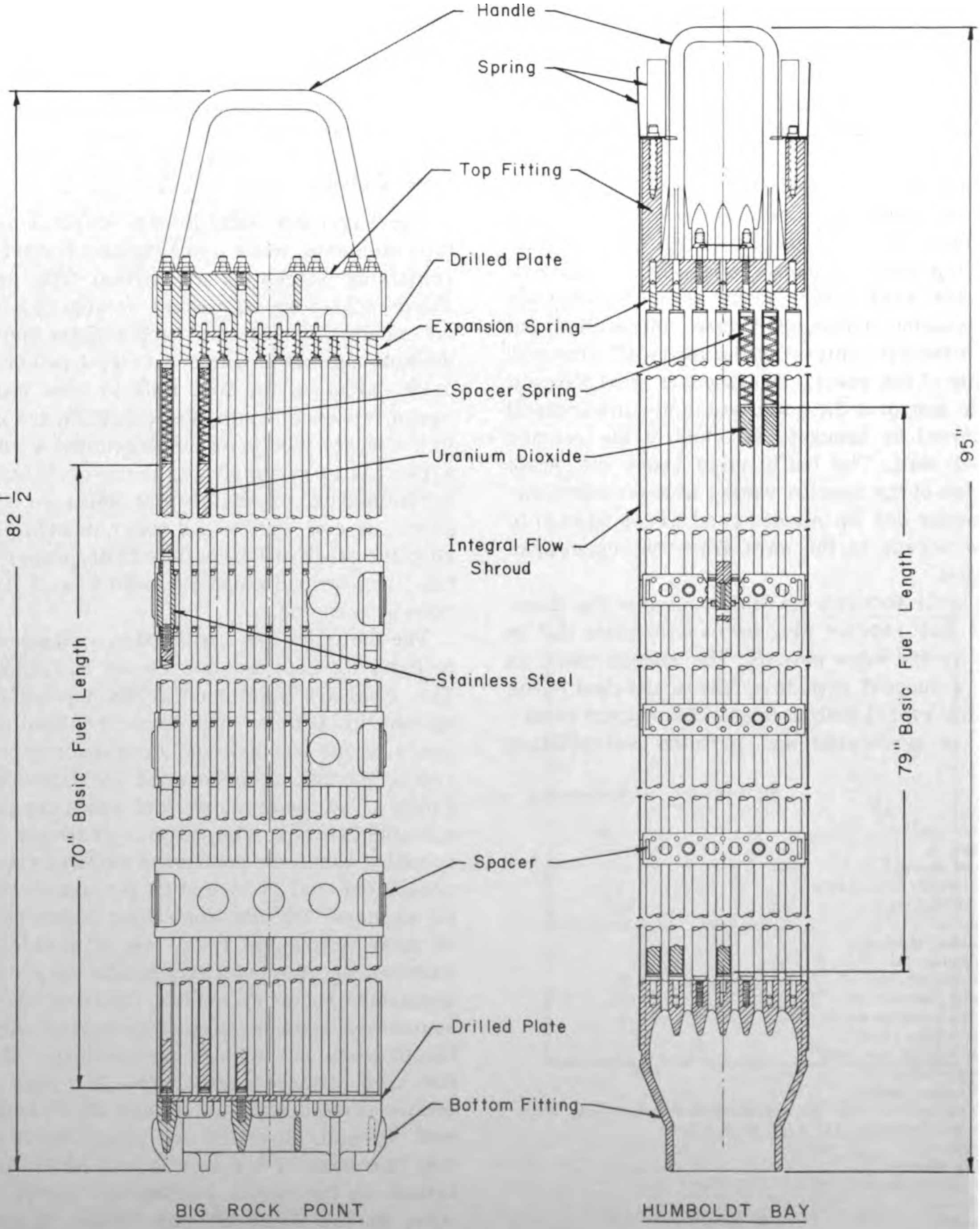

Fig. VIII-4 Fuel bundles.

than the standard rods, to reduce the power peaking caused by the water in the control-rod channel (see Fig. VIII-5). These 12 special rods include the four segmented rods used to support the wire-spacer assemblies. Their dimensions are shown in Fig. VIII-5, which is a horizontal section through a typical portion of the core.

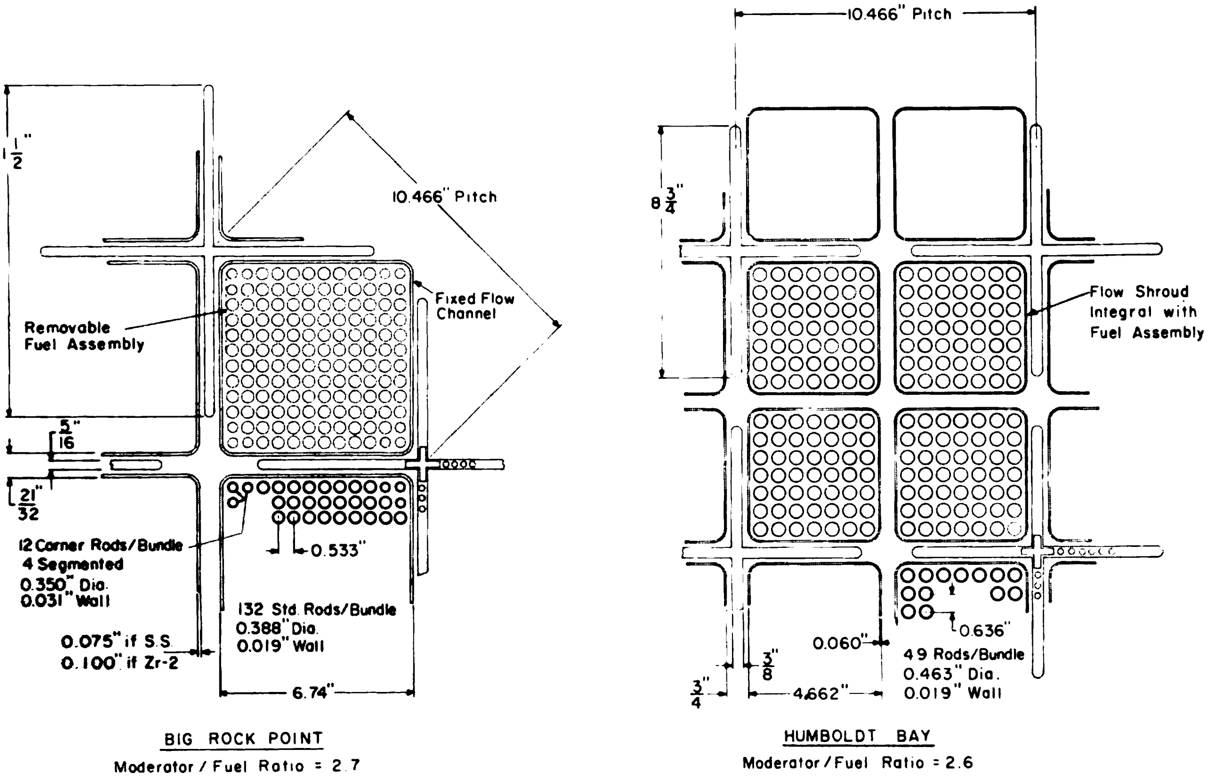

BIG ROCK POINT
Moderator / Fuel Ratio = 2.7

HUMBOLDT BAY
Moderator/Fuel Ratio = 2.6

Fig. VIII-5 Horizontal cross sections through typical core regions.

The geometrical relations between the major components of the cores of the two reactors are illustrated by Fig. VIII-5. The components include the groups of fuel rods, as provided by the fuel bundles; the flow channels, which are defined by the integral fuel-bundle shrouds in the Humboldt Bay core and by the preinstalled flow channels in Big Rock Point; the control-rod passages, formed by the radial spacing of the fuel-element or flow-channel assemblies; and the control rods themselves. In the Big Rock Point core, the flow channels may be either stainless steel or Zircaloy, depending on the core loading and the shutdown control requirements. The thicknesses of the channels of both materials are shown in Fig. VIII-5.

The control rods for both reactors are made up of poison tubes containing boron carbide which are assembled into a cruciform structure by a surrounding steel sheath, as indicated in Fig. VIII-5. These control elements are similar to those in the Dresden reactor which were described in *Power Reactor Technology*, 5(3): 34. The control rods are guided on the four core channels that they contact by stellite rollers at the top and bottom of each blade. Heat generated in the poison rods is removed by coolant that flows through holes in the sheaths and by contact heat transfer from the rods to the sheaths.

In addition to the regular, bottom-driven control rods shown in Fig. VIII-5, the Humboldt Bay reactor can be equipped with a system of peripheral control rods. These cruciform rods enter the core from the top and are provided to assure that an adequate cold shutdown margin is available even if any one of the central, bottom-driven control rods sticks in the withdrawn position. It was found that the peripheral control rods were not needed with the first core of the Humboldt Bay reactor. Consequently rods and drives were removed from the vessel prior to power operation.

Both reactors are provided with liquid-poison injection systems that provide a backup means of shutting the reactor down and holding it subcritical in the event that the control rods are not able to do so. Both systems, which are pressurized by bottled nitrogen gas, utilize sodium pentaborate solutions.

As mentioned above, either stainless-steel or Zircaloy flow channels can be used in the core structure of the Big Rock Point reactor. It is intended that the stainless-steel channels be used during initial operation of the reactor to reduce the excess reactivity that will exist prior to the establishment of an equilibrium program of partial-core refueling. The initial core of the Humboldt Bay reactor will contain up to 96 poison curtains which are made of borated stainless steel and which are hung from the top grid in such a way that they surround groups of four fuel assemblies. The curtains will be removed during the life of the first core to maintain reactivity.

	Big Rock Point	Humboldt Bay
Fuel and core		
Fuel material	UO_2	UO_2
Initial enrichment, % U^{235}	3.2	2.6
Weight of UO_2 in core, lb	19,300	34,600
Average fuel exposure, first core load, Mwd/ton of U	10,000	10,000
Equivalent core diameter, in.	62.5	77.5
Active core height, in.	70	79
Fuel-rod array in bundle	12 by 12 square	7 by 7 square
Number of bundles in core	56	172
Reactivity requirements		
Temperature, Δk_{eff}	0.025	0.015
Voids, Δk_{eff}	0.019	0.021
Xenon and samarium, Δk_{eff}	0.031	0.031
Fuel depletion and maneuvering, Δk_{eff}	0.127	0.133
Initial reactivity requirement, Δk_{eff}	1.202	1.200
Control elements		
Number of central control rods	32	32
Number of peripheral control rods		8
Shape of peripheral control rods		Cruciform
Control-rod poison material	B_4C	B_4C
Number of poison curtains (maximum)		96
Shape of poison curtains		Plate
Poison-curtain material		Borated S.S.
Single control rod, maximum worth, $\Delta k/k$	0.042	0.038
Liquid poison		
Material	Sodium pentaborate solution	
Volume, gal	850	365
Worth, $\Delta k/k$	0.25	0.20

Heat Removal

In view of the differences in the basic modes of operation of the reactor plants, their heat-removal and steam-generation characteristics are of particular interest. A comparison of the principal thermal characteristics of the two systems is given in the following table.

	Big Rock Point	Humboldt Bay
Average power density, kw/liter	45	27
Peaking factors		
Gross	1.94	2.62
Local	1.65	1.38
Overpower	1.27	1.25
Maximum at overpower	4.07	4.53
Linear power density, kw/ft of fuel rod		
Average	3.34	2.97
Maximum	10.5	10.8
Maximum at overpower	13.3	13.5
Fuel-jacket heat flux, Btu/(hr)(sq ft)		
Average	110,000	80,600
Maximum	352,000	292,100
Maximum at overpower	447,000	365,100
Burnout ratio, minimum at overpower	1.5	2.0
Coolant flow rate through core, 10^6 lb/hr	11.8	11.25
Core inlet subcooling, Btu/lb	14.0	12.1
Core inlet velocity, ft/sec		
Maximum	6.3	4.56
Minimum	5.1	4.37
Steam volume fraction		
Average core exit	0.41	0.48
Maximum channel exit	0.57	0.64
Average over core length	0.21	0.20
Average steam quality, core exit, %	4.9	6.3
Steam quality entering drum, %	5.2	
Average steam surface separation velocity, ft/sec		0.90
Average downcomer velocity, ft/sec		1.73

Effects of Circulation Mode on Reactor Design

The difference in performances that are achievable with natural and forced circulation is most clearly apparent in the comparison of core power densities in the preceding tabulation, where the power density in the Big Rock core is shown to be 1.67 times that in the Humboldt Bay core. Since the inlet subcooling is nearly the same in both cases and since the steam-void fractions do not differ greatly, the improvement in power density in the Big Rock reactor can be regarded rather directly as the benefit received from forced circulation — at least to a first approximation. That is to say, both reactors use about the same total coolant flow rate (see table), but to achieve this total, the natural-circulation core must provide a larger cross-sectional area for coolant flow. The actual situation is not quite as simple as that, since the Humboldt Bay core is some 13% longer than that at Big Rock Point, and the design relations that involve core length as a variable are not simple ones.

The fuel arrangement and design must, of course, be compatible with the heat-transport capabilities of the coolant system. Apparently the fuel centerline temperature is the limiting consideration in heat removal from the fuel elements in both cores. For ceramic fuel elements of a given basic design this consideration sets, to a good first approximation, the maximum power that can be extracted from a unit length of fuel element. The preceding table shows that the maximum power generation per foot of fuel element is very nearly the same for the two cores. If one considers, for simplicity, that the designer has fixed the coolant-flow area in a way that is characteristic for the type of recirculation (natural or forced) to be used, then he has left the interdependent design variables of fuel-rod diameter and moderator-to-fuel ratio to vary in order to match the required total length of fuel rod with the required coolant-flow area. Either one of these may be chosen freely but not both. In the cases considered here, the designers have chosen very nearly the same moderator-to-fuel ratio for the two cores (see Fig. VIII-5). This choice strongly involves the interrelated reactor physics characteristics of steam-void coefficient of reactivity, temperature defect, and fuel enrichment. Once a moderator-to-fuel ratio has been chosen, there is no longer any room for variation of fuel-rod diameter. In the cases considered here, where the moderator-to-fuel ratios are nearly equal, it is clear that the fuel-rod diameter must be smaller in the Big Rock core if advantage is to be taken of the higher coolant-flow velocity provided by the forced-circulation system.

In the forced-circulation case the coolant-flow velocity is a design parameter that the designer may vary at will for design optimization. Presumably the power density in a core like that of Big Rock Point could be increased still further by increasing the coolant-flow velocity along with other design modifications. If the linear power-generation limit for the fuel elements is considered fixed, one might increase the power density by moving the fuel rods closer together and increasing the coolant-flow velocity. This would decrease the moderator-to-fuel ratio and increase the steam-void coefficient of reactivity, the temperature defect, and the fuel-enrichment requirement. Or one might hold the moderator-to-fuel ratio constant, decrease the fuel-rod diameter, and increase the coolant flow. The major considerations in such a design variation would be the increase in fuel-fabrication cost (per kilowatt-hour), the increased neutron absorption in the fuel jackets (unless they were made proportionately thinner), and possibly the fuel-rod support problems.

Naturally the attractive way of increasing the power density in the forced-circulation case is to employ increased coolant flow (if necessary) in conjunction with fuel elements of the same size but higher power rating. Work toward the development of fuel elements of higher capability for the Big Rock Point reactor is reviewed in Sec. III of this issue of *Power Reactor Technology*.

Although high power density in the core has some advantages per se, the more important consideration is perhaps the size of the reactor vessel required for a given power generation. Here the external steam separation employed in the Big Rock Point plant would be expected to show an additional difference because considerations of recirculation flow do not determine the amount of space that must be left between the reactor core and the pressure-vessel wall. The consideration of fast-neutron shielding for the vessel wall does, of course, remain and is quite significant in determining the pressure-vessel diameter.

The comparison of reactor cross sections in Fig. VIII-5 does not show any important difference in the thickness of annulus between core and vessel. The reason for this is not apparent, but, in this case of relatively new, relatively small reactors, a number of possibilities could be visualized having little fundamental significance. It is in reactors of dimensions that begin to push the limits of pressure-vessel size that large incentives for high effective power density may develop. Now it is perhaps more to the point to examine the details of the recirculation phenomena in the natural-circulation circuit of the Humboldt Bay reactor.

The average velocity in the downcomer of the Humboldt Bay reactor is given[2] as 1.73 ft/sec.

One would judge, from quoted dimensions and flow rates, that this downcomer velocity occurs in the annular area around the chimney, and that the term "average" indicates an average over the flow area at that level. In the regions below the feedwater inlet sparger and opposite the active core region, where the core shroud forms the inner boundary of the downcomer, the flow area is decreased, and the average velocity must be considerably higher. The velocity near the top of the chimney has, of course, the greatest interest because it is in that region that the effects of velocity on gravitational separation determine the amount of carry-under in the recirculation flow. Apparently the degree of carry-under experienced is much less than that found in the small-scale steam separation tests at Argonne National Laboratory, which have been reported in Ref. 3 [reviewed in *Power Reactor Technology*, 6(2): 69-74]. In those tests the ratio of steam quality in the downcomer to that in the riser was found to be about 0.7 at 1000 psi for a downcomer velocity of 1.73 ft/sec. The successful operation of the Humboldt Bay plant can be taken as evidence that the actual ratio is not nearly that high. Estimates based on the data given in Ref. 2 indicate that the design expectation for the downcomer-to-riser quality ratio was no higher than 0.28.

The different coolant-recirculation approaches at Big Rock Point and Humboldt Bay give rise to certain incidental features of reactor design which are worth notice in passing.

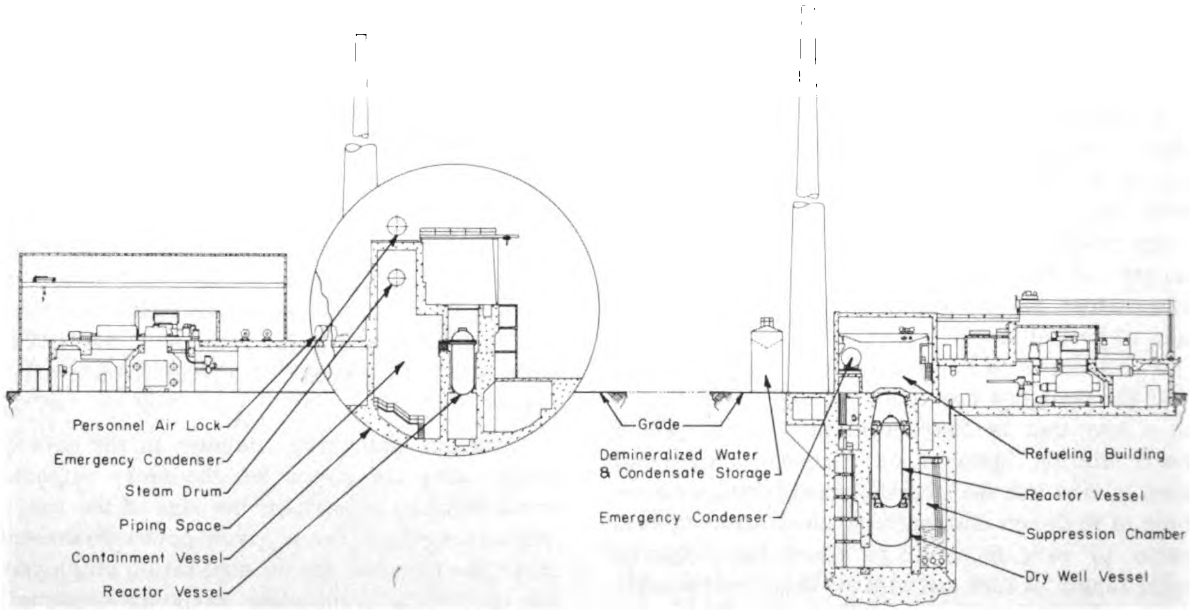

BIG ROCK POINT

HUMBOLDT BAY

Fig. VIII-6 Plant cross sections.

Since the forced-circulation scheme of the Big Rock Point reactor permits the core to have a relatively high pressure drop, each flow channel in the core is provided with an orifice at its bottom. Although the orifices could be used to match the flow distribution to the radial power distribution, they are installed primarily to increase the single-phase pressure drop of the core. The effect of the increased single-phase pressure drop is to make individual channel flow less dependent on power, thus improving the burnout ratio and parallel channel stability. The pressure drop across the orifice is equal to slightly more than one-third of the pressure drop across the remainder of the core channel.

The lifting forces imparted to the fuel bundles by the upward-flowing coolant are small enough in both reactors that no positive fuel hold-down mechanism is required. In the Big Rock Point reactor, whose fuel bundles fit in semipermanent flow channels of the reactor core structure, no bundle hold-down is used. In the Humboldt Bay core, where the control-rod channels are formed by the integral shrouds of surrounding fuel bundles, hold-down latches are provided for those fuel bundles which adjoin bottom-driven control rods. Consequently, if a control rod jams against a fuel bundle, the bundle cannot be lifted from the core as insertion of the rod is attempted.

One of the differences in the plants is the accessibility of the core for shutdown operations such as refueling. In Big Rock Point, ports in the vessel top head provide access to the core, although the normal refueling procedures include removal of the head. The steam dryer in the Humboldt Bay reactor has a removable center section, which permits access to the vessel internals without the necessity of removing the head.

Plant Arrangement and Containment

The basic differences in coolant schemes in the two reactors lead to striking differences in plant arrangement and containment design, for the external steam drum approach used at Big Rock Point would not fit gracefully into the pressure-suppression concept employed at Humboldt Bay. The differences are illustrated in Fig. VIII-6, which gives simplified vertical cross sections of the two plants to the same scale. In addition to showing the inherent differences in appearance of the forced-circulation plant and the internal natural-circulation plant, the drawing illustrates the conventional containment scheme employed in the Big Rock Point plant and the pressure-suppression containment utilized for Humboldt Bay.

The Big Rock Point containment vessel was designed and constructed in accordance with the *ASME Boiler and Pressure Vessel Code*, Secs. II, VIII, and IX, as modified by applicable nuclear code cases. The vessel is typical of the conventional type, except that its exposed exterior surface is insulated with a cork mastic coating protected by acrylic resin. The insulation prevents excessive temperatures inside the vessel that are caused by solar radiation, reduces heat loss in winter, provides atmospheric corrosion protection, and reduces inside surface condensation. The application of the pressure-suppression concept to the Humboldt Bay reactor was described in *Power Reactor Technology*, 6(3): 27, and will not be discussed further.

Big Rock Point	
Diameter of containment sphere, ft	130
Height above grade, ft	103
Approximate free volume, cu ft	940,000
Design pressure, psia	41.7
Design maximum temperature, °F	235
Maximum leakage rate at design pressure, %/day	0.5
Number of access air locks	3
Total number of penetrations	100
Diameter of nozzle penetrations, in.	
Maximum	24
Minimum	0.75
Humboldt Bay	
Dry well	
Vessel inside diameter, ft	17.5
Vessel overall height, ft	68
Design pressure, psia	86.7
Maximum leakage rate at design pressure, %/day	0.1
Suppression chamber and pool	
Chamber total volume, cu ft	54,300
Air space volume, cu ft	33,400
Water volume, cu ft	20,900
Vent pipe submergence, ft of water	6
Water temperature, °F	80
Air space internal pressure rating, psia	24.7
Internal pressure capability of concrete structure, psia	39.5
Maximum leakage rate at 24.7 psia, % of free-air volume per day	1.0
Refueling building	
Volume, cu ft	192,000
Minimum exterior wall thickness, in.	12
Maximum inleakage rate at a negative pressure of $^1/_4$ in. water, cfm	134

Turbine-Generator, Condensate, and Feedwater Systems

The power system for each plant includes those components which convert steam into electric power and which provide feedwater for the reactor. The major components of the systems are shown on Fig. VIII-7, which presents simplified flow diagrams for each plant. Each system utilizes a tandem-compound double-flow

	Big Rock Point	Humboldt Bay
Turbines		
Speed, rpm	3600	3600
Rating, kw	54,500	50,000
Inlet pressure, psia	1015	1015
Exhaust pressure, in. Hg abs.	3.5	3.5
Generators		
Rating, kva	70,588	70,588
Voltage	13,800	13,800
Power factor	0.85	0.85
Short-circuit ratio	0.80	0.70
Hydrogen pressure, psia	45	45
Main condensers		
Condensing surface area, sq ft	27,500	30,700
Condensing capacity during load rejection, lb/hr	948,000	810,000
Hot well capacity, gal	6000	6500
Condensate demineralizers		
Number	3	3
Size, each	Half capacity	Half capacity
Maximum flow rate, gal/(min)(sq ft)	50	50

saturated-steam turbine, which is connected directly to a hydrogen-cooled generator. Each turbine is equipped with external moisture separators in the crossover between the high-pressure and low-pressure sections, and three extraction points are provided. At its initial power rating, the Humboldt Bay system uses only two extractions: the third point can be used with a high-pressure feedwater heater to increase efficiency. The main condenser in each

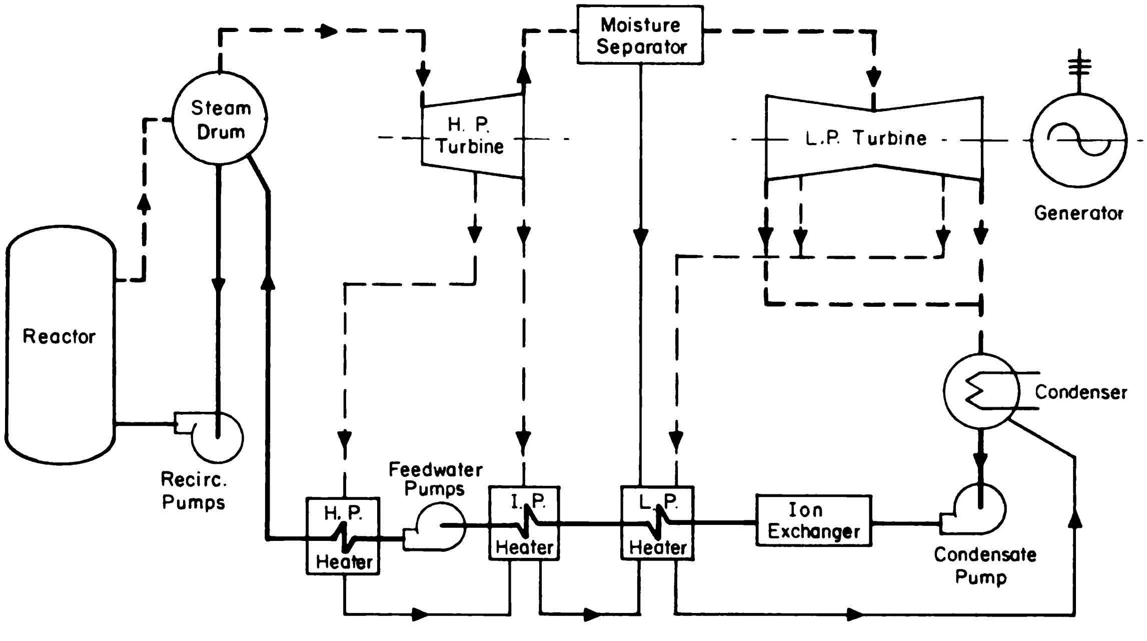

BIG ROCK POINT

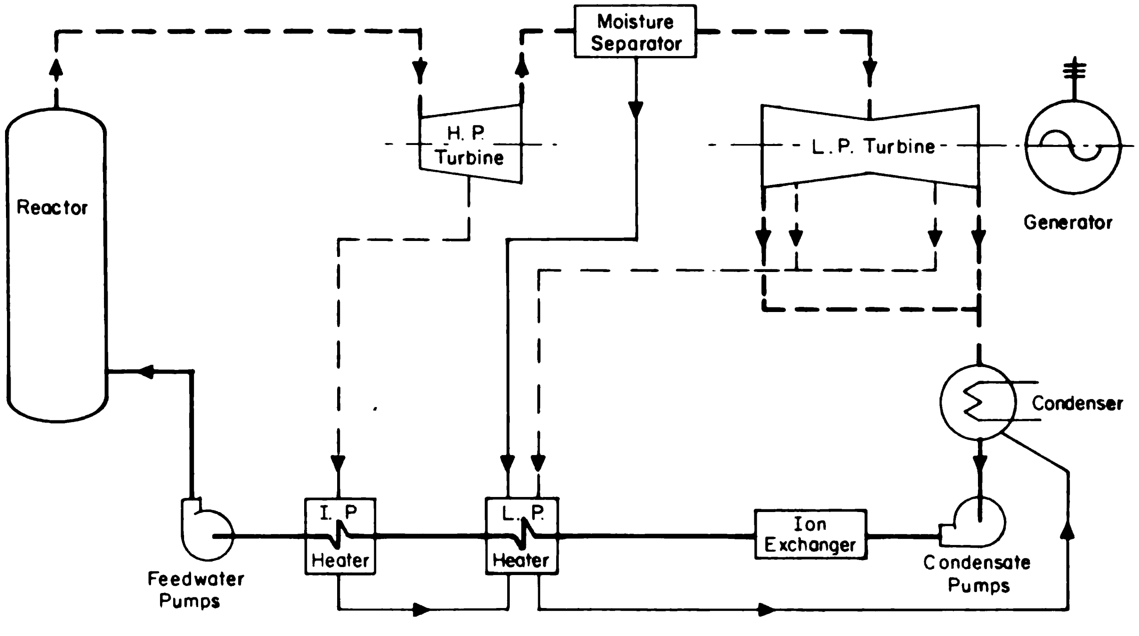

HUMBOLDT BAY

Fig. VIII-7 Simplified flow diagrams.

system is a horizontal, single-pass divided-water-box deaerating type unit of conventional construction. The condensers can accept bypass steam at reduced pressure, and they have oversize, baffled, storage type hot wells that provide a holdup time for the decay of short-lived radioactivity in the condensate. The air- and gas-removal equipment of the condensers discharges to the main exhaust stacks through oversize pipes that provide en route holdup time for further decay of radioactivity. Full-flow ion exchangers are located in the condensate system of each plant.

Control and Instrumentation

The mode of control for the plants is one in which the turbine follows the reactor output rather than system load changes. The basic control device for the turbine is an initial pressure regulator, and during normal operation the turbine admission valves are controlled by this regulator. The steam bypass valve is normally closed, and so all reactor steam flow is passed through the turbine. The occurrence of abnormal conditions, such as turbine trip, results in the opening of the bypass valve and the dumping of steam directly to the condenser. If a sudden loss of electrical load results in turbine overspeed, a speed-governor signal overrides the initial pressure-regulator signal. The governor signal initiates sufficient closure of the turbine admission valves to obtain acceptable turbine speed, but this admission-valve closure causes the reactor pressure and reactivity to rise. The increase in reactor pressure generates another signal, which opens the turbine bypass valve and dumps steam to the condenser, thereby lowering reactor pressure.

The reactor operator adjusts reactor power level by manual operation of the bottom-driven control rods. Each rod is provided with its own hydraulically operated drive mechanism that is mounted vertically in a thimble welded to one of the reactor bottom head nozzles. The basic concept of the drive mechanism is one in which a double-acting piston and a drive shaft are attached to each cruciform control element. Differential pressures across the piston are used to drive the rod into or out of the core, and a ratchet type locking device is used to hold the drive (and rod) at set positions when driving pressures have been removed. The ratchet does not interfere with insertion of the control rod into the core but must be unlatched in order to withdraw the rod. Maximum withdrawal rate of a rod is 3 in./sec, and speed of movement is controlled by a flow-metering device in the hydraulic circuit. Signals indicating control-rod positions are initiated by indicator mechanisms housed within the drive sections of the rods. A mechanism consists of a series of fixed, magnetically operated switches, each of which indicates a discrete rod position, and a permanent magnet which is carried on the rod-drive piston and which actuates the switches.

A vertical cross section of a control-rod-drive mechanism of the Big Rock Point reactor is given in Fig. VIII-8. The mechanism is representative of the assembly used in Humboldt Bay as well as Big Rock Point, and both drives are modified versions of a design originally developed for the Dresden reactor. High-pressure water, which is the actuating fluid for the hydraulic drive unit, is introduced at one of two inlet ports of the mechanism, depending on the desired direction of movement of the control rod. Internal passages in the unit direct the actuating fluid to either the top or the bottom of the piston, resulting in an unbalanced force that causes the piston to move.

The components of the ratchet type locking device are shown near the top of the mechanism in Fig. VIII-8. A collet assembly, which consists of a piston and locking fingers, is spring and gravity loaded to remain in the down position as shown on the drawing. In this position, the collet fingers engage ratchet notches in the drive piston and lock the control rod in place, thereby permitting the hydraulic driving pressures to be removed from the drive mechanism. If scram or normal insertion of the rod is desired, admission of hydraulic fluid to the up inlet will accomplish the desired movement without interference from the collet assembly. However, inadvertent opening of the valve in the down hydraulic line cannot cause rod movement out of the core. To withdraw the rod from the core, a momentary up pressure must be applied to the mechanism; this up pressure causes the collet fingers to move outward and to unlatch as the rod begins to move upward. The admission of down fluid to the unit then places a downward-acting force on the drive piston and an upward-acting force on the collet assembly. Consequently the collet assembly moves up, causing the collet fingers to be held clear of the ratchet notches of the piston rod, thereby permitting the drive piston to move down. When the control rod has moved down to the desired position, the control valve of the down hydraulic fluid line is closed, and the drive mechanism is isolated from the control pressure. With the pressure removed the collet assembly returns to its normal position, and the collet fingers reenter the locking notches on the piston rod. Pressure within the control-rod drives is such that approximately 30 psi differential above reactor pressure is applied to the bottom of the pistons. This is not enough pressure to force the control rods into the core, but it does provide leakage past the drive seals for cooling.

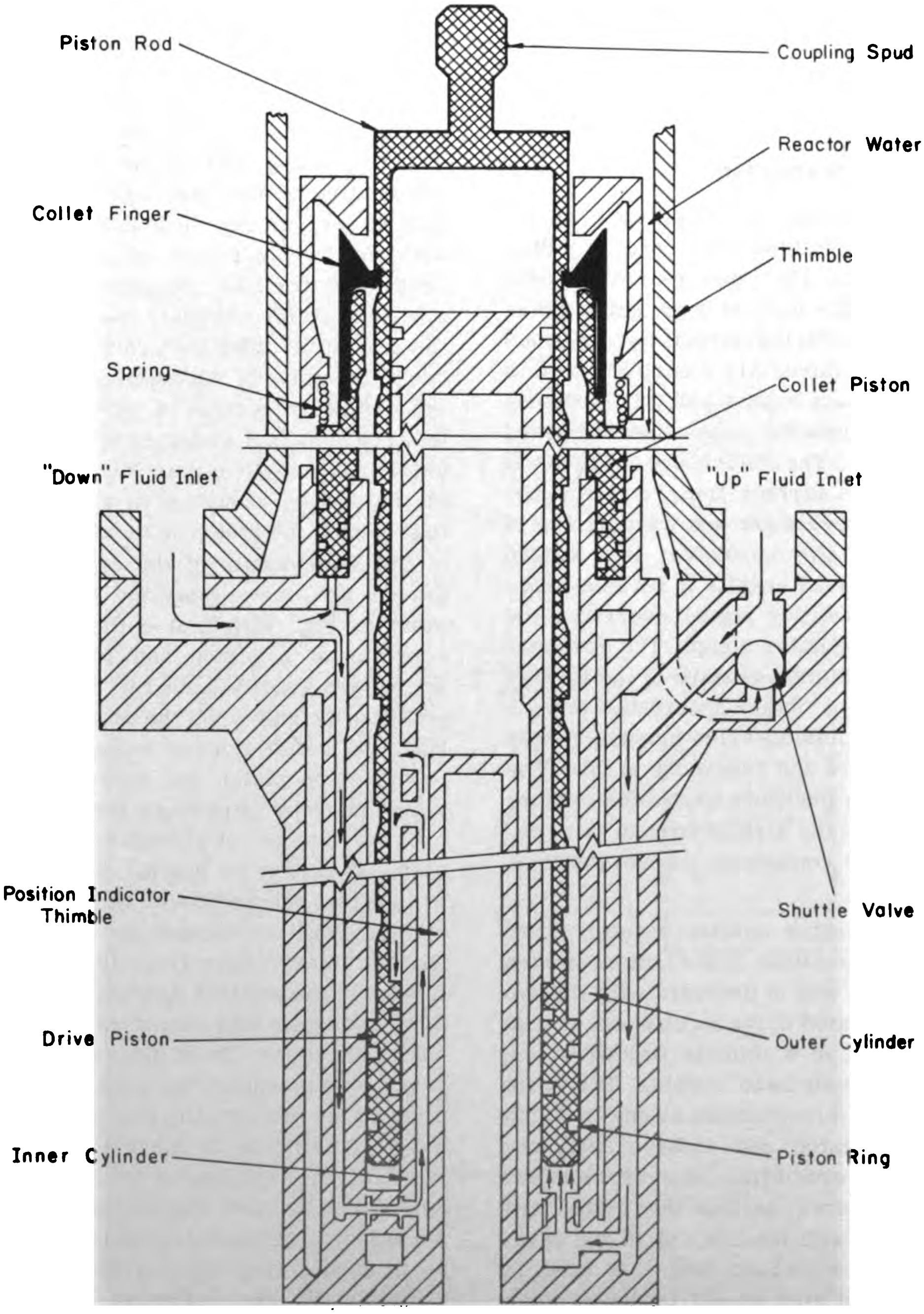

Fig. VIII-8 Control-rod-drive mechanism, Big Rock Point reactor.

In each plant the reactor neutron-monitor system consists of two separate sets of detectors: the out-of-core monitors, which provide the operators with immediate indications of neutron level within the reactor from startup to full power and which are connected to the reactor safety system, and the in-core monitors, which are used to determine the neutron-flux distribution in the core and periodically to provide data for verification of analytical predictions and major rod programming. The out-of-core monitors cover a range of nine decades by use of three subsystems that cover the start-up range, the period or intermediate range, and the power range. A block diagram of the out-of-core nuclear instrumentation of the Big Rock Point reactor, shown in Fig. VIII-9, illustrates the major features of the system provided for each plant. Although the Humboldt Bay system differs slightly from that of Big Rock Point, the principal components and interrelations between the channels are the same. Both systems incorporate revisions to earlier system drawings that were shown in *Power Reactor Technology*, 5(2): 66-67.

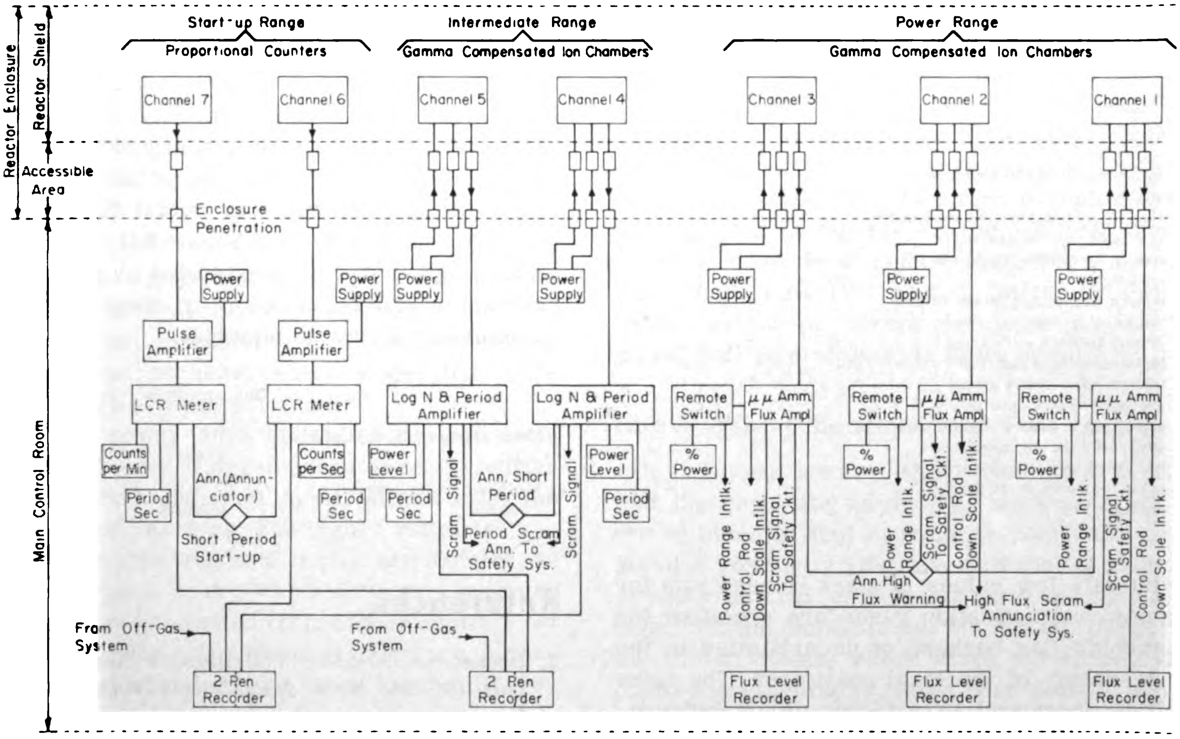

Fig. VIII-9 Out-of-core nuclear instrumentation diagram, Big Rock Point reactor.

The in-core flux-monitor system uses miniature fission chambers as detectors and determines neutron flux in eight radial positions of the core. Detectors are located at three elevations in each radial position, so that a total of 24 in-core measurements can be taken. The three detectors for each radial core position are fabricated into a single assembly that is inserted into the core from the top. Calibration wires are inserted through nozzles located in the bottom head of the reactor pressure vessel.

Radioactive Waste Disposal

The principal sources of gaseous radioactivity are the off-gases from the main condenser air ejectors, the gland seal condenser, and the mechanical vacuum pumps. The air-ejector gases, which are carried to the plant stack through a holdup line to provide decay time, are passed through a high-efficiency filter prior to entering the stack. Gases from the gland seal condenser and the mechanical vacuum pumps flow through a separate holdup pipe, which provides a shorter holdup period, and are discharged to the stack. Before release from the stack, the process gases are mixed with ventilating air, giving a significant dilution of the airborne radioactivity.

The limits on the annual average rates of release of fission and activation gases from the stacks of Big Rock Point and Humboldt Bay, as given in the Technical Specifications,[4,5] are tabulated below:

	Big Rock Point	Humboldt Bay
Holdup time for air-ejector gases, min	30	18
Holdup time for gland-seal condenser and vacuum-pump gases, sec	90	50
Minimum air flow in stack, cfm	30,000	12,000
Stack height, ft	240	250
Maximum permissible stack release rate		
Annual average, curies/sec	1.0	0.05
Instantaneous, curies/sec	10	0.5
Maximum permissible annual average stack release rate, expressed in units of μc/sec, does not exceed the permissible air concentrations for unrestricted areas, as given in 10CFR20, multiplied by	1.2×10^{10} cm^3/sec	6×10^8 cm^3/sec

Relatively low values of stack release rate for fission and activation gases are specified for Humboldt Bay because of uncertainties in the meteorology of the local coast area. The rates will be increased by a factor of 5 if meteorological tests confirm that the increase is reasonable.

The general procedures followed in liquid waste disposal are collection, dilution, and discharge, or storage following concentration by evaporation. Effluent from the liquid radioactive waste system is released under batch control, and storage tanks are provided for retreatment of effluent if required prior to discharge. The effluent is pumped to the circulating-water discharge duct, so that a large volume of nonradioactive water is available for use as a diluent.

	Big Rock Point	Humboldt Bay
Minimum waste treatment	Filtration	Filtration
Waste-filter capacity, maximum, gal/min	50	50
Nonradioactive water available for diluting waste effluent, full power, gal/min	50,000	104,000
Maximum waste inventory in system, curies	5000	10,000

Solid wastes include spent demineralizer resins, contaminated tools, equipment, and clothes, used filters, and used process equipment such as control rods or core components. Demineralizer resins are normally sluiced to a storage tank that is sufficiently large to receive wastes for approximately five years. Other solid wastes are stored in an underground concrete burial vault. Room is available for additional storage tanks or burial vaults, and, when the current facilities are full, additional storage space will be constructed or a licensed contractor will be called in to remove the accumulated solid waste material.

	Big Rock Point	Humboldt Bay
Resin storage-tank capacity, gal	10,000	10,000
Maximum waste inventory, curies	40,000	50,000

References

1. Docket No. 50-155, Final Hazards Summary Report for Big Rock Point Plant, Vols. 1 and 2, Nov. 14, 1961, and Amendments.
2. Docket No. 50-133, Final Hazards Summary Report, Humboldt Bay Power Plant Unit No. 3, Sept. 1, 1961, and Amendments.
3. M. Petrick, A Study of Vapor Carryunder and Associated Problems, USAEC Report ANL-6581, Argonne National Laboratory, July 1962.
4. Appendix A (Technical Specifications) to Provisional Operating License No. DPR-6, granted to Consumers Power Company by the United States Atomic Energy Commission.
5. Appendix A (Technical Specifications) to Provisional Operating License No. DPR-7, granted to Pacific Gas & Electric Company by the United States Atomic Energy Commission.

Section IX

Power Reactor Technology

Specific Reactor Types

Heavy-Water Reactors

By J. R. Dietrich

The last comprehensive review of heavy-water reactors in *Power Reactor Technology* was in 4(2): 62-77. Among the points discussed in that review were the following:

1. To the extent that there is a concern about the possible depletion of nuclear fuel resources, this concern constitutes an incentive for the development of heavy-water-moderated reactors of high neutron economy.
2. The power cost estimates arrived at in studies of heavy-water-moderated reactors have tended to be higher than those estimated for the light-water reactors. The higher estimates result from the costs directly attributable to heavy water—heavy-water inventory charges and losses—and often from higher capital cost estimates. The estimated fuel costs are, in general, considerably below those for the H_2O reactors and are less dependent on uranium costs, plutonium buy-back prices, and fuel-processing costs.
3. It is generally recognized that the difference in economic environment for nuclear power generation which exists between the United States and Canada is responsible to a large degree for the differences in preference for light-water and heavy-water reactors in the two countries. It is also true, but not so generally recognized, that this difference in economic environment may also strongly affect the direction of preferred development of the D_2O reactor in the two countries.

Since the issuance of the preceding review, there have been some critical reexaminations of the heavy-water reactor type, as well as some significant technical developments, which have sharpened and illuminated these points. The reexaminations have strengthened the position of the liquid-D_2O-cooled reactor for the near term, and have, mostly by omission, deemphasized the direct-cycle boiling-D_2O pressure-tube system. Many other coolant possibilities have been examined, and several seem promising, but the organic-cooled system appears to emerge as the one most likely to give an early economic improvement over the pressurized D_2O system. In the following brief review of recent developments, these points will be discussed in more detail.

Heavy-Water Reactors and Fuel Supplies

It has long been recognized in a general way that the capability of the D_2O-moderated reactor to achieve high neutron economy and substantial reactivity lifetime with fuel of natural or near-natural enrichment is a real advantage; but the implications of that advantage in the United States, where large enrichment facilities are available, have been slow in being noticed. The AEC Report to the President[1] states that the U. S. resources of fissile isotope appear to be small in relation to the hoped-for development of nuclear power generation, and the recognition of this fact in that report has helped to give the proper emphasis to the wise use of nuclear fuel. Ironically, the relation of low-enrichment operation to fuel resource utilization had not been clearly defined prior to the Report to the President, and the report, although establishing the basis of importance for heavy-water reactors, placed no emphasis on the need for that reactor type. Since the publication of the report, heavy-water systems have been examined more carefully in relation to efficient fuel utilization, and a more precise appreciation of their conservation advantages has developed. These advantages, which were brought out in a general way in the discussion of nuclear fuel utilization in the previous issue of *Power Reactor Technology* [6(4): 1-38], may be summarized as follows:

1. Because the heavy-water-moderated reactor can achieve high neutron economy with fuel of low enrichment, it possesses the unique ability to utilize fissile isotope effectively (i.e., to extract a large amount of energy per net gram of fissile isotope destroyed) and at the same time to minimize the amount of fissile isotope required in inventory. In a rapidly expanding nuclear power-generation system, the tie-up of fissile isotope in reactor inventory represents as effective a drain on the resource as does the actual destruction of the isotope.

2. Because of its ability to achieve long exposures with fuel of low enrichment, the D_2O-moderated reactor can minimize the effective loss of fissile isotope that results from the degradation of enrichment in the tailings from isotope separation plants and spent reactor fuel elements.

3. Because the epithermal component of the neutron energy spectrum can be low in a reactor of low enrichment, and because a low effective neutron temperature can be achieved by the use of cool moderator, D_2O reactors of the pressure-tube type can minimize the effects of the high capture-to-fission ratio (α) which afflicts plutonium in the epithermal-neutron energy regions and hence can utilize plutonium more effectively than other thermal reactors.

4. The natural-uranium D_2O-moderated reactor is probably more efficient than a diffusion plant in converting raw natural uranium to fissile isotope for the fueling of fast breeders. That is to say, if a given quantity of natural uranium is used in a natural-uranium D_2O-moderated reactor, the plutonium produced will probably provide inventory for a larger power capacity of fast breeder than would the U^{235} that could be extracted from the same quantity of natural uranium by a diffusion plant operating with a practical value of tails enrichment.

5. If it should prove desirable to operate on a thorium fuel cycle, the D_2O-moderated reactor would still retain the relative advantage of achieving high conversion ratio with low inventory requirement. Furthermore, it apparently has the capability of utilizing plutonium efficiently as a means of starting the U^{233}-thorium cycle, and its chances of breeding on that cycle are as good as or better than those of other solid-fuel reactors operating in the thermal or near-thermal energy range.

Power Cost Estimates

In the more recent studies of nuclear power plants employing heavy-water reactors, the estimated power costs have improved relative to estimates for light-water plants of comparable output, and the prospects appear good for competitiveness in plants of large size. Designers who have some experience with the uncertainties in power cost estimates are likely to discount the significance of such estimates if they are based on anything short of detailed construction drawings. However, if the current, rather favorable estimates are discounted because of uncertainties, at least the earlier, less favorable estimates should be viewed with equal, or greater, reservation.

Actually there are good reasons for improvements in the estimated economic performance. Not the least of these is the advancement of the technology, most clearly demonstrated by the operation of the NPD plant[2-5] and the advanced stage of construction of the Douglas Point Station[6,7] (scheduled[6] for full-scale commercial operation in 1965) in Canada and by the startup of the Carolinas-Virginia Tube Reactor (CVTR) in the U. S. [see *Power Reactor Technology*, 6(4): 63-81, for a review of the CVTR design]. Another important factor is the development of more favorable design concepts and the optimization of design of the particular concepts. As pointed out in the previous review, optimization and attention to design detail are of the highest importance in those reactors (for example, the heavy-water reactors) whose attractive features depend on good neutron performance. Finally, most of the more recent power cost studies have been made at higher power levels [500 Mw(e)] than the earlier studies. The economic performance of the heavy-water reactors improves relative to that of the light-water reactors as plant size increases and presumably would experience a step increase if plant size were increased further to the point that a single light-water reactor could not supply the required thermal power.

The recent power cost estimates for reactors cooled and moderated by D_2O have been made by the Du Pont Company at the Savannah River Laboratory,[8] by a joint team from the American Electric Power Service Corporation (AEPSC) and the General Nuclear Engineering Corporation (GNEC)[9] and by the AECL Chalk River Laboratory.[10] Although each of these groups has considered several D_2O-moderated reactor types, the results for the liquid-D_2O-cooled type will suffice to show the trend of the estimates. Table IX-1 summarizes the characteristics of the reactors which were described by the three groups at a joint USAEC-AECL review[11] in May 1963. Table IX-2 summarizes the capital and fuel cost estimates for the three plants. These are somewhat more susceptible to comparison than are the estimates of power-generation cost, inasmuch as they are less affected by ground rules. However, it is clear that different groups use different criteria for the breakdown between direct and indirect costs. The inclusion of D_2O inventory at $20 per pound is for the sake of comparison only. The power cost estimates of the various groups covered D_2O prices from $17 per pound to $28 per pound, with and without depreciation, and, of course, included allowances for D_2O losses. The references should be consulted for the understanding of the ground rules necessary for the interpretation of power cost estimates. However, for purposes of orientation, it may be mentioned that the Du Pont and AEPSC-GNEC estimates were, respectively, 5.8 and 6.9 mills/kw-hr for the case of private utility financing with nondepreciating D_2O.

Other economic studies of very large heavy-water reactors have considered the production of process heat for water desalinization—in most cases with concurrent electric generation by backpressure turbines. Reference 12 (see also Ref. 13), reporting work at the Oak Ridge National Laboratory (ORNL), considers a plant of 25,000 Mw(t), employing three heavy-water-moderated reactors, each of 8333 Mw(t) capacity, cooled by boiling light water.* With municipal financing and a plutonium credit of $6.7 per gram (as nitrate), the plant is estimated to produce electric power at 1.55 mills/kw-hr and fresh water at 11.0 cents per 1000 gal, when water and electricity are sold in the ratio of 9 gal per kilowatt-hour.

Reference 12 does not make comparisons with other reactor types for the desalinization application, but a recently issued report[14] gives the results of a study of sea-water distillation by nuclear heat (with electric power production by backpressure turbines), carried out by the Bechtel Corporation for AEC. In the study[14] light-water reactors and water-cooled graphite-moderated reactors were considered in addition to organic-cooled D_2O-moderated reactors. The study utilized reactor and fuel cost information supplied by ORNL and by various contractors through the AEC Division of Reactor Development and the Savannah River and Hanford Operations Offices. The D_2O-moderated reactor was found to give the lowest cost heat, primarily because of its low estimated fuel cost.

Canadian and U. S. Approaches

The differences between the economic environments of nuclear plants in the U. S. and Canada are well known, and it has become a cliché to point out that the low capital charge rate applicable to the Canadian reactor (about 6.5% per annum) causes the balance between capital costs and fuel costs, which usually must be struck in economic optimizations, to be tipped in favor of low fuel costs. It has been recognized that this circumstance plays a large part in the Canadian choice of the heavy-water reactor and that, in combination with some other nontechnical considerations, it plays a large part in the favorable performance shown by the natural-uranium designs in the Canadian environment. What is not so generally recognized is the extent to which these effects permeate the entire Canadian design approach, making it uniquely fitted for the Canadian power economy and for the use of natural uranium. This effect may be seen by examining the characteristics of the Canadian and U. S. designs listed in Table IX-1, and it will become even more obvious if the designs are examined in detail. The most straightforward comparisons can be made between the Canadian design and the AEPSC-GNEC design, since both have rod type fuel

---

*This reactor is of particular interest technically, for it appears to achieve a negative coolant-void coefficient of reactivity. This has not been previously reported for D_2O-moderated reactors cooled by H_2O and, in general, has been considered very difficult, if not impossible, with natural-uranium fuel. The design described in the reference is unusual in that it uses quite massive fuel elements and a high fuel-to-moderator ratio. This entails the penalties of low specific power and reduced reactivity lifetime, but these penalties appear to be tolerable in the economics of the very large reactor system.

Table IX-1 COMPARISON OF DESIGNS FOR 500-Mw(e) LIQUID-D_2O-COOLED REACTORS*[11]

	Canadian (AECL-1730)[10]	Du Pont (DP-830)[8]	AEPSC-GNEC (NP-12344)[9]
General			
Gross thermal output, Mw(t)	1570	1838	1850
Net electrical output, Mw(e)	491	491	489
Net thermal efficiency, %	31.3	26.7	26.4
Total D_2O inventory, metric tons	350	325	390
Refueling method	On-line	Shutdown	On-line
Primary coolant system			
Design pressure, psia	1830	1730	1760
Coolant inlet temperature, °C	266	260	257
Coolant outlet temperature, °C	310	310	302
Coolant flow rate, gal/min	122,000	138,000	128,000
Maximum coolant velocity, ft/sec	30	30	40
Fuel			
Fuel material	UO_2	UO_2	UO_2
Fuel cladding	Zircaloy	Zircaloy	Zircaloy–2.5% Nb
Fuel configuration	Solid rods	Coaxial tubes	Hollow rods
Fuel bundle length, ft	1.7	15	4.5
Concentration of U^{235}, %	0.71	1.19	1.41†
Average fuel burnup, Mwd/metric ton of U	8680	14,000	19,700
Number of fuel positions	387	226	560
Core fuel inventory, metric tons of U	95.7	27.1	51.4
Reactor core			
Pressure-tube concept	Hot	Cold	Cold
Core length (including reflector), ft	21.4	19	20
Reactor diameter (including reflector), ft	~23.9	18	22
Control method	Rods	Rods	Ball columns
Number of control positions	16	23	187
Pressure-tube inside diameter, in.	4.0	4.4	3.5
Maximum heat flux, Btu/(hr)(sq ft)	330,000	850,000	620,000
Average specific power, Mw/metric ton of U	16	68	36
Mw/metric ton of total D_2O	4.5	5.2	4.8
D_2O moderator inventory, metric tons	265	163	242
Turbine plant			
Throttle steam pressure, psia	762	522	540
Throttle steam temperature, °C	265	245	246
Type of steam cycle	Reheat	Nonreheat	Nonreheat
Feedwater return temperature, °C	182	200	188
Condenser pressure, in. Hg	1.0(?)	1.5	1.5
Gross cycle efficiency, %	34.6	30.0	28.4

*Basic numbers are from Refs. 8 to 10. However, the AECL numbers, where appropriate, have been adjusted upward from the 457-Mw(e) output of Ref. 10 to the 491-Mw(e) value appropriate for this comparison.

†Optional operation to 5000 Mwd/metric ton of U possible with natural uranium.

elements in 19-rod bundles. Some of the significant items are the following:

1. Although the important coolant temperatures are not greatly different in the Canadian and U. S. designs, the thermal efficiency of the Canadian plant is substantially higher, with the result that the U. S. designs generate some 18% more thermal power for a given electrical output. The higher thermal efficiency appears to result from a slightly lower condenser pressure, the use of a reheat steam cycle, and the use of U-tube U-shell steam generators that do not restrict the temperature of the generated steam to a value less than the coolant inlet temperature to the reactor. The latter point is illustrated in Fig. IX-1. The U-tube U-shell generators are avoided in the U. S. design studies because of their estimated high capital cost.

2. The Canadian designs use a larger quantity of heavy water in the reactor tank—part of it to afford a generous 2-ft reflector—but they use a much smaller quantity of heavy water in the external coolant system to reach a total that is intermediate between that for the Du Pont and the AEPSC-GNEC designs (Table IX-1). The low external inventory results from the use of the counterflow coolant arrangement in adjacent pressure tubes, illustrated in Fig. IX-2,

which eliminates the need for return lines from one end of the reactor to the other, and apparently also from a design approach that weights very heavily the considerations of minimizing the external D_2O inventory. This approach is illustrated in Fig. IX-3, showing a bank of pumps and steam generators for the 200-Mw(e) CANDU reactor (the reactor for the Douglas Point Station). The unit shown in the figure, comprised of five pumps and four steam generators, each of the latter utilizing 10 vertical U-tube heat exchangers, serves one end of the reactor and is duplicated at the other end. The holdup of D_2O in headers and other parasitic volumes is comparatively small. Again, U. S. practice would indicate a smaller number of larger units on capital cost considerations.

3. The Canadian design produces more power per unit length of fuel element than does the U. S. design (AEPSC-GNEC) that utilizes fuel assemblies of the same (rod bundle) type. Primarily this is the result of a flatter power distribution in the Canadian reactor (apparently a maximum-to-average ratio of 1.5 vs. 2.6 in the U. S. design). The immediate reasons for the excellent power flattening achieved in the Canadian design are primarily the thick reflector and the bidirectional push-through scheme of fuel reloading. The latter is illustrated in Fig. IX-4. There is, however, a more fundamental reason why better power flattening can be achieved in a reactor designed for relatively low fuel burnup than in one designed for high fuel burnup.

Table IX-2 CAPITAL AND FUEL COST ESTIMATES FOR 500-Mw(e) LIQUID-D_2O-COOLED REACTORS[11]

	Canadian (AECL-1730)[10]	Du Pont (DP-830)[8]	AEPSC-GNEC (NP-12344)[9]
Capital costs [all costs are in millions of U. S. dollars and apply to single units of 500 Mw(e) capacity]			
Land and land rights		0.4	0.4
Structure and improvements		6.0	12.1
Reactor plant equipment		21.7	37.2
Turbine-generator equipment		27.8	25.2
Total direct cost	55.0	55.9	74.9
Indirect costs (including contingency)	36.7	29.9	27.0
Total construction cost	91.7*	85.8	101.9
Total construction cost, $/kw(e)	202	175	208
D_2O inventory at $20/lb	14.3	15.4	17.2
Total plant cost	106.0	101.2	119.1
Total plant cost, $/kw(e)	232	206	244
Fuel characteristics			
Fuel material	UO_2	UO_2	UO_2
Fuel shape	Rod	Tube	Hollow rod
Cladding	Zircaloy	Zircaloy	Zircaloy–2.5% niobium
Fabrication method	Pelletizing	Mechanical compaction	Pelletizing
Concentration of U^{235}, %	0.715	1.19	1.41
Average exposure, Mwd/metric ton of U	8680	14,000	19,700
Fuel-cycle costs, $/kg of U†			
Conversion and fabrication		21.60	71.44
Shipping (fresh and spent fuel)		2.50	19.01
Depletion of U^{235}		66.10	88.12
Reprocessing		26.08	28.88
Use of U^{235}		3.21	7.23
Net plutonium credit		(36.43)	(46.35)
Other		1.19	
Total, $/kg of U	52‡	84	168
Total, mills/kw-hr	0.80	0.94	1.35

*For a 454-Mw(e) plant.

†Costs tabulated under "Du Pont" and "AEPSC-GNEC" are for U. S. Government ownership of fuel; the AEPSC-GNEC estimate of total fuel cost under private ownership is 1.29 mills/kw-hr.

‡Throwaway fuel cycle.

In uranium-cycle reactors with reasonably high conversion ratios, the initial effect of fuel exposure is to increase the macroscopic fission cross section, because the macroscopic fission cross section of Pu^{239} is considerably higher than that of U^{235}. This usually occurs even though the reactivity may be decreasing because of the lower η of Pu^{239} and the buildup of fission products. In such reactors the macroscopic fission cross section of the fuel will go through a maximum as exposure continues and as the Pu^{239} content approaches an equilibrium value, and it will eventually decrease to a value far below its initial value. Until the fission cross section decreases below its initial value, power flattening by appropriate fuel shuffling or incremental reloading procedures may be very effective. However, when a reactor contains old fuel with substantially decreased fission cross section, the best the fuel-shuffling program can do is to flatten the neutron-flux distribution; it cannot make the old fuel bundles produce as much power, on the average, as the new ones.

At a given conversion ratio, this effect is more pronounced in low-enrichment reactors (e.g., the heavy-water reactors) than in the reactors that inherently use higher enrichment (e.g., the light-water reactors), simply because the fractional burnup of fissile isotope, for a given exposure in megawatt-days per ton, is larger in the low-enrichment reactor. The effect is felt rather strongly in the AEPSC-GNEC design.

The other effect of high-burnup fuel on power distribution occurs in the initial period of operation: not only is the initial fuel composition far different from that which characterizes the final equilibrium reloading cycle, but the nonequilibrium period lasts so long that compromises in either fuel or reactor performance during that period are quite expensive. The designer must then solve the double problem of finding a favorable equilibrium power dis-

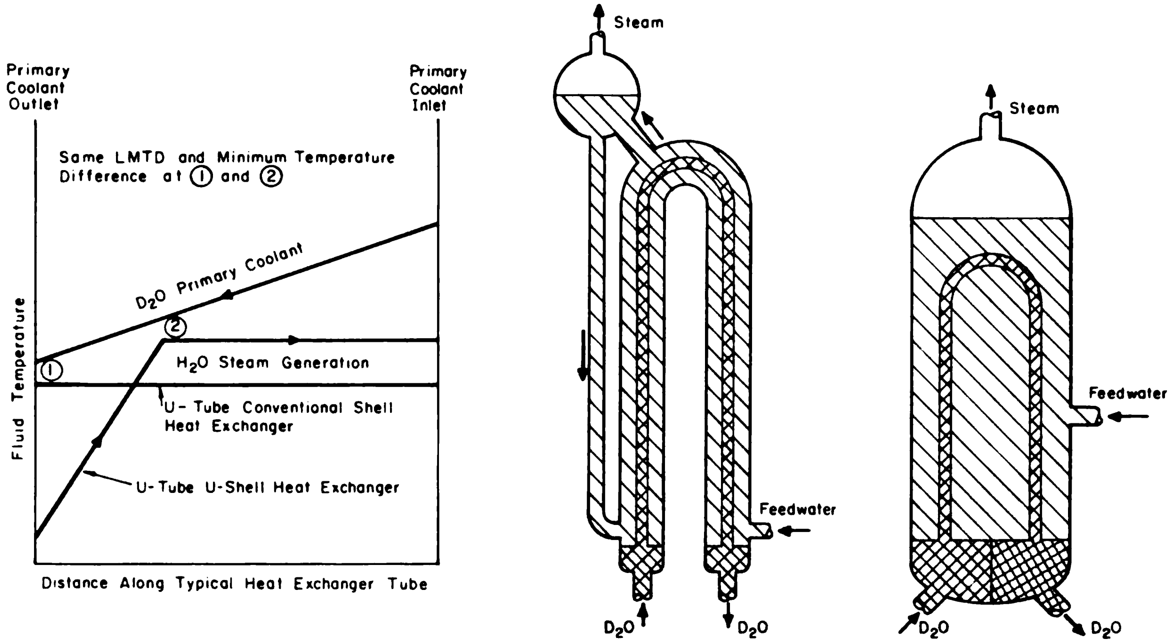
Primary Coolant Outlet
Primary Coolant Inlet
Same LMTD and Minimum Temperature Difference at ① and ②
D_2O Primary Coolant
②
①
H_2O Steam Generation
U-Tube Conventional Shell Heat Exchanger
U-Tube U-Shell Heat Exchanger
Fluid Temperature
Distance Along Typical Heat Exchanger Tube
Steam
Feedwater
D_2O
D_2O
Steam
Feedwater
D_2O
D_2O

Comparison of Temperatures

U-Tube U-Shell Heat Exchanger

U-Tube, Conventional-Shell Heat Exchanger

Fig. IX-1 Comparison of U-tube U-shell and U-tube conventional-shell heat exchanger. The U-shell design produces hotter steam principally because of the countercurrent flow in the feedwater—D_2O-outlet leg of the U: this countercurrent flow, in conjunction with a low feedwater inlet temperature, is used to cause the point of minimum temperature difference to occur where the D_2O temperature is relatively high.

tribution and of establishing that distribution without creating a less favorable distribution during the nonequilibrium period.

The Canadian design (relative to the AEPSC-GNEC design) utilizes much more massive fuel elements, with a consequent reduction in fabrication cost per pound of uranium. Partly this results from several of the points discussed above. The high value of average power per unit length of fuel element, along with the low cost of the natural-uranium fuel, allows the use of massive elements without an important penalty in fuel inventory charges. At the same time, the economical use of D_2O in the external circuit gives a reasonably high value of specific power relative to total D_2O, despite the fact that a low specific power relative to fuel implies also a low specific power relative to that D_2O which is in the reactor tank.

The use of the large fuel rods results also from Canadian developments directed specifically toward the problems of fuel bundles for heavy-water reactors. The fundamental difference between fuel designed for this application and fuel designed for the typical U. S. light-water reactors is that space for fission-gas accumulation cannot be provided in the heavy-water case without incurring an undesirable power peaking due to the end-peaking or Wilkins effect. Much of the Canadian fuel research has been directed toward the understanding of the behavior of fission gases in oxide fuel elements, and presumably these developments, along with the relatively low burnup of the fuel, are factored into the Canadian design. The elements specified in Ref. 10 (diameter, 0.74 in.), are considerably larger than the 0.60-in. elements specified for the CANDU reactor. In contrast to this rather massive design, the U. S. design utilizes a smaller element, with a central hole that serves the dual purpose of reducing the maximum oxide temperature and providing a space for the fission gases that may be released (Fig. IX-5).

The other U. S. design, produced by the Du Pont group, utilizes the Savannah River fuel-element approach that has been under development for some time. The massive full-length fuel elements consist of coaxial Zircaloy-clad tubes of uranium oxide (Fig. IX-6). They are fabricated by pouring fused uranium oxide powder into prefabricated Zircaloy sheaths, consolidating the powder by vibratory compaction, and swaging the composite tube over a mandrel to increase the oxide density above 90% of theoretical. At the present time the di-

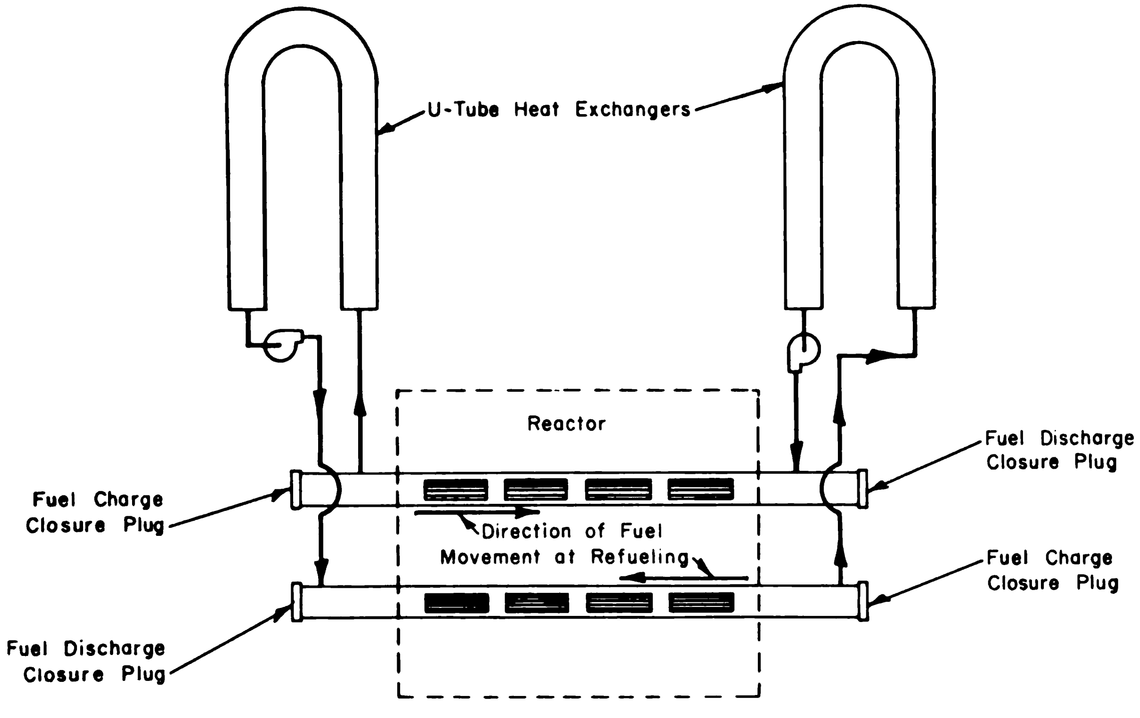
U-Tube Heat Exchangers
Reactor
Fuel Charge Closure Plug
Fuel Discharge Closure Plug
Direction of Fuel Movement at Refueling
Fuel Discharge Closure Plug
Fuel Charge Closure Plug

Fig. IX-2 Coolant-flow paths and fuel movement directions, CANDU reactor.

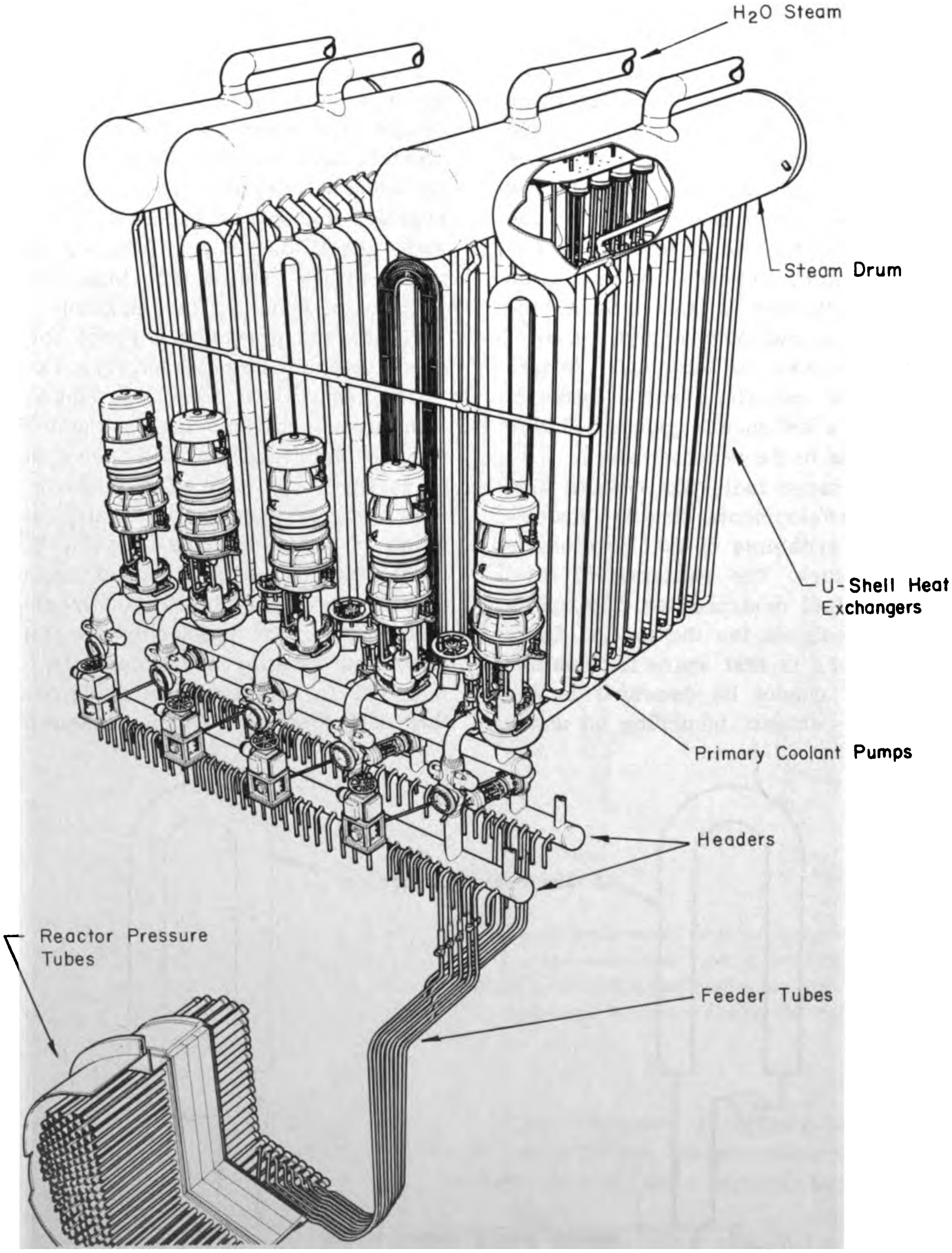

Fig. IX-3 CANDU boiler and circulating pump arrangement.[7] This bank of equipment serves one end of the reactor, and an identical bank serves the other end. The D_2O primary coolant passes through the tubes of the heat exchangers. The headers are 16 in. in outside diameter by 32 ft long, with 1.5-in. walls. The feeder tubes are of four sizes, $1\frac{1}{4}$, $1\frac{1}{2}$, 2, and $2\frac{1}{2}$ in. (normal), according to the coolant-flow requirements of the pressure tubes served.

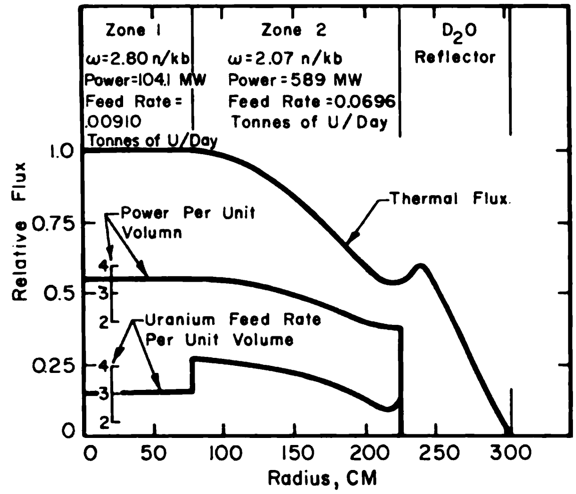

Fig. IX-4 Radial flux, power, and fuel feed distributions in CANDU.[7] Here ω is the discharge fuel exposure in neutrons per kilobarn; nvt = (neutrons/kilobarn)(10^{21}).

rect development effort on heavy-water power reactors in the U. S. consists largely of the development and testing of the tubular fuel elements, in both metal and oxide versions, at Savannah River. Some irradiation tests have been made in the Vallecitos Boiling-Water Reactor, but currently all testing is being done in the Heavy-Water Components Test Reactor (HWCTR),[15] which was constructed primarily for the development of fuel elements for heavy-water reactors. The status of elements currently under test is summarized in Table IX-3. The experience to date has been encouraging for the tubular elements containing oxide of relatively high density, but failures have been experienced in elements containing oxide in the 83% of theoretical density range. The following quotation is from Ref. 16:

> By the end of June, the maximum exposure attained by any of the fuel elements in the HWCTR was 7400 MWD/ton U in oxide tubes that were operating at a maximum $\int k\,dt$ of 22 watts/cm. However, fuel testing in HWCTR during the May-June period was interrupted three times by failures of oxide fuel assemblies. The cause of these failures has not yet been determined. Information available while this report was in preparation indicates that the failures were due to the collapse (under the hydraulic pressure of the coolant— 1200 psi max.) of the outer sheathing of Zircaloy. The failures occurred only in fuel tubes that were filled with UO_2 having a density of about 83% of theoretical; oxide of 88% density gave sufficient support to the cladding that failure has not occurred. The first failure, which occurred during a power ascension on May 31, was in an assembly of eight short oxide tubes, the hottest of which had operated at a maximum $\int k\,dt$ of 50 watts/cm to a maximum exposure of about 3000 MWD/ton U. Another failure of this type of UO_2 element had occurred on April 3 shortly after a reactor shutdown. The other full-length oxide tubes failed during subsequent reactor operation: one during a startup, the other during normal operation. These latter tubes had operated at a maximum $\int k\,dt$ of 28 watts/cm and had attained maximum exposures of 4800 and 5600 MWD/ton U.

Reference 16 also describes a new vibrator that has been installed at the Savannah River Laboratory. It is expected to facilitate the attainment of high oxide density, as well as to make possible the fabrication of larger elements.

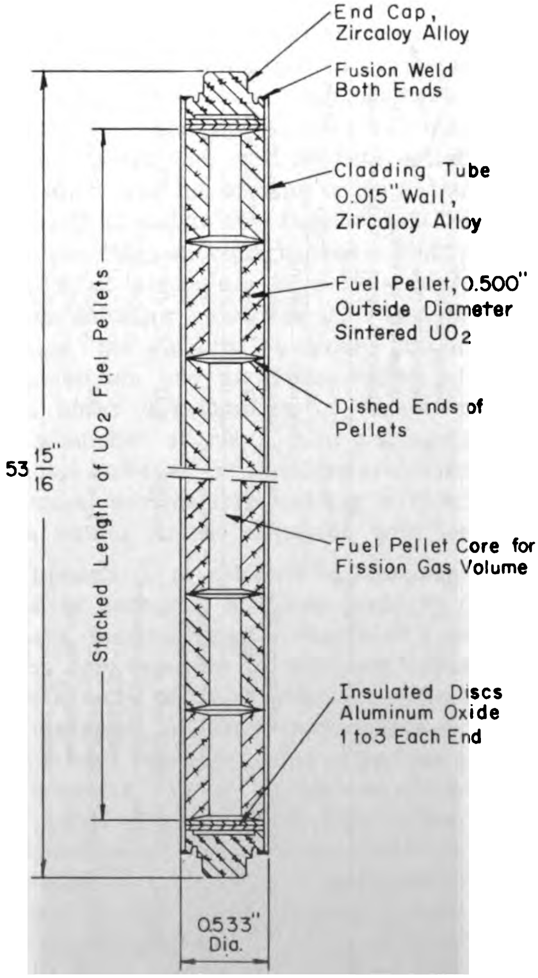

Fig. IX-5 Details of the fuel rod in the AEPSC-GNEC design.[9]

Table IX-3 FUEL IRRADIATION TESTS IN THE HWCTR,[16] JUNE 1963[*]

Reactor power	36 Mw
Coolant pressure	1200 psig
Coolant inlet temperature	238°C
Moderator outlet temperature	249.5°C

					Maximum nominal conditions								Maximum exposure,[‡] Mwd/ton of U	
Position	Element number	Fuel type	Fuel assembly description	Starting date	Assembly power,[†] Mw	Specific power,[‡] Mw/ton of U	Heat flux, pcu/(hr)(sq ft)	Outlet temp., °C	Surface temp., °C	Core-cladding temp., °C	Core temp., °C	$\int k\,dt$, watts/cm	Attained	Planned
37	CANDU	Oxide rod	Five 19-rod bundles of natural UO_2 pellets	10-5-62	0.83	21	117,000	262	270	289	1,250	25	2,908	9,000
38[§]	OT-3-2	Oxide tube	Single tube of vibratory-compacted natural UO_2	5-19-63	0.41	40	178,000	256	286	340	800	15	543	[§]
39	2ETWO-2	Metal tube	Unalloyed, 2.1% enriched, 2-in. OD, single tube	5-19-63	1.01	80	459,000	252	306[¶]	424	491		1,170	8,000
40	SOT-1-2	Oxide tube	Eight 14-in.-long tubes of 1.5% enriched UO_2	10-5-62	0.49	57	274,000	246	292	371	1,100	22	7,418	23,000
42	2ETWO-3	Metal tube	Same as position 39	6-11-63	0.96	76	436,000	251	306	418	482		533	10,000
55	SOT-5-2	Oxide tube	Eight 14-in. tubes of natural UO_2; 4 swaged, 4 vibratory compacted	5-19-63	0.48	31	292,000	249	300	393	2,030	46	457	6,000
56	SOT-1-3	Oxide tube	Same as position 40	1-6-63	0.47	53	253,000	246	288	361	1,060	21	5,665	10,000
57	SMT-1-2	Metal tube	Ten $11\frac{1}{4}$-in. alloyed (Fe,Al) natural-U tubes	5-19-63	0.47	29	249,000	250	301	357	408		436	7,500
58	OT-1-5	Oxide tube	Single tube of vibratory-compacted 1.5% enriched UO_2	1-6-63	0.60	57	262,000	248	291	367	1,120	22	5,656	23,000
59	OT-1-3	Oxide tube	Single tube of vibratory- and swage-compacted 1.5% enriched UO_2	[**]	0.64	55	275,000	249	294	376	1,120	22	4,832	5,000
60	OT-1-2	Oxide tube	Same as position 59	10-5-62[††]	0.59	51	254,000	248	287	363	1,060	21	7,041	11,000

[*] Data taken on June 18, 1963; exposures as of June 31, 1963.

[†] Based on ΔT and flow calculations; does not include gamma heating of moderator.

[‡] Based on an assembly power that includes gamma heating of moderator (1.09 times the power based on ΔT and flow calculations).

[§] Liquid loop position. The OT-3-2 fuel element is being used to commission the loop; this is not an irradiation test of fuel.

[¶] Temperature limited by surface boiling.

[**] Starting date 1-6-63; discharged 4-3-63; recharged 6-6-63; failed 6-20-63.

[††] Irradiated from 10-5-62 to 6-7-63 in position 42; moved to position 60 on 6-11-63.

The typical reactor design prepared by the Du Pont group[8] differs quite markedly from the typical Canadian designs (Table IX-1). The use of tubular elements rather than rod bundles and the use of slightly enriched rather than natural uranium lead to quite high specific power relative to the fuel and relative to the D_2O in the reactor because of the favorable geometry of the fuel for heat removal and the relatively thin oxide sections that were used. In the Du Pont design, on-power refueling is not used. Partial core reloading is contemplated, and radial power flattening is achieved by using higher average fuel exposures (or lower enrichments) near the center rather than near the edge of the reactor.

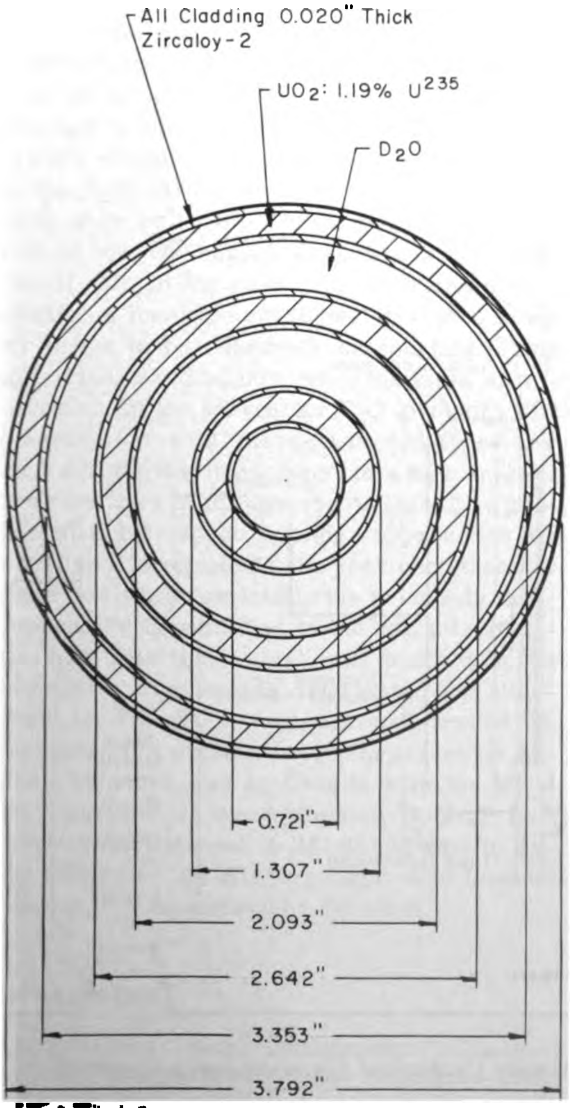

Fig. IX-6 Du Pont fuel element.

Organic-Cooled Heavy-Water Reactors

It must, of course, be recognized that the organic-cooled system has not reached nearly the same stage of development as the liquid-D_2O-cooled system. The problem of organic fouling of fuel elements is well known. Recent results indicate that the problem may be controlled by careful attention to the initial cleanup of the system, control of the halogen (chlorine) content of the coolant,[11] and suitable filtration. Fuel elements suitable for the desired operating temperatures have not been demonstrated, although the possibilities of utilizing carbide fuels, or even metallic uranium, offer some promises of nuclear and thermal performance which are absent in the aqueous-coolant cases; however, the area of uncertainty in the development of a usable fuel element lies not in the fuel material but in the cladding material. Also, a pressure-tube design has not been proved. In both of these problems a key question is whether zirconium will operate satisfactorily in contact with hot organic in the reactor environment. Canadian investigations of this question have been encouraging but are not yet conclusive. If zirconium or a low-cross-section zirconium alloy cannot be used in these applications, the sintered aluminum product (SAP) of aluminum and aluminum oxide, which has been under development for organic reactors for a number of years, provides another possibility; however, it presents problems of fabrication, particularly welding problems, and is a rather brittle material, with less high-

Although it is difficult to compare the results of economic analyses made by different groups, the comparative results of a particular group for reactors of different types should have a more straightforward interpretation. It is, therefore, the more striking that the groups which have recently looked at various advanced heavy-water reactor types have all estimated the lowest power-generation costs for the organic-cooled type. These results are listed in Table IX-4. This list includes the results of studies[17] on the organic-cooled type by Combustion Engineering, Inc., under ground rules identical to those used earlier by the AEPSC-GNEC group for studies of the D_2O-cooled and gas-cooled types.

Table IX-4 ESTIMATED FUEL CYCLE AND POWER COSTS FOR SINGLE-REACTOR PLANTS IN THE 450- to 500-Mw(e) RANGE, UTILIZING D_2O-MODERATED REACTORS WITH VARIOUS COOLANTS

Reactor coolant	Estimating group	Type of financing	Fuel	Fuel-cycle cost, mills/kw-hr	Total energy cost, mills/kw-hr
Liquid D_2O	Du Pont[8]	Private plant, AEC fuel ownership	Enriched uranium	0.94	5.79
Boiling D_2O				0.68	5.94
H_2O fog				0.68	5.65
Organic				0.69	5.02
Liquid D_2O	AEPSC-GNEC*[9]	Private plant, private fuel ownership	Enriched uranium	1.29	6.94
Boiling D_2O				1.09	6.84
CO_2 gas				1.66	9.08
Organic	Combustion Engineering*[17]	Private plant, private fuel ownership	Enriched uranium	0.72	5.50
Liquid D_2O	AECL[10]	Canadian utility	Natural uranium	0.80	3.86
H_2O fog				0.86	3.89
Boiling H_2O				0.69	3.77
Organic				0.42	3.45

*These two studies used identical ground rules.

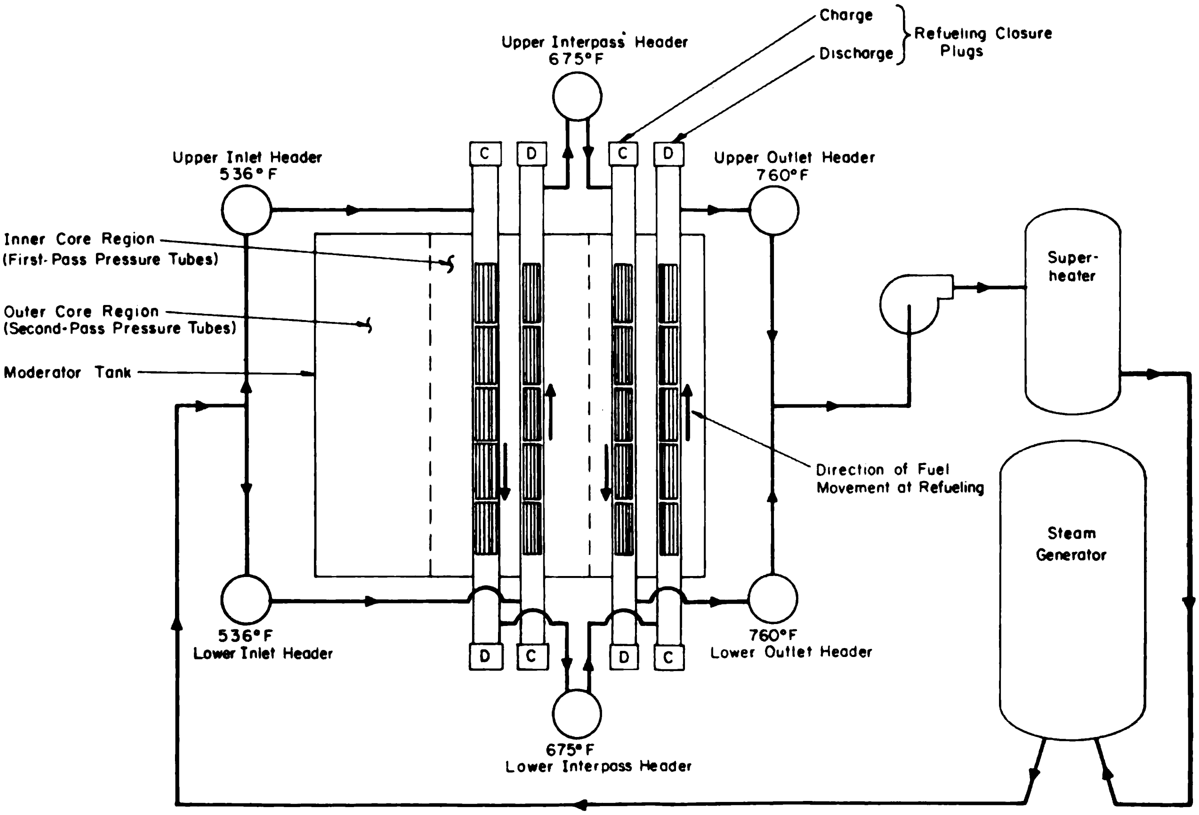

Fig. IX-7 Coolant-flow paths and fuel movement directions, Combustion Engineering organic-cooled reactor.

temperature strength than would be desirable. The organic-cooled design studies that have served as the basis for the economic evaluations discussed here have all utilized SAP-clad fuel elements. All of them have had also, either as the reference design or as a backup design, composite pressure tubes that, in one way or another, place SAP in contact with the organic but utilize Zircaloy for its strength properties and low neutron absorption.

It is hardly surprising that the organic coolant appears attractive in this application, for the low-vapor-pressure characteristic of the organic is particularly attractive in the pressure-tube concept. The use of a separate nonorganic moderator reduces the rate of organic decomposition to a fraction of that experienced in a reactor that is both moderated and cooled by an organic liquid. Further, as discussed above in connection with the D_2O-cooled reactors, the traditional approach of attempting to improve economic performance through working the fuel harder and increasing the specific power may well yield limited returns when applied to low-enrichment D_2O-moderated reactors. If this is the case, the well-known deficiencies of the organics as heat-transfer fluids may prove to be relatively unimportant in this application, particularly since their use eliminates most of the ex-reactor D_2O inventory that is associated with the D_2O-cooled types and thus reduces the importance of a high specific power relative to the in-reactor D_2O. It is possible also that specific design approaches can be utilized to minimize the poor heat-transfer properties while exploiting the relatively high-temperature capabilities of the coolant. An approach of this type, which was utilized in the Combustion Engineering design study, is illustrated in Fig. IX-7. Serious work toward the development of organic-cooled heavy-water reactors is under way in Canada with the WR-1 Test Reactor[18] at the Whiteshell Nuclear Research Establishment in Manitoba, and in Europe under the ORGEL (Organique-Eau Lourde) program,[19-21] sponsored by Euratom.

References

1. U. S. Atomic Energy Commission, Civilian Nuclear Power, a Report to the President—1962, Nov. 20, 1962.
2. Nuclear Canada Issue of *Nucleonics*, 18(10): (October 1960).
3. Nucleonics Reactor File... No. 13, NPD on the Line, *Nucleonics*, 20(11): 47 (November 1962).
4. I. N. MacKay, General Description of Nuclear Power Demonstration Plant, paper presented at the Winter Meeting of the American Nuclear Society, Washington, D. C., November 1962 (and other papers on NPD details presented at the same session).
5. L. G. McConnell, Commissioning and Initial Operation of NPD, The Eighth AECL Symposium on Atomic Power, Held at Chalk River, Ontario, Sept. 24, 1962, Canadian Report AECL-1599, pp. 40-42, September 1962, (This report also contains papers on NPD development and construction.)
6. D. L. S. Bate, Status Report on the Douglas Point Project, The Eighth AECL Symposium on Atomic Power, Held at Chalk River, Ontario, Sept. 24, 1962, Canadian Report AECL-1599, pp. 54-68, September 1962.
7. Atomic Energy of Canada Ltd., Douglas Point Nuclear Generating Station, Canadian Report AECL-1596.
8. D. F. Babcock, R. R. Hood, L. Isakoff, J. C. Jensen, D. S. St. John, and J. W. Wade, An Evaluation of Heavy-Water-Moderated Power Reactors, Status Report as of March 1963, USAEC Report DP-830, Savannah River Laboratory, June 1963.
9. American Electric Power Service Corp. and General Nuclear Engineering Corp., East Central Nuclear Group Inc. Heavy Water Moderated Reactors Evaluation Study, Report NP-12344, Oct. 15, 1962, in three volumes: I, Summary and Conclusions; II, Design Bases and Plant Comparisons; III, Plant Designs.
10. Atomic Energy of Canada Ltd., Power Reactor Development Evaluation, A Summary Report by a Committee of AECL Staff, Canadian Report AECL-1730, May 1, 1963.
11. D. G. Boyer and D. P. Dunlop, USAEC/AECL Review of Heavy Water Reactor Evaluation Studies, Minutes of Meeting Held at Toronto, Ontario, May 23–24, 1963.
12. Irving Spiewak, A Large Desalinization Reactor Based on Current Technology, *Nucleonics*, 21(7): 64 (July 1963).
13. Sargent & Lundy, Saline Water Conversion Power Reactor Plants, USAEC Report SL-1998, Jan. 11, 1963.
14. Bechtel Corp., Large Reactor Study for Sea Water Distillation. Final Report, USAEC Report TID-19267, July 1963.
15. L. M. Arnett, D. Randall, C. P. Ross, B. C. Rusche, and C. D. Taylor, Final Hazards Evaluation of the Heavy Water Components Test Reactor (HWCTR), USAEC Report DP-600, Savannah River Laboratory, December 1962.
16. R. R. Hood and L. Isakoff (Comps.), Heavy Water Moderated Power Reactors Progress Report,

May-June 1963, USAEC Report DP-855, Savannah River Laboratory, August 1963.

17. Combustion Engineering, Inc., March 1963. (Unpublished)

18. F. W. Gilbert, WR-1 Fits Organic Coolant to Canadian Program, *Can. Nucl. Tech.*, 2(2): 37 (Spring 1963).

19. J. C. Leny, ORGEL—A European Concept, *Nucl. Eng.*, 6(67): 508 (December 1961).

20. J. C. Leny, ORGEL: A European Power Reactor Design, *Trans. Am. Nucl. Soc.*, 5(1): 103 (June 1962).

21. J. C. Leny, ESSOR: Specific Test Reactor for the ORGEL Program, *Trans. Am. Nucl. Soc.*, 5(1): 104 (June 1962).

Section X

Power Reactor Technology

Unconventional Approaches

Design Study of Thermionic Nuclear Plant

A recent report[1] describes a feasibility study of a water-cooled thermionic nuclear power plant of the portable medium-power (PM) class, which was carried out for the Atomic Energy Commission by the Martin Co.

The major design criteria established before the beginning-of-life study were:[1]

(1) The plant is to have a net power output of 1000 kwe, 60-cycle 3-phase ac at 480 volts. The plant is to be of the preassembled type, meeting the air-transportability requirements of the C-130A aircraft (i.e., maximum size—8½ ft × 8½ × 30 ft; maximum weight—30,000 lb). In addition, the plant and modules are to be designed for minimum on-site erection and operating requirements.

(2) The reactor is to be cooled with either a natural or forced circulation water system.

(3) Thermionic converters are to be incorporated within the fuel elements. They are to be of the low temperature cesium plasma type, utilizing a refractory metal cathode that also serves as cladding for the fuel in each device.

(4) The reactor core is to be designed for a minimum of 10,000 fueled power hours.

(5) An air-cooled heat rejection system for minimum size and weight (air at 80°F maximum, −60°F minimum) is to be incorporated in the design.

(6) A theoretical analysis is to be conducted to determine plant nuclear, thermal, and electrical responses during startup, gradual load changes, and step transients.

The study included a cost analysis; however, this review will confine its attention to the reactor design features. Previous reviews in *Power Reactor Technology*, which covered only the principles of thermionic electric generation, may be found in 3(1): 6-14 and 3(3): 48-50. Reference 2 is a good discussion of general principles and is of more recent date.

A thermionic converter transforms nuclear heat directly into electricity without the intermediate step of conversion to mechanical energy. It accepts heat at a high temperature T (in a nuclear thermionic reactor, this heat is sup-

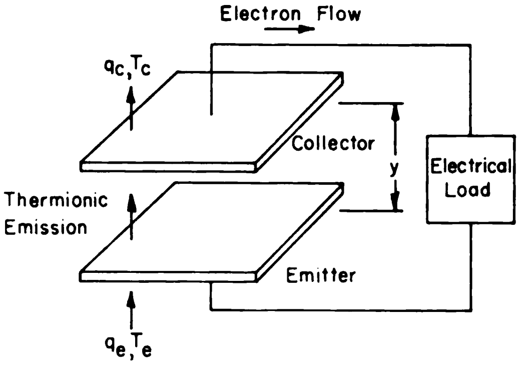

(a) Schematic of Thermionic Converter Diode.

q_e — Heat Rate from Nuclear Fuel Emitter.

T_e – Temperature of Emitter.

q_c – Heat Rate Rejected from Collector.

T_c – Temperature of Collector.

y – Interelectrode Spacing.

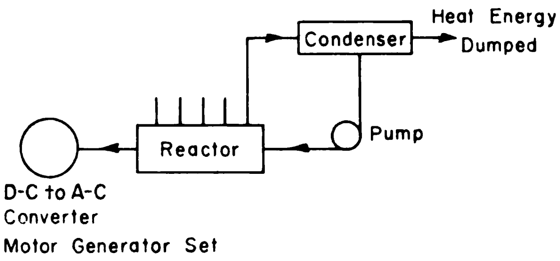

(b) BWR, Direct Cycle, Forced Circulation.

Fig. X-1 Schematic of nuclear thermionic converter.

plied by the fissioning fuel), rejects heat at a lower temperature T_c, and generates electric energy. It also performs according to the thermodynamic principles applicable to all heat cycles. The converter consists of two electrodes (part *a* of Fig. X-1), the emitter or cathode and the collector or anode. The emitter receives heat, q_e, and delivers electrons with positive kinetic energy. The emitted electrons cross the interelectrode spacing, y, to the collector, doing work against the electrical load and dissipating additional energy, which must be rejected as heat, in the collector. The characteristic space-charge barrier formed in the interelectrode spacing, which can place a severe limit on the current density, can be alleviated by reducing the spacing to a few microns and/or by the introduction of positive ions. The latter remedy is usually applied by filling the gap with an easily ionized gas (e.g., cesium) that becomes partially ionized by electron collisions.

The main characteristics of the reactor described in Ref. 1 are listed in Table X-1. All the electrical generation is by thermionic means. The heat rejection is by means of a forced-circulation boiling-water system in a direct

Table X-1 NUCLEAR THERMIONIC POWER PLANT: SUMMARY OF CONCEPTUAL DESIGN CHARACTERISTICS[1]

Overall performance data	
Thermal power, Mw(t)	16
Electric power, Mw(e), net	1
Core life, full-power hours	10,000
Design pressure, psia	150
Average core coolant temperature, °F	358
Core design characteristics	
Geometry	Right-circular cylinder (approximately)
Diameter, average, in.	40.2
Active length, in.	44
Overall length of fuel element, in.	48
Core structural material	Stainless steel
Fuel-element data	Cylindrical, series-connected diodes, UO_2-Mo fuel, Mo alloy electrodes, ZrO_2 insulator, stainless-steel sheath
Sheath outside diameter, in.	0.620
Sheath thickness, in.	0.015
Insulator (ZrO_2) thickness, in.	0.100
Collector thickness, in.	0.020
Plasma (Cs) gap thickness, in.	0.010
Emitter (fuel-pellet cladding) thickness, in.	0.020
Fuel-pellet diameter, unclad, in.	0.290
U^{235} loading, core total, kg	117
UO_2 concentration in fuel pellets, g/cm^3	
Central zone	1.7
End zones	4.3
Burnable poison-element data, cylindrical zirconium boride-zirconium	
Diameter of rods, in.	0.43
Number of rods	129
Boron (natural) loading per rod, g	1.85
Total boron (natural) loading, g	240
Reflector control data	
Number of drums	18
Diameter of drums, in.	6
Drum composition	
Poison facing material	Ag-In-Cd
Drum body	BeO
Nuclear worth of control drum system, %	
Cold	2.0
Hot	2.5
Nuclear worth of control fuel-bundle system, %	3.0
Average thermal core flux, initial, nv	7×10^{12}
Control requirements, %	
Cold-hot	0.5
Equilibrium poisons	1.5
Maximum poisons	0.3
Lifetime	1.0
Core heat-transfer and hydraulic characteristics	
Heat flux, Btu/(hr)(sq ft)	
Average	66,400
Maximum	197,200
DNB ratio	6.4
Exit quality, %	
Average	15
Hot channel	30
Reactor flow rate, lb/hr	403,000
Mass flow rate, lb/(hr)(sq ft)	234,000
Thermionic characteristics	
Electrical power density, watts/cm^2	4.0
Diode efficiency, %	10
Emitter temperature	
Average, °C	1450
Average, °F	2642
Maximum, °C	1500
Maximum, °F	2732
Collector temperature	
Average, °C	650
Average, °F	1202

cycle, i.e., steam from the reactor coolant is sent directly to an air-steam condenser (part *b* of Fig. X-1). The relatively low steam pressure is chosen on the basis of overall practicability and transportability, inasmuch as high pressure is not required for thermodynamic reasons.

The solid moderator (zirconium hydride) is used to minimize the temperature defect of reactivity and to minimize the variation of the

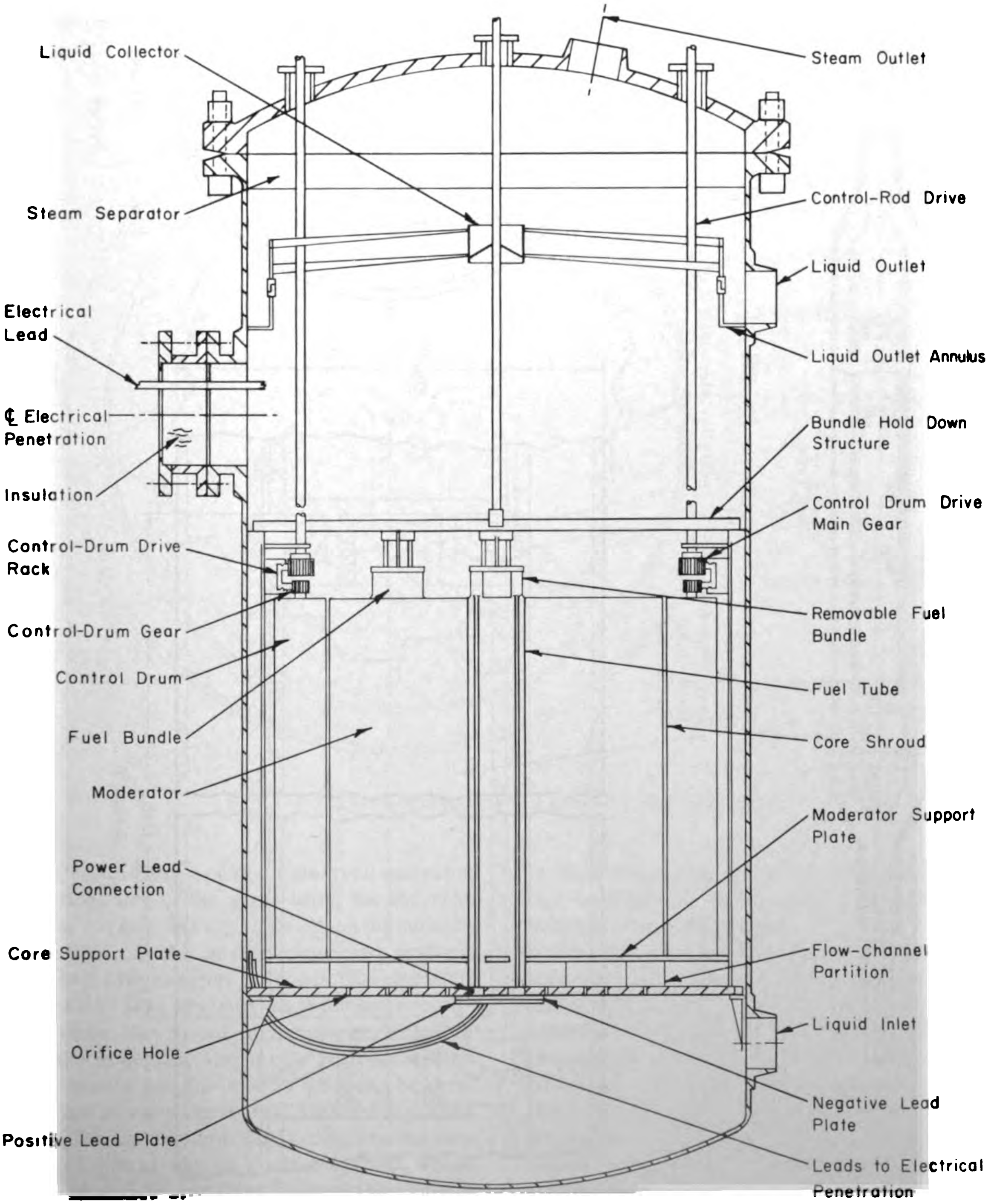

Fig. X-2 Pressure vessel and internals.[1]

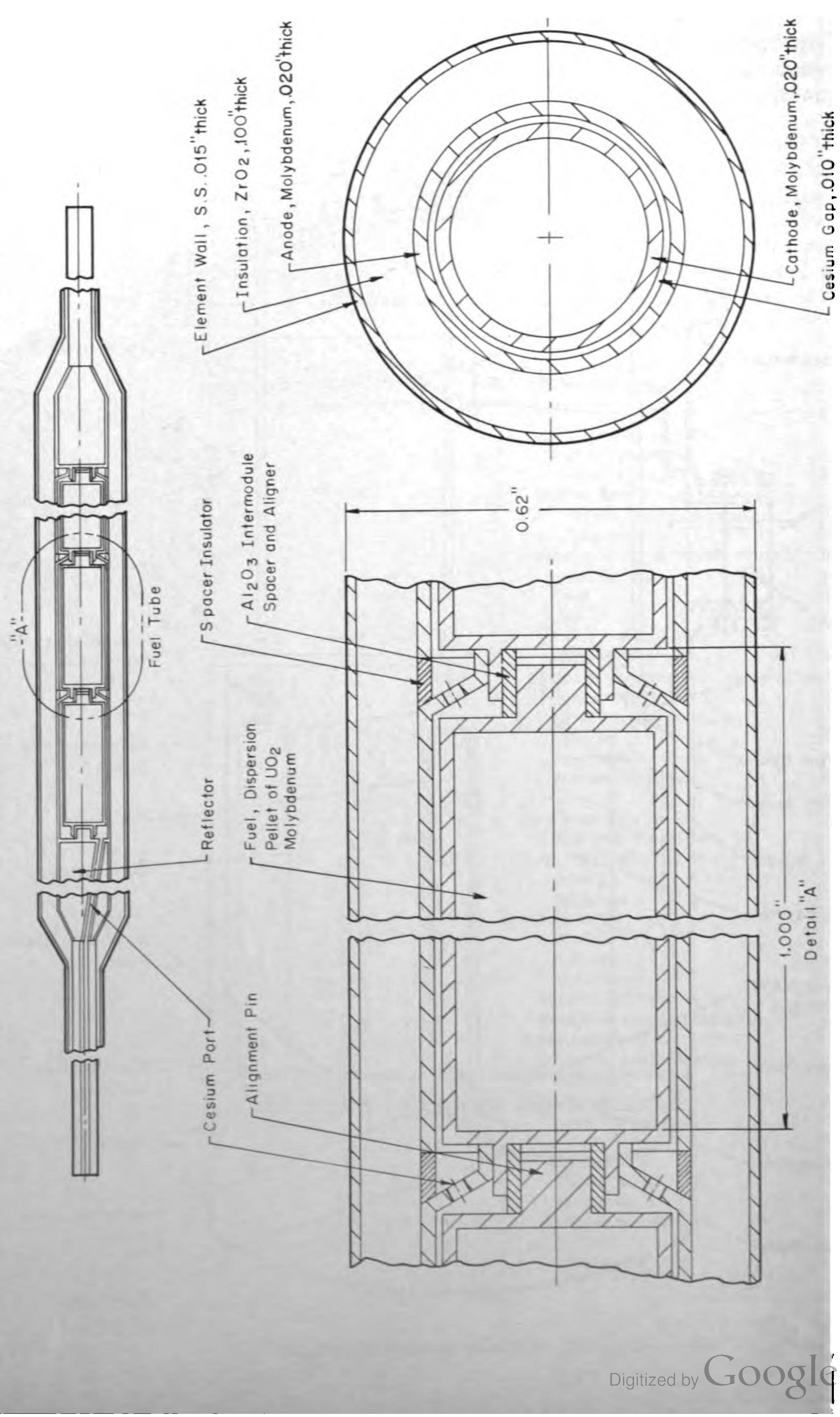
"A"
Fuel Tube
Cesium Port
Alignment Pin
Reflector
Fuel, Dispersion Pellet of UO_2 Molybdenum
Spacer Insulator
Al_2O_3 Intermodule Spacer and Aligner
Element Wall, S.S. .015" thick
Insulation, ZrO_2, .100" thick
Anode, Molybdenum, .020" thick
Cathode, Molybdenum, .020" thick
Cesium Gap, .010" thick
0.62"
1.000"
Detail "A"

Fig. X-3 Fuel element for thermionic nuclear power plant.[1]

spatial power distribution with power level. A spatial power distribution that stays constant with time, particularly in the axial direction, is highly desirable in this reactor type to obtain the best performance from the in-core thermionic diodes. As indicated in later paragraphs, the diodes in a given fuel element are connected in series electrically. The fission-heated cathodes of the diodes depend on electron emission for cooling, and, at the same time, the electron emission current density depends on the cathode temperature. In the series-connected system, the cooler, lower-power cathodes can choke off the "coolant" flow of electrons to the hotter cathodes unless the areas of the several diodes, which are in series, are carefully proportioned to compensate for the effect. This can be done only if the power distribution among the diodes remains nearly constant. This consideration also influenced the choice of control system, which utilizes rotatable absorbing drums in the reflector (along with burnable poison) for operating control and movable fuel bundles for shutdown.

The core and associated components of the reactor are contained within the pressure vessel (see Fig. X-2). The control-drive mechanisms are attached directly to the pressure-vessel head. The basic internal structure is the core barrel, which locates and supports the core, moderator, reflector, and additional structure. Appended to the bottom of the core barrel is the core support plate that transmits the entire load to the core support brackets integral with the pressure vessel.

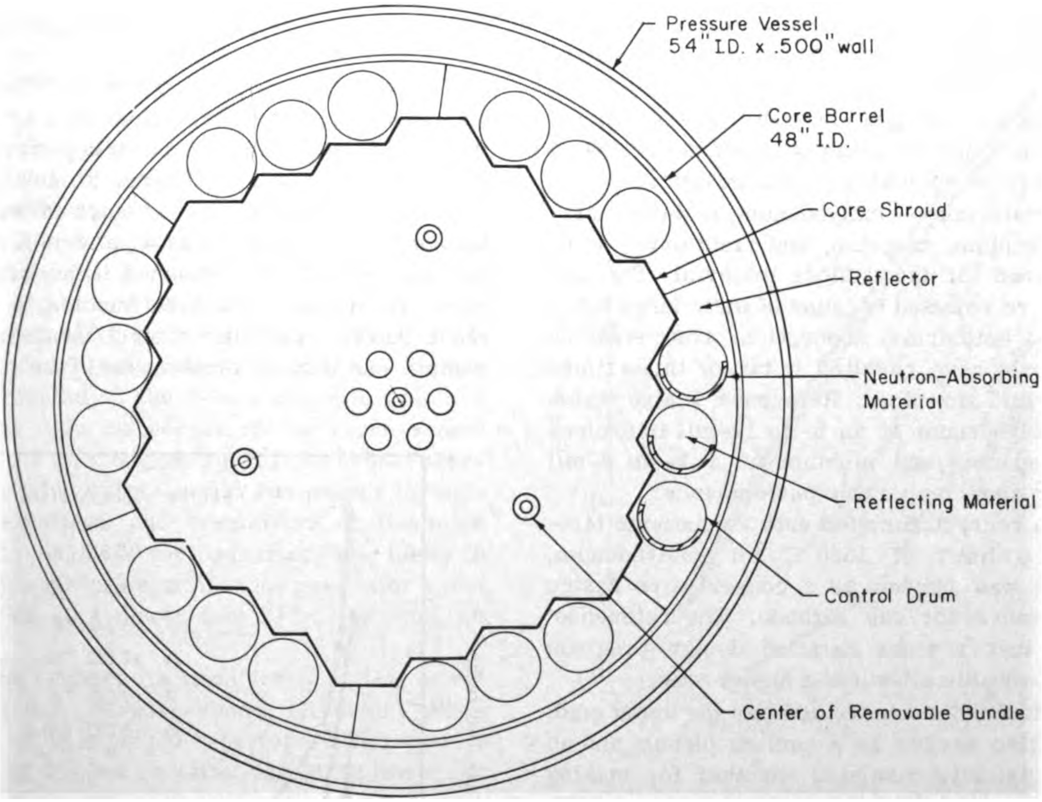

Fig. X-4 Cross-sectional view of pressure vessel and core.[1]

The construction of the fuel elements is shown in Fig. X-3. A dispersion pellet of UO_2-molybdenum serves as the fuel, and the molybdenum cladding serves as the emitter. A cesium gap separates the emitter from the molybdenum collector, which is electrically attached to the emitter of the adjacent fuel pellet. Outside the collector is a zirconium oxide sleeve enclosed by a stainless-steel tube. The zirconium oxide not only must isolate the collectors electrically from each other and the stainless-steel tube, but it must also provide a medium for conducting the collector heat to the stainless-steel tube and thence to the coolant. The diode collectors are separated by Al_2O_3 spacers that serve as electrical insulators. At the end of each fuel element is a reflector section composed of beryllium oxide. The current-conducting loads from the ends are made of molybdenum.

The UO_2-molybdenum cermet was chosen because of the good compatibility of UO_2 and molybdenum. In addition, molybdenum has a moderate neutron-capture cross section (relative to other possible materials) and good high-temperature strength. UO_2 was chosen in preference to other uranium compounds because of its proven performance characteristics.

Six materials — molybdenum, niobium, iridium, rhenium, tungsten, and tantalum — were considered for the cathode material. The last four were rejected because of their large thermal and epithermal absorption cross sections that would have resulted in two or three times higher fuel inventory. Reference 1 also states that molybdenum at an 8- to 12-mil interelectrode spacing and niobium at a 2- to 4-mil spacing give comparable performance.

Since recrystallization sets a maximum temperature limit of 1550°C for molybdenum, 1450°C was chosen as a conservative design temperature for the cathode. The reference[1] states that a more detailed design program would probably allow for a higher value.

The fuel tubes are welded into the upper grid, which also serves as a cesium plenum and as an electrically insulated chamber for making interelement electrical connections between the power-producing fuel elements. The cesium reservoir, supported several inches above the upper grid by three support rods, contains the cesium supply required by the thermionic diodes, which is carried from the top of the reservoir down to the upper grid by a tube. Each cesium reservoir contains a thermocouple, an electric heater, and the required electrical connections needed for control of the cesium pressure.

The lower end of each fuel element is formed into an electrical receptacle that mates with a banana plug that projects from, but is electrically insulated from, the core support plate. Each banana plug is electrically connected to one of two (positive and negative) lead plates attached below the core support plate. Two fuel elements, serially connected, form individual circuits. Thus one of the two serially connected fuel elements connects to one lead plate, and the other element connects to the electrically opposite lead plate. The lower ends of the elements in one cluster are bound together by a tube structure for rigidity. A spacer tube is inserted in the center of the cluster to distribute the coolant flow around the elements. These tubes will contain solid moderator or burnable poison. All the elements are separated from the spacer tube and from each other by spirally wound wire spacers located along the length of the elements.

The fuel elements are grouped in clusters of five. Seven clusters are joined in a triangular pattern to a hexagonally shaped upper grid. This grouping forms a fuel bundle. No lower grids are used; therefore the clusters of each fuel bundle can be lowered into a pattern of holes in the solid moderator designed to accommodate them. An array of 32 such bundles, a 34-element bundle, and four control bundles, which contain six instead of seven fuel tube clusters,

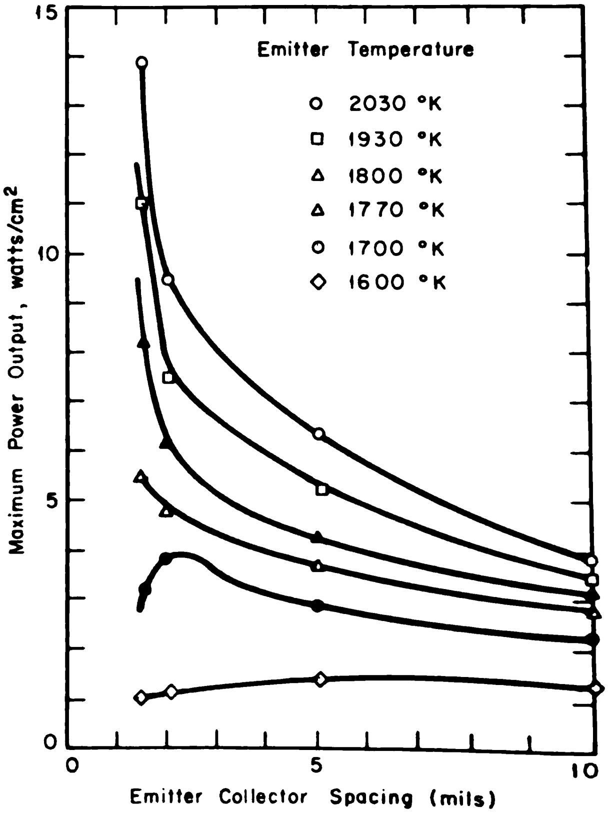

Fig. X-5 Optimum electric power density as a function of interelectrode spacing and emitter temperature.[2]

comprise the 1274-fuel-element core. The following is a summary of the fuel arrangement in the core.

Number of thermionic modules (diodes) per fuel element	44
Number of fuel elements per cluster	5
Number of seven-cluster fuel bundles (35 fuel elements)	32
Number of six-cluster fuel bundles (30 fuel elements)	4
Number of 34-fuel-element bundles	1
Total number of fuel elements	1274
Total number of fuel bundles	37

There is a positive and a negative lead plate for each fuel bundle. The 74 leads make a total of 37 individual circuits leaving the reactor, and each circuit nominally carries 1100 amp of direct current at 32 volts. The power leads from the lead plates are taken out along the bottom of the support plate to the pressure-vessel wall, and up the wall in a water-cooled aluminum bus that is located in the 2-in. annulus formed between the core barrel and the pressure-vessel wall, to the two insulated pressure-vessel penetrations. The water-cooled bus passes through the penetrations and terminates at the input terminals of the power converter. The latter is an acyclic motor – synchronous generator rated at 1350 kw (0.8 power factor) at 480 volts, 60 cycles.

Silicone rubber is used for a potting compound at the pressure-vessel electrical penetrations. It is expected to perform satisfactorily because of the low radiation level and low pressure.

Eighteen revolvable drums (see Fig. X-4) in the reflector provide control for operation and scram. These drums are ganged in sets of three so that one drive mechanism can control a set of three drums. The drums are made of either solid beryllium or cans of BeO, with a $\frac{1}{4}$- to $\frac{3}{8}$-in. thickness of Ag-Cd-In wrapped around 180° of the drum. The drums are located in reflector cutouts and are supported at the bottom by the moderator support plate and at the top by extensions from the core barrel.

General Thermionic Considerations

Reference 2 is a recent report on thermionic power generation which gives details of operating experience with practical thermionic converters as well as general principles. Figure X-5, from the reference, illustrates the sensitivity of the power output of a thermionic converter to the emitter-collector spacing, and Fig. X-6 illustrates comparisons between ideal converters and several thermionic converters developed to date. Above about 1800°K, for the case of a niobium emitter and a molybdenum

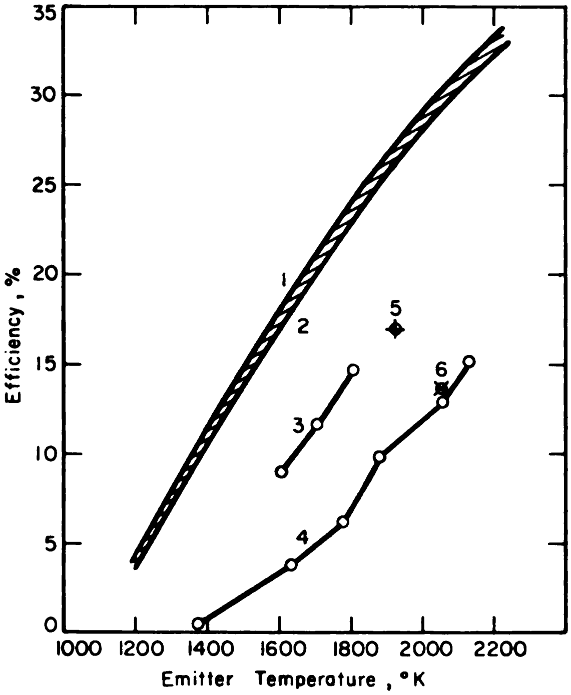

1. Efficiency of ideal converter including only radiation losses, emissivity 0.25
2. Efficiency of ideal converter including only radiation losses, emissivity 0.33
3. Calculated efficiency of molybdenum emitter converter, not including radiation from back of emitter — Thermo Electron Engineering Corp., private communication
4. Calculated efficiency of tungsten emitter converter, not including radiation from back of emitter — V. C. Wilson and J. Lawrence, General Electric Company Scientific Report No. 3, Contract AF 19-(694)-5472, August 1960
5. Measured efficiency of molybdenum emitter converter — N. S. Rasor, IAS Paper No. 61-72, January 1961
6. Measured efficiency of tantalum emitter converter — Thermo Electron Engineering Corp., private communication

Fig. X-6 Thermal efficiency of thermionic converters.[2]

collector, the maximum power output increases rapidly with decreasing interelectrode spacing (Fig. X-5), and the maintenance of small spacings has given rise to structural problems. The reference states that these problems currently limit the life of practical devices to about 1000 hr, but it expresses confidence that the structural problems will be solved after sufficient development work and that eventually the life of converters probably will be limited only by the corrosive effects of cesium and the evaporation of the emitter. The reference[2] also presents concepts of several thermionic nuclear reactors and discusses the following problems:

1. Diffusion of gaseous fission products into the cesium, and its effects on converter performance
2. Metallurgical compatibility of emitter and nuclear fuel materials
3. Extent and effects of distortion of emitter-clad fuel elements
4. Corrosive effect of cesium on electrode materials
5. Development of high-temperature electrical insulation metallurgically bondable to collector and structural materials

Thermoelectric Power Supply

Reference 3 gives a conceptual design for a 200-watt reactor-powered thermoelectric power supply for space applications. It employs an unshielded reactor that consists of a split sphere of pure U^{233} metal reflected by beryllium metal (Fig. X-7). U^{233} was chosen over U^{235} because of its considerably lower critical mass (giving a lower total weight), and it was chosen over plutonium because of its higher melting point. The core, which transfers its heat to the beryllium reflector and cooling radiator by conduction, operates with a central temperature of 764°C and at a thermal power of 5 kw, as required by the generator efficiency of 4%. Reactivity is controlled by varying the separation of the uranium hemispheres by means of the cleft in the complete unit, which is indicated in Fig. X-7.

Lead telluride was chosen as the thermoelectric material because: "...there is, however, only one material, lead telluride, which is truly operational from the standpoint of having operated satisfactorily in power supplies and having fairly well-known operating limits and properties."[3] The reference concludes that the final feasibility of the device is dependent on the radiation-damage effects to the thermoelements. It also concludes that the upper limit for the power level of the particular reactor discussed is the thermal-stress limit of the thermoelements. If the allowable temperature gradients in the thermoelements could be doubled, the power output could be doubled by the addition of a larger radiator.

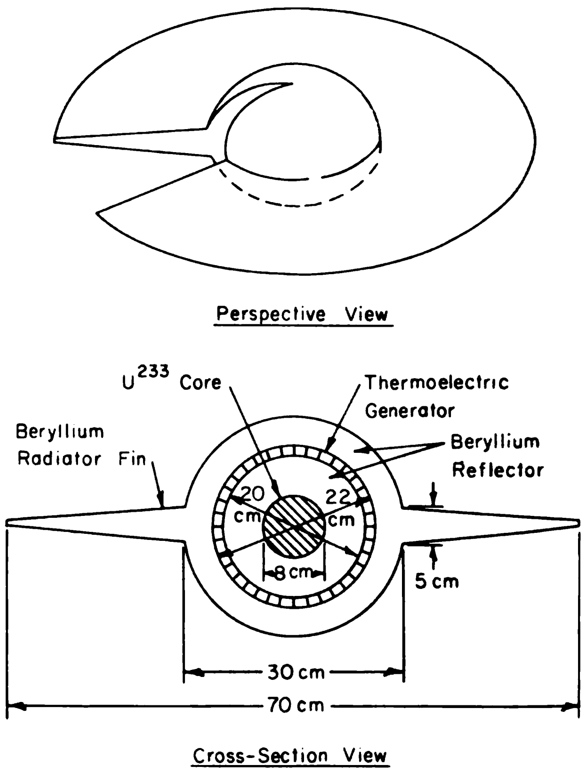

Fig. X-7 Conduction-cooled reactor system.[3]

References

1. Martin-Marietta Corporation, Aerospace Division, Feasibility Study of Water-Cooled Thermionic Nuclear Power Plant, USAEC Report MND-2903 (Vol. 1), November 1962.
2. E. P. Gyftopoulos and G. N. Hatsopoulos, Thermionic Nuclear Reactors, *IEEE Trans. Commun. Electron.*, 65: 98-108 (March 1963).
3. D. R. MacFarlane, A 200-Watt Conduction-Cooled Reactor Power Supply for Space Application, USAEC Report ANL-6694, Argonne National Laboratory, March 1963.

LEGAL NOTICE

This document was prepared under the sponsorship of the U. S. Atomic Energy Commission. Neither the United States, nor the Commission, nor any person acting on behalf of the Commission:

A. Makes any warranty or representation, expressed or implied, with respect to the accuracy, completeness, or usefulness of the information contained in this report, or that the use of any information, apparatus, method, or process disclosed in this report may not infringe privately owned rights; or

B. Assumes any liabilities with respect to the use of, or for damages resulting from the use of any information, apparatus, method, or process disclosed in this report.

As used in the above, "person acting on behalf of the Commission" includes any employee or contractor of the Commission, or employee of such contractor, to the extent that such employee or contractor of the Commission, or employee of such contractor prepares, disseminates, or provides access to, any information pursuant to his employment or contract with the Commission, or his employment with such contractor.

NUCLEAR SCIENCE ABSTRACTS

The U. S. Atomic Energy Commission, Division of Technical Information, publishes *Nuclear Science Abstracts (NSA)*, a semimonthly journal containing abstracts of the literature of nuclear science and engineering.

NSA covers (1) research reports of the U. S. Atomic Energy Commission and its contractors; (2) research reports of government agencies, universities, and industrial research organizations on a world-wide basis; and (3) translations, patents, books, and articles appearing in technical and scientific journals.

Complete indexes covering subject, author, source, and report number are included in each issue. These are cumulated quarterly, semiannually, and annually providing a detailed and convenient key to the literature.

Availability of *NSA*

SALE *NSA* is available on subscription from the Superintendent of Documents, U. S. Government Printing Office, Washington, D. C., 20402, at $30.00 per year for the semimonthly abstract issues and $22.00 per year for the four cumulated-index issues. Subscriptions are postpaid within the United States, Canada, Mexico, and all Central and South American countries, except Argentina, Brazil, British and French Guiana, Surinam, and British Honduras. Subscribers in these Central and South American countries, and in all other countries throughout the world, should remit $37.00 per year for subscriptions to semimonthly abstract issues and $25.00 per year for the four cumulated-index issues.

EXCHANGE *NSA* is also available on an exchange basis to universities, research institutions, industrial firms, and publishers of scientific information. Inquiries should be directed to the Division of Technical Information Extension, U. S. Atomic Energy Commission, P. O. Box 62, Oak Ridge, Tennessee, 37831.

TECHNICAL PROGRESS REVIEWS may be purchased from Superintendent of Documents, U. S. Government Printing Office, Washington, D. C., 20402. *Isotopes and Radiation Technology* at $2.00 per year for each subscription or $0.55 per issue; the other four journals at $2.50 per year and $0.70 per issue. The use of the coupon below will facilitate the handling of your order.

POSTAGE AND REMITTANCE: Postpaid within the United States, Canada, Mexico, and all Central and South American countries except as hereinafter noted. Add $0.50 per year, or $0.15 per single issue for the *Isotopes and Radiation Technology* journal and $0.75 per year or $0.20 per single issue for the other four journals for postage to all other countries, including Argentina, Brazil, British and French Guiana, Surinam, and British Honduras. Payment should be by check, money order, or document coupons, and MUST accompany order. Remittances from foreign countries should be made by international money order, or draft on an American bank, payable to the Superintendent of Documents, or by UNESCO book coupons.

order form

SUPERINTENDENT OF DOCUMENTS
U. S. GOVERNMENT PRINTING OFFICE
WASHINGTON, D. C., 20402

Enclosed:

document coupons ☐ check ☐ money order ☐

Charge to Superintendent of Documents No. ____________

Please send a one-year subscription to

- ☐ NUCLEAR SAFETY
- ☐ POWER REACTOR TECHNOLOGY
- ☐ REACTOR FUEL PROCESSING
- ☐ REACTOR MATERIALS

(Each subscription $2.50 per year; $0.70 per issue.)

- ☐ ISOTOPES AND RADIATION TECHNOLOGY

(Each subscription $2.00 a year; $0.55 per issue.)

SUPERINTENDENT OF DOCUMENTS
U. S. GOVERNMENT PRINTING OFFICE
WASHINGTON, D. C., 20402

(Print clearly)

Name ______________________________

Street ______________________________

City ______________ Zone ____ State ________

THE UNIVERSITY
OF MICHIGAN
MAY 25 1964
PHOENIX
LIBRARY

POWER REACTOR TECHNOLOGY

A Quarterly Technical Progress Review

Prepared for DIVISION OF TECHNICAL INFORMATION, USAEC, by
W. H. ZINN and J. R. DIETRICH, GENERAL NUCLEAR ENGINEERING CORPORATION

Spring 1964

FEATURE ARTICLE:

Neutron Physics Considerations
in Large Fast Reactors

● VOLUME 7

● NUMBER 2

TECHNICAL PROGRESS REVIEWS

To meet the needs of industry for concise summaries of current atomic developments, the Atomic Energy Commission is publishing this series, Technical Progress Reviews. Issued quarterly, each of the reviews digests and evaluates the latest findings in a specific area of nuclear technology and science.

The five journals published in this series are:

Isotopes and Radiation Technology, P. S. Baker, A. F. Rupp, and associates, Oak Ridge National Laboratory

Nuclear Safety, Wm. B. Cottrell, W. H. Jordan, and associates, Oak Ridge National Laboratory

Power Reactor Technology, W. H. Zinn and J. R. Dietrich, General Nuclear Engineering Corporation

Reactor Fuel Processing, Stephen Lawroski and associates, Chemical Engineering Division, Argonne National Laboratory

Reactor Materials, R. W. Dayton, E. M. Simons, and associates, Battelle Memorial Institute

Each journal may be purchased from the Superintendent of Documents, U. S. Government Printing Office, Washington, D. C., 20402. *Isotopes and Radiation Technology* at $2.00 per year for subscription or $0.55 for individual issues; the other four journals at $2.50 per year and $0.70 per issue. See back cover for remittance instructions and foreign postage requirements.

The views expressed in this publication do not necessarily represent those of the United States Atomic Energy Commission, its divisions or offices, or of any Commission advisory committee or contractor.

Availability of Reports Cited in This Review

Unclassified AEC reports are available for inspection at AEC depository libraries and are sold by the Office of Technical Services, Department of Commerce, Washington, D. C., 20230. Some of the reports cited are not available owing to their preliminary nature; however, the information contained in them will eventually be made available in formal progress or topical reports.

Unclassified reports issued by other Government agencies or private organizations should be requested from the originator.

Unclassified British and Canadian reports may be inspected at AEC depository libraries. British reports are sold by the British Information Service, 45 Rockefeller Plaza, New York, N. Y.; Canadian reports (AECL series) are sold by the Scientific Document Distribution Office, Atomic Energy of Canada, Ltd., Chalk River, Ontario, Canada.

Classified U. S. and foreign reports identified in this journal as Classified may be purchased by properly cleared Access Permit Holders from the Division of Technical Information Extension, U. S. Atomic Energy Commission, P. O. Box 1001, Oak Ridge, Tenn., 37831. Such reports may be inspected at classified AEC depository libraries.

POWER REACTOR TECHNOLOGY

A REVIEW OF RECENT DEVELOPMENTS

Prepared for DIVISION OF TECHNICAL INFORMATION, USAEC,
by W. H. ZINN and J. R. DIETRICH,
GENERAL NUCLEAR ENGINEERING CORPORATION

SPRING 1964

VOLUME 7

NUMBER 2

Foreword

This quarterly review of reactor development has been prepared at the request of the Division of Technical Information of the U. S. Atomic Energy Commission. Its purpose is to assist interested organizations in the task of keeping abreast of new results in reactor technology for civilian application.

Power Reactor Technology contains reviews of selected recently published reports that are judged noteworthy in the fields of power-reactor research and development, power-reactor applications, design practice, and operating experience. It is not meant to be a comprehensive abstract of all material published during the quarter, nor is it meant to be a treatise on any part of the subject. However, related reports from different sources are often treated together to yield reviews having some breadth of scope, and background material may be added to place recent developments in perspective. Occasionally the reviews are written by guest authors. Reviews having unusual breadth or significance are placed at the front of the issue as Feature Articles.

The intention is to cover the various areas of reactor development from the general viewpoint of the reactor designer rather than from the more detailed points of view of specialists in the individual areas. To whatever extent the coverage of *Power Reactor Technology* may occasionally overlap the fields of the other Technical Progress Reviews, the overlaps will be motivated by this objective of viewing current progress through the eyes of the reactor designer.

A degree of critical appraisal and some interpretation of results are often necessary to define the significance of reported work. Any such appraisal or interpretation represents only the opinion of the reviewer and (in the usual case, when the review is written by General Nuclear Engineering Corporation staff) the Editor. When the review is predominantly interpretive, the reviewer is named; unless identified as a guest author, he is a member of the General Nuclear Engineering Corporation staff. Readers are urged to consult the original references to obtain all the background of the work reported and to obtain the interpretation of the results given by the original authors.

For timely coverage, *Power Reactor Technology* must often review fragmentary material. The fixed subject headings listed below have been adopted in the hope of maintaining some continuity and order in the material from one issue to another: all reviews except Feature Articles will be arranged under these headings. A particular issue will not necessarily contain all the headings but only those under which material is reviewed.

Economics, Applications, Programs
Resources and Fuel Cycles
Physics
Fluid and Thermal Technology
Fuel Elements
Materials
Control and Dynamics
Containment, Radiation Control, and Siting
Systems Technology
Components
Design and Construction Practice
Operating Experience
Specific Reactor Types
Specific Applications
Unconventional Approaches

W. H. Zinn, President
J. R. Dietrich, Vice-President and Editor
General Nuclear Engineering Corporation

DEPOSITED BY THE
UNITED STATES OF AMERICA

Contents

FEATURE ARTICLE

Neutron Physics Considerations in Large Fast Reactors **107**
by David Okrent, Argonne National Laboratory

Foreword

I ECONOMICS, APPLICATIONS, PROGRAMS 138
Desalinization of Water 138
References 144

II PHYSICS 145
Thermal-Neutron Diffusion Parameters 145
References 152

III FLUID AND THERMAL TECHNOLOGY 154
Burnout in Multirod Geometry 154
References 165

IV FUEL ELEMENTS 167
Plutonium-Bearing Fuels 167
References 183

V MATERIALS 187
Neutron Irradiation of Type 347 Stainless Steel 187
References 191

VI OPERATING EXPERIENCE 193
Shippingport 193
References 196

VII SPECIFIC REACTOR TYPES . . . 197
Seed and Blanket 197
References 200

(Note: The pagination of this journal will henceforth be consecutive throughout the four issues of each volume.)

Issued quarterly by the U. S. Atomic Energy Commission. Use of funds for printing this publication approved by the Director of the Bureau of the Budget on October 14, 1963.

FEATURE ARTICLE

Neutron Physics Considerations in Large Fast Reactors

By David Okrent[*]

(Editor's Note: Of all reactor types the fast reactor probably depends most strongly for successful design on correct and adequate consideration of the neutron physics relations. We are fortunate to have Dr. Okrent as a guest reviewer for that subject. Because of his long experience and his familiarity with a broad range of both calculational and experimental results, he has been able to cover even the subtler aspects of neutron-physics behavior without demanding of the reader more than a qualitative knowledge of reactor physics. We believe the review will be interesting and useful to the general reader as well as to the reactor physicist, and we expect to make good use of it as a background for future reviews of progress in fast reactor development.)

Introduction

The term "fast reactor" is a broad one, covering a host of reactor types and sizes. The common attribute of fast reactors has usually[†] been taken to be the absence of moderating material deliberately introduced to lower the neutron energy. The sodium, oxygen, or carbon that may be incidentally present does affect the neutron energy spectrum, but the moderating power of these elements is too small to reduce neutron energies to thermal values before capture or leakage occurs. In a very small, high-metal-density fast reactor, inelastic scattering will reduce the average fission energy of about 2 Mev only to several hundred kilovolts before fission or leakage occurs. In a very large ceramic-fueled fast reactor, on the other hand, a large fraction of the fission events in the fissile isotope, such as Pu^{239}, may occur at energies between 1 and 100 kv, and some neutrons may be found in the few-electron-volt range. In general, inelastic scattering is effective in reducing the energy of neutrons above 100 kv. The number of neutrons found much below this energy will depend directly on the ratio of moderating power to total absorption.

---

[*] David Okrent received the Mechanical Engineering degree from Stevens Institute of Technology in 1943 and the Ph.D. in Physics from Harvard University in 1951. Since January 1951 he has been with the Argonne National Laboratory. He served as chief physicist in the design and startup of ZPR-III and as chief physicist during the design of EBR-II. As manager of the Fast Reactor Safety Program for several years, he originated the TREAT Reactor and experimental program and also worked on theoretical problems in the physics and safety of fast reactors. Dr. Okrent became a Senior Physicist at Argonne in 1957 and is currently a member of the Laboratory Director's Office. He is also a member of the AEC Advisory Committee on Reactor Safeguards.

In 1955 he was a delegate to the first Atoms for Peace conference in Geneva. In 1958 he served with the United Nations as a Scientific Secretary for the second Geneva Conference. In 1961–1962 he held a Guggenheim fellowship at the University of Cambridge. Dr. Okrent is a Fellow of the American Physical Society and a member of the American Nuclear Society. He is currently vice-chairman of the Mathematics and Computing Division of ANS.

[†] In conceptual designs of some large metal and ceramic fueled fast reactors, modest amounts of moderating material have recently been deliberately added to the reactor core to enhance the Doppler coefficient and to modify other physics parameters. The moderation introduced is insufficient to thermalize a significant fraction of the neutrons.

Fast reactors differ from thermal reactors in that the cross sections for fission at these energies are of the order of 100 times smaller than at thermal energies. However, the high concentration of fissionable atoms needed to maintain criticality is what permits the use of large quantities of structural materials, such as steel, in the core with only slight effect on the breeding ratio. Per atom, the ratio of capture in iron to fission in plutonium is similar for fast and for thermal reactors. The effect on breeding then depends primarily on the relative numbers of atoms of steel and plutonium; 50 times as much plutonium per unit volume of fast reactor core permits the use of 50 times as much steel.

Relatively speaking, the fission and capture cross sections are slowly varying in this energy range. There are no huge capture resonances, and hence no special reactivity effects are associated with xenon and samarium. There is no very strong absorber, such as cadmium in a thermal reactor, which is black to neutrons and from which one can design control rods in the form of thin plates. The neutron absorption cross section for B^{10}, the usual fast reactor control-rod poison, is less than 1 barn at 500 kev. Total cross sections are relatively small, and neutron mean free paths are relatively long. To a first approximation the reactor can usually be considered homogeneous for purposes of reactor physics analysis. There are no very steep gradients in flux, even near control rods.

The absence of thermal neutrons means that there is no thermal group whose mean energy will change with changes in moderator temperature. Small but important changes in spectrum can occur, however, with gross changes in core composition, such as partial or complete loss or expulsion of the sodium coolant from the core. Changes in the relative probability of fission and capture with such a shift in spectrum can be accompanied by important reactivity effects.

Fast reactors are relatively small, and, excepting the Doppler effect and the spectral shift on loss of sodium, most changes in reactivity with increase in temperature are associated with changes in leakage probability attributable to sodium and fuel expansion or to small motions of the fuel elements. A reduction in the fuel density in the core leads to a loss of reactivity. A reduction in sodium density allows more neutrons to leak; however, for large fast reactors this reactivity loss may be counterbalanced by a reactivity gain associated with the hardening of the neutron energy spectrum.

Table 1 VARIATION IN NEUTRON ENERGY SPECTRUM WITH REACTOR SIZE AND COMPOSITION

	Fraction of flux in each range			
Energy range	Fission spectrum	EBR-II	Large metal	Large oxide
1 to 10 Mev	0.69	0.20	0.09	0.08
0.1 to 1	0.30	0.70	0.67	0.54
0.01 to 0.1	0.01	0.10	0.22	0.30
0 to 0.01			0.02	0.08

There is a correlation between the size of the reactor, its k_∞,* and the mechanisms of control that are available. Very small reactors must be highly enriched; they will have a high k_∞ in the vicinity of 2 and hence a high leakage probability. Large changes in reactivity can be accomplished by the motion of reasonable masses of material next to the core, i.e., by reflector control. As core size increases, k_∞ and the probability of neutron leakage decrease. Increasingly impractical quantities of reflector material must be moved to achieve the necessary degree of reactor control. One then ordinarily resorts to fuel removal or the introduction of a strong neutron absorber, usually B^{10}.

The amount of control required can vary considerably with reactor type, design, and manner of operation. Things such as temperature and power coefficients, internal breeding ratio, maximum allowable burnup, and frequency of partial reloading all play major roles.

Although cross sections do vary relatively slowly, both the absolute and the relative values of cross sections change significantly over the broad energy range of importance, and this has a direct effect on the performance of various reactors. In Table 1 the relative amounts of neutron flux to be found in four different energy ranges are given for the EBR-II reactor, for a large metal-fueled reactor, and for a large ceramic-fueled reactor. In Fig. 1 the neutron energy spectra of these reactors are compared graphically. The differences are considerable. Note that the curves of Fig. 1 represent smoothed-out versions of the true spectra. As is illustrated in Fig. 2 for an 800-liter metal-fueled reactor, the scattering resonances in materials like sodium and iron produce many more large wiggles in the curve than are shown in Fig. 1.

---

*The term k_∞ is the number of neutrons emitted per neutron absorbed, averaged over all materials of the core.

Many aspects of fast reactor performance depend strongly on reactor size and spectrum. Some reactors will be sensitive to neutron cross sections at high energies, whereas others will depend strongly on cross sections below 10 kv. The high concentration of fissile isotopes in very small reactors may allow the use of considerable quantities of structural materials that have high capture cross sections, whereas in a large ceramic-fueled reactor, equal volume fractions of the same structural material would prove disastrous to the breeding ratio. Similarly, the hard spectrum of small reactors will lead to small Doppler coefficients, and large reactors that have some extra moderation may have large Doppler coefficients.

Most of the nuclear safety studies on fast reactors in the past[1] have dealt with moderate-sized reactors using one-piece, freely expanding uranium metal fuel elements. The rapid shutoff coefficient with axial expansion, the absence of an appreciably positive Doppler coefficient, and the presence of a negative reactivity coefficient for loss of sodium all helped in efforts to demonstrate the safety of this reactor type.

However, development work for large fast reactors today is centered primarily on a restrained metallic fuel element or on some form of ceramic fuel, neither of which seems certain to provide a reliable, negative, prompt thermal-expansion effect on reactivity of sufficient mag-

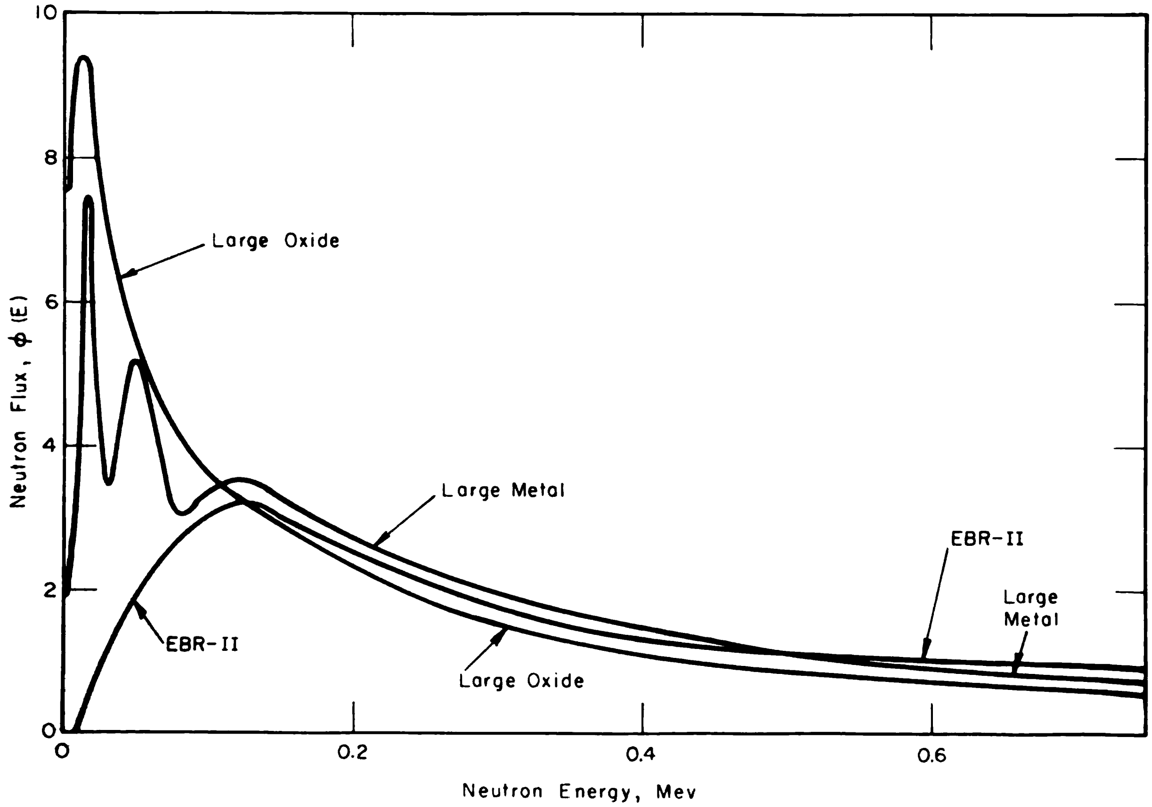

Fig. 1 Neutron energy spectra for EBR-II, for a large metal-fueled reactor, and for a very large oxide-fueled reactor.

nitude. Hence attention has shifted, and increased importance has been attached, to the Doppler effect, which promises to be large, and to the sodium void coefficient, which threatens to be positive.

Reviews of physics of small and intermediate-sized fast reactors were made by Okrent et al.[2] in 1955, by Codd et al.[3] in 1956, and by Loewenstein and Okrent[4] in 1958. Several papers on varied topics in fast reactor physics were given at the Second United Nations International Conference on the Peaceful Uses of Atomic Energy in 1958[5–8] and at the Conference on the Physics of Breeding in 1959.[9]

A major review of work on small fast critical assemblies was given by Paxton[10] in 1959 and in the series of papers by members of the Los Alamos Scientific Laboratory in the December 1960 issue of *Nuclear Science and Engineering*. Fast reactor cross sections were examined in detail by Yiftah et al.[11] in 1960. The most extensive collection of papers in the field of fast reactor physics is in the proceedings of a seminar, *Physics of Fast and Intermediate Reactors*, sponsored by the IAEA in Vienna in 1961.[12] Physics problems of large fast power reactors received considerable attention at that seminar, as they did at the Conference on Breeding, Economics, and Safety in Large Fast Power Reactors in 1963.[13]

This review article deals primarily with the steady-state nuclear performance characteristics of large fast power reactors. The treatment given is descriptive and qualitative. Most of the results used for purposes of illustration are drawn from the published literature. The subsections that follow deal with:

1. The important cross sections of the major fissile and fertile isotopes in relation to the neutron energy spectrum in typical fast reactors. The relative reactivity worth and breeding potential of the various isotopes are explained in terms of these cross sections.
2. Performance-related characteristics, such as breeding ratio, critical mass, and long-term reactivity changes, as functions of reactor size and composition.
3. Safety-related characteristics, namely, the reactivity coefficients.
4. A number of design variables and design considerations in relation to these neutron physics characteristics. Included among the

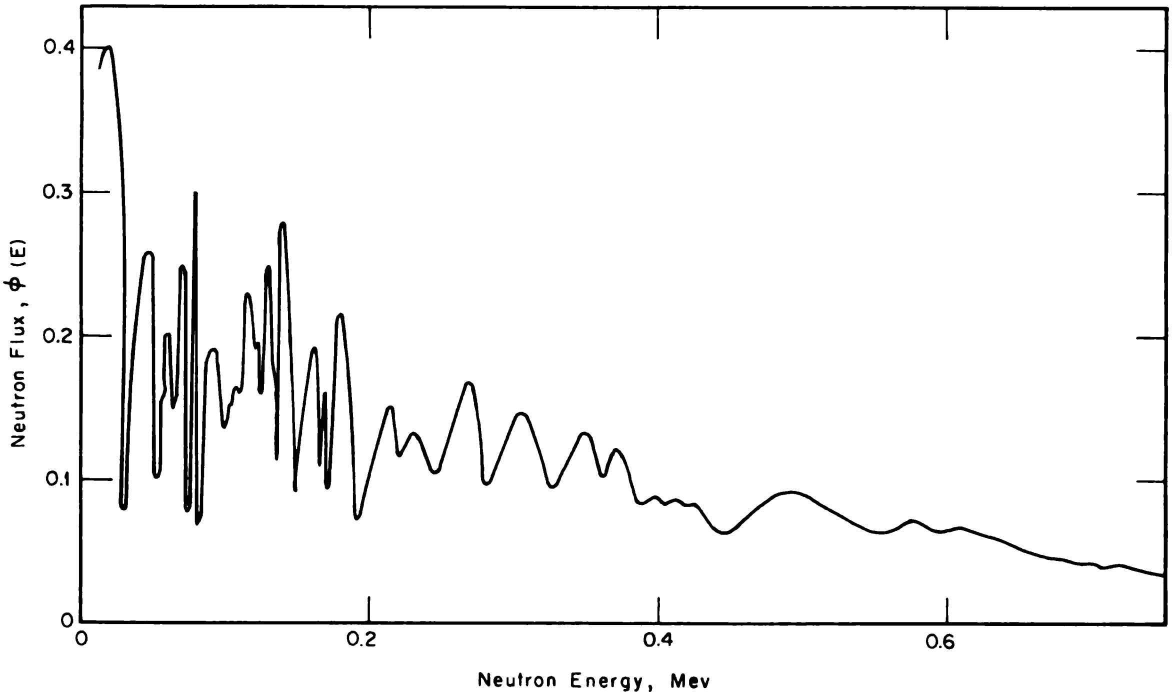

Fig. 2 Detailed neutron energy spectrum for a large metal-fueled reactor.

topics treated are hybrid fuel systems and the relative nuclear performance of various cladding and structural materials.

Basic Cross Sections

The fission cross sections for Pu^{239}, U^{233}, and U^{235} are plotted in Fig. 3 as functions of neutron energy. The cross sections are rather flat at high energies and rise slowly with decreasing energy below 100 kv. At low energies, U^{233} is seen to have a considerably higher cross section than Pu^{239}. The cross section for Pu^{241} is roughly similar to that for U^{233}.

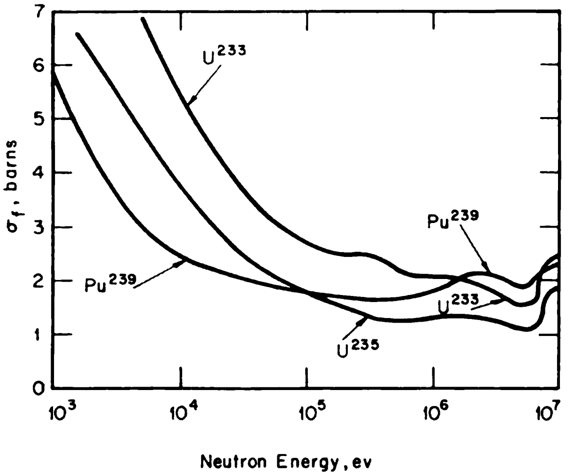

Fig. 3 Fission cross sections of U^{233}, U^{235}, and Pu^{239}.

The fission cross sections for Th^{232}, U^{238}, and Pu^{240} are compared in Fig. 4. The cross section for the plutonium isotope, which is very similar to that for U^{234}, has a much lower threshold energy and a much greater magnitude than that for U^{238}. Thorium has a very high threshold energy and a very small cross section, so that fission in thorium will be very small.

The ratios of capture to fission (α) for Pu^{239}, U^{233}, and U^{235} are plotted as functions of energy[14] in Fig. 5. This ratio has a major effect on breeding potential. Alpha for U^{233} is small and shows very little variation with energy above 10 kev. Alpha for Pu^{239}, on the other hand, is quite large and furthermore exhibits a large change with energy in the vicinity of 50 kv. One can expect considerable differences in breeding ratio for plutonium-fueled reactors that have fluxes lying primarily above or primarily below this energy.

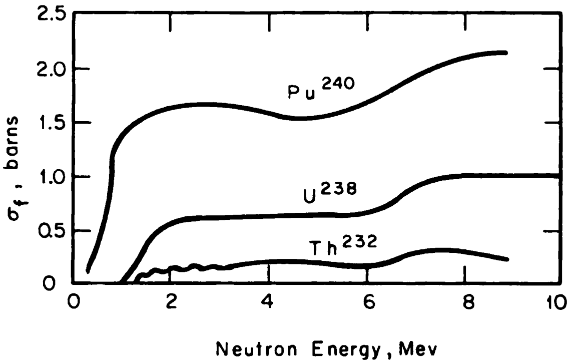

Fig. 4 Fission cross sections of Th^{232}, U^{238}, and Pu^{240}.

The capture cross section for U^{238} is plotted in Fig. 6. The capture cross section for thorium is similar. Over much of the energy range, the ratio of capture in the fertile materials to the sum of fission plus capture in the fissile isotope is roughly 1:10. Hence a fuel enrichment of 10% gives an internal breeding ratio in the vicinity of unity.

The number of neutrons emitted per fission, ν, rises with energy, as is demonstrated[11,15] for Pu^{239} in Fig. 7. A similar behavior is expected for all fissionable isotopes. However, the number of neutrons emitted per fission varies from isotope to isotope, as is illustrated in Table 2 for a specific neutron energy, 1.5 Mev.

Direct consequences of the cross sections, for example, are that Pu^{241} is more reactive

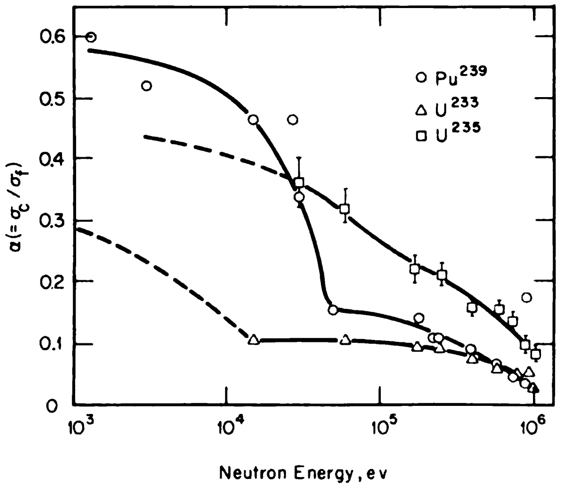

Fig. 5 Alpha for U^{233}, U^{235}, and Pu^{239}.

than Pu^{239} and that Pu^{240} is more reactive than U^{238}. The parameter ($\nu\sigma_{\text{fission}} - \sigma_{\text{fission}} - \sigma_{\text{capture}}$), which provides a partial measure of the relative reactivity worth of these isotopes, has been plotted (per atom) for U^{233}, U^{235}, and Pu^{239} in Fig. 8, and for U^{238} and Pu^{240} in Fig. 9. The curve for thorium would be similar to that for U^{238}, except that it would show less rise at higher energies because of its smaller fission cross section. Of course, below the threshold energy for fission, the parameter is negative ($= -\sigma_c$) for the fertile isotopes.

The same parameter has been averaged over the core spectrum for four reactors that have widely different spectra. The results are listed in Table 3 for U^{238}, Pu^{239}, Pu^{240}, and Pu^{241}. The rapid variation with reactor spectrum for threshold fissionable materials is obvious. Indeed, for large reactors, where the effect of scattering on neutron leakage is not very great, the total reactivity effect of the U^{238} in the core may be a loss of reactivity; in other words, reactors that have less U^{238} in the core will have a lower critical mass, other things being equal.

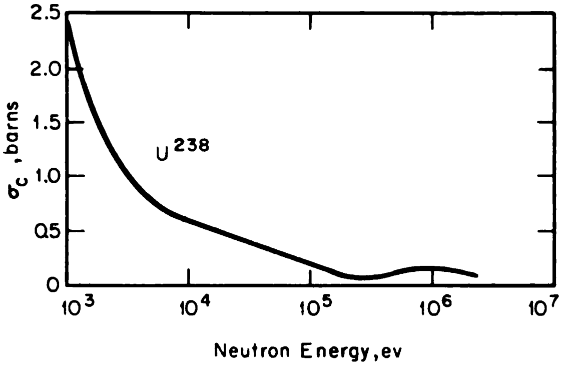

Fig. 6 Capture cross section of U^{238}.

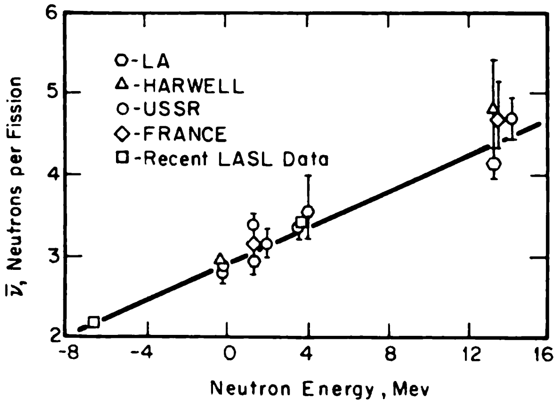

Fig. 7 ν (neutrons per fission) for Pu^{239}.

Table 2 NEUTRONS EMITTED PER FISSION (ν) PRODUCED BY 1.5-Mev NEUTRONS

Isotope	ν
Thorium	2.2
U^{233}	2.66
U^{235}	2.58
U^{238}	2.57
Pu^{239}	3.09
Pu^{240}	3.1
Pu^{241}	3.2

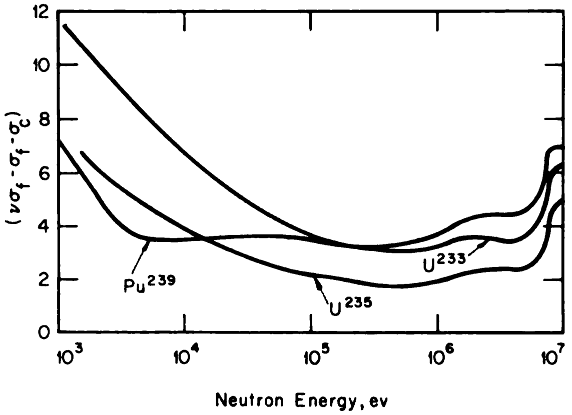

Fig. 8 Reactivity parameter ($\nu\sigma_f - \sigma_f - \sigma_c$) for U^{233}, U^{235}, and Pu^{239}.

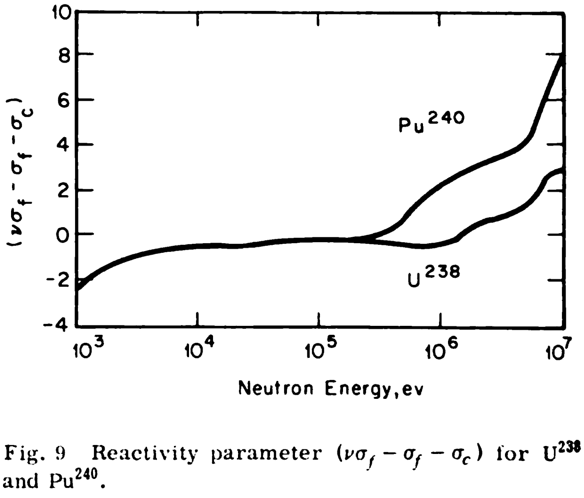

Fig. 9 Reactivity parameter ($\nu\sigma_f - \sigma_f - \sigma_c$) for U^{238} and Pu^{240}.

The breeding ratio of any particular reactor can be expressed by the formula

$$\text{Breeding ratio} = \frac{\nu - 1 - \alpha - A - L + (\nu' - 1)F}{1 + \alpha}$$

where the numerator measures the number of neutrons left for breeding purposes (by capture in fertile material) per fission in the thermally fissionable isotope. The symbols A, L, and F each signify the number of neutron events of a specific kind per fission in the thermally fissionable isotope. A is the parasitic absorption of neutrons in nonfissile and nonfertile materials, L is the leakage of neutrons from the blanket, and F is the number of fissions in fertile material, each giving off ν' neutrons.

Table 3 AVERAGE VALUES OF $(\nu\sigma_f - \sigma_f - \sigma_c)$ IN SEVERAL FAST-REACTOR SPECTRA

Reactor spectrum type	U^{238}	Pu^{239}	Pu^{240}	Pu^{241}
EBR-II	0.03	3.47	1.05	4.00
Fermi	−0.06	3.39	0.66	4.25
800-liter metal	−0.19	3.44	0.26	5.13
1500-liter oxide	−0.19	3.44	0.22	5.24

The term $[(\nu - 1 - \alpha)/(1 + \alpha)]$ measures the breeding potential of the primary fissionable material. The term $(\nu' - 1)\sigma_{\text{fission}}$ measures the fast fission bonus to breeding from the fertile material. These terms, averaged over the spectra of four different reactors, are compared for the appropriate isotopes in Table 4. For these reactors Pu^{239} and Pu^{241} have a considerably greater breeding potential than that of U^{233}. The breeding potential for U^{235} is below all of these. All the isotopes show some loss of breeding potential as the neutron spectrum is lowered. However, since the alpha for U^{233} is relatively flat with neutron energy, it is possible that for intermediate spectrum reactors having an average energy considerably lower than any of those examined in Table 4, the breeding potential for U^{233} will exceed that of Pu^{239}.

Table 4 BREEDING POTENTIAL OF VARIOUS ISOTOPES IN DIFFERING SPECTRA

Reactor spectrum	$(\nu - 1 - \alpha)/1 + \alpha$				$(\nu_f - 1)\sigma_f$			
	Pu^{239}	Pu^{241}	U^{233}	U^{235}	U^{238}	Pu^{240}	Pu^{242}	Th
EBR-II	1.79	1.86	1.44	1.17	0.19	1.35	1.30	0.034
Fermi	1.71	1.81	1.39	1.12	0.12	1.01	0.98	0.021
800-liter metal	1.56	1.76	1.33	1.04	0.081	0.75	0.72	0.014
1500-liter oxide	1.55	1.75	1.32	1.03	0.087	0.71	0.69	0.015

Table 5 NEUTRON BALANCE FOR 800-LITER METAL-FUELED REACTORS*

(On Basis of 1 Fission in Plutonium

	25% steel in core		25% tantalum in core	
	Core	Blanket	Core	Blanket
Fissions in Pu^{239}	1.0		1.0	
Captures in Pu^{239}	0.19		0.17	
Fissions in U^{238}	0.21	0.076	0.13	0.051
Captures in U^{238}	0.87	1.29	0.44	0.75
Na captures	0.005	0.001	0.001	
Structural captures	0.053	0.023	0.90	0.013
Neutrons escaping from blanket	0.038		0.025	
Ratio of fertile to fissile atoms in core	7.9		5.5	

*Core contains 25% fuel (Pu^{239} + U^{238}), 25% structure, and 50% sodium. Blanket is 45 cm thick and is well reflected. Blanket contains 60% U^{238}, 20% steel, and 20% sodium.

Among the fertile materials Pu^{240} can provide a much greater fast fission bonus than that of U^{238}, thanks to its higher fission cross section. The fast fission bonus from thorium is very small.

Some orientation as to the relative size of different contributions to the breeding ratio formula, given earlier, can be obtained from Table 5. The neutron balance for an 800 liter metal-fueled reactor, having an efficient well-reflected blanket, is presented here for two cases involving different structural and cladding materials—steel and tantalum. Capture in the sodium is very small, but the structural parasitic absorption depends very strongly on the material used. Leakage from the blanket can be kept small, but whether it is economical to do this must be evaluated separately. An appreciable fast fission bonus is achievable with either structural material.

Performance: Related Characteristics

Critical Mass and Breeding Ratio

Knowledge of the critical mass and breeding ratio is basic to a determination of the economic performance of a fast reactor. The total fuel inventory will consist of a critical mass plus the requirements for fuel held up in cooling, shipping, reprocessing, refabrication, etc. Frequently an estimate of two critical masses as the total inventory is made for computing interest charges on the fuel.

The breeding gain (i.e., the breeding ratio minus 1) enters into a determination of reactor income through sale of excess fissile isotope. Also, for a given specific power (say, in units of kilowatts per kilogram of fissile isotope) the doubling time of the reactor is inversely proportional to the ratio of the breeding gain to the critical mass.[16]

Breeding may take place primarily in the core, primarily in the blanket, or may be divided roughly equally between the two, depending on reactor design. From the long-term reactivity point of view, an internal breeding ratio of about unity is desirable. However, accomplishing this characteristic may lead to an undesirable safety-related effect, namely, a sodium reactivity coefficient that corresponds to an increase of reactivity upon loss of sodium. This will be discussed later.

The performance of a broad range of large fast power reactors was computed by Yiftah and Okrent[17] in 1960, using cross sections representing the then best evaluation of available cross-section measurements.[11] Some representative results are reproduced herein to demonstrate performance trends. The calculations were all made in spherical geometry on reactor systems having typical but arbitrary compositions. The breeding ratio has been defined as the ratio of thermally fissionable isotopes made to those used, and the breeding ratio and critical mass of thermally fissionable isotopes are for the new, clean just-critical reactor. The details of geometry, composition, and density are given in Table 6.

Equal core volume does not signify equal reactor-power capability for different kinds of fuel. It should also be observed that the blanket material was always assumed to be metallic, and that the blanket fertile material volume fractions used in these calculations are quite high, probably too high when one allows for the low-density blankets usually required in the path of core coolant flow. The core volume fraction of 0.25 for structural material may also be on the high side. No allowance could be made in these idealized calculations for control-rod holes and transition regions. However, for reactors using stainless steel as the structural material, the results obtained are nevertheless typical.

The critical mass, breeding ratio, internal breeding ratio, and average alpha of Pu^{239} are listed for Pu^{239}-U^{238} metal-, oxide-, and carbide-fueled reactors as functions of core volume in the first section of Table 7.

Table 6 REACTOR SPECIFICATIONS FOR PERFORMANCE CALCULATIONS[17]

Core volume fractions	
Fuel and fertile material	0.25
Structural material	0.25
Sodium	0.5
Assumed density fuels, g/cm^3	
Pu-U^{238}	19.0
U^{235}-U^{238}	18.7
PuO_2-UO_2	8.4
PuC-UC	11.4
Thorium	11.6
ThO_2-UO_2	8.4
Blanket thickness, cm	45 (U); 54 (Th)
Blanket volume fractions	
U^{238} or Th	0.6
Steel	0.2
Sodium	0.2

The plutonium is pure Pu^{239}. The critical masses rise with reactor size, whereas the breeding ratios fall off slightly because of a rise in alpha of Pu^{239}, with a degradation in average neutron energy. The absence of a moderator such as oxygen or carbon and the higher concentration of a strong absorber such as U^{238} both cause the metal-fueled reactor to have fewer neutrons in the low energy range. Consequently the average alpha is lower for the metal fuel. This factor, plus the larger fast fission bonus that accompanies a higher concentration of U^{238}, leads to a considerably higher breeding ratio for the metal fuels, other things being equal.

A similar set of results for U^{233}-thorium fueled reactors is also listed in Table 7. For these reactors the breeding ratio is found generally to lie between 1.2 and 1.3. Alpha for U^{233} is found to vary only slightly over the wide range of reactors studied. The breeding ratio is lower for these reactors than for the Pu^{239}-U^{238} fueled systems, not only because of the

Table 7 PERFORMANCE CHARACTERISTICS OF FAST REACTORS* USING STEEL STRUCTURE, SODIUM COOLANT, AND METAL, OXIDE, OR CARBIDE FUEL[17]

(See Table 6 for Reactor Specifications)

Reactor core volume, liters	Fuel	Critical mass, kg	Breeding ratio	Internal breeding ratio	α of fissile isotope
		U^{238}-Pu^{239} Fuel			
800	Metal	430	1.82	0.73	0.19
	Oxide	370	1.55	0.31	0.23
	Carbide	400	1.62	0.46	0.22
1500	Metal	690	1.79	0.91	0.20
	Oxide	560	1.47	0.44	0.25
	Carbide	610	1.56	0.61	0.24
2500	Metal	1030	1.76	1.04	0.21
	Oxide	810	1.42	0.54	0.27
	Carbide	900	1.52	0.73	0.25
		U^{238}-U^{235} Fuel			
800	Metal	650	1.32	0.49	0.21
1500	Metal	1010	1.30	0.62	0.22
	Oxide	790	1.09	0.27	0.24
	Carbide	860	1.15	0.40	0.24
2500	Oxide	1110	1.05	0.35	0.25
		Th-U^{233} Fuel			
800	Metal	450	1.29	0.38	0.09
	Oxide	370	1.23	0.27	0.10
	Carbide	410	1.26	0.38	0.10
1500	Metal	680	1.28	0.50	0.09
	Oxide	540	1.21	0.39	0.11
	Carbide	620	1.24	0.52	0.10
2500	Metal	970	1.28	0.61	0.09
	Oxide	760	1.19	0.49	0.11
	Carbide	890	1.23	0.62	0.11
		Th-U^{235} Fuel			
800	Metal	790	1.03	0.28	0.20
1500	Metal	1190	1.02	0.37	0.20
	Carbide	1060	0.97	0.36	0.23

$$\text{Breeding ratio} = \frac{U^{238}\ (\text{or } Th^{232})\ \text{captures in reactor}}{Pu^{239}\ (\text{or } U^{233}\ \text{or } U^{235})\ \text{captures + fissions in reactor}}$$

$$\text{Internal breeding ratio} = \frac{\text{production of thermally fissionable isotopes in core}}{\text{destruction of thermally fissionable isotopes}}$$

$$\alpha = \frac{\sigma_{\text{capture}}}{\sigma_{\text{fission}}}$$

---

* All reactors have 25% fuel, 25% steel, and 50% sodium in the core. Blankets have 60% fertile isotope (metallic), 20% steel, and 20% sodium. Calculations were made in spherical geometry.

reduced breeding potential of U^{233} at these neutron energies but because of the very small fast fission bonus obtained with thorium as the fertile material in the core.

For comparative purposes the performances of some U^{235}-fueled reactors are also given in Table 7. In general, with U^{235} the critical mass is higher and the breeding ratio lower. This is directly attributable to its smaller fission cross section, its smaller ν relative to that measured for Pu^{239}, and its higher α relative to that for U^{233}.

Effects of Fission Products

The detailed capture cross sections of all the fission products have not been measured, but one can make theoretical estimates thereof.[illegible] The effect of fission products on breeding ratio and critical mass are listed in Table 8 for typical metal-, oxide-, and carbide-fueled plutonium reactors of 1500 liters core volume.[22] In each case the same number of fission products, 0.0008×10^{24} atoms/cm^3, have been added to the core. This many atoms would accumulate if 3[illegible]% of the combined Pu – U^{238} had fissioned in the metal reactor considered. The corresponding heavy atom burnup is 8.6% for the carbide case. The effect on breeding of this considerable fission-product accumulation is small, although not negligible.

The performance of reactors lacking any internal breeding is not examined here in detail. Enriched oxide or metal dispersions in a matrix of stainless steel would fall into this category. In large sizes, reactors of this type will generally have much lower critical masses and much lower breeding ratios. In a very large reactor, capture in U^{238} or thorium causes the reactor to lose reactivity, hence the reduction in critical mass for systems without fertile material in the core. However, there is a nearly complete loss of fast-fission bonus (a small blanket contribution remains), and parasitic capture in plutonium fuel would rise appreciably. The result can be a drop of 0.6 in the breeding ratio of the usual plutonium metal-fueled system. A U^{233}-fueled reactor would not be hurt as much on breeding ratio.

Table 8 EFFECT OF FISSION PRODUCTS (0.0008×10^{24} atoms/cm^3) ON PERFORMANCE OF 1500-LITER REACTORS*[22]

Reactor type	Critical mass: New reactor	Critical mass: With fission products	Breeding ratio: New reactor	Breeding ratio: With fission products
Metal	[illegible]	[illegible]	1.73	1.74
Oxide	[illegible]	582	1.47	[illegible]
Carbide	[illegible]	[illegible]	1.54	1.47

* All reactors have [illegible] fuel, [illegible] steel, and [illegible] sodium in core. The blankets all have [illegible] uranium metal, [illegible] steel and [illegible] sodium.

Long-Term Reactivity Effects

The reactivity loss associated with a net uniform burnout of a fraction $\delta M_c/M_c$ of the original critical mass is given approximately by the relation

$$\left(\frac{\delta k/k}{\delta M_c/M_c} \approx 0.4 \text{ to } 0.5\right)$$

$$\delta M_c = M_c \times \frac{\%\text{ burnup of fuel alloy}}{\%\text{ enrichment of fuel alloy}} \times \left(\frac{1}{1 - F_c}\right) \times (1 + \alpha)(1 - \text{IBR})$$

where F_c = fissions in core fertile isotopes per fission in core fissile isotopes

α = ratio of capture to fission in fissile isotope

IBR = internal breeding ratio = (fissile atoms produced in core)/[fissile atoms destroyed (by capture and fission) in core]

In this report burnup means fission. The definition of IBR used herein applies to this formula, even if some thermally fissile isotope exists and is destroyed in the blanket. The real definition of the term "internal breeding ratio" becomes somewhat obscure in that event.

The change in reactivity is a function primarily of the product of the percent burnup of fuel alloy and the term (1 – IBR). Of course, if the fissile isotope produced is different from that destroyed, the relative reactivity worths of the two isotopes must be factored into the equation.

Radial growth of the fuel within its jacket under irradiation should produce only slight reactivity effects, corresponding to a small displacement of sodium bond, for example. Axial growth, on the other hand, corresponds to a net reduction in the fuel density in the overall core. Its reactivity effect can be estimated roughly by a relation like

$$\frac{\delta k}{k} \approx -0.3 \frac{\delta L}{L}$$

where $\delta L/L$ is the fractional increase in core length with fixed core radius and fixed mass of fuel. The numerical coefficient in the equation will vary with parameters like core size and ratio of core height to diameter.

Table 9 LONG-TERM REACTIVITY EFFECTS*[22]

Reactor type	Breeding ratio	Internal breeding ratio	Atoms/cm^3 of Pu + U ($\times 10^{-24}$)	Burnup, % of Pu + U fissioned	$\delta k/k$ Burnout in core	$\delta k/k$ Buildup in blanket	$\delta k/k$ Fission product buildup	$\delta k/k$ Total
800-liter metal	1.82	0.73	0.012	5	−0.054	+0.026	−0.017	−0.045
1500-liter oxide	1.47	0.44	0.00467	10	−0.169	+0.025	−0.037	−0.181
1500-liter carbide	1.56	0.61	0.0069	10	−0.147	+0.031	−0.028	−0.144

*All reactors have 25% fuel, 25% steel, and 50% coolant in the core.

The long-term reactivity losses due to a net burnup of fuel and fission-product accumulation in the core, and the reactivity gain due to buildup of plutonium in the blanket, have been listed for three typical reactors[22] in Table 9. Heavy atom burnups of 5% for the metal fuel and 10% for the oxide and carbide have been arbitrarily chosen for purposes of illustration. The major reactivity loss lies in net core burnup for all three reactors. The loss is huge for the oxide and carbide since the chosen compositions yield relatively low internal breeding ratios. The fission-product buildup has only a moderate effect on reactivity and is approximately balanced by the gain associated with blanket plutonium buildup.

Changes in plutonium isotopic composition with recycle affect the long-term reactivity loss by changing the net core burnup of fuel. The reactivity loss is generally greater for pure Pu^{239} than for the equilibrium plutonium mixture obtained with recycle. The difference between the two is about the same order of magnitude as the loss due to fission-product accumulation.[22]

Even a 2 or 3% reactivity loss can be a considerable amount to balance with control rods in a fast reactor. The small core dimensions and the unavailability of strong absorbers for control-rod materials, coupled with complicating considerations of reactor safety, all tend strongly toward placing conservative limits on the shim reactivity requirements. Partial reloading helps in this respect but not without costs in shutdown time. (Fortunately, there is no xenon-override problem.) But a constant reactivity core seems highly desirable, and, in principle, it is not beyond reach in large fast power reactors. Internal breeding ratios can be raised simply by increasing either the density or volume fraction of the fuel mixture. There is relatively little change in critical mass or overall breeding ratio as a consequence. The move would be an obvious one except for the adverse effect it has on a vital dynamic characteristic, the sodium reactivity coefficient, which will be discussed in the following section.

Safety-Related Characteristics

The prompt-neutron lifetime in fast reactors is relatively short, i.e., the time between successive generations of neutrons emitted promptly at the time of fission will usually be less than 5×10^{-7} sec. For such a reactor an excess reactivity of only 0.0035 $\delta k/k$ above prompt critical would lead to a doubling of the power every 100 μsec. Hence any single super-prompt-critical burst in a fast reactor will take its course long before mechanically induced control-rod motion can be effective, and the inherent fast-acting reactivity coefficients of the reactor will determine whether the burst will be terminated without excessive damage or will lead to a violent disassembly with pressures comparable to those generated by a high explosive.

Thus nuclear safety must be factored into the design of the fast reactor from its very inception. A major portion of this safety consideration deals with the three reactivity coefficients due to fuel expansion, to coolant expansion, and to the Doppler effect.

Fuel Expansion

Fuel expansion leading to an increase in core length and a decrease in fuel density reduces reactivity. For a one-piece, unrestrained metallic fuel pin in a reactor such as EBR-II, this mechanism provides a large, negative prompt-acting reactivity effect that plays a major role in guaranteeing the safety of the reactor. Calculations indicate that the fuel expansion effect for a fuel element of similar type in a large reactor having a core height-to-diameter ratio of unity would still be appreciable, as is illustrated[23] in Table 10. For pancake-shaped reactors with an $H:D$ ratio of $\frac{1}{4}$, however, the fuel expansion reactivity coefficient may be much reduced.

Table 10 FUEL EXPANSION REACTIVITY COEFFICIENTS*[23]

Core size, liters	$H:D$	$\frac{\Delta k/k}{\Delta T} \times 10^6$
50	1	−4.5
	$\frac{1}{4}$	−0.9
3000	1	−3.4
	$\frac{1}{4}$	−0.9

*All reactors contain 25% PuC-U^{238}C, 16% steel, and 59% Na in the core.

Unfortunately most of the fuel-element types actively under development for use in large fast power reactors may be unable to provide a large prompt-acting axial expansion of the fuel. The fuel may be restrained, preventing axial motion. It may be multipiece with no definite average reduction in fuel density upon local expansion. It may crumble or crack with irradiation and thermal cycling. Care must be taken to ensure that fuel motion with heating does not add reactivity for some fuel-element types.

Sodium Void Reactivity Effects[17,24–27]

The loss of some or all the sodium from the reactor influences reactivity in three ways:

—Less neutrons are captured in sodium, adding reactivity. This is generally a small effect, since the sodium capture cross section is very small. Sodium has a large resonance at 3 kev, however, and the reactivity gained from the reduction in absorption cannot be neglected for large ceramic-fueled fast reactors.

—Neutrons tending to escape from the core will no longer be scattered into different directions by the sodium. Their leakage probability is increased, and their reactivity is decreased. The major contribution to this effect will come from the sodium near the core boundary; a change in neutron direction near the core center has less influence on the chance of its leaking. Small reactors having more leakage will be more sensitive than large reactors to the change in scattering probability. Reactors in which sodium contributes a higher fraction of the scattering will have a greater increase in neutron leakage with sodium loss.

—The loss of inelastic scattering and elastic moderation by the sodium results in a harder neutron energy spectrum. Fission becomes more probable in the fertile isotopes like U^{238} and Pu^{240}, and capture and fission in all isotopes occur at a higher average energy. However, the capture cross section of Pu^{239} falls off much more rapidly with increasing energy than does the Pu^{239} fission cross section, as do also the capture cross sections of most other highly absorbing isotopes, for example, niobium and U^{238}. Hence the average number of neutrons produced per absorption (fission and capture)

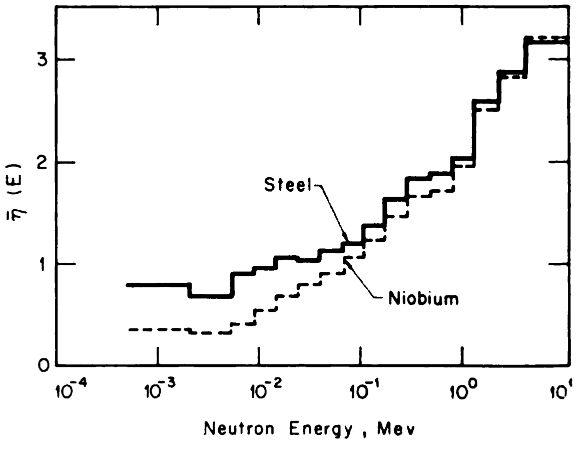

Fig. 10 $\bar{\eta}$ as a function of neutron energy for 1500-liter plutonium carbide-fueled reactors with steel or niobium structure. $\bar{\eta}$ is the average number of neutrons emitted per absorption in all core materials.

in all core materials rises as the spectrum hardens, and this effect generally produces a reactivity gain. The effect is illustrated in Fig. 10 for 1500-liter reactors fueled with PuC-UC and using steel or niobium as the structural material.[17] Using more sophisticated calculation techniques,[25] Hummel et al.[28] recently reported a similar result, as illustrated in Fig. 11, where the adjoint flux (i.e., the relative reactivity worth of a neutron) is plotted for two large oxide-fueled reactors. The situation is much aggravated when the enrichment is reduced, or when Pu^{240} and fission products are present.

The net sodium void reactivity effect will be negative if the contribution from enhanced neutron leakage predominates. This is the case for the EBR-II and the Enrico Fermi reactors. As is shown in Fig. 12, the sodium void coefficient becomes less negative (or more positive) as reactor size is increased for a given reactor composition.[17] For each composition there is some size at which the spectral effect predominates and the net effect becomes positive. The reactors of Fig. 12 are fueled with plutonium-uranium metal, using steel or niobium as the structural material. Sodium occupies 50% of the core. With steel structure the threshold for a positive coefficient is about 1200 liters, whereas with niobium the threshold falls below 500 liters. The calculations were made in spherical geometry, and the sodium coefficient was computed for the loss of core sodium only.

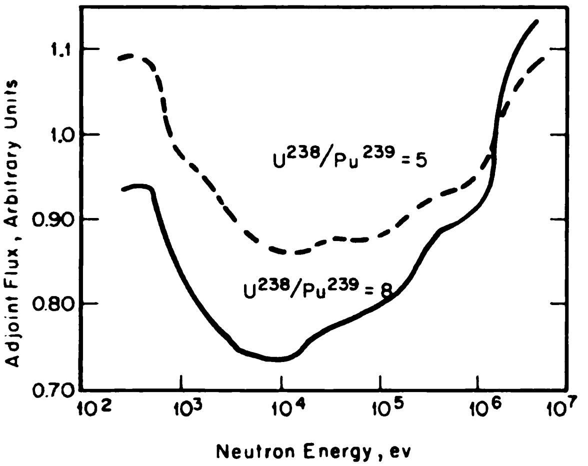

Fig. 11 Adjoint flux (neutron reactivity worth) for large $Pu^{239}O_2$-$U^{238}O_2$ fueled reactors. (Reactors have 70 vol.% sodium effect of Pu^{240} and fission products if not included.)

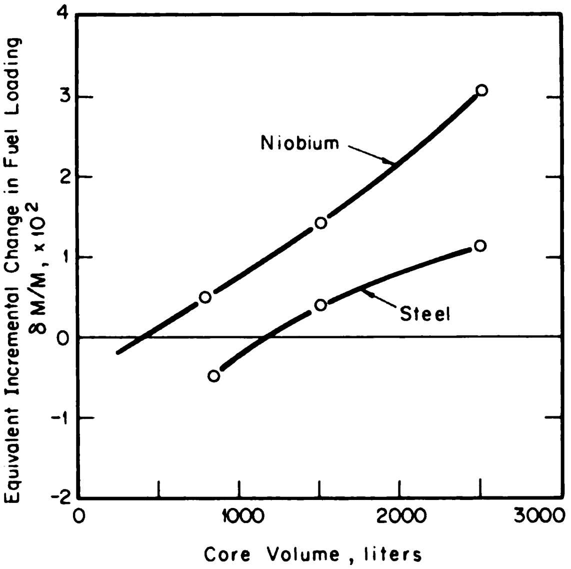

Fig. 12 Reactivity change effected by removal of 40% of sodium from plutonium-metal-fueled cores with steel or niobium structure.

When a fuel material of lower density is used, less U^{238} will be present in the fuel elements, and the sodium void coefficient turns positive at a larger core size. In Fig. 13 the coefficient has been plotted against reactor size for some specific carbide- and oxide-fueled reactors. In the case of PuC-UC the threshold volume for a positive coefficient was calculated to be near 2000 liters, whereas for the oxide it was above 3000 liters.

The spatial dependence of the sodium void coefficient is also an important consideration. As shown in Fig. 14, Nims and Zweifel[24] calculated that the net coefficient for the Fermi reactor was negative at all core radii. In this relatively small U^{235}-fueled* reactor, spectral hardening was calculated to cause a reactivity loss rather than a gain. In a larger reactor fueled with PuO_2 dispersed in a uranium-molybdenum matrix, however, as is shown in Fig. 15, only neutron leakage contributed nega-tively to the sodium void coefficient. The net coefficient varied from highly positive at the core center to slightly negative at the core edge.

---

*The flatter variation of α with energy and the rapid fall of σ_f with increasing neutron energy for energies below 300 kev with U^{235} lead one to expect this isotope to be less inclined toward positive sodium coefficients than is Pu^{239}.

Hence for a reactor having a zero value for the overall sodium coefficient, there is a strong positive component from the inner portions of the core which is balanced by a negative contribution from the blanket and from outer parts of the core. Thus expulsion of sodium initially from the center of the core can lead to a reactivity excursion. This effect is illustrated[29] in Fig. 16. The change in reactivity with progressive axial loss of sodium is plotted for each of two oxide-fueled reactors. In Case A, where a total loss of sodium leads to a gain of reactivity of 0.008 $\Delta k/k$, there is a peak gain of more than twice this amount when two-thirds of the core is the only region voided. Case B describes a reactor to which some beryllium oxide has been added. The addition of this small amount of moderator serves two purposes. First, it makes the sodium coefficient less positive by shifting the neutron energy spectrum downward and by reducing the dependence of the spectrum on the presence or absence of sodium. Second, by increasing the fraction of low-energy neutrons present at all times—both in the presence and absence of sodium—it ensures a considerably larger negative Doppler coefficient than would be present in Case A. However, the beryllium oxide addition has a bad side effect. The breeding ratio[29] drops from about 1.3 to about 1.1.

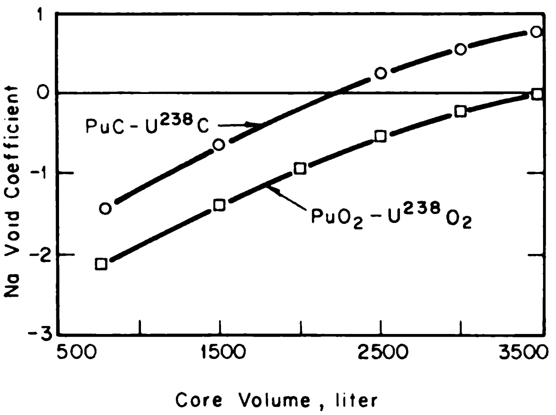

Fig. 13 Sodium coefficient as a function of core volume for oxide and carbide-fueled reactors. (Reactor composition is 25% fuel, 25% steel, and 50% sodium.)

If the magnitude of the reactivity which might be gained through the loss of sodium were always less than that which could be balanced by other reactivity effects, the sodium void reactivity effect might not assume very great importance in large fast power-reactor design. However, one generally has only a fraction of 1% $\Delta k/k$ available for shutdown from the Doppler effect or from fuel expansion, even if the latter mechanism is still operative at high fuel temperatures. On the other hand, the reactivity gains from the total loss of sodium have been calculated to be well in excess of 3% $\Delta k/k$ for some core compositions in large sizes.

What are the avenues available if one wishes to achieve a negative sodium coefficient, or a coefficient that is only slightly positive, in a 1000-Mw(e) reactor fueled with plutonium plus U^{238}? Core volumes ranging from 3000 to 6000 liters and perhaps more are needed for such an output.

As shown[27] in Fig. 17, the sodium coefficient depends strongly on the sodium volume fraction for a given core composition and volume. For compositions typical of large reactors, the sodium coefficient is slightly positive for small sodium volume fractions, increasing as the volume fraction of sodium is increased, until, somewhere between 50 and 70 vol.% sodium, the coefficient falls sharply and becomes negative. The greater the core height (the greater

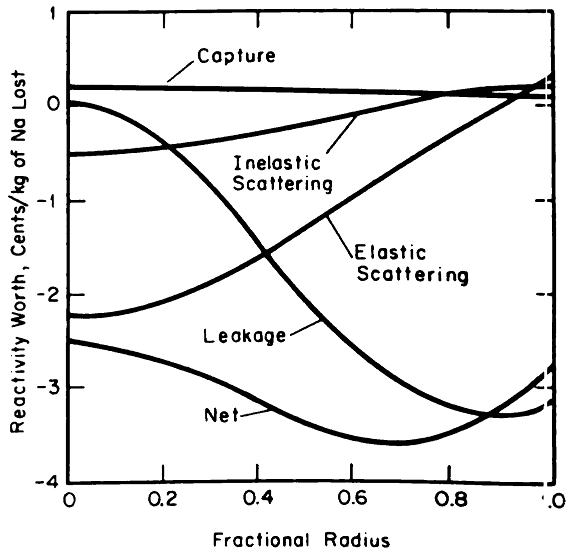

Fig. 14 Components of sodium density coefficient of reactivity for Fermi reactor as a function of core radius.

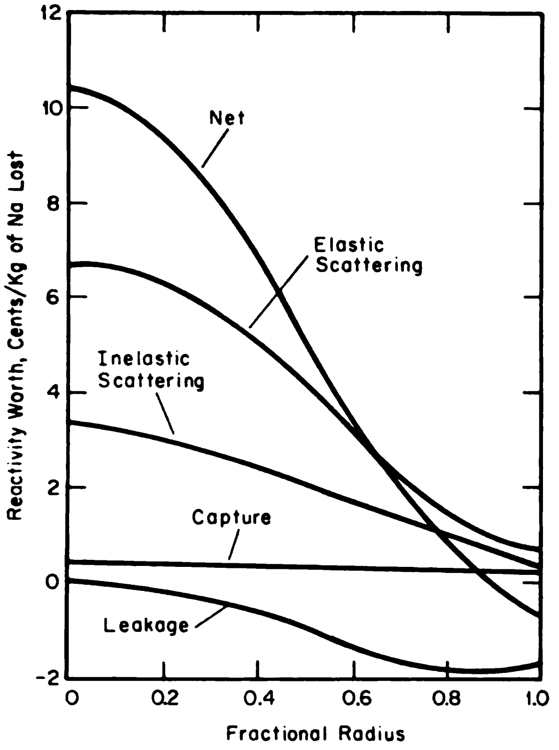

Fig. 15 Components of sodium density coefficient of reactivity for a 800-liter cermet-fueled (PuO_2 in U^{238} + Mo) reactor as a function of core radius.

the core volume) the greater the sodium volume fraction needed to achieve a negative sodium coefficient.

Figure 17 is for oxide-fueled reactors. For plutonium-U^{238} metal-fueled reactors that have the same overall volume fractions in the core, the sodium coefficients would be more positive for each reactor design, thanks to the higher concentration of U^{238} in the fuel.

The high sodium volume fractions necessary to give a negative coefficient will lead to reduced breeding ratios. A lower fast fission bonus from the U^{238} is a major cause. The efficiency of the blanket for capturing neutrons may also be impaired. And the internal breeding in the core will drop in direct relation to the ratio of U^{238} to Pu^{239}, leading to greater reactivity losses for the same degree of heavy atom burnup.

Also, high sodium volume fractions may lead to undesirably large positive reactivity contributions, in the event that only the central regions of the core should lose sodium.

Various geometric configurations may afford the opportunity of tailoring the sodium coefficient to more desirable specifications. Pancake-shaped, or thin, annular cores lead to higher enrichment, greater neutron leakage, and hence some improvement in the sodium coefficient.

Calculations indicate that the reactivity effect due to loss of sodium from the core alone tends to be relatively insensitive to the blanket design.[28,30] However, the reactivity loss accompanying loss of sodium from the blanket is quite large for a relatively thin blanket having a high volume fraction of sodium. Unfortunately such a blanket is not efficient in capturing neutrons, and its use might lead to an appreciable reduction in breeding ratio. Modifications in the relation between blanket and core, i.e., the introduction of a sodium transition region between the two, may be a better way to help achieve an overall negative sodium void effect.

At the Argonne conference on large fast power reactors[13] in October 1963, studies were reported by Cohen[29] and by Zaleski[31] on the safety characteristics of large fast reactors having positive sodium void effects. Zaleski found that with a large negative Doppler coefficient the reactor would still be stable in the presence of a positive sodium void coefficient. Cohen and Zaleski both found that the course of an accident involving the expulsion of sodium by boiling depends very strongly on the manner in which the sodium is lost from the reactor. For a mild power transient or a partial loss of flow, boiling might be limited to the upper core regions

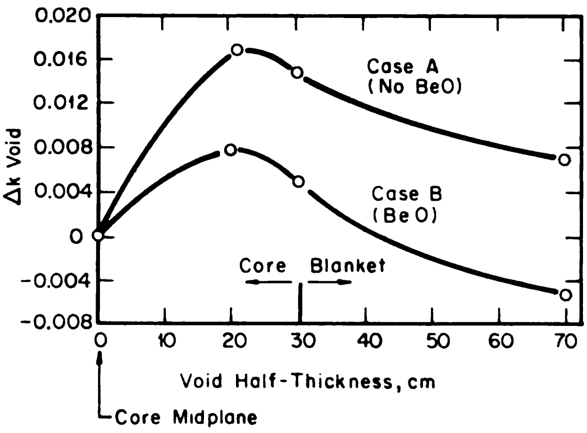

Fig. 16 Spatial dependence of reactivity change for progressive axial loss of sodium, starting at core midplane. (Case *A* is a large oxide-fueled reactor. Case *B* is a similar reactor to which some BeO has been added to improve Doppler and sodium density coefficients.)

and upper blanket. In this case boiling would decrease reactivity. However, model experiments, using water,[32] have exhibited a chugging behavior that leads to periodic voiding of the central regions of subassemblies; hence further study is needed here.

For the hypothetical accident involving full loss of coolant flow and a delay in scram, boiling may begin at the core center. The course of such an event would depend strongly on the magnitude of the Doppler effect and the variation in sodium void reactivity effect with position in the reactor.[29]

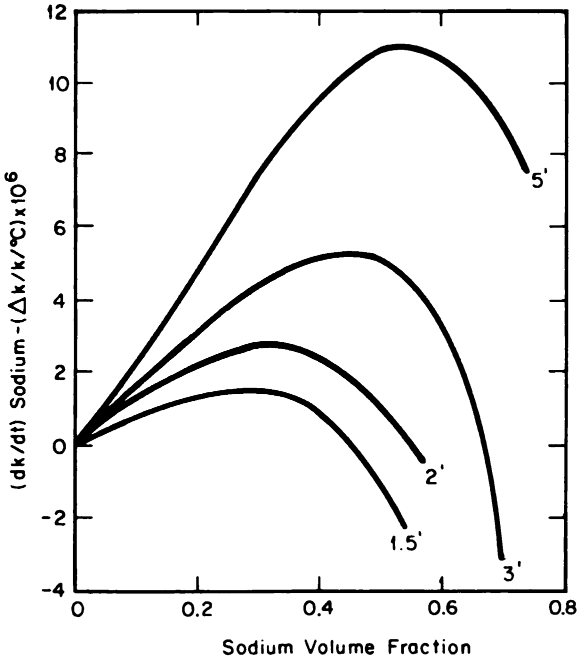

Fig. 17 Sodium coefficient as a function of core height and sodium volume fraction for pancake-shaped reactors (vol.% fuel/vol.% steel = 2).

Clearly, intensive study is needed on the role of positive sodium void effects in the safety of large fast power reactors. If, in order to go to the 1000-Mw(e) size, one has to pay a large penalty in the form of reduced breeding ratio, higher fuel-cycle costs, or greater capital investment for containment purposes, it may be that two 500-Mw(e) reactors at a common site will prove more desirable. Or an increased emphasis on higher power densities, leading to smaller reactor sizes, may result.

In any event, it is clear that the determination of the sodium void effect, the evaluation of the effect to determine what are its acceptable magnitudes, and the accomplishment of acceptable effects without spoiling other reactor performance characteristics combine to form one of the major reactor physics problems of large fast power-reactor design today.

Other Coolants

Since the positive character of the sodium void coefficient is introduced primarily by its moderating power, it might be expected that this effect would be alleviated with the use of a heavy coolant. Calculations have been made of coolant void coefficient for several large reactors cooled with a lead-bismuth eutectic.[17] These magic number elements have low neutron-capture cross sections and high thresholds for inelastic scattering, making them ideal in this respect. Highly negative coolant void coefficients were obtained with lead-bismuth for reactors in which sodium coolant would lead to a highly positive coefficient. A coolant like potassium should also have a less positive tendency than sodium.

Lithium has also been examined as a potential fast reactor coolant.[33] As one expects, even the weakly absorbing Li^7 isotope gives a more positive coolant void coefficient in large reactors than sodium, as a consequence of its stronger moderating powers. The presence of Li^6 isotope in small amounts in the lithium makes the situation still less attractive. Since Li^6 is a strong neutron absorber, its explusion, of course, leads to considerable reactivity gains.

Fast reactors cooled with helium gas or carbon dioxide are not expected to have sizable reactivity effects associated with coolant pressure changes.[34] Fast reactors cooled with steam or water at supercritical pressure, however, apparently can face a problem similar to that encountered with sodium.[35]

Doppler Effect[27,36–41]

Heating of the fuel changes the velocity of atomic vibration, leading to a changed distribution of relative velocities between neutron and atom. Any self-shielding in cross-section resonances is reduced, and the increased reaction rates are reflected in reactivity changes. If only fissile material is heated, it has been expected that a gain in reactivity would result, due to the increased probability of absorption compared to leakage. When an isotope like U^{238}, having a high cross section for neutron capture, is intimately mixed with the fissile isotope in sufficient quantity, the Doppler effect associated with fuel heating will lead to a reactivity loss.

The EBR-I reactor with the Mark I and II loadings exhibited a prompt positive power coefficient of reactivity[42] that was thought possibly to arise from a positive Doppler coefficient. Although later experiments demonstrated that the positive coefficient arose from bowing of the fuel rods,[43,44] attempts were made to calculate and to measure[45,46] a Doppler effect. The results of both calculation and experiment indicated that the Doppler coefficient was so small as to be negligible in EBR-I.

Self-shielding of resonances is small at the higher neutron energies. A greater resonance width, a higher level density, and a reduced resonance strength combine to produce a generally overlapping character. In reactors of moderate size such as the EBR-II and the Enrico Fermi, with relatively high fuel enrichment and a hard neutron energy spectrum, the Doppler effect on reactivity is believed to be small, much smaller than the negative reactivity effect of fuel expansion for these reactors.

In large fast reactors, on the other hand, particularly those fueled with a ceramic such as the oxide or carbide, the ratio of moderating power to neutron absorption is large enough to provide significant fractions of neutrons below 10 kev, and the Doppler effect can be appreciable. Doppler coefficients such as $-1 \times 10^{-5}\ \Delta k/k$ per °C at fuel operating temperatures have been calculated for some designs.[27] Such a reactor would lose about 0.015 $\Delta k/k$ when the fuel went from room temperature to operating temperatures, and would lose about 0.007 $\Delta k/k$ when the fuel went from operating temperatures to the melting point. In this temperature range the Doppler coefficient of such a reactor falls off with rising temperatures roughly as $1/T$.

A prompt-acting, large negative Doppler coefficient imposes some extra control requirements. However, it affords a powerful tool for reactor safety and eases the problem of reactor stability.[31] It reduces the chances that the accidental rapid insertion of reactivity will lead to excessive fuel temperatures. If the accident is so severe that explosive pressures and violent disassembly are needed to terminate the affair, an appreciably negative Doppler effect can markedly reduce the severity of the accident.[47,48] Hence the Doppler effect is a very important parameter to consider when optimizing overall performance. For example, the neutron energy spectrum in a large metal-fueled fast reactor can be adjusted downward by the deliberate introduction of small quantities of moderating material. The reactor would then have both the Doppler effect and the breeding ratio of a ceramic-fueled reactor that has the same ratio of fertile-to-fissile material.

Conversely the loss of sodium from the core hardens the spectrum and reduces the Doppler effect that would result from further fuel heating. Bhide and Hummel[49] have calculated that the Doppler coefficient may be reduced by a factor of 2 on loss of sodium from large ceramic-fueled reactors that have an initial sodium fraction of 52 vol.%. Some of their results are reproduced in Table 11.

For reactors having 70 vol.% sodium initially present, Hummel has recently calculated a reduction in Doppler coefficient by nearly a factor of 5 upon loss of sodium.[50] This sharp reduction in the Doppler effect is serious, since the effect is already smaller than the possible total amount of reactivity to be gained from the loss of sodium for some larger reactor concepts. Moreover, the reduction of Doppler effect itself corresponds to an increase in the reactivity gained upon loss of sodium, if this loss occurs when the fuel is hotter than normal. The problem has led to the consideration of the deliberate introduction of some fixed moderator, possibly in the form of beryllium oxide.[51] The moderation augments the normal Doppler coefficient by providing more neutrons between 500 and 5000 volts, and it does make the Doppler coefficient less sensitive to the loss of sodium. However, as mentioned earlier, it also results in a considerable reduction in the breeding ratio for plutonium-fueled reactors.

It seems very likely that large fast power reactors can be designed to have a substantially negative Doppler coefficient. The fertile U^{238} (or thorium) has been calculated to provide large negative reactivity effects upon heating (see Refs. 27, 40, 49, 52–54), and this is being confirmed in recent experiments.[52,55] Also, a negative Doppler effect has been measured upon heating a U^{235} sample in a U^{235}-thorium fast assembly.[52] Furthermore, recent improvements in theoretical methods,[56–60] in which allowance has been made for the overlapping effect be-

Table 11 DOPPLER REACTIVITY EFFECTS AND COEFFICIENTS FOR LARGE[49] FAST REACTORS FUELED WITH PuO_2-$U^{238}O_2$ AND PuC-U^{238}C

Ratio of Pu to U^{238}	Sodium present?	300 to 2500°K		300 to 750°K		1500 to 2500°K	
		$-\%\ \Delta k$	$-\frac{\Delta k}{\Delta T} \times 10^5$	$-\%\ \Delta k$	$-\frac{\Delta k}{\Delta T} \times 10^5$	$-\%\ \Delta k$	$-\frac{\Delta k}{\Delta T} \times 10^5$
				Oxide Case			
1:9	Yes	2.63	1.15	1.09	2.40	0.59	0.59
1:9	No	1.44	0.65	0.63	1.40	0.29	0.29
1:7	Yes	1.81	0.79	0.77	1.73	0.40	0.40
1:7	No	0.92	0.40	0.39	0.87	0.18	0.18
				Carbide Case			
1:9	Yes	1.95	0.89	0.82	1.82	0.40	0.40
1:9	No	1.11	0.48	0.47	1.05	0.20	0.20
1:7	Yes	1.30	0.59	0.54	1.20	0.29	0.29
1:7	No	0.63	0.29	0.27	0.60	0.12	0.12

tween resonances of the same isotope, as well as for overlapping between resonances of different isotopes, indicate that the reactivity contribution from the fissile isotope should be very small and possibly slightly negative upon heating a mixture of fertile and fissile material, typifying the fuel of a large reactor.

For reactors of medium enrichment (30 to 50%), a small negative Doppler effect has usually been calculated.[50,61] Of course, detailed analysis is required for each design.

Other Fuel Cycles

Since the world's fission-energy resources consist primarily of thorium and U^{238}, one can anticipate that each of these fertile isotopes will find its way into future breeder reactors and that both U^{233} and Pu^{239} will serve as fissionable isotopes. It has been conventional to speak in terms of the U^{238}-Pu^{239} cycle and the Th^{232}-U^{233} cycle. The latter combination has been calculated to provide a breeding ratio of 1.20 : 1.25 in clean large fast reactors, smaller than that for U^{238}-Pu^{239} but still well above unity. However, it may be that a more desirable set of overall performance characteristics can be obtained with mixed fuel systems such as Th-Pu^{239} or U^{238}-U^{233}.

The fission cross section of U^{233} falls off more steeply with increasing energy between 5 and 100 kev than that of Pu^{239}. Also, the ratio of capture to fission for fast neutrons is thought to be small and slowly varying with energy for U^{233}, whereas that of Pu^{239} shows a rapid decrease between 30 and 300 kev. Consequently the reactivity increase due to the spectral hardening that accompanies the loss of sodium should be much smaller when U^{233} rather than Pu^{239} is used as the fissionable isotope. A reactor fueled with U^{233} should therefore exhibit less difficulty with positive sodium coefficients.

Thorium has a much smaller fission cross section and a higher threshold energy for fission than U^{238}. Consequently thorium provides very little fast fission bonus to the breeding ratio. However, it also contributes a smaller reactivity gain due to increased fast fission upon loss of sodium; hence it should tend to give a more negative sodium void coefficient. Also, in the metallic form thorium is less dense than uranium. Two metal-fueled reactors that use the same volume fractions of thorium or uranium will exhibit less capture and scattering from the fertile isotope in the thorium case. This again makes the sodium void coefficient more negative for thorium than for uranium.

Reactors using thorium in the core do suffer from an important control problem. Upon capture of a neutron in thorium, Pa^{233} is first formed; it decays to U^{233} with a 27.4-day half-life. (The corresponding link in the U^{238}-Pu^{239} chain, Np^{239}, decays with only a 2.33-day half-life.) Consequently a considerable buildup of Pa^{233} will occur in a thorium-bearing reactor. When such a reactor is shut down after long-term operation at high power, considerable reactivity will be released if this Pa^{233} is allowed to decay in the core. For one Th-U^{233} conceptual design, Goldman[61] has calculated that $1\frac{3}{4}\%$ $\Delta k/k$ would be released in 22 days and that a total of 4% $\Delta k/k$ was available. This reactivity, of course, is initially lost during operation of the reactor, leading to greater reactivity shim requirements for burnup. Goldman has estimated that even with an internal breeding ratio of unity, such a reactor would lose considerable reactivity during operation. In the concept studied, a large portion of the thorium absorptions would not produce U^{233} until after the fuel element had been unloaded. Thus considerably more shutdown and operational reactivity are required if thorium is the fertile material in the core. Thorium in the blanket would produce an effect much smaller in magnitude, since the reactivity worth of fissionable isotopes there is less.

The buildup of Pu^{240} or U^{234} with recycle generally makes the sodium coefficient more positive. Both these isotopes have larger fission cross sections and lower threshold energies for fission than U^{238}. In this respect, U^{233} can again be expected to fare better than Pu^{239}. Because of the lower ratio of capture to fission in U^{233}, the buildup of U^{234} at equilibrium, when U^{233} is the fuel, will be much less than the buildup of Pu^{240} when Pu^{239} is the fuel, other things being equal.

What does this all mean so far as hybrid fuel cycles are concerned? In Table 12 the breeding ratio and sodium void reactivity effect are compared for 3000-liter metal-fueled spherical reactors for different fertile-fissile combinations.[30][*] The sodium void effect for uniform loss from the core is negative for all but the U^{238}-Pu^{239} fuel type. The breeding ratio is about 0.2 higher when U^{238} rather than thorium is used in the cores of these reactors.

This is at least preliminary evidence that for metal-fueled large reactors, the sodium void problem with Pu^{239} may be significantly eased if thorium is used as the fertile material in the core, at some expense to breeding ratio and with the creation of some additional control problems. Less improvement in the sodium coefficient would be expected upon the substitution of thorium into oxide or carbide fuels, since the density advantage would not be present.

Table 12 CRITICAL MASS, BREEDING RATIO, AND SODIUM VOID[30] EFFECT FOR 3000-LITER METAL-FUELED FAST REACTORS[*]

Fuel type	Critical mass, kg	Breeding ratio	Sodium void effect, $\Delta k/k$[†]
Th-U^{233}	918	1.27	−0.031
U^{238}-U^{233}	878	1.50	−0.012
Th-Pu^{239}	1060	1.36	−0.013
U^{238}-Pu^{239}	1030	1.60	+0.0025
Th-U^{235}	1580	1.02	−0.030
U^{238}-U^{235}	1460	1.16	−0.016

[*] All reactors have 15 vol.% fuel, 18 vol.% steel, and 67 vol.% sodium in the core. The blanket has 40% uranium, is 45 in. thick, and is reflected.

[†] Reactivity effect produced by removing 40% of sodium in core.

The excellent characteristics of the U^{238}-U^{233}-fueled reactor are of particular interest. The breeding ratio is much better than for the conventional thorium-U^{233} concept, the control problem due to Pa^{233} buildup is alleviated,[*] and the sodium coefficient is quite negative. Thus one can reasonably expect to be able to go to somewhat higher fuel alloy concentrations (and a still higher breeding ratio) or to larger core volumes, or to both, without getting a positive sodium void coefficient. An internal breeding ratio of about unity may be possible. Furthermore, the relatively flat alpha of U^{233} leads one to expect only a moderate drop in breeding ratio upon going from the metallic form to the oxide or carbide of the U^{238}-U^{233} mixture. Also, only moderate differences in sodium coefficient are expected for equal concentrations of U^{238} in metal, oxide, or carbide reactors of the same size.

These expectations are confirmed by the calculated results listed in Table 13. At 3000 liters and fuel concentrations up to 27%, the U^{238}-U^{233} combination in metal, oxide, or carbide form gives negative core sodium void effects. With the metal an internal breeding ratio above unity is calculated, with an overall breeding ratio of 1.67. Even for the oxide the breeding ratio exceeds 1.4. At 6000 liters in spherical geometry, negative sodium coefficients are calculated for fuel concentrations between 15 and 20%.

It may be that nature has been doubly kind. Fuel elements of uranium in metallic, oxide,

---

[*] For ready comparison, the sodium coefficient and other characteristics are also listed in Table 12 for U^{235}-fueled reactors of similar composition. Note that U^{235} seems to give a sodium coefficient similar to that with U^{233}.

[*] The U^{238}-U^{233} reactor would also have a larger delayed-neutron fraction than the corresponding thorium-U^{233} reactor, thanks to the appreciable delayed-neutron contribution from U^{238}.

Table 13 PERFORMANCE CHARACTERISTICS OF REACTORS USING U^{238}-U^{233} FUEL IN METALLIC, OXIDE, OR CARBIDE FORM*

	Blanket of 40% U^{238}, 45% Na					
			Na void effect, $\Delta k/k$		Breeding ratio	
Reactor type	Ratio U^{238} to U^{233}	Critical mass, kg	Core only	Core + blanket	Internal	Total
3000-liter metal						
20% fuel, 67% Na	11.1	940	−0.0068	−0.0091	0.87	1.61
27% fuel, 57% Na	13.7	1050	−0.0001	−0.0016	1.05	1.67
6000-liter metal						
20% fuel, 67% Na	13.1	1620	+0.0020	+0.0007	1.04	1.61
27% fuel, 57% Na	15.6	1850	+0.0061	+0.0053	1.22	1.67
3000-liter oxide						
20% fuel, 67% Na	6.1	840	−0.0150	−0.0180		
27% fuel, 57% Na	8.0	900	−0.0048	−0.0068	0.69	1.41
6000-liter oxide						
20% fuel, 67% Na	7.7	1390	−0.0034	−0.0051	0.69	1.35
27% fuel, 57% Na	9.6	1540	+0.0040	+0.0029	0.85	1.39
3000-liter carbide						
20% fuel, 67% Na	8.0	870	−0.0096	−0.0121	0.68	1.45
27% fuel, 57% Na	10.1	950	−0.0015	−0.0033	0.85	1.50
6000-liter carbide						
15% fuel, 70% Na	7.7	1350	−0.0059	−0.0078	0.68	1.35
20% fuel, 67% Na	10.0	1470	+0.0006	−0.0008	0.87	1.46
27% fuel, 57% Na	11.7	1660	+0.0058	+0.0048	1.01	1.48

*Structure is steel in core and blanket. Blanket is 45 cm thick and reflected. Density of metal, oxide, and carbide are 19, 10, and 13 g/cm^3, respectively. The sodium void effect is computed by removing 40% of the sodium originally present in region.

carbide, and sulfide form have all exhibited considerable potential in irradiation tests to date.

Thus there is reason to believe that, in the long run, U^{238}-U^{233} in some form may well be one of the two primary fuel types for fast power reactors. Such a reactor type, in concert with the optimum plutonium-burning design, could consume the world's supply of fissionable material. The blanket of each reactor type could be built with thorium or U^{238}, or both, as the need arose for specific fissile isotopes.

Very Large Reactors

From the point of view of coolant void coefficients, the thorium-U^{233} combination should lend itself particularly well to the very large reactors mentioned in connection with the desalinization of water. In Table 14 sodium void coefficients and other nuclear characteristics are given for 25,000- and 50,000-liter spherical reactors containing 15% thorium-U^{233} and 70% sodium in the core.[62] The sodium void effect for the core alone still appears to be negative at 25,000 liters.

With lead as the coolant, the coolant void effect is more negative than for sodium. At 25,000 liters, where the sodium void effect is essentially zero, lead (or lead-bismuth) gives a substantially negative result. By 50,000 liters in spherical geometry, however, even lead is calculated to have a slightly positive void coefficient with U^{233}-thorium fuel. The coefficient would be more strongly positive if U^{238} were the fertile material.

It must be noted that the multigroup cross sections[11] used in these calculations were prepared with smaller reactors, having a harder

Table 14 PERFORMANCE OF VERY LARGE REACTORS[62] USING THORIUM-U^{233}*

Core size, liters	Coolant	Critical mass, kg	Breeding ratio		Coolant void effect,† $\Delta k/k$
			Internal	Total	
25,000	Na	4600	0.82	1.03	−0.00005
50,000	Na	8440	0.91	1.06	+0.012
25,000	Pb	4070	0.89	1.08	−0.010
50,000	Pb	7600	0.97	1.10	+0.0005

*All reactors are spherical and contain 15% metal fuel, 15% steel, and 70% coolant in core.

†Reactivity change on removing 40% of coolant from core.

spectrum, in mind. Particularly for the very large sodium-cooled reactors, the results can only be taken as indicative, not definitive.

Fuel Recycle Effects

The equilibrium fuel isotopic composition with continuous recycling will depend only on the reactor design and the feed material used to replenish core burnout. The initial composition will influence the time needed to get close to equilibrium but not the final composition.

The equilibrium composition upon recycle has been computed with three different feed materials for some of the Pu^{239}-U^{238}-fueled reactors discussed earlier in the section on reactor performance, assuming in each case that the feed plutonium composition is the same as that initially present in the core.[22] Representative results are given in Table 15. When the feed material is Pu-A (pure Pu^{239}), very little Pu^{242} has a chance to build up, and only about 5% of Pu^{241} is present at equilibrium for all the cases considered. When the feed material has a large proportion of higher isotopes, the final constitution depends sharply on the internal breeding ratio. Internal breeding adds primarily Pu^{239}, and, when the internal breeding ratio is high, less of the feed material rich in higher isotopes is used. Thus the metal-fueled core, with larger internal breeding, has less Pu^{241} and Pu^{242} at equilibrium than the oxide, when Pu-C is the feed.

Table 16 COMPARISON OF INITIAL AND EQUILIBRIUM CRITICAL MASS AND BREEDING RATIO FOR 1500-LITER OXIDE REACTOR[22]

Feed type	Critical mass*		Breeding ratio†	
	Initial	Equilibrium	Initial	Equilibrium
Pu-A	562	496	1.47	1.67
Pu-B	514	468	1.57	1.80
Pu-C	442	421	1.72	1.96

* Kilograms of (Pu^{239} + Pu^{241}).
† (Pu^{239} + Pu^{241} produced)/(Pu^{239} + Pu^{241} consumed.)

A comparison of initial and equilibrium critical mass and breeding ratio is given in Table 16 for a 1500-liter oxide-fuel reactor using Pu-A, -B, or -C, respectively, as the initial fuel and the feed. In all three cases the critical mass is lowered and the breeding ratio is increased on the transition to an equilibrium composition. It is interesting to note that the breeding ratio for equilibrium composition with Pu-C feed is 0.49 above that for a reactor using pure Pu^{239}, whereas the critical mass (of thermally fissile isotopes) is only three-fourths as large. The large fast fission bonus in Pu^{240} and Pu^{242} leads to some of this large difference in performance. The remainder is attributable to the relatively greater reactivity and breeding potential which Pu^{241} is believed to have, relative to Pu^{239}.

However, not all qualities of a reactor improve with the change in plutonium isotopic composition on recycle. If pure Pu^{239} is taken

Table 15 EQUILIBRIUM COMPOSITION OF FUEL WITH PLUTONIUM RECYCLE[22]

Reactor type	Type of feed Pu	Pu^{239}	Pu^{240}	Pu^{241}	Pu^{242}	Atoms of Pu/ atoms of U^{238} (at equilibrium)	Atoms of Pu/ atoms of Pu^{238} (initially)
800-liter metal	Pu-A	0.653	0.293	0.041	0.013	0.172	0.128
800-liter metal	Pu-C	0.544	0.281	0.066	0.109	0.189	0.163
800-liter oxide	Pu-A	0.609	0.324	0.049	0.018	0.510	0.336
800-liter oxide	Pu-C	0.288	0.266	0.121	0.325	0.795	0.439
1500-liter oxide	Pu-A	0.582	0.343	0.054	0.021	0.391	0.253
1500-liter oxide	Pu-B	0.481	0.372	0.088	0.059	0.425	0.269
1500-liter oxide	Pu-C	0.329	0.287	0.109	0.275	0.542	0.323

Pu Composition of Feed

Feed type	Atom %			
	Pu^{239}	Pu^{240}	Pu^{241}	Pu^{242}
Pu-A	100	0	0	0
Pu-B	74.7	10.2	12.4	2.7
Pu-C	40.0	10.0	25.0	25.0

as the starting point, the sodium void reactivity coefficient gets appreciably more positive (or less negative) during the transition to equilibrium composition.

Some Considerations of Practical Design and Blanket Management

The performance figures presented earlier were all for idealized spherical reactors. Actual reactors of the same core volume will all have larger critical masses for a variety of reasons. Control-rod channels, coolant-flow transition regions, and, in particular, the transition from spherical to cylindrical geometry, may combine to raise the critical mass by 20% or more.

The overall breeding ratio should not be affected significantly by these considerations if the blanket is kept an efficient capturer of neutrons. However, various practical considerations also enter herein. If the residence time of the upper and lower blanket is determined by fuel-element burnup considerations rather than by optimum blanket economics, thick end blankets may prove to be uneconomical. Again, if blanket fabrication and reprocessing costs are excessive, or if the blanket fluxes are very low because of a low core power density, the outer portions of a radial blanket may prove uneconomical.[63]

In the cases where flux levels are low or residence times are limited, the introduction of moderator into the blanket, with a consequent reduction in fertile material requirements, may help appreciably. A blanket cycle involving inward radial motion of elements during their total residence time may sometimes improve the economics, but this depends strongly on the specific conditions present.

In an unmoderated blanket of a fast reactor, one can expect a buildup of 2 or 3% Pu^{240} in the bred Pu^{239} for optimum cycling. Since the core physics performance is good for essentially any plutonium isotopic composition (disregarding sodium coefficient and possibly Doppler effect considerations), the reactor can be used to convert "dirty" plutonium* to "clean" plutonium by feeding the core with the former from thermal reactors and extracting the latter from the blanket for use in thermal reactors, should suitable designs develop.

Burnout does not appear to be limited by considerations of reactivity in fast reactors, even if the internal breeding ratios are low. There will be economic penalties imposed, however, due to (1) the higher frequency of reactor shutdown imposed by the need of partial reloading and (2) the loss of neutrons to shim type control rods, which will be needed to supply the reactivity loss between partial unloadings, assuming control is via a neutron absorber such as boron, tantalum, or tungsten.

If the latter problem becomes important, the use of moderator (or moderator plus fertile material) type shim rods may help.[30]

Neutron Physics Effects of Structural Materials

General Cross-Section Considerations

The effect of structural materials on fast reactor performance is determined by the magnitude and variation with energy of three cross sections: those for elastic scattering, inelastic scattering, and neutron capture.

The use of a structural material with a high cross section for elastic scattering reduces the leakage reactivity controlled by the sodium coolant, other things being equal. That phenomenon leading to a negative component in the sodium void reactivity effect is thus reduced, making the overall sodium void coefficient more positive.

Inelastic scattering affects the critical mass by moving neutrons from a higher energy to a lower energy, where the probability of leakage from the core is usually smaller but the probability of producing a fission may be smaller or larger, depending on the particular conditions involved. The introduction of a structural material with much inelastic scattering can also influence the sodium coefficient or the Doppler coefficient by producing more low-energy neutrons.

Inelastic scattering affects the breeding ratio in two ways: (1) by moving neutrons to a region of lower energy where alpha for Pu^{239} is higher and (2) by reducing the probability of fast fission in the fertile material and hence the fast fission bonus.

---

* The expression "dirty plutonium" is used to categorize plutonium having a considerable buildup of the higher isotopes.

Neutron capture in the structural materials exhibits a regular behavior and a systematic variation with atomic number, Z. For all structural materials neutron capture is usually much smaller than the fission cross section of Pu^{239} over the energy range from 10 kev to 10 Mev. There are no huge resonances as are found for xenon and samarium in the thermal-energy region. Only tantalum has a cross section about equal to that for fission in Pu^{239}, and this is only below 15 kev.

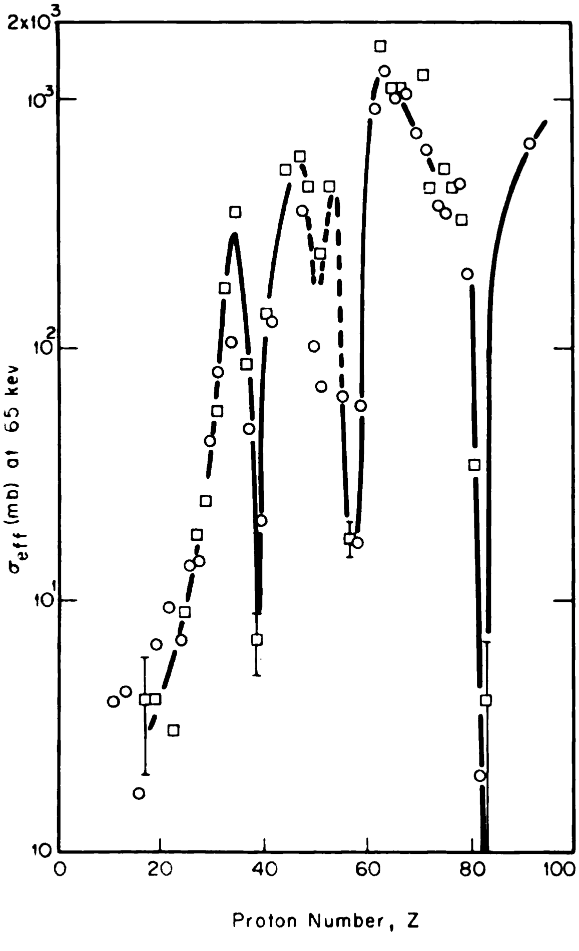

(The squares correspond to results for odd-Z elements. The circles, corresponding to results for even-Z elements, would generally fall below the curve drawn through the squares, except that the results for even-Z elements have been multiplied by a factor of 2.2, to make the data overlap. This even-odd effect is related to the average difference in resonance-level spacing for even vs. odd nuclei. The large dips in the cross section occur for isotopes with complete neutron shells, corresponding to the "magic" numbers 50, 82, and 126.)

Fig. 18 Average radiative capture cross sections for 65-kev neutrons as a function of atomic number.

The capture cross section will vary from element to element, as well as among isotopes of a particular element, but there is a general behavior pattern. The capture cross section tends to increase with atomic number. It is larger for nuclei having an odd number of protons or neutrons (odd-even) than for those having even numbers of both protons and neutrons (even-even). And it is very small for the so-called "magic nuclei." This systematic behavior pattern of neutron capture is illustrated in Fig. 18, where measurements of σ_c at 65 kev are plotted against Z over a large range of elements.[64] The values plotted in Fig. 18 are listed in Table 17, along with similar measurements of 30 kev.

In Fig. 19 the capture cross sections of three important structural elements, iron, niobium, and tantalum, are plotted vs. neutron energy. Of the two odd-even isotopes, the heavier Ta^{181} exhibits more capture than Nb^{93}. The capture cross section of U^{238} has been included for comparison purposes. Iron has a small σ_c, as one expects for a lighter element of primarily even-even nuclear structure.

The capture cross sections of tungsten, molybdenum, zirconium, and vanadium are plotted vs. energy in Fig. 20. Tungsten and molybdenum are both even-Z nuclei; the heavier tungsten captures more neutrons. Zirconium and vanadium both have "magic" character; hence one expects them to have small capture cross sections.

The capture cross section usually falls off quite rapidly with increasing neutron energy. Fission cross sections do the same below 100 kv; however, they reach a plateau region and then rise with increasing energy, as illustrated in Fig. 3.

Some Specific Cases

The capture cross sections of various structural* materials have been averaged over the

---

*The term "structural" is used loosely herein to cover cladding, jacket liners, or subassembly structural components. The calculations, of course, would also apply if the particular element is used as the matrix material for a cermet fuel or as an alloying or additive agent.

Table 17 CAPTURE CROSS SECTION MEASUREMENTS[64] AT 30 AND 65 KEV*

Z	Element	$\sigma_{n,\gamma}(30)$, mb	$\sigma_{n,\gamma}(65)$, mb
6	C	<0.2	0.0 ± 0.3
9	F	4.5 ± 1.0	
11	Na	5.0 ± 0.7	0.7 ± 0.3
12	Mg	0.4 ± 0.2	2.1 ± 0.7
13	Al	2.8 ± 0.7	
14	Si	13.0 ± 4.0	2.0 ± 0.7
15	P	7.0 ± 1.0	0.5 ± 0.2
16	S	25.0 ± 8.0	0.8 ± 0.6
17	Cl	11.0 ± 4.0	4.0 ± 2.0
19	K	16.0 ± 2.0	4.0 ± 1.0
20	Ca	10.0 ± 1.0	3.0 ± 1.0
22	Ti	29.0 ± 3.0	5.0 ± 1.0
23	V	23.0 ± 8.0	3.0 ± 1.0
24	Cr	10.0 ± 3.0	3.5 ± 1.0
25	Mn	22	9.0 ± 1.0
26	Fe	12.0 ± 3.0	6.3 ± 2.0
27	Co	88.0 ± 30.0	18
28	Ni	16.0 ± 4.0	6.5 ± 2.0
29	Cu	39.0 ± 7.0	25.0 ± 5.0
30	Zn	31.0 ± 6.0	20.0 ± 5.0
31	Ga	103	56
32	Ge	74	39.0 ± 6.0
33	As	350	175
34	Se	94	51
35	Br	650	345
37	Rb	180	89
38	Sr	155	24
39	Y	13.5 ± 3.0	6.9 ± 2.0
40	Zr	14.0 ± 3.0	10.3 ± 2.0
41	Cb	264	135
42	Mo	140	69
45	Rh	850	540
46	Pd	454	265
47	Ag	951	586
48	Cd	330	183
49	In	(763)	(448)
50	Sn	88.0 ± 15.0	51.0 ± 10.0
51	Sb	436	245
52	Te	97	35
53	I	733	440
56	Ba	61	33
57	La	55.0 ± 10.0	18.0 ± 3.0
58	Ce	35.0 ± 5.0	8.0 ± 2.0
59	Pr	115	59
62	Sm	875	450
63	Eu	2560	1580
64	Gd	1175	670
65	Tb	1850	1070
66	Dy	775	570
67	Ho	1720	1070
68	Er	960	540
69	Tm	1310	700
70	Yb	575	390
71	Lu	2520	1200
72	Hf	510	330
73	Ta	735	440
74	W	270	190
75	Re	900	525
76	Os	300	175
77	Ir	795	450
78	Pt	330	234
79	Au	515	332
80	Hg	295	103
81	Tl	71	35
82	Pb	3.0 ± 3.0	1.0 ± 2.0
83	Bi	1.0 ± 4.0	4.0 ± 3.0
92	U^{238}	473	302

* The neutron energy resolution was ±7 and ±20 kev at 30 and 65 kev, respectively. The estimated absolute error is ±9% except where noted.

neutron energy spectra of two typical large fast power reactors, one an 800-liter metal-fueled reactor with a relatively hard spectrum and the other a 6000-liter oxide-fueled reactor with a considerably more degraded spectrum. The results are listed in Table 18. Spectrum-averaged values for capture in U^{238} and fission in Pu^{239} are also presented.

The cross sections are listed per atom in units of barns. To compare their effects on reactor performance, one must multiply them by the appropriate concentrations of atoms. These are listed for the pure materials at full density (N) in an adjoining column. For example, 10 vol.% nickel or iron gives about twice the atom concentration that 10 vol.% zirconium would give.

The capture cross sections for thermal neutrons (0.025 ev) have also been listed in Table 17 for the various elements, as has the ratio of $\sigma_{c,\text{thermal}}$ to $\sigma_{c,6000\ \text{liters}}$. Except for titanium this ratio is less than the corresponding ratio of the cross section for fission in Pu^{239}. Thus, per atom, capture in structural materials is relatively greater for large fast reactors than for thermal reactors. What makes the use of the various structural materials conceivable is the much higher atom concentration of fissile isotope in fast reactors. The effect on breeding ratio will depend essentially on the ratio

$$\frac{N^{\text{structural}} \cdot \bar{\sigma}_c^{\text{structural}}}{N^{\text{fissile}} \cdot (\bar{\sigma}_f + \bar{\sigma}_c)^{\text{fissile}}}$$

The effect of various structural materials on the critical mass and breeding ratio[17] of an 800-liter U^{238}-Pu^{239} metal-fueled reactor is given in Table 19. Steel, titanium, and zirconium give the lowest critical masses and highest breeding ratios. They are similar in their effect. The higher inelastic scattering cross section in vanadium leads to some reduction in breeding ratio and a small increase in critical mass. Niobium and molybdenum have appreciable capture cross sections, and the breeding ratio is depressed considerably, whereas the large capture cross section of tantalum drops the breeding ratio to near unity. These reactors were all assumed to have 25 vol.% of the structural material; the trends would be similar but the relative differences smaller if, say, 15 vol.% of the structural material were used in the calculation.

The effects of 15 vol.% of various structural elements on a 3000-liter PuC-U^{238}C-fueled reactor are given in Table 20. The general trends are similar to those observed with the smaller metal-fueled reactor. The (n,p) cross section for nickel makes it somewhat less favorable to breeding than iron or chromium.

The choice of structural material in the core also can influence important reactivity coefficients. For example, the magnitude of the Doppler effect is very sensitive to the amount of low-energy flux present. The use of a structural material with a considerable capture cross section, which in turn leads to a higher critical mass, results in a harder neutron energy spectrum. In one large carbide-fuel concept, for example, the use of niobium rather than stainless steel as the cladding material in the core led to a reduction[33] of the Doppler coefficient by a factor of 7 (i.e., the coefficient remained negative but was much smaller in magnitude). On the other hand, the use of vanadium or Inconel X instead of steel was calculated to produce little change in the Doppler coefficient for this particular concept.

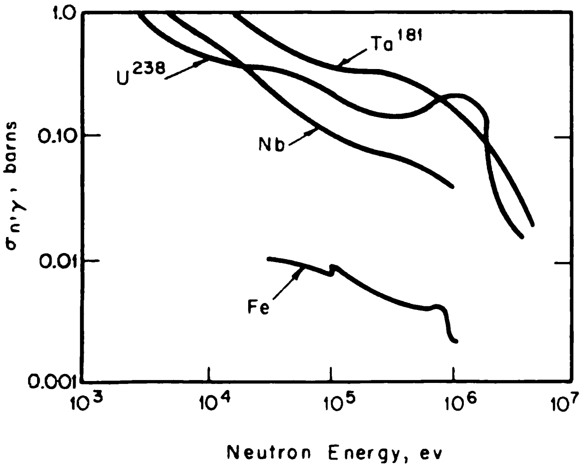

Fig. 19 Capture cross sections of iron, niobium, tantalum, and U^{238}.

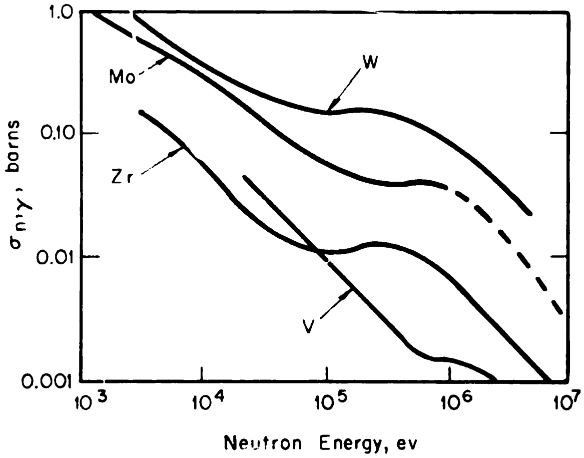

Fig. 20 Capture cross sections of vanadium, zirconium, molybdenum, and tungsten.

The effect of various structural materials on the sodium void effect for a 3000-liter PuC-U^{238}C-fueled reactor is illustrated in Table 21. The calculations indicate that the structural elements of low atomic mass are roughly the same in their influence on sodium void effect, at least for this particular reactor choice. A similar behavior among steel, nickel, and vanadium has also been reported for an oxide-fueled concept.[33]

However, it must be emphasized that the results given in Table 20 (as well as in earlier tables on sodium void effect for large reactors) are only qualitative. The techniques used for these calculations were not the most sophisticated,[25] and cross-section information at the lower neutron energies, in particular, is un-

Table 18 AVERAGE CAPTURE CROSS SECTIONS OF STRUCTURAL MATERIALS IN TYPICAL FAST REACTOR SPECTRA

Element	N, atoms per cm^3 of pure element $\times 10^{-24}$	Average capture cross section, barns		Capture at 0.025 ev (thermal)	$\frac{\sigma_{c,\text{ thermal}}}{\sigma_{c,6000\text{ liters}}}$
		800-liter metal fuel reactor	6000-liter oxide fuel reactor		
Ti	0.0566	0.006	0.012	5.8	483
V	0.0704	0.009	0.019	5.0	263
Cr	0.0822	0.009	0.014	3.1	221
Fe	0.0847	0.006	0.008	2.5	313
Ni	0.0913	0.02*	0.025*	4.8	194
Zr	0.0425	0.011	0.018	0.18	10
Nb	0.0545	0.107	0.245	1.2	5
Mo	0.0640	0.073	0.118	2.7	23
Ta	0.0553	0.322	0.617	21.0	34
U^{238}	0.048	0.202	0.296	2.7	9
$\sigma_f Pu^{239}$		1.8	2.0	746.0	373

*Includes 0.01 barn for σ_{np} reaction.

Table 19 EFFECT OF VARIOUS STRUCTURAL MATERIALS ON PERFORMANCE[17] OF 800-LITER U^{238}-Pu^{239} METAL-FUELED REACTOR*

Structural material	Critical mass, kg	Breeding ratio	Alpha	A†	F†
Stainless steel	431	1.82	0.188	0.082	0.29
Ti	425	1.92	0.180	0.073	0.33
V	456	1.68	0.222	0.11	0.25
Zr	415	1.89	0.181	0.076	0.31
Nb	494	1.51	0.169	0.44	0.25
Mo	502	1.46	0.185	0.41	0.22
Ta	716	1.02	0.170	0.91	0.18

*The core contains 25 vol.% fuel, 25 vol.% structural material, and 50 vol.% sodium. The blanket contains 60% U^{238}, 20% steel, and 20% sodium.

†A = absorptions in structure and coolant per fission in Pu^{239}; F = fissions in U^{238} per fission in Pu^{239}.

Table 20 EFFECT OF VARIOUS STRUCTURAL MATERIALS ON PERFORMANCE OF 3000-LITER PuC-U^{238}C-FUELED REACTOR*

Element	Critical mass, kg	Breeding ratio
Ti	950	1.47
V	1010	1.32
Cr	960	1.42
Fe	950	1.44
Ni	970†	1.33†
Zr	930	1.48
Nb	1190	1.14
Mo	1150	1.14
Ta	1720	0.80

*The core contains 15 vol.% fuel, 15 vol.% structure, and 70 vol.% sodium. The blanket contains 40% U^{238}, 15% steel, and 45% sodium.

†Estimated correction has been made for σ_{np} in nickel.

Table 21 SODIUM VOID EFFECT FOR 3000-LITER PuC-U^{238}C-FUELED REACTORS* WITH VARIOUS STRUCTURAL MATERIALS

Structural material	Sodium void effect, $\delta k/k$†
Ti	−0.003
V	−0.002
Cr	−0.003
Fe	−0.004
Ni	−0.001‡
Zr	−0.002
Nb	+0.012
Mo	+0.006
Ta	+0.011

*All reactors have 15 vol.% fuel, 15 vol.% structure, and 70 vol.% sodium in core.

†Reactivity change corresponding to removal of 40% sodium initially present in core.

‡Correction has been estimated and included for $\sigma_{n,p}$ in nickel.

Table 22 EFFECT OF NIOBIUM ON PERFORMANCE OF 6000-LITER THORIUM-U^{233}-FUELED FAST REACTORS*

Vol.% structure in core	Steel structure in core		Niobium structure in core	
	Sodium void effect, $\Delta k/k$ (core only)	Breeding ratio	Sodium void effect, $\Delta k/k$ (core only)	Breeding ratio
15	−0.0258	1.24	−0.0019	0.97
25	−0.0175	1.18	+0.0092	0.79

*All reactors have 15% fuel. All reactors have reflected blanket of 40% U^{238}, 15% steel, and 45% sodium. Sodium void effect is the result of removing 40% of the sodium originally present.

certain. Since the sodium void effect is the result of a balance between two large competing phenomena, considerable error is likely at the present time. Sharper distinctions between the various structural elements of low atomic number may become evident as accuracy of prediction improves.

Molybdenum, niobium, and tantalum all lead to positive sodium void effects, as might be expected from the curves given in Figs. 10 and 11. The capture cross sections for molybdenum and niobium are particularly uncertain at low energies, and the magnitude of these coefficients could change appreciably. It is not expected that they will behave like steel, however, in regard to the sodium coefficient.

The relative effect of steel and niobium structure in the core is again illustrated in Table 22 for 6000-liter thorium-U^{233}-fueled fast reactors. With 15 vol.% structure in the core, for reactors using 15 vol.% fuel, the sodium void effect changes from highly negative with steel to almost zero with niobium. If the core structure is raised to 25 vol.% at the expense of sodium, the sodium void effect is highly negative with steel and is quite positive with niobium. The breeding ratio drops from about 1.2 to below unity upon the change from steel to niobium.

In summary, the choice of materials for purposes of structure, fuel containment, or alloying in large fast power reactors has become increasingly complex from the nuclear point of view. Both the type of fuel and the reactor size can affect the choice. Questions of sodium void reactivity effect and Doppler coefficient, as well as breeding ratio and critical mass, must enter into the judgment. A structural material like niobium may be quite tolerable in all nuclear respects for a small U^{238}-plutonium-fueled reactor of EBR-II size. In a large U^{238}-plutonium metal-fueled reactor, the effect of the niobium on breeding ratio may be acceptable but its effect on sodium void coefficient intolerable. In a large U^{238}-plutonium oxide-fueled reactor, niobium may be intolerable in appreciable quantities on both these counts, as well as because of a large reduction in the Doppler coefficient relative to that which one would have had with steel. In a large thorium-U^{233}-fueled reactor, on the other hand, the influence of niobium on the sodium coefficient may be tolerable, but not its effect on breeding ratio.

Uncertainties in Theoretical Prediction

Although a major improvement in our knowledge of fast-neutron cross sections has come about in the last several years, there remain large gaps in the available information. For Pu^{239}, for example, $\nu(E)$ (neutrons per fission) is believed to be known to 1½ or 2% except at higher energies; σ_{fission} is probably known to about 5% except at lower energies where a 10% or greater uncertainty is likely; and the capture cross section is known to about 20% except at lower energies, where the uncertainty is greater. If these few uncertainties all contributed cross-section errors to a calculation in the same direction, the error in reactivity from these sources alone would be 6 or 7% $\Delta k/k$.

The cross sections of most other isotopes and materials of interest to fast reactors are inadequately measured, particularly the capture cross sections. If all these uncertainties were to add up in the same direction, the error in critical mass would be huge. If a careful, objective review of cross sections is made, the errors introduced should be partly random and tend to cancel to a considerable degree. However, considerable discrepancies can and do remain. In one particular 1960 study of this kind on the better measured U^{235}-fueled fast criticals,[11] discrepancies in the prediction of reactivity as large as 4% $\Delta k/k$ appeared between the experiments and calculated results based on an objective cross-section evaluation. Fortunately, recent cross-section measurements have narrowed these differences sharply (see Refs. 11, 15, 65, and 66).

The existence of a considerable body of data from U^{235}-fueled critical experiments enables one to adjust calculations empirically, helping in the prediction of systems not too different in size or composition. However, no similar body of information now exists for plutonium or U^{233}.

The breeding ratio is relatively insensitive to most of the cross-section uncertainties. However, for large oxide- or carbide-fueled reactors, and again for reactors using the thorium-U^{233} cycle, the breeding ratio lies near enough to unity that the uncertainty becomes serious, particularly when doubling time is being evaluated.

Most sensitive to cross-section uncertainties and still in need of further improvement in calculational techniques are the Doppler and sodium void reactivity effects. Both are sensitive to details of reactor spectrum and to the details of cross-section structure in the resonance region. Estimates indicate errors of 50% in the sodium coefficient to be plausible, and even the calculated sign of the coefficient may be in error near the threshold of a positive coefficient.[22] Uncertainties up to 50% are estimated to exist also in the prediction of the Doppler effect.[50,53]

Hence the precise specification of the nuclear characteristics of a large fast power reactor today is essentially impossible. One can only hope to bracket the important parameters.

Concluding Remarks

Only part of the story of large fast power reactor performance has been given here. Conflicts in the simultaneous optimization of design for breeding, for economics, and for safety have been indicated. However, the general subjects of fast reactor safety and fast reactor economics have not been treated. Nor have other considerations, such as heat-transfer characteristics and fuel-element performance, been factored into the discussion.

It has been shown, with reasonable certainty, that breeding is quite feasible in large fast reactors fueled with U^{238}-Pu^{239} or Th^{232}-U^{233}, using any of several structural materials and cooled with sodium. However, materials with large capture cross sections, such as niobium, molybdenum, and tantalum, affect breeding seriously. They also make the attainment of a negative sodium coefficient considerably more difficult for the large reactors.

Breeding is also quite feasible using hybrid fuel systems, such as the combination U^{238}-U^{233}.

It is reasonably certain that large fast reactors can be designed to have significantly negative Doppler coefficients. This desirable characteristic is achievable, in principle, for metal, oxide, or carbide. Small amounts of moderator can be added to enhance the Doppler effect achieved ordinarily but at some penalty to the breeding gain.

It is apparently very difficult to design large fast reactors, especially those fueled with U^{238}-Pu^{239} in some form, so that there is no semblance of a positive sodium void coefficient, even locally. The real importance of the sodium coefficient to fast reactor safety has become the focal point for considerable analysis. Criteria for the determination of safe sodium coefficients (and for safe reactivity gains with the loss of sodium by boiling or other causes) are being sought, always in the light of other existing reactivity coefficients. Despite the difficulties introduced by positive void coefficients, sodium remains, by far, the favorite coolant for large fast power reactors, primarily because of its favorable heat-removal characteristics.

In the process of optimizing the design of large fast power reactors for safety, for economics, and for doubling time, one can anticipate the comparison of reactors having both low and high power densities, of reactors having widely differing geometries, of large reactors with reactors half their size, and of reactors designed with widely differing combinations of reactivity coefficients.

References

1. W. J. McCarthy, Jr., R. B. Nicholson, D. Okrent, and V. Z. Jankus, Studies of Nuclear Accidents in Fast Power Reactors, *Proceedings of the Second United Nations International Conference on the Peaceful Uses of Atomic Energy, Geneva, 1958*, Vol. 12, p. 207, United Nations, Geneva, 1958.
2. D. Okrent, R. Avery, and H. H. Hummel, A Survey of the Theoretical and Experimental Aspects of Fast Reactor Physics, *Proceedings of the International Conference on the Peaceful Uses of Atomic Energy, Geneva*, 1955, Vol. 5, p. 347, United Nations, New York, 1956.
3. J. Codd, L. R. Shepherd, and J. H. Tait, The Physics of Fast Reactors, *Progr. Nucl. Energy*, Ser. I, 1: 251-310 (1956).
4. W. B. Loewenstein and D. Okrent, Physics of Fast Power Reactors, *Proceedings of the Second United Nations International Conference on the Peaceful Uses of Atomic Energy, Geneva*, 1958, Vol. 12, p. 16, United Nations, Geneva, 1958.
5. A. I. Leipunsky, A. I. Abramov, V. N. Andreev, A. I. Baryshnikov, I. I. Bondarenko, N. I. Fetisov, V. I. Galkov, V. I. Golubev, A. D. Gulko, A. G. Guseinov, O. D. Kazachkovsky, N. V. Kozlova, N. V. Krasnoyarov, B. D. Kuziminov, V. N. Morozov, M. N. Nikolaev, L. E. Sherman, G. N. Smirenkin, Iu. Ya. Stavissky, F. I. Ukraintsev, and L. N. Usachev, Studies in the Physics of Fast Neutron Reactors, *Proceedings of the Second United Nations International Conference on the Peaceful*

Uses of Atomic Energy, Geneva, 1958, Vol. 12, p. 3, United Nations, Geneva, 1958.

6. G. E. Hansen, Properties of Elementary Fast-Neutron Critical Assemblies, *Proceedings of the Second United Nations International Conference on the Peaceful Uses of Atomic Energy, Geneva*, 1958, Vol. 12, p. 6, United Nations, Geneva, 1958.
7. R. D. Smith and J. E. Sanders, Experimental Work with Zero Energy Fast Reactors, *Proceedings of the Second United Nations International Conference on the Peaceful Uses of Atomic Energy, Geneva*, 1958, Vol. 12, p. 89, United Nations, Geneva, 1958.
8. J. K. Long, W. B. Loewenstein, C. E. Branyan, G. C. Brunson, F. S. Kirn, D. Okrent, R. E. Rice, and F. W. Thalgott, Fast Neutron Power Reactor Studies with ZPR-III, *Proceedings of the Second United Nations International Conference on the Peaceful Uses of Atomic Energy, Geneva*, 1958, Vol. 12, p. 119, United Nations, Geneva, 1958.
9. G. Fischer, C. Kelber, D. Meneghetti, P. Persiani, D. Shaftman, and A. B. Smith (Eds.), Proceedings of the Conference on the Physics of Breeding, October 19–21, 1959, USAEC Report ANL-6122, Argonne National Laboratory.
10. L. J. Koch and H. C. Paxton, Fast Reactors, in *Ann. Rev. Nucl. Sci.*, 9: 437-472 (1959).
11. S. Yiftah, D. Okrent, and P. A. Moldauer, *Fast Reactor Cross Sections*, Pergamon Press, Inc., New York, 1960.
12. *Physics of Fast and Intermediate Reactors* (3 vols.), International Atomic Energy Agency, Vienna, 1961.
13. Proceedings of the Conference on Breeding, Economics, and Safety in Large, Fast Power Reactors, Report ANL-6792, Argonne National Laboratory, 1963 (to be published).
14. J. C. Hopkins and B. C. Diven, Neutron Capture to Fission Ratios in U^{233}, U^{235} and Pu^{239}, *Nucl. Sci. Eng.*, 12(2): 169 (February 1962).
15. A. B. Smith, Recent Changes in Heavy Element Cross Sections, in Proceedings of the Conference on Breeding, Economics, and Safety in Large, Fast Power Reactors, Report ANL-6792, Argonne National Laboratory, 1963 (to be published).
16. J. R. Dietrich, The Efficient Utilization of Nuclear Fuels, *Power Reactor Technol.*, 6(4): 1 (Fall 1963).
17. S. Yiftah and D. Okrent, Some Physics Calculations on the Performance of Large Fast Breeder Power Reactors, USAEC Report ANL-6212, Argonne National Laboratory, December 1960.
18. P. Greebler, H. Hurwitz, and M. L. Storm, Statistical Evaluation of Fission-Product Absorption Cross Sections of Intermediate and High Energies, *Nucl. Sci. Eng.*, 2(3): 334 (May 1957).
19. U. L. Businaro, S. Gallone, and D. Morgan, On the Dependence upon Energy of Fission Product Poisoning of U^{235}, *J. Nucl. Energy: Pt. A & B*, 4(3): 319 (March 1957).
20. P. A. Moldauer, On the Estimation of Fast Neutron Cross Sections, Proceedings of the Conference on the Physics of Breeding, USAEC Report ANL-6122, pp. 67-76, Argonne National Laboratory, 1959.
21. J. D. Garrison and B. W. Roos, Estimation of Fission Product Capture Cross Sections, *Trans. Am. Nucl. Soc.*, 3(1): 299 (June 1960).
22. D. Okrent, Performance of Large Fast Power Reactors, Including Effects of Higher Isotopes, Recycling and Fission Products, *Physics of Fast and Intermediate Reactors*, Vol. II, International Atomic Energy Agency, Vienna, 1961.
23. A. Smaardyk, T. R. Bump, J. Handwerk, W. J. Kann, E. L. Martinec, P. J. Persiani, G. F. Popper, and S. B. Skladzien, Interim Report: FARET Experimental Program, USAEC Report ANL-6708, Argonne National Laboratory, April 1963.
24. J. B. Nims and P. F. Zweifel, Preliminary Report on Sodium Temperature Coefficients in Large Fast Reactors, USAEC Report APDA-135, Atomic Power Development Associates, Inc., November 1959.
25. H. Hummel and A. Rago, An Accurate Treatment of Resonance Scattering in Light Elements in Fast Reactors, *Physics of Fast and Intermediate Reactors*, Vol. I, International Atomic Energy Agency, Vienna, 1961.
26. M. Bhide and H. H. Hummel, Reactivity Coefficients of Sodium in Some Large Fast Reactors, *Physics of Fast and Intermediate Reactors*, Vol. I, International Atomic Energy Agency, Vienna, 1961.
27. P. Greebler, B. A. Hutchins, and J. R. Sueoka, Calculation of Doppler Coefficient and Other Safety Parameters for A Large Fast Oxide Reactor, USAEC Report GEAP-3646, General Electric Company, Atomic Power Equipment Department, Mar. 23, 1961.
28. H. H. Hummel, K. Phillips, and A. Rago, Calculations of Sodium Void Reactivity Effect for Large Fast Oxide Reactors in Spherical and Slab Geometry, in Proceedings of the Conference on Breeding, Economics, and Safety in Large, Fast Power Reactors, Report ANL-6792, Argonne National Laboratory, 1963 (to be published).
29. K. Cohen et al., Reactor Safety and Considerations of Fuel Cycle Economics for Fast Reactors, in Proceedings of the Conference on Breeding, Economics, and Safety in Large, Fast Power Reactors, Report ANL-6792, Argonne National Laboratory, 1963 (to be published).
30. D. Okrent, Breeding, Safety, and Fuel Cycles, Rome Symposium, 1963.
31. C. P. Zaleski, Some Ideas on the Reactivity Coefficients in Large, Fast Reactors, in Proceedings of the Conference on Breeding, Economics and Safety in Large, Fast Power Reactors, Report ANL-6792, Argonne National Laboratory, 1963 (to be published).

32. P. R. Huebotter, Studies of Simulated Sodium Boiling and Fuel Meltdown, in Proceedings of the Conference on Breeding, Economics, and Safety in Large, Fast Power Reactors, Report ANL-6792, Argonne National Laboratory, 1963 (to be published).
33. K. Horst and B. A. Hutchins, Comparative Study of PuC-UC and PuO_2-UO_2 as Fast Reactor Fuel, Part I, USAEC Report GEAP-3880, General Electric Company, Atomic Power Equipment Department, Jan. 19, 1962.
34. D. Smidt, Discussion, in Proceedings of the Conference on Breeding, Economics, and Safety in Large, Fast Power Reactors, Report ANL-6792, Argonne National Laboratory, 1963 (to be published).
35. R. E. Peterson and S. L. Stewart, Moderator Segmentation: A Core Design for Counteracting Positive Coolant Coefficients in Large Fast Reactors, *Trans. Am. Nucl. Soc.*, 6(2): 260 (November 1963).
36. G. Goertzel, An Estimation of Doppler Effect in Intermediate and Fast Neutron Reactors, *Proceedings of the International Conference on the Peaceful Uses of Atomic Energy, Geneva, 1958,* Vol. 5, p. 472, United Nations, New York, 1956.
37. H. Feshbach, G. Goertzel, and H. Yamauchi, Estimation of Doppler Effect in Fast Reactors, *Nucl. Sci. Eng.*, 1(1): 4 (March 1956).
38. A. M. Lane, J. E. Lynn, and J. S. Syory, An Estimation of the Doppler Effect in Fast Neutron Reactors, British Report AERE-T/M-137, July 1956.
39. H. A. Bethe, On the Doppler Effect in Fast Reactors, USAEC Report APDA-119, Atomic Power Development Associates, Inc., Mar. 11, 1957.
40. R. B. Nicholson, The Doppler Effect in Fast Neutron Reactors (thesis), Report APDA-139, Atomic Power Development Associates, Inc., June 1960.
41. E. A. Fossoul, Effet Doppler du Plutonium 239 dans les Reacteurs Rapides, *Physics of Fast and Intermediate Reactors,* Vol. III, International Atomic Energy Agency, Vienna, 1961.
42. H. V. Lichtenberger, F. W. Thalgott, W. Y. Kato, and M. Novick, Operating Experience and Experimental Results Obtained from a NaK-Cooled Fast Reactor, *Proceedings of the International Conference on the Peaceful Uses of Atomic Energy, Geneva,* 1955, Vol. 3, p. 345, United Nations, New York, 1956.
43. F. W. Thalgott, J. F. Boland, R. O. Brittan, J. C. Carter, F. D. McGinnis, M. Novick, D. Okrent, H. A. Sandmeier, R. R. Smith, and R. E. Rice, Stability Studies on EBR-I, *Proceedings of the Second United Nations International Conference on the Peaceful Uses of Atomic Energy, Geneva,* 1958, Vol. 12, p. 242, United Nations, Geneva, 1958.
44. R. R. Smith, J. F. Boland, F. D. McGinnis, M. Novick, and F. W. Thalgott, Instability Studies with EBR-I, Mark III, USAEC Report ANL-6266, Argonne National Laboratory, December 1960.
45. W. Y. Kato and D. K. Butler, Measurement of the Doppler Temperature Effect in an EBR-I Type Assembly, USAEC Report ANL-5809, Argonne National Laboratory, July 1958.
46. A. R. Baker and T. A. J. Jaques, A Measurement of the Contribution of the Doppler Effect to the Temperature Coefficient of Reactivity in a Fast Reactor, British Report AERE-R/M-168, June 1958.
47. R. B. Nicholson, Methods for Determining the Energy Release in Hypothetical Reactor Meltdown Accidents (thesis), USAEC Report APDA-150, Atomic Power Development Associates, Inc., December 1962.
48. B. Wolfe, N. Friedman, and D. Riley, Influence of the Doppler Effect on the Meltdown Accident, in Proceedings of the Conference on Breeding, Economics, and Safety in Large, Fast Power Reactors, Report ANL-6792, Argonne National Laboratory, 1963 (to be published).
49. M. G. Bhide and H. H. Hummel, Calculations of the Doppler Coefficients of Large Ceramic-Fueled Fast Reactors, USAEC Report ANL-6601, Argonne National Laboratory, August 1962.
50. H. H. Hummel and A. L. Rago, Effect of Parameter Variation in Doppler Effect Calculations, in Proceedings of the Conference on Breeding, Economics, and Safety in Large, Fast Power Reactors, Report ANL-6792, Argonne National Laboratory, 1963 (to be published).
51. P. Greebler, Recent Improvements in Calculations of Doppler and Sodium Reactivity Effects for Large Fast Reactors, in Proceedings of the Conference on Breeding, Economics, and Safety in Large, Fast Reactors, Report ANL-6792, Argonne National Laboratory, 1963 (to be published).
52. T. H. Springer and S. G. Carpenter, Fast Spectrum Doppler Measurements, in Proceedings of the Conference on Breeding, Economics, and Safety in Large, Fast Power Reactors, Report ANL-6792, Argonne National Laboratory, 1963 (to be published).
53. R. Froelich, K. Ott, and J. J. Schmidt, Dependence of Fast Doppler Coefficients on Nuclear Data Uncertainties, in Proceedings of the Conference on Breeding, Economics, and Safety in Large, Fast Power Reactors, Report ANL-6792, Argonne National Laboratory, 1963 (to be published).
54. P. Greebler and E. Goldman, Doppler Calculations for Large, Fast Ceramic Reactors — Effects of Improved Methods and Recent Cross-Section Information, USAEC Report GEAP-4092, General Electric Company, Atomic Power Equipment Department, Dec. 19, 1962.
55. G. J. Fischer, H. H. Hummel, J. R. Folkrod, and D. A. Meneley, Experimental Results for U^{238} Doppler Measurements in Fast Reactor Spectra, in Proceedings of the Conference on Breeding, Economics, and Safety in Large, Fast Power Re-

actors, Report ANL-6792, Argonne National Laboratory, 1963 (to be published).

56. J. Codd and J. P. Collins, Plutonium-239 and Uranium-238 Resonance Interaction Effects in a Dilute Fast Reactor, European Atomic Energy Society Symposium on Advances in Reactor Theory, Karlsruhe, 1963.
57. J. Codd and J. P. Collins, The Influences of Resonance Overlapping on the Doppler Effect in a Dilute Fast Reactor, in Proceedings of the Conference on Breeding, Economics, and Safety in Large, Fast Power Reactors, Report ANL-6792, Argonne National Laboratory, 1963 (to be published).
58. R. N. Hwang, An Improved Method of Doppler Effect Calculations for Fissile Materials in the Intermediate Energy Region, in Proceedings of the Conference on Breeding, Economics, and Safety in Large, Fast Power Reactors, Report ANL-6792, Argonne National Laboratory, 1963 (to be published).
59. R. Froelich, K. Ott, and J. J. Schmidt, Calculation of Doppler Coefficients of Dilute Fast Reactors, in Proceedings of the Conference on Breeding, Economics, and Safety in Large, Fast Power Reactors, Report ANL-6792, Argonne National Laboratory, 1963 (to be published).
60. D. B. Adler and F. T. Adler, Theoretical Representation of Cross Sections of Fissile Isotopes, in Proceedings of the Conference on Breeding, Economics, and Safety in Large, Fast Power Reactors, Report ANL-6792, Argonne National Laboratory, 1963 (to be published).
61. A. J. Goldman, A Feasibility Study of Fast U^{233}-Th Breeder Reactors, USAEC Report NDA-2134-3, Nuclear Development Corporation of America, Oct. 10, 1960.
62. D. Okrent, Nuclear Considerations in the Selection of Materials for Fast Power Reactors, in *Nuclear Metallurgy*, Vol. IX, AIME, 1963.
63. S. A. Hasnain and D. Okrent, On The Design and Management of Fast Reactor Blankets, *Nucl. Sci. Eng.*, 9(3): 314 (March 1961).
64. R. L. Macklin, J. H. Gibbons, and T. Inada, Average Radiative Capture Cross Sections for 30- and 65-keV Neutrons, *Phys. Rev.*, 129(6): 2695 (Mar. 15, 1963).
65. D. Meneghetti, Effect of Resonance Scattering on Criticality Calculations of Fast Assemblies, USAEC Report ANL-6466, Argonne National Laboratory, December 1961.
66. W. G. Davey, k Calculations for 22 ZPR-III Fast Reactor Assemblies Using ANL Cross Section Set 635, USAEC Report ANL-6570, Argonne National Laboratory, May 1962. (See also ANL-6682.)

Section I

Power Reactor Technology

Economics, Applications, Programs

Desalinization of Water

The use of large blocks of nuclear (thermal) power to produce fresh water from saline water has been under discussion for several months past.[1–6] Both fast[1,2] and thermal[3,4] reactors have been proposed for this purpose, and a recent study[7] has considered a wide range of reactor types and sizes. The reader interested in the general state of water resources in this country—without regard to the nuclear question—may find Refs. 8 and 9 helpful. The discussion here will center around the nuclear energy sources that have been considered for the application.

The plant discussed in Ref. 1 utilizes a fast reactor, fueled with vibration-compacted UO_2-PuO_2, which is described in more detail in Ref. 2. Core specifications are given in Table I-1, and a schematic of the core arrangement is in Fig. I-1. The energy is used entirely for producing distilled water, and the amount produced, 10^9 gal/day, represents about half the consumption of New York City. The water conversion plant discussed in Ref. 2 is a multistage flash evaporation unit consisting of 30 stages, although the seawater plant used in Ref. 1 (Fig. I-2) is a quadruple-effect evaporator. A figure of merit used to describe the relative performance of evaporator plants is the so-called "performance ratio." This is the weight of water evaporated per unit weight of steam consumed and is approximately equal to the number of effects used in a multiple-effect evaporator plant. The performance ratio can also be defined as the weight of fresh water produced per 1000 Btu of heat consumed, and this latter definition is particularly useful for the following conversion:

(Cost of steam, cents/10^6 Btu)(8.33)/(performance ratio)
= cost of energy used for distillation, cents/1000 gal of fresh water produced

Table I-1 CORE SPECIFICATIONS[2] OF A PROPOSED FAST REACTOR FOR A WATER DESALINIZATION PLANT

Power, Mw(t) (blanket power neglected)	25,000
Core volume, liters	50,000
Core height, ft	4
Core diameter, ft	24
Core composition	
Fuel material, vol. %	34 (UO_2 + PuO_2)
Coolant, Na, vol. %	50
Steel, vol. %	16
Fuel enrichment, %	15 (total Pu)
Critical mass, kg of Pu (total)	22,000 (at equilibrium)
Fuel and core	
Cladding, outside diameter, in.	0.300
Cladding, thickness, in.	0.020
Fuel diameter, in.	0.260
Pitch, in.	0.396
Elements per subassembly	400
Number of subassemblies (25,000-Mw reference)	1016
Coolant and core	
Maximum/average power density	1.5
Maximum heat flux, Btu/(hr)(sq ft)	10^6
Coolant velocity, ft/sec	25
Average coolant temperature rise, °F	257
Inlet temperature, °F	593
Blanket specifications	
Axial blankets (top and bottom)	
Diameter, ft	24
Thickness, each, ft	3
Composition	34 vol. % UO_2 50 vol. % Na 16 vol. % steel
Radial blanket	
Thickness, ft	1.5
Composition	65 vol. % UO_2 20 vol. % Na 15 vol. % steel
Reactor performance characteristics	
Specific power, Mw/kg of Pu	1.1
Power density, Mw/liter	0.5
Fuel burnup, Mwd/metric ton	100,000
Plutonium production ratio (breeding ratio)	
Total, core and blanket	1.3
Internal (core) breeding ratio	0.75

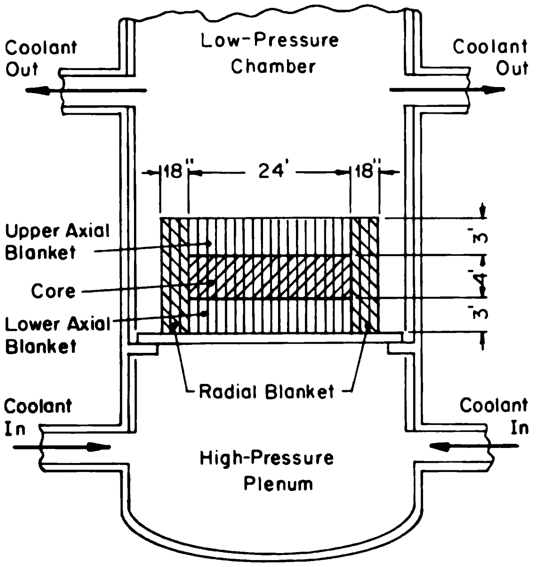

Fig. I-1 Core arrangement of the proposed fast 25,000-Mw reference reactor[2] for conversion of seawater.

This equation expresses the connection between the reactor portion of the seawater conversion plant and the evaporation portion of the plant, at least as far as costs are concerned. If the heat source is expensive, then the cheapest water is produced by an evaporator plant with a high performance ratio. If heat is relatively cheap, then a low performance ratio may be used; the evaporator plant can be cheap also, and the total cost of the fresh water is reduced accordingly. Thus there is an optimum value for the performance ratio which is lower as the cost of heat is lower. For the plant described in Ref. 1, only four effects are postulated, since the cost of steam from the reactor is calculated to be low.

Reference 3 discusses thermal reactors as applied to the production of both electricity and distilled water. The reactor plant consists of three heavy-water-moderated boiling-H_2O reactors, each generating 8333 Mw(t). A simplified flow diagram of the plant is shown in Fig. I-3. The water portion of the plant consumes about 19,800 Mw(t) and 500 Mw(e), and the net power to the switchyard is 4500 Mw(e). Detailed plant designs of the reactors discussed in Ref. 3 are given in Ref. 4. Table I-2 summarizes one of the designs. The heavy-water reactors are refueled under power and employ fuel elements of the concentric tubular type, containing two rings of UO_2 that are each about 0.6 in. thick.

Reference 7 represents a portion of a cooperative effort of a number of governmental agencies to define more closely the costs associated with the dual-purpose plants. Those participating in the overall study are the Atomic Energy Commission (AEC), the Bureau of Reclamation, the Office of Saline Water (Department of Interior), and the Federal Power Commission. The Bechtel Corporation was engaged by the AEC to act as architect-engineer in connection with the AEC portion of the program, and Ref. 7 is the Bechtel report. The total of nine different cases that were studied covered a wide variety of reactors and encompassed a time period from the present to 1980.

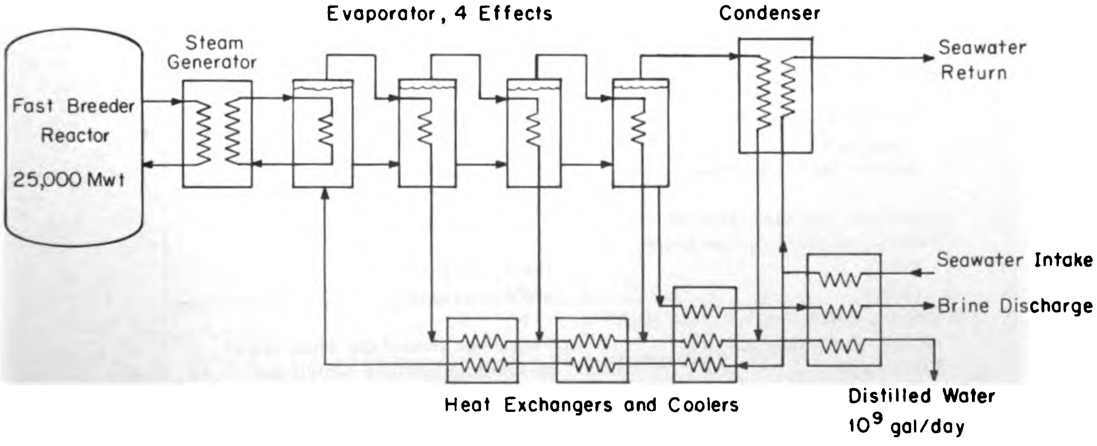

Fig. I-2 Seawater distillation plant employing a fast-breeder reactor.[1]

Table I-2 DESIGN DATA[4] FOR A DUAL-PURPOSE 8333-MW(T) REACTOR

Reactor type	Pressure tube, D_2O moderated, boiling light-water cooled		
Fuel	Vibratory-packed natural UO_2 (below 0.8% U^{235})		
Moderator	D_2O		
Reflector	2 ft of graphite on bottom and sides; 2 ft of D_2O on top of reactor		
Reactor thermal power	25,000 Mw, three 8333-Mw(t) reactors		
Type of refueling	On-line, from below reactor		
Materials			
Density of UO_2 fuel	9.81 g UO_2/cm^3		
Pressure-tube material	Zircaloy-2 tubing; stainless-steel end plugs		
Calandria tube material	Aluminum 6061T6		
Calandria material	Aluminum-clad steel		
Gas between tubes	CO_2		
Reactor dimensions			
Reactor shape	Rectangular parallelepiped with corners removed		
Lattice spacing	Square array on 9-in. pitch		
Nuclear material inventory, each of three reactors			
Uranium, metric tons	747		
D_2O, metric tons	545		
Graphite, metric tons	486		
Core size			
Total number of tubes	1308		
Active core length, ft	28.5		
Active core width, ft	27		
Active core height (along tube length), ft	30		
Calandria vessel			
Length, ft	34.5		
Width, ft	33		
Height, ft	35		
Fuel elements			
Form	Nested concentric tubes of UO_2		
Cladding	0.020-in. Zircaloy-2		
Dimensions of fuel element	Inside diameter, in.	Outside diameter, in.	Length, in.
Inner tube	1.424	2.718	72 nominal
Outer tube	3.152	4.326	72 nominal
Reactor cooling system			
Specific power in uranium	11.2 watts/g (average)		
Heat flux, Btu/(hr)(sq ft)	Average	Maximum	
Inner tube	216,000	248,000	
Outer tube	263,000	303,000	
Burnout (at 12.5% quality)	754,000		
Mass flow rate of coolant, lb/hr	2.21×10^8		
Reactor temperature, pressure			
Inlet	464°F, 720 psia		
Outlet	486°F, 620 psia		
Steam separation system, 8333 Mw(t)			
Method of steam separation	Two-stage centrifugal separators		
First stage	In-line impingement centrifugal separators, one located at end of each pressure tube; exit quality, 90%		
Second stage	Centrifugal separator, 24 per 8333-Mw(t) reactor; exit quality >99.25%		

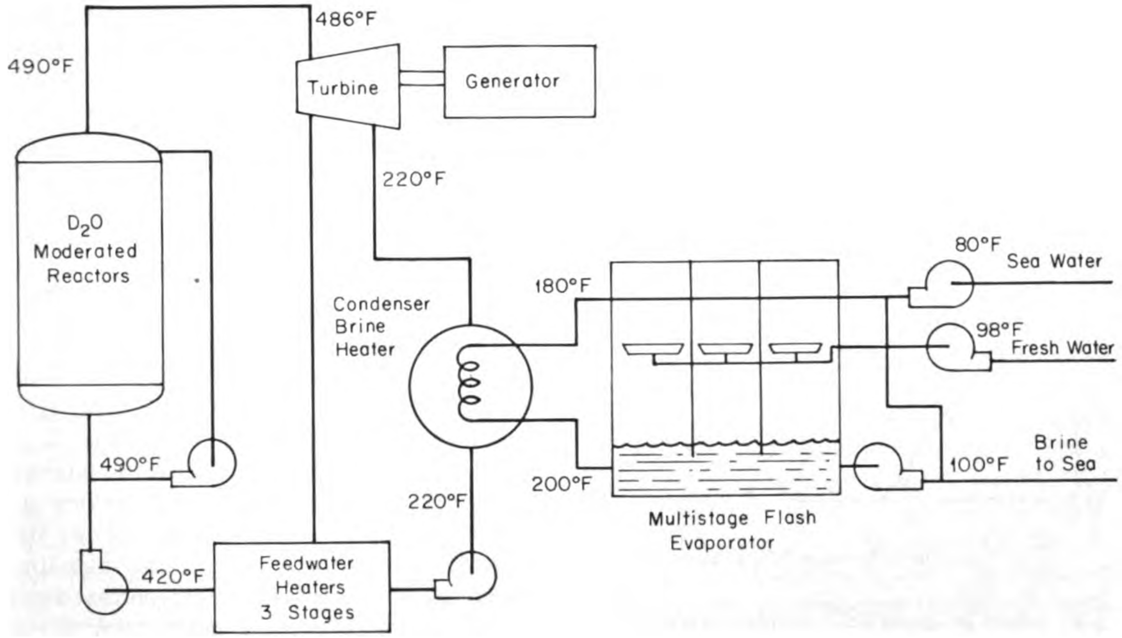

Fig. I-3 Schematic of dual-purpose plant.[3]

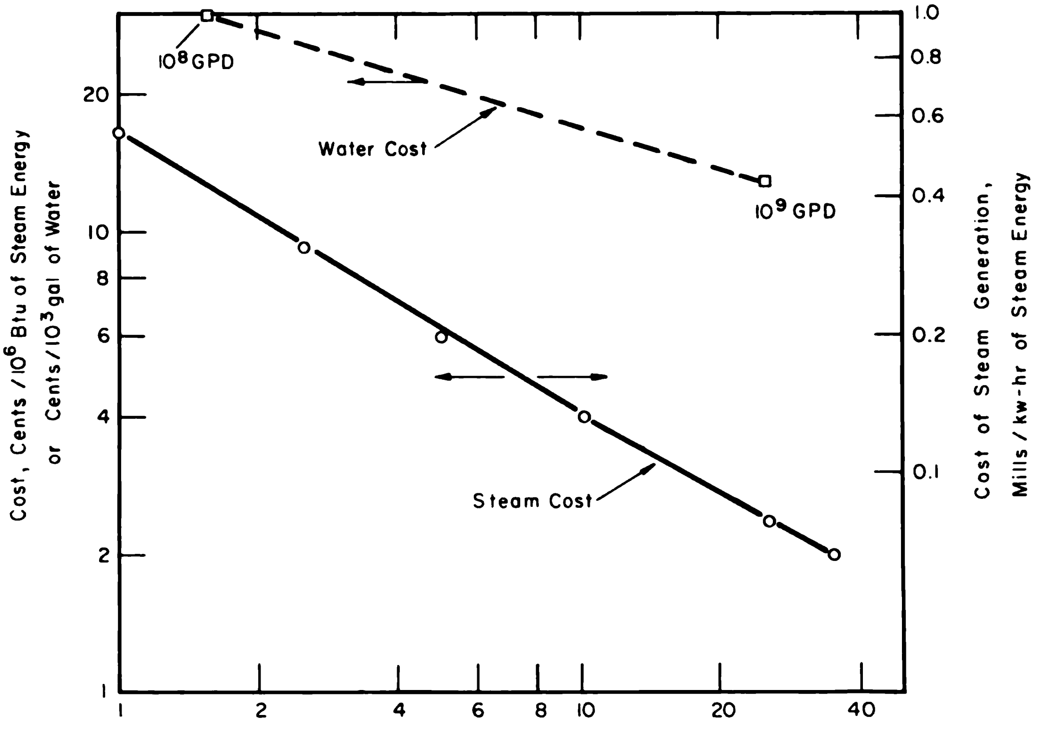

Fig. I-4 Estimated costs of steam production by fast-breeder reactors and corresponding costs of desalinizing seawater.[2] Single-purpose operation; 90% plant factor; municipal financing: 7.75% on depreciating capital, 5.5% on working capital, 3.75% on fuel inventories.

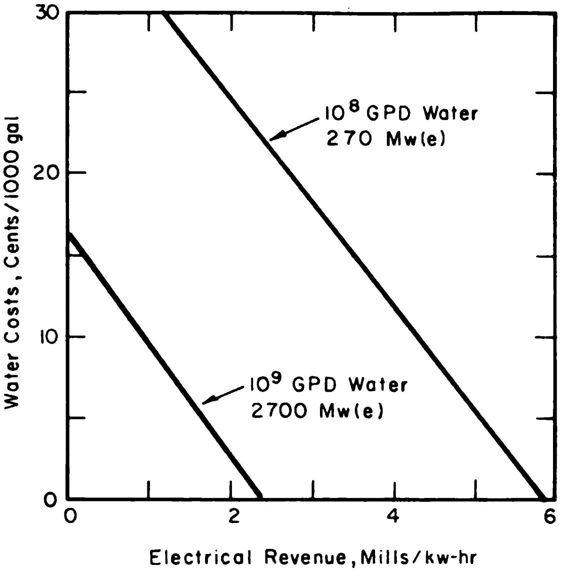

Fig. I-5 Effect of electrical revenue on water production costs.[2] Reactors and ground rules are the same as for Fig. I-4.

When one considers the possibilities of very large desalinization plants, along with the possibilities of concurrent electric power production under the various conceivable financing schemes, the situation becomes so complex and so far removed from past nuclear experience that a casual assessment of the proposals has little value. It is at least possible, however, to gain some understanding of the goals and requirements of the application by examining selected results from the studies mentioned above.

Figure I-4, constructed from the results of Ref. 2, shows estimated steam and fresh water costs for single-purpose plants in the 10^8 to 10^9 gal/day range, for plants utilizing fast-breeder reactors. Regardless of how one views the accuracy of the estimates, it seems clear that, for very low desalinization costs, one is speaking of the nuclear generation of steam energy at costs of about 10 cents per million Btu or less, corresponding to thermal-power generation costs of about 0.35 mill/kw-hr or less.

For current desalinization technology, high steam temperatures are not required, since the use of temperatures above about 300°F leads to scaling problems in the evaporators. If the reactor type used for steam production is capable of producing steam at considerably higher temperature, it seems obvious that the use of backpressure turbines for the production of electricity in conjunction with the desalinization process would be economically attractive in any case where there is a market for the power. Since the thermal energy in the exhaust steam from the backpressure turbines is still usable in the desalinization process, the economics of power generation are particularly favorable if the electricity can be considered as a byproduct; for the use of energy in the power cycle is effectively 100% efficient, and only a fraction of the total plant cost is attributable to the electrical generation. The estimated improvement in economics is illustrated in Fig. I-5, from Ref. 2, which shows the 10^8 gal/day plant producing fresh water at about 18 cents per thousand gallons if electric power is sold at 3 mills/kw-hr. The 10^9 gal/day plant is estimated to produce fresh water at about 7 cents per thousand gallons if electricity is sold at

Table I-3 ESTIMATED STEAM, ELECTRICITY, AND WATER COSTS FOR 25,000-Mw(t) STATION* USING THREE H_2O-COOLED, D_2O-MODERATED REACTORS[3]

Steam cost (600 psi), cents/10^6 Btu		Electricity cost, mills/kw-hr	Water cost, cents/10^3 gal	
Capital	3.8	1.16	Heat	1.4
D_2O inventory	0.8	0.10	Electricity	1.8
Fuel cycle	0.9	0.11	Capital	6.0
Operation and maintenance, insurance	1.0	0.18	Operation and maintenance	0.8
			Chemicals	1.0
Totals	6.5	1.55		11.0

*Economic ground rules: plant investment at 7.7%/year; fuel and D_2O at 5.5%/year; natural U_3O_8 at \$5/lb; Pu as nitrate at \$6.7/g; D_2O at \$20/lb; load factor = 90%; size of fueling industry = 10 tons/day; fuel owned by plant operator.

1.5 mills/kw-hr. These numbers are somewhat lower, but not drastically so, than those estimated in Ref. 3 for a station of comparable size utilizing the heavy-water-moderated reactors (Table I-3).

The results of Ref. 7 can be used, conceptually, to examine a transition from reactors of currently contemplated sizes to the very large reactors such as those considered in Refs. 2 and 3 and to throw some light on the effects of the dual-purpose (vs. power only) application and methods of financing. The nine reactor types considered in the study are described in Table I-4. The uncertainties in estimating the very large plants may be inferred from the lack of specificity in their descriptions. In Table I-5 the estimated costs of producing steam energy for water desalinization are given for the nine types in a way that compares dual-purpose operation with power-only operation. For each of the plant types, Ref. 7 gives curves similar to that of Fig. I-6, which applies to the plant utilizing fast-breeder reactors (Case 9). The reference also gives for each case the estimated cost of electric power generation if the plant is designed for that purpose only. In Table I-5 the costs of steam production listed are those for the dual-purpose plant which correspond to the sale of electricity at a price equal to its production cost in the single-purpose plant. This is illustrated in Fig. I-6. The estimates for the very large plants (Cases 7-9) are not greatly different than those given in Table I-3.

Table I-4 REACTOR TYPES USED IN STUDIES OF NINE DIFFERENT ELECTRIC GENERATION-DESALINIZATION CASES IN REF. 7

1. One 1500-Mw(t) light-water reactor of current technology.
2. Three 1500-Mw(t) light-water reactors in a single plant, current technology.
3. One 3220-Mw(t) light-water reactor, current technology.
4. One 3500-Mw(t) heavy-water-moderated organic-cooled reactor, current technology.
5. One 3500-Mw(t) graphite-moderated light-water-cooled reactor, current technology.
6. One 8300-Mw(t) heavy-water-moderated organic-cooled reactor; 1975 technology.
7. A multiunit 25,000-Mw(t) station with high-conversion-ratio reactors, such as: heavy-water-moderated organic-, light-water-, or heavy-water-cooled reactors; graphite-moderated organic-, or light-water-cooled reactors; or graphite-moderated gas-cooled thorium-cycle reactors; 1980 technology.
8. A 25,000-Mw(t) station utilizing an unspecified number of slightly enriched reactors such as: light-water-moderated in combination with graphite-moderated steam-cooled reactors, graphite-moderated sodium-cooled reactors, or graphite-moderated gas-cooled reactors; 1980 technology.
9. An unspecified number of fast-breeder reactors of 25,000 Mw(t) total capacity; 1980 technology.

Since the costs of steam production in the large plants of Table I-5 do not appear to be substantially less than the costs necessary for the economic large-scale desalinization of water, one might conclude, at least tentatively, that revenue from the sale of steam for de-

Table I-5 ESTIMATED COSTS OF PRODUCING ELECTRICITY AND HEAT IN THE FORM OF STEAM FOR SEAWATER DISTILLATION[7]

Case (see Table I-4)	Cost of electricity from plant designed for power only, mills/kw(e)-hr		Cost of heat in steam from dual-purpose plant if electricity is sold at the cost of its production in the power-only plant, cents/10^6 Btu		Net electrical output of power-only plant, Mw(t)	Net electrical output of dual-purpose plant, Mw(e)
	7% to 5% financing	14% to 12.5% financing	7% to 5% financing	14% to 12.5% financing		
1	3.97	6.16	20	30	470	240
2	3.67	5.65	18.5	27	1410	720
3	3.45	5.28	18	26	1002	510
4	3.01	4.88	13	20	1110	620
5	3.03	4.89	15	22	1140	600
6	2.18	3.53	10	16	2770	1600
7*	1.87 to 1.67	3.20 to 3.01	9 to 8	14 to 6	8300	4800
8*	2.20 to 2.14	3.61 to 3.46	8 to 7.5	12 to 12	9000	6350
9*	1.78 to 1.57	3.30 to 3.07	6 to 5	11 to 10	9000	6350

*The range of the estimates results from a range of assumptions as to natural-uranium cost, plutonium value, and capacity of fuel reprocessing plant.

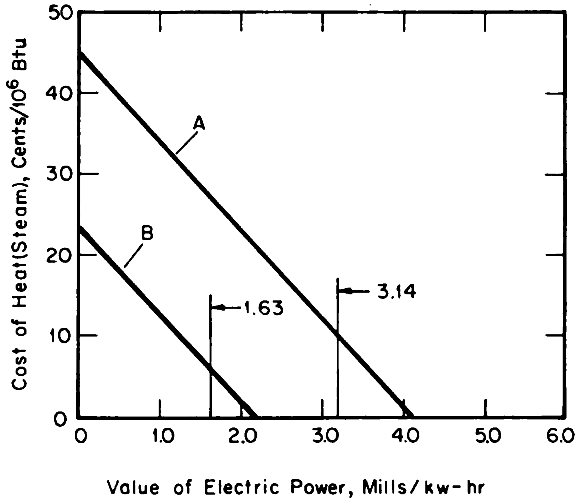

Fig. I-6 Effect of electrical revenue on cost of producing steam heat for desalinization by fast-breeder reactors, from Ref. 7 (Case 9). Curve A is for annual fixed charge rates of 14% and 12.5% for depreciating and nondepreciating capital, respectively; curve B is for rates of 7% and 5%. Plant factor is 80%. The vertical lines show the estimated electric power costs if the plant is designed for power only.

salinization is unlikely to make possible large reductions in the cost of electrical generation from a reactor of given thermal capacity. The more important aspect of the dual-purpose application may be that it increases the opportunities for utilizing plants of very large energy output.

References

1. R. P. Hammond, Large Reactors May Distill Sea Water Economically, *Nucleonics*, 20(12): 45 (December 1962).
2. A. Sesonske and R. P. Hammond, A Preliminary Evaluation of Fast Oxide Breeder Reactors for Sea Water Conversion, USAEC Report LA-2733, Los Alamos Scientific Laboratory of the University of California, August 1962.
3. I. Spiewak, A Large Desalinization Reactor Based on Current Technology, *Nucleonics*, 21(7): 64 (July 1963).
4. Sargent and Lundy, Saline Water Conversion Power Reactor Plants, USAEC Report SL-1998, Jan. 11, 1963.
5. Edging Toward Desalination, *The Forum Memo to Members*, Atomic Industrial Forum, Inc., 10(10): 8 (October 1963).
6. Nuclear Desalter Called Too Costly, *Engineering News-Record*, 17(19): 23 (Nov. 7, 1963).
7. Bechtel Corp., Large Reactor Study for Sea Water Distillation, Final Report for Office of Program Evaluation, Division of Reactor Development, U. S. Atomic Energy Commission, July 1963.
8. R. Revelle, Water-Resources Research in the Federal Government, *Science*, 142(3595): 1027 (Nov. 22, 1963).
9. D. G. Stephan, Water Renovation ... What It Means to You, *Chem. Eng. Progr.*, 59(11): 19 (November 1963).

Section II

Physics

Thermal-Neutron Diffusion Parameters

The good agreement between the measurement and calculation of neutron diffusion parameters, which was indicated several years ago, has been found to be somewhat premature with the advent of more advanced experimental techniques and more sophisticated methods of analysis. The purpose of this article is to review some of the recent papers pertaining to the measurement and calculation of diffusion parameters and to present the current status. Many of the papers reviewed were presented at the Neutron Thermalization Conference held at the Brookhaven National Laboratory in the spring of 1962.

The various aspects of the thermal diffusion problem are best seen by examining the space-time-energy-dependent diffusion equation in a nonmultiplying scattering medium:

$$1/v \frac{\partial \phi(E,r,t)}{\partial t} = -\Sigma_a(E,r)\phi(E,r,t) + D(E,r)\,\nabla^2\,\phi(E,r,t) + H(E,r)\,\phi(E,r,t) + S(E,r,t) \qquad (1)$$

where

$$H(E,r)\,\phi(E,r,t) = \int_{r'}\int_{E} \phi(E',r',t)\,\Sigma_s(E',r' \rightarrow E,r)\,dE'dr' - \phi(E,r,t)\,\Sigma_s(E)$$

and v = neutron velocity corresponding to the energy E

ϕ = neutron flux

D = diffusion coefficient

∇^2 = thermalization operator

Σ_a = absorption cross section

S = source term

$\Sigma_s(E',r' \rightarrow E,r)$ = differential cross section for scattering

$\Sigma_s(E)$ = total cross section for scattering

In a pulsed medium at large times after the injection of the neutron burst, the asymptotic solutions of Eq. 1 can be written as:

$$\phi(r,E,t) = R(r)\;\phi_\alpha(E)e^{-\alpha t} \qquad (2)$$

where α is the lowest eigenvalue of the equation

$$\left(-\frac{\alpha}{v} + \Sigma_a + DB^2\right)\phi(E) = H\phi(E) \qquad (3)$$

and $\phi_\alpha(E)$ is the eigenfunction.

Integrating Eq. 3 over all energies, and considering only $1/v$ absorbers, gives

$$B^2\;\overline{Dv} + \alpha_0 - \alpha = 0 \qquad (4)$$

where $\overline{Dv} = \dfrac{\int n(v)v\;Ddv}{\int n(v)\;dv}$

$\alpha_0 = v(kT)\;\Sigma_a(kT) = v_0\Sigma_a(kT)$

k = the Boltzmann constant

T = the absolute temperature

For $B^2 = 0$ (pulsed infinite medium), the solution to Eq. 3 is a Maxwellian flux distribution and $\alpha = \alpha_0$. When $B^2 > 0$, the spectrum $n(v)$ is displaced to lower energies, and diffusion cooling results. If $B^2 < 0$, the spectrum is shifted to higher energies, and diffusion hardening is the result. Therefore $\overline{Dv}$ is a continuous function of B^2 and can be expanded in the power series:

$$\overline{Dv}(B^2) = D_0 - CB^2 + FB^4 \ldots \qquad (5)$$

where C is known as the diffusion cooling constant. If Eq. 4 is substituted in Eq. 5, the relation between α and B^2 is found as

$$\alpha = \alpha_0 + D_0B^2 - CB^4 + FB^6 + \ldots \qquad (6)$$

Here B^2 is the geometrical buckling and is given as the lowest eigenvalue of the equation

$$\nabla^2 R + B^2 R = 0 \tag{7}$$

In the stationary or time-independent case, there may be asymptotic solutions of Eq. 1 at large distances from the source of the form

$$\phi(r,E) = e^{-\kappa z} \phi_\kappa(E) \tag{8}$$

where κ is the smallest eigenvalue of

$$(\Sigma_a - D\kappa^2)\ \phi(E) = H\phi(E) \tag{9}$$

and ϕ_κ is the eigenfunction. The term κ^2 can be expressed as

$$\kappa^2 = a_1\Sigma_a(kT) + a_2\Sigma_a^2(kT) + a_3\Sigma_a^3(kT) + \ldots \tag{10}$$

and κ^{-1} can be defined as the thermal diffusion length when it is the eigenvalue corresponding to a positive eigenfunction $e^{-\kappa x}\ \phi_\kappa(E)$ describing the exponential decay of the thermal flux in an infinite source-free region, with no variation in the transverse y or z directions. For very weak absorption and at a large distance from the source, $n(v) = \phi(E)/v$ has a Maxwellian distribution at room temperature and deviates progressively and becomes hardened as the absorption in the medium is increased.

Equations 3 and 9 are of the form

$$\left(Dk_1 - \frac{k_2}{v_0}\right)\phi(E) = H\phi(E) \tag{11}$$

where

Pulsed-source experiment $k_1 = B^2$,

$$k_2 = \alpha - \alpha_0;\ \alpha_0 = v_0\Sigma_a(kT) \tag{12a}$$

Diffusion-length experiment $k_1 = -\kappa^2$,

$$k_2 = -v_0\Sigma_a(kT) \tag{12b}$$

A schematic of these functions is shown in Fig. II-1. Here α_0 is v_0 times the cross section in pure moderator at the temperature T, and κ_0^2 is the inverse diffusion length in the pure moderator. The uniform addition of a $1/v$ poison $\Delta\Sigma_a(kT)$ shifts the curve a distance $v_0\Delta\Sigma_a(kT)$ in the direction of positive α without changing the shape of the curve. Thus a larger value of κ^2, namely κ_1^2, is obtained on the abscissa. The dotted curve in the pulsed-neutron experiment region in Fig. II-1 relates the value of the decay constant α to the geometrical buckling of a medium that has an intrinsic $1/v$ absorption cross section $\Sigma_{a_0}(kT) = \alpha_0/v_0$ and to which a uniform $1/v$ poison cross section $\Delta\Sigma_a(kT)$ has been added. The solid curve in the diffusion-length experiment region relates κ^2, or the inverse length $1/L^2$, to the added poison $\Delta\Sigma_a(kT)$ in an infinite medium having an intrinsic $1/v$ cross section $\Sigma_{a_0}(kT) = \alpha_0/v_0$. Only the small segment between the intercepts cannot be measured by either of the techniques.

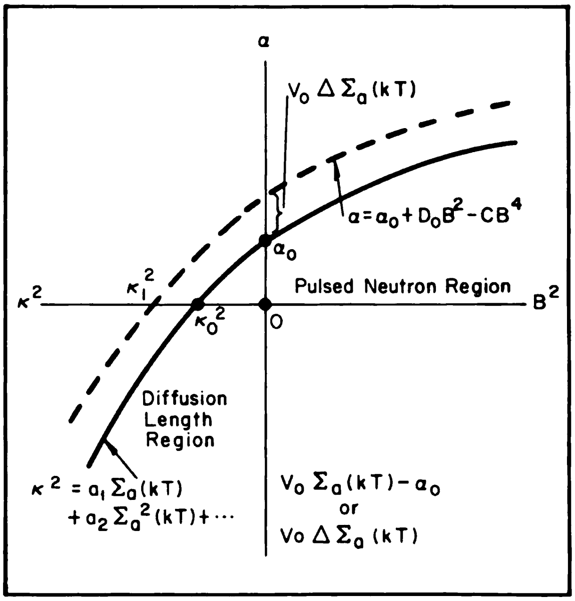
α
$V_0\ \Delta\Sigma_a(kT)$
$\alpha = \alpha_0 + D_0B^2 - CB^4$
α_0
Pulsed Neutron Region
κ^2
κ_1^2
κ_0^2
0
B^2
Diffusion Length Region
$\kappa^2 = a_1\Sigma_a(kT) + a_2\Sigma_a^2(kT) + \cdots$
$V_0\ \Sigma_a(kT) - \alpha_0$
or
$V_0\ \Delta\Sigma_a(kT)$

Fig. II-1 Schematic[12] of the functions $\alpha\ (B^2)$ and $\kappa^2[v_0\ \Sigma_a(kT)]$.

The nonasymptotic solutions of Eq. 1 describe the neutron flux and spectral distribution near discontinuities in the time-independent form of Eq. 1 and the flux and spectrum during the thermalization process in the time-dependent form.

Diffusion-Length Measurements in H_2O

Three techniques have been used to measure the thermal diffusion length in water, differentiated by the source of thermal neutrons as follows: (1) thermal neutrons from a thermal column; (2) a point source of low-energy neutrons; and (3) a pulsed neutron source. One of the recent measurements is that made by Ballowe et al.,[1,2] at the Vallecitos Atomic Laboratory of the General Electric Company. In this measurement the thermal column of the General Electric Nuclear Test Reactor (NTR) was used as a source of thermal neutrons. The experimental arrangement consisted of a cylindrical cadmium-lined water tank, 23.75 in. in diameter, containing a close-fitting piston that was faced with cadmium except for a thin aluminum window at its center. The neutron detector, a thin B^{10}-ZnS(Ag) scintillator, was mounted behind the window. Varying the position of the piston permitted the length of the column of water between the end of the tank and the piston to be varied as desired. The end of the cylindrical water tank abutted the transition region to the graphite thermal column of the NTR, which served as the neutron source. The relaxation length of the thermal neutrons emanating from the thermal column was evaluated by measuring the thermal-neutron flux as a function of the length of the water column between the piston and the end of the water tank.

Because of the cadmium facing, the logarithmic shape of the curve of flux vs. distance remained the same regardless of the length of the water column, and the slope of this curve was the same as that measured in a medium of infinite length. The slope determined the relaxation length and hence the diffusion length in the medium when corrections were made for geometry and background.

Table II-1 DIFFUSION-LENGTH MEASUREMENTS ON THERMAL NEUTRONS IN WATER

Authors	Year	Reference	Method	Temp. at which measurement was made, °C	Diffusion length L, cm	Diffusion length L (at 22°C),* cm
J. L. Russell et al.	1962	1,2	Thermal column	24.55	2.873 ± 0.008	2.858 ± 0.012
Starr and Koppel	1961	3	Thermal column	21	2.754 ± 0.008	2.760 ± 0.008
Reier and DeJuren	1961	4	Sb-Be	23	2.781 ± 0.006	2.775 ± 0.006
Rockey and Skolnik	1961	5	Sb-Be	25.9	2.859 ± 0.018	2.835 ± 0.018
Rohr	1962	7	Sb-Be	16	2.742 ± 0.011	2.778 ± 0.011
Lopez and Beyster	1962	6	Pulsed source	26.7	2.828 ± 0.016	2.803 ± 0.016
Küchle	1960	8	Pulsed source	22	2.744 ± 0.080	2.744 ± 0.080
Dio	1958	9	Pulsed source	22	2.739 ± 0.06	2.739 ± 0.06

*Conversion to 22°C made using $dL/dT = 0.006$ cm/°C.

The measurements were made at temperatures ranging from 25 to 93°C in pure water. Measurements were also made over essentially the same range in H_3BO_3, $CdSO_4$, and $Gd(NO_3)_3$ solutions. The water result at room temperature is one of those listed in Table II-1.

Starr and Koppel[3] have measured the diffusion lengths, using thermal neutrons from a thermal column in H_2O poisoned by various concentrations of H_3BO_3. The measurements were made in a cylindrical water tank situated atop the Brookhaven Research Reactor, using small, bare indium foils spaced at intervals of 0.375 in. (or for heavily poisoned water, 0.250 in.) along a direction perpendicular to the thermal column. The value obtained for pure water at 21°C is also listed in Table II-1.

M. Reier and J. A. DeJuren[4] made diffusion measurements in pure water over the range from 23 to 244.4°C. They also made diffusion measurements at 23°C with various amounts of boron poison in the water and with one cadmium solution, using an Sb^{124}-Be photoneutron source. They used the inhomogeneous form of the diffusion equation (which contains a source term) to determine corrections to the measured relaxation length because of the significant thermalization of the 24-kev neutrons, even at considerable distances from the source where the cadmium ratios were greater than 100. The solution to the inhomogeneous equation, on the assumption of spherical symmetry, consisted of the solution $n = Ge^{-r/L}/r$, the source-free diffusion equation multiplied by a slowly varying correction term involving exponential integrals. The details of the source correction are given in Ref. 4. The measured diffusion length corrected for source effects at 23°C and the corrected value inferred for 22°C are listed in Table II-1. The source corrections at 23°C and 49°C reduced the uncorrected values of L by 0.8%. At 70 and 90°C the correction was 0.6%.

The diffusion length was measured in water over the range from 25.9 to 295.3°C in the pressure vessel of the Knolls Atomic Power Laboratory high-temperature critical assembly by K. S. Rockey and W. Skolnik.[5] They used 5- and 10-mil foils made of P metal, an alloy of manganese (71%), copper (18%), and nickel (10%). The room-temperature result is listed in Table II-1. It is possible that the somewhat high value measured can be attributed to the neglect of source-neutron corrections.

The third technique for measurement of the thermal diffusion length consists in injecting pulses of fast neutrons into moderator regions of different sizes and measuring the decay constant of the leakage neutrons distributed in the fundamental spatial mode. The asymptotic decay constant α is generally fitted to the series expansion given in Eq. 6:

$$\alpha = \alpha_0 + D_0 B^2 - C B^4 + \ldots$$

where α_0 = thermal-neutron density absorption probability of the unpoisoned medium, $v_0 \Sigma_{a_0}(kT)$, at the ambient temperature, T

D_0 = thermal-neutron density coefficient*

C = diffusion cooling coefficient

B^2 = geometrical buckling

The expression for the diffusion length may be found by using the prescription in Eqs. 12*a* and 12*b* to obtain stationary diffusion parameters from pulsed diffusion parameters. Substituting $-1/L^2 = \kappa^2$ for B^2 in Eq. 6 gives the relation

$$L^2 = \frac{D_0}{v_0 \Sigma_a(kT)} \left[1 + \frac{v_0 C \Sigma_a(kT)}{D_0^2}\right] \qquad (13)$$

when $4\Sigma_a(kT) v_0 C \ll D_0^2$. This equation should yield values of L that are directly comparable to values measured by stationary methods.

Lopez and Beyster[6] measured the thermal-neutron diffusion length in water at 26.7°C by the pulsed-source technique. The measured value of the diffusion length lies between values measured by Rohr[7] and Rockey and Skolnik (Table II-1). Küchle and Dio,[8,9] who earlier used the pulsed-source technique to measure the diffusion length, obtained values that were somewhat low, as are shown in Table II-1. These lower values may have been the result of underestimation of the effects of higher harmonic modes or to a container reflection phenomenon. Both of these sources of error are discussed in Ref. 6.

Other Neutron-Diffusion Parameters in H_2O

The close relation between the equations governing pulsed-source experiments and diffusion-length measurements in poisoned water permits the evaluation of the characteristic pulsed-source diffusion parameters α_0, D_0, and C from stationary measurements. Although this has been known for many years, the measurements of Starr and Koppel[3] are the first to yield data of sufficient accuracy to yield a determination of the diffusion cooling C term (see Eq. 6). Thus the stationary and pulsed experimental results may be compared directly by comparing the diffusion parameters.

In evaluating the diffusion parameters, Starr and Koppel[3] made a least-squares fit of the experimental data $[\kappa_i^2, \Sigma_{a_i}(kT)]$ to Eq. 6 and to Eq. 10, substituting $-\kappa^2$ for B^2 and $-v_0\Sigma_a(kT)$ for $\alpha - \alpha_0$ as prescribed in relations 12*a* and 12*b*, to obtain for Eq. 6

$$\frac{\Sigma_a(kT)}{\kappa^2} = \frac{D_0}{v_0} + \frac{C}{v_0}\kappa^2 \qquad (14)$$

and to obtain for Eq. 10

$$\frac{\kappa^2}{\Sigma_a(kT)} = a_1 + a_2 \Sigma_a(kT) \qquad (15)$$

The coefficients a_1 and a_2 of Eq. 15 may be evaluated in terms of the diffusion parameters by recognizing the inverse series expansion of Eq. 6 to be

$$B^2 = \frac{\alpha - \alpha_0}{D_0} + \frac{C}{D_0}\left(\frac{\alpha - \alpha_0}{D_0}\right)^2 + \ldots \qquad (16)$$

and making the substitutions prescribed in relations 12*a* and 12*b* for B^2 and $\alpha - \alpha_0$ to obtain

$$\frac{\kappa^2}{\Sigma_a(kT)} = \frac{v_0}{D_0} - \frac{C}{D_0^3} v_0^2 \, \Sigma_a(kT) \qquad (17)$$

for Eq. 15. In this equation κ is the inverse diffusion length measured in the poisoned medium, having the total macroscopic cross section $\Sigma_a(kT) = \Sigma_H + \Sigma_B$. The value of the hydrogen cross section was found by varying the value of Σ_H in the expression

---

*The value D_0 cm^2/sec is related to the more familiar average diffusion coefficient for neutron flux $\bar{D}$ having the dimension (cm^2) by the average neutron velocity $\bar{v}_0$, namely $D_0 = \bar{v}_0 \bar{D}$, where the averages are over the ambient temperature Maxwellian spectrum.

$$\sum_n \left[\frac{K^2}{\Sigma_a} - \frac{K^2}{\Sigma_a}(\text{calc})\right]$$

until the variance from the least squares fit to the coefficients in Eq. 17 was a minimum. Using the linear functions, Eqs. 14 and 17, the diffusion parameters can then be obtained from the intercept and slope of these functions evaluated at the zero values of κ^2 or $\Sigma_a(kT)$. The results that were obtained from each equation are:

Equation No.	D_0	C/D_0
14	35,506 cm^2/sec	0.11045 cm^2
17	35,852	0.07648

Although the values of D_0 are in good agreement, the values of C/D_0 are not. This is the result of the neglect of the higher order terms and is not surprising in the light of the 20% spectral shift in the most heavily poisoned medium.

For a particular experimental error on the experimental points, there is apparently an optimum range of poison concentration beyond which no further accuracy would be obtained in the determination of the diffusion parameters, D_0 and C Actually, if higher order terms were included in Eqs. 14 and 17 in order to fit the large poison concentrations better, the uncertainty in the first two terms would remain roughly constant. Thus a fit over a small range of poison concentration seems to be as good as a fit over a wider range, so far as the determination of D_0 and C is concerned. Therefore, to obtain an estimate of the error in the value of the diffusion parameters resulting from truncating the series, Starr and Koppel[3] repeatedly fitted Eqs. 14 and 17 with progressively fewer points, dropping those corresponding to the highest poison concentrations and, at the same time, obviously increasing the uncertainty in both D_0 and C. Since the values of C as evaluated using Eqs. 14 and 17 would tend toward the same limit, and the ends of the error bars would tend to approach one another as the equations are fitted over a range of progressively lighter poison concentrations, the fitting of the equations with fewer points was continued until the upper end of the error bar corresponding to the lesser value of C just touched the lower end of the error bar corresponding to the greater value of C. At this point a minimum total uncertainty could be assigned to the diffusion cooling coefficient C. The results obtained using this method of analysis are listed in Table II-2. When C/D_0 was determined from Eq. 17, the dropping of points caused much less shift in the values than when Eq. 14 was used; this indicates that the data are described better by Eq. 17.

The thermal-column measurements of D_0 reported by Reier[10] are also listed in Table II-2.

The Beyster and Lopez neutron diffusion parameter data, listed in Table II-2, were measured, using a high-intensity pulsed neutron source obtained by bombarding a water-cooled lead or tungsten alloy target with 23- to 25-Mev

Table II-2 MEASURED AND CALCULATED DIFFUSION PARAMETERS IN WATER

Author	Year	Reference	Method	Temp. at which measurement was made, °C	D_0, cm^2/sec	D_0 (at 21°C) cm^2/sec	C	$\sigma_a H_2O$, mb	F
Starr and Koppel	1961	3	Thermal column	21	35,850 ± 100	35,850 ± 100	2,900 ± 350	326.9 ± 1.6	
Reier	1960	10	Thermal column	22	37,618 ± 205	37,488 ± 205*		328 ± 6	
Beyster and Lopez	1961	6,11	Pulsed source	26.7	37,426 ± 368† 37,630 ± 404‡	36,685 ± 368 36,889 ± 404*	4,852 ± 763 4,153 ± 852	325.3 ± 1.6 324.8 ± 1.6	
Küchle	1960	8	Pulsed source	22	35,400 ± 700	35,300 ± 700*	4,200 ± 800	326 ± 6	
Honeck		12	Calculation			37,460	2,878		180

*D_0 was corrected to 21°C, using dD_0/dT = 130 cm^2/(sec)(°C). No attempt was made to correct C, since this would shift C by a fraction of the error limits.

†Extrapolation length = 0.32 cm.

‡Extrapolation length = $f(B^2)$.

electron pulses to produce bursts of 2×10^{10} neutrons each by the (γ,n) process. Neutron lifetime measurements were performed on small and large water samples that ranged in geometrical buckling from 0.014 to 0.59 cm^{-2}. Reference 11 lists additional data obtained over the buckling range 0.6 to 1.5 cm^{-2}. The effects of harmonic modes in the large water geometries were determined by measurements of the time-dependent spatial flux. It was found that these flux distributions were also adequately described by simple diffusion-theory calculations.

A three-parameter fit was made to the data, using Eq. 6. The extrapolation distance was calculated in two different ways. In case 1 the extrapolation distance was taken to be a constant $d = 2.131\ D_0/\bar{v}$ with $\bar{v} = 2/\sqrt{\pi}\ 2.2 \times 10^5$ cm/sec. In case 2, d was assumed to vary with B^2. The method of treatment of the extrapolation length did not greatly affect the results. The results of Küchle[8] are also listed in Table II-2. These results were obtained by a three-parameter analysis in the buckling range $B^2 = 0$ to 0.7 cm^{-2}.

Comparison of Experimental and Calculated Diffusion Parameters

Extensive calculations of diffusion parameters in H_2O, D_2O, and graphite have been made by Honeck.[12] He solved the eigenvalue equation, Eq. 3, using the transport formulation for different amounts of poison and employing the Nelkin bound-proton scattering kernel with oxygen included. The calculated eigenvalues were then expanded into a power series to obtain values of D_0, C, and F (Eq. 6). These values are listed in Table II-2.

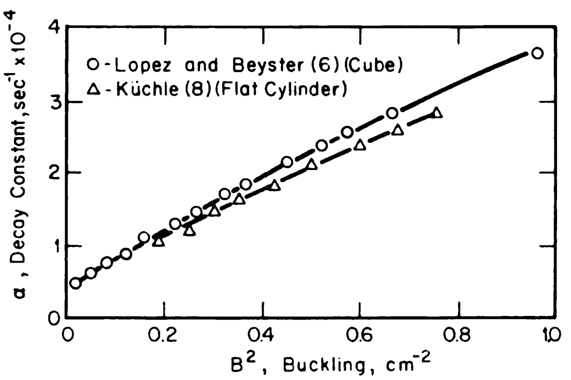

Fig. II-2 α vs. B^2 for H_2O at 26.7°C.[13]

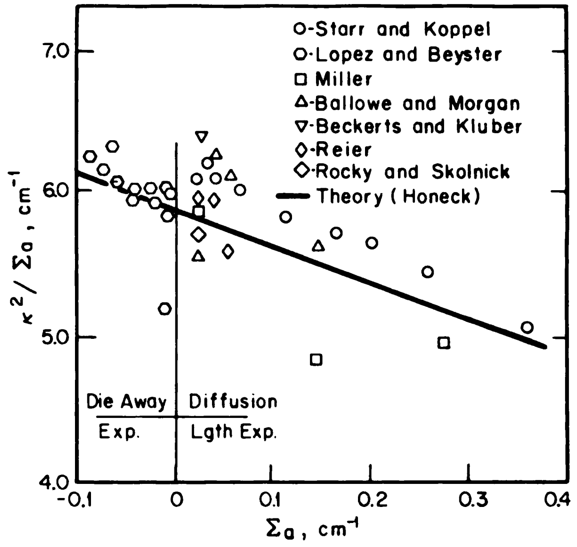

Fig. II-3 Computed and measured diffusion parameters in water.[12]

A comparison of the α vs. B^2 curves for H_2O from the pulsed-source results of Lopez and Beyster and those of Küchle[8] are given in Fig. II-2. Since the shape of Küchle's curve is very similar to that found by earlier investigators, Beckurts[13] concludes that background, backscattering, and even higher spatial modes cannot be the reason for the discrepancy. According to Buckurts the discrepancy must arise from the fact that Küchle and the other investigators made the measurements in flat cylindrical assemblies, whereas Lopez and Beyster used cubical assemblies. This contention is supported by the very strong effect of the extrapolation length in small water geometries found by Hall et al.,[14] who did pulsed measurements on square and flat systems with quite different results. Since there are problems in connection with specifying the buckling in small water systems, Beckurts[13] is of the opinion that there are, at present, doubts as to the accuracy of pulsed measurements in water and that more confidence should be placed in the poisoning experiments. Although both the pulsed-source and poisoning techniques are suitable methods for measuring D_0 and $\sigma_{a\,H_2O}$, there is uncertainty in determining the higher order coefficients in the power series Eqs. 6 and 10. Therefore it is preferable to compare the different measurements point by point rather than by the coefficients of a least-squares fit. Some of the measured and computed diffusion parameters discussed above are compared in this way in Fig. II-3.

Neutron-Diffusion Coefficient in D_2O

Brown and Hennelly[15] measured the thermal-neutron diffusion coefficient as a function of temperature in D_2O lattices. These measurements were made over the temperature range from 20 to 220°C by measuring the relaxation length of thermal neutrons in D_2O containing known amounts of heterogeneous poison in the form of thin-walled copper tubes spaced on a variety of square lattice pitches. The measurements were corrected for the volume displacement and scattering of the copper as well as for the thermal-expansion coefficients. The measured values of $D = D_0/v_0$ are plotted in Fig. II-4.

The value of D obtained from pulsed source measurements in D_2O by Ganguly and Waltner[16] are also plotted in Fig. II-4. These experiments gave a value of $C = 37{,}200 \pm 5000$ for the diffusion cooling coefficient, which compares favorably with Sjöstrand's[17] preliminary value of preliminary value of $35{,}000 \pm 8000$ cm^4/sec.

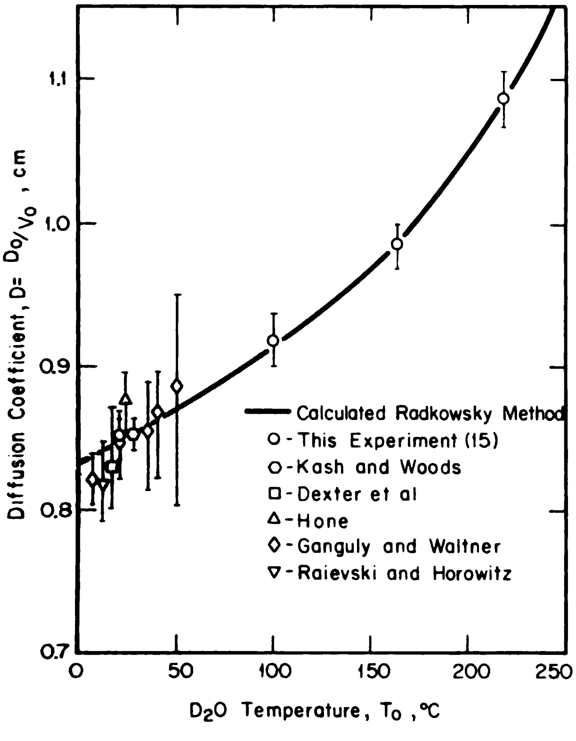

Fig. II-4 Diffusion coefficient of D_2O as a function of temperature.[15]

The experimental values of the neutron diffusion coefficient D obtained by boron poisoning, measurement of extrapolation distance, and pile oscillation are also indicated. The agreement among all the measurements is good. The temperature dependence of the thermal diffusion coefficient was calculated using Radkowsky's method in Ref. 15. This result is plotted in Fig. II-4; the variation of D with temperature is well described by this simple calculational model.

Diffusion Parameters in Graphite

Early pulsed-source measurements in graphite systems resulted in a value of C, the diffusion cooling coefficient, in the range of 12 to 16×10^5 cm^4/sec at a graphite density of 1.6 g/cm^3. These values are in good agreement with the theoretical value of $C = 14 \times 10^5$ calculated by Nelkin.[18] Later French and German measurements have indicated a C value about twice as large, as well as discrepancies in other parameters. Therefore careful remeasurements have been made by Klose, et al.,[19] Starr and Price,[21] and Starr and de Villiers.[20]

Klose made pulsed-source measurements on 45 graphite piles that ranged in buckling from 7×10^{-4} cm^{-2} to 240×10^{-4} cm^{-2}. A three-parameter least-squares fit of the decay constants to the B^2 power series for α (Eq. 6) was obtained with the α values weighted according to their relative accuracy. The fitting procedure was repeated, dropping all measured points with B^2 larger than a fixed B^2_{max}, in order to investigate the dependence of the diffusion parameters on the buckling range used. By this analytical procedure it was concluded that, if the B^2 ranged included in the fitting procedure is small (i.e., only a few points are used), low values for D_0 and C are obtained, whereas, when B^2 exceeds about 60×10^{-4} cm^{-2}, D_0 and C increase continuously, indicating that the three-parameter fit is no longer adequate. With a four-parameter fit, no definite tendencies were noted, but the D_0 and C values were somewhat lower over the entire range of B^2_{max}. These values are listed in Table II-3. It was surprising that a large negative value was obtained for the F parameter, since previous theoretical estimations have predicted a small positive value. However, recent calculations by Honeck[12] confirm the negative sign and the order of magnitude of this coefficient. The calculated results are listed in Table II-3. The large size and the negative sign of

F may arise because the thermalization power of graphite decreases strongly with the decreasing neutron "temperature" or spectral softening (diffusion cooling) that occurs with increasing buckling.

Starr and de Villiers[20] have determined the diffusion cooling parameter C in graphite by measurement of the average neutron velocity in graphite. The asymptotic neutron decay of a neutron burst in a series of graphite piles of differing bucklings was measured, using simultaneously a detector in which every incident neutron was counted and a detector which had a $1/v$ response sensitivity. Thus, at long times after the pulsed-source neutron burst, the ratio of the counting rate of the thermally black detector to that of the $1/v$ response detector is proportional to the density-weighted average velocity $\bar{v}$. The detectors used were two physically identical BF_3 proportional counters. The black detector contained 96% enriched B^{10} and the gray detector contained 11% B^{10}. The diffusion cooling constant C was determined by assuming that D is a constant in the expression $\overline{Dv}$ in Eq. 5. Since D_0 equals $\bar{v}_0\bar{D}$, D can be written as $D_0/\bar{v}_0$, and Eq. 5 can be rearranged as follows:

$$\bar{v} = \bar{v}_0\left(1 - \frac{C}{D_0} B + \ldots\right)$$

Therefore a direct measurement of the average velocity as a function of buckling will yield the diffusion cooling coefficient C in terms of the more precisely known D_0. The results of this measurement are listed in Table II-3.

Starr and Price[21] measured the diffusion length in graphite and various graphite-bismuth assemblies by exponential measurements in connection with an investigation of liquid-metal-fueled reactor systems. The diffusion parameters of these systems were subsequently measured by pulsed-source methods, and the results were compared. The results were then combined to obtain a more accurate set of parameters. In all cases the diffusion length determined from pulsed-source experiments agreed within statistical error with the diffusion length determined by exponential experiments.

Table II-3 MEASURED AND CALCULATED DIFFUSION PARAMETERS IN GRAPHITE

Author	Year	Ref.	Method	Fitting	Density	D, cm^2/sec	C, cm^4/sec	F, cm^6/sec	σ_a^c, mb
Klose, Küchle, and Reichardt	1962	19	Pulsed source	3-parameter	ρ = 1.6 g/cm^3	$2.13 \pm 0.02 \times 10^5$	$26 \pm 5 \times 10^5$	$-20 \pm 10 \times 10^7$	4.77 ± 0.07
				4-parameter	ρ = 1.6 g/cm^3	$2.11 \pm 0.02 \times 10^5$	$16 \pm 5 \times 10^5$		4.80 ± 0.07
Honeck	1962	12	Calculation	4-parameter		2.178×10^5	24.57×10^5	-8.31×10^7	
Starr and de Villiers	1962	20	Pulsed source (average velocity measurements)						
Starr and Price	1962	21	Pulsed source		AA graphite, ρ = 1.674 g/cm^3	$2.09 \pm 0.03 \times 10^5$	$41 \pm 4 \times 10^5$		3.83 ± 0.06
Starr and Price	1962	21	Pulsed source		GBF graphite, ρ = 1.697 g/cm^3	$2.02 \pm 0.01 \times 10^5$	$34 \pm 3 \times 10^5$		
Starr and Price	1962	21	Exponential measurements		AA graphite	Diffusion-length average 54.5 ± 0.5 cm			
					GBF graphite	Diffusion-length average 50.7 ± 0.3 cm			

Since the pulsed-source experiments yield an accurate value of the diffusion constant, and the exponential experiments yield an accurate value of the diffusion length, the combined data should result in a more accurate determination of the thermal absorption cross sections. The experimental results are listed in Table II-3.

The disparity of the values for the diffusion cooling parameter, C, listed in Table II-3, may result from variations in density and from anisotropy effects in the graphite. However, the experiments indicate that the diffusion cooling parameter is substantially greater than was previously estimated.

References

1. W. C. Ballowe, Measurement of the Diffusion Length of Thermal Neutrons in Light Water, in Proceedings of the Brookhaven Conference on Neutron Thermalization, April 30 to May 2, 1962, Vol. III, Experimental Aspects of Tran-

sient and Asymptotic Phenomena, USAEC Report BNL-719, pp. 799-804, Brookhaven National Laboratory, November 1962.

2. J. L. Russell, Jr., W. C. Ballowe, W. R. Morgan, and M. V. Mosgovoy, Thermal Neutron Diffusion Length Measurements in Light Water from 20°C to 90°C, USAEC Report GEAP-4018, Vallecitos Atomic Laboratory, April 1962.
3. E. Starr and J. Koppel, Determination of Diffusion Hardening in Water, *Nucl. Sci. Eng.*, 14(3): 224 (November 1962); also in USAEC Report BNL-719, pp. 1012-1033, Vol. III.
4. M. Reier and J. A. DeJuren, Diffusion Length Measurements of Thermal Neutrons in Water from 23°C to 244°C, *J. Nucl. Energy: Pt. A & B,* 14(1): 18 (April 1961); also in USAEC Report BNL-719, pp. 977-980, Vol. III.
5. K. S. Rockey and W. Skolnik, Measurements on the Diffusion Length of Thermal Neutrons in Water from 25 to 296°C, *Nucl. Sci. Eng.*, 8(1): 62 (July 1960).
6. W. M. Lopez and J. R. Beyster, Measurement of Neutron Diffusion Parameters in Water by the Pulsed Neutron Method, *Nucl. Sci. Eng.*, 12(2): 190 (February 1962).
7. Personal communication between K. H. Beckurts, Kernforschungszentrum Karlsruhe, Germany, and G. Rohr, Brookhaven National Laboratory, 1962 (referenced in BNL-719, Vol. III).
8. M. Küchle, *Nukleonik,* 2: 131 (1960) (as referenced in BNL-719, Vol. III, p. RE-60.
9. W. H. Dio, *Nukleonik,* 1: 13 (1958) (as referenced in BNL-719, Vol. III, p. RE-71).
10. M. Reier, WAPD-T-1140, 1960. [As referenced in USAEC Report BNL-719 (Vol. IV), p. 1202, Brookhaven National Laboratory.]
11. J. R. Beyster, J. R. Brown, H. C. Honeck, D. H. Houston, J. U. Koppel, W. M. Lopez, Y. D. Naliboff, D. E. Parks, G. D. Trimble, F. Wikner, and J. C. Young, Integral Neutron Thermalization, Annual Summary Report, October 1, 1961 – September 30, 1962, USAEC Report GA-3542, p. 187, General Dynamics Corp., General Atomic Division, Mar. 15, 1963.
12. H. C. Honeck, On the Calculation of Thermal Neutron Diffusion Parameters, in Proceedings of the Brookhaven Conference on Neutron Thermalization April 30 to May 2, 1962, Vol. IV, Theoretical Aspects of Transient and Asymptotic Phenomena, USAEC Report BNL-719, pp. 1186-1210, Brookhaven National Laboratory, December 1962.
13. K. H. Beckurts, Transient Effects in Space, Time, and Energy, in Proceedings of the Brookhaven Conference on Neutron Thermalization April 30 to May 2, 1962, Vol. III, Experimental Aspects of Transient and Asymptotic Phenomena, USAEC Report BNL-719, pp. RE1-62, Brookhaven National Laboratory, November 1962.
14. R. S. Hall, S. A. Scott, and J. Walker, *Proc. Phys. Soc. (London),* 79: 257 (1962) (as referenced in BNL-719, Vol. III, p. RE-60).
15. H. D. Brown and E. J. Hennelly, Neutron Thermalization Studies at Savannah River, in Proceedings of the Brookhaven Conference on Neutron Thermalization April 30 to May 2, 1962, Vol. III, Experimental Aspects of Transient and Asymptotic Phenomena, USAEC Report BNL-719, pp, 879-894, Brookhaven National Laboratory, November 1962.
16. N. K. Ganguly and A. W. Waltner, Measurement of Neutron Diffusion Parameters of Heavy Water at Different Temperatures by Pulsed Source Method, *Trans. Am. Nucl. Soc.*, 4(2): 282 (November 1961).
17. N. G. Sjöstrand, *Arkiv Fysik,* 15: 145 (1958) (as referenced in BNL-719, Vol. III, p. RE-61).
18. M. Nelkin, The Diffusion Cooling of Neutrons in a Finite Moderator, *J. Nucl. Energy: Pt. A&B,* 8 (1-3): 48 (November 1958).
19. H. Klose, M. Küchle, and W. Reichardt, Pulsed Neutron Measurements on Graphite, in Proceedings of the Brookhaven Conference on Neutron Thermalization, April 30 to May 2, 1962, Vol. III, Experimental Aspects of Transient and Asymptotic Phenomena, USAEC Report BNL-719, pp. 935-945, Brookhaven National Laboratory, November 1962.
20. E. Starr and J. W. L. de Villiers, Determination of Diffusion Cooling in Graphite by Measurement of the Average Neutron Velocity, in Proceedings of the Brookhaven Conference on Neutron Thermalization April 30 to May 2, 1962, Vol. III, Experimental Aspects of Transient and Asymptotic Phenomena, USAEC Report BNL-719, pp. 997-1011, Brookhaven National Laboratory, November 1962.
21. E. Starr and G. A. Price, Measurement of the Diffusion Parameters of Graphite and Graphite-Bismuth by Pulsed Neutron Methods, in Proceedings of the Brookhaven Conference on Neutron Thermalization April 30 to May 2, 1962, Vol. III, Experimental Aspects of Transient and Asymptotic Phenomena, USAEC Report BNL-719, pp. 1034-1073, Brookhaven National Laboratory, November 1962.

Section
III
Power Reactor Technology

Fluid and Thermal Technology

Burnout in Multirod Geometry

By John S. Wiley

Introduction

An article in the last issue of *Power Reactor Technology* compared two burnout heat-flux correlations[1,2] with data taken using channels of relatively simple cross section. The purpose of this article is to extend consideration to more complex geometries, namely, those involving a bundle of heated rods. Instead of considering the correlations themselves, this article compares the multirod data, where possible, with data taken in the simpler test sections. The annular test-section data are from Refs. 3 and 10, and the rectangular-channel data and circular test-section data are from Ref. 4.

A basic difficulty in understanding flow phenomena in multirod bundles is illustrated by looking at a cross section of a typical bundle, Fig. III-1. The various flow subchannels, which are numbered in Fig. III-1, offer ample opportunity for mixing of their contents. One of the points made in Fig. III-14 of the last issue was that the test section's equivalent diameter was an important variable.* Consideration of Fig. III-1 reveals that there are a number of equivalent diameters, and some of the flow channels are bounded by unheated surfaces. The varying equivalent diameters give rise to mixing, of course, and thus any diameter effect is inseparably tied to the amount of mixing between subchannels.

Presentation of Data

The first multirod data to be considered are found in Ref. 5. A total of five test sections

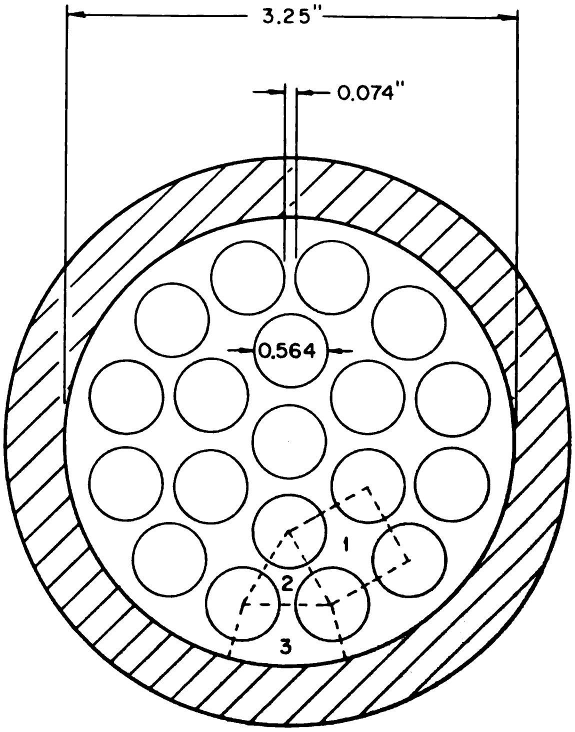

$$\bar{D}_e = \frac{4(\text{Total Flow Area})}{(\text{Total Wetted Perimeter})} = 0.32''$$

$$D_{e_1} = 0.36''$$

$$D_{e_2} = 0.23''$$

$$D_{e_3} = 0.35''$$

Fig. III-1 Cross section of one of the multirod test sections used for burnout studies at Hanford Atomic Products Operation (HAPO).

---

*The diameter effect shown on that figure can be approximated by $(0.18/D)^{0.4}$. This approximation will be used to extrapolate data to different equivalent diameters.

Table III-1 DESCRIPTION OF EXPERIMENTAL TEST SECTIONS[5]

Test-section designation	Spacing between rods within bundle, in.	Spacing between outer rod and pressure tube, in.		Heater rod outside diameter, in.	Heater length, in.	Radial heat-flux variation, outer/inner/center rod	Wire wraps					Type of thermocouple
		Nominal	Minimum				Test-section orientation	Diameter, in.	Pitch, in.	Material	Heat generated in wire wrap	
I	0.074	0.112	0.074	0.564 ±0.001	18.5	1/0.83/0.83	Vertical	0.074	10	Ceramic beads on 0.028 wire	No	Single-point contact, no water thermocouples
II	0.015	0.060	0.050	0.629 ±0.001	19.5	1/1/1	Horizontal	0.015	10	Inconel wire	Yes, ~1/3 of rod flux or ~2% of total power	Single-point contact, no water thermocouples
III	0.050	0.101	0.074	0.587 ±0.001	19.5	1/1/1	Horizontal	0.050	9	Ceramic beads on 0.024 wire	No	Copper plug, no water thermocouples
IV	0.050	0.101	0.074	0.587 ±0.001	19.5	1/1/1	Horizontal	0.050	9	MgO-filled tubing	Yes, ~1/3 rod flux or ~2% of total power	Copper plug, 5 water thermocouples
V	0.050	0.101	0.085	0.587 ±0.001	76.0	1/1/1	Horizontal	0.050	9	MgO-filled tubing	Yes, ~1/10 rod flux or ~0.5% of total power	Copper plug, 10 water thermocouples

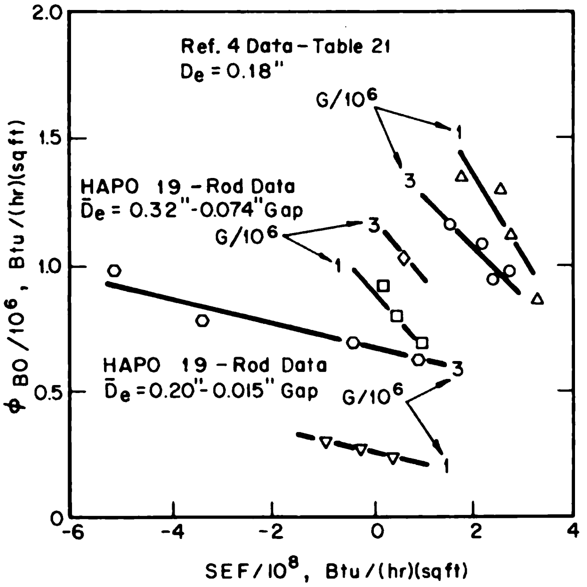

Fig. III-2 Comparison of Hanford multirod test-section data[5] with rectangular-channel data given in Ref. 4. Pressure = 1200 psi.

were utilized in the study, and the description of each is given in Table III-1. The cross section of test section I is shown in Fig. III-1, and the various equivalent diameters are given on the figure. Burnout data taken with test sections I* and II are shown in Fig. III-2, and burnout data taken with test sections III and V are shown in Fig. III-3. Also plotted on Fig. III-3 are burnout data taken with test sections of annular and rectangular cross section. The annular-channel data were interpolated from the data given in Fig. III-4. The rectangular-channel data at an equivalent diameter of 0.28 in. were extrapolated from the data taken with a channel having an equivalent diameter of 0.19 in., using the following relation:

$$\phi_{BO_{D=D_0}} = \phi_{BO_{D=0.18}} (0.18/D_0)^{0.4} \quad (1)$$

where $\phi_{BO_{D=D_0}}$ is the burnout heat flux at diameter D_0, Btu/(hr)(sq ft); $\phi_{BO_{D=0.18}}$ is the burnout heat flux at a diameter of 0.18 in., Btu/(hr)(sq ft); and D_0 is the equivalent diameter, in.

Consideration of Fig. III-2 reveals that increasing the average equivalent diameter, $\overline{D}_e$, increases the burnout heat flux, which is opposite to the trend observed for the simpler channels, and is expressed in Eq. 1. This probably is caused by improved mixing as the rod-to-rod spacing is increased, although it is not possible to establish this quantitatively. Some mixing data for test section V have been reported.[6] These data were obtained[7] by measuring local water temperatures just downstream of the heated section, and the data were taken employing single-phase flow. A total of 10 thermocouples were utilized. The data were treated as though the rod bundle consisted of two regions, one being within the bundle and the other being a region between the bundle and the pressure tube. This is shown schematically in Fig. III-5. The results of the mixing study are quoted as follows:[6]

> ... The data show that, over the 6.3-foot length, the average increase in the enthalpy of the coolant in sub-channels within the bundle is about 1.4 times the enthalpy increase of the coolant in the sub-channels between the bundle and the pressure tube wall. If no interchannel mixing had occurred, the enthalpy increase ratio should be about 3.0 ...

If mass and energy balances are written for the bundle and wall regions, it is possible to solve for m_1, m_2, H_1, and H_2 if the relation between m_1 and m_2 or H_1 and H_2 are known. The equations are as follows:

$$m_t = \phi\left(\frac{A_1}{H_1 - H_{in}} + \frac{A_2}{H_2 - H_{in}}\right) \quad (2)$$

$$H_1 = H_{in} + \frac{\phi A_1}{m_1} \quad (3)$$

$$H_2 = H_{in} + \frac{\phi A_2}{m_2} \quad (4)$$

$$(H_1 - H_{in}) = k(H_2 - H_{in}) \quad (5)$$

where $m_{1,2}$ = steam-water flow rate in bundle and wall regions, lb/hr
m_t = total steam-water flow rate, lb/hr
ϕ = heat flux, Btu/(hr)(sq ft)
$A_{1,2}$ = heat-transfer areas in bundle and wall regions, sq ft
$H_{1,2}$ = outlet enthalpy of steam-water mixture from bundle and wall regions, Btu/lb
H_{in} = inlet enthalpy, Btu/lb
k = constant expressing relation between H_1 and H_2

---

*The heat fluxes plotted in Fig. III-2 correspond to the average burnout heat fluxes for test section I.

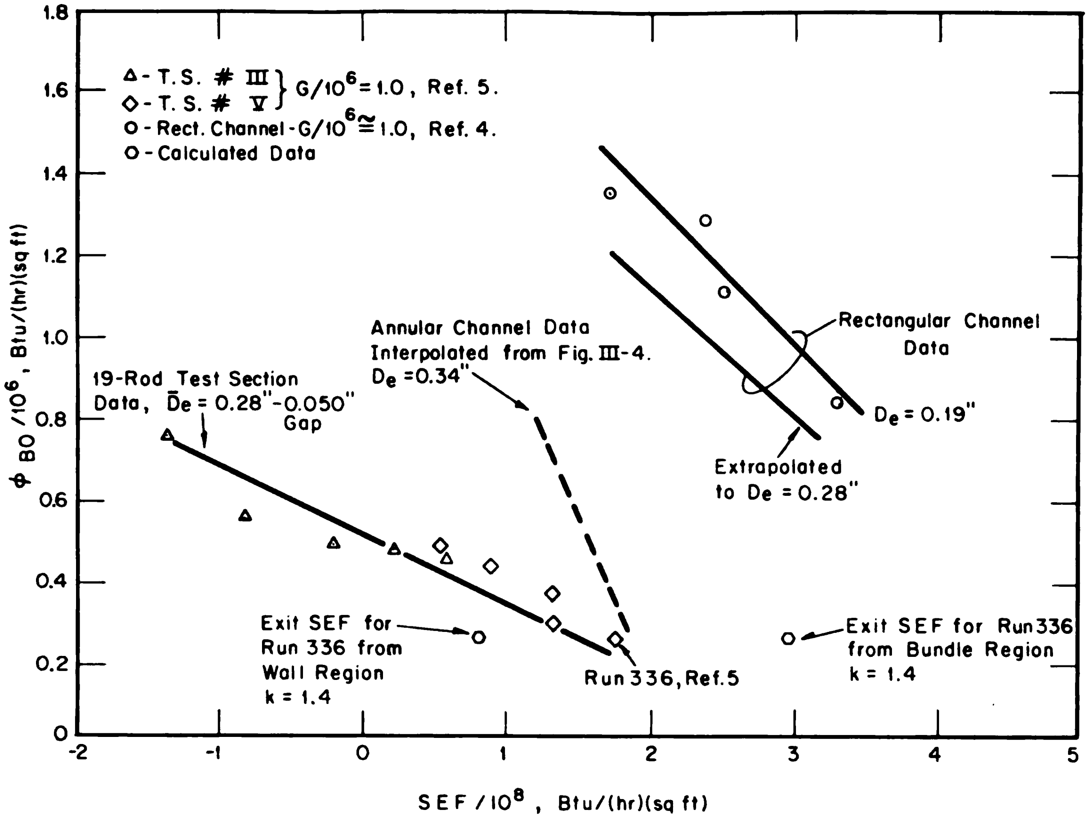

Fig. III-3 Comparison of Hanford multirod test-section (T.S.) data[5] with data given in Refs. 3 and 4. Pressure = 1200 psi.

With $k = 1.4$, solving Eqs. 2 to 4 for run 336 (Ref. 5) results in the data shown in Table III-2. The calculations shown in Table III-2 are approximate, since the division of flow area and heat-transfer area between the bundle region and the wall region was arbitrarily set and the area of the wire wraps was neglected. It was also assumed that mixing as measured with single-phase flow is representative of the behavior of two-phase flow. The outlet steam energy flows for the bundle, and wall regions are plotted on Fig. III-3; however, the agreement with rectangular-channel data is still lacking. Although agreement with the annular-channel data is not good either, the figure illustrates that local conditions may be quite different from average conditions in a bundle with interconnected flow passages.

The Westinghouse multirod burnout data are contained in Ref. 8. The cross section of the bundle is shown in Fig. III-6, and the test pressure was 2000 psia. The Westinghouse multirod data correlate well with the rectangular-channel data given in Tables 21 and 15 of Ref. 4, and this is shown in Fig. III-7. The figure illustrates one burnout point and several scanning points. The Westinghouse nine-rod test section was instrumented to measure wall-temperature increases at the exit of the center tube. These thermocouples did not function satisfactorily; hence the protection afforded by these thermocouples was lacking. The burnout run resulted in physical destruction of the test section, whereas the scanning runs were designed to approach the rectangular-channel correlation but with a heat flux about 15 to 20% lower. That this procedure was satisfactory is illustrated by Fig. III-7. The circular-channel data, illustrated in Fig. III-8, appear to be conservative compared with the multirod burnout points. The test section was equipped with pressure taps located within the rod bundle as well as within the shroud (the area between the rod bundle and the walls defining the flow channel). An approximate analysis of the data resulted in the following conclusion:[8]

... (a) At the entrance, the velocity in the rod area is lower because the entrance pressure-loss coefficient is larger; (b) in the center region, where boiling has not yet started, the velocity in the rod area is greater because the equivalent diameter in this area is larger; (c) near the end of the rod bundle, the velocity in the rod area decreases because of the increased flow resistance caused by boiling and because the exit-loss coefficient is higher in the rod area. Since these flow patterns are only qualitative, their effect on DNB is not known, and depends upon many factors such as radial flux gradient, rod length and pitch, flow rates, entrance and exit losses and two-phase densities. In the present tests, axial-flow redistribution apparently had little effect upon axial pressure drop and burnout.

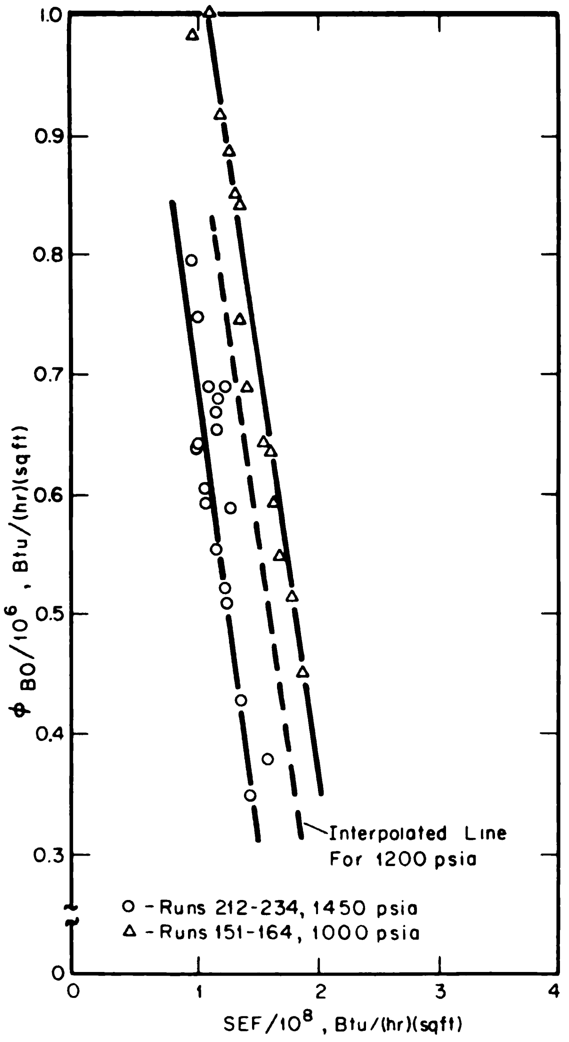

Fig. III-4 Burnout heat-flux data from Ref. 3. Annular-channel geometry: equivalent diameter = 0.34 in.; mass flow = 1.1×10^6 lb/(hr)(sq ft).

Additional data that will be discussed can be found in Ref. 9. The test section used employed nine heated rods and is shown in Fig. III-9. It is quite similar to the Westinghouse nine-rod test section except that the rod-to-rod spacing was quite a bit larger, about 0.19 in., as was the rod-to-shroud spacing, 0.17 in. The actual values for these spacings are given in the reference. The above quoted numbers, as well as the equivalent diameters shown on Fig. III-9, are only approximate. Four test sections were constructed with a cross section as given in Fig. III-9 and a heated length of 18 in. The relative heater-rod powers were as follows:

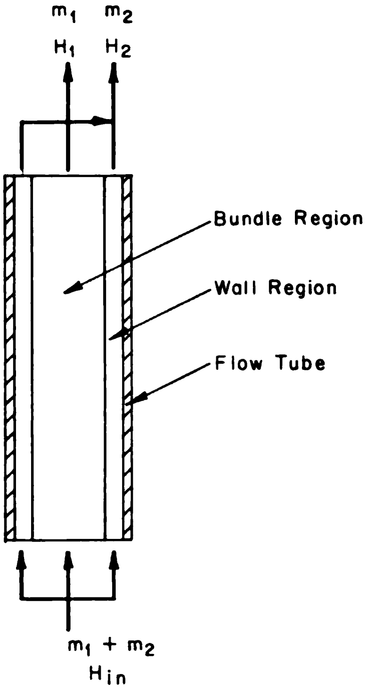

Fig. III-5 Schematic of pressure tube and rod bundle. Here m = flow rate in pounds per hour; H = enthalpy in Btu's per pound.

Test-section No.	Relative heater-rod power			
	Rod A	Rod B	Rod C	All others
1, 3, 4	1.00	1.00	1.00	0.80
2	1.22	1.00	1.00	0.80

Assemblies 3 and 4 were destroyed because rod A bowed at midspan and caused an electrical short to the shroud. The spacers for electrical insulation shown on Fig. III-9 were made of Rulon. One set of spacers was positioned about 10 in. upstream of the heated end of the test section, and a second set was positioned about 1 in. downstream of the end of the test section.

Table III-2 RESULTS OF MIXING CALCULATIONS WITH $k = 1.4$, RUN 336 OF REF. 5

[H_{in} = 503 Btu/lb, m_t = 22,120 lb/hr, ϕ = 284,000 Btu/(hr)(sq ft)]

Outlet enthalpies, Btu/lb	
Bundle	769 (32.2)*
Wall region	693 (19.8)*
Average	746 (28.3)*
Outlet mass flow, lb/(hr)(sq ft)	
Bundle region	1.49×10^6 (13,430)†
Wall region	0.67×10^6 (8,690)†
Average	1.01×10^6
Outlet steam energy flow, Btu/(hr)(sq ft)	
Bundle region	2.94×10^8
Wall region	0.81×10^8
Average	1.74×10^8

*Number in parentheses is outlet quality in percent.

†Number in parentheses is outlet mass flow in pounds per hour.

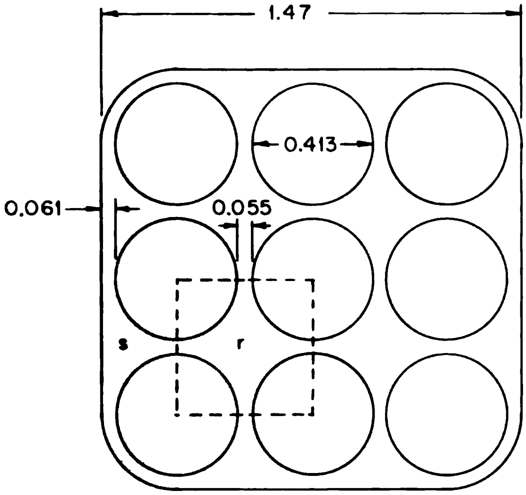

$$\bar{D}_e = \frac{4(\text{Total Flow Area})}{(\text{Total Wetted Perimeter})} = 0.20''$$

$D_{e_r} = 0.26''$

$D_{e_s} = 0.18''$

Fig. III-6 Cross section of multirod test section used for burnout studies at Bettis Atomic Power Laboratory.

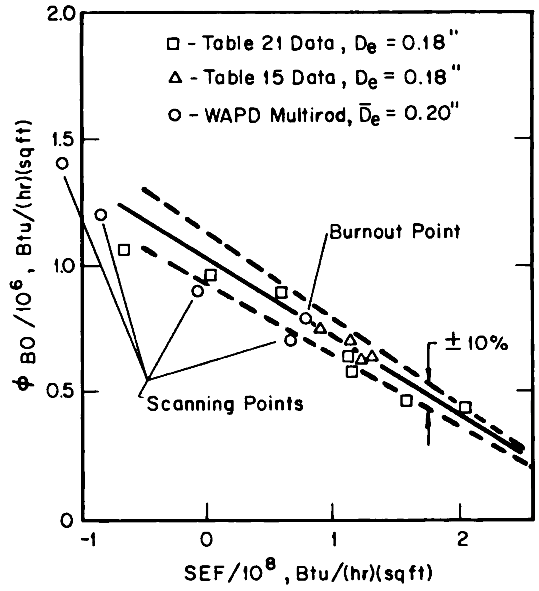

Fig. III-7 Comparison of nine-rod test-section data[8] with rectangular-channel data appearing in Tables 15 and 21 of Ref. 4. Pressure = 2000 psia; mass flow = 1.0×10^6 lb/(hr)(sq ft).

Data were taken at nominal pressures of 1000 and 1400 psia, and the 1000-psia data are illustrated in Fig. III-10. Also plotted in Fig. III-10 are rectangular-channel data from Ref. 10. It is evident that the kind of agreement between rectangular-channel data and nine-rod test-section data shown in Fig. III-7 is not present. The combination of an unknown amount of bowing of rod A and the presence of the spacers as shown in Fig. III-9, however, make detailed analyses difficult. Although the upstream spacer was about 20 hydraulic diameters upstream of the burnout point, the downstream spacer was only about two hydraulic diameters downstream of the burnout point, and it seems likely that any flow redistribution caused by the downstream spacer would be evident only several equivalent diameters upstream.

The steam-energy flows plotted on Fig. III-10 were computed using the bulk exit qualities given in Table 4 of Ref. 9. Of particular interest are the five points taken with test section No. 2, where the relative power of rod A was 22% higher than in the data taken with test section No. 1. In all but three of the points plotted on Fig. III-10 for the nine-rod section, burnout was detected as occurring on rod A, and the authors of the reference conclude that "... turbulent cross flow is sufficient to maintain a distributed quality pattern regardless of the distribution of quality generation for the clear-

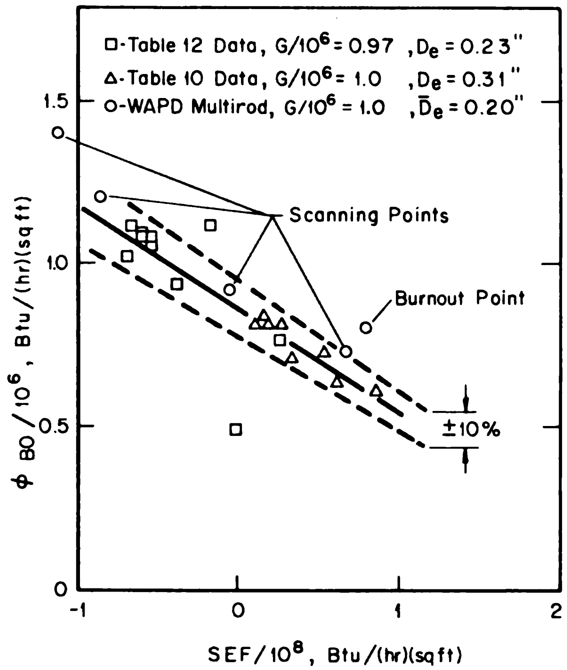

Fig. III-8 Comparison of nine-rod test-section data[8] with circular-channel data appearing in Tables 10 and 12 of Ref. 4. Pressure = 2000 psia.

ances of this test section." Although this may be true, there is almost a 22% spread in the data about the appropriate line drawn on Fig. III-10.

Figure III-11 compares the multirod data appearing in Fig. III-10 with annular-channel data taken from Ref. 3. Although the comparison is not exact, it appears that the annular-channel data are a better representation of the burnout behavior of the multirod geometry than are the data taken in the rectangular test section. The two curves at a *G* of 1.1 × 10⁶ lb/(hr)(sq ft) show good agreement. Unfortunately it is difficult to tell whether this is accidental or not since, as shown in Fig. III-9, the multirod test section had a variety of equivalent diameters.

The test section used to obtain the data given in Ref. 11* was similar in cross section to Fig. III-1 and was called the "high-heat-flux" test section. The shroud inside diameter was 3.195 in., and the rods had an outside diameter of 0.550 in. Twelve of the rods were wrapped with stainless-steel spirals, and the test section was equipped with a burnout detector. The rod-to-rod spacing was 0.083 in. (the diameter of the spacer wires), whereas the rod-to-shroud spacing was about 0.1 in. minimum. The system pressure was a nominal 1000 psia; the data are shown in Fig. III-12. The particular values plotted are those termed "good validity of the burnout point" in the reference. Other data having low or questionable validity are not shown. The heater tube material was Inconel X, having a heated length of 36 in. The relative heat fluxes were:

Outer rod	1.0
Inner rod	0.854
Center rod	0.807

The burnout heat fluxes plotted on Fig. III-12 are those corresponding to the power dissipated via the outer ring of rods.

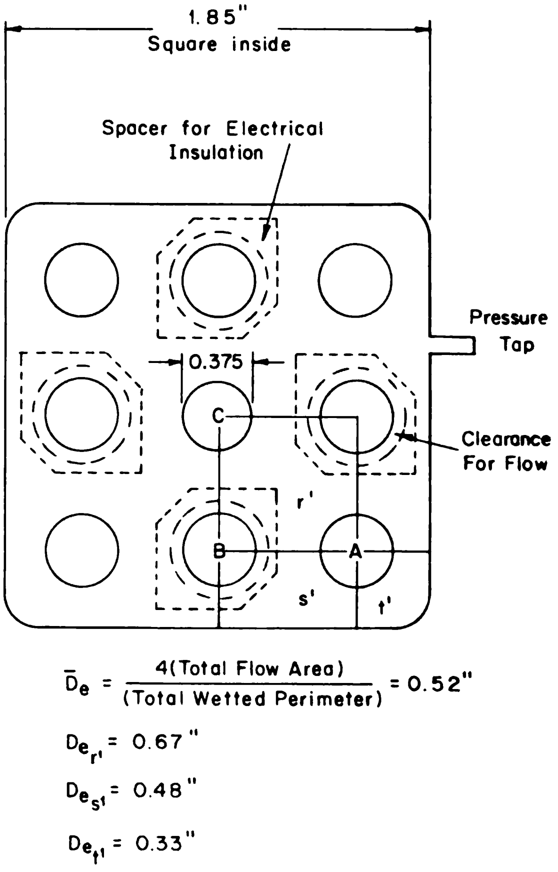

Fig. III-9 Cross section of multirod test section used for burnout studies at General Electric's Atomic Power Equipment Department (GE-APED).

---

*The results of the Columbia program have been summarized and published as Ref. 14, which will be discussed shortly.

If Fig. III-12 were superimposed on Fig. III-11, it would be found that the data for the multirod test sections were very close together for a mass flow of 0.5 and 1.0 × 10^6 Btu/(hr)(sq ft). Thus the burnout behavior of the two-rod bundles appears to be reasonably well approximated by the annular test-section data.

Other multirod burnout data to be discussed will be found in Ref. 12. A cross section of the four-rod test section is shown in Fig. III-13, and a summary of the parameters of importance is shown in Table III-3. The spacers were designed to present as little restriction to flow as possible. They consisted of small cylindrical pins, oriented as shown in Fig. III-13. The spacers were located in planes 2 in. above the upper end and 9 in. below the upper end of the heated section. The spacers are quite different than the ones shown in Fig. III-9 and do appear to present little flow restriction. As shown in Table III-3, one rod had a slightly thicker wall to increase the heat flux, and the critical heat-flux detection thermocouples were welded to the hot rod. Some data were taken with all rods having an identical wall thickness; "... the data obtained with one rod hotter were compared with the data with all rods the same, and there was no difference in critical heat flux values, when the hot rod heat flux and average bulk steam qualities were used ..."[12]

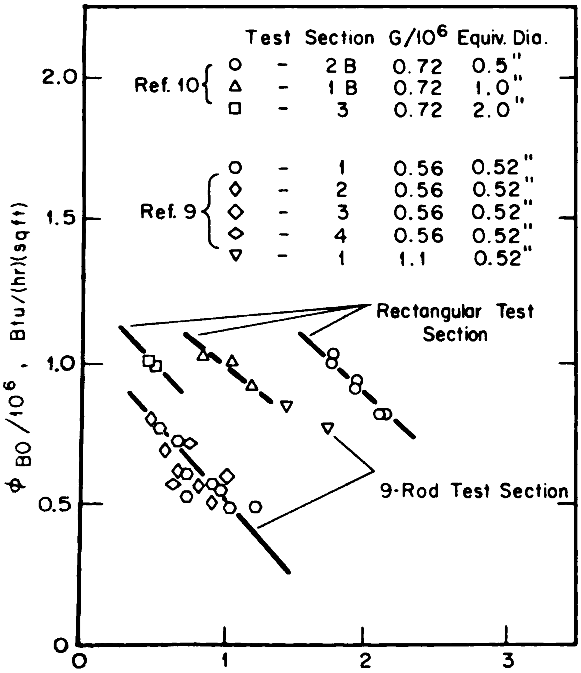

Fig. III-10 Comparison of nine-rod test-section data[9] with rectangular-channel data appearing in Ref. 10. Pressure = 1000 psia.

Results obtained with the four-rod test section are shown in Fig. III-14. Presumably these data were taken with one rod slightly hotter, although no distinction was given in Ref. 12 as to which data were which. In Fig. III-14 a hysteresis effect was noted in plotting the $G = 0.2 \times 10^6$ lb/(hr)(sq ft) data. This is noted in Fig. III-14 by two straight, dotted lines running through the appropriate points. Although the differences in the locations of the two dotted lines are of minor importance, it would be of interest to know why there is a difference. Comparative annular-channel data are shown in Fig. III-15. Although the annular-channel data do not exactly reproduce the four-rod data, there is a good correspondence at mass velocities in excess of 0.5 × 10^6 lb/(hr)(sq ft).

Table III-3 TEST-SECTION PARAMETERS: FOUR-ROD GEOMETRY[12]

Heated length	3 and 4 ft
Hydraulic diameter	0.419 in.
Heater tube wall thickness	0.020 and 0.022 in.
Heater tube material	Inconel X, heat-treated to 1300°F for 20 hr, air cooled
Rod-to-rod spacing	0.187 in.
Rod-to-wall spacing	0.135 in.
L/D ratio	86 for 3-ft heated length; 104 for 4-ft heated length
Flow direction	Vertical, upward
Electric power	Single-phase, alternating current
Distance between spacers	11 in.

Discussion

The use of rectangular cross-section test-section burnout data may not be conservative in the thermal design of power reactors employing bundles of fuel rods. The Westinghouse data suggest that it is possible to design a multirod test section to yield good agreement between rectangular-channel and multirod burnout data, although not many experimental points are reported in Ref. 8. Lack of mixing might be blamed for the relatively poor multirod burnout performance shown in Figs. III-2, III-10, and III-12 (compared to rectangular test-section data), but it is difficult to make quantitative

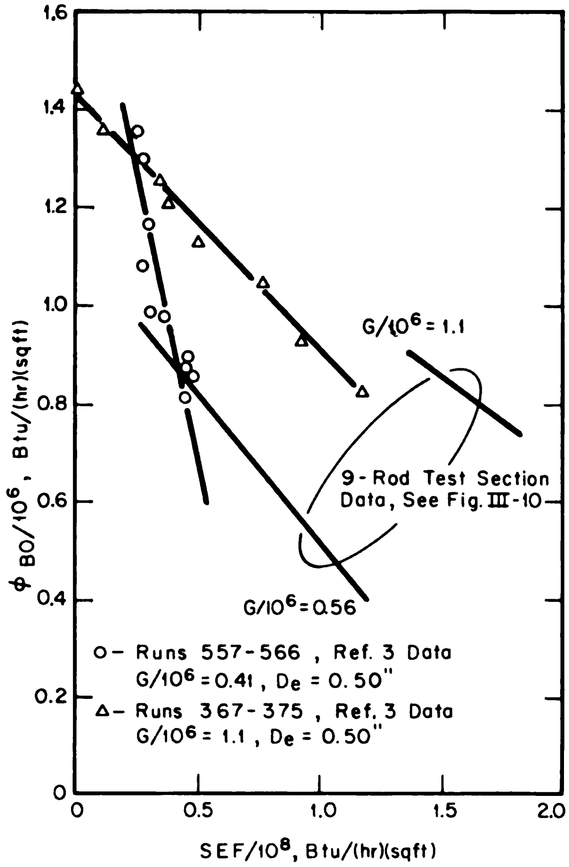

Fig. III-11 Comparison of nine-rod test-section data[9] with annular-channel data appearing in Ref. 3. Pressure = 1000 psia.

statements since few analytical or experimental mixing data are available for comparison. Reference 13 contains results of mixing experiments done with the fuel element for the Carolinas-Virginia Tube Reactor (CVTR). The CVTR bundle is similar to the bundle shown in Fig. III-1 except that the outer ring of rods is on a hexagonal geometry instead of a circle, and a hexagonal flow liner surrounds the bundle. Boiling did not take place. Mixing was evaluated by injecting lithium nitrate into various subchannels at the test-section inlet and measuring its concentration in various subchannels at positions along the length of the test section. The results will not be discussed herein; however, this type of experiment may represent a method of obtaining two-phase mixing and burnout data in a single test setup.

The applicability of the annular-channel data to the prediction of rod-bundle burnout can best be considered by looking at the individual plots and comparing the two. Figure III-11 shows good agreement at a $G/10^6$ of 1.1 between GE-APED nine-rod-bundle data and annular test-section data, although only two runs were reported for the nine-rod bundle at this value of mass flow. At a mass flow of about 0.5×10^6, the DNB-1 lines for annular and rod-bundle geometries have different slopes. Figure III-15 illustrates good correlation between GE-APED four-rod and annular-geometry data at mass flows from 1.0 to 1.5×10^6 and fair agreement at a mass flow of 0.5×10^6.

The Hanford and Columbia University experiments with 19-rod test sections are compared in Fig. III-16. The data originating at Columbia plotted therein were taken with the "six-foot-long" test section; this was similar to the "high-heat-flux" test section discussed earlier but had a heated length of 6.0 ft and the relative heat fluxes were as follows:

Outer rod	1.0
Inner rod	0.806
Center rod	0.766

The values of ϕ_{BO} plotted on Fig. III-16 for the "six-foot-long" test section are those corresponding to the heat flux impressed on the outer rods. The Columbia University data are available in Ref. 14.

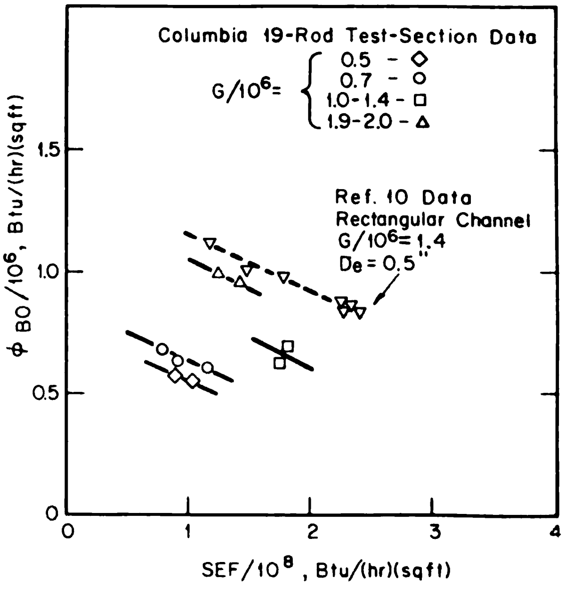

Fig. III-12 Comparison of Columbia 19-rod test-section data[11] with rectangular-channel data appearing in Ref. 10. Pressure = 1000 psia.

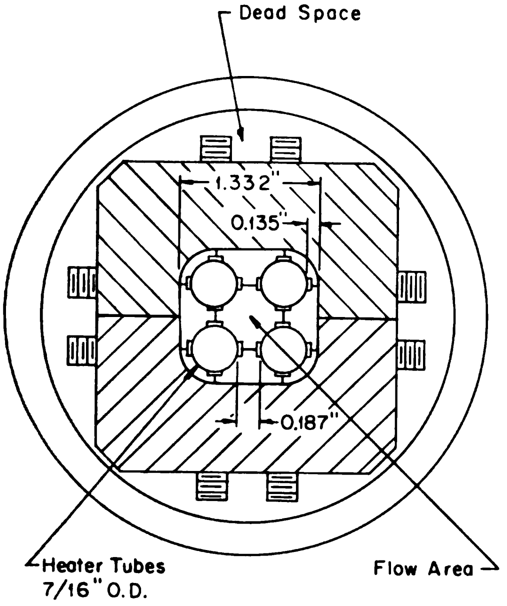

Fig. III-13 Cross section of four-rod test section used for burnout studies at GE-APED.

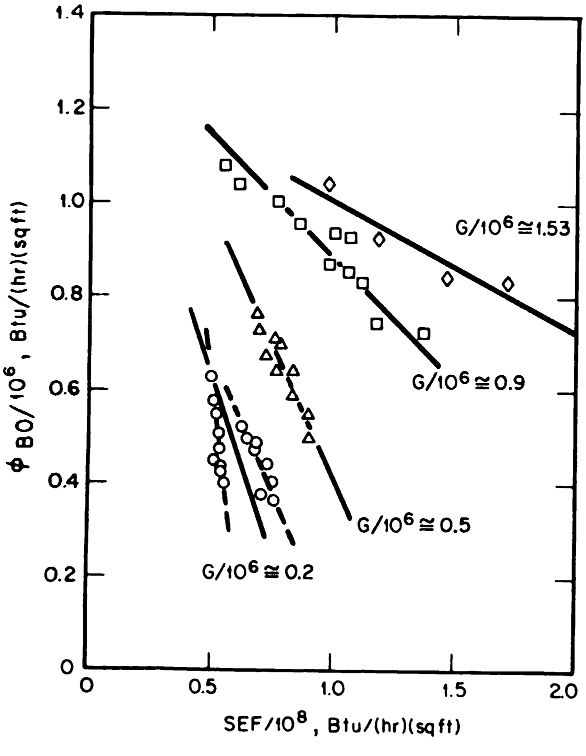

Fig. III-14 Steam-energy flow plot of burnout data taken with 4-rod test section and reported in Ref. 12. Pressure = 1000 psia.

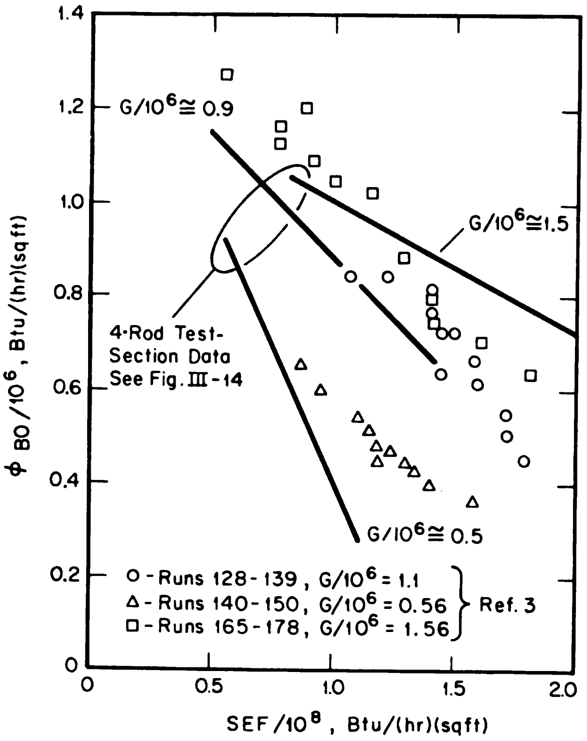

Fig. III-15 Comparison of four-rod test-section data[12] with annular-channel data appearing in Ref. 3. Pressure = 1000 psia.

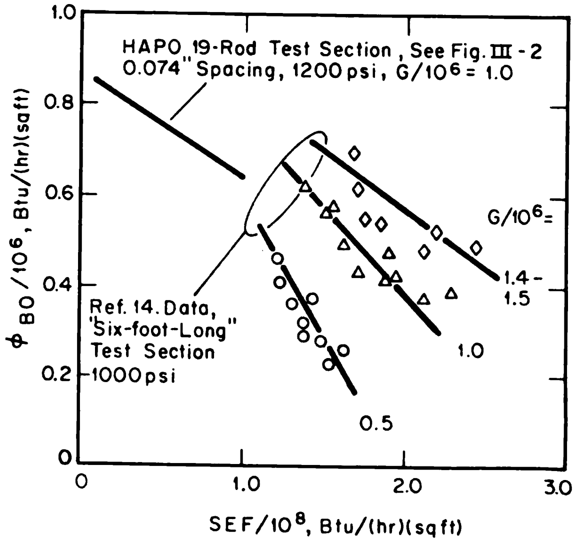

Fig. III-16 Comparison of Hanford[5] and Columbia[14] University 19-rod test-section burnout data.

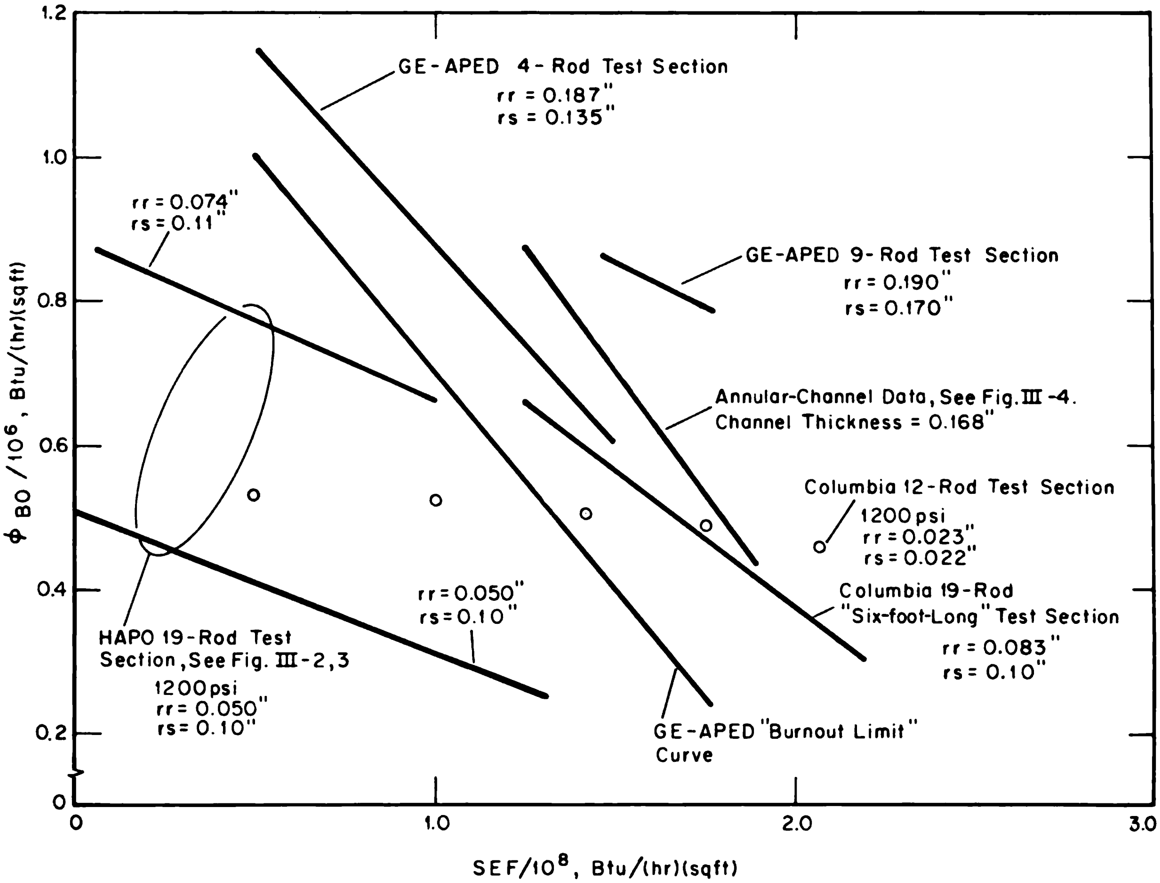

Fig. III-17 Summary of burnout data. Pressure = 1000 psia except where noted. Here *rr* = rod-to-rod spacing in inches; *rs* = rod-to-shroud spacing in inches; $G/10^6 \cong 1.0$ lb/(hr)(sq ft).

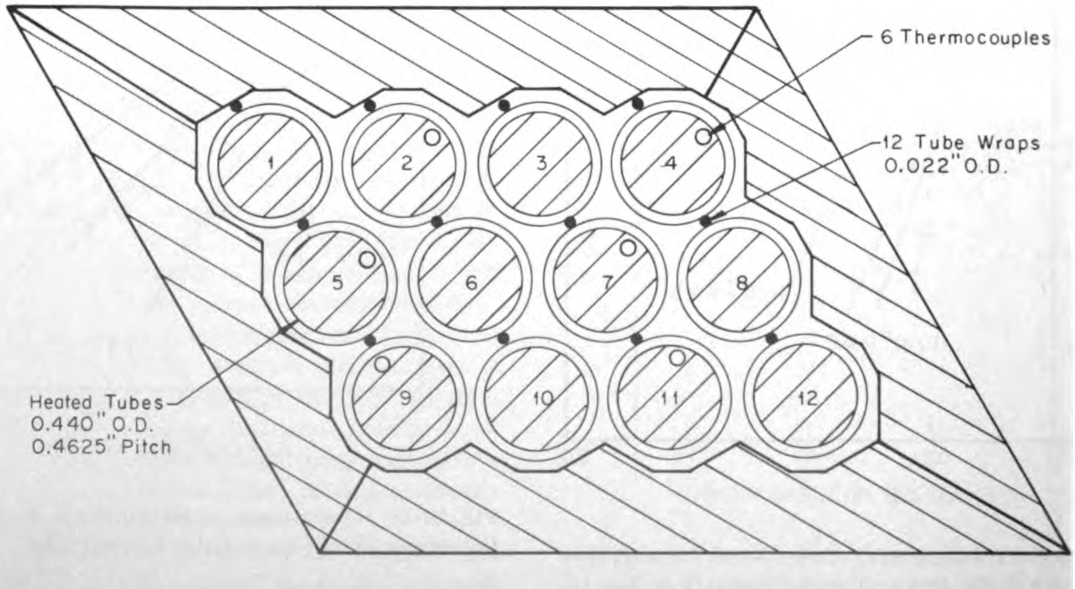

Fig. III-18 Cross section of Columbia 12-rod test section at ½ in. from exit end of heated length.

The Hanford and Columbia data show fairly good agreement provided the rod-to-rod spacing of the Hanford 19-rod test section is at least 0.074 in. Consideration of Figs. III-2 and III-16 suggests that the rod-to-rod spacing is an important parameter and that ϕ_{BO} increases with an increase in this spacing, other variables remaining constant. The Hanford data fall under the (extrapolated) Columbia data at a mass flow of 1.0×10^6. This is reasonable, however, since the average heat flux across the Hanford bundle is plotted as a comparison to the heat flux for the outer ring of rods of the Columbia University test section, and the Hanford test section operated at 1200 psi compared to 1000 psi for the Columbia test section.

Conclusions

Figure III-17 is offered as a conclusion to this article. In this figure are plotted rod-bundle data, annular test-section data, and the GE-APED burnout limit curve of Ref. 2. The only previously unpresented data appearing in Fig. III-17 are those taken with the Columbia 12-rod test section, shown in Fig. III-18. The test pressure was 1200 psia, and the heated length was 12 in. The burnout limit curve appears to adequately represent the rod-bundle data from the standpoint of safety except for the Hanford and the Columbia 12-rod test-section data. Although the Hanford runs were at a different pressure, there is no other evidence for such a large effect of pressure, and therefore the reason for the low burnout behavior of the Hanford 19-rod test section must be due to another variable. This could possibly be the relatively close rod-to-rod spacing, but the Hanford experiments on test sections II to V were done with the section horizontal, and this also might have had an effect on the results. The rod-to-rod spacing is noted on Fig. III-17, and it can be noted that ϕ_{BO} does improve, in general, as the spacing is increased. The Columbia 12-rod test section is, of course, the exception. It is possible that ϕ_{BO} is not a simple function of rod-to-rod and rod-to-shroud spacing, and ϕ_{BO} goes through a minimum corresponding to the values of *rr* and *rs* of the Hanford test section with the 50-mil rod-to-rod spacing. On the other hand, the data from the Columbia 12-rod section are the first report for an entirely triangular pitch; the GE-APED test sections had square pitch, and the 19-rod test sections had a mixture of triangular and square flow channels. The relative confusion present in Fig. III-17 will probably continue until mixing data are available on these several test sections.

References

1. L. S. Tong, H. B. Currin, and A. G. Thorp II, New Correlations Predict DNB Conditions, *Nucleonics*, 21(5): 43 (May 1963).
2. E. Janssen and S. Levy, Burnout Limit Curves for Boiling Water Reactors, Report APED-3892, General Electric Company, Atomic Power Equipment Department, Apr. 1, 1962.
3. E. Janssen and J. A. Kervinen, Burnout Conditions for Single Rod in Annular Geometry, Water at 600 to 1400 psia, USAEC Report GEAP-3899, General Electric Company, Atomic Power Equipment Department, February 1963.
4. R. A. DeBortoli, S. J. Green, B. W. LeTourneau, M. Troy, and A. Weiss, Forced-Convection Heat Transfer Burnout Studies for Water in Rectangular Channels and Round Tubes at Pressures Above 500 psia, USAEC Report WAPD-188, Westinghouse Electric Corp., Bettis Plant, October 1958.
5. E. D. Waters, G. M. Hesson, D. E. Fitzsimmons, and J. M. Batch, Boiling Burnout Experiments with 19-Rod Bundles in Axial Flow, USAEC Report HW-77303, Hanford Atomic Products Operation, August 1963.
6. J. K. Green and J. E. Brown, Hanford Atomic Products Operation, Mar. 26, 1963. (Unpublished)
7. Hanford Atomic Products Operation, Jan. 17, 1963. (Unpublished)
8. S. J. Green, G. W. Mauer, and A. Weiss, Burnout and Pressure-Drop Studies for Forced-Convection Flow of Water Parallel to Rod Bundles, ASME Paper No. 62-HT-43, presented at the ASME-AIChE Heat Transfer Conference and Exhibit, Houston, Texas, August 5–8, 1962.
9. E. E. Polomik and E. P. Quinn, Multi-Rod Burnout at High Pressure, USAEC Report GEAP-3940, General Electric Company, Atomic Power Equipment Department, September 1962.
10. F. E. Tippets, Critical Heat Flux and Flow Pattern Characteristics of High Pressure Boiling Water in Forced Convection, USAEC Report GEAP-3766, General Electric Company, Atomic Power Equipment Department, April 1962.
11. B. Matzner, Basic Experimental Studies on Boiling Fluid Flow and Heat Transfer at Elevated Pressures. Monthly Progress Report, April 1962, USAEC Report TID-15637, Columbia University, Engineering Research Laboratories, April 1962.
12. J. E. Hench, Multirod (Four-Rod) Critical Heat Flux at 1000 psia, USAEC Report GEAP-4358, General Electric Company, Atomic Power Equipment Department, September 1963.

13. A. A. Bishop, P. A. Nelson, and E. A. McCabe, Jr., Thermal and Hydraulic Design of the CVTR Fuel Assemblies, USAEC Report CVNA-115, Westinghouse Electric Corp., Atomic Power Division, June 1962.
14. B. Matzner and J. S. Neill, Forced-Flow Boiling in Rod Bundles at High Pressure, USAEC Report DP-857, Savannah River Laboratory, September 1963.
15. B. Matzner, Heat Transfer and Hydraulic Studies for SNAP-4 Fuel Element Geometries, Topical Report No. 2, USAEC Report TID-19563, Columbia University, Engineering Research Laboratories, September 1963.

Section

IV

Power Reactor Technology

Fuel Elements

Plutonium-Bearing Fuels

The potential use of plutonium for recycle in power reactors has been discussed in several previous issues of *Power Reactor Technology*. The development of satisfactory plutonium-bearing elements is of vital significance to the fast-breeder reactor, but development is under way for both fast and thermal reactor applications. The purpose of this review is to give a reasonably comprehensive picture of the present status of plutonium-bearing fuel-element development. The importance accorded plutonium as a fuel can be judged from the number of laboratories in the United States that are working on plutonium-bearing fuel development; these include Argonne National Laboratory, Hanford Atomic Products Operation, Los Alamos Scientific Laboratory, Mound Laboratory, General Electric's Atomic Power Equipment Department (GE-APED), Battelle Memorial Institute, Nuclear Materials & Equipment Corporation, and United Nuclear Corporation. In addition, most other countries supporting power-reactor programs are conducting developmental work on plutonium fuels.

This review includes discussions of the fabrication, properties, and irradiation behavior of plutonium compounds and their use in plutonium-bearing fuel elements. Basic metallurgical and physical property information is not included, in general, since another Technical Progress Review, *Reactor Materials*, has a section devoted to this type of information. Reference 47 contains a quite detailed account of the history of the discovery of the element plutonium and some recent developments.

Oxides: PuO_2 and PuO_2-UO_2

The applicability of PuO_2 is suggested by the widespread success that UO_2 has achieved as a fuel for power reactors. The French fast reactor Rapsodie may employ UO_2-PuO_2 as a fuel,[1] and the Plutonium Recycle Test Reactor (PRTR) has operated principally with fuel rods[2] containing UO_2 and PuO_2. The latter reactor is of the pressure-tube heavy-water-moderated type. These two programs are of particular interest since the fabrication processes for producing the elements are quite different. The French technique produces the basic fuel rod shown in Fig. IV-1 via a pelletizing process. The fuel-pin dimensions are shown in Table IV-1, which also includes the dimensions of a pin fabricated of an alternate fuel material, U-Pu-Mo alloy. The oxide process is based on the fabrication of pellets of the mixed oxides entirely in a glove-box line. The raw materials are ammonium diuranate precipitated UO_2 (ADU) and calcined plutonium oxalate for the PuO_2. The materials are ball-milled and mixed to a paste after the addition of alcohol, camphor, and stearine. The paste is granulated and fed to a pellet-forming machine. The pellets are baked under vacuum and sintered at 1700°C under hydrogen. The final pellets contain 25 wt.% UO_2 and are loaded into the stainless-steel jacket tubes that are closed by electron welded end plugs. As of the writing of Ref. 1, the production line had been tested with UO_2.

The production of fuel elements containing PuO_2 at Hanford Atomic Products Operation (HAPO) has been the subject of a considerable amount of research.[4] The various methods considered are summarized in Fig. IV-2, and a number of different shapes have been produced. This discussion will concentrate on the fabrication methods used for those elements irradiated in the PRTR. The first core of the PRTR consisted of 52 natural UO_2 assemblies and 33 enriched spike assemblies of 1.8 wt.% plutonium (low exposure) alloyed with aluminum.[2,5] Both types of elements employed 19-rod clusters of

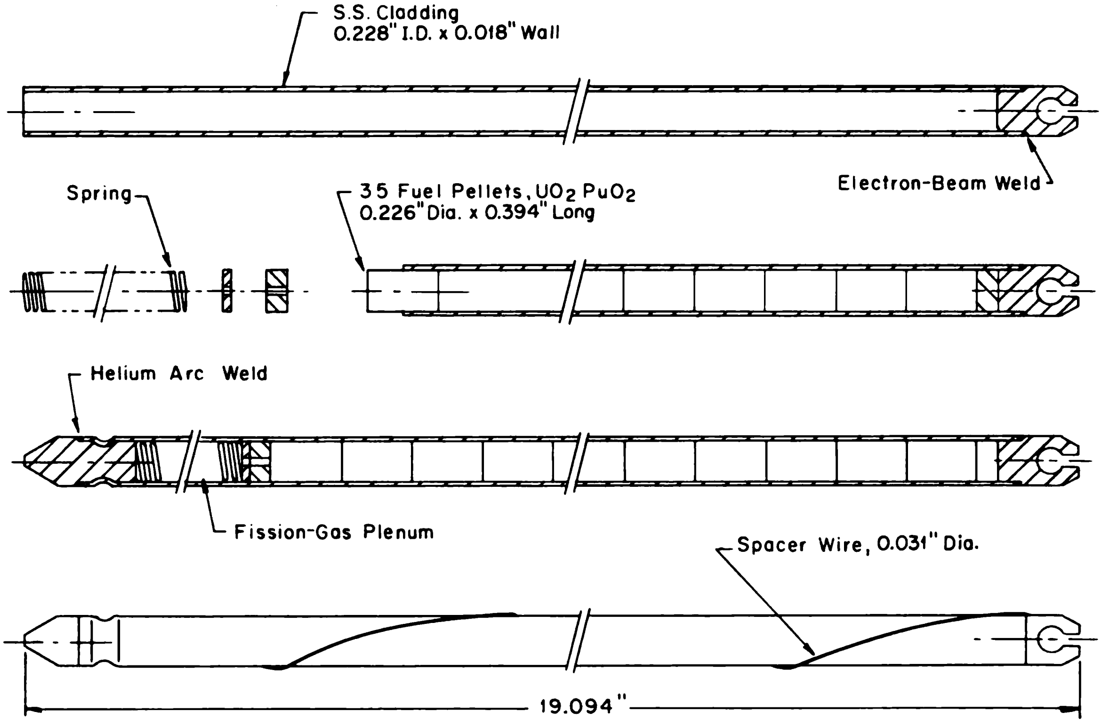

Fig. IV-1 Ceramic fuel rod for the French fast reactor Rapsodie.[1]

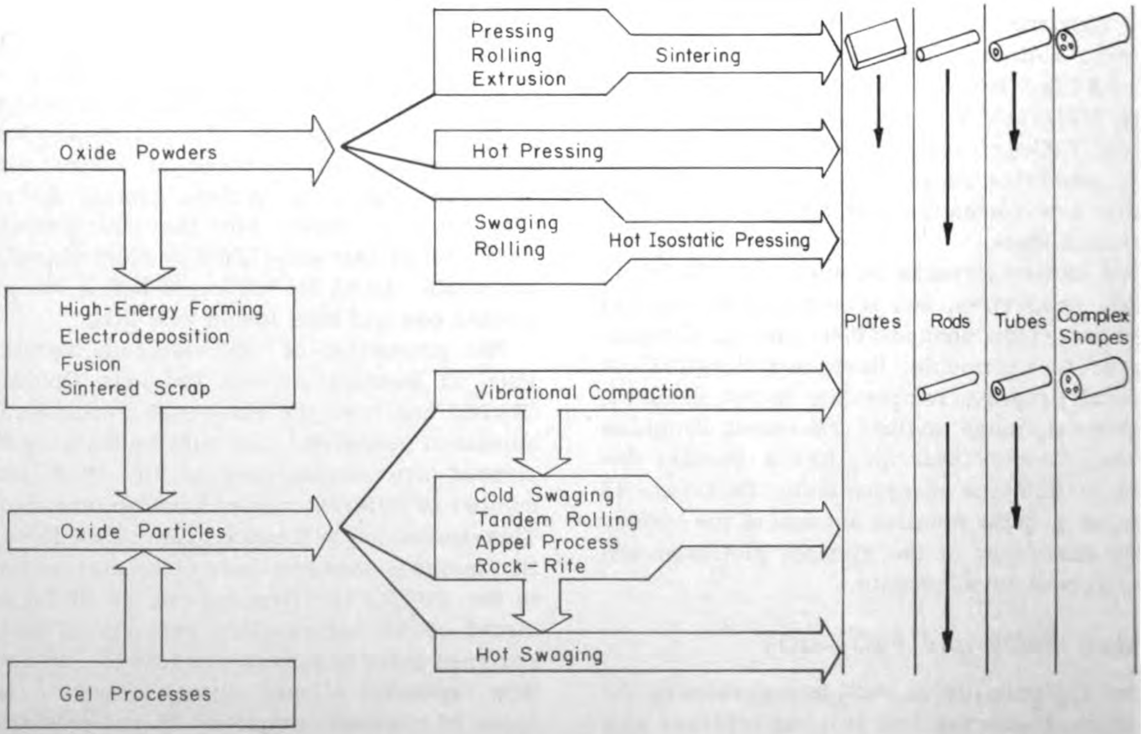

Fig. IV-2 Oxide fabrication methods under study at Hanford Atomic Products Operation.[4]

Table IV-1 FUEL-PIN DIMENSIONS[3] IN INCHES AT 20°C

	Alloy fuel	Oxide fuel
Rod length	15.75	13.39
Rod diameter	0.216	0.226
Niobium cladding outside diameter	0.232	
Niobium cladding thickness	0.008	
Stainless-steel cladding outside diameter	0.264	0.264
Stainless-steel cladding thickness	0.0157	0.019
Expansion space height	1.968	4.685

$^{9}/_{16}$-in.-diameter rods that had a length of 8 ft and employed Zircaloy cladding. The natural UO_2 elements were prepared by cold swaging.

The histories of the PRTR fuel elements and the development work connected with the plutonium program at HAPO have been reported in a variety of Hanford publications. Prior to October of 1962, the results of the plutonium programs at Hanford were reported in the quarterly progress reports of the Fuels Development Operation[6–9] and the Plutonium Metallurgy Operation.[10–13] With the quarter starting October 1962, the information appeared in the quarterly progress report of the Ceramics Research and Development Operation.[14–16] The power operation[17] of the PRTR commenced in May 1961, and during the next year the reactor output was 7261 Mwd(t). The following quotation[12] summarizes the status of the fuel-element program early in 1962:

> In the early part of 1962 the Plutonium Recycle Program (PRP) was advanced almost a year by a change in the core loading schedule for the Plutonium Recycle Test Reactor (PRTR). This was accomplished by eliminating the spike core loading of thirty high exposure aluminum-plutonium fuel elements and by advancing the charging date and charging rate of uniformly enriched Urania-Plutonia (UO_2-PuO_2) fuel elements. The new schedule resulted in a concerted fabrication effort and thirty UO_2-PuO_2 19-rod cluster fuel elements were produced from March through June, 1962. Eighteen of these elements were produced by a cold swage compaction process and twelve by a vibratory compaction process. In addition, during this period three high exposure aluminum-plutonium, four low exposure aluminum-plutonium, and one swaged MgO-PuO_2 spike fuel element were assembled and transferred to the PRTR for irradiation.

In September 1962 the several special fuel elements had been inserted into the PRTR (see Table IV-2), and as of March 1963 the PRTR core contained 44 UO_2-PuO_2, 22 Al-Pu, and 19 UO_2 elements, of which four UO_2-PuO_2, one Al-Pu, and seven UO_2 elements were considered as test elements.[18] The composition of the PRTR core as a function of irradiation history is shown in Fig. IV-3. The fabrication of the Pu-Al spike elements is summarized in Refs. 19 and 20, and Ref. 21 gives details on swageable end-cap design for the UO_2-PuO_2 elements. Reference 22 contains details on vibratory-compaction fabrication techniques.

The MgO-PuO_2 fuel element mentioned in Table IV-2 proved to be a particularly interesting one. In August of 1962 high coolant activity led to the examination of that fuel bundle, with the following results:[14]

> Postirradiation examination revealed a longitudinal split ($1\frac{1}{2}$-inches long and $\frac{1}{4}$-inch wide) in the cladding of one rod, and washout of approximately 9 inches of fuel material. There is no nonuniform discoloration of the cladding that would indicate overheating.

Table IV-2 SPECIAL TEST FUEL ELEMENTS[2]

Fuel type	Fabrication method	Fuel geometry	No. of elements	Average exposure (Sept. 1, 1962)
UO_2	Vipac	Tubular	1	1338 Mwd/ton of U
UO_2	Vipac	19-rod	1	1129 Mwd/ton of U
UO_2	Hot swage	19-rod	1	1010 Mwd/ton of U
Pu-Al (HX)*	Extrusion	19-rod	3	34.8 Mwd
UO_2-PuO_2 (HX)	Cold swage	19-rod	2	16.6 Mwd
UO_2-PuO_2 (HX)	Vipac	19-rod	2	17.0 Mwd
MgO-PuO_2 (HX)	Cold swage	19-rod	1	7.5 Mwd

Maximum exposure to date for the UO_2 element, 2650 Mwd/ton of U
Total reactor exposure to date, 8550 Mwd

* (HX) = high-exposure plutonium, 10 to 17 at.% Pu^{240}.

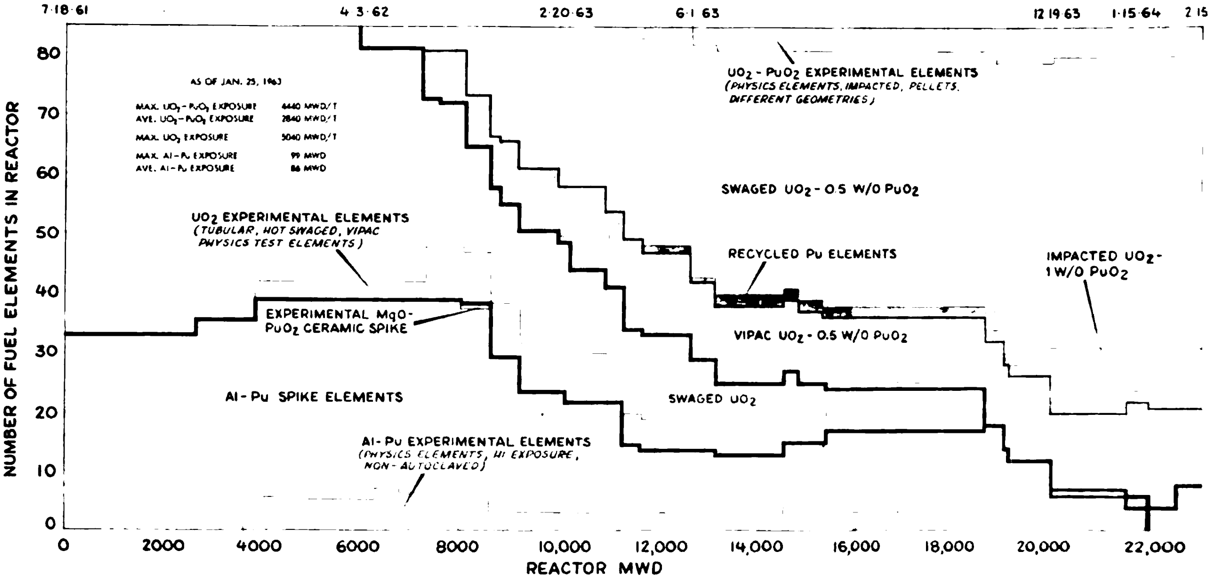

Fig. IV-3 PRTR fuel-element history.

The causes of the failure have been postulated as follows:[23]

> A combination of three factors probably caused the PuO_2-MgO rod failure in the PRTR last August according to a tentative mechanism based on post-irradiation analyses: High localized temperatures were generated at several points of unexplained higher-than-normal plutonium concentration distributed at six-inch intervals along the rods; autoradiographs of some of the rods, including the failed one, revealed the high localized plutonium concentrations. Moisture released by the MgO at excessive operating temperatures attacked the inside of the Zircaloy cladding. A trace of impurity, possibly fluoride from an etchant trapped in an internal cladding defect, caused the water to react much more rapidly than otherwise; severe pitting corrosion, not normally associated with water corrosion of Zircaloy, was found on the inside of the cladding around the failure. The hypothesis goes on to state that corrosion-generated hydrogen dissolved in the cladding and migrated to the cooler outside surface where it precipitated to form a massive hydride layer, since observed metallographically. The weakened cladding failed in a brittle manner, producing a "leaker". Continued irradiation permitted waterlogging and/or hydration of the MgO to cause further splitting of the cladding in a ductile manner. This resulted in exposure of a section of the core to the heavy water coolant and a significant amount of core washout.

Specifications for the MgO-PuO_2 are given in Table IV-3 along with another developmental element containing ZrO_2-PuO_2.

Preirradiation autoclave tests of deliberately defected (drilled holes) rods containing samples of the fuel used in the test elements were conducted. No evidence indicated that swelling of

Table IV-3 SPECIFICATIONS FOR MgO-PuO_2 AND ZrO_2-PuO_2 19-ROD PRTR ELEMENTS[12]

	Swage-compacted ZrO_2-PuO_2	Swage-compacted MgO-PuO_2
Rod outside diameter, in.	0.565 to 0.570	0.565 to 0.570
Core outside diameter, in.	0.503 ± 0.002	0.503 ± 0.002
Cladding thickness, in.	0.032	0.032
Core length, in.	88	88
Fuel core volume, cm^3/element	5449	5449
Core density, % of theoretical	90	90
Weight of core material, kg/element	27.217	17.928
Weight of PuO_2, g/element	371	371
Percentage of PuO, wt.%	1.3	2.1
Maximum core temperature, °F	2923 (1606°C)	1652 (900°C)

the high-fired magnesia would occur under PRTR operating conditions. However, additional tests after the failure of the PRTR element showed that swelling behavior was sensitive to the shape of the defect. As before, capsules defected with drilled holes did not swell, but those having splits milled in the cladding to simulate longitudinal cladding splits did swell.

The PuO_2-MgO fuel rods, made by the incremental loading technique, provided an interesting evaluation of the effect of fissionable fuel distribution on postfailure washout behavior. Nonfissionable magnesia was readily washed from regions of low plutonium concentration, but further loss of fuel was prevented where plutonium concentration was high. In general, where fissionable materials are uniformly distributed, experience has shown that in-reactor sintering of particle fuels effectively prevents loss of significant quantities through cladding defects.

Following the failure of the MgO-PuO_2 element all the PRTR fuel elements were ultrasonically decontaminated, inspected, and recharged into the reactor. No significant damage was discovered, although several bundles had missing or broken spacers. The reactor itself, and primary loop components, were also decontaminated. The details are given in Ref. 22. A total time of 15 weeks was used for this cleanup, and the residual contamination was estimated to be less than 10 mg of Pu, out of an original washout of about 1.8 g. Reference 16 reports on two additional bundles with failed fuel rods. One bundle (5113) contained a rod with a $^3\!/_{16}$-in. by $^3\!/_{32}$-in. hole about a yard down from the top of the rod. The second bundle (5174) contained three failed rods, with the holes adjacent to the top end cap weld.

In extensive postirradiation examination and analysis, the failures were shown to be related to specific, small batches of fuel. Evidence points to three separate types of fuel contamination suffered during the summer and fall of 1963. These were: (1) fluoride and chloride impurities introduced as contaminants in plutonium metal that was to be oxidized; (2) high moisture content sorbed from glove-box atmospheres during periods of high outdoor humidity; and (3) traces of hydrocarbon introduced by failure of a bearing seal. The halide concentration of plutonium was experienced when a change was made in the source of supply. Purification processes were developed to adequately remove these halides. Diffusion of water vapor through rubber gloves and plastic glove-box bags raised the moisture content of glove-box atmospheres to an undesirably high level (PuO_2-containing fuel appears to sorb and hold moisture more tenaciously than does UO_2 alone). Failure of mechanical processing equipment is an obvious possibility that must be considered by any fuel fabricator. The unsuspected introduction of traces of oil from such mechanical failures points out the necessity for careful examination and possible redesign of commercially available equipment that may cause trouble in semiremote operations.

Table IV-4 DESIGN DATA FOR EBWR PLUTONIUM-BEARING CORE[14]

Reactor loading	
Central core region	Plutonium fuel, 36 fuel assemblies in 6 by 6 array
Outer core region	UO_2 fuel, 148 assemblies
Total number of plutonium assemblies	42 (6 spares)
Number of rods per assembly	36 (6 by 6 geometry)
Core composition	UO_2−1.5 wt.% PuO_2 (depleted UO_2, 0.2% U^{235}; high-exposure PuO_2, 8% Pu^{240})
Core length, in.	48.5
Core weight, g	830
Core density, % of theoretical density	86 to 89
Cladding	Zircaloy-2 tubing
Inside diameter, in.	0.372
Wall thickness, in.	0.025

The use of mixed oxides in the form of powder in the loading of fuel rods has one advantage in that it is possible to vary the concentration of plutonium along the length of the rods to shape the axial power profile. This is accomplished by simultaneously loading small increments of PuO_2, mixed with fine UO_2, along with increments of a coarse UO_2 fraction. The incremental loading can be done either during vibratory compaction or prior to a swaged-compaction step. One of the Hanford research programs reported[24] involved the fabrication of a variable enrichment element for irradiation in the Engineering Test Reactor (ETR), and other programs[14] have involved incrementally loading rods with the increments varying from 80 to 150 increments of PuO_2-UO_2 per rod. In general, the results have indicated that this incremental loading may produce segregation of the plutonium-bearing material, and in one PRTR incrementally loaded rod the PuO_2 segregation made temperatures sufficiently high to cause center void formation and columnar grain growth[16,25] in a limited region.

Another common way of loading the PuO_2-UO_2 mixtures is called "bottle loading." In this procedure all the fuel materials for one rod are preblended by mixing for a given period of time. This method produces a blend with a constant PuO_2 distribution to within ±0.1 wt.% when finally loaded into a fuel rod.[16]

A plutonium-bearing core for the Experimental Boiling-Water Reactor (EBWR) is being fabricated at Hanford. Table IV-4 shows design data for the fuel loading. The fabrication technique consists of blending PuO_2 with depleted UO_2 that has been pulverized and air roasted. This material is then put through the Dynapak process, which is described in Ref. 15. This process involves pneumatic impaction of the oxides at a temperature of 1200°C and an impact pressure of about 250,000 psi. Following the Dynapak operation the mixed oxides are loaded via vibrational compaction to 86 to 89% of theoretical density. Irradiations in the ETR of PuO_2-UO_2 fuel rods have been accomplished, and details are given in Table IV-5.

Table IV-5 DETAILS OF EBWR-ETR CAPSULES[16]
GEH-14-421, -422, -423, AND -424

Fuel composition	UO_2–2.5 wt.% PuO_2
UO_2	Arc-fused; depleted U contains 0.22 wt.% U^{235}
PuO_2	Pu contains 7.8 wt.% Pu^{240}
GEH-14-421, -422	Impacted physical mixture
GEH-14-423, -424	Physical mixture
Dimensions, in.	
Fuel, outside diameter/length	0.383/3.00
Zircaloy-2 outside diameter/thickness/length	0.420/0.019/3.70
Aluminum outside diameter/inside diameter/length	1.125/0.420/4.38
Complete assembly with bail, length	5.00
Requested irradiation conditions	
Thermal-neutron flux, neutrons/(cm²)(sec)	0.62×10^{14}
Rod power, kw/ft	16.2
Heat flux, Btu/(hr)(sq ft)	500,000
Exposure, Mwd/ton of fuel	1430

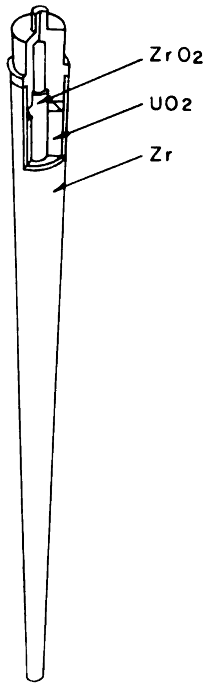

Fig. IV-4 Rod for fuel-element rejuvenation studies.[14]

Another project under way at Hanford is one pertaining to fuel-element rejuvenation.[14] Fuel rejuvenation is defined as reenrichment of the fuel without total reprocessing and is being studied with the help of the fuel rod shown in Fig. IV-4. The element is designed to be reenriched after irradiation by opening the rod and inserting PuO_2, or enriched UO_2, into the concentric ⅛-in.-ID ZrO_2 tube. One irradiation cycle had been accomplished at the time of writing of Ref. 16. The ZrO_2 tube was filled with vibratory-compacted enriched UO_2, resealed, and returned to the Materials Testing Reactor (MTR) for irradiation. Another concept involves the fast reactor to thermal reactor exchange element. This concept consists of "... enriching depleted uranium fuel elements in the blanket of a fast reactor and then irradiating them in the core of a thermal reactor without intervening separation and refabrication processes ..."[16] This element was designed to be irradiated in an existing fast reactor and the PRTR. Details of the element are given in Table IV-6.

A number of capsule irradiations have been conducted to study various aspects of the mixed-oxide fuel elements. Table IV-7, for example, gives data on a series of irradiation tests with the following purposes:[14]

> (a) determining the effect of PuO_2 content on the irradiation stability of the fuel, (b) comparing the in-reactor performance of fuel pellets prepared from mixtures of UO_2 and PuO_2 and from mixtures of UO_2 and $(U, Pu)O_2$ (from calcination of $Pu(OH)_4$ and $(NH_4)_2U_2O_7$ coprecipitated from hot ammonium hydroxide), and (c) investigating the in-reactor sintering of low density (63–65% TD) uranium-plutonium oxide pellets.

The high-density oxide capsules were designed to operate with a surface heat flux of 440,000 Btu/(hr)(sq ft), whereas the low-density capsules were designed to operate with a surface heat flux of 275,000 Btu/(hr)(sq ft). After irradiation to an exposure of 166×10^{18} fissions/cm^3, capsule GEH-14-86 was cross sectioned and samples were taken, with the aid of a diamond-tipped microdrill, from various radial locations within the pellet.* These samples were analyzed radiochemically, with the results as shown in Table IV-8. These data show that Pu, Ce^{144}-Pr^{144}, Zr^{95}-Nb^{95}, and Sr^{90} were relatively fixed within the capsule (little relocation), but the concentrations of the more volatile Cs^{137} and Ru^{106} were greater by orders of magnitude near the periphery of the pellet.

Table IV-6 FAST-THERMAL REACTOR EXCHANGE ELEMENT[16]

Fuel rods	
Cladding material	Zircaloy-2
Fuel	Depleted UO_2
Fuel density	86 to 89% of theoretical density
Rod outside diameter	0.563 in.
Rod inside diameter	0.505 in.
Overall length	$71^3/_8$ in.
Fuel length	$68^5/_8$ in.
Wire wrap material	Zircaloy-2
Wire wrap diameter	0.35 in.
Wire wrap pitch	10 in.
Assembly	
No. of rods	16
Array	Square, 4 by 4
Rod centerline spacing	0.598 in.
Can material	304L stainless steel
End hanger material	304L stainless steel
Overall length	$96^1/_2$ in.

Table IV-7 CAPSULE IRRADIATION TESTS[14] OF UO_2-PuO_2

Capsule data	
UO_2-PuO_2 pellet size	$^1/_2$ in. in diameter
Diametral gap	0.001 to 0.003 in.
Cladding	Zircaloy-2, 0.031 in. thick
Atmosphere	Helium
Size of capsule	$^9/_{16}$ in. in outside diameter by $2^1/_2$ in. in length
High-density pellet capsules (6 pairs)	
Identity number	GEH-14-19, -20, -85 to -91
PuO_2 content	0.0259 to 5.67 mole %
PuO_2 type	4 MCO,* 8 MM†
Sintering conditions	1600°C in H_2, to 11 hr
Density	90 to 93% of theoretical density
Low-density pellet capsules (6 pairs)	
Identity number	GEH-14-21, -22, -65 to -74
PuO_2 content	0.0259 to 7.45 mole %
PuO_2 type	2 MCO, 10 MM
Heating conditions	1000°C in H_2
Density	63 to 65% of theoretical density

* MCO, mixed crystal oxide; ratio of UO_2 to PuO_2 is 5 to 1.
† MM, mechanical mixture of UO_2 (natural) and PuO_2.

GE-APED has conducted a series of irradiation experiments with PuO_2-UO_2 fuel. These experiments were done in the General Electric Test Reactor (GETR), the irradiations taking place during part of the year 1960. The results of the experiments are reported in Ref. 26. References 27 and 28 describe studies done to compare oxide and carbide fuels for use in a fast reactor; they use the results obtained in Ref. 26.

A total of 40 stainless-steel-clad specimens were fabricated[29] and irradiated to burnups from 5000 to 99,000 Mwd/ton at heat fluxes ranging from 0.5×10^6 to 1.6×10^6 Btu/(hr)(sq ft). Following irradiations the specimens were given gamma scans, dimensional measurements were taken, and the fission-gas re-

---

* This burnup corresponds to approximately 5600 Mwd/ton of UO_2 and PuO_2.

Table IV-8 FISSION-PRODUCT DISTRIBUTION IN IRRADIATED[16] UO_2–4.13 MOLE % PuO_2 CAPSULE (GEH-14-86)

Sample	Radius, cm	Radius, in.	Plutonium, dis/(min)(μg U)	Uranium, μg/sample	Ru^{106}, dis/(min)(μg U)	$Ce^{144}Pr^{144}$, dis/(min)(μg U)	$Zr^{95}Nb^{95}$, dis/(min)(μg U)	Ce^{137}, dis/(min)(μg U)
1	0.378	0.147	8.6×10^3	1.8×10^2	7.7×10^5	1.3×10^6	5.3×10^6	2.5×10^3
2	0.142	0.056	1.1×10^4	1.5×10^2	1.9×10^3	1.3×10^6	5.3×10^6	4.0×10^3
3	0.262	0.103	7.6×10^3	1.4×10^2	3.7×10^2	1.1×10^6	4.1×10^6	1.7×10^3
4	0.373	0.147	8.9×10^3	1.6×10^2	5.6×10^5	1.1×10^6	4.5×10^6	2.9×10^3
5	0.462	0.182	7.7×10^3	1.1×10^2	2.2×10^5	1.1×10^6	4.5×10^6	5.0×10^3
6	0.538	0.212	9.6×10^3	1.6×10^2	7.8×10^5	1.6×10^6	5.7×10^6	2.1×10^4
7	0.599	0.236	7.0×10^3	1.3×10^2	5.3×10^5	1.2×10^6	4.1×10^6	6.4×10^4

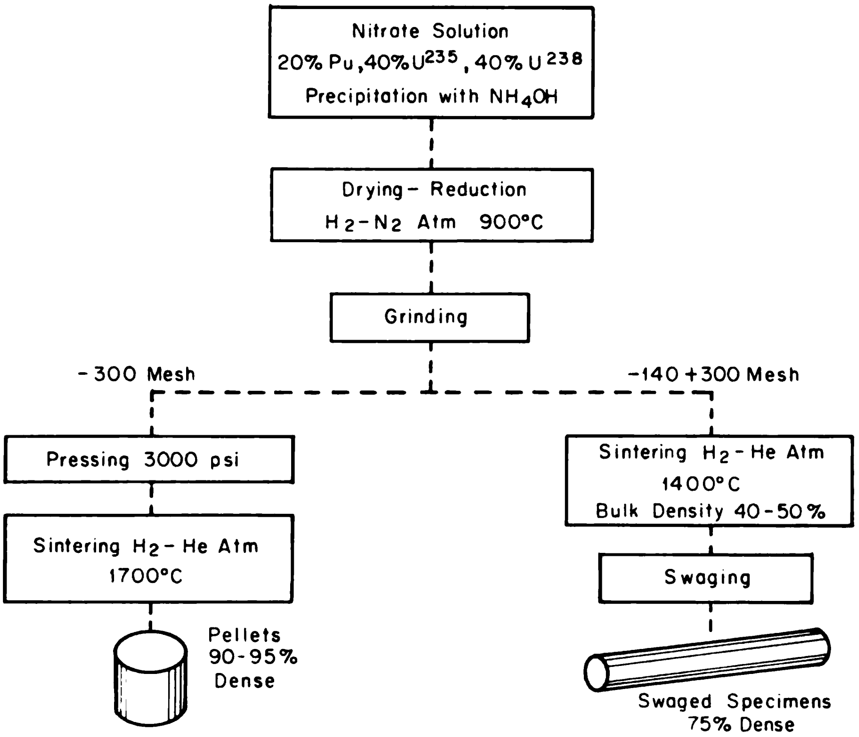

Fig. IV-5 Fuel preparation and fabrication flow sheet.[26]

lease was determined. Central voids were measured, and some metallographic examinations were made. The fuel preparation is shown in Fig. IV-5, and the test specimens are shown in Fig. IV-6. The actual composition of the fuel is shown in Table IV-9. A total of 10 irradiation capsules were fabricated, each containing four of the fuel specimens. These capsules were placed in the GETR, which is cooled by water. Details of the irradiation conditions are shown in Table IV-10. The results of the fuel-element measurements are shown in Table IV-11. The fission-gas release data are given in parts *a* and *b* of Fig. IV-7. Assumptions used to compute the data shown in the figure can be found in Ref. 26.

Possibly the most interesting result is the presence of the void formed during irradiation. As indicated in Table IV-11, only 4 out of the 40 specimens went through the experiment without forming a central void. In the case of the swaged specimens, it was possible to ascertain an approximate correlation between void size and heat flux, and this relation is shown in part *a* of Fig. IV-8. It can be seen that no void formed in the swaged specimens for heat fluxes below about 500,000 Btu/(hr)(sq ft). Part *b* of Fig. IV-8 shows similar data for the pelleted specimens. The voids are smaller for the pelleted than for the swaged specimens at a given value of heat flux, and the void size is not so strongly correlated with heat flux. In a comment on the void formation in the pelleted specimens, the reference[26] states: "... since the pelleted specimens were fabricated with a 6–8 mil diametral gap between the fuel and the cladding, and it is not known whether or not this gap closed during irradiation, this might explain the anomalies in the void formation in the pelleted specimens ..." The mechanism of the formation of the central void is postulated to be[26] grain growth brought about by sintering and/or vaporization and redeposition rather than melting. Two of the specimens had off-center "central" voids, and these same samples also had fuel-to-cladding gaps that may have allowed the fuel to contact the cladding at an isolated spot. Interestingly, a fuel-to-cladding gap in a swaged specimen during operation is postulated.

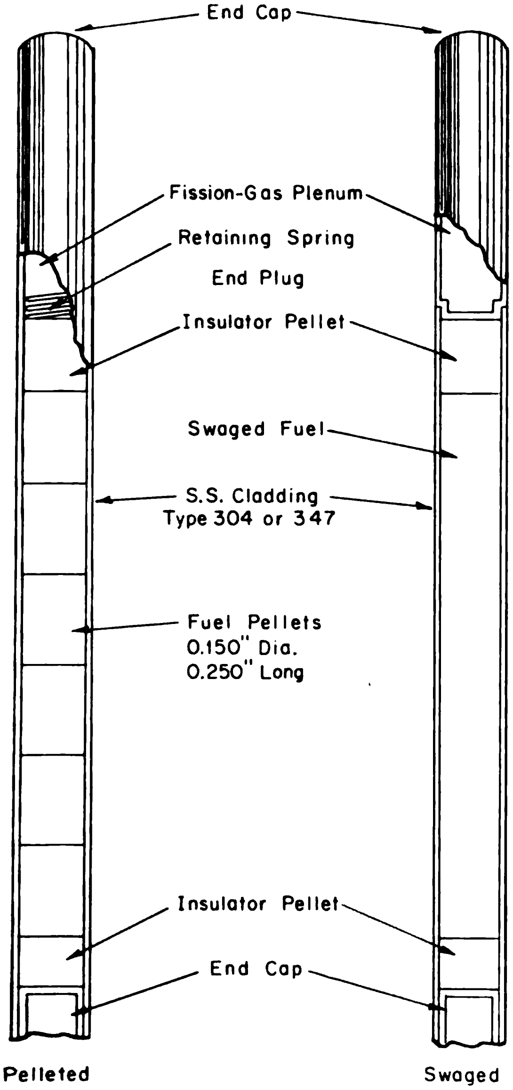

Fig. IV-6 Typical test specimens.[26]

Table IV-9 FUEL COMPOSITION[26] OF GE-APED TEST SPECIMENS

Isotope	Wt.%
Pu^{239}	18.81
Pu^{240}	1.20
U^{235}	37.86
U^{238}	42.13

Two unidentified phases were found in the fuel, and additional results of the metallographic observations are given in Table IV-12. The two phases are called "silver" and "gray" in Table IV-12, and Ref. 26 gives some information on their behavior. In 1961 a paper was presented[30] at a symposium on Radiation Effects in Refractory Fuel Compounds that is, substantially, Ref. 26. The paper is discussed in Ref. 30, and this discussion would be of interest to the specialist.

Information on PuO_2 properties is given in the Battelle Memorial Institute reports listed as Refs. 31 to 33. The first of these references lists, in tabular form, information on composition; physical, mechanical, thermal, electrical, and chemical properties; and irradiation properties for a number of fuel materials, among which is PuO_2. Unfortunately the most common entry for this latter fuel material is "no data available." References 32 to 34 deal with the stability of PuO_2 under various conditions.

Carbides

The carbides are receiving considerable attention as potential plutonium-bearing fuels because their thermal conductivity is high compared to that of the plutonium-bearing oxides. In this country the Argonne National Laboratory (ANL) and the United Nuclear Corporation appear to have done the most development of (PuU)C.[35] In general, the fabrication method enjoying greatest popularity involves reacting

UO_2 and PuO_2 with carbon to produce the carbides. The mixed carbides can then be pelleted by cold pressing and sintering; densities up to 95% of theoretical density have been achieved by the use of nickel as a sintering aid. Los Alamos Scientific Laboratory (LASL) has prepared various UC-PuC compounds by the direct comelting of uranium and plutonium metal with carbon in an arc furnace.[36]

The results of ANL irradiations of UC-PuC fuel rods have been reported in the 1961 and 1962 annual reports of the Metallurgy Division

Table IV-10 EXPERIMENTAL PARAMETERS FOR GETR IRRADIATIONS[26]

Specimen No.	Burnup, Mwd/ton*	Heat flux, Btu/(hr)(sq ft) × 10^6		$\int k\, d\theta$,† Btu/(hr)(ft)		Surface temperature, °F‡	
		Maximum	Average	Maximum	Average	Maximum	Average
I-1-P§	16,600	1.41	1.30	5,600	5,200	1,040	970
I-2-P	13,600	1.36	1.10	5,400	4,400	1,010	830
I-3-P	8,700	1.03	0.75	4,100	3,000	1,040	750
I-4-P	4,700	0.62	0.40	2,500	1,600	1,010	650
II-1-S§	19,400	1.33	1.28	5,300	5,100	1,080	1,050
II-2-S	16,100	1.34	1.09	5,400	4,400	1,120	940
II-3-S	10,700	1.06	0.73	4,300	2,900	1,160	830
II-4-S	6,600	0.72	0.45	2,900	1,800	1,130	750
III-1-S	26,000	1.14	1.06	4,600	4,200	810	760
III-2-P	18,800	1.10	0.96	4,300	3,800	790	730
III-3-P	15,100	1.02	0.77	4,000	3,000	820	670
III-4-S	11,700	0.75	0.48	3,000	1,900	710	500
IV-1-S	19,100	0.91	0.78	3,600	3,100	890	820
IV-2-P	14,000	0.82	0.71	3,200	2,800	1,030	910
IV-3-P	10,900	0.69	0.55	2,700	2,100	990	820
IV-4-S	9,000	0.53	0.37	2,100	1,500	880	660
V-1-S	99,000	1.52	1.27	6,000	5,100	1,260	1,060
V-2-P	77,400	1.58	1.30	6,200	5,100	1,180	1,020
V-3-P	54,400	1.28	0.92	5,000	3,600	1,130	880
V-4-S	42,700	0.86	0.55	3,400	2,200	930	650
VI-1-S	69,100	1.00	0.89	4,000	3,500	1,140	1,030
VI-2-P	41,600	0.79	0.68	3,100	2,700	1,060	950
VI-3-P	34,900	0.76	0.57	3,000	2,200	1,210	950
VI-4-S	30,900	0.62	0.40	2,400	1,600	980	680
VII-1-S	70,300	1.44	1.31	5,700	5,200	1,220	990
VII-2-P	49,900	1.50	1.32	5,900	5,200	1,170	950
VII-3-P	38,900	1.24	0.92	4,800	3,600	1,080	790
VII-4-S	29,600	0.86	0.55	3,400	2,200	950	630
VIII-1-S	45,200	1.07	0.83	4,200	3,300	1,180	930
VIII-2-P	28,300	0.85	0.66	3,300	2,600	1,220	920
VIII-3-P	23,100	0.75	0.54	2,900	2,100	1,150	840
VIII-4-S	19,300	0.50	0.36	2,000	1,400	820	590
IX-1-P	47,600	1.40	1.36	5,460	5,270	1,060	930
IX-2-P¶	38,300	1.36	1.19	5,300	4,700	**	**
IX-3-P	34,500	1.21	0.95	4,850	3,200	990	740
IX-4-P¶	17,600	0.86	0.56	3,350	2,160	**	**
X-1-S††	36,300	0.91	0.88	3,600	3,500	**	**
X-2-P	23,700	0.85	0.75	3,400	3,000	**	**
X-3-P	16,800	0.71	0.54	2,800	2,200	**	**
X-4-S	15,000	0.57	0.37	2,300	1,500	**	**

* Tons of plutonium and uranium (2000 lb/ton).
† Linear power generation = $4\pi \int k\, d\theta$.
‡ Temperature at inner surface of cladding.
§ P, pelleted specimen; S, swaged specimen.
¶ These specimens had no gas plenum.
** Cladding thermocouple failed.
†† Estimated data; majority of thermocouples failed during irradiation.

of ANL.[37] Arc-melted PuC and PuC-UC, and pressed and sintered pellets of PuC-UC, were irradiated in the EBR-I. The burnups achieved were all the order of 1000 Mwd/metric ton. The arc-melted material was very friable and fractured into large numbers of pieces on removal from the stainless-steel cladding or during subsequent handling. Minor dimensional changes were measured, with the densities, in general, decreasing on the order of 1%. The pressed and sintered material was stated to be "very durable" with minor dimensional changes. The

Table IV-11 POSTIRRADIATION FUEL MEASUREMENTS[26]

Specimen No.	Preirradiation density, % of theoretical	Active fuel length, in.			Central void data			
		Pre-irradiation	Post-irradiation	Postirradiation/ preirradiation	Diameter, in.	% of cross-sectional area	Length, in.	% of post-irradiation length
I-1-P*	93.5	1.605	†		0.034 to 0.044	5.0 to 9.7	1.60	100
I-2-P	92.5	1.605	†		0.019 to 0.041	1.7 to 7.5	1.60	100
I-3-P	93.3	1.605	†		†		†	
I-4-P	92.7	1.600	†		No void			
II-1-S	75	1.825	†		0.051 to 0.071	11.7 to 21.3	1.67	90
II-2-S	75	1.825	†		†		†	
II-3-S	75	1.825	†		†		†	
II-4-S	75	1.825	†		0.017 to 0.021	1.4 to 2.0	1.18	63
III-1-S	75	1.825	1.91	1.05	0.056 to 0.057	12.5	1.30	68
III-2-P	93.3	1.544	1.65	1.07	0.014 to 0.018	1.0 to 1.1	0.50	30
III-3-P	92.3	1.553	1.63	1.05	0.020 to 0.023	2.0 to 2.3	1.32	81
III-4-S	75	1.825	1.91	1.05	0.014 to 0.050	1.0 to 11.0	1.33	70
IV-1-S	75	1.825	2.07	1.13	0.036	5.7		
IV-2-P	90.7	1.552	1.65	1.06	0.034 to 0.035	5.1 to 5.4	1.55	94
IV-3-P	89.0	1.564	1.63	1.04	0.031 to 0.035	4.0 to 5.4	0.70	43
IV-4-S	75	1.835	2.04	1.13	No void			
V-1-S	75	1.825	1.99	1.09	0.047 to 0.067	9.8 to 19.5	1.50	75
V-2-P	95.8	1.495	1.58	1.06	0.022 to 0.031	2.0 to 4.0	0.81	51
V-3-P	94.5	1.473	1.53	1.04	0.005 to 0.009	0.2 to 0.4	0.86	56
V-4-S	75	1.825	1.89	1.03	0.031 to 0.045	4.0 to 9.1	1.78	94
VI-1-S	75	1.825	1.96	1.07	0.042 to 0.054	7.8 to 13.0	1.26	664
VI-2-P	96	1.527	1.59	1.04	0.029 to 0.031	3.5 to 4.0	0.62	39
VI-3-P	95.3	1.531	1.58	1.03	0.013 to 0.031	0.7 to 4.0	0.75	47
VI-4-S	75	1.825	1.96	1.07	0.026 to 0.034	3.0 to 5.1	0.75	38
VII-1-S	75	1.825	1.90	1.04	0.051 to 0.060	11.6 to 16.0	1.61	84
VII-2-P	94.7	1.520	1.63	1.07	0.028 to 0.036	3.2 to 5.3	0.88	55
VII-3-P	96	1.516	1.58	1.04	0.033 to 0.038	4.5 to 5.9	0.57	36
VII-4-S	75	1.825	1.98	1.08	0.022 to 0.036	2.2 to 5.8	1.32	67
VIII-1-S	75	1.825	1.82	1.00	0.040 to 0.049	7.1 to 10.8	1.44	79
VIII-2-P	94.2	1.530	1.57	1.03	0.013 to 0.013	0.7	1.17	74
VIII-3-P	94.3	1.529	1.59	1.04	No void			
VIII-4-S	75	1.825	1.82	1.00	0.027 to 0.027	3.0	0.28	15
IX-1-P	86.5	1.333	1.36	1.02	0.026 to 0.040	2.8 to 6.6	0.95	70
IX-2-P‡	94.8	1.521	1.58	1.04	0.022 to 0.031	2.2 to 4.2	1.10	70
IX-3-P	83.7	1.348	1.36	1.01	0.027 to 0.036	3.2 to 5.7	1.36	100
IX-4-P‡	95.8	1.774	1.83	1.03	No void			
X-1-S§	75	1.825	1.85	1.01	0.040 to 0.054	7.1 to 13.0	1.72	93
X-2-P	96	1.517	1.52	1.00	0.009 to 0.018	0.3 to 1.3	0.61	41
X-3-P	96.5	1.514	1.57	1.04	0.013 to 0.027	0.7 to 3.0	0.42	27
X-4-S	75	1.825	1.84	1.01	0.008	0.3		

*P, pelletized specimen; S, swaged specimen.

† No measurements taken.

‡ These specimens had no gas plenum.

§ Estimated data; majority of thermocouples failed during irradiation.

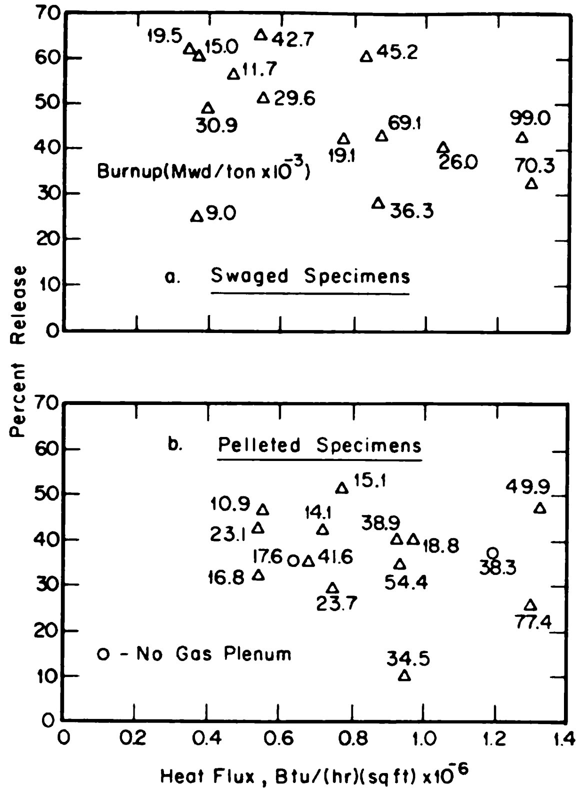

Fig. IV-7 Fission-gas release data.[26]

pressed and sintered pellets released 12% of the theoretical fission-gas release, and this was attributed[38] to the low density of the pellets, about 55%. LASL has reported data on a number of the properties of (UPu)C.[36,39]

The UKAEA has been studying mixed carbides for fast reactor applications.[40] Specimens of (UPu)C have been prepared by arc-melting uranium, plutonium, and carbon and casting in massive copper molds. Pellets have been prepared by cold pressing and sintering to greater than 95% of theoretical density. Data are shown in Table IV-13. Thermal conductivity of the carbides is given in Table IV-14. These data indicate that the addition of PuC to UC has the effect of reducing the thermal conductivity of the latter substance to about 70% of its former value.

Additional information on the preparation of PuC and (UPu)C can be found in Ref. 41, and Ref. 42 reports on the examination of irradiated (PuU)C fuel pellets. Irradiation data on (UPu)C pellets contained in Ref. 40 apparently came from the same experiments described in Ref. 42, and since the latter reference was issued later, the irradiation data contained therein will be cited. The reference[42] reports on the irradiation of nine stainless-steel-clad carbide fuel elements in the PLUTO reactor. Four of the elements contained arc-cast $(U_{90}Pu_{10})C$ pellets fabricated by direct arc-melting U-Pu metal with graphite. The pellets had a diameter of 0.1 in. They were ground to size and were incorporated in 20 Cr–20 Ni titanium-stabilized double-vacuum-melted stainless-steel tubing. Fission-gas space was allowed at one end of the assembly. Details on the sizes of the elements and conditions during irradiation are given in Table IV-15. Following irradiation, dimensional measurements were taken and no significant changes in dimensions were recorded. As stated in Ref. 42: "... it was concluded that no noticeable distortion of the sheathing had occurred during irradiation ..." Gas-release data are given in Table IV-16. It is evident that sample 8024 exhibited considerably more gas release than a comparable sample, 8025. No reasons for this difference are given in the reference, although metallographic examinations were done to see if an explanation could be found. The

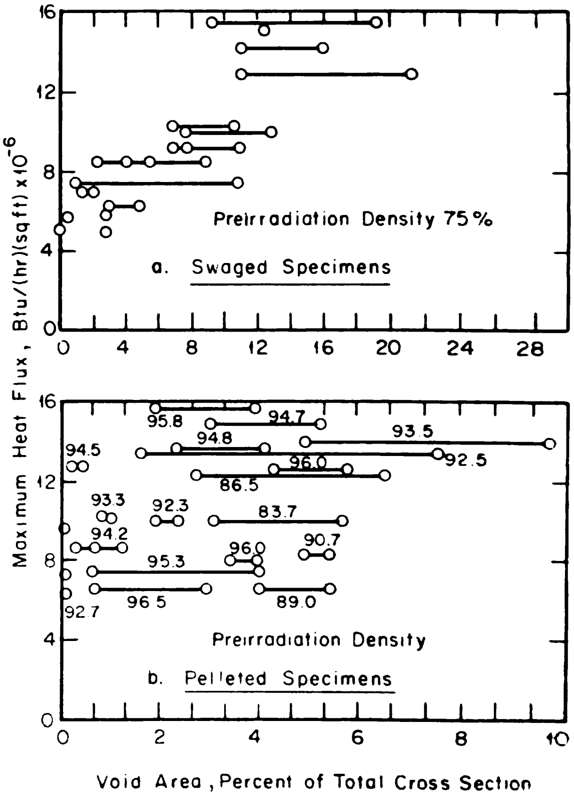

Fig. IV-8 Central void data, heat flux vs. void area.[26]

Table IV-12 SUMMARY OF METALLOGRAPHIC OBSERVATIONS[26]

Specimen	Burnup, Mwd/ton	Average heat flux, Btu/(hr)(sq ft)	Preirradiation density, % of theoretical	Approx. diameter of central void, in.	Fuel cracking	Structure	Other phases and constituents	Fuel-to-cladding gap
V-1-S	99,000	1.27×10^6	~75	0.060	Mainly radial with some circumferential	Small grains at OD; long columnar grains extending out from central void, porous band along OD of fuel, little or no grain growth at OD	Silver phase present throughout fuel	Fuel in contact with cladding
VI-1-S	69,100	0.89×10^6	~75	0.055	Mainly radial with some circumferential	Equiaxed grains at OD; long columnar grains extending out from central void; some grain growth at OD	Silver phase present throughout fuel. Gray phase present along OD of fuel	Fuel-to-cladding gap with particles of fuel adhering to cladding
V-4-S	42,700	0.55×10^6	~75	0.050	Radial	Equiaxed grains at OD; columnar grains extending out from central void; grain growth at OD	Silver phase present throughout fuel	Fuel-to-cladding gap exists
IV-4-S	9,000	0.37×10^6	~75	Small irregular shape	Radial	Unsintered or partially sintered fuel at OD; small columnar grains at central void	Large deposits of silver phase throughout fuel	Fuel-to-cladding gap exists
V-2-P	77,400	1.30×10^6	95.8	0.030	Mainly radial with some circumferential	Small grains at OD; long columnar grains extending out from central void; porous band along OD of fuel, little or no grain growth at OD	Silver phase present throughout fuel. Polygon-shaped crystals within columnar grains	Fuel in contact with cladding
V-3-P	54,400	0.92×10^6	94.5	Very small irregular shape	Mainly circumferential, some radial	Small grains at OD; equiaxed grains in mid-radius region, short columnar grains around central void	Silver phase present throughout fuel	Fuel in contact with cladding
IX-3-P	34,500	0.84×10^6	83.7	0.070	Mainly radial with some wide circumferential cracks near OD	Equiaxed grains at OD; long columnar grains extending out from central void; grain growth at OD	Silver phase present throughout fuel. Gray phase present along OD	Fuel-to-cladding gap exists
IV-3-P	10,900	0.55×10^6	89.0	0.035	Radial and wide circumferential cracks	Equiaxed grains at OD; long columnar grains extending out from central void; grain growth at OD	Silver phase present throughout fuel. Gray phase present along OD	Fuel-to-cladding gap exists
Unirradiated pellet			93.7		None	Uniform cross section	Two small deposits of silver phase	

reference notes that the lack of fuel swelling can possibly be explained by the fact that the 0.020-in.-thick cladding effectively restrains the fuel material.

The plutonium fuel programs at the United Nuclear Corporation (UNC) are described in Ref. 43. The fabrication technique involves the reaction of a pelletized mechanical mixture of UO_2, PuO_2, and carbon. The resulting material, called a clinker, is ground, cold pressed, and sintered. The advantage of using the nickel sintering aid can be seen in Table IV-17.

Table IV-13 EFFECT OF SOME SINTERING VARIABLES ON THE DENSITY OF UC AND $(U_{85}Pu_{15})C$ PELLETS[40]

Pellet	Carbon content, wt.%	Sintering time, hr	Sintering temp., °C	Bulk density, g/cm³
(UPu)C	4.69	4	1585	13.11
(UPu)C	4.89	4	1585	13.11
(UPu)C	5.25	4	1550	13.12
UC	4.70	5	1550	12.99
UC	4.70	12	1550	12.94

Table IV-14 THERMAL CONDUCTIVITIES OF UC AND $(U_{85}Pu_{15})C$ CYLINDERS[40]

Fabrication method	Density, g/cm³	Carbon content, wt.%	Thermal conductivity,* cal/(sec)(cm)(°C)
Uranium carbide			
Arc cast	13.87	4.40	0.052
Arc cast	13.64	3.77	0.052
Arc cast	13.40	5.06	0.058
Hot pressed	13.08	4.91	0.041
Uranium plutonium carbide			
Arc cast	13.67	4.55	0.031
Arc cast	13.55	4.71	0.036
Arc cast	13.24	4.84	0.041
Hot pressed	13.21	4.92	0.030
Arc cast		5.03	0.040
Hot pressed	12.90	~5.2	0.030
Hot pressed	13.04	5.41	0.030

* Uncorrected for porosity.

Metallic Fuels: Alloys

These fuels are of particular interest since a plutonium-containing alloy is proposed for use in the EBR-II for core 2. This alloy has the composition shown in Table IV-18. The goal mentioned in Ref. 44 for design of the plutonium-bearing element is a burnup of 5% (about 45,000 Mwd/metric ton) with central metal temperatures up to about 700°C. Unfortunately the reference alloy (Table IV-18) undergoes serious swelling at lower burnups and lower temperatures. One suggested method of attacking the problem has been the use of a strong jacket to restrain the fuel material mechanically. The strong-jacket concept was discussed in *Power Reactor Technology*, 4(4): 86, and Ref. 55 is a more recent publication dealing, in part, with the subject. Another suggested solution has been reduction of the plutonium content to 10 to 15%, which also improves radiation stability.[44] Results of irradiation of prototype EBR-II core 2 fuel elements were reported at a recent meeting of the American Nuclear Society.[45] This reference states that the minimum desired fuel burnup is 1.5 to 2 at.% and gives results of irradiations conducted in capsules in the CP-5 reactor. The cladding had a wall thickness of 0.009 in. and was separated from the fuel material by a sodium-filled gap with a (radial) dimension of 0.0006 in. Results are quoted as follows:

> The initial irradiations were conducted primarily with commercially obtained Nb/1 wt% cladding. The cladding had an internal void volume amounting to

Table IV-15 IRRADIATION DETAILS OF CARBIDE FUELS[42]

(Specimen Composition in Each Case Is 10 Wt.% PuC-90 Wt.% Natural UC)

Specimen No.	Carbon content, wt.%	Specimen size, in.		Specimen density, g/cm³	Capsule total heat output, watts	Calculated specimen rating, watts/g	Measured mean burnup, provisional Mwd/metric ton of fuel	Gas bond	Measured can surface temp., °C	Estimated specimen temp., °C	
		Diameter	Length							Surface	Center
8024	4.53 to 4.64	0.10	0.963	13.40 to 13.54	140	38	5,650	Ar	545	980	1010
8025	No analysis	0.10	1.00	10.22 to 13.42		38	6,550	Ar	545	980	1010
8013	4.54 to 4.61	0.10	1.94	13.35 to 13.59	252*	76.5†	12,500	He	420	462	480
8014	4.52 to 4.65	0.10	1.34	13.24 to 13.59	196	91.5‡	16,500	Ar	520	752	777

* Estimated heat output.
† Actually 54 watts/g.
‡ Actually 21 watts/g.

13 per cent of the fuel volume. Other cladding materials were also evaluated as they became available. Among these were niobium, Nb/1 wt% V alloy, Nb/33 wt% Ta/1 wt% Zr alloy, vanadium, molybdenum, and Ta/0.1 wt% W alloy. Cladding failures during irradiation could not be correlated with reported rupture strengths of the materials, and were generally traced to defects in the tubing materials. The failures occurred at burnups in the range of 1.0 to 1.5 atom per cent and were characterized by fracture or splitting of the cladding, originating at the hottest portion of the specimen and extending along the length of the specimen. Once a fissure had been established, the fuel generally extruded through the opening. The majority of cladding failures were by brittle fracture of the material. Vanadium cladding in the fully annealed condition failed in a ductile manner.

By improving the quality of the jacketing material and increasing the void volume within the cladding, the attainable burnup of the fuel prior to clad failure was extended from 1.3 atom per cent to 1.9 atom per cent. The attainable burnup was further extended to 2.1 atom per cent by venting the cladding to permit escape of entrapped fission gas or bond sodium.

Duplex tubing consisting of austenitic nickel alloys coated on the inside surface with 0.002-in. of tungsten is also under evaluation. The tungsten barrier is used to isolate the plutonium alloy from the austenitic nickel, thereby preventing formation of a molten eutectic. With this configuration it has been possible to achieve a 2.6 atom per cent burnup without failure.

A tertiary alloy is being considered for the French fast reactor Rapsodie.[3] The philosophy of canning the alloy, U-Mo-Pu, in a strong can is also being followed by the French, and a schematic of the Rapsodie fuel pin, using the alloy fuel, is shown in Fig. IV-9. The alloy will be injection cast into the niobium tube and capped with a resistance-welded niobium capsule. The niobium rod is then placed inside a stainless-steel can, using sodium as a thermal bonding material. Apparently a whole fuel pin such as is shown in Fig. IV-9 had not been fabricated when Ref. 3 was written, and the authors express concern as to the success of the double canning operation. Irradiation of U-Mo-Pu has also been done for the United Kingdom reactor program with the following quoted results: "... the avoidance of severe swelling at temperatures as high as 600°C presents a difficult problem..."[40]

There are, of course, potentially a large number of alloys with plutonium. The Pu-Al alloy was used as the spike enrichment elements for the PRTR, although these elements, as designed, had short reactivity lifetimes and high throughput rates.[2] The PRTR spike enrichment fuel elements are 8-ft-long 19-rod clusters. Additional data on the elements are given in Table IV-19. Irradiation of the Pu-Al elements in the PRTR has produced shortening

Table IV-16 FISSION-GAS RELEASE MEASUREMENTS[42]

(Composition of Each Fuel Specimen Is 10 Wt.% PuC–90 Wt.% Natural UC)

Specimen No.	Estimated volume of Xe produced, cm^3 at NTP	Recoil contribution, cm^3 at NTP	Measured volume of Xe on puncture, cm^3 at NTP	Percentage gas release [(measured/total produced) × 100]
8013	1.052	3.6×10^{-3}	3.4×10^{-4}	3.2×10^{-2}
8014	0.953	3.3×10^{-3}	1.3×10^{-5}	1.4×10^{-3}
8024	0.238	8.55×10^{-4}	4.7×10^{-3}	1.96
8025	0.279	9.9×10^{-4}	8.1×10^{-5}	2.9×10^{-3}

Table IV-17 DENSITIES OF (UPu)C OBTAINED WITH AND WITHOUT NICKEL SINTERING AID[43]

Material	Sintering temp. for 1 hr, °C	Approximate number of pellets made	Average density		Maximum density	
			g/cm^3	% of theoretical	g/cm^3	% of theoretical
$(U_{0.8}Pu_{0.2})C_{0.95}$	1965	200	12.54	92.4	12.83	94.4
$(U_{0.8}Pu_{0.2})C_{0.95}$ + 0.1 wt.% Ni	1590	200	13.15	96.8	13.30	97.8

of the fuel rods, which has been made apparent by the loosening of the spiral spacing wires around the rods.[11,15] Although the reason for the shortening of the rod apparently is not known in detail, Ref. 11 suggests that it is due to interaction between the Pu-Al core and the Zircaloy cladding. The shortening is a progressive phenomenon affected by the number of thermal cycles and/or fuel-element exposure. The lack of wear and/or fretting corrosion as a result of the loose wires suggests that at operating temperature the wires are tightened by the differential expansion between the core and the cladding.[11] The shortening has been noticed at an exposure of 54 Mwd, and one element with an average exposure of 74.2 Mwd exhibits a 0.28% shortening of a rod.[15]

Table IV-18 FUEL ALLOY FOR INITIAL CORE 2 LOADING: EBR-II[44]

Element	Wt.%
Zirconium	1.0
Molybdenum	2.9
Ruthenium	4.2
Rhodium	0.7
Palladium	2.2
U^{238}	Bal.
U^{235}	15 to 18
Plutonium	18 to 15

A number of intermetallic compounds such as U-Pu, Th-Pu, Bi-Pu, Co-Pu, and Fe-Pu have been prepared,[36] and some have been irradiated.[46] The irradiations were at maximum fuel temperatures of about 450°C, and burnups of about 2% were attained. Cast alloys of thorium containing 5 and 10 wt.% plutonium exhibited excellent dimensional stability, but cold-rolled zirconium that contained 5 and 7 wt.% plutonium exhibited poor dimensional stability.[46]

Metallic Plutonium, Cermets, and Miscellaneous Compounds

One application for nearly pure plutonium for power-reactor fuel is in the Los Alamos Molten-Plutonium Reactor Experiment I (LAMPRE-I). The fuel for this experiment is 90 at.% Pu–10 at.% Fe contained in a tantalum capsule. The nominal rod size[48] is 0.36 in. in inside diameter by 6¼ in. in length, with a wall thickness of 0.025 in. The alloys considered for LAMPRE-I are shown in Table IV-20. The addition of the alloying elements lowers the melting point of the fuel with respect to that of unalloyed plutonium (about 640°C). The tantalum capsule material suffers intergranular attack if the fuel is operated above 575°C. The Pu-Ce-Co alloy is of particular interest, since the plutonium content can be varied from 20 to 88 at.% with a corresponding reduction in the cerium concentration.

An alloy of Pu–1.25 wt.% Al was used in core IV of EBR-I.[38] The slugs of Pu-Al were 0.232 in. in diameter and 2.121 in. long. They were contained in a Zircaloy-2 jacket, and a NaK bond was provided for heat transfer purposes. A total of 420 fuel rods and 10 thermo-

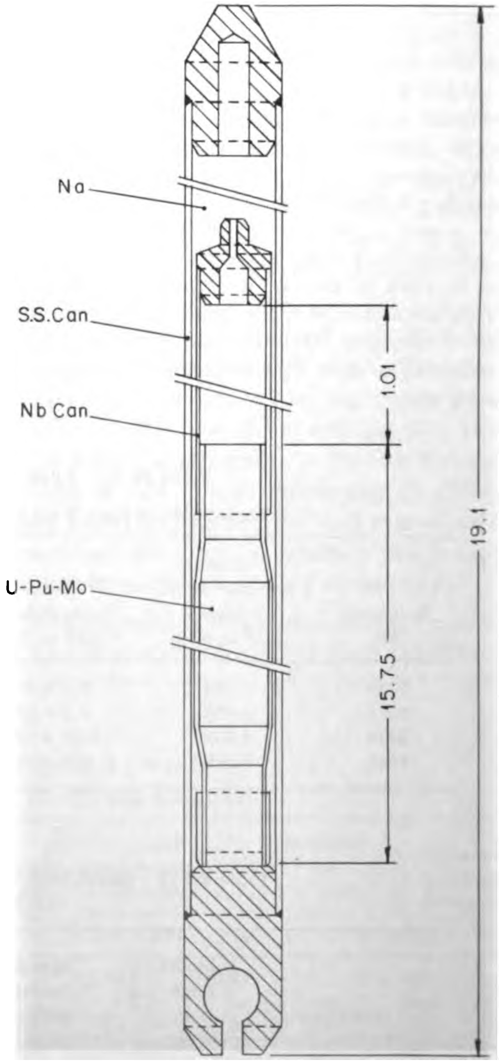

Fig. IV-9 The U-Pu-Mo fuel pin for the French fast reactor Rapsodie.[3]

couple rods containing the alloy were fabricated and successfully irradiated in the EBR-I.

Plutonium-bearing cermets have received considerable study. Researchers in the United Kingdom have prepared $(UPu)O_2$–stainless-steel and (UPu)C-Fe cermets.[40,41] The former material was fabricated by coating spheroids of $(UPu)O_2$ with stainless-steel powder and pressing into compacts. Plates were then formed by roll bonding. Some irradiations have been performed of 30, 40, and 50 vol.% oxide in stainless steel in the form of plates and pellets. The carbide-iron cermets were in a less advanced stage of study at the time of writing of Ref. 40. Oxide–stainless-steel cermets have been fabricated and irradiated in support of the Dounreay fast reactor program.[50] They are made by coating $(UPu)O_2$ granules with stainless-steel powder, pressing into pellets, and sintering in hydrogen. Preliminary irradiations have given mixed results, but the data given in Ref. 50 are of a preliminary nature. Cermets of PuO_2 and PuC in a zirconium-niobium base alloy are receiving study at the BelgoNucléaire Laboratories.[51] Hanford reports on properties of PuN-Pu, PuN-W, PuO_2-Zr, PuO_2-Mo, and PuO_2-W cermets in Refs. 14 and 16. LASL has prepared sintered pellets of PuO_2–stainless steel and PuO_2-Mo.[52,53]

Table IV-19 MARK I-G ALUMINUM-PLUTONIUM FUEL-ELEMENT DATA[20]

Core composition, wt.%	Pu, 1.81; Al, 95.40; Ni, 1.35; Si, 1.10; Fe, 0.33
Pu composition tolerance (standard deviation), wt.% Pu	0.04
Core density, g/cm^3	2.77
Average core weight (single rod), g	780
Average Pu weight per core (single rod), g	14.15
Average core weight per element, (19-rod cluster), g	14,820
Average Pu weight per element, (19-rod cluster), g	269.04
Core diameter, in.	0.500 ± 0.0002
Core length, in.	87.500 ± 0.020
Cladding material	Zircaloy-2
Cladding inside diameter, in.	0.505 ± 0.001
Cladding outside diameter (nominal), in.	0.565
Cladding thickness (nominal), in.	0.030
Cladding length, in.	89.115 ± 0.010
Rod length (overall), in.	
Regular rods	92.56
Center rod	93.11
Element length (overall), in.	$97\frac{5}{8}$
Rod weight (approximately), lb	3
Fuel-element weight, 19-rod cluster (approximately), lb	59
Wire wrap material	Zircaloy-2
Wrapping wire diameter, in.	0.072
Number of bands per element	4

Table IV-20 LOW-MELTING ALLOYS SUITABLE FOR MOLTEN-PLUTONIUM FUELS[49]

Alloy	Solidus point, °C
Pu–9.5 at.% Fe	409
Pu–12 at.% Co	405
Pu–12.5 at.% Ni	465
Pu–Ce–12 at.% Co	<450

In summary, metallic fuels face formidable swelling problems in a reactor designed to operate with high-temperature fuel irradiated to large burnups. Reference 54, in fact, concludes that "... the potential of metallic systems appears now to be very limited ..." On the other hand, the author of Ref. 55 favors a simple U-Pu metallic fuel element containing 25 to 30% internal void, and states that Nimonic-clad pins such as these have been successfully tested to 5% burnup (about 45,000 Mwd/metric ton) at 700°C temperature.

The mixed-oxides system has been irradiated to high burnup in the GETR. Although the results are encouraging, the irradiation of full-length fuel elements has only just started in the PRTR. It is concluded in Ref. 54 that PuO_2-UO_2 mixtures behave similarly to UO_2 alone but with somewhat higher fission-gas release for the mixed oxides. Of the remaining Pu-bearing fuels, the solid solution of PuC and UC has promise, but few basic data are presently available.

References

1. P. Bussy, The Plutonium-Based Fuel Production Programmes in France, in Proceedings Plutonium as a Power Reactor Fuel, American Nuclear Society Topical Meeting, Richland, Washington, September 13 and 14, 1962, USAEC Report HW-75007, p. 3.1, Hanford Laboratories, December 1962.
2. R. I. Smith and R. E. Peterson, Experience with the Plutonium Recycle Test Reactor, in Proceedings Plutonium as a Power Reactor Fuel, American Nuclear Society Topical Meeting, Richland, Washington, September 13 and 14, 1962, USAEC Report HW-75007, p. 11.1, Hanford Laboratories, December 1962.

3. F. Sebilleau and C. P. Zaleski, Plutonium as a Fuel for the Fast Reactor RAPSODIE, in Proceedings Plutonium as a Power Reactor Fuel, American Nuclear Society Topical Meeting, Richland, Washington, September 13 and 14, 1962, USAEC Report HW-75007, p. 15.1, Hanford Laboratories, December 1962.
4. E. A. Evans, Hanford Programs for Advanced Plutonium Fuel Designs and Fabrication Methods, in Proceedings Plutonium as a Power Reactor Fuel, American Nuclear Society Topical Meeting, Richland, Washington, September 13 and 14, 1962, USAEC Report HW-75007, p. 5.1, Hanford Laboratories, December 1962.
5. W. J. Bailey, Investigation of Plutonium-Bearing Fuel Elements for the Plutonium Recycle Test Reactor, Part 1, USAEC Report HW-70158 (Pt. 1) Hanford Atomic Products Operation, June 1961.
6. Hanford Atomic Products Operation, Fuels Development Operation Quarterly Progress Report, October–December 1961, USAEC Report HW-72346. (Classified)
7. Hanford Atomic Products Operation, Fuels Development Operation Quarterly Progress Report, January–March 1962, USAEC Report HW-72347, Apr. 16, 1962. (Classified)
8. Hanford Atomic Products Operation, Fuels Development Operation Quarterly Progress Report, April–June 1962, USAEC Report HW-74377, July 20, 1962. (Classified)
9. Hanford Atomic Products Operation, Fuels Development Operation Quarterly Progress Report, July–September 1962, USAEC Report HW-74378, Oct. 15, 1962. (Classified)
10. Hanford Atomic Products Operation, Plutonium Metallurgy Operation Quarterly Progress Report, October–December 1961, USAEC Report HW-72161, Jan. 15, 1962. (Classified)
11. Hanford Atomic Products Operation, Plutonium Metallurgy Operation Quarterly Progress Report, January–March 1962, USAEC Report HW-73318, Apr. 16, 1962.
12. Hanford Atomic Products Operation, Plutonium Metallurgy Operation Quarterly Progress Report, April–June 1962, USAEC Report HW-74162, July 16, 1962. (Classified)
13. Hanford Atomic Products Operation, Plutonium Metallurgy Operation Quarterly Progress Report, July–September 1962, USAEC Report HW-74718, Oct. 15, 1962. (Classified)
14. Hanford Atomic Products Operation, Ceramics Research and Development Operation Quarterly Progress Report, October–December 1962, USAEC Report HW-76300.
15. Hanford Atomic Products Operation, Ceramics Research and Development Operation Quarterly Progress Report, January–March 1963, USAEC Report HW-76301, Aug. 23, 1963.
16. Hanford Atomic Products Operation, Ceramics Research and Development Operation Quarterly Progress Report, April–June 1963, USAEC Report HW-76302, Nov. 4, 1963.
17. J. C. Fox, D. J. Foley, and J. F. Fletcher, Startup Experience with the Plutonium Recycle Test Reactor, Paper No. 62-WA-247 presented at Winter Annual Meeting of The American Society of Mechanical Engineers, Nov. 25–30, 1962.
18. Hanford Atomic Products Operation, Quarterly Progress Report, Research and Development Programs Executed for the Division of Reactor Development, January–March 1963, USAEC Report HW-78118, April 1963.
19. R. K. Koler, Pneumatic Injection Casting of Aluminum-Plutonium Fuel Elements, USAEC Report HW-69204, Hanford Atomic Products Operation, April 1961.
20. M. D. Freshley, Plutonium Spike Fuel Elements for the PRTR. Part I. The MARK I-G, USAEC Report HW-69200 (Pt. 1), Hanford Atomic Products Operation, March 1961.
21. L. C. Lemon and W. T. Ross, Head-Welded Swageable End Cap for UO_2-PuO_2 Fuel Elements, USAEC Report HW-74287, Hanford Atomic Products Operation, July 13, 1962.
22. H. E. Hanthorn, Calculated Costs of Fabrication of Plutonium-Enriched Fuel Elements, USAEC Report HW-74304, Hanford Atomic Products Operation, August 1962.
23. Hanford Laboratories, PuO_2-MgO Failure Mechanism Postulated, in Plutonium R&D Newsletter, Issue No. 2, January 1963.
24. I. D. Thomas, Plutonium Fuel Experience at Hanford, in Proceedings Plutonium as a Power Reactor Fuel, American Nuclear Society Topical Meeting, Richland, Washington, September 13 and 14, 1962, USAEC Report HW-75007, p. 6.1, Hanford Laboratories, December 1962.
25. Hanford Laboratories, Plutonium R&D Newsletter, Issue No. 3, April 1963.
26. J. M. Gerhart, The Post-Irradiation Examination of a PuO_2-UO_2 Fast Reactor Fuel, USAEC Report GEAP-3833, General Electric Company, Vallecitos Atomic Laboratory, November 1961.
27. K. M. Horst and B. A. Hutchins, Comparative Study of PuC-UC and PuO_2-UO_2 as Fast Reactor Fuel. Part I. Technical Considerations, USAEC Report GEAP-3880, General Electric Company, Atomic Power Equipment Department, Jan. 19, 1962.
28. G. D. Collins, Comparative Study of PuC-UC and PuO_2-UO_2 as Fast Reactor Fuel. Part II. Economic Considerations, USAEC Report GEAP-3880 (Pt. II), General Electric Company, Atomic Power Equipment Department, Nov. 15, 1962.
29. J. M. Cleveland, W. C. Cavannaugh, M. E. Snyder, and W. C. Cowden, Fast Oxide Breeder Project I—Fuel Fabrication. Part I. Plutonium-Uranium Dioxide Preparation and Pelletized Fuel Fabrication, Part II. Fabrication of Plutonium-Uranium Dioxide Specimens by Swaging, USAEC Report

GEAP-3486, General Electric Company, Vallecitos Atomic Laboratory, Aug. 15, 1960.

30. J. M. Gerhart, J. N. Siltanen, and J. S. Cochran, The Irradiation and Examination of a Plutonium-Uranium Oxide Fast Reactor Fuel, in Sixty-fourth Annual Meeting Papers: Symposium on Radiation Effects in Refractory Fuel Compounds, *Am. Soc. Testing Mater. Spec. Tech. Publ.*, No. 306, p. 154, American Society for Testing and Materials, Philadelphia.
31. Roy W. Endebrock (Ed.), Properties of Fuels for High-Temperature Reactor Concepts, USAEC Report BMI-1598, Battelle Memorial Institute, Nov. 1, 1962.
32. S. J. Paprocki, D. L. Keller, and W. M. Pardue, The Chemical Reactions of PuO_2 with Reactor Materials, USAEC Report BMI-1580, Battelle Memorial Institute, May 29, 1962.
33. S. J. Paprocki, D. L. Keller, C. A. Alexander, and W. M. Pardue, The Volatility of PuO_2 in Nonreducing Atmospheres, USAEC Report BMI-1591, Battelle Memorial Institute, Aug. 16, 1962.
34. E. E. Jackson and M. H. Rand, The Oxidation Behaviour of Plutonium Dioxide and Solid Solutions Containing Plutonium Dioxide, British Report AERE-R-3636, June 1963.
35. Nuclear Fuels and Materials Development, USAEC Report TID-11295(2nd ed.), September 1962.
36. J. A. Leary, W. J. Maraman, W. N. Miner, and F. W. Schonfeld, Quarterly Status Report on Solid Plutonium Fuels Program for Period Up to June 30, 1963, USAEC Report LAMS-2949, Los Alamos Scientific Laboratory, July 1963.
37. J. H. Kittel, L. A. Neimark, R. Carlander, O. L. Kruger, and R. C. Lied, Preliminary Irradiations of PuC and UC-PuC, USAEC Report ANL-6678, Argonne National Laboratory, September 1963.
38. W. R. Burt, Jr., A. G. Hins, R. M. Mayfield, and A. B. Shuck, Manufacture of EBR-I Core IV Fuel and Blanket Rods, Metallurgy Division Annual Report for 1962, USAEC Report ANL-6677, pp. 53-55, Argonne National Laboratory.
39. A. E. Ogard, C. C. Land, and J. A. Leary, The Thermal Expansion of PuC and PuC-UC Solid Solution, USAEC Report LA-2768, Los Alamos Scientific Laboratory, October 1962.
40. B. R. T. Frost, P. G. Mardon, and L. E. Russell, Research on the Fabrication, Properties, and Irradiation Behaviour of Plutonium Fuels for the U.K. Reactor Programme, in Proceedings Plutonium as a Power Reactor Fuel, American Nuclear Society Topical Meeting, Richland, Washington, September 13 and 14, 1962, USAEC Report HW-75007, p. 4.1, Hanford Laboratories, December 1962.
41. M. Palfreyman and G. A. Keig, Some Investigations on the Preparation and Properties of Plutonium Monocarbide, (UPu)C Solid Solutions and (UPu)C/Fe Cermets, British Report AERE-M-1106, September 1962.
42. B. T. Bradbury, J. E. Cole, B. R. T. Frost, and J. D. B. Lambert, Post Irradiation Examination of Stainless Steel Clad UC, UC-UFe_2 and PuC-UC Fuel Pellets, British Report AERE-R-4323, May 1963.
43. A. A. Strasser, Plutonium Fuel Programs of the United Nuclear Corporation, in Proceedings Plutonium as a Power Reactor Fuel, American Nuclear Society Topical Meeting, Richland, Washington, September 13 and 14, 1962, USAEC Report HW-75007, p. D3.1, Hanford Laboratories, December 1962.
44. F. G. Foote, Plutonium Fuel Programs at Argonne National Laboratory, in Proceedings Plutonium as a Power Reactor Fuel, American Nuclear Society Topical Meeting, Richland, Washington, September 13 and 14, 1962, USAEC Report HW-75007, p. 7.1, Hanford Laboratories, December 1962.
45. W. N. Beck, J. H. Kittel, and R. Carlander, Irradiation Behavior of Refractory-Alloy-Clad Plutonium Alloys, *Trans. Am. Nucl. Soc.*, 6(2): 375 (November 1963).
46. J. A. Horak, J. H. Kittel, and H. V. Rhude, The Effects of Irradiation on Some Binary Alloys of Thorium-Plutonium and Zirconium-Plutonium, USAEC Report ANL-6428, Argonne National Laboratory, July 1962.
47. A. S. Coffinberry and W. N. Miner (Eds.), *The Metal Plutonium*, University of Chicago Press, Chicago, 1961.
48. Los Alamos Scientific Laboratory, LAMPRE I Final Design Status Report, USAEC Report LA-2833, January 1962.
49. J. W. Anderson, W. D. McNeese, and J. A. Leary, Preparation and Fabrication of Plutonium Fuel Alloy for Los Alamos Molten Plutonium Reactor Experiment No. 1, USAEC Report LA-2439, Los Alamos Scientific Laboratory, Apr. 15, 1960.
50. P. Brock, L. H. Cope, and K. Q. Bagley, Fuel Elements for Fast Reactors, in Proceedings Plutonium as a Power Reactor Fuel, American Nuclear Society Topical Meeting, Richland, Washington, September 13 and 14, 1962, USAEC Report HW-75007, p. 18.1, Hanford Laboratories, December 1962.
51. E. Vanden Bemden, Description of the Belgonucleaire, in Proceedings Plutonium as a Power Reactor Fuel, American Nuclear Society Topical Meeting, Richland, Washington, September 13 and 14, 1962, USAEC Report HW-75007, p. 22.1, Hanford Laboratories, December 1962.
52. W. C. Pritchard, K. A. Johnson, J. A. Leary, and W. J. Maraman, Compaction and Sintering of PuO_2-Mo Powder Mixtures, USAEC Report LA-2621, Los Alamos Scientific Laboratory, Nov. 6, 1961.
53. W. C. Pritchard, K. A. Johnson, and J. A. Leary, Compaction and Sintering of PuO_2-Type 302B

Stainless Steel Powder Mixtures, USAEC Report LAMS-2898, Los Alamos Scientific Laboratory, Jan. 3, 1963.
54. A. A. Johnson, J. M. Hoffmann, J. E. Crawley, R. T. Huntoon, and D. A. Orth, Commercial Fabrication of Plutonium Fuel, USAEC Report DP-838, Savannah River Laboratory, June 1963.
55. L. R. Blake, Fast Reactor Design for Economic Power Production, *J. Nucl. Energy: Pt. A & B*, 16(11/12): 509 (November/December 1962).

Section V

Power Reactor Technology

Materials

Neutron Irradiation of Type 347 Stainless Steel

Type 347 stainless steel is widely used in reactor core structures and fuel elements and in the construction of test loops for the in-pile testing of reactor materials and components. Information previously available in the literature[1–4] indicates that fast-neutron irradiation of stainless steels to exposures of about 3×10^{21} to 4×10^{21} nvt results in changes in mechanical properties such as increases of about 13% in ultimate tensile strength, increases of 60% in yield strength, and decreases of about 44% in total elongation. The study reported in Refs. 5 and 6 was undertaken to determine the effect of neutron exposures in excess of 4×10^{21} nvt. The study is of interest to designers, not only because it reports on the mechanical properties of encapsulated stainless-steel specimens after massive exposure to fast neutrons (1.1×10^{22} nvt), but also because it describes very interesting effects on test samples cut from sections of the operating J-10 pressure loop of the Engineering Test Reactor (ETR).

For the encapsulated sample tests, AISI type 347 stainless steel in the form of $^5/_8$-in.-diameter rod, annealed and cold finished, meeting the specifications of ASTM A-276-55 (with an additional specification that the yield strength should be in the 50,000- to 65,000-psi range) was purchased for the test material. The composition of the type 347 stainless steel employed in the test program is given in Table V-1. Table V-2 gives the results of tensile tests on the material.

Two of the 11 capsules included in the surveillance program contained full-size Charpy V-notch and modified subsize Izod specimens. The specimens were arranged in three clusters spaced over the 8-in. capsule length. Each cluster contained two Charpy and four Izod specimens held in place by stainless-steel clip holders.

The estimated fast-neutron flux exposures for capsules in the surveillance program, as of the end of ETR cycle 40 (Oct. 2, 1961), are given in Table V-3. The subsize tensile specimens contained in capsules BMI-24-6 and BMI-24-18 were examined and tested. It was noted visually that all specimens were in good condition. Those removed from the longer exposure capsule (capsule BMI-24-6) were more discolored with a deposit of light-reddish oxide than those removed from the shorter exposure capsule. Two specimens from each capsule were tested at room temperature (about 75°F), and two were tested at 600°F. The two remaining specimens of each capsule were annealed for a period of 1 hr at 1800°F and were then tested at room temperature or 600°F. The results of the mechanical tests are given in Table V-4.

Table V-1 MANUFACTURERS' ANALYSIS OF AISI TYPE 347 STAINLESS STEEL USED FOR IRRADIATION TEST SPECIMENS[5]

Chemical analysis, wt.%							
Carbon	Manganese	Phosphorus	Sulfur	Silicon	Nickel	Chromium	Tantalum and niobium
0.057	1.72	0.024	0.016	0.65	10.41	17.91	0.67

Table V-2 ROOM-TEMPERATURE MECHANICAL PROPERTIES OF AISI TYPE 347 STAINLESS STEEL USED FOR IRRADIATION TEST SPECIMENS[5]

Specimen	Tester	Tensile strength, psi	Yield strength, psi	Elongation, % in 1.1 in.	Reduction in area, %	Rockwell hardness
Standard (0.505 in. in diameter)	Manufacturer	88,000	53,000	43.0	65.0	B 92
	KAPL	91,300	56,000	63.0		B 84 to 87
Subsize (0.16 in. in diameter)	KAPL	92,600	38,800	64.3	75.6	A 48 to 52
	BMI	89,100	35,000	61.0	73.5	

Examination of the data in Table V-4 shows that irradiation increased the 0.2% offset yield strength about 190% at room temperature, increased the ultimate strength about 24%, and decreased the total elongation about 50%. Similar changes in these properties were also observed in tests at 600°F. The data indicated that the effects of increasing the neutron exposure from 6.5×10^{21} to 1.1×10^{22} nvt were minor at both test temperatures, being reflected chiefly in differences in yield strength and total elongation.

The properties of specimens irradiated to different levels of exposure and subsequently annealed for 1 hr at 1800°F before testing are also given in Table V-4. These results indicate that the annealing treatment was sufficient to remove nearly all effects of irradiation on the specimens. In particular, recovery of the yield and ultimate strengths of the stainless-steel specimens was facilitated, whereas recovery of preirradiation ductility was not quite so complete, especially in the specimens that received the higher irradiation exposure. A typical stress-strain curve of type 347 stainless steel, tested in the unirradiated condition at 75°F, after irradiation to an estimated exposure of 1.1×10^{22} nvt, and after irradiation and annealing, is shown in Fig. V-1. The slope of the stress-strain curve obtained from irradiated specimens after a 1-hr anneal at 1800°F is almost identical to that of an unirradiated specimen.

The results of impact and tensile tests on AISI type 347 stainless steel have been determined for exposures up to about 1.1×10^{22} nvt.

Table V-3 SUMMARY OF BMI-24 SURVEILLANCE-CAPSULE EXPOSURES[5] AS OF END OF CYCLE 40

Capsule	Type of specimens in capsule	Total exposure as of end of cycle 40 (10-2-61), $\times 10^{21}$ nvt		Remarks
		Top	Bottom	
BMI-24-2	Tensile and fatigue	8.7	10.3	In-pile since cycle 4
BMI-24-4	Tensile and fatigue	7.0	9.3	In-pile since cycle 4
BMI-24-6	Tensile and fatigue	11.0*	8.4*	In-pile since cycle 4
BMI-24-8	Tensile and fatigue	8.4	9.0	In-pile since cycle 4
BMI-24-10	Tensile and fatigue	9.1	7.4	In-pile since cycle 4
BMI-24-12	Tensile and fatigue	9.7	9.7	In-pile since cycle 4
BMI-24-14†	Impact	5.8	5.6	Discharged from reactor at end of cycle 28, and specimens tested
BMI-24-16†	Impact	9.7	8.4	In-pile since cycle 4
BMI-24-18	Tensile and fatigue	4.4*	6.4*	In-pile since cycle 19
BMI-24-20	Tensile and fatigue	4.4	6.4	In-pile since cycle 19
BMI-24-22	Tensile and fatigue	4.6	6.2	In-pile since cycle 19

*Capsules BMI-24-6 and BMI-24-18 were discharged from the reactor at the end of cycle 42 (about Jan. 15, 1962) with exposures of about 0.93×10^{22} to 1.1×10^{22} and 5.1×10^{21} to 7.4×10^{21} nvt, respectively.

†Capsules BMI-24-14 and BMI-24-16 contain 12 subsize modified Izod specimens and 6 regular-size Charpy V-notch specimens. All other capsules contain 6 each subsize tensile and cycle-strain fatigue specimens.

This exposure level is, to date, the highest for which tensile properties of type 347 stainless-steel specimens have been reported. At an exposure of about 6.5×10^{21} nvt, the impact strength was reduced by about 50% at room temperature and considerably more at liquid-nitrogen temperatures. The fracture produced at room temperature was generally of the ductile type. At liquid-nitrogen test temperatures, the fracture was a combination of cleavage and shear types, more indicative of brittle fracture.

Tensile tests performed on subsize specimens of type 347 stainless steel showed increases of nearly 200% in the 0.2% offset yield values and increases in the ultimate strength of about 25%, as results of irradiation to 1.1×10^{22} nvt. Conversely, very large decreases in total elongation were observed. The hardness of specimens irradiated to exposures of 6.5×10^{21} nvt increased approximately 15% over the hardness of similar unirradiated material. Little change in hardness occurred as the result of increasing the neutron exposure from 6.5×10^{21} to 1.1×10^{22} nvt. These data and the results of tensile tests indicate a trend to saturation of irradiation effects in type 347 stainless steel when irradiated at process-water temperature with neutron exposures near 6.5×10^{21} nvt.

The ability to remove most of the effects of neutron irradiation by postirradiation annealing was demonstrated. Annealing for 1 hr at 1800°F, in most cases, caused the recovery of the pre-irradiation properties, but complete recovery of ductility was not achieved, particularly in the specimens that received the higher neutron exposure.

In addition to the tests described above, Refs. 5 and 6 report the results of tests conducted on specimens cut from sections of the J-10

Table V-4 COMPARISON OF THE TENSILE PROPERTIES AT 75 AND 600°F OF UNIRRADIATED, IRRADIATED, AND IRRADIATED AND ANNEALED TYPE 347 STAINLESS STEEL[5]

Total integrated fast flux (>1 Mev), nvt	Capsule	Condition	Yield strength (0.2% offset), 10^3 psi	Ultimate tensile strength, 10^3 psi	Uniform elongation, %	Total elongation, % in 1.1 in.	Reduction of area, %
		Tested at 75°F					
0		Unirradiated	34.5	87.7	>40.0	61.8	75.0
0		Unirradiated	36.0	90.0	>40.0	62.6	73.5
0		Unirradiated	34.5	89.5	>40.0	66.3	72.0
0*		Unirradiated	38.3	92.5		63.4	75.0
0*		Unirradiated	38.7	92.8		64.7	76.0
0*		Unirradiated	39.3	92.4		64.7	75.6
7.6×10^{21}†	BMI-24-18	As irradiated	104.0	112.0	25.8	34.5	68.5
5.5×10^{21}‡	BMI-24-18	As irradiated	88.7	111.5	24.7	32.7	70.0
1.1×10^{22}‡	BMI-24-6	As irradiated	103.5	112.5	24.3	30.9	70.0
9.2×10^{21}†	BMI-24-6	As irradiated	109.0	113.0	25.4	30.9	78.0
1.1×10^{22}‡	BMI-24-18	Irradiated and annealed at 1800°F for 1 hr	33.0	87.1	52.1	55.5	75.0
6.6×10^{21}†	BMI-24-6	Irradiated and annealed at 1800°F for 1 hr	33.8	87.5	57.5	61.0	77.0
		Tested at 600°F					
0*		Unirradiated	26.9	63.8		36.4	71.0
0*		Unirradiated	28.5	66.5		34.9	71.6
0*		Unirradiated	28.0	65.9		34.9	69.4
7.2×10^{21}†	BMI-24-18	As irradiated	81.8	83.0	10.7	14.5	61.0
5.5×10^{21}‡	BMI-24-18	As irradiated	80.0	84.0	13.2	16.4	60.0
1.1×10^{22}‡	BMI-24-6	As irradiated	86.8	89.0	10.1	13.3	60.7
8.7×10^{21}†	BMI-24-6	As irradiated	85.3	87.5	9.0	11.9	60.7
1.0×10^{22}†	BMI-24-6	Irradiated and annealed at 1800°F for 1 hr	28.2	64.3	27.7	30.0	68.0
5.5×10^{21}‡	BMI-24-18	Irradiated and annealed at 1800°F for 1 hr	27.4	65.0	28.7	31.7	68.0

*Tests made by Knolls Atomic Power Laboratory.

†Values based on $Fe^{54} \rightarrow Mn^{54}$ reaction.

‡Values based on cycle-to-cycle determination of $Ni^{58} \rightarrow Co^{58}$ reaction.

loop that operated in the ETR at the National Reactor Testing Station for about 17 months. The loop components from which the test samples were cut consisted of two basic capsules or tubes, an inner tube containing test specimens in a pressurized-water or -steam atmosphere, and an outer surrounding tube (or jacket) separated from the inner tube by a helium gas annulus. The outside of the outer tube was in contact with the 120°F process water. Thus the inner or pressure tube underwent irradiation at a temperature of about 750°F under significant pressure and thermal stresses, whereas the outer tube was exposed to the same irradiation but at a temperature of about 120°F with no significant stresses present.

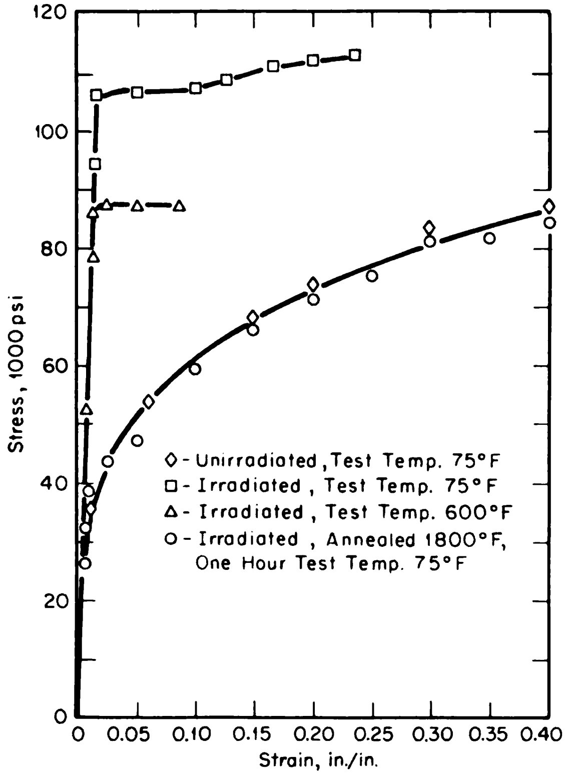

Fig. V-1 Stress vs. strain for AISI type 347 stainless steel before and after irradiation to 1.1 × 10^{22} nvt.

The J-10 test loop was placed in service in the ETR in October 1959 and was removed on Mar. 16, 1961. During this time the loop was exposed to approximately 222 effective full-power days (approximately 38,800 Mwd) at an estimated maximum flux (above 1 Mev) of 3.8 × 10^{14} nv. The 36-in.-long section, which had resided in the ETR core, was removed from both inner and outer loop sections and was examined at Battelle.

The initial chemical and physical properties of the material from which the pressure tube and the gas jacket were fabricated indicated that the compositions and fabrication conditions of both the pressure tube and the gas jacket were similar, although forging of the pressure tube was accomplished at a higher temperature. The tensile strength of the inner pressure tube was slightly higher, and the 0.2% offset yield strength was appreciably higher than that of the gas jacket. The ductilities of both loop sections were approximately equal in the preirradiation condition.

Table V-5 gives the results of tensile tests on 3 unirradiated, and 18 irradiated, type 347 stainless-steel specimens that were machined from the inner and outer loop sections and tested at room temperature and 600 or 750°F. The procedure employed for the elevated-temperature tests was to heat the specimen to 600 or 750°F and maintain this temperature for 30 min before beginning the test. The unirradiated values listed in the table are for comparison and include handbook data, results of tensile tests from specimens machined from an uncontaminated outer loop section, and data from McInnes Steel Co. personnel who prepared the inner J-10 pressure tube.

All the test specimens fractured within the 2-in. gauge length and exhibited necking in the area of fracture. However, the inner loop specimens gave evidence of reduced ductility as shown by small uniform elongations, a severe reduction in total elongation, and decreases in the reduction in area. Tests made at room temperature on specimens from the outer jacket indicated that the yield strength and ultimate strength had been increased about 120 and 80%, respectively, over the unirradiated material. The total elongation and the reduction in area were decreased approximately 50 and 12%, respectively.

The outer jacket material when tested at 750°F showed about the same degree of increase in the ultimate strength, a slightly smaller increase in yield strength, and further decreases in total elongation and reduction in area as compared with unirradiated specimens. The decrease in total-elongation values as a function of increasing test temperature to about 900°F

Table V-5 TEST RESULTS OBTAINED ON IRRADIATED TENSILE SPECIMENS MACHINED FROM SECTIONS OF THE J-10 LOOP[5]

Specimen	Approx. peak irradiation test temp., °F	Fast-neutron (>1 Mev) exposure*		Test temp., °F	Yield strength (0.2% offset), 10^3 psi	Ultimate tensile strength, 10^3 psi	Total elongation (in 2 in.), %	Reduction of area, %
		10^{14} nv	10^{21} nvt					
				Inner Loop, Initial Tests				
ST-3-L	510	1.0	1.9	75	132.0	132.0	4.25	53.5
ST-2-I	625	2.0	3.9	75	145.0	145.0	6.50	54.5
ST-2-H	735	3.7	7.1	75	149.0	149.0	10.30	58.2
ST-2-L	540	1.1	2.1	750	103.0	103.0	4.50	42.7
SB-2-I	740	2.7	5.1	750	115.0	115.0	1.50	40.8
SB-2-H	760	3.6	6.9	750	120.0	120.0	2.50	50.5
Control†				70	52.5 to 60.7	91.3 to 93	53 to 61	68 to 72
Handbook data‡				750	40 to 50	70 to 80	45 to 50	
				Inner Loop, Duplicate Tests				
ST-7-L	540	0.87	1.7	75	130.0	134.0	6.5	59.1
ST-7-I	675	2.9	5.57	75	139.5	144.8	10.6	59.8
ST-7-H§	735	1.7	3.26	75	143.0	147.0	9.4	61.5
SB-7-L	700	1.2	2.3	750	115.3	115.3	4.2	64.0
SB-7-I	760	1.9	3.65	750	123.0	123.5	4.2	45.5
SB-7-H	760	3.4	6.5	750	125.4	125.8	4.1	40.5
				Outer Loop				
LT-4-L	120	0.91	1.8	75	100.0	103.5	31.5	54.0
LT-4-I	120	1.8	3.5	75	95.2	101.3	26.0	57.0
LB-3-H	120	3.4	6.5	75	102.5	108.0	25.0	60.5
LT-3-L	120	3.1	2.0	750	62.5	66.7	13.3	54.0
LT-3-I	120	2.4	4.5	750	65.4	69.3	11.4	54.6
LT-3-H¶	120	2.7	5.1	600	71.8	73.3	12.5	48.3
Control 1**				75	46.8	99.7	50.4	61.8
Control 2**				750	36.5	67.6	26.2	62.9

*Exposures based on Mn^{54}.

†From McInnes Steel Co. reports on samples cut from as-machined J-10 pressure tube.

‡*Metals Handbook*, Vol. 1, 8th ed., p. 503.

§Less than 1 mg of sample was submitted for analysis; therefore the analysis may be inaccurate due to small weighing errors. On the basis of the location of the specimen, a value of ~7 × 10^{21} nvt would be expected.

¶Only 1.5 mg of sample was analyzed. Small weighing errors could have caused significant errors in analysis. It is believed that the actual value would duplicate LB-3-I since the specimen came from adjacent position.

**Samples cut from portion of J-10 pressure tube above reactor core.

is characteristic of unirradiated stainless steel and should not be considered a result of irradiation. However, the extreme difference between the results from the inner loop and outer jacket (much greater) at similar levels of exposure, at the same test temperature, does appear to be the result of irradiation under stress and/or temperature. The shape of the stress-strain curves for the inner loop and the outer jacket was entirely different.

The examination of the J-10 loop was of considerable value, since the data revealed the mechanical-property changes that occurred in a structural material under actual operating conditions of pressure, temperature, and neutron flux. Irradiation of encapsulated specimens can never duplicate *in situ* irradiations of reactor components, since the specimens are not subjected to variations in temperature and stress, two parameters that may contribute to property changes in irradiated structures. The data indicate that the stress state and irradiation temperature may play a very important role in property changes during irradiation.

References

1. M. J. Graber and J. H. Ronsick, ETR Radiation Damage Surveillance Programs. Progress Re-

port I, USAEC Report IDO-16628, Phillips Petroleum Co., Jan. 27, 1961.

2. D.O. Leeser, *Mater. Methods*, Manual 107, August 1954.
3. W. F. Murphy and S. H. Payne, Fast Neutron Effects on Tensile and Hardness Properties of Type 347 Stainless Steel, in *Symposium on Radiation Effects on Materials*, Vol. I, p. 162, American Society for Testing and Materials, 1956.
4. M. H. Bartz, Performance of Metals During Six Years Service in the Materials Testing Reactor, *Proceedings of the Second United Nations International Conference on the Peaceful Uses of Atomic Energy, Geneva, 1958*, Vol. 5, pp. 466-474, United Nations, New York, 1958.
5. W.E. Murr, F.R. Shober, R. Lieberman, and R.F. Dickerson, Effects of Large Neutron Doses and Elevated Temperature on Type 347 Stainless, USAEC Report BMI-1609, Battelle Memorial Institute, Jan. 21, 1963.
6. W. E. Murr and F. R. Shober, Annealing Studies on Irradiated Type 347 Stainless, USAEC Report BMI-1621, Battelle Memorial Institute, Mar. 6, 1963.

Section

VI

Power Reactor Technology

Operating Experience

Shippingport

A recent report[1] summarizes approximately five years of operating experience with the Shippingport Atomic Power Station: from its startup in December 1957, through the installation of, and the initial operation of, the fourth core seed, to the end of March 1963. Some 1650 reports are available on the Shippingport project and work related to it. The reports are listed in Ref. 2. A number of the previous reports on operating experience have been reviewed in past issues of *Power Reactor Technology*, 2(4): 74-77; 4(2): 52-58; 5(4): 61-72; 6(2): 64-67; and 6(3): 49-55. The Shippingport plant is described in detail in Ref. 3.

Figure VI-1 shows the operating history of the plant. Most of the nonroutine events cited on the figure have been covered in the reviews listed above. It is notable that the time required for refueling (with a new seed; the original blanket, called core 1, is still in place) decreased from five months for the first refueling to 44 days for the second and to 32 working days for the third. Most of this improvement is attributed to increased experience and improved planning, although 20 days of the first, long refueling period was devoted to modification of the vessel head instrumentation. The average load factor between refueling periods was 37% for the first seed, 70% for the second, and 77% for the third. If the periods used for testing and training are excluded, these factors increase to 75, 97, and 97%, respectively.

The third seed, which, like seed 2, initially contained 90 kg of U^{235} with 170 g of natural boron as a burnable poison, was operated for 7329 equivalent full-power hours (EFPH) during its lifetime. At the end of March 1963, the plant had delivered 1.225×10^9 net kw-hr of electricity and had operated for a total of 22,366 EFPH. The original core (i.e., the natural-uranium blanket) was still in operation, with seed 4. The average exposure of the blanket fuel was 9000 Mwd/metric ton of uranium, and its peak exposure was 30,100 Mwd/metric ton of uranium.

The five years of operating experience have demonstrated that the plant meets satisfactorily the operational requirements for practical integration into a utility system. These include: "...(1) the capability of operating as a base-loaded station for extending periods, (2) the capability of accepting its share of the load swings necessitated by system disturbance, and (3) the capability of operating on a peak-load basis when station-system efficiency conditions justified such use..."[1] Operation has shown that, when used as a peak-load facility, the station follows all system load changes in the power range; it can also be shut down and started up under controlled conditions at a faster rate than that of any conventional, modern station on the Duquesne system. In relation to the effectiveness of the station for base-load operation, it is significant that the frequency of safety shutdowns (scrams) has decreased with time, as indicated by Fig. VI-2. Some of the safety shutdowns are attributed to personnel error and some to equipment problems.

The fast-neutron exposure of the reactor pressure vessel is causing some increase in the ductile-brittle transition temperature, which places a limit on the permissible stress levels at temperatures below 250°F. These limitations are being observed by the control of operating procedures during plant startups and during the periodic hydrostatic testing. It is concluded, on the basis of present materials data, that neutron damage will not limit operation at normal operating temperatures at any time through the life of the second core.

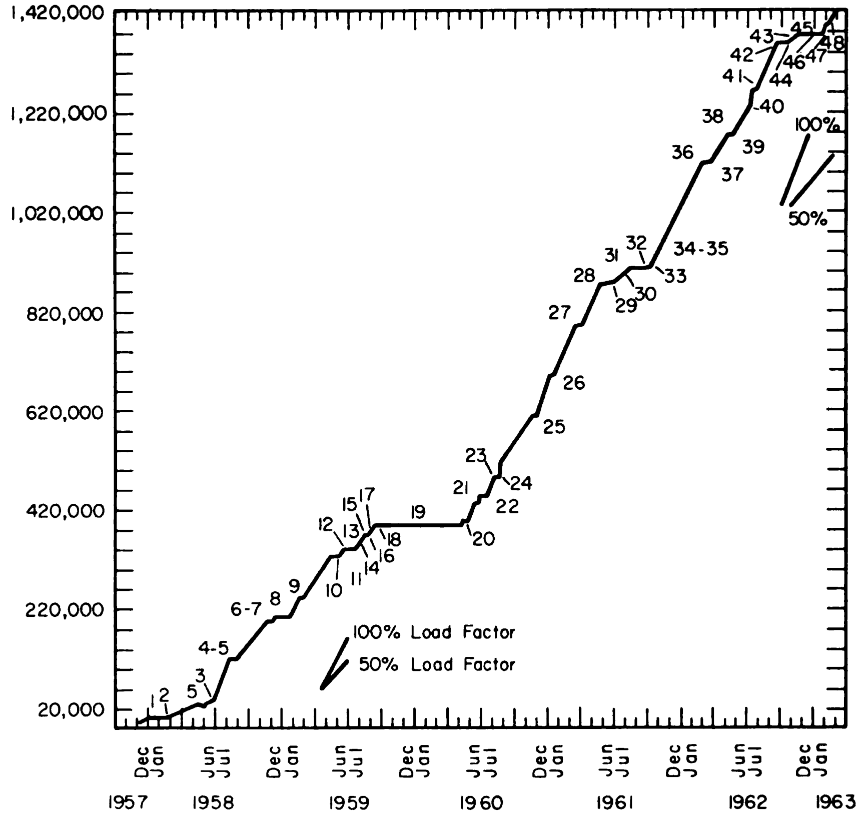

1. Reactor Shut Down for Test and Training
2. Leak Discovered in Steam Generator
3. Coolant Loop Pump Failed
4. First 1000-Hr Reactivity Lifetime Test
5. Shut Down for Maintenance and Testing
6. Second 1000-Hr Reactivity Lifetime Test
7. Shut Down for Maintenance and Testing
8. Moisture-Separator Failure Discovered; Plant Remained Shut Down Through January 1959
9. Repair of Turbine Governor
10. Periodic Operation for Training Purposes
11. Shut Down for Maintenance and Testing
12. Periodic Operation for Testing Plant Dynamic Response
13. Shut Down for Capacity Reduction and Hot Subpower Tests
14. Final Reactivity Lifetime Test; Final Run at Full Power for Core 1, Seed 1
15. Low-Power Physics Testing
16. 50-Mw Operation for End of Core Life Tests
17. Shut Down Because of Xenon Buildup
18. Final Power Run at 20 Mw
19. Shut Down To Replace Core Seed 1; Full Power Resumed
20. Low-Power Physics Testing
21. Maintenance—Replacement of E-12 Control-Rod-Drive Mechanism
22. Low-Power Physics Testing
23. Testing and Student Training
24. Return of 1-B Loop to Service
25. Low-Power Physics Testing
26. Low-Power Physics Testing and Maintenance
27. Low-Power Physics Testing—240-Hr Samarium Transient Test; Start of Final Full-Power Run
28. End of Seed 2 Ability to Override Equilibrium Xenon at 100% Power—Physics Testing
29. Testing, Maintenance, and Operator Training
30. Core Physics Testing—End of Seed 2 Life Tests
31. Start of Refueling and Replacing Seed 2
32. Initial Approach to Criticality, Seed 3
33. Full-Power Operation with Seed 3
34. Low-Power Physics Tests
35. A 3000-Hr Reactivity Lifetime Test
36. Shutdown Low-Power Physics Test, Rod Mechanism Test, Reactor Protection System Response Test
37. Student Training, Tests
38. Shutdown Xenon Transient Test
39. Operations Supervisor Training
40. Reduced Output on Generator Due to Feedwater Heater Outage
41. Shutdown Low-Power Physics Test—Rod-Mechanism Exercise
42. Shutdown End of Seed 3 Ability to Override Equilibrium Xenon at 100% Reactor Power
43. Operation at Reduced Power and Lower Average Coolant Temperature
44. End of Seed 3 Operation
45. Seed 3 and Seed 4 Refueling
46. Initial Approach to Criticality—Seed 4
47. Physics Tests
48. Shut Down for Testing and Begin 3600-Hr Reactivity Lifetime Test

Fig. VI-1 Operating history of Shippingport Atomic Power Station.[1]

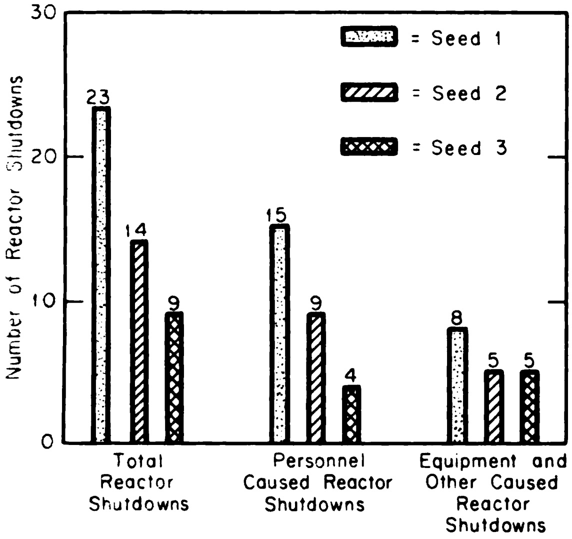

Fig. VI-2 Analysis of Shippingport safety shutdowns during operation with seeds 1 to 3.[1]

The history of power sharing between the seed and blanket is indicated in Fig. VI-3. The power fraction produced in the natural-uranium blanket during the first three seed lives averaged about 54%. Of the energy generated in the blanket, about half has been generated by the burning of plutonium in place, about 8% by the direct fissioning of U^{238}, and the remainder from the burning of U^{235}. The U^{235} content of the blanket has now decreased to about one-third its original (natural uranium) value. The temperature coefficient of reactivity (at rated power) has been nearly the same for all three seeds under comparable conditions of control-rod configuration. The coefficient becomes less highly negative as seed exposure progresses and control rods are withdrawn, as is to be expected. It changes from about $-2.0 \times 10^{-4}/°F$ for a new seed to about $-0.7 \times 10^{-4}/°F$ at the end of seed life.

During the operation of seed 1, asymmetries in the radial power distribution were observed to develop for certain configurations of control-rod insertion and to oscillate with a period of about 24 hr if no action was taken to control them. This phenomenon could be controlled rather easily by suitable manipulation of the control rods. Self-sustained oscillations of this type could not be generated in seed 2, even by deliberate unbalancing of the power distribution, and no oscillations were observed during seed 3 operation. Oscillation has, however, occurred in seed 4. The occurrence of the oscillation is presumably promoted by poor reactivity coupling of the various core regions in the azimuthal coordinate and is more apt to occur when the reactivity of the blanket is low than when it is high.

The performance of the blanket fuel elements has been very encouraging. Postirradiation examination of blanket rod bundles removed after seed 1, seed 2, and seed 3 operations has shown them to be in good condition. Detailed metallurgical examinations of elements removed at the second refueling have been made, and examination of a rod removed at the third refueling, with an estimated exposure of 23,000 Mwd/metric ton of uranium is under way. The examination of a rod removed, at the second refueling, with an exposure of 16,000 Mwd/metric ton of uranium, showed[1] that the average hydrogen content of the cladding was less than 80 ppm, that there was no abnormal cracking of grain growth in the UO_2, and that the 4-mil radial annulus between fuel and cladding was still intact. Reference 4 reports examinations of several elements removed at the second reloading and presumably includes the element mentioned above. The highest value of the estimated central temperature, for any of the elements, is 1320°F, corresponding to a time average heat flux of 152,000 Btu/(hr)(sq ft). For the blanket element diameter (0.411 in.), this heat flux corresponds to a conductivity integral ($\int k\, d\theta$) of 12.5 watts/cm..

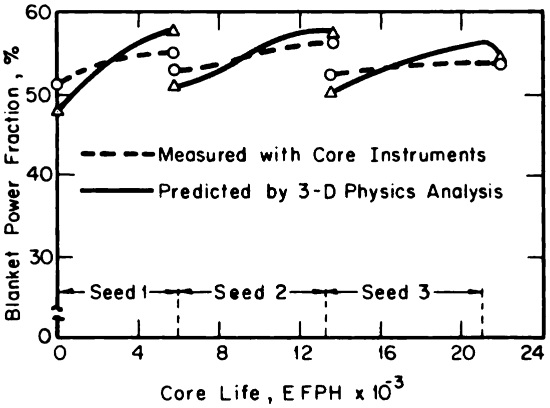

Fig. VI-3 Percentage of core energy from natural-uranium blanket during Shippingport core 1 life.[1]

Tests have been made of samples of the hafnium control rods removed after each seed life.

Figure VI-4 shows the changes in mechanical properties which were observed up to the end of life of seed 2. Excessive corrosion of the weld joint between the hafnium blades and the Zircaloy-2 control-rod hub was attributable to welding difficulties that resulted in contamination of the weld metal during rod manufacture. Improved welding procedures were developed, and all but two of the original rods (which showed low corrosion) were replaced at the second refueling.

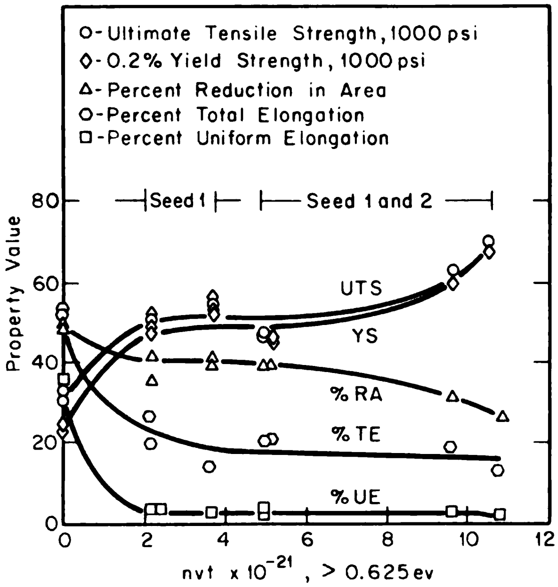

Fig. VI-4 Effect of neutron exposure on the 600°F tensile properties of Shippingport hafnium control rod after two seed lives.[1]

The primary coolant water is demineralized water adjusted to a *p*H of 9.5 to 10.5 with lithium hydroxide. A hydrogen overpressure is used to give 15 to 60 cm^3 of hydrogen per kilogram of water and an oxygen content less than 0.14 ppm. These conditions have minimized corrosion of the reactor plant piping and components and have kept the crud concentration low (about 5 ppb). The control of *p*H by the ion exchanger has been excellent, with infrequent additions of lithium hydroxide of less than 0.5 lb every four to five weeks. The use of isotopically pure lithium (99.99% Li^7) was begun in December 1960 and has reduced the tritium concentration in the coolant from a maximum of 280 μc/liter to about 2 μc/liter. Until recent repairs to leaky relief valves, the rate of hydrogen addition was approximately 100 cu ft/week. No excursions of oxygen concentrations above 0.14 ppm have occurred during power operation.

Seed 4 is scheduled to operate for the remainder of its reactivity lifetime, at which time the entire core is to be removed and the reactor is to be modified to accept a core of new design. The new core will raise the reactor capability from 67 Mw(e) to 150 Mw(e)(gross). Part of the power is to be dissipated, since the station turbine is rated for only 100 Mw(e).

References

1. J. T. Stiefel, H. Feinroth, and G. M. Oldham, Shippingport Atomic Power Station Operating Experience, Developments, and Future Plans, USAEC Report WAPD-TM-390, Westinghouse Electric Corp., Bettis Atomic Power Laboratory, April 1963.
2. Westinghouse Electric Corp., Bettis Atomic Power Laboratory, The Shippingport Pressurized Water Reactor Project Catalog of Document Abstracts, USAEC Reports WAPD-PWR-1606(Rev.), December 1961, and WAPD-PWR-1606(Add. 1), May 1, 1963.
3. AEC Naval Reactors Branch, Westinghouse Electric Corp., and Duquesne Light Co., *The Shippingport Pressurized Water Reactor*, Addison-Wesley Publishing Company, Inc., Reading, Mass., September 1958.
4. L. R. Lynam, Examination of PWR Core 1 Blanket Fuel Rods for Microstructure Changes, Hydrogen Pickup, Burst Strength, and Fission Gas Release at the End of the Second Seed Life, USAEC Report WAPD-TM-326, Westinghouse Electric Corp., Bettis Atomic Power Laboratory, April 1963.

Section

VII

Power Reactor Technology

Specific Reactor Types

Seed and Blanket

The most recent operating experience with the Shippingport Pressurized-Water Reactor is reviewed in Sec. VI of this issue of *Power Reactor Technology*. The further work on seed-and-blanket technology by the Bettis Atomic Power Laboratory has been proceeding from this reactor in two main directions: the development of a second core for Shippingport and the study of large power reactors of the seed-and-blanket type (the Large Power Reactor Program). The following review covers three recent reports[1–3] relating to the second core program.

The Shippingport reactor is currently operating with its fourth enriched seed and with the natural-uranium blanket that was originally installed. The term "second core" refers to a replacement of the entire core, including the blanket, by a new core of different design. The replacement is to be made at the end of life of seed 4, which is expected early in 1964.

The new core is to yield large increases in both power output and total energy output, as summarized in Table VII-1. The major changes in design features are the following:

1. The fuel elements are to be of the plate type, composed of oxide wafers encased in Zircaloy-4 cladding, as illustrated in Fig. VII-1. The plates will be assembled into square fuel assemblies by welding at their edges. The blanket plates, which will replace rod type UO_2 elements in the present core, will be 0.140 in. thick and will contain natural UO_2 wafers 0.100 in. thick. The seed plates will be 0.076 in. thick and will contain wafers, 0.036 in. thick, of highly enriched UO_2 sintered with ZrO_2. They will replace the current seed plates of uranium-zirconium alloy clad with Zircaloy-2.

2. The seed of core 2 contains sufficient highly enriched uranium, compensated by lumped burnable poison, to achieve a lifetime of 10,000 EFPH for this first seed. The burnable poison is in the form of wafers of austenitic stainless-steel alloy containing 0.8% B^{10}. These wafers are used instead of the fuel wafers in some of the compartments of the seed fuel elements.

3. The fuel assemblies are to be somewhat larger in size and fewer in number (see Table VII-1).

4. The length of the core is to be increased from 6 to 8 ft. This requires lengthening of the pressure vessel by means of an extension ring, which also serves as a support flange for the core support barrel, clamped between the vessel proper and the head by the head bolts.

These changes were reviewed briefly in *Power Reactor Technology*, 5(4): 70-72. The most far-reaching change is the use of the plate type oxide elements. A long program of development has shown that these elements are capable of very long exposure lifetime if the center temperature of the fuel is not too high. When normal failure eventually occurs, it is as a result of excessive bulging of the walls of the plate compartment. Initially this bulging results from swelling of the oxide, due to the precipitation of fission gases within the oxide. Eventually, however, the pressure of the fission gas released by the oxide causes the compartment walls to bulge away from the oxide; the latter then overheats, releasing still more fission gas, and the process advances fairly rapidly to ultimate failure of the compartment wall.

The exposure lifetime has been found to vary with fuel operating temperature, internal porosity of the fuel body, and external fuel restraint, with the practical importance of the variables decreasing in the order named. Figure VII-2 shows the results of irradiation tests on elements comparable to those for the blanket of core 2. Figure VII-3 shows the results of tests in which

Table VII-1 COMPARISON OF CORE 1 AND CORE 2 DESIGN FEATURES, SHIPPINGPORT[1]

	Core 1	Core 2
Rating	231 Mw(t); 67 Mw(e) with three primary coolant loops	505 Mw(t); 150 Mw(e)* with four primary coolant loops†
Average power density, kw/liter		
Seed	75	157
Blanket	25	33
Total core	43	60
Design core lifetime, EFPH		
Seed 1	3000	10,000
Blanket	8000	20,000
Fuel elements		
Seed	Zircaloy-2-clad enriched metal alloy U-Zr plates	Zircaloy-4-clad enriched UO_2-ZrO_2 compartmented plates
Blanket	Zircaloy-2-clad UO_2 rods	Zircaloy-4-clad UO_2 compartmented plates
Fuel assemblies, number and size (cross section)		
Seed	32; 5.6 by 5.6 in.	20; 7.376 by 7.376 in.
Blanket	113; 5.5 by 5.5 in.	77; 7.376 by 7.40 in.
Number of coolant passes in core		
Seed	1	1
Blanket	1	2
Core height, ft	6	8
Nuclear control	32 rods and distributed burnable poison in the seed (seeds 2, 3, and 4)	20 rods and lumped burnable poison in the seed
Orifices	Fixed	Adjustable
Number of ports in reactor vessel head (for refueling)	10	1

*The 150-Mw(e) capability will be demonstrated by means of the existing 100-Mw(e) turbine plus a heat-dump system.

†New impellers and drive motors will be installed in the existing primary pump volutes to increase the head capability by 45%.

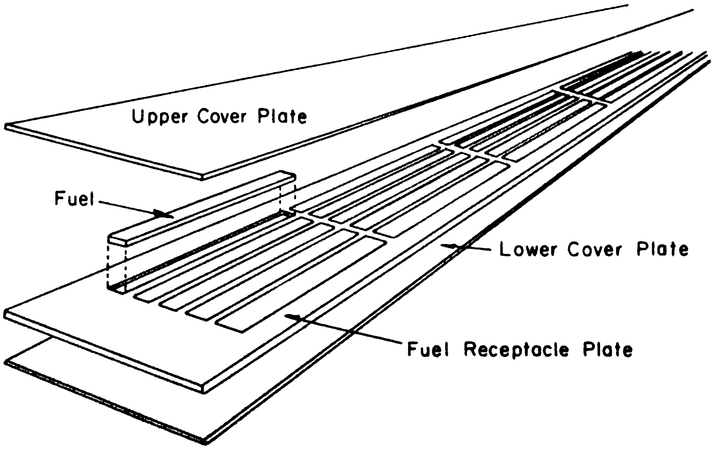

Fig. VII-1 Schematic representation of cladding and fuel components for a compartmented oxide plate type fuel element.[2]

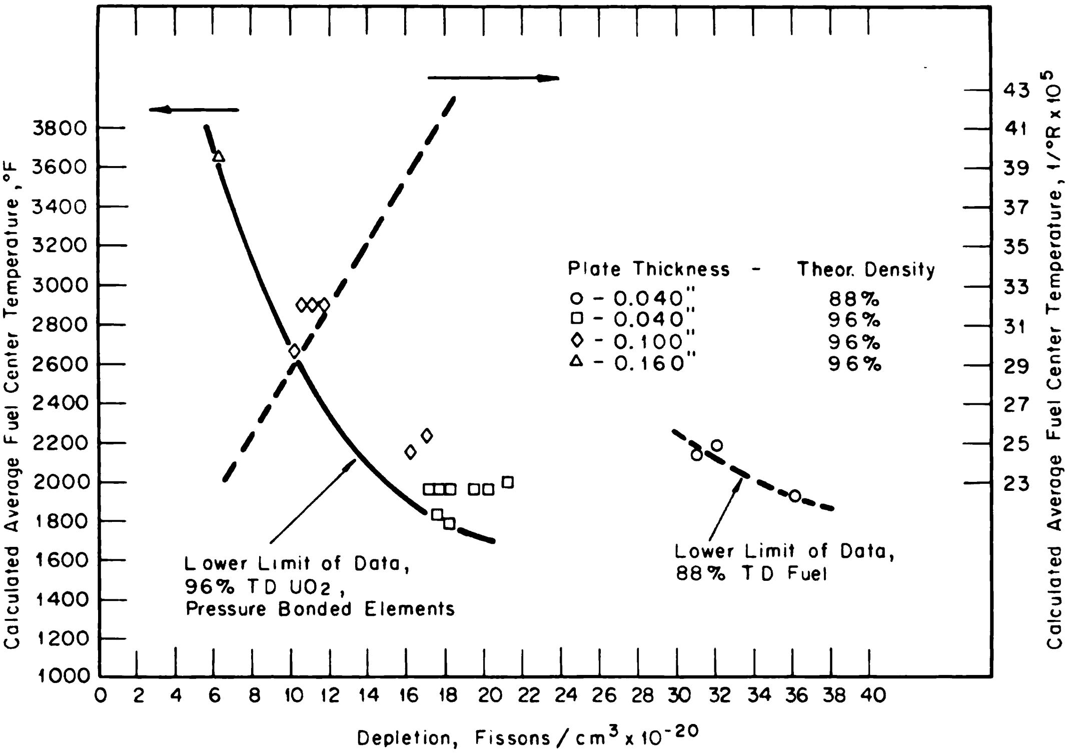

Fig. VII-2 Effects of center temperatures and oxide density on exposure lifetime of compartmented plate type UO_2 elements.[2]

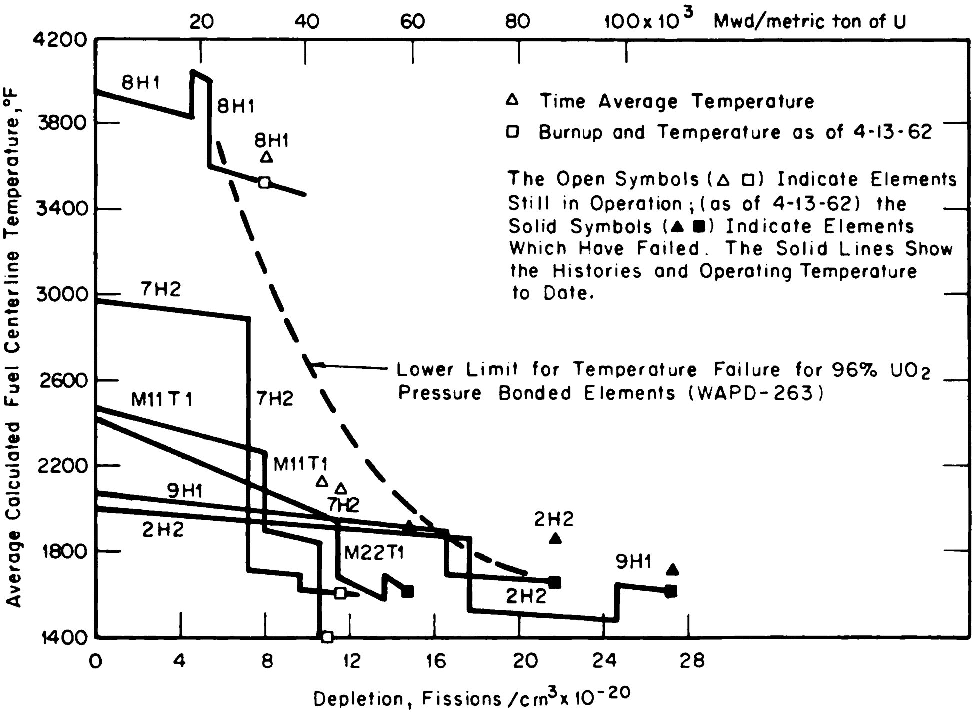

Fig. VII-3 Effects of temperature history on fuel-element life for 96% of theoretical density UO_2 fuel.[3]

elements operated for initial periods at high values of center temperature were subsequently operated at lower temperature (lower power density). The results show that the decrease of center temperature definitely improves the life expectancy and suggest that, within limits, it is reasonable to base an estimate of the life expectancy for such an element on its time-averaged center temperature—at least if the nature of the temperature variation is a decrease with time.

Figure VII-4 shows the calculated maximum exposure in the blanket of core 2 and the calculated fuel center temperature at the location of maximum exposure at the ends of four seed lives. The failure curve derived from the test program is also shown. The conclusion is that the blanket will last through four seed lives; at that time the maximum exposure in the blanket will correspond to about 70,000 Mwd/metric ton of uranium. The results of a similar analysis for the seed fuel are shown in Fig. VII-5.

It is clear from Figs. VII-4 and VII-5 that the fuel center temperatures in the Shippingport core 2 will be much lower than those customarily used in other reactors, which employ UO_2 elements of the rod type. The temperatures are, of course, low because of the thin oxide sections used in the fuel elements. The center temperature of one of the 0.10-in. oxide wafers in the blanket elements would be about the same as that of a rod pellet of 0.14-in. diameter if it were operating at the same specific power. The compartmented plates represent one method of utilizing very thin oxide sections in a structure of manageable size.

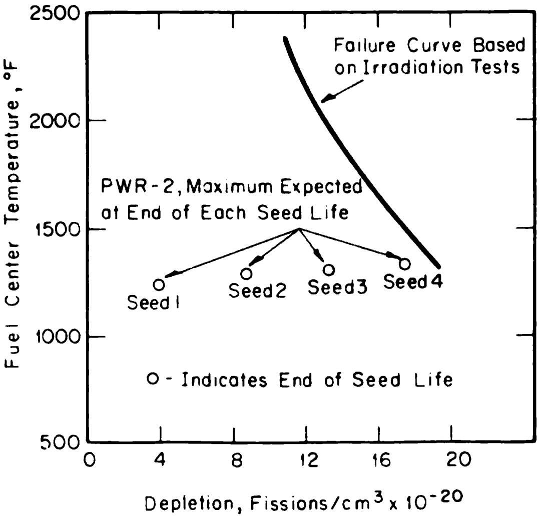

Fig. VII-4 Comparison of center-line fuel temperatures for failed UO_2 compartments with those expected in the Shippingport core 2 blanket.[1]

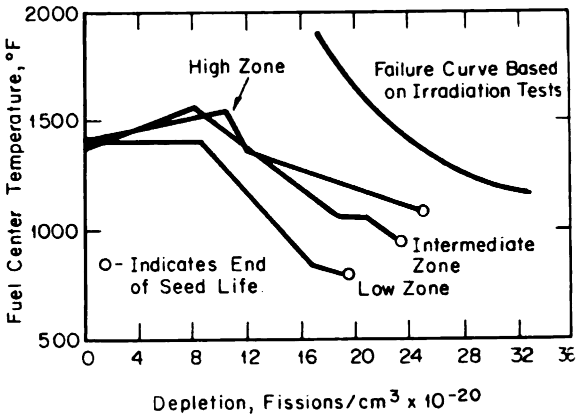

Fig. VII-5 Comparison of center-line fuel temperature in seed fuel elements tests with those expected for the Shippingport[2] core 2.

References

1. J. T. Stiefel, H. Feinroth, and G. M. Oldham, Shippingport Atomic Power Station Operating Experience, Developments, and Future Plans, USAEC Report WAPD-TM-390, Westinghouse Electric Corp., Bettis Atomic Power Laboratory, April 1963.
2. R. C. Daniel, M. L. Bleiberg, H. B. Meieran, and W. Yeniscavich, Effects of High Burnup on Zircaloy-Clad Bulk UO_2, Plate Fuel Element Samples, USAEC Report WAPD-263, Westinghouse Electric Corp., Bettis Atomic Power Laboratory, September 1962.
3. H. B. Meieran, Post-Irradiation Evaluation of a Plate-Type UO_2 Fuel Element, USAEC Report WAPD-TM-332, Westinghouse Electric Corp., Bettis Atomic Power Laboratory, January 1963.

LEGAL NOTICE

This document was prepared under the sponsorship of the U. S. Atomic Energy Commission. Neither the United States, nor the Commission, nor any person acting on behalf of the Commission:

A. Makes any warranty or representation, expressed or implied, with respect to the accuracy, completeness, or usefulness of the information contained in this report, or that the use of any information, apparatus, method, or process disclosed in this report may not infringe privately owned rights; or

B. Assumes any liabilities with respect to the use of, or for damages resulting from the use of any information, apparatus, method, or process disclosed in this report.

As used in the above, "person acting on behalf of the Commission" includes any employee or contractor of the Commission, or employee of such contractor, to the extent that such employee or contractor of the Commission, or employee of such contractor prepares, disseminates, or provides access to, any information pursuant to his employment or contract with the Commission, or his employment with such contractor.

NUCLEAR SCIENCE ABSTRACTS

The U. S. Atomic Energy Commission, Division of Technical Information, publishes *Nuclear Science Abstracts (NSA),* a semimonthly journal containing abstracts of the literature of nuclear science and engineering.

NSA covers (1) research reports of the U. S. Atomic Energy Commission and its contractors; (2) research reports of government agencies, universities, and industrial research organizations on a world-wide basis; and (3) translations, patents, books, and articles appearing in technical and scientific journals.

Complete indexes covering subject, author, source, and report number are included in each issue. These are cumulated quarterly, semiannually, and annually providing a detailed and convenient key to the literature.

Availability of *NSA*

SALE *NSA* is available on subscription from the Superintendent of Documents, U. S. Government Printing Office, Washington, D. C., 20402, at $30.00 per year for the semimonthly abstract issues and $22.00 per year for the four cumulated-index issues. Subscriptions are postpaid within the United States, Canada, Mexico, and all Central and South American countries, except Argentina, Brazil, British and French Guiana, Surinam, and British Honduras. Subscribers in these Central and South American countries, and in all other countries throughout the world, should remit $37.00 per year for subscriptions to semimonthly abstract issues and $25.00 per year for the four cumulated-index issues.

EXCHANGE *NSA* is also available on an exchange basis to universities, research institutions, industrial firms, and publishers of scientific information. Inquiries should be directed to the Division of Technical Information Extension, U. S. Atomic Energy Commission, P. O. Box 62, Oak Ridge, Tennessee, 37831.

TECHNICAL PROGRESS REVIEWS

To meet the needs of industry for concise summaries of current atomic developments, the Atomic Energy Commission is publishing this series, Technical Progress Reviews. Issued quarterly, each of the reviews digests and evaluates the latest findings in a specific area of nuclear technology and science.

The five journals published in this series are:

Isotopes and Radiation Technology, P. S. Baker, A. F. Rupp, and associates, Oak Ridge National Laboratory

Nuclear Safety, Wm. B. Cottrell, W. H. Jordan, and associates, Oak Ridge National Laboratory

Power Reactor Technology, W. H. Zinn and J. R. Dietrich, General Nuclear Engineering Corporation

Reactor Fuel Processing, Stephen Lawroski and associates, Chemical Engineering Division, Argonne National Laboratory

Reactor Materials, R. W. Dayton, E. M. Simons, and associates, Battelle Memorial Institute

Each journal may be purchased from the Superintendent of Documents, U. S. Government Printing Office, Washington, D. C., 20402. *Isotopes and Radiation Technology* at $2.00 per year for subscription or $0.55 for individual issues; the other four journals at $2.50 per year and $0.70 per issue. See back cover for remittance instructions and foreign postage requirements.

The views expressed in this publication do not necessarily represent those of the United States Atomic Energy Commission, its divisions or offices, or of any Commission advisory committee or contractor.

Availability of Reports Cited in This Review

Unclassified AEC reports are available for inspection at AEC depository libraries and are sold by the Office of Technical Services, Department of Commerce, Washington, D. C., 20230. Some of the reports cited are not available owing to their preliminary nature; however, the information contained in them will eventually be made available in formal progress or topical reports.

Unclassified reports issued by other Government agencies or private organizations should be requested from the originator.

Unclassified British and Canadian reports may be inspected at AEC depository libraries. British reports are sold by the British Information Service, 45 Rockefeller Plaza, New York, N. Y.; Canadian reports (AECL series) are sold by the Scientific Document Distribution Office, Atomic Energy of Canada, Ltd., Chalk River, Ontario, Canada.

Classified U. S. and foreign reports identified in this journal as Classified may be purchased by properly cleared Access Permit Holders from the Division of Technical Information Extension, U. S. Atomic Energy Commission, P. O. Box 1001, Oak Ridge, Tenn., 37831. Such reports may be inspected at classified AEC depository libraries.

POWER REACTOR TECHNOLOGY

A REVIEW OF RECENT DEVELOPMENTS

Prepared for DIVISION OF TECHNICAL INFORMATION, USAEC,
by W. H. ZINN and J. R. DIETRICH,
GENERAL NUCLEAR ENGINEERING CORPORATION

SUMMER 1964

VOLUME 7

NUMBER 3

Foreword

This quarterly review of reactor development has been prepared at the request of the Division of Technical Information of the U. S. Atomic Energy Commission. Its purpose is to assist interested organizations in the task of keeping abreast of new results in reactor technology for civilian application.

Power Reactor Technology contains reviews of selected recently published reports that are judged noteworthy in the fields of power-reactor research and development, power-reactor applications, design practice, and operating experience. It is not meant to be a comprehensive abstract of all material published during the quarter; nor is it meant to be a treatise on any part of the subject. However, related reports from different sources are often treated together to yield reviews having some breadth of scope, and background material may be added to place recent developments in perspective. Occasionally the reviews are written by guest authors. Reviews having unusual breadth or significance are placed at the front of the issue as Feature Articles.

The intention is to cover the various areas of reactor development from the general viewpoint of the reactor designer rather than from the more detailed points of view of specialists in the individual areas. To whatever extent the coverage of *Power Reactor Technology* may occasionally overlap the fields of the other Technical Progress Reviews, the overlaps will be motivated by this objective of viewing current progress through the eyes of the reactor designer.

A degree of critical appraisal and some interpretation of results are often necessary to define the significance of reported work. Any such appraisal or interpretation represents only the opinion of the reviewer and (in the usual case, when the review is written by General Nuclear Engineering Corporation staff) the Editor. When the review is predominantly interpretive, the reviewer is named; unless identified as a guest author, he is a member of the General Nuclear Engineering Corporation staff. Readers are urged to consult the original references to obtain all the background of the work reported and to obtain the interpretation of the results given by the original authors.

For timely coverage, *Power Reactor Technology* must often review fragmentary material. The fixed subject headings listed below have been adopted in the hope of maintaining some continuity and order in the material from one issue to another: all reviews except Feature Articles will be arranged under these headings. A particular issue will not necessarily contain all the headings but only those under which material is reviewed.

Economics, Applications, Programs
Resources and Fuel Cycles
Physics
Fluid and Thermal Technology
Fuel Elements
Materials
Control and Dynamics
Containment, Radiation Control, and Siting
Systems Technology
Components
Design and Construction Practice
Operating Experience
Specific Reactor Types
Specific Applications
Unconventional Approaches

W. H. Zinn, President
J. R. Dietrich, Vice-President and Editor
General Nuclear Engineering Corporation

DEPOSITED BY THE
UNITED STATES OF AMERICA

Contents

I Resources and Fuel Cycles 201
Fuel Management 201
References 205

II Physics 206
Critical and Exponential Experiments . . 206
Physics of Heavy-Water Lattices . . . 212
Resonance Integrals in Fertile Isotopes 214
Effective Cross Sections 215
Physics of Control Materials 216
Shielding 218
References 220

III Fluid and Thermal Technology . . . 223
Burnout Correlations from the Russian Literature 223
References 235

IV Fuel Elements 237
Fabrication by Novel Methods 237
References 246

V Control and Dynamics 248
Conference on Noise Analysis in Nuclear Systems 248
References 263

VI Containment, Radiation Control, and Siting 265
Vented-Containment Concept for the New Production Reactor 265
References 267

VII Components 269
Pumps for Liquid Metal 269
Flow Controller for Sodium Service . . 271
Control Rods and Drives 271
References 275

VIII Design and Construction Practice: Pathfinder and BONUS 276
Introduction 276
Pathfinder Atomic Power Plant 276
BONUS Power Station 292
Discussion 310
References 312

IX Operating Experience 313
Consolidated Edison Nuclear Steam Generating Station 313
Plutonium Recycle Test Reactor: Primary Coolant Pumps . . 315
Heavy-Water Components Test Reactor: Control- and Safety-Rod Drive Systems 316
Performance of the EBWR at Powers Up to 100 Mw(t). 317
References 320

X Specific Reactor Types 322
Pressurized Water: Study of Zircaloy Core Structure for N.S. *Savannah* . . 322
Organic-Cooled Reactors: The Tripartite Meeting 324
References 326

Issued quarterly by the Atomic Energy Commission. Use of funds for printing this publication approved by the Director of the Bureau of the Budget on October 14, 1963.

Section

I

Power Reactor Technology

Resources and Fuel Cycles

Fuel Management

The proceedings of a fuel management symposium that was held at the New York Operations Office of the AEC on Sept. 27, 1962, have been published.[1] Although considerable time has elapsed since the symposium, the material is still of interest, and selected results are noted briefly below.

The benefits to be derived from a program of partial-core reloading were studied in a project carried out by Jackson and Moreland, Inc., and Allis-Chalmers Mfg. Co. under AEC-Euratom sponsorship. The study was made in terms of the SENN reactor,[2] a dual-cycle boiling-water reactor which was designed by the General Electric Company and which is nearly identical to the Dresden reactor.

Of the refueling programs investigated, the out-in refueling shuffle proved most attractive. This involves unloading fuel from the centermost region of the core, shifting the remaining, partially exposed fuel inward to occupy the unloaded region, and adding fresh fuel in the resulting empty peripheral core positions. The advantage of partial reloading is an increase in the reactivity lifetime for a given feed enrichment (or for a given control capability), and the out-in shuffle gives the further advantage of flattening the radial power distribution by placing the most highly exposed fuel elements near the center of the core. The first of these advantages increases continuously, but at a decreasing rate, as the frequency of refueling is increased and the size of the reload batch is decreased. The second advantage increases with the frequency of refueling, at least up to a point, although there may be an optimum frequency for this effect, depending on the feed enrichment and the resulting fuel lifetime.

These relations are illustrated in Fig. I-1, which shows the power peaking factors and the discharge exposure of the fuel in the equilibrium cycle as functions of the number of reload batches into which the core is divided. The feed enrichment is held constant at 1.84% ^{235}U. Up to three or four batches, both the radial and axial peaking factors decrease as the number of batches is increased. Presumably the improvement in the axial factor is due partly

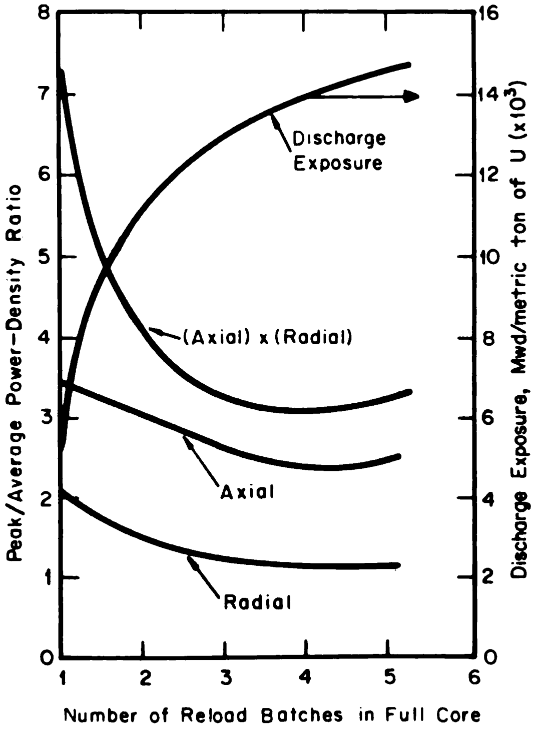

Fig. I-1 The fuel exposure at discharge and the power peaking factors calculated for the SENN reactor with out-in partial-core reloading.[3] The feed enrichment is held constant at 1.84% ^{235}U. All control rods are operated as a bank, and the curves apply to the equilibrium reloading cycle.

to the decreasing depth of insertion of the control rods (which are assumed to be operated as a bank) as the reactivity swing between loadings is reduced and partly to the increasing self-flattening by preferential fuel burnup as the fuel exposure increases. Eventually the exposure becomes so high that the power drops off drastically in the most highly exposed fuel, and both the radial and axial factors increase slightly with further increases in the number of batches.

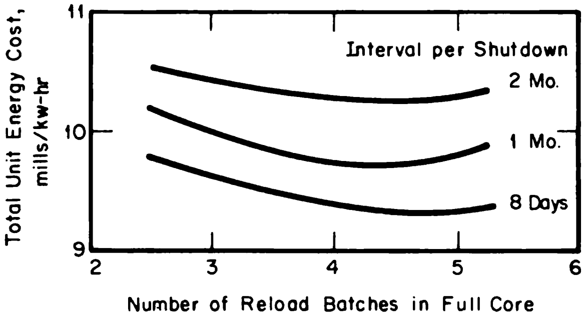

Fig. I-2 Calculated effect of the number of reload batches per core on total power-generation cost in the SENN reactor, for out-in reloading with constant feed enrichment of 1.84% ^{235}U.

As the number of reload batches is increased, the main effects on the total power-generation cost are the following:

—the decrease in fuel-cycle cost due to the increasing exposure at discharge

—the decrease in capital cost component (up to the point of minimum power peaking factor) due to the increasing power capability of the reactor

—the decrease in plant factor caused by the increasing frequency of shutdown for reloading

In Fig. I-2 the net effect of energy cost has been estimated for three different values of the shutdown time required per refueling. The importance of this shutdown time is apparent. Crowley[3] emphasized the importance of designing the reactor for rapid refueling. In the discussion following the presentation of his paper, he indicated that, although refueling times from four to eight days have been used as "reference" values for some reactors, they have not yet been achieved. He did consider it reasonable, however, to consider routine refueling operations of one-month duration as compatible with the present state of the art.

In a study carried out at the Massachusetts Institute of Technology,[4] fuel cycles in the Canadian CANDU reactor were investigated. The CANDU reactor is a pressure-tube heavy-water type designed for fueling with natural uranium. The basic cost assumptions used are listed in Table I-1. For the study the enrichment of the fuel was considered to be open to variation, and one of the questions investigated was the effect of enrichment on fuel-cycle cost and total energy cost in the basic CANDU fuel management program of bidirectional push-through. The results are given in Table I-2.

As the fuel enrichment is changed, the degree of power flattening attainable in the equilibrium reactor, by adjusting the rate of push-through to give higher average exposure in the central region of the reactor, is changed. This is taken into account in the total (overall) power cost by assuming that the reactor size, and hence the capital cost, can be adjusted to take advantage of the maximum attainable power flattening. The study did not consider, however, any other changes in design variables, such as changes in lattice pitch.

In Table I-2 it is shown that one of the methods investigated for achieving the desired feed enrichment is by blending. This method is attractive primarily because the Canadian price for natural uranium is lower than the natural-uranium price used in fixing the price scale for

Table I-1 PRINCIPAL COST BASES FOR STUDY OF FUEL MANAGEMENT IN THE CANDU REACTOR[4]

Natural UO_2, \$/kg U	13.55
Enriched UF_6	USAEC price scale, 7/1/62
Plutonium nitrate credit, \$/g Pu	8.00
Conversion of UF_6 to UO_2, \$/kg U	12.50
Fabrication of fuel from UO_2, \$/kg U	42.78
Shipping of irradiated fuel, \$/kg U	15.45
Reprocessing of fuel to nitrates, \$/kg U	20.68
Conversion of UNH to UF_6, \$/kg U	5.60
Annual charges on	
Fuel fabrication working capital, %/yr	4.5
Uranium, %/yr	4.5
Plant investment, %/yr	7.76
Operation and maintenance, mills/kw-hr	1.02

slightly enriched uranium in the United States. The blending scheme involves mixing uranium of 3.2% enrichment, purchased in the United States, with Canadian natural uranium to produce uranium of the desired enrichment. This possibility involves both technical and regulatory problems that have not been explored in practice. In Table I-2 it is shown that the optimum enrichment for overall power cost is about 1.0%. This is true whether or not blending is used, although the improvement is large only for the blending case. A comparable or somewhat greater improvement would, of course, be available without blending if the U. S. enriched-fuel price schedule were based upon the Canadian price for natural uranium.

Table I-2 CALCULATED EFFECTS OF FUEL COST VARIABLES ON POWER COSTS IN THE CANDU REACTOR, WITH CONTINUOUS BIDIRECTIONAL FUELING[4]

	Fuel prepared by blending		Fuel not prepared by blending	
Fuel enrichment	Fuel reprocessed	Fuel not reprocessed	Fuel reprocessed	Fuel not reprocessed
		Fuel-cycle costs, mills/kw-hr		
Natural U			(1.03)*	0.99
1.0 at.% ^{235}U	0.83	0.89	0.99	1.05
1.3 at.% ^{235}U	0.86	0.92	0.93	0.99
1.5 at.% ^{235}U	0.93	0.96	0.97	1.00
		Overall power costs, mills/kw-hr		
Natural U			(6.56)	6.52
1.0 at.% ^{235}U	6.21	6.27	6.37	6.43
1.3 at.% ^{235}U	6.30	6.36	6.38	6.44
1.5 at.% ^{235}U	6.45	6.48	6.50	6.53

*Numbers in parentheses are for cases where reprocessing is not economically justified.

Table I-3 shows the results of the investigation of other refueling methods in the CANDU reactor. For each of these cases, an investigation similar to that recorded in Table I-2 was carried out. In Table I-3 the results are recorded for the enrichments calculated to give the minimum total power cost in each case. The advantage of the bidirectional push-through program appears to be clearly confirmed, although it must be remembered that the study was confined to the basic CANDU design, and no investigation was made of qualitative variations in the plant design which might turn the other fuel-cycle approaches to particular advantage.

The paper by Puechl[5] of Nuclear Materials & Equipment Corporation is worthy of particular attention; this paper is more readily available, and in greater detail, in Refs. 6 and 7. The paper is a fuel management study of water-moderated reactors fueled with mixtures of natural uranium and plutonium isotopes. The plutonium mixtures considered are typical of those discharged from thermal power reactors and contain substantial fractions of ^{240}Pu. The author points out that quite long reactivity lifetimes can be achieved with these mixtures at relatively modest values of initial excess reactivity. Basically this is because the ^{240}Pu acts in much the same way as a burnable poison, but with the accentuated effect, since the absorption of a neutron in ^{240}Pu not only removes a ^{240}Pu atom (a poison) but also produces a fissile atom of ^{241}Pu. The effect, however, is a complex one since the cross sections of both ^{239}Pu and ^{240}Pu vary strongly with neutron energy and, therefore, the behavior of the neutron energy spectrum during the fuel exposure is important. Figure I-3 shows the computed reactivity lifetimes for two different cases, and in each the initial plutonium loading contained 12% ^{240}Pu. The details of these cases are given in Table I-4.

Puechl[5] also shows that the reactivity lifetime is quite sensitive to the fuel-to-moderator ratio and that the optimum ratios tend to be

Table I-3 CALCULATED EFFECTS OF DIFFERENT REFUELING METHODS ON POWER COSTS IN THE CANDU REACTOR[4]

	Fuel prepared by blending		Fuel not prepared by blending	
	Fuel reprocessed	Fuel not reprocessed	Fuel reprocessed	Fuel not reprocessed
Continuous bidirectional refueling				
Feed enrichment for lowest power cost,* % ^{235}U	1.0	1.0	1.0	1.0
Fuel-cycle cost for lowest power cost, mills/kw-hr	0.83	0.89	0.99	1.05
Lowest total power cost, mills/kw-hr	6.21	6.27	6.37	6.43
Discontinuous out-in refueling				
Feed enrichment for lowest power cost,* % ^{235}U	1.3	1.3	1.3	1.3
Fuel-cycle cost for lowest power cost, mills/kw-hr	1.33	1.34	1.44	1.45
Lowest total power cost, mills/kw-hr	6.78	6.79	6.89	6.90
Single-batch refueling				
Seed enrichment for lowest power cost,* % ^{235}U	1.75	1.75	1.75	1.75
Fuel-cycle cost for lowest power cost, mills/kw-hr	1.74	1.75	1.79	1.80
Lowest total power cost, mills/kw-hr	7.18	7.18	7.23	7.23

*The enrichments considered were natural uranium, 1.0%, 1.3%, 1.5%, and 1.75%.

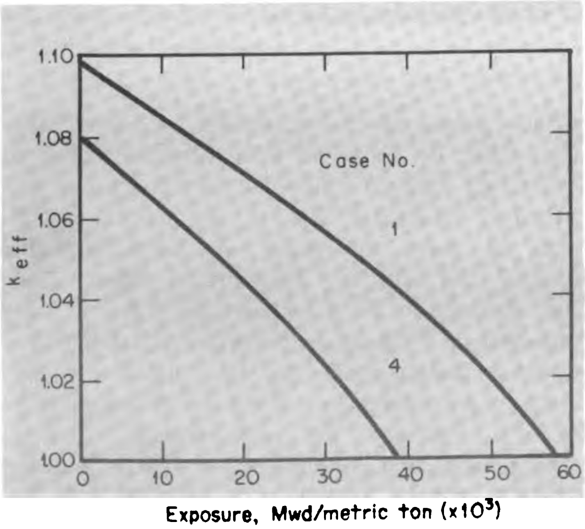

Fig. I-3 Reactivity lifetimes[5] of two H_2O-moderated cores fueled with natural uranium plus plutonium containing 12% ^{240}Pu. See Table I-4 for further characteristics.

Table I-4 CHARACTERISTICS OF THE PLUTONIUM-FUELED CORES[5] GIVING REACTIVITY LIFETIMES SHOWN IN FIG. I-3

	Case 1	Case 4
Surface-to-volume ratio of fuel elements, cm^{-1}	5.36	7.00
Moderating ratio, $\xi\Sigma_s$ per fuel* atom, barns	150	150
Σ_a (moderator) per fuel* atom, barns	2.84	2.84
Σ_a (cladding) per fuel* atom, barns	3.0	3.92
Core life, Mwd/metric ton	57,500	39,400
Initial k_{eff}	1.0983	1.0806
Initial Pu content of fuel,* at.%	7.84	6.33
Final Pu content of fuel,* at.%	5.52	4.90
Final isotopic composition of Pu, at.%		
^{239}Pu	49.6	53.6
^{240}Pu	22.4	20.8
^{241}Pu	19.0	19.0
^{242}Pu	9.0	6.6
Initial U enrichment	Natural	Natural
Final U enrichment, (atoms ^{235}U/atoms U) × 100	0.346	0.413
Net Pu change, kg/metric ton	26.9	17.3
Net U change, kg/metric ton	28	24

*The "fuel" comprises all the uranium and plutonium present.

lower than is desirable from the point of view of power density in the reactor core. Another point that is suggested by Table I-4 is that the loss of reactivity which does occur is due not so much to the net burnup of plutonium but to the degradation of the plutonium isotope mixture to one which contains a higher percentage of nonfissile isotopes. One wonders what method would be optimum for reenriching the discharged fuel for further recycle.

Puechl[5] suggests that the recycle of plutonium is not simply a matter of producing plutonium-bearing fuel elements but that there may be unique advantages to be exploited in the plutonium-fuel concept, as well as unique considerations of reactor design to be taken into account.

References

1. Fuel Management Symposium Held at New York Operations Office, New York, N.Y., September 27, 1962, USAEC Report TID-7665, October 1963.
2. C. Matteini, The Garigliano Nuclear Power Station, *Nucl. Eng.*, 4(38): 200-203 (May 1959).
3. J.H. Crowley, Fuel Management Study of the SENN Reactor, in Fuel Management Symposium Held at New York Operations Office, New York, N. Y., September 27, 1962, USAEC Report TID-7665, pp. 1-12, October 1963.
4. M. Benedict, Physics Model for Fuel Management Study of the Spectral Shift Reactor and Recalculations of Costs of the Heavy Water Reactor, in Fuel Management Symposium Held at New York Operations Office, New York, N.Y., September 27, 1962, USAEC Report TID-7665, pp. 40-56, October 1963.
5. K. Puechl, Fuel Management Study of a Water Moderated UO_2PuO_2 System, in Fuel Management Symposium Held at New York Operations Office, New York, N. Y., September 27, 1962, USAEC Report TID-7665, pp. 103-137, October 1963.
6. K. H. Puechl, The Potential of Plutonium as a Fuel in Near-Thermal Converter Reactors, *Nucl. Sci. Eng.*, 12(2): 135 (February 1962).
7. K. H. Puechl, The Potential of Plutonium as a Fuel in Near-Thermal Burner Reactors, *Nucl. Sci. Eng.*, 12(2): 151 (February 1962).

Section II

Power Reactor Technology

Physics

Critical and Exponential Experiments

Boiling Reactors

Experiments relating to exponential work on the BORAX-V reactor were cited in *Power Reactor Technology*, 7(1): 7. Further work on this reactor, covering the zero-power critical experiments performed with boiling core B-1, is recorded in Ref. 1. The fuel rods for core B-1 consist of type 304 stainless-steel tubes with an outside diameter of 0.375 in. and a wall thickness of 0.015 in. These rods contain UO_2 that is enriched to 4.95 wt.% ^{235}U. The active fuel height is 2 ft. The square fuel bundles, $3\frac{7}{8}$ in. on a side, may contain any number of fuel rods from 0 to 49. The full core (Fig. II-1) contains 60 fuel bundles on an 8 by 8 array, with the corner bundles missing, and has an effective diameter of 39 in. Poison rods having the same dimensions as the fuel rods could be substituted for fuel rods for flux-flattening purposes and to control excess reactivity. The core contained nine control rods of boral canned in stainless steel; the central rod and four intermediate rods were cruciform in shape, and the four outer rods were T shaped. The zero-power experiments covered the range from room temperature to the operating condition at 489°F and 600 psig. The major core characteristics measured included critical mass, control-rod calibrations, excess reactivity, shutdown reactivity margin, reactivity effects of various core components, reactivity effects of temperature and voids, neutron-flux and power distributions, and cadmium ratios. Also, some development work was done on a rotating oscillator rod that was installed toward the end of the experimental program.

The experiments indicated that the available excess reactivity at 489°F and 600 psig was 3.2%. Because the void coefficient measurements were made at room temperature and it was expected that the void worth would be higher at operating temperature, it was estimated that the rated full power of 20 Mw(t) could not be achieved. This condition resulted from the requirement that the reactor must be subcritical, in its most reactive state, with eight control rods inserted fully and the ninth control rod withdrawn fully. To accomplish this, a number of boron–stainless-steel poison rods were substituted for fuel rods, thus reducing the reactivity available for power operation. As a result of this, the planned power operation of the core was canceled and changes in the design of core B-2 were undertaken to achieve more excess reactivity.

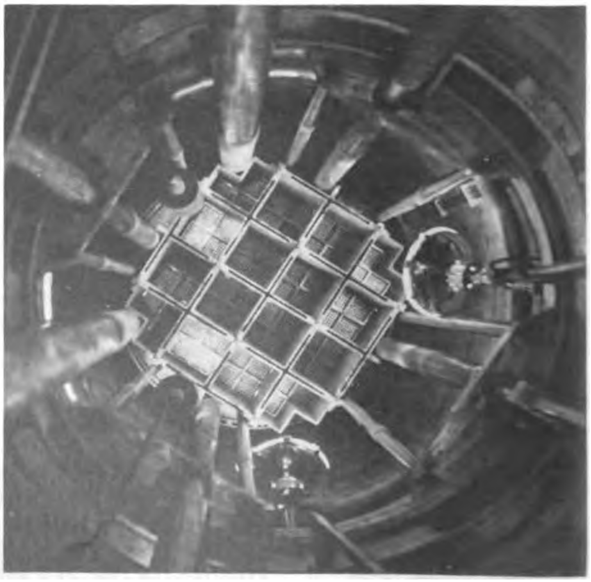

Fig. II-1 Boiling core B-1 of BORAX-V.[1]

Experiments to provide tests of analytical techniques used for predicting reactivity coefficients, detailed power distributions, and spectral variations, with special emphasis on control augmentation in boiling-water reactors, were performed at Vallecitos by the General Electric Company.[2] It is pointed out in Ref. 2 that the control augmentation is sought in order to improve power-reactor designs in the following areas:

1. Reduction in the worth of the movable control required, which in turn leads to increased plant safety
2. Extension of the average fuel exposure made possible with the increased reactivity in the initial core load
3. Flattening of the power distribution by more desirable control distribution

The particular method of control augmentation investigated utilized temporary poison slabs of boron steel. The core characteristics of interest were measured for a range of poison concentrations in the slabs. Two types of fuel rods were used in these experiments. The central zone of the core contained type 304 stainless-steel tubes that had an outside diameter of 0.500 in. and a wall thickness of 0.028 in. The tubes were filled with UO_2 pellets enriched to 2.01 wt.% U. The pellet density was 9.41 g/cm^3, and the pellet outside diameter was 0.444 in. The active fuel height was 67 in. In experiments requiring a driver region, the central core region was surrounded by fuel tubes made of 2S aluminum. The driver tubes had an outside diameter of 0.502 in.; the UO_2 pellets had an outside diameter of 0.491 in., a density of 10.0 g/cm^3, and an enrichment of 1.6 wt.% ^{235}U. The active fuel height in these tubes was 48.0 in. A typical core arrangement is shown in Fig. II-2. The core configurations studied were typical of boiling-water reactor lattices and included assemblies with black and gray absorbing slabs and control-rod cruciforms. Differential reactivity and spectrum effects were investigated for various poison and void tube perturbations. The spatial variation of the neutron spectrum and density in a typical boiling-water lattice was studied by means of the resonance spectral indicator method. This method utilizes foils of materials with well-defined resonances in the energy range of 0.5 to 5.0 ev. Strong spectral variations across the fuel bundles were observed. These variations exist in power reactors and are important in reactor design.

Light-Water-Moderated Assemblies

Critical approach and exponential experiments were performed by General Electric at Hanford on 1.82 wt.% plutonium-aluminum fuel rods. The purpose of these experiments was to determine the effect on criticality of small differences in the concentration of the ^{240}Pu isotope. Reference 3 describes the cylindrical lattice array that was studied. The fuel rods used in this experiment were 0.500 in. in diameter and 44 in. in length. They were sealed in Zircaloy-2 tubes that had an outside diameter of 0.566 in. and a wall thickness of 0.030 in. The average plutonium content was 7.12 g per rod. The amount of the ^{240}Pu isotope varied, but there were two principal groups of rods. One group contained an average of 5.05 wt.% ^{240}Pu in the plutonium, and the other group contained an average of 6.0 wt.% ^{240}Pu. Experiments were performed with the two groups of rods alternately in either an inner or outer

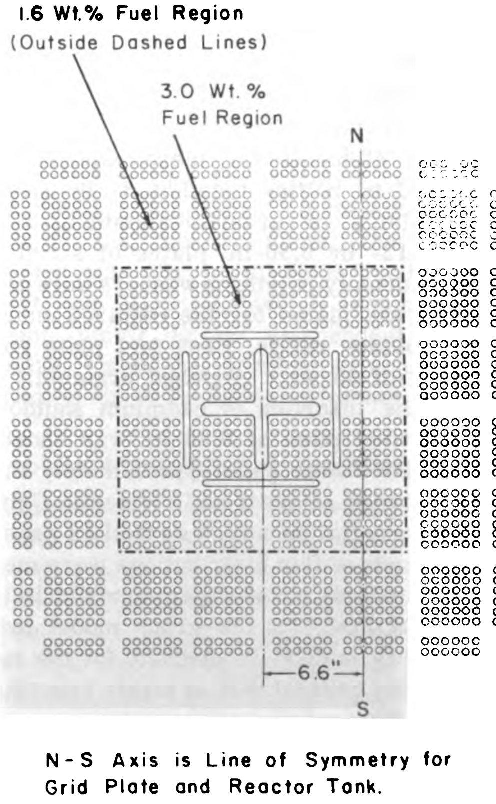

Fig. II-2 Fuel regions for the poison-curtain study.[2]

zone. Calculations were fitted to those two experiments to yield an average ^{240}Pu concentration that could be associated with each experiment; i.e., an average ^{240}Pu concentration was specified as a function of the critical number of rods in both cases. A plot was made of the number of fuel rods vs. ^{240}Pu content and extrapolated linearly to the number of rods for criticality of the mixed loading. The number of rods for criticality of a loading that contained a mixed ^{240}Pu content is also reported in Ref. 3. This extrapolation indicated that the average ^{240}Pu content in the mixed loading was greater than that for any rod in the mixed lattice. It is concluded that either there is a systematic error that has not been detected in the results from the mixed loadings or that the critical mass of plutonium varies more strongly with ^{240}Pu concentration than the calculations predict.

Also given in Ref. 3 are the results of measurements of the relative plutonium content of plutonium-aluminum fuel elements using reactivity coefficients measured in the Physical Constants Testing Reactor (PCTR). These measurements were compared with chemical analysis, and rods were selected on this basis for use in lattice experiments.

Results of critical and exponential experiments performed on small, highly enriched light-water-moderated cores are given in Ref. 4. The fuel elements for these experiments were formed by bolting together 3- by 12- by 0.018-in. plates of uranium-aluminum alloy and 3- by 12- by 0.30-in. plates of stainless steel. High-density polythene washers were used to separate the plates for the required metal-to-water volume ratios. Each fuel plate contained 11 g of 93 wt.% enriched uranium. To allow for the insertion of cadmium shutdown plates, a lattice pitch of 0.35 in. was chosen. This pitch left water gaps approximately 0.35 in. wide between adjacent fuel elements. Critical and exponential bucklings as well as gross- and fine-structure flux distributions were measured. An analysis of the experiments utilizing the MUFT-SOFOCATE few-group model indicates that this method is adequate for the calculation of the critical size of highly absorbing light-water-moderated lattices. Other conclusions inferred from these experiments are

(b) In reactor systems with critical heights down to a minimum of 12 in. there is no evidence that separation of spatial variable in the macroscopic flux distribution is invalid to within the experimental accuracies of ±1 cm. (vertical) and ±1.5 cm. (horizontal) in the determination of the extrapolated core dimensions.

(c) The theoretical mode underestimates thermal flux peaking due to wide water gaps (0.35 in.) in the core. Although this may be significant in calculations of fuel power peaking, the theoretical predictions are adequate to provide "flux weighting factors" for the calculation of reactivity and critical size.

(d) Measurements of material buckling and thermal fine structure can be made in light water moderated exponential assemblies as small as 12 in. sq. and 24 in. high.* Measurements in smaller assemblies diverge significantly from the critical determinations.

---

*In terms of migration lengths these dimensions are equivalent to five migration lengths square and ten migration lengths high.

A report of a panel on light-water lattices held in Vienna May 28–June 1, 1962, is given in Ref. 5. Physicists from most of the well-known laboratories in the field attended this meeting. The formal papers prepared for the meeting were not read but rather served as a basis for information discussion in which other relevant matters could be introduced which had not been formally prepared. The formal papers are, however, printed in their entirety in Ref. 5. Most of the experimental work cited has been reviewed either in *Power Reactor Technology* or elsewhere, and no attempt will be made here to describe each of the experiments. However, the reader should consult Ref. 5 for a systematic tabulation of experimental results on light-water lattices. It was pointed out in the discussions that reasonably uniform practices are used at the present time for the calculation of light-water lattices, and toward the end of the discussion the panel tried to estimate the uncertainties in the calculation of eigenvalues. These uncertainties depend on such things as the water-to-fuel ratio, the rod size, and the fuel enrichment. Although the estimates of uncertainties were largely intuitive, they are of interest (see Table II-1). If these uncertainties were really present and if they all acted in the same direction, they would amount to 3.1% in the eigenvalue. If they were combined statistically (being nearly independent), they would amount to 1.3%. The observed difference between calculation and experiment is somewhat smaller than the 1.3%, indicating that there is

Table II-1 EFFECT OF UNCERTAINTIES ON THE EIGENVALUE[5]

Source of uncertainty	Effect on eigenvalue, %
Resonance absorption	0.5
Thermal-flux spatial distribution	0.3
Thermal η (^{235}U)	0.7
Fast fission factor calculation	0.3
Leakage calculation	0.5
Epithermal η (^{235}U)	0.7
Cross sections used in thermal utilization	0.1

either a canceling of errors in the calculations or that overestimates are given in Table II-1.

Heavy-Water Assemblies

Critical bucklings were measured for heavy-water-moderated lattices of natural-uranium-metal rod clusters in the Process Development Pile at Savannah River Laboratory. The results of these measurements are given in Ref. 6. Fuel for these assemblies consisted of uranium-metal slugs having a diameter of 0.988 in. The slugs were 8.07 in. long and had an average density of 18.9 g/cm^3; they were loaded into air-filled aluminum tubes 12 ft long, with outside and inside diameters of 1.090 and 1.026 in., respectively. These rods were suspended in the reactor tank either individually or in clusters of 3, 7, or 19 rods. With one exception the rods in each cluster were spaced in a triangular array on 1.5-in. centers. The exception was a special 7-rod cluster in which the rods were spaced on 2.0-in. centers. The fuel assemblies were loaded in the reactor on triangular pitches ranging from 7.0 in. to 21.0 in.

Reference 6*a* presents the results of material buckling measurements with the same rods. These measurements were made in an exponential facility, and the results were compared with measurements in the critical facility. A systematic difference in the bucklings was noted. Although the exact nature of the processes involved are not well understood, the effect has been shown (see Ref. 22) to be systematic changes in the exponential buckling which exceed those that can be calculated from simple two-group theory.

Reference 7 gives the results of critical buckling measurements of 25 heavy-water-moderated lattices of natural-uranium oxide rod clusters. These measurements were made in the Process Development Pile at Savannah River. The fuel rods consisted of 9-ft-long aluminum tubes that had an outside diameter of 0.547 in. and a wall thickness of 0.02 in. These tubes were filled with sintered uranium oxide pellets which were ½ in. in diameter and which had an average density of 10.4 g/cm^3. Fuel assemblies containing 19, 31, and 48 rods were built up from the fuel rods. The assemblies were loaded in the reactor on triangular lattice pitches that ranged from 8.08 to 16.17 in. In some experiments the fuel clusters were encased in housing tubes made of aluminum, with outside diameters of 4.00, 5.00, and 6.00 in. and wall thicknesses of 0.054, 0.056, and 0.058 in., respectively. Migration areas were also measured. This was accomplished by measuring the pile periods resulting from small increases in water height, converting these periods to changes in k_{eff} by means of the inhour equation, and then using two-group theory to calculate the migration area from the $\Delta k_{eff}/\Delta B^2$ values. It is pointed out that the buckling measurements should be accurate to about 1% and that the measured migration areas are in good agreement with those obtained from the Benoist theory. (The appropriate references for the Benoist theory are Refs. 8 and 9).

Measurements of initial conversion ratios and fast fission factors at five hexagonal lattice spacings in a 19-element UO_2 CANDU type fuel bundle have been made in a ZED-II lattice at Chalk River. The fuel bundles contained cold D_2O coolant. Reference 10 describes the details of the measurements. One conclusion reached was that a previous model used by Duret and Marriott,* which assumed the fast fission factor to be independent of lattice spacing, should be modified to account for the variation shown by the experiments.

Graphite-Moderated Assemblies

Reference 11 gives the results of critical measurements on systems that are thorium loaded, graphite moderated, and oralloy fueled (93.16% ^{235}U). These experiments are a part of a program to study the characteristics of long-life high-temperature gas-cooled reactors. In particular, the experiments were designed for the comparison of graphite-moderated critical assemblies with and without thorium, in hopes that the effects of uncertainties in uranium cross sections would cancel to yield more accurate information about resonance capture in thorium. The assembly for these experiments consisted of a lattice of thin oralloy foils equally spaced between graphite moderator blocks 0.5 and 1.0 in. thick. Thorium-metal foils that had the same dimensions as the oralloy foils were also placed within the assembly at regular intervals. Results of the experiments were compared with earlier experiments that had the same composition except for the thorium foils. Resonance group cross sections are deduced from the experiments and are compared with calculations from basic resonance parameter data.

---

*The model used by Duret and Marriott is described in the Canadian Report CRRP-873, A Computer Program for Reactor Studies, 1959.

The PCTR small-lattice techniques have been discussed in earlier issues of *Power Reactor Technology*, in particular 7(1): 4 and 8. Reference 12 gives results of PCTR measurements on the lattice of the Experimental Gas-Cooled Reactor being built at Oak Ridge. The fuel assembly is a cluster of seven uranium oxide rods clad with stainless steel. The steel cladding has an outside diameter of 0.705 in. and a wall thickness of 0.020 in. The fuel consists of UO_2 pellets, enriched in the ^{235}U isotope, having an outside diameter of 0.323 in. and a density of 10.4 g/cm^3. Two fuel enrichments were studied: 1.8 and 2.5 wt.% ^{235}U. The fuel rods were spaced on an 8-in.-square pitch in a graphite moderator. The infinite multiplication factor and thermal utilization were measured for both enrichments. In addition, both the resonance escape probability and the fast fission factor were measured for the 1.8% enrichment. Results of this work provide a basis for reactor calculations on lattices of this type.

Results of similar measurements utilizing the PCTR techniques are given in Ref. 13 for lattice parameters of solid and concentric tubes of natural-uranium fuel in graphite lattices. The basic measurements were made for the concentric tube in a 10.5-in. graphite lattice as well as in an 8.375-in. lattice. Measurements were made with both water and air in the coolant channels for the 10.5-in. lattice and with water only in the smaller lattice. Basic measurements on the solid fuel were limited to the 10.5-in. water- and air-cooled lattice. Fuel dimensions and associated data are given in Table II-2.

Table II-2 DIMENSIONS AND RELATED DATA ON LATTICES STUDIED IN REF. 13

	Concentric tube fuel		Solid fuel	
Radii of cell components, cm				
	Inside	Outside	Inside	Outside
Fuel	1.422	2.108		
	2.540	3.175		3.175
Cladding	1.237	1.400		
	2.133	2.205		
	2.439	2.528		
	3.189	3.278	3.189	3.273
Coolant tube	3.840	4.003	3.840	4.003
Graphite				
10.5-in. lattice	4.035	15.050*	4.035	15.050*
8.375-in. lattice	4.035	12.001*		
Densities, g/cm^3				
Fuel	18.81		18.86	
Aluminum	2.7		2.7	
Graphite	1.615		1.610	
Water	1.0		1.0	
Weights in central cell, g				
Fuel	18,164		30,347	
Cladding	755.5		255.9	
Process tube	531.0		531.0	
Water	1,060		631.0	
Graphite				
10.5-in. lattice	54,193		54,007	
8.375-in. lattice	32,874			

*Radius of cylindrical cell of equal area.

Zirconium Hydride Assemblies

Critical experiments performed to evaluate results of the consequences of water immersion of SNAP-2/10A reactor cores are given in Ref. 14. The fuel for these experiments was an alloy of zirconium–10 wt.% (93.2% enriched) uranium, hydrided to a concentration of 6.5 × 10^{22} atoms of hydrogen/cm^3. The fuel rods were clad with Hastelloy that had an outside diameter of 1.250 in. and a wall thickness of 0.011. The fuel diameter was 1.212 in., and the rod length was 12.225 in. The rods were arranged on a triangular pitch of 1.260 in. in the full core, which contained 37 fuel rods and was hexagonal in shape. The coolant for the SNAP-2/10A reactors normally is NaK, but the experiments reported on in Ref. 14 were conducted with the core flooded with water or voided with the aid of Styrofoam displacers. To simulate immersion the core was surrounded by several tanks which could be filled with water to various levels. Pulsed-neutron techniques were used to measure the excess reactivity of the fully loaded, fully water-reflected assemblies that were studied. The measurements were compared with diffusion theory and transport calculations. It was shown that much better agreement was obtained between theory and experiment when the experiments were compared with transport calculations that assumed anisotropic scattering rather than diffusion theory or transport theory with isotropic scattering.

Fast-Neutron Assemblies

The ZPR-III critical facility was described in *Power Reactor Technology*, 7(1): 11. Reference 15 gives a further comparison of experimental parameters of assemblies studied in this facility with calculations utilizing a set of cross sections deduced from the published set by Yiftah et al.* Critical masses of a large number of assemblies were calculated to an accuracy of about 5%. Other conclusions are quoted as follows:[15]

> (2) The calculated relative fission rates of U^{233}, Pu^{239}, Pu^{240}, U^{236}, and U^{238} are in good agreement with the measured data, but the calculated rates for U^{235} and U^{234} are 6% low and 7% high, respectively, relative to those of the other five isotopes. The disagreement between the calculated and experimental fission rates of U^{235} and those of U^{233} and Pu^{239} is insensitive to errors in the calculated spectrum and may be due to erroneous intercalibration of these chambers. This uncertainty regarding the intercalibration of the fission chambers must be removed before the fission-ratio data can be interpreted.
>
> (3) In every case examined, the experimental prompt-neutron lifetime was larger than the calculated value. On the average, the experimental value was 34% greater than the calculated and was moderately constant for all the assemblies, with extreme values of 24% and 48%. The discrepancy is too large to be attributed to experimental errors, and it appears that all the calculated spectra are too hard.
>
> (4) The lack of data on the effect of the sample size upon the measured central reactivities is held to be a serious drawback to the interpretation of much of the reactivity data. It is argued that this should not be important in the comparison of the relative reactivity effects of U^{233}, U^{235}, and Pu^{239}, and also should not affect the general conclusions to be drawn from cases such as carbon and boron-10 in which the discrepancies between experiment and calculation are very large.
>
> (5) The calculated relative central reactivities of U^{233}, U^{235}, and Pu^{239} are in moderately good agreement with experimental data. These data are not sensitive to the calculated spectra. The agreement indicates that the assumed nuclear data for these isotopes are reasonably accurate.
>
> (6) The reactivity effects of the scatterers carbon, oxygen, aluminum, and sodium are shown to be principally dependent upon the importance spectrum and, hence, can be considered as principally importance-spectrum indices. There are large discrepancies between the experimental and calculated reactivities, particularly in the systems with soft importance spectra, and it is inferred that the calculated importance spectra are too hard.
>
> (7) The experimental and calculated central reactivities of steel are in excellent agreement, and those for zirconium are in quite good agreement. In view of the evidence of appreciable errors in the calculated real flux and importance spectra, it appears that this agreement might be fortuitous.
>
> (8) There are large discrepancies between the experimental and calculated central reactivities of the heavy absorbers Mo, Nb, Ta, Th^{232} and B^{10}. Of particular note is the experimental reactivity of B^{10}, 31% greater than calculated. Since the $\sigma(n,\alpha)$ for B^{10} is roughly $1/v$ in dependence, this is strong corroboration of the prompt-neutron lifetime data for which the discrepancy is 34%. Thus, the B^{10} central reactivity data also show that the calculated spectra are too hard.

---

*These cross sections appear in: S. Yiftah, D. Okrent, and P. A. Moldauer, *Fast Reactor Cross Sections*, Pergamon Press, Inc., New York, 1960.

The data for Mo, Nb, Ta and Th^{232} do not generally support the B^{10} data, but it is suggested that this may be due to uncertainty in the knowledge of $\sigma(n,\gamma)$ for these materials.

(9) The calculation of the reactivity effect of U^{238} is shown to be quite sensitive to the assumed cross sections due to competing reactions, and it is not possible to identify errors in U^{238} data. The agreement between results of experiment and calculation would be improved if the calculated spectrum were not so hard.

Spectral Shift

Experimental work under the Spectral Shift Control Reactor (SSCR) Basic Physics Program was reviewed in *Power Reactor Technology*, 5(4): 17; 6(2): 13; 6(3): 81; and 7(1): 8. References 16 to 19 are topical reports containing summaries of the experimental work as well as some analysis and interpretation of the experiments. Reference 16 summarizes results of 20 uniform lattice measurements that utilize 4.02% enriched UO_2 clad in stainless steel as fuel as well as 2.46% enriched UO_2 clad in aluminum. Lattice nonmoderator-to-moderator volume ratios varied from 0.65 to 1.2. The moderator mixtures of light and heavy water ranged from 0 to 77 mole % D_2O. Theoretical interpretation has shown that these systems are very sensitive to the resonance integral of ^{238}U. Also, it was pointed out that the multiregion, few-group diffusion model provides an adequate means of predicting lattice criticality as well as space and energy flux distributions over a large range of lattice parameters.

Reference 17 gives a summary of the perturbation experiments as well as an analysis of these experiments. The PDQ-4 four-group two-dimensional code and the TKO four-group three-dimensional code were used for the analysis. Coefficients for the diffusion equation were calculated utilizing the BPG computer code. In general, the agreement between calculations and experiment is good.

Reference 18 is a summary of the small-lattice work. In addition to the work reviewed in *Power Reactor Technology*, 7(1): 8, lattice parameters for fuel rods containing thorium as the fertile material were measured at two heavy-water concentrations, namely, 70.4 and 80.4 mole %. Although critical experiments were not available for comparison as was the case with the UO_2 measurements, the results appear to be consistent and are in reasonably good agreement with theoretical predictions.

In spectral shift reactors the large epithermal absorption by the fertile material leads to cadmium ratios close to unity for this material. Errors in cadmium ratios of this magnitude lead to very large errors in ρ_{28}, the ratio of epicadmium to subcadmium absorptions. This has given incentive for the development of a method of measuring this quantity with some degree of accuracy. Reference 19 describes such a technique, which has been demonstrated by measurements to 1% in 12 water-moderated lattices. The principal advantages of the method are[19]

1. Uranium activities are measured by chemically processing the irradiated fuel to avoid problems associated with the use of ^{238}U foils.
2. Cadmium-covered uranium measurements are eliminated to avoid cadmium perturbations.
3. ρ_{28} is obtained directly, rather than by the difference between the cadmium ratio and unity, to avoid large errors when the cadmium ratio approaches unity.

Physics of Heavy-Water Lattices

Several analytical schemes have been employed in the past to determine D_2O lattice bucklings from test-lattice data obtained by fuel assembly substitution measurements. Reference 20 presents a comparison between experiment and predictions of three such analytical schemes for test lattices that have bucklings known from previous one-region pile measurements.

A typical substitution measurement of a lattice buckling has three steps: (1) a reference measurement in a one-region lattice, (2) the substitution of one or more test fuel assemblies for reference fuel assemblies, and (3) a remeasurement in the mixed lattice. Three methods of analysis are described and compared with experiment. The first is a one-group three-region perturbation method (after Persson)* which requires experimental data for test regions of at least two different sizes. These results are then used to extrapolate to the case in which the test lattice extends through the pile. The second method is a two-region two-group approach which utilizes a single measurement of the critical moderator height with test assemblies present and a measurement of the critical moderator height with the one-region reference loading. This analysis requires a knowledge of the fast and slow diffusion coefficients, the fast and slow migration areas, and the resonance escape probability for both the reference and test lattices. The third method involves two-group three-region calculations and thus combines features of the two preceding methods. At least two differently sized substitution loadings are made and the results analyzed in concert by two-group theory to eliminate the effect of the intermediate zone of immediately adjoining test and reference fuel assemblies while obtaining the buckling for the test region.

---

*Persson's work is referenced in the following report: R. Persson, One-Group Perturbation Theory Applied to Substitution Measurements with Void, Swedish Report RFX-74, 1961.

All experimental measurements were performed in the Process Development Pile on a 9.33-in. triangular pitch. The fuel assemblies employed in the test lattices were of four types: (1) a 31-element UO_2 rod cluster in a 5-in.-OD aluminum housing tube (0.056 in. thick); (2) a 19-element UO_2 rod cluster in a 4-in.-OD aluminum housing tube (0.054 in. thick); (3) a 19-element UO_2 rod cluster in a 5-in.-OD aluminum housing tube (0.056 in. thick); and (4) a single natural-uranium-metal rod. The 0.50-in.-OD natural-UO_2 columns had a density of 10.4 g/cm^3, were clad in a 0.547-in.-OD 0.02-in.-thick 6063 aluminum tube, and were spaced on a 0.650-in. triangular pitch within a cluster. The 0.998-in.-OD metal rod was clad in a 1.090-in.-OD 0.032-in.-wall 6063 aluminum tube. Reference fuel assemblies consisted of the 31-element UO_2 rod clusters with either D_2O or air-filled housing tubes. Extrapolated pile radii and vertical extrapolation distances were measured by the flux profile method. The perturbation method included measurements of the change in diffusion coefficients, $\delta D_z/D_z$, resulting from voiding the coolant channels of test assemblies. Conclusions on the applicability of the analytical methods were as follows: (1) the successive-substitution one-group perturbation method gave satisfactory results in all cases; (2) the two-region two-group method gave satisfactory results under limited conditions; and (3) the three-region two-group method worked well but did not offer any advantage over the one-group perturbation method to justify its greater complexity.

Further comparisons between experiment and predicted reactivity parameters for clusters of natural-uranium and oxide rods are presented in Ref. 21. The first part of this report is concerned with a comparison between the present calculational method employed at United Nuclear Corp. and two other methods in use during the period around 1959, i.e., prior to the existence of reliable data (k_∞ and B^2) on large clusters of natural-uranium rods, for normalization of calculational methods over the complete range of practical interest. The results of the three calculational methods are compared over the relatively broad range of parameters contained in the following experimental data: (1) measurements of k_∞ and material buckling for D_2O-cooled 7- and 19-element metal rod (0.515-in. diameter) and UO_2 rod (0.520-in. diameter) clusters at the Zero Energy Experimental Pile, Chalk River; (2) measurements of k_∞ for D_2O- and air-cooled 19-element UO_2 rod (0.504-in. diameter) clusters at the PCTR, Hanford; (3) measurements of material buckling for D_2O-cooled 7-element metal rod (1.0-in. diameter) clusters at the Process Development Pile, Savannah River; and (4) measurements of k_∞ for 19-, 31-, and 37-element UO_2 rod (0.5-in. diameter) clusters at the Pawling Lattice Test Rig (PLATR), United Nuclear Corp. In the latter group the experiments were chosen to check the ability of the calculational methods to calculate: k_∞ for D_2O-cooled lattices, coolant density coefficients, and the effect of replacing D_2O with low-density H_2O.

The second part of the report[21] contains a comparison between predictions of the calculational method presently employed at United Nuclear Corp. and the results of measurements of thermal utilization and k_∞ made in the PLATR. The latter facility was specially constructed for D_2O studies; k_∞ measurements are performed by the void-substitution or null-reactivity technique, similar to the method employed at the PCTR. Results are presented for 19-, 31-, and 37-element clusters of 0.5-in.-diameter UO_2 rods, for a series of experiments with fuel elements consisting of concentric tubes of UO_2 (inside diameters of 0.56, 1.24, 1.54, 2.52, 2.52, and 3.50 in. and outside diameters of 1.06, 2.04, 2.04, 3.02, 3.32, and 4.00 in., respectively), and 7-, 19-, and 31-element clusters of 0.5-in.-diameter UC rods. Coolants used include air, D_2O, low-density H_2O (fog), and organic (Dowtherm A).

Reference 22 provides a review of the requirements, methods, and accuracy of experimental physics studies performed on heavy-water lattices. The types of measurements discussed include those of buckling, multiplication constant, intracell lattice parameter, migration area, spectrum, and operating coefficients. Within each category the experimental methods and accuracy of measurement are discussed, and, where possible, the discussion is illustrated with examples taken from the heavy-water power-reactor studies at the Savannah River Laboratory. A broad spectrum of experimental methods and their interpretation is covered in a concise manner with a minimum of mathematical detail. An extensive bibliography is provided to supplement the mathematical aspects of the subject.

Resonance Integrals in Fertile Isotopes

Because the results of measurements of resonance integrals as a function of rod size have been sufficiently inconsistent to indicate the presence of large systematic errors in some of the measurements or in some of the interpretations, Pettus et al.[23,24] have measured the effective resonance integrals for the two fertile isotopes, ^{238}U and ^{232}Th, in both their metal and oxide forms as functions of lump size in the Lynchburg Pool Reactor at the Babcock & Wilcox Co. Nuclear Development Center. See Figs. II-3 to II-5. In addition to the resonance-integral measurements, Refs. 23 and 24 give measurements of temperature effects and determinations of the Dancoff factor. The Dancoff factor measurements substantiate calculations that utilize the Bell[25] approximation.

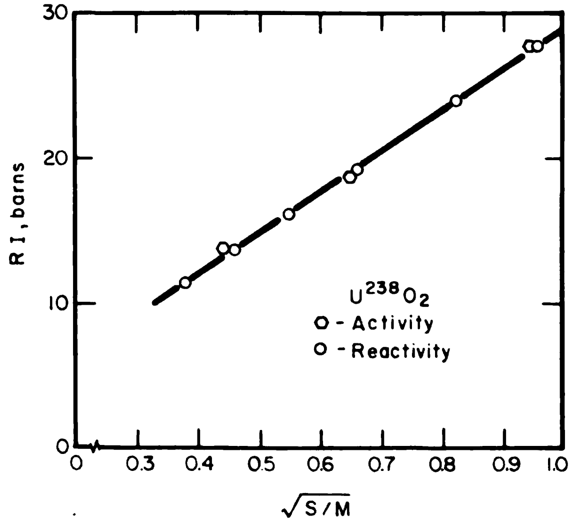

Fig. II-3 Uranium oxide effective resonance integral (RI) vs. $\sqrt{S/M}$.[23]

It is of particular interest that both activation and reactivity techniques were used to measure the resonance integrals independently and that results of the two techniques compared favorably. Apparently no comparable work using both techniques at the same facility has been reported. Linear fits to results obtained for the resonance integrals as a function of the square root of the surface-to-mass ratio are given below:

$$^{238}\text{U (metal)}\, RI = 2.4 + 26.2\ \sqrt{S/M}$$

$$^{238}\text{U (oxide)}\, RI = 0.8 + 28.2\ \sqrt{S/M}$$

$$^{232}\text{Th (metal)}\, RI = 3.91 + 14.81\ \sqrt{S/M}$$

$$^{232}\text{Th (oxide)}\, RI = 3.41 + 17.32\ \sqrt{S/M}$$

Note that no $1/v$ contributions are included in these expressions. The formulas for uranium were obtained from fits to both the reactivity and activation measurements, whereas the formulas for thorium are from the activation results only. The activation results are preferred because many complex calculations are required for the proper interpretation of the reactivity measurements. In particular, the neutron spectrum as well as the importance function must be calculated as a function of the lethargy within the cadmium sleeve where the measurements are made.

As an indication of the agreement between the activation and reactivity measurements, results are presented for uranium oxide in Fig. II-3. A comparison of this work on uranium with other recent measurements (Refs. 26 and 27 cited for comparison purposes) indicates that the uranium-metal results are in good agreement but that the uranium oxide results are systematically several barns lower. Although the differences in the uranium oxide results are not fully explained, note that in this work the same ratio of oxide-to-metal capture was obtained by both activation and reactivity measurements and that this ratio is independent of calibration errors. A comparison of the results for thorium metal and oxide with recent measurements at other facilities is given in Figs. II-4 and II-5.

Reference 23 gives the results of measurement of the uranium metal and uranium oxide resonance integrals by activation techniques. A comparison of this work with previous measurements of Hellstrand indicates good agreement for uranium oxide and poorer agreement for uranium metal. It is pointed out,[28] however, that the difference between results for uranium metal is judged to be within the over-all uncertainty. Results of these measurements are given below.

For ^{238}U (metal):

$$RI = 6.09 + 24.8\sqrt{S/M} \qquad 0.4 < \sqrt{S/M} < 0.75$$

For ^{238}U (oxide):

$$RI = 3.91 + 27.8\sqrt{S/M} \qquad 0.2 < \sqrt{S/M} < 0.6$$

The $1/v$ part of the integral is included in these expressions.

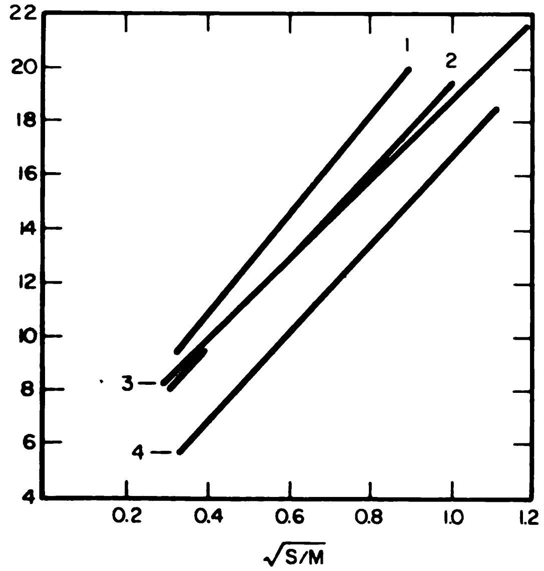

1. - Moore et al,
British Report AEEW - R 57, 1961
2. - Hellstrand and Weitman,
Swedish Report AE-99, 1962
3. - Present Work
4. - Rothman and Ward,
Nuc. Sci. & Eng., I ; 293, 1962

Fig. II-4 Comparison of thorium-metal results with other recent measurements.[24]

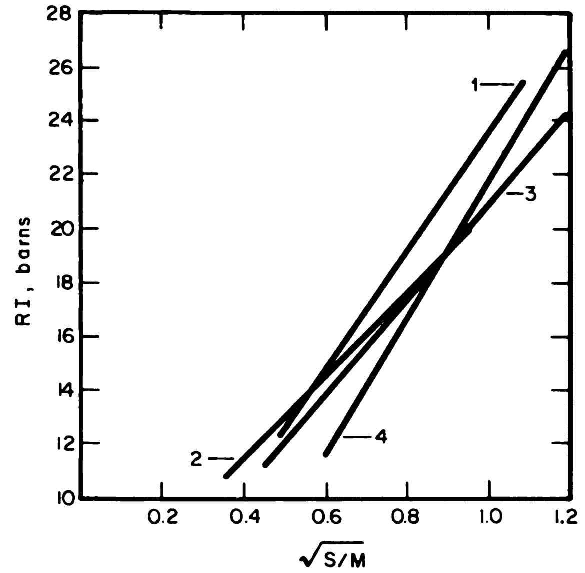

1. - Moore, et al,
British Report AEEW-R57, 1961
2. - Hellstrand and Weitman,
Swedish Report AE-99, 1962
3. - Present Work
4. - Thie, "Heavy Water Exponential Expts. Using ThO$_2$ and UO$_2$", Pergamon Press, 1961

Fig. II-5 Comparison of thorium oxide results with other recent measurements.[24]

Recent measurements of the effective resonance integral of thorium oxide rods are reported in Ref. 29. In the activation technique used, activities obtained in thermal and slowing-down neutron fluxes were compared and gold was utilized as a standard. The results of these thorium oxide measurements are expressed by:

$$RI = (4.9 + 15.5\sqrt{S/M}) \pm 5.0\%$$

The $1/v$ part of the integral is excluded from this expression.

Effective Cross Sections

The need for an accurate description of the time-dependent concentrations of fission products and their macroscopic cross sections prompted the formulation of the CINDER one-point depletion and fission-product program. Reference 30 presents the analytical and physical basis for this program and a comparison with experimental results for enriched-uranium samples exposed to a fuel depletion of 87%.

An exact analytical method is outlined[30] for calculating the detailed time-dependent concentration of each fission product and other generated nuclides. The analytical treatment is general and applicable to all fuels. It includes the formation of nuclides by both radioactive decay (β^- and γ) and neutron capture. Flexibility is built into the calculation by the use of linear chains coupling each nuclide to a single parent (contains no branches). This approach results in a unique set of coupled equations which can be solved independently of particular nuclide parameters and which can be applied to all chains. The chains are independent in the sense that the concentrations in each chain can be calculated without regard to the other chains; the total concentration of each nuclide is given by the sum of the partial concentrations from each chain. The CINDER program embodies this approach in determining the concentration of the nth nuclide, assuming a constant flux and an average fission rate during a given time increment. The program employs one to four arbitrary energy groups and will handle up to 300 nuclides grouped into linear chains as specified by the requester. Up to 99 fission-product chains and 40 fuel chains containing a maximum of 15 nuclides each are permitted. The direct fission yields for the nuclides in the fission-product chains can be specified for up to 10 fissile nuclides appearing in the fuel chains. These limitations are arbitrary and readily changed. The calculation is performed in a sequence of time increments with each increment being of arbitrary length. At each of these increments, the power density (or, optionally, the thermal flux), the fast-to-thermal flux ratios, a thermal spectrum (or shielding) factor, and an epithermal shielding factor (per nuclide) can be specified. The parameters needed to calculate the concentrations, i.e., decay constants, cross sections, type of coupling, yields, etc., must be specified by the requester. At the end of each time step, the program output provides the individual nuclide concentrations, the barns per fission and macroscopic absorption cross sections in each energy group (total and summed over selected nuclides), and other quantities of interest. Given is a recommended set of data (cross sections, half-lives, yield fractions, and nuclide chains) necessary to describe the products resulting from fission of ^{235}U, ^{238}U, and ^{239}Pu. The tabulation includes 67 chains and 256 nuclides of which only 163 are actually different nuclides. The more important nuclides and chains are discussed in detail.

The calculational method is demonstrated by calculating both the individual and total thermal and resonance cross sections per fission of 163 fission products from ^{235}U, natural uranium, enriched uranium, and ^{239}Pu, in a variety of irradiation flux histories and spectra. All known fission products of significance are included in the analysis, i.e., those formed by direct fission yields and by neutron absorption and radioactive decay. A comparison of the aggregate absorption cross sections, determined by both calculation and experiment for a highly enriched sample, shows agreement to within 2% thermally and 15% epithermally.

Reference 31 presents a compilation of neutron cross sections for 6-, 16-, 18-, 24-, and 25-group problems, with neutron energies ranging from fast to thermal. A conspicuous feature of this report is the lack of definitions, discussion, source of contents, and references.

Physics of Control Materials

Reference 32 is a topical report on the absorber burnup experimental program carried out at the Vallecitos Atomic Laboratory. The purpose of the program is to provide information about the change in effective absorption cross section of reactor control-element materials due to transmutation by neutron capture. Test samples were in the form of cylinders, $^1/_4$ in. in diameter and 2 in. in length. Most of the absorber materials were diluted in glass to provide samples of three different self-shielding factors for each element (corresponding to $\Sigma_a t$ of ~ 0.2, 1, and 5). The samples were irradiated in a region adjacent to the core of the General Electric Test Reactor pool facility, and the flux was monitored by aluminum-cobalt wires. After each irradiation the reactivity effect due to the individual samples was measured by pile oscillator techniques in the General Electric Nuclear Test Reactor. Resonance and subcadmium effects were measured by oscillating the samples with and without a fixed 20-mil cadmium sleeve. A detailed description of the experimental technique and method of interpreting the experimental data is given for each element investigated. Figure II-6

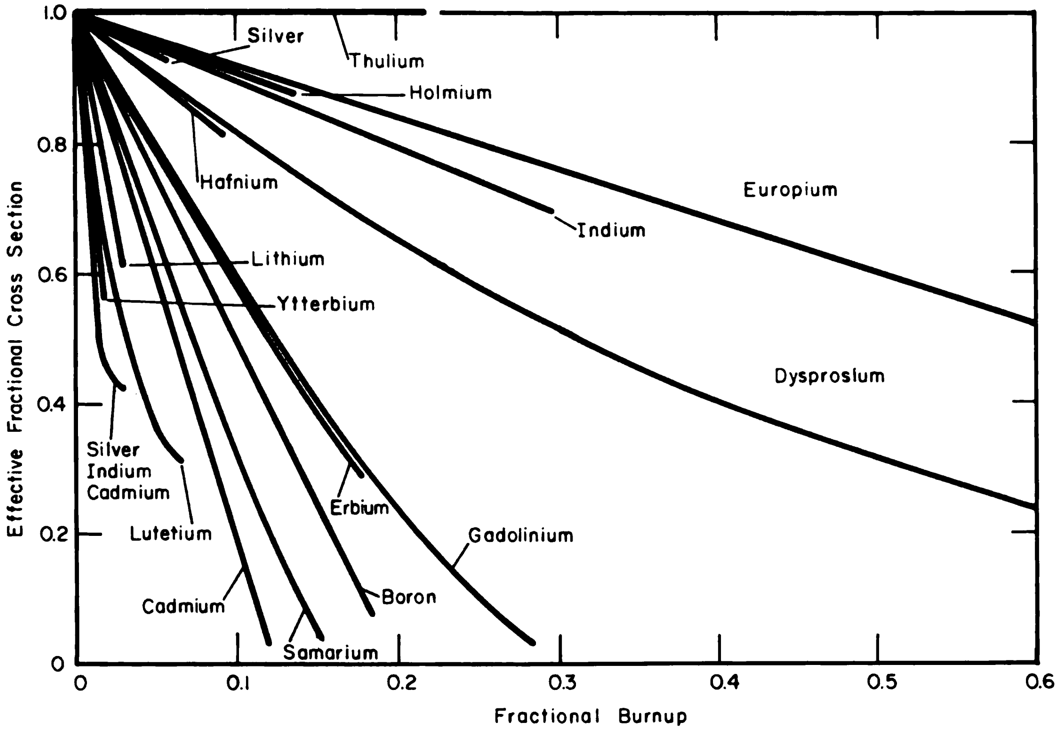

Fig. II-6 Fractional cross section vs. fractional burnup.[32]

presents curves of the effective fractional cross section, $\sigma(n)/\sigma(0)$, vs. fractional burnup, n/N_0, where

$\sigma(n)$ = isotopically weighted element cross section after capturing n neutrons per atom

$\sigma(0)$ = isotopically weighted element cross section for no irradiation

n = number of neutrons captured by the absorbing element (per atom of the element)

N_0 = number of initial atoms of a given element

The curves neglect all resonance capture effects. They are computed on the basis of thermal burnup, and the experimental verification was with a thermal flux.

A theoretical investigation has been made regarding the effect of binary poison mixtures on the temperature defect and temperature coefficient with a simple reactor model.[33] The poison mixtures investigated were Gd-Er, Gd-Eu, Eu-Er, and Eu-Cd. The reactor model consists of an infinite homogeneous mixture of ^{235}U, carbon, and poison, thus eliminating the need for consideration of lattice effects. The change in an operating characteristic at a given operating temperature is defined in terms of the behavior of the reactor system poisoned with the binary mixture relative to one poisoned with boron. Both reactors use the same fuel and structure density and the same multiplication factor at operating temperature; consequently both reactors have the same percentage of parasitic absorption. To simplify computations the Westcott scheme for computing reaction rates was adopted. All materials other than ^{235}U and the binary poison mixtures were assumed to have cross sections of the $1/v$ type.

In the analytical model adopted, changes in the poison cross section are dependent solely on changes in the moderator temperature. Restrictions on the temperature dependence of the poison cross sections necessary to give a decrease in both the temperature defect and temperature coefficient were derived. It was found, for a fixed macroscopic poison cross section, that the largest decrease in the temperature coefficient is produced by the element or isotope having the largest value of $d\sigma/(\sigma dT)$, whereas the poison that gives the largest decrease in the temperature defect is one having the highest ratio of cross section at room temperature to cross section at operating temperature. This result seems hardly surprising. It was also found that in this model the magnitude of the negative temperature coefficient could be increased and the temperature defect could be decreased simultaneously, and a suitably selected binary mixture could decrease the temperature defect without changing the temperature coefficient of reactivity.

One objective when selecting a burnable poison for use in a reactor is to match the reactivity curve throughout the life of the reactor. In many cases not only does a mismatch occur, but a sizable residue of poison remains at the end of life. These effects are of particular importance for the case of slightly enriched cores, where the desired burnout curve departs quite widely from that of an unshielded poison. Reference 34 presents the results of an investigation to find a burnable poison element that can be used to match essentially any decreasing reactivity curve and still have a tolerable residue. The approach taken by the author exploits geometrical effects for highly self-shielded poison materials rather than adjustment of unshielded elemental cross sections. The use of highly self-shielded poisons allows the shape of the burnout curve to be nearly independent of the particular (high cross section) element used.

It is assumed in the analysis that the total effective cross section is proportional to the absorber surface, and, for the case of cylinders or slabs, one dimension (optical thickness) is smaller than the other dimensions. With these assumptions it is shown that spherical particles yield little improvement over an unshielded poison, that cylinders are limited to a linear reactivity shape, but that slabs allow the synthesis of any decreasing burnout characteristics by a combination of samples with different initial blackness factors. Typical fuel cycles were evaluated to determine additional requirements on the burnable poison; both irradiation lifetime and burnout shape were determined. The physical characteristics of four poison materials (cadmium, samarium, europium, and gadolinium) were examined, and gadolinium was selected for further investigation. To retain the desirable geometric properties associated with a slab geometry as well as the requirement of a high neutron absorption cross section, the actual shape of the absorber lumps was taken to be that of a right-circular disk. The effect of disk geometry on both the self-shielding factor and external medium was investigated first for monoenergetic reactions; the analysis was then extended to include spectral effects. The dependence of the self-shielding factor and effective cross section (on irradiation) were evaluated for disks of different dimensions. Experiments were performed to obtain information on (1) the amount of poison residue from gadolinium, (2) self-shielding factors for gadolinium disks, and (3) the burnout behavior of gadolinium disks. A description of the experimental procedures and data interpretation are given.

Shielding

ML-1 Shield Design

A complete report on the ML-1 radiation shield has been published.[35] The ML-1 is a closed-cycle gas-cooled nuclear power plant developed to demonstrate the feasibility of using such a plant in the field; it was reviewed in *Power Reactor Technology*, 6(3): 57-60. Since the plant was to be transportable, the shielding was designed primarily to allow access around the reactor after shutdown. Accordingly it is of interest to review the field operating characteristics of the plant:[35]

> The plant unit (connected reactor and power conversion packages) shall be assembled on a standard military semi-trailer... and all preparations completed for relocation to an operating site within six (6) hours after unloading from any aircraft.
>
> The plant shall be capable of being installed and delivering rated power within twelve (12) hours after arrival at an operating site.
>
> The plant shall be capable of relocation to a new site beginning twenty-four (24) hours after reactor shutdown following operation for extended periods at full power. Completion of disassembly and loading shall be within thirty-six (36) hours after reactor shutdown.
>
> Nuclear radiation allowed: (1) Allowable radiation, twenty-four (24) hours after shutdown at twenty-five (25) ft from the reactor in the direction of the (truck) cab (without water shield), is fifteen (15) mr/hr with the power conversion package in place. (2) No personnel shall receive greater than 3 rem/quarter.
>
> During plant operation, radiation shielding integral to the plant may be supplemented by field expedient materials (earth, gravel, wood, water) sufficient to reduce radiation levels outside the

combined shield to within dosage levels prescribed by the Surgeon General D/A. The integral plant shield (excluding supplemental expedient shielding) shall be adequate to reduce the residual radiation level following full power operation for extended periods to safe levels in time to permit relocation twenty-four (24) hours after reactor shutdown.

A discussion of the shield design changes that took place as the reactor system was developed is presented[35] in chronological order with a listing of the reasons for each significant change in design. The reasons include a change in performance specifications, unacceptable materials, and the incorporation of Lid Tank Shielding Facility (LTSF) test results into the final shield design. The original shield design, for example, used canned crystalline ammonium pentaborate as a solid shielding material, but during testing it was found not acceptable because of deterioration under thermal cycling and radiation. Ammonium pentaborate in aqueous solution was considered; however, during testing it was found to be unacceptable because it was corrosive to aluminum alloys and unstable above 150°F. The final choice was a boric acid solution.

The complete analysis of the final shield design, as shown in Fig. II-7, is presented in the report. The analysis is in two parts. One part deals with the after-shutdown dose rate, which is of prime importance in this shield design, and the other part deals with the expected dose rates during reactor operation. An outline of the methods used in these calculations is presented. The report also presents the data from a series of experiments which were conducted in the LTSF at Oak Ridge National Laboratory in support of the ML-1 shield design. The tests included both operational and shutdown measurements. Also included were variations of the shielding materials, changing of shielding-material thicknesses, and variation of boron content in the water annulus.

Of particular interest is the operational dose-rate data taken during power runs of the ML-1 system. The shielding was that of the reference design (Fig. II-7), with the exception that an expedient shield consisting of 17½ in. of wood (Douglas fir) was positioned directly over the reactor to help reduce the air-scattered dose rate. The operational data agreed fairly well with the analysis and proved that the system

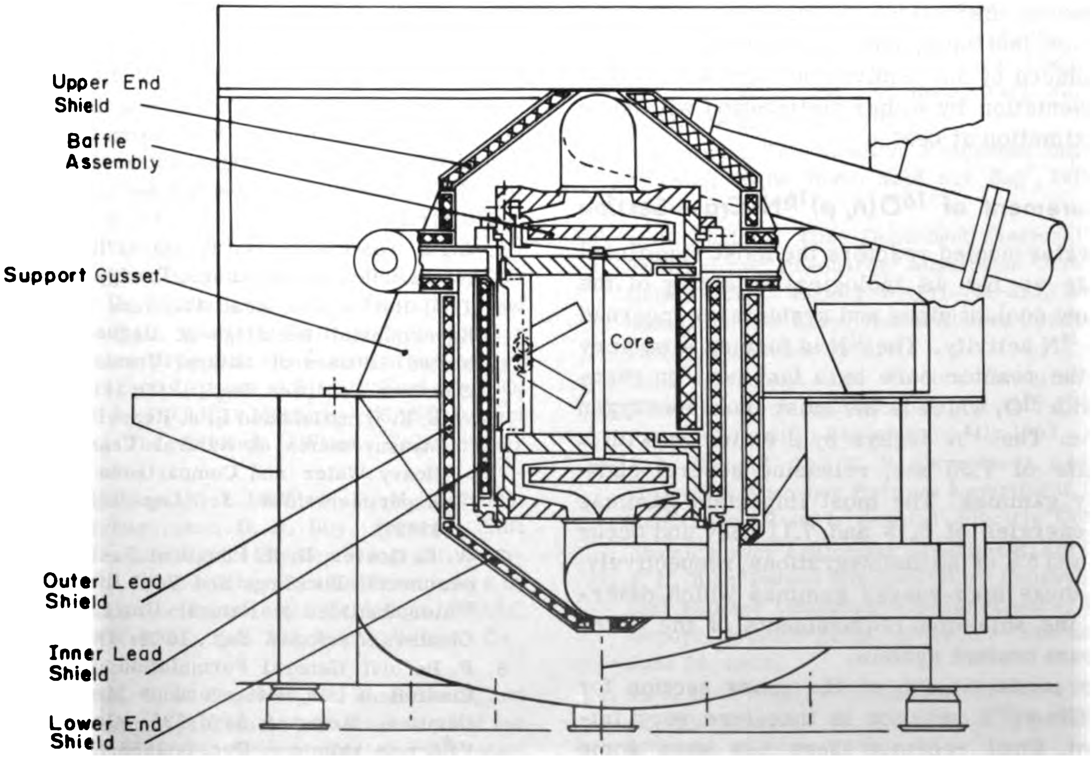

Fig. II-7 Final design of the ML-1 shield.[35]

could operate in the field without exceeding the dose-rate limits set forth in the specifications.

Geometrical Attenuation Factors

The analysis of many shielding problems can be reduced to surface sources that require only a geometrical attenuation factor to determine the radiation flux at the detector location. There are actually very few instances in which a true surface source exists, but there are several instances in which a volume source can be represented as a surface source. As an aid in quickly determining the radiation flux from either a cylindrical or concave spherical surface source, a recent report[36] presents the geometrical attenuation factors in the form of sets of curves. The attenuation factors are plotted as functions of the ratio $d:R$, where d is the source-detector separation distance and R is the radius of the source. The cylindrical source data are further broken down into separate curves for different length-to-radius ratios. Curves are also presented for concave spherical surfaces with different polar angles. For the two geometries, curves are presented for both isotropic and cosine source distributions. The choice of which set of curves to use is left to the user's discretion. A true surface source would be isotropic, but, when a volume source is replaced by an "equivalent" surface source, representation by either distribution will be an approximation at best.

Measurement of $^{16}O(n, p)^{16}N$ Cross Section

In water-cooled reactors the most significant activity as far as biological shielding of the primary coolant pipes and systems is concerned is the ^{16}N activity. The ^{16}N is formed in or very near the reactor core by a fast-neutron reaction with ^{16}O, which is the most abundant oxygen isotope. The ^{16}N decays by β emission with a half-life of 7.35 sec, releasing several high-energy gammas. The most important gammas have energies of 6.13 and 7.11 Mev and occur in 69 and 5% of the disintegrations, respectively. It is these high-energy gammas which determine the shielding requirements of the water or steam coolant system.

The measurement of the cross section for the $^{16}O(n,p)^{16}N$ reaction is therefore very important. Until recently there has been some discrepancy in the cross section at about 14.7 Mev. To resolve the discrepancies an experiment was run to remeasure the cross section between the neutron energies of 12.6 and 16.3 Mev.[37] When these cross sections were combined with previously measured cross sections from 10.24 Mev (the reaction threshold) to 12.6 Mev,[38] a curve was obtained which could be integrated over the Watt fission spectrum to yield an effective cross section for fission neutrons. This effective cross section was evaluated as 19.5 μb, an effective cross section in agreement with most previously calculated and measured effective values. Care is necessary in the choice of fits to the Watt spectrum as this alone can vary the effective cross section from 16.5 μb to 24.3 μb.

References

1. Argonne National Laboratory, Zero-Power Experiments with Boiling Core B-1, BORAX-V, USAEC Report ANL-6689, June 1963.
2. T. R. Jaworowski, P. G. Aline, and H. D. Kosanke, Control Augmentation Critical Experiments, USAEC Report APED-4236, Vallecitos Atomic Laboratory, July 15, 1963.
3. F. G. Dawson, Jr., J. L. Carter, W. A. Reardon, J. E. Faulkner, E. D. Clayton, R. E. Heineman, H. L. Henry, and B. R. Leonard, Jr., Physics Research Quarterly Report, October–December 1962, USAEC Report HW-76128, Hanford Atomic Products Operation, Jan. 15, 1963.
4. I. Johnstone, W. H. Taylor, and S. K. Wallace, Critical Size and Flux Distribution Measurements in Highly Enriched, Light Water Moderated Lattices, *J. Brit. Nucl. Energy Soc.*, 2(4): 379 (October 1963).
5. *Light Water Lattices*, Technical Reports Series No. 12, International Atomic Energy Agency, 1962.
6. T. J. Hurley, Jr., H. R. Fike, and G. F. O'Neill, Experimental Bucklings of Heavy Water Moderated Lattices of Natural Uranium Metal Rod Clusters, *Nucl. Sci. Eng.*, 12(3): 341 (March 1962).
   a. E. E. Wingfield and E. J. Hennelly, Exponential Measurements of Natural Uranium Rods in Heavy Water and Comparisons with Critical Experiments, *Nucl. Sci. Eng.*, 12(3): 348 (March 1962).
7. W. E. Graves, H. R. Fike, and F. G. O'Neill, Experimental Bucklings and Void Effects in Heavy Water Lattices of Natural Uranium Oxide Rod Clusters, *Nucl. Sci. Eng.*, 16(2): 186 (June 1963).
8. P. Benoist, General Formulation of the Diffusion Coefficient in a Heterogeneous Medium Allowing Cavities, Report SPM-522, Commissariat à l'Énergie Atomique, Dec. 2, 1958.
9. P. Benoist, A Simple New Expression of the Radial Diffusion Coefficient for Fueled Channels,

Report SPM-710, Commissariat à l'Énergie Atomique, 1962.

10. B. G. Chidley, T. J. Manuel, and P. R. Tunnicliffe, Initial Conversion Ratios and Fast Fission Factors in Heavy-Water Natural-Uranium Lattices Using 19-Element UO_2 Fuel Rods, *Nucl. Sci. Eng.*, 17(1): 47 (September 1963).

11. G. M. Benson and R. H. Fox, Room Temperature Critical Measurements on Thorium-Loaded, Graphite-Moderated, Oralloy-Fueled Systems, USAEC Report UCRL-6901, University of California, Lawrence Radiation Laboratory, June 30, 1962.

12. P. F. Nichols, J. R. Worden, F. C. Engesser, and R. E. Heineman, The Measurement of the Lattice Parameters of a Gas Cooled Reactor Lattice, *Nucl. Sci. Eng.*, 15(3): 233 (March 1963).

13. D. E. Wood, K. R. Birney, and E. Z. Block, Lattice-Parameter Measurements for Solid and Concentric Tubes of Uranium Fuel in Graphite Lattices, *Nucl. Sci. Eng.*, 18(1): 116 (January 1964).

14. L. I. Moss, Experiments with Water-Reflected, Undermoderated, Zirconium Hydride Critical Assemblies, USAEC Report NAA-SR-8490, Atomics International, Sept. 15, 1963.

15. W. G. Davey, A Comparison of Experimental and Calculated Prompt Neutron Lifetimes and Central Reactivity Coefficients in ZPR-III Assemblies and Their Relationship to Other Reactor Parameters, USAEC Report ANL-6682, Argonne National Laboratory, June 1963.

16. T. C. Engelder, R. H. Clark, M. N. Baldwin, E. J. DeRoche, G. T. Fairburn, J. W. Hallam, D. H. Roy, N. Vutz, and T. M. Schuler, Spectral Shift Control Reactor Basic Physics Program. Measurement and Analysis of Uniform Lattices of Slightly Enriched UO_2 Moderated by D_2O-H_2O Mixtures, USAEC Report BAW-1273, The Babcock & Wilcox Co., November 1963.

17. T. C. Engelder, R. H. Clark, E. J. DeRoche, G. T. Fairburn, J. W. Hallam, D. R. Hostetler, and C. B. Woodhall, Spectral Shift Control Reactor Basic Physics Program. Measurement and Analysis of Perturbed Lattices of Slightly Enriched UO_2 Moderated by D_2O-H_2O Mixtures, USAEC Report BAW-1274, The Babcock & Wilcox Co., October 1963.

18. T. C. Engelder, N. L. Snidow, D. M. Roberts, G. T. Fairburn, and D. H. Roy, Spectral Shift Control Reactor Basic Physics Program. Measurement of k_∞ and Other Lattice Parameters by the Small Lattice Experiment Technique, USAEC Report BAW-1283, The Babcock & Wilcox Co., November 1963.

19. R. H. Lewis, T. C. Engelder, D. M. Roberts, and D. B. Wehmeyer, Thermal Activation Method for ρ_{28} Measurements in Slightly Enriched Uranium Oxide Lattices, USAEC Report BAW-1268, The Babcock & Wilcox Co., May 1963.

20. W. E. Graves, Analysis of the Substitution Technique for the Determination of D_2O Lattice Bucklings, USAEC Report DP-832, Savannah River Laboratory, June 1963.

21. W. L. Brooks, M. Raber, and G. Sofer, Present Status of Calculation and Experiment for D_2O-Moderated Natural Uranium Lattices, Report UNC-5062, United Nuclear Corp., Sept. 13, 1963.

22. J. L. Crandall, Efficacy of Experimental Physics Studies on Heavy Water Lattices, USAEC Report DP-833, Savannah River Laboratory, July 1963.

23. W. G. Pettus, M. N. Baldwin, and C. Samuel, Resonance Absorption in U^{238} Metal and Oxide Rods, USAEC Report BAW-1244, The Babcock & Wilcox Co., April 1962.

24. W. G. Pettus, M. N. Baldwin, and C. Samuel, Resonance Absorption in Thorium Metal and Oxide Rods, Final Report, USAEC Report BAW-1286, The Babcock & Wilcox Co., November 1963.

25. G. I. Bell, A Simple Treatment for Effective Resonance Absorption Cross Sections in Dense Lattices, *Nucl. Sci. Eng.*, 5(2): 138 (February 1959).

26. E. Hellstrand, Measurements of the Effective Resonance Integral in Uranium Metal and Oxide in Different Geometries, *J. Appl. Phys.*, 28: 1493-1502 (December 1957).

27. P. G. F. Moore, S. K. Pattenden, and R. B. Tattersall, The Measurement of the Effective Resonance Integrals of Uranium and Thorium Using the Pile Oscillator Operating Inside a Cadmium Tube, British Report AEEW-R-57, August 1961.

28. J. Hardy, Jr., G. G. Smith, and D. Klein, The Effective U-238 Resonance Capture Integrals of Uranium Metal and UO_2 Rods, *Nucl. Sci. Eng.*, 14(4): 358 (December 1962).

29. J. Weitman, The Effective Resonance Integral of Thorium Oxide Rods, *Nucl. Sci. Eng.*, 18(2): 246 (February 1964).

30. T. R. England, Time-Dependent Fission-Product Thermal and Resonance Absorption Cross Sections, USAEC Report WAPD-TM-333, Westinghouse Electric Corp., Bettis Atomic Power Laboratory, November 1962.

31. L. D. Connolly, Los Alamos Group-Averaged Cross Sections, USAEC Report LAMS-2941, Los Alamos Scientific Laboratory, July 1963.

32. J. L. Russell, Jr., M. R. Carrothers, and W. V. Mosgovoy, Absorber Burn-up Experiment, USAEC Report GEAP-4017, General Electric Company, Atomic Power Equipment Department, April 1962.

33. J. H. Bick, Poison Mixtures Which Improve Thermal Reactor Operating Characteristics, USAEC Report NAA-SR-8225, Atomics International, June 30, 1963.

34. R. J. Holl, Highly Self-Shielded Burnable Poisons, USAEC Report ACNP-63003, Allis-Chalmers Mfg. Co., Mar. 6, 1963.

35. Aerojet-General Nucleonics, Army Gas-Cooled Reactor Systems Program. ML-1 Shielding De-

sign Report, USAEC Report IDO-28609, October 1963.

36. K. M. Campe, Geometrical Attenuation Factors for Gamma Radiation from Cylindrical and Spherical Surface Sources, USAEC Report PWAC-397, Pratt & Whitney Aircraft, Sept. 15, 1962.
37. K. W. Seemann and W. E. Moore, The $O^{16}(n,p)N^{16}$ Cross Section from 12.6 to 16.3 Mev, USAEC Report KAPL-2214, Knolls Atomic Power Laboratory, Sept. 21, 1962.
38. J. A. DeJuren, R. W. Stooksberry, and M. Wallis, Measurement of the $O^{16}(n,p)N^{16}$ Cross Section from 11 to 19 MeV, *Phys. Rev.*, 127(4): 1229 (Aug. 15, 1962).

Section

III

Power Reactor Technology

Fluid and Thermal Technology

Burnout Correlations from the Russian Literature

By John S. Wiley

In an earlier discussion of burnout limits [*Power Reactor Technology*, 7(1): 14-26], two circumstances were pointed out which are well known to heat-transfer investigators but which may not be emphasized strongly enough when thermal limits are set for a particular reactor. They are:

—Burnout correlations that are arrived at empirically to cover a wide range of operating variables provide no means of distinguishing between deviations which result from experimental errors and those which result from true functional relations neglected in the correlation.

—The burnout ratio, as ordinarily used in reactor design, represents not so much a safety factor on reactor heat flux (and hence on reactor power) as an uncertainty factor, related to the uncertainty as to whether the burnout correlation used is truly applicable to the situation in the reactor core.

Both of these considerations emphasize the desirability of comparing correlations and burnout data that have been developed by investigators who are widely separated in background and in approach. The Russian work provides a useful comparison of this kind with the U. S. work that has been reviewed more frequently in *Power Reactor Technology*. The purpose of this review is to make such a comparison. Some work by British investigators is also covered[21] because it illuminates the effect of length and diameter on the burnout heat flux in tubular test sections, a question that has particular significance in the comparison.

Table III-1 RUSSIAN BURNOUT CORRELATIONS EXAMINED

Correlator	Reference
Kutateladze	1
Ornatskii and Kichigin	2
Povarnin and Semenov	3
Zenkevich	4,5
Zenkevich and Subbotin	6

Burnout Correlations for Subcooled Water: Tubular Geometry

The correlations considered here are listed in Table III-1. It is not clear whether U. S. burnout data were used to any important extent in developing the correlations. Direct references to data from USAEC documents are not often cited in the Russian heat-transfer literature, although there are references to journals of the U. S. technical societies, such as the American Society of Mechanical Engineers and the American Institute of Chemical Engineers.

One of the surprising things discovered was that those correlations in which the surface tension of water was a parameter were quite dependent on the value of surface tension used, particularly at pressures approaching the critical pressure where the surface tension approaches zero. Accordingly values of surface tension were taken from Ref. 7. At pressures approaching critical the Russian values differ appreciably from numbers in the *International Critical Tables*, at least as presented in Ref. 8.

Another difficulty in comparing the various correlations arises in converting pressure from metric to British units. The usual unit used in the Russian literature is the atmosphere, which is defined in either of two ways:[7]

$$1 \text{ atm} = 1 \text{ kg/cm}^2 = 735.6 \text{ mm Hg}$$

$$1 \text{ atm(phys)} = 1.034 \text{ kg/cm}^2 = 760 \text{ mm Hg}$$

The former definition (1 atm = 1 kg/cm²) seems, on the basis of some spot checks of saturation-pressure data, to be the one most often used in the Russian literature, and it was used for the conversions made in this review.

Table III-2 LIST OF SYMBOLS USED BY ZENKEVICH

Russian symbol	Definition	Units	USA symbol
q_{cr}	Critical heat flux	kcal/(hr)(m²)	ϕ_{BO}, etc.
r	Vaporization enthalpy	kcal/kg	h_{fg}
ν	Kinematic viscosity*	m²/hr	μ/ρ
σ	Surface tension†	kg/m	σ
W_g	Mass velocity	kg/(hr)(m²)	G
γ'	Density of water at saturation temperature	kg/m³	$1/v_f$
γ''	Density of steam at saturation temperature	kg/m³	$1/v_g$
γ_{sub}	Density of water*	kg/m³	ρ
i_{sat}	Enthalpy of saturated water	kcal/kg	h_f
i_{sub}	Enthalpy of subcooled water*	kcal/kg	h

*Taken for mean water temperature at test-section exit.

†Taken at saturation temperature.

The correlation by Zenkevich and Subbotin is stated[4] to lie within ±10% of the Zenkevich correlation, and attention will therefore be devoted to the latter. The Zenkevich correlation is as follows:

$$K = K_1^{0.65}\,(95 + 420K_2) \times \left(1 + \frac{0.32 \times 10^6}{R^{1.1} + 2.6K_1 + 0.9K_2}\right)(10^{-5}) \qquad (1)$$

where $K = \dfrac{q_{cr}}{r}\left(\dfrac{\nu}{\sigma g\, W_g}\right)^{1/2}$

$$K_1 = \gamma''/\gamma_{sub}$$

$$K_2 = \frac{i_{sat} - i_{sub}}{r}$$

$$R = \frac{W_g\,[\sigma/(\gamma' - \gamma'')]^{1/2}}{\gamma_{sub}\,\nu}$$

The definitions of K, K_1, K_2, and R involve the Russian symbols usually found in their heat-transfer–fluid-dynamics technical articles. A list of these symbols and their usual U. S. equivalents is given in Table III-2. In correlations like that of Zenkevich, Eq. 1, where dimensionless groupings are utilized, it is relatively easy to handle the units. On the other hand, strictly empirical correlations, typified by that of Zenkevich and Subbotin,* require careful attention to the units to ensure correct answers.

The correlation of Zenkevich is plotted in Figs. III-1 and III-2. Again the concept of steam-energy flow (SEF) is utilized to compare the correlation with data given in *Power Reactor Technology*, 7(1): 14-26. SEF is calculated as the product of the mass flow through the test section and the difference between the enthalpy at the burnout point and that of saturated water at the test-section pressure. Also plotted in Figs. III-1 and III-2 are (dotted) DNB-1 lines for corresponding pressures taken from *Power Reactor Technology*, 7(1). The agreement between the solid and dotted lines (which are based on Ref. 9 data) is fairly good. Data of Buchberg were used in developing the Zenkevich correlation; Ref. 10 contains these data in graphs, and Zenkevich states that the graphs were used in the development of Eq. 1. These data are given as "UCLA burnout data for subcooled water at tube exit" in Table II of Ref. 11 and finally appear in Table 12 of Ref. 9. For some reason, however, the Table 12 data are

---

*The Zenkevich-Subbotin correlation is as follows:

$$q_c = 590\, W_g^{1/2}\, \Delta t_H^{1/3} \left(\frac{v''}{v'' - v'}\right)^{-1.8} \qquad (2)$$

where Δt_H = subcooling at point of burnout, °C
v'' = specific volume of saturated steam at test-section pressure, m³/kg
v' = specific volume of saturated water at test-section pressure, m³/kg

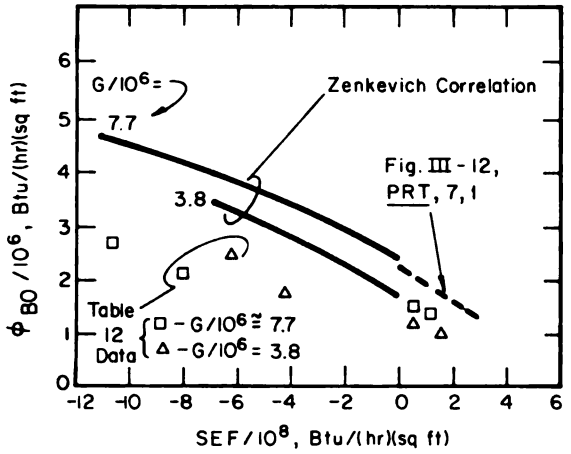

Fig. III-1 Comparison of correlation of Zenkevich[4,5] with data appearing in Table 12 of Ref. 9. Also plotted is a curve taken from Fig. III-12, *Power Reactor Technology*, 7(1): 22. Pressure = 1000 psia.

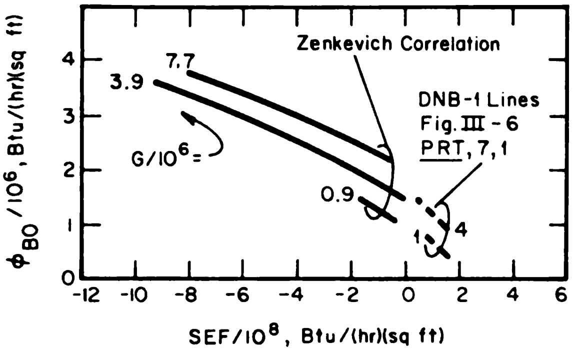

Fig. III-2 Comparison of correlation of Zenkevich[4,5] with data taken from Fig. III-6, *Power Reactor Technology*, 7(1): 18. Pressure = 2000 psia.

slightly different from the data that originally appeared in Ref. 10.

One wonders why, if Zenkevich used Buchberg's data in developing his correlation, the correlation does not agree more closely with the Buchberg data. A comparison is given in Table III-3, and Fig. III-1 also shows Table 12 data of Ref. 9. It can be seen that the Zenkevich correlation overpredicts ϕ_{BO} by as much as a factor of 2. It is possible that only the 2000-psia data of Buchberg were used by Zenkevich, since the agreement for the 2000-psia data is relatively good (as shown in Table III-3). Figure 3 of Ref. 4, page 139, shows a comparison of Buchberg's data with Eq. 1, and a total of 26 points is shown. Table 12 of Ref. 9 contains results of 27 experiments at 2000 psia in the subcooled regime. In addition, Zenkevich concluded that the critical heat flux is not affected by tube diameter in the range from 4 to 12 mm. This is questioned in Ref. 12. The diameter effect will be considered in this article in a later section.

Several correlations, which are listed in Table III-4, are compared in Fig. III-3. The correlation of U. S. origin (WCAP) is included for purposes of comparison. It is believed likely that the differences in the values of ϕ_{BO} predicted by the various correlations is primarily due to a lack of inclusion (or improper inclusion) of terms for the effect of *L* and *D*. The values of *L* and *D* used by the various experimenters are indicated on Fig. III-3, and it is evident that Ornatskii and Kichigin achieve quite high values of ϕ_{BO} with their short, small-diameter tube. Interestingly, Kutateladze in writing his correlation stated that he used data

Table III-3 COMPARISON OF ZENKEVICH CORRELATION WITH TABLE 12 DATA OF REF. 9

Table 12* run No.	Pressure, psia	Mass flow, lb/(hr)(sq ft) × 10^{-6}	Burnout enthalpy, experimental, Btu/lb	$\phi_{BO_{predicted}}$, Btu/(hr)(sq ft) × 10^{-6}	$\phi_{BO_{experimental}}$, Btu/(hr)(sq ft) × 10^{-6}	$\frac{\phi_{BO_{experimental}} - \phi_{BO_{predicted}}}{\phi_{BO_{experimental}}}$, %
002	500	3.87	390	1.76	2.68	34
006	500	3.87	434	1.51	2.28	34
012	500	7.73	438	2.09	2.04	−2.5
008	500	7.65	398	2.42	2.70	10.4
023	1000	3.87	385	3.29	2.54	−30
026	1000	3.84	436	2.89	1.77	−63
027	1000	7.71	404	4.46	2.74	−63
029	1000	7.65	437	4.07	2.05	−99
038	2000	3.95	473	3.42	2.96	−16
054	2000	3.88	659	1.63	1.42	−15
049	2000	7.74	573	3.66	3.34	−10
055	2000	7.76	652	2.44	2.28	−7

*Table 12 of Ref. 9.

of Zenkevich, Zenkevich and Subbotin, and Buchberg, although the publications of the first two experimenters do not seem to be any of those cited in this article. Note that the correlations of Povarnin and Semenov[3] and of Kutateladze,[1] as given in the cited references, involved the flow velocity rather than the mass flow W_g, as shown in Table III-4. Kutateladze[1] calls this, in fact, the "reduced flow velocity of liquid." The substitution of the term W_g/γ_{sub} was done by the present author and may involve some error, since the flow velocity varies along the entire length of the heated test section. A few data are included from Table 12 of Ref. 8 for comparative purposes.

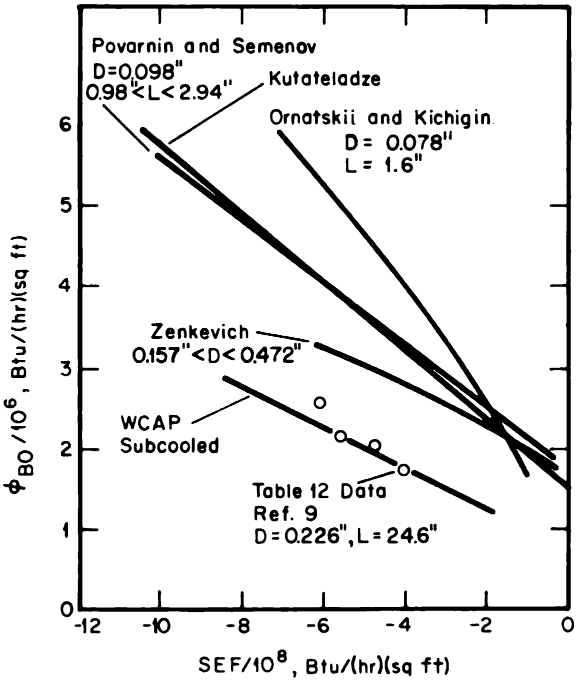

Fig. III-3 Comparison of various burnout heat-flux correlations. Pressure = 1000 psia, $G = 3.7 \times 10^6$ lb/(hr)(sq ft).

Burnout Correlations for Subcooled Water: Rod–Bundle Geometry

Reference 13 contains the results of one of the few experiments conducted to study burnout in the subcooled regime with a bundle of heated rods. The bundle consisted of 7 or 19 rods having an outside diameter of 5 mm (0.197 in.) on a triangular pitch of 6 mm (0.236 in.). A cross section of the bundle is given in part *a* of Fig. III-4, and an individual heater element is shown in part *b* of Fig. III-4. Burnout-detecting thermocouples were attached to the central rod and three peripheral rods. Experiments were conducted within the following ranges of variables:

Pressure: 180 to 210 atm (2560 to 2987 psia)
Flow rate: 0.65 to 4.65 m/sec (2.1 to 15.3 ft/sec)
Subcooling (exit): 10 to 40°C

It was found that the data were correlated by the Zenkevich correlation, Eq. 1. Some difficulty was experienced in reproducing the data when a fresh bundle of tubes was tested, and the

Table III-4 BURNOUT CORRELATIONS PLOTTED IN FIG. III-3

Correlator	Correlation
Povarnin and Semenov[3] (metric units)	$q_{cr} = 2.85 \times 10^6 (1 + 0.017\ \Delta t_{sub}) \left(1 + \frac{W_g}{24{,}660\ \gamma_{sub}}\right)^{0.8}$ (3)
Ornatskii and Kichigin[2] (metric units)	$q_{cr} = 2.5 \times 10^4\ W_g^{0.44}\ \Delta t_{sub}^{0.6}$ (4)
Kutateladze[1] (metric units)	$\frac{q_{cr}}{r\sqrt{g\gamma''}\ \sqrt[4]{\sigma(\gamma' - \gamma'')}} = 0.023 \left(\frac{W_g}{3600\ \gamma_{sub}} \sqrt[4]{\frac{\gamma' - \gamma''}{g^2\ \sigma}}\right)^{0.5}$ $\times \left[1 + 0.45 \left(\frac{\gamma'}{\gamma''}\right)^{0.85} \left(\frac{i_{sat} - i_{sub}}{r}\right)\right]$ (5)
WCAP* subcooled[14] (British units)	$\phi_{BO} = (0.23 \times 10^6 + 0.094\ G)\ (3 + 0.01\ \Delta T_{sub})$ $\times (0.435 + 1.23\ e^{-0.0093L/D_e})\ (1.7 - 1.4\ e^{-a})$ (6) where: $a = (0.532)\ [(H_f - H_{in})/H_{fg}]^{1/3} \left(\frac{\rho_g}{\rho_f}\right)^{-1/2}$

*The term *a* in this correlation has been given three different definitions.[14–16] The particular form used above is the one published first and appears in Ref. 14. Reference 16 presumably corrected the definition given in Ref. 15 but gave the constant as 0.0532.

authors state that "... after several successive transitions (of regime in boiling), the critical heat flux q_{cr} attained a steady value."

What is not clear, however, is how the subcooling was measured. The following quotation serves to illustrate this:[13]

> The results are in satisfactory agreement with the equation, although there are marked differences in the patterns of water flow for the bundles of seven and nineteen tubes. This agreement is probably related to the discrepancy for both types of bundle(s) between the mean temperature of the water after mixing at the exit of the bundle and the temperature actually measured.

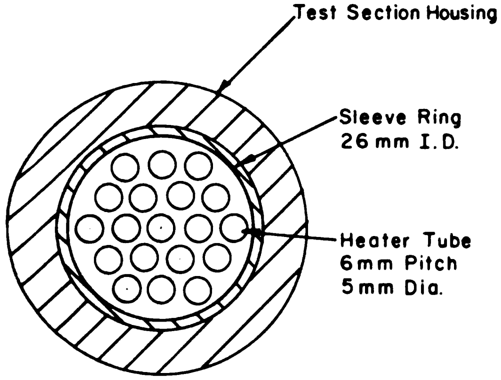

A. Cross Section of 19-Rod Bundle.

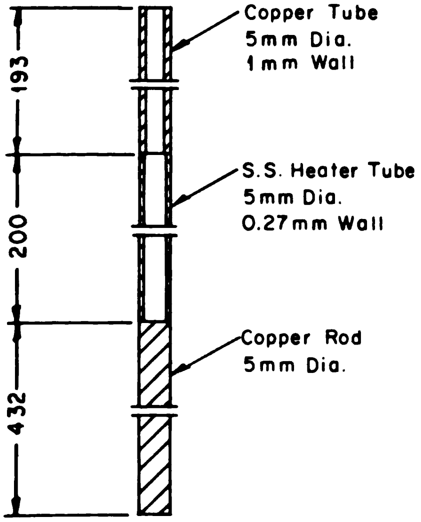
Copper Tube 5mm Dia. 1mm Wall
S.S. Heater Tube 5mm Dia. 0.27mm Wall
Copper Rod 5mm Dia.
193
200
432

B. Cross Section of Heater Tube Used in 19-Rod Bundle.

Fig. III-4 Details of test section used to take data appearing in Ref. 13.

The quotation suggests that subcooling was measured at the location of burnout with a waterside thermocouple and that the exit, mixed-mean water temperature was not used. This is a somewhat crucial point, of course. The importance of mixing was discussed in Sec. III of the last issue of *Power Reactor Technology.*

Reference 17 contains the results of burnout experiments that were run with a test section which had a cross section as shown in Fig. III-5. This test section is, of course, a mockup of a rod bundle, at least of the central and surrounding rods. The inner and outer walls could be heated independently, and the data plotted in Fig. III-5 are for ϕ_{exterior} both zero and finite. The heated exterior walls apparently act like a film tripper and promote transfer of liquid from the walls to the central rod. The improvement in ϕ_{BO} caused by heating the exterior walls is of the same order of magnitude as that obtained[18] by placing washers on the unheated (outer) flow tube in annular geometry. Reference 18 was reviewed in *Power Reactor Technology,* 6(3): 10. The beneficial effect on ϕ_{BO} of bilateral heating has also been observed in annular geometry. The following is quoted from Collier[19] (page 16):

> The Italian ... and Swedish ... experiments with annuli heated on both walls have indicated that the heating of the external surface of the annulus causes an increase in the burnout heat flux value of the inner surface at the same nominal channel exit conditions ... The increase appears to be proportional to the value of the heat flux applied to the secondary surface.

Burnout Correlations for Net Boiling: Tubular Geometry

The correlations of interest for the net boiling region are those of Kon'kov and Modnikova,[20] Ivashkevich,[21,22] and Shitsman.[23] Also included for comparative purposes is a recently developed correlation by British experimenters Lee and Obertelli.[24]

The Kon'kov and Modnikova correlation is quite a specialized one, dealing with the phenomenon of the deterioration of heat transfer during the flow of a steam-water mixture in vertical, tubular test sections. The original article (or translation) should be consulted for details on this phenomenon, but, briefly, it involves the breaking-away of the film of water on the internal surface of the tube during annular flow. The following quotation serves to define this phenomenon more fully.[20]

> ... the wall temperature is initially almost constant and only differs by a few degrees from the saturation temperature. When the steam content reaches a certain level, the wall temperature rises sharply, reaches a maximum and then falls, the magnitude of the maximum rise being a function of the flow rate, the specific heat load and the pressure. The reduction in the wall temperature after the maximum is apparently to be explained by the increase in the flow rate as a result of the evaporation of the liquid phase in the flow.
>
> In contrast to the experiments with film boiling, where as a rule very large temperature jumps occur and the destruction of the tube makes it impossible to determine the maximum temperature, in our present experiments the temperature jumps varied from t = 25°C to t = 300°C.

The correlation is as follows:

$$x_d = \left[\frac{q}{r\gamma''}\,\frac{\left(\dfrac{\sigma}{\gamma' - \gamma''}\right)^{1/2}}{\nu'}\right]^{-0.125} \left(\mathrm{Pr}_{\mathrm{liquid}}\right)^{-0.5}\left(\frac{\mu'}{\mu''}\right)^{-0.2}$$

$$\times\left[\frac{d}{\left(\dfrac{\sigma}{\gamma' - \gamma''}\right)^{1/2}}\right]^{0.2}\left(\frac{500}{\mathrm{Re}_{\mathrm{liquid}}\,\dfrac{\gamma''}{\gamma'} + 350} + 0.35\right) \qquad (7)$$

The units employed in Eq. 7 have been defined in Table III-2 with only a few exceptions. The term d is the diameter of the tube, and $\mathrm{Pr}_{\mathrm{liquid}}$ is obvious. The term $\mathrm{Re}_{\mathrm{liquid}}$ is called the "Reynolds number for the liquid film, on the assumption that the liquid phase is flowing wholly along the surface of the tube":

$$\mathrm{Re}_{\mathrm{liquid}} = \frac{M(1 - x_{\mathrm{mean}})\,v'}{\pi d_{\mathrm{internal}}\,\nu'} \qquad (8)$$

where M = flow rate (mass of steam-water mixture, kg/hr
$v' = 1/\gamma'$, m^3/kg
ν' = kinematic viscosity of saturated water, m^2/hr

The term x_d is the quality at which the deterioration of heat transfer takes place, and, if x_{mean} (which is not defined in either translation cited as Ref. 20) can be taken as x_d, then Eq. 8 becomes

$$\mathrm{Re}_{\mathrm{liquid}} = \frac{dW_g\,(1 - x_d)}{4\mu'} \qquad (9)$$

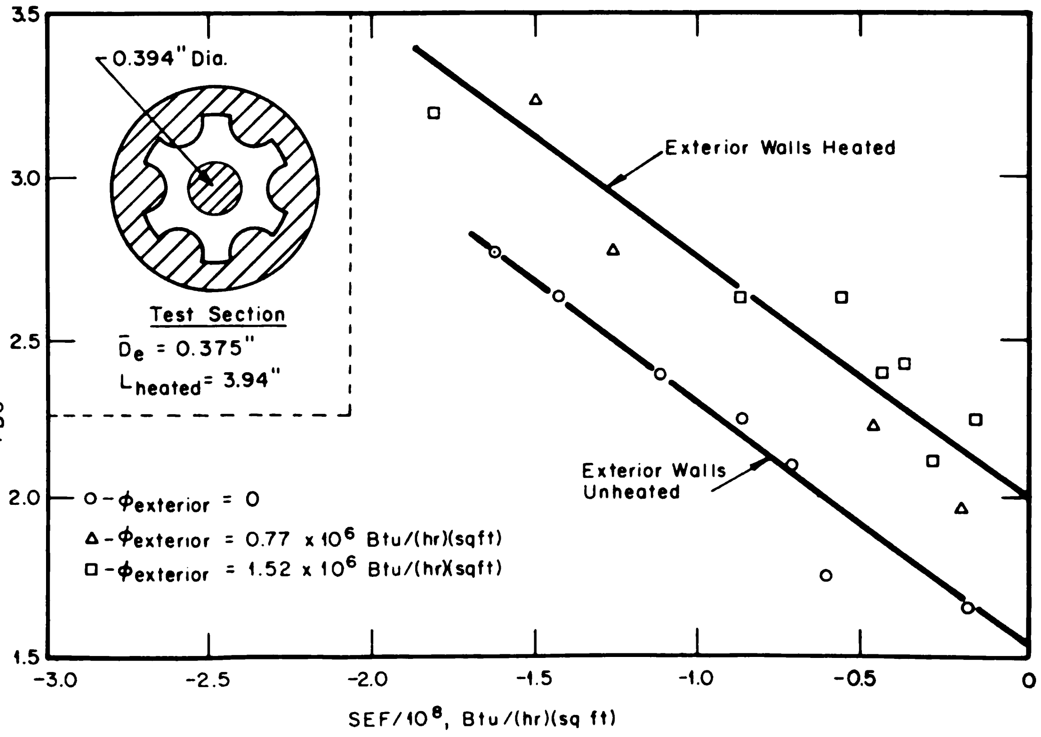

Fig. III-5 SEF plot of data of Alad'yev and Dodonov. Data taken from Table 2 of Ref. 17. Pressure = 1421 psia; ϕ_{exterior} = heat flux impressed on scalloped flow tube; ϕ_{BO} = burnout heat flux for center rod; and $G \cong 0.6 \times 10^6$ lb/(hr)(sq ft).

Table III-5 VALUES OF x_d PREDICTED BY KON'KOV-MODNIKOVA CORRELATION

Mass flow, lb/(hr)(sq ft)	x_d, lb/lb
Pressure = 2000 psia	
0.5×10^6	0.27
1.0×10^6	0.21
2.0×10^6	0.18
Pressure = 1000 psia	
0.5×10^6	0.66
1.0×10^6	0.45
2.0×10^6	0.32

where μ' equals $\nu'\gamma'$. The units on M are not given in Ref. 20, and in fact the translations show this symbol as G; the units for M were derived by the present author to make the Reynolds number of Eq. 8 dimensionless.

Equation 9 was substituted in Eq. 7, and values of x_d were calculated by trial and error for various pressures and values of W_g. These are shown in Table III-5.

The phenomenon of disruption of a thin liquid flowing in the annular regime has been discussed in Ref. 25, which was reviewed in *Power Reactor Technology*, 5(2): 17-18. What appears to correspond to the values of x_d for an internally heated annular test section appear in Table II-7 of that issue of *Power Reactor Technology*, and, in general, they are somewhat lower than the values shown in Table III-5. In any case the values shown in Table III-5 are considerably higher than typical qualities used in boiling-water reactors designed in the USA, although they are about right for exit qualities from proposed fog-cooled reactors. The Russian experiments were done with both steam-water mixtures or water alone fed to the test section, and the following conclusion was reached:[20]

> . . . No effect on the conditions of deterioration of heat transfer could be detected as a result of the different methods.

The correlations of Ivashkevich[21,22] allow for nonuniform heating of the test section, but the present discussion will be restricted to the form applicable directly to uniform heating.[21] The correlation is as follows:

$$\frac{q_c}{r^* (g\gamma'')^{½} [\sigma(\gamma' - \gamma'')]^{¼}} = \frac{1.9 \times 10^{-5} R_e}{1 + 1.8 \times 10^{-8} [K_3(1 + K_2) + K_4] R_e} \qquad (10)$$

where $K_2 = \dfrac{i_{\text{sat}} - i_c}{r}$

$$K_3 = l_1 \left(\frac{\gamma' - \gamma''}{\sigma}\right)^{½}$$

$$K_4 = l_2/d$$

$$R_e = \frac{w}{\nu'}\left(\frac{\sigma}{\gamma' - \gamma''}\right)^{½} \quad \text{when } \frac{d}{2}\left(\frac{\gamma' - \gamma''}{\sigma}\right)^{½} \geq 1$$

$$= \frac{wd}{2\nu'} \quad \text{when } \frac{d}{2}\left(\frac{\gamma' - \gamma''}{\sigma}\right)^{½} < 1$$

$$r^* = r\ (1 - x) \text{ for } x \geq 0$$

$$r^* = r\ [1 + A\ (i_{\text{sat}} - i_c)/r] \quad \text{for } T_z < T_{\text{sat}}$$

$$A = 1 + 0.065\ (\gamma'/\gamma'')^{0.8}$$

The preceding units are consistent with those given in Table III-2. Two of the terms not yet defined are i_c and T_z, which are the enthalpy and temperature, respectively, of the liquid at the center of the stream. Thus, for net vapor generation, $i_c = i_{\text{sat}}$ and K_2 is zero. The term l_1 is defined as the "distance between section at which surface boiling begins and section under consideration . . .," and l_2 is the ". . . distance between section at which $x = 0$ and section under consideration . . ." The only other term open to question is w. In Ref. 22 this is termed the velocity of the liquid, and in Ref. 21 it is termed the velocity of flow. For purposes of this review, the term w will be set equal to W_g/γ'.

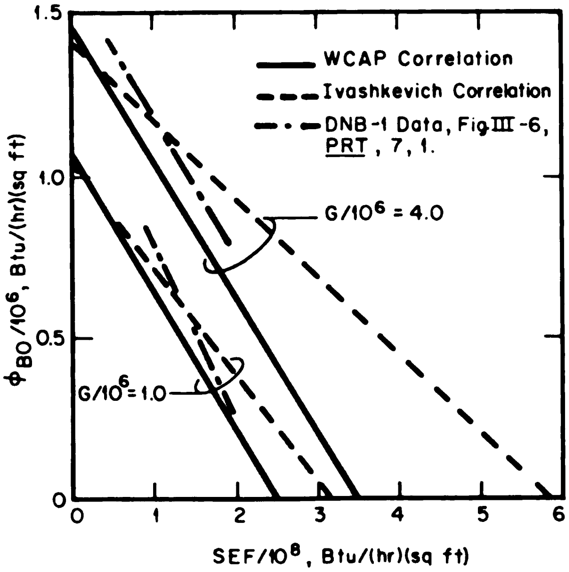

Fig. III-6 Comparison of correlation of Ivashkevich (Eq. 10) with the WCAP correlation (Table III-6). Pressure = 2000 psia. Also shown are DNB-1 data from Fig. III-6, *Power Reactor Technology*, 7(1): 18.

The constant K_3 has an upper limit of 50 and is related to the velocity profile. The constant involves a determination of the position where subcooled boiling is initiated. Fortunately for runs employing net steam generation over only a few inches of test-section length, the value of 50 is quickly achieved. The constant K_4 is the ratio of the boiling length to the test-section diameter. This ratio† can be shown to be

$$L_B/D = \mathrm{SEF}/4\phi \qquad (11)$$

For the moment attention is restricted to the net quality regime where

$$\gamma^* = \gamma(1 - x) \qquad (12)$$

and to tubular test sections with an internal diameter of 0.18 in. At pressures between 1000 and 2000 psia, the parameter

$$\frac{d}{2}\left(\frac{\gamma' - \gamma''}{\sigma}\right)^{1/2}$$

exceeds unity; the value of Reynolds number is as follows:

$$\mathrm{Re} = \frac{W_g}{\gamma' \nu'}\left(\frac{\sigma}{\gamma' - \gamma''}\right)^{1/2} \qquad (13)$$

Substitution of physical property data, a value of 50 for K_3, and Eqs. 11 to 13 into Eq. 10, and rearranging,‡ yields Eq. 14 at a pressure of 2000 psia,

$$\phi_{\mathrm{BO}} = \frac{0.5309G - (1.15 \times 10^{-4} + 1.647 \times 10^{-9}G)\ \mathrm{SEF}}{0.1907 + 3.294 \times 10^{-7}G} \qquad (14)$$

and Eq. 15 at a pressure of 1000 psia,

$$\phi_{\mathrm{BO}} = \frac{1.484G - (2.285 \times 10^{-3} + 2.385 \times 10^{-9}G)\ \mathrm{SEF}}{0.233 + 4.77 \times 10^{-7}G} \qquad (15)$$

Equations 14 and 15 have been plotted in Figs. III-6 and III-7. Also plotted in these figures is the so-called "WCAP correlation" in the form used in *Power Reactor Technology*, 7(1). Another comparison is in Table III-6.

When Figs. III-6 and III-7 are considered, it is important to remember that the burnout correlations illustrated are equations, and that actually very few burnout data exist at high SEF's such as those in the vicinity of the intersections of the correlations with the SEF axis. The reason for this is probably best explained by considering Eq. 11. If one attempts to explore the region around an SEF of 5 × 10^8 and a ϕ_{BO} of 0.5 × 10^6 (see Fig. III-7), then L_B/D must be equal to 250. Not many test sections employing only single-phase water as feed have been

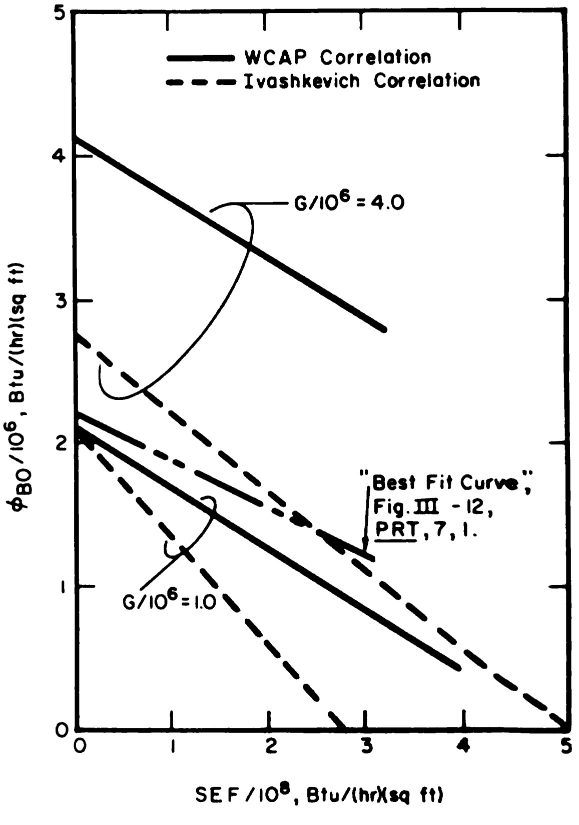

Fig. III-7 Comparison of correlation of Ivashkevich (Eq. 10) with the WCAP correlation (Table III-6). Pressure = 1000 psia. Also shown is the curve from Fig. III-12, *Power Reactor Technology*, 7(1): 22.

---

†The heat balance across a uniformly heated test section can be written as follows: [See Fig. III-1, *Power Reactor Technology*, 7(1), for nomenclature.]

$$\phi = \frac{GD}{4L}(x_e H_{fg} + H_f - H_{in}) = \frac{D}{4L}[\mathrm{SEF} + G\ (H_f - H_{in})]$$

Therefore

$$H_f - H_{in} = \frac{4\phi L}{GD} - \frac{\mathrm{SEF}}{G}$$

if $H_{in} = H_f$, $L = L_B$. Hence

$$\frac{L_B}{D} = \frac{\mathrm{SEF}}{4\phi}$$

‡The system of units in Eqs. 14 and 15 is British.

operated with such a large value of L_B/D to produce DNB-1 data. In particular, Tables 13 and 23 of Ref. 9 contain data taken with test sections that had values of L_T/D of 365 and 242, respectively. The data shown in Table 13, however, were taken in the subcooled region, whereas the data in Table 23 plot as DNB-2 curves. The reader's attention is directed to Fig. III-12, which will be discussed later. The data shown thereon were taken in a tubular test section with a total length-to-diameter ratio, L_T/D, of about 151. At the high mass velocities employed for some of the experiments, it can be seen that the DNB-1 line eventually becomes about parallel with the x axis as SEF increases. This behavior is not predicted by either the WCAP or Ivashkevich correlations, but then neither is the existence of the DNB-2 lines such as are shown in Fig. III-6, *Power Reactor Technology*, 7(1).

Table III-6 COMPARISON OF WCAP BURNOUT CORRELATION WITH THE CORRELATION OF IVASHKEVICH

Mass flow (G), lb/(hr)(sq ft)	WCAP* correlation	Ivashkevich correlation
	Pressure = 2000 psia	
1.0×10^6	$\phi_{BO} = 1.12 \times 10^6 - 0.0042$ SEF	$\phi_{BO} = 1.02 \times 10^6 - 0.0034$ SEF
4.0×10^6	$\phi_{BO} = 1.47 \times 10^6 - 0.0042$ SEF	$\phi_{BO} = 1.41 \times 10^6 - 0.0024$ SEF
	Pressure = 1000 psia	
1.0×10^6	$\phi_{BO} = 2.07 \times 10^6 - 0.0042$ SEF	$\phi_{BO} = 2.09 \times 10^6 - 0.0074$ SEF
4.0×10^6	$\phi_{BO} = 4.09 \times 10^6 - 0.0042$ SEF	$\phi_{BO} = 2.77 \times 10^6 - 0.0055$ SEF

*These are taken from Fig. III-11 and Table III-2 (bottom equation) of *Power Reactor Technology*, 7(1).

The correlation by Shitsman[23] is as follows:

$$q_c/q_0 = 1/[1 + K(L_B/D)^{0.8}] \tag{16}$$

where q_c = critical heat flux, kcal/(m²)(hr)

$$K = 2.2\ D^{0.8} \exp\left(\frac{0.1}{1 - \dfrac{P_{crit}}{P}}\right) \tag{17}$$

P_{crit} = critical pressure, kg/cm²
P = system pressure, kg/cm²
L_B = boiling length, m
D = tube diameter, m
q_0 = constant, kcal/(m²)(hr)

Values of the constant q_0 are given in Ref. 23 as a function of pressure and mass flow. These data are reproduced in Fig. III-8. Substitution of Eq. 11 into Eq. 16 yields the equations shown in Table III-7. Figure III-9 illustrates Eqs. 18 and 19 and compares them with data previously cited in Sec. III of *Power Reactor Technology*, 7(1). The Shitsman correlation reproduces the illustrated Ref. 9 data quite well at a diameter of 0.18 in., but the dependence of ϕ_{BO} on diameter as given in Eq. 17 does not agree with the data as the quality (or SEF) approaches zero.

Table III-7 SHITSMAN BURNOUT CORRELATIONS

[Pressure = 1000 psia, and q_0 Is Taken as 6×10^6 kcal/(hr)(m²)]

Tube diameter, in./mm	Correlation*	
0.18/4.57	$\phi_{BO} = \dfrac{2.21 \times 10^6}{1 + 0.0282\left(\dfrac{SEF}{\phi_{BO}}\right)^{0.8}}$	(18)
0.32/8.13	$\phi_{BO} = \dfrac{2.21 \times 10^6}{1 + 0.0448\left(\dfrac{SEF}{\phi_{BO}}\right)^{0.8}}$	(19)

*Units on ϕ and SEF are Btu/(hr)(sq ft).

The Lee-Obertelli correlation is given as an appendix to Ref. 24. It is as follows:

$$q_{BO}/10^6 = 0.45\left(1 + \frac{0.546}{G/10^6}\right)\left(\frac{H_{BO}}{10^3}\right)^{-2} \frac{e^{-0.00165L/D}}{0.77 + 12D} \tag{20}$$

The units are straightforward and are in terms of British thermal units, pounds, hours, and feet. The heat balance across the test section can be written as follows:

$$H_{exit} \equiv H_{BO} = \frac{4\phi_{BO}L}{GD} + (H_{in} - H_f) + H_f \tag{21}$$

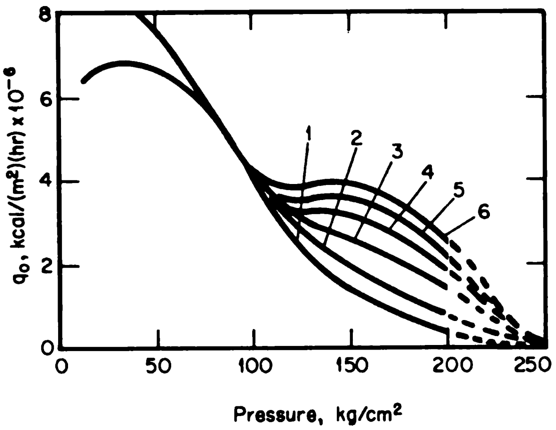

Curve	Mass flow, kg/(sec)(m²)	Mass flow, lb/(hr)(sq ft) × 10⁶
①	500	0.37
②	1000	0.74
③	2000	1.47
④	3000	2.21
⑤	4000	2.95
⑥	5000	3.68

Fig. III-8 The functional relation between the constant q_0 and pressure. (Taken from Ref. 23.)

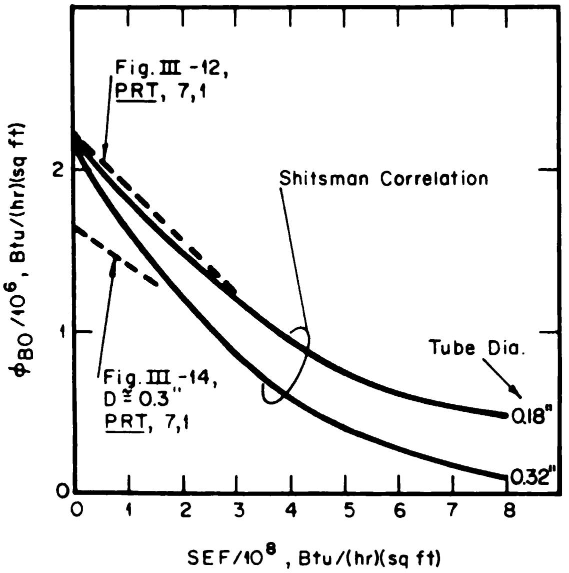

Fig. III-9 Comparison of the Shitsman correlation[23] with data taken from Sec. III of *Power Reactor Technology*, 7(1). Pressure = 1000 psia.

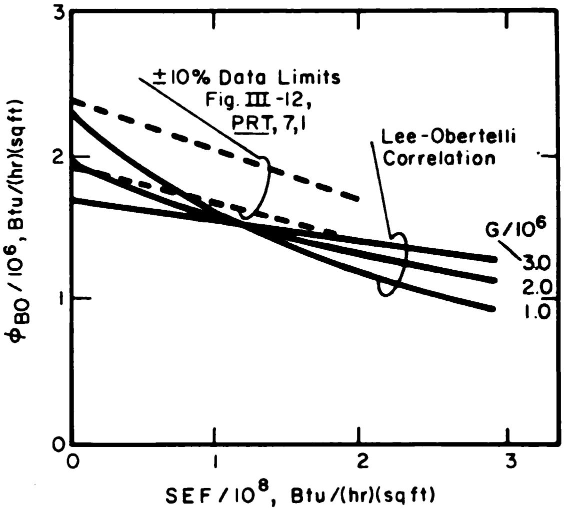

Fig. III-10 Comparison of the Lee-Obertelli correlation[24] with data taken from Fig. III-12, *Power Reactor Technology*, 7(1): 22. Pressure = 1000 psia.

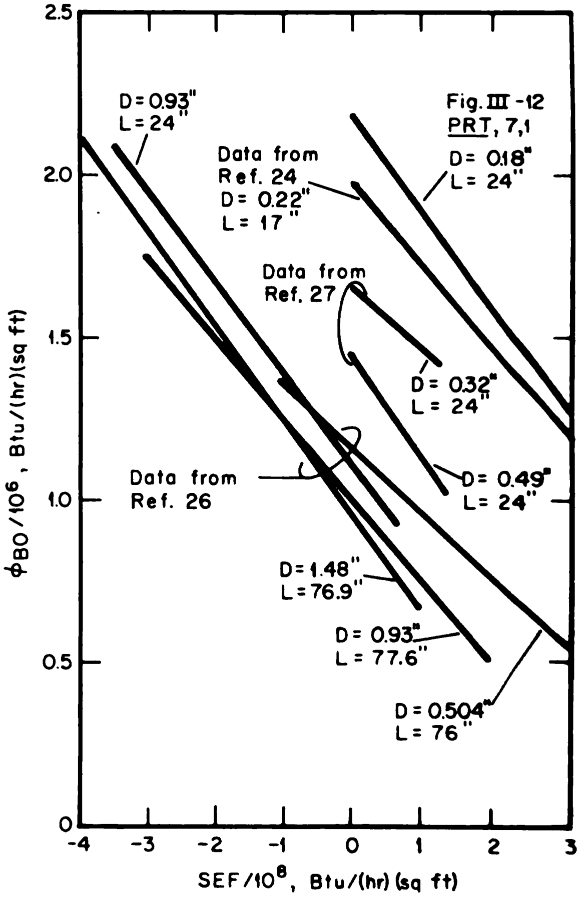

Fig. III-11 Comparison of data from various sources showing effects of length and diameter changes on ϕ_{BO}. Pressure = 1000 psia.

Table III-8 COMMENTS ON DATA PLOTTED IN FIG. III-11

(Pressure = 1000 psia)

Source	Diameter, in.	Length, in.	Effect of G on DNB-1 line position on SEF plot	ϕ_{BO} at SEF = 0, Btu/(hr)(sq ft)*
Reference 24, runs 56 to 90	0.22	17.0	None for $0.7 \times 10^6 < G < 3 \times 10^6$	1.99×10^6
Reference 26, runs C-1 to C-2	0.504	76.0	Some effect for $5.5 \times 10^6 < G < 10 \times 10^6$ None for $0.7 \times 10^6 < G < 4 \times 10^6$	1.18×10^6
Reference 26, runs B-1 to B-49	0.93	77.62	None for $0.5 \times 10^6 < G < 4 \times 10^6$	1.01×10^6
Reference 26, runs D-1 to D-38	0.93	24.0	Some effect for $0.5 \times 10^6 < G < 1 \times 10^6$ and $5.5 \times 10^6 < G < 7 \times 10^6$ None for $1.4 \times 10^6 < G < 4 \times 10^6$	1.12×10^6
Reference 26, runs A-1 to A-47	1.475	76.88	Some effect for $0.7 \times 10^6 < G < 1 \times 10^6$ None for $1.4 \times 10^6 < G < 4 \times 10^6$	0.91×10^6
Reference 27	0.32 (av.)	24	None for† $1.2 \times 10^6 < G < 1.9 \times 10^6$	1.66×10^6
Reference 27	0.49 (av.)	24	Some effect for $G = 0.5 \times 10^6$ None for† $1 \times 10^6 < G < 2 \times 10^6$	1.44×10^6

*These data are taken from Fig. III-11.
†Upper limit on G was about 2×10^6.

Substitution of the second equation in the footnote on page 230 for $H_{in} - H_f$ yields

$$H_{BO} = H_f + \frac{\text{SEF}}{G} \tag{22}$$

If Eq. 22 is substituted in Eq. 20, rearrangement yields

$$\phi_{BO} = \frac{0.45 \times 10^{12} (G^2 + 0.546 \times 10^6 G) f(D,L/D)}{G^2 H_f^2 + 2(GH_f)(\text{SEF}) + \text{SEF}^2} \tag{23}$$

where

$$f(D,L/D) = \frac{e^{-0.00165L/D}}{0.77 + 12D} \tag{24}$$

Equation 23 is plotted in Fig. III-10 for a pressure of 1000 psia with $f(D,L/D)$ taken as 0.95 (the value of 0.95 is an average of the f values for the dimensions of the test sections used to obtain data in Tables 3, 5, and 8 of Ref. 9). Also plotted are the data-limit lines taken from an earlier *Power Reactor Technology* article. The correlation predicts ϕ_{BO} quite well. The effect of G shown by the correlation is approximately within the ±10% scatter of the experimental data plotted in Fig. III-12, *Power Reactor Technology,* 7(1). The correlation is somewhat under the experimental data, but the authors mention that the correlation (in the form given by Eq. 20) also underpredicted ϕ_{BO} for their own data at a diameter of 0.22 in. and total lengths of 8.5 and 17 in.

The $f(D,L/D)$ function is very interesting, and its application is one of the few where such a correction has been attempted. Accordingly an attempt was made by the present author to ascertain its accuracy when applied to other data, since the Lee-Obertelli correlation was developed by the authors from their own data by modifying a correlation presented in Ref. 9. The data that were used for comparative purposes are shown in Fig. III-11 and originate from the sources indicated in Table III-8. This table shows that there is a wide

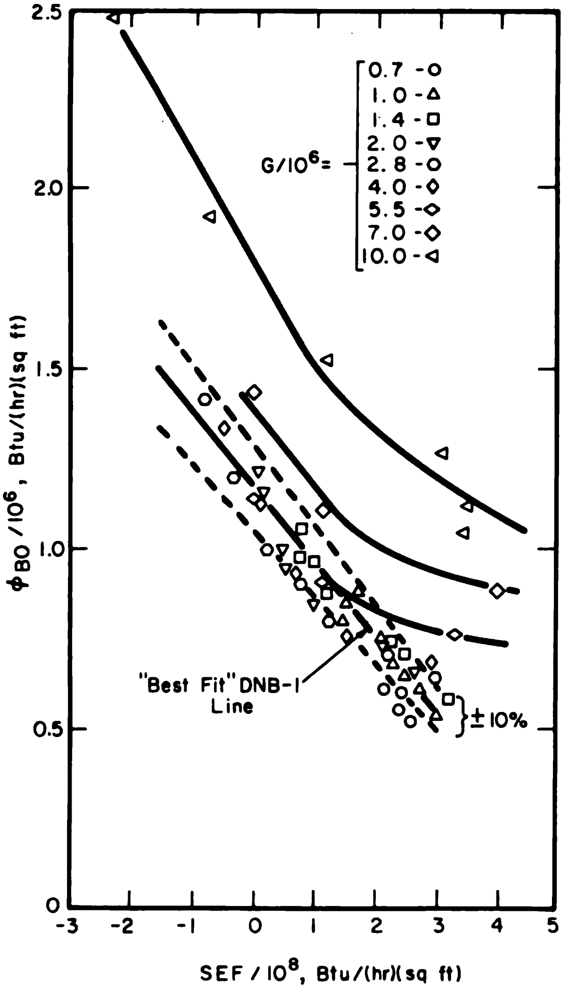

Fig. III-12 Burnout heat-flux data from Ref. 26. Pressure = 1000 psia. Test-section length is 76 in. Test-section diameter is 0.504 in. (tubular).

range of mass flow, G, over which the position of the DNB-1 line is independent of G. The range is roughly from 1×10^6 to 4×10^6 lb/(hr)(sq ft). This G-independent range is illustrated in Fig. III-12 for one of the test sections used to take data appearing in Ref. 26. A variation of $G/10^6$ between 0.7 and 4.0 affects the position of the DNB-1 line within ±10% as $G/10^6$ is increased to a value of 10.0, the position of the DNB-1 line is affected markedly. Figure III-11, therefore, is a collection of the G-independent DNB-1 curves. The intersection of these DNB-1 lines with the SEF-equals-zero axis yields a value termed $\phi_{BO_{SEF=0}}$, and these values are shown in Table III-8.

If, in Eq. 23, SEF is taken as zero, then ϕ_{BC} becomes a function of $f(D,L/D)$ and, according to the correlation, of G. What we have just done, however, is assemble some data where ϕ_{BO} is not a function of G within certain ranges, and let us pretend that the Lee-Obertelli correlation says this, i.e.,

$$\phi_{BO_{SEF=0}} = f(D,L/D) \times (\text{constant}) \qquad (25)$$

The comparison of the Lee-Obertelli $f(D,L/D)$ term with the burnout data shown in Fig. III-11 is illustrated in the last two columns of Table III-9. The f term correlates the data, at least at SEF = 0, to within ±10%, which is about the spread in ϕ_{BO} anyway.

Discussion and Conclusions

Figures III-1 and III-2 show that, if the correlation of Zenkevich were extrapolated into the

Table III-9 APPLICATION OF THE LEE-OBERTELLI $f(D,L/D)$ TERM TO DATA APPEARING IN REFERENCES 9, 24, 27, AND 26

Test-section length (L), in.	Test-section diameter (D), in.	$f(D,L/D)$	ϕ_{BO} at SEF = 0, Btu/(hr)(sq ft)	$\dfrac{\phi_{BO_{SEF=0}}}{f(D,L/D)}$	$\dfrac{\dfrac{\phi_{BO_{SEF=0}}}{f(D,L/D)} - \left[\dfrac{\phi_{BO_{SEF=0}}}{f(D,L/D)}\right]_{av.}}{\left[\dfrac{\phi_{BO_{SEF=0}}}{f(D,L/D)}\right]_{av.}}$
12	0.18	0.943	2.20×10^6	2.33×10^6	0.11
17	0.22	0.889	1.99×10^6	2.24×10^6	0.07
76	0.504	0.612	1.18×10^6	1.93×10^6	−0.08
77.6	0.93	0.513	1.01×10^6	1.97×10^6	−0.06
76.9	1.48	0.409	0.91×10^6	2.22×10^6	0.06
24	0.93	0.564	1.12×10^6	1.99×10^6	−0.05
24	0.32	0.811	1.66×10^6	2.05×10^6	−0.02
24	0.49	0.732	1.44×10^6	1.97×10^6	−0.06
			$\left[\dfrac{\phi_{BO_{SEF=0}}}{f(D,L/D)}\right]_{av.}$	$= 2.09 \times 10^6$	

quality range, it would agree fairly well with the DNB-1 data plotted thereon from Ref. 9, especially at 2000 psia. Zenkevich did use a few data that now appear in Ref. 9, and it is of interest to speculate whether Ref. 9 was available in the Soviet Union when Zenkevich was deriving his correlation. If it was, the "agreement" may be less significant. The remaining correlations shown in Fig. III-3 illustrate the confusion arising from lack of inclusion of a term dealing with a length and diameter effect on ϕ_{BO}. If the data, taken with the exterior walls heated, were plotted from Fig. III-5 to Fig. III-3, they would lie above even the correlation of Ornatskii and Kichigin. Again this is believed to be the result of working with a short test section.

The agreement between the correlations of Ivashkevich and WCAP is rather remarkable and illustrates the utility of an SEF treatment for comparing rather difficult correlations. At 2000 psia (Fig. III-6) both correlations do well with respect to the Ref. 9 data that were plotted; at 1000 psia (Fig. III-7) both correlations do less well. This might be because the functional form of the correlations was developed from the 2000-psia, or at least the relatively higher pressure, data.

The correlations of Shitsman and Lee-Obertelli are in rather good agreement for a tube diameter of 0.18 in. (Figs. III-9 and III-10), although the diameter effect predicted by the former correlation is not correct at SEF's approaching zero. Shitsman predicts no effect of mass flow on burnout for pressures between about 70 and 100 kg/cm^2 (Fig. III-8), and this is substantiated by data plotted in Fig. III-12, *Power Reactor Technology*, 7(1). The $f(D,L/D)$ term suggested by Lee-Obertelli to account for the effect of these variables on ϕ_{BO} is quite good, as is evidenced by the last column of Table III-9.

References

1. S. S. Kutateladze, Critical Heat Fluxes in the Flow of a Wetting Liquid with the Core (of the Stream) Below the Saturation Temperature, USAEC Translation AEC-tr-5518, Aug. 28, 1962. [Translated from *Nauchn. Dokl. Vysshei Shkoly, Energ.*, 2: 229-239 (1959).]
2. A. P. Ornatskii and A. M. Kichigin, An Investigation of the Dependence of the Critical Heat Load on Mass Flow Rate, Subcooling, and Pressure, USAEC Translation AEC-tr-5710. [Translated from *Teploenerg.*, 8(2): 75-79 (1961).]
3. P. I. Povarnin and S. T. Semenov, An Investigation of Burnout During the Flow of Subcooled Water Through Small-Diameter Tubes at High Pressures, USAEC Translation AEC-tr-5602. [Translated from *Teploenerg.*, 7(1): 79-85 (1960).]
4. B. A. Zenkevich, Similarity Criteria for Critical Heat Loading in Forced Liquid Flow, *J. Nucl. Energy: Pt. B*, 1(2): 137 (August 1959).
5. B. A. Zenkevich, The Generalization of Experimental Data on Critical Heat Fluxes in Forced Convection of Subcooled Water, *J. Nucl. Energy: Pt. B*, 1(2): 130 (August 1959).
6. B. A. Zenkevich and B. I. Subbotin, Critical Heat Fluxes in Subcooled Water with Forced Circulation, *J. Nucl. Energy: Pt. B*, 1(2): 134 (August 1959).
7. S. S. Kutateladze and V. M. Borishanskii, Handbook of Heat Transfer, Translation NP-tr-917, Aug. 16, 1962. (Translation of *Spravochnik po Teploperedache*, State Publishing House of Power Engineering, Moscow, 1958.)
8. Knolls Atomic Power Laboratory, Basic Sub-Cooled Light Water Properties, USAEC Report KAPL-M-SMS-3, April 1955 (reissued October 1959).
9. R. A. DeBortoli, S. J. Green, B. W. LeTourneau, M. Troy, and A. Weiss, Forced-Convection Heat Transfer Burnout Studies for Water in Rectangular Channels and Round Tubes at Pressures Above 500 Psia, USAEC Report WAPD-188, Westinghouse Electric Corp., Bettis Plant, October 1958.
10. H. Buchberg et al., Final Report on Studies in Boiling Heat Transfer, USAEC Report COO-24, University of California, March 1951.
11. W. H. Jens and P. A. Lottes, Analysis of Heat Transfer, Burnout, Pressure Drop, and Density Data for High-Pressure Water, USAEC Report ANL-4627, Argonne National Laboratory, May 1, 1951.
12. I. T. Alad'yev, L. D. Dodonov, and V. S. Udalov, Critical Heat Fluxes for Water Flowing in Tubes, *J. Nucl. Energy: Pt. B*, 1(3): 181 (March 1960).
13. B. A. Zenkevich, V. I. Subbotin, and M. F. Troyanov, Critical Heat Fluxes for a Bundle of Tubes Cooled in Pressurized Water, *J. Nucl. Energy: Pt. B*, 1(3): 197 (March 1960).
14. L. S. Tong, H. B. Currin, and A. G. Thorp II, New DNB (Burnout) Correlations, USAEC Report WCAP-1997(Rev.), Westinghouse Electric Corp., Atomic Power Division, September 1962.
15. L. S. Tong, H. B. Currin, and A. G. Thorp II, New Correlations Predict DNB Conditions, *Nucleonics*, 21(5): 43 (May 1963).
16. L. S. Tong, H. B. Currin, and A. G. Thorp II, Comments on Letter by W. R. Gambill, *Nucleonics*, 21(7): 7 (July 1963).
17. I. T. Alad'yev and L. D. Dodonov, Critical Heat Flows in the Boiling of Underheated Water in Channels of Complex Shape (Pressure 100 atm

abs), in Convection and Radiation Heat Transfer. Translation of *Konvektiviyy I Luchistyy Teploobmen*. Report FTD-TT-61-395, pp. 79-99 (a publication of Publishing House of the Academy of Sciences, USSR, Moscow, 1960).

18. J. A. Hodde (Ed.), Fuel Cycle Program. A Boiling Water Reactor Research and Development Program, Quarterly Report No. 5, July 1961–September 1961, USAEC Report GEAP-3835, General Electric Company, Atomic Power Equipment Department, Oct. 10, 1961.
19. J. G. Collier, Heat Transfer and Fluid Dynamic Research as Applied to Fog Cooled Power Reactors, Canadian Report AECL-1631, June 1962.
20. A. S. Kon'kov and V. V. Modnikova, Experimental Investigation of the Conditions of Deterioration of Heat Transfer During Boiling in Tubes, USAEC Translation AEC-tr-5539 [Translated from *Teploenerg.*, 9(8): 77-81 (1962).] See also the Central Electricity Generating Board (British) translation, C.E. Trans. 2932, O.T.S. Document 63-23966.
21. A. A. Ivashkevich, Critical Heat Flux and Heat Transfer Coefficient During Boiling of Liquids in Channels Under Conditions of Forced Flow, USAEC Translation AEC-tr-5038. [Translated from *Teploenerg.*, 8(10): 74-78 (1961).]
22. A. A. Ivashkevich, Critical Heat Fluxes for Forced Convection of Liquid in Channels, *J. Nucl. Energy: Pts. A & B*, 16: 171 (March 1962).
23. M. E. Shitsman, Heat-Transfer Crisis in Steam-Generating Channels, British Report TRG Information Series 267(R). [Translated from *Inzh.-Fiz. Zhur., Akad. Nauk Belorussk. SSR*, 5(9): 9-15 (1962).
24. D. H. Lee and J. D. Obertelli, An Experimental Investigation of Forced Convection Burnout in High-Pressure Water, Part I. Round Tubes with Uniform Flux Distribution, British Report AEEW-R-213, August 1963.
25. A. W. Bennett, J. G. Collier, and P. M. C. Lacey, Heat Transfer to Mixtures of High Pressure Steam and Water in an Annulus, Part II. The Effect of Steam Quality and Mass Velocity on the "Burnout" Heat Flux for an Internally Heated Unit at 1000 psia, British Report AERE-R-3804, August 1961.
26. R. R. Hood and L. Isakoff (Comps.), Heavy Water Moderated Power Reactors Progress Report, May–June 1963, USAEC Report DP-855, E. I. du Pont de Nemours & Co., Inc., August 1963.
27. R. R. Hood and L. Isakoff (Comps.), Heavy Water Moderated Power Reactors Progress Report, June 1962, USAEC Report DP-755, E. I. du Pont de Nemours & Co., Inc., July 1962.

Section

IV

Power Reactor Technology

Fuel Elements

Fabrication by Novel Methods

The oxide-bearing fuel elements in currently operating water-cooled power reactors have all been fabricated by the technique of loading pressed-and-sintered pellets of UO_2 into cladding tubes and welding end caps onto the ends of the tubes for sealing purposes. Research has continued, however, into alternate methods of fabricating fuel elements, and the purpose of this review is to discuss several recent publications dealing with these novel methods. For supporting background information the reader may wish to consult the following articles published in *Power Reactor Technology,* 6(1): 26-37 and 6(2): 28-42.

References 1 through 3 are recent Battelle Memorial Institute reports concerned with fabrication details of several different fuel elements. The references report on work done to develop fabrication techniques for producing low-cost fuel elements of specific types. As such, applications to specific reactors are not discussed; the work, however, is of general interest because of the variety of fabrication methods studied. Of the two elements described in Ref. 1, emphasis herein will be placed on the so-called "concentric-component" element, as this was the most successful. The concentric-component element is of tubular geometry and employs a UO_2–stainless-steel cermet as "meat," clad on both sides with stainless steel. The core materials were 20 and 30 wt.% loadings of −325-mesh, spherical UO_2 particles in a matrix of −325-mesh, type 316 stainless-steel powder. The cladding material was 0.006-in. type 316 stainless steel, and the end plugs were also made of type 316 stainless steel.

Attempts were made to incorporate a plastic binder into the core material to allow for forming or extruding into a tubular shape, but the final elements were made by the loading of loose powder into the annular space formed between the concentric stainless-steel cladding tubes. As-loaded densities from 50 to 60% were attained. Tamp packing, powder wetting after partial loading, vibrational packing, and step packing with periodic thermal cycling of the tubes were studied to try to attain a uniform loading density.

When loading was completed, a consolidation and bonding step was accomplished. This was designed to densify the fuel cermet, size the fuel element, and form a bond between the meat and the cladding. Three processes were considered: (1) explosive compaction, (2) cold hydrostatic pressing, and (3) gas-pressure bonding. These processes were employed either singly or in combination. Figure IV-1 shows a schematic view of an assembled specimen ready for implosive consolidation. In this process a sheet of explosive (PETN) was wrapped around the outside jacket and detonated in a housing submerged in a tank of water. The mild-steel jackets were then removed by an acid bath. Experiments were also done using a backup die with the explosive charge (Primacord) placed inside the tube. A mild-steel insert was used between the specimen and the explosive to smooth out the shock wave.

Cold hydrostatic pressing was accomplished at 100,000 psi. No mandrels were necessary because the outer tube yielded before the inner cladding tube, and densification of the meat took place from the outside in. The gas-pressure bonding was done at 2100°F and 10,000 psi for 3 hr.

Test elements of lengths 6 and 10 in. were made by combinations of the above-discussed fabrication techniques, and full-scale elements having an outside diameter of $^3/_4$ in. and a length of 27 in. also were fabricated. The conclusions are quoted[1] as follows:

> (1) Tubular fuel elements approximately 3/4 in. in diameter and 27 in. long can be fabricated by the assembly, consolidation, and bonding of concentric components.
>
> (2) These elements possess dense fuel cores and almost complete core-cladding bonding when explosively sized and gas-pressure bonded.
>
> (3) Additional study is needed to optimize the blending and loading procedures to insure a uniform dispersion of UO_2 in the stainless steel matrix and to achieve a uniform loading density along the length of the elements, which later influences the surface condition of the bonded elements.
>
> (4) A densification step after powder loading is needed to attain sufficient density in the fuel annulus to prevent wrinkling of the outside cladding during pressure bonding of the element.

References 2 and 3 deal with fabrication techniques applicable to the production of UO_2-fueled rods. Specifically, the work was done as a part of the USAEC Fuel-Cycle Development Program. Reference 2 describes a fabrication technique that is a combination of vibrational compaction and gas-pressure bonding. The fuel material was UO_2, consisting of high-density particles of coarse sizings mixed with varying amounts of micronized UO_2. The latter material is a powder prepared by a fluid jet-grinding process to reduce the particle size.[4] The coarse particles included fused, high-energy-impacted, and electrodeposited oxides. The cladding materials included Zircaloy, types 304L and 406 stainless steel, and Inconel X, with cladding thicknesses varying from 0.007 in. (304L) to 0.030 in. (Zircaloy).

Some results of the program are given in Table IV-1. An improvement was achieved by the use of an intermediate swage to increase the prebonded density to the point where pleating and surface roughening would not occur during the gas-pressure bonding step. The effect of intermediate swaging is shown in Table IV-2. To summarize:

> The swaging operation was found to be particularly advantageous in the aforementioned work and its combination with vibrational compaction, using inexpensive vibrational equipment and pressure bonding may be advantageous although somewhat more involved. These studies have shown, however, that gas-pressure bonding following a single-step preliminary densification by vibrational compaction is feasible. The requirements for fabricating stainless steel-clad UO_2 rods by the combined processes are:
>
> (1) Oxide mixtures of fused and Micronized UO_2 in which the high-surface-area Micronized UO_2 constitutes approximately 30 to 40 w/o

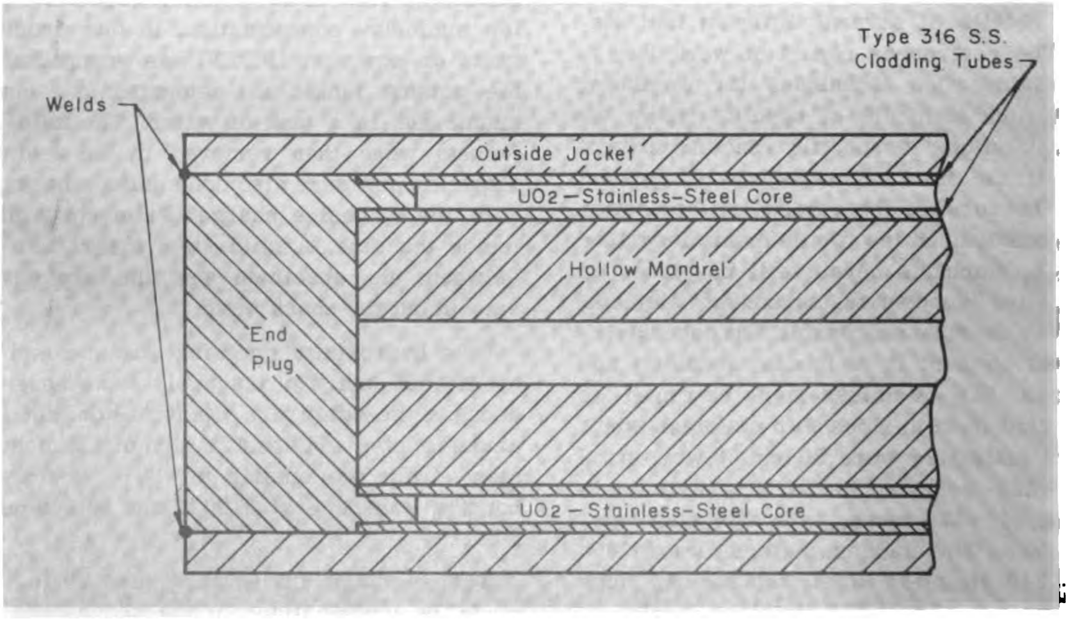

Fig. IV-1 Schematic of assembled specimen for implosive consolidation.[1] Explosive sheet is wrapped around the outside jacket to the desired charge density, and the fuel annulus is densified from the outside in.

Table IV-1 EFFECTS OF FUSED PARTICLE-SIZE VARIATIONS ON VIBRATIONALLY COMPACTED AND PRESSURE-BONDED RODS[2]

Oxide composition			Average density after vibrational compaction, % of theoretical	Results of gas-pressure bonding 3 hr at 2100°F and 10,000 psi			
Amount, wt.%	Type of powder	Mesh size		Rod appearance	Outside diameter, in.	Oxygen/ uranium ratio	Average density, % of theoretical
40	Micronized		64.3	Rods were bowed, and cladding was rough and distorted	Could not be taken	2.007	94.1
60	Fused	−6 +10					
40	Micronized		60.5	Rods were bowed, and cladding was rough and distorted by wrinkling	Could not be taken	2.010	94
40	Fused	−6 +10					
20	Fused	−35 +65					
20	Micronized		73.7	Rods were only slightly bowed and cladding slightly roughened; these were areas where uneven packing was in evidence	0.535 (av.),* rods out of round	2.008	87.7†
60	Fused	−10 +20				2.010	89.0
20	Fused	−35 +65				2.010	86.5
25	Micronized		71.9	Rods were only slightly bowed; cladding was roughened slightly, and there was some evidence of uneven packing	0.536 (av.),* rods out of round	2.006	87.8†
60	Fused	−10 +20				2.006	88.4
15	Fused	−35 +65				2.012	87.4
30	Micronized		66.5	Rods were bowed and badly distorted by wrinkling; there was evidence of uneven packing	Could not be taken	2.008	92.0
50	Fused	−10 +20					
20	Fused	−35 +65					
30	Micronized		70.0	Rods were only slightly bowed, and cladding surfaces were only slightly distorted; there was some wrinkling of the cladding	0.532 (av.), rods slightly out of round	2.002	93.5
70	Fused	−20 +35					
20	Micronized		74.2	Rods retained a high degree of straightness, and cladding was only slightly distorted	0.563 (av.)	2.004	92.4
70	Fused	−20 +35					
10	Fused	−35 +65					
25	Micronized		72.2	Rods retained a high degree of straightness, and cladding was only slightly distorted	0.562 (av.)	2.003	94.3
60	Fused	−20 +35					
15	Fused	−65 +200					

*All oxide materials were contained in 0.563-in.-OD type 304L stainless-steel tubes with a 0.015-in. wall.

†Samples taken at three locations down the length of the rod.

Table IV-2 EFFECTS OF INTERMEDIATE SWAGING ON VIBRATIONALLY COMPACTED AND PRESSURE-BONDED RODS[2]

Oxide composition				Type 304L cladding diameter prior to bonding, in.			Cladding wall thickness, in.	Average density before bonding, % of theoretical			Results of gas-pressure bonding 3 hr at 2100°F and 10,000 psi			
Amount, wt.%	Type of powder	Mesh size	Prefabrication method	Vibratory packed	Cold swaged	Hot swaged		Vibratory packed	Cold swaged	Hot swaged	Rod appearance	Outside diameter, in.	Oxygen/uranium ratio	Average density, % of theoretical
30 70	Micronized Fused	−20 +200	Vibrationally compacted and cold swaged	0.590	0.563		0.007	64.9	71.7		Rods retained straightness, but there was some surface roughness and a wrinkle down entire length of cladding	5.515 (av.) (wrinkled)	2.001	95.4
30 70	Micronized Fused	−35 +65	Vibrationally compacted and cold swaged	0.750	0.575		0.010		81.0		Rods retained straightness, and cladding remained smooth	5.568 (av.)	2.006 2.008 2.004	95.4* 95.1 94.5
30 70	Micronized Fused	−100 +200	Vibrationally compacted and cold swaged	0.750	0.573		0.010	58.0	72.0		Rods remained straight and had smooth surfaces	0.555 (av.)	2.017	96.3
30 70	Micronized Fused	−20	Vibrationally compacted, cold swaged, and hot swaged	0.750		0.570	0.010			84.0	Rods were slightly bowed, but cladding retained a smooth surface	0.547 (av.)	2.014 2.012 2.000	95.6* 96.3 95.3
30 70	Micronized Fused	−65 +100	Vibrationally compacted, cold swaged, and hot swaged	0.750		0.573	0.010			84.6	Rods were slightly bowed, but cladding retained a smooth surface	0.552 (av.)	2.012 2.016 2.004	95.2* 94.5 92.6
30 70	Micronized Fused	−100 +200	Vibrationally compacted, cold swaged, and hot swaged	0.750		0.573	0.010			83.3	Rod retained its straightness and smooth surface	0.550 (av.)	2.002 2.010 2.006	95.6* 95.1 94.3

*Samples taken at three locations down the length of the rod.

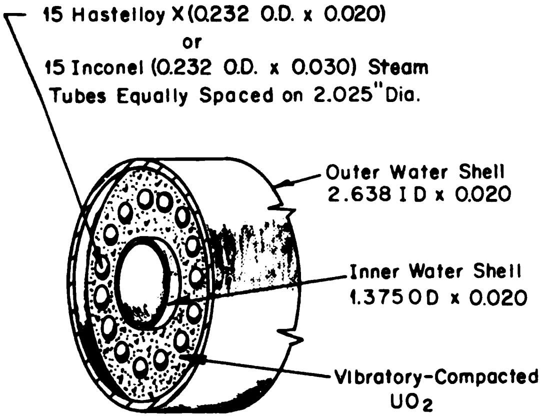
15 Hastelloy X (0.232 O.D. x 0.020)
or
15 Inconel (0.232 O.D. x 0.030) Steam Tubes Equally Spaced on 2.025"Dia.
Outer Water Shell 2.638 I D x 0.020
Inner Water Shell 1.375 O D x 0.020
Vibratory-Compacted UO2

Fig. IV-2 Cross section of an annular multitube element.[5] In the particular application envisioned in Ref. 5, water is boiled on the inner and outer cladding surfaces, and steam is superheated within the steam tubes.

(2) A maximum fused UO_2 particle size of minus 20 plus 35 mesh and uniform bulk densities of 75 per cent of theoretical or greater

(3) A pressure-bonding cycle consisting of pressurizing to approximately 6,000 psi prior to heating to 2100 F and holding for 3 hr at 2100 F and 10,000 psi.

The reference[2] concludes with a discussion of the effect of pressure bonding on the cladding.

Reference 5 describes developmental work leading to the fabrication of an "annular multitube fuel element." A cross section of the element is shown in Fig. IV-2. The element is quite specialized, in that it was designed to be used with an integral boiling-superheating reactor. Fuel elements for steam-cooled reactors have been discussed in *Power Reactor Technology*, 6(2): 75-80. The small tubes serve as flow channels for steam, whereas boiling takes place on the external and internal heat-transfer surfaces of the annulus itself. The element represents the application of vibrational compaction to the fabrication of a fuel element of a relatively complex shape.

The fuel powder used was vacuum-outgassed arc-fused UO_2 having a particle density greater than or equal to 98% of theoretical. Several blends were tried, but the final experiments were done with powder that was 60% $^{8}/_{16}$ mesh, 15% $^{30}/_{100}$ mesh, and 25% 200 mesh. The fuel subassembly ready for loading is shown in Fig. IV-3. Details for the welding of the various tubes into the bottom tube sheet are given in the reference[5] but will not be discussed here. The assembly at the top is not part of the fuel element proper but was utilized to ensure that the steam tubes retained their proper relative positions with respect to each other and to the internal and external cladding tubes. The tension rods (carbon steel) were inserted through the steam tubes and held in tension by tightening the locknuts. The center column absorbed

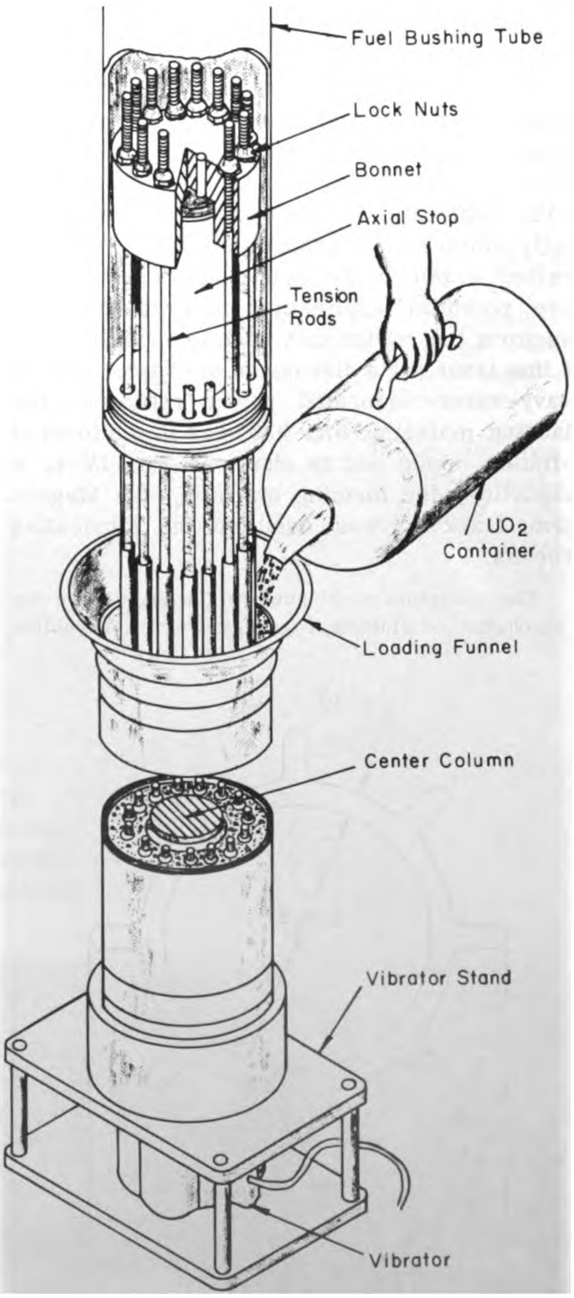

Fig. IV-3 The UO_2 fuel loading of multitube shell subassembly.[5]

the load developed by the tension rods and provided the basis for straightness of the whole subassembly.

The maximum density attained during the compaction step was 84.3% and was accomplished by dividing the fuel charge into eight equal increments. Dimensional inspection indicated that the small tubes were within ±0.030 in. from their intended axes. The ovality of the outside cladding was reduced from about 0.020 in. initially to about 0.010 in. after compaction, and the assembly had a runout of about 0.010 in. along the 36-in. fuel length. The upper end closure of the fuel element is peculiar to the boiling-superheating function and will not be discussed here.

The fabrication of fuel rods clad with Al-Al_2O_3 [sintered aluminum powder (SAP)] is described in Ref. 6. Fuel elements clad with SAP have potential application in organic-cooled reactors; the reader may wish to consult Sec. X of this issue for a discussion of organic-cooled heavy-water-moderated power reactors. The cladding material, SAP 930, was in the form of 8-finned tubing and is shown in Fig. IV-4. A magnetic-pulse forming machine,[6] the Magneform Mark I, was used in the fabrication process.

> The operation of Magneform is based upon the discharge of electrical energy from a capacitor bank through a coil. The collapsing magnetic field causes eddy currents to be induced into a conductive workpiece placed in, around, or near the coil. This results in a repulsive force between the coil and the workpiece due to the interaction of their magnetic fields, in accordance with Lenz's law. Various forming operations are possible depending on the location of the coil with respect to the workpiece. For example, coils may be selected for swaging and expanding of tubular shapes and forming all sheet materials. Coils for magnetic pulse forming must be rigidly constructed to withstand the force equal and opposite to that exerted on the workpiece.

Table IV-3 SPECIFICATIONS FOR MAGNEFORM MARK I MAGNETIC-PULSE FORMING MACHINE[6]

Power consumption	220 volts, 60 cps, single phase, 1500 watts (maximum average)
Maximum energy released per pulse	6000 joules
Maximum input current to work coil	90,000 amp
Maximum pulse rate at maximum power	10/min
Operating-level control	Continuously adjustable
Maximum pressure on workpiece	$\frac{4 \times 10^5}{\text{Work area, sq in.}}$ psi
Time of applied pressure	10 to 100 μsec, depending on coil and workpiece
Work-coil application	Work-coil size
Swaging	4- and 6-in. in inside diameter (with corresponding field shapers)
Expanding	1 in. in outside diameter (minimum)
Flat forming	3- and 6-in.-diameter "pancake" coils

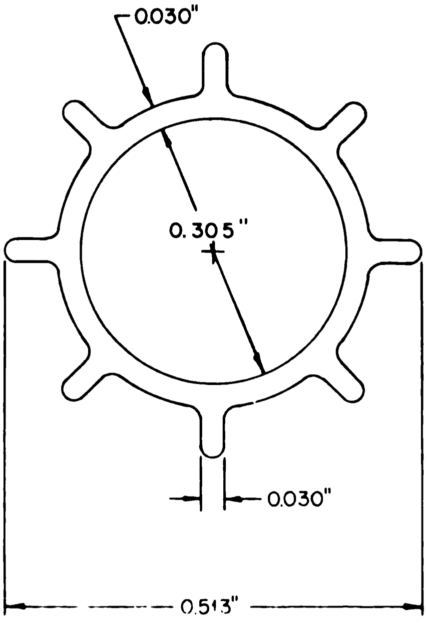

Fig. IV-4 Cross-sectional dimensions of SAP extruded tubing.[6]

The specifications for the machine are given in Table IV-3.

The study of magnetic swaging was initiated to develop techniques for producing fuel rods with cladding-to-fuel contact in order to improve heat transfer between the fuel and cladding. A design of an organic-moderated reactor which is briefly mentioned in the reference specifies a fuel-to-cladding annulus of 0.0015 in. This was stated[6] to be difficult to obtain over the design fueled length of 96 in. because of diametral variations in the components, chipping of the fuel pellets, and internal galling of the cladding. Various techniques were considered for collapsing the cladding onto the pellets, and the magnetic swaging was selected for investigation as the most promising. The swaging reduces the fuel-to-cladding clearance to approximately zero, which should produce a higher gap conductance than the 0.0015-in. annulus, but the reference states that little is known of the overall heat-transfer effect of having no clearance between fuel and cladding.

Table IV-4 SIMULATED FUEL-ROD COMPONENTS[6]

	Rod 1	Rod 2	Rod 3
Pellet material	Stainless steel	Grade A Lavite	Natural UO_2
Pellet diameter, in.	0.300 ± 0.001	$0.300^{+0.001}_{-0.000}$	$0.300^{+0.001}_{-0.000}$
Pellet length, in.	1.000	0.500	0.350
Number of pellets	32	64	90
Pellet column length, in.	32	32	31.5
Tube length, in.	40	40	40

Several simulated fuel rods were fabricated, and dimensional details are given in Table IV-4. Figure IV-5 shows the simulated fuel rod undergoing the swaging step in the Magneform machine. The operation was done at room temperature. Swaging of rods 2 and 3 (Table IV-4) took place in increments of $^3/_8$ in., and swaging was extended about $^1/_2$ in. beyond the ends of each pellet column. Rod 3 was filled with helium, sealed with hot, pressure-bonded aluminum end plugs, and thermal cycled between 350 and 900°F in a vacuum retort. No leaks were detected. The conclusions are as follows:

> It is concluded that magnetic pulse swaging is a feasible method of reducing the fuel-cladding annuli in APM-clad UO_2 fuel rods to essentially zero. Intimate fuel-cladding contact is retained after thermal cycling, and is believed to be a result of tensile hoop stresses remaining in the Magneformed cladding.

Reference 7 gives comparative cost data for various processes used to fabricate fuel elements for the General Electric High Power Density Development Project. This project was discussed in *Power Reactor Technology*, 7(1): 34-42. The processes are as follows:

Pellet Fuel

Ground pellet, cladding-to-pellet gap of 4 to 9 mils
Ground pellet, gap reduced by swaging
Unground pellet, gap reduced by swaging

Compacted Powder Fuel

Two-pass cold-swaged powder
Three-pass cold-swaged powder
Three-pass hot-swaged powder
Tandem-rolled powder
Vibratory-compacted powder

Fabrication flow sheets are shown[7] for the various processes, and Fig. IV-6 illustrates the three-pass swaged-powder fuel method. The fuel-fabrication costs were those associated with the process from the receipt of tubing and fuel, through the fabrication of fuel segments, loading of rods into a fuel assembly, and packing for shipment. The bases for the cost figures are quoted as follows:

> ... Costs are based on actual labor measurements made during semi-production laboratory fabrication of two and three-pass swaged powder fuel and swaged ground and unground pellet fuel. The unmeasured fabrication steps of the tandem rolling and the vibratory compaction processes are estimated based on laboratory fabrication experience.

Table IV-5 shows a breakdown for the labor for the three-pass cold-swaged-powder fuel-fabrication process. Similar tables are given for the other processes. Table IV-6 summarizes the various fuel-fabrication processes and their relative labor requirements. It must be remembered that the cost of direct labor is only a portion of the cost of the final fuel element, even if the fuel rods fabricated by the various processes had identical in-core lifetimes. Besides overhead charges on the direct labor, the cost of amortizing capital equipment must be included. Losses may also be an important cost consideration, and the unit fabrication cost increases with the enrichment of the fuel.[7]

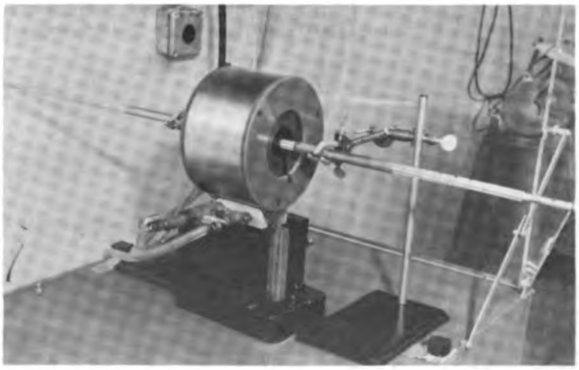

Fig. IV-5 Swaging simulated APM-UO_2 fuel rod.[6]

Interestingly, almost any fabrication process appears to be cheaper labor-wise than assembly of a ground pellet into a clad tube. Whether the less expensive processes can be used, however, depends on their in-reactor performance. One of the objectives of the High Power Density Development Project is to obtain in-pile performance data. Although a large number of fuel assemblies have been classed as failed,[8] the reasons for these failures do not appear to be known and may or may not be related to the various fabrication procedures used.

The remaining reports deal with two fuel-element components, the cladding tubing and the end closures.[9,10] The importance of maintaining cladding integrity in an operating fuel element is obvious. The tubing evaluation program outlined in Ref. 9 had the following objectives:

1. Determine the influence of defects upon tubing burst strengths and thereby define an "acceptable defect." This information is necessary to establish an inspection procedure for tubing quality control.
2. Determine the "expected defect level" of commercial tubing as indicated by ultrasonic testing techniques, thus allowing a correlation between the expected and acceptable defect levels.
3. Determine tubing tensile properties at elevated temperatures and thus provide information applicable to fuel geometries desired for nuclear superheat designs.

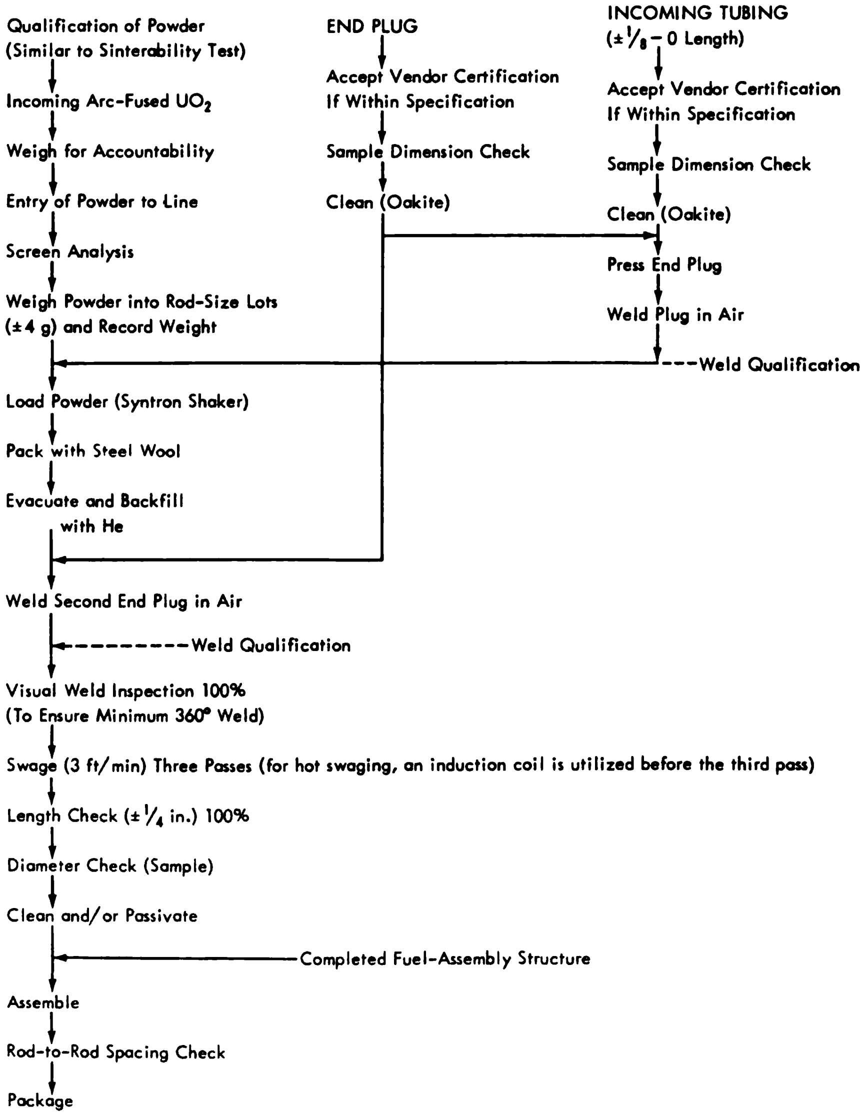
Qualification of Powder (Similar to Sinterability Test)
Incoming Arc-Fused UO₂
Weigh for Accountability
Entry of Powder to Line
Screen Analysis
Weigh Powder into Rod-Size Lots (±4 g) and Record Weight
Load Powder (Syntron Shaker)
Pack with Steel Wool
Evacuate and Backfill with He
Weld Second End Plug in Air
Weld Qualification
Visual Weld Inspection 100% (To Ensure Minimum 360° Weld)
Swage (3 ft/min) Three Passes (for hot swaging, an induction coil is utilized before the third pass)
Length Check (± 1/4 in.) 100%
Diameter Check (Sample)
Clean and/or Passivate
Completed Fuel-Assembly Structure
Assemble
Rod-to-Rod Spacing Check
Package
END PLUG
Accept Vendor Certification If Within Specification
Sample Dimension Check
Clean (Oakite)
INCOMING TUBING (± 1/8 − 0 Length)
Accept Vendor Certification If Within Specification
Sample Dimension Check
Clean (Oakite)
Press End Plug
Weld Plug in Air
Weld Qualification

Fig. IV-6 Three-pass swaged powder fuel.[7]

Table IV-5 LABOR REQUIRED IN FABRICATING THREE-PASS COLD-SWAGED-POWDER FUEL[7]

Process step	Labor man-hours/ pound of uranium
Sample; weigh; crush; screen; weigh for accountability; blend	0.166
Fuel transfer and accountability;	0.020
clean tubing (ultrasonic); cut tube to length; press and weld first end plug	0.101
Load, vibrate, and compact	0.140
Helium backfill; press and weld second end plug	0.104
Swage (3 pass)	0.164
Check diameter and length	0.088
Leak check	0.022
Assemble	0.023
Package	0.024
Total process	0.852

A number of feet of types 304, 316, and 316L stainless-steel tubing were purchased from several manufacturers. The tubes were subject to burst and tensile tests and given ultrasonic inspections. Since the tubing evaluation program was done in support of the Nuclear Superheater Development Effort, the burst and tensile tests were done at about 1300°F. The ultrasonic evaluation was done by the immersion-ultrasonic method using equipment calibrated to detect longitudinally oriented defects on the outer and inner wall surfaces of the tubing. The results of the ultrasonic evaluation are shown in Table IV-7. The conclusions of the study are quoted as follows:[9]

> 1. Tubing defects which are 10 percent of the wall thickness or less do not significantly affect the location of tubing failures induced in a laboratory burst test apparatus. In other words, there is not a direct correspondence between burst test failures and location of tubing defects if the defects are 10 percent or less of the tubing wall thickness.
>
> 2. Artificially defecting tubing to less than 20 percent of the wall thickness does not affect the average burst strength but tends to reduce the minimum in a group of data points. This may be explained by the low probability of coinciding the defect with the weakest portion of the tube.
>
> 3. Defects greater than 20 percent of the tubing wall will cause a reduction in the average ultimate tubing strength with the defect serving as the point of initial failure.
>
> 4. Differences in tubing geometry, temper, and type material appear to have no significant effect upon the quality of the tubing as determined by ultrasonic methods.
>
> 5. The average expected rate of occurrence of defects in commercial tubing is one defect in 22 feet of tubing for those defects greater than 5 percent of the wall, and one defect in 50 feet for those in excess of 10 percent.
>
> 6. In view of the data obtained from this study, a realistic acceptance limit has been established for incoming tubing slated for fuel element fabrication. This limit (defects having a magnitude not greater than 10 percent of the wall thickness) can be used in tubing inspection practices where the ultrasonic technique is recommended. The cost penalty that such a specification may incur is expected to be minimum based on results obtained from a sampling of tubing purchased from representative qualified tube vendors using a variety of in-plant non-destructive testing techniques.

Reference 10 is somewhat specialized, dealing with end-closure development for the superheater fuel rods for the Pathfinder reactor. The Pathfinder reactor is discussed in detail in Sec. VIII of this issue. The report does bring attention to bear on the many details that may be important in producing satisfactory fuel

Table IV-6 RELATIVE LABOR REQUIREMENTS FOR VARIOUS UO_2 FUEL-FABRICATION PROCESSES[7]

Process	Man-hours/lb U	Large core (25,000 lb U), man-hours/lb U*	Very large core (352,000 lb U), man-hours/lb U†
Tandem rolled	0.689	0.459	0.306
Three-pass swaged powder	0.852	0.568	0.379
Three-pass hot swaged powder	0.853	0.569	0.379
Swaged unground pellet	0.972	0.648	0.432
Two-pass swaged powder	0.978	0.652	0.435
Vibratory compacted	1.026	0.684	0.456
Ground pellet with gap	1.106	0.737	0.491
Swaged ground pellet	1.172	0.781	0.521

*A 33% labor and overhead decrease from the value shown in column 2.

†A 33% labor and overhead decrease from the value shown in column 3.

Table IV-7 ULTRASONIC EVALUATION OF STAINLESS-STEEL TUBING—SUMMARY SHEET*

Vendor	Wall thickness, in.	Outside diameter, in.	Type material	Quantity tested, ft	Number of defects: Greater than 5% of wall	Number of defects: Greater than 10% of wall	Defects/ft of tubing
A	0.028	3/4	304L	34	1	1	1/17
A	0.028	3/4	316L	36	1	1	1/18
A	0.028	5/8	304	22	0	0	0/22
A	0.028	5/8	316L	48	2	0	1/24
B	0.028	1 1/4	304L	32	0	0	0/32
A	0.016	3/4	304L	48	1	1	1/24
A	0.016	3/4	316L	42	0	0	0/42
B	0.016	5/8	304	168	8	7	1/11.2
A	0.010	3/4	304	36	1	2	1/12
D	0.010	7/16	304	48	3	1	1/12
C	0.010	3/8	316 annealed	48	0	0	0/48
C	0.010	3/8	316 1/8 hard	36	0	1	1/36
C	0.010	3/8	316 1/4 hard	42	0	0	0/42
C	0.008	3/8	316 annealed	48	1	2	1/16
C	0.008	3/8	316 1/8 hard	18	0	0	0/18
C	0.008	3/8	316 1/4 hard	54	0	0	0/54

rods. The end-cap designs studied are shown in Fig. IV-7. The conclusions are quoted as follows:

1. Design is one of the major considerations for welding components which have large mass differences. Proper attention to heat balance of components at the design stage can mean the difference between a process which is hypercritical to parameter variation and one which provides a practical latitude for production application.

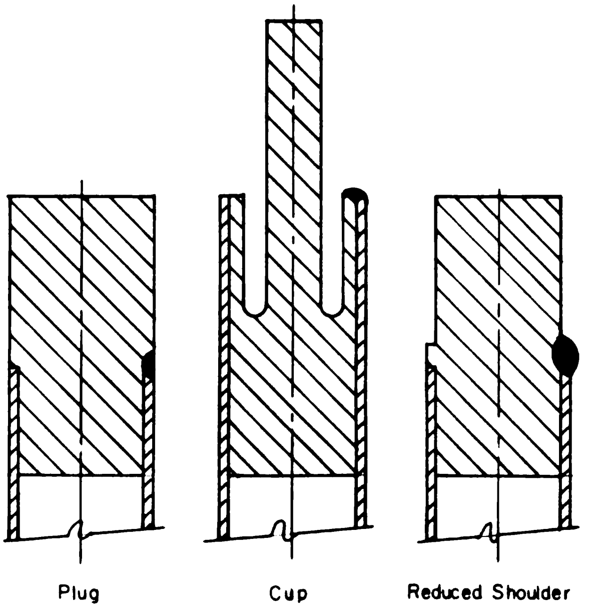

Fig. IV-7 Schematic of modified end caps with improved heat balance.[10]

2. Weld puddle geometry and weld microstructure can be greatly improved with the proper use of chills on the fuel tube. An integral chill which rotates with the tube during welding is the most effective.
3. Entrapped air or gas between the end plug and fuel can cause serious weld defects if heat buildup becomes great during welding. This can be minimized by venting, increasing weld speed or reducing the welding mass by end cap design. The most satisfactory method was found to be a combination of speed and design.
4. Preheat and decay cycles change outer appearances, but do not significantly affect weld penetration in the range studied ... in the case of this material and this geometry.
5. Satisfactory welds can be made on Pathfinder-type fuel rods by using straight plug caps with vent holes, reduced shoulder caps or cup caps. The plug caps, however, are the most sensitive to welding parameters.
6. Both the reduced shoulder and the cup-cap end closures are relatively insensitive to process variations. From a design standpoint the reduced shoulder cap is most desirable for Pathfinder.

References

1. E. S. Hodge, R. J. Carlson, and E. G. Smith, Jr., Investigation of Fabrication Techniques for Tubular Fuel Elements, USAEC Report BMI-1652, Battelle Memorial Institute, Oct. 28, 1963.

2. S. W. Porembka, C. B. Boyer, and J. J. Hauth, Fabrication of UO_2 Fuel Rods by Vibrational Compaction and Pressure Bonding, USAEC Report BMI-1637, Battelle Memorial Institute, June 28, 1963.
3. E. S. Hodge, S. W. Porembka, C. B. Boyer, and R. J. Diersing, Use of Agglomerated UO_2 in Pressure-Bonded Stainless Steel-Clad Fuel Rods, USAEC Report BMI-1640, Battelle Memorial Institute, July 23, 1963.
4. G. R. Cole, Evaluation of Fused UO_2, USAEC Report DP-819, Savannah River Laboratory, April 1963.
5. H. V. Lichtenberger, C. D. Sedlak, and B. E. Murtha, Annular Multitube Fuel Element Design and Development, USAEC Report CEND-187, Combustion Engineering, Inc., Apr. 30, 1963.
6. E. C. Supan, Magnetic Pulse Swaging of APM-UO_2 Fuel Rods, USAEC Report NAA-SR-8263, Atomics International, Sept. 30, 1963.
7. R. B. Hoffman, Economic Comparison of Fuel Fabrication Processes Used in the High Power Density Program, USAEC Report GEAP-4294, General Electric Company, Atomic Power Equipment Department, June 25, 1963.
8. R. L. Holladay (Comp.), High Power Density Development Project Fourteenth Quarterly Progress Report July–September 1963, USAEC Report GEAP-4391, General Electric Company, Atomic Power Equipment Department, Sept. 1, 1963.
9. R. F. Kirby, Evaluation of 300 Series Stainless Steel Tubing for Fuel Cladding, USAEC Report GEAP-4095, General Electric Company, Atomic Power Equipment Department, October 1962.
10. R. A. Boschke and R. J. Wiggins, Pathfinder Atomic Power Plant. End Closure Development for Low Enrichment Superheater Fuel Rods, USAEC Report ACNP-63023, Allis-Chalmers Mfg. Co., July 30, 1963.

Section
V

Power Reactor Technology

Control and Dynamics

Conference on Noise Analysis in Nuclear Systems

By M. F. Valerino

On November 4–6, 1963, a symposium on Noise Analysis in Nuclear Systems was held at the University of Florida, Gainesville. The objectives of the symposium were to define the present state of the art and to stimulate maximum exchange of ideas and information through informal discussions. From the proceedings it was evident that the field of reactor noise analysis has steadily grown to the point that routine noise measurements are now generally accepted as part of power-reactor startup procedures, although the results have not proved to be useful in all cases. Noise measurements have been made as part of the standard operational analyses performed on such power reactors as the Saxton, Savannah, Consolidated Edison, Yankee, and Dresden reactors. From an overall consideration, it was apparent that much exploratory experimentation remains to be done in order to realize the full potentialities of noise-analysis techniques.

Data-handling systems have been developed for rapid acquisition and digitizing of the data for processing with digital computer codes. The use of commercially available electronic analyzers (on-line or off-line in conjunction with the tape-recorded noise fluctuations) have proved to be highly satisfactory in the analysis of the noise data.

The fundamental soundness of noise-analysis techniques, from both the theoretical and experimental points of view, has been amply tested by extensive measurements on numerous zero-power reactors and subcritical assemblies whose dynamic characteristics are thoroughly understood. Hence a firm foundation exists for extension of present noise-analysis techniques to the study and physical interpretations of the variety of noise sources prevalent in reactor power-plant systems. The interacting dynamics of the numerous components of the reactor power-plant system, as ultimately reflected in the reactor through the various reactivity coefficients, result in an extremely complicated behavior of the overall system which, in most cases, cannot be analyzed in terms of the individual physical processes involved. In general, the additional understanding obtained by application of current noise-analysis techniques and interpretations has been more qualitative than quantitative. This limitation reflects the existing limitation on the amount of useful information contained in the noise signals which can presently be extracted and reliably interpreted in terms of system kinetic parameters, however, it has not prevented the acquisition of useful results in a number of important cases. In several instances extrapolation of the results of noise measurements clearly indicated the reactor operating conditions for onset of instability. In the Saxton power reactor, an empirical correlation was obtained between the area under a well-defined resonance in the power spectra and the fraction of the reactor heat-transfer surface over which nucleate boiling is occurring. This unexpected result demonstrates the fact that the full potentialities of noise-measurement results are currently being realized as continued experimentation is under way in the application and further refinement of presently developed methods.

Development work on reactor noise analyses utilizing zero-power reactors and subcritical assemblies is continuing in several important areas. In particular, investigations of spatial effects upon the noise measurements are currently being emphasized, which involve considerations of such basic phenomena as neutron-wave propagation and the associated spatially dependent impulse and transfer functions. Several methods for generating neutron-source driving functions having a random or pseudo-random output are in various stages of practical development for use in noise experiments. A coordinated effort is presently under way to improve on the noise measurements for specific determination of reactor shutdown margin.

The underlying principles of random-noise theory have been formulated on a sound mathematical basis and are well documented in the scientific literature. Applications of the theory have been carried out in the fields of communication engineering, systems analyses, automatic controls, meterology, etc. References 1 through 12 represent a portion of the bibliography on this subject. The recently published book *Reactor Noise*, by J. A. Thie,[1] presents a thorough and concise exposition of the fundamentals of noise analysis and of the important reactor noise experiments performed up to 1962.

A brief review is presented herein of the papers given at the Conference on Noise Analysis in Nuclear Systems. Abstracts of these papers are published in Ref. 13. Prior to the review, the general methods of noise analysis are briefly described to provide background information on the subject. For a comprehensive treatment of noise analysis, reference should be made to the literature, notably Thie's book[1] (and references listed therein) for the specific application to reactors.

Methods of Reactor Noise Analysis

Analysis of a stationary random process is performed by means of various characteristic functions that describe in a statistical manner the regularity of the process. Repeated measurements of a stationary random process under identical conditions would reveal no apparent similarity in the instantaneous variations (wave form) of the random function with time. However, the characteristic functions calculated from the different wave forms would be closely similar (within a statistically defined precision) and hence would reveal that the different wave forms were indeed member functions of the same stationary random process. Two characteristic functions, which have proven to be highly useful in the analysis of random functions, are the autocorrelation function and the power spectral density. These two functions are determinable one from the other. In the case of two stationary random processes that are in some manner related to each other, the comparable characteristic functions calculated from the two wave forms are the cross-correlation function and the cross power spectral density.

AUTO- AND CROSS-CORRELATION FUNCTIONS

Assume that $x(t)$ is some frequency-rich random disturbance in some system variable, such as fission rate, control-rod position, coolant flow rate, coolant inlet temperature, or void density, which is being generated either intrinsically within the system or by some external source. Let $y(t)$ be the observed system response signal, such as neutron level, coolant outlet temperature, or fuel temperature. The autocorrelation function of the measured output signal is defined as

$$C_y(\tau) = \lim_{T \to \infty} \frac{1}{T} \int_{-T/2}^{T/2} y(t)\, y(t+\tau)\, dt \qquad (1)$$

In practice, a finite number of data of total time duration T are treated. The data record is subdivided by N equally spaced discrete points of time interval Δt, where $T = N\,\Delta t$. The lag time τ is then represented by a shift of m points (so as to equal $m\,\Delta t$) up to the maximum lag time $\tau_m = M\,\Delta t$, where $M < N$. It is evident that with this method of treatment the continuous data record is handled in a digitized manner over the finite time T. The expression for the approximation to the autocorrelation function defined in Eq. 1 is hence given as

$$C_y(\tau) = \frac{1}{N - \frac{\tau}{\Delta t}} \sum_{j=1}^{N-\frac{\tau}{\Delta t}} y_j y_j + \frac{\tau}{\Delta t} \qquad (2)$$

The autocorrelation function is a measure of the degree of correlation present in successive values of $y(t)$. If the function is normalized to $C_y(0) = 1$, strong correlation exists between the signal variations occurring at time interval τ apart when $C_y(\tau) \approx 1$. Zero correlation exists when $C_y(\tau) = 0$.

The cross-correlation function of output y on input x is defined in a similar manner as

$$C_{xy} = \lim_{T\to\infty} \frac{1}{T} \int_{-T/2}^{T/2} x(t)\, y(t+\tau)\, dt \qquad (3)$$

In practice, data records of $x(t)$ and $y(t)$ are digitized and the cross-correlation function is obtained in the same way as indicated by Eq. 2 for the autocorrelation function. The cross-correlation function is a measure of the interrelation between two random variables. Figure V-1 is a plot of the cross-correlation function between input-source and output-detector random signals obtained in noise measurements at the University of Florida. The input variations are mainly felt by the detector at a time 1.533 msec later. In this particular application (study of space-dependent kinetics), the lag time is related to the time for neutron-wave propagation between source and detector in the critical assembly. Thie[1] gives other examples of cross correlations which have been obtained from noise measurements, e.g., between reactor power and primary steam flow in the Halden Boiling-Water Reactor.

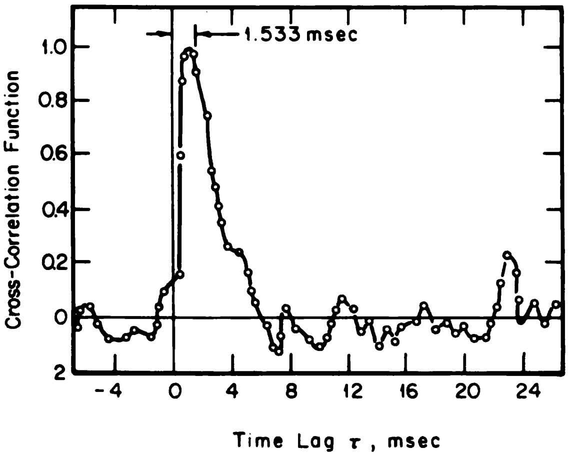

Fig. V-1 Cross correlations between source and detector, with detector located 32.6 cm from source.[19]

POWER SPECTRAL DENSITY

The correlation functions, which are in the time domain, may be Fourier analyzed to obtain corresponding functions in the frequency domain. For the more familiar case of a periodic function $f(t)$, the Fourier representation is given by

$$f(t) = \sum_{n=-\infty}^{\infty} F(n) \exp(jn\omega_1 t) \qquad (4)$$

where ω_1 is the fundamental frequency $2\pi/T$ and $F(n)$ is the complex Fourier amplitude at frequency $n\omega_1$, which is given by

$$F(n) = \frac{1}{T} \int_{-T/2}^{T/2} f(t) \exp(-jn\omega_1 t)\, dt \qquad (5)$$

Here $f(t)$ is simply characterized by a superposition of sine waves at various frequencies $n\omega_1$ with appropriate amplitudes and phase angles given by $F(n)$. If $f(t)$ is considered to be a time-varying current through a unit resistance, it can be shown[1] that the total dissipated power is simply given by

$$P_t = \sum_{n=-\infty}^{\infty} |F(n)|^2 \qquad (6)$$

Here $|F(n)|^2$ represents the square of the magnitude of the Fourier amplitude for frequency $n\omega_1$. A plot of the individual values of $|F(n)|^2$ vs. integer n displays the spectrum of the power, i.e., the frequency-dependent power spectra for $f(t)$.

As opposed to the discrete line-spectral characteristic of periodic functions, continuous frequency distributions are required to represent nonperiodic functions of time, e.g., random-noise functions from which any periodicities present in the fluctuations have been removed. For the random function of time $y(t)$, the Fourier series representation becomes a Fourier integral representation.

$$y(t) = \int_{-\infty}^{\infty} Y(f) \exp(j\omega t)\, df \qquad (7)$$

Here $\omega = 2\pi f$. Equation 7 differs from Eq. 4 only in that the summation over discrete frequencies is replaced by integration over a continuous frequency spectrum.

An extremely useful result is obtained by Fourier analysis of the autocorrelation function.

$$C_y(\tau) = \int_{-\infty}^{\infty} P_y(f) \exp(j\omega\tau)\, df \qquad (8)$$

It has been proved that the Fourier amplitude $P_y(f)$ of the autocorrelation function $C_y(\tau)$ is the frequency-dependent power spectral density of the original random function $y(t)$. This important result is known as Wiener's theorem.[14]

The total power in the random-noise fluctuations (the analogy that $y(t)$ represents a current through a unit resistor is retained throughout) is given by

$$P_t = \int_{-\infty}^{\infty} P_y(f)\, df \qquad (9)$$

A plot of $P_y(f)/P_t$ vs. f gives the normalized power spectral density for the noise fluctuations. Obviously, if the resulting plot is peaked at, say, frequency f_0 over a narrow frequency bandwidth Δf, a resonance is indicated in the system behavior for $f = f_0$.

To evaluate $P_y(f)$ from knowledge of $C_y(\tau)$, the Fourier theorem analogous to Eq. 5 for periodic functions is applied. In this case the relation is

$$P_y(f) = \int_{-\infty}^{\infty} C_y(\tau) \exp(-j\omega\tau)\, d\tau \qquad (10)$$

Note that in the analysis of data by digital methods, the integral is actually approximated as a sum of discrete values. Because of the finite length of the signal analyzed in any practical digital application, the summation is terminated over some finite time interval T. Thie[1] discusses the general effects of these and other analysis approximations on such factors as precision, frequency resolution, and high-frequency cutoff of the calculated results.

Fourier analysis of the cross-correlation function C_{xy} gives similar results; in this case the cross power spectral density $P_{xy}(f)$ is obtained rather than $P_y(f)$ as indicated above for the autocorrelation function. An important difference between $P_y(f)$ and $P_{xy}(f)$ is that $P_{xy}(f)$ is complex and contains important phase information, whereas $P_y(f)$ is real and so actually represents only the magnitude of the power as a function of frequency.

TRANSFER FUNCTION

The transfer function between output $y(t)$ and input $x(t)$ relates the amplitudes and the phase-angle differences of the input and output signals as a function of input-signal frequency. The transfer function can be obtained from noise measurements by application of the cross-correlation technique to the random-noise signals. The result obtained is

$$H(f) = \frac{P_{xy}(f)}{P_x(f)} \qquad (11)$$

where $H(f)$ is the desired transfer function, $P_x(f)$ is the power spectral density of the input noise signal, and $P_{xy}(f)$ is the cross power spectral density.

In the practical application of noise-analysis techniques, the effect on the correlation results of extraneous system noises or disturbances, $n(t)$, must be considered. The sources for $n(t)$ could be instrumentation noise or system noise generated by some unknown driving function. Obviously $n(t)$ affects the observed signal $y(t)$.

If the fluctuations $x(t)$ and $n(t)$, which determine $y(t)$, are completely unrelated so that they are mutually nondependent variations, then the fluctuations $x(t)$ and $n(t)$ are statistically uncorrelated with each other, i.e., $C_{xn}(\tau) = 0$. In this case the input-output cross-correlation function obtained is independent of the presence of the uncorrelated noise $n(t)$ and hence is actually equal to $C_{xy}(\tau)$. As a result, the cross power spectral density $P_{xy}(f)$, and hence the transfer function $H(f)$, does not reflect the existence of the uncorrelated noise $n(t)$.

Generally, it is much easier to measure the power spectral density of the output, $P_y(f)$, rather than the cross power spectral density, $P_{xy}(f)$. For no extraneous noise in the system, the amplitude of the transfer function of the system, $|H(f)|$, is given by the following relation:

$$|H(f)|^2 = \frac{P_y(f)}{P_x(f)} \qquad (12)$$

If, further, $P_x(f)$ is white, i.e., is frequency independent over the range of frequencies of interest, then $\sqrt{P_y(f)}$ is directly proportional to the amplitude of the transfer function.[15]

In the presence of extraneous noise sources, reliable and meaningful interpretation of the noise measurements requires that either the unwanted noise be negligible, i.e., $P_n(f) \ll P_y(f)$, or that the experiment be designed so that the uncorrelated noise component can be determined and accounted for in obtaining the final results. Further, it is important that the frequency response of the instrumentation system be reasonably flat over the range of frequencies of interest in the investigation. The instrumentation frequency response can be measured to thereby permit appropriate corrections for the instrumentation effects.

NOISE SOURCES

In zero-power reactors and subcritical assemblies, two important noise sources are detected,[16,17] namely, (1) the natural statistical fluctuations of the neutron-chain reaction as filtered by the reactor transfer function and (2) the random neutron bombardment of the detector. The first noise source contains information on the reactor transfer function and, accordingly, is referred to as the correlated noise component of the detector output. The second noise source represents an interfering background noise and, accordingly, is referred to as the white- or uncorrelated-noise component of the detector output. To satisfactorily determine the reactor transfer function (and associated reactor characteristics, such as the neutron lifetime and degree of subcriticality), it is necessary to have a high ratio of correlated to white-noise content in the detector output. This ratio is proportional to the detector efficiency ϵ, which is defined as the number of detector pulse counts per reactor fission. For suitable measurements ϵ must be at least 10^{-4} and preferably greater. To meet this requirement the detection chambers are heavily loaded with ^{10}B and are placed within or at the edge of the active core.

In power reactors, additional reactivity noise sources, $\rho_{in}(f)$, are usually present to excite the reactor. These reactivity variations may arise as the result of random fluctuations in coolant temperature, coolant flow, steam-void content, electrical signal actuating the control rods, etc. The neutron detectors in power reactors are generally far removed from the reactor core so that the natural statistical fluctuations of the chain reaction are masked by the white noise. Useful information can be obtained if the noise component at the detector output associated with the random driving function, $\rho_{in}(f)$, is sufficiently large compared to the white-noise component discussed above. Thie[1] obtains an estimate of the order of magnitude of reactivity fluctuations required to observe the correlated-noise component for a typical case. Thie's estimate indicates, for example, that random coolant-temperature fluctuations of the order of 0.1°C, as typically producing about a 0.1-cent reactivity effect, would provide a suitably strong signal at the detector output (above the white-noise component) for observing the spectrum of the reactivity driving function as filtered by the reactor transfer function. In the typically noisy boiling-water reactors, reactivity excitations of the order of 1 cent are obtained from the random steam-void fluctuations.

Recent Work on Noise Analysis

A review of the conference papers follows. Reference is made to the individual papers by using the conference-assigned paper number, which was retained in the abstracts published in Ref. 13.

NOISE MEASUREMENTS IN ZERO-POWER REACTORS

D. H. Bryce[18] described how measurements of neutron-detection probabilities (defined as the probability per unit time of detecting a neutron at time t following detection of an arbitrary neutron at time $t = 0$) were utilized in zero-power experiments on the Cornell University reactor to obtain subcritical calibration of control elements, to measure shutdown margin, and to estimate detector efficiency (and hence reactor power). The measurements were made using a neutron-triggered time-sequenced multiple-scaler system, the output of which permitted construction of a quantity proportional to the neutron-detection probability function. A heavily loaded BF_3 detector was mounted at the periphery of the small-diameter core so as to obtain the high detector efficiency required for reliable interpretation of the measurements. The estimated detector efficiency was about 10^{-2} (believed accurate to within a factor of 2). The measured control-rod worth vs. rod position was found to agree well with results obtained by the inhour method. Good agreement of shutdown margin (10 cents reactivity difference for shutdown of 12.70 dollars) was obtained between the measured results and the results of application of other methods, including consideration of the reactivity worths of the individual control rods. Cohn of Argonne National Laboratory cautioned on the interpretation of the measurement results down to large subcriticalities. In particular, he pointed out that the prompt-neutron generation time, which was assumed constant in the data interpretation, is a function of the magnitude of the shutdown reactivity and that changes in generation time as high as 30% have been calculated for some reactor configurations.

Uhrig[19] described the research program at the University of Florida on noise-analysis techniques, as specifically applied to both critical and subcritical assemblies. This program began about 1957 with attempts to measure the source transfer function, i.e., the output variation of neutron density in a subcritical assembly due to an input variation of neutron-source strength. Mathematically it is readily shown that the frequency-dependent portion of the source transfer function and the frequency-dependent portion of the reactivity transfer function (defined as the output neutron-density variation due to an input reactivity variation) are identical, to a good approximation. For k less than about 0.98, the source transfer function of a subcritical assembly can be represented as

$$\frac{1}{j\omega + \alpha}$$

where

$$\alpha = \frac{1 - k(1 - \beta)}{l}$$

Hence the prompt subcriticality is obtained from the source transfer function if the neutron lifetime, l is known. The ratio β/l can be obtained from reactivity transfer-function measurements performed on the critical assembly; from knowledge of the effective delayed-neutron fraction β, the neutron lifetime is determined.

Uhrig described the details of the power-spectral-density measurements performed in subcritical assemblies. The primary input to the system was the statistical fluctuations in the rate with which neutrons were emitted from the artificial neutron source. The data curves obtained exhibit the shape predicted by theory. Internal consistency between these measurements of $\Delta k/k$ and control-rod calibration was obtained. An absolute comparison was not possible because the reactor would not go critical for the test configuration.

Cross power-spectral-density measurements were carried out in the two-slab critical core of the University of Florida Training Reactor wherein the disturbance input was introduced by a random reactivity generator. The cross power spectral density was measured between the outputs of two ionization chambers located adjacent to the two slabs comprising the reactor core. A mathematical model was formulated for this experimental configuration which includes coupling between the two slabs; the coupling is delayed by a transit time related to the time for neutron-wave propagation between the two slabs. The experimental results support the general features of the proposed model and further show that the frequency dependence of the velocity of the neutron wave must be taken into account.

As a result of the demonstrated importance of the neutron-wave phenomenon, more elaborate experiments were devised to measure the spatially dependent impulse-response function. These measurements were performed on both light- and heavy-water-moderated subcritical assemblies. The results obtained are given in Ref. 20 and are reviewed later. The impulse-response function is proportional to the cross-correlation function between a random input and the output. In these experiments an accelerator type neutron source was used. The input source intensity into the system was of the pseudorandom binary off-on type. Cross correlations were performed between the input source variation and the output neutron flux at several positions in the assembly. Figure V-1 shows the cross-correlation function obtained between the input source and the output of the detector located 32.6 cm above the source in a heavy-water assembly. The peak value of the function is reached in about 1.5 msec, after which it decreases to almost zero and vacillates about the zero value. The reciprocal of the decay constant defining the curve falloff immediately after attainment of the peak value is equal to the effective neutron lifetime. The value indicated by the data curve is in good agreement with the lifetime obtained from pulsed neutron experiments in the same assembly. Present effort at the University of Florida is concentrated on continuation of the theoretical and experimental investigations of the spatially dependent effects.

Kylstra and Uhrig[20] described the results of the measurements of the spatially dependent transfer function between two detectors at different locations in the assembly. For the light-water assembly, reasonable agreement for the amplitude of the transfer function is obtained between the experimental data and a theoretical spatially dependent transfer function which is based on a Fermi-age diffusion-theory point-source model. The measured phase shift was somewhat less than the theoretical phase shift, although the agreement is still reasonable. The transfer function measured in the heavy-water subcritical assembly agrees very well in both amplitude and phase shift with the theoretical model to 250 cps. At that point other effects become important and cause large changes in the measured transfer function. Selfridge[21] described the details of the mechanized data-handling procedures developed for noise analysis at the University of Florida.

The results of reactor noise and other kinetic experiments are frequently interpreted in terms of the simple point-reactor kinetics model utilizing one neutron energy group. Cohn[22] presented derivations of source transfer functions corresponding to more complex models. The primary interest is to determine what effect departures from the simple model would have on the interpretation of noise measurements, in particular, with respect to the determination of the ratio of delayed-neutron fraction to prompt-neutron lifetime. The more complex models considered were (1) a two-group point-reactor model, (2) a two-region reactor model in which fissions may occur in both regions, and (3) a three-region reactor model in which neutrons could pass between the two multiplying regions by way of a nonmultiplying intermediate region only. The application of these models to the fitting of noise data that were available from appropriate zero-power critical assemblies were presented.

Danofsky[23] described the measurements of the cross power-spectral-density function between the neutron outputs of the two fuel regions of the Iowa State University Training Reactor. The measurements were taken with the reactor critical and no external signal input into either region. In the reactor configuration the two slab fuel regions are surrounded with graphite and separated by approximately 18 in. of graphite. An attempt was made to relate the cross power-spectral-density function between the two fuel regions to the power-spectral-density function of the output of one of the regions. In this relation a coupling term is involved which includes the phase shift resulting from the time lag required for a disturbance to travel between the two fuel regions. A non-spatial model was used for theoretical interpretation of the results, although clearly the problem is one of space-dependent kinetics.

SHUTDOWN REACTIVITY MEASUREMENTS

Schultz[24] described how reactor noise measurements can be utilized to determine shutdown reactivity. The principle involved (limited to the high-frequency range of the output signal) is based on these two facts: (1) the frequency dependence of the reactor power fluctuations on input variations of reactivity and neutron-source strength is the same, and (2) the ratio of reactor power fluctuations (or of the magnitudes of the Fourier amplitudes of the neutron-flux noise) obtained at a high frequency to those obtained at a low frequency (but nevertheless in the high-frequency range) is related to the shutdown reactivity. The theoretical relation is obtained from the zero-power transfer function. The theoretical ratios of the amplitudes of the transfer function, corresponding to various combinations of high- and low-frequency values, are plotted in Fig. V-2 (dashed curves) as a function of subcriticality. To check the practical application of noise techniques for shutdown reactivity measurements, power-spectral-density measurements were accomplished on the cold, clean reactor at the Westinghouse Reactor Evaluation Center Critical Experiment Station (CES), Waltz Mill, Pa., for various amounts of shutdown reactivity and for several source, detector, and control-rod configurations. Initial measurement results

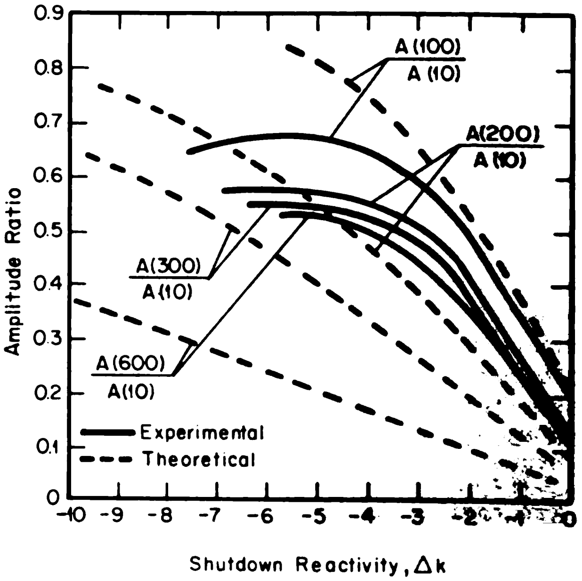

Fig. V-2 Power-spectral-density ratios for various frequency combinations vs. shutdown Δk.[24]

gave extremely poor agreement with the theoretical curves. These results emphasized the importance of decreasing the relative magnitude of the uncorrelated noise in the output signal, particularly if it is desired to infer the shutdown margin from the measurement by use of the theoretical zero-power transfer function. The high level of uncorrelated noise in the system also significantly altered the shape of the experimentally derived curves of amplitude ratio vs. shutdown margin, as compared to the theoretically derived curves.

Uncorrelated noise consists of (1) bombardment noise or counting randomness, (2) neutrons arriving at the detector after such a long distance or after so many interactions that any fission information has been wiped out, and (3) neutrons resulting from (γ, n) reactions that would be uncorrelated with the fission process, as would be the noise arising in the input circuit of the electronic measuring equipment. Because of the small signals generally involved in such measurements, the counting statistics are poor and bombardment noise makes up a large portion of the total uncorrelated noise. In general, detector efficiencies greater than 10^{-4} are required if reactor noise measurements are to be made in the presence of bombardment noise.

Attempts were made to obtain larger useful signals. The solid curves of Fig. V-2 represent the results of measurements taken with the detector in the center of the core. It is seen that the amplitude ratio, $A(100)/A(10)$, closely approximates the theoretical ratio for shutdown reactivities less than about −3%. However, as the magnitude of the shutdown reactivity increased, the amplitude ratios flattened out instead of approaching unity, as indicated by the theory.

In one special set of measurements, wherein two parallel-connected detectors were placed in the center of the core (resulting in a detector efficiency of approximately 10^{-3}), the experimental curves of amplitude ratio vs. shutdown reactivity, as shown in Fig. V-3, are much closer to the theoretical curves. The experimental curves also approached unity as the subcriticality was increased.

In the practical application of the noise techniques to power reactors, the locations at which the detectors can be placed relative to the core are limited so that the attainment of detector efficiencies near the required 10^{-4} value is extremely difficult in any practical installation. The intense fission-product and activation gamma sources prevalent after power operation add to the problem of minimizing the uncorrelated noise relative to the useful fission fluctuation noise.

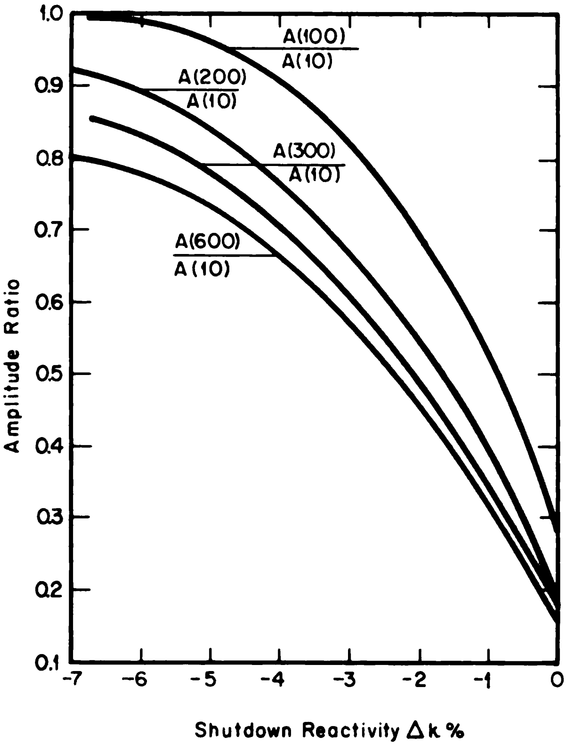

Fig. V-3 Variation of power-spectral-density ratio with Δk, as achieved with two parallel-connected ionization chambers in center of core.[24]

In general, the results presented by Schultz verify the principles involved in the shutdown reactivity measurements and show that even in the presence of a significant amount of uncorrelated noise, a useful reactivity meter might still be derived empirically. This conclusion is illustrated by the experimental results plotted in Fig. V-4, which show that true subcriticality readings were being obtained and that the apparatus was not functioning as a simple counting-rate meter. These results were obtained with the single detector in the center of the core and with the reactor subcritical and later made critical at several different power levels. Once the reactor is critical the amplitude ratio does not change. This characteristic distinguishes the true shutdown reactivity meter from the ordinary counting-rate meter.

The empiricism in the use of a shutdown reactivity meter is introduced by the requirement for a calibration of amplitude ratio vs. shutdown reactivity (as initially measured by other experimental techniques). The calibration curve obtained, which will depend on the geometrical location of the ion chamber in or near the core, is then utilized for future monitoring of the shutdown margin. On the basis of the measurements Schultz concludes that, given a favorable detector location, a relatively simple and inexpensive direct-reading shutdown reactivity meter can be built which will operate down to -5% in shutdown reactivity for a cold, clean reactor.

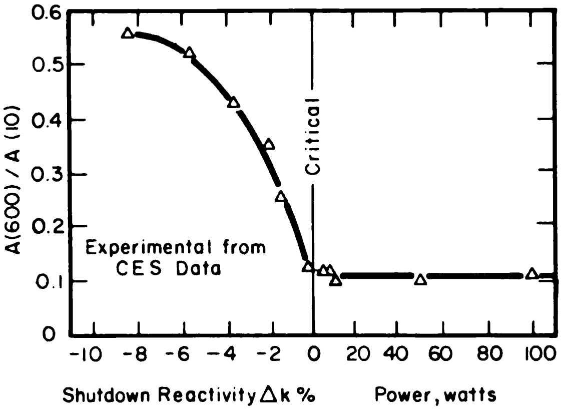

Fig. V-4 Operation of shutdown reactivity meter in subcritical and power ranges.[24]

Ricker et al.,[25] described the research program that was set up at the Oak Ridge National Laboratory (ORNL) in order to (1) obtain a more thorough understanding of the nature of the neutron fluctuations in a shutdown reactor, (2) ascertain the need for specialized instrumentation for spectral-density measurements, and (3) acquire the fundamental information necessary for the development of a practical shutdown margin monitor. In the first phase of the program, the fluctuations in a reactor whose physical characteristics are well understood will be investigated. In the final phase various reactor types under normal operating conditions will be investigated. The first phase of research is presently under way. Negative reactivity determinations will be made by using the spectral-density analyzer at the ORNL Pool Critical Assembly, which has been carefully calibrated by pulsed-neutron and distributed-poison techniques. The required specialized instrumentation for accurate analysis of the fluctuations by the spectral-density techniques is being developed and checked.

NOISE MEASUREMENTS IN POWER REACTORS

Randall and Griffith[26] summarized the noise-measurement and -analysis techniques and equipment developed at Atomics International for reactor parameter determinations and dynamic-stability analyses. The mathematical concepts involved in the determination of transfer functions from power spectra were briefly outlined. Wherever extraneous system noise is excessive, the cross power-spectral-density techniques should be used. It is pointed out, however, that, if the spectral density of the disturbance, $P_n(f)$, is a large portion of $P_y(f)$, then even the cross spectral-density technique (expressed by Eq. 11) is subject to serious statistical errors. An expression is given for estimating the relative confidence limits for the phase and gain components of a transfer-function measurement from a finite sample of data. This expression contains the coherence function, $R^2(f)$, the use of which enables qualitative representation of the noise-to-signal ratio for the system.

$$\frac{P_n(f)}{|H(f)|^2 P_x(f)} = \frac{1-R^2(f)}{R^2(f)} \tag{13}$$

The characteristic frequency modes of importance in reactor systems lie within the span of 10^{-4} to 10^5 cps. Randall and Griffith divide this wide range into three overlapping regions. The first region, from 1 to 10^5 cps, is that in which prompt-neutron lifetime and reactor shutdown margin are generally determined. The second region, from 0.05 to 50 cps, includes the natural frequency modes of nearly all mechanical components and hydraulic parameters, i.e., mechanical vibrations, fuel bowing, pump oscillations, nucleate boiling, gas entrainment, and hydraulic disturbances. The third region, 10^{-4} to 1 cps, is dominated by the time dependence of the temperature coefficients of reactivity, delayed-neutron effects, and xenon instabilities. Randall and Griffith emphasize that specific techniques and equipment must be considered for application in each frequency region. Each region has certain unique technical problems associated with system excitation, data acquisition, data reduction, and interpretation of results. A brief discussion is presented of each of these technical problems, and experimental examples are described to illustrate the differences in the equipment and techniques used in each frequency region.

As an illustration of inherent system excitation which can be utilized, it is pointed out that transfer functions between flow rate and several output variables (power level, coolant outlet temperature, and fuel temperature) were measured on a SNAP-2 power-reactor system wherein inherent random fluctuations in coolant flow rate provided the only system driving function. However, because of the low driving-function strength, other sources of system noise, such as instrumentation noise, severely limited the accuracy of many of these measurements. Hence a strong incentive exists for perturbing the system with an externally generated random disturbance if accurate noise analyses are desired.

Three stages of data acquisition are involved. These are signal detection, conditioning, and recording. Flow diagrams are presented for the data-acquisition systems used in the high- and low-frequency ranges. Data reduction to obtain the desired power spectral densities from the recorded noise signals is accomplished with either analog or digital techniques. Precise analog measurements can be obtained with a wave-analyzer system that normally operates over the frequency range from 4 to 10^4 cps; the frequency range can be extended from 0.0003 to 10^5 cps by use of signal tape recordings with appropriate speed controls for expanding or compressing the time scale of the data to be analyzed. A sample power-spectral-density measurement of high-frequency noise in the range from 10 to 7×10^4 cps is shown for illustration. The relative standard deviation for statistical errors was less than 1%, and the machine accuracy was also of the order of 1%.

For digital-computer analysis of the data, the noise signals are passed through signal-conditioning networks, coupled to an analog-to-digital converter, and sampled in regular time intervals. As a result, the digital results are recorded on magnetic tape to provide the input information for a cross spectral computer code which calculates the gain, phase, and coherence estimates at each frequency.

Ball[27] described the noise measurements performed on three pressurized-water power reactors. The noise studies were primarily motivated by a desire to check experimentally the stability of the nuclear reactor system in the N.S. *Savannah.* However, the available equipment was also utilized for measurements on the Yankee reactor and on the Indian Point reactor of Consolidated Edison. The ion-chamber signals were amplified, filtered through band-pass filters, and used to provide the integral of the absolute value of the noise at selected frequencies. The resultant output power spectral density represents the combination of the reactivity driving function and the reactor transfer function.

Prior to the noise measurements at power, the zero-power transfer function was measured on a group of N.S. *Savannah* elements to confirm the feasibility of the analog method of analysis. In these measurements the spectral reactivity fluctuations are very small so that the transfer function could be easily masked by the white-noise component of the average current. Hence the ion chamber was located in the center of the zero-power assembly. The data follow the expected transfer-function curve very closely, as shown in Fig. V-5, thereby verifying the technique used.

The power spectral densities measured at power operation indicated no tendency toward instability for any of the three power reactors. The source of the broad-band reactivity driving function was not definitely determined, but the most likely cause in each of the reactor systems is the random fluctuation in water-temperature distribution. Experiments on the N.S.

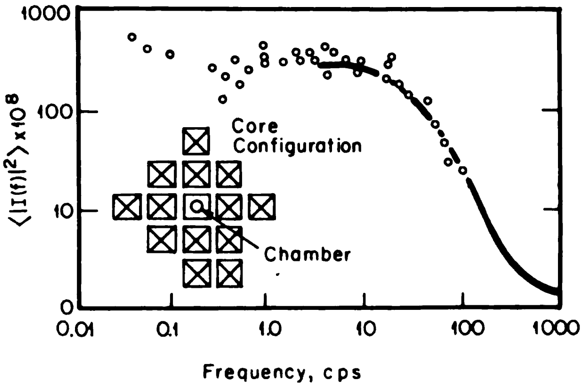

Fig. V-5 Zero-power transfer function obtained from power spectral density.[27] Empirical curve fit, using theoretical form of the functional relation, gives $l/\beta = 0.00394$.

Savannah at 50% power and in a rolling sea (ship gyro stabilizers off) indicated a resonance at the frequency of the ship roll (0.1 cps). The resonance is clearly evident in Fig. V-6, where the product of the spectral density of input reactivity fluctuations and the squared modulus of the reactor transfer function is plotted against frequency. This reactivity driving effect is definitely associated with the side-to-side movement of the control rods ("rod slosh"), occurring in the rolling sea; however, the amplitude of the effect was too small to require any remedial action. In general, no specific application of the information obtained was found insofar as setting operating criteria for these pressurized-water systems. Work at Babcock & Wilcox is presently centered on using the spectral-density change at high powers as an indication of the onset of boiling in pressurized-water systems.

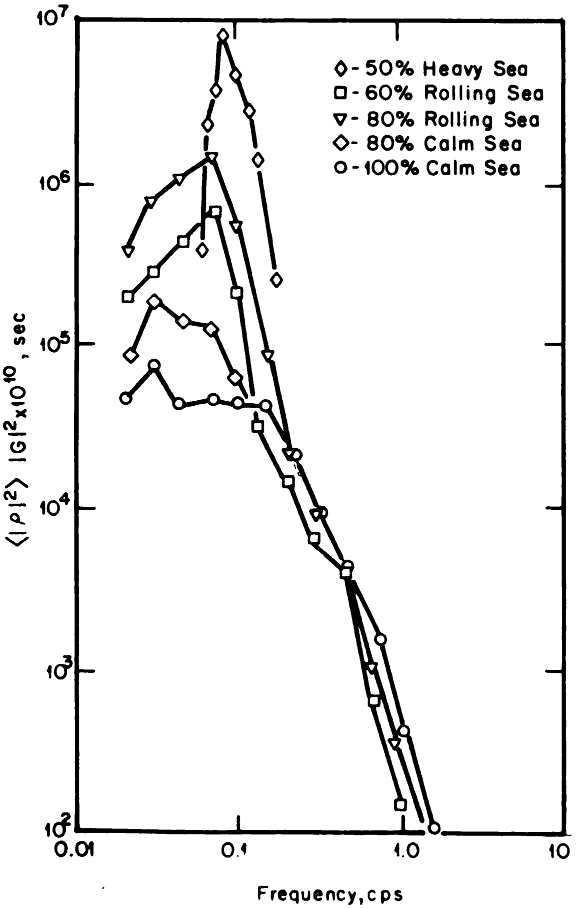

Fig. V-6 N.S. *Savannah* sea trial data showing reactivity driving function as filtered by the reactor transfer function.[27]

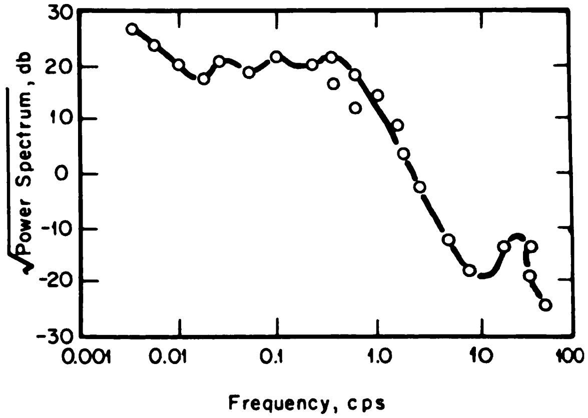

Fig. V-7 Spectrum of nuclear power fluctuations in the Saxton reactor at 20 Mw.[28]

Rajagopal[28] described the noise measurements performed on the Saxton pressurized light-water reactor. The major objectives of the noise studies were to (1) detect nucleate boiling and determine its relation to changes in reactor operating conditions and (2) study the applicability of noise measurements in determining reactor time constants, shutdown reactivity, and any other kinetic parameters.

The primary side of the Saxton reactor is provided with extensive instrumentation, including miniature in-core detectors, instrumented (with cladding thermocouples) fuel rods, Pitot flow tubes at the inlet and outlet nozzles of selected fuel assemblies, and inlet and outlet plenum thermocouples. Standard plant instrumentation, such as the compensated ion chambers and the flow meters, is also available to provide signals for noise measurements. The power spectral and cross power spectral analyses were performed in a commercial electronic spectrum analyzer. Comparison of results obtained from immediately successive measurements demonstrated a surprising degree of resolution and repeatability.

The most interesting results were obtained on the spectral density of the power fluctuations, which exhibit a well-defined resonance between 10 and 20 cps as shown in Fig. V-7. An investigation was therefore conducted to determine the effect on the resonance of reactor power at constant average coolant temperature and of average coolant temperature at constant reactor power. Some of the results obtained are presented in Fig. V-8. Detailed analysis of the resonance at these various reactor operating

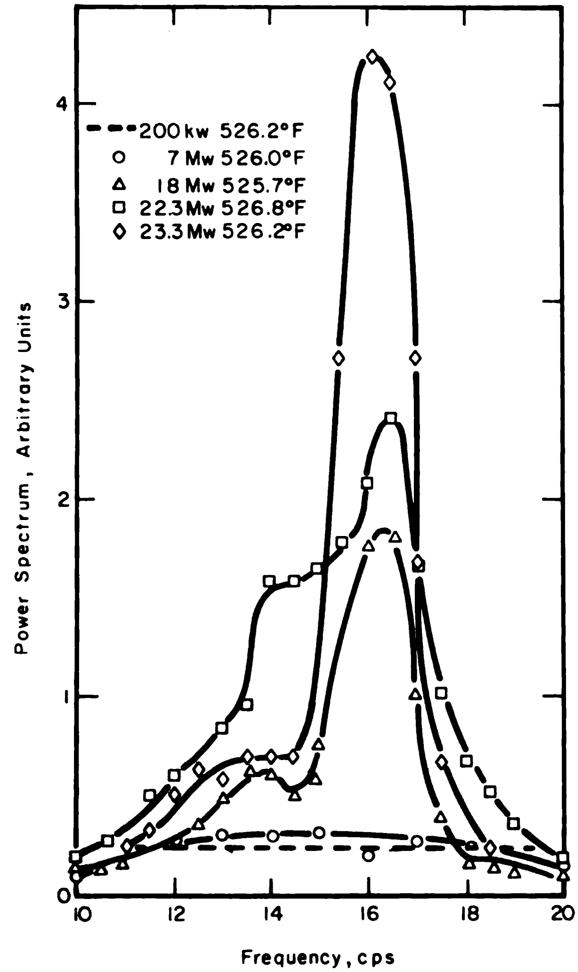

Fig. V-8 Effect of reactor power on resonance present in the power spectrum of the Saxton reactor.[28]

conditions showed that the resonance is related to nucleate boiling. The frequency at which the resonance occurs corresponds to the expected bubble formation and collapse rates at the operating temperature and pressure. In attempts to correlate the measured properties of the resonance with calculations on nucleate boiling, a plot was made of the measured area under the resonance curves vs. the estimated averaged surface area in nucleate boiling (see Fig. V-9). The estimated surface area in nucleate boiling is based on calculations made by an available digital-computer code. The plot shows a linear dependence between the variables. These results indicate that, by power spectral analysis of the fluctuations in nuclear power, it is possible to detect and obtain a relative measure of nucleate boiling occurring in the reactor. In addition to the foregoing analyses, cross power spectral analyses of the various measured signals were performed. It was concluded that significant information and insight as to the dynamic behavior of a power reactor can be obtained by noise analysis.

Pluta[29] summarized the preliminary results of statistical analyses of limited neutron-flux and core-flow noise data taken from the Vallecitos Boiling-Water Reactor. Both digital and Fourier analog analyses of the data were performed; the power-spectral-density functions

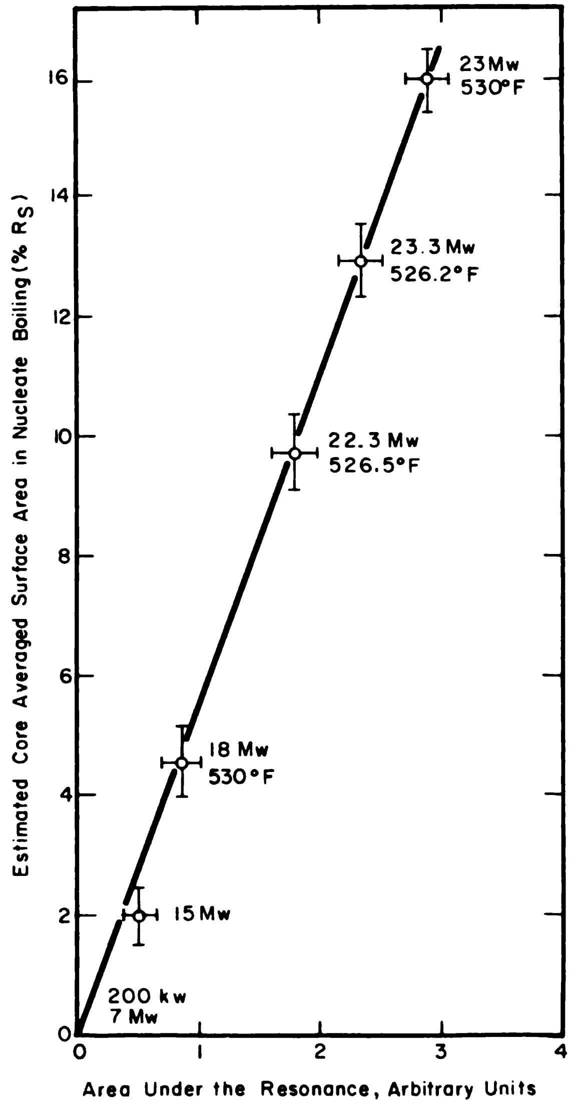

Fig. V-9 Relation between measured resonance and calculated fraction of heat-transfer surface in nucleate boiling for the Saxton reactor.[28]

obtained are in agreement within the statistical confidence associated with the data. Because of the lack of a quantitative model of the reactor kinetic characteristics and the reactivity driving mechanisms, it was not possible to infer the value of a significant system parameter (e.g., the exit steam fraction) from the correlation functions. Hence the results obtained were limited in usefulness.

For the same reactor conditions, measurements were made of (1) the power-spectral-density function of the neutron flux utilizing noise analysis and (2) the closed-loop reactivity-flux transfer function, utilizing a rod oscillator as the reactivity driving function and an in-core ionization chamber for the flux measurements. It had been previously demonstrated that the in-core and out-of-core ionization chambers gave nearly the same noise-analysis results. From the magnitude of the transfer function, $|T(j\omega)|$, and the measured power-spectral-density function of the neutron flux, G, the reactivity driving–power-spectral-density function of the system was determined from the relation $G = |T|^2 G_{\text{driving}}$. The frequency dependence of the reactivity driving function obtained by this procedure is plotted in Fig. V-10. These results demonstrate the fact that the reactivity driving function is not white over the frequency range of interest. Since no techniques are known at this time for predicting G_{driving}, it is not possible to determine $|T|$ from boiling-water reactor-flux noise by means of autocorrelation techniques.

The application of cross-correlation techniques using a known random reactivity function or the classical rod-oscillator experiment is the obvious way to circumvent the lack of a comprehensive theoretical model. The present theoretical background is adequate to justify application of the cross-correlation technique to a boiling-water reactor as a substitute method for obtaining the closed-loop transfer function of the system.

A paper presented by Eurola[30] summarized the reactor noise measurements performed during power operation with the first fuel charge in the Halden Boiling-Water Reactor (HBWR) and described the scope of the noise measurements with the second fuel charge. The HBWR is a D_2O-boiling power reactor, which has been in power operation since October 1960. The primary purpose of the reactor noise measurements was to detect any appearance of substained oscillations in the statistical fluctuations of the neutron flux. In addition, an attempt is being made to utilize these measurements as a tool to get information on the reactor dynamic behavior in the high-frequency range. The measurements conducted during the first fuel charge revealed (1) a kind of hysteresis that made the nuclear power noise and the noise in the differential pressure between the reactor vessel and the primary side of the steam generator behave in two entirely different ways under almost identical reactor conditions and (2) an acoustical oscillation (which was predicted) in the primary steam circuit at a frequency of about 3 cps and with an amplitude reaching 30% of the mean flow. With respect to the measurements with the second fuel charge, the results obtained are still being analyzed so that the information derived to date must be considered tentative. Of particular interest is the plot in Fig. V-11 of the reciprocal mean-square value of the nuclear power noise vs. reactor power. A linear relation is obtained which, when linearly extrapolated to zero ordinate, predicts the instability to be at 16 Mw for the specific conditions of reactor operation.

Boardman[31] described the attempts to analyze the noise from the Dounreay Fast-Breeder Reactor. During a high-power run, recordings were made of the fluctuations in reactor power and in the inlet and outlet coolant temperatures (through plenum thermocouples). The cross-correlation function between reactor power and

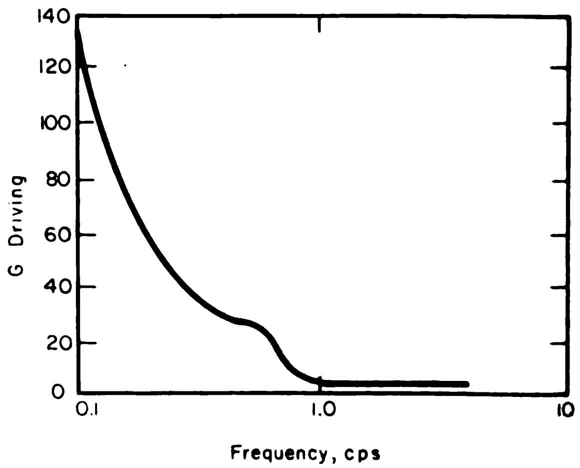

Fig. V-10 Frequency dependence of the reactivity driving function in the Vallecitos Boiling-Water Reactor.[29]

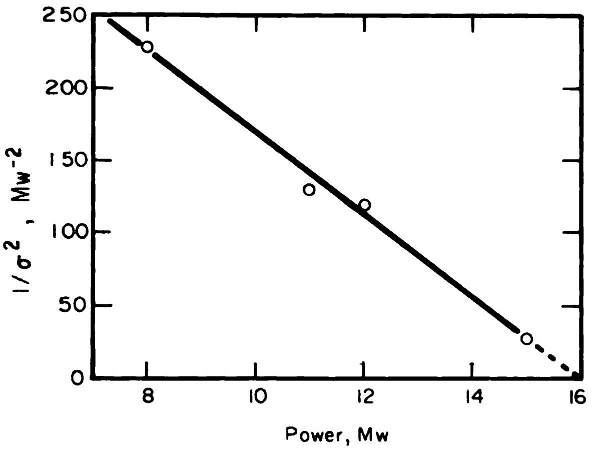

Fig. V-11 Reciprocal of the mean-square value of reactor power noise vs. power level in the Halden Boiling-Water Reactor.[30]

inlet coolant temperature was determined in order to obtain an indication of the mean fraction of the noise in the reactor power which is due to the noise measured by the thermocouple. The very small magnitude of the cross-correlation function indicates that very little of the reactor power fluctuation is actually due to changes in inlet coolant temperature, as measured by the plenum thermocouple. The most significant features of the cross-correlation results are that: (1) the correlation, although small, is positive, thereby implying a positive coefficient of reactivity; and (2) there is no indication of the long-term correlation appearing in the autocorrelation function of the reactor power, which had been previously evaluated. This latter result suggests that the long-term correlation obtained in the autocorrelation function of the reactor power is not due to fluctuations in inlet coolant temperature but rather to some other cause, e.g., reactor operator. On the basis of various reasonable assumptions that were indicated by the overall measurement results, it is suggested that the combined reactivity coefficient of fuel and coolant, α, is about $+5 \times 10^{-6}\,(^\circ\mathrm{C})^{-1}$, as compared with the value of $-1.3 \times 10^{-5}\,(^\circ\mathrm{C})^{-1}$ obtained from oscillator measurements for the combined coefficients averaged over the core. However, because of the approximate nature of the noise-data interpretations, the deduced value of α may have quite a large error. More refined calculations are being carried out. Also, it is recognized that the plenum thermocouple measures only fluctuations in temperature of the coolant in its immediate vicinity and not the average fluctuation over the core.

The possibilities of noise-analysis techniques are discussed in Ref. 31 as: (1) an aid in determining the kinetics of the reactor, e.g., the power feedback mechanism, and (2) an on-line reactor monitor. It is emphasized that much more experience with noise-analysis techniques is required for accurate evaluation and interpretation of reactor noise data of the type obtained on the Dounreay reactor.

A paper by Miida[32] was presented which reviewed the status of noise analysis in nuclear systems in Japan. Considerable activity is under way in research work on noise-analysis techniques and in measurements and analyses of power spectra from operating reactors in Japan. The measurements are directed at obtaining the zero-power transfer function, neutron-generation time, and power spectra of reactors at high power levels for stability information. Combination of the results of noise and pile oscillator measurements performed on a water-boiler reactor revealed that the input noise spectrum had a peak at 0.03 to 0.04 cps; this peak was shown to be associated with the void fluctuations due to radiolytic water decomposition. The results indicated that the void fluctuation noise was nonwhite, i.e., the noise amplitude was sharply peaked at a frequency that was determimed by the void-residence time in the reactor core. Power spectral measurements on a power reactor revealed that the reactor noise increased by a factor of 3 more with coolant flow relative to values without coolant flow. This is mainly due to mechanical vibration of the fuel rods and control rods.

GENERAL INVESTIGATIONS

Osborn and Yip[33] presented a highly theoretical and generalized treatment of the subject of neutron-noise interpretation. The purpose was to develop, from first principles, the theoretical basis underlying the more commonly used phenomenological interpretation of measurements of fluctuations and correlations in neutron distributions. In the reduction of the generally intractable theoretical equations to "working level" equations, which involved the usual "point reactor" approximation, it is demonstrated that the cross sections appearing in the reduced equations differ from those appearing in the commonly used phenomenological equations. Osborn concludes that the effort to deduce kinetic parameters for reactors from measurements on steady-state systems must proceed with caution.

Moore[34] presented a theoretical paper on the general properties of noise fields in a reactor. In the usual point reactor approximation, the random fluctuations of the neutron population are interpreted in terms of the usual lumped-parameter model. In this case the dynamic characteristics are described by means of the transfer function. Moore points out that in a large reactor the transit time across the reactor for disturbances, such as thermal-neutron-wave propagation, becomes important; hence the random fluctuations of the neutron population can no longer be described by lumped-parameter models, and, instead, the fluctuations in neutron density must be regarded as a stochastic function of both space and time, i.e., a noise field. The general mathematical properties of such fields were presented.[34] The space-time autocorrelation function of any field and the cross correlation between two fields were defined. Relations between the correlation functions were obtained which are generalizations of the usual relations for lumped-parameter systems. In the case of a noise field, the spectral relations are characterized by a dispersion function in a manner analogous to the appearance of the transfer function in the lumped-parameter system. The dispersion function essentially describes how a sharp pulse, initiated at time $t = 0$ and at a given point in the medium, is dispersed (i.e., how the pulse peak is attenuated and the pulse width broadened) as its effects are propagated in time and space.

Balcomb[35] presented a summary of the cross-correlation method for measuring system dynamic response. The use of the method was illustrated by various appropriate examples. One example involved the utilization of a Gaussian input signal. The results were carried through to system transfer functions and included examples both with and without extraneous noise. It was demonstrated that excellent results can be obtained using purely random input signals provided the computations are carried to the frequency domain. Included was a discussion of the use of idealized input signals constructed from special pseudorandom binary sequences. The resulting input signal is a binary square-like wave form which has been modified so that the sign in each time interval is chosen at random. Also included was a discussion of the factors involved in the choice of either the digital or analog method for performing the cross-correlation computations. Valat[36] discussed autocorrelation techniques with random source excitation (random square waves, rectangular Poisson pulses) as means of reducing statistical error in highly negative reactivity measurements. Extraction of the desired information from the measurements is, however, difficult. Encouraging experiments are under way. It is emphasized that a high detector efficiency is essential to significant measurements. Mohler[37] discussed the problems involved in the measurement of power spectrum and in the estimation of power spectral density (average power per unit of frequency bandwidth) from noise records. Error analysis and methods for reducing error in measurement were emphasized.

Gyftopoulos and Hooper[38] described some work on the synthesis of test signals for the measurement of kernels in nonlinear systems. A number of periodic signals have been designed which allow the exact measurement of the linear kernel by means of cross-correlation measurements between input and output. The spectrum of the linear kernel is the transfer function of the first-order approximation of the system. Efforts are currently under way to design signals for the measurement of the linear kernel in the presence of the higher order kernels as well as measurement of the higher order kernels themselves. Surdin and Kassimatis[39] considered, in great detail, the problem of measurement of subcritical reactivity using the correlation functions. Several cases of external source modulation were considered, namely, (1) random short pulses of equal amplitude and m zero crossings; (2) short periodic pulses of large constant amplitude; (3) sinusoidally modulated source; (4) large periodic pulses of constant amplitude. The authors conclude that the possible applications of the correlation functions appear to be more extensive than those specifically treated in the paper.

Kemeny and Murgatroyd[40] were primarily concerned with the formulation of stochastic models to represent some of the important physical aspects of nuclear reactor theory. The noise produced in a zero-power reactor is mainly associated with the neutron-fission fluctuations. For analyses of the physical processes related to these neutron-fission fluctuations, it is possible to synthesize the stochastic analog of many of the well-known relations of reactor theory. It was pointed out, however, that the principal source of noise produced in power reactors is associated with mechanical vibrations, flow fluctuations, etc. In this case the input noise is not necessarily Gaussian, and it is not known how this affects the interpretation of the noise-analysis results.

Weaver[41] considered the problem of minimizing the mean-square value of the neutron-noise output of a reactor by appropriate design of the control system. By noise minimization it was felt that an increase in reactor stability would be realized. Albrecht[42] derived, by use of a simple model, the general equations for the variance of the neutron density in systems undergoing transient changes, without solving for the distribution itself. The variance is a measure of the statistical uncertainty (i.e., the spread of the data), which is sufficient information for many excursion and pulsed-neutron experiments.

References

1. J. A. Thie, *Reactor Noise,* Rowman and Littlefield, Inc., New York.
2. R. B. Blackman and J. W. Tukey, *The Measurement of Power Spectra,* Dover Publications, Inc., New York.
3. J. S. Bendat, *Principles & Applications of Random Noise Theory,* John Wiley & Sons, Inc., New York.
4. Y. W. Lee, *Statistical Theory of Communication,* John Wiley & Sons, Inc., New York.
5. L. A. Wainstein and V. P. Zubakov, *Extraction of Signals from Noise,* Prentice-Hall, Inc., Englewood Cliffs, N. J.
6. W. R. Bennett, *Electrical Noise,* McGraw-Hill Book Company, Inc., New York.
7. D. K. C. MacDonald, *Noise and Fluctuations: An Introduction,* John Wiley & Sons, Inc., New York.
8. A. M. Yaglom, *An Introduction to the Theory of Stationary Random Functions* (translated by R. A. Silverman), Prentice-Hall, Inc., Englewood Cliffs, N. J., 1962.
9. E. L. Peterson, *Statistical Analysis and Optimization of Systems,* John Wiley & Sons, Inc., New York.
10. S. H. Crandall and W. D. Mark, *Random Vibration in Mechanical Systems,* Academic Press Inc., New York.
11. A. A. Kharkevich, *Spectra and Analysis,* (translated from Russian), Consultants Bureau, New York, 1960.
12. R. C. Jennison, *Fourier Transforms and Convolutions for the Experimentalist,* Pergamon Press, Inc., New York.
13. *J. Nucl. Energy, Pt. A & B,* 18(1): (1964).
14. N. Wiener, Generalized Harmonic Analysis, *Acta Math.,* 55: 117 (1930).
15. M. N. Moore, The Determination of Reactor Transfer Functions from Measurements at Steady Operation, *Nucl. Sci. Eng.,* 3: 387 (1958).
16. C. E. Cohn, A Simplified Theory of Pile Noise, *Nucl. Sci. Eng.,* 7: 472 (1960).
17. F. de Hoffmann, Statistical Aspects of Pile Theory, *The Science and Engineering of Nuclear Power,* Vol. II, edited by Clark Goodman, Addison-Wesley Publishing Company, Inc., Cambridge, Mass., 1949.

References 18 through 42 are papers presented at the Conference on Noise Analysis in Nuclear Systems; these papers will be published as USAEC Report TID-7679.

18. D. H. Bryce, Measurement of Reactivity and Power Through Neutron Detection Probabilities, Paper No. 1-1.
19. R. E. Uhrig, The Nuclear Noise Research Program at the University of Florida, Paper No. 4-3.
20. C. D. Kylstra and R. E. Uhrig, Measurement of the Spatial Dependent Transfer Function of Nuclear Systems by Noise Analysis, Paper No. 4-1.
21. R. G. Selfridge, Digital Data Reduction in Noise Analysis, Paper No. 4-2.
22. C. E. Cohn, Applicability of Simple Reactor Kinetics to the Interpretation of Reactor Noise Experiments, Paper No. 5-2.
23. R. A. Danofsky, Cross-Power Spectral Measurements in the Two Core University Training Reactor-10, Paper No. 3-3.
24. M. A. Schultz, Shutdown Reactivity Measurements Using Noise Techniques, Paper No. 2-3.
25. C. W. Ricker, D. N. Fry, E. R. Mann, and S. H. Hanauer, Investigation of Negative Reactivity Measurement by Neutron Fluctuation Analysis, Paper No. 2-4.
26. R. L. Randall and C. W. Griffith, Application of Power Spectra to Reactor System Analysis, Paper No. 2-2.
27. R. M. Ball, Noise Results on Yankee, Savannah, and Con Ed Reactors, Paper No. 6-1.
28. V. Rajagopal, Noise Measurements on the Saxton Reactor, Paper No. 6-2.
29. P. R. Pluta, Preliminary Results of VBWR Noise Analysis, Paper No. 6-3.
30. T. Eurola, Reactor Noise Experiments on HBWR (Paper No. unassigned).
31. F. D. Boardman, Noise Measurements in the Dounreay Fast Reactor, Paper No. 6-4.
32. J. Miida, A Review of Noise Analysis in Nuclear Systems in Japan (Paper No. unassigned).

33. R. K. Osborn and S. Yip, The Physical Theory of Noise in Reactors and Reactor-Like Systems, Paper No. 1-2.
34. M. N. Moore, The Noise Field of a Reactor, Paper No. 1-3.
35. J. D. Balcomb, The Crosscorrelation Method of Measuring System Dynamic Response, Paper No. 3-1.
36. J. Valat, Negative Reactivity Measurements Using Random Source Excitation and Autocorrelation Techniques, Paper No. 3-2.
37. R. R. Mohler, Power Spectrum Measurement and the Estimation of Power Spectral Density, Paper No. 2-1.
38. E. P. Gyftopoulos and R. J. Hooper, Signals for Transfer Function Measurements in Nonlinear Systems, Paper No. 3-4.
39. M. Surdin and C. Kassimatis, Some Applications of Correlation Functions to Nuclear Reactor Control, Paper No. 3-5.
40. L. G. Kemeny and W. Murgatroyd, Stochastic Models for Fission Reactors, Paper No. 5-1.
41. L. E. Weaver, Minimization of Reactor Noise Through Minimum Bandwidth Control, Paper No. 5-3.
42. R. W. Albrecht, Statistical Uncertainties in Pulsed Neutron and Excursion Experiments, Paper No. 5-4.

Section VI

Power Reactor Technology

Containment, Radiation Control, and Siting

Vented-Containment Concept for the New Production Reactor

The New Production Reactor (NPR) is a dual-purpose power-plus-plutonium reactor located at Hanford.[1–3] It was briefly discussed in *Power Reactor Technology*, 3(4): 75-76. Reference 1 is a discussion of the containment concept used for the reactor. Although the NPR is a dual-purpose reactor located at a relatively remote site, the technical features of the use of vented containment hold considerable interest for the power-reactor designer.

Table VI-1 MODES OF OPERATION FOR THE NPR[2]

Phase	Products	Period used as basis of design, years
I	Plutonium	2
II	Plutonium and steam	8 or more
III	Steam	Remaining life

The NPR is only one of a number of production reactors located at the Hanford site, and none of the others are contained.[1] The author states that a decision was made to open some land across from the site to farming and that this would make it necessary to provide a containment system that would preclude the spread of radioactive contamination in the event of a failure of the reactor cooling system. Since a total containment sphere would have been several hundred feet in diameter, it was decided that the initial pressure surge resulting

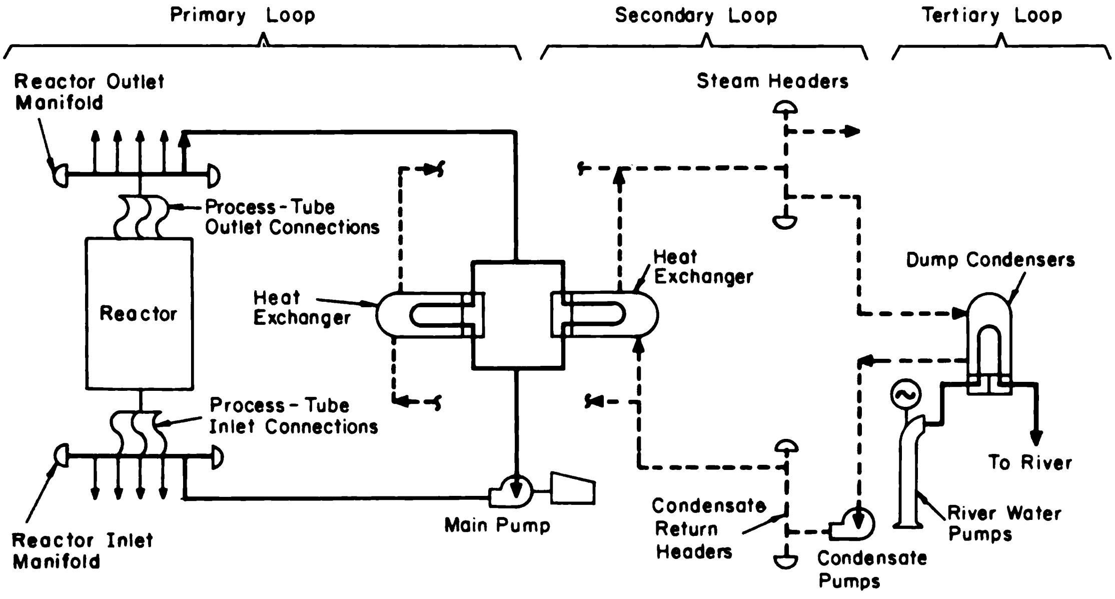

Fig. VI-1 Simplified flow diagram for the NPR.[1]

from a coolant-system failure would be released to the atmosphere. Before release of fission products from the reactor core could occur, a number of pressure-tight valves would be closed to isolate the reactor. The reactor is a pressurized-water-cooled graphite-moderated reactor designed to produce both plutonium and power. The operation of the reactor is divided into phases I, II, and III. The mode of operation during the various phases is shown in Table VI-1. Phase I operation actually will be only for about a year. The NPR was scheduled for final completion[4] in March 1964, and construction of an 800-Mw(e) power plant to utilize the steam is in progress. Completion and operation of the power plant are scheduled for the fall[4] of 1965.

Table VI-2 gives design data on the NPR, and Fig. VI-1 illustrates the simplified NPR flow diagram. The reactor and heat exchangers are arranged in different, adjacent buildings. This is illustrated in Fig. VI-2. The reactor building, pipe gallery, and cells housing individual primary coolant loop components are connected by means of double-hinged flapper-valve type shutters located between the buildings. These shutters ordinarily allow the buildings to maintain their separate identities for ventilation purposes but allow passage of the initial pressure surge in the event of an accident.

The construction material used for the confinement-volume walls, etc. (Fig. VI-2), is reinforced concrete coated with an elastomer.[3] The heat-exchanger cells can withstand an internal pressure of 8 psig. The initial pressure-relief vent valves are located in the pipe-gallery area and in the reactor building. The

Table VI-2 DESIGN DATA FOR THE NPR[2]

Reactor type and size	Pressurized-water-cooled graphite-moderated pressure-tube design; approximate dimensions are 33 by 33 by 39 ft
Pressure tubes	
Material	Zircaloy-2
Number	1004
Inside diameter, in.	2.7
Wall thickness, in.	0.25
Lattice spacing, in.	8 by 9
Controls	
Horizontal rods	87
Vertical ball channels	108
Fuel	
Phases I and II	Metallic uranium, Zircaloy-2 cladding
Phase III	Uranium oxide, Zircaloy-2 cladding
Heat-dissipation plant	
Number of loops	5 in phase I; 6 in phases II and III
Number of evaporators	10 in phase I; 12 in phases II and III
Surface area of each, sq ft	16,000
Dump condensers	16
Capacity, lb/hr	12.6×10^6
Generating plant	
Number of generators	2
Capacity of each, Mw(e)	400 in phase II; 430 in phase III

	Operating phase		
	I (5 loops)	II (6 loops)	III (6 loops)
Design capacity, gross			
Mw(t)			3290
Mw(e)	0	800	860
Operating data			
Bulk coolant temperature, °F			
Reactor inlet/outlet			469/572*
Coolant flow, lb/hr			86×10^6
Steam temperature at evaporation, °F	320	359	435
Steam pressure at evaporation, psia	90	150	375
Steam flow, lb/hr			11.4×10^6

*These numbers are reversed in the reference.

thickness of the pipe-gallery roof was sized to withstand 5 psig. These design values resulted from calculations which indicated that a rupture in one of the cells would cause a pressure drop of 3 psi between the cell wherein the rupture occurred and the gallery. In turn, the vent area provided in the pipe-gallery roof was sized to limit the pressure within to a maximum of 5 psig.

The maximum credible accident postulates a complete fracture of a main coolant line and the escape of the entire volume of primary water without condensing. When the pressure within the confinement area builds up to 1 in. of water, the ventilating supply and discharge valves will be closed by pressure switches, thus sealing the ventilation system. When the pressure rises to 2 in., the pressure switches initiate a fog spray that sprays water in the pipe gallery and the cells. The fog-spray pumps are driven by both electric motors and diesels for maximum reliability. At a pressure of 2 psig, the counterweighted weather hoods on the vent stacks blow off. These stacks are shown in Fig. VI-3. After approximately 300 sec the butterfly valves close automatically, sealing the building and preventing release of any fission products released by fuel meltdown. The fog-spray system starts delivering water about 10 sec after the pressure surge to prevent further pressure buildup within the confined building. This spray system is the only means of preventing excessive pressure buildup.

There are a total of 13 butterfly vent valves (Fig. VI-3), 11 of which are located in the gallery and 2 in the reactor building. The inflatable plastic bag serves as a backup, should the butterfly valve fail to close. A vacuum-breaker system is provided which consists of 4 check valves, 2 in the reactor building and 2 in the heat-exchanger building. These check valves open if the differential pressure exceeds 2 psig.

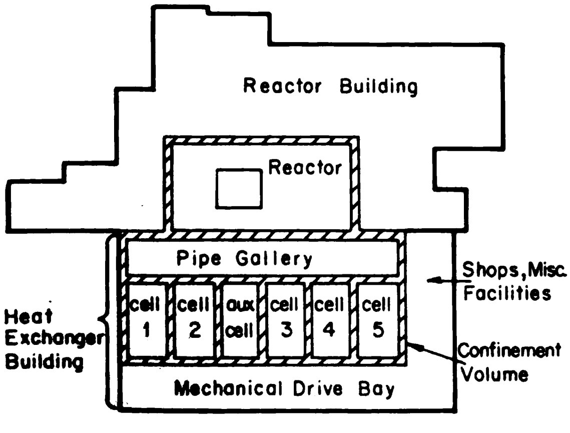

Fig. VI-2 Plan view of reactor and heat-exchanger buildings of the NPR plant.[1]

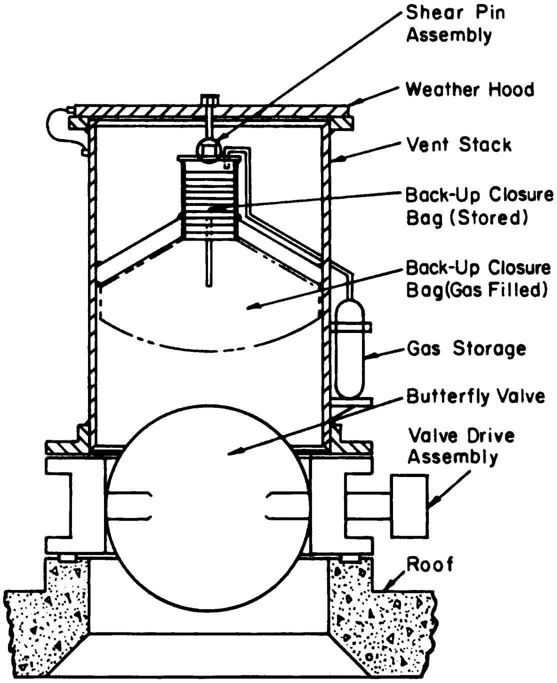

Fig. VI-3 Simplified arrangement of an individual confinement vent-valve assembly.[1]

The whole concept of confinement is tied rather explicitly to an accident wherein no fission products will be liberated during the first 300 sec when the reactor is blowing down. The meltdown of fuel was studied analytically and is reported on in Ref. 3. For the most serious incident studied, a period of 100 sec was available between closure of the building vent valves and potential fission-product release. A containment exhaust system is provided with filters of high particulate efficiency. These would be used after the initial venting and control of building pressure by the fog-spray system. The filtered exhaust air would be released through a 200-ft stack to the atmosphere.

References

1. G. T. Lewis, Jr., The Vented-Containment Concept Used for the New Production Reactor, Paper 63-WA-229 presented at the Winter Annual Meeting of the ASME, November 17–22, 1963.

2. W. J. Dowis, Basis of Design—Hanford New Production Reactor (NPR), USAEC Report HW-SA-2981, Hanford Atomic Products Operation, Apr. 19, 1963.
3. H. S. Davis, D. D. Stepnewski, G. E. Wade, and D. L. Condotta, Fission-Product Confinement for the New Hanford Production Reactor, *Trans. Am. Nucl. Soc.*, 6(1): 118 (June 1963).
4. New Production Reactor, in *Annual Report to Congress of the Atomic Energy Commission for 1963*, p. 46, U. S. Government Printing Office, Washington, January 1964.

Section VII

Components

Power Reactor Technology

Pumps for Liquid Metal

The Lithium-Cooled Reactor Experiment (LCRE) is an outgrowth of the Aircraft Nuclear Propulsion Program (ANP). References 1 and 2 discuss the design of the primary coolant pump[1] and the reflector coolant pump[2] for the LCRE. The two pumps appear to be quite similar, and only the primary coolant pump will be discussed here. The pumps were designed during the ANP program and incorporate design features of a flight type reactor coolant pump for a nuclear aircraft power plant. The "spin-off" of the ANP technology into other areas is an interesting development, although it must be realized that the design of a liquid-metal pump for a central-station power plant might be different from a pump designed for use in flight.

Table VII-1 lists design characteristics of the primary coolant pump, termed the LP-1. Figure VII-1 shows a simplified section of the liquid lithium pump. The design goal of a 10,000-hr operation without maintenance[1] is not a modest one, and it is of interest to note that four LP-1 test units have accumulated a total of 32,254 hr at design conditions. Two of the units have completed their scheduled 10,000-hr test.[1] Whether these were free of maintenance is not specified in the reference.

The major problem in the design of the pump is the sealing system, which is shown schematically in Fig. VII-1. Figure VII-2 shows additional details of the construction of the dynamic seal. The following quotation[1] serves to explain the operation of the seals:

> A major design feature of the LP-1 pump is the sealing system, which is shown on the simplified schematic in Fig. [VII-1]. The objective of the sealing system is to prevent any contamination of the hot liquid metal with oxygen, moisture, or carbonaceous material. Absolute minimum contamination levels are required to assure proper operation of the pump for the design total operating life of 15,000 hours. Primary sealing of the hot lithium is accomplished by establishing a liquid metal to inert gas interface on the rotating vanes of a radial vaned impeller, termed a dynamic seal, which is located on the shaft above the main pump impeller. The

Table VII-1 SUMMARY OF DESIGN CRITERIA FOR LP-1 PRIMARY COOLANT PUMP[1]

Hydraulic criteria	
Type of pump	Single stage, centrifugal
Fluid	Lithium
Fluid temperature, °F	Maximum, 1600; nominal, 1000
Flow rate, gal/min	390 total; 195 per pump
Head rise, ft	115
Design shaft speed, rpm	4500
Pump hydraulic efficiency, %	69
Inlet pressure, psia	36
Design specific speed	1830
Design suction specific speed	1310

Structural criteria
- Operating life: 15,000 hr total; 1000 hr at design conditions
- Material, predominantly niobium–1% zirconium alloy and type 316 stainless steel

Radiation dosage
- 10^8 rads of gamma; 5×10^{14} fast neutrons/cm^2

Maximum allowable design-stress levels for niobium–1% zirconium alloy (forgings and extrusions)
- 15,200 psi for 10,000-hr operation at 1000°F; 5500 psi for 1000-hr operation at 1600°F

Mechanical design criteria
- Design critical speed of pump shaft, 11,850 rpm
- Pump mounting: vertical, with two pumps mounted in a common sump
- Pump-shaft bearing support: single roller bearing at top end, duplex ball thrust bearing at lower end
- Pump-shaft sealing system: centrifugal type of dynamic seal for primary liquid-metal seal; helium sweep-gas flow and mechanical shaft face seals for secondary sealing
- Pump thermal insulation: sealed can filled with zirconium wool type insulation
- Pump lubrication system: forced feed; total flow of 2.2 gal/min of MIL-L-7808D oil
- Dry weights: each pump, excluding motor, 226 lb; sump without pumps, 630 lb

Pump drive-motor design criteria
- Type of drive: two pole, variable frequency, a-c induction motor
- Shaft speed range, 0 to 7200 rpm
- Electrical system: 3 phase; 110 volts at 60 cps; 0 to 120 cps
- Shaft bearing support, single ball bearings at top and lower end
- Drive lubrication system, bearing packed with NRRG 159 grease
- Motor weight, 320 lb

pump discharge pressure is sealed by permitting the liquid metal to partially flood the vaned side of the rotating dynamic seal impeller to a selected radial interface location where a pressure balance is obtained by utilizing the sweep gas pressure above the dynamic seal, as shown in Fig. [VII-1]. At this equilibrium condition, the sum of the sweep gas pressure plus the pressure rise developed in the rotating annulus of liquid on the dynamic seal impeller vanes is equal to the pressure existing at the top of the impeller due to the pump discharge pressure. The helium sweep gas discharges into the sump at essentially the same pressure as that existing at the interface on the dynamic seal, so that a common inlet pressure is sensed by both the dynamic seal and main pump impellers. In this manner, the dynamic seal interface position is insensitive to the pump shaft speed for a given pump throttle setting as both impellers generate a head rise as a common function of the pump shaft speed. The sweep gas exits from the top of the sump through a vapor trap and then through a pressure regulator, which establishes the pressure level in the sump. From the regulator the helium sweep gas is discharged overboard to the atmosphere.

The secondary sealing of the pump is accomplished by the helium sweep gas flow in conjunction with the cermet faced, bellows mounted mechanical shaft face seals. A single, oil cooled, shaft face seal is located at each end of the pump bearing compartment to effectively seal against leakage of oil or inert gas from the lubrication system and prevent contamination of the inert gas blanketed oil system from the ambient air at the top of the shaft. A dry gas cermet shaft face seal is utilized below the lower shaft face seal to form a purge cavity as indicated in Fig. [VII-1]. A flow of about 6 SCFH of helium is introduced into the purge cavity directly above the dry gas face seal and flows upward through a single tooth shaft labyrinth, which produces an effective acceleration of the helium purge gas to prevent the diffusion of oil vapors below the labyrinth. The purge gas and any oil vapor leakage from the oil cooled face seal are swept overboard to an extennal containment vessel. To prevent gross leakage of oil into the liquid metal region in the

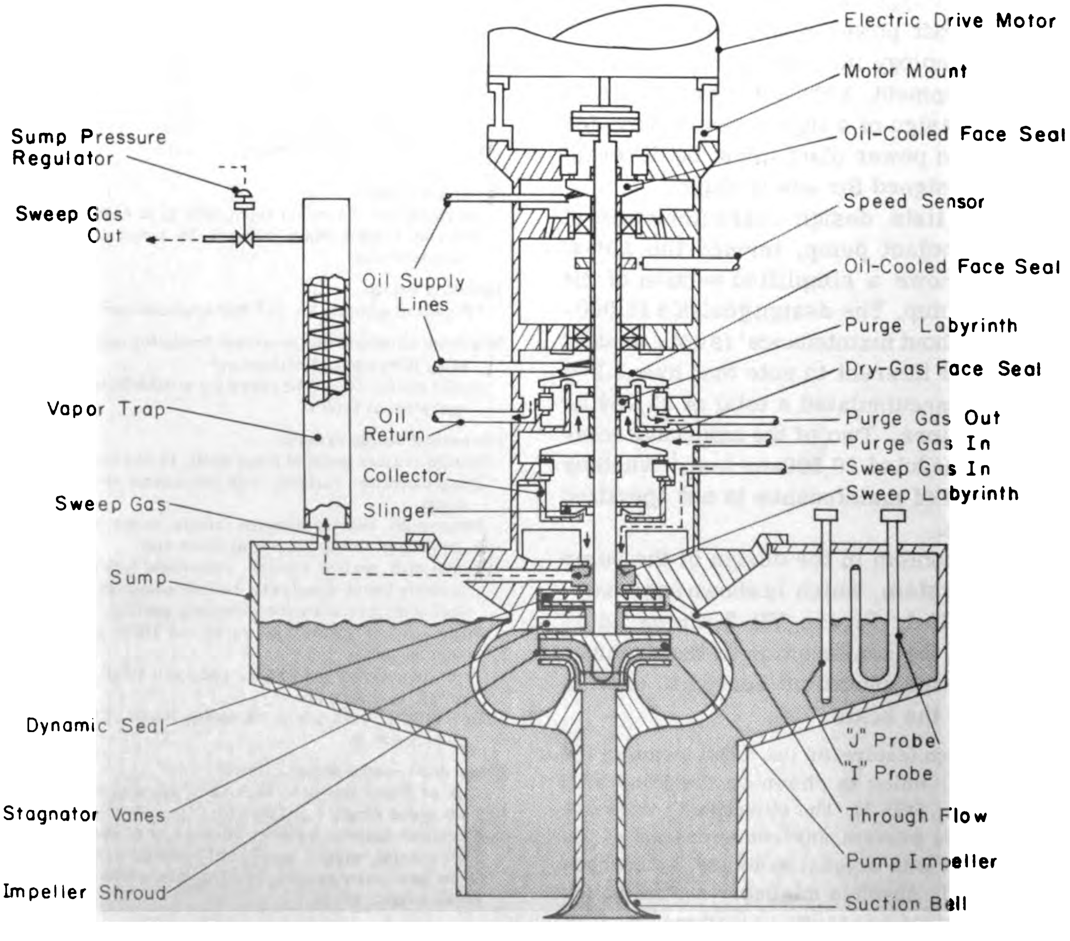

Fig. VII-1 Cross section of the primary coolant pump and sump.[1]

event of a major failure of both lower shaft face seals and the purge gas flow, a secondary dynamic seal, termed a slinger, is installed below the dry gas shaft face seal. The helium sweep gas flow is introduced down the shaft tunnel below the slinger to prevent the diffusion of lithium vapors up the shaft above the single tooth labyrinth shown in Fig. [VII-1]. A sweep gas flow rate of about 25 SCFH is utilized to provide an effective sweep gas velocity through the labyrinth. To prevent the introduction of contaminants into the pump system through the sweep gas circuit, the helium is purified to less than two parts per million of oxygen and two parts per million of moisture contaminants prior to introduction into the pump sealing system.

Two primary pumps are arranged on a common sump, as shown in Fig. VII-3.

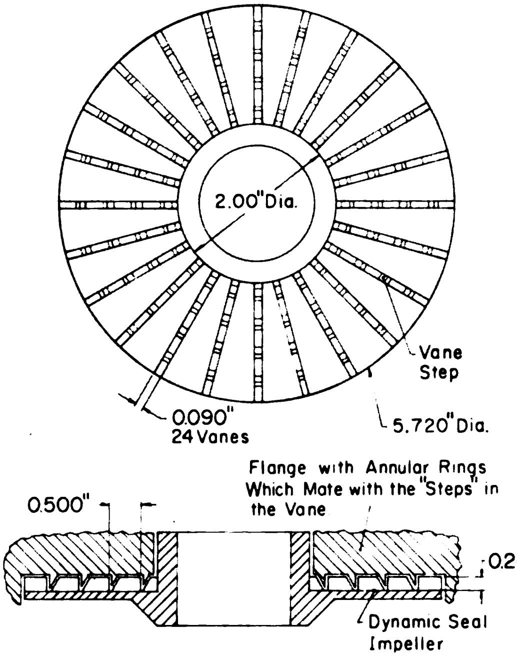

Fig. VII-2 Schematic of the dynamic seal for the primary coolant pump.[1]

Flow Controller for Sodium Service

Reference 3 describes a throttle valve that was constructed for possible use in the primary or secondary systems of a sodium-cooled reactor. The major parts of the controller are the valve body with one entrance and two exit ports, an orifice-closing member or gate, and a torque-tube seal. A cross-sectional view of the valve assembly is shown in Fig. VII-4. Type 304 stainless steel was utilized for the valve parts, and the valve body walls were $^5/_8$ in. thick. The design of the gate was an important feature of the controller. As the gate rotated, the flow area of one of the exit ports was approximately equal to the area of the other port available for flow. A turn from the fully open to the completely closed position required about a 30° rotation of the gate in either direction from the midposition.

The sealing of the valve was accomplished by means of seal welds as shown in Fig. VII-5. The torque tube allowed the drive shaft to turn within the necessary ±30° swing and still provided a positive barrier between the sodium and the helium fill gas. The sodium freeze seal at the top of the drive shaft was used for backup purposes. In case of rupture or damage of the torque tube, the sodium flowing into the small, annular clearance would freeze and seize the drive shaft.

The flow controller was tested with flowing sodium in a test loop at flows to 5000 gal/min in the temperature range from 825 to 1000°F. The two exit orifices were contoured, and the flow rate was shown to be nearly linear with respect to the degree of valve opening. Thermal shocking was done to the flow controller by allowing colder sodium to flow through a hot valve. The valve performed satisfactorily for 500 shocks after some modifications to increase clearances between the gate and the bore. The performance of the torque-tube drive-shaft seal was satisfactory.

Control Rods and Drives

A hydraulic control-rod actuator is described in Ref. 4. This mechanism utilizes reactor primary water as an actuating mechanism and has the design characteristics shown in Table VII-2.

Table VII-2 DESIGN CHARACTERISTICS FOR HYDRAULIC CONTROL-ROD ACTUATOR[4]

Criterion	Design value
Stroke, in.	60
Scram time, maximum, sec	1
Positioning speeds, in./min	6 and 12
Incremental positioning, in./step	1/8
Rod-position indication, in.	±1/8
System environmental pressure, psig	2000
System environmental temperature, °F	500
Maximum outside diameter, in.	14
Design lifting capacity, lb	2300

The operating principle of the hydraulic control-rod actuator is shown in parts *a* through *d* of Fig. VII-6. Part *e* of Fig. VII-6 is a simplified schematic of the actuator.

The supply water for the actuator is furnished by a canned rotor pump at a pressure that is about 125 psi above the reactor pressure. The linear-motion mechanical-transfer coupling is formed by a shaft having spiral keyways of two different pitches, which are in turn coupled to the pistons. The reference[4] compares the action of this shaft and the pistons to that of a "Yankee" screwdriver: "... As the power piston moves upward the shaft rotates, thus the angular position of the shaft is a function of the power piston position. This rotary motion of the shaft is translated back to a linear motion of the servo piston by the 'Yankee' screwdriver action. The ratio of motion between the pistons is approximately 38 to 1 so that a 3-in. motion of the servo piston represents the full stroke of the power piston." Rod withdrawal is accomplished by driving (or stepping) the control sleeve in an up direction. The increase in the pressure beneath the power piston moves it, and (by means of the transfer coupling) the servo piston, in a withdrawal direction. When the control port is again uncovered the proper amount, the motion ceases

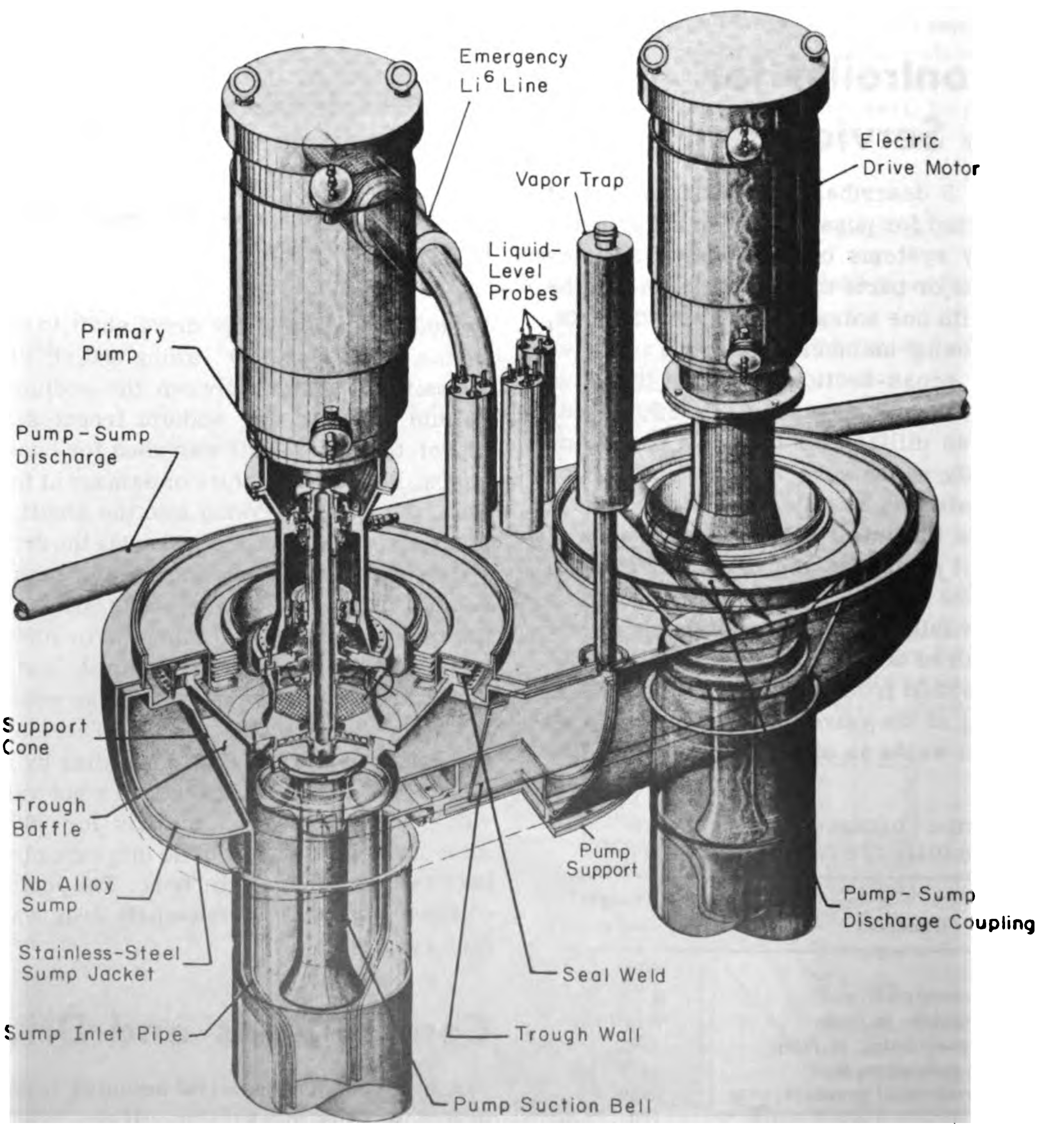

Fig. VII-3 Cutaway illustration of LP-1 pumps and sump.[1]

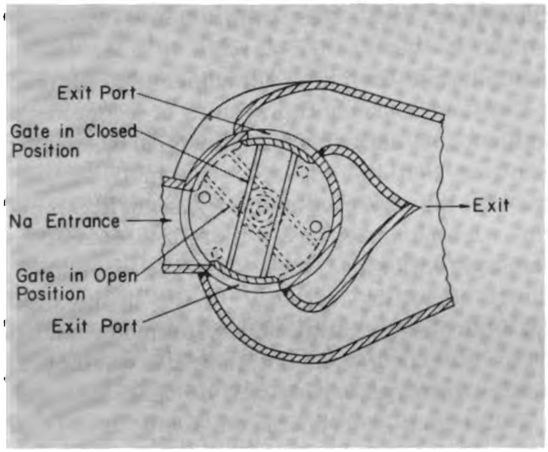

Fig. VII-4 Cross section of the sodium-flow controller valve.[3]

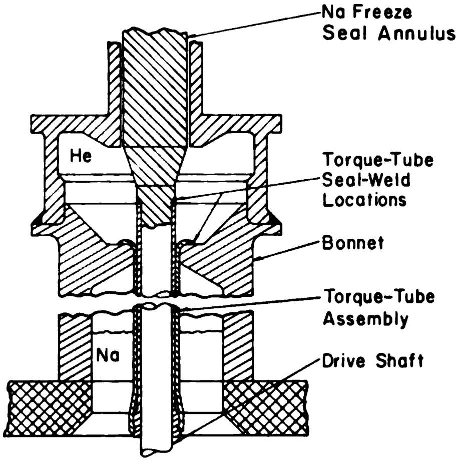

Fig. VII-5 Torque-tube seal and sodium-flow controller valve.[3]

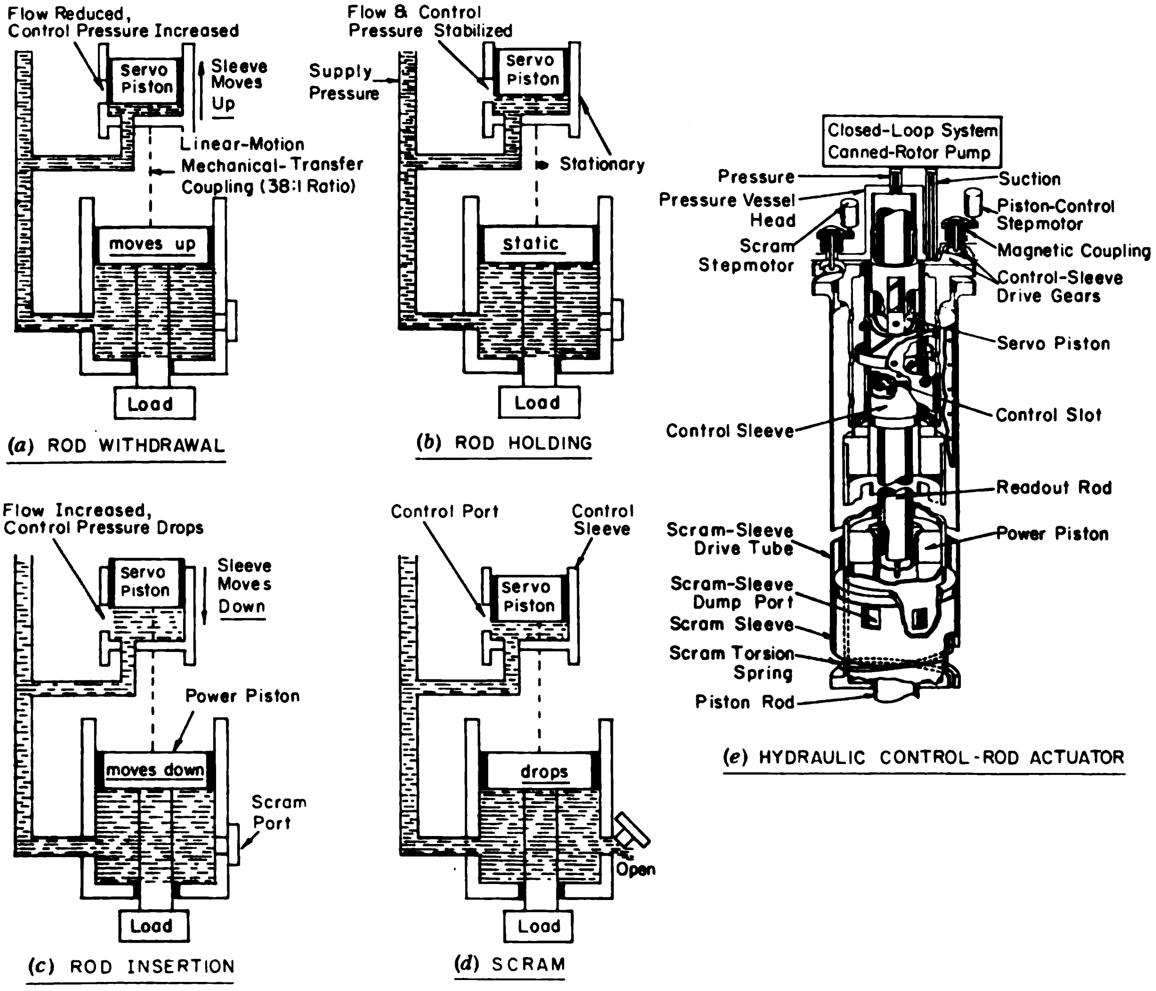

(*a*) ROD WITHDRAWAL

(*b*) ROD HOLDING

(*c*) ROD INSERTION

(*d*) SCRAM

(*e*) HYDRAULIC CONTROL-ROD ACTUATOR

Fig. VII-6 Schematic diagram of the hydraulic control-rod actuator and illustrations of its operating principles.[4]

and the rod is held in a fixed position. The rod is inserted by reversing the initial direction of motion of the control sleeve. Scram is accomplished by opening the scram ports and allowing the water to drain away.

All signals in and out of the mechanism are transmitted by magnetic couplings so that no seals are required between the reactor water and the exterior. Scram is accomplished by any one of the following operations:

—deenergizing the magnetic clutches
—interrupting all electric power
—shutting off the hydraulic supply

In the first two scram options, the magnetic clutch disconnects the scram stepmotor from the scram sleeve-drive gears, and the scram torsion spring rotates the scram sleeve until the scram ports are uncovered. This results in the action shown in part *d* of Fig. VII-6. No controls are moved for the last scram option, and scram occurs at about one-half the normal rate. When pressure is restored, the control rod moves to its original position. A prototype mechanism was built and operated to demonstrate proof of principle.

Reference 5 describes a pressure-balanced control rod, designed originally for the Experimental Organic-Cooled Reactor (EOCR). The reference is an analytical study only and does not describe any hardware. The particular control rod studied employed a fueled follower, and it is this feature which makes a pressure-balanced rod particularly important. If the coolant-flow direction normally is opposite to the direction of rod-fuel motion for scram, then the attainment of an acceptable scram time may be difficult owing to the resistance of passage of the assembly through the relatively rapidly flowing water. The solution offered in Ref. 5 can be explained by study of Fig. VII-7. During normal operation the absorbing section is raised out of the core, and its place is taken by fuel. Coolant enters the side of the lower boot through the slots and flows into an annular passage sealed from the exterior of the element by the rubbing shoes. The coolant then flows through an orifice and into the movable lower plenum; from there it cools the fuel element, exiting at the top into an upper plenum. Since the lower end of the lower plenum is sealed, there is no need for the element to force its way through rapidly moving coolant in the event of a scram.

In the event of scram, the movable assembly displaces the water trapped between itself and the lower boot. This water flows in the paths shown by the dashed arrows in Fig. VII-7 and exits above the top of the upper grid plate. The reference contains the results of a considerable amount of mathematical study of the system, showing that the movable assembly should behave in the expected manner. It would seem that the rubbing shoes are a most important part of the system, since they keep the coolant from short-circuiting directly to the upper plenum for both the operating and scrammed conditions. The reference does not indicate whether full-scale prototype testing will be undertaken.

Reference 6 reports on tests done with a control-rod-drive prototype for the Pathfinder power reactor. The drive system uses a rack-

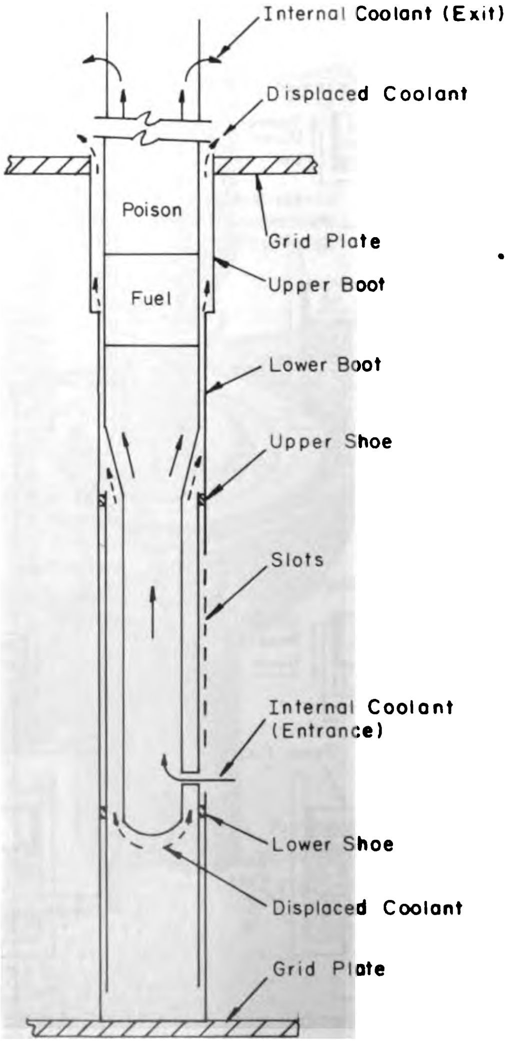

Fig. VII-7 Flow paths for internal coolant and displaced coolant during a scram.[5]

and-pinion drive, and it was designed to operate in a pool of shielding water. The Pathfinder plant is discussed in Sec. VIII of this issue of *Power Reactor Technology*. The installation contains an interesting mechanism to prevent the formation of a void in the rack housing due to rapid removal of the rack during a scram. This mechanism consists of a steam line from the reactor to the upper end of the rack housing; as steam flows through this line during a scram, it is condensed by the relatively cooler shield water. To prevent a convection path from being set up during normal operation, a spring-loaded piston type accumulator is provided near the top of the rack housing. The reference contains the results of a number of tests performed on the rod-drive prototype to demonstrate satisfactory performance under all operating conditions.

References

1. C. Ferguson, L. K. Knudsen, R. P. Lamers, B. R. Lucas, D. V. Manfredi, and H. P. Odom, Design Summary Report of LCRE Primary Coolant Pumps and Sump, USAEC Report PWAC-383, Pratt & Whitney Aircraft Division, United Aircraft Corp., Nov. 22, 1963.
2. C. Ferguson, L. K. Knudsen, R. P. Lamers, B. R. Lucas, D. V. Manfredi, and H. P. Odom, Design Summary Report of LCRE Reflector Coolant Pumps and Sump, USAEC Report PWAC-384, Pratt & Whitney Aircraft Division, United Aircraft Corp., Dec. 6, 1963.
3. R. A. Winborne, Flow Controller Evaluation for Sodium Service, USAEC Report NAA-SR-7534, Atomics International, Nov. 30, 1963.
4. F. C. Legler and R. B. Hussey, A New Hydraulic Control-Rod Actuator for Nuclear-Reactor Power Plants, ASME Paper 63WA88, 1963.
5. F. K. Clements, A. D. Kartchner, R. S. Kerr, and W. B. Lewis, Design of a Pressure Balanced Control Rod, *Nucl. Sci. Eng.*, 18(2): 200 (February 1964).
6. J. Patterson, E. Duewel, R. Kern, M. Jury, R. Grenda, A. McIlheran, and M. McDermott, Control Rod Drive Prototype Test Report, USAEC Report ACNP-63018, Allis-Chalmers Mfg. Co., Oct. 25, 1963.

Section

VIII

Power Reactor Technology

Design and Construction Practice: Pathfinder and BONUS

By Walter Mitchell III

Introduction

The Nuclear Superheat Program of the U. S. Atomic Energy Commission includes the construction of two central-station power reactors, the Pathfinder reactor near Sioux Falls, S. D., and the Boiling Nuclear Superheater (BONUS) reactor at Punta Higuera, P. R. These two reactors are in the process of startup at this writing. If they fulfill expectations, they will establish the feasibility of generating high-temperature steam in water-cooled water-moderated reactors. Since water-reactor technology has so far shown economic promise in the United States, the development of nuclear superheat reactors may have important consequences.

The design approaches to many of the problems of nuclear superheat are different in the two reactors. The designs are described here, in a single review, because their diversity itself serves to illuminate the problems and relations of nuclear superheat. The major part of the review is devoted to summaries of the two designs. A brief discussion of the two in relation to the development of nuclear superheat is given at the end, but any critical comparison given before the establishment of the operating characteristics would be premature.

Pathfinder Atomic Power Plant

The integral nuclear superheat reactor of the Pathfinder Atomic Power Plant[1,2] reached criticality in March 1964. The evolution of the plant type and the administrative organization of the project were described in *Power Reactor Technology*, 2(3): 51; hence the emphasis in this article is on design features and operating parameters. The plant, which is located near Sioux Falls, S. D., was designed and constructed by the Allis-Chalmers Mfg. Co. for the owners and operators, the Northern States Power Co. of Minneapolis, Minn. Architect and engineering services for the project were provided by the Pioneer Service and Engineering Co. of Chicago.

Although a bulk-steam exit temperature of 825°F from the superheater is specified for the reference design, this temperature cannot be realized with the first-core loading. The basis for design of the first core is a 725°F bulk-steam exit temperature from the superheater, and the safeguards report for the plant, as well as the following discussion, is based on the lower value.

The two-region core of the heterogeneous, boiling-water type reactor contains a central superheater region that is surrounded by an annular boiler region. Superheated steam from the reactor is passed directly to a condensing steam turbine, and feedwater from the condensate system is mixed with the boiler recirculated water. Forced, controlled recirculation of water through the boiler region is accomplished by pumps and piping located outside the reactor vessel. The stainless-steel-clad superheater fuel elements contain highly enriched uranium dioxide in a stainless-steel cermet, whereas the Zircaloy-2-clad boiler elements are fueled with slightly enriched uranium dioxide. The steam-generating portion of the plant is housed in a vertical, cylindrical containment vessel, and the power-conversion equipment is located in an adjoining building.

A simplified flow diagram of the plant is given in Fig. VIII-1, and the principal characteristics are listed as follows:

Power, boiler region, kw	157,400
Power, superheater region, kw	31,500
Total core power, kw	188,900

Gross electrical capability, kw	62,500
Gross heat rate, Btu/kw-hr	10,780
Net electrical output, kw	58,500
Net efficiency, %	31
Steam outlet pressure, psig	535
Reactor operating pressure, psig	600
Temperature, boiler region, °F	489
Outlet temperature, superheater region, °F	725
Reactor steam flow at rated power (approximate), lb/hr	616,125
Recirculation rate, gal/min	65,000
Containment vessel size, ft	50 (dia.) by 120
Reactor vessel size, ft	11.5 (OD) by 31.5
Overall core dimensions, height and diameter, ft	6 by 6
Dimensions of superheater region, height and diameter, ft–in.	6 by 30
Fuel, boiler region (Zircaloy-clad)	2.2% enriched UO_2
Fuel, superheater region (S.S.-clad)	93% enriched UO_2–S.S. cermet
Fuel loading, boiler region, kg ^{235}U	144.3
Fuel loading superheater region, kg ^{235}U	50.0
Average heat flux, boiler region, Btu/(hr)(sq ft)	122,000
Average heat flux, superheater region, Btu/(hr)(sq ft)	59,100
Maximum heat flux, boiler region, Btu/(hr)(sq ft)	447,000
Maximum heat flux, superheater region, Btu/(hr)(sq ft)	219,000
Neutron flux, approximate, neutrons/(cm^2)(sec)	3.5×10^{13}

General Reactor Features

The reactor vessel and its internals, the recirculation loops, and the control-rod drives constitute the reactor system. Figure VIII-2, a vertical section through the reactor vessel, shows the arrangement of internal components of the vessel, the mounting position for the control-rod drives, and the connecting points at the vessel for feedwater piping, recirculation water piping, and the main steam line. As shown in the figure, recirculation water enters the reactor vessel at its bottom and flows upward through the annular boiler region. Most of the steam formed in the boiler region continues to flow upward in the pressure vessel and is separated from the water at the steam-water interface located above the active core. The water and some entrained steam flow into steam separators that are located in the annular space between the boiler core and the pressure-vessel wall. The entrained steam is separated from the water, and the water then flows down through the downcomer annulus to the lower portion of the pressure vessel. The steam flows upward into the steam dome, passes through the steam dryer, flows down through the superheater region, and flows out the bottom of the reactor

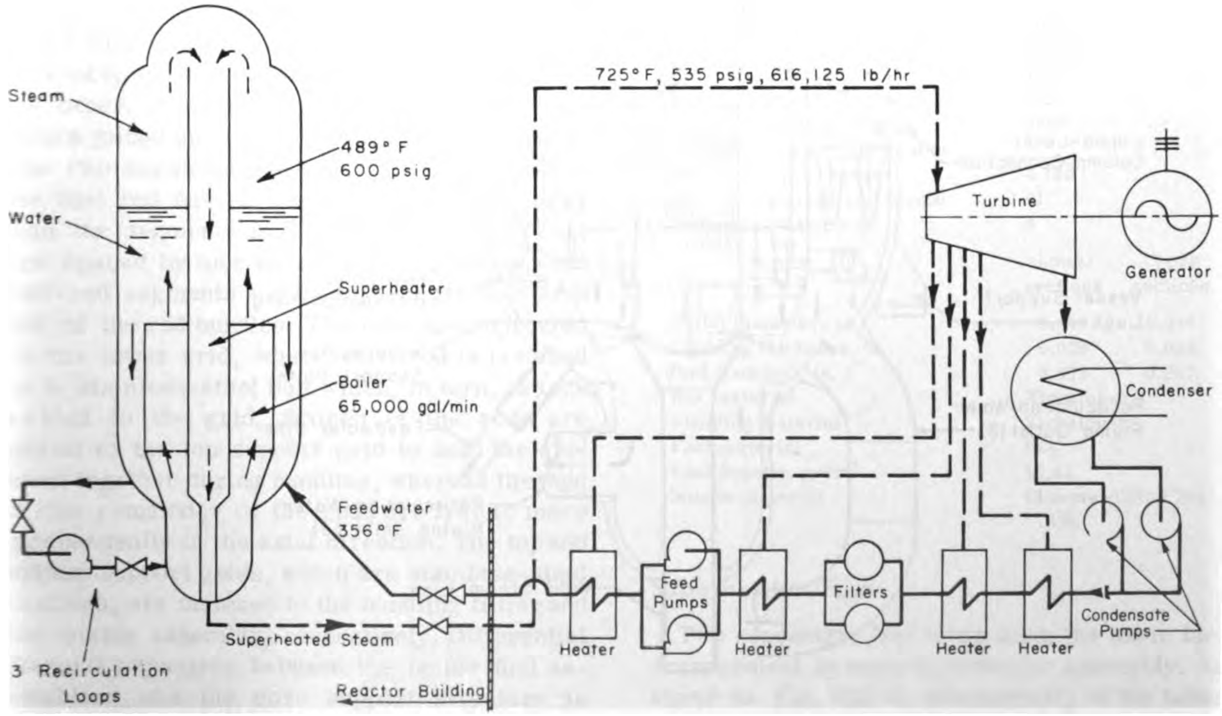

Fig. VIII-1 Simplified flow diagram of the Pathfinder Atomic Power Plant.

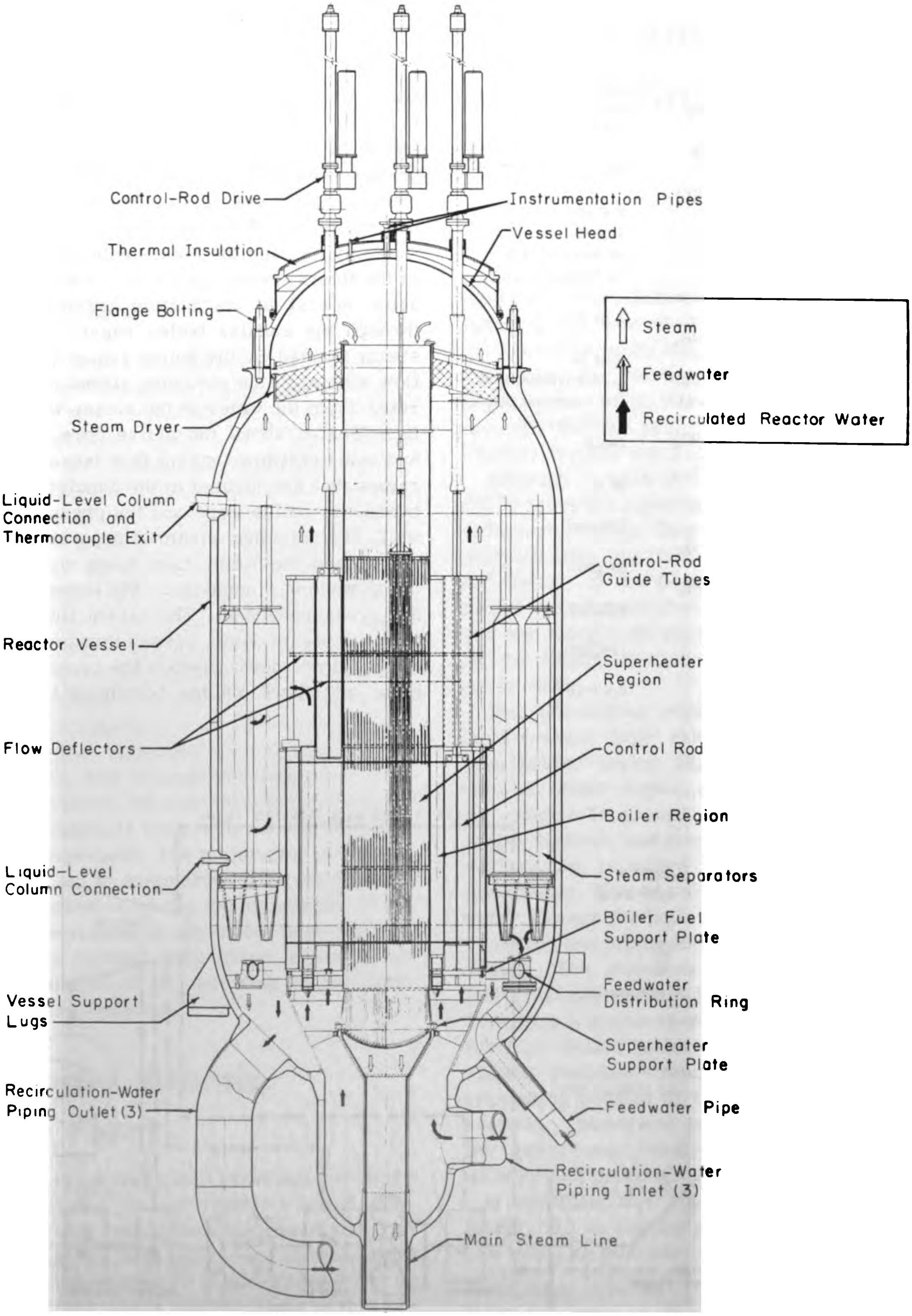

Fig. VIII-2 Vertical section of the Pathfinder reactor.

vessel through the main steam line. Feedwater enters the reactor vessel near its bottom and is mixed with the downcomer flow by means of a sparger shown in Fig. VIII-2. The recirculation flow, which consists of the downcomer flow and the feedwater, leaves the vessel through piping outlets, passes through recirculation pumps where its pressure is raised approximately 25 psi, and then reenters the reactor vessel through the recirculation-water piping inlets.

The boiler region contains 96 fuel-element assemblies, each approximately 5 in. square by 99 in. long overall. The superheater region of the core, which resembles a tube type heat exchanger, contains 412 positions for 1-in.-diameter fuel assemblies. Reactor power level is controlled by a system of rods located in both the boiler and superheater regions of the core. The rack-and-pinion type drives employed for all control rods are mounted on top of the reactor pressure vessel.

The reactor vessel is carbon steel and is internally clad with stainless steel. Internal support structures and baffles are stainless steel, and the recirculation piping is stainless steel or is clad with stainless steel.

Boiler Fuel

Each boiler fuel assembly contains a bundle of 81 fuel rods in a 9 by 9 array, with a nozzle assembly on one end and a handling fitting on the other. Each fuel rod consists of four segments joined end to end as shown in Fig. VIII-3. The two segments that comprise the top half of the fuel rod have a slightly smaller diameter than the segments in the bottom half. The rods are spaced by tube sheets at the joints between fuel-rod segments and by support grids at each end of the rod bundles. The rods are supported on the lower grid, where each rod is fastened by a stainless-steel bolt which, in turn, is tack welded to the grid. Sixteen of the rods are bolted to the top support grid to hold the element together during handling, whereas the tops of the remainder of the rods are free to move independently in the axial direction. The top and bottom support grids, which are stainless-steel castings, are fastened to the handling fitting and the nozzle assembly, respectively. Differential thermal expansion between the boiler fuel assemblies and the core support structure is accommodated at the bottom core support plate by a spring-loaded sliding fit between the fuel-element nozzles and the receiving sleeves in the bottom support structure.

Specifications and performance data for the boiler fuel assemblies and for the boiler region of the reactor are given in the following tabulation:

Core, boiler region		
Mean outside diameter, in.	69.0	
Mean inside diameter, in.	31.3	
Active fuel length, in.	72	
Volume, cu ft	123	
Number of fuel-element assemblies	96	
Average power density, kw/cu ft core volume	1280 (∼45 kw/liter)	
Average specific power, kw/kg of uranium	24.0	
Average heat flux, Btu/(hr)(sq ft)	122,000	
Maximum heat flux, Btu/(hr)(sq ft)	447,000	
Steady-state minimum burnout ratio	1.9	
Maximum fuel temperature, °F	4215	
Maximum surface-cladding temperature, °F	514	
Inlet coolant velocity, ft/sec	13.6	
Exit voids, average and maximum, %	45.5 and 56	
Pressure drop, psi	13.6	
Thermal power generated, Mw	157.4	
Thermal power to coolant, Mw	159.1	
Heat-transfer area, sq ft	4397	
Coolant flow area, lower half, sq ft	9.43	
Coolant flow area, upper half, sq ft	10.81	
Fuel burnup, Mwd/ton	10,000	
Core lifetime, year	1.5	
Fuel enrichment ^{235}U, wt.%	2.2	
Fuel loading, uranium, kg	6560	
Boiler fuel-element assemblies		
Bundle size, in. square	4.735	
Number fuel rods per bundle	81	
Rod sections per rod	4	
	Lower sections	Upper sections
Pellet diameter, in.	0.348	0.310
Cladding thickness, in.	0.028	0.026
Rod diameter, in.	0.408	0.367
Box material	Zircaloy-2	
Cladding material	Zircaloy-2	
Fuel material	UO_2	
Fuel density, g/cm^3	10.41	
Nozzle material	Chrome-plated 304L S.S.	

Superheater Fuel

Two concentric fuel tubes form the basic fuel arrangement in each superheater assembly. As shown in Fig. VIII-4, concentricity of the tubes is maintained by full-length straight-wire spacers, and spacing of the assembly proper in pre-

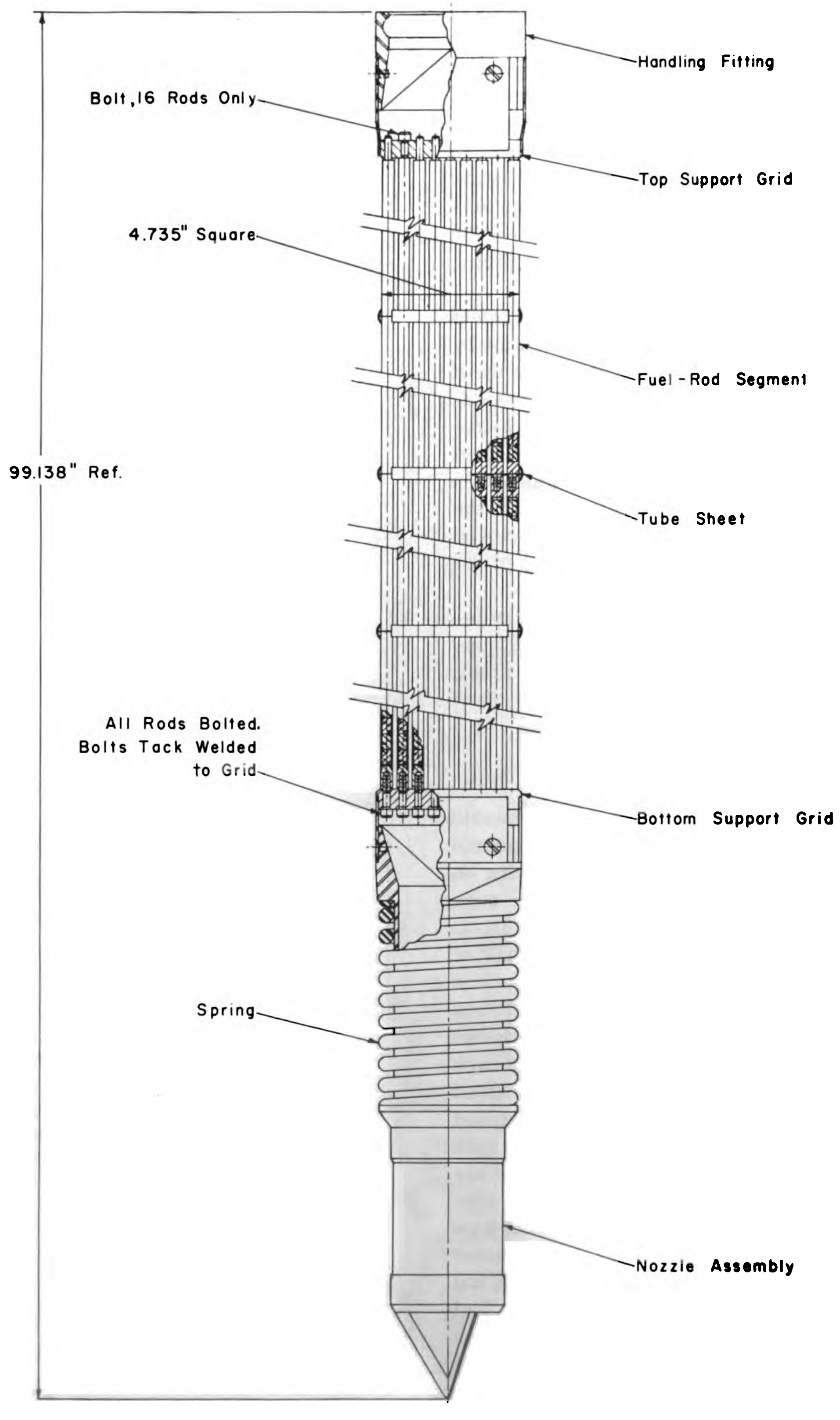

Fig. VIII-3 Boiler fuel assembly of the Pathfinder reactor.

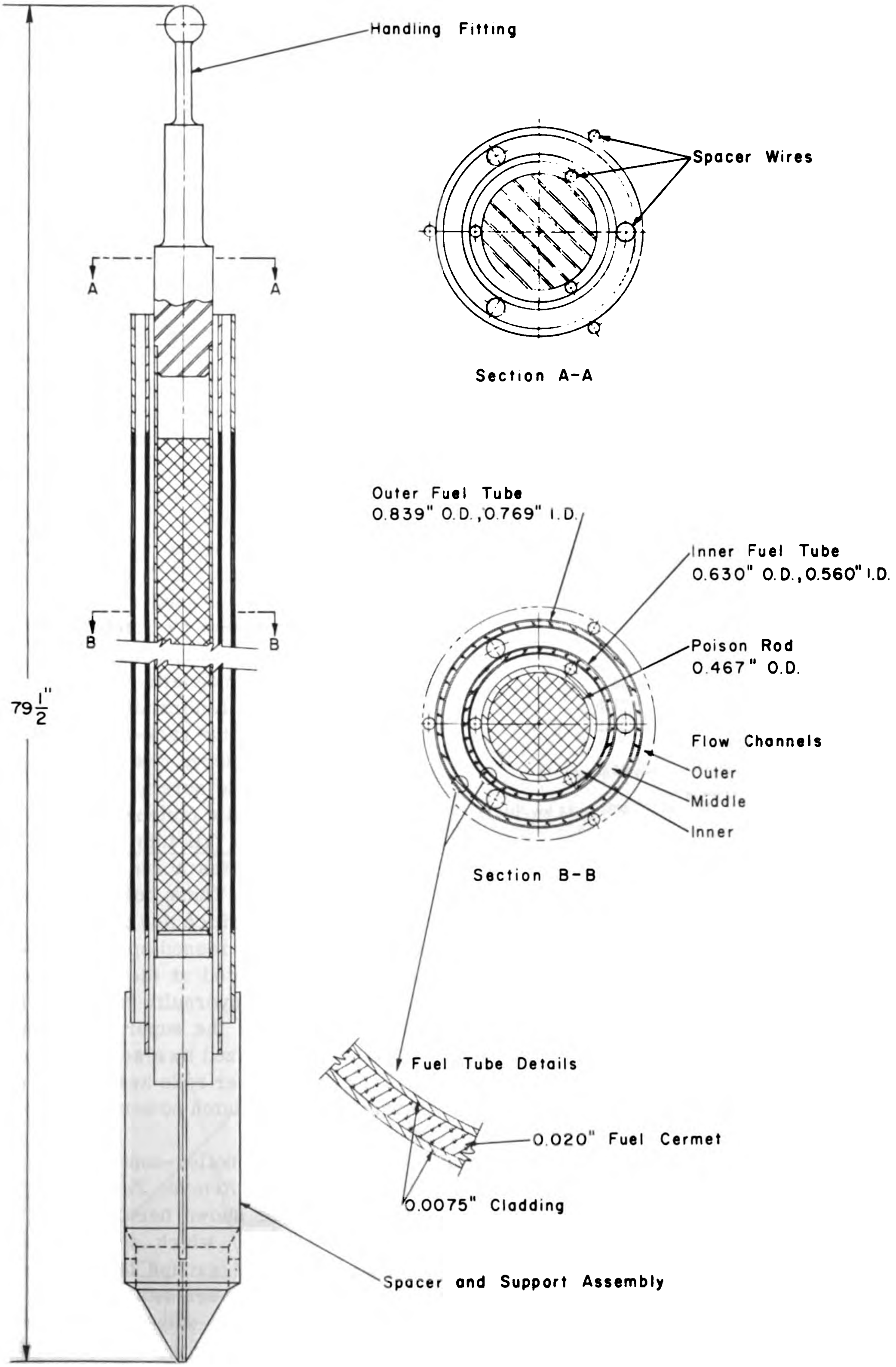

Fig. VIII-4 Superheater fuel assembly of the Pathfinder reactor.

installed flow channels is accomplished in the same manner. Most of the superheater elements contain a central burnable poison rod, but up to 100 unpoisoned elements can be used for flux shaping and reactivity adjustment. The fueled and poisoned sections of each element are welded to end fittings. At the lower end of the element, the fitting consists of a spacer and support assembly that plugs into a support plate in the core structure. At the upper end of the assembly, the central-rod portion is welded to a handling fitting, and the fuel tubes are not axially restrained and are free to expand.

Each superheater fuel tube consists of a UO_2–stainless-steel cermet that is sandwiched between two thin stainless-steel-cladding tubes. Heat transfer from the cermet to the cladding is improved by diffusion bonding of the two. The central poison rod, which consists of a compact containing about 0.35 wt.% natural boron carbide in alumina at about 70% of theoretical density, is clad with relatively thick stainless steel.

Superheater data are given in the following tabulation:

Core, superheater region	
Mean outside diameter, in.	30
Active fuel elength, in.	71.5
Volume, cu ft	32.5
Number of fuel-element assemblies	412
Average power density, kw/cu ft core volume	970 (~34 kw/liter)
Average heat flux, Btu/(hr)(sq ft)	59,100
Maximum heat flux, Btu/(hr)(sq ft)	219,000
Power generated, Mw(t)	31.5
Power to coolant, Mw(t)	29.8
Heat-transfer area, sq ft	1817
Coolant-flow area, sq ft	0.993
Maximum fuel temperature, °F	1280
Maximum cladding surface temperature, °F	1270
Average flow rate in element, lb/hr	1478
Maximum flow rate in element, lb/hr	1626
Average exit bulk temperature, °F	725
Average inlet velocity in coolant channels, steam, ft/sec	128
Average exit velocity in coolant channels, steam, ft/sec	207
Core pressure drop, psi	61
Fuel burnup, average, %	18.5
Core lifetime, months	9
Fuel enrichment, wt.% ^{235}U	93
Fuel loading, kg ^{235}U	50
Superheater fuel-element assemblies	
Outer insulating tubes	
Outside diameter, in.	1.076
Inside diameter, in.	1.024
Inner insulating tubes	
Outside diameter, in.	0.967
Inside diameter, in.	0.937
Outer fuel tubes	
Outside diameter, in.	0.839
Inside diameter, in.	0.769
Inner fuel tubes	
Outside diameter, in.	0.630
Inside diameter, in.	0.560
Poison-tube outside diameter, in.	0.467
Cladding and structural material	Type 316L S.S.
Cladding thickness	
Fuel tubes, in.	0.0075
Poison tube, in.	0.028
Cermet thickness, in.	0.020
Cermet composition, wt.% UO_2	17.5

Control Elements

Pathfinder control elements consist of cruciform blades and poison shims in the boiler region and round rods in the superheater region. The poison shims are located between boiler-fuel-assembly positions. They are locked in position by the assemblies and cannot be moved unless the two adjacent fuel assemblies are first removed. The boiler and superheater control elements are driven by mechanisms mounted on the vessel head, and, although all rod drives are equipped with magnetic clutches, the superheater elements will normally not be scrammed. The drives are of the rack-and-pinion type and are equipped with servo position indicators.

On receipt of a scram signal, the boiler control-rod magnetic clutches release and allow the boiler rods to fall into the core, while the same signal initiates a run-in of all control-rod-drive motors. Those boiler rods which are in the full-out position are accelerated, during a scram by a compressed spring; all scrammed rods are decelerated at the end of their downward strokes by hydraulic dashpots. The magnetic clutches for the superheater control-rod drives are energized by a separate supply, and thus the superheater rods are not automatically scrammed when clutch power to the boiler rods is interrupted.

The cruciform boiler-control rods were described in *Power Reactor Technology*, 5(2): 46, and will not be shown here. The superheater control elements, which are shown in Fig. VIII-5, consist of groups of small rods. The rods in each group are attached to a cruciform structure called the superheater control-rod support yoke, and this yoke, holding 13 rods, is driven by a single drive unit mounted on top of the reactor vessel. There are four such control elements in the superheater region.

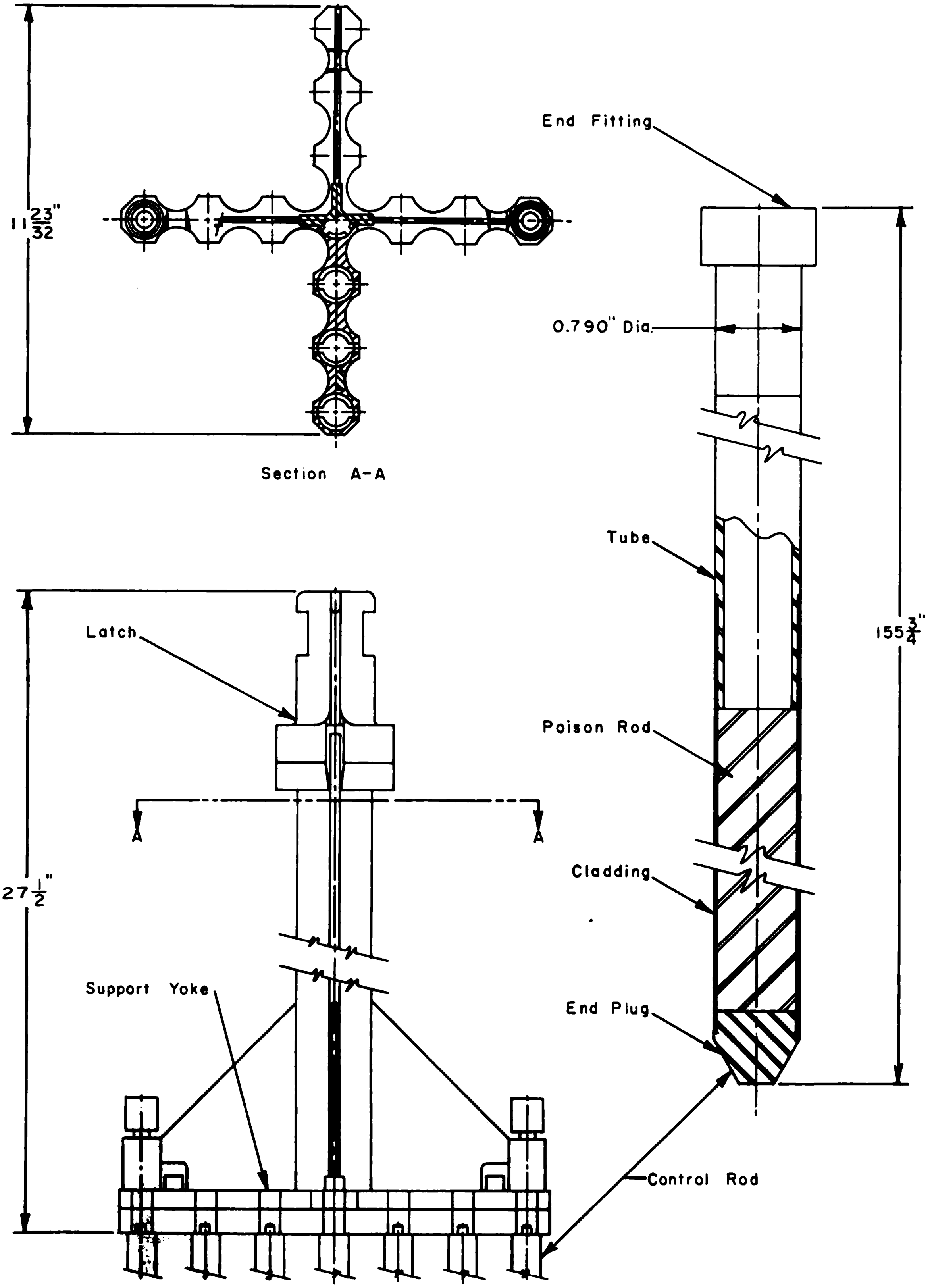

Fig. VIII-5 Superheater control element of the Pathfinder reactor.

All control elements in the Pathfinder core are provided with guide channels in the core structure, and none can contact a fuel assembly. Specifications for the control rods are given in the table that follows this section, and the manner in which the rods are integrated with the remainder of the core is described in a later section.

All control-rod drives are basically the same rack-and-pinion type, but the normal drive speed of those boiler rods closest to the superheater region is about one-third that of the speed of other rods in order to keep the cold startup reactivity-increase rate about the same for all rods.

Boiler control rods	
Number	16
Number of drives	16
Shape	Cruciform
Material	2 wt.% boron in 304 S.S.
Blade dimensions, in.	
Thickness	$\frac{1}{4}$
Width	$10\frac{7}{16}$
Poison length	72
Superheater control rods	
Number	52, ganged into 4 groups
Number of drives	4
Shape	Cylindrical
Material	2 wt.% boron in 304 stainless steel, clad in 304L S.S.
Rod dimensions, in.	
Poison diameter	0.75
Cladding thickness	0.020
Poison length	72
Poison shims	
Number, maximum	56
Shape	Rectangular strip
Material	0.20 wt.% boron in 304 S.S.
Shim dimensions, in.	
Thickness	0.10
Width	$2\frac{25}{32}$
Poison length	74

Pressure Vessel and Core Structure

The reactor pressure vessel, shown in Fig. VIII-2, has an inside diameter of 11 ft and an overall height of about 36 ft. The vessel and head are designed, constructed, and tested in accordance with Secs. VIII and IX of the *ASME Boiler and Pressure Vessel Code* as modified by Special Code Cases 1270N, 1271N, and 1273N. The design pressure is 700 psig at 500°F, and the integrated fast-neutron flux (>1 Mev) at the point of maximum exposure is calculated to be 2×10^{18} neutrons/cm^2 in 30 years. The vessel shell and lower head sections are fabricated from 3-in.-thick composite plate consisting of ASTM A-212 grade B carbon-steel base material clad on the inside with $\frac{1}{4}$-in.-thick type 304L stainless steel. The hemispherical portion of the upper head is formed from $2\frac{3}{8}$-in.-thick A-212 grade B plate with $\frac{1}{8}$-in. 304L cladding. The bond between the stainless steel and carbon steel of the composite plate is effected by hot rolling, and weld joints and carbon-steel forgings are clad with weld-deposited niobium-stabilized stainless steel.

The upper vessel opening has a clearance diameter of 7 ft 7 in., which provides sufficient space for the removal of the core grid plate. Three positioning studs in the vessel flange locate the head with respect to the vessel, and the main closure bolting consists of 48 studs and nuts that are 3 in. in diameter. The vessel-closure seal utilizes two concentric, corrugated, stainless-jacketed soft-iron-core gaskets.

The reactor vessel head and closure region are separated from the shield-pool water by a steel cover that contains a layer of metallic thermal insulation. The arrangement of this cover and its connection to the shield-pool floor are shown in Fig. VIII-6. The space between the vessel and concrete biological shield beneath the shield pool is sealed off by the pool floor and a stainless-steel expansion bellows that permits a 1-in. differential expansion between the vessel and shield-pool floor. The vessel proper is insulated with 4 in. of calcium silicate and is held in its cavity by five steel support columns that transfer the vessel load to spread footings embedded in reinforced concrete. Thermal expansion of the vessel in the radial direction is absorbed by flexing of the columns.

The following are the 32 penetrations of the vessel:

Description	No.	Inside diameter, in.	Location
Nozzles to recirculation pumps	3	$20\frac{1}{2}$	Below core
Nozzles from recirculation pumps	3	$20\frac{1}{2}$	Below core
Steam-outlet nozzle	1	$16\frac{1}{2}$	Below superheater
Feedwater nozzle	1	$9\frac{3}{4}$	Below core
Boiler-core instrument nozzle	1	$6\frac{3}{8}$	Above core
Lower liquid-level nozzle	1	$2\frac{3}{8}$	Below core
Control-rod-drive nozzles	20	$3\frac{1}{2}$	Vessel head
Superheater core-instrument nozzle	1	$1\frac{1}{2}$	Vessel head
Upper liquid-level nozzle	1	$\frac{1}{2}$	Vessel head

The arrangement of major components within the pressure vessel is illustrated by Figs. VIII-2 and VIII-7. The principal components that are not part of the core structure are the feedwater distribution ring, the steam separators, and the steam dryer.

As shown in Fig. VIII-2, the feedwater distribution ring, which is a 5-in.-diameter pipe, is supported by brackets attached to the vessel wall. Steam separators, shown in Fig. VIII-8, occupy the annular downcomer region in the Pathfinder reactor. These separators, which handle about 20% of the steam produced, help reduce steam carryunder into the recirculation pump suctions to about 0.1% by volume. At normal operating conditions the total maximum-pressure drop through the separators is $5\frac{1}{2}$ ft of water. The steam separators, which are installed in groups, rest on a support shelf mounted on brackets welded directly to the lower portion of the reactor vessel. They are aligned near their tops and are held down axially by brackets that extend under the boiler-element hold-down structure described in a subsequent paragraph.

The steam-dryer assembly, which can be seen in Fig. VIII-2, occupies the annular space between the superheater chimney and the inside

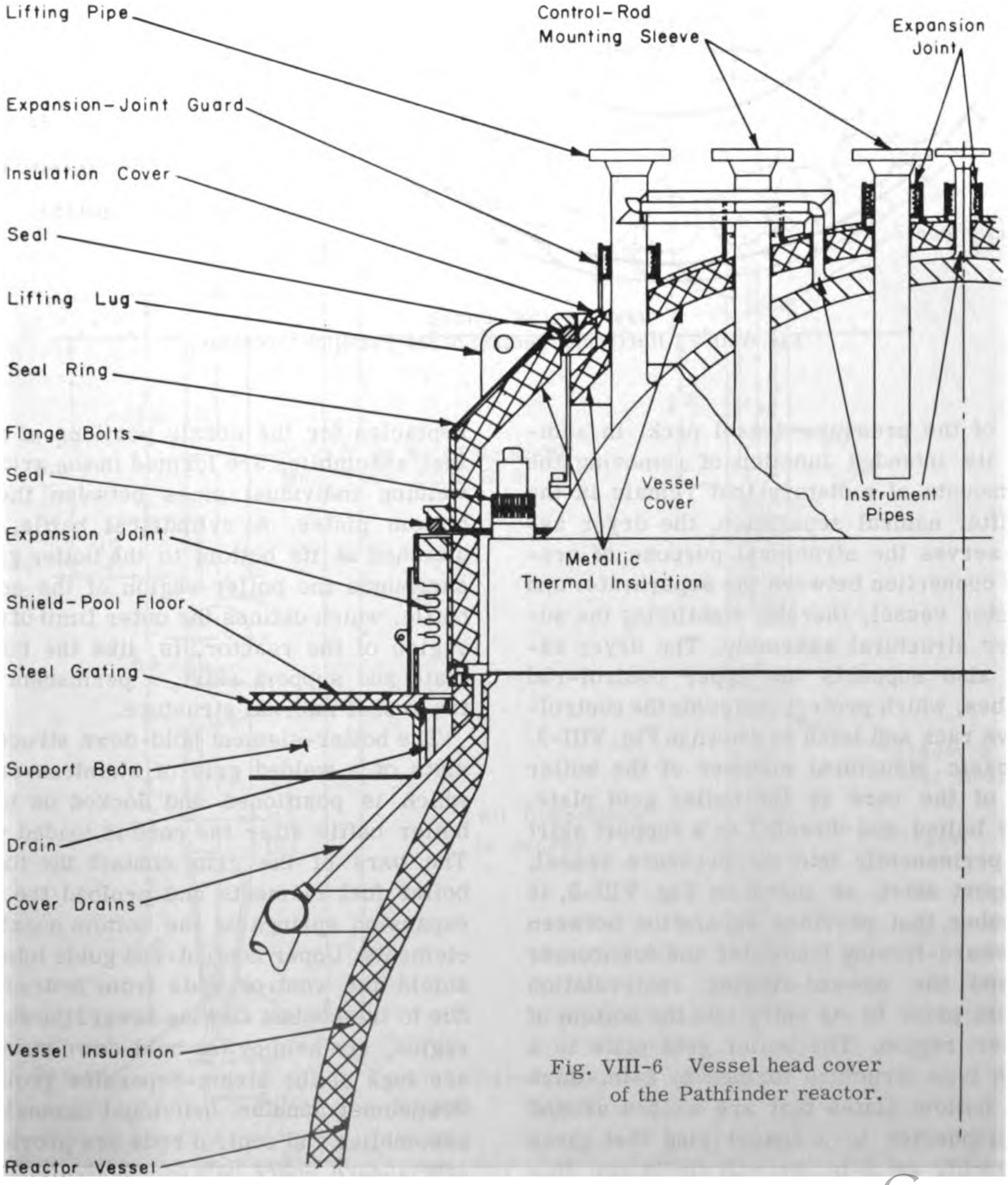

Fig. VIII-6 Vessel head cover of the Pathfinder reactor.

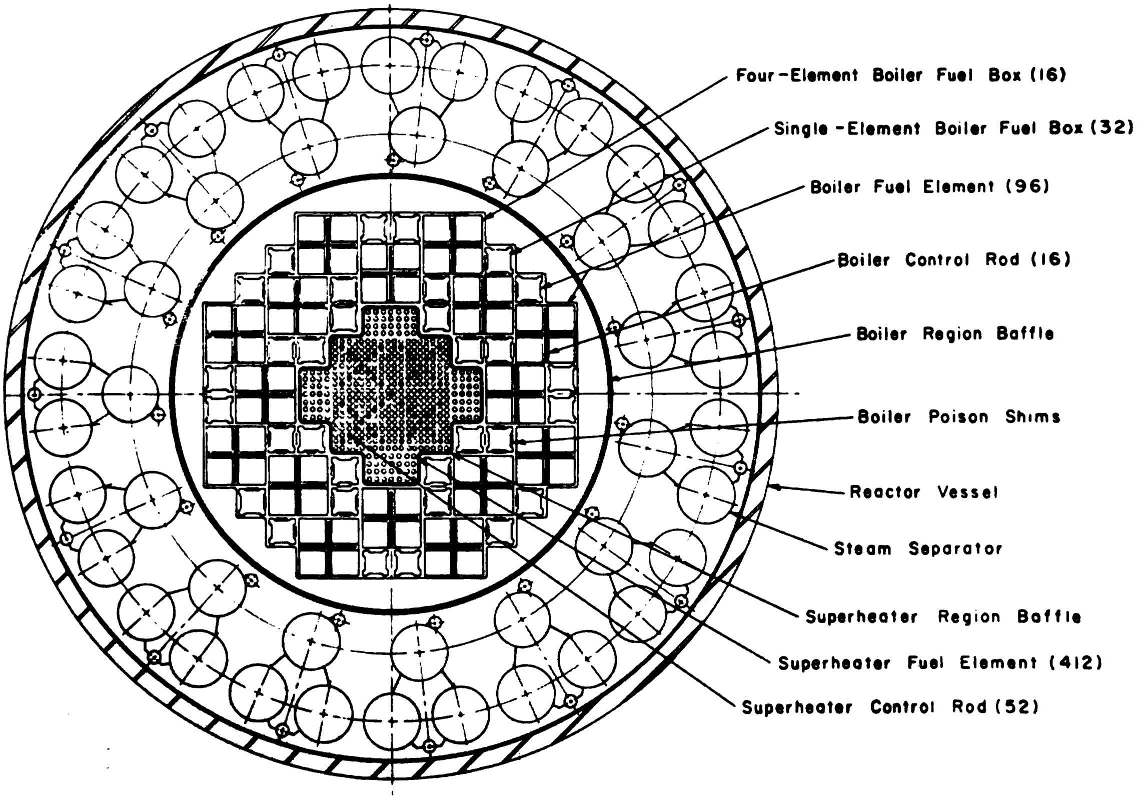
Four-Element Boiler Fuel Box (16)
Single-Element Boiler Fuel Box (32)
Boiler Fuel Element (96)
Boiler Control Rod (16)
Boiler Region Baffle
Boiler Poison Shims
Reactor Vessel
Steam Separator
Superheater Region Baffle
Superheater Fuel Element (412)
Superheater Control Rod (52)

Fig. VIII-7 Horizontal section of the Pathfinder reactor.

surface of the pressure-vessel neck. In addition to its intended function of removing the trace amounts of moisture that remain in the steam after natural separation, the dryer assembly serves the structural purpose of providing a connection between the superheater and the reactor vessel, thereby stabilizing the superheater structural assembly. The dryer assembly also supports the upper control-rod guide tubes, which protect and guide the control-rod-drive rack and latch as shown in Fig. VIII-2.

The basic structural member of the boiler section of the core is the boiler grid plate, which is bolted and doweled to a support skirt welded permanently into the pressure vessel. The support skirt, as shown in Fig. VIII-2, is the member that provides separation between the downward-flowing feedwater and downcomer water and the upward-flowing recirculation water just prior to its entry into the bottom of the boiler region. The boiler grid plate is a sandwich type structure formed by 2-in.-thick top and bottom plates that are welded around their peripheries to a spacer ring that gives the assembly an 8-in. overall thickness. Receptacles for the nozzle portions of the boiler fuel assemblies are formed in the grid plate by welding individual pipes between the top and bottom plates. A cylindrical baffle, which is attached at its bottom to the boiler grid plate, surrounds the boiler region of the core. This baffle, which defines the outer limit of the fueled region of the reactor, is, like the boiler grid plate and support skirt, a permanent piece of the vessel internal structure.

The boiler-element hold-down structure consists of a welded grid of stainless-steel bars which is positioned and locked on top of the boiler baffle after the core is loaded with fuel. The bars of the grid contact the tops of the boiler fuel elements and preload the thermal-expansion springs at the bottom nozzles of the elements. Upper control-rod guide tubes, which shield the control rods from hydraulic loads due to the coolant flowing toward the downcomer region, are held by the hold-down structure, as are lugs of the steam-separator groups in the downcomer annulus. Individual channels for fuel assemblies and control rods are provided in the active core space between the boiler grid plate and the boiler-element hold-down structure. These channels are formed by components called boiler fuel boxes, which are of two different types. There are 16 four-element boxes and 32 single-element boxes, all formed of Zircaloy-2. The four-element boxes are about $10\frac{3}{4}$ in. square, and contain, in addition to the four square channels for boiler fuel assemblies, a cruciform channel for a boiler control rod. The single-element boxes, which are about 5 in. square and hold one boiler fuel assembly each, have slots milled in their outer surfaces to accommodate burnable-poison shims.

The superheater structure, which resembles a tube type heat exchanger, is shown in Figs. VIII-2 and VIII-7. The assembly contains tubes for fuel elements, for control-rod guidance, and for a neutron source. All tubes are held in vertical alignment by a top tube sheet, by intermediate steady plates, and by a bottom grid plate. The fueled portion of the superheater is surrounded by a vertical baffle, and other vertical structural members extend the overall height of the assembly from a point below the active core region (at the superheater support plate shown in Fig. VIII-2) to the steam-dryer assembly at the top of the reactor vessel. The space between the tubes in the superheater region is filled with water moderator that mixes with the recirculation water above and below the boiler core. Each superheater fuel assembly fits inside a double-walled process tube

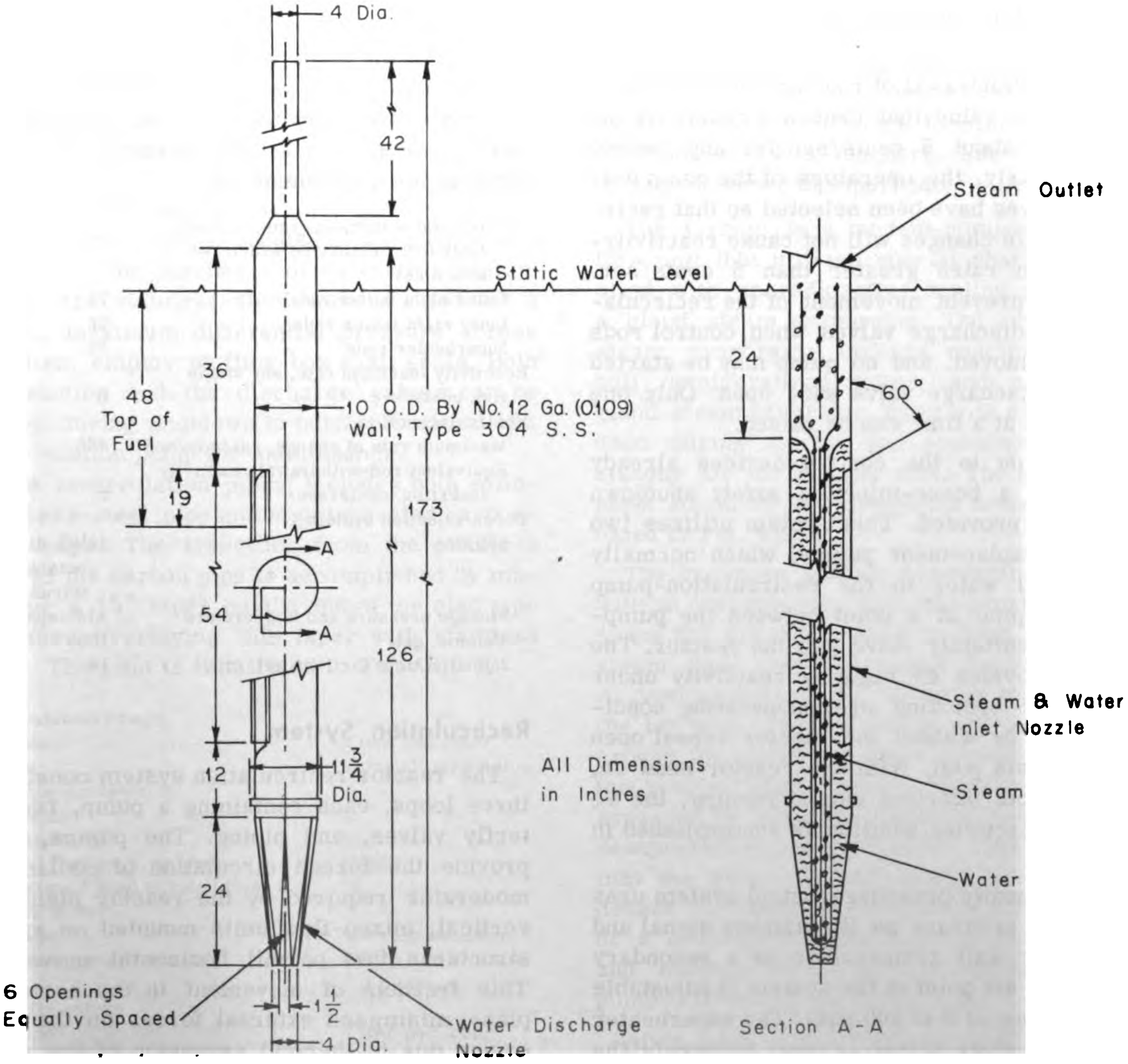

Fig. VIII-8 Steam separator of the Pathfinder reactor.

that contains a layer of stagnant steam for thermal insulation between the water moderator and the superheated-steam coolant.

Control and Instrumentation

The specified mode of operation of the plant calls for manual control of reactivity and for automatic control of pressure. Reactor power is controlled by movement of the control rods or by positioning the recirculation-pump discharge valves (the amount of moderator passing through the core can be varied by throttling recirculation flow with butterfly valves installed on the recirculation-pump discharge side). Reactor pressure is normally controlled by positioning the turbine inlet valves or by a regulating dump valve. If necessary, reactor steam can be dumped to the condenser through the regulating dump valve.

Rate of withdrawal of reactor control rods is limited to a value that causes a reactivity insertion of about 5 cents/sec for any control rod. Similarly, the operators of the pump discharge valves have been selected so that recirculation rate changes will not cause reactivity-insertion rates greater than 5 cents/sec. Interlocks prevent movement of the recirculation-pump discharge valves when control rods are being moved, and no pump may be started with its discharge valve wide open. Only one control rod at a time can be raised.

In addition to the control devices already mentioned, a boron-injection safety shutdown system is provided. This system utilizes two positive displacement pumps, which normally supply seal water to the recirculation-pump discharge pipe at a point between the pump-discharge butterfly valve and the reactor. The system provides 4% negative reactivity under all reactor operating or nonoperating conditions, with or without the reactor vessel open to the shield pool. With the reactor head on, and with both injection pumps running, the 4% negative-reactivity addition is accomplished in 4 min.

The automatic pressure-control system uses steam-line pressure as its primary signal and superheater exit temperature as a secondary signal. The set point of the system is adjustable over a range of 0 to 800 psig. The superheater exit-temperature signal is used to modify the primary pressure signal in order to speed the response of steam flow to reactor power during transients, thereby reducing the temperature rise in the transient.

A block diagram of the Pathfinder nuclear-instrumentation system was given in *Power Reactor Technology*, 5(2): 69, as was the range covered by each of the eight neutron-detecting channels. The two functions of the nuclear instrumentation system are (1) to provide information to the reactor operator so that he can manually adjust the reactivity level in the reactor and (2) to furnish input information to the plant's automatic shutdown system.

Although the first core will contain in-core neutron-flux monitors to obtain experimental information, it is not planned to include such devices in subsequent cores. The first-core installation consists of nine ionization chambers, placed at three radial locations in three superheater process tubes that contain no fuel. At each of the three radial locations, chambers will be placed at three axial positions. Readout instrumentation provides for the simultaneous reading or recording of information from any three of the nine chambers.

Control-rod withdrawal rate, in./min (only one rod may be withdrawn at a time)	
Outer eight boiler rods	72
Inner eight boiler rods	26
Superheater rods	72
Reactivity insertion rate, any single rod, cents/sec	5
Recirculation flow	
Maximum rate of change, gal/min/sec	455
Equivalent rod-withdrawal reactivity insertion, cents/sec	5
Boron-injection system	
Solution	12½% disodium octaborate tetrahydrate
Storage pressure and temperature	Atmospheric
Volume, gal	1000
Injection time for 1000 gal, min	18

Recirculation System

The reactor recirculation system consists of three loops, each containing a pump, two butterfly valves, and piping. The pumps, which provide the forced circulation of coolant and moderator required by the reactor plant, are vertical, mixed-flow units mounted on special structures that permit horizontal movement. This freedom of movement in the horizontal plane minimizes external forces on the pump casing due to thermal expansion of the piping. Bushing type shaft seals, with water injection, prevent leakage of the primary coolant to the

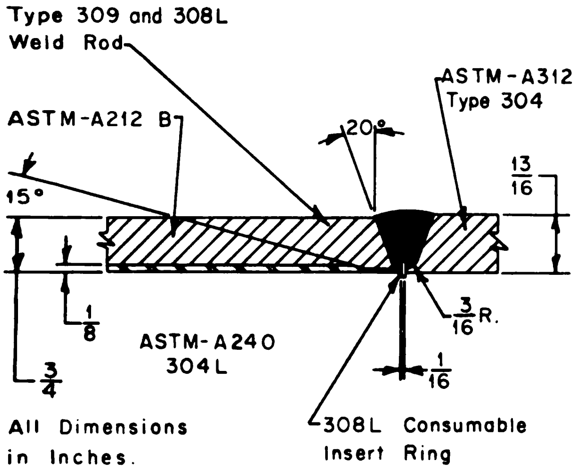
Type 309 and 308L Weld Rod
ASTM-A212 B
ASTM-A312 Type 304
20°
13/16
15°
1/8
ASTM-A240 304L
3/4
3/16 R.
1/16
All Dimensions in Inches.
308L Consumable Insert Ring

Fig. VIII-9 Transition joint in recirculation piping in the Pathfinder reactor.

atmosphere. Backup sealing is provided by mechanical, spring-loaded face seals and labyrinth bushings on each shaft. Dual seal-injection pumps are provided, with automatic transfer from one pump to the other.

A butterfly valve is located at the suction and another at the discharge of each recirculation pump. The stainless-steel valves, rated for a 50-psi maximum differential pressure across the disk, employ stuffing-box shaft seals. Both the suction and the discharge valves can be closed during shutdown to permit isolation of a recirculation pump for maintenance.

The recirculation piping includes both solid-stainless-steel pipe and stainless-clad carbon-steel pipe. The transition from the stainless pipe to the carbon pipe is accomplished by machining a 15° taper on the end of the clad pipe and then overlaying this taper with stainless steel. The joint is illustrated in Fig. VIII-9.

Recirculation pumps	
Number	3 (one per loop)
Type	Vertical, mixed flow
Nozzle diameter, in.	
Suction	22
Discharge	22
Rated flow each, gal/min	21,600
Developed head at rated flow, ft	71
Drive motor	
Type	600 rpm induction
Power requirements	400 hp, 2300 volt, 3 phase
Butterfly valves	
Number	6 (two per loop)
Pressure rating, psig	700
Maximum ΔP across disk, psi	50
Drives	Electric motors
Piping	
Outside diameter, in.	
Reactor to pumps	22
Pumps to reactor	22
Minimum fundamental natural frequency of piping loops	1.5 × pump rpm

Turbine-Generator, Condensate, and Feedwater Systems

Superheated steam flows from the reactor to the turbine through a single main line. The line is equipped with a motor-operated isolation valve which is located within the reactor building and which is tripped on scrams requiring isolation of the containment building. At the turbine the main steam line divides into two smaller lines, each of which is equipped with a turbine trip valve. Four bellows-sealed safety valves, installed on a common 10-in. header, are located in the main steam line between the reactor and the isolation valve. The safety valves discharge through flexible connections to a common 14-in. discharge line that connects to the condenser desuperheater pipe.

The turbine is a tandem-compound double-flow unit that utilizes special shaft seals supplied with nonradioactive sealing steam from a gland steam evaporator. The regular gland steam evaporator utilizes reactor steam to boil demineralized water, and an auxiliary gland steam generator, fired with oil or gas, is used during startup and shutdown and as a standby for the regular unit. The turbine supplies steam to four feedwater heaters as indicated in Fig. VIII-1.

The two-pass surface condenser is equipped with an oversized hot well that provides storage space for the water used to flood the reactor steam dome and superheater during shutdown. A desuperheater pipe, which is located above the hot well, accepts steam which is bypassed around the turbine or which is relieved through the reactor safety valves. Temperature of the bypassed or relieved steam is reduced in the desuperheater by condensate that is injected into the steam through spray nozzles. Condenser circulating water comes from the basin of a cross-flow induced-draft cooling tower, and makeup water for the cooling tower is pumped from the Big Sioux River.

After being drawn from the hot well by condensate pumps, the feedwater passes through three low-pressure heaters, a full-flow filter, a feed pump, and a high-pressure heater. A parallel arrangement is employed for all pumps and filters, and, since each unit is sized for full normal flow, a standby is provided. Each feedwater heater is equipped with a bypass line. Makeup water is supplied to the condenser hot well from a demineralized-water storage tank.

An emergency shutdown condenser, cooled by shield-pool water, is used to condense reactor steam following a scram that requires isolation of the containment building.

Steam line	
Diameter, in.	16
Thickness	Schedule 60
Steel	A-335 grade P11
Insulation thickness, in.	5
Turbine-generator	
Speed, rpm	3600
Rating, Mw(e)	66
Generator	Direct-coupled hydrogen-cooled type
Condenser	
Design heat load, 10^6 Btu/hr	435
Vacuum for design heat load, in. Hg	28.5

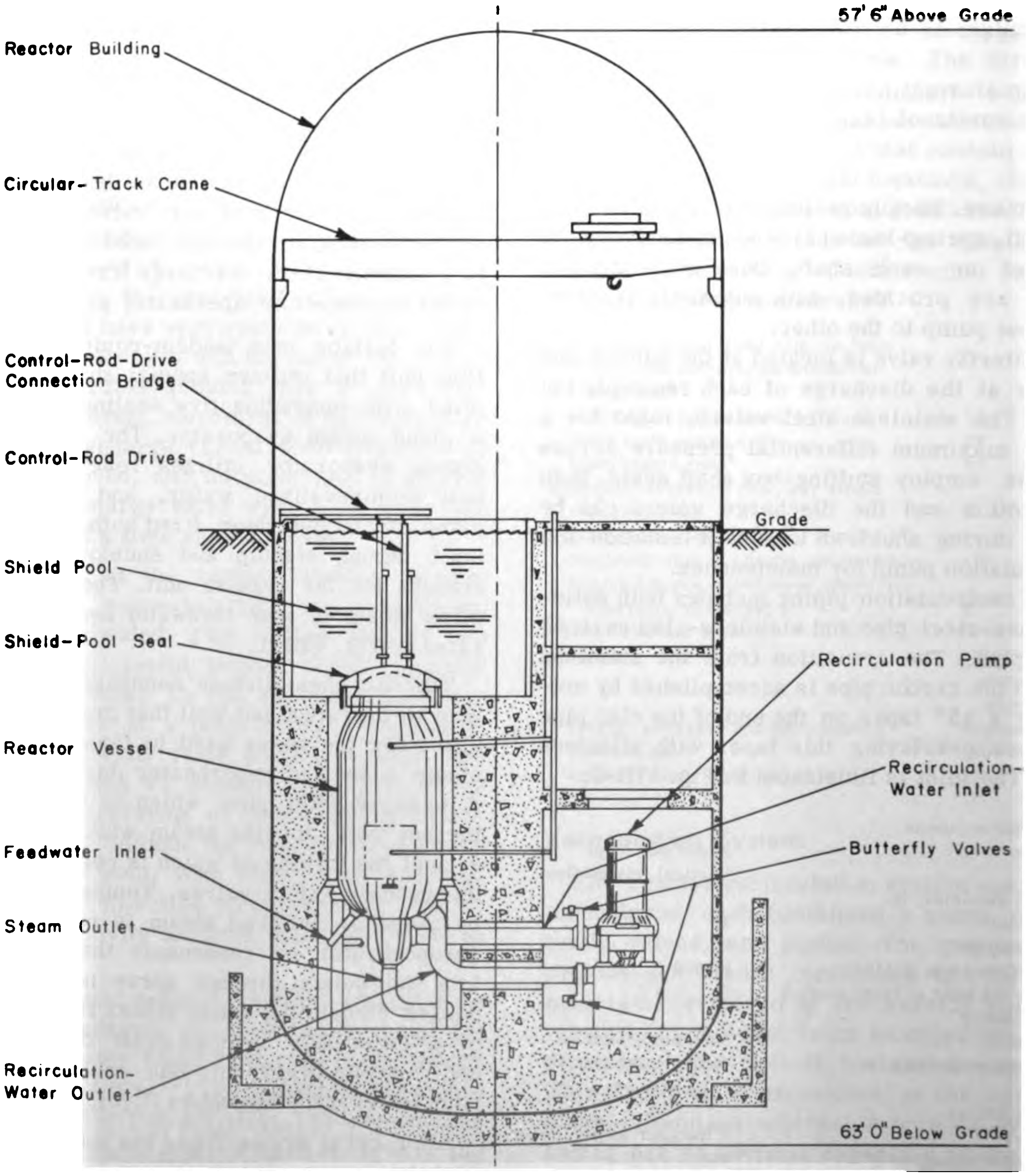

Fig. VIII-10 Vertical section through the containment building of the Pathfinder Atomic Power Plant.

Plant Arrangement and Containment

The reactor and recirculation system are enclosed in a cylindrical containment vessel. Figure VIII-10, a vertical section through the containment vessel, and Fig. VIII-11, a horizontal section through the plant, illustrate the arrangement of the major components. Access to the containment is through a normal airlock, an emergency airlock, or an 11-ft-diameter circular equipment door that is bolted and sealed to the shell. Approximately the bottom half of the reactor containment vessel is below grade: the upper half of the vessel is insulated on its outside down to an elevation 5 ft below ground level.

Containment vessel	
Shape	Cylindrical, with hemispherical top and ellipsoidal bottom
Inside diameter, ft	50
Inside height, ft	120.5
Height of cylindrical section, ft	83
Height of portion below grade, ft	63
Material	Carbon steel
Thickness, in.	
Top	$^{11}/_{16}$
Walls and bottom	$1^{3}/_{8}$
Design internal pressure, psig	78
Maximum leakage rate at design pressure, % of contained volume per day	0.2

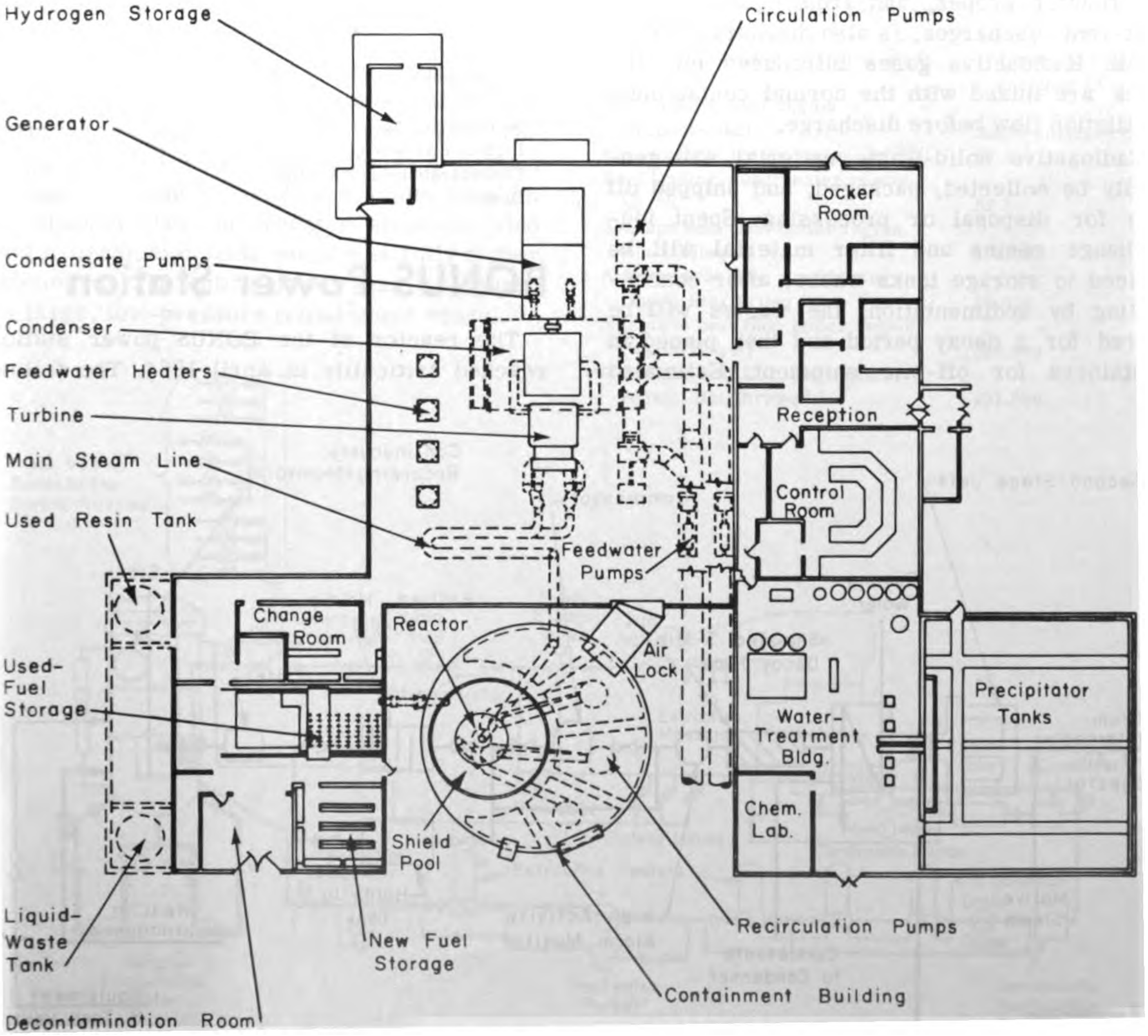

Fig. VIII-11 Horizontal section of the Pathfinder Atomic Power Plant.

Purification and Radioactive Waste Disposal

Noncondensable radioactive gases, which originate in the reactor, pass with the steam to the main condenser where they are removed by air ejectors. The oxygen and hydrogen formed by dissociation of water in the reactor are passed through a catalytic recombiner located after the second-stage nozzle of the air ejector, as shown in Fig. VIII-12. The discharged gas stream from the recombiner is passed through a shielded holdup pipe that provides decay time for short-lived radioactive nuclides. The gases are then moved by a compressor through a baffled holdup tank that provides additional decay time, thence through a filter, and finally to the plant stack. Ventilation air from the area around the reactor proper, and from equipment and tank-vent discharges, is also discharged to the stack. Radioactive gases introduced into the stack are mixed with the normal containment ventilation flow before discharge.

Radioactive solid-waste material will generally be collected, packaged, and shipped off site for disposal or processing. Spent ion-exchange resins and filter material will be sluiced to storage tanks where, after concentrating by sedimentation, the wastes will be stored for a decay period and then placed in containers for off-site shipment. Estimated quantities of solid waste are shown in the tabulation below.

Radioactive liquid wastes will be processed by filtration, demineralization, sedimentation, decay, and/or dilution. After processing has reduced radioactivity levels to acceptable values, the processed water will be returned to its system for reuse or will be discharged to the river. The capacities of tanks in the liquid-waste systems are given in the following tabulation:

Plant stack	
Height above grade, ft	107
Minimum flow during operation, cfm	25,000
Estimated quantities of solid wastes	
Combustible wastes, lb/year	10,000
Noncombustible wastes, lb/year	2000
Filter cartridges, lb/year	1000
Spent resins, cu ft/year	350
Filter backwash materials, lb/year	1000
Liquid-waste system tank capacities, gal	
Four tanks for low solids holdup	3000 each
Waste surge	1000
Reclaimed water	3000
Neutralizing holdup	300
Neutralizing tank	1500
High-solids holdup	2000
Concentrated waste storage	2000
Sumps	7200

BONUS Power Station

The reactor of the BONUS power station[3] reached criticality in April 1964. The follow-

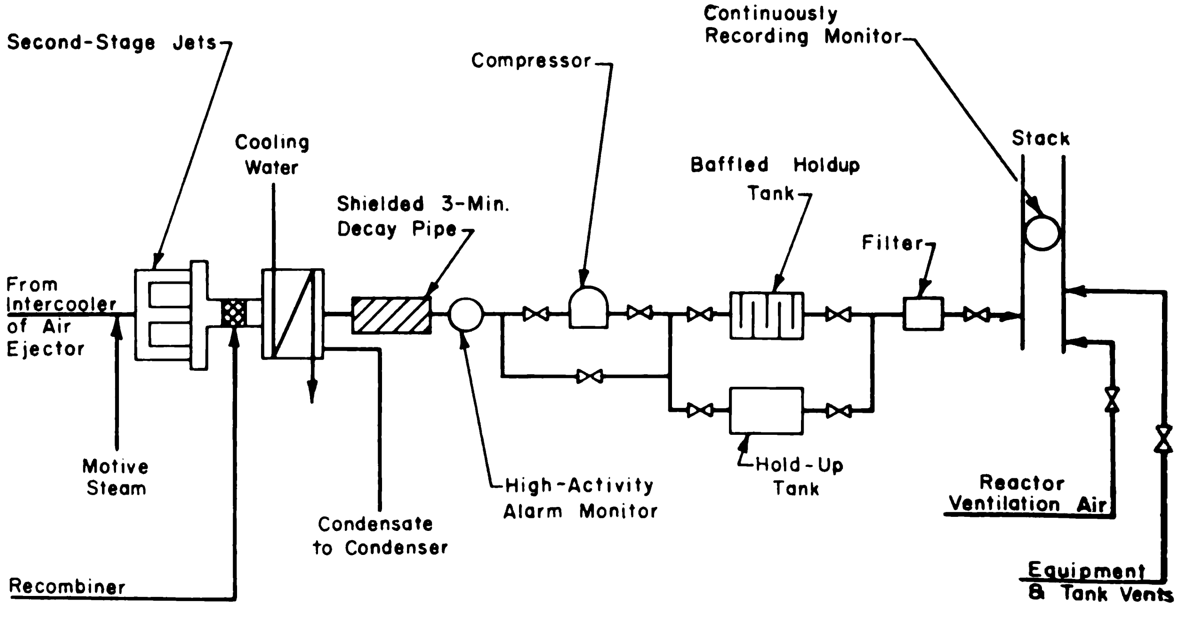

Fig. VIII-12 Gaseous waste-disposal system of the Pathfinder Atomic Power Plant.

ing material on BONUS is presented, for the reader's convenience, in the same general format as in the above description of the Pathfinder plant. Another review, in considerably less detail, appeared in *Power Reactor Technology*, 3(4): 68-74.

The BONUS plant, a joint construction project of the Puerto Rico Water Resources Authority (PRWRA) and the USAEC, is located at Punta Higuera, near Rincon, P. R. It was designed by the General Nuclear Engineering Corporation and PRWRA. Its operation, after testing, will be the responsibility of the PRWRA.

The two-region core of the reactor consists of a central boiler region and a peripheral superheater region. Superheated steam produced in the reactor is fed directly to a condensing steam turbine, and feedwater from the condensate system is returned to the reactor vessel, where it mixes with the reactor recirculating water. Recirculation loops located external to the reactor vessel provide forced coolant flow through the boiler region of the core. The Zircaloy-2-clad boiler fuel elements contain natural or slightly enriched uranium dioxide. The Inconel-clad superheater elements also contain uranium dioxide but of a slightly higher enrichment. The entire power plant is housed in a large, low-pressure containment vessel.

A simplified flow diagram of the plant is given in Fig. VIII-13, and the following are the principal characteristics:

Power, boiler region, kw	37,000
Power, superheater region, kw	13,000
Total core power, kw	50,000
Gross electrical capability, kw	17,500
Net electrical output, kw	16,500
Net efficiency, %	33
Steam outlet pressure, psig	865
Reactor operating pressure, psig	950
Temperature, boiler region, °F	540
Outlet temperature, superheater region, °F	900
Reactor steam flow at rated power (approximate), lb/hr	152,000
Recirculation rate, gal/min	8660
Containment-vessel size, ft	Hemisphere on top of short cylinder, 167 (dia.)
Reactor vessel size, ft	7.5 (OD) by 27
Overall core dimensions, height and diameter, ft	4.55 by 4.83
Fuel, boiler region (Zircaloy-clad)	Natural and 2.4% enriched UO_2
Fuel, superheater region (Inconel-clad)	3.25% enriched UO_2
Fuel loading, boiler region, kg ^{235}U	61.2
Fuel loading, superheater region, kg ^{235}U	52.8
Average heat flux, boiler region, Btu/(hr)(sq ft)	106,000
Average heat flux, superheater region Btu/(hr)(sq ft)	66,000
Maximum heat flux, boiler region, Btu/(hr)(sq ft)	367,000
Maximum heat flux, superheater region, Btu/(hr)(sq ft)	201,000

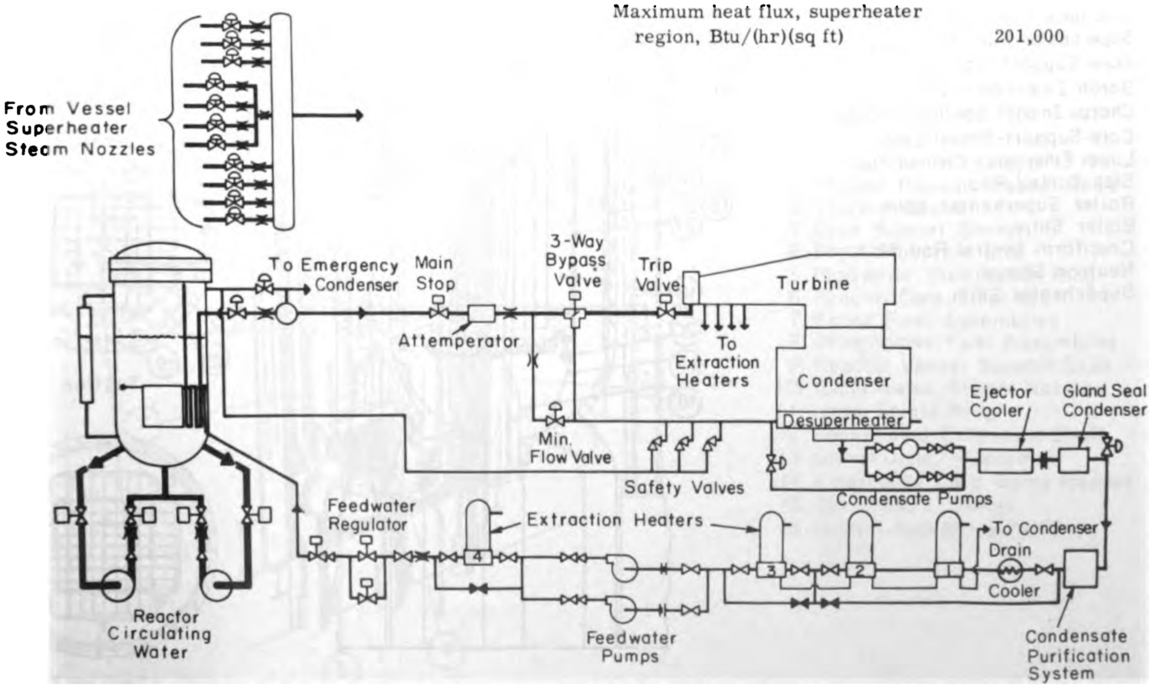

Fig. VIII-13 Simplified flow diagram, BONUS power station.

General Reactor Features

The arrangement of the major reactor components and the locations of piping connections to the pressure vessel are shown in Figs. VIII-14 and VIII-15. Recirculation water enters the reactor vessel through a bottom central nozzle and flows upward within the vessel to enter the bottom of the boiler fuel assemblies. The slightly subcooled water is heated as it progresses upward through the boiler assemblies, and a net steam generation occurs. The steam-water mixture formed in the boiler fuel assemblies continues to move upward after it leaves the active core region and passes through the cells of the eggcrate superstructure. At the steam-water interface and in the steam dome above the interface, gravitational separation of water and steam takes place. The water then passes downward through the annular down-

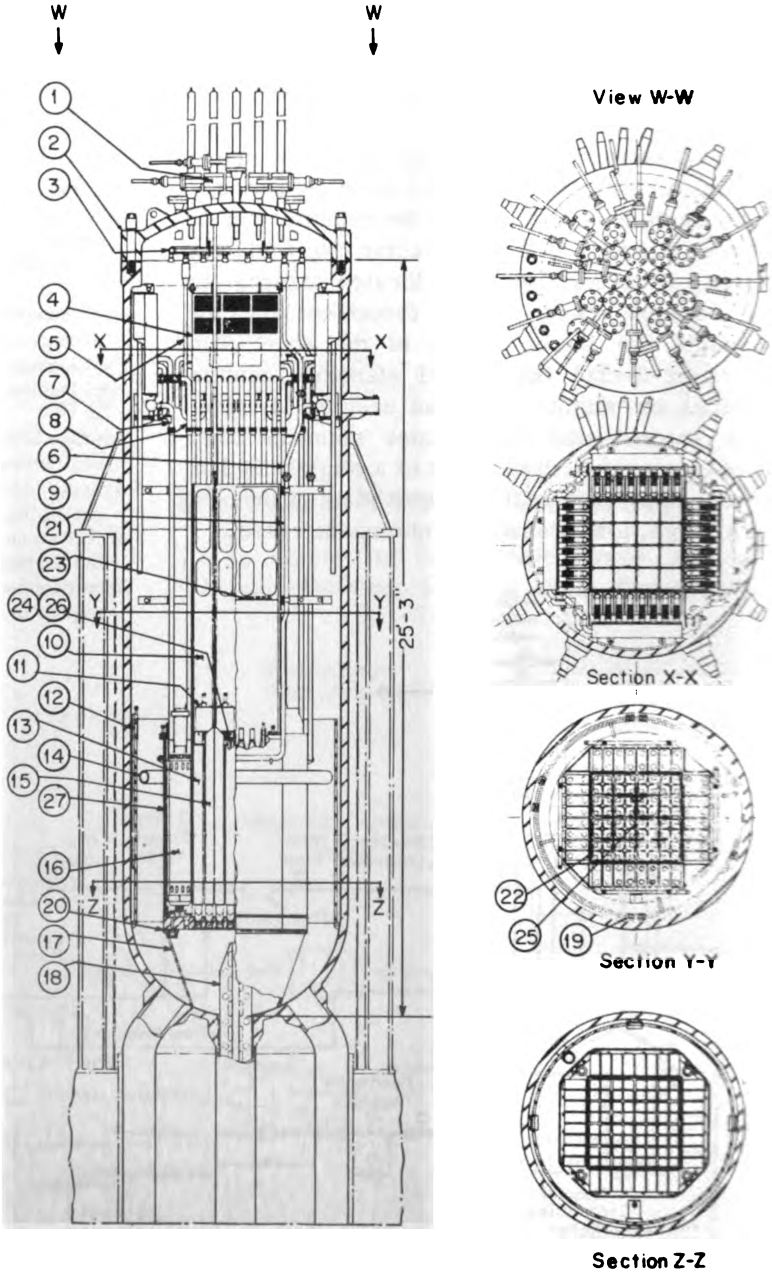

1 Control-Rod Actuator Assembly
2 Closure Head
3 Boiler Spray
4 Steam-Dryer Preheater Assembly
5 Upper Emergency Cooling Pipe
6 Center Emergency Cooling Pipe
7 Superheater Outlet Connector Pipe
8 Superheater Inlet Connector Pipe
9 Reactor Vessel
10 Core Structure
11 Boiler Fuel Holddown Assembly
12 Thermal Shield
13 Boiler Fuel Assembly
14 Feedwater Spray Ring
15 Cruciform Control Rod (2 thru 9)
16 Superheater Fuel Assembly
17 Core Support Barrel
18 Boron Injection Pipe
19 Charpy Impact Specimen Holder
20 Core-Support-Barrel Shim
21 Lower Emergency Cooling Pipe
22 Slab Control Rod
23 Boiler Superheater Shim
24 Boiler Shim
25 Cruciform Control Rod No. 1
26 Neutron Source
27 Superheater Shim

Fig. VIII-14 Pressure-vessel cross sections of the BONUS reactor.

comer region between the reactor core and the pressure-vessel wall, where it mixes with the feedwater. The recirculation flow, consisting of the downcomer and feedwater flows, then leaves the pressure vessel through two outlet pipes. The steam, which still contains traces of water, passes through dryer/preheater units located near the top of the reactor vessel, after which it enters individual superheater inlet pipes. It then flows downward through these individual pipes to the superheater fuel assemblies that are at the elevation of the active core. The steam passes through the superheater fuel assemblies and then returns, through individual superheater-assembly outlet pipes, to the upper portion of the pressure vessel. It is then fed from the outlet pipes to collection headers, from which several small pipes leave the reactor vessel through superheated-steam outlet nozzles.

The boiler region of the core contains 64 fuel assemblies, each about $4\frac{1}{2}$ in. square by $5\frac{1}{2}$ ft long. The 32 fuel assemblies of the superheater region are arranged in 4 groups of 8 assemblies each around the square boiler region of the core. Reactor power level is controlled by a system of control rods that are located in the boiler region and in the space between the

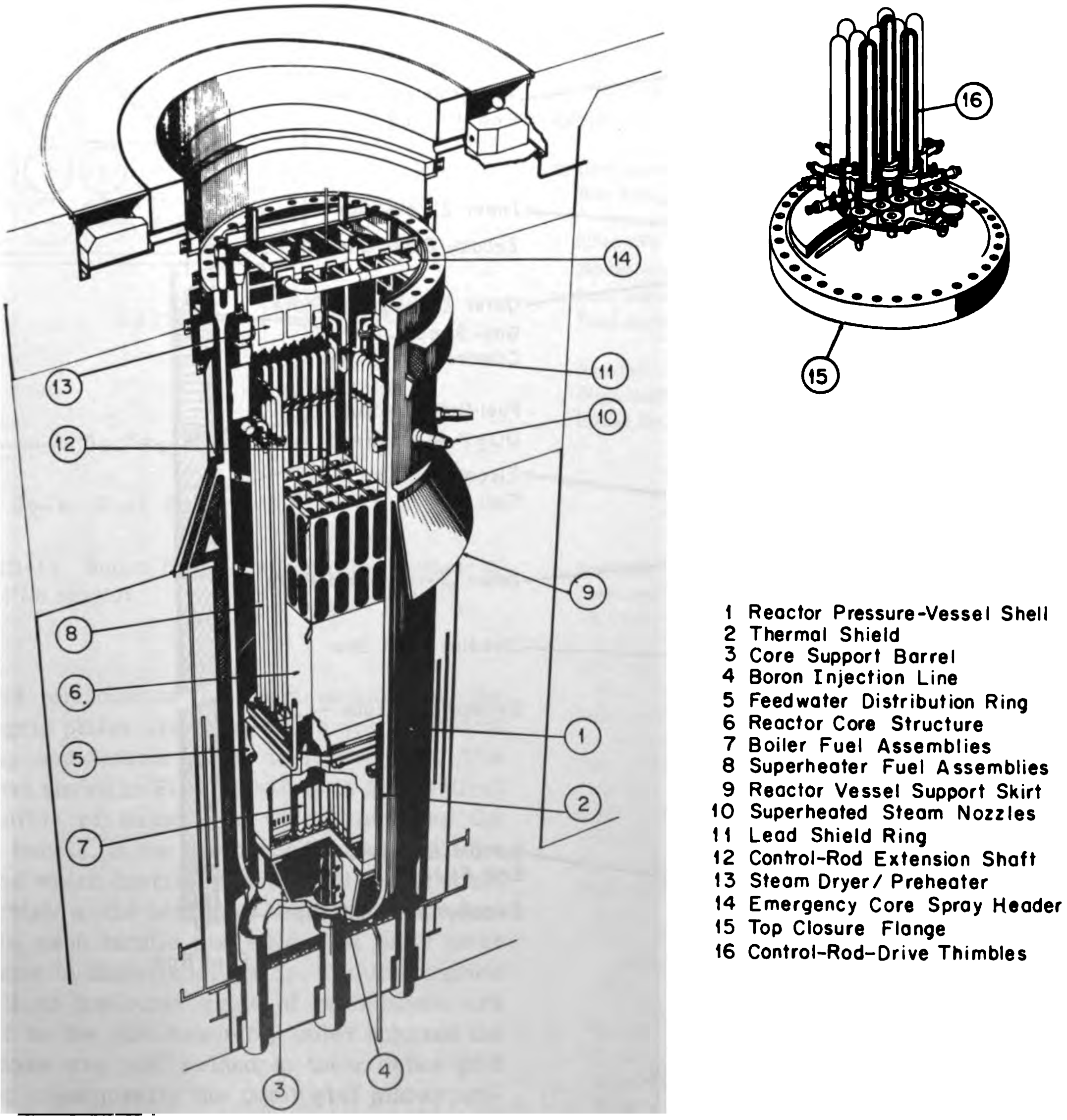
16
15
14
13
12
11
10
9
8
6
5
7
1
2
3
4
1 Reactor Pressure-Vessel Shell
2 Thermal Shield
3 Core Support Barrel
4 Boron Injection Line
5 Feedwater Distribution Ring
6 Reactor Core Structure
7 Boiler Fuel Assemblies
8 Superheater Fuel Assemblies
9 Reactor Vessel Support Skirt
10 Superheated Steam Nozzles
11 Lead Shield Ring
12 Control-Rod Extension Shaft
13 Steam Dryer/ Preheater
14 Emergency Core Spray Header
15 Top Closure Flange
16 Control-Rod-Drive Thimbles

Fig. VIII-15 Perspective view of pressure vessel and internals of the BONUS reactor.

boiler and superheater regions. The rods are top-driven, and their actuators are mounted on the reactor vessel head.

The reactor vessel is carbon steel and is clad internally with stainless steel; the major internal structural members and the recirculation piping are stainless steel.

Boiler Fuel

A boiler fuel assembly and a boiler fuel rod are shown in perspective in Fig. VIII-16, and horizontal cross sections through the rod and the assembly are given in Fig. VIII-17. Each assembly consists of a square Zircaloy-2 outer box, stainless-steel top and bottom end fittings, and two bundles of Zircaloy-clad fuel rods. The two bundles of rods are placed one on top of the other inside the Zircaloy-2 outer box, and each bundle consists of an inner and an outer Zircaloy-2 grid plate, a central square Zircaloy-2 tube, and 32 Zircaloy-clad fuel rods that contain the UO_2 fuel. The inner grid plates are those which occupy positions nearer the

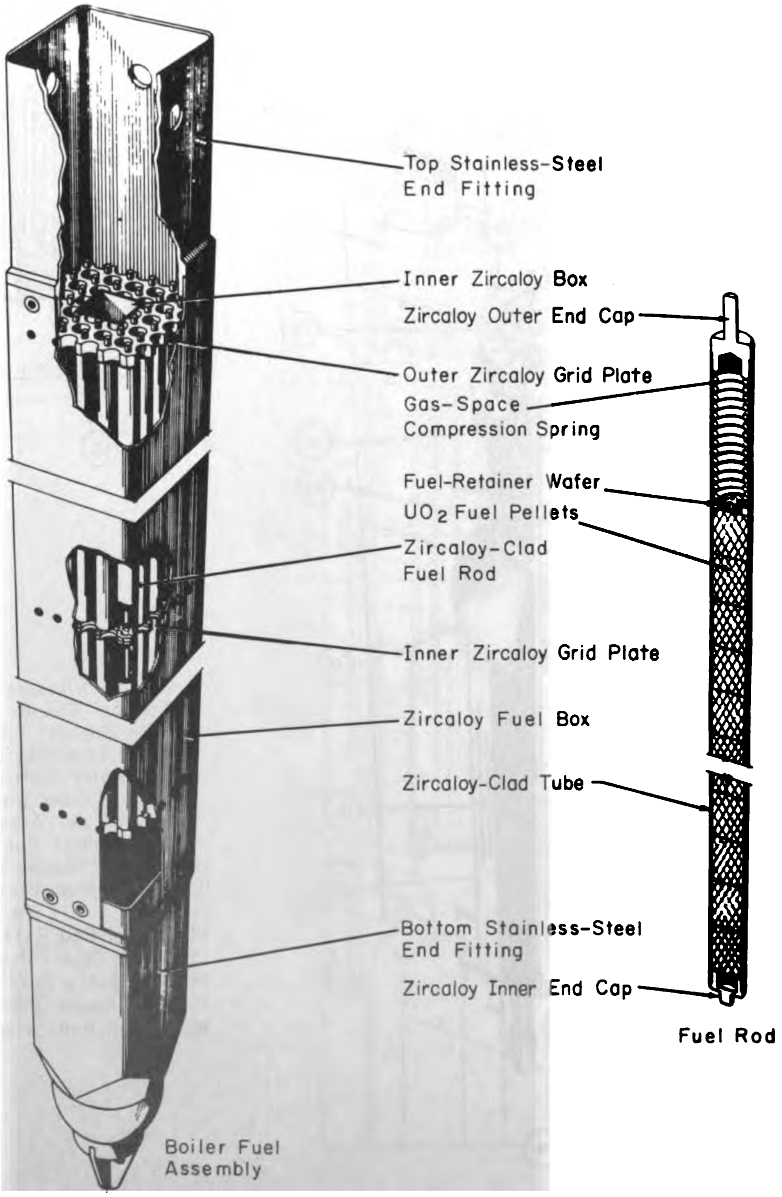

Fig. VIII-16 Perspective view of boiler fuel assembly of the BONUS reactor.

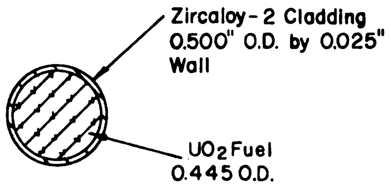

Boiler Fuel Element

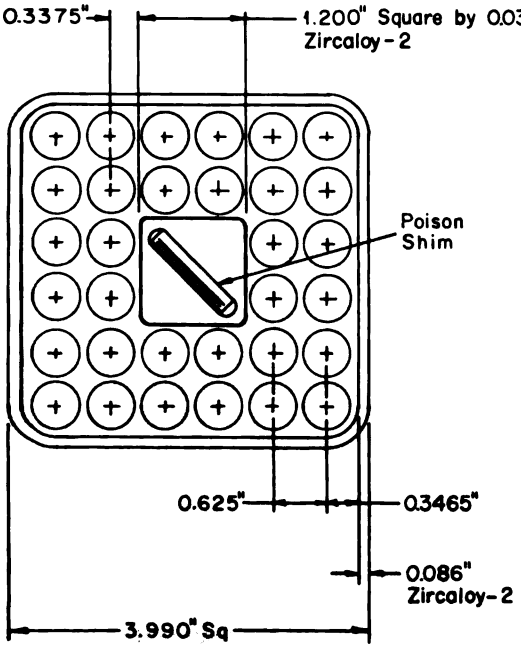

Boiler Fuel Assembly

Fig. VIII-17 Boiler fuel-assembly cross sections of the BONUS reactor.

vertical midpoint of the fuel assembly, and the outer grid plates are those which are located at the top and bottom of the fuel assembly. The fuel rod shown in Fig. VIII-16 is in the vertical orientation of those rods which comprise the upper bundle. In the lower bundle the end of the fuel rod which contains the internal spring would be located at the bottom of the bundle. The fuel rods in each bundle are welded at their inner end caps to their inner grids. The inner grids as well as the outer grids of each bundle are welded to the fuel-assembly outer box, but the fuel rods are not welded to their outer grid plates; consequently the outer grid plates provide only radial spacing of the fuel rods, and the rods are free to expand axially to accommodate differential thermal growth. The upper-bundle rods expand upward, whereas the lower-bundle rods expand downward from the center of the boiler fuel assembly.

The fuel rods are arranged in 6 by 6 square lattice with the four central rods removed. This nonfueled axial region along the center line of the fuel assembly is occupied by a central Zircaloy box. The volume inside the central box is occupied by water that enters the region through an orifice at the inlet end of the bottom fuel bundle. The flow to the region is sufficient to prevent formation of steam by gamma and neutron heating. The central-box region can also contain removable poison shims that are used for axial and radial shaping of the power pattern in the boiling zone.

Boiler-region-component specifications and performance data are given in the following table.

Boiler core region	
Size and geometry of active core, in.	35.4 square by 54.6 high
Effective outside diameter, ft	3.34
Moderator and reflector material	H_2O
Structural metal within active core	Zircaloy-2
Fuel material	UO_2, sintered pellets
Number of fuel assemblies	64
Fuel loading, tons uranium element	2.81
Initial fuel enrichment, wt.% ^{235}U	0.71 (natural U) in four central assemblies; 2.4 in remaining 60 assemblies
Average specific power, Mw(t)/ton uranium element	13.2
Average region power density, kw(t)/liter of region	33.6
H_2O/UO_2 volume ratio (without control rods; superheater unflooded)	2.4
Total steam flow from coolant channels, lb/hr	143,000
Total steam flow from moderator, lb/hr	9000
Total water flow to coolant channels, lb/hr	3.226×10^6
Total water flow to moderator, lb/hr	134,000
Total water flow to reactor vessel, lb/hr	3.360×10^6
Volume composition of active core, %	
Water moderator other than coolant	25.2
UO_2 fuel	25.4
Coolant, steam-water	35.1
Structural metal, Zircaloy-2	7.6
Fuel cladding, Zircaloy-2	6.1
Helium fuel-to-cladding thermal bond	0.6

Boiler fuel assembly	
Fuel elements per assembly	32
Fuel-element pitch, in.	0.625
Assembly structural material	Zircaloy-2
Assembly-can outside dimensions, in.	3.990 square
Can wall thickness, in.	0.086
Central-moderator tube	Square
Moderator-tube outside dimensions, in.	1.200 by 1.200
Moderator-tube wall thickness, in.	0.030
Fuel-cladding outside diameter, in.	0.500
Boiler fuel element	
Element type	Rod, segmented
Fuel type	UO_2, sintered pellets
Total length of fuel, in.	54.0
Fuel length per rod segment, in.	27.0
Fuel-cladding material	Zircaloy-2
Fuel-cladding outside diameter, in.	0.500
Fuel-cladding thickness, in.	0.025
Fuel-to-cladding thermal bond	Helium
Thermal bond thickness, in.	0.0025
UO_2 fuel-pellet diameter, in.	0.445
Boiler heat transfer and fluid flow	
Net heat generation in fuel at 100% full power, Mw(t)	37.0
Heat loss to moderator by gamma and neutron radiation, Mw(t)	0.44
Heat transferred through fuel cladding, Mw(t)	36.3
Net heat transferred to moderator, Mw(t)	0.7
Average heat flux, Btu/(hr)(sq ft)	106,000
Maximum heat flux, Btu/(hr)(sq ft)	367,000
Burnout heat flux, Btu/(hr)(sq ft)	>750,000
Nominal operating pressure, psig	950 (exit)
Water saturation temperature, °F	540
Coolant exit temperature, °F	540
Coolant inlet temperature, °F	532
Feedwater temperature, °F	354
Inlet subcooling, °F	8
Inlet subcooling, Btu/lb	9.8
Average inlet velocity in coolant channels, water, ft/sec	6.3
Average exit velocity in coolant channels, water, ft/sec	9.3
Maximum exit velocity in coolant channels, water, ft/sec	16.0
Maximum fuel-cladding temp., °F	650
Fuel-cladding melting point, °F	3350
Maximum UO_2 fuel centerline temp., °F	4140
Maximum UO_2 fuel surface temperature, °F	1040
Average UO_2 fuel temperature over region, °F	1200
UO_2 fuel melting point, °F	5000
Fraction of total active coolant-channel height in boiling	0.80
Fraction of water-coolant-channel volume in total water of region	0.58
Average steam volume fraction in total water of region	0.147
Average steam volume fraction over total active height of coolant channels	0.23
Average steam volume fraction in boiling section of coolant channels	0.28
Average steam volume fraction at exit of coolant channels	0.42
Maximum steam volume fraction at exit of coolant channels	0.450
Average exit steam volume fraction in total water of region	0.290
Average steam quality at exit of coolant channels	0.0443
Minimum inlet operating pressure, psig	950
Region pressure drop, psi	8.4

Superheater Fuel

A perspective drawing of the superheater fuel assembly is given as Fig. VIII-18, and cross-section dimensions of the assembly and a fuel rod are shown in Fig. VIII-19. Overall height of the assembly, including the standpipes and connectors, is 18 ft 8 in., and its total weight is 325 lb. Steam makes four passes in traversing the superheater assembly, so the flow velocity is relatively high and the heat-transfer coefficient is relatively good. Steam is channeled to the assembly through the inlet standpipe and commences its first pass through the assembly from the top. At the bottom of the assembly, the steam reverses direction and flows upward through the second-pass fuel elements, reverses again at the top of the assembly, flows downward through the third-pass elements, reverses again at the bottom of the assembly, and completes its passage through the fueled region by flowing upward through the fourth-, and final, pass elements to the outlet standpipe. Each of the four passes in an individual fuel assembly contains eight superheater fuel rods spaced in two clusters of four each, as shown in Fig. VIII-19. The standpipes are equpped with connectors that permit the fueled portion of the assembly to be uncoupled, rotated 180°, and recoupled, thereby reversing the position of the individual fuel rods relative to the radial power distribution and permitting a more nearly uniform burnup of the fuel.

The basic flow channels in the superheater assembly are formed by stainless-steel pressure tubes that are brazed to top and bottom tube-sheet structures. The stainless-steel castings that form the top and bottom tube-sheet assemblies are similar in design except for the number and location of pass-divider walls. The lower tube sheet has a single, split-wall pass divider that separates the crossover plenum for the first and second passes from the crossover plenum of the last two passes. The upper tube sheet has two divider walls that separate the inlet and outlet connection plenums from the crossover plenum between the second and third passes. Each plenum in the assembly is lined with a thin-walled member that prevents contact between the superheated steam and the relatively cool walls of the tube-sheet structure. The space between the liner and the structural walls is filled with stagnant steam and acts as an insulator to reduce heat losses to the moderator. The liners slide over the coolant tubes to accommodate differential expansion. The tube portion of the superheater fuel assembly is enclosed by a protective Zircaloy-2 shroud.

The basic fuel element of the superheater assembly consists of a clad fuel rod, formed from cylindrical pellets of UO_2, and a concen-

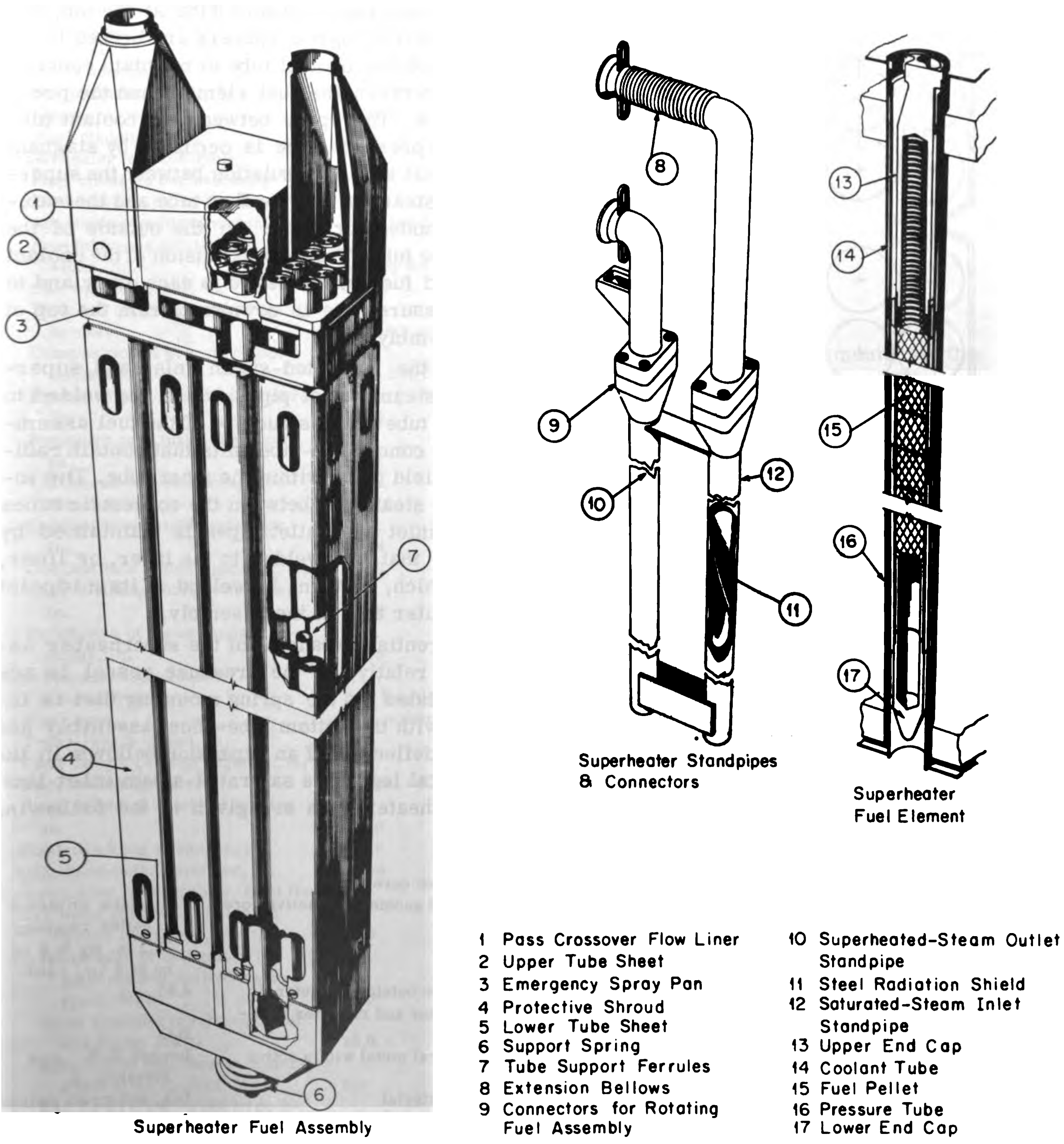

Superheater Fuel Assembly

Superheater Standpipes & Connectors

Superheater Fuel Element

Fig. VIII-18 Perspective view of superheater fuel assembly of the BONUS reactor.

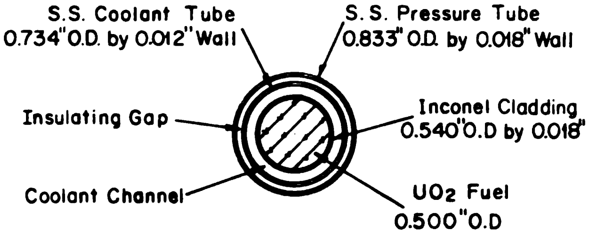

Superheater Fuel Element

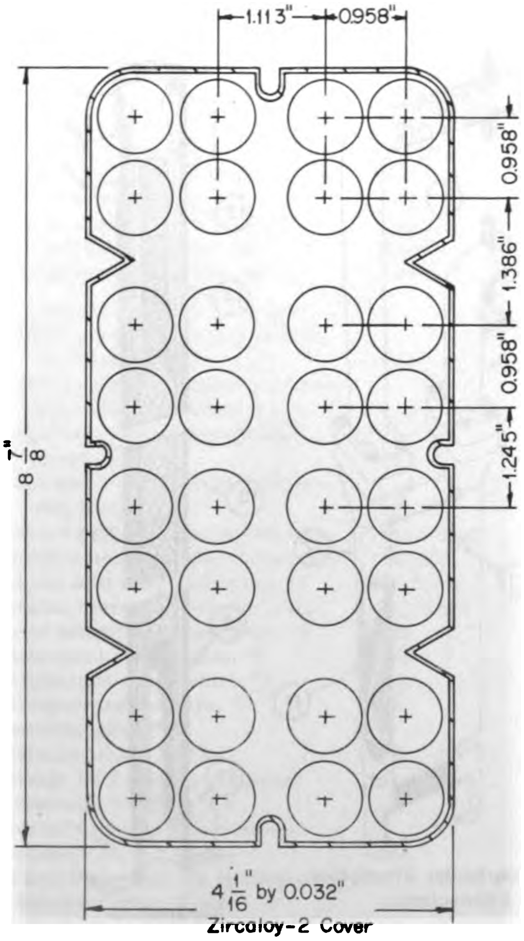

Superheater Fuel Assembly

Fig. VIII-19 Superheater fuel-assembly details, BONUS reactor.

tric coolant tube that forms an annular flow channel. The pellets are concave at each end to permit thermal growth of the central, hottest zone of the pellet relative to the cooler, cladding-restrained surface. Fission-gas space is provided at each end of the fueled portion of the rod between the last pellet and the welded end closure.

The coolant tube, which forms the flow annulus around the superheater rod, is welded to the top end closure of the rod. Radial positioning of the coolant tube relative to the fuel rod is accomplished by four spacer rings with radial guides that are brazed to the fuel cladding and by similar type radial lugs that are cast integral with the bottom closure of the rod. The coolant tube is not affixed to these radial guides.

Each fuel element is brazed to its superheater-assembly pressure tube at the top, and four split-ring spring spacers are brazed to the outside of the coolant tube to maintain concentricity between the fuel element and the pressure tube. The space between the coolant tube and the pressure tube is occupied by stagnant steam that acts as insulation between the superheated steam within the flow tube and the saturated moderator water on the outside of the pressure tube. Thermal expansion of the coolant tube and fuel tube relative to each other and to the pressure tube is downward from the top of the assembly.

Both the saturated-steam inlet and superheated-steam outlet pipes, which are welded to the top tube-sheet structure of the fuel assembly, are concentric-tube units that contain radiation shield plugs within the inner tube. The insulating steam gap between the concentric tubes of the inlet and outlet pipes is maintained by spacers that are welded to the inner, or liner, tube, which, in turn, is welded at its midpoint to the outer tube of the assembly.

Differential expansion of the superheater assembly relative to the pressure vessel is accommodated by the spring mounting that is integral with the bottom tube-sheet assembly and by the deflection of an expansion bellows in the horizontal leg of the saturated-steam inlet line.

Superheater data are given in the following table:

Superheater core region	
Size and geometry of active core	Four slabs adjacent to boiler region: 35.2 in. by 9.8 in by 54.6 in each
Effective outside diameter, ft	4.83
Moderator and reflector material	H_2O
Structural metal within active core	Inconel, S.S and Zircaloy-2
Fuel material	UO_2, sintered pellets
Number of fuel assemblies	32
Fuel loading, tons of uranium element	1.79
Initial fuel enrichment, wt.% ^{235}U	3.25

Average specific power, Mw(t)/ton of uranium element	7.25
Average region power density, kw(t)/liter of region	11.5
H_2O/UO_2 volume ratio (without control rods; superheater unflooded)	3.85
Total steam flow from coolant channels, lb/hr	152,000
Total steam flow from moderator, lb/hr	9000
Approximate volume composition of active core, %	
Water moderator other than coolant	58
UO_2 fuel	15
Coolant, steam	13
Steam insulation	6
Structural metal	2 Zircaloy-2; 5 S.S.
Fuel cladding	2 Inconel
Superheater fuel assembly	
Fuel elements per assembly	32
Fuel-element pitch, in.	0.958
Assembly structural material	Type 348 S.S.
Assembly-can outside dimensions, in.	8.87 by 4.05
Can wall thickness, in.	0.032
Thermal insulation within assembly	Stagnant steam
Composition of pressure and coolant tubes	Type 348 S.S.
Pressure tube outside diameter, in.	0.833
Pressure tube inside diameter, in.	0.797
Thickness of steam insulation annulus, in.	0.0315
Coolant tube outside diameter, in.	0.734
Coolant tube inside diameter, in.	0.710
Fuel cladding outside diameter, in.	0.540
Thickness of steam coolant annulus, in.	0.089
Superheater fuel element	
Element type	Full length
Fuel type	UO_2, sintered pellets
Total length of fuel, in.	54.6
Fuel length per rod segment, in.	54.6
Fuel cladding material	Inconel 600
Fuel cladding outside diameter, in.	0.540
Fuel cladding thickness, in.	0.018
UO_2 fuel-pellet diameter, in.	0.500
Superheater heat transfer, fluid flow	
Net heat generation in fuel at 100% full power, Mw(t)	13.0
Heat loss to moderator by gamma and neutron radiation, Mw(t)	0.50
Heat transferred through fuel cladding, Mw(t)	13.0
Insulation heat loss to moderator from coolant, Mw(t)	0.9
Net heat transferred to coolant, Mw(t)	11.6
Net heat transferred to moderator, Mw(t)	1.4
Average heat flux, Btu/(hr)(sq ft)	66,000
Maximum heat flux, Btu/(hr)(sq ft)	201,000
Nominal operating pressure, inlet, psig	950
Water-saturation temperature, °F	540
Coolant exit temperature, °F	900
Coolant inlet temperature, °F	540
Average inlet velocity in coolant channels, steam, ft/sec	76.0
Average exit velocity in coolant channels, steam, ft/sec	122
Maximum exit velocity in coolant channels, steam, ft/sec	145
Maximum fuel cladding temperature, °F	1175
Maximum UO_2 fuel centerline temperature., °F	3160
Maximum UO_2 fuel surface temperature, °F	1300
Average UO_2 fuel temperature over region, °F	1400
UO_2 fuel melting point, °F	5000
Region pressure drop, psi	79.3

Control Elements

Reactivity control elements in the BONUS core include cruciform control rods located in the boiler region, slab control rods in the space between the boiler and superheater regions, boiler poison shims, boiler-superheater poison shims, and, possibly, superheater poison shims. In addition, the four natural-uranium boiler fuel assemblies located at the center of the core serve as rather massive elements which shim the reactivity and flatten the power.

The poison subassembly of the cruciform control rod consists of four thin, boron–stainless-steel angles that are spot welded together to form a member with a cruciform cross section. The cruciform poison section is joined to a cruciform guide shaft that in turn is welded to an extension shaft equipped with a disconnect fitting for the drive mechanism. In the fully inserted position, the cruciform control rods extend downward to a level 2 in. above the bottom of the fuel region. When fully withdrawn from the core, the rods extend downward to a point 3 in. above the top of the fuel region.

The slab control rods, which occupy channels located between the boiler and superheater regions of the core, are formed from boron–stainless-steel plate. The slab, which is stiffened by a tee reinforcement, is joined to a tee-section guide shaft. As with the cruciform rods, the guide shaft of the slab rod is joined to an extension shaft that has the lower half of the drive-mechanism disconnect fitting at its upper end. Vertical disposition of the slab control rods relative to the active core region, in the fully inserted and the fully withdrawn positions, is the same as for the cruciform control rods.

The boiler shim assemblies are positioned diagonally inside the central boxes of the boiler fuel assemblies as shown in Fig. VIII-17. The shim assembly, shown in perspective in Fig. VIII-20*a*, is basically a holder of boron–stainless-steel strips. The assembly is designed so that different thicknesses and widths of shim strip may be accommodated in a standard mechanical unit. Consequently the shim loading

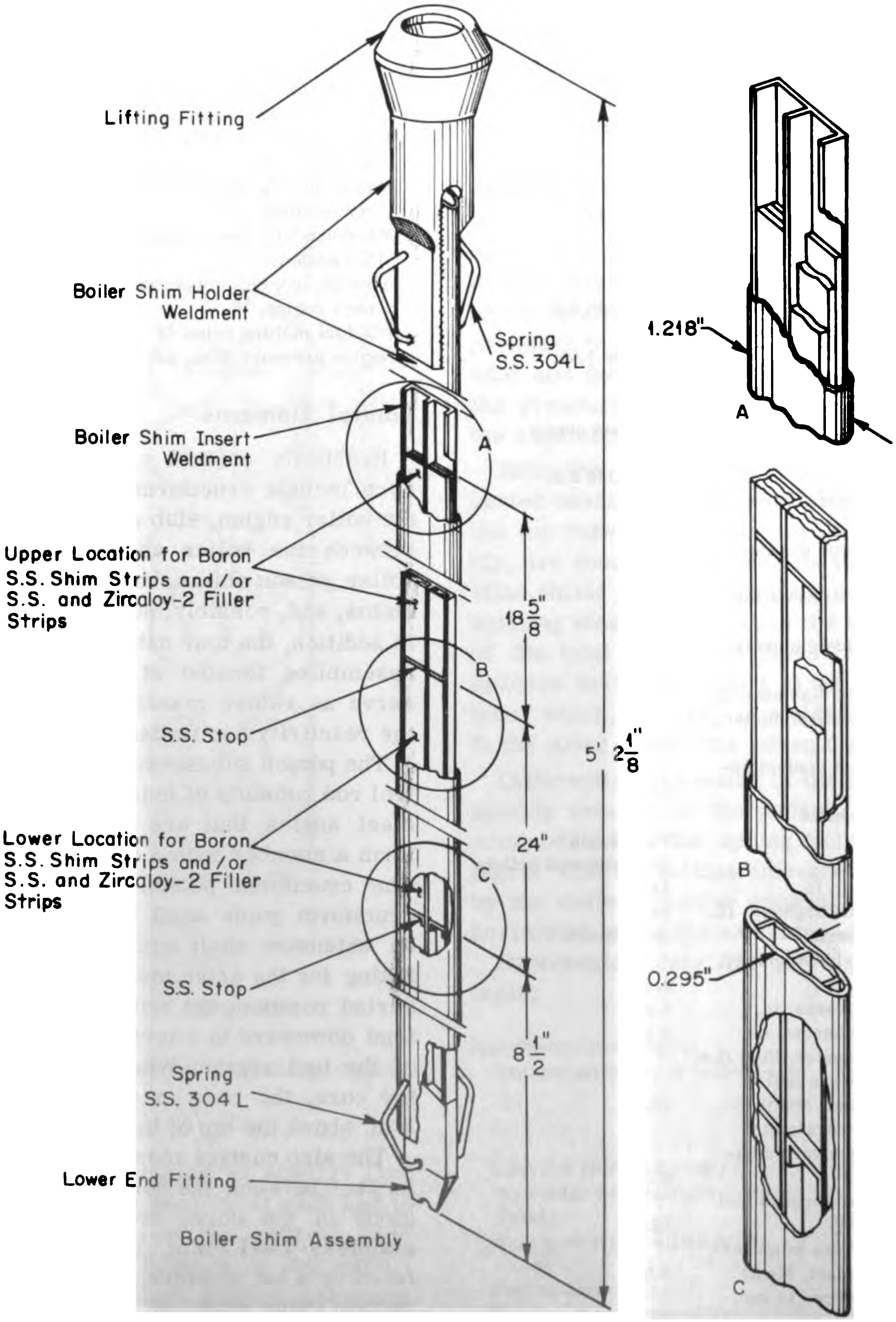
Lifting Fitting
Boiler Shim Holder Weldment
Spring S.S. 304L
Boiler Shim Insert Weldment
A
Upper Location for Boron S.S. Shim Strips and / or S.S. and Zircaloy-2 Filler Strips
$18\frac{5}{8}$"
B
S.S. Stop
5' $2\frac{1}{8}$"
Lower Location for Boron S.S. Shim Strips and / or S.S. and Zircaloy-2 Filler Strips
24"
C
S.S. Stop
$8\frac{1}{2}$"
Spring S.S. 304 L
Lower End Fitting
Boiler Shim Assembly
1.218"
A
B
0.295"
C

Fig. VIII-20*a* Boiler shim assembly of the BONUS reactor.

can be adjusted in fine steps to match closely the requirements for power shaping, etc.

The boiler-superheater shim assembly, shown in Fig. VIII-20*b*, is used to maintain the proper power distribution between the boiler and the superheater regions during the approach to equilibrium fuel cycle. As in the boiler shim assemblies, the poison strength of the assembly can be preselected by loading it with various combinations of shim strips.

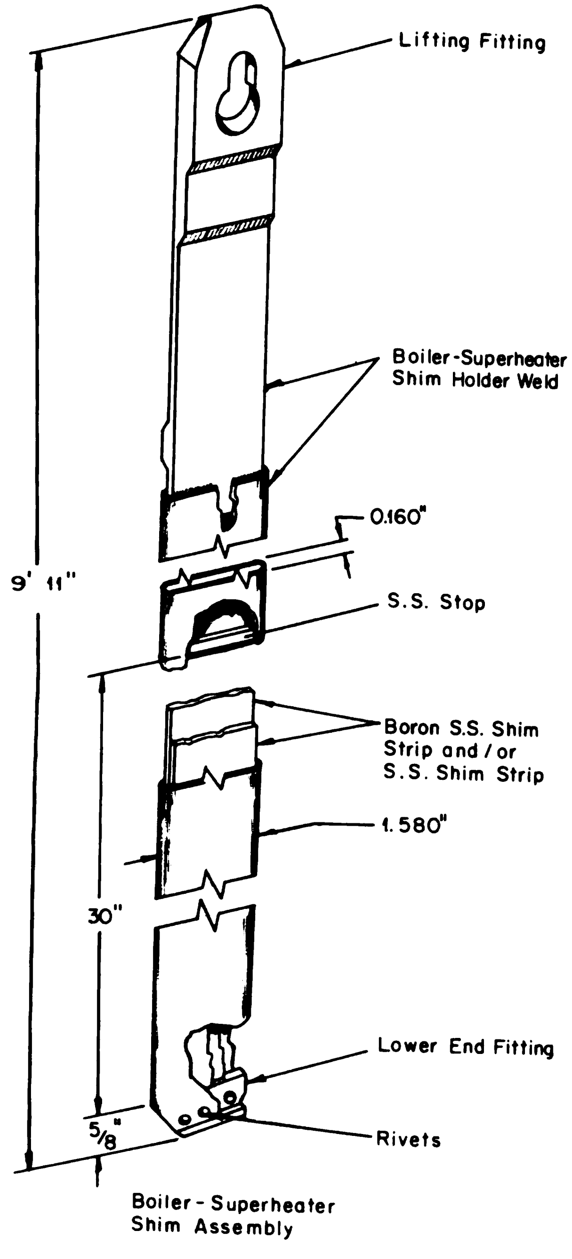
Lifting Fitting
Boiler-Superheater Shim Holder Weld
0.160"
9' 11"
S.S. Stop
Boron S.S. Shim Strip and / or S.S. Shim Strip
1.580"
30"
Lower End Fitting
5/8"
Rivets
Boiler - Superheater Shim Assembly

Fig. VIII-20*b* Boiler-superheater shim assembly of the BONUS reactor.

If it is necessary to decrease the power generation in the superheater fuel zone relative to power generation in the boiler fuel zone, superheater shim assemblies will be employed. The superheater shim assembly is a relatively simple piece, consisting of a boron–stainless-steel shim bar attached to a lifting fitting.

Boiler control rods	
Number	9
Number of drives	9
Shape	Cruciform
Material	1.09 wt.% enriched boron S.S. (92 wt.% ^{10}B)
Span, in.	$7\frac{3}{4}$
Blade thickness, in.	0.125
Poison length, in.	$62\frac{3}{8}$
Superheater control rods	
Number	8
Number of drives	8
Shape	Slab
Material	1.09 wt.% enriched boron S.S. (92 wt.% ^{10}B)
Span, in.	$14\frac{1}{4}$
Blade thickness, in.	0.125
Poison length, in.	$62\frac{3}{8}$
Boiler and boiler-superheater shims	
Poison material	1.25 wt.% natural boron S.S. or type 304L S.S.
Superheater shims	
Width, in.	1.0
Thickness, in.	$\frac{1}{2}$
Material	0.5 wt.% natural boron S.S.

Pressure Vessel and Core Structure

The BONUS reactor pressure vessel is a hollow right-circular cylinder with an integral lower head and a removable upper head. The structural material of the vessel is carbon steel, and a weld-overlaid stainless-steel inside lining provides long-term corrosion resistance. At the closure end of the vessel, where the clear opening is 6 ft 4 in. in diameter, the seal is effected by double, stainless-steel O-rings. Thirty-six $3\frac{1}{2}$-in.-diameter studs are used to secure the vessel top to the shell, and a leak-off connection is provided between the O-ring seal members to prevent leakage outside the vessel. The vessel is supported by a conical steel skirt welded to its outer wall. The skirt rests on a portion of the external shield and is welded to it to prevent lifting of the reactor vessel in the event of a primary-system rupture accident.

An internal thermal shield, consisting of a cylindrical piece of stainless steel, is supported by brackets welded to the lower portions of the vessel wall. A unique feature in the BONUS reactor vessel is the arrangement in the superheated-steam outlet nozzles; the connecting steam piping not only extends outward from the nozzles but internal piping extends inward to the superheated-steam headers. The internal piping, which carries the superheated steam, is insulated from the nozzle forging by seven layers of stainless-steel foil. A summary of reactor-vessel data and a list of nozzles are given at the end of this section.

Figure VIII-21 is a perspective drawing of the reactor core structure. As shown in this figure and in Figs. VIII-14 and VIII-15, the load of the reactor core structure is transferred to the bottom of the reactor pressure vessel by a conical support barrel. This barrel, which is

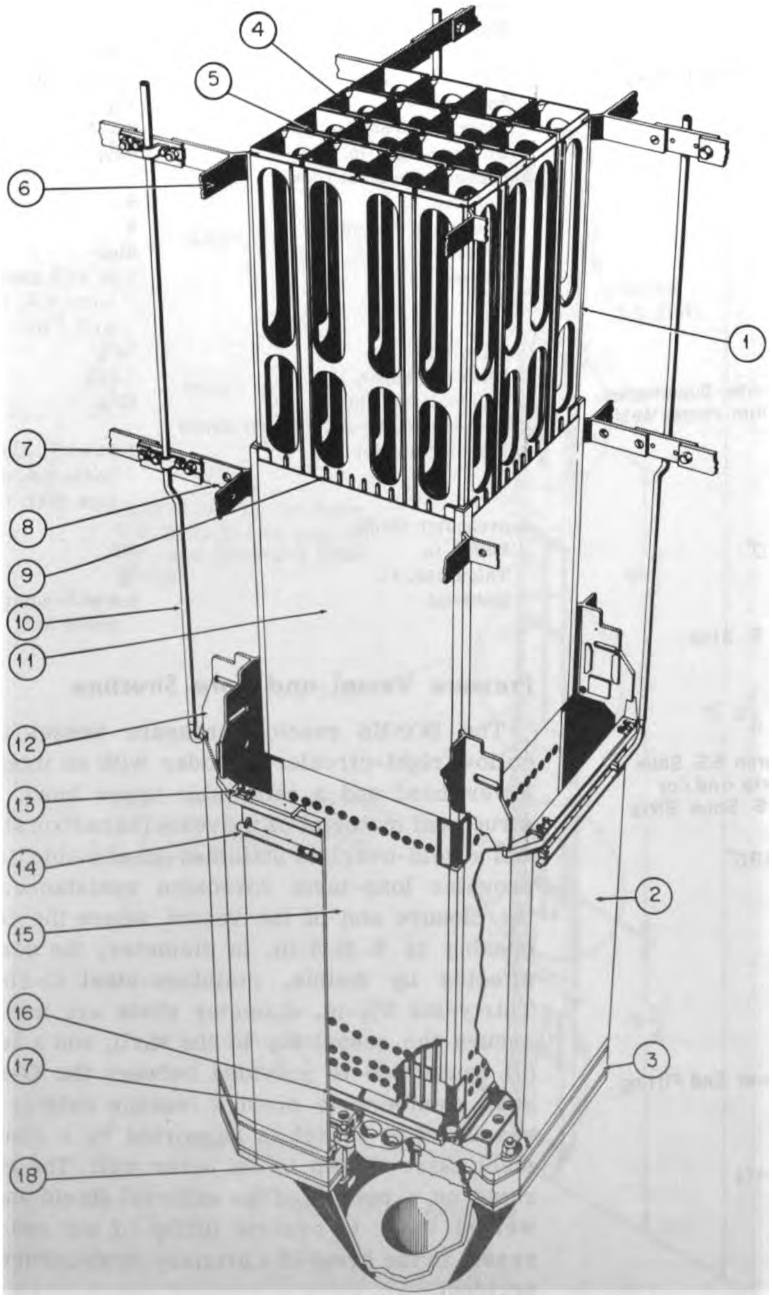

1 Rod Guide Structure
2 Baffle Support
3 Core Plate & Attachments
4 Boxes
5 Spacer Bar
6 Upper Sway Lug
7 Sway Link
8 Lower Sway Lug
9 Shim Channel
10 Superheater Emergency Coolant Pipe
11 Upper Panel Assembly
12 Support Lug
13 Superheater Spacer
14 Emergency Coolant Header
15 Lower Panel Assembly
16 Panel Support
17 Superheater Support
18 T Bolt

Fig. VIII-21 Perspective view of core structure of the BONUS reactor.

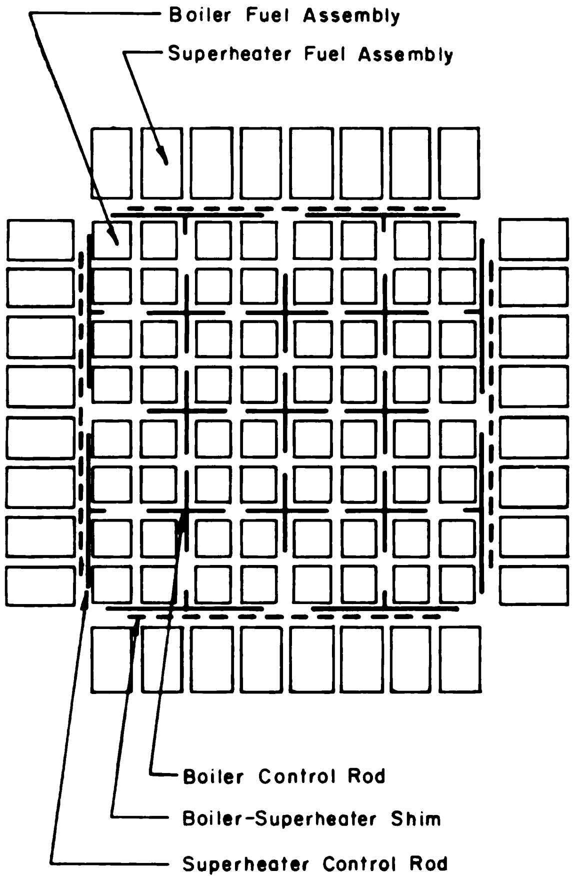

Fig. VIII-22 Control-element locations in the BONUS reactor.

welded to the carbon-steel reactor vessel, contains an Inconel section that acts as a welded transition piece between the stainless-steel upper section of the barrel and the reactor vessel so that stresses due to differential expansion are minimized. The core support barrel is attached at its upper end to the core support plate and supports this plate and the full core load. The barrel also serves as a flow barrier between the coolant-water inlet and the recirculation-water outlets. The stainless-steel core plate contains holes that accept the bottom fittings of the boiler fuel assemblies, provides a mounting space for the superheater fuel-assembly supports, and furnishes a mounting for the core baffle support. The core baffle support transmits the load of the upper superheater grid structure and the control-guide structure to the core support grid. Sway lugs are attached to brackets welded to the vessel wall at two elevations, and four emergency cooling line brackets are welded to the vessel wall. Superheated-steam headers are mounted high in the reactor vessel, as are superheated-steam outlet pipes. Each header has four connector flanges to which superheater-assembly outlet standpipes are attached, and each superheated steam outlet pipe has a single connector flange. The headers are supported by brackets that also serve to support the dryer/preheaters and to furnish the main alignment surface for the reactor-vessel internals.

A boiler emergency spray header is attached by brackets to the underside of the vessel closure head.

Each boiler fuel assembly is supported directly by the bottom grid and is held in place by a hold-down assembly that exerts a lateral force on each of four boiler assemblies through a wedging and spacing action. This force aligns the assemblies under the control-rod guide structure so that they cannot be removed as long as the hold-down assembly is in place.

At each slab type control-rod position, Zircaloy-2 double-walled panels extend downward from the upper guide structure to the bottom grid. These panels serve the dual purpose of defining the slab control-rod channels and providing positions for the boiler-superheater shims. A horizontal cross section through the reactor core, which shows the locations of fuel and control assemblies, is shown in Fig. VIII-22.

Pressure vessel	
Vessel shape	Cylindrical
Vessel wall composition	ASTM A-212 grade B carbon steel; S.S. weld overlay type ER 308L over type ER 309
Vessel inside diameter	7 ft
Vessel overall height	26 ft 7 in.
Vessel wall thickness, base metal	3$\frac{1}{8}$ in.
Vessel cladding thickness	$\frac{1}{4}$ in.
Design pressure	1150 psig
Design temperature	600°F
Operating pressure	950 psig
Operating temperature	540°F
Internal thermal-shield material	AISI type 304 S.S.
Internal thermal-shield thickness	1 in.
External thermal insulation	Fiberglass
External thermal-insulation thickness	3$\frac{1}{2}$ in.
Nozzle list	
Recirculating-water inlet	1, 16-in. schedule 100
Recirculating-water outlets	2, 12-in. schedule 100
Feedwater inlet	1, 4-in. schedule 80
Large superheated-steam outlets	7, 3-in. schedule 80

Small superheated-steam outlets	4, 2-in. schedule 160
Control-rod thimbles	17, 3-in. double extra heavy
Instrumentation thimbles	4, 3-in. double extra heavy
Pressure-relief nozzle	1, 6-in. schedule 80
Upper liquid-level nozzle	1, 2-in. schedule 80S
Lower liquid-level nozzle	1, 2-in. schedule 80S
Vent nozzle	1, 1-in. schedule 80S
Emergency coolant inlet	1, 2-in. schedule 80S
Gasket leak-off nozzle	2, 1-in. schedule 80S
Spare nozzle	1, 2-in. schedule 80S

Control and Instrumentation

The control concept employed in the BONUS station is one in which the reactor establishes the plant output, and control of the turbine admission valves is made responsive to reactor pressure. The turbine accepts the steam generated by the reactor and maintains a load such that the reactor pressure is held constant at its set point. Control of reactor power level is accomplished by movement of the cruciform-shaped and slab type control rods. Although the recirculation flow loops in the BONUS plant are provided with flow-control valves that can be used for making initial adjustments of the recirculation rate, reactor power will not normally be controlled by varying recirculation flow.

The superheated-steam exit temperature of the reactor is allowed to vary between 900 and 950°F, and an automatic attemperator spray-control system is provided in the main steam-supply line to maintain steam temperature at the inlet of the turbine essentially constant and equal to a nominal value of 900°F.

Pressure control is accomplished by an integrated master system composed of three valve-control systems: the turbine-admission-valve control system, the turbine-bypass-valve control system, and the minimum-flow bypass-valve control system. The functional interconnection of these systems, which provides control of reactor pressure, is such that the proper system or combination of systems is brought into use as the particular pressure set point and operating conditions demand.

A block diagram of the 10-channel nuclear instrumentation system of the BONUS reactor was given in *Power Reactor Technology*, 5(2): 68. The reactor contains no in-core instrumentation.

All control rods are provided with rack-and-pinion type top-mounted drives. Only one rod can be moved at a time, which results in a maximum reactivity-addition rate of approximately 0.01% k_{eff}/sec.

The reactor system is provided with a manually operated, gravity-flow liquid-poison system. A 20 wt.% solution of boric acid in water is stored in a pressure vessel mounted about 18 ft above the normal reactor water level. The 114 gal of boric acid solution are kept hot (193°F) during storage to prevent thermal shock to the reactor vessel during poison injection. Injection of all the poison solution into the reactor requires about 3 min and results in a reactivity decrease of such magnitude that the reactor is 1.5% subcritical when cold, clean, with normal water level, and all rods and shims out of the core.

Recirculation System

The major components of the recirculation loops are shown schematically in Fig. VIII-13. Slightly subcooled water is pumped into the core via the bottom inlet nozzle and plenum. The water rises through the boiler assemblies where it is heated to saturation, after which steam is separated from the water, and the water flows radially outward and then down between the reactor core and pressure-vessel wall. As the saturated water descends in the vessel, it mixes with relatively cold feedwater that reduces the overall temperature of the recirculation mixture to a subcooled level. The subcooled water leaves the vessel at the bottom through two nozzles and descends through downcomers to the reactor circulating-water pumps, which are located in a pump room beneath the reactor vessel. Discharge lines from the circulating pumps feed a common, single riser that returns the recirculation water to the reactor vessel.

The two downcomer pipes are equipped with motor-operated gate valves, and the discharge line from each pump is equipped with a motor-operated gate valve, a check valve, and a flowmeter. Either pump can be isolated from the reactor by closing its gate valves. The check valves prevent reverse flow through a pump if it fails, and the other pump continues to operate.

Of the total water flow to the reactor vessel, 95% passes through the coolant channels and the remaining 5% flows to the moderator and to the control-rod channels between the boiler fuel-assembly boxes. Characteristics of the recirculation-system components are listed in the following table:

Recirculation pumps	
Number	2 (one per loop)
Type	Vertical, single stage, single volute, centrifugal
Nozzle diameter	
Suction	12 in.
Discharge	10 in.
Rated flow each	4500 gal/min
Developed head at rated flow	67 ft
Piping diameter	
Reactor to pumps	12 in.
Pumps to riser	10 in.
Riser to reactor	16 in.

Turbine-Generator, Condensate, and Feedwater Systems

The power-conversion cycle and equipment of the BONUS plant are essentially the same as those of a conventional power plant. Steam flows from the reactor through the main steam line to the turbine-condenser unit. Condensate pumps take water from the condenser hot well and pump it through the air ejector after coolers, a gland-seal condenser, condensate purification units, and three low-pressure feedwater heaters, to the main feed pumps. The feed pumps raise the pressure of the condensate and force it through the high-pressure feedwater heater and the feedwater regulating valve back into the reactor.

The single-casing single-flow turbine, which has four extraction openings for feedwater heating, drives a standard 13.8-kv 3-phase 60-cycle hydrogen-cooled generator. The gland-seal system used for the turbine shaft seals is a standard pressure-breakdown type. Steam leakoff from the high-pressure packing at the high-pressure end of the turbine is fed to the extraction line leading to feedwater heater No. 1. During turbine operation the seal gland at the low-pressure end of the turbine is normally fed by steam that is bled from the leak-off connection on the high-pressure seal gland; however, with the turbine shut down, reactor steam is supplied to the seals through the seal steam regulator. The outer chamber of all seal glands is maintained at a negative pressure with respect to the building atmosphere by means of gland-seal exhausters.

The reactor is equipped with a saturated steam line that leads to an emergency condenser, and on a branch from this line a series of safety valves is installed to prevent excessive pressures in the reactor system. The location of these valves is shown in Fig. VIII-13.

The two-pass main condenser is capable of condensing the full output of the reactor when the turbine bypass valves are open and a condenser pressure of 3.5 in. Hg abs. is available. The condenser has a divided hot well and divided water boxes, and its condensate storage capacity is sufficient for a 4- to 9-min holdup at full-flow conditions. Condenser cooling is accomplished with pumped seawater.

Turbine	
Number	1
Description	Single-casing ASME-AIEE preferred standard
Nameplate rating	16,500 kw
Turbine throttle conditions at full full load	
Superheated-steam weight flow	151,000 lb/hr
Pressure	850 psig
Temperature	900°F
First extraction	163 psia; 6734 lb/hr
Second extraction	64 psia; 7312 lb/hr
Third extraction	27.2 psia; 8251 lb/hr
Fourth extraction	8.14 psia; 7703 lb/hr
Exhaust-steam enthalpy, CEP	1010.3 Btu/lb
Exhaust-steam weight flow	117,285 lb/hr
Generator	
Number	1
Description	13,800-volt, 3ϕ, 60 cps, 3600 rpm, ASME-AIEE preferred standard
Terminal output	17,506 kw
Capability at 0.85 lb-ft and 30 psig H_2 pressure	22,059 kva
Main condenser	
Number	1
Description	Two-pass single-shell divided waterbox and hot well
Heat-transfer surface	20,000 sq ft
Capacity	119,000 lb/hr
Operating pressure with 85°F cooling water	2 in. Hg abs.
Tube description	
Material	Aluminum and brass
Number	4368
Outside diameter	$\frac{7}{8}$ in.
Wall thickness, BWG	16
Length	20 ft
Cooling-water flow rate	17,800 gal/min
Cooling-water temperature, inlet	85°F

Plant Arrangement and Containment

A total-containment design philosophy is employed in the BONUS plant. The general containment type that results from this philosophy was compared to other types in *Power Reactor Technology*, 5(1): 34-35, and a discussion of the actual BONUS containment appeared in *Power Reactor Technology*, 5(2): 54-55.

The basic components of the containment building are a steel dome, a short cylindrical steel section, and a concrete foundation slab. A perspective view of the building, showing the arrangement of plant equipment, is given as Fig. VIII-23, and dimensions and specifications are listed in the following table:

Containment building	
Shape	Cylindrical steel and concrete wall, hemispherical steel dome, flat concrete-floor slab
Overall dimensions	
Diameter	166 ft 8 in.
Height inside	107 ft 4 in.
Building height above ground	84 ft 4 in.
Concrete-wall dimension	
Minimum thickness	18 in.
Height	26 ft 6 in.
Dome	
Diameter	166 ft 8 in.
Wall thickness	$\frac{5}{16}$ in.
Material	Carbon steel, ASTM A-201 grade B
Cylindrical shell	
Height	26 ft 4 in.
Wall thickness	$\frac{3}{8}$ in.
Material	Carbon steel, ASTM A-201 grade B

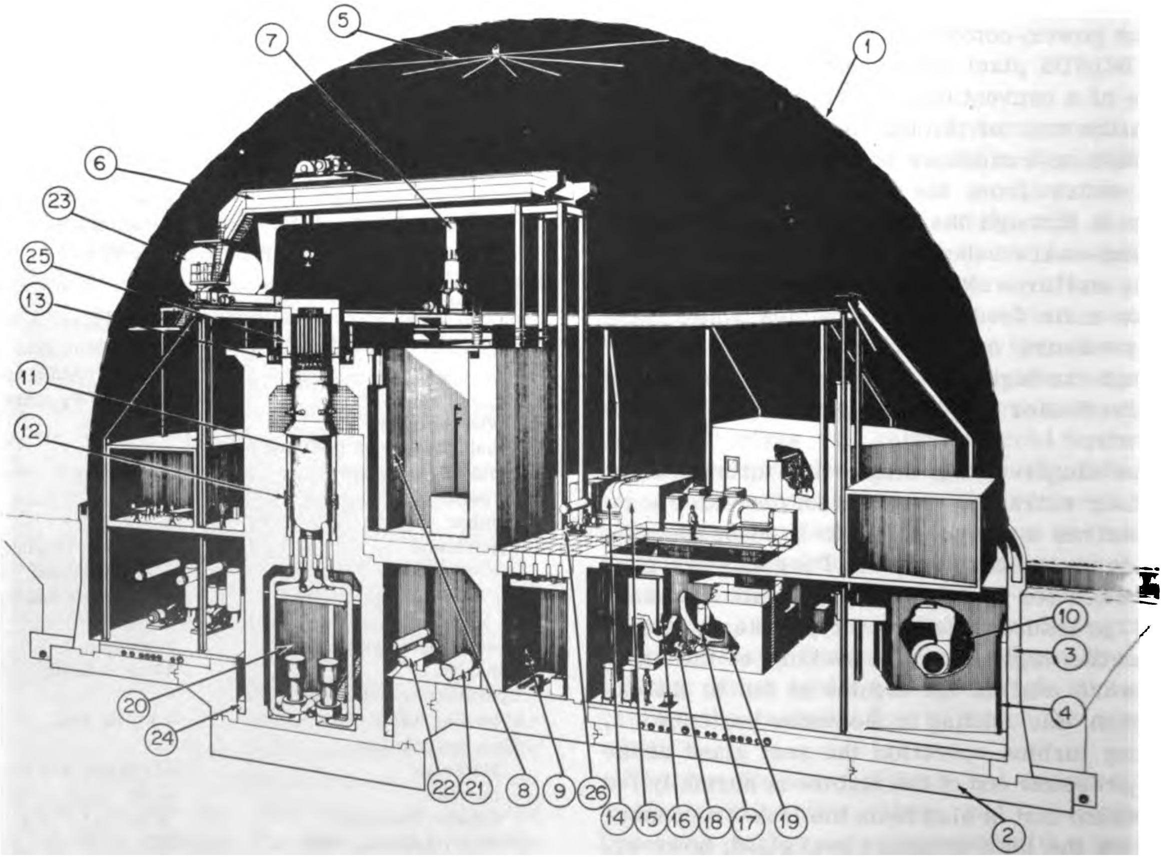

1 Steel Dome
2 Foundation Mat
3 Retainer Wall
4 Freight Door
5 Building Spray
6 Polar Gantry Crane
7 Fuel Unloading Coffin
8 Spent-Fuel Storage Pool
9 Solid Radioactive-Waste Storage
10 Building Ventilation Intake Fan
11 Reactor Pressure Vessel
12 Neutron Shield Tank
13 Control-Rod-Drive Motor Trench
14 Turbine Generator
15 Turbine Shield
16 Condenser
17 Condensate Pumps
18 Evactor Pump
19 Gland Seal Condenser
20 Reactor Circulating-Water Pump Room
21 Startup Heater
22 Reactor Water-Purification Coolers
23 Emergency Condenser
24 Reactor Pit Water Moat
25 Removable Concrete Shield
26 Fuel Pool Cooling System

Fig. VIII-23 Perspective view of containment building, BONUS power station.

Design pressure	5 psig
Design temperature	140°F
Free volume of containment barrier	1.59×10^6 cu ft
Design leak rate of steel shell, % of building vol./day at 5 psig	0.2
Maximum permissible leak rate, including floor slab and all penetrations, % of building vol./day at 5 psig	0.4

Purification and Radioactive Waste Disposal

The scheme of disposing of the noncondensable gases formed during reactor operation is one in which radiolytic and radioactive gases are removed from the main condenser by the air ejector and then are subjected to a series of holdups and filtrations before being discharged to the reactor building exhaust. A schematic diagram of the system is shown in Fig. VIII-24.

The principal liquid wastes are expected to be low-level wastes that can be processed at the plant and discharged to the sea. Any liquid wastes containing high levels of radioactivity will be converted to solid waste by the addition of absorbent solids or by casting in cement.

Solid wastes from the BONUS plant will be handled by bailing or by drum storage. A hot-waste storage area, with sufficient capacity to handle the waste generated over a period of several years, will be used as a collection point for material awaiting off-site shipment for permanent disposal. The estimated rates of generation of solid wastes are given in the following table:

Waste source	Quantity of waste, 66-gal drums/year
Filters, condensate, reactor, and pool	5
IX resins	4
Charcoal traps	1
Liquid-waste concentrate	6
Baled-paper waste	7
Miscellaneous, air filters, etc.	2
Total (estimated)	25

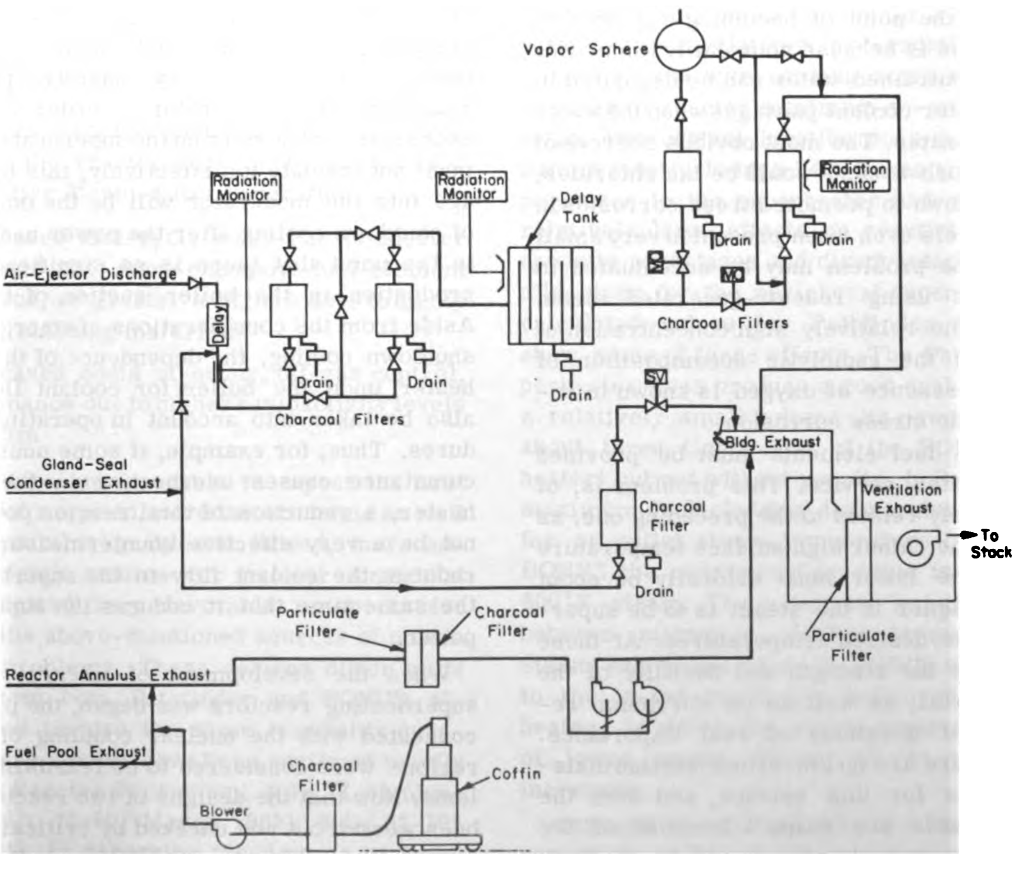

Fig. VIII-24 Gaseous waste-disposal system of the BONUS power station.

Discussion

The incorporation of integral nuclear superheat into the basic concept of the direct-cycle boiling-water reactor appears to be the most straightforward way of attaining the modern steam conditions that are generally regarded as an important goal for nuclear steam generation. Designers can build on the established boiling-water technology to eliminate some of the developmental problems that usually accompany the proving of a new concept and can use the direct cycle (no heat exchangers) to minimize the reactor temperatures necessary for a given steam temperature, although the direct-cycle steam may prove to be a difficult reactor coolant.

Relative to the direct-cycle saturated-steam boiling reactor, the provision of integral nuclear superheat seems to have added at least the four new questions of feasibility that follow.

1. Effective steam-water separation, and, in particular, the problem of water carry-over in the steam, assumes much greater importance, probably to the point of becoming a feasibility problem. This is because nonvolatile impurities carried by entrained water can be deposited in the superheater coolant passages when the water finally evaporates. The most obvious sources of trouble in such a case would be the chlorides, which are known to promote stress corrosion in stainless steels even when present in very small amounts. The problem may be accentuated in superheaters using reactor-generated steam because of the relatively high concentration of oxygen from the radiolytic decomposition of water; the presence of oxygen is known to enhance chloride stress corrosion.

2. Suitable fuel elements must be provided for superheater service. This problem is, of course, closely related to the preceding one, as well as to the rather high surface temperature required. The latter must evidently be about 1200°F or higher if the steam is to be superheated to the desired temperatures. At these temperatures the strength and ductility of the jacket material, as well as its corrosion resistance, are questions of real importance. Currently there are no low-cross-section materials suitable for this service, and even the stainless steels are suspect because of the stress-corrosion problem.

3. The question of radioactive carry-over into the turbine and the off-gas system of the superheat reactor cannot be assumed to be settled by the favorable past experience with direct-cycle saturated-steam boiling reactors. This is true because the boilers benefit from a large decontamination factor: when the steam evaporates, nearly all the nonvolatile impurities are left behind in the water. The boiler sections of integral superheat reactors will enjoy the same effect, but any radioactive products that are added to the steam in the superheater — as from a failed or leaky fuel element — will pass on into the turbine.

4. The coupling of the two sections of the reactor — the boiler and the superheater — in terms of both the neutron chain reaction and the coolant flow introduces unique relations of core design and plant operation. It is essential to provide means for adjusting and maintaining the division of power between the boiler and the superheater, over the reactivity lifetime of both, at proper values to yield the desired steam outlet temperature.

The superheater normally has no independent coolant supply of its own, but is dependent upon steam generated by the boiler. Therefore the designer, although he must thermally insulate the superheater coolant passages from the surrounding water moderator in order to prevent excessive heat loss from the superheated steam, must not insulate too effectively; this heat leakage into the moderator will be the only means of shutdown cooling after the power has decayed to the point that there is no significant steam production in the boiler section of the core. Aside from the considerations of emergency and shutdown cooling, the dependence of the superheater upon the boiler for coolant flow must also be taken into account in operating procedures. Thus, for example, if some unusual circumstance causes overheating in the superheater, a reduction of total reactor power may not be a very effective countermeasure, for it reduces the coolant flow to the superheater at the same time that it reduces the superheater power.

When the development of integral boiling-superheating reactors was begun, the problems connected with the nuclear coupling of the two regions were considered to be feasibility problems. Now that the designs of two reactors have been worked out and checked by critical experiments, the problems are no longer in that category, but the measures taken for their solution have played important roles in determining the core designs and must be taken into account in any assessment of the designs.

The nature of the preceding problems is such that they cannot be completely resolved except by operation of the reactor itself. For this reason the performances of the Pathfinder and BONUS reactors will be of great interest, and if utilized effectively these reactors may provide invaluable information for reactor development for some years to come.

For the successful development of a reactor type, it is not enough that the feasibility problems be solved; rather, they must be solved in a manner that will make the reactor type economically competitive. Since the integral nuclear superheat reactor represents an extension of direct-cycle boiling-water technology, the economic requirements in this case can perhaps be stated more directly than in most cases of a new reactor type. Economic advantages will accrue from the higher thermal efficiency and from the savings in cost of the turbine and associated equipment. For economic success of the reactor type, it is necessary that these advantages not be nullified by costs associated with the superheating feature. Conceivable sources of such costs include:

—increased capital costs due to lower power density in the reactor core or to the need for very effective steam-water separation

—increased fuel-cycle costs due to shorter fuel-element life, more expensive fuel-element construction, or greater neutron losses to highly absorbing cladding materials

—increased costs of siting, off-gas control, or maintenance due to higher radioactivity levels in the steam

It would be unreasonable to expect the first reactors of a type to solve the economic as well as the feasibility problems. Indeed, more advanced design studies for nuclear superheat have indicated very favorable prospects for avoiding the above-mentioned sources of possible cost problems. These designs differ quite widely from both Pathfinder and BONUS, although they involve the same feasibility questions. These studies have been reviewed briefly in *Power Reactor Technology*, 4(3): 71-85 (June 1961); 6(2): 75-80 (March 1963); 6(4): 97-105 (Fall 1963). In assessing the designs of Pathfinder and BONUS, it is reasonable to ask whether they advance the technology in the directions that are most likely to lead to good economic performance.

The differences between the two designs are substantial. Some of these differences are due to the design power output, and some are rather incidental. It would not be feasible, for example, to employ the BONUS system of superheater power-level control, which utilizes sheets (blades) of absorbing material between the boiler and superheater, in a very much larger reactor. On the other hand, the use of this system rather than a set of control rods within the superheater is a rather incidental design choice. The difference in reactor size may have been of greater significance in fostering a somewhat bolder approach in the smaller BONUS reactor. This approach is reflected by the higher design values of steam temperature and pressure in BONUS relative to Pathfinder.

The question of a central or peripheral location for the superheater section generates many pros and cons for each approach. When the question is considered in a general way, the central location is usually credited with requiring a relatively small volume for a given power, with having a relatively flat radial power distribution, and with causing some reduction in the overall reactor maximum-to-average power ratio. The central location does, however, result in relatively high heat fluxes and fuel temperatures in the superheater and does lead to relatively large effects on reactivity. Just the opposite advantages and disadvantages are usually given for the peripheral superheater. The calculated values for Pathfinder and BONUS show some of these effects. The Pathfinder superheater does produce a good deal of power in a relatively small volume (its power density is about three times that of the BONUS superheater) but not without penalty. In Pathfinder the maximum fuel-cladding temperature is 1270°F for an outlet steam temperature of 725°F; in BONUS the corresponding value is 1175°F for 900°F steam. The relatively small difference between maximum cladding temperature and steam exit temperature in BONUS is due partly to the in-out multipass design of the superheater, in which the steam traverses regions of lower power density as its temperature increases.

Although the Pathfinder fuel operates at a somewhat higher maximum surface temperature than the BONUS fuel, its required lifetime is much shorter (nine months, about one-sixth that of the BONUS fuel). This is due partly to the shorter reactivity lifetime of the highly enriched superheater fuel. From the long-range standpoint, it is questionable whether highly enriched fuel has an economic future in central-station power reactors, and in this respect the BONUS development, if it is successful, may represent a more direct approach to ultimate economic success. In some ways the oxide-pellet slightly enriched fuel appears also to offer advantages in solving the corrosion problems, for it allows considerable flexibility in the choice of jacket material. It was a relatively straightforward matter, for example, to modify the BONUS fuel-element jacket, from stainless steel to Inconel, after the seriousness of the stress-corrosion problem in stainless steel became apparent.

The nuclear designs of the two reactors are characteristic of their basic geometrical arrangements. As mentioned above, the power split between boiler and superheater is controlled in BONUS by means of blade type control rods at the boiler-superheater boundary, whereas Pathfinder has control rods in both the boiler and the superheater. The nuclear design of each reactor is such that reactivity effects from flooding or voiding of the superheater regions are minimized by suitable choice of the fuel-to-water ratio. Under operating conditions, flooding of the Pathfinder superheater causes a reactivity change of $-0.66\%\ \Delta k/k$, whereas flooding of the BONUS superheater results in a reactivity gain of $0.16\%\ k_{\text{eff}}$.

The problem of obtaining the required degree of steam-water separation is handled differently in the two plants. Pathfinder has centrifugal separators in its downcomer region to remove entrained steam from the recirculation water, whereas BONUS, with no such mechanical devices, relies on gravitational separation. Pathfinder has a mesh type steam dryer through which saturated steam must pass on its way to the superheater region of the core, and BONUS has dryer units in the same relative location and preheats the steam slightly before its entrance to the superheater proper by regenerative heat exchange with the exit steam.

The BONUS reactor is provided with a gravity-actuated emergency core spray that will cool the boiler and superheater fuel elements in the event all primary cooling water is lost from the vessel. Pathfinder, on the other hand, relies on the normal feedwater supply to provide cooling water to the reactor vessel faster than it is lost.

In summary, it can be said that the integral-superheat reactors of the Pathfinder and BONUS plants show originality of concept and reflect interesting differences in design approach. With the plants now in the process of startup, speculation as to their probable performance is pointless, since experience should soon provide the answers to questions of operational capabilities.

References

1. Northern States Power Co., Pathfinder Atomic Power Plant Safeguards Report, Part II. License Application, USAEC Report ACNP-5905, Jan. 15, 1962, and addenda.
2. Northern States Power Co., Technical Specifications for Pathfinder Atomic Power Plant, May 28, 1963.
3. General Nuclear Engineering Corp. and the Puerto Rico Water Resources Authority, Boiling Nuclear Superheater (BONUS) Power Station, Final Hazards Summary Report, USAEC Report PRWRA-GNEC-5, Feb. 1, 1962, and addenda.

Section

IX

Operating Experience

Consolidated Edison Nuclear Steam-Generating Station

The Consolidated Edison Thorium Reactor (CETR) was described in detail in *Power Reactor Technology*, 6(3): 28-40. Since that review a number of articles dealing with the operating experience of the CETR have been published.[1–6] Reference 1 is a paper from a conference on operating experience with power reactors; the conference was sponsored by the International Atomic Energy Agency in June 1963. References 2 to 6 are papers that were presented at the Winter Meeting of the American Nuclear Society, November 1963. In 1962, the provisional operating license for the CETR was issued in March, the facility was completed in May, criticality was achieved on August 2, and the unit was placed on-line on September 16. Operation at full power occurred on Jan. 25, 1963; as of March 1964, a total of about 1.2×10^6 Mw-hr had been generated.

An early trouble was experienced with the coating of the fuel-transfer canal. This coating was a phenolic paint, and leakage of water occurred through defects in the paint or around inadequately sealed points of attachment of anchors. A similar problem was also experienced at the Shippingport reactor and is reviewed in *Power Reactor Technology*, 6(3): 51. In Ref. 2 it is stated that work was done on the CETR fuel-transfer pool during August and September of 1963; however, no details of this work are given. Difficulties were noted in the ability to produce and maintain water in the fuel-transfer-system pool of sufficient visual clarity for satisfactory handling of the core and core components. The fuel-transfer system was designed to be flooded with water from condensed bleed steam; before power operation the system used treated water. Algae were found to be present in the fuel pools, and it is postulated[2] that the algae fed on the cyclohexylamine present in water as a corrosion inhibitor. The following temporary measures were instituted to clarify the water:[2]

1. Drain the pools and treat the pool walls with hydrogen peroxide for algae control.
2. Abandon cyclohexylamine treatment of the particular tank furnishing makeup water for this purpose.
3. Install a temporary wood cellulose filter to remove the fine silt and corrosion products present in the unevaporated makeup water. These steps were successful in making fuel loading under a full head of water possible.

Tests of the reactor head joint revealed a leak-free seal. Although provision had been made for seal-welding the top head closure, the seal ring was welded to the head only and not to the body of the vessel. However, other bolted-joint components were seal welded. These items included the pressurizer vent-valve bonnet and the hinge-pin covers on all eight discharge check valves for the primary coolant pumps. Not all hinge-pin covers experienced leakage, but all were welded as a precaution.

During the first six months of operation, 187 automatic shutdowns occurred. They were not occasioned by a reactor safety problem but were the result of malfunctions of associated equipment and conservative settings of the nuclear instruments. Of these shutdowns, about 20% were from malfunctions in nuclear instrumentation systems, 25% originated in the control system for the control-rod drives, and about 30% were caused by malfunctions in the conventional plant equipment. The remaining 25% were from miscellaneous causes, generally nonrepetitive in nature.

THE UNIVERSITY OF MICHIGAN LIBRARIES

The control-rod-drive system appears to be the most interesting area of operating experience reported. The drive system, shown in Fig. V-6 of *Power Reactor Technology*, 6(3), is sealed in an 1800-psi pressure-tight housing. Experience demonstrated that the small amount of leakage past the shaft seal, plus the water that was carried down into the housing by a wet shaft, produced a high-humidity condition. This atmosphere seemed particularly hard on the miniature switch that reported disengagement of the drive shaft from its carriage and the one that operated when full insertion was reached. The following is quoted from Ref. 2:

> ... Various corrective measures were made including the use of a switch redesigned to reduce its susceptibility to moisture interference, and a system to purge the drive mechanism housing with dry nitrogen to limit humidity. These measures were partially successful, and recently, further improvements have been made to provide for an arrangement allowing individual nitrogen flow control to each housing in accordance with certain electrical circuit resistance readings periodically made as an indicator of moisture in the housing, and to provide a new set of hermetically sealed switches.

Reference 1 reports the virtual elimination of troubles with the rod-drive system as a result of these actions.

A number of the difficulties experienced were peculiar to the CETR. These included some piping reruns and failures of tubes in the fossil-fired superheater. Some activity has been detected on the secondary side of the primary steam generators. Up to the time Ref. 2 was written, a level of about 10^{-5} μc/ml had been detected, and this appeared to be steadily rising. This activity leak apparently occurred within the period from June to November 1963, since a particular point made in Ref. 1 is that no measurable leakage had been observed.

The ion-exchange and filtration portions of the primary coolant purification system have been kept in almost continuous operation, but the purification gas stripper was not required to be in operation.[2] At the outlet of the mixed-bed ion exchanger, the activity was about 2×10^{-5} μc/ml due to noble-gas activity; operation of the degasser decreased this to about 10^{-5} μc/ml. No gaseous waste had been discharged as of the writing of Ref. 1, and the ventilation of the containment building, prior to access, has required no exceptional precautions.

The operation of the automatic control system for the CETR is briefly described in Ref. 3. The plant was designed to accept a ± 18% power step or a ± 9% per minute power ramp. Although an actual step could not be studied because the turbine throttle could not be stepped, a power change of 50 Mw(e) in 12 sec was reviewed. Figures IX-1 and IX-2 show the results with the steam-flow gain constant set at its recommended design value. The author concludes that the plant can actually accept a step of ± 27% in power or a ramp of ± 15% per minute.

References 4 to 6 present results of physics and thermal measurements done on the CETR. Temperature coefficients of reactivity were determined by doubling time differences for several temperatures, both with and without boric acid in the moderator. Control-rod worths were determined, and power coefficients were measured. Table IX-1 shows a summary of the CETR reactivity coefficients.

A series of flow measurements and heat balances were made on the CETR, and it was of interest to find that the heat balances indicated that the actual flow was higher than the design flow by about 13%. The actual flow, which is equivalent to 60×10^6 lb/hr, is obtained with eight pumps in operation and at

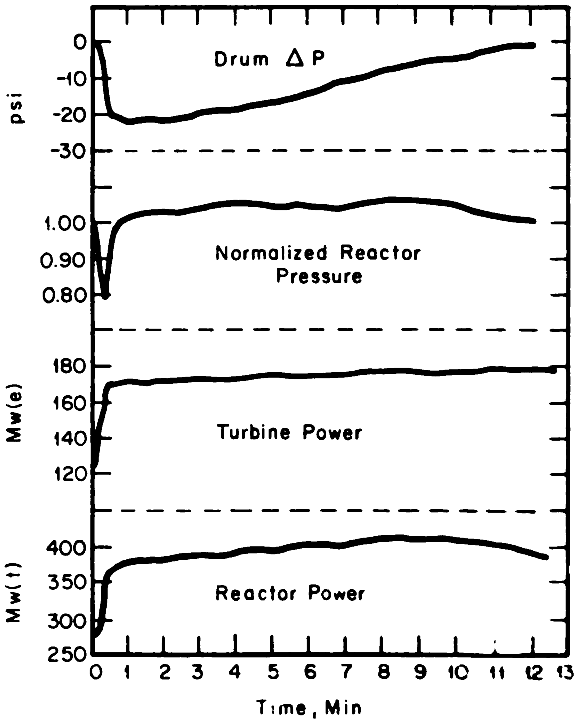

Fig. IX-1 Response of the CETR plant to a simulated step in power of +5 Mw(e).[3]

temperatures between 475 and 500°F. The measured core pressure drop was 49 psi, compared to the predicted value of 54 psi. Deddens concludes that[6]

> ...most of the decreased core pressure drop is accounted for by a revised method for computing pressure drop in the flow annulus between the fuel element bundle and the fuel element can... The significance of this is that not all of the increased flow is effective in cooling the fuel rods...

Deddens also concludes that the steam-generator performance is "significantly" better than predicted and that the CETR has excess thermal capacity; therefore the CETR could be operated at rated power [585 Mw(t)] with six pumps in three boiler loops in operation.[6]

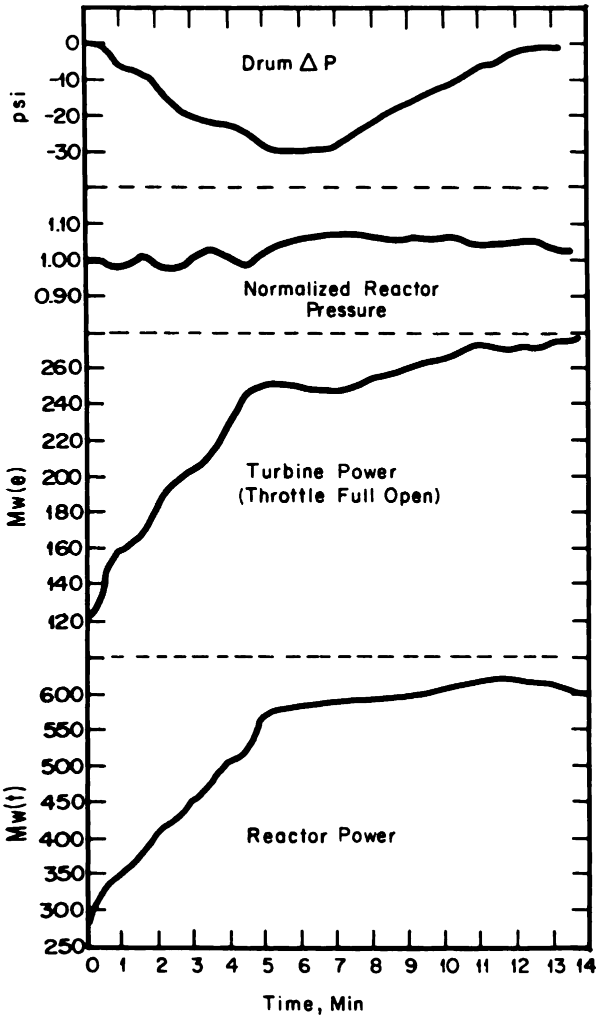

Fig. IX-2 Response of the CETR plant to a ramp[3] of +25 Mw(e)/min.

Table IX-1 SUMMARY OF CETR REACTIVITY COEFFICIENTS[5]

Parameter	Reactivity coefficient $dk/k \times 10^5$	Core conditions
Temperature, uniform	−17.1/°F ± 8%	Initial, 450°F, no poison
Boric acid	−14.8 ± 0.7/10 ppm	Initial, 450°F
Pressure coefficient	+13.3/100 psi	Initial, 450°F, 1450 to 1650 psig
Power coefficient	−2.2 ± 0.07/Mw	Initial

Plutonium Recycle Test Reactor: Primary Coolant Pumps

The Plutonium Recycle Test Reactor (PRTR) is not a power reactor in the strict sense, but the primary coolant pressure and temperature are high enough to be representative of power-reactor conditions. The PRTR primary coolant is heavy water at a temperature of about 480°F and a pressure of 1050 psi. Prototypes of the PRTR primary coolant pumps have been extensively tested, and these earlier tests have been reviewed in *Power Reactor Technology*, 4(4): 71-73. Reference 7 is a report on the operating experience with the pumps used with the reactor. The reader may wish to consult Fig. XI-1 in the previously mentioned article in *Power Reactor Technology* for a schematic diagram of the mechanical pump seals used on the prototype PRTR pumps and, presumably, the actual pumps used with the reactor.

The problems encountered with the pumps are summarized as follows:

1. Stationary mechanical seal face distortion.
   (a) Differential thermal expansion of the massive pump cover plate which supported this member.
   (b) Hydraulic-pressure distortion of the stationary face.
2. Large amounts of corrosion products collected in the mechanical seal chamber from carbon-steel test loops.
3. Misalignment of mechanical seal faces from insert cocking; unseating the seal face from O-ring expansion.
4. Excessive vibration of the pump rotating assembly which includes the 2400-lb flywheel; vibration resulting from hydraulic instability of

the pumps causing lack of positive seating in the thrust bearings; and motor vibration.

5. Helium evolving between seal faces.
6. Inadequate venting of the seal chamber and the pump bowl.

Of these problems, all but the last two were encountered and corrected during the test program; the last two were peculiar to operation of the PRTR. In the reference are several tables that give detailed comments on pump-seal failures during PRTR operations. The helium that is dissolved in the PRTR coolant comes from the pressurization of the primary coolant with helium,[8] and this caused rapid failure of the pump seals during initial PRTR operations. The problem was solved by injecting helium-free water into the seal chamber and venting the pump bowl and seal chamber to remove helium collected at these points during primary system cooldown, depressurization, or other circumstances resulting in excessive gassing. The PRTR primary pumps are located at a high point of the piping and serve as collection points for any evolved helium. The vent flow is 3 gal/min from the pump bowl, and the vent pipe is drilled into the highest point of the high-pressure seal chamber to allow seal venting during pump operation.

As a result of the studies just described, the life of the PRTR pump seals has been improved. The following quotation serves to define the improvement:[7]

> Seal life has increased from an average of 1250 for 15 of the first 20 PRTR runs to an average of 2050 hr for the last completed run of each pump. The longest completed run was for 7 months with 4094 hr total operation. Mockup runs have shown seal life of more than a year attainable. Longer than average runs are currently in progress. It should be noted that PRTR is a test reactor with operating periods of 1 week to 10 days. Longer life, as with the test loop, is predicted for continual operation.

Heavy-Water Components Test Reactor: Control- and Safety-Rod Drive Systems

The Heavy-Water Components Test Reactor (HWCTR) also is not a power reactor but, like the PRTR, has the capability of operation with coolant pressure and temperatures approaching those of a power reactor. The HWCTR is cooled with D_2O at 1500 psi and 600°F, nominally, and is equipped with 18 control rods and 6 safety rods. Reference 9 reports on operating experience with the HWCTR rod-drive systems.

The rod drives are motor-driven rack-and-pinion drives located at the top of the reactor. Pressure breakdown, floating-ring labyrinth seals are employed. Figure IX-3 shows a simplified section of the safety-rod-drive arrangement. The six central control rods are arranged in a cluster and are attached to a common rack-drive housing. The remaining control rods and the safety rods are individually driven. The rack-drive housings are about 20 ft long and consist of a stainless-steel drive housing welded to two sections of 2-in. stainless-steel pipe. Latches for gripping the rod poison sections

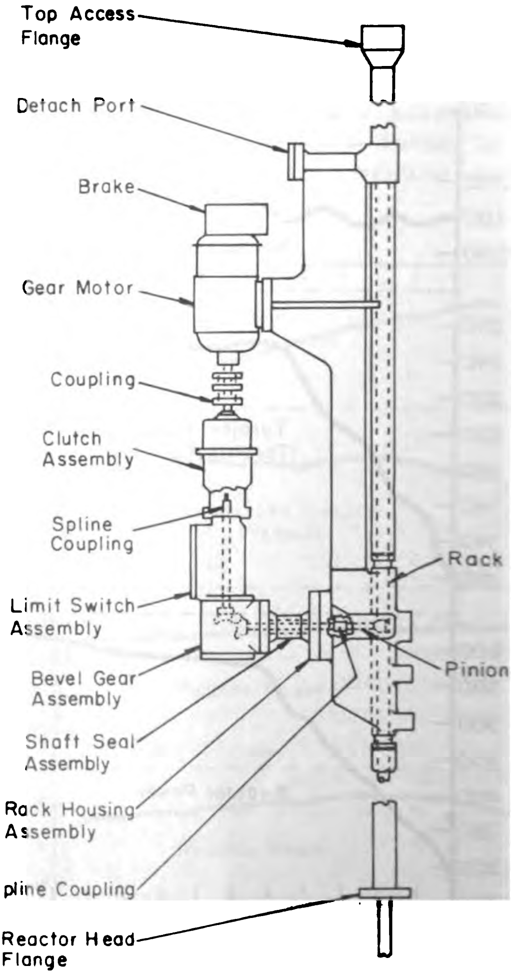

Fig. IX-3 Safety-rod-drive arrangement for the HWCTR.[9]

are at the lower end of the rack assembly, but the latch-actuating mechanism is located in the upper end, where it can be operated through the delatch port (Fig. IX-3).

During the first 1.5 years of operation of the HWCTR, there have been 34 incidents involving abnormal operation of the rod drives. These are summarized in Table IX-2. Most of the incidents (19) occurred during the first month of operation at low power, and 25, including the 19, occurred before power operation. Table IX-3 shows the breakdown of failures and operating difficulties. The seized clutch and seal that caused the stuck rods during scram were repaired and modified to prevent further difficulties. On four occasions (Table IX-3) the rods drove in an uncontrolled manner, although the reference does not say in which direction. This action was caused by a broken rod-drive control switch at the reactor control panel. The switches originally were double-block selector switches with a stiff spring return. No mechanical stops were incorporated, and, if the operator applied too much torque to the handle of the switch, the plastic cam mechanism causing the rod motion could be broken in the last-demanded position. All switches were replaced in March 1962 with ones employing metal cams and mechanical stops.

Table IX-2 SUMMARY OF HWCTR ROD-DRIVE DIFFICULTIES[9]

Operating difficulties	
Mechanical failures	10
Electrical failures	18
Others	6
Difficulties occurring in March 1962	19
Total rod drops (approximate)	1200
Failures to drop properly	
Slow times	6
Stuck	3
Electrical component revisions	4
Mechanical component revisions	4

The performance of the seals was satisfactory. Table IX-4 illustrates the seal leak rates. One case of seal failure was found. The failure was due to improper seal assembly. The seal leakage is especially important for reactors employing heavy water as a coolant, and it should be noted that the total seal outleakage in the HWCTR was collected. Inspection of the seals indicated absence of crud. This was due to the filtration of the seal water before injection into the seal.

Table IX-3 LIST OF HWCTR FAILURES AND OPERATING DIFFICULTIES[9]

Description	Causes
Failure of safety rod to scram completely (3 times)	Unknown; seized clutch; seized seal
Broken and bent latch fingers; rod could not be driven out of reactor	Rack scrammed six times without attached poison section; broken finger jammed in guide tube
Broken limit switch actuating cam nut (3 times)	Understrength cam surface; switches improperly adjusted
Rod drove in or out uncontrolled (4 times)	Broken control switch actuating the cam jammed the switch
Inoperative electrical system (16 times)	Shorted clutch coils, shorted relay coils, faulty relays, loose wires
Broken limit switch "Microswitch" (3 times)	Cracked during assembly and improper adjustment
Difficulty in latch or delatching rods (5 times)	Guide tubes too long; improper use of latching tool
Control rod driving abnormally (4 times)	Unknown
Failure of safety rod to scram within time limits (6 times)	Gear misalignment; inadequate limit switch lubrication; improper switch adjustment

Table IX-4 SEAL LEAK RATES FOR THE HWCTR

Total seal outleakage, lb/hr	7.1
Average seal outleakage, lb/hr per seal	0.3
Smallest outleakage of any seal, lb/hr	0.1
Total seal inleakage to reactor, lb/hr	171.0
Average seal inleakage to reactor, lb/hr per seal	7.1

Performance of the EBWR at Powers Up to 100 Mw(t)

As originally designed, the Experimental Boiling-Water Reactor (EBWR) was to be a prototype boiling-water reactor to produce 20 Mw(t) in the form of 600-psig steam. It eventually attained a power level of 61.7 Mw(t).

Information is given in Refs. 10 and 11 on modifications to the EBWR and on results of experiments in an attempt to reach a power of 100 Mw(t). Since Ref. 10 is a more up-to-date report, its review will be emphasized here.

Figure IX-4 is a schematic of the EBWR pressure vessel and internals as modified for operation up to 100 Mw(t). One of the basic changes made was to increase the number of fuel elements from 110 to 147, still maintaining a 4-ft core height. As shown in the figure, the core was encased in a shroud to prevent bypass flow, and a riser was installed. Increased riser height was provided to step up the flow rate through the core, since the reactor was operated as a natural-circulation device. A new feedwater ring was installed near the top of the riser to attempt to rapidly quench any steam carried over into the downcomer, and a new steam discharge duct was provided. The new steam duct withdrew the steam from the very top of the reactor in order to obtain as large a distance as practical between the water level and the steam-withdrawal point. The thermal power of the EBWR was distributed as follows: 20 Mw(t) was utilized by the turbine plant, and the balance [up to 80 Mw(t)] was absorbed by the reboiler plant. Steam generated in the boilers was condensed in air-cooled condensers. A steam dryer, which was part of the original EBWR equipment, was utilized to ensure a supply of dry steam for the turbine. Performance characteristics of the EBWR from zero to 100 Mw(t) are given in Ref. 12.

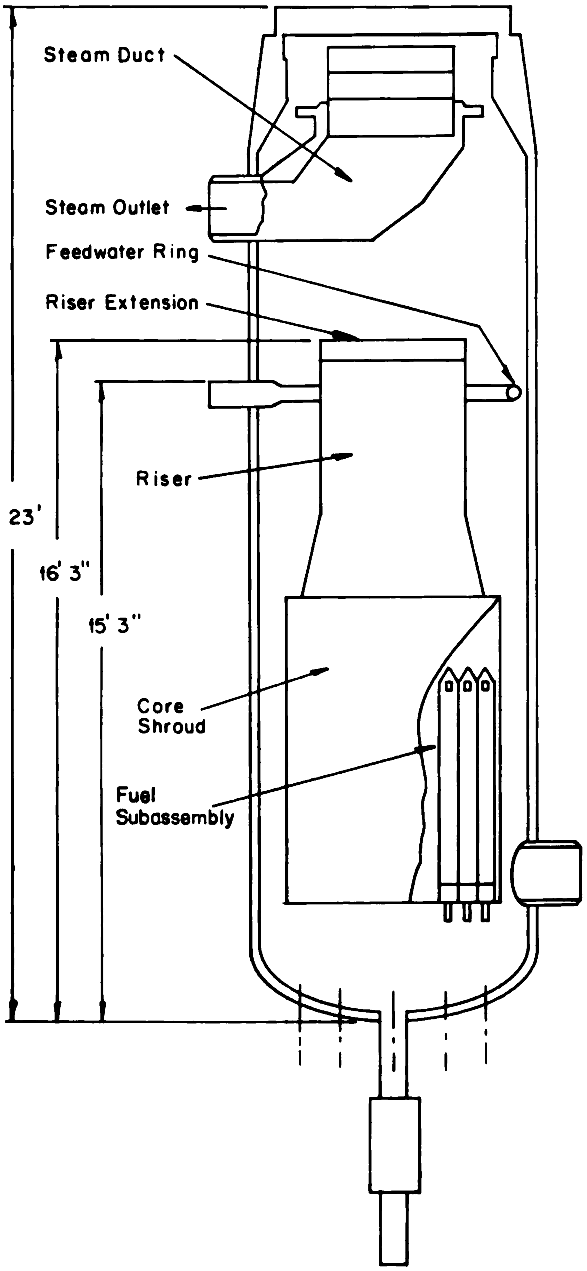

Fig. IX-4 Schematic of the EBWR pressure vessel and internals as modified for operation at power levels up to 100 Mw(t).[10]

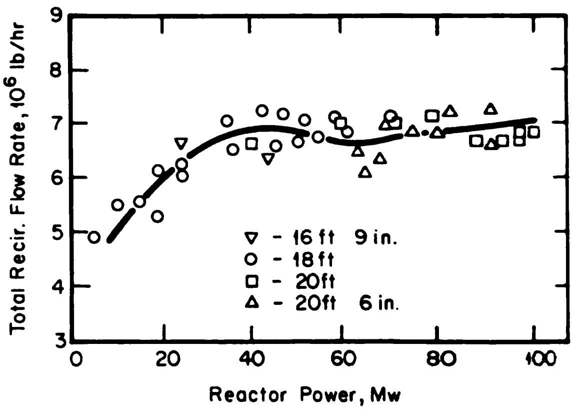

Fig. IX-5 Total recirculation flow rate as a function of reactor power at 600 psig and various true-mixture interface levels.[10]

Extensive instrumentation was installed within the vessel to provide data on the recirculation flow rate, volumetric and weight fraction of vapor carry-under in the downcomer, reactor subcooling, riser void fractions, quenching rate of the entrained vapor in the downcomer, location of the true two-phase mixture interface within the reactor, and liquid carry-over in the effluent steam. The reader's attention is directed to the references[10,11] for design details on the instrumentation.

Three series of tests were conducted with the modified EBWR. The first series was of an exploratory nature and was run at 300 psig to simulate operation at higher power density. The maximum power level attained during the series was 20 Mw(t). During test series 2, the reactor power was varied from 5 to 60 Mw(t), and the pressure was held at 600 psig. Prior to the start of the second series of tests, the top foot of the riser was removed to increase the steam dome volume, and the saturated water level was maintained 7 in. above the top of the riser during the series. Test series 2 ended with all control rods fully out of the core and with some boric acid (equivalent to 0.5% *k*) remaining in the coolant. Boron strips were removed from some of the fuel elements in order to attain the desired 100-Mw(t) power level during test series 3.

The more important results of the test series are contained in Figs. IX-5 through IX-8. These figures, in general, show how the performance characteristics of the EBWR are governed by steam carry-under in the downcomer, liquid carry-over in the effluent steam and, indirectly, by the location of the water-steam interface in the pressure vessel. For example, Fig. IX-5 illustrates the total recirculation flow rate as a function of reactor power. Although the data pertinent to operation with the old riser configuration are not shown in the figure, they are illustrated in Ref. 10. The additional riser height was successful in increasing the recirculation flow rate. The reason for the inflection point of the flow rate vs. power curve (Fig. IX-5) can be explained by a consideration of Fig. IX-6. This latter figure is a map of the subcooling of the reactor coolant, and an understanding of the figure is most helpful in gaining an insight into the operation of the EBWR at high power.

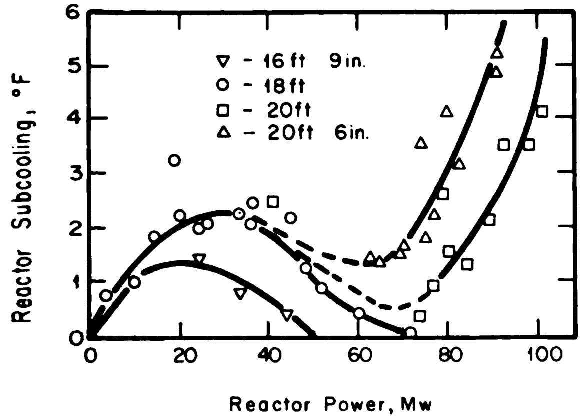

Fig. IX-6 Map of reactor subcooling as a function of reactor power and various true-mixture interface levels.[10]

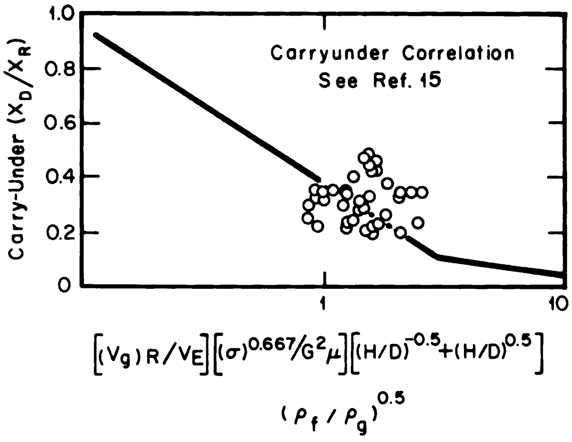

Fig. IX-7 Comparison of carry-under data with the correlation, using measured steam volume fraction.[10]

For reactor operation with no carry-under of steam into the downcomer, the core inlet subcooling increases continuously with power. This can be qualitatively explained by considering the data shown in Fig. IX-5 for powers up to about 20 Mw(t)—as power doubles, say from 10 to 20 Mw, the recirculation flow rate increases somewhat, but not by a factor of 2. A doubling of power is accompanied, however, by a doubling of the flow rate of the relatively cold feedwater, if steady state exists. Thus, as power increases, the core subcooling increases until the point is reached where steam starts to be carried into the downcomer. The effect of carry-under can be noticed in Fig. IX-6 at powers of about 20 to 30 Mw(t). The carry-under of saturated steam decreases the subcooling as power is increased. It can be seen from Fig. IX-6 that the subcooling increases sharply at a power of about 70 Mw(t) for an interface height of 20 ft. At this point liquid carry-over in the steam commences, and its effect is noticed in Fig. IX-6 by a rapidly increasing subcooling at the core inlet. It is of interest to note the sensitivity of the reactor subcooling to the interface height. At an interface height of 20 ft 6 in., the point of carry-over is reached at a lower power level (about 60 Mw) because of the reduced steam dome height. Reference 10 presents a prediction of the reactor subcooling curve in the region where carry-over is important, and the agreement between the prediction and the experimental data (a typical example is shown in Fig. IX-6 at powers in excess of 60 to 70 Mw) is good.

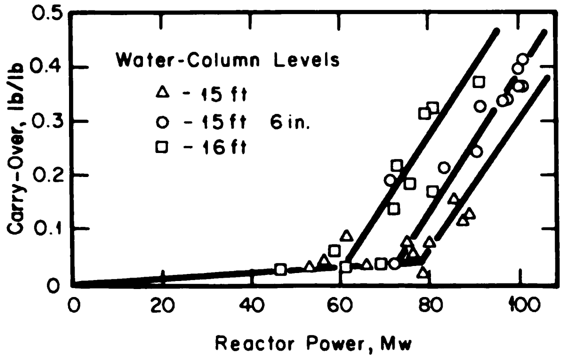

Fig. IX-8 Liquid carry-over as a function of reactor power and various water-column levels. (Data from Heat Balance on Primary Reboiler)[10]

In Fig. IX-5 the shape of the flow vs. power curve can be explained by the effect of inlet subcooling; as subcooling increases, the recirculation flow rates tend to increase.[10] Between roughly 40 and 60 Mw(t), Fig. IX-6 shows decreasing subcooling due to carry-under, and this is reflected in Fig. IX-5 in decreasing recirculation flow rates. Above about 60 Mw(t), subcooling increases due to carry-over, and this is reflected in Fig. IX-5 by increasing recirculation flow rates.

The vapor carry-under in the EBWR was calculated with the aid of a heat balance, using measured flow rates and subcooling. The carry-under in this reactor was substantial, even at low power, and varied from about 20% at 10 Mw to about 40% at 100 Mw. The value of 40% means that 40 wt.% of all steam generated in the core ends up entrained in the downcomer. What is of particular value, however, is the comparison of the analytical carry-under prediction given in Ref. 13 with the experimental data derived from the EBWR operation. This comparison is shown in Fig. IX-7. Steam-water separation was reviewed in *Power Reactor Technology*, 6(2): 69-74, and Ref. 13 was included in this earlier review. The scatter of the data shown in Fig. IX-7 is believed[10] to be caused by inaccuracies in determining the steam volume fraction in the upper part of the downcomer because of the quenching process and the resulting high degree of turbulence around the measuring probe.

Figure IX-8 illustrates liquid carry-over as a function of reactor power and water-column level. The water-column level is a measure of the true fluid-interface level, and, in the power range from 70 to 100 Mw, other data presented in Ref. 10 show that the true mixture interface is about 4.8 ft above the water-column-level readings. The figure illustrates that the initiation of carry-over, the break-points in the curves, occurs at different power levels for different interface heights. The figure also illustrates the large amount of carry-over that attended the operation of the modified EBWR at high power.

References

1. W. C. Beattie and R. H. Freyberg, Operating Experience with Indian Point Nuclear Electric Generating Station, in *Operating Experience with Power Reactors*, Vol. 1, pp. 307-324, International Atomic Energy Agency, Vienna, 1963.
2. R. H. Freyberg, Jr., Operating Experience at Indian Point, Consolidated Edison Company of New York, *Trans. Am. Nucl. Soc.*, 6(2): 340 (November 1963).
3. S. H. Esleeck, Performance of the Indian Point Reactor Plant, *Trans. Am. Nucl. Soc.*, 6(2): 341 (November 1963).
4. M. L. Batch and F. E. Fisher, Indian Point Reactor Reactivity and Flux-Distribution Measurements, *Trans. Am. Nucl. Soc.*, 6(2): 343 (November 1963).
5. R. M. Ball, J. M. Makepeace, and J. P. Farrar, Operating Coefficients and Reactivity Behavior at Indian Point, *Trans. Am. Nucl. Soc.*, 6(2): 343-344 (November 1963).
6. J. C. Deddens, Indian Point Reactor Primary-System Thermal and Hydraulic Evaluation, *Trans. Am. Nucl. Soc.*, 6(2): 340-341 (November 1963).
7. P. A. Scott, Plutonium Recycle Test Reactor Primary Coolant Pumps, Paper No. 63-WA-234 presented at the Winter Annual Meeting of the ASME, Nov. 17-22, 1963.
8. N. G. Wittenbrock (Ed.), Plutonium Recycle Test Reactor Preliminary Safeguards Analysis, USAEC Report HW-48800(Rev.), Hanford Atomic Products Operation, June 5, 1958.
9. S. H. Kale, HWCTR Control-Rod and Safety-Rod Drive Systems, Paper No. 63-WA-257 presented at the Winter Annual Meeting of the ASME, Nov. 17-22, 1963.
10. M. Petrick and E. A. Spleha, Thermal Hydraulic

Performance Characteristics of EBWR [0 to 100 Mw(t)], USAEC Report ANL-6693, Argonne National Laboratory, May 1963.

11. D. Miller (Ed.), Thermal Operating Performance of Nuclear Reactors, A Panel Discussion Held at the Fifth National Heat Transfer Conference, Houston, Texas, August 8, 1962, USAEC Report TID-7669.

12. E. A. Wimunc, M. Petrick, W. C. Lipinski, and H. Iskenderian, Performance Characteristics of EBWR from 0–100 Mwt, USAEC Report ANL-6775, Argonne National Laboratory, September 1963.

13. M. Petrick, A Study of Vapor Carryunder and Associated Problems, USAEC Report ANL-6581, Argonne National Laboratory, July 1962.

Section X

Power Reactor Technology

Specific Reactor Types

Pressurized Water: Study of Zircaloy Core Structure for N.S. Savannah

The reactor for the N. S. *Savannah* was described in detail in *Power Reactor Technology*, 6(1): 43-54. As built, the reactor contained a stainless-steel core structure, and Ref. 1 is an evaluation of the substitution of Zircaloy in the fuel-element containers.

Figure X-1 shows the core structure for the reactor. The boxlike structures contain the fuel elements and presently account for about one-third of the total quantity of stainless steel in the active core. The remaining steel (which is type 304) is accounted for primarily by the cladding of the fuel rods. The substitution of Zircaloy for the element containers would be expected to lower the ^{235}U inventory for a given reactivity lifetime and increase the control-rod worth. Physics calculations and structural analyses were done for the various core compositions considered, and the results were used in an economic study of the fuel cycle. Supporting studies were on the compatibility of Zircaloy with the reactor environment, and a brief safeguards analysis was made.

The results of the nuclear calculations are summarized in Table X-1. The four cases studied were the reference case, S-420, which

Table X-1 SUMMARY OF CALCULATED NUCLEAR CHARACTERISTICS[1] FOR VARIOUS FUEL-ELEMENT CONTAINERS

	Stainless-steel containers, reference case S-420*	Zircaloy fuel-element containers		
		Case Z-420†	Case Z-386‡	Case Z-338§
One-zone enrichment, wt. % ^{235}U	4.20	4.20	3.86	3.38
Multiplication factor of clean core with rods out (followers in)				
Cold	1.132	1.195	1.172	1.135
Hot	1.079	1.138	1.114	1.079
Multiplication factor of clean core with rods in				
Cold	0.972	0.991	0.969	0.934
Hot	0.882	0.910	0.886	0.848
Cold worth of all control rods, % Δk	16	20	20	20
Shutdown margin of cold, clean core with central rod out, % Δk	1.4	Supercritical	1.4	4.9
Lifetime, years at 63 Mw(t)	1.63	3.20	2.52	1.63

*Case S-420 was the reference case, with core 1 type fuel elements (uniform enrichment of 4.20 wt.%) in stainless-steel containers.

†Case Z-420 was the same as the reference case except that the containers were Zircaloy.

‡Case Z-386 had core 1 type fuel elements (uniform enrichment of 3.86 wt. %) in Zircaloy containers; enrichment was adjusted to give the same shutdown margin with the central rod out as the reference case.

§Case Z-338 had core 1 type fuel elements (uniform enrichment of 3.38 wt. %) in Zircaloy containers; enrichment was adjusted to give the same lifetime as the reference case.

represented the as-designed reactor, and three cases employing Zircaloy fuel-element boxes, cases Z-420, Z-386, and Z-338. These cases are described in the table. The results of the economic evaluation of the various cases are summarized in Table X-2. The savings are substantial in all the cases; it was concluded that the Zircaloy boxes would cost about $ 130,000 more than the stainless-steel boxes, but this cost was amortized over a 20-year core life and was insignificant in the final results.

Zircaloy-2 and Zircaloy-4 were evaluated for applicability over the expected 20-year life of the core. Corrosion, wear, and long-lived crud activity were found to be acceptable with the only area of uncertainty being the susceptibility of Zircaloy to fretting corrosion. This problem might be accentuated on the N. S. *Savannah* reactor because of its mobile nature, but the problem of fretting corrosion is potentially present in any reactor employing Zircaloy as structural material. Reference 1 includes a review of previous investigations on fretting corrosion of Zircaloy, which are considered inconclusive for the proposed application. The material appears susceptible to impact corrosion that might arise owing to repeated contact between fuel elements and their Zircaloy containers. The conclusion[1] is that this can only be answered by testing a mockup of a portion of the core under the proposed system conditions.

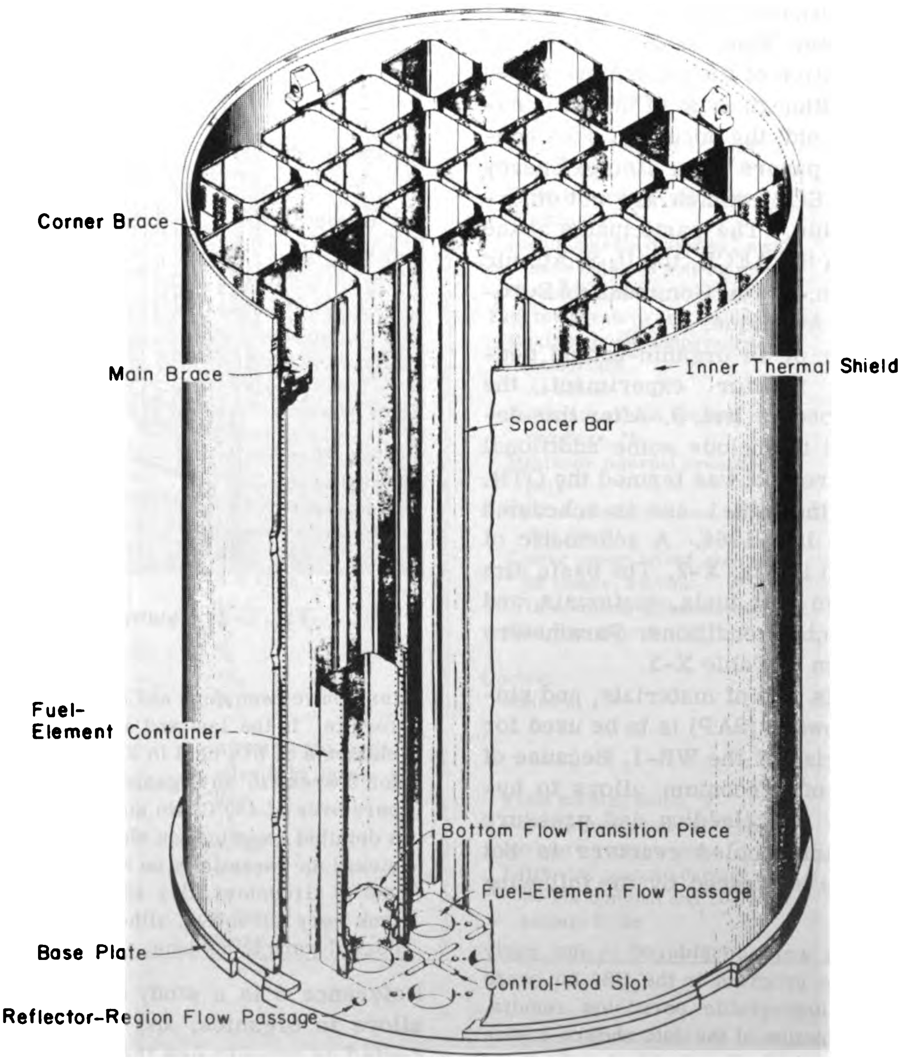

Fig. X-1 Fuel-element container assembly.[1]

Table X-2 COST REDUCTIONS RESULTING FROM SUBSTITUTING ZIRCALOY FOR STAINLESS STEEL IN FUEL-ELEMENT CONTAINERS[1]

	Cost reduction, % (based on cost for reference case S-420)*		
Cost component	Case Z-420	Case Z-386	Case Z-338
Fabrication	49	38	9
Net burnup	1	4	2
Reprocessing	49	37	7
Uranium use charge	7	15	26
Working capital	2	5	9
Total fuel cycle	32	26	10

*See the Table X-1 footnotes for a description of the cases.

Organic-Cooled Reactors: The Tripartite Meeting

The Tripartite Organic-Cooled Heavy-Water Reactor Meeting was held in June 1962, and Ref. 2 is the collection of the papers presented at this meeting. Although most of the information is now rather old, the document does contain a collection of papers from Atomic Energy of Canada, Ltd. (AECL), which are not otherwise widely available. The participants at the meeting were from the AECL, the U. S. Atomic Energy Commission, and the Communauté Européene de l'Énergie Atomique.

An early design of an organic-cooled deuterium-moderated reactor experiment, the OCDRE, is described in Ref. 3. After this design was reworked to include some additional experimental features, it was termed the OTR. It is now called the WR-1 and is scheduled for completion[4] in late 1964. A schematic of the WR-1 is shown in Fig. X-2. The basic aim of the reactor is to test fuels, materials, and coolants under reactor conditions. Parameters of interest are given in Table X-3.

A key problem is one of materials, and sintered aluminum powder (SAP) is to be used for the cladding material of the WR-1. Because of the susceptibility of zirconium alloys to hydriding, their use for cladding and pressure tubes in the organic-cooled reactors is not straightforward, as evidenced by the following quotation:[4]

> Zirconium alloys were considered in the early days of the organic program in the USA but were discarded due to unfavorable corrosion results. However, re-examination of the data showed a wide scatter in the results with some indication of promise under certain conditions. Over the past two-year period several in-reactor and out-reactor tests have been done at Chalk River with promising results. In the last and most severe test two fuel elements of UO_2 clad in Zircaloy-2 were irradiated for 3 weeks in an organic coolant with sheath temperatures of 460°C. No visible change occurred and a detailed examination showed that the sheaths had picked up essentially no hydrogen. This makes the use of zirconium alloy sheaths and pressure tubes look very attractive, although there still is a great deal of work to be done.

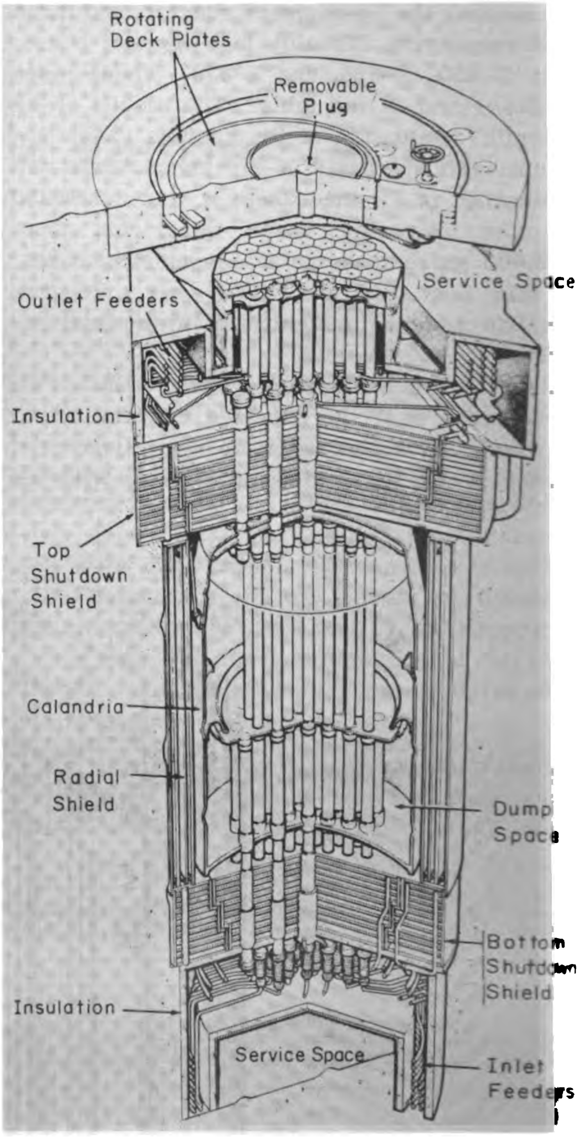

Fig. X-2 Cutaway[4] of the WR-1.

Reference 6 is a study of the use of zirconium alloys in organics, and the following are suggested as ways to use the alloys:

—insulate the zirconium alloy from the organic material

Table X-3 DESIGN PARAMETERS FOR THE WR-1 REACTOR

Reactor type	Uranium oxide fuel, heavy-water moderator, organic coolant, vertical construction
Total nuclear power, Mw(t)	30.0
Reactor power, Mw(t)	28.6
Number of fuel sites	37 at 2.23% enrichment
Power per site, maximum fuel rating, Mw	1.07
Core data	
Lattice type	Triangular
Lattice pitch, in.	9.25
Cell area, cm^2	478
Nominal hot core radius, in.	29.54
Nominal core height, ft	7
Actual core height, ft	8
Maximum thermal-neutron flux, neutrons/(cm^2)(sec)	1.08×10^{14}
Average/maximum axial flux	0.637
Average/maximum radial flux	0.776
Fuel-channel assembly	
Geometry	
Internal diameter, core region, in.	3.25
Overall length	33 ft 1.5 in.
Minimum wall thickness, core region, in.	0.0315
Approximate dry weight, lb	
Without fuel	400
With fuel and coolant	700
Material	S.S. (initially)
Fuel closure	Standard mechanical type closure
Fuel support	Fuel is hung from the fuel closure
Calandria form	Vertical cylinder tapered on top side with dished top and bottom
Material	304L S.S.
Nominal inside diameter	8 ft 10 in.
Overall height, ft	16.5
Wall thickness, in.	$\frac{1}{2}$
Top head thickness, in.	$\frac{3}{4}$
Bottom head thickness, in.	$1\frac{3}{8}$
Dry weight, less extensions, lb	32,200
Calandria tubes	
Material	ASTM B-210-60T-alloy 5052 aluminum
Quantity	13
Inside diameter, in.	4.755
Wall thickness, in.	0.060
Quantity	24
Inside diameter, in.	3.695
Wall thickness, in.	0.050
Heavy-water inventory at 120°F, lb	
Calandria	31,500
Moderator system pipes	2470
Main pumps	120
Demineralizer circuit	323
Heat exchanger	1050
Helium pumps	106
Instrumentation system	20
Approximately 3% reserve	1111
Total	36,700
Reactor heat transport system	
Total flow, lb/hr × 10^{-6}	3.3
Outlet temperature, °F	700
Inlet temperature, °F	640
Maximum velocity through coolant tubes, ft/sec	30
Design pressure drop across fuel, psi	150
Channel outlet pressure, psi	165
Fuel	
Fuel density at 20°C, g/cm^3	10.4 to 10.7
Sheath material	SAP
Type of assembly	19-element bundle
Bundles/site	1
Number of bundles in core	37
Fuel length, hot, in.	96
Overall bundle length, approximate in.	106
Sheath outside diameter, maximum cold and hot, in.	0.6035 and 0.6095
Sheath thickness, average in.	0.0235
Fuel temperature and ratings	
Maximum fuel temperature, °F	
At surface	1380
At center	3730
Maximum sheath surface temperature, °F	895
Maximum internal pressure, psia	350 to 450
Maximum surface heat flux, Btu/(hr) (sq ft)	298,000
Linear power rating, normal	
Of bundle, kw/cm	7.85
Of element, $Q/4\pi$, watts/cm	36.4
Heat flux distribution	Sinusoidal in axial direction
Coolant	
Material	Mixture by weight of 70% Santowax OM and 30% radiolytic tars
Final melting point, °F	152
Vapor pressure at 700°F, psia	39
Moisture content, ppm	Less than 100
Estimated organic damage rate at 30 Mw nominal and 30% high boiler, lb/hr	11.2

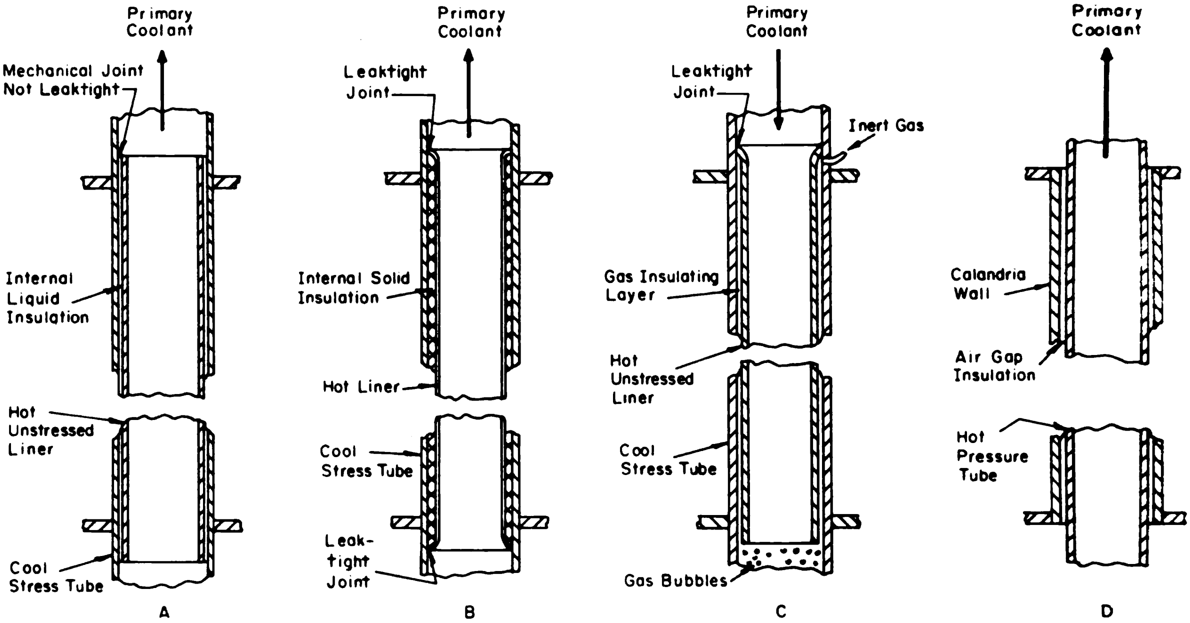

Internal Liquid Insulation

Internal Solid Insulation

Internal Gas Insulation

External Insulation

Fig. X-3 Pressure-tube designs.[4]

—coat the alloy with a material impervious to hydrogen, to prevent hydrogen pickup

— control coolant conditions to maintain a protective oxide film on the zirconium alloy

—reduce the hydrogen content until pickup is reduced to a tolerable rate

Reference 6 is a progress report. It discusses experiments done with Zircaloy-2 and a Zirconium – 0.5 copper–0.4 molybdenum alloy, called "ATR." The authors came to the decision that the evidence is not conclusively against the use of zirconium alloys in organic environments.

The basic design problem of a pressure-tube reactor is that of the pressure tube. The WR-1 utilizes, for example, an aluminum calandria tube to keep the relatively cool moderator (90–200°F) from contacting the pressure tube (about 650°F). In contrast, the Carolinas-Virginia Tube Reactor (the CVTR, a D_2O-cooled reactor) uses internal insulation between the fuel bundle and the pressure tube, so that the pressure-tube temperature approaches that of the moderator [see *Power Reactor Technology*, 6(4): 63-81]. Several possible approaches are summarized in Fig. X-3. The design employing the internal liquid insulation is simple in concept but difficult in practice; it is the concept used in the CVTR, which employs a multiplicity of thermal baffles, some attached to the pressure tube and some to the fuel bundle. The design employing internal solid insulation poses materials problems. The Canadian workers have been studying the use of fibrous compressed silica insulation, known as MinK, for this application.[7] The internal gas insulation approach is not a natural one for a liquid-cooled reactor and did not receive much attention in Refs. 4 and 7. The external insulation concept, which is used for the WR-1, results in operation with a hot pressure tube. Operation of the tube at elevated temperature accentuates corrosion problems and reduces greatly the probability of finding a successful zirconium alloy for the application. It also reduces the strength of the tube material and increases the required wall thickness. This consideration may be a less important one when an organic coolant is used, since the coolant pressure is not high.

References

1. T. D. Anderson, E. E. Gross, H. C. McCurdy, L. D. Schaffer, L. R. Shobe, and C. L. Whitmarsh, Summary Report, An Evaluation of the Substitution of Zircaloy for Stainless Steel in N.S. *Savannah* Fuel-

Element Containers, USAEC Report ORNL-3476, Oak Ridge National Laboratory, Nov. 6, 1963.

2. The Tripartite Organic Cooled Heavy Water Reactor Meeting, Santa Monica, California, June 11–13 1962, USAEC Report TID-7648 (Pt. 1).
3. I. MacKay, Organic-Cooled Deuterium-Moderated Reactors, *Nucleonics*, 18(10): 78 (October 1960).
4. W. M. Campbell, Canada's Organic Cooled Reactor Program, in The Tripartite Organic Cooled Heavy Water Reactor Meeting, Santa Monica, California, June 11–13, 1962, USAEC Report TID-7648 (Pt. 1), pp. 1-16.
5. L. R. Haywood, WR-1 Station Data, in The Tripartite Organic Cooled Heavy Water Reactor Meeting, Santa Monica, California, June 11–13, 1962, USAEC Report TID-7648 (Pt. 1), pp. 137-161.
6. A. Sawatzky and F. H. Krenz, Zirconium Alloys in Organics: A Possibility, in The Tripartite Organic Cooled Heavy Water Reactor Meeting, Santa Monica, California, June 11–13, 1962, USAEC Report TID-7648 (Pt. 1), pp. 72-91.
7. E. J. Adams, OCDR Coolant Tube Assembly Development, in The Tripartite Organic Cooled Heavy Water Reactor Meeting, Santa Monica, California, June 11–13, 1962, USAEC Report TID-7648 (Pt. 1), pp. 41-56.

LEGAL NOTICE

This journal was prepared under the sponsorship of the U. S. Atomic Energy Commission. Neither the United States, nor the Commission, nor any person acting on behalf of the Commission:

A. Makes any warranty or representation, expressed or implied, with respect to the accuracy, completeness, or usefulness of the information contained in this journal, or that the use of any information, apparatus, method, or process disclosed in this journal may not infringe privately owned rights; or

B. Assumes any liabilities with respect to the use of, or for damages resulting from the use of any information, apparatus, method, or process disclosed in this journal.

As used in the above, "person acting on behalf of the Commission" includes any employee or contractor of the Commission, or employee of such contractor, to the extent that such employee or contractor of the Commission, or employee of such contractor prepares, disseminates, or provides access to, any information pursuant to his employment or contract with the Commission, or his employment with such contractor.

NUCLEAR SCIENCE ABSTRACTS

The U. S. Atomic Energy Commission, Division of Technical Information, publishes *Nuclear Science Abstracts (NSA)*, a semimonthly journal containing abstracts of the literature of nuclear science and engineering.

NSA covers (1) research reports of the U. S. Atomic Energy Commission and its contractors; (2) research reports of government agencies, universities, and industrial research organizations on a world-wide basis; and (3) translations, patents, books, and articles appearing in technical and scientific journals.

Complete indexes covering subject, author, source, and report number are included in each issue. These are cumulated quarterly, semiannually, and annually providing a detailed and convenient key to the literature.

Availability of *NSA*

SALE *NSA* is available on subscription from the Superintendent of Documents, U. S. Government Printing Office, Washington, D. C., 20402, at $30.00 per year for the semimonthly abstract issues and $22.00 per year for the four cumulated-index issues. Subscriptions are postpaid within the United States, Canada, Mexico, and all Central and South American countries, except Argentina, Brazil, British and French Guiana, Surinam, and British Honduras. Subscribers in these Central and South American countries, and in all other countries throughout the world, should remit $37.00 per year for subscriptions to semimonthly abstract issues and $25.00 per year for the four cumulated-index issues.

EXCHANGE *NSA* is also available on an exchange basis to universities, research institutions, industrial firms, and publishers of scientific information. Inquiries should be directed to the Division of Technical Information Extension, U. S. Atomic Energy Commission, P. O. Box 62, Oak Ridge, Tennessee, 37831.

TECHNICAL PROGRESS REVIEWS may be purchased from Superintendent of Documents, U. S. Gov ment Printing Office, Washington, D. C., 20402. *Isotopes and Radiation Technology* at $2.00 per year each subscription or $0.55 per issue; the other four journals at $2.50 per year and $0.70 per issue. T use of the coupon below will facilitate the handling of your order.

POSTAGE AND REMITTANCE: Postpaid within the United States, Canada, Mexico, and all Central South American countries except as hereinafter noted. Add $0.50 per year, or $0.15 per single issue the *Isotopes and Radiation Technology* journal and $0.75 per year or $0.20 per single issue for the four journals for postage to all other countries, including Argentina, Brazil, British and French Gui Surinam, and British Honduras. Payment should be by check, money order, or document coupons, MUST accompany order. Remittances from foreign countries should be made by international order, or draft on an American bank, payable to the Superintendent of Documents, or by UNESCO coupons.

order form

SUPERINTENDENT OF DOCUMENTS
U. S. GOVERNMENT PRINTING OFFICE
WASHINGTON, D. C., 20402

Enclosed:

document coupons ☐ check ☐ money order ☐

Charge to Superintendent of Documents No. ____________

Please send a one-year subscription to

☐ NUCLEAR SAFETY

☐ POWER REACTOR TECHNOLOGY

☐ REACTOR FUEL PROCESSING

☐ REACTOR MATERIALS

(Each subscription $2.50 per year; $0.70 per issue.)

☐ ISOTOPES AND RADIATION TECHNOLOGY

(Each subscription $2.00 a year; $0.55 per issue.)

SUPERINTENDENT OF DOCUMENTS
U. S. GOVERNMENT PRINTING OFFICE
WASHINGTON, D. C., 20402

(Print clearly)

Name ______________________________

Street ______________________________

City ____________________ Zone ____ State ____

Phoenix

POWER REACTOR TECHNOLOGY

THE UNIVERSITY
OF MICHIGAN
DEC 21 1965
PHOENIX
LIBRARY

Prepared for DIVISION OF TECHNICAL INFORMATION, USAEC, by
W. H. ZINN and J. R. DIETRICH, GENERAL NUCLEAR ENGINEERING CORPORATION

Fall 1964

● VOLUME 7

● NUMBER 4

TECHNICAL PROGRESS REVIEWS

To meet the needs of industry for concise summaries of current atomic developments, the Atomic Energy Commission is publishing this series, Technical Progress Reviews. Issued quarterly, each of the reviews digests and evaluates the latest findings in a specific area of nuclear technology and science.

The five journals published in this series are:

Isotopes and Radiation Technology, P. S. Baker, A. F. Rupp, and associates, Oak Ridge National Laboratory

Nuclear Safety, Wm. B. Cottrell, W. H. Jordan, and associates, Oak Ridge National Laboratory

Power Reactor Technology, W. H. Zinn and J. R. Dietrich, General Nuclear Engineering Corporation

Reactor Fuel Processing, Stephen Lawroski and associates, Chemical Engineering Division, Argonne National Laboratory

Reactor Materials, R. W. Dayton, E. M. Simons, and associates, Battelle Memorial Institute

Each journal may be purchased from the Superintendent of Documents, U. S. Government Printing Office, Washington, D. C., 20402. *Isotopes and Radiation Technology* at $2.00 per year for subscription or $0.55 for individual issues; the other four journals at $2.50 per year and $0.70 per issue. See back cover for remittance instructions and foreign postage requirements.

The views expressed in this publication do not necessarily represent those of the United States Atomic Energy Commission, its divisions or offices, or of any Commission advisory committee or contractor.

Availability of Reports Cited in This Review

Unclassified AEC reports are available for inspection at AEC depository libraries and are sold by the Office of Technical Services, Department of Commerce, Washington, D. C., 20230. Some of the reports cited are not available owing to their preliminary nature; however, the information contained in them will eventually be made available in formal progress or topical reports.

Unclassified reports issued by other Government agencies or private organizations should be requested from the originator.

Unclassified British and Canadian reports may be inspected at AEC depository libraries. British reports are sold by the British Information Service, 45 Rockefeller Plaza, New York, N. Y.; Canadian reports (AECL series) are sold by the Scientific Document Distribution Office, Atomic Energy of Canada, Ltd., Chalk River, Ontario, Canada.

Classified U. S. and foreign reports identified in this journal as Classified may be purchased by properly cleared Access Permit Holders from the Division of Technical Information Extension, U. S. Atomic Energy Commission, P. O. Box 1001, Oak Ridge, Tenn., 37831. Such reports may be inspected at classified AEC depository libraries.

POWER
REACTOR
TECHNOLOGY

A REVIEW OF RECENT DEVELOPMENTS

Prepared for DIVISION OF TECHNICAL INFORMATION, USAEC,
by W. H. ZINN and J. R. DIETRICH,
GENERAL NUCLEAR ENGINEERING CORPORATION

FALL 1964

VOLUME 7

NUMBER 4

Foreword

This quarterly review of reactor development has been prepared at the request of the Division of Technical Information of the U. S. Atomic Energy Commission. Its purpose is to assist interested organizations in the task of keeping abreast of new results in reactor technology for civilian application.

Power Reactor Technology contains reviews of selected recently published reports that are judged noteworthy in the fields of power-reactor research and development, power-reactor applications, design practice, and operating experience. It is not meant to be a comprehensive abstract of all material published during the quarter, nor is it meant to be a treatise on any part of the subject. However, related reports from different sources are often treated together to yield reviews having some breadth of scope, and background material may be added to place recent developments in perspective. Occasionally the reviews are written by guest authors. Reviews having unusual breadth or significance are placed at the front of the issue as Feature Articles.

The intention is to cover the various areas of reactor development from the general viewpoint of the reactor designer rather than from the more detailed points of view of specialists in the individual areas. To whatever extent the coverage of *Power Reactor Technology* may occasionally overlap the fields of the other Technical Progress Reviews, the overlaps will be motivated by this objective of viewing current progress through the eyes of the reactor designer.

A degree of critical appraisal and some interpretation of results are often necessary to define the significance of reported work. Any such appraisal or interpretation represents only the opinion of the reviewer and (in the usual case, when the review is written by General Nuclear Engineering Corporation staff) the Editor. When the review is predominantly interpretive the reviewer is named; unless identified as a guest author, he is a member of the General Nuclear Engineering Corporation staff. Readers are urged to consult the original references to obtain all the background of the work reported and to obtain the interpretation of the results given by the original authors.

For timely coverage, *Power Reactor Technology* must often review fragmentary material. The fixed subject headings listed below have been adopted in the hope of maintaining some continuity and order in the material from one issue to another: all reviews except Feature Articles will be arranged under these headings. A particular issue will not necessarily contain all the headings but only those under which material is reviewed.

Economics, Applications, Programs
Resources and Fuel Cycles
Physics
Fluid and Thermal Technology
Fuel Elements
Materials
Control and Dynamics
Containment, Radiation Control, and Siting
Systems Technology
Components
Design and Construction Practice
Operating Experience
Specific Reactor Types
Specific Applications
Unconventional Approaches

W. H. Zinn, President
J. R. Dietrich, Vice-President and Editor
General Nuclear Engineering Corporation

DEPOSITED BY THE
UNITED STATES OF AMERICA

Contents

Foreword

I Physics 329
Doppler Effect 329
Control-Rod Programming 330
Short Notes 331
References 333

II Fluid and Thermal Technology . . 335
Burnout in Steam-Water Mixtures . . 335
References 352

III Fuel Elements 354
Stainless-Steel-Cladding Failures in VBWR 354
Fission-Product Helium 355
Steel-Lined Zircaloy-2-Clad Fuel Elements 356
Boron-Containing Fuel Elements . . 356
Electron-Beam Welding 358
Irradiation Effects in UO_2 359
References 363

IV Materials 365
Boron for Control Rods 365
Transition Joints of Zircaloy to Stainless Steel 368
References 369

V Containment, Radiation Control, and Siting 370
Effect of Fission-Product Release . . 370
Effect of Temperature on Fission-Product Deposition 371
References 371

VI Components 372
Pumps 372
Heat Exchangers 374
References 375

VII Design and Construction Practice 376
EGCR Control Rods 376
SRE Rod Drop-Time Measurement . . 377
Pressure-Tube Reactor Components . 379
Systems Design 384
References 384

VIII Operating Experience 385
Moderator-Level Control 385
References 399

IX Specific Reactor Types 401
Heavy-Water Reactors 401
Pressurized-Water Reactors: Chemical Shim 411
Pressurized-Water Reactors: Natural-Circulation Startup 421
Pressurized-Water Reactors: The Large Power Reactor Program . . 422
References 431

Index, Volume 7 433

Issued quarterly by the U. S. Atomic Energy Commission. Use of funds for printing this publication approved by the Director of the Bureau of the Budget on October 14, 1963.

Section
I

Power Reactor Technology

Physics

Doppler Effect

Results of recent transient tests on oxide-fueled cores in the SPERT reactor[1,2] have proved the efficacy of the Doppler effect — more specifically the Doppler broadening of neutron-absorption resonances — as a shutdown agency in the event of accidental power excursions. The phenomenon is, of course, important only if strong resonance absorption is present in the reactor (usually absorption by a fertile isotope, ^{238}U, or thorium) and if the substantial increase of fuel temperature which is necessary to increase the Doppler broadening by a significant amount can be tolerated. The slightly enriched oxide fuels usually meet the requirements. However, even with these fuels the temperature margin available for Doppler shutdown may not be large if the hypothetical accident occurs when the reactor is already operating at a power level high enough to cause fuel temperatures near the permissible limit. For this reason, the evaluation of the Doppler effect as a protective mechanism in practical cases requires considerable attention to detail and particular attention to the evaluation of the effects of temperature distribution — both the gross distribution from fuel element to fuel element and the local distribution within individual elements — on the amount of reactivity compensation available before destructive temperatures are reached. Similar considerations of detail are involved in the evaluation of the Doppler contribution to the power coefficient of reactivity.

Recent work that is applicable to practical Doppler evaluations is reported in Refs. 3 and 4. References 5 to 36 constitute a short bibliography of background material on the Doppler effect and related questions of resonance absorption in thermal and fast reactors.

Reference 1 describes the detailed mathematical methods developed for analysis of temperature effects on the Doppler coefficient of reactivity and the resonance capture probability, including the important cases of a nonuniform temperature distribution in fuel rods arrayed in a reactor lattice. The analytical techniques used for solution of this problem consist in: (1) transformation of the Boltzmann equation, which describes the steady-state transport of neutrons, into an integral equation whose solution can be expressed as a Neumann series; and (2) establishment of a relation between Monte Carlo histories and the Neumann series to determine the proper form for the random variables that depend on the paths of the neutron histories. By application of this technique, it is possible to evaluate the various reactor parameters and their derivatives, e.g., the Doppler coefficient, by a new and direct method that has not been utilized before.

On the basis of the new method, a computer program, REPAD, was written for a cylindrical lattice cell containing a centrally located cylindrical fuel rod with an arbitrary radial temperature distribution. Several specific cases for different fuel temperatures were investigated with REPAD, using water moderator and UO_2 fuel; both uniform and radially parabolic fuel-temperature distributions were treated. For each case, 12,000 histories were used. Running time on the IBM-709 is about 0.01 min per history for uniform fuel temperature and 0.02 min per history for nonuniform fuel temperature. In the latter case, 24 temperature regions in the fuel were used.

In the interpretation of the specific results obtained in the investigation, it is instructive to define

$$T_{av} = \frac{T_s + T_p}{2}$$

and
$$T_{\mathrm{rm}} = \left(\frac{\sqrt{T_s} + \sqrt{T_p}}{2}\right)^2$$

where T_s is the surface temperature and T_p is the peak temperature at the center line of the fuel rod. Also, an effective temperature, T_{eff}, is defined as that spatially constant fuel temperature which gives the same value of the reactor parameter (in this case the Doppler coefficient of reactivity or the resonance capture probability) as obtained for a parabolic temperature distribution in the fuel. It is not expected that T_{eff} for the resonance capture probability $(1-p)$ will be the same as T_{eff} for the Doppler coefficient of reactivity, $(1/p)(\partial p/\partial T)$. Values of T_{eff} calculated for two cases of parabolic fuel-temperature distribution are tabulated as follows:

T_s, °K	T_p, °K	T_p/T_s	T_{av}, °K	T_{rm}, °K	T_{eff}, °K
840	2800	3.34	1820	1670	1520 for $(1-p)$ 1400 for $(1/p)(\partial p/\partial T)$
1820	3780	2.08	2800	2720	2730 for $(1-p)$ 2800 for $(1/p)(\partial p/\partial T)$

For the higher temperature case, the parabolic temperature distribution can be characterized by the average temperature, because T_{av}, T_{rm}, and T_{eff} appear to give the same values of $(1-p)$ and $(1/p)(\partial p/\partial T)$ within the limits of statistical error. However, for the lower temperature run, which corresponds more nearly to practical operating fuel temperatures in a power reactor, the average temperature is a poorer approximation to the effective temperature. Use of the average temperature to characterize the parabolic distribution would, in this case, cause the following errors:

T_s, °K	T_p, °K	Parameter	Percentage error caused by replacing T_{eff} with	
			T_{av}	T_{rm}
840	2800	$(1-p)$ $(1/p)(\partial p/\partial T)$	1.7 −9.0	1.0 −6.5

A qualitative explanation in Ref. 3 gives reasons why the average temperature appears to be a much better approximation to the effective temperature for the case at the higher temperatures.

Tabular data of the Doppler-broadened neutron cross sections of ^{241}Pu below 11 ev are given in Ref. 4 for temperatures ranging from 27 to 3000°C. The capture, fission, and scattering cross sections represent theoretical predictions based on the resonance parameters obtained from a multilevel analysis of the ^{241}Pu total cross sections. The total cross-section data fitted in the analysis are those measured by Simpson and Schuman in 1960, as tabulated in Ref. 37. More recent measurements of the fission cross section of ^{241}Pu by T. Watanabe and O. D. Simpson [*Phys. Rev.* (to be published)] and of the total cross section of ^{241}Pu by N. J. Pattenden and by D. S. Craig and C. H. Westcott (unpublished) indicate that the older data of Simpson and Schuman, which were fitted in the analysis, are not accurate over the peaks of the narrow resonances. For the fission cross section, the recent fission measurements indicate that the theoretical fission data, i.e., as predicted from the total cross-section data, are in agreement with the experimental fission data to the order of 10 to 20%. No experimental data are available to enable a similar comparison for the capture and scattering cross sections of ^{241}Pu.

Control-Rod Programming

Calculational work performed in obtaining a control-rod program for a large multiregion core of the pressurized-water reactor type is summarized in Ref. 38. The purpose was to predict the limitations on power when a given group of control rods is moved or to ascertain which control rods can be moved when the maximum reactor power is limited to a given value. The control rods are arranged in subgroups that can be moved independently, and there are many different orders in which the subgroups can be withdrawn. However, the rod-withdrawal programs considered involved only sequential withdrawals from one rod pattern to a successive pattern in such a way that any rod, once withdrawn from the core, need never be inserted again.

The core used as a model for the study was an 8-ft-diameter 3-region core. It was loaded nonuniformly in the radial direction to give the most uniform radial power distribution when chemical shim was used for control. The additional restriction was imposed that the ^{235}U loading used be the greatest that could be controlled by movable cruciform control rods. This method of choosing the loading for the chemical-shim core was employed to provide a backup to the chemical-shim control concept in the event that movable control rods would be necessary for reactor operation. For the case of the core controlled by movable control rods, two concepts were studied: (1) partial control by chemical shim and 44 movable control rods, and (2) control by 44 movable control rods plus 8 fixed shims.

In the development of a suitable rod-withdrawal program, consideration was given to the restrictions imposed by the limiting peak-to-average power-density ratio in the core corresponding to full-power rating. A restriction imposed upon the rod-withdrawal program is that the nuclear radial peak-to-average power-density ratio must never exceed 2.30. The resulting permissible axial power distribution then imposes the restriction that the worth of any rod subgroup used cannot be greater than 2.5%; otherwise the perturbation of the axial power distribution would restrict the power capability of the core.

Reference 4 describes the method of analysis and results obtained in arriving at a control-rod-withdrawal program (with partial chemical shim and fixed shims) which satisfies restrictions and considerations imposed as basic ground rules for the study. First, the number of control rods needed to shut down the reactor is determined for the case in which the most reactive rod is stuck in its fully withdrawn position. Various orders of rod withdrawal are then investigated, and the two-dimensional power distributions are compared to obtain the most desirable ratio of peak-to-average power. Effects on power distribution of nonuniform buildup of plutonium and fission products and of fuel depletion are not considered. The rod-withdrawal program resulting from the study is displayed in Fig. I-1. Also given are the reactivity associated with each control-rod subgroup that is withdrawn (k) and the radial power-peaking factor associated with the pattern of rods remaining in the core (F). Figure I-1 applies to control by 44 movable control rods plus chemical shim for equilibrium xenon. If control were effected by 44 rods and 8 fixed shims, reactivities would be about 3% higher than values shown in Fig. I-1. When operating with fixed shims, the vessel would be opened when the 16-rod pattern was reached for removal of the shims. After shim removal 44 rods would be employed for control.

Short Notes

Results of a survey of experimental cross sections and other nuclear data for zirconium are presented in Ref. 39. The sources of information are given, and the interpretations made to produce a tabulation of nuclear data for use in neutronic calculations are described.

Measurements in water of the age of fission neutrons to indium resonance energy (1.46 ev) are described in Ref. 40. The measurements utilized a finite plane fission source and essentially infinite plane detectors so as to be equivalent to a measurement using axial detectors and an infinite plane source. The advantage of this experimental approach is that the measured results do not require calculated corrections to extrapolate to infinite source geometry, as is the case in measurements using axial detectors with a finite plane or point source. The remaining corrections to the data are small and well understoood. The reference describes the details of the experimental setup, experimental procedures, and methods of data reduction. The fission-neutron age measured in the experiment (to 1.46 ev) was 26.45 ± 0.32 cm^2 at a water density of 1.0 g/ml. For comparison, the comparable calculated age is given, as obtained with the Monte Carlo computer code TYCHE[41] which includes the effects of both inelastic scattering and anisotropic elastic scattering in oxygen. The calculated age is 25.62 ± 0.24 cm^2.

A review of neutron thermalization in Ref. 42 describes briefly the various techniques developed, their relation to one another, and their applications. Emphasis is placed on those aspects which are closely related to reactor design and, since digital computer codes are frequently used, to the numerical methods and codes that have been developed. The individual methods are surveyed in just sufficient detail to reveal the essential physics or the key to each method. An extensive bibliography is included, and it covers specific topics related to the neutron thermalization problem.

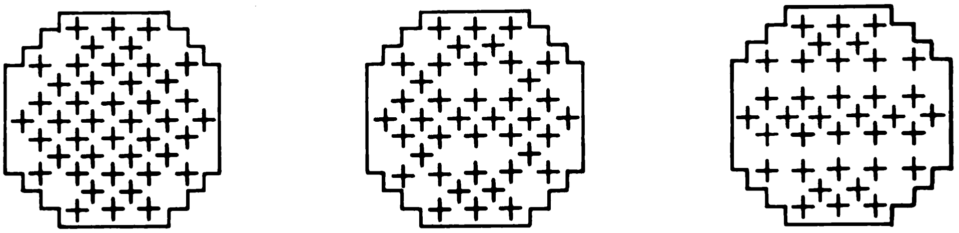

44 Rods
k = 0.956
F = 3.19

40 Rods
k = 0.974
F = 2.19

36 Rods
k = 0.997
F = 2.29

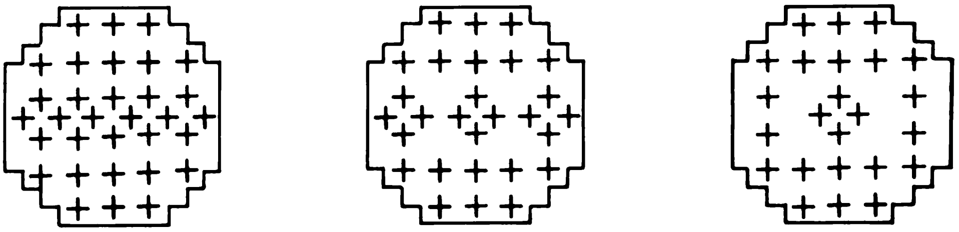

32 Rods
k = 1.011
F = 2.03

28 Rods
k = 1.029
F = 2.07

24 Rods
k = 1.045
F = 2.25

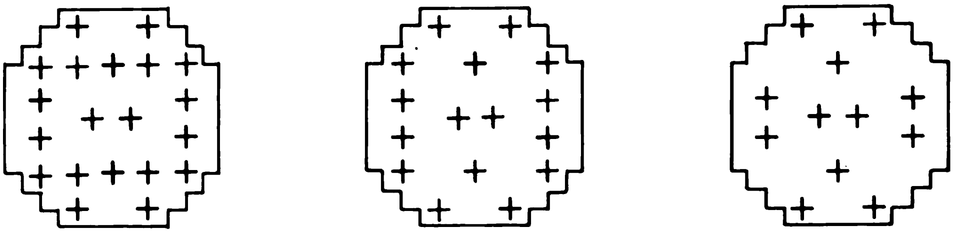

20 Rods
k = 1.057
F = 1.88

16 Rods
k = 1.076
F = 1.93

12 Rods
k = 1.086
F = 1.74

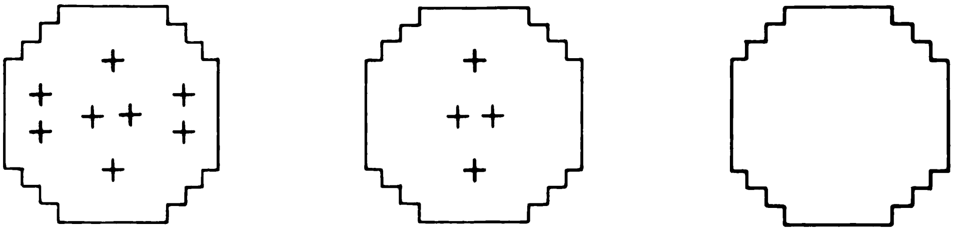

8 Rods
k = 1.096
F = 1.97

4 Rods
k = 1.108
F = 1.71

No Rods
k = 1.121
F = 1.40

Fig. I-1 Control-rod-withdrawal program.[6] Here k is the neutron multiplication factor, hot at zero power, with boron to control the equilibrium xenon swing, and F is the radial peak-to-average power factor.

References

1. A. H. Spano, Self-Limiting Power Excursion Tests of a Water-Moderated Low-Enrichment UO_2 Core, *Nucl. Sci. Eng.*, 15(1): 37 (January 1963).
2. A. H. Spano, J. E. Barry, L. A. Stephan, and J. C. Young, Self-Limiting Power Excursion Tests of a Water-Moderated Low-Enrichment UO_2 Core in SPERT I, USAEC Report IDO-16751, Phillips Petroleum Co., 1962.
3. J. E. Olhoeft, The Doppler Effect for a Non-Uniform Temperature Distribution in Reactor Fuel Elements, USAEC Report WCAP-2048, Westinghouse Electric Corp., Atomic Power Division, July 1962.
4. N. H. Marshall and O. D. Simpson, Doppler Broadening of the Total Fission, Capture, and Scattering Neutron Cross Sections of Pu-241, USAEC Report IDO-16954, Phillips Petroleum Co., Dec. 16, 1963.
5. E. Creutz, H. Jupnik, T. Snyder, and E. P. Wigner, Review of the Measurements of the Resonance Absorption of Neutrons by Uranium in Bulk, *J. Appl. Phys.*, 26: 257 (1955).
6. E. Hellstrand, Measurements of the Effective Resonance Integral in Uranium Metal and Oxide in Different Geometries, *J. Appl. Phys.*, 28: 1493 (1957).
7. R. M. Pearce and D. H. Walker, A Direct Measurement of the Uranium Metal Temperature Coefficient of Reactivity, *Nucl. Sci. Eng.*, 2(1): 24-32 (February 1957).
8. J. Chernick and A. R. Vernon, Some Refinements in the Calculation of Resonance Integrals, *Nucl. Sci. Eng.*, 4(5): 649 (November 1958).
9. F. T. Adler, G. W. Hinman, and L. W. Nordheim, The Quantitative Evaluation of Resonance Integrals, in *Proceedings of the Second United Nations International Conference on the Peaceful Uses of Atomic Energy, Geneva, 1958,* Vol. 16, p. 142, United Nations, Geneva, 1958.
10. R. D. Richtmyer, R. Van Norton, and A. Wolfe, The Monte Carlo Calculation of Resonance Capture in Reactor Lattices, in *Proceedings of the Second United Nations International Conference on the Peaceful Uses of Atomic Energy, Geneva,* 1958, Vol. 16, p. 180, United Nations, Geneva, 1958.
11. L. Dresner, *Resonance Absorption in Nuclear Reactors*, Pergamon Press, Inc., New York, 1960.
12. W. H. Arnold, Jr., and R. A. Dannels, The Doppler Coefficient of $U^{238}O_2$, *Trans. Am. Nucl. Soc.*, 3(1): 229 (1960).
13. W. H. Arnold, Jr. and R. A. Dannels, Westinghouse Electric Corp., 1960. (Unpublished).
14. A. R. Vernon, Calculation of the Effective Resonance Integral of U^{238}, *Nucl. Sci. Eng.*, 7(3): 252 (March 1960).
15. M. Wagner, Spatial Distribution of Resonance Absorption in Fuel Elements, *Nucl. Sci. Eng.*, 8(3): 278 (September 1960).
16. E. Hellstrand, P. Blomberg, and S. Horner, The Temperature Coefficient of the Resonance Integral for Uranium Metal and Oxide, *Nucl. Sci. Eng.*, 8(6): 497 (December 1960).
17. L. W. Nordheim, The Contribution of the Individual Resonances to the Resonance Integrals in Uranium and Thorium, USAEC Report GA-2563, General Dynamics Corp., General Atomic Division, Oct. 26, 1961.
18. E. Hellstrand and J. Weitman, The Resonance Integral of Thorium Metal Rods, *Nucl. Sci. Eng.*, 9(4): 507 (April 1961).
19. R. M. Pearce, The Doppler Effect in Thermal Reactors, *J. Nucl. Energy, Pt. A*, 13: 150 (1961).
20. L. Dresner, Some Remarks on the Effect of a Nonuniform Temperature Distribution on the Temperature Dependence of Resonance Absorption, *Nucl. Sci. Eng.*, 11(1): 39 (September 1961).
21. R. Goldstein and E. R. Cohen, Theory of Resonance Absorption of Neutrons, *Nucl. Sci. Eng.*, 13(2): 132 (June 1962).
22. J. H, Ferziger, Resonance Absorptions in Lumps with Nonuniform Temperature Distributions, *Nucl. Sci. Eng.*, 14(3): 244 (November 1962).
23. E. Hellstrand and G. Lundgren, The Resonance Integral for Uranium Metal and Oxide, *Nucl. Sci. Eng.*, 12(3): 435 (March 1962).
24. L. W. Nordheim, A New Calculation of Resonance Integrals, *Nucl. Sci. Eng.*, 12(4): 457 (April 1962).
25. G. W. Hinman, G. F. Kuncir, J. B. Sampson, and G. B. West, Accurate Doppler Broadened Absorption, *Nucl. Sci. Eng.*, 16(2): 202 (June 1963).
26. M. M. Levine, Resonance Integral Calculations for U^{238} Lattices, *Nucl. Sci. Eng.*, 16(3): 271 (July 1963).
27. S. Iijima, Resonance Absorption and the Resonance Disadvantage Factor, *Nucl. Sci. Eng.*, 17(1): 42 (September 1963).
28. A. Reichel, The Temperature Dependence of Effective Resonance Integrals, *J. Nucl. Energy, Pt. A & B*, 17(7): 281 (September 1963).
29. H. Feshbach, G. Goertzel, and H. Yamauchi, Estimation of Doppler Effect in Fast Reactors, *Nucl. Sci. Eng.*, 1(1): 4-19 (March 1956).
30. H. A. Bethe, On the Doppler Effect in Fast Reactors, USAEC Report APDA-119, Atomic Power Development Associates, Inc., Mar. 11, 1957.
31. R. B. Nicholson, The Doppler Effect in Fast Neutron Reactors, USAEC Report APDA-139, Atomic Power Development Associates, Inc., June 1960.
32. P. Greebler, B. A. Hutchins, and J. R. Sueoka, Calculations of Doppler Coefficient and Other Safety Parameters for a Large Fast Oxide Reactor, USAEC Report GEAP-3646, General Electric Compnay, Atomic Power Equipment Department, Mar. 23, 1961.
33. P. Greebler and B. A. Hutchins, The Doppler Effect in a Large Fast Oxide Reactor, Its Calculation and Significance for Reactor Safety, in

Proceedings of the Seminar on the Physics of Fast and Intermediate Reactors, Vienna, Austria, August 3-11, 1961, Vol. III, p. 121, IAEA, Vienna, 1962.

34. M. G. Bhide and H. H. Hummel, Calculations of the Doppler Coefficient of Large Ceramic-Fueled Fast Reactors, USAEC Report ANL-6601, Argonne National Laboratory, August 1962.
35. P. Greebler and E. Goldman, Doppler Calculations for Large Fast Ceramic Reactors—Effects of Improved Methods and Recent Cross Section Information, USAEC Report GEAP-4092, General Electric Company, Atomic Power Equipment Department, Dec. 19, 1962.
36. Proceedings of the Conference on Breeding, Economics, and Safety in Large Fast Power Reactors, October 7–10, 1963, USAEC Report ANL-6792, Argonne National Laboratory, December 1963:
    a. B. Wolfe, N. Friedman, and D. Riley, Influence of the Doppler Effect on the Meltdown Accident, pp. 170-190.
    b. J. Codd and P. J. Collins, Some Calculations Concerning the Influence of Resonance Overlapping on the Doppler Effect in a Dilute Fast Reactor, pp. 711-724.
    c. R. N. Hwang, An Improved Method of Doppler-Effect Calculation for Fission Materials in the Intermediate Energy Region, pp. 727-742.
    d. H. H. Hummel and A. L. Rago, Effect of Parameter Variation in Doppler Effect Calculations, pp. 747-761.
    e. R. Froelich, K. Ott, and J. J. Schmidt, Calculation of Doppler Coefficients of Dilute Fast Reactors, pp. 777-789.
    f. C. Graves, Methods of Evaluation of Effective Cross Section for Doppler Coefficient Calculation in Large Fast Breeder Reactors, pp. 791-802.
    g. E. A. Fossoul, Doppler Effect in Fast Reactors for Nonuniform Heating and Temperature Distribution, pp. 803-819.
37. O. D. Simpson and N. H. Marshall, Doppler Broadening of the Low Energy Total Neutron Cross Section of Pu-241, USAEC Report IDO-16679, Phillips Petroleum Co., Aug. 4, 1961.
38. D. L. Miller, Control Rod Programming in a Large Multiregion Core, USAEC Report WCAP-3719, Westinghouse Electric Corp., Atomic Power Division, October 1962.
39. P. J. Hemmings, A Compilation of Nuclear Data for Natural Zirconium, British Report AHSB(S)-R-62, 1963.
40. R. K. Paschall, The Age of Fission Neutrons to Indium Resonance Energy in Water, Part I, Experiment, USAEC Report NAA-SR-8621, Atomics International, Nov. 30, 1963.
41. H. Alter, The Age of Fission Neutrons to Indium Resonance Energy in Water, Part II, Theoretical, USAEC Report NAA-SR-8662, Atomics International (to be published).
42. H. C. Honeck, A Review of the Methods for Computing Thermal Neutron Spectra, USAEC Report BNL-821 (T-319), Brookhaven National Laboratory, June 1963.

Section

II

Power Reactor Technology

Fluid and Thermal Technology

Burnout in Steam-Water Mixtures

By John S. Wiley

The DNB-2 Curve and Its Significance

The first article in this series on two-phase burnout, Sec. III, *Power Reactor Technology*, 7(1), presented data (Figs. III-6 and III-7 of that article) showing lines arbitrarily called DNB-1 and DNB-2. The discussion in the succeeding two articles was directed to typical DNB-1 behavior; the purpose of this review is to discuss the significance of the DNB-2 line. The terms "DNB-1" and "DNB-2" were coined by Levedahl,[1] who first published burnout data on a steam-energy flow (SEF) plot.* The application of the terms to the constant inlet-temperature data shown in Fig. II-1, however, is somewhat arbitrary since the data indicate a transition zone between the DNB-1 and DNB-2 curves. Data taken at an inlet subcooling (SC) or 62°F, for example, plot in a nearly vertical curve.

When DNB data are considered on an SEF plot, remember that the abscissa and ordinate of the plot are always related by the heat balance

$$\phi = D/4L_T[\mathrm{SEF} + G(H_f - H_{\mathrm{in}})] \qquad (1)$$

$$= D/4L_T\,(\mathrm{SEF} + G\Delta H_{sc}) \qquad (2)$$

The experimenter may take data on burnout heat flux by setting G, for example, and varying H_{in}, or he may vary G at given values of H_{in}. Figure II-1 illustrates burnout data at 2000 psia from Table 21 of Ref. 2. The way the data are presented in the table suggests that the DNB points were established by making a series of runs with varying mass flow and constant inlet temperature, and the solid lines on Fig. II-1 depict this method of operation. The dashed lines, which are cross plotted, suggest that the experiments could have been run equally well by setting the mass flow at a constant value and varying the inlet temperature to find the DNB point. Thus DNB-2 lines on Fig. II-1 do not appear unique and could have been obtained by cross-plotting data taken at constant mass flow. The question this review attempts to answer, therefore, is whether the DNB-2 curves ever do represent some unique behavior that would contribute to our understanding of burnout phenomena.

Figure II-2 illustrates additional 2000-psia data appearing in Table 10 of Ref. 2. The few points were taken at a mass flow of about 0.5 × 10^6 lb/(hr)(sq ft), and a possible "best-fit" curve through the several points is shown as curve *A* in Fig. II-2. If curve *A* did represent the behavior of ϕ_{BO} with SEF at constant mass flow, then the deviation of the runs from the curve could be attributed to statistics. If more Table 10 data were plotted,* however, it would become evident that curve *A* is not really the best-fit curve and that the data could be better represented by DNB-1 and DNB-2 curves. If a constant-*G* curve is drawn on Fig. II-2, it takes a nose dive, as shown by curve *B*. This sort of behavior is not what is observed in Fig. II-1, where the constant-*G* curves are all quite straight. The writer therefore concludes that at least two different burnout mechanisms are illustrated in Fig. II-2, whereas the burnouts plotted in Fig. II-1 probably were all caused by a single mechanism. This argument is not particularly convincing at present because only a few points are shown on Fig. II-2. Further data, from experiments at 1000 psia, will be considered in an attempt to substantiate that burnouts giving DNB-2 lines can be caused by a different burnout mechanism than burnouts giving DNB-1 lines.

---

*Steam-energy flow is the product Gx_eh_{fg}, where G is the mass flow in pounds per hour per square foot, x_e is the exit quality, and h_{fg} is the vaporization enthalpy in British thermal units per hour per square foot.

*A presentation of Table 10 data is shown in Fig. III-7, *Power Reactor Technology*, 7(1).

It is instructive to assume that one has available a number of test sections, of a given diameter but a variety of lengths, and to proceed to conduct, conceptually, a number of experiments to determine the burnout heat flux. Such programs have, in fact, been carried out many times in laboratories all over the world. Typical data for a test section having a length of 17 in. and an inside diameter of 0.220 in. are shown in Fig. II-3. These are data of Lee and Obertelli[3] and were taken at a nominal pressure of 1000 psia. It is evident that data taken at subcoolings from about 10 to 135°F plot on a single DNB-1 line.

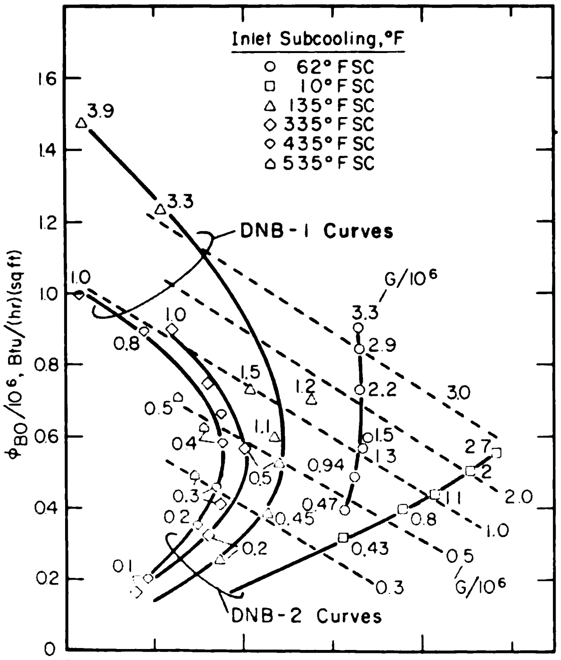

Fig. II-1 Steam-energy flow plot of data from Table 21 of Ref. 2. Pressure = 2000 psia, $L_T = 27$ in., and flow-channel thickness = 0.097 in.

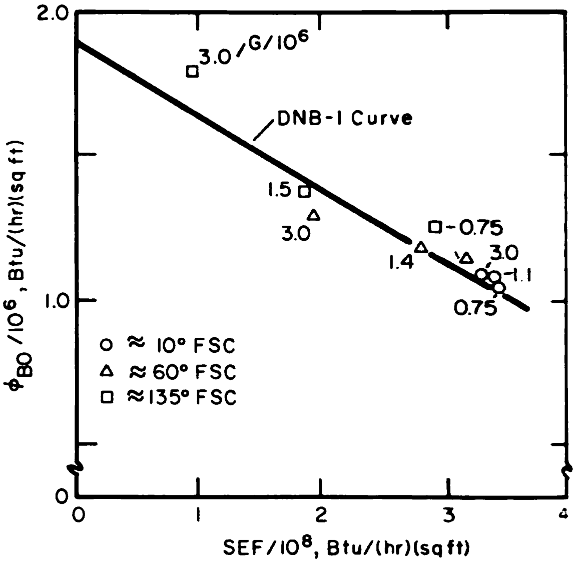

Fig. II-2 Steam-energy flow plot of burnout data from Table 10 of Ref. 2. $G/10^6 \cong 0.5$ lb/(hr)(sq ft) and pressure = 2000 psia.

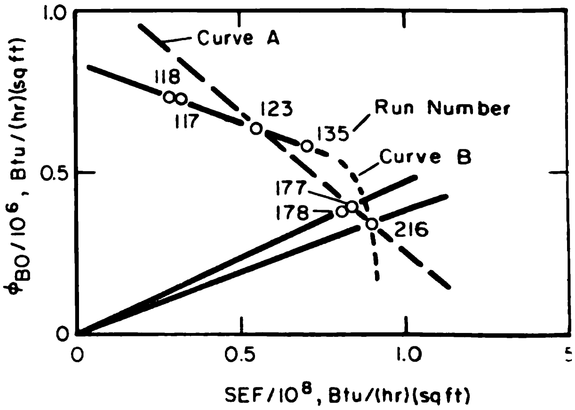

Fig. II-3 Steam-energy flow plot of runs 56 to 90 of Ref. 3. Pressure = 1000 psia (nominal), $L_T = 17.0$ in., and $D = 0.220$ in.

As tube length is increased to 34 in., the data take the appearance shown in Fig. II-4. The DNB-1 line is depressed, and this length effect has been discussed in Sec. III of *Power React Technology*, 7(3). As the tube is lengthened to 53.5 in., data plotted in Fig. II-5 are obtained. At first glance the DNB-2 data plotted in Fig. II-5 suggest no unusual behavior and, indeed, look quite similar to data shown in Fig. II-1. The spread of the data seems to call for some attention, however, for at 1000 psi the SEF plot rdinarily pulls together the data for a tubular st section, so that data for a rather wide ange of mass flows falls on a single line, at ast in the DNB-1 range.

Figure II-6 compares Lee-Obertelli data with ata appearing in Ref. 4, which reports work one by the Centro Informazioni Studi Esperi- ize (CISE). The particular Ref. 4 data plotted ere taken with a steam-water mixture fed to e test section, and, if burnout is independent of upstream history, then the 31.4-in. CISE test section should be equivalent to the last few feet of the 79-in. Lee-Obertelli test section.* Curves, arbitrarily called DNB-2′, have been placed through the CISE data (neglecting, for the moment, the portion labeled "instability branch"), and it is evident that they coincide fairly well with the Lee-Obertelli data at the corresponding mass flows. The DNB-2′ curves have been extrapolated to the DNB-1 curve with a shape suggested by data appearing in Ref. 5. The vertical, extrapolated portion of the DNB-2′ curves plotted on Fig. II-5 represent what Collier[5] calls "dryout," where the heat-transfer coefficient is reduced from a high value in the forced convective region to a value near that

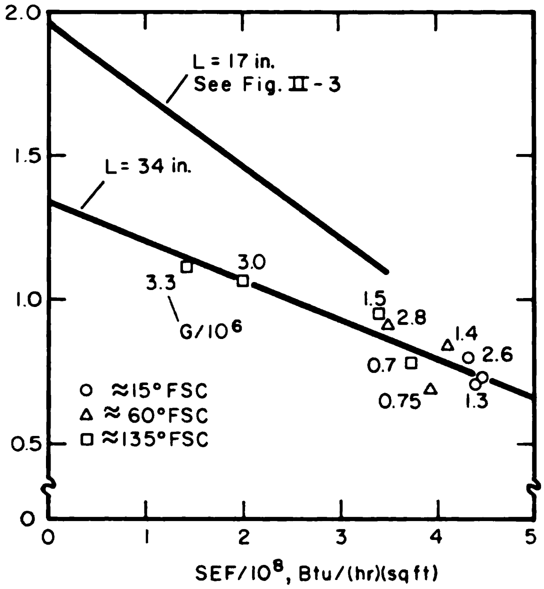

.g. II-4 Steam-energy flow plot of runs 117 to 134 Ref. 3. Pressure = 1000 psia (nominal), L_T = 34.0 ., and D = 0.220 in.

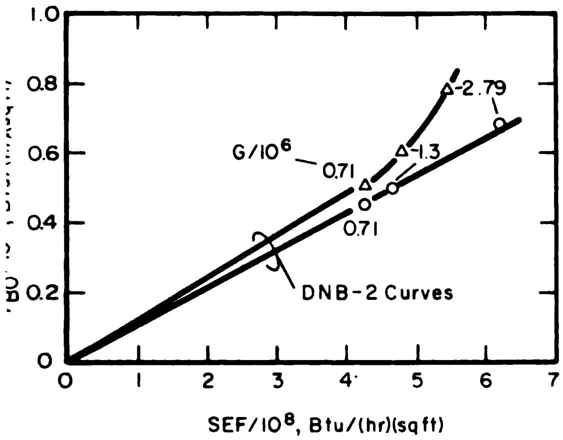

g. II-5 Steam-energy flow plot of runs 135 to 152 Ref. 3. Pressure = 1000 psia (nominal), L_T = 53.5 ., and D = 0.220 in.

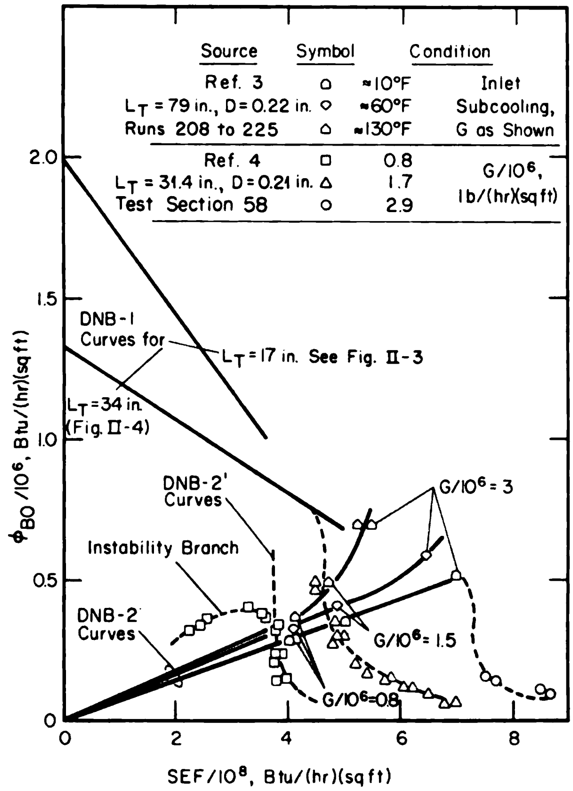

Fig. II-6 Comparison of data in Ref. 3 (Lee and Obertelli) and Ref. 4 (CISE data). Pressure = 1000 psia (nominal).

---

*The test sections used to take burnout data reported in Ref. 3 had lengths of 3.9, 8.3, 15.8, and 31.4 in. Although there is a length effect observable in the SEF plots of CISE data, changing the length from 15.8 to 31.4 in. has but little effect on the positions of the DNB-2′ curves.

expected for heat transfer by forced convection to dry steam.

In Fig. II-6 is shown an attempt to reconcile burnout data taken with test sections employing both single- and two-phase feed. This possibility has been considered on page II-184 of Ref. 4, which is quoted as follows:

> ... experiments in the quality region carried out with subcooled water at the inlet, cannot be directly compared with data taken with water and steam entering the test section...

The above quotation might be interpreted as stating that it is difficult to obtain the complete set of DNB curves with but one test section of given dimensions. For example, the DNB-1 data usually come from low L/D test sections, whereas the DNB-2 data come from high L/D test sections. As L and D are changed to explore different regions, they in themselves affect ϕ_{BO}, and, until the effects of L and D on ϕ_{BO} are known precisely, this confounding effect makes analyses difficult. The importance of this should not be underestimated, for it acts as a restraint of great binding power on the experimenter. Suppose, for example, the objective is to determine the position of the DNB-1 line with a test section having an L_T/D of 300 and mass flows of about 1 million lb/(hr)(sq ft). Experience indicates that ϕ_{BO} will be of the order of 1 million Btu/(hr)(sq ft) at a value of SEF = 0. If these numbers are put into Eq. 1, it can be shown that the experiment must be conducted with the water at an inlet subcooling of about 1200 Btu/lb. To avoid working with cryogenic fluids, the experimenter must therefore explore the DNB-1 region with test sections of low L/D. However, he then is unable to explore the DNB-2 region without using two-phase feed to the test section. Accordingly the constant-G curves implied in Fig. II-6 will probably be difficult to obtain with a single test section of given dimensions employing only single-phase feed.

Figure II-6 bears a striking resemblance to curve B of Fig. II-2 with respect to the "droop" in the constant-G curves and lends credibility to the hypothesis that some DNB-2 type burnouts are caused by a different burnout mechanism than that operating to cause DNB-1 type burnouts. Unfortunately a discussion of burnout mechanisms usually is of a qualitative nature, and the state of the art is such that it would be hazardous to say which burnout mechanism was responsible for the termination of a given burnout experiment.

From the standpoint of simplifying the variables that must be considered by the designer, it would be fortunate if all DNB-2 type burnouts at the pressure under consideration (1000 psia) were caused by a single mechanism. Unfortunately there appears to be at least one other mechanism that gives burnout data which, when plotted on an SEF plot, exhibits curves of the DNB-2 type. This is labeled "instability branch" in Fig. II-6. This particular set of data is typical of behavior experienced in a relatively large number of runs at pressures from 580 to 1200 psia (nominal) and mass flow rates of about 0.8×10^6 lb/(hr)(sq ft). The region of the intersection of the instability branch with the appropriate DNB-2′ curve line is discussed in Ref. 4 and is termed the "maximum ϕ_{BO}," although it pertains only to a particular value of mass flow. The authors of Ref. 4 state that this maximum in burnout heat flux is related to a change in flow and heat-transfer mechanisms, and they suggest that the behavior near the maximum is related to some kind of instability due to a change in flow pattern at the inlet of the heated tube. The following is quoted from Ref. 4:

> Rather strong pressure oscillations were observed at low qualities. These oscillations, much more relevant at low flowrates, are probably due to flow instabilities; it must however be noted that the efficiency of the pressure control loop decreases with flowrate. The oscillations were seen both at the absolute and at the differential manometers; no quantitative measurements were made of their amplitude, frequency and of the flow conditions at which they appeared. Usually, experiments were not performed when oscillations higher than ±1 kg/cm^2 were detected at the absolute manometer, and in this case more stable conditions were reached by increasing inlet quality.

Not many experiments have been reported in the open literature wherein carefully controlled observations were made to explore oscillatory behavior in heated sections. The designer is usually given burnout data, which consists of values of mass flow, inlet enthalpy, pressure, burnout heat flux, and exit quality at burnout. Because the experimenter does not ordinarily know the more detailed conditions inside the tube at burnout, such as phase distributions and burnout mechanisms, this information is not presented. The method of detecting burnout varies widely, and the final value of ϕ_{BO} set down by the experimenter in his data table may involve subjective considerations.* Often the experimental equipment is not set up to detect fast transients in flow, pressure drop, or wall temperature. These considerations lead the designer to apply relatively large safety factors on burnout because the experimental data, when reduced to a correlation, may not be particularly applicable to his case; for example, hydraulic instability rather than steam blanketing of heat-transfer surfaces may be the limit on his particular design, whereas the correlation he is using may pertain to burnout caused by transition to film boiling.

Accordingly the experiments of Quandt[6] are of interest because they are one of the few reported studies on flow oscillations in a test section producing a steam-water mixture. The experimental equipment used was modified to make it more suitable for measurement of flow oscillations. Special high-speed instrumentation was employed to measure test-section flow and pressure drop, overall pressure drop, total pressure, inlet plenum temperature, and test-section outside wall temperature. Tests were run in Bettis High-Pressure Loop No. 23, which was modified; a high-flow bypass was used in parallel with the test section to ensure a constant overall pressure drop.

The following quotation[6] serves to define what was observed during the course of burnout runs:

> Experimental Observations of Flow Oscillations
>
> This discussion will supplement the quantitative data previously presented with a qualitative description of an oscillation test conducted at constant over-all pressure drop and increasing heat flux. First the total pressure drop was established at a zero power condition corresponding to the desired initial flow. From this point the heat flux was increased in small steps with steady-state conditions being established after each step in order to record the flow decrease and the various test section and coolant temperatures. Since the flow through the unheated by-pass was about 20-30 times the heated-section flow, minor adjustments were sufficient to maintain a constant over-all pressure drop. During this increase in power, the fast-response instruments showed relatively steady flows and pressure drops with a normal amount of noise appearing on the traces due to turbulent flow (approximately 15-25% of the reading and at roughly the natural frequency of the transducer system ...). Due to this rather high noise level the fast-response instruments were not used to measure absolute values.
>
> When the flux was high enough for the channel to be near an oscillating condition the increments in power from one steady-state point to another were reduced to 2% of the existing flux. Eventually a steady-state condition was reached where the normal small drift of loop variables such as inlet temperature, total pressure, heat flux, etc., was sufficient to cause the flow and channel pressure drop to begin a well-defined sinusoidal oscillation, die out, and start again. These "incipient oscillations" would appear with amplitudes roughly 30% of the average flow reading, while the other variables which were being recorded with high-speed instruments showed no variation other than normal noise. If, at this point the flux was increased by 2%, self-sustained flow oscillations of constant amplitude would result. If the flux was lowered by 2%, the flow would resume the normal noise pattern. Therefore it was possible to determine rather precisely the conditions at which flow oscillations began. Upon further small increases in heat flux the amplitude of the flow oscillation increased rapidly, then leveled out with the instruments showing an extremely reproducible, and now nonlinear, oscillation of definite frequency. At this point both heated channel flow and pressure drop showed the oscillations while the over-all pressure drop, channel outside wall temperatures, and inlet temperature remained steady.
>
> Continuing increases in heat flux finally caused the over-all pressure drop and the test-section-wall temperature to pick up the oscillation. Hence the oscillation had become strong enough to influence the external loop and the test section inside surface was passing in and out of a burnout condition every cycle. Continued increases in heat flux caused the inlet water temperature to begin to oscillate, indicating that the flow had begun to pulse out the inlet of the channel. This last point might occur at 10-20% higher power than the point of initial oscillation. Further increases in heat flux resulted finally in a wall-temperature excursion (burnout) superimposed on top of the oscillation. In some runs burnout occurred before any of the secondary oscillations began, and this complete pattern did not occur.

Results of the experiments are plotted in Fig. II-7. These data are called "values at last stable condition" and presumably correspond to data taken at the point (in time) "at which flow oscillations began." The data line up nicely into DNB-2 curves with the exception of the two 1200-psia runs at a subcooling of 115°F. Their behavior suggests that they may lie on a DNB-1 curve or at least near the intersection of the DNB-1 and DNB-2 curves. The data in Fig. II-7 are replotted in Figs. II-8 to II-10; however, in these curves, instead of ϕ_{BO}, the fractionable length of the test section undergoing boiling at burnout, $(L_B/L_T)_{BO}$ is plotted as a function of mass flow with inlet subcooling as a parameter.

---

*Pages II-174 to II-177 of Ref. 4 contain an excellent description of the problems besetting the determination of which value of ϕ represents ϕ_{BO}.

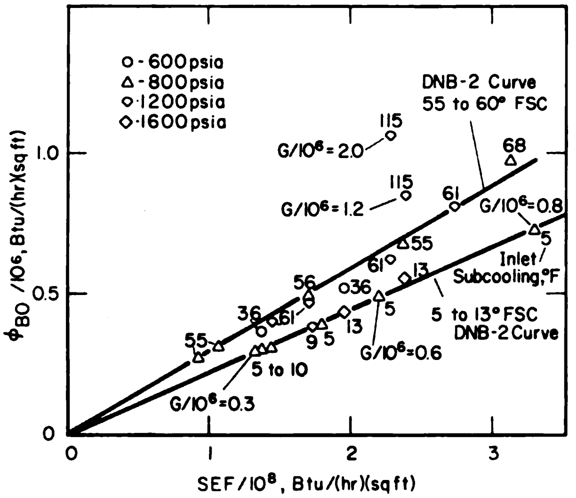

Fig. II-7 Steam-energy flow plot of data from Quandt.[6] Pressure, mass flow, and inlet subcooling as indicated.

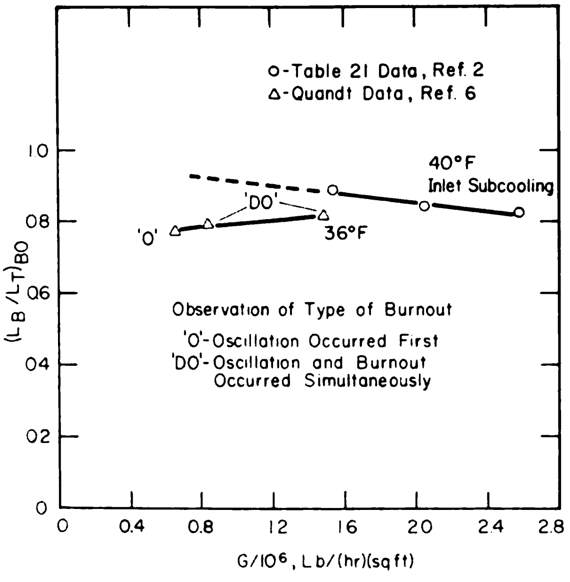

Fig. II-8 Fractional length of test section undergoing boiling at point of burnout vs. mass flow. Comparison of data in Refs. 2 and 6. Pressure = 600 psia and inlet subcooling as indicated.

The call-outs "D," "DO," and "O" signify whether the runs were terminated by burnout occurring first, burnout and oscillation occurring simultaneously, or an oscillation occurring first, respectively. These results were taken from Table 1 of Ref. 6. Also plotted on Figs. II-8 to II-10 are data taken from Table 21 of Ref. 2. The Table 21 data were taken in a test section whose nominal dimensions were the same as those of the of the test section used to take the Ref. 6 data, and the data originally appeared in Refs. 7 to 9. The latter references suggest that the Table 21 data were taken in test loops without a parallel channel flow, although the loops

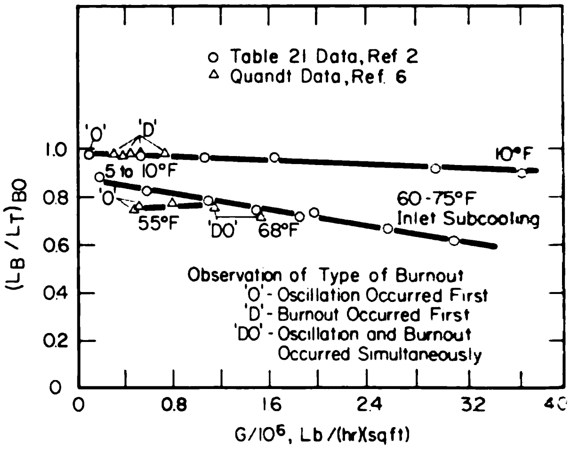

Fig. II-9 Fractional length of test section undergoing boiling at point of burnout vs. mass flow. Comparison of data in Refs. 2 and 6. Pressure ~800 psia and inlet subcooling as indicated.

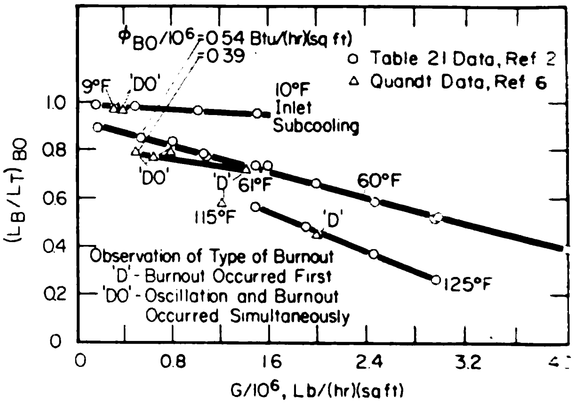

Fig. II-10 Fractional length of test section undergoing boiling at point of burnout vs. mass flow. Comparison of data in Refs. 2 and 6. Pressure = 1200 psia and inlet subcooling as indicated.

utilized could have provided an alternate flow path.

It is of interest to speculate as to whether the same instability or oscillatory behavior was operating in the Table 21 experiments as in those of Quandt. Figure II-8 reveals some disparity between the $(L_B/L_T)_{BO}$ values from Table 21 and those from Quandt. In the Quandt runs, which exhibited some sort of oscillatory behavior, burnout always occurred at lower values of $(L_B/L_T)_{BO}$ than in the Table 21 runs. This is also true at the higher pressures (Figs. II-9 and II-10), although at low subcooling the difference is minor. Values of ϕ_{BO} are indicated for two of the runs plotted in Fig. II-10. Whatever was happening within the Table 21 test section for the burnout run with $\phi_{BO} = 0.54 \times 10^6$ Btu/(hr)(sq ft), it represents a 38% increase in heat flux compared to the corresponding value observed by Quandt of 0.39×10^6 Btu/(hr)(sq ft).

An interesting series of experiments is described in Ref. 10. The authors had noticed that values of ϕ_{BO} taken in various laboratories exhibited "very considerable divergences." Although test sections of different lengths were utilized for the various runs, the divergences were greater than could reasonably be assigned to the effect of that variable. Accordingly a test loop was fabricated which produced feed for the test section by condensing high-pressure steam, as shown schematically in Fig. II-11. It was discovered that ϕ_{BO} (or q_{cr} in the terminology usually used in Russian heat-transfer literature) depended on which valve was used to throttle the high-pressure steam. This is illustrated in Fig. II-12. Burnout was indicated by reddening of the test section, and the authors state that they believe the lower branch of the burnout curve was due to the presence of pulsations. Traces of flow-time curves shown in the reference illustrate the oscillatory behavior of the coolant flow rate upon approaching burnout with the flow rate controlled by valve No. 1 (Fig. II-11). Similar behavior was evidenced when the compressible volume shown in Fig. II-11 was filled with steam or water with a temperature above 572°F. In Figs. II-13 and II-14 are shown the results of hundreds of runs leading to burnout in pulsating and nonpulsating systems.

The variety of DNB-1 lines shown in Fig. II-13 is interesting. At qualities less than zero, q_{cr} is length independent; this could be the region where film boiling causes burnout, as it would seem reasonable that formation of a patch of steam over a local, heated area would be independent of upstream conditions. In the quality region, q_{cr} becomes length dependent, suggest-

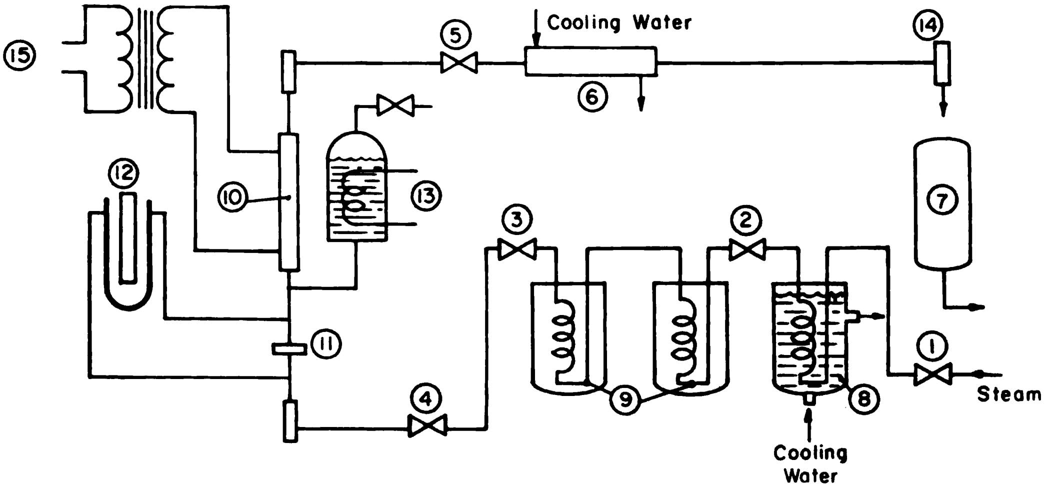

Fig. II-11 Schematic of experimental apparatus used to take data reported in Ref. 10.

1 to 5	Throttling valves	11	Measuring orifice
6	Condenser	12	Differential manometer
7	Weighing tank	13	Electrically heated buffer volume
8	Vapor cooler	14	Thermocouple wells
9	Coils	15	Power supply
10	Test section		

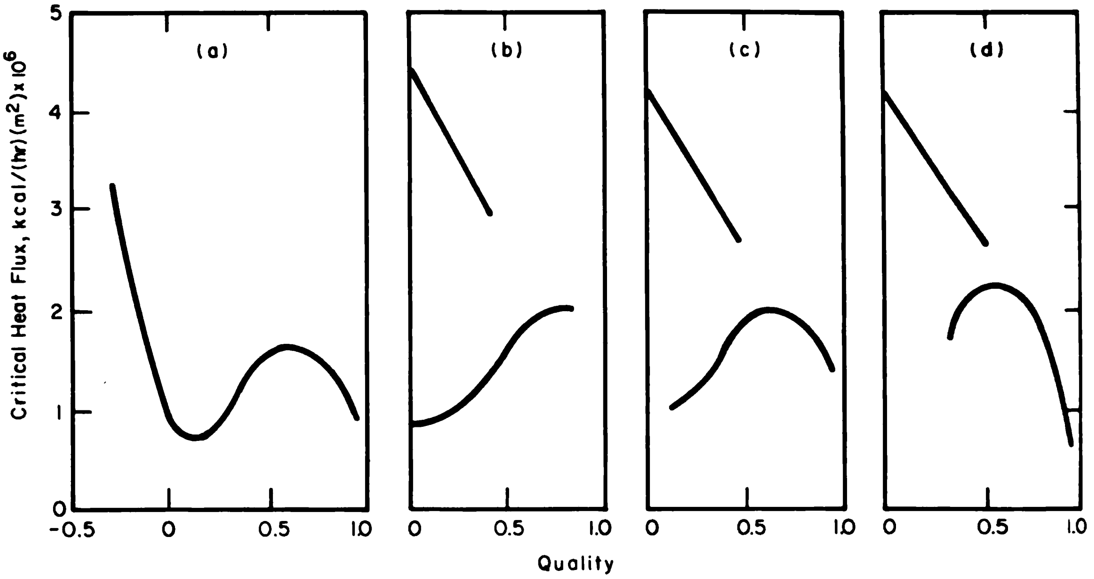

Fig. II-12 Critical burnout heat flux vs. quality.[10] Pressure = 100 atm abs., mass flow = 400 kg/(m^2)(sec), tube inside diameter = 8 mm, and L_T/D = 20. (Data not shown.)

Fig. II-12 part	Valve used for flow control (see Fig. II-11)	Volume upstream of test section, liters
a	1	1.87
b	2	1.41
c	3	0.56
d	4	0.05

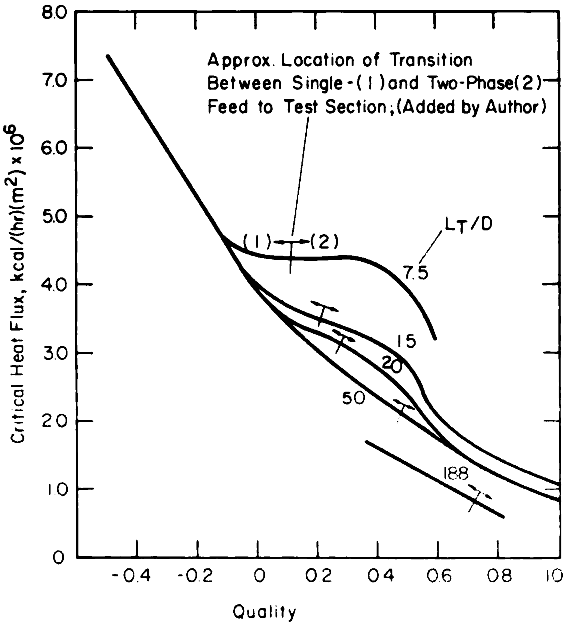

Fig. II-13 Critical burnout heat flux vs. quality for a nonpulsating system.[10] Pressure = 100 atm abs., mass flow = 750 kg/(m^2)(sec), tube inside diameter = 8 mm, and L_T/D is as indicated. (Data not shown.)

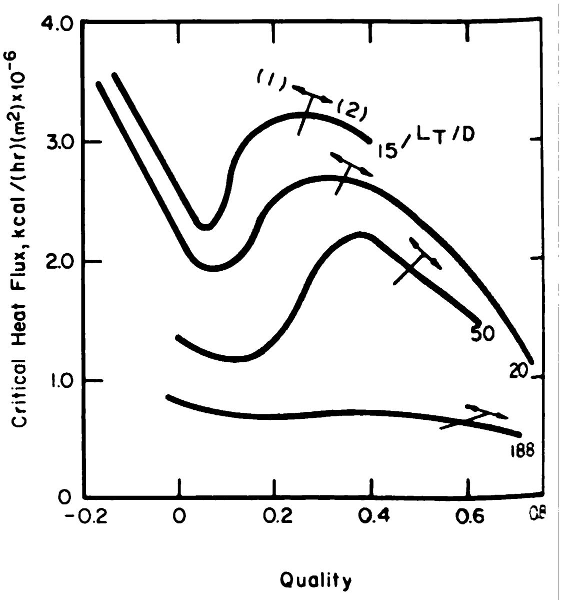

Fig. II-14 Critical burnout heat flux vs. quality for a pulsating system.[10] Pressure = 100 atm abs., mass flow = 750 kg/(m^2)(sec), tube inside diameter ~8 mm, and L_T/D is as indicated. (Data not shown.)

ing that an entrance effect is important, although it certainly extends to large values of L_T/D. Tick marks are shown on the curves to show the transition point from single-phase to two-phase feed to the test section. These tick marks were added by the reviewer. A relatively large number of "instability branches" are shown in Fig. II-14, all arising from runs with single-phase feed.

The "stabilizing" of an otherwise unstable burnout is discussed in Ref. 11. This consists in orificing the test section between its inlet and the expander (Fig. II-11). The following is quoted from Ref. 11:

> ... The throttles between the expander and heated channel do not always exclude the undesired conditions as transition from type 1 to type 2 can be effected only if the pressure drop in the throttle separating the heated channel from the preceding section is rather substantial. Thus, for example, in runs ... at $P = 100$ atm and $W_g = 400$ kg/m^2 sec the pressure drop needed amounted to about 10 kg/cm^2 ...

A pressure drop through an inlet orifice of about 140 psi is considerably more than design practice would dictate in this country, and it is of interest to note that orifices with a resistance of about 30 psi were used in the Russian First Atomic Power Station for the boiling channels.[12]

> ... Successful working in the boiling regime made it possible towards the middle of 1957 to transfer more than half of the channels of the reactor (70), into the boiling regime.
>
> Beginning at that time, spent channels were replaced by channels with the resistance disk at the entrance end of the fuel element. The resistance of the disk was 2 atm at a flow 250 kg/hr. Lengthy operation of the majority of the channels in the boiling regime showed that no hydraulic pulsation or instability of flow would occur under these conditions.
>
> Working in the boiling regime gives typically a steam content at the exit end of the channels of 5-25 wt.% with thermal ratings of 0.6-1.3 × 10^6 kcal/m^2 hr with water flows along the channel of 0.7-1 m/hr at a pressure of 100 atm and a temperperature at the inlet end of 190°C.

The First Atomic Power Station is a pressure-tube graphite-moderated reactor.

In summary, the DNB-2 lines are of little use for design purposes. Some DNB-2 type burnouts are caused by instabilities within the test section, but it is difficult to apply these data to reactor design. Some DNB-2 type burnouts appear to be caused by a different burnout mechanism than DNB-1 type burnouts, but in any case little is known about the details of what happens within the test section. Possibly the best use of the DNB-2 line is as a signal to the experimenter that, if his data fall on DNB-2 curves, he may be generating ambiguous information, which will probably prove difficult for the designer to use with confidence.

Burnout in Nonuniformly Heated Channels

Much information is available on the burnout of channels of various shapes for an axially uniform power-generation rate, but axial uniformity is never encountered in actual nuclear reactors. Several reports have been written about burnout in connection with nonuniform axial power generation,[13–15] and this section will review those publications.

Work done at General Electric's Atomic Power Equipment Department (GEAP) utilized a heated rod in annular geometry. Test sections were fabricated to give both a cosine and truncated cosine distribution of heat flux. This was accomplished by a technique of axially varying the wall thickness of the tube, and the method was common to experiments done at the other laboratories. The relative heat generation in the cosine and truncated cosine rods is shown in Figs. II-15 and II-16. A number of thermocouples were spot welded to the inside diameter of the test section and served as temperature or

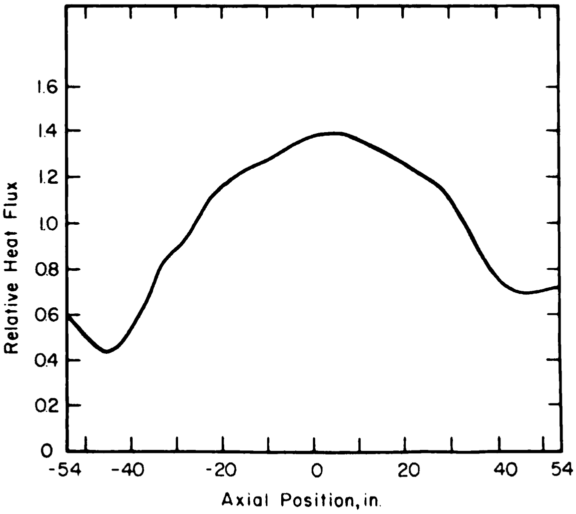

Fig. II-15 Relative heat-flux distribution—cosine rod No. 4.[13]

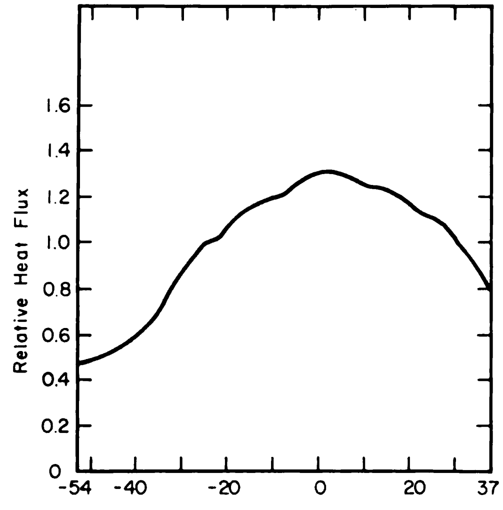

Fig. II-16 Relative heat-flux distribution—truncated cosine rod No. 20.[13]

voltage detection devices. Burnout was detected by a bridge that measured imbalance in the resistance of two adjacent segments of the heated rod and with the thermocouples. Details of the apparatus and other parameters of interest are shown in Table II-1.

Reference 13 gives the test-section average heat flux and exit quality at burnout-detector trip and the local heat flux and quality for those thermocouple positions at which a temperature rise was indicated.* The local data are plotted in Figs. II-17 to II-19, where they are compared with data for a similar test section heated uniformly. The data for the uniformly heated test section are from Ref. 16. In Ref. 13 the conclusion is that the nonuniformly heated rod data averaged 9 to 20% low compared to a correlation of the uniformly heated rod data given in Ref. 16. It was concluded[13]

> ... that the uniform rod burnout correlation can be used to predict burnout for cosine heat flux distribution. It is tacit in this conclusion that burnout depends only on local conditions of quality and flow ... The nonuniform rod data points averaged 9 to 20 percent low. The magnitude of this deviation is considered small, and of the same order as that for the uniform rod data upon which the correlation was originally based.

Figures II-20 and II-21 show the average heat flux at burnout plotted as a function of the exit quality at burnout. This particular method of showing nonuniform heat-flux burnout data is recommended in another reference and will be discussed later. Also plotted in Figs. II-20 and II-21 are the results of the uniformly heated test-section burnout runs. A difference is evident between the burnout data, for example Fig. II-17, from the uniformly and nonuniformly heated test sections. Whether this is due to the

Table II-1 CONDITIONS FOR GEAP BURNOUT TESTS[13]

Rod outside diameter, in.	0.540
Flow-tube inside diameter, in.	0.875
Hydraulic diameter, in.	0.335
Heated length, in.	
Cosine rod	108
Truncated cosine rod	91
Pressure, psia	1000
Flow rates, lb/(hr)(sq ft) × 10^{-6}	0.84 to 1.40
Exit quality range, %	12 to 35
Peak to average power generation (approx.)	
Cosine rod	1.4
Truncated cosine rod	1.3

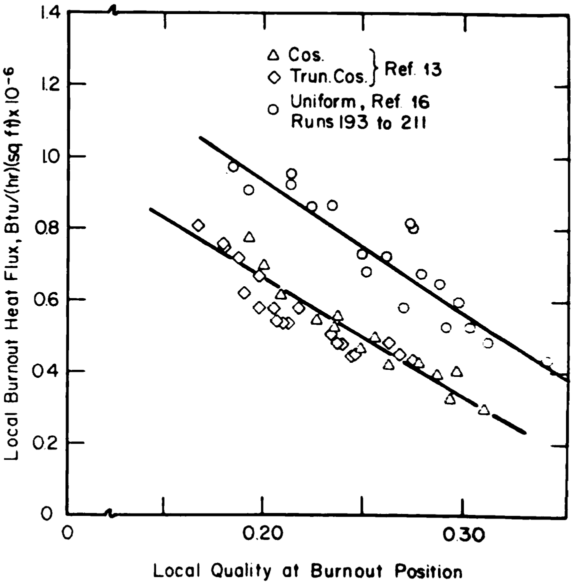

Fig. II-17 Comparison of uniformly and nonuniformly heated test-section burnout data. Pressure = 1000 psia and mass flow = 0.84 × 10^6 lb/(hr)(sq ft).

---

*The thermocouples were positioned at finite locations along the heated length of the test section, and there would seem to be no guarantee that burnout would take place at a position immediately adjacent to a thermocouple. This source of error is not discussed in the reference. Possibly it is a minor one, because in many runs wall-temperature increases were observed by several thermocouples simultaneously.

nonuniform shape of the heat-generation rate is not necessarily obvious, for other variables may be involved. An indication of another variable is given by the series of cosine rod-burnout data, starting with run 16 and terminating with run 23; these runs are shown in Figs. II-19 and II-21. Runs 16 to 20 utilized heated rod No. 59, which was destroyed during run 20 by a burnout. Rod No. 42 was then employed for runs 21 to 23, which were close duplicates of the mass flow, inlet subcooling, and pressure of runs 17, 18, and 16, respectively. These duplicate runs are marked on Fig. II-19 with dashed connecting curves, and it can be seen that runs 21 to 23 produced slightly different results than runs 16 to 18. This is particularly evident in Fig. II-21. Test section 59 had been used for at least 15

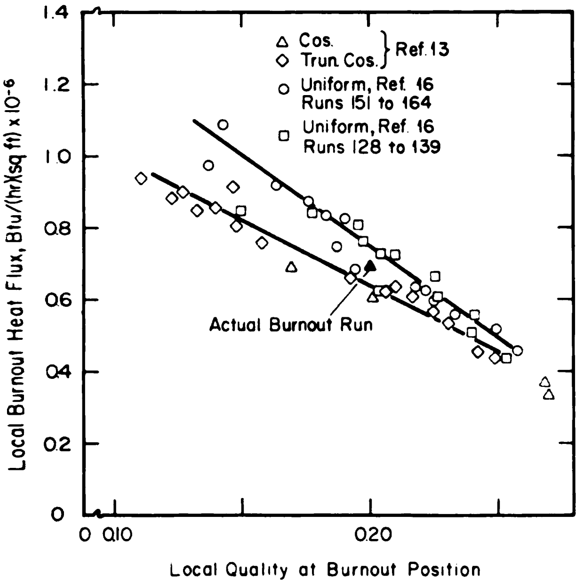

Fig. II-18 Comparison of uniformly and nonuniformly heated test-section burnout data. Pressure = 1000 psia and mass flow = 1.1×10^6 lb/(hr)(sq ft).

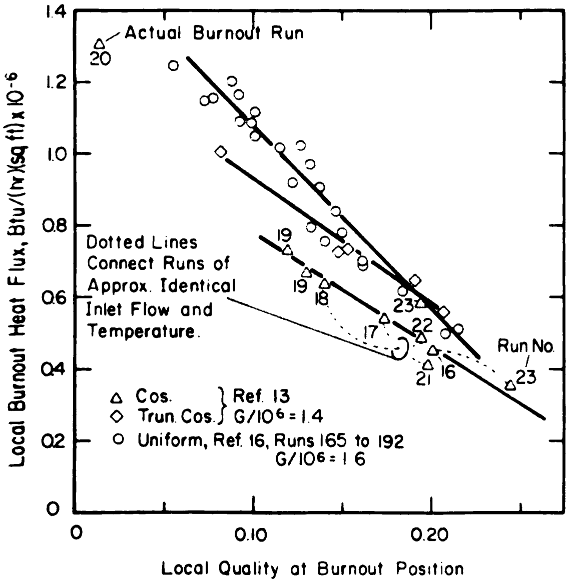

Fig. II-19 Comparison of uniformly and nonuniformly heated test-section burnout data. Pressure = 1000 psia and mass flow is as indicated.

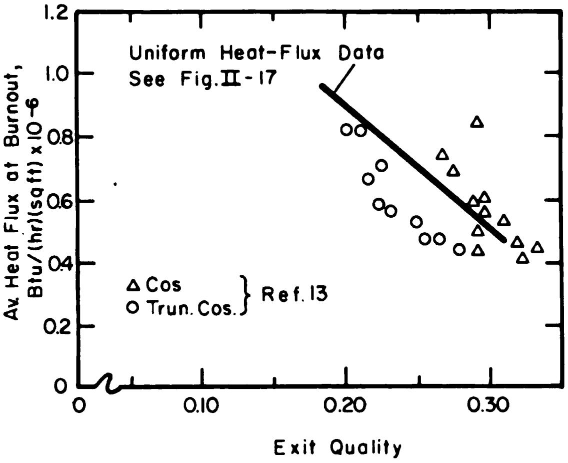

Fig. II-20 Comparison of uniformly and nonuniformly heated test-section burnout data. Pressure = 1000 psia and mass flow = 0.84×10^6 lb/(hr)(sq ft).

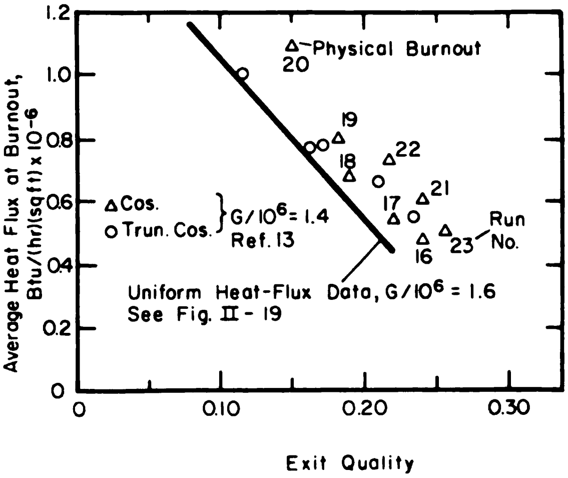

Fig. II-21 Comparison of uniformly and nonuniformly heated test-section burnout data. Pressure = 1000 psia and mass flow is as indicated.

runs prior to run 16; thus there may have been some "aging" effect, as reported by Zenkevich et al.[17] A further difference was that test section 59 was fabricated of type 347 stainless steel, whereas test section 42 was fabricated of Incoloy.

The reference concludes with a discussion of a prediction of the power level and position of burnout for a nonuniformly heated rod. It is assumed that the burnout heat flux is a linear function of quality, e.g.,

$$\phi_{BO} = A - Bx \qquad (3)$$

where ϕ_{BO} is the burnout heat flux, x is the quality, and A and B are constants. If $f(y)$ is the relative heat flux along the length, y, of the tube, then the burnout location is given by the following relation:

$$\left[\frac{d\ \ln f(y)}{dy}\right]_{y=y_1} = -\frac{B\pi D_1}{\dot{W}h_{fg}} \qquad (4)$$

where y_1 = location of position of burnout
D_1 = diameter of heated tube
h_{fg} = vaporization enthalpy
$\dot{W}$ = flow rate, lb/unit time

After the position of burnout is obtained, the test-section average power at burnout can be determined:

$$\bar{\phi}_{BO} = \frac{1}{f(y)_{y=y_1}}\left[\frac{A + B\dfrac{\Delta h_s}{h_{fg}}}{\dfrac{B\pi D_1}{\dot{W}\,h_{fg}}\;\dfrac{\int_{y_0}^{y_1} f(y)\,dy}{f(y)_{y=y_1}}}\right] \qquad (5)$$

where y_0 is the value of y at the entrance to heated portion of the test section, and Δh_s is the inlet subcooling in British thermal units per pound. The predicted average burnout heat flux for the several runs reported in Ref. 13 was determined from Eq. 5 and compared with the experimental data, and the agreement was within +11 to −2.5%. Unfortunately the authors of the reference do not give the values of A and B used in their calculations.

The experiments performed at The Babcock & Wilcox Co. (B&W) are reported in Ref. 14. These were done with uniformly and nonuniformly heated tubes having an inside diameter of 0.41 to 0.45 in. and a heated length of 72 in. The pressure was 2000 psia, and the various nonuniform axial power-generation profiles used are shown in Fig. II-22. The test sections were fabricated from type 304 stainless steel, and a number of thermocouples were fastened to the exterior of the test section for detection of burnout by means of temperature fluctuations or ex-

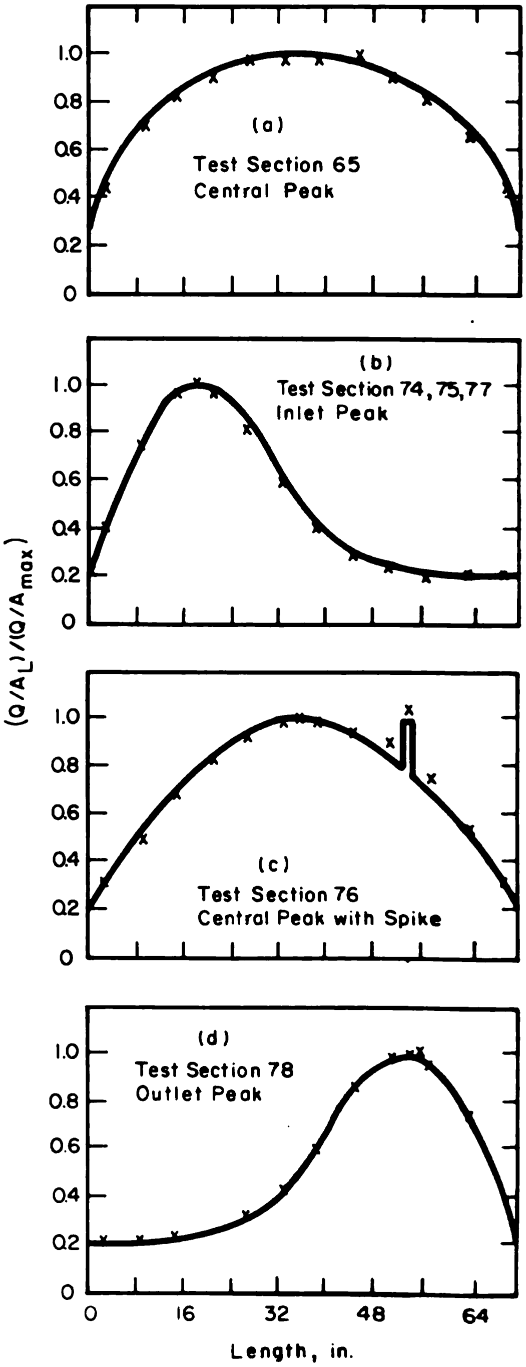

Fig. II-22 Axial power profiles of various test sections used to take data appearing in Ref. 14. Crosses on figures indicate test results.

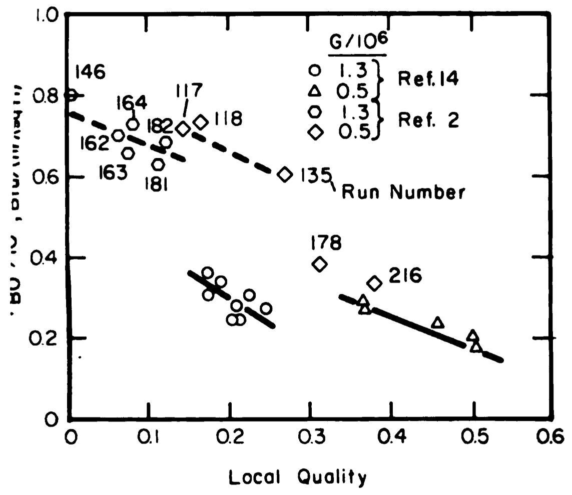

ig. II-23 Comparison of burnout data from Ref. 14 ıd Table 10 of Ref. 2. Pressure = 2000 psia. Test-ection dimensions are as follows:

Ref.	Inside diameter, in.	Length, in. (heated)
14	~0.41	72
2	0.306	23.25

ursions. Runs were accomplished at mass flows f 0.5, 0.7, 1.0, and 1.3 × 10^6 lb/(hr)(sq ft) and arying inlet subcooling.

Data taken with the uniformly heated* test ection are shown in Fig. II-23 for mass flow f 0.5 and 1.3 × 10^6 lb/(hr)(sq ft). Also plotted n Fig. II-23 are data from Table 10 of Ref. 2.

It is evident that the Table 10 data plotted in ig. II-23 lie above the Ref. 14 data. This could e explained by the fact that the test section sed to take the Table 10 data had a length of bout 24 in., whereas the test section used to ıke the Ref. 14 data had a length of about 72 in. he effect of length is an important one and was iscussed in Sec. III of *Power Reactor Tech-ology*, 7(3). However, on an SEF plot, runs 178 nd 216 are on a DNB-2 line (Fig. II-2), and it ; possible that the B&W data shown in Fig. -23 also would plot on DNB-2 lines. The NB-2 lines are best obtained by plotting con-tant inlet-temperature data. Unfortunately most f the B&W experiments were not done at constant inlet temperature, and only a few runs can be exhibited on an SEF plot. These will be presented later.

The data are presented[14] in terms of burnout heat flux vs. quality plots. Part *a* of Fig. II-24 shows local heat flux vs. local quality, and part

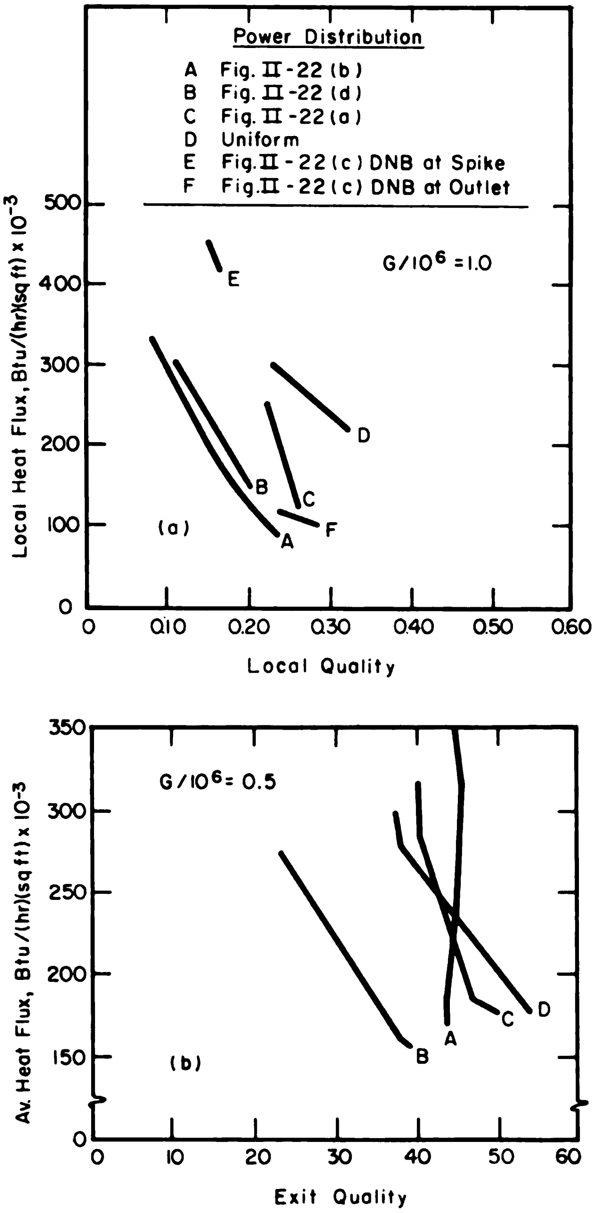

Fig. II-24 Comparison of effects of axial heat-flux distribution and burnout heat flux vs. quality.[14] Pressure = 2000 psia and mass flow is as indicated. The average heat flux plotted on the ordinate of (*b*) is defined as

$$\text{Average heat flux} \equiv \frac{1}{L_T}\int_0^{L_T} \phi(x)\,dx$$

---

* The uniformly heated test sections burned out 1 to in. upstream of their ends; the use of local quality ır the uniformly heated test sections introduces neg-gible differences compared to the use of exit quality.

b of Fig. II-24 shows average heat flux vs. exit quality. The authors conclude that:

> 2 For a given enthalpy at the point of DNB, the nonuniform heat-flux distributions have lower allowable local heat flux than does the uniformly heated tube. However, on very small areas of the heat-transfer surface (heat-flux spikes smaller than 1 sq in.), it appears possible to approach or even exceed the heat flux that would normally result in DNB with uniform heated flux.
>
> 3 For a given enthalpy at the outlet of the channel:
>
> (a) The outlet peak flux distribution has the lowest channel power at DNB for all mass velocities tested.
>
> (b) At the lower mass velocities, higher channel power is permissible with inlet peak and central peak flux distributions than with uniform distribution.
>
> (c) At higher mass velocities the channel power at DNB for inlet peak, central peak, and uniform flux distribution has nearly the same value.

A comparison of the 1000-psia data just cited and the 2000-psia data under discussion is impressive. The test sections used in the APED and B&W work have about the same length and hydraulic diameter. Comparison of Fig. II-18 and part *a* of Fig. II-24, however, shows that the 2000-psia operation results in a much greater difference between the uniformly and nonuniformly heated test-section data than does the 1000-psia operation. Also, the values of ϕ_{BO} shown in part *a* of Fig. II-24 are quite low. The B&W test loop was conceptually similar to the one shown in Fig. II-11. Steam from a boiler could be mixed with water to provide the desired inlet temperature. The experiments described in Ref. 14 were all done with subcooled water at the test-section inlet, but the reference does not state whether this was achieved by mixing steam with relatively cooler water or by merely using the boiler to produce hot water for feed to the test section. If the boiler were used to generate steam, possibly the same instabilities that led to the low values of ϕ_{BO} shown in Fig. II-12 were also present in the B&W runs.

SEF plots were made for some of the data in Ref. 14 at subcoolings of about 12 to 60°F. These plots are shown in Figs. II-25 and II-26; only runs that burned out with L_{BO} greater than 66 in. are plotted in these figures. Because the SEF plot is intimately tied into the heat-balance equation, the ordinate of Fig. II-25 is $(q/A)_{av.}$, defined as follows:

$$(q/A)_{av.} = \frac{1}{L_{BO}} \int_0^{L_{BO}} (q/A)\, dx$$ (6

where q/A = axially dependent heat flux, Btu (hr)(sq ft)
x = distance along heated channel, ft
L_{BO} = value of x at burnout, ft

The inlet-peak section exhibited many upstream burnouts about 33 in. downstream from the point of start of heating. These data are presented in Figs. II-27 and II-28. Also included in Fig. II-27 are the two runs for the central-peak-with-spike test section wherein burnout occurred at the position of the spike (L = 54 in.), and the curve shown in Fig. II-27 was arbitrarily drawn through these two points.

In considering Figs. II-27 and II-28, the reviewer was impressed not so much by the difference in heat flux at which the uniformly and nonuniformly heated test sections exhibited burnout (for given inlet conditions), but rather by the difference in local qualities at burnout. Figure II-25 illustrates that at an inlet subcooling of about 10°F the data group into a DNB-2 curve; variation of mass flow moves the SEF at burnout over a rather wide range for the uniformly heated tube, but the tube with the outlet peak exhibits burnout at roughly a constant value of SEF, namely, ~0.9 × 10^6 Btu/(hr)(sq ft). When subcooling is increased to about 60°F

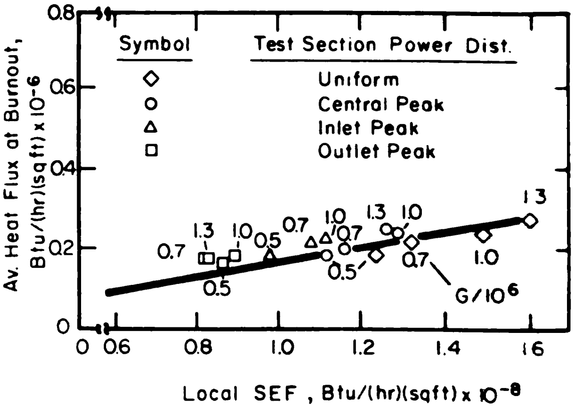

Fig. II-25 Steam-energy flow plot of data from Re 14. Pressure = 2000 psia, inlet subcooling = ~12°F, and mass flow is as indicated. The average heat flu plotted on ordinate is defined as

$$\text{Average heat flux} \equiv \frac{1}{L_{BO}} \int_0^{L_{BO}} \phi(x)\, dx$$

Runs shown were terminated by burnout at $L_{BO} \geq 69$ in.

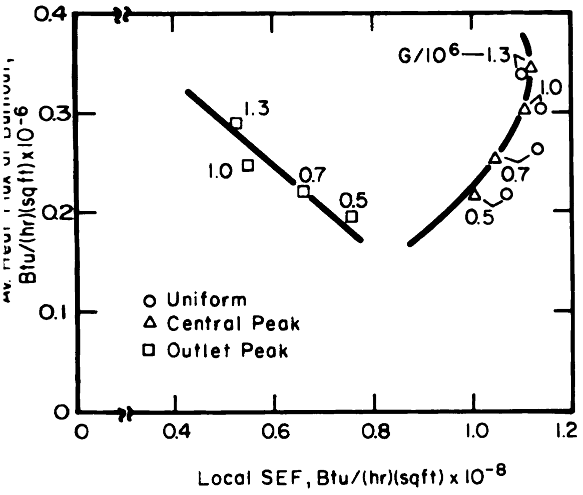

Fig. II-26 Steam-energy flow plot of data of Ref. 14. Pressure = 2000 psia, mass flow is as indicated, inlet subcooling = 60°F (approximately), L_{BO} = 66 to 69 in., and the average heat flux at burnout is defined as in Fig. II-25.

Fig. II-26), the uniformly heated test section and the test section with the central peak exhibit burnout at almost identical values of $\phi_{BO_{ab.}}$ and SEF_{local}. Only when the power distribution is peaked toward the outlet does the character of the burnout curve change, and then it takes a characteristic DNB-1 shape.

Reference 15, which contains nonuniformly heated test-section data, is a companion to Ref. 3. A total of four nonuniformly heated test sections were utilized with an axial heat-generation rate given by Eq. 7.

$$\phi = \phi_{\max} \cos \frac{\pi x}{L_T} \qquad (7)$$

where $\phi_{\max}$ is the heat flux at the center of the test section in British thermal units per hour per square foot, x is the length along the test section measured from the center in feet, and L_T is the extrapolated length in feet. Two of the test sections, Mark I and II, had the wall-thickness variations accomplished by a series of "steps," each 4 in. long, machined on the outside. Test sections III and IIIa were machined to give a smooth variation in wall thickness rather than a series of steps. One inside diameter was 0.383 in.; other pertinent data are given in Table II-2.

Burnout was detected by a bridge type detector with one lead each connected to the center and exit of the tube and with the third lead positioned to give approximately equal resistances in each arm of the bridge. Several runs were made with thermocouples to detect temperature increases:

> . . . these showed that within ¼ of a second a temperature excursion could be taking place over several zones of the tube and, within this time scale, not starting at one unique point and spreading along the tube. The series of tests on the Mk I tube was concluded by isolating the detector and allowing the tube to overheat sufficiently to rupture the tube: this confirmed that the power previously indicated

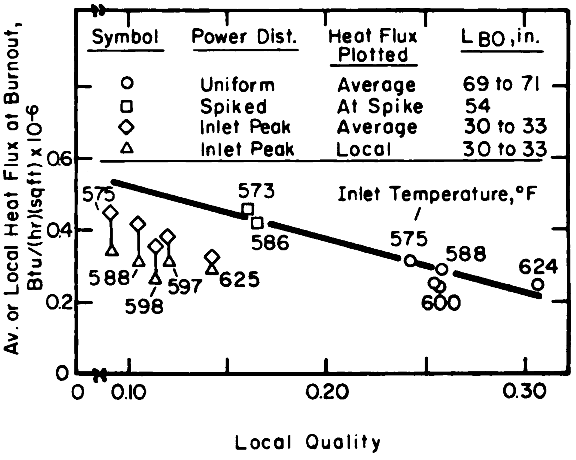

Fig. II-27 Burnout heat flux vs. quality; Ref. 14 data. Pressure = 2000 psia, inlet temperature is as indicated, and mass flow = 1 × 10^6 lb/(hr)(sq ft).

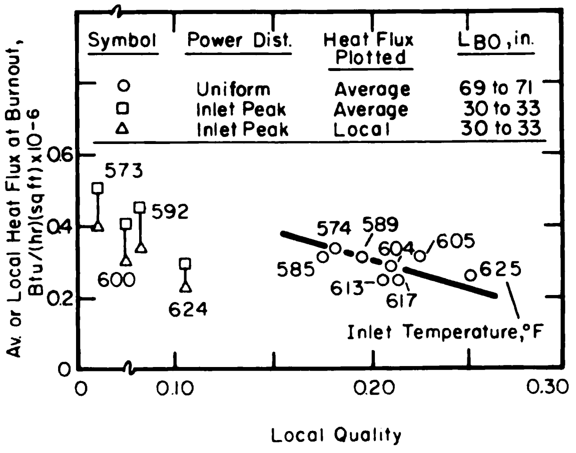

Fig. II-28 Burnout heat flux vs. local quality; Ref. 14 data. Pressure = 2000 psia, inlet temperature is as indicated, mass flow = 1.3 × 10^6 lb/(hr)(sq ft), and the average heat flux at burnout is defined as in Fig. II-25.

at trip-off would have resulted in a substantial rise of temperature.

Runs were made at 560, 1000, and 1600 psia, with mass velocities from 0.75 to 3.0×10^6 lb/(hr)(sq ft) and inlet subcoolings from 0 to 250 Btu/lb. Data presented in tabular form include the burnout power, mean exit quality, and axial zone wherein burnout occurred, as well as inlet pressure, mass velocity, and inlet subcooling.

A number of methods are considered to correlate the nonuniform flux data with uniform flux data. Three sources of uniform flux burnout data are considered: data in Ref. 3, calculated values of ϕ_{BO} using Barnett's equation,[19] and calculated values using the round-tube best-fit equation of Ref. 2. Barnett's correlation* is as follows, using the nomenclature of Ref. 3:

$$\phi = \frac{A + \left(\frac{DGC}{4}\,\Delta H_i\right)}{1 + CL}$$

$$= A - \left(\frac{DGC}{4}\,h_{fg}\right)\frac{x}{100}$$

where $A = \alpha D^a G^b$ and $C = \beta D^c G^d$. Here α, β, a, b, c, and d are dependent on pressure as follows:

	560 psia	1000 psia	1600 psia
α	1.507	0.994	0.790
a	−0.724	−0.555	−0.42
b	−0.419	−0.161	0.079
β	0.0144	0.00841	0.0101
c	−1.471	−0.430	−1.606
d	−0.819	−0.490	0.0715
No. of experiments	135	317	97
Rms, % error	4.76	5.36	2.26
Max. errors, %	+17, −16	+24, −17	+6, −7

With these sources of uniformly heated test-section burnout data, three recipes were tried to see how closely each would duplicate the nonuniform burnout data:[15]

> ### Methods A, B and C (Overall Length Concept)
>
> The basis of these three methods is to use the overall channel length of the cosine flux tube as the length of the uniform flux tube: using uniform flux data, *a*, *b* and *c* above, comparison being then made of the burnout power or average flux over the whole channel length in each case, regardless of the position of burnout. This method has been suggested by others to give fair agreement for tubes at 2000 p.s.i.(7)[†] and 1000 p.s.i.(8). Comparison of cosine flux and uniform flux data (9, 10) for an annular section at 1000 p.s.i. confirms this hypothesis. It is appreciated that this is somewhat empirical since no account is taken of the location of burnout. These methods are subsequently referred to as the "overall length concept".
>
> ### Methods D, E and F (Local Length Concept)
>
> These three methods consider the possibility of burnout at a series of stations along the cosine flux tube: at each point considered, the distance, l, from the inlet is used as the length of tube with uniform flux, which from data *a*, *b*, or *c* above, and the same inlet condition, gives the predicted burnout flux at that point. By varying the distance l, the burnout line *AB* ... is plotted and the particular value of l, at which burnout takes place is where the cosine flux profile is tangential to the line *AB*. In evaluating the tests, the point at the end of each zone is considered. These methods are subsequently referred to as the "local length concept".
>
> ### Methods G and H (Equivalent Length Concept)
>
> These two methods are similar to D, E, and F in that they enable the burnout line *AB* to be plotted and hence the predicted burnout flux to be determined. In place of the actual distance of any point from inlet, however, an associated "equivalent length, L_e", is considered, defined as follows:-
>
> $$L_e = \frac{1}{\phi_1}\int_0^1 \phi \, dl$$
>
> where ϕ_1 = local value of flux on the cosine profile distance l from inlet.

---

*For a pressure of 1000 psia and a tube inside diameter of 0.18 in., Barnett's correlation can be shown to have the following form:

Mass flow, lb/(hr)(sq ft) $\times 10^{-6}$	Correlation
1.0	$\phi_{BO} = 2.58 \times 10^6 - 0.0044$ SEF
4.0	$\phi_{BO} = 2.06 \times 10^6 - 0.0022$ SEF

These correlations can be compared with the ones shown in Table III-6 and III-7, *Power Reactor Technology*, 7(3).

[†] Numbers in parentheses refer to references in the original article.

he recommended method of predicting the iagnitude of ϕ_{BO} and the location of burnout is uoted as follows:[15]

> If the requirement is for the prediction of burnout power regardless of the accuracy of predicting its location along the channel, then the local length concept using Barnett's equation for uniform flux data is recommended.
>
> If, however, accuracy of predicting the location of burnout has to be considered, as might well be the case when the channel length differs from available test data, then the recommendation is to use the equivalent length concept with Barnett's equation for uniform flux data. This, in general, gives a predicted burnout power higher than the local length concept and an allowance—say a reduction of 10% in the predicted power should then be made.
>
> For an approximate estimate, however, the burnout power can be predicted by considering the power on a uniform flux tube of same overall length and diameter. The experimental burnout power was then found to be predicted well at 560 p.s.i., to be 10-15% lower than the predicted power at 1000 p.s.i. and 0-10% higher at 1600 p.s.i.

Figure II-29 illustrates Lee-Obertelli uniormly and nonuniformly heated burnout data or nearly identical test sections. The average est-section heat flux at burnout is plotted gainst the steam-energy flow calculated using he exit quality at burnout. Although only a relaively small sample of the Lee-Obertelli data s shown in Fig. II-28, it is interesting to note hat Ref. 15 contains DNB-2 type burnout data. few runs in Fig. II-29 are plotted from Table 0 of Ref. 2, and it is evident that the Table 10 lata plot above the Lee-Obertelli data (similar o the behavior shown in Fig. II-23). This is robably a length effect because the 1000-psia lata shown in Fig. II-29 were taken in a test section having a length of 76 in. and an inside liameter of 0.540 in. These data from the 76-in. est section are from Ref. 19 and are plotted in Fig. III-12, *Power Reactor Technology*, 7(3). The Ref. 19 data in Fig. II-29 fall somewhat under the Mark I test-section data, but this is probably the effect of a slightly bigger inside diameter.

Discussion and Conclusions

The most direct way to treat nonuniformly heated test sections is possibly by Methods A, B, and C of Lee and Obertelli. This is based on treating the nonuniformly heated test section as one operating at the average heat flux and neglects the position of burnout. The results of this method are illustrated in Figs. II-20, II-21, part *b* of II-24, and II-29. With the exception of the data for the outlet-peak distribution in part *b* of Fig. II-24, this method is not as much in error as might be expected. Several of the inlet-peak and central-peak runs fell below the uniformly heated test-section results (part *b* of Fig. II-24), although the shape of curve *A* in that figure suggests rather peculiar behavior in any event.

The other somewhat obvious method of treating nonuniformly heated test sections is that of considering only local conditions—quality, mass flow, and heat flux. Figures II-17 to II-19 substantiate that this is not a bad approximation, although at lower mass flows (Fig. II-17) the data derived from the nonuniformly heated test section diverge significantly from data from uniformly heated test sections. Local conditions at burnout are not listed in Ref. 15, although the Lee-Obertelli Methods D, E, and F appear to be based on this concept and are recommended by them. Those runs (listed in Ref. 14) exhibiting burnout near the end of the test section are illustrated in Figs. II-25 and II-26. Although there are differences between the uniformly and nonuniformly heated test-section data, these are most noticeable with the outlet-peak test section (Fig. II-26). Figures II-27 and II-28 il-

Table II-2 DESIGN DATA ON TEST SECTIONS USED IN REF. 15

Designation	Flux profile	Ratio of maximum to average flux	Ratio of maximum to minimum flux	Heated length, in.	Extrapolated length, in.
Mark I	Stepped	1.25	2.4	72	100
Mark II	Stepped	1.43	8.0	72	78.8
Mark III	Smooth	1.45	9.7	72	76.8
Mark III*a*	Smooth	*	*	60	76.8

*The Mark III*a* tube was the Mark III tube with no power applied to the last foot of the tube.

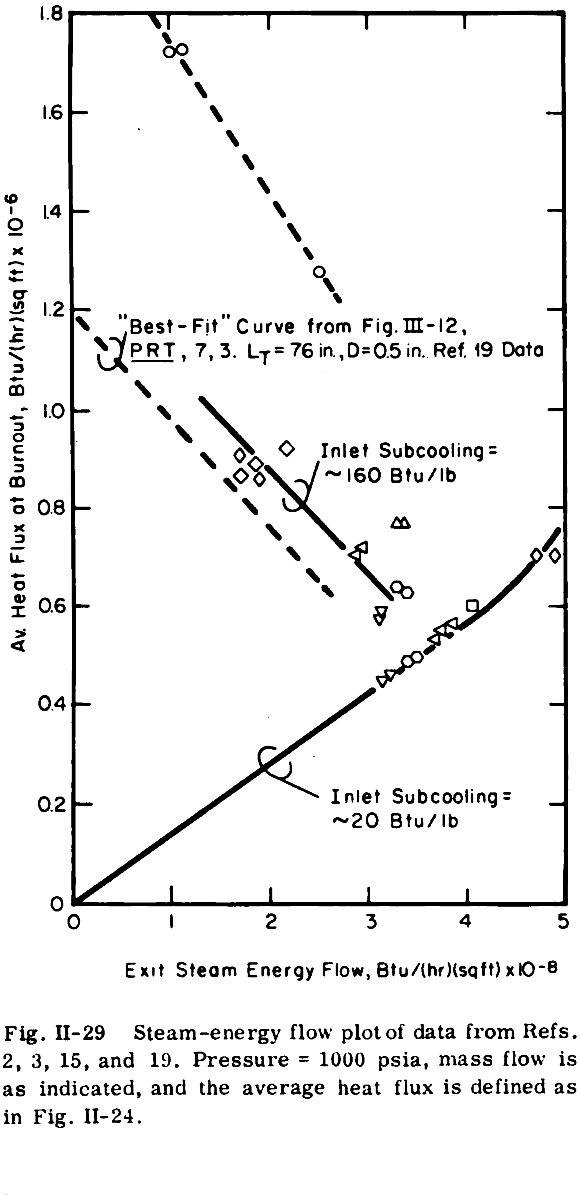

Fig. II-29 Steam-energy flow plot of data from Refs. 2, 3, 15, and 19. Pressure = 1000 psia, mass flow is as indicated, and the average heat flux is defined as in Fig. II-24.

lustrate the burnout data for those nonuniformly heated test sections exhibiting burnout well upstream of the exit. It is difficult to compare these upstream burnout data with uniformly heated test-section data because a substantial extrapolation of the uniformly heated data given in Ref. 14 is necessary. Burnout data from other sources for long, cylindrical test sections at 2000 psia were not readily available to the reviewer, although they may exist.

When the preceding data are considered, it appears that the designer is forced to a rather large degree of conservatism in trying to assess the effect of nonaxial power distributions in a reactor. Some of the uncertainty may be inevitable, but the situation might be helped by experiments designed to study the DNB-2 region in detail.

References

1. W. J. Levedahl, Application of Steam Energy Flow to Reactor Design, *Trans. Am. Nucl. Soc.*, 5(1): 149-150 (June 1962).
2. R. A. DeBortoli, S. J. Green, B. W. LeTourneau, M. Troy, and A. Weiss, Forced-Convection Heat Transfer Burnout Studies for Water in Rectangular Channels and Round Tubes at Pressures Above 500 psia, USAEC Report WAPD-188, Westinghouse Electric Corp., Bettis Plant, October 1958.
3. D. H. Lee and J. D. Obertelli, An Experimental Investigation of Forced Convection Burnout in High Pressure Water. Part I. Round Tubes with Uniform Flux Distribution, British Report AEEW-R-213, August 1963.
4. A Research Program in Two-Phase Flow, CISE (Centro Informazioni Studi Esperienze), Segrate (Milano), Italy, Jan. 31, 1963.
5. J. G. Collier, Heat Transfer and Fluid Dynamic Research as Applied to Fog Cooled Power Reactors, Canadian Report AECL-1631 (CRARE-1108), June 1962.
6. E. R. Quandt, Analysis and Measurement of Flow Oscillations, in *Heat Transfer—Buffalo, Chem. Eng. Prog. Symp. Ser.*, 57(32): 111 (1961).
7. M. Troy, Upflow Burnout Data for Water at 2000 psia in 0.097 in. × 1 in. × 27 in. Long Rectangular Channels, USAEC Report WAPD-TH-340, Westinghouse Electric Corp., Bettis Plant, July 1957.
8. H. S. Jacket, J. D. Roarty, and J. E. Zerbe, Investigation of Burnout Heat Flux in Rectangular Channels at 2000 psia, USAEC Report WAPD-AIW(IM)-3, Westinghouse Electric Corp., Bettis Plant, Dec. 5, 1955.
9. M. Troy, Upflow Burnout Data for Water in Rectangular Channels at Pressures from 600 to 1570 psia, USAEC Report WAPD-TH-321, Westinghouse Electric Corp., Atomic Power Division, September 1957.
10. M. A. Styrikovich et al., Effect of Upstream Elements on Critical Boiling in a Vapor Generating Pipe, USAEC Translation AEC-tr-474 [*Teploenerg.*, 7(5): 81-87 (1960)].
11. I. T. Aladyev, Z. L. Miropolsky, V. E. Doroshchuk, and M. A. Styrikovich, Boiling Crisis in Tubes, in *International Developments in Heat Transfer*, Part II, pp. 237-243, American Society of Mechanical Engineers, 1961.
12. Yu. V. Evdokimov, V. Ya. Kozlov, V. G. Konochkin, L. A. Kocheltkov, A. K. Krasin, V. V. Litkin, V. S. Severyanov, B. A. Semenov, and G. N. Ushakov, Experience in the Operation of the First Atomic Power Station, *J. Nucl. Energy: Pts. A & B*, 18(3): 148-155 (March 1964).

13. E. Janssen and J. A. Kervinen, Burnout Conditions for Nonuniformly Heated Rod in Annular Geometry, Water at 1000 psia, USAEC Report GEAP-3755, General Electric Company, Atomic Power Equipment Department, June 1963.
14. H. S. Swenson, J. R. Carver, and C. R. Kakarala, The Influence of Axial Heat-Flux Distribution on the Departure from Nucleate Boiling in a Water-Cooled Tube, ASME Paper 62-WA-297, Nov. 25, 1962.
15. D. H. Lee and J. D. Obertelli, An Experimental Investigation of Forced Convection Burnout in High Pressure Water. Part II. Preliminary Results for Round Tubes with Non-uniform Axial Heat Flux Distribution, British Report AEEW-R-309, November 1963.
16. E. Janssen and J. A. Kervinen, Burnout Conditions for Single Rod in Annular Geometry, Water at 600 to 1400 psia, USAEC Report GEAP-3899, General Electric Company, Atomic Power Equipment Department, February 1963.
17. Letter to the Editors: Critical Heat Fluxes for a Bundle of Tubes Cooled in Pressurized Water, *J. Nucl. Energy: Pt. B*, 1(3): 197 (March 1960).
18. P. G. Barnett, An Investigation into the Validity of Certain Hypotheses Implied by Various Burnout Correlations, British Report AEEW-R-214, June 1963.
19. R. R. Hood and L. Isakoff (Comps.), Heavy Water Moderated Power Reactors Progress Report, May–June 1963, USAEC Report DP-855, E. I. du Pont de Nemours & Co., Inc., August 1962.

Section III

Fuel Elements

Power Reactor Technology

Stainless-Steel-Cladding Failures in VBWR

The fuel elements under irradiation in the Vallecitos Boiling-Water Reactor (VBWR) as part of the AEC-sponsored Fuel-Cycle Program were described in *Power Reactor Technology*, 7(1) (see Table IV-1, page 28, of that issue and the accompanying description). These fuel elements comprised 50 assemblies, each made up of 16 metal-jacketed rods containing pressed and sintered UO_2 pellets of 0.376-in. diameter. The jackets were all designed to be freestanding. Twenty-four of the assemblies employed Zircaloy jackets 22 mils thick, and the remainder employed 20-mil annealed 304 stainless steel (10 assemblies) or 15-mil cold-worked 304 stainless steel (16 assemblies). A recent paper[1] describes the condition of these elements at the end of operation of the VBWR in December 1963, after the irradiation program had run for three years. The findings are summarized in Table III-1.

The two failures listed in Table III-1 for Zircaloy-jacketed rods appeared to be incidental; one was attributed to fretting wear and the other to some unknown cause. The larger number of failures of steel-jacketed rods, on the other hand, apparently resulted from some specific failure process. A performance limit apparently existed[1] for the 304-stainless-steel-jacketed rods at an exposure level of about 2.6×10^{20} fissions/cm^3. According to Ref. 1, cracking of the jackets caused the failures, which consistently occurred in the peak flux zone. Typically, the cold-worked material cracked longitudinally, whereas the annealed material cracked mostly in the circumferential direction and usually at pellet interfaces.

In Ref. 2 the failures are characterized as intergranular corrosion. The authors state that the characteristic failure is not limited to the elements tested under the Fuel-Cycle Program, but has been observed in essentially all the types of stainless-steel-clad elements irradiated in the VBWR. The cause of the cracking has not yet been determined, but evaluation of the data thus far indicates[2] that it results from a stress-assisted corrosion attack of the grain boundaries and that the mechanism becomes operative only after a long time in the reactor environment. The latter observation suggests that either a long crack-nucleation stage is involved or a material change takes place as a result of radiation damage or coolant environment which eventually makes the material sensitive to cracking. The occurrence of both circumferential ridging and cracking at the pellet interfaces of annealed cladding points to a relation between localized high stresses and strains and susceptibility to cracking. It is also stated in Ref. 2 that this is similar to cracking experienced in a pressurized-water-reactor environment, in which intergranular cracking occurred in unsensitized type 304 stainless steel that had been stressed beyond the yield point.*

Whether or not the cracking phenomenon is understood completely, a question of great practical importance is the extent to which the experience in VBWR is typical. Steel-jacketed elements are performing satisfactorily in the Yankee reactor, in which jackets of type 348 stainless steel are used. Thus we can ask whether the difference in behavior of the steel jackets results from typical differences between the boiling-water and the pressurized-water environments, whether it results from inci-

---

*Reference 2 cites the following report: T. J Pashos, Experience with Stainless Steel as a Fuel Clad Material in Water-Cooled Power Reactors, Report APED-4260, September 1963.

Table III-1 FUEL-ELEMENT FAILURES OBSERVED IN VBWR UNDER THE FUEL-CYCLE PROGRAM[5]

Cladding material	Type designation	Cladding thickness, cm	No. of rods irradiated	No. of failures detected		Type of failure	Probable cause of failure	Average exposure, fissions/cm^3 × 10^{-20} (Mwd/ton)		
				Assembly sipping*	Rods visual			Failed assembly	Lead assembly	Group average
Zircaloy-2	J	0.0588	381	1	1	Small hole	Fretting wear	2.41 (8358)	2.78 (9643)	1.8 (6250)
Zircaloy-4	J	0.0588	5	1	1	Small hole	Unknown	1.66 (5774)	Same	Same
Type 304 S.S., cold worked (75,000 psi yield strength at room temperature)	I	0.0381	252	1	1	Longitudinal crack 18 cm long	Intergranular corrosion	2.38 (8252)	2.65 (9193)	1.92 (6780)
				1	1	Longitudinal crack 1 cm long		2.03 (7044)		
				1	†	Unknown		2.65 (9193)		
				1	†	Unknown		2.32 (9042)		
Type 304 S.S., annealed (40,000 psi yield strength at room temperature)	H	0.0507	160	1	1	Circumferential cracks	Intergranular corrosion	2.24 (7770)	2.48 (8599)	2.13 (7400)
				1	1	Circumferential cracks		2.48 (8599)		
				1	2	Circumferential cracks		2.44 (8485)		

*Coolant water surrounding the fuel rods in an assembly is trapped and a sample withdrawn. The sample is analyzed for fission-product iodine and compared to results obtained from a nondefective assembly sampled in a similar manner. A higher concentration of radioactive iodine is interpreted as being indicative of a failure in the fuel-rod cladding.

†Inspection not yet performed.

dental differences in fuel-element design or operating conditions (such as the heat-flux level), or whether it is representative of the difference between types 304 and 348 stainless steels. The VBWR experience focuses interest on the fuel performance of the boiling reactors that do utilize steel-jacketed elements, notably Humboldt Bay, Big Rock Point, and Elk River. The first two reactors use type 304 stainless steel, whereas the Elk River reactor uses type 304 with an admixture of 600 ppm of boron as burnable poison.

Fission-Product Helium

As reported in a Westinghouse paper[3] presented at the June meeting of the American Nuclear Society, helium is in some cases one of the major gaseous constituents within the void spaces of irradiated oxide fuel rods. The gas has been found in fuel elements that have had no opportunity to acquire helium as part of the fabrication process. In some irradiated elements that have operated with UO_2 center temperatures below that at which equiaxed grain growth occurs (1500 to 1700°C), the helium has been found to be more abundant than the fission-product gases xenon and krypton in the void spaces. In these low-temperature cases, the fractional release of xenon and krypton from the UO_2 was less than 0.5%.

The primary source of helium is the ternary fission of ^{235}U, thus giving an alpha particle plus two larger fission fragments. The helium resulting from such ternary fissions has a reported[4] fission yield of about 0.3%, whereas the fission yield of xenon plus krypton ranges from 25 to 30%. The high fractional content of helium in the free gases within the elements is explained as the result of a high diffusivity of the helium in UO_2. As stated in Ref. 3, the observed fractional release of helium from UO_2 during irradiation of various experimental fuel rods ranges from about 10 to almost 100%, but no clear-cut correlation has been found between the fractional release and UO_2 temperature or burnup level. To account for the concentration of helium relative to xenon and krypton in fuel elements operating at low temperature (less than 1500°C center temperature), the rate of diffusion of helium in UO_2 must be about 100 times greater than that of xenon and krypton. The helium phenomenon is thought to be significant as a contribution to the internal pressure within fuel-element jackets, and possibly, in some cases, as a contribution to the thermal conductivity of the gases in the pellet-jacket gap.

Steel-Lined Zircaloy-2-Clad Fuel Elements

The extensive fuel-element development programs at General Electric's Atomic Power Equipment Department (APED) were reviewed in Sec. IV of *Power Reactor Technology*, 7(1). One of the elements fabricated for irradiation in the VBWR under the Fuel-Cycle Program incorporated fuel rods clad with stainless-steel-lined Zircaloy-2. Reference 5 details the techniques used for fabrication of these rods.

Reasons for development of the lined Zircaloy-2-clad rods are briefly as follows. Early experiences at APED indicated that Zircaloy-2-clad rods were susceptible to failure by attack by fluorides contained as an impurity in the UO_2 fuel pellets and by hydrogen liberated in a chemical reaction within leaking fuel elements. It was postulated that a stainless-steel-lined Zircaloy-2 fuel rod would solve the hydriding and fluoride problems by interposing a nonreactive barrier (the stainless steel) between the fuel and cladding. Subsequent research, however (since 1961), indicated that defected Zircaloy-clad fuel rods could operate satisfactorily for long periods of time provided the UO_2 contained less than 35 ppm of fluoride.[5] Development work was, nevertheless, continued on the fabrication of lined elements and culminated in the VBWR irradiations.

The lined fuel rods contained pressed and sintered UO_2 pellets centerless ground to a diameter of about 0.37 in. The tubing was produced by a subcontractor using coextrusion; the fabrication involved the following steps:

> a. Zircaloy-2 and 304L stainless-steel sleeves of the appropriate size were prepared and cleaned.
>
> b. Mild steel canning components, which completely enveloped the stainless steel and Zircaloy, were prepared.
>
> c. The various components were assembled and the mild steel can was welded shut, except for the opening in the evacuation tube.
>
> d. The mild steel can was evacuated and sealed.
>
> e. The assembled parts were then heated to 871 C (1600 F) and extruded, using an extrusion force of 136 to 182 metric tons and an extrusion ratio of 15.7 to 1.
>
> f. The carbon steel canning was removed and the tubing was etched to remove any surface contamination.
>
> g. The tubing was visually inspected, and prepared for shipping. No other inspection was performed...

The tubing was ordered early in 1961, and it is stated in Ref. 5 that commercial processes for the production of this type of tubing were not available at that time. Imperfections of various sorts were noted, but only 3 tubes out of the 20 received were bad enough to be rejected. The lining, which was type 304 stainless steel, had thicknesses varying from about 2 to 6 mils. It was metallurgically bonded to the Zircaloy-2, although the reaction zone was not extensive. Some blisters, which did not interfere with pellet loading, were noted on the inside diameter of the tubes where bonding had not taken place; the nominal cladding-to-pellet gap was about 0.004 in. Calculational techniques for sizing the cladding thickness and for the plenum design are presented.[5]

Irradiation of the lined fuel rods ended with the shutdown of the VBWR in December of 1963. At that time the rods had received an average exposure of about 6700 Mwd/ton, and no failures have been reported.

Boron-Containing Fuel Elements

The use of boron as a burnable poison in power-reactor cores usually involves a problem of how to incorporate the boron in the core composition. In a number of cases discrete shim strips containing boron have been installed specifically for the purpose, but a more desirable approach usually is to add the boron to one of the normally present core materials. This has been done in the Elk River reactor, which is supplied with 600 ppm of boron as an admixture to the type 304 stainless steel used for the fuel-element jackets. However, this approach has not yet been proved out by experience. Several recent reports describe development work at the General Electric Company[6] and at Combustion Engineering, Inc.,[7–10] on the incorporation of boron in fuel-element jackets and in the uranium oxide fuel material. The experimental fuel elements produced at General Electric have been previously cited in *Power Reactor Technology*, 7(1): 34-35 (Table IV-8) in the discussion of the Fuel-Cycle Program at General Electric. These fuel elements were incorporated in the Special Assembly 12L described in that program.

Special Assembly 12L contained some fuel elements with boron in the cladding and some with boron in the UO_2, as well as some elements without boron, for purposes of comparison. The borated cladding consisted of type 304 stainless-steel tubing, in either the annealed or the cold-worked condition and contained either 500 or 750 ppm of natural boron. The fuel was in the form of sintered pellets of UO_2 or in the form of powder, placed by vibratory compaction. The fabrication of the fuel rods with the borated stainless steel appeared to involve no special problems except the welding of the upper end-plug closure seal. Cracks appeared at the center of the weld bead due to the hot short condition of the high-boron alloy. The cracking was eliminated by a redesign of the weld configuration to control the stresses during the cooling period and by modifying the welding procedure to cause dilution of the weld metal to reduce the overall boron content.

The fuel rods fabricated with the burnable poison within the UO_2 fuel material are somewhat more interesting. Before the start of the in-pile test program, laboratory studies showed boron to have a migratory behavior at temperatures greater than 1000°F. Migration is undesirable because it results in changes in the self-shielding of the boron, or otherwise modifies the neutron flux level seen by the boron, and hence changes the reactivity worth and the rate of boron burnup. The APED experimenters therefore utilized boron as zirconium diboride, either as a fine, uncoated powder (−325 mesh) or as larger sintered particles sized between 100 and 200 μ and coated individually with a film of molybdenum metal or BeO.

The designs of two types of fuel rods (designated F and G) containing poisoned oxide are shown in Fig. III-1. The poison-bearing fuel was loaded into the tubes by vibratory compaction, and, as illustrated in the figure, three

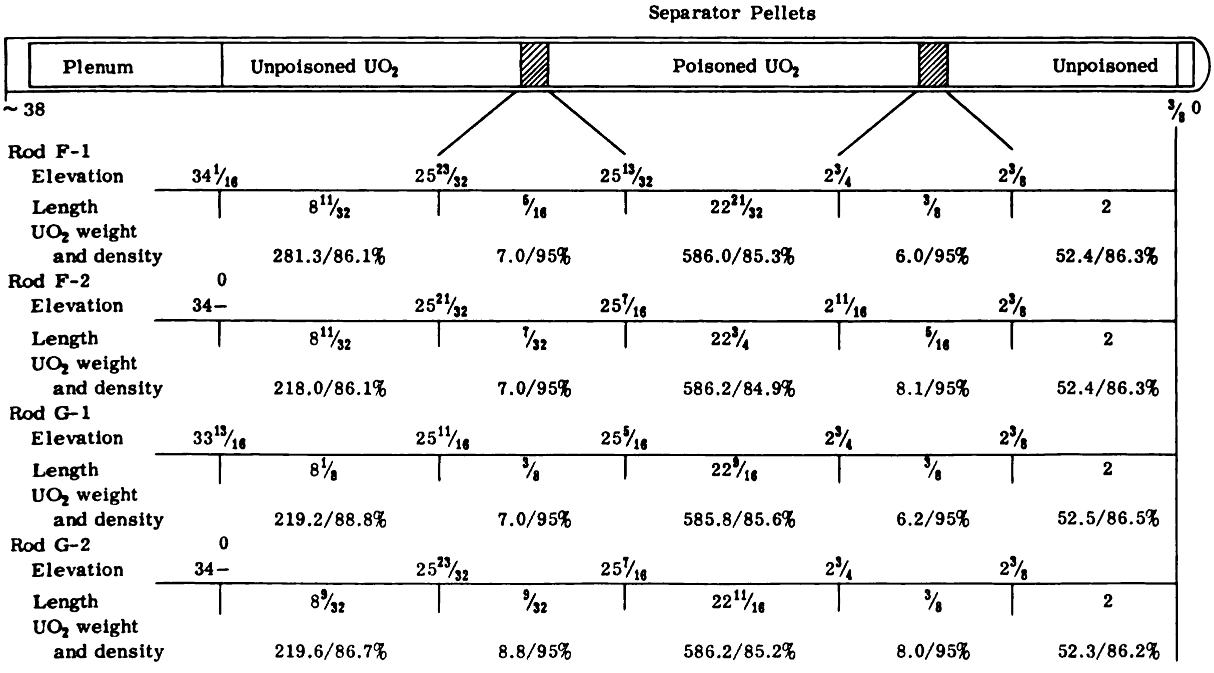

Rod F-1										
Elevation	$34\frac{1}{16}$		$25\frac{23}{32}$		$25\frac{13}{32}$		$2\frac{3}{4}$		$2\frac{3}{8}$	
Length		$8\frac{11}{32}$		$\frac{5}{16}$		$22\frac{21}{32}$		$\frac{3}{8}$		2
UO_2 weight and density		281.3/86.1%		7.0/95%		586.0/85.3%		6.0/95%		52.4/86.3%
Rod F-2	0									
Elevation	34–		$25\frac{21}{32}$		$25\frac{7}{16}$		$2\frac{11}{16}$		$2\frac{3}{8}$	
Length		$8\frac{11}{32}$		$\frac{7}{32}$		$22\frac{3}{4}$		$\frac{5}{16}$		2
UO_2 weight and density		218.0/86.1%		7.0/95%		586.2/84.9%		8.1/95%		52.4/86.3%
Rod G-1										
Elevation	$33\frac{13}{16}$		$25\frac{11}{16}$		$25\frac{5}{16}$		$2\frac{3}{4}$		$2\frac{3}{8}$	
Length		$8\frac{1}{8}$		$\frac{3}{8}$		$22\frac{9}{16}$		$\frac{3}{8}$		2
UO_2 weight and density		219.2/88.8%		7.0/95%		585.8/85.6%		6.2/95%		52.5/86.5%
Rod G-2	0									
Elevation	34–		$25\frac{23}{32}$		$25\frac{7}{16}$		$2\frac{3}{4}$		$2\frac{3}{8}$	
Length		$8\frac{9}{32}$		$\frac{9}{32}$		$22\frac{11}{16}$		$\frac{3}{8}$		2
UO_2 weight and density		219.6/86.7%		8.8/95%		586.2/85.2%		8.0/95%		52.3/86.2%

Fig. III-1 Locations and dimensions of fuel sections in rods[6] with poison in the UO_2. (Elevation and length are in inches.)

axial zones were provided. An additional two rods (designated type E) were fabricated of UO_2 containing BeO-coated ZrB_2 powder, but at the time of writing of Ref. 6 these rods had not been completed. The zoned loading indicated in Fig. III-1 was begun by filling and compacting the lower portion of the cladding tube. A $^1/_4$-in. sintered UO_2 pellet was then placed on top of the lower portion to act as a separator, and the fuel containing a mixture of UO_2 and coated or uncoated poison particles was compacted in place. Low *g*-level vibration was used during the initial loading of the poisoned zone to lock the sintered pellet in place and prevent its relative motion. After compaction of the middle zone, another separator was seated and the upper regions of the tube interior were cleaned of traces of poisoned fuel by means of a suction probe and swabs. The top zone was then loaded and compacted with unpoisoned fuel. A sleeve, not shown in Fig. III-1, was used to support the cladding in the region of the plenum. A perforated disk of stainless steel was welded to the lower end of the sleeve and served to prevent the powder from falling into the plenum or becoming loose during subsequent handling operations. The rods were evacuated, backfilled with helium at room temperature to a pressure of 1 atm, and sealed by welding on an end plug.

The shutdown of the VBWR also interrupted irradiation on the assembly incorporating the burnable-poison rods. An average exposure of 2972 Mwd/ton was attained.[11]

The Combustion Engineering work[7-9] to date has been with boron carbide, although other poisons are presumably to be investigated. The fabrication of boron carbide–UO_2 mixtures has been studied, as well as the mechanics of boron migration. Neutron physics studies are reported in Ref. 8 to determine B_4C particle sizes that would provide desired degrees of self-shielding. These results are contained in Table III-2. It is indicated in the reference that self-shielding factors from 0.5 to 0.6 are necessary to achieve burnable-poison utilization throughout the core lifetime, and hence the larger particles in Table III-2 are of interest. However, −325 mesh particles were used for the initial studies reported in Refs. 7–10.

A number of fuel rods have been prepared by electromagnetic and pneumatic vibratory-compaction methods, using admixtures of UO_2 and B_4C. Densities from 87 to 89% of theoretical were attained with the −325 mesh B_4C particles, although it is stated in Ref. 8 that the establishment of a uniform distribution of large particles of B_4C at low concentrations may be a problem. Local boron-concentration variations of less than ±20% from nominal were maintained; this was within the prescribed limits.

Table III-2 SELF-SHIELDING OF B_4C SPHERES[8]

Average particle diameter, in.	Self-shielding factors
0.001	0.98
0.005	0.90
0.010	0.79
0.020	0.63
0.030	0.50

The addition of boron compounds to UO_2 during fabrication of sintered pellets has been studied in the past, and Ref. 6 contains a brief bibliography on the subject. Boron losses discussed in Refs. 12 and 13 occurred during fabrication of fuel plates for the SM-1 reactor (the Army Package Power Reactor)[12] and during the sintering of UO_2 pellets containing boron compounds.[13] The approach at Combustion Engineering involves consideration of the various chemical reactions in which boron and its compounds can participate, as well as experimental investigations of volatilization by heating the boron-bearing UO_2. The following reaction is believed responsible for boron volatilization:

$$UO_{2(s)} + B_4C_{(s)} \rightarrow UB_{4(s)} + CO_{2(g)} \text{ or } CO + {}^1/_2O_2$$

Subsequent dissociation of UB_4 may provide a volatile boron species, but both analytical and experimental results indicate that the formation of significant amounts of volatile boron species is improbable in an operating fuel element. An irradiation program has been formulated[10] for the testing of boron-bearing UO_2 in-pile.

Electron-Beam Welding

Fabrication of fuel-element components of substantial length by means of electron-beam welding is reported in Ref. 14. Figure III-2 illustrates the various types of weld joints studied, and Table III-3 gives the relative sizes used. The material employed was exclusively reactor-grade Zircaloy-2.

Problems associated with each type of weld shown in Fig. III-2 are discussed, and examples are given of welds produced with the equipment used.[14] Because weldments of about 9 ft were studied, fitup, fixturing, and work-carriage operation were important, for any distortion tended to magnify the positioning error of, for example, a burn-through weld where the inner rib might not be visible. The authors conclude that the electron-beam welding process has proved highly successful. Several 9-ft-long assemblies were fabricated with the use of this process, and a number of shorter test weldments of considerable complexity are illustrated.[14] An earlier discussion of the electron-beam welding is contained in *Power Reactor Technology*, 2(2): 33-34 (March 1959).

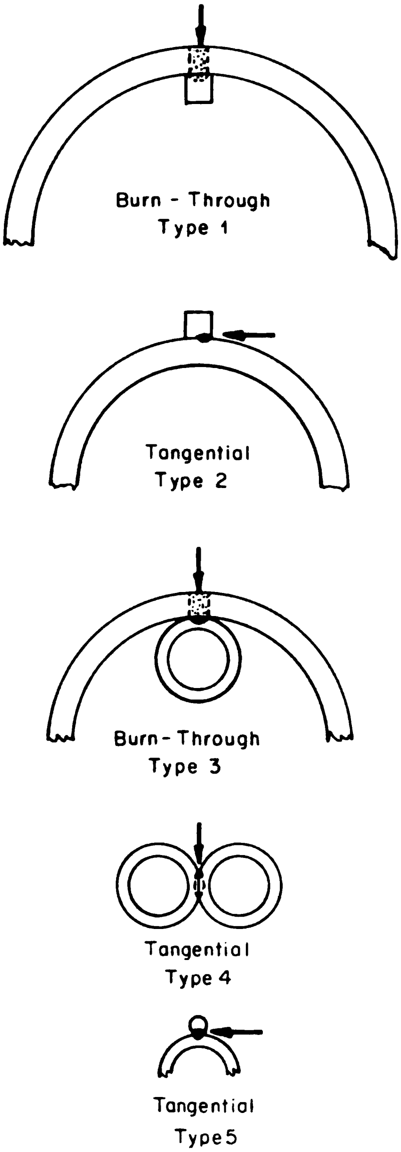

Fig. III-2 Weld-joint descriptions and designations.[14]

Table III-3 DIMENSIONS OF TYPICAL WELDMENT COMPONENTS[14]

Type of joint	Part	Dimensions
1	Tubular cladding	3.070 in. OD by 0.060 in. wall
	Rib	0.062 in. thick
2	Tubular cladding	2.330 in. OD by 0.060 in. wall
	Rib	0.062 in. thick
3	Large tubular cladding	2.330 in. OD by 0.060 in. wall
	Small tubular cladding	0.565 in. OD by 0.30 in. wall
4	Both pieces of tubular cladding	0.565 in. OD by 0.030 in. wall
5	Tubular cladding	0.565 in. OD by 0.030 in. wall
	Round wire	0.072 in. diameter

Irradiation Effects in UO_2

Information continues to accumulate to aid the designer in predicting the performance of UO_2-bearing fuel elements. References 15 and 16, in particular, are review articles that contain a wealth of material on UO_2 and, in the case of Ref. 15, on a number of other uranium compounds. In addition, *Reactor Materials*, 6(4), contains a feature article on the behavior of fission gases in ceramic reactor materials.

Reference 17 is a report on the emission of ^{133}Xe from irradiated UO_2 in the form of spheroids and powders. The materials are characterized in Table III-4; they were prepared as follows:

> Powder specimens were prepared by precipitation of ammonium diuranate from nitrate solution and calcination at 900°C in air, followed by reduction in hydrogen at the same temperature. The preparation was divided into two portions; both were annealed in hydrogen for 5 hrs., one at 1250°C and the other at 1650°C. The latter preparation sintered during annealing and was therefore crushed to pass 400 mesh. Finally, both preparations were reduced in carbon monoxide at 800°C immediately prior to irradiation.
>
> Sintered spheroids, Group A. These were prepared by spheroidising fragments of green compacts

of uranium dioxide in a gyratory mill. Densification was achieved by sintering in cracked ammonia at 1650°C. Finally the required size fractions were produced by sieving.

Sintered spheroids, Group B. These were prepared by blending uranium dioxide powder with binder to produce a granular mix. After sieving out the appropriate size range, the granules were densified by rotation in a gyratory mill and finally sintered.

Fused spheroids were prepared by passing fragments of sintered compacts through the flame of a plasma torch. Any material which had by-passed the torch was separated by rolling the product down an inclined plane. A portion of each of the two preparations studied was annealed in vacuo for 2 hours at 1650°C and cooled slowly in order to relieve any stress.

Table III-4 PHYSICAL PROPERTIES OF UO_2 SPHEROIDS AND POWDERS[17]

Sample type and No.	Mean radius, μ	BET* area, cm²/g	Equivalent sphere radius, μ	Roughness factor
Sintered spheroid Group A				
A1	150	25	114	1.3
A2	40	103	29	1.5
Sintered spheroid Group B				
B1(a)	>200			
B1(b)	110	88	33	3.3
B2	150	23	125	1.2
B3	120	55	52	2.3
Fused spheroid				
F1	60	200	14	4.3
F2	60	115	25	2.4
Fused spheroid, annealed				
F1/A	60	75	38	1.6
F2/A	60	77	37	1.6
Powder				
P1		9100	0.31	
P2		1300	2.2	

*Brunauer, Emmett, Teller.

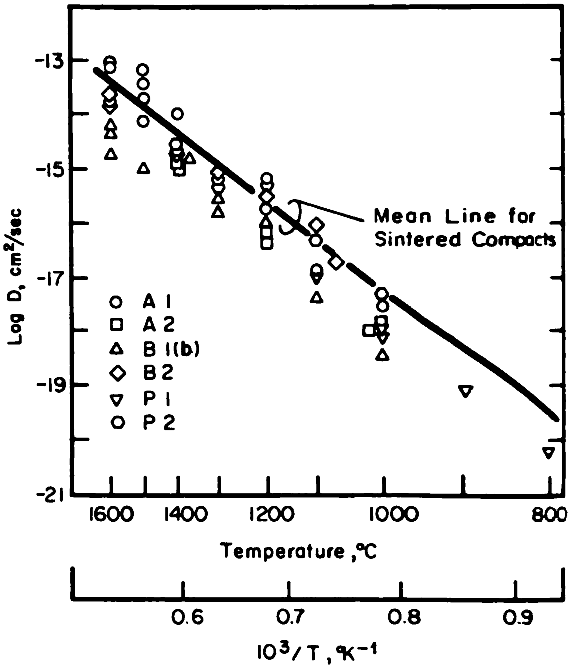

Fig. III-3 Plot of log D (cm²/sec) vs. $1/T$°K for sintered spheroids and powders.[17]

The results of the experiments are shown in Fig. III-3. It is stated in Ref. 17: "...any differences between sintered compacts of gram size, sintered spheroids of about 50 microgram size and fine powders are experimentally undetectable." The fractional release of xenon, to a first approximation, is proportional to the product of the diffusion coefficient, the square of the sample density, and the square of the BET surface area. The powdered materials have a larger BET area by several orders of magnitude than do the sintered and fused samples (Table III-4) and therefore release fractionally more xenon than the fused and sintered materials.

The release of other fission products from powdered UO_2, sintered compacts, and sintered or fused spheroids of UO_2 is detailed in Ref. 18. Fission products studied were iodine, tellurium, and cesium. The results are shown in Table III-5. Samples were also heated in the range 2000 to 2200°C to determine the effect of grain growth on the emission of fission products. These results are shown in Table III-6.

It is interesting to compare the release of ^{133}Xe from the conventional UO_2 fuels with the release from zirconia-urania plates. The latter fuel has been selected for the seed portion of the second core of the Shippingport Pressurized-Water Reactor, and Ref. 19 presents the results of the irradiation experiments. The plates were prepared by mechanically blending ZrO_2 and slightly enriched UO_2 and heating the blend at about 1700°C, in hydrogen, to form a solid solution. The comminuted powders were pressed into plates, with a binder, and sintered in hydrogen at 1750°F. Table III-7 lists the properties of the ZrO_2-UO_2 plates along with those of

Table III-5 EMISSION OF FISSION-PRODUCT[18] IODINE, TELLURIUM, AND CESIUM FROM UO_2

(Results Expressed as the Ratio $\sqrt{D_i'/D_{Xe}'}$)

Sample No.	Density, g/cm^3	Surface area, cm^2/g	Temp., °C	I	Te	Cs
Powder						
P/2		1,300	1,400	0.98	1.05	0.9
Sintered compact						
S/1	6.40	23,000	930*	0.55		0.45
S/2	6.75	19,200	1,000	0.9	1.1	>0.03
S/3	7.07	17,200	1,000	0.7	0.4	0.3
S/5	8.85	7,800	1,000	1.3	0.9	0.9
			1,000	0.7		
			1,200	0.7	0.8	0.8
			1,200	0.6		
			1,200	0.8	0.8	
S/7	8.15	1,370	1,200	1.3	1.9	0.6
			1,600	1.1	1.1	0.9
S/8	8.50	730	1,600*	1.1	1.1	0.3
			1,600*	1.5	1.5	0.7
S/9	10.3	140	1,000	3.9	2.8	2.4
			1,000	6.3	4.9	5.1
			1,200	2.9	3.9	1.4
			1,400	2.3	2.7	1.4
S/19		~100	1,600*	1.3		2.3
S/18	10.3	10	1,600*	4.4	10	6.3
S/14	10.8	5	1,600*	2.5	11	0.8
S/15	10.16	4	1,300	7.3	6.7	15.2
Sintered spheroid						
A1		25	1,200	2.1	2.6	1.0
			1,400	5.3	6.3	4.6
			1,600	2.7	10.5	0.6
			1,600	4.1	14.0	2.5
			1,600	3.5	21.0	0.8
			1,600	1.4	21.0	0.6
A2		103	1,400	2.5	3.3	2.5
Fused spheroid						
F2/A	10.6	77	1,200	2.0	5.7	1.0
			1,600	4.1	16.1	1.8

*Data obtained from a single analysis at the end of a 2-hr run.

Table III-6 FISSION-PRODUCT AND URANIUM EMISSION FROM UO_2 DURING GRAIN GROWTH[18]

(Sample No. S/13, Surface Area 7 cm^2/g, Density 10.7 g/cm^3)

Temperature, °C (±50°C)	Time, hr	Fraction released of								
		^{133}Xe	^{131}I	^{132}Te	^{137}Cs	^{89}Sr	^{140}Ba	^{106}Ru	^{144}Ce	U
2000	2.1	0.05	0.14	0.18	0.11	0.09	0.05	0.01	0.02	
2000	4.5	0.34		0.59	0.12	0.14	0.17	0.12	0.05	0.04
2050	1.5	0.23		0.66	0.21	0.19	0.20	0.22	0.08	0.10
2150	1.5	0.16	0.19	0.39	0.06	0.15	0.15	0.15	0.06	
2200	1.5	0.72		0.68	0.11	0.52	0.54	0.63	0.25	0.26
2200	5.0	0.99		0.94	0.33	0.83	0.74	0.78	0.47	0.45

Table III-7 CHEMICAL AND PHYSICAL PROPERTIES OF SINTERED ZrO_2-UO_2 PLATES[19]

Nominal composition	Isotopic analysis, at.% ^{235}U	Chemical analyses: Wt.% U	Wt.% Zr	Ppm Al	Ppm Fe	Ppm Si	Density, % of theoretical	Grain size, μ	Roughness factor	Geometrical size, in.
ZrO_2−26 wt.% UO_2	3.75	22.7	54.9	39	180	170	98.0	10 to 25	0.9	1.5 by 0.25 by 0.05
ZrO_2−35 wt.% UO_2	3.75	31.0	47.9	120	350	64	96.5	9 to 18	1.2	1.5 by 0.25 by 0.05
UO_2	0.71	88.1		10	21	20	97.0	20 to 100	2.2	1.5 by 0.25 by 0.10

some plates made only of UO_2. The plates were sealed in quartz tubes and irradiated at nominal room temperature in the Brookhaven Research Reactor. The ^{133}Xe was then collected in charcoal traps during isothermal high-temperature anneals.

Diffusion coefficients for the various materials tested are shown in Fig. III-4. The slightly irradiated ZrO_2-UO_2 solid solutions exhibited higher ^{133}Xe release rates, diffusion coefficients, and activation energies than unalloyed UO_2. Microstructure was determined both before and after irradiation. In the as-fabricated condition, the 26 wt.% material showed only a single phase present (face-centered tetragonal), whereas the 35 wt.% material showed two phases (major phase was equiaxed face-centered tetragonal, and minor phase was transformed tetragonal). The phase transformations during irradiation and the post-irradiation heat-treatment are discussed in Ref. 19. This discussion would be of interest to the specialist.

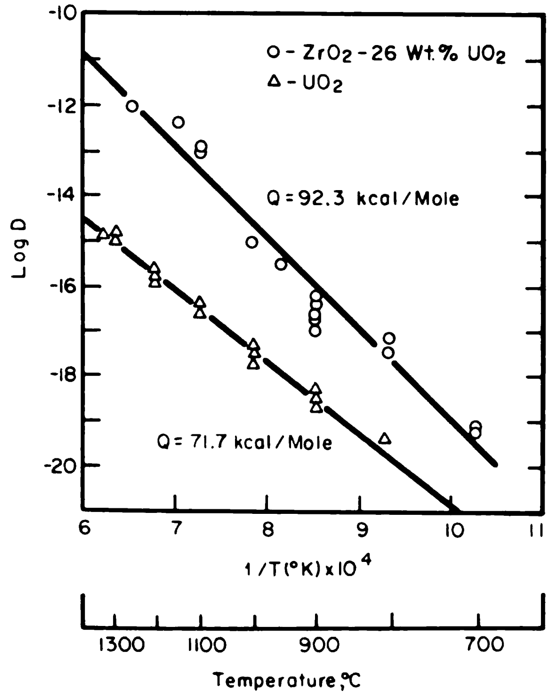

Fig. III-4 Variation of *D* with temperature: comparison[19] of cubic UO_2 and tetragonal ZrO_2−26 wt.% UO_2.

A number of Hanford reports deal with the change in physical properties of UO_2 under irradiation.[20–22] These reports contain much specialized information but are also of general interest. The melting point of UO_2, for example, depends on irradiation.[20] Samples of irradiated UO_2 from 0.005 to 11.3 at.% uranium were obtained from a variety of test capsules with different fabrication and irradiation histories. Aliquots of tens of milligrams were heated in a resistance furnace in direct contact with a tungsten heating element. The aliquots were observed through an external microscope, and the temperatures were measured with an optical pyrometer. Crystal growth and vaporization were observed photographically.

A melting point of 2790 ± 20°C was observed for 95% dense UO_2 that was pressed and sintered in hydrogen for 12 hr at 1750°C. Figure III-5 illustrates the behavior of the melting point with irradiation. Although there is considerable scatter of the data, a justification for the shape of the curve at exposures less than 0.4 at. burnup is given.[20] Measurements were also made on nonstoichiometric UO_2, and these data are contained in Ref. 20. References 21 and 22 report physical property data for irradiated and nonirradiated polycrystalline and single-crystal UO_2.

Reference 23 is related to Ref. 20 and is cited here for completeness, although it is not concerned with irradiated UO_2. It reports on the density changes exhibited by UO_2 upon melting. Single crystal pins of UO_2 were heated in sealed tungsten capsules. With the use of ^{60}Co source and photographic film, the density of the crystals was determined radiographically

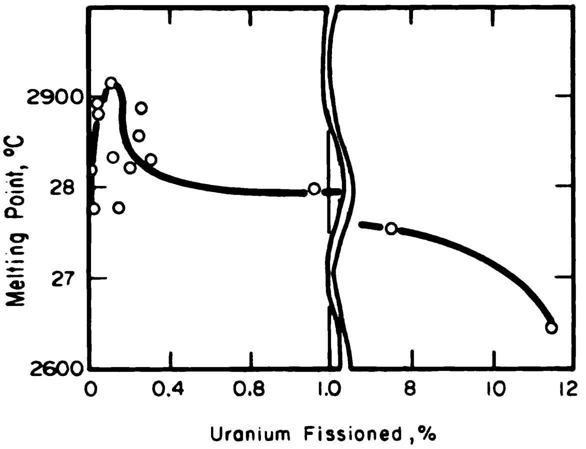

Fig. III-5 Melting point vs. in-reactor exposure[20] for irradiated UO_2.

Data were taken at temperatures from 1280 to 3100°C, and the results are shown in Fig. III-6. The density of the solid at 2800°C was determined to be 9.67 ± 0.13 g/cm^3, and that of the liquid was determined to be 8.7 ± 0.16 g/cm^3. The coefficient of expansion of the molten UO_2 was 3.5×10^{-5}/°C between 2800 and 3100°C. An empirical formula is presented for specific volume as a function of temperature between 0 and 2800°C.

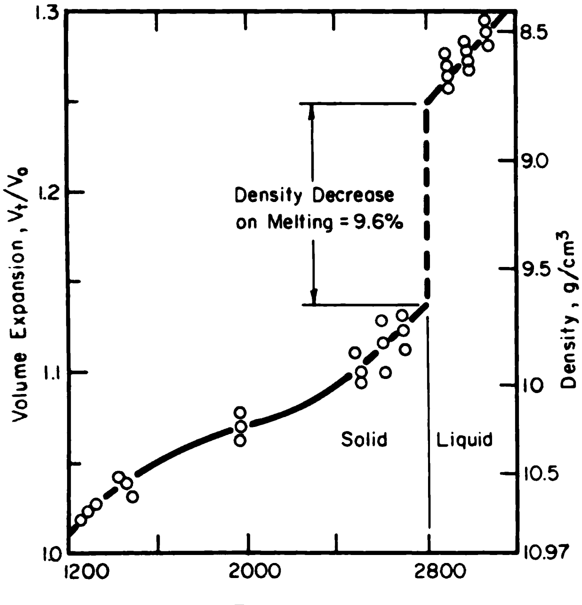

Fig. III-6 Volume and density change[23] of UO_2.

References

1. H. E. Williamson, J. P. Hoffman, C. J. Baroch, and T. J. Pashos, Comparative Performance of Similar Zircaloy- and Stainless-Steel-Clad Fuels in the VBWR, *Trans. Am. Nucl. Soc.*, 7(1): 105 (June 1964).
2. T. J. Pashos, W. H. Arlt, C. J. Baroch, and H. E. Williamson, The Intergranular Corrosion of Stainless Steel Cladding in Water Reactor Environments, *Trans. Am. Nucl. Soc.*, 7(1): 119 (June 1964).
3. R. N. Duncan, C. J. Kubit, D. R. McClintock, and W. R. Smalley, The Formation and Release of Helium from UO_2 Fuel During Irradiation, *Trans. Am. Nucl. Soc.*, 7(1): 89-90 (June 1964).
4. S. Katcoff, Fission-Product Yields from Neutron-Induced Fission, *Nucleonics*, 18(11): 201-208 (November 1960).
5. C. J. Baroch, Design and Fabrication of Fuel Rods Clad with Stainless-Steel-Lined Zircaloy-2, USAEC Report GEAP-4555, Vallecitos Atomic Laboratory, Feb. 7, 1964.
6. S. Y. Ogawa and H. E. Williamson, Design and Fabrication of Special Assembly 12-L. Two Designs for Utilizing Boron as Burnable Poison, USAEC Report GEAP-4312, General Electric Company, Atomic Power Equipment Department, July 15, 1963.
7. G. Zuromsky, R. C. Brayer, W. C. Taylor, and W. P. Chernock, Burnable Poison Additions to UO_2, Quarterly Progress Report for Period Ending March 31, 1963, USAEC Report CEND-179, Combustion Engineering, Inc., April 1963.
8. G. Zuromsky, R. C. Brayer, and W. P. Chernock, Burnable Poison Additions to UO_2, Summary Report, July 1, 1962–June 30, 1963, USAEC Report CEND-181, Combustion Engineering, Inc., November 1963.
9. R. C. Brayer and W. P. Chernock, Burnable Poison Additions to UO_2, Progress Report, Period Ending December 31, 1963, USAEC Report CEND-203, Combustion Engineering, Inc., January 1964.
10. R. C. Brayer and W. P. Chernock, Burnable Poison Additions to UO_2, Progress Report, Period Ending March 31, 1964, USAEC Report CEND-3107-210, Combustion Engineering, Inc., April 1964.
11. C. L. Howard (Comp.), Fuel Cycle Program—A Boiling Water Reactor Research and Development Program, Fourteenth Quarterly Progress Report, October–December 1963, USAEC Report GEAP-4481, General Electric Company, Atomic Power Equipment Department, Jan. 7, 1964.
12. Oak Ridge National Laboratory, Army Package Power Reactor Project Annual Progress Report for Period Ending January 31, 1960, USAEC Report ORNL-2907, Apr. 4, 1960.
13. G. L. Ploetz and H. G. Sowman, Burnable Poison Additives to Uranium Dioxide, USAEC Report

KAPL-1447, Knolls Atomic Power Laboratory, Nov. 17, 1955.

14. R. F. Klein, Electron Beam Welding of Nuclear Fuel Cladding Components, USAEC Report HW-79143, Hanford Laboratories, October 1963.
15. J. B. Melehan, V. W. Storhok, R. J. Burian, M. Kangilaski, and R. A. Wullaert, The Effect of Nuclear Radiation on Ceramic Reactor-Fuel Materials, Report REIC-27, Battelle Memorial Institute, Radiation Effects Information Center, June 30, 1963.
16. B. G. Childs, Review Article, Fission Product Effects in Uranium Dioxide, *J. Nucl. Mater.*, 9(3): 217 (August 1963).
17. D. Davies and G. Long, The Emission of Xenon-133 from Lightly Irradiated Uranium Dioxide Spheroids and Powders, British Report AERE-R-4347, June 1963.
18. D. Davies, G. Long, and W. P. Stanaway, The Emission of Volatile Fission Products from Uranium Dioxide, British Report AERE-R-4342, June 1963.
19. J. C. Clayton, The Evolution of Xenon-133 from Slightly Irradiated Zirconia-Urania Plates, USAEC Report WAPD-TM-313, Westinghouse Electric Corp., Bettis Atomic Power Laboratory, August 1963.
20. J. A. Christensen, Irradiation Effects on Uranium Dioxide Melting, USAEC Report HW-69234, Hanford Laboratories, March 1962.
21. J. L. Bates, Microhardness of Uranium Dioxide, USAEC Report HW-77799, Hanford Laboratories, June 1963.
22. J. L. Bates, J. A. Christensen, and J. L. Daniel, Irradiation Effects in Uranium Dioxide Single Crystal, USAEC Report HW-73959, Hanford Laboratories, September 1962.
23. J. A. Christensen, Thermal Expansion of Uranium Dioxide, USAEC Report HW-75148, Hanford Laboratories, Oct. 4, 1962.

Section
IV

Power Reactor Technology

Materials

Boron for Control Rods

That boron is still the most important control material is borne out by the number of power reactors in which it is used as a neutron absorber and by the amount of work reported on its properties. Several recent reports give further information on its use as a control absorber.

The Pathfinder nuclear superheat reactor, one of the more interesting concepts presently in the late development stage, has boron in both the boiler and superheat control rods. [The Pathfinder design was reviewed in *Power Reactor Technology*, 7(3).] The boiler control rods[1] are cruciform with a blade thickness of ¼ in. They are made of type 304 stainless steel containing 2 wt.% natural boron. The blade surfaces are bare to the coolant water. The overall poisoned length of the blades is 72 in., and additional short nose and tail sections are of 304 stainless steel. The superheater control rods, unlike the boiler rods, are not required to scram and are expected to be fully withdrawn from the core during normal operation. These are cylindrical rods, ¾ in. in diameter, consisting of a core of 304 stainless steel containing 2 wt.% natural boron and a mechanically bonded cladding of 304L stainless-steel tubing 0.020 in. thick. The poisoned length is again 72 in., and the rods have a short nose of 304 stainless steel and a gas space above the poison at the top of the rod.

The mechanical properties of the two boron–stainless-steel alloys are as follows:

	Boiler rod	Superheater rods
Tensile strength, psi	82,300	94,200
Yield strength, psi	42,700	64,100
Elongation, %	7.9	11.5
Rockwell B hardness	96.8 ± 3	
Impact strength, ft-lb	6.5 ± 5	

Impact strengths on the boiler material were determined on unnotched specimens. Similar specimens of boron-free 304 stainless steel gave impact values of 27.7 ft-lb.

The cruciform boiler blades were assembled in special fixtures by manual arc welding with the use of coated E-308-16 rods. The blades were subsequently stress relieved at high temperature. Stress relief is of obvious importance for such a component, but the selection of a suitable temperature demands a choice between moderate temperatures, which require long treatment times and introduce the danger of sensitization, and higher temperatures, with the attendant difficulties of distortion during cooling. Specific data on the stress-relief procedure for the Pathfinder rods would be of interest.

Analysis showed that distortion of the rods due to thermal gradients in the rod channels would not be excessive. Calculated impact stresses for the boiler rods at a maximum velocity of 22 in./sec at scram gave a maximum value of 5980 psi. In test a prototype boiler rod underwent 990 scram cycles and 22,388 cycles through a 6-ft stroke. Because the prototype differed from the reactor rods in that it did not have the 304L stainless-steel tip at the contact end, impact conditions were particularly severe, but dye-penetrant inspection showed no cracks in the unirradiated prototype. The superheat control rod, although not intended to undergo scram operation, was also tested for 20 scram cycles with no adverse effects.

Since the ex-pile behavior of the rods appeared to be satisfactory, a literature search was conducted to supply data from which the operating behavior could be predicted. The tabular data, as compiled in Ref. 2, are given in Tables IV-1 and IV-2. The hardness of boron stainless steel was also found to increase rapidly up to 8×10^{19} neutrons/cm^2 (nvt) and

Table IV-1 MECHANICAL PROPERTIES OF UNIRRADIATED AND IRRADIATED BORON STAINLESS STEEL[2]

Wt.% boron*	Test temperature, °C	Core at.% burnup† or nvt dose	Yield strength, psi	Tensile strength, psi	Elongation, %	Ref.
0	23	0	37,500	90,000	50	2
0	23	2.7×10^{20} nvt	82,000	104,000	40	2
1.0^{10}	23	0	93,400	121,000	15.6	3
1.0^{10}	23	0.7	149,500	153,500	3.4	3
1.0^{10}	23	1.1		137,100	1.6	3
1.8^{N}	23	0	41,300	84,200	8	4
1.8^{N}	23	0.5	136,000	151,000	0.5	4
1.8^{N}	315	0.5	85,500	119,000		4
2.0^{10}	23	0		88,400	8.1	5
2.0^{10}	23	0.3		93,300	0.5	5
2.0^{10}	23	0.8		78,800	0.4	5
2.04^{N}	23	0	47,000	89,000	5.4	4
2.04^{N}	23	0.6	97,800	120,000		4
2.04^{N}	315	0.6	71,300	106,000		4

*Superscripts refer to whether the boron was natural (N) or enriched to 93% in the ^{10}B isotope (10).

†Core at.% is the concentration of one particular element or isotope in terms of all the atoms in the boron–stainless-steel alloy.

Table IV-2 IMPACT STRENGTH OF UNIRRADIATED AND IRRADIATED BORON STAINLESS STEEL[2]

Wt.% boron	Test temp., °C	Core at.% burnup or nvt dose	Unirradiated ft-lb	Irradiated ft-lb	Ref.
0	23	3.0×10^{20} nvt	15.9	15.7	4
1.8^{N}	23	0.3	1.0	0.44	4
1.8^{N}	315	0.3	1.0	0.35	4
2.0^{10}	23	0.8	4.4	0.16	5
2.0^{10}	315	0.8	2.3	0.24	5
2.04^{N}	23	0.6	0.64	0.22	4
2.04^{N}	315	0.6	0.64	0.05	4

then remain nearly constant at higher doses. No correlations between hardness and mechanical properties were found in the literature, but the notch sensitivity of the material was emphasized. Although the tables indicate that losses in both elongation and impact resistance are large for relatively small burnups, the Pathfinder discussion places considerable emphasis on the fact that, in use, control-rod boron is burned preferentially from the surface to the center. The figures given in Ref. 2 are for an average burnup of 1 at.% in the boron-containing portions of the rod; at this average burnup the surface burnup would be 1.3 at.% and the center only 0.6 at.%. The designers would thus expect the rod to retain more ductility at the center, although the tables indicate that even this ductility would be quite limited. In this regard the method of fabrication of the control rod may be quite important. The Pathfinder rod design is such that no stress raisers or notch formers are introduced at the surface. With spot-welded designs, if cracks are initiated at these welds on the surface, propagation through even a low-burnup central region would seem possible.

Crack initiation at spot-welded areas is likely, as shown by some EBWR experience in which 60% of the spot welds showed $\frac{1}{4}$-in. or larger cracks in 2 wt.% boron stainless steel at only 0.4 at.% burnup. Cracks were also initiated in the weld areas of Dresden control rods employing stainless steel with 2 wt.% boron. The welds in this core were fusion welds of the general type used in Pathfinder, but the boron stainless steel was cold rolled rather than annealed, and the Pathfinder stress relief is expected to provide crack resistance.

The data on swelling as provided by the literature survey[2] are presented in Fig. IV-1. Because the data were taken from various sources employing different experimental techniques, the spread in values is not unexpected. The points grouped at 1 core at.% burnup show a swelling rate of between 1 and 4% between 450 and 600°F. For temperatures above 600°F, swelling behavior was inferred from work on postirradiation annealing. These data are given in Fig. IV-2 and are pertinent to superheat control-rod behavior. The swelling at 600°C, for instance, would be assumed to be equal to the sum of the volume increase at lower temperatures (Fig. IV-1) plus the volume increase on annealing (Fig. IV-2).

From the literature survey it was concluded that 1 core at.% burnup is the threshold for observable effects under Pathfinder conditions and that cracking should not occur below 1.5 core at.% burnup. Swelling of from 2 to 3 vol.% is to be expected per 1 core at.% burnup in the boiler rods, with possibly larger rates of swelling in the higher temperature superheater rods. Burnup limits of 1 core at.% were set for the boiler control rods and $\frac{1}{2}$ core at.% for the superheater.

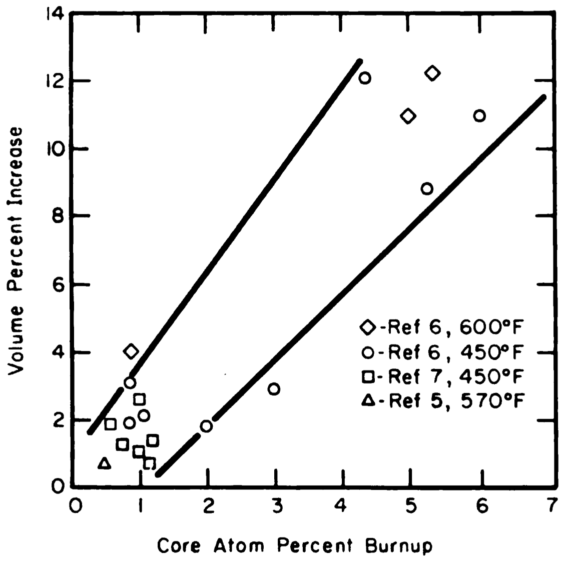

Fig. IV-1 Volume percent increase vs. core atom percent burnup for irradiated boron stainless steel.[2]

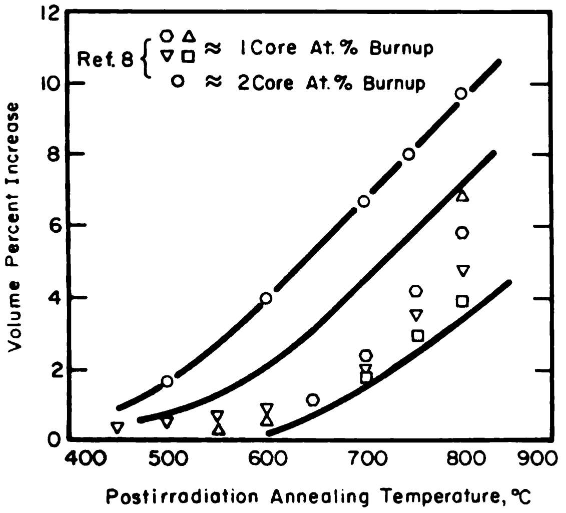

Fig. IV-2 Volume percent increase vs. postirradiation annealing temperature for 1 and 2 core atom percent burnup.[2]

For control-rod applications, boron may also be used in the form of boron carbide, B_4C, which is presumably more stable than the elemental form. A report from Atomics International[9] describes work on the compatibility of boron carbide with copper, types 430 and 304 stainless steels, and AISI 4130 steel at temperatures from 750 to 1300°F. Diffusion couples of B_4C and the alloy under study were prepared by hot-pressing the powdered carbide into a cavity in the alloy under vacuum. The sealed couples were then soaked at the test temperatures for periods up to 10,000 hr. Compatibility was determined by metallographic examination and hardness traverses. Copper and type 430 stainless steel were compatible with B_4C for 10,000 hr at 1300°F, whereas type 304 stainless steel was compatible for the same period at 1100°F but not at 1300°F. The 4130 steel was compatible for 10,000 hr at 750°F but not at 950°F and above. Also, with copper and types 430 and 410 stainless steels, little or no difference occurred in the behavior of normal B_4C (21.7% carbon), hypostoichiometric B_4C (18% carbon), and hyperstoichiometric B_4C (28% carbon) under similar but shorter tests.

The results of irradiation of boron carbide and zirconium boride dispersions in Zircaloy-2 and aluminum oxide have been reported by Battelle.[10] Pellets of Al_2O_3 containing B_4C, and hot-extruded pellets of Zircaloy-2 containing either B_4C or ZrB_2, were irradiated in the 450 to 500°F temperature range to ^{10}B burnups of 81 to 96%. The alumina pellets showed excessive cracking and poor corrosion resistance in water at 600°F. The Zircaloy-2 containing B_4C was superior to the materials containing ZrB_2 with regard to radiation stability and swelling. Both types of Zircaloy-2 pellets showed good gas retention and corrosion behavior.

Boron carbide might be usable as a burnable poison in the form of solid bodies, or lumps, as well as in the dispersion form. Reports from Westinghouse[11,12] discuss the fabrication of wafers of high-density B_4C, and B_4C plus silicon carbide, and their subsequent irradiation. The preparation of the compacts by hot pressing is described in detail in Ref. 11. The need to develop a product that could cover a wide range of ^{10}B contents led to a study of enriched boron, depleted boron, and natural boron in the form of B_4C. Also studied were mixtures of B_4C and SiC. High densities (99%) were sought and obtained because of the requirement for corrosion resistance and gas retention. Both B_4C and B_4C-plus-SiC pellets of high density were shown to have excellent corrosion resistance to 680°F water ex-pile. Because the pellets were intended for use in the Shippingport PWR compartmental fuel elements, methods of diffusion bonding and gas-pressure bonding were developed to seal the Zircaloy-2 compartments around the B_4C pellets. During bonding the pellets were coated with carbon to prevent interaction between the pellet and the cladding. [The compartmented fuel plates for Shippingport were discussed in *Power Reactor Technology*, 7(2).]

Clad elements were irradiated in 450 to 510°F water to depletions as high as 97% of ^{10}B atoms.[12] Swelling and buckling of the pellets occurred within the compartments, and the B_4C-plus-SiC elements showed greater swelling, due to excessive cracking, than the B_4C elements. Irradiation reduced the corrosion resistance of the B_4C elements to the point that all intentionally defected elements showed a complete loss of poison. Although B_4C elements would permit higher ^{10}B loadings than are possible with boron stainless steel, the plasticity and deformation of the carbide under irradiation and its loss of corrosion resistance in-pile raise some question as to the application of B_4C elements.

Transition Joints of Zircaloy to Stainless Steel

For pressure tubes and similar applications within reactor cores, Zircaloy is, of course, extremely attractive because of its low cross section and other properties. Satisfactory methods for joining Zircaloy to stainless steel or other alloys would make it possible to secure the advantage of neutron economy in the core, and at the same time much cheaper and more readily fabricated materials could be used in regions where their cross sections are of little importance. One of the more interesting methods for joining Zircaloy to stainless steel, particularly for tubular products, is the technique of coextrusion, or tandem extrusion. The tandem extrusion method for preparing a Zircaloy-stainless-steel joint was reviewed in *Power Reactor Technology*, 6(2): 51-52. The method consists in the extrusion of a canned composite fillet made up of a cone-shaped length of stainless steel followed by a cone of Zircaloy canned in mild steel. For the production of tubes, the composite fillet is pierced for a mandrel as in conventional tube extrusions. Extrusion temperatures must be selected so that the "stiffnesses" of the two alloys match as closely as possible. But the temperatures cannot be so high that there is interaction between the alloys or that the beta transition for the Zircaloy is exceeded. Interfaces between the Zircaloy and stainless steel in such extrusions are quite thin, just a few microns thick, and no trouble is experienced with the formation of nickel-zirconium eutectics.

A number of tandem tubular extrusions were prepared for Savannah River Laboratory by Nuclear Metals. These extrusions were found to have satisfactory mechanical and other properties when tested ex-pile.[13] Some of the results were mentioned in the earlier *Power Reactor Technology* review. Data have now become available on the properties of such joints tested after irradiation.[14] In the work reported, six tandem-extruded joints prepared by the methods described in Ref. 15 were irradiated at 50°C to exposures as high as 7.8×10^{20} neutrons/cm^2 (>0.1 Mev). Integrated fluxes were calculated from previous measurements, and the specimen temperatures were calculated from gamma fluxes and coolant flows. The specimens were mounted with longitudinal loading bolts so that the differential thermal expansion on heating, plus a preloading stress applied to the bolts, placed the joints under stresses that ranged from 3800 psi for the specimen under lowest load to 20,500 psi for the most highly stressed specimen. Three of the specimens were tested as extruded, but the remaining three had received 15, 18, and 20% cold reductions. The unworked specimens were approximately 1.9 in. in outside diameter with 0.2-in. walls. In the cold-worked specimens these measurements decreased slightly. Postirradiation measurements showed a maximum diameter decrease of 13 mils. Interface lengths were from 9 to 12 in. Four of the irradiated joints showed no defects, but some evidence of corrosion attack was found at the internal joint interfaces on the two remaining specimens. The penetration along the interface was as much as 10 mils. The two specimens that had been fabricated by a technique (not described) designed to prevent this difficulty did not show attack. The bond interfaces exhibited no changes due to irradiation.

One as-extruded and one cold-worked specimen were tensile tested. At the limit of the machine, the 56,000-psi nominal stress placed on the as-extruded tube was not sufficient to cause it to fail. Instead, deformation apparently occurred in the Zircaloy. The cold-worked specimen had a slightly thinner wall, so that failure was achieved at a nominal stress of 91,000 psi. The failure occurred in the Zircaloy at the grips. The strength up to the point of failure was similar to values previously found for unirradiated material, so that either no strengthening of the Zircaloy due to irradiation was indicated or the grip failure was below the true strength of the material. The tests show promising behavior for the tandem-extruded joints at the test temperatures under moderately high irradiation levels, but extrapolation of this behavior to much higher temperatures would probably be unwise.

The preparation of coextruded tubular joints and other coextrusion-joining techniques for bonding dissimilar metals is described in a recent review paper.[16]

References

1. D. A. Patterson, D. A. Nehrig, R. H. Klumb, and T. E. Peterson, Pathfinder Atomic Power Plant. Boron-Stainless Steel Control Rods for Pathfinder Reactor. Final Summary Report, USAEC Report ACNP-63001, Allis-Chalmers Mfg. Co., Feb. 15, 1963.
2. D. A. Patterson and D. A. Nehrig, Burnup Limits for Pathfinder Two Weight Per Cent Natural Boron-Stainless Steel Control Rods, USAEC Report ACNP-63006, Allis-Chalmers Mfg. Co., Dec. 19, 1963.
3. W. O. Schaffnit, Radiation Damage Studies of Boron Stainless Steel, Final Report, USAEC Report IDO-16502, Phillips Petroleum Co., Jan. 28, 1959.
4. General Electric Company, Atomic Power Equipment Department, Survey of the Physics, Metallurgy, and Engineering Aspects of Reactor Control Materials, USAEC Report GEAP-3183, June 12, 1959.
5. J. D. Eichenberg, The Effect of Irradiation on the Properties of Boron–Stainless-Steel Powder Dispersion Samples, USAEC Report WAPD-160, Westinghouse Electric Corp., Bettis Plant, Jan. 2, 1957.
6. W. E. Ray, The Effects of Neutron Capture on Reactor Control Materials, Report-11708, Dresser Products, Inc., 1960.
7. W. E. Ray, W. A. Neisz, and H. W. Cooper, Discrete Fixed Poison Rods Containing Boron, *Nucl. Sci. Eng.*, 4(3): 386-401 (September 1958).
8. W. V. Johnston and J. E. Noonan, Reactor Technology Report No. 8, Metallurgy, The Effect of Temperature on the Volume and Structural Stability of Irradiated Boron-Containing Materials, USAEC Report KAPL-2000-5, pp. 35-92, Knolls Atomic Power Laboratory, March 1959.
9. R. D. Hahn, Compatibility of Boron Carbide with Potential AOMR Control Rod Cladding Materials, USAEC Report NAA-SR-8702, Atomics International, Mar. 1, 1964.
10. R. J. Burian, E. O. Fromm, and J. E. Gates, Effect of High Boron Burnups on B_4C and ZrB_2 Dispersions in Al_2O_3 and Zircaloy-2, USAEC Report BMI-1627, Battelle Memorial Institute, Apr. 24, 1963.
11. S. F. Kaufman, Fabrication Development of Boron Carbide and Boron Carbide + Silicon Carbide Mixtures for Possible Application as Lumped Burnable Poisons in PWR-2, USAEC Report WAPD-244, Westinghouse Electric Corp., Bettis Atomic Power Laboratory, January 1964.
12. R. G. Gray and L. R. Lynam, Irradiation Behavior of Bulk B_4C and B_4C + SiC Burnable Poison Plates, USAEC Report WAPD-261, Westinghouse Electric Corp., Bettis Atomic Power Laboratory, October 1963.
13. J. W. Joseph, Jr., Evaluation of Tandem-Extruded Joints Between Zircaloy and Stainless Steel, USAEC Report DP-723, Savannah River Laboratory, June 1962.
14. J. W. Joseph, Jr., Irradiation of Tandem-Extruded Joints Between Zircaloy and Stainless Steel, USAEC Report DP-859, Savannah River Laboratory, October 1963.
15. W. B. Tuffin, A. R. Gilman, and S. Isserow, Tubular Stainless Steel-Zircaloy Transition Joints Prepared by Tandem Extrusion, USAEC Report NMI-7216, Nuclear Metals, Inc., Feb. 2, 1962.
16. P. Loewenstein and W. B. Tuffin, Metallurgical Bonding of Dissimilar Metals by Co-Extrusion, American Society for Metals Technical Report W4-3.2, 1964.

Section
V
Power Reactor Technology

Containment, Radiation Control, and Siting

Effect of Fission-Product Release

A report on the environmental hazard from fission-product releases has been issued by the United Kingdom Atomic Energy Authority.[1] The fission products included in the study are the same volatile fission products that would be expected to be released during a uranium fire, but they should not be much different from those expected during a fuel melt. The percentages of each isotope released are estimates obtained primarily from the Windscale accident.[2] The isotopes and elements involved and the percentage release of each used in the investigation are shown in Table V-1.

One part of the investigation was devoted to the determination of how the radioactivity would be dispersed in the atmosphere, with particular regard to conditions in the United Kingdom. The investigation indicated that Pasquill's extension of Sutton's theory of turbulent diffusion was the better representation of the dispersion, particularly at large distances. Briefly, Pasquill's method reduces the lateral and vertical spread of the Sutton theory cloud after a travel of 1 mile from the release point. For comparison of the effects of meteorological stability on the dispersion of radioactivity, two stability conditions were included in all environmental hazards evaluations. One was an average United Kingdom weather condition, and the other was an inversion condition, which in most cases represents the worst condition as far as dispersion is concerned. The effects of ground deposition on the cloud dosage and the amount of deposited activity were also investigated and included in the environmental hazard evaluations. Tests have shown that values for the "velocity of deposition" are in the range of 0.01 to 5 cm/sec, where the velocity of deposition, V_g, is defined as

$$V_g = \frac{\text{total deposited activity per unit area of ground}}{\text{cloud dosage}}$$

Analysis of the Windscale accident led to deposition velocities of 0.1 to 0.5 cm/sec. Any possibility of underestimating the cloud dosage was avoided by choosing a deposition velocity of 0.1 cm/sec for both stability conditions. For average weather conditions, the cloud dosage is indistinguishable from the $V_g = 0$ condition. For inversion conditions, deposition reduces the cloud dosage no more than a factor of 4 or 5 at 60 miles. In the deposited-activity calculations, deposition velocities were selected to give the maximum deposition at each particular distance from the release point. Deposition velocities used were 1 cm/sec for average weather conditions and 0 to 1 cm/sec for inversion conditions.

From the calculated cloud and ground concentrations, the following determinations were made:

1. Dosage as a function of distance from gamma and beta radiation released external to an individual from the cloud
2. Dosage from activity deposited on the ground
3. Dosage from activity deposited on the individual's skin
4. Internal dose rate from inhaled iodine, including the contribution from ^{132}Te
5. Hazards from food exposed to ^{131}I deposition, such as green vegetables
6. Hazards of consumption of milk and eggs that had been contaminated with ^{131}I
7. Inhalation and ingestion hazards of ^{137}Cs
8. Inhalation and ingestion hazards of ^{89}Sr and ^{90}Sr

9. A tentative assessment of the inhalation ıd ingestion hazards from ^{106}Pu, ^{140}Ba, and ^{4}Ce

10. Possible hazard from inhaled insolubles Sr, ^{106}Ru, and ^{144}Ce

On the basis of the Medical Research Council- commended dosages during emergencies here available), the maximum permissible ncentrations are reported for airborne radio- tive hazards. Also reported are the ground ncentration levels to give the maximum nergency dose rates either from direct con- ct or by eating foodstuffs that have been ntaminated. Included are descriptions of the tions required to safeguard the public from e hazards brought on by the activity release.

Table V-1 ELEMENTS OR ISOTOPES UNDER INVESTIGATION[1]

Element or isotope	Amount released, %
Bromine Krypton Xenon	60
^{132}Te	15
^{131}I, ^{132}I, ^{133}I, ^{134}I, ^{135}I	25
^{89}Sr, ^{90}Sr	0.1
^{106}Ru	4
^{137}Cs	15
^{144}Ce	0.15
^{140}Ba	0.2

In summary, the most important isotope re- ted to public health hazards following a re- tor accident is ^{131}I. Therefore all the other tivities are reported in terms of the ^{131}I tivity. Because ^{131}I has a half-life of eight ys, the deposition dose will have decayed fficiently in a few weeks to permit reoccupa- n of most of the affected area except those rtions which are contaminated by ^{137}Cs and r. The ^{137}Cs and ^{90}Sr portions of the area e expected to be much smaller than the rtions affected by the ^{131}I release.

All calculated data on the external and internal zards and on the areas of food contamination e presented in terms of the distance affected each isotope. Since the amount released pends on a number of variable factors, the magnitude of the release of all isotopes is specified for several levels of ^{131}I, ranging from 1 to 10^5 curies. The consequences of the various releases are discussed. In view of the maximum amount of ^{131}I that can accumulate in a reactor, it is evident that a complete release would be disastrous, and assurance of some retention of fission products is a matter of considerable importance.

Effect of Temperature on Fission-Product Deposition

A report has been published on the development of an analytical model to calculate the steady-state deposition of fission products from gas streams onto surfaces.[3] Included in the analytical procedure are the effects of nonisothermal regions on the steady-state deposition rate. A computer code is described which is used to evaluate the equations (derived in the report) representing the deposition. The report also gives sample results that are compared with experimental data. In general, the agreement of the experimental and analytical results for relative deposition in nonisothermal regions was reasonably good for ^{95}Zr, ^{103}Ru, ^{141}Ce, ^{140}Ba, and ^{132}Te. The experimental data for the deposition of ^{131}I were higher than was estimated by roughly a factor of 10. Although the reason for this disagreement was not fully explained in the report, the author states that it may have been caused by compound formation resulting from collision of iodine with the cold wall, with subsequent rapid condensation or deposition.

References

1. J. R. Beattie, An Assessment of Environmental Hazard from Fission-Product Releases, British Report AHSB(S)R-64, May 16, 1961.
2. H. J. Dunster, H. Howells, and W. L. Templeton, District Surveys Following the Windscale Incident, October 1957, *Proceedings of the Second United Nations International Conference on the Peaceful Uses of Atomic Energy, Geneva, 1958*, Vol. 18, pp. 296-308, United Nations, Geneva, 1958.
3. M. N. Ozisik, Effects of Temperature on Fission-Product Deposition, USAEC Report ORNL-3542, Oak Ridge National Laboratory, March 1964.

Section VI

Components

Power Reactor Technology

Pumps

The design and test of a diaphragm pump for use with liquid metals are described in Ref. 1. This type of pump is often used as a feed pump, where its high-pressure and low-capacity characteristics make it suitable for feeding solutions or slurries into the reactor system. Figure VI-1 is a schematic illustration of the pump as used for pumping liquid metals. The particular application of this pump was in the laboratory to pump a lead-bismuth eutectic within a test loop, although the pump is expected to have value for reactor applications.

The prime mover for the pump was a pulse generator utilizing hydraulic fluid to transmit the pulses to the first diaphragm. A NaK intermediate system then transmitted the pulses from the first diaphragm to the remote high-temperature diaphragm assembly, in which the diaphragm served to separate the NaK from the process fluid, which was lead-bismuth eutectic in the application described in Ref. 1. The remote head was designed to meet four requirements:

Operation at 300 to 600°C
No external or internal leakage of fluids
Ease of disassembly
Continuous operation for extended periods of time

As illustrated in Fig. VI-1, the remote head was of bolted construction and was designed to operate at 50 psig discharge pressure and 816°C. The diaphragm was 0.030 in. thick and was of type 446 stainless steel, as were the rest of the remote high-temperature components. Polished, raised bearing surfaces ensured adequate sealing between the rather massive components of the remote head and the diaphragm itself. The remote head was entirely immersed in a liquid bath for temperature-control purposes.

A key component of the pump was the valve assembly, which contained ball type check valves and seats. The 0.75-in.-diameter balls were of type 440 stainless steel, and the valve body was type 446 except for some type 316 tie bars. As illustrated in Fig. VI-1, the valve was operated with the direction of flow from top to bottom. This was done because the balls were of lower density than the pumped fluid (lead-bismuth eutectic) and thus would be normally positioned on the valve seats when the pump was not operating. The pressure-time curve was designed to be sinusoidal in nature so as to reduce accelerations of the fluid at the beginning and end of each stroke and promote quiet operation.

The pump was operated continuously for 5376 hr without difficulty at a eutectic temperature of 575°C, an outlet pressure of 20 psig, and a flow rate of 0.6 gal/min. On two occasions, however, the temperature was briefly reduced because of failure of the cooling-water supply to the low-temperature head. Postoperation examination revealed slight wear on the valve seats, but they still maintained a tight seal.

An interesting pump described in Ref. 2 is capable of pumping boiling fluids without damage due to cavitation or noise. Although the tests described in the reference were nominally at standard conditions, the operating principles seem equally applicable at elevated pressures and temperatures. Figure VI-2 gives cross-sectional views of the device.

The following quotation[2] serves to define the operating principles of the pump (the figure numbers have been changed to be consistent with this section):

> This pump is a two-stage centrifugal-displacement unit with one rotating element — a one-piece centrifugal rotor-impeller.[P] The first stage in-

---

[P] U. S. Patents Nos. 2,940,657 and 3,102,083.

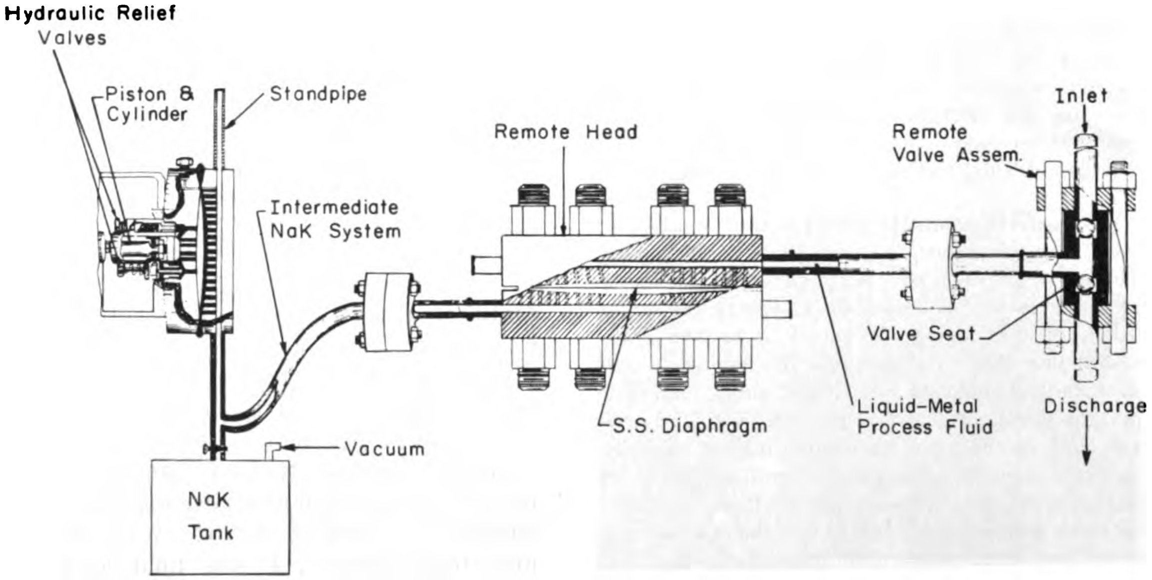

Fig. VI-1 Schematic illustration of a two-stage diaphragm pump.[1]

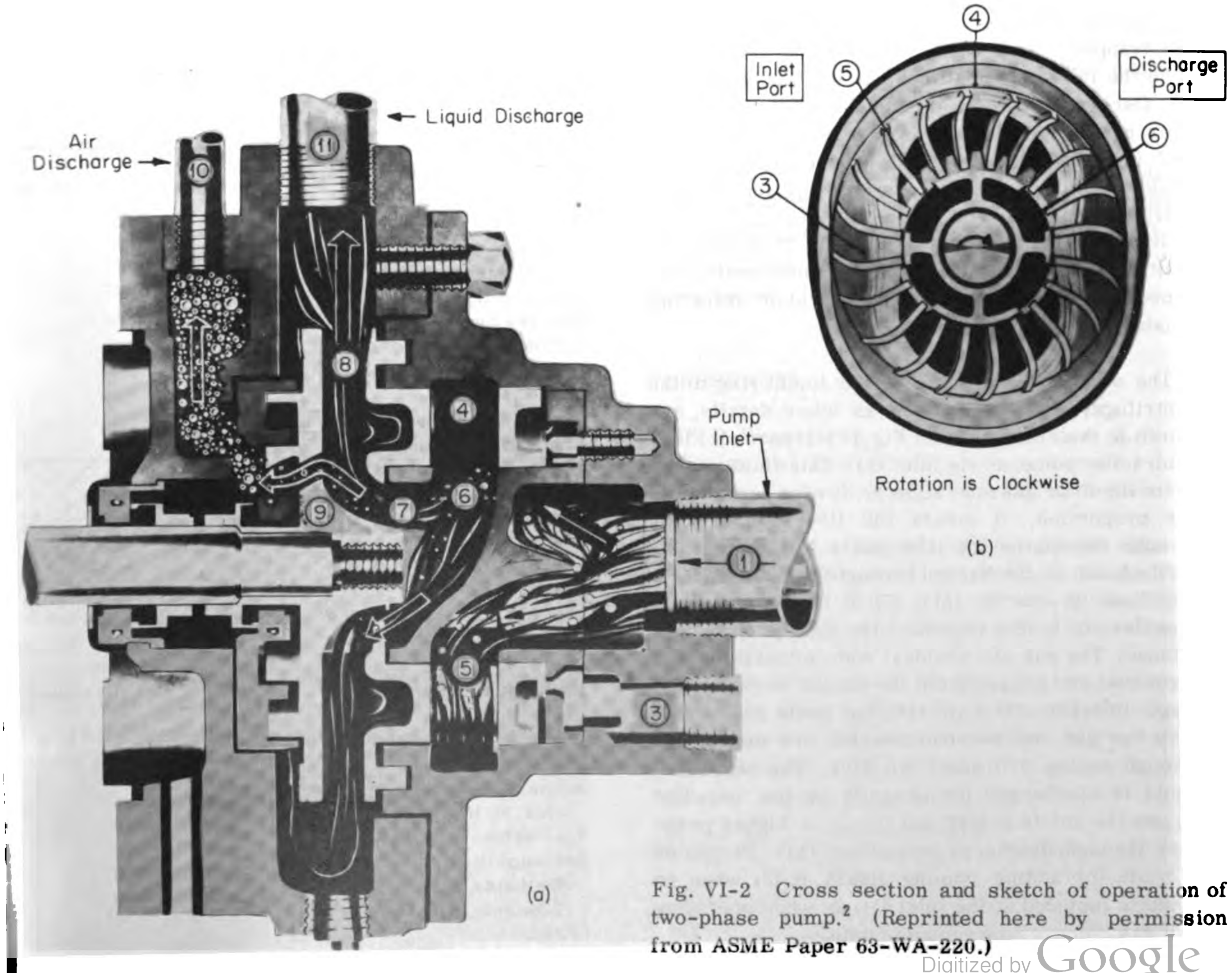

Fig. VI-2 Cross section and sketch of operation of two-phase pump.[2] (Reprinted here by permission from ASME Paper 63-WA-220.)

cludes a liquid-ring-principle compressor while the second stage is a centrifugal liquid pump. The unit has one inlet and two discharge connections, one for the second-stage discharge of liquid and the other for the interstage discharge of air or vapor. Other connections provide for liquid make-up when required, drains, and so on, Fig. [VI-2, part *a*].

The centrifugal-displacement action of a typical liquid ring compressor as used in the first stage is shown in Fig. [VI-2, part *b*]. A series of buckets in the rotor is full of liquid when leaving the minor radius of the casing, as shown at 3. The rotor throws this liquid out and into the casing as at 4, much as in a standard centrifugal pump, but after this, the similarity between the two ends. The central inlet to the rotor is ported instead of being open continuously, as in a centrifugal, and the outer casing curves inwardly to direct the liquid back into the rotor instead of delivering it to the conventional centrifugal pump casing discharge.

The centrifugal kinetic energy imparted by the rotor to each bucket of liquid in traveling from position (3) to (4) at first creates an outward piston or displacement action in each bucket. This action draws gas, vapor and/or liquid into the rotor as it passes the open inlet port (5). This liquid and vapor are trapped within each bucket and carried around from the inlet port position (5) to the discharge port (6). During the transit, the accelerated liquid ring, after passing station (4) is directed by the casing back into the rotor, where it expends its acquired liquid kinetic energy in compressing the trapped charge in each bucket and in discharging this centrally through the discharge port (6). Thus, a semi-positive displacement action is centrifugally obtained that will pump fluids of widely differing densities.

The staged relationship of the liquid ring to the centrifugal impeller, as well as other details, are shown in the cross section Fig. [VI-2, part *a*]. Fluid enters the pump at its inlet (1). This fluid may be in its liquid or gaseous state or it may be mixed in any proportion. It enters the first stage rotor through the stationary inlet ports (5), as just described, and is discharged through the central ports (6), directly into the inlet (7) of the second stage impeller (8). In this impeller, the fluid is first centrifuged. The gas and residual noncondensables are separated and escape from the center of the second stage impeller through rotating ports (9). From here the gas and noncondensables are discharged through casing connection (10). The separated liquid is discharged peripherally by the impeller (8) into the volute casing and thence to higher pressure through discharge connection (11). Provision is made for adding cooling liquid at (3) when no liquid is included at the inlet (1), as when operating as a gas compressor vacuum pump. The advantages of this pump are compared to those of other types of pumps, and a brief history of operating experience is included.

Heat Exchangers

The fabrication of the primary heat exchanger for the Molten-Salt Reactor Experiment (MSRE is discussed in Ref. 3. The molten fuel of the MSRE is pumped through the shell side of the exchanger, while nonfuel-bearing molten salt circulates through the tube side. Details on the heat exchanger are given in Table VI-1.

The major problem in the design of the heat exchanger seems to have been the tube-to-header joint, which experience had shown to be subject to cracking during cyclic service at high temperatures. In the final joint design,

Table VI-1 DESIGN DATA[3] FOR THE MSRE PRIMARY HEAT EXCHANGER

Structural material	INOR-8
Heat load, Mw	10
Shell-side fluid	Fuel salt
Tube-side fluid	Coolant salt
Layout	25% cut, cross-baffled shell and U tube
Baffle pitch, in.	12
Tube pitch, in.	0.775
Tube	
Outside diameter, in.	0.5
Wall thickness, in.	0.042
Active shell length, ft	6
Average tube length, ft (approximately)	14
No. of U tubes	163
Shell diameter, in.	16
Overall length, ft (approximately)	8
Tube-sheet thickness, in.	1½
Design temperature, °F	1300
Design pressure	
Shell, psig	75
Tube, psig	125
Terminal temperatures	
Fuel salt, °F	Inlet 1225; outlet 1175
Coolant salt, °F	Inlet 1025; outlet 1100
Exchange geometry	Parallel and counter flow
Effective log mean temperature difference, °F	133
Active heat-transfer surface area, sq ft	259
Fuel-salt holdup, cu ft	6.1
Pressure drop	
Shell side, psig	24
Tube side, psig	29

shown in Fig. VI-3, both welding and brazing are used so as to remove stress concentration near the weld area and provide support at the base of the weld. In addition, the brazing will reinforce defective welds, should any occur during fabrication.

The brazing alloy was 82 wt.% gold–18 wt.% nickel, and the welding electrode was thoriated tungsten. A number of test specimens were made so that optimum welding and brazing conditions could be studied, and the results of the tests are given in the reference. Fabrication of the full-size exchanger proceeded without apparent difficulty; Fig. VI-4 shows the exchanger positioned in the furnace pit. A cover was added and seal welded in place, and the assembly was brazed in a hydrogen atmosphere at about 1850°F. Final inspection included ultrasonic inspections in the braze areas after the tubes had been filled with water, a helium leak test, and an 800-psi hydrostatic test. No leaks were found.

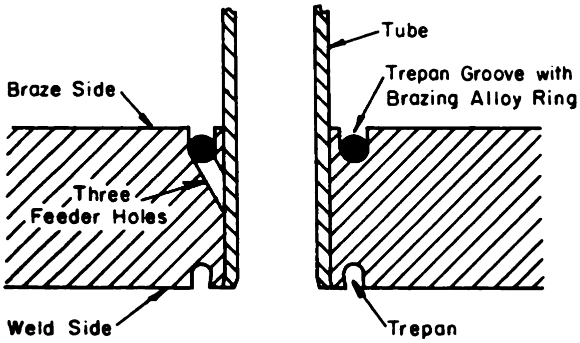

(a) Before Welding and Brazing

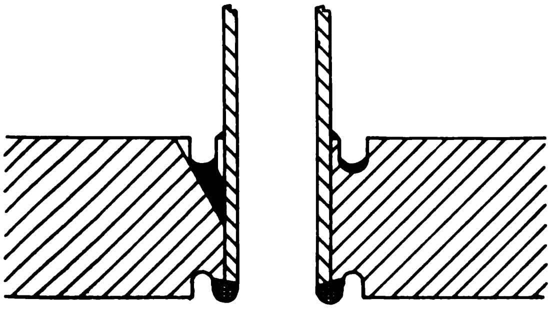

(b) After Welding and Brazing

Fig. VI-3 Schematic drawing of welded and back-brazed joint design for the MSRE heat exchanger.[3]

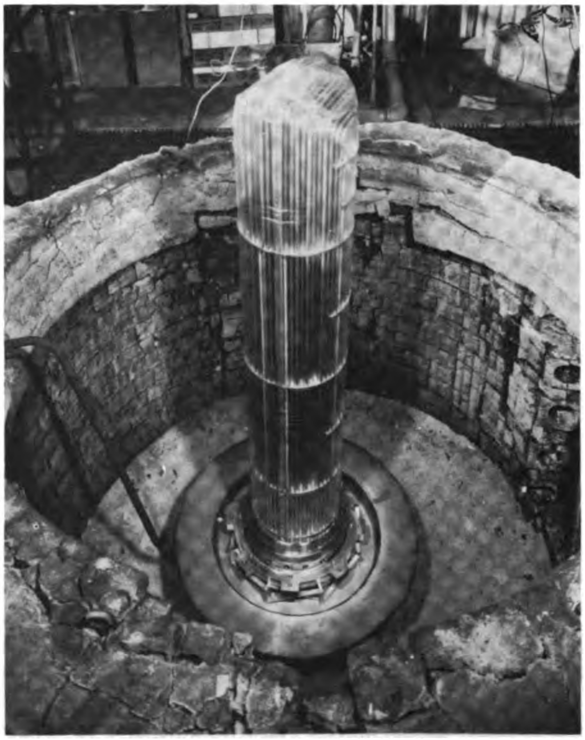

Fig. VI-4 Tube bundle of the MSRE heat exchanger positioned in furnace pit prior to brazing.[3]

REFERENCES

1. D. E. Westerheide, J. C. Clifford, and G. Burnet, Design and Test of a Diaphragm Pump for Liquid Metals, *Nucl. Sci. Eng.*, 17(4): 523-527 (December 1963).
2. H. E. Adams, Pumping Boiling Fluids When the Available Static Head is Zero or Less, Paper ASME No. 63-WA-220 presented at the Winter Annual Meeting, Philadelphia, Pa., November 17–22, 1963.
3. R. G. Donnelly and G. M. Slaughter, Fabrication of the Heat Exchanger Tube Bundle for the Molten-Salt Reactor Experiment, USAEC Report ORNL-3500, Oak Ridge National Laboratory, Dec. 9, 1963.

Section VII

Power Reactor Technology

Design Practice

EGCR Control Rods

Control rods that are sufficiently flexible to move in bowed channels have been developed for the Experimental Gas-Cooled Reactor (EGCR). The design and thermal analysis of the rods are described in detail in Ref. 1, a recent ORNL report.

The requirement for a rod capable of moving in a bowed passage is brought about by the dimensional changes that are anticipated in the graphite-moderator structure of the EGCR. The 21 control rods, which are placed on 24-in. centers throughout the core, move in 4-in.-diameter channels. The channels are located principally at intersections of graphite columns. Some of the physical relations that exist between the core, the pressure vessel, and a control rod and its drive mechanism are illustrated in Fig. VII-1. Although restraint bands are shown around the graphite columns that form the moderator structure, the control-rod channels will become bowed because of nonuniform graphite shrinkage induced by fast-neutron flux gradients across the core. If the graphite blocks do not crack, the restraint bands should limit the maximum bow to about 1 in.; the blocks may crack, however, and an offset in the rod channel could result. In addition to the irradiation-induced dimensional changes, thermal and pressurization effects may cause misalignment of the channels.

The required diameter for the EGCR rods is 3.25 in. Their normal rate of movement is 1.8 in./min, and the maximum velocity reached during the free-fall portion of a scram is about 18 ft/sec. As shown in Fig. VII-1, the rods are suspended on stainless-steel cables that are connected to drive mechanisms located near the top extension of the rod nozzles. A shroud tube, hung from the nozzle at the pressure-vessel head, guides each control rod into its core channel and holds one portion of the rod shock absorber. Consequently the shock load involved in stopping a free-falling control rod is borne by the pressure vessel.

The rod design, which evolved from considerations of the rather stringent design requirements, is a particularly interesting one. An articulated design was adopted to achieve a very long rod capable of moving in a bowed channel. Boron carbide (B_4C) was chosen as the nuclear poison, principally because of the required 20-year lifetime of the rod. Also, to avoid the problems that may occur with external cooling of rods that can become eccentric in their channels, the rods are provided with internal, forced-circulation cooling. In addition to meeting the design requirements that the control rods be compatible with the high-pressure-helium reactor environment and that the cladding material be compatible with the core and shroud structural materials, the rod designers were called on to provide a diffusion barrier (see Sec. IV of this issue of *Power Reactor Technology*) between the boron carbide poison material and the rod cladding material to prevent the high-temperature reaction that occurs between boron and nickel. The final design of the rod, shown in Fig. VII-2, is described in the next paragraph by a paraphrased excerpt from Ref. 1.

The 3.25-in.-diameter rod has a poisoned length of about 15 ft and an overall length of about 20 ft. The rod is made up of four segments that are supported by an internal rod of type 347 stainless steel; the bottom three segments, which comprise the poison section of the rod, contain annular rings of hot-pressed B_4C. The B_4C is contained in type 304 stainless-steel-cladding tubes, and all surfaces of the stainless steel which contact the B_4C are copper plated to prevent the high-temperature boron-

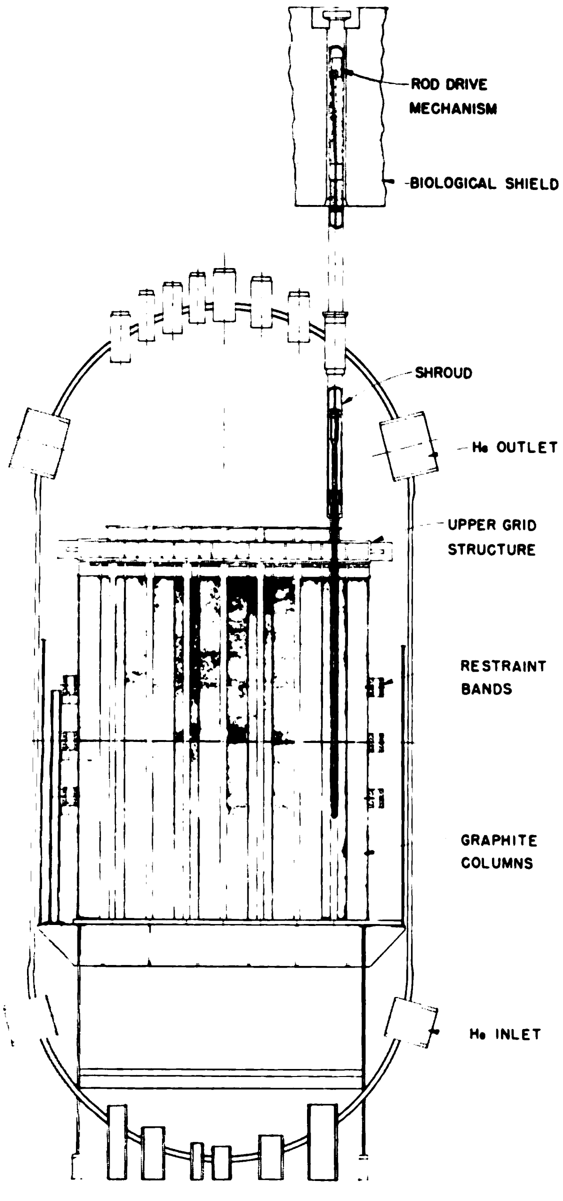

Fig. VII-1 Vertical section through the EGCR core.[1]

nickel reaction mentioned in the preceding paragraph. Flexibility of the overall assembly is achieved by elastic bending of the central rod between spacer support plates, whereas the segments of the rod can move relative to one another by means of connecting ball-and-socket joints. One face of each ball-and-socket joint is overlaid with Hastelloy C to prevent self-welding. The woven stainless-steel filter attached to the top of each poison segment of the rod vents the inner volume of the segment to the reactor, thereby equalizing pressures and avoiding the pressure differentials that could exist because of helium-gas generation in the B_4C during irradiation. The rod segments are kept in contact at their ball-and-socket joints by a top Inconel X compression spring; the joints maintain an essentially leaktight flow channel for the internal, forced-circulation coolant. The Inconel X spring and a top slip joint accommodate the relative movement that will occur between the central support rod and the tubing caused by differential thermal expansion during normal operation.

The forced-circulation helium coolant for each rod assembly enters the control-rod nozzle at the top, flows down over the rod-drive mechanism, then down the shroud, and into the center of the control rod. The wire-brush seal, shown at the top of the assembly in Fig. VII-2, prevents bypassing of the cool helium directly into the top plenum of the reactor and ensures that it flows into the center of the rod assembly. Tests of a mockup control rod showed that these wire brushes and the ball-and-socket joints between rod segments are effective seals and that the rod coolant is channeled down the interior of the rod as intended.

No major problems were encountered in manufacturing the 21 rods required in the EGCR. The finished rods weighed between 137 and 142 lb.

SRE Rod Drop-Time Measurement

A system has been developed for determining the scram, or drop, times of the safety rods in the Sodium Reactor Experiment (SRE). Total drop time of the top-driven SRE rods consists of two components: the time during which the rod is in free gravity fall into the core, and the time during which a snubbing effect slows and stops the rod at the end of the fall. If the free-fall component of total drop time is measured and then compared with calculated free-fall time, mechanical interference with rod insertion, such as that caused by warpage of the thimble in which the rods move, can be detected. Satisfactory operation of the piston-cylinder snubber, which must stop the rods without damaging them, can be verified by measuring the second, or snubber, component of total drop

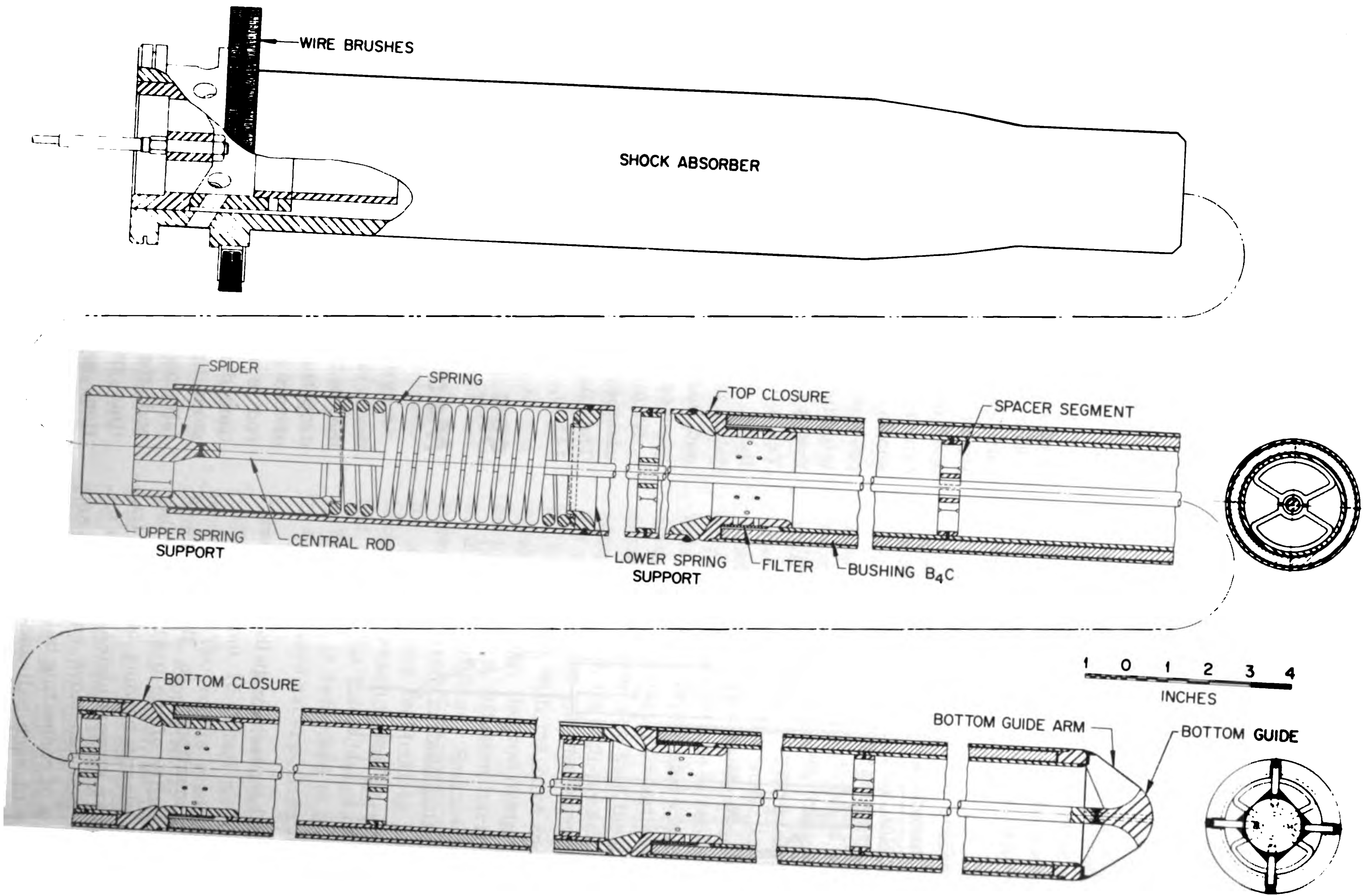

Fig. VII-2 Details and general arrangement of segmented EGCR control rod.[1]

time. The system developed for the SRE is capable of measuring each time component; furthermore, the time required is short enough that the measurements can be performed routinely.

A conceptual drawing of the SRE timing system is shown in Fig. VII-3. In this drawing a safety rod is shown held in the fully withdrawn position by an electromagnet. When the reactor is scrammed, the energizing current to the electromagnet is interrupted, and the rod, with the snubber piston at its uppermost end, falls downward into the core. As the rod nears the bottom of its stroke, the snubber piston is guided into a snubber cylinder by the tapered section of the drive housing shown in Fig. VII-3. When the rod reaches its fully inserted position, the snubber piston actuates a limit switch which indicates that the rod has reached the full-in position. As shown in the figure, the SRE timing system utilizes two timers to measure the individual components of the total scram time. When a scram is initiated and the current to a safety-rod holding magnet is interrupted, the first time-interval meter is triggered. At the entrance to the snubber cylinder, an electromagnetic pickup is actuated by the snubber piston and generates a signal that stops the first electronic timer and starts the second. The second timer is stopped when the snubber piston actuates the down-limit switch at the bottom of the snubber cylinder. Thus the free-fall component of total drop time and the snubber component of total drop time are measured.

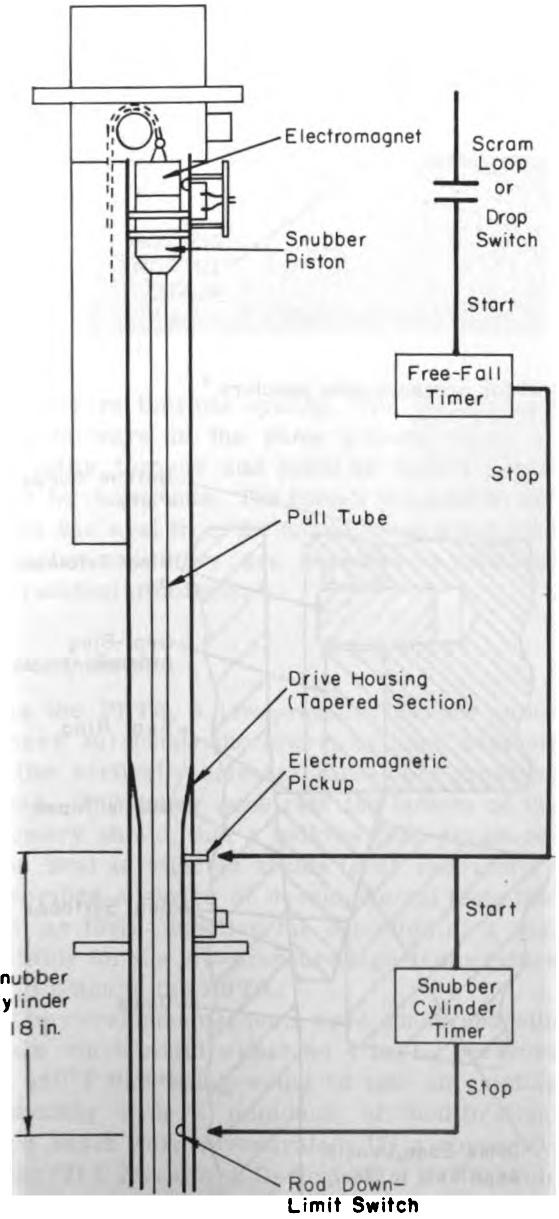

Fig. VII-3 Mark II safety rod and timing circuit of the SRE.[2]

The timing-system panel is mounted in the reactor control room, and complete drop-time measurements for the four safety rods of the SRE can be made at this panel by one person in less than 10 min. The snubber time and free-fall time are displayed directly in units of time on four-decade lighted dials on the two timers. The timing system appears to be one that would be adaptable to various reactors.

Pressure-Tube Reactor Components

Dome-Seal Tube Closure

During the period 1957 to 1958, when studies of high-performance nozzle closures for the pressure tubes of the Plutonium Recycle Test Reactor (PRTR) were undertaken, a dome type nozzle seal was conceived. The seal was subsequently developed and used in the PRTR gas loop at service conditions of 1500°F and 500 psi. Reference 3 is a description of recent work directed toward determining the suitability of the dome seal as an alternate pressure-tube nozzle closure for the heavy-water-cooled CANDU reactor. As a result of the developmental work on the dome type closure, it was concluded that

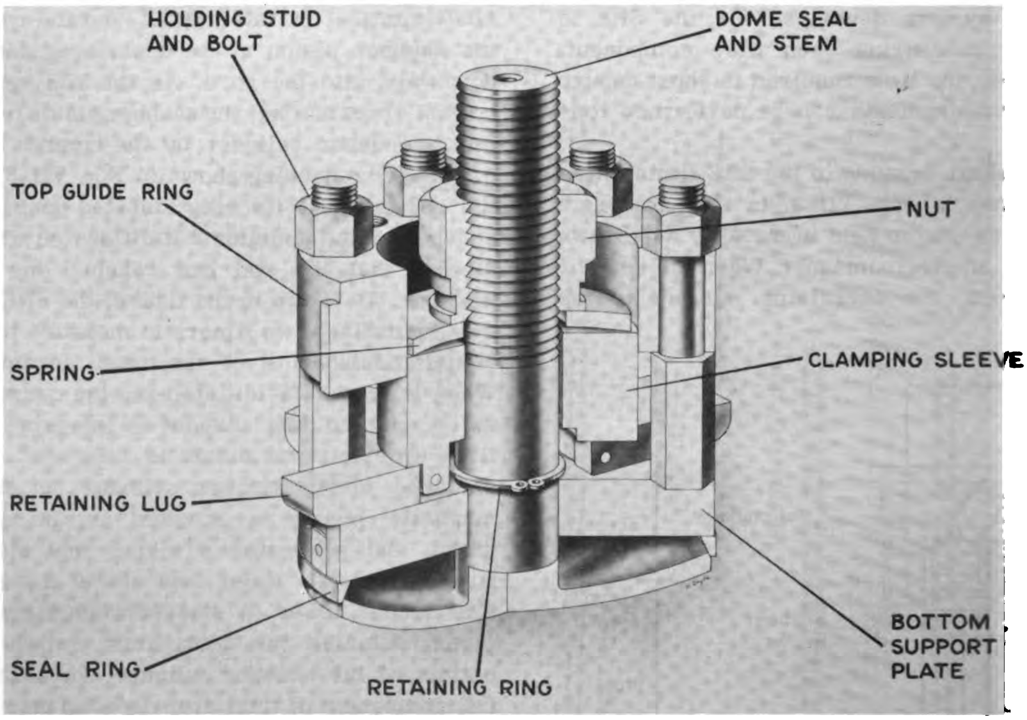

Fig. VII-4 Cutaway view of the dome seal for pressure-tube reactors.[3]

the closure is a promising type for high-pressure high-temperature water applications.

A cutaway view of the dome seal is given in Fig. VII-4. The entire assembly shown in the figure is inserted into the end of the open pressure tube to be sealed. In the simplest terms the operation of the seal can be described as follows: the large nut that is threaded to the dome-seal stem is tightened, thereby deflecting the dome and causing it to exert pressure on the seal ring. The sealing action of the assembly is illustrated in Fig. VII-5, which shows the principal components involved in the sealing process. The load exerted by the dome on the seal ring causes the ring to yield locally and effect the seal. A Belleville-spring washer installed between the dome-stem nut and the clamping sleeve, as shown in Fig. VII-4, allows the dome to expand when heated while permitting forces high enough for effective sealing in the cold condition. A schematic representation of the deflection of the dome, both with and without the Belleville spring, is shown for the cold and hot conditions in Fig. VII-6.

The dome seal did not leak during a test program that included steady-state operation, frequent assembly-disassembly operations,

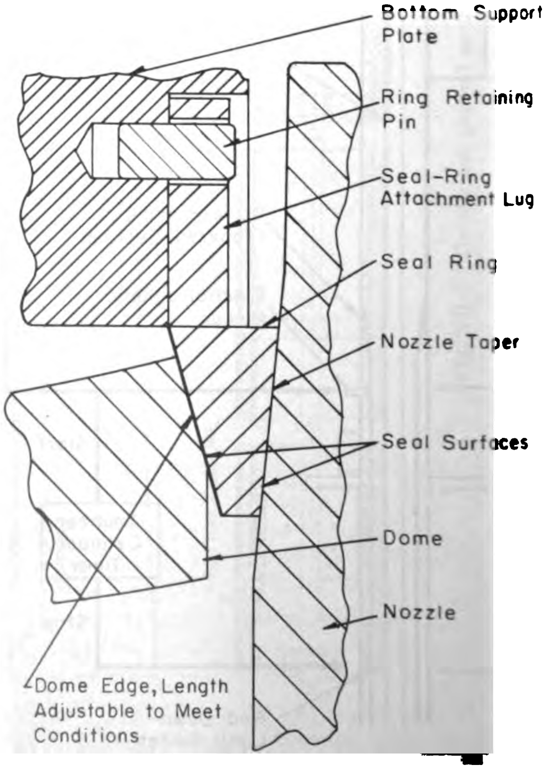

Fig. VII-5 Schematic of [illegible] dome seal.[3]

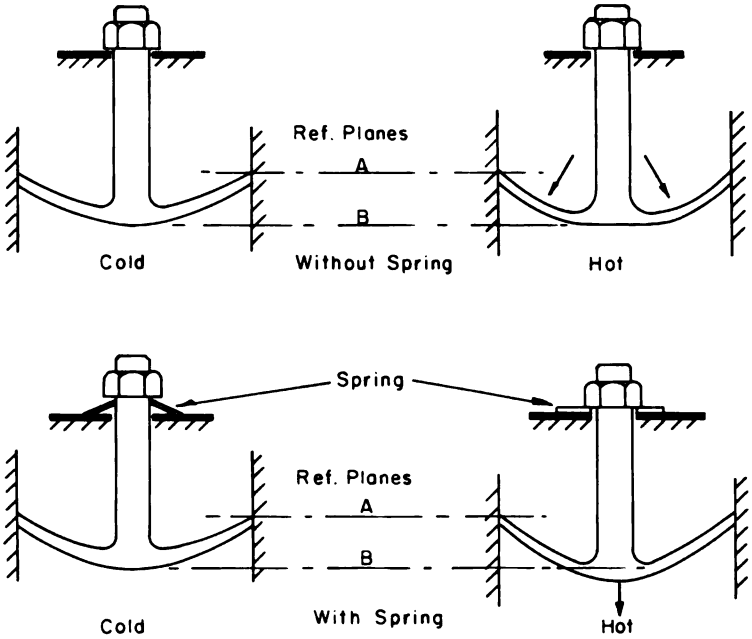

Fig. VII-6 Theory of dome deflection with and without Belleville-spring washer.[3]

and severe thermal cycling. The disassembly torques were in the same general range as assembly torques and could be varied somewhat by lubricants. The forces required to remove the seal from the nozzle were lower than expected, and they are expected to cause no operational problems.

Helium Seals

In the PRTR, a low-pressure helium atmosphere surrounds the lower, or inlet, sections of the vertically oriented Zircaloy-2 pressure tubes. The tubes penetrate the bottom of the primary shield, and a bellows type pressure-tube seal is effected at this level. Reference 4 describes a series of developmental tests that had as their objective the selection of a seal suitable for the low-pressure high-temperature application in the PRTR.

The developmental tests were concerned with seals which could withstand 4 in. Hg pressure at 480°F and which would fit into an existing assembly with a minimum of modification. Five seals were investigated: (1) a copper O-ring; (2) a Zircaloy-2 D-ring; (3) a B-F ferrule seal; (4) a stainless-steel, pressurized O-ring; (5) a Zircaloy-2 O-ring. The results of the seven tests performed (three utilized the Zircaloy-2 O-rings) are given in Table VII-1. Although the B-F ferrule seal shown in Fig. VII-7 was the most effective of those tested, the Zircaloy-2 O-ring shown in Fig. VII-8 was chosen for use in the PRTR because of its lower cost and easier installation in the existing reactor components. The following are observations on the different seal tests taken from Ref. 4.

1. Copper O-ring. Low leak rates were obtained at the beginning and ending of each cycle; maximum leak rates were at operating temperatures. Low leakage was measured during the first cycle but rapidly increased during subsequent cycles.
2. Zircaloy D-ring. Maximum leak rates were 270 and 266 liters/hr during the first two cycles. Because of these excessive rates, testing was terminated.
3. B-F Ferrule. After the first three tests, the test assembly was disassembled. Later it was reassembled and Tests 4, 5, and 6 were run. This seal had the lowest leakage of any tested. However, the shape is complex and the fabrication cost is relatively high. Maximum leak rates were obtained during the cooling portion of the cycle.
4. Stainless Steel O-ring. A good seal was obtained with the silver-coated pressurized ring during the first two cycles, but leakage increased as the number of cycles increased. Maximum leak rates were measured at steady-state conditions.
5. Zircaloy-2 O-ring. This seal had a diametrical clearance of 0.002 in. and was used with a standard PRTR flange. Leakage was low on all tests with a tendency for leak rates to decrease as cycles

Table VII-1 AVERAGE HELIUM LEAK RATES OF FIVE SEALS TESTED FOR PRTR,[4] LITERS PER HOUR

	Cycle 1	Cycle 2	Cycle 3	Cycle 4	Cycle 5	Cycle 6
Copper O-ring (standard PRTR flange; makeup torque, 30 in.-lb; 6/20/62, 6/21/62, 6/22/62; pressure, 2.0 to 3.0 in. Hg)	0.020* 0.180†	2.900* 0.880†	12.30* 2.43†	44.50* 17.00†	61.80* 14.05†	
Zircaloy-2 D-ring (special flange; makeup torque, 30 in.-lb; 6/5/62, 6/13/62)	55.0* 141.0†	144.0* 161.0†				
B-F ferrule seal (makeup torque, 15 in.-lb; 6/15/62, 6/16/62, 7/3/62; pressure, 2.0 to 3.0 in. Hg)	2.48* 2.68†	1.02* 1.239†	1.001* 1.29†	0.075* 0.381†	0.0901* 0.385†	0.127* 0.48†
S.S. pressurized O-ring (standard flange; makeup torque, 15 in.-lb; 6/15/62, 7/2/63; pressure, 2.0 to 3.0 in. Hg)	0.248* 0.350†	0.168* 0.330†	13.7* 6.70†	31.21* 7.1†		
Zircaloy-2 O-ring (standard flange; ID, 2.0574 in.; 10/4/62 to 10/5/62; makeup torque, 27 in.-lb; disassembly torque, 15 to 20 in.-lb; pressure, 3.8 to 4.4 in. Hg)	1.42* 1.61†	1.32* 1.45†	1.12* 1.33†	1.13* 1.45†		0.728* 1.00†
Zircaloy-2 O-ring (relieved flange; same O-ring as Test 5; 10/10/62; makeup torque, 30 in.-lb; disassembly torque, 15 to 20 in.-lb; pressure, 3.8 to 4.2 in. Hg)	1.830* 1.40†	0.925* 1.21†	0.735* 1.11†	0.616* 0.980†		
Zircaloy-2 O-ring (standard flange; ID, 2.059; makeup torque, 30 in.-lb; disassembly torque, 20 to 25 in.-lb; pressure, 3.8 to 4.2 in. Hg)	0.704* 1.18†	0.680* 0.995†	0.600* 0.940†	0.785* 1.07†		0.612* 0.935†

*Steady-state and rising-temperature conditions.
†Falling-temperature conditions.

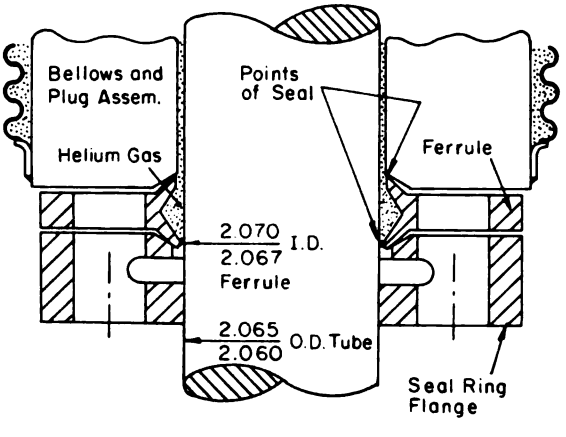

Fig. VII-7 Cross section of ferrule seal.[4]

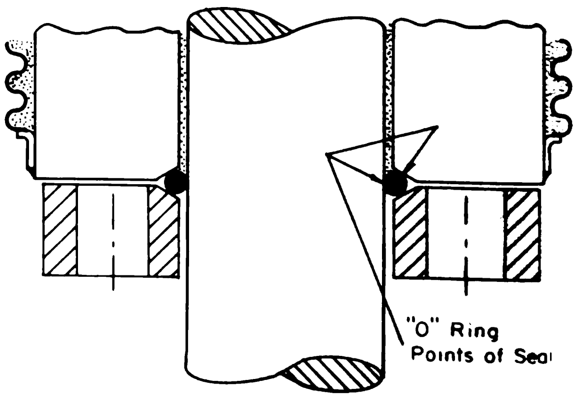

Fig. VII-8 Cross section of the PRTR Zircaloy-2 O-ring seal.[4]

increased. Small leak rates were noted during heating and steady-state conditions and maximum rates occurred during cooling.

6. Zircaloy-2 O-ring. This test was to determine the effect of a modified flange. The modification was a circumferential groove on the ID, designed to allow cantilever flexing of the flange lip. The O-ring was unchanged from Test Number 5. No significant improvement in leak rate was observed.

7. Zircaloy-2 O-ring. This test was to determine whether maximum allowable reactor tolerance conditions would adversely affect the low leak rates obtained in Test Number 5. An O-ring with a diametrical clearance of 0.015 in. was tested successfully with no significant change in results; that is, (*a*) low leak rates, (*b*) lower leak rates as cycles increased, and (*c*) maximum leakage during cooling.

Surge Suppressors in Flow-Monitor Sensing Lines

One advantage of pressure-tube reactors is the relative ease with which coolant flows and temperatures in individual process channels can be measured. In the PRTR, each of the 85 process channels is provided with flow-monitoring equipment capable of furnishing a visual readout of the flow rate in the channel, providing an electrical signal for recording, and supplying a signal to the safety circuit that initiates a reactor scram on receipt of a high-flow or low-flow signal. The flow-monitoring equipment for each process channel includes a Venturi flowmeter in the inlet piping, sensing lines containing valves, and a flow transmitter. Reference 5 gives details of an experimental program that was undertaken to devise means of reducing oscillations encountered in the PRTR flow monitors. The following quotation[5] describes the problem:

> During startup of the PRTR, it was found that the readings of flow meters on those pressure tubes which connect near the inlet of the bottom ring header were fluctuating excessively. The fluctuations were as much as ±8% which is nearly as large as the ±10% span between the high and low flow trips. When superimposed on the normal reactor flow changes, the fluctuations would cause spurious flow trips. During preliminary testing, the meter fluctuations were reduced by throttling the valves in the sensing lines from the flow venturi to the flow meter. This was recognized as being unsatisfactory for a permanent solution since this practice introduces an unknown variable lengthening of the response characteristics of the meter. It also introduces an error of unknown magnitude due to the nonuniform flow passage in the valve seat when throttled. An experimental program was therefore undertaken to determine the degree of valve throttling which might be appropriate for fluctuation suppression and to devise other and better methods of suppression.

The experimental program led to the conclusion that throttling of valves in the flow-transmitter sensing lines is not a satisfactory way of decreasing the fluctuations, principally because the flow indications are extremely sensitive to valve position and because there is a very narrow range of usable positions. A satisfactory method of damping the oscillations is to increase the hydraulic flow resistance in the pressure-sensing lines by installing (for the PRTR case) 3- to 4-ft lengths of $^1/_{16}$-in. tubing.

The addition of the short lengths of small-diameter tubing to the pressure-sensing lines in the PRTR flow-monitoring system has caused the flow transmitter to have time-response characteristics similar to those illustrated by curve *B* of Fig. VII-9. This curve, which is nearly critically damped, can be seen to reflect a happy medium between the time-response characteristics illustrated by curve *A*, in which the underdamped or oscillatory system has a fast response but also a very large overshoot, and the time-response characteristics shown by curve *C*, which is representative of an overdamped system in which the response is so slow that the system is unsatisfactory.

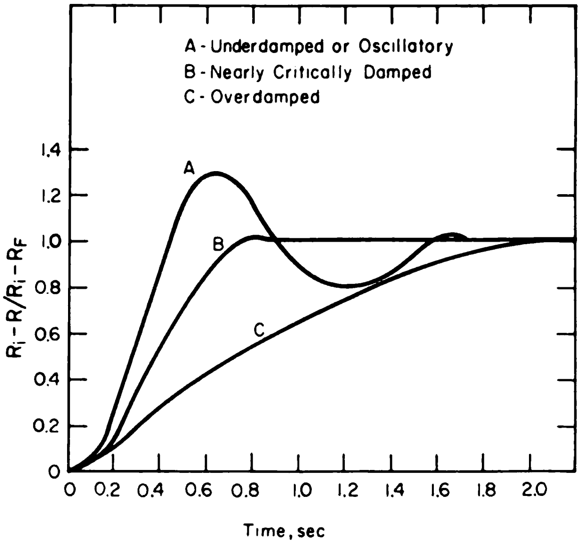

Fig. VII-9 Typical PRTR flow-transmitter response curves. R = transmitter reading, R_i = initial transmitter reading, and R_F = final transmitter reading.

Systems Design

Pathfinder Recirculation-Piping Design

A forced-recirculation mode of operation is employed for the reactor of the Pathfinder Atomic Power Plant. The recirculation system, which is described in some detail in Sec. VIII of *Power Reactor Technology,* 7(3), consists basically of three parallel coolant loops, each with a single mixed-flow centrifugal pump. Calculations and analyses to determine flexibility, vibration, and stresses in the loops are reported in Ref. 6. The majority of the information presented in the reference treats rather routine calculational methods and the results obtained by applying these methods. However, one interesting section is devoted to a description of the analysis performed to determine discontinuity stresses at dissimilar metal joints. These temperature-induced stresses occur in the primary loop piping at the junction between solid stainless-steel piping and stainless-steel-clad carbon piping. The joint was described in the above-mentioned *Power Reactor Technology* article.

LCRE Auxiliary Systems

The Lithium-Cooled Reactor Experiment (LCRE), which was to be located at the National Reactor Testing Station, was conceived as a test for a lithium-cooled high-temperature 10-Mw reactor. Reference 7 describes the functional design of the LCRE auxiliary systems and the development work and tests that were completed, in process, or planned at the time the program was canceled. The report, which is well organized and satisfyingly complete, gives the procurement and fabrication status of the auxiliary systems and includes manpower and cost expenditures and estimates. An indication of the degree of completeness which the author of Ref. 7 has attained in the report is given by the inclusion of a section in which all drawings associated with the LCRE auxiliary systems are listed, are grouped by systems, and are coded to indicate status, source, and use. The auxiliary systems include all reactor systems except the main liquid-metal coolant loops and the reactor control and safety systems.

References

1. J. W. Michel, Design and Thermal Analysis of EGCR Control Rods, USAEC Report ORNL-350, Oak Ridge National Laboratory, March 1964.
2. J. G. Radcliff, Design and Development of the Safety-Rod Drop-Time Test System, USAEC Report NAA-SR-7880, Atomics International, Oct. 31, 1963.
3. D. H. White, Dome Seal Performance Tests, USAEC Report HW-79205, Hanford Atomic Products Operation, November 1963.
4. D. H. White, Tests on Reactor Helium Seals—PRTR Inlet, USAEC Report HW-76008, Hanford Atomic Products Operation, December 1963.
5. G. M. Hesson, W. L. Thorne, and J. M. Batch, Surge Suppressors for the PRTR Process Tube Meters, USAEC Report HW-70711(Rev.), Hanford Atomic Products Operation, May 1963.
6. D. J. Nolan and J. F. Patterson, Pathfinder Atomic Power Plant. Recirculation Piping Design, USAEC Report ACNP-63026, Allis-Chalmers Mfg. Co., Jan. 10, 1964.
7. H. J. Banach (Comp.), LCRE Auxiliary Systems Termination Report, USAEC Report PWAC-416, Pratt & Whitney Aircraft, Division of United Aircraft Corp., Mar. 9, 1964.

Section

VIII

Power Reactor Technology

Operating Experience

Moderator-Level Control

By Walter Mitchell III

Regulation of moderator height can be an attractive means of reactor control. Among the advantages enjoyed by the level-control system are its lack of strong control rods and, except for possible shim elements, any in-core hardware. Consequently local flux perturbations are small, and the reliability of the system is enhanced by not having crucial components in the reactor-core environment.

A reactor must have a fluid moderator to be able to use level control. Although several reactor types fulfill this requirement, there are many other considerations that limit the practical use of level control. A reactor that has a hydrogenous moderator, for example, is not a likely prospect for such a control scheme because the short neutron-migration length in its moderator material makes the reactivity of the system extremely sensitive to level variations. Furthermore, in a reactor without some sort of segregation between primary coolant and moderator, it is hard to assure that coolant flow is provided to the fuel elements regardless of moderator level.

The basic considerations mentioned above indicate rather strongly that the heavy-water-moderated pressure-tube reactor is the single type currently being developed which can use moderator-level control. Even within this fairly specific reactor category, however, the ease with which level control can be employed and its degree of usefulness vary. If the heavy-water-moderated pressure-tube reactor is to retain its identity as a machine in which the high-pressure components are small (i.e., pressure tubes instead of a large pressure vessel), then the temperature of the moderator must be low. If high temperatures were permitted, the moderator pressure would have to be high to prevent bulk boiling, and the moderator tank would have to embody the undesirable features of a reactor pressure vessel. Also, the usual negative reactivity effect associated with an increase in temperature indicates the desirability of a relatively cool heavy-water moderator. If it is accepted that the moderator will operate at a temperature some several hundred degrees Fahrenheit below that of the primary coolant (which must be quite hot if the plant is to produce decent steam), then there must be a thermal-insulation barrier between the two. By his placement of this insulation, the designer selects one of the two basic variations of the heavy-water-moderated pressure-tube reactor. This selection affects to some extent the ease with which moderator-level control can be incorporated in the design. One variation has internally insulated pressure tubes that are immersed in the relatively cool moderator, thereby earning the title "cool tube." The other basic variation permits contact between the hot primary coolant and the pressure tubes but limits heat conduction to the moderator by providing an insulating gap between the pressure tube and the cool moderator, which is contained in a calandria type tank. It is to this second variation that level-control schemes are more easily applied because consideration need not be given to the external cooling of pressure tubes during normal operation. Thus, for simplicity and general applicability, the heavy-water-moderated reactor using a calandria type tank with gas-gap insulation around the pressure tubes is a logical choice for reactivity control by means of moderator-level regulation.

Two operating heavy-water reactors of the type described above, the U. S.'s Plutonium Recycle Test Reactor[1] (PRTR) and Canada's Nuclear Power Demonstration[2] (NPD) reactor, utilize moderator-level regulation as the primary means of reactivity control. In the following paragraphs the designs of these reactors are described, and operating experience with their level-control systems is discussed. Both plants are relatively small because they have thermal powers of less than 100 Mw. Units of this size can employ level-control schemes that are somewhat simpler, and at the same time more useful, than those applicable to large reactors. Large-reactor installations are discussed later in this article, with the CANDU control system used as an example.

Plutonium Recycle Test Reactor

The PRTR is a vertical pressure-tube type reactor that is moderated with heavy water and cooled by pressurized heavy water. The reactor has a thermal power of 70 Mw, and, although the plant does not produce electric power, the primary-circuit temperature and pressure conditions are typical of those which might exist in power reactors of this type. The primary coolant enters the core at 478°F, leaves at 530°F, and is maintained at a nominal pressure of 1050 psig. The arrangement of the major components of the reactor is shown in Fig. VIII-1, which illustrates the placement of the 85 Zircaloy-2 process tubes relative to the aluminum calandria type tank that contains the heavy-water moderator. In addition to the pressure tubes and 13 flux-monitor channels, the core region contains channels for 18 shim assemblies whose active elements will be described later. Full-core-length fuel assemblies are placed in the Zircaloy-2 process tubes and consist of bundles of rod type elements or of a concentric assembly containing a central fuel rod surrounded by two concentric fuel tubes. Several types of nuclear fuel material, including aluminum-plutonium alloys, UO_2, and a mixture of PuO_2-UO_2, have been used, and Zircaloy-2 has served as cladding material.

As shown in Fig. VIII-1, the calandria of the PRTR consists of several sections or compartments. The calandria is about 115 in. high and has a central, cylindrical section which contains the moderator and which is pierced by 85 vertical tubes forming dry channels for the primary-system pressure tubes. The space between the calandria tubes and the pressure tubes provides the gas-gap thermal insulation mentioned earlier. An annular compartment about 2 ft thick surrounds the 7-ft-diameter moderator portion of the calandria and contains a heavy-water reflector. The reflector and moderator systems are separate, and the reflector is held at a constant level in the reactor.

The annular reflector extends downward to a point about 2 ft above the bottom of the calandria. The bottom 2 ft of the annulus around the moderator cylinder forms a dump chamber that houses a circular weir over which the moderator flows in leaving the reactor core.[3] During an emergency shutdown of the reactor, caused by removing the heavy-water moderator from the calandria, the dump chamber serves as a temporary holdup volume that permits a rapid initial decrease in moderator level and, consequently, a rapid decrease in the reactivity of the system. Four large vertical lines connect the dump chamber to a moderator storage tank that is located beneath the reactor. Four additional lines of the same diameter connect the storage tank with the helium-gas space above the moderator in the calandria. One of the four lines that connect the dump chamber to the moderator storage tank is set flush with the base of the chamber and accommodates the normal flow of heavy water which spills over the circular weir. The other three lines are called the bottom gas lines and extend upward in the dump chamber to various heights. During normal operation these three lines equalize helium-gas pressure between the dump chamber and the storage tank. When the moderator is dumped from the calandria, the bottom lines facilitate escape of the helium from the dump chamber, thereby permitting the chamber to fill rapidly with heavy water; the lines then provide flow paths through which the moderator drains to the storage tank. The four lines that connect the moderator storage tank to the gas space above the moderator in the calandria are called the top gas lines, and each contains a fast-acting dump valve that is held closed during normal operation. The top gas lines, the bottom gas lines, and the fast-acting valves form the basis for the rapid moderator dump that scrams the reactor. During normal operation the moderator is held in the calandria by a differential gas pressure between the dump chamber and the blanket-gas space in the top of the calandria. When the fast-acting dump valves are opened, the gas pressure above the moderator in the calandria is equalized with that in the storage tank and dump chamber, and therefore the moderator falls from the calandria.

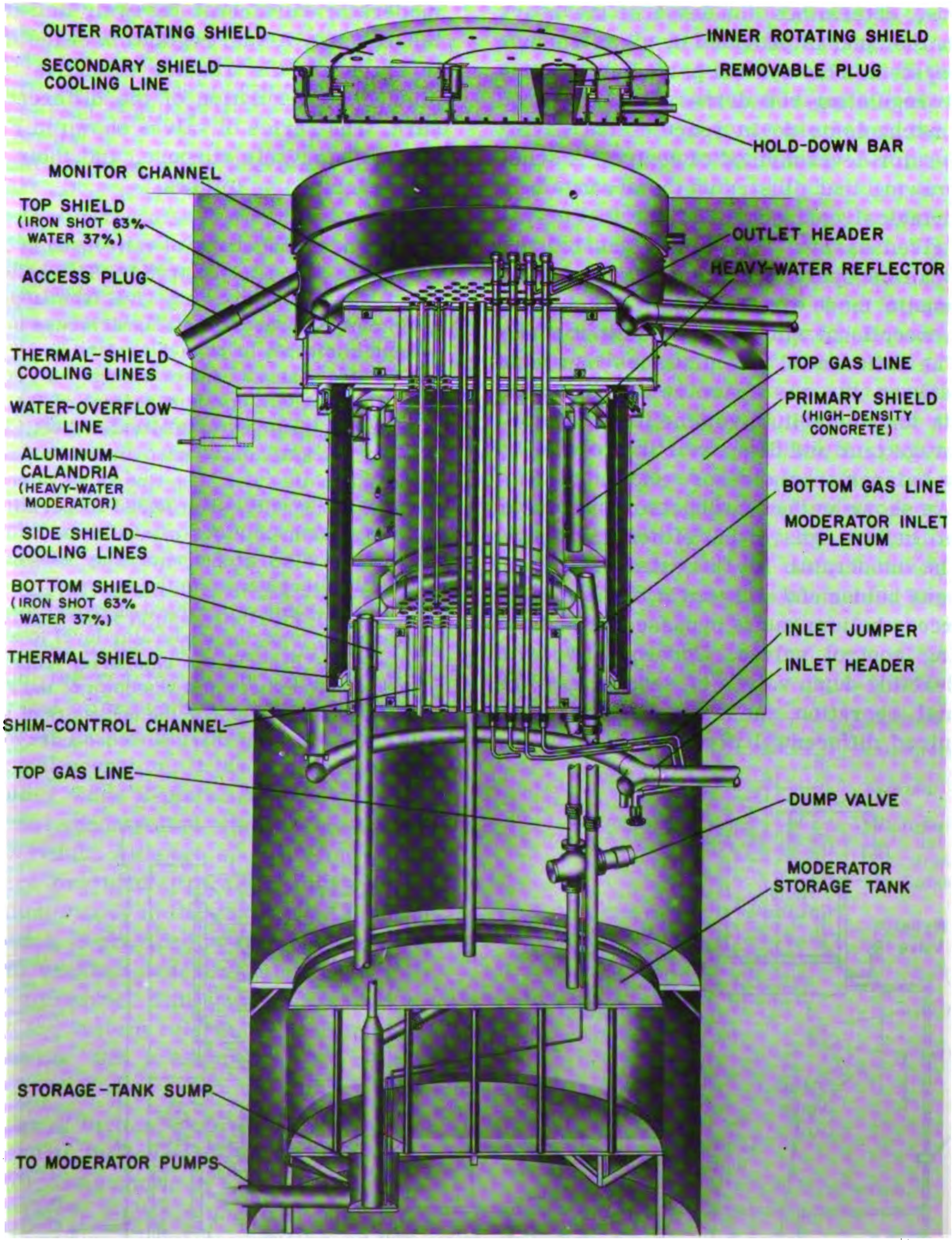

Fig. VIII-1 Cutaway view of the PRTR.[1]

The heavy-water moderator is maintained at a temperature range of 115 to 135°F by continuous circulation through a heat-removal system. Cool moderator enters the calandria at its base, picks up heat, and leaves the calandria over the weir at its base or through discharge ports in its upper regions. The warm moderator drains to the storage tank, from which it is pumped at a rate of 1100 gal/min through a heat exchanger and then returned to the bottom of the calandria. A specified minimum flow is always maintained over the weir to ensure a constant reference for static moderator level.

The differential pressure, which exerts the force necessary to hold the moderator in the calandria tank and which, as a function of its magnitude, determines the level of the heavy water in the tank, is provided by a gas-balance control system. This system performs the same job that regulating-rod drives and safety-rod scram mechanisms do in reactors not having the moderator-level method of control. A schematic drawing that illustrates the arrangement of the principal components of the PRTR system is given as Fig. VIII-2. The gas-balance system can be operated automatically, and, in its automatic mode of operation, it has demonstrated exceptional stability at constant power level. The differential gas pressure that must exist between the gas space at the top of the calandria and the helium volume in the moderator storage tank and dump weir is provided by the gas-balance compressor shown in Fig. VIII-2. As shown in the drawing, the compressor receives helium gas from either the space above the moderator in the calandria or the helium-gas holder and delivers it to the storage tank. Excess helium gas is bypassed through the regulating control valves. Consequently, with the fast-acting dump valves closed, as they are in normal operation, the compressor creates the required differential pressure between the moderator surface at the weir and that within the reactor. Actual regulation of the moderator level within the reactor calandria is accomplished by regulation of the differential pressure. The series of valves shown in Fig. VIII-2 is used for this purpose, and their functions are described as follows:[3]

1) An automatic control valve, used in conjunction with the automatic controller. This valve can control the moderator at any level from approximately (76 cm) 30 in. above the calandria base to the maximum attainable level in the calandria.

2) Two manual control valves—a "coarse" and a "fine" valve—used in control of the reactor by manual adjustment of moderator level. The coarse valve has a capacity approximately equal to that of the automatic valve. The fine valve, of considerably smaller capacity, is provided to permit smoother level adjustment under manual control. The manual control valves are considerably slower in action than the other valves in the system.

3) A "shutdown" valve—a quick-opening valve capable of lowering moderator level to about 75 cm above the base of the calandria. This valve was provided to effect rapid shutdown of the reactor and if possible to preclude the necessity of scramming the reactor, if a short period occurs or (on auto-

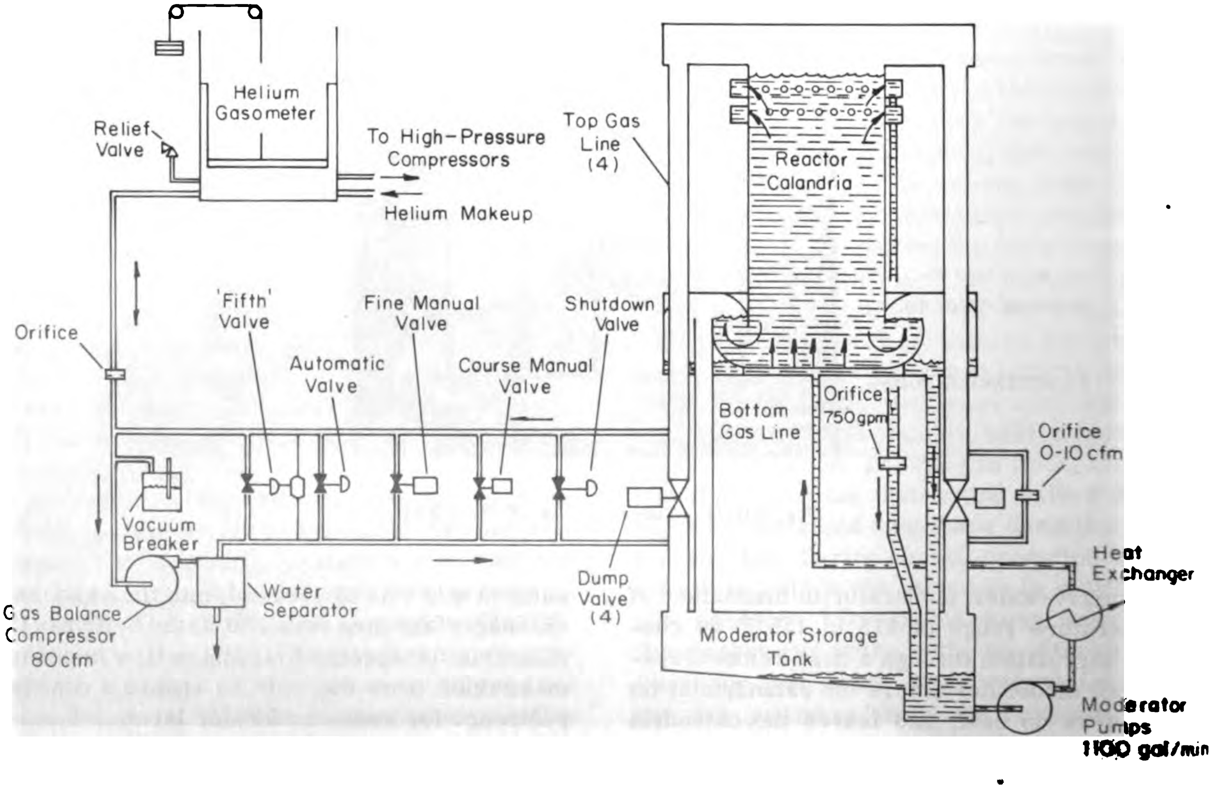

Fig. VIII-2 The PRTR moderator-level-control system.[3]

matic control) if power level varies excessively from the set point. This valve may also be opened manually by the reactor operator; in addition, it is opened (and the gas balance compressor stopped) by safety circuit interlocks at the time moderator dumping occurs.

4) A characterizing valve, referred to simply as the "fifth" valve, which is actuated in a positive feedback loop in response to the differential pressure in the gas balance system. This valve is adjusted to be fully open when pressures are equalized (i.e., when moderator is at weir level) and to be closed when moderator level reaches about 200 cm. The effects of this valve are to further limit the maximum rate of moderator rise (and thus of reactivity increase) at low moderator levels, and to extend the range of the "manual" and "automatic" control valves to lower moderator levels.

The helium gasholder (gasometer) shown in Fig. VIII-2 furnishes a pressure reference for the gas-balance system and is held at a pressure very slightly greater than the air pressure in the building that houses the PRTR. The orifice in the line to the gasholder limits the flow of gas from the reactor during dumping of the moderator but offers no appreciable resistance to the flow of gas at the flow rates that occur during normal operation. If the helium supply in the gasholder were depleted and its pressure lowered, an uncontrolled rise in moderator level could result. Although specific control interlocks are provided to prevent the depletion of the helium supply in the gasholder, a backup safety feature is provided by the installation of the vacuum breaker near the inlet to the gas-balance compressor. This vacuum breaker ensures that the system reference pressure does not fall below the pressure in the reactor building.

The design of the fast-acting dump valves that are installed in the four top gas lines deserves some attention. As shown in Fig. VIII-3, a drawing of the valve, a plug is normally held in the closed (up) position by a spring at its base. The valve plunger is not attached to the plug but is normally held free of the plug by an electromagnet located at the end of the actuator assembly. Opening of the valve is accomplished by deenergizing the electromagnet. This permits a strong spring to force the plunger against the plug, thereby overcoming the upward-acting force of the plug spring and opening the valve. The dump valves are capable of opening in 30 to 50 msec after the solenoids of the electromagnet are deenergized. The actuating plunger is recocked subsequent to opening of the valve by energizing the holding electromagnet and feeding compressed air to the bottom side of the piston; the force thus generated is capable of overcoming the downward force exerted on the pushrod by the valve-opening spring. Air pressure is bled from the cocking cylinder after the opening spring is compressed and the plunger is brought into contact with the electromagnet. The spring-loaded air piston then contracts to its normal position, leaving the valve free to open if the electromagnet is deenergized. Because failure of the cocking piston to retract could prevent or materially slow down the opening up of the valve, limit switches prevent starting of the gas-balance compressor unless the pistons of all four dump valves are in the retracted position.

Although regulating and safety rods are replaced in the PRTR by its moderator-level-control system (and its dump feature), the reactor still requires shim elements. These shim elements maintain the moderator level within its normal operating range, compensate for fuel burnout, provide for xenon override, and flatten the neutron flux. The shim elements also provide for depressing the flux for experimental purposes in portions of the reactor. Operation of the units is manual, and they are not intended as a safety device. Eighteen shim assemblies[4] of the type shown in Fig. VIII-4 are provided in the PRTR core. Each of the 18 assemblies contains three Inconel elements that are "gray" to

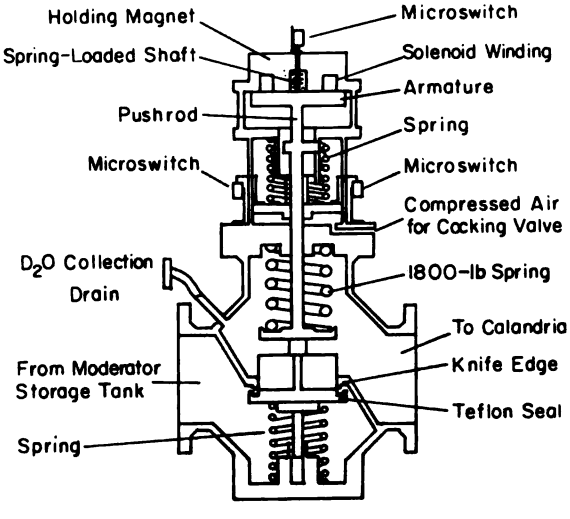

Fig. VIII-3 PRTR dump valve.[3]

neutrons. The basic frame, or structural members, of the shim assemblies does not move in and out of the core. Instead, the frame remains fixed in its position in the core, and the three Inconel elements are moved. Actuating force for the absorber elements is provided by electric motors that drive lead screws through suitable transmissions. The absorber elements are supported on the lead screw by recirculating-ball nuts. The overall height of the shim-rod assembly is such that the assembly extends from above the top primary shield into the bottom primary shield shown on Fig. VIII-1. The rod assembly has three basic zones that correspond to locations in the top shield, the calandria, and the bottom shield. The zone that extends through the top primary shield contains the driving head and electrical components of the control assembly. In the calandria region, the support framework provides guidance for the elements, and the lower-primary-shield zone of the assembly is used for storage of the shim elements when they are out of the core. The frame member of the shim assembly, which

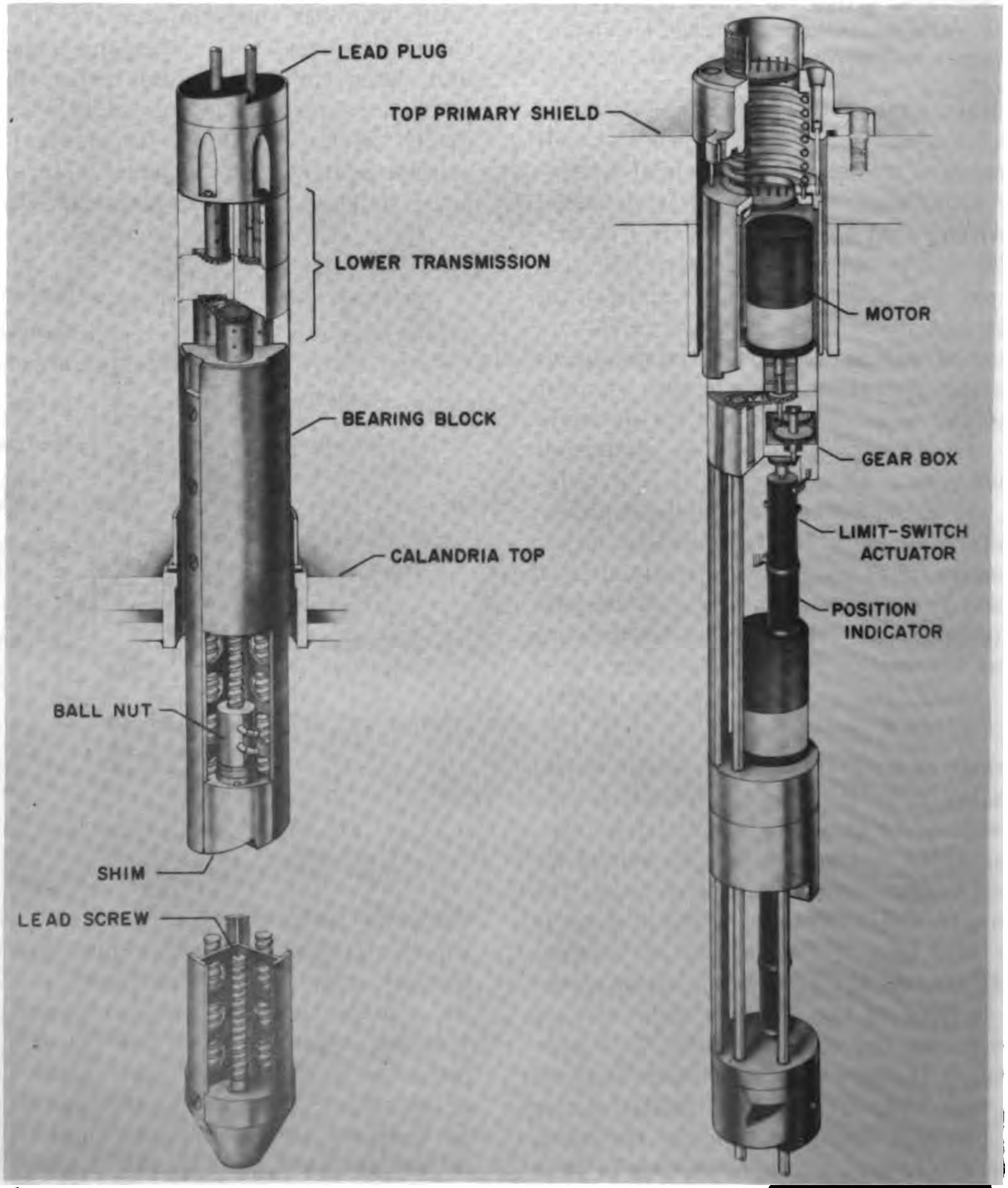

Fig. VIII-4 PRTR shim-control unit.[1]

remains in the core at all times, is fabricated from an aluminum extrusion with numerous punched holes as shown in Fig. VIII-4. The lead screws are aluminum or zirconium, and thus the absorption in the shim-assembly channel is minimized when the shim elements are in the out-of-core position. Each of the three elements in a shim assembly is 36 in. long and has an average worth of about 2 m*k*. Two motors are used to drive the three lead screws, and the mechanical arrangement is such that there are two mutually powered elements and one independently powered element. One of the mutually powered lead screws turns $\frac{2}{3}$ as fast as the other, so that when one of the elements is fully inserted in the core the other is immediately below it. Second-generation shim-rod assemblies[4] being developed for the PRTR will use the same lower unit (frame structure and absorber elements) as the first-generation assemblies. The driving heads, although considerably different, perform the same basic functions.

Nuclear Power Demonstration Reactor

A second reactor that utilizes moderator-level regulation as the primary means of reactivity control is the Nuclear Power Demonstration (NPD) reactor.[5,6] This reactor, which uses natural-uranium fuel and has horizontal pressure tubes, was developed and built during roughly the period that the PRTR was undergoing design and construction. Unlike the PRTR, NPD produces electric power. As its name implies, the NPD was built to prove the feasibility of the heavy-water power-reactor concept embraced by the Canadians.

The pressurized heavy-water-cooled NPD generates about 20 Mw of electric power from a thermal-power production of nearly 90 Mw and has primary coolant parameters similar to those of the PRTR. Primary coolant enters the reactor at 485°F, leaves at 530°F, and is maintained at a nominal pressure of 1040 psig. Although the appearance of NPD, as shown in Fig. VIII-5, is markedly different from that of the PRTR, the principle of operation of the moderator-level-regulation system is the same; i.e., NPD uses a gas-balance system that will be described shortly. Fuel elements in NPD consist of 7- or 19-rod bundles, with each rod containing pellets of natural UO_2 encased in cylindrical Zircaloy-2 cladding tubes. Fuel channels in the core are formed by 132 Zircaloy-2

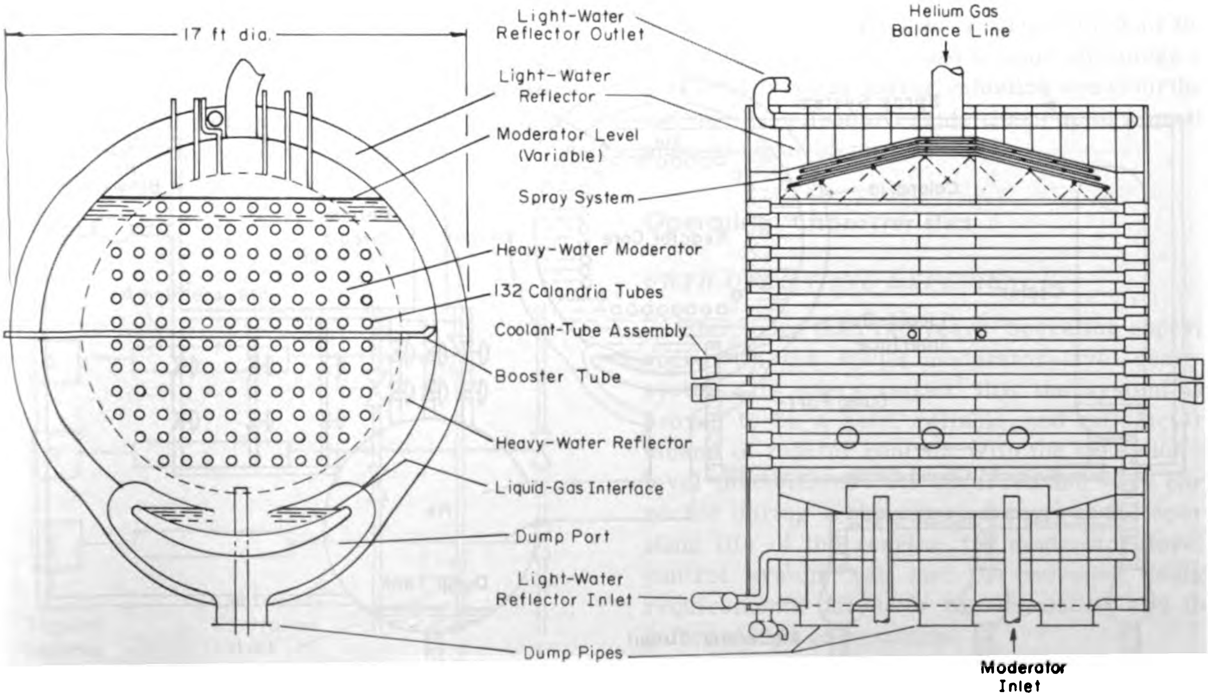

Fig. VIII-5 Vertical sections of the NPD reactor.[6]

pressure tubes, each having an inside diameter of 3.25 in. As in the PRTR, the pressure tubes penetrate the core through low-pressure calandria tubes that are part of the heavy-water core tank.

As shown in Fig. VIII-5, the calandria of the NPD reactor is a compartmented tank. However, the sections within the tank are not used to separate the moderator and reflector portions of the core as in the PRTR but, rather, to separate the two types of reflector used in NPD. As shown in the figure, the active core region of NPD is surrounded by a heavy-water reflector that is integral with, and a part of, the moderator system. It is this heavy-water reflector which the inner compartment of the calandria tank bounds, so that when the NPD moderator level is changed, the heavy-water-reflector level changes too. The incorporation of the heavy-water moderator-reflector liquid into a single system in the NPD, in which the reflector is actually quite thick (~21 in.), illustrates an interesting difference in design approach from that employed in the PRTR. In the PRTR the inner tank which surrounds the process channels and which contains the heavy-water moderator is only slightly larger than the distance across the outermost process tubes. The annular heavy-water reflector, whose level is not varied, remains in its portion of the calandria following a moderator dump and provides postdump shielding. Comparable shielding in NPD is furnished by the light-water reflector that surrounds the heavy-water moderator-reflector section of the calandria. In spite of the reactivity effects, the scheme employed in NPD appears to be the simpler one: a single heavy-water system suffices for both moderator and inner reflector, and, although a relatively large volume of heavy water must be moved to achieve a given change in moderator height, the provision of sufficient pipes, etc., to handle the relatively large flow seems to be a straightforward step.

The moderator-level-control system of the NPD reactor,[7] although utilizing the same gas-balance principle used in the PRTR, has interesting features and differences. The NPD system (shown in Fig. VIII-6) contains the same basic components as its counterpart in the PRTR: a reactor tank containing a dump region that has a relatively large volume into which heavy water can flow at the initiation of a moderator dump, large interconnecting pipes between the reactor tank and the dump or storage tank, and gas connecting lines between the top of the reactor tank and the dump tank. Fast-

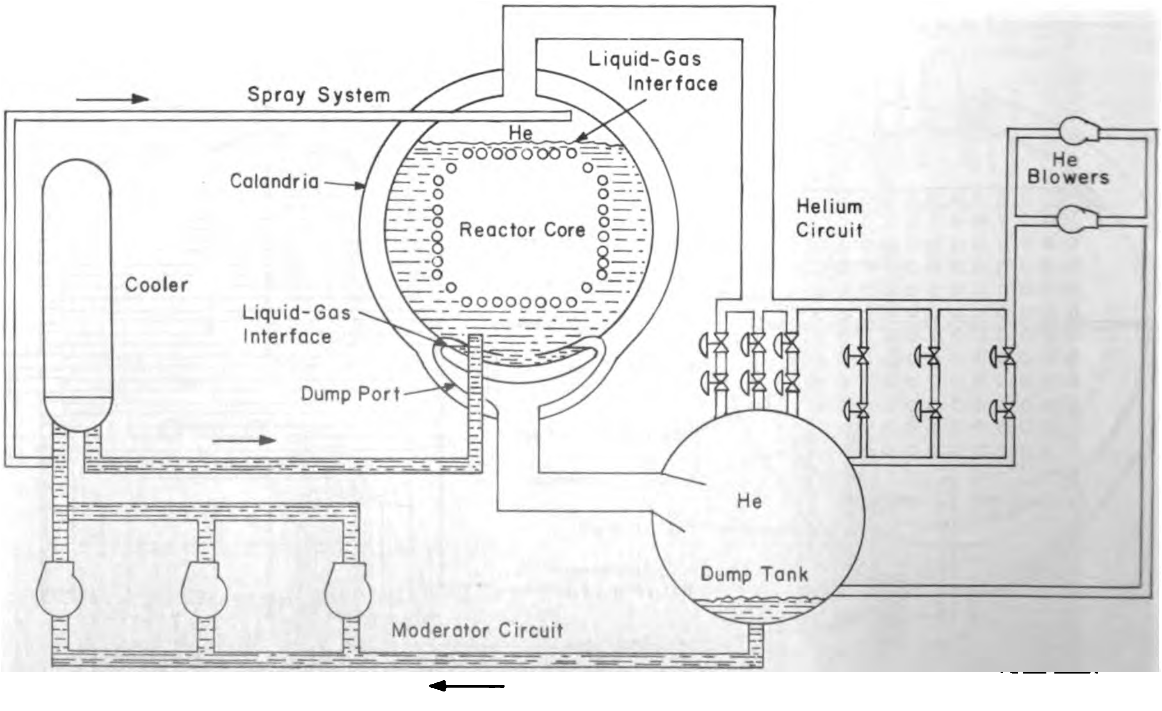

Fig. VIII-6 The NPD reactor moderator and helium systems.[7]

opening valves, which are opened to equalize pressure between the moderator and storage tanks and thereby cause the dumping of the moderator, are located in the top gas line. The pressure differential, which establishes the level of moderator in the tank, is developed around these normally closed valves by helium compressors. Since the operation of the NPD system is similar to that of the PRTR system, it will not be described here. However, the arrangement employed in valving the main gas-balance or top gas line is important. As shown in Fig. VIII-6, and as indicated in Fig. VIII-5, a single large gas line leads most of the way from the top of the calandria tank to the top of the dump tank. However, prior to entering the dump tank, the single large line branches into three parallel lines. Each of the three parallel lines is provided with two valves in series, so that, to dump the heavy-water moderator from the reactor tank to the storage tank, two valves in one of three lines must open. The opening of a single one of the three parallel lines results in a sufficiently fast lowering of the moderator level for scram purposes. The three parallel lines with double valves in each line are used in the NPD because a triplicated system[8] is employed in the scram as well as the regulating circuitry of the reactor. The triplicated safety system, which is shown schematically in Fig. VIII-7, minimizes the number of false trips and gives the advantage that all equipment can be tested routinely, one channel at a time, from the primary sensing element through to actual operation of the dump valves.

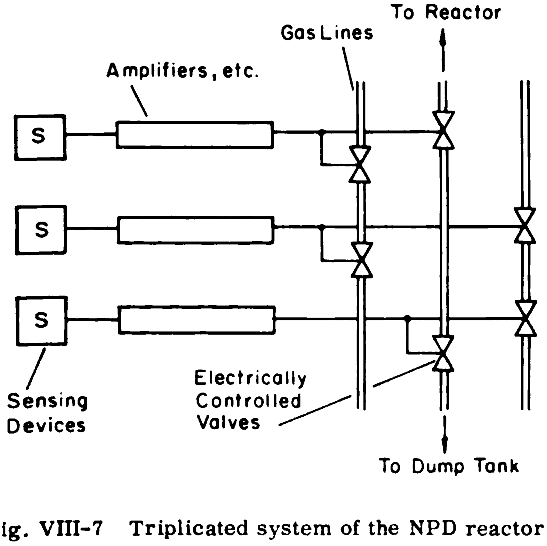

Fig. VIII-7 Triplicated system of the NPD reactor.[8]

In addition to the primary mode of reactor control, i.e., the variation of moderator level, NPD has other means of reactivity management. By virtue of the on-power refueling scheme used, the amount of excess reactivity available at any time in plant life can be held to a minimum. Although not actually a control feature as such, the on-line refueling scheme does make the job of the control-system components relatively easy once the reactor has attained an equilibrium core condition. In addition to the reactivity control methods already mentioned, NPD has the capability of changing reactivity by two other means: insertion of a booster rod and variation of moderator temperature. The booster rod, whose location is shown in Fig. VIII-5, is a fissile assembly that can be inserted into the core to give a boost in reactivity. The rod is worth 2.5 mk and, when inserted following an emergency shutdown, partially overrides xenon poison and permits the reactor to be below 60% of full power for up to 35 min while retaining a restart capability. Although moderator-temperature variation is ineffective as a control mechanism once an equilibrium fuel-burnup condition has been reached (since its reactivity coefficient is essentially zero at that condition), it is useful during the first year of operation of the reactor. With a fresh pile the temperature coefficient of reactivity for the moderator is -0.04 mk/°F. The effect of this characteristic can be used to good advantage as a reactivity shim during refueling and to further extend the poison override times up to a maximum of about 55 min.

Operating Characteristics

PRTR OPERATING EXPERIENCE

After more than two years' operating experience with the PRTR moderator-level-control system, its users report[3] that the system has proved to be a safe, reliable, and satisfactory means of reactor control. With the exception of level instabilities that occurred and were corrected during a short period early in the operating life of the reactor, the moderator-level-control system has met or exceeded design requirements for both the regulating and the safety modes of operation.

Control-System Characteristics. Startup tests performed with the PRTR verified the control-system characteristics that were predicted in analyses and tests performed during the design of the system. The moderator level is controllable over a range of about 80 cm to the maximum capacity of the calandria, which is at a level of about 287 cm. The normal range of levels for operation of the reactor at power is 260 to 270 cm. Reactor operating procedures require that criticality be attained only at moderator levels exceeding 182 cm. The worth of the moderator as a function of its height is shown in Fig. VIII-8 for a level range of 140 to 270 cm. As can be determined from the figure, the moderator-level coefficient of reactivity is approximately 5 cents/cm in the normal range of levels for power operation.

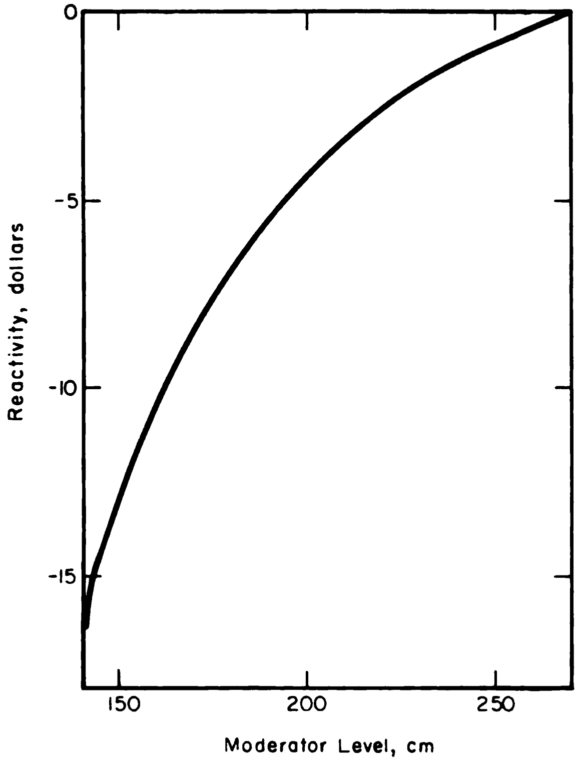

Fig. VIII-8 Reactivity variation with moderator level in the PRTR.[3]

Test data on the control system obtained during the reactor startup period show that the limiting rates of moderator-level change attainable with the system are as shown in Fig. VIII-9. One of the curves is for an increasing moderator level, and the other two curves represent level change rates corresponding to decreasing levels. The perturbations that occur in all curves at about the 220-cm level are caused by the capacity of a header located behind the moderator recirculation (outflow) ports located at that level. These perturbations, which show so clearly on the maximum rate of level-change curves, are not observed at level-change rates that normally occur in the system, and, furthermore, do not affect control of the reactor.

For the limiting level change rates shown in Fig. VIII-9, there are corresponding limiting rates of change in reactivity. Figure VIII-10 shows the limiting rates of reactivity change attainable with the PRTR control system. As shown in the figure, the maximum reactivity change rate at a moderator level of around 182 cm, which is the minimum criticality level as set by reactor operating procedures, is slightly more than 2 cents/sec, and the maximum rate at the normal range of levels for operation at power is about 1 cent/sec.

Although the PRTR control system had been operated principally in a manual mode up to the

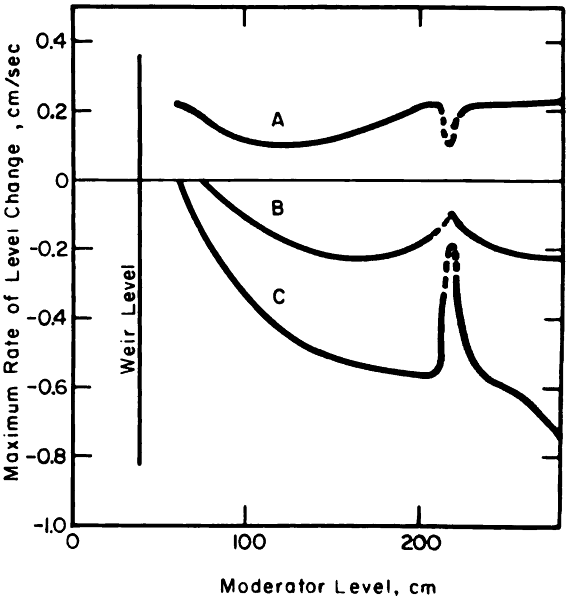

Fig. VIII-9 Limiting rates of moderator-level change with control system in the PRTR.[3] *A*, all control valves closed, increasing level. *B*, automatic or manual valve open, decreasing level. *C*, automatic and shutdown valves open, decreasing level. ("Fifth" valve is operating in all cases.) The spikes that appear in these curves are due to effects of the header volume behind the top discharge orifices. These are seen only in maximum-change-rate tests, such as produced the data, and never in actual operation where rates of level change (at this level) are well below maximum.

time of writing of Ref. 3, indications were that the stability of control would be very good in both manual and automatic modes of operation. During all phases of reactor operation under the manual option, the system provides stable control, and the limited experience obtained with the automatic controller indicates that it will provide a marked improvement and smoothness and precision of control over the manual mode at the power levels (2 to 70 Mw) at which it had been used. Although the stability of the system is entirely acceptable, minor fluctuations in moderator level (which may represent wave action at the surface rather than true variation in level) do tend to obscure measurements of reactor noise and make period measurement involving long periods difficult.

The moderator-dump feature of the PRTR control system has been demonstrated to be a rapid, reliable, and essentially fail-safe means of reactor scram. Figure VIII-11 shows the height of moderator as a function of time after tripping the reactor safety circuit. The curve shown in the figure is a composite drawn from data obtained from timed tests performed during the reactor startup. Since the times are given as time after tripping of the safety circuit, they include delays in the safety circuit and in opening of the dump valves. The decrease in reactivity, which occurs as a result of the lowering of the moderator level in the calandria, is related to the time after tripping the safety circuit by the curve shown in Fig. VIII-12. The design requirements for the safety system specified a 2-ft decrease in level from normal operating levels within 1 sec after tripping of the safety circuit. The reactivity associated with this decrease in level is about 3 dollars

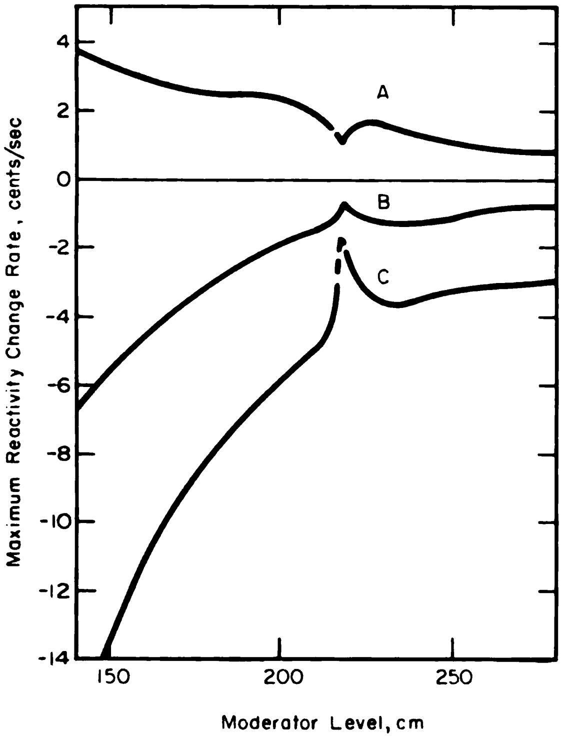

Fig. VIII-10 Limiting rates of reactivity change with control system of the PRTR.[3] *A*, all control valves closed. *B*, automatic or manual valve open. *C*, automatic and shutdown valves open. ("Fifth" valve is operating in all cases.) The spikes that appear in these curves are due to effects of the header volume behind the top discharge orifices. These are seen only in maximum-change-rate tests, such as produced the data, and never in actual operation where rates of level change (at this level) are well below maximum.

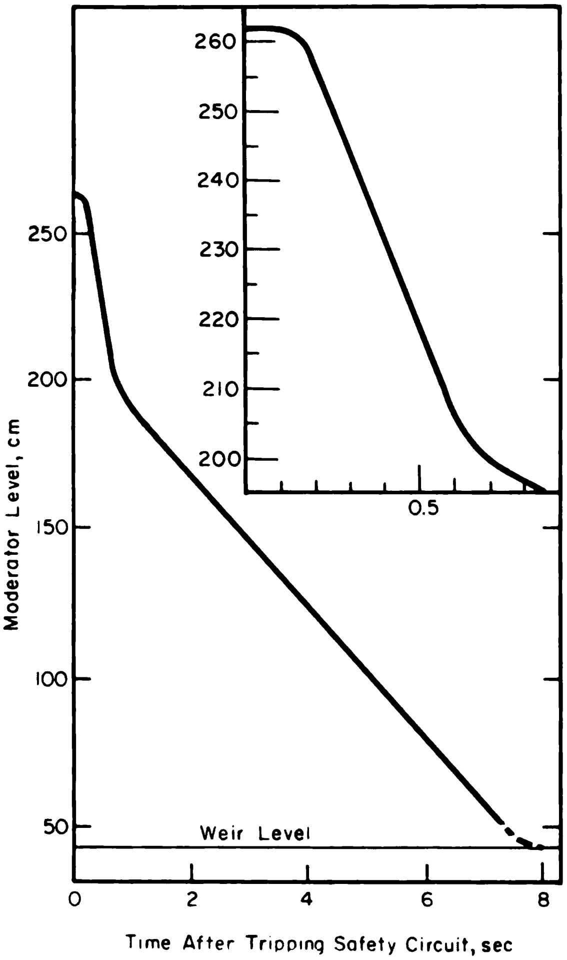

Fig. VIII-11 Typical moderator-level decrease during dump of the PRTR.[3]

and 50 cents. As can be seen in Figs. VIII-11 and VIII-12, these requirements are bettered by the system, with the required 2-ft change in level accomplished in less than 0.7 sec. At the end of the first second after tripping the safety circuit, where the reactivity decrease was required to be about 3 dollars and 50 cents, the actual reduction amounts to about 5 dollars. Although the moderator rate of level decrease may be somewhat slower than shown in Fig. VIII-11 for cases in which the moderator is dumped from levels below the normal operating range, the net rate of reactivity decrease is as great as that shown in Fig. VIII-12 owing to the increase in moderator-level coefficient of reactivity at the lower levels.

Although the dump time and effectiveness just discussed are based on the satisfactory operation of all four moderator dump valves, it is interesting to note that failure of some of the valves to open does not materially affect the initial (and most important, of course) rate of dump. Tests showed that the design requirement of a 2-ft drop within 1 sec could easily be met with two valves operating and could almost be met with only a single operable valve. Figure VIII-13 shows the difference in moderator level as a function of time after tripping the safety circuit for the normal, or four-valves-working, case and for the situation in which only one valve opens.

Problems During Early Operation. Early in the control-system test period, oscillations occurred in the moderator level.[3] These oscillations, which were up to 2 cm in height, were stopped by the addition of a water separator to the discharge of the gas-balance compressor, as shown in Fig. VIII-2, and by changes in the inventory of the helium gasholder and in helium-addition procedures, although the specific mechanism causing the oscillations was not identified. Subsequent to the stopping of the oscillations in moderator level, a pressurized helium system associated with the primary coolant loop was placed in service. Whenever the helium compressors in the system associated with the primary coolant loop were operated, the oscillations in moderator level recurred. Because the gasholder shown in Fig. VIII-2 is a common component of several systems, including the primary-loop helium system that was apparently causing the later oscillations in moderator level, it became evident that there was some interaction between the

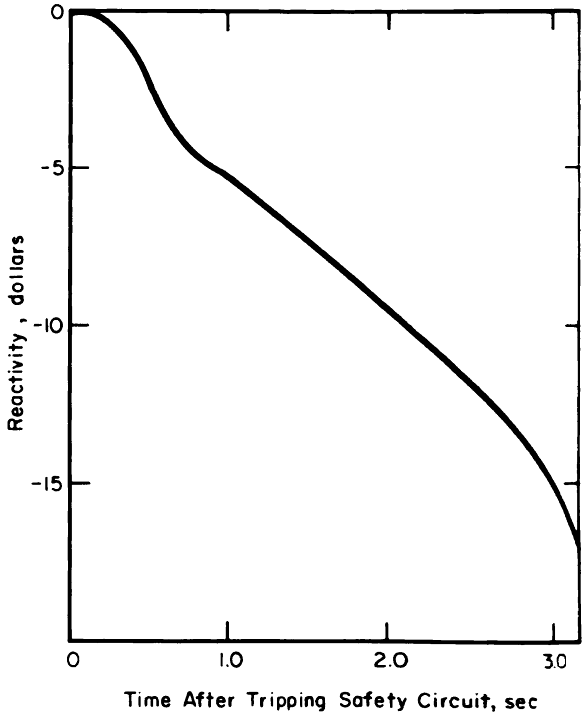

Fig. VIII-12 Reactivity decrease during moderator dump in the PRTR.[3]

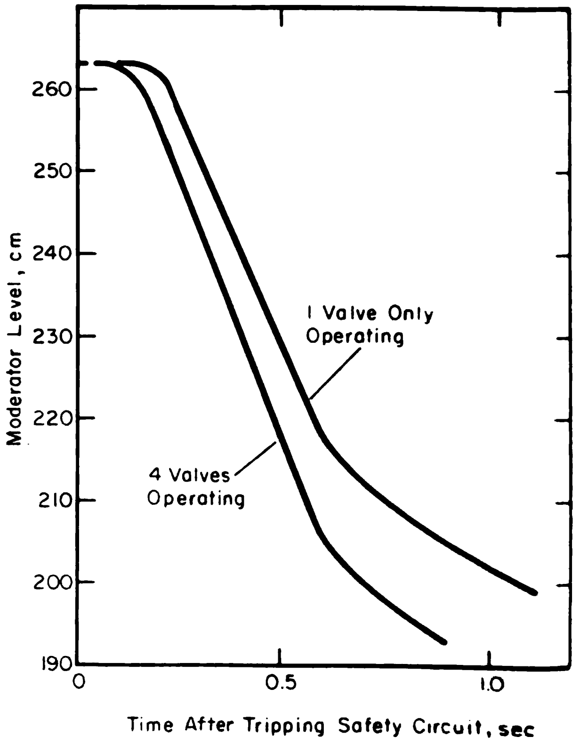

Fig. VIII-13 Effect of dump-valve malfunction on moderator dump rate in the PRTR.[3]

level-control system and other reactor systems. The causative mechanism for the second series of oscillations was determined to be fluctuations in pressure within the helium gasholder, which resulted in fluctuations in moderator level. Significant oscillations in moderator level were eliminated by modifying the gasholder cover so that the gasholder gave relatively even response to changes in inventory, and by replacing a common manifold that had served the control system as well as the primary loop system with a separate line from the gasholder to the level-control system. This latter step was taken as a precaution against pressure pulsations from other sources.

With the helium-gasholder arrangement used in the PRTR level-control system, a decrease in gasholder pressure is accompanied by a corresponding decrease in gas pressure within the reactor calandria. This decrease of pressure within the calandria results in an increase in the differential pressure between the calandria and the moderator storage tank and causes an increase in moderator level. On two separate occasions, spontaneous rises in moderator level were caused by rather sudden decreases in helium pressure in the gasholder. These spontaneous rises in level illustrate rather dramatically the strong interaction that can exist between remotely related systems. The first spontaneous rise in moderator level occurred during a critical test that was made at a time when modifications to the ventilation-exhaust system of the containment vessel were being carried out. A containment valve was closed to seal off the exhaust duct during the modification, and the ventilation supply fan was left in operation, causing the containment-vessel pressure to increase gradually. Consequently helium pressure in the gasholder increased gradually (not at a rate sufficiently fast to decrease the differential pressure across the calandria tank but, rather, so slowly that the level-control system did not "feel" the increase). When work on the containment exhaust system was completed, the valve that had been closed to seal off the exhaust duct was opened, and building pressure rapidly dropped to normal. The gasholder pressure decreased with the building pressure, thereby increasing the differential pressure across the calandria and causing a rapid rise of the moderator level of about 1 cm, followed by a slower rise to about 2.5 cm. The shutdown valve of the level-control system was opened, and the rise in moderator level stopped. On another occasion a spontaneous rise in moderator level of about 8 cm occurred. This time the reactor was ready for startup, and the control valves had been closed, but the gas-balance compressor had not been started. The rise, which had again been caused by changes in helium pressure in the gasholder, was stopped by opening the control valves. In the second instance, the sudden change in gasholder pressure had apparently been caused by the rather rapid charging of the helium into the gasholder and the inability of the pressure-relief mechanism of the gasholder to prevent an overpressure upon the injection of such large amounts of helium. Consequently the gasholder pressure increased slowly for some time, again causing no discernible change in the differential pressure across the reactor calandria. Then the gasholder inventory was rapidly reduced, probably by starting the helium compressors, thus relieving the overpressure condition and causing a rapid increase in calandria differential pressure.

A number of steps were taken to prevent the recurrence of spontaneous moderator-level rises such as those described above. These steps included the procedural requirement that the air pressure in the containment vessel must be less than atmospheric pressure by at least 0.3 in. H_2O before reactor operation is permitted. This provision prevents the occurrence of a sudden decrease in containment-vessel pressure (and, consequently, gasholder pressure) due to venting to the atmosphere. The only other step that will be mentioned here is the one taken to prevent a transient rise in moderator level caused by a rupture of the gasholder or its connecting piping. The magnitude of such a rise is limited by keeping the operating pressure of the gasholder to a value of 1 in. H_2O or less above the building pressure.

Some difficulty was encountered with leakage through the dump valves in the top helium-gas lines. This leakage caused the rate of rise of moderator level during startup to markedly decrease, and, often, the moderator could not be raised above a level of about 150 cm. Although the results of such a leak do not present a hazard, it is conceivable that a sudden stoppage of the leak could cause an increase in the differential pressure across the calandria tank and a subsequent rise in moderator level. Therefore startup procedures were specified which required that the rate of rise of moderator level during startup be within prescribed limits. A program of planned maintenance of the valves has essentially eliminated the leakage problem.

NPD OPERATING EXPERIENCE

The moderator-level-control system of NPD has performed its functions satisfactorily.[7,9–11] Utilization of the system has proceeded somewhat differently than in PRTR, in that NPD's automatic-control mode of operation was brought into use immediately after first achieving criticality. This early use of the automatic system is not too unexpected, however, since the NPD design incorporates the triplicated-components arrangement in the regulating as well as in the safety portions of the system. Another factor that probably hastened the use of the automatic system was that manual control of moderator level, which was carried out with five of the valves shown in Fig. VIII-6 in an equilibrium position and the sixth valve used for fine control, proved to be simple but slow.

Apparently the NPD control system was brought into service with a minimum of difficulty. The object of the load-following scheme used in the on-power mode of operation of NPD is to have the reactor follow changes in turbine load so that constant steam pressure is maintained at the turbine throttle valve. The reactor satisfactorily assumes load at the limiting rate of 20% full load/min; it shuts down to a low power, without excessive steam bypass, on a loss of electrical connection to the grid or loss of the turbine. Early experience with the system can probably be summarized best by the following sentence from Ref. 7: "Perhaps the most difficult commissioning operation was bringing the triplicated input signals into sufficient agreement."

Table VIII-1 COMPARISON OF DESIGN AND MEASURED PARAMETERS IN NPD[9]

Parameter	Design value	Measured value
Clean critical level	89.3 in.*	97.5 in.
Moderator temp. coefficient	−0.06 mk/°F	−0.04 mk/°F
Heat-transport system temp. coefficient	−0.024 mk/°F	−0.02 mk/°F
Light-water reflector savings	3 mk	3.6 mk
$\Delta k_{\text{eff}}/k_{\text{eff}}$		
For clean critical condition to full tank	37 mk	39 mk
For enriched booster	2.5 mk	2.4 mk
Dump rate in first second	3 mk†	5 mk

*Error due to underestimate of depleted uranium; now reconciled.

†Conservative value; measured results more favorable.

It is shown by measurements that the installed blower capacity of the NPD level-control system, in conjunction with the piping arrangement employed, can cause a maximum rate of rise of moderator level which corresponds to a rate of reactivity increase at cold, clean critical conditions of slightly less than 0.3 mk/sec. At this rate, it takes 12 min to fill the calandria tank, and the rate of reactivity increase at full-tank conditions is 0.06 mk/sec. Moderator dump tests showed that with two out of three protective channels in operation (that is, with only one gas-balance line opening), reactivity could be reduced 5 mk in the first second and 15 mk in 2 sec. The dump valves had fully opened 0.3 sec after receiving a trip signal. Table VIII-1 is a comparison of pertinent design and measured parameters in NPD, and Fig. VIII-14 shows the variation of moderator temperature coefficient with fuel irradiation. As mentioned earlier, the coefficient is essentially zero with equilibrium fuel burnup, and Ref. 11 contains a statement that there is no detectable change in

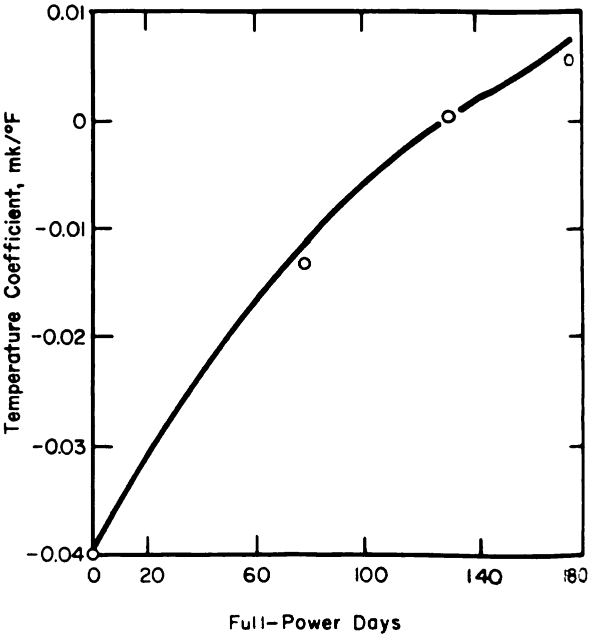

Fig. VIII-14 Variation of moderator temperature coefficient with fuel irradiation in the NPD reactor.[11]

moderator temperature coefficient with changes in moderator level. The value of 39 m*k*, shown in Table VIII-1 as the measured value of reactivity change from the clean critical moderator level to full tank level, corresponds to a change in level from 97.5 in., as indicated in Table VIII-1, to a full tank height of approximately 173 in.

Large Reactors

The operating experience gained with the reactor control systems of PRTR and NPD has shown the suitability of moderator-level control for small, heavy-water-moderated pressure-tube reactors. The NPD system, in particular, rather epitomizes the useful application of moderator-level control by its extreme simplicity and almost complete lack of ancillary systems, components, or gadgets for reactor control. Despite the obvious utility of moderator-level control in NPD, however, its use in future reactors is by no means certain because there appears to be no great demand for reactors of the NPD type and size and because moderator-level-control systems lose a great deal of their attractiveness when applied to large reactors. A brief discussion of the CANDU reactor,[6,12,13] which qualifies as both a large reactor and one which uses moderator-level control, serves to illustrate the complications which occur in larger reactors and which begin to nullify the advantages of a concept that is simple in practice as well as in principle in smaller reactors.

The 200-Mw(e) CANDU is similar in appearance to the NPD reactor. It utilizes a calandria pierced by horizontal process tubes, is fueled with rod type bundles containing natural UO_2, is moderated by heavy water, and is cooled by pressurized heavy water. Nominal coolant temperature at the reactor inlet is 480°F, that at the reactor outlet is 560°F, and the primary coolant pressure is about 1400 psi. As in NPD, emergency shutdown is accomplished by a moderator dump system operating on the gas-balance principle.[14] In a sense, moderator-level control is also used in CANDU, since after a shutdown the reactor must be brought back to critical by raising the moderator. However, the use of level control alone can result in the requirement that the reactor operate for significant periods at reduced power output because of xenon oscillations induced by flux distortions resulting from operation at low moderator levels. In CANDU, cadmium sulfate will be added to the moderator to permit operation at full tank at all times.[14] This moderator-poison expedient will be employed at times prior to the full build-in of xenon or if fuel reactivity is higher than usual. As the xenon builds up after an extended shutdown, the cadmium in the moderator will be removed by ion exchange.

CANDU is provided with four small absorber rods, moving in two through tubes, to give a means of local control in each of the four quadrants of the reactor.[14] These absorbers, which can be moved collectively or independently, will be used to adjust the overall reactivity as well as to exert local influence on the flux in any particular quadrant.

The last accessory control mechanism that will be described for CANDU consists of booster rods similar to the rod installed in NPD. The CANDU system consists of eight booster elements that are capable of moving independently in four through tubes.[14] The proposed total worth of the eight elements, when fully inserted, is about 10 m*k*. The worth of the rods is expected to be sufficient to give the reactor restart capability after being shut down for about 30 min from equilibrium full power or to allow power to be reduced to about 65% for an indefinite period.

With the exception of the on-line refueling process that is a feature of the CANDU design, all the reactivity-control methods will be integrated into an automatic system. When we consider the several major control devices which will be parts of this system, and which have been mentioned previously, it is obvious that the rather simple concept of moderator-level control loses a great deal of its simplicity when applied to reactors in the CANDU size range. The CANDU case is an example of the simple concept being a little too simple to meet the requirements of a large core, and it is unfortunate that the uncomplicated implementation of the scheme, as exemplified by the NPD system, is not applicable to the larger reactors.

References

1. N. G. Wittenbrock, P. C. Walkup, and J. K. Anderson (Eds.), Plutonium Recycle Test Reactor Final Safeguards Analysis, USAEC Report HW-61236, Hanford Atomic Products Operation, Oct. 1, 1959.

2. I. N. MacKay, The Canadian NPD-2 Nuclear Power Station, in *Proceedings of the Second United Nations International Conference on the Peaceful Uses of Atomic Energy, Geneva, 1958,* Vol. 8, pp. 313-321, United Nations, New York, 1958.
3. J. F. Fletcher and R. I. Smith, Moderator Level Control in the Plutonium Recycle Test Reactor, USAEC Report HW-79669, Hanford Atomic Products Operation, December 1963.
4. D. E. Rasmussen and L. D. Gustafson, The PRTR and PRCF Control and Safety Rod Drives, ASME Paper 62-WA-235, November 1963.
5. Reactors on the Line NPD, *Nucleonics,* 20(11): Reactor File ... No. 13.
6. *Directory of Nuclear Reactors, Vol. IV, Power Reactors,* International Atomic Energy Agency, Vienna, 1962.
7. W. S. Brown, Reactor Control of NPD, paper presented at the Winter Meeting of the American Nuclear Society, Washington, November 1962.
8. G. C. Laurence, Reactor Safety in Canada, *Nucleonics,* 18(10): 73-77 (October 1960).
9. L. G. McConnell, Commissioning and Initial Operation of NPD, in The Eighth AECL Symposium on Atomic Power, Held at Chalk River, Ontario, September 24, 1962, Canadian Report AECL-1599, September 1962.
10. L. G. McConnell, Initial Operating Experience with the "NPD" Reactor, in *Operating Experience with Power Reactors,* Vol. I, pp. 139-150, International Atomic Energy Agency, Vienna, 1963.
11. A. C. Whittier, Nuclear Performance of NPD, in ANS Topical Meeting on Nuclear Performance of Power-Reactor Cores, September 26—27, 1963, Sponsored by the Northern California Local Section of the American Nuclear Society, USAEC Report TID-7672, pp. 95-122, February 1964.
12. Atomic Energy of Canada Ltd., Douglas Point Nuclear Generating Station, Canadian Report AECL-1596.
13. C. E. Benyon, Douglas Point: The CANDU Reactor, in The Ninth AECL Symposium on Atomic Power at Toronto, Ontario, September 23, 1963, Canadian Report AECL-1807, pp. 25-30.
14. E. Siddall, Reactivity Control in the CANDU Reactor, in Papers Presented by A.E.C.L. to the International Conference of the Canada Nuclear Association, Held at Ottawa, Ontario, May 28–30, 1962, Canadian Report AECL-1962 (Paper I, Atomic Energy of Canada Ltd., February 1963.

Section IX

Power Reactor Technology

Specific Reactor Types

Heavy-Water Reactors

Large-Plant Studies

The design of the Carolinas-Virginia Tube Reactor (CVTR) was reviewed in *Power Reactor Technology*, 6(4). This plant was designed as the prototype of a full-scale plant, and Ref. 1 is a report on a study of the larger plant. The CVTR was designed to produce 17 Mw(e), whereas the large plant nominally produces 300 Mw(e).

Although the CVTR had not produced a significant amount of operating experience at the time Ref. 1 was issued, the influence of the small reactor can be seen in the design of the large reactor, especially in the following areas:

1. The pressure-tube reactor concept (cold-tube design)
2. Heavy water as moderator and coolant
3. Pressure-tube joints, including a Zircaloy–stainless-steel joint
4. Fuel-assembly design
5. Stagnant-water (D_2O) baffle design for thermal insulation
6. Primary-system temperatures and pressures
7. Primary-system pressure drop
8. The basic reactor layout (e.g., moderator tank and header-cavity layout)
9. Refueling method
10. Closed-system ventilation of the vapor container with D_2O recovery

A set of four large plants (cases) was studied using four different fuel assemblies, as shown in Table IX-1. Design data on cases II and IV are presented in Table IX-2.

Table IX-1 FUEL ASSEMBLIES SPECIFIED FOR LARGE-PLANT STUDIES

Case	Rods/cluster	Fuel
I	19	Natural UO_2
II	19	Enriched UO_2
III	37	Natural UO_2
IV	37	Enriched UO_2

The CVTR and the large plant are both U-ube designs, although the CVTR uses a gasketed oint and the large plant uses a coextruded Zircaloy–stainless-steel transition joint. Each plant has a mechanical joint for pressure-tube closure without seal welding. The CVTR fuel element is about 8 ft long, and the large plant is fueled with a 13- to 16-ft-long fuel element, possibly made of subassemblies. Cross-sectional views of the 19- and 37-rod fuel bundles and pressure tubes are shown in Fig. IX-1.

Steam conditions of the CVTR secondary plant were dictated by the existence of a steam plant previously constructed. The large plant was designed with a primary-system pressure of 1000 psia for the natural-uranium reactor and 1500 psia for the enriched-uranium reactor. The lower pressure was selected to minimize the wall thickness of pressure tubes and fuel-rod cladding for the reactor using natural uranium, whereas the upper pressure is identical with that of the CVTR. There are some differences between the refueling concept for the large plant and that of the CVTR. The CVTR is refueled by removing the pressure tubes (from which the fuel elements have been removed) from the reactor during one of the refueling steps and replacing them by fully loaded pressure tubes, whereas the large plant would be refueled without moving the pressure tubes except in the case of pressure-tube damage. The two plants also differ in the method of pressure-tube support. The CVTR supports the pressure tubes on a core support plate by means of jumper blocks and support columns.* However,

---

*Figure III-7 of the previously mentioned CVTR review illustrates the method of pressure-tube support.

Table IX-2 CVTR LARGE-PLANT DATA: 300 Mw(e) NOMINAL POWER[1]

	Case II (enriched)	Case IV (enriched)
Heat output, Mw(t)		
From core	1136	1136
From fuel rods in maximum-power U tube	4.72	8.69
Coolant flow, lb/hr		
Total coolant flow rate	38.3 × 10^6	38.3 × 10^6
Flow per maximum-power U tube	147,200	272,300
Pressure, psia		
System pressure minimum (U-tube exit)	1480	1480
U-tube pressure drop	105 ± 5	105 ± 5
Steam pressure	481	481
Hot-channel factors		
Heat flux (F_q)	3.10	3.10
Radial	1.50	1.42
Axial	1.62	1.62
Maximum-to-average rod in cluster	1.18	1.25
Flux (F_q^E) engineering	1.08	1.08
($F_{\Delta H}^E$) engineering	1.05	1.05
Flow effectiveness*	1.05	1.05
Heat transfer		
Active core surface area, sq ft	32,748	32,197
Average flux, Btu/(hr)(sq ft)	124,600	124,600
Maximum steady-state flux, Btu/(hr)(sq ft)	386,000	386,000
Average film coefficient in maximum-power tube, Btu/(hr)(sq ft)(°F)	9900	10,000
Minimum DNB ratio at full power	2.3	2.3
Temperatures, °F		
Moderator, average	155	155
Moderator, inlet	130	130
Coolant, inlet-to-pressure tubes	488	488
Coolant, discharge from pressure tubes	570.8	570.8
Saturation temperature	592.7	592.7
Fuel-rod surface, maximum steady	602	602
Maximum center temperature at 100% power	3930	3930
Fuel rod		
Outside diameter, in.	0.54	0.54
Pellet diameter, in.	0.5	0.5
Cladding wall thickness, in.	0.0163	0.0163
Fuel length per rod, ft	16.04	16.03
Rod lattice, in.	0.672	0.672
Rods per assembly	19	37
Pressure tube		
Total No. of pressure tubes	760	384
No. of U-tube assemblies	380	192
No. of fuel elements	760	384
Inside diameter, in.	3.959	5.303
Wall thickness, in.	0.207	0.277

*Ratio of hot-tube enthalpy rise to corewise average enthalpy rise. Dependent on timewise nuclear factor for low-power tubes.

the major difference between the CVTR and the large plant is the number of pressure tubes, the number being larger by an order of magnitude in the large plant. This increased number results in a greatly increased jumper stack height (Fig. IX-2). In the large plant the pressure tubes are supported on the top neutron-shield tank to minimize stresses due to thermal

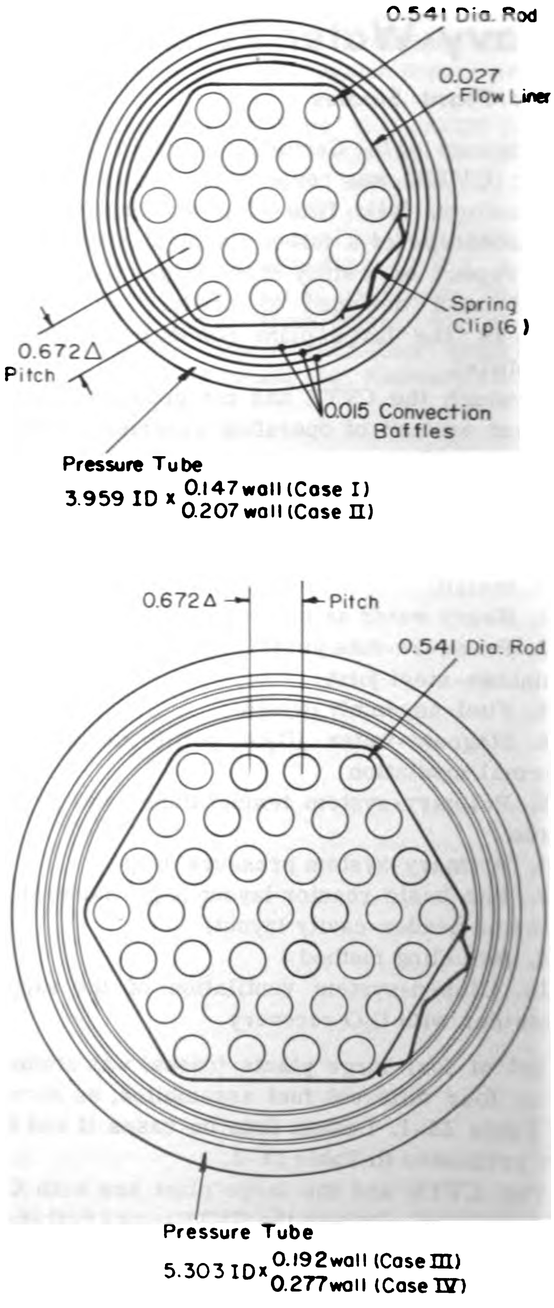

Fig. IX-1 Cross section of pressure tubes containing 19- and 37-rod fuel clusters (dimensions in inches).[1]

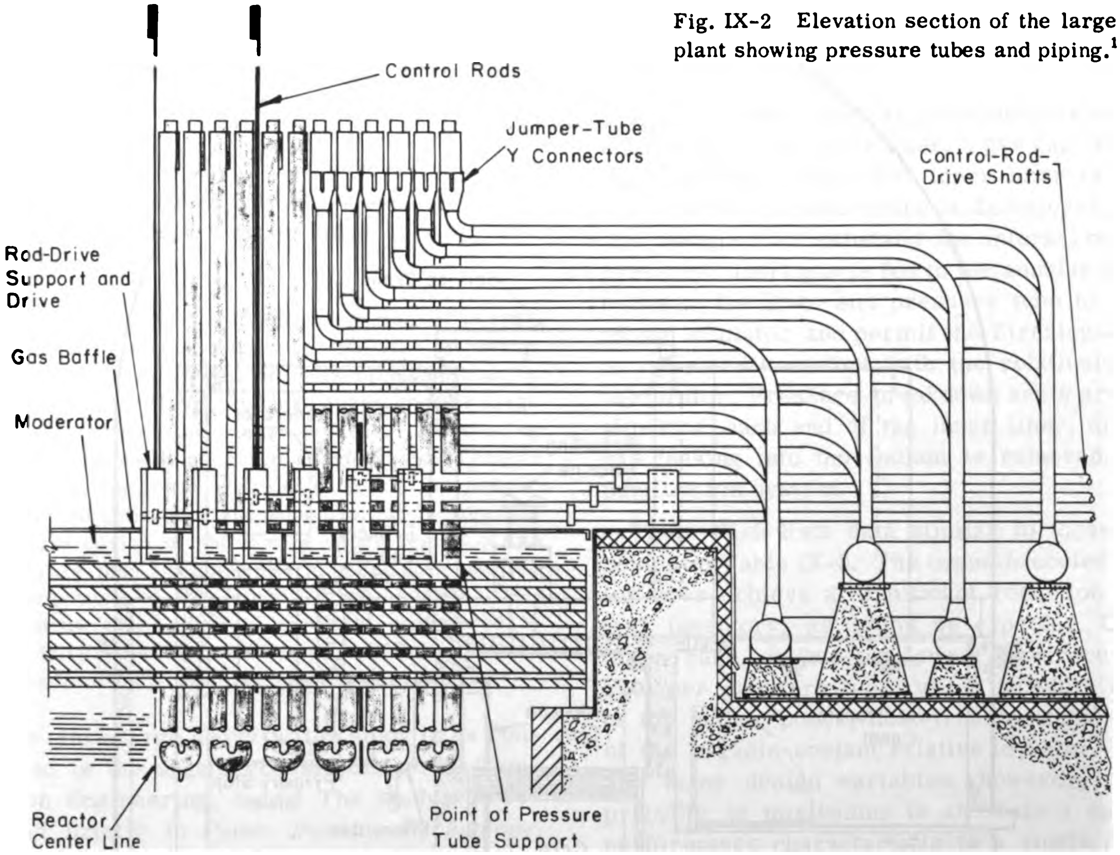

Fig. IX-2 Elevation section of the large plant showing pressure tubes and piping.[1]

expansions. It is noted in Ref. 1 that the U-tube design for the pressure tubes is not necessarily the best arrangement for the large plant. Advantages and disadvantages of U tubes relative to through-tubes and bayonet or reentrant tubes are also discussed. The U-tube design does confine all the jumper tubes and their associated joints to the top of the reactor where they are probably more readily accessible, and it avoids penetrations of the moderator tank below the D_2O level. But the U tubes also have an inherently large pressure drop (because they constitute a two-pass system) and are expensive.

Figure IX-3 is a schematic diagram of the equipment arrangement in the vapor container. The reference contains some cost data on the arge-plant designs and the following quotation probably best serves to illustrate the results:[1]

> An estimate of the cost of each of the four large plants was made primarily to indicate areas where improvements must be made to lower costs. Since no concerted effort was made to achieve optimum conditions or designs, it was anticipated that the estimated costs of these four plants would be higher than estimates by others in the industry for comparable plants. Thus comparisons should be made with caution.
>
> The costs for each of the four plants are listed below.

Item	Cost* mills/kw-hr			
	Case I	Case II	Case III	Case IV
Plant	6.06	5.89	5.53	5.27
D_2O	1.53	1.48	1.42	1.32
D_2O losses (2% per year)	0.24	0.23	0.22	0.20
Fuel cost	3.74	2.15	3.85	1.98
Operation & maintenance	0.80	0.80	0.80	0.80
Total	12.37	10.55	11.82	9.57

*Costs based on 14.5% yearly rate on capital investment and 13.0% yearly rate on the D_2O.

The fuel assemblies for each of these four cases are described in Table IX-1. Although comparisons of cost data are often not significant, there are a few comparisons of important design parameters that probably can be made with validity. These comparisons are illustrated in Table IX-3. The data for the Canadian, Du

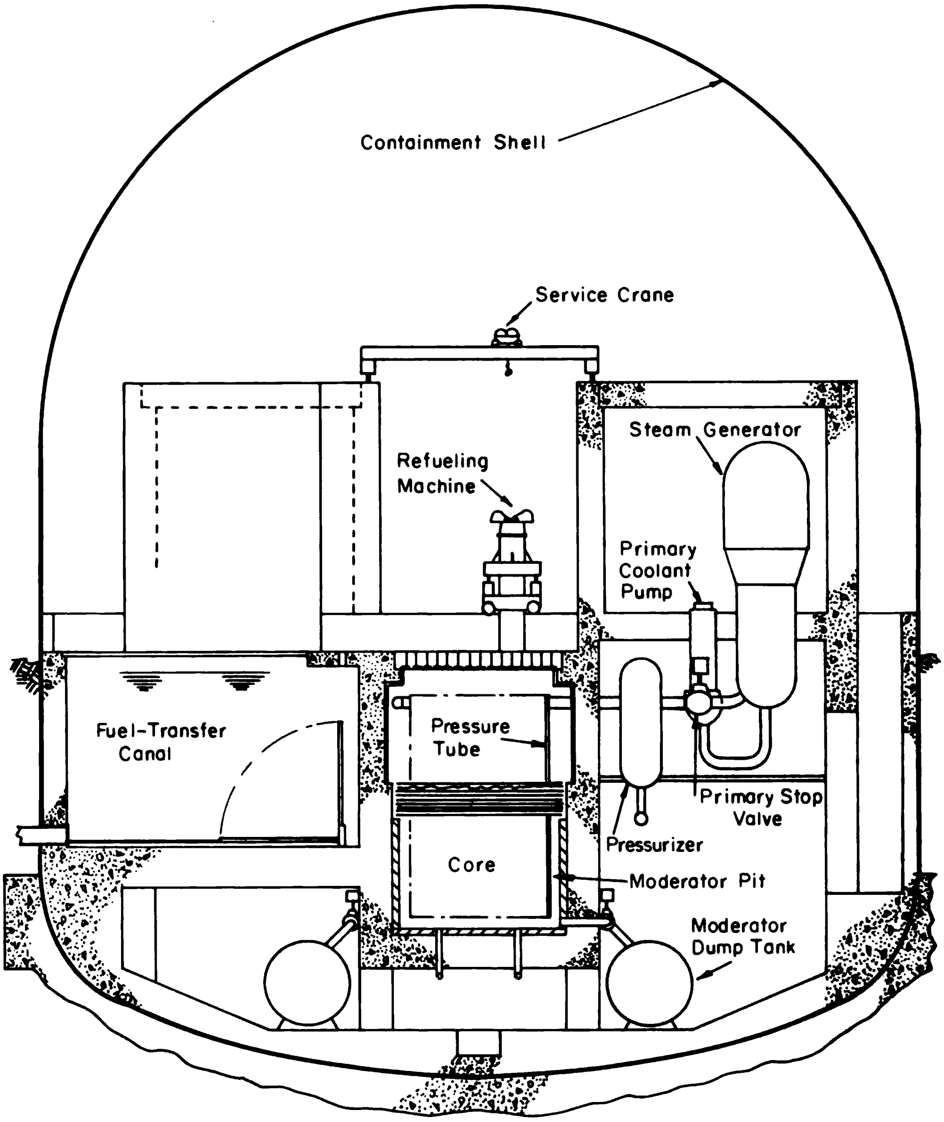

Fig. IX-3 Elevation section of vapor container.[1]

Table IX-3 COMPARISON OF DESIGNS FOR LIQUID D_2O-COOLED REACTORS

	Canadian	Du Pont	AEPSC-GNEC	Westinghouse case IV
Gross power, Mw(t)	1570	1838	1850	1135
Total D_2O inventory, metric tons	350	325	390	485
Maximum heat flux, Btu/(hr)(sq ft)	330,000	850,000	620,000	386,000
Uranium inventory, metric tons	95.7	27.1	51.4	76.7
Average specific power, Mw(t)/metric tons of U	16	68	36	14.8
No. of pressure tubes	387	226	560	384 (192 U tubes)
Average power/pressure tube, Mw(t)	4.1	8.1	3.3	3.0

Pont, and American Electric Power Service Corporation–General Nuclear Engineering Corporation (AEPSC-GNEC) designs were taken from Table IX-1, *Power Reactor Technology*, 7(1): 88.

The relatively high D_2O inventory of the U-tube design results from a large number of pressure tubes with a large tube-to-tube spacing:[1]

> The quantity of heavy water in the reactor is very large, with the consequence that the inventory charges are very high. This is brought about by the large quantity of pressure tubes and the large spacing between the pressure tubes. The spacing of the U-tubes is governed by mechanical considerations concerned with locating all the jumper tubes and pressure tube supports. It is apparent that the design of the entire upper region of the pressure tube including the jumper tubes and the arrangement of the jumper tubes, control rods, supports, etc., must be carefully engineered to give the proper balance between D_2O inventory and pressure drop without mechanical interference.

The other large heavy-water study to be considered is the organic-cooled design by Combustion Engineering, Inc.[2,3] The study was reviewed briefly in *Power Reactor Technology*, 7(1): 95-97, and this review will emphasize some of the technical details of the concept. The characteristics of the plant are summarized in Table IX-4. The reactor, shown in its containment building in Fig. IX-4, has 600 pressure tubes, each containing five fuel elements (Fig. IX-5). Interestingly, a two-pass flow through the core is used, as in the CVTR [this is shown in Fig. IX-7, *Power Reactor Technology*, 7(1)]; although the CVTR uses a U tube, the organic-cooled design connects the two passes via a lower, interpass header, so that the allocation of pressure tubes to the two passes can be made for optimum thermal performance. The fuel element contains 37 rods, but not all are of identical size. Thirty-one rods have an outside diameter of 0.513 in., and the remaining rods have an outside diameter of 0.313 in. to achieve a circular configuration. Rod-to-rod spacing is maintained by small square "wires" wound helically around each rod. These wires are extruded as an integral part of the cladding tube, which is sintered aluminum (SAP), XAP-001. Each rod was designed to be freestanding, and the assembly is secured by stainless-steel bands around the outside of the bundle. The bundle was designed with staggered ends (Fig. IX-5) that intermesh with the adjacent bundles to minimize end flux peaks and orient the elements azimuthally.

The pressure tubes are of composite design, consisting of an inner liner, a gas gap, and the outer pressure tube. The inner liner is XAP-001, and the pressure tube is Zircaloy-2. Both are designed to withstand the internal organic pressure. Inert gas is fed to the annular region between the liner and pressure tube to serve as an insulator and permit the Zircaloy-2 tube to operate in contact with the relatively cold moderator. Pressure-breakdown seals are provided at each end of the inner liner, and any gas leaking into the coolant is removed in the purification system.

Table IX-5 lists data similar to those presented in Table IX-3. The organic-cooled reactor does achieve a significant reduction of the D_2O inventory, as might be expected. On the other hand, it has the lowest power-removal rate per pressure tube, which possibly is due to the rather poorer heat-transfer capabilities of the organic coolant relative to water. There are many design variables, however, and it probably is misleading to attribute a specific performance characteristic to a single design variable. The average specific powers of the Canadian, the Westinghouse, and the Combustion Engineering designs are comparable; the relatively high specific powers of the Du Pont and AEPSC-GNEC designs are probably due to the different fuel-element designs. The Canadian, Westinghouse, and Combustion Engineering designs utilize solid pellets, whereas the Du Pont design specifies coaxial cylinders of fuel (UO_2) of relatively thin oxide sections, and the AEPSC-GNEC design specifies hollow, sintered pellets of UO_2. The Du Pont fuel element is shown and discussed in *Power Reactor Technology*, 7(1): 95. The coaxial design is mentioned in Ref. 1 as a fertile area for further study. In Ref. 2 it is recognized that the 37-rod fuel element may not be an optimum one, and the coaxial design and several others are discussed.

Reference 2 includes power cost estimates. Results are summarized in Table IX-6. Note that the organic-cooled heavy-water-moderated reactor (OHWR) was designed to operate on either enriched or natural fuel. It is stated in Ref. 2 that the resultant plant, therefore, cannot be considered as an optimum design for operation with only one type of fuel.

Table IX-4 500-Mw(e) D_2O-MODERATED ORGANIC-COOLED REACTOR-PLANT CHARACTERISTICS[2]

General		
Reactor type	D_2O moderated, organic cooled	
Steam-cycle type	Nonreheat with turbine moisture extraction	
Total fission power, including moderator heat loss, Mw	1550	
Station net output, Mw(e)	Enriched	512.2
	Natural	510.3
Net plant efficiency, %	Enriched	33.05
	Natural	32.92
Fuel and core		
Type of fuel	UO_2	
Fuel density, % of theoretical	91	
Design burnup, Mwd/metric ton	Enriched	20,000
	Natural	5,000
Cladding material	XAP-001	
Cladding thickness, in.	0.010 and 0.016	
Fuel-rod outside diameter, in.	0.313 and 0.513	
No. of fuel rods/bundle	6 plus 31	
Overall length of fuel bundle, in.	40	
No. of bundles/pressure tube	5	
Pressure tubes		
Number	600	
Lattice arrangement	Square	
Pitch, in.	$9\frac{3}{4}$	
Material	Zircaloy-2 and XAP-001	
Outside diameter, in.	$4\frac{1}{32}$	
Wall thickness, in.	Zircaloy-2, 0.036; XAP, 0.062	
Insulation material	0.100 in. inert-gas annulus	
Core length, in.	192	
Core equivalent diameter, in.	269	
Radial-reflector thickness, in.	12	
Axial-reflector thickness, in.	12	
Total UO_2 loading, lb	246,000	
Type of control unit	Hy-Ball	
No. of control units	200	
Nuclear fuel inventory and burnup	Enriched	Natural
Uranium total, metric tons	98.7	98.7
Initial enrichment, wt.% ^{235}U	1.25	0.7115
Discharge enrichment, wt.% ^{235}U	0.05	0.30
Discharge plutonium, g/kg of U initial	6.09	3.23
Design life, Mwd/metric ton of U	20,000	5000
Nuclear fuel inventory and burnup	Enriched	Na
Fuel conversion ratio by weight for gross lifetime		
Total plutonium generated/^{235}U lost	1.40	1.24
Fissionable plutonium generated/^{235}U lost	1.23	1.0
Fuel conversion ratio by weight for net lifetime, plutonium remaining/^{235}U lost	0.51	0.7
Lifetime energy-production fractions		
^{235}U fission	0.49	0.64
^{238}U fission	0.01	0.0
Plutonium fission	0.50	0.35
Thermal		
Average heat flux, Btu/(hr)(sq ft)	115,000	115.
Maximum heat flux, Btu/(hr)(sq ft)	298,400	352.
Maximum cladding-surface temperature, °F	< 850	<
Maximum UO_2 fuel temperature including all hot-spot factors, °F	< 3450	< 375
Primary coolant system		
Coolant material	Santowax OMP, 10% high boilers	
Total coolant flow, lb/hr	42,900,000	
Reactor inlet temperature, °F	536	
Reactor outlet temperature, °F	760	
Reactor pressure drop (header to header), psi	223	259
No. of loops	4	
Coolant inventory, lb	790,000	
Makeup, lb/day	7200	
Blanket gas	Nitrogen	
Materials in contact with coolant	Carbon steel, XAP-001, S.S.	
Moderator system		
Medium	D_2O	
Moderator-tank inlet temperature, °F	130	
Moderator-tank outlet temperature, °F	190	
Design temperature, °F	250	
Total flow rate, lb/hr	4,350,000	
System design pressure, psig	150	
Blanket gas	Helium	
Materials in contact with moderator	S.S., Zircaloy	
Total inventory, lb	519,000	
Makeup, lb/year	5000	
Cooling arrangement	Nonregenerative	

Thermal Breeder Reactors

Two recently published studies deal with the subject of D_2O reactors and their potential as breeders or near breeders.[4,5] These studies are of particular interest because one examines the thorium-^{233}U system[4] and the other considers the uranium-plutonium system.[5]

No reactor designs, as such, are presented in Ref. 4. The reference is more a discussion of the philosophy behind the thermal breeder reactor. The reactors that are discussed are D_2O-moderated and D_2O-cooled machines fueled with the coaxial fuel elements of either metal or oxide, clad in a zirconium alloy.[6] A brief description of the preliminary designs is given in Table IX-7. The thorium-fueled reactor has a number of somewhat unusual features. An outer ring of pressure tubes is placed in the

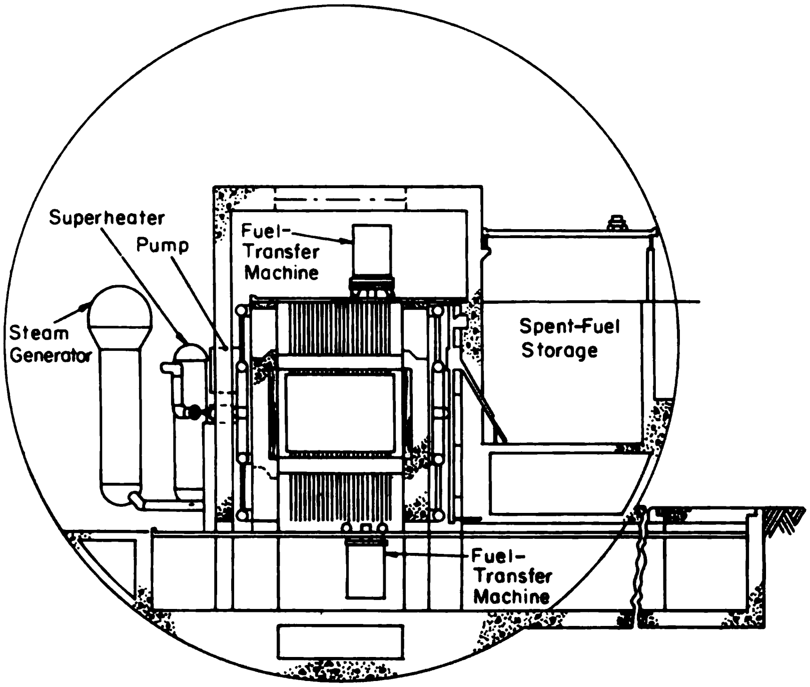

Fig. IX-4 Reactor plant elevation.[2]

reflector region to serve as a converter blanket and is fueled with thorium containing, initially, no fissile isotope. Short elements of uranium-free thorium also are placed at the top and bottom of the fuel column in the axial reflector region, and some of the control rods are fabricated of thorium.

The following quotation[4] serves to highlight the discussion presented in Ref. 4 on breeding in thermal reactors:

> In considerations of breeding in thermal reactors with the thorium-^{233}U fuel cycle, a clear distinction must be made as to the significance of the following four factors: breeding ratio, doubling time, conservation of fuel resources, and fuel economics. A high breeding ratio is of value only if it leads to a short doubling time; a short doubling time serves little purpose if it does not conserve fuel resources; and fuel conservation itself is of questionable value unless for some postulated set of economic conditions this conservation leads to lower fuel cycle costs.
>
> The D_2O-moderated thermal breeders discussed in this report are based on consideration of all four of these factors. The reactors do not represent the maximum possible breeding ratio or the minimum doubling time achievable with solid-fueled D_2O reactors. Instead, they represent a judgment of the compromises that will be necessary to achieve excellent conservation of fuel resources while retaining those features of D_2O reactors that are essential to low-cost power generation in the near future. It will be shown that the breeding gain in any of the D_2O systems considered is too small to be an important factor in fuel cycle costs during the next 50 years or so.

A fixed-fuel reactor employing thorium as the fertile material suffers from the immobility of ^{233}Pa, which may absorb neutrons prior to decay to ^{233}U. This has led to reactor concepts in which the thorium would be placed in a "blanket" where a low neutron flux would minimize ^{233}Pa losses. This principle is employed to some extent in the design shown in Table IX-7, but its use is limited by the economic disadvantages of devoting D_2O moderator and reactor volume to blanket functions, or even to power-producing functions when the specific power is low. Also, resonance absorption in ^{233}U causes significant reductions in eta and the breeding ratio.[4] Consequently the highest breeding ratios are apt to be obtained with moderator/fuel ratios higher than those which currently give the best economic performance. Taken together, these reasons have led the authors of Ref. 4 to deemphasize breeding and to emphasize low inventory and long fuel life, at least for the near future.

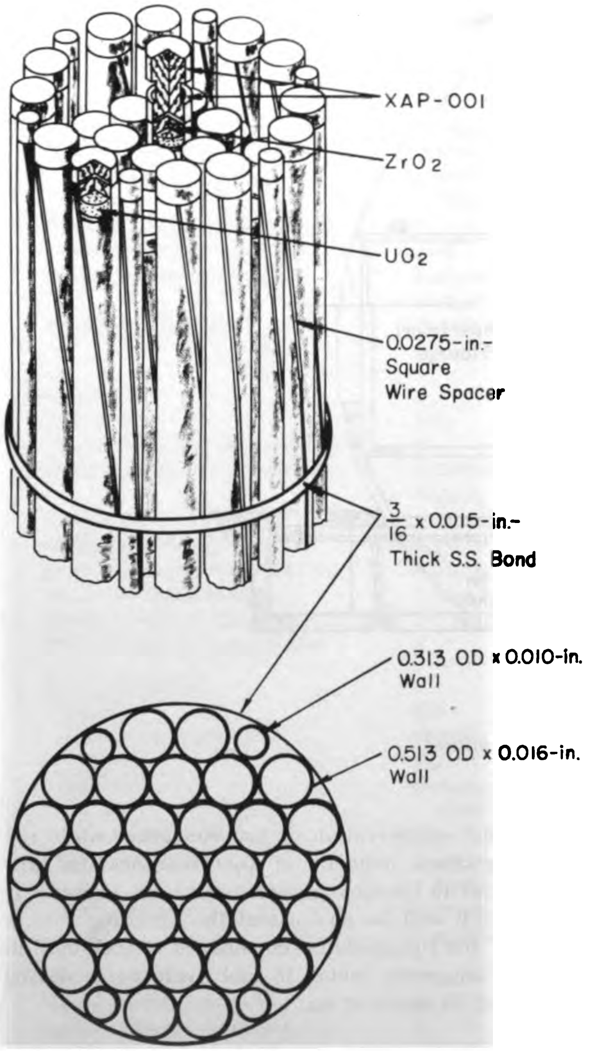
XAP-001
ZrO_2
UO_2
0.0275-in.-Square Wire Spacer
$\frac{3}{16}$ x 0.015-in.-Thick S.S. Bond
0.313 OD x 0.010-in. Wall
0.513 OD x 0.016-in. Wall

Fig. IX-5 Perspective and cross-sectional view of 37-rod fuel element.[2]

Table IX-5 COMPARATIVE DESIGN DATA FOR THE HEAVY-WATER-MODERATED ORGANIC-COOLED REACTOR: ENRICHED-FUEL DESIGN

Gross power, Mw(t)	1550
Total D_2O inventory, metric tons	235
Maximum heat flux, Btu/(hr)(sq ft)	352,5
Uranium inventory, metric tons	98.7
Average specific power, Mw(t)/metric ton of U	15.7
No. of pressure tubes	600
Average power/pressure tube, Mw(t)	2.6

The following reactor system is postulated for the orderly development of D_2O-thorium breeders:[4]

> Until 1975, all new reactors are H_2O converters with Pu recycle.
>
> From 1975 to 1985, all new reactors are D_2O converters operating on uranium fuel with Pu recycle.
>
> In the years 1985 to 2000, all new reactors are D_2O-thorium reactors with a conversion ratio of 1.00. The old D_2O converter reactors remain on uranium fuel with Pu recycle.
>
> After the year 2000, all new reactors are D_2O-thorium breeders, with an effective breeding ratio (including reprocessing losses) of 1.05. This breeding ratio leads to a doubling time of 32 years, which will meet the estimated growth of nuclear power beyond the year 2030.

In Fig. IX-6 are shown the uranium and thorium requirements for the above system (termed "D_2O-thorium" in the figure) and for three other systems that were postulated and discussed in a previous article in *Power Reactor Technology*, 6(4). Subject to the assumptions used in deriving the data shown in Fig. IX-6, it is evident that the D_2O-thorium system will be more conserva-

Table IX-6 OHWR TOTAL-ENERGY-GENERATION COST SUMMARY[2]

(Costs Are in Mills/kw-hr at 90% Plant Factor)

	Natural fuel with private ownership	Enriched fuel	
		Government ownership	Private ownership
Capital	2.99	2.99	2.99
Amortization of initial core fuel and fabrication	0.23	0.20	0.25
Fuel cycle	1.88	0.77	0.72
Heavy water (at \$24.50/lb)			
Amortization charge	0.43	0.43	0.43
Losses (1% of inventory)	0.03	0.03	0.03
Organic makeup	0.12	0.12	0.12
Operation and maintenance	0.36	0.36	0.36
Nuclear liability insurance	0.08	0.08	0.08
Total	6.12	4.98	4.98

Table IX-7 DESCRIPTION OF 1000-Mw(e) PRELIMINARY DESIGNS OF D_2O-MODERATED POWER REACTORS[4]

Fuel	UO_2	Th metal
Initial enrichment, wt.%	1.2 (^{235}U)	1.5 (^{233}U)
Reactor coolant	Liquid D_2O	Liquid D_2O
Lattice pitch, in.	10	10
No. of fuel positions	489	678
Core radius, ft	10.8	12.6
Core length, ft	15	15
Coolant inlet temp., °C	264	264
Coolant outlet temp., °C	304	304
Maximum heat flux, pcu/(hr)(sq ft)	434,000	340,000
No. of coolant loops	8	8
Throttle steam pressure (saturated), psia	495	500
Net plant efficiency, %	26.7	26.1
Net power production, Mw(e)	1000	981
D_2O inventory, tons	660	872
Thorium or uranium inventory, metric tons	64.5	103
^{233}U or ^{235}U inventory, kg	765	1540

tive of uranium resources for the next century than will the other systems.

Fuel-cycle cost data are given in Table IX-8. In any of the cases estimated, it appears that breeding is a relatively small economic factor in fuel-cycle costs and that an attractive way to reduce near-term costs is to increase the exposure in the thorium fuel even at the expense of reduced conversion ratios. It is also indicated that thorium-fueled D_2O reactors still have an attractive fuel-cycle cost even if the cost of natural uranium should increase to $100 per kilogram. The use of uranium in the thorium fuel cycles having breeding ratios of 1.00 or greater is not obvious from Table IX-8, but the uranium is used as a source of ^{235}U for startup of the fuel cycle. As the cost of uranium increases to a high value, the inventory charge for the uranium becomes the major component of the fuel-cycle cost.

The breeding potential of thermal reactors fueled with plutonium is described in Ref. 5. The reference, primarily the result of a physics study, considers the breeding ratio in infinite homogeneous systems, presents a conceptual design for a plutonium-fueled D_2O-moderated thermal power reactor, and treats the buildup of higher plutonium isotopes and their effect on conversion ratios. The details of the various calculational procedures will not be discussed here; however, they would be of interest to the specialist. The author considers D_2O-, H_2O-, graphite-, and beryllium-moderated reactors and concludes that heavy water is the most desirable moderator and that it is essential to keep the moderator at a low temperature. The moderator temperature and resulting neutron temperature have a large effect on the value of eta of plutonium. Figure IX-7 gives $\bar{\eta}$ as a function of moderator temperature for two different values of moderating power per plutonium atom.

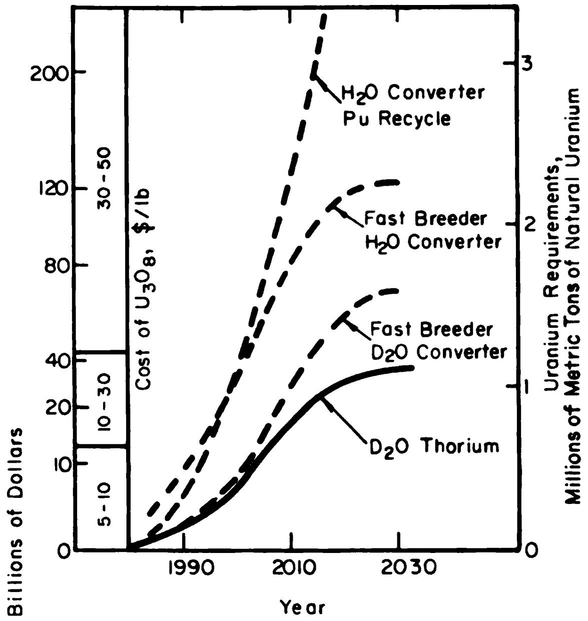

a. Uranium Requirements

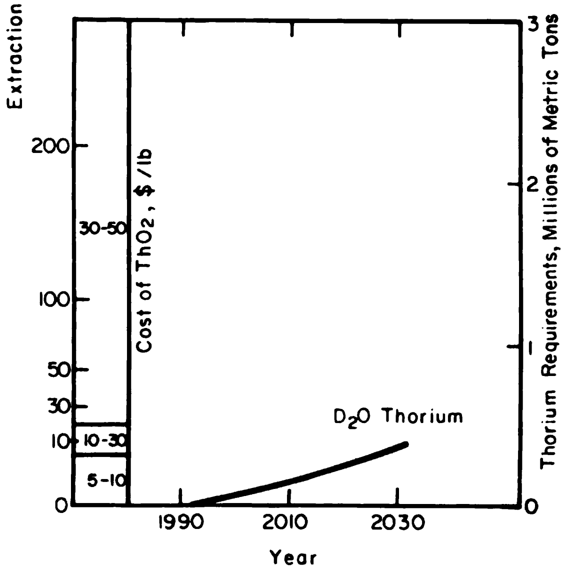

b. Thorium Requirements

Fig. IX-6 Uranium and thorium requirements for the D_2O-moderated power reactors through 2030 A.D.[4]

Table IX-8 ESTIMATED FUEL-CYCLE COSTS FOR D_2O REACTORS[4]

		Current costs			Future costs		
Fuel	UO_2	Th	Th	Th	Th	Th	Th
Equivalent breeding ratio*		1.00	1.05	1.00	1.00	1.05	1.00
Uranium cost, \$/kg of uranium	13	13	13	13	100	100	100
Thorium cost, \$/kg of thorium		20	20	20	20	20	20
Exposure, 10^3 Mwd/metric ton	14	15	15	30	15	15	30
Costs, \$/kg of fuel							
Fabrication	22	30	30	30	30	30	30
Shipping	2	5	5	5	5	5	5
Reprocessing		35	35	35	10	10	10
Burnup or credit	49	0	−3.6†	0	0	−27†	0
Subtotal, \$/kg	73	70	66	70	45	18	45
Subtotal, mill/kw-hr†	0.81	0.74	0.70	0.37	0.48	0.19	0.24
Uranium inventory charge, mills/kw-hr‡,§	0.05	0.15	0.15	0.15	1.12	1.12	1.12
Thorium inventory charge, mill/kw-hr‡	0	0.05	0.05	0.05	0.05	0.05	0.05
Total, mills/kw-hr	0.86	0.94	0.90	0.57	1.65	1.36	1.41

*Includes allowance for reprocessing and refabrication losses; "equivalent breeding ratio" equals breeding ratio in reactor − 0.01.

†At net thermal efficiencies shown in Table IX-7.

‡At a charge rate of 10% per year; total inventory assumed 50% greater than reactor inventory.

§It is assumed that ^{233}U is worth only the cost of the natural uranium required to produce it and that 3 kg of ^{233}U can be obtained from 1 metric ton of mined uranium.

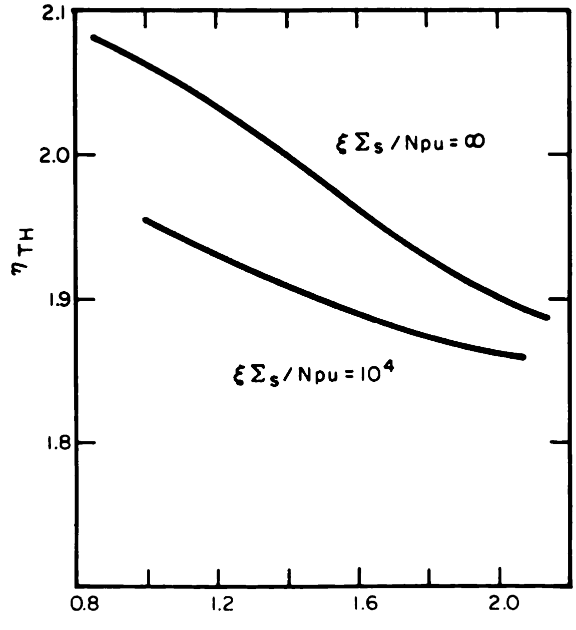

Fig. IX-7 Effect of moderator temperature on thermal average value of eta of ^{239}Pu (heavy-water moderator).[5]

Since moderator temperatures of the order of room temperature are indicated, the author concludes that the reactor should be a heterogeneous one of the pressure-tube type.

The limiting value of the attainable breeding ratio is given by

$$\bar{\eta}\epsilon - 1$$

where $\bar{\eta}$ is the number of neutrons produced per neutron absorbed in the fuel and ϵ is the fast fission factor, including $(n,2n)$ reactions. It is shown[5] that values of epsilon approaching 1.1 are necessary to obtain high conversion ratios in the plutonium-fueled thermal reactors and that these values are obtained only with close-packed large-diameter clusters of metallic (uranium-plutonium) fuel elements. The use of oxides reduces epsilon considerably. The use of large-diameter fuel clusters is reconciled with the usual heat-transfer requirement of large surface areas by conceiving the rod bundle as a cluster of at least 91 fuel rods, each having a diameter of about 0.4 in. Plutonium-bearing fuel elements were discussed in Sec. IV of *Power Reactor Technology*, 7(2), and although the uranium-plutonium type elements have not undergone extensive experimentation, the experience to date has been mixed.

The coolants considered in the study were D_2O, helium, and steam, and Table IX-9 summarizes the conversion ratios calculated to be attainable in these reactors. The choice of beryllium as a pressure-tube material has quite an effect on the attainable conversion

Table IX-9 ESTIMATES OF FINAL CONVERSION RATIOS IN URANIUM-PLUTONIUM HEAVY-WATER SYSTEMS[5]

(Beryllium Pressure Tubes, Zircaloy-2 Cladding)

Type	Initial conversion ratio	Operating conversion ratio	Final conversion ratio	Specific power, Mw/kg of plutonium (central channel)	Channel power, Mw(e)	Pumping power, % of channel electric power
D_2O coolant	1.0415	0.9784	0.9184	5.5	2.87	1.74
Steam coolant	1.0645	1.0014	0.9414	0.83	0.277	12.0
Helium coolant	1.0439	0.9808	0.9208	1.74	0.59	8.5

ratios, since they would decrease about 8% if Zircaloy-2 were employed. Beryllium cladding, in the case of the helium-cooled reactor, would increase the initial conversion ratio about 5% over the data shown in Table IX-9. If allowances were made for such items as leakage, extra parasitic absorption, and control requirements, the author concludes that reactors could be designed to yield conversion ratios of about 0.90.

Pressurized-Water Reactors: Chemical Shim

The use of soluble neutron absorber in the primary coolant system seems destined to play an increasing role in the control of reactivity in pressurized-water reactors. Although first used as an emergency shutdown measure to "back up" the control-rod system in water-moderated reactors, the soluble-absorber concept was extended, in the Yankee reactor design, to provide the normal cold shutdown margin. Because of a number of uncertainties about its behavior under conditions of power operation, dissolved absorber has up to now been restricted to use for shutdown in routine applications; it has, however, been used at full power during relatively short tests in the BORAX-II, BORAX-III, EBWR, and Yankee reactors. Also, it has been in use during several months of power operation in the Saxton reactor. The potential advantages for reactivity shimming by dissolved absorber under power are such that an extensive development effort has been directed toward that end. The application poses safety questions that have been investigated generally and in sample reactor designs. These questions will have to be answered specifically for any reactor intended for operation with dissolved absorber. It seems highly probable that this will be done and that reactivity control by dissolved absorber, otherwise known as chemical shim, will come into general use for pressurized-water reactors.

The main development effort on chemical shim has been made at the Westinghouse Atomic Power Department (WAPD), under AEC contract, as part of the AEC's Large Reactor Development Program. A survey paper on the subject was published in a recent issue of *Nucleonics*.[7] This, and a number of topical reports that have become available from the WAPD project, forms the basis for the review that follows. The review is restricted to the application and behavior of the chemical-shim system in the operating reactor, and it will not consider related plant-design questions, such as methods of fuel handling for a reactor that depends on dissolved absorber for shutdown.

The direct advantage of chemical shim is the reduction of the number and size of control rods required for the reactor installation. Although this effect is desirable in itself, the more important result is the improvement in spatial distribution of power (and hence in average power density in the core) that can be realized by minimizing the number and size of control rods in the core. The total improvement may be made up of several increments, but the main opportunity for improvement arises because a change in the concentration of dissolved absorber does not strongly affect the spatial power distribution, whereas a change in the number of control rods inserted, or in the depth of insertion of a bank of control rods, may influence the distribution profoundly. To realize the importance of this effect, one must consider the power distribution over the entire life of the core rather than at some particular instant in the life. In designing a control-rod installation, the designer can usually achieve a rather favorable power distribution for one particular condition of reactivity by utilizing those control rods which must be in the core to flatten the distribution. Inevitably, however, the control rods must be moved as the reactivity changes (because of fuel burnup or other effects), and the power distribution then becomes less favorable. If, instead of control rods, dissolved absorber is used to compensate for reactivity changes, the initial flattening of the power distribution can be accomplished by spatial variations in fuel enrichment or by other permanently installed spatial variations of core composition. Since the concentration of dissolved absorber is changed during reactor operation to compensate reactivity changes, the effect on power distribution is relatively small because the change in concentration is distributed uniformly over the core volume, and the initial favorable power distribution is preserved reasonably well.

At the present time, at least, the complete replacement of control rods by dissolved absorber is not contemplated. The rapid-scram requirement cannot easily be met by a soluble absorber system. At this time it does not seem desirable to make rather frequent large changes in the dissolved absorber concentration, as would be necessary, for example, if it were used to compensate the reactivity changes associated with power changes. The optimum division of the control function between control rods and soluble absorber will no doubt vary from one reactor design to another. The question is discussed later in this review, but at this point, for purposes of orientation, the system described in Ref. 8 may be considered briefly. That system, which probably represents about the minimum use of control rods likely in the near future, incorporates rods for the dual purpose of covering the power defect and the power maneuvering requirements and of providing rapid power-reduction capability. The required reactivity capability of the rod installation for these purposes is estimated to be 4.4% k_{eff}. An installation of 24 cruciform rods in the 8-ft-diameter core is calculated to provide this strength with a stuck-rod margin of 1 rod; the total worth of the 24-rod installation is 6.6% k_{eff}. The installation in the core is illustrated in Fig. IX-8. The soluble absorber shown in the figure (2000 ppm boron) has a reactivity worth[9] of 14 to 15% k_{eff} at room temperature and a worth of 18 to 19% k_{eff} at 522°F.

In the following sections some of the specific characteristics and problems of the chemical-shim concept are discussed at greater length under appropriate headings.

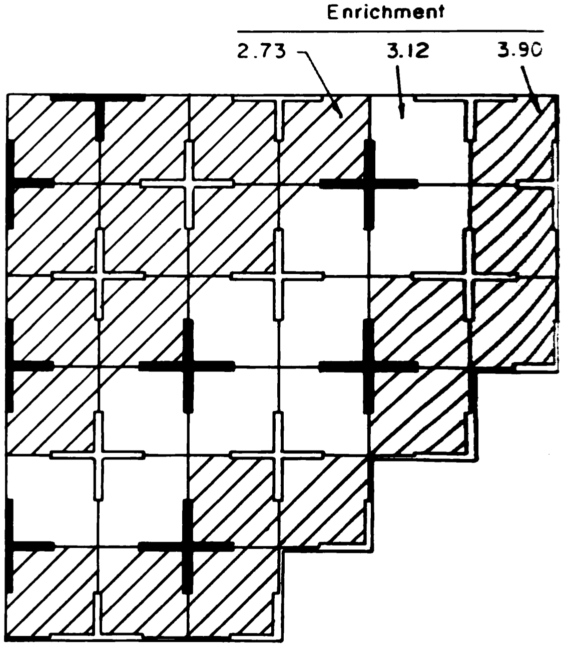

Fig. IX-8 Quarter-core diagram of control-rod installation in a reactor utilizing chemical shim.[8] The core, fueled with UO_2 clad in stainless steel, is intended for an output of 825 Mw(t). Its effective diameter is 98 in., and its height is 105 in. The equivalent H_2O/uranium volume ratio at room temperature is 3.34.

The solid cruciforms represent absorbing control rods, and the open cruciforms represent fueled "[illegible] followers," fueled with UO_2 of 2.73% enrichment. The absorbing control rods have a total worth of 6.6% in the hot reactor. The calculation is made for the case of 2000 ppm of dissolved boron in the water; under this condition k_{eff} for the hot, rodded core is 0.975.

Reactor Physics Effects

The most obvious question related to the reactor physics of chemical shim is how much dissolved absorber may be required to compensate a given excess reactivity. The major variables affecting this relation are the water fuel ratio of the core, the fuel enrichment, and the reactor temperature. Calculations for three representative cores for large pressurized-water reactors are given in Ref. 9; the pertinent characteristics of these cores are summarized in Table IX-10. Figure IX-9 shows the calculated reactivity worth of the dissolved absorber (natural boron) as a function of the absorber con-

Table IX-10 CHARACTERISTICS OF PRESSURIZED-WATER REACTOR CORES USED IN ANALYSIS OF DISSOLVED-BORON REACTIVITY EFFECTS[9]

	Core 1	Core 2	Core 3
Water/UO_2 volume ratio (68°F)	1.7:1	1.7:1	1.4:1
Water/U* volume ratio (68°F)	3.4:1	3.4:1	2.9:1
^{35}U enrichment, wt.%†			
Inner	2.56	2.94	2.94
Middle	2.93	3.36	3.36
Outer	3.66	4.20	4.20
Average	3.05	3.50	3.50
Fuel-rod pitch, in.	0.553	0.553	0.554
Pellet diameter, in.	0.375	0.375	0.393
Cladding thickness, in.	0.015	0.015	0.015
Material volume fractions‡ (68°F)			
UO_2	0.33590	0.33590	0.36866
304 stainless steel	0.08612	0.08612	0.09138
H_2O	0.56412	0.56412	0.52325
Void	0.01386	0.01386	0.01671
Core height, ft	8.5	8.5	8.5
Core diameter, ft	8.1	8.1	8.1
Extrapolation distance, cm	7.5	7.5	7.5
Thickness of steel baffle around core, in.	0.6	0.6	0.6
H_2O reflector thickness, in.	4	4	4

*It is assumed that $\rho_{H_2O} = 1.0$ g/cm³ and $\rho_U = 18.7$ g/cm³.

†Each core has three radial zones of enrichment, of equal volumes. The enrichments in the inner, middle, and outer zones are in the ratios 7:8:10.

‡This includes structure and additional water associated with typical cores.

centration in the coolant-moderator. Curves are given for the three reactors of Table IX-10, at room temperature and at operating temperature.

The curves in Fig. IX-9 illustrate some effects besides the obvious relation between boron content and reactivity. It is clear, for example, that the effectiveness of the boron decreases slightly as the fuel enrichment is increased. This is to be expected because the more highly enriched fuel competes more favorably against the boron for the absorption of neutrons. A larger effect, however, is the effect of water/fuel ratio. The "wetter" core (No. 2) is affected considerably more than the "drier" core (No. 3) by a given concentration of boron in the water. The major part of this effect is due to the simple fact that a given concentration represents a greater total amount of boron in the wetter core.

Since the amount of boron in the core is proportional to the amount of water in the core (for a given boron concentration), it is clear that the thermal expansion of water which accompanies a rise in temperature will remove some boron from the core. This effect gives rise to a positive component of the temperature coefficient of reactivity in cores utilizing soluble absorber. The effect is apparent in Fig. IX-9, since the curves for 522°F lie well below the curves for 68°F. In reactor 3, for example, the reactivity effect of 2000 ppm of boron at 68°F is 15.8% k_{eff}, whereas the effect of the same concentration at 522°F is only 12.3% k_{eff}. The positive component of the coefficient increases with the concentration of dissolved absorber and places a limit on the amount of dissolved absorber that may be used without encountering a net positive temperature coefficient of reactivity. This limiting concentration of dissolved absorber depends on the reactor temperature, the enrichment, and the fuel/water ratio. However, the two latter variables do not affect strongly the positive-coefficient limit on the amount of reactivity that can be compensated by dissolved absorber. The latter point is illustrated by Fig. IX-10, which, for two different reactors, shows little difference in the value of "cumulative boron worth" at which the temperature coefficient of reactivity changes sign. The operating temperature, on the other

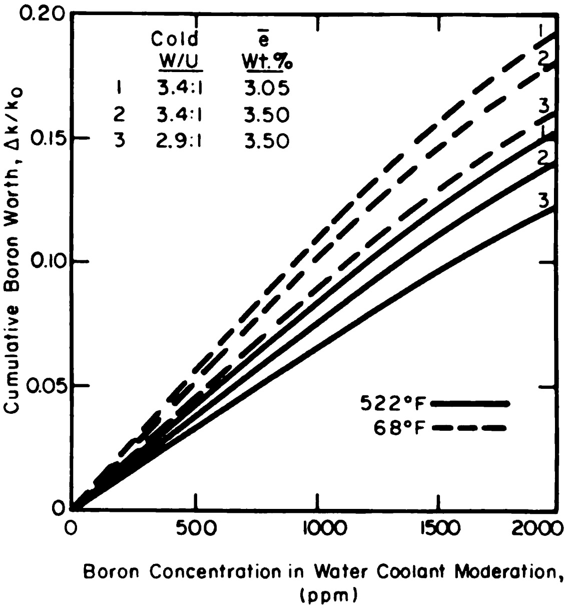

Fig. IX-9 Calculated reactivity worth of dissolved natural boron in three pressurized-water reactors.[9] The reactors are those described in Table IX-10.

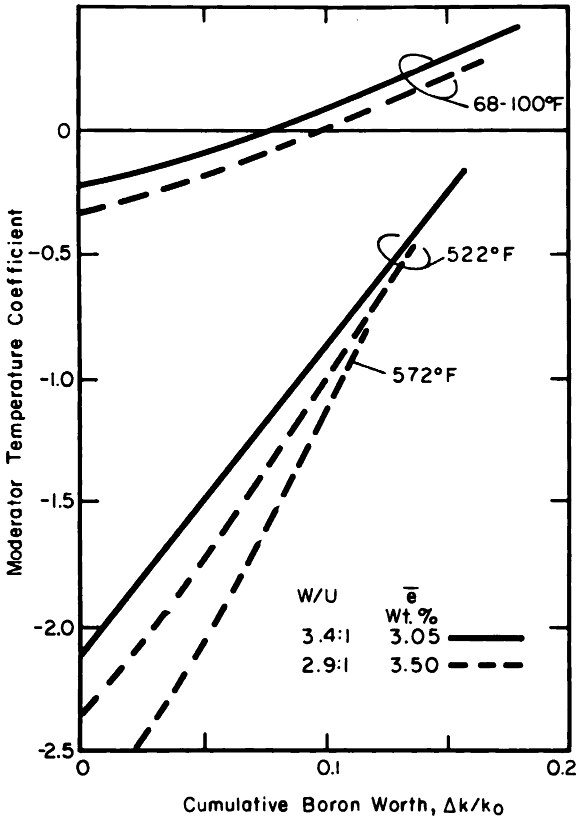

Fig. IX-10 Variation of moderator-temperature coefficient of reactivity with cumulative reactivity worth of dissolved boron in pressurized-water reactors.[9] The characteristics of the two reactors considered are given in Table IX-10.

Although the two reactors differ considerably in the reactivity effect of a given concentration of boron (see Fig. IX-9), their temperature coefficients of reactivity do not differ much if both have the same amount of reactivity compensated by dissolved boron.

hand, has a large effect. Figures IX-9 and IX-10 indicate that substantial reactivity compensation can be accomplished with soluble poison over a wide range of reactor-design variables without encountering the undesirable condition of a positive temperature (or void) coefficient of reactivity. The dissolved absorber will, however, reduce the value of the negative temperature coefficient as well as the temperature defect of reactivity from room temperature to operating temperature. These changes may affect the details of the reactor control system.

The degree of improvement in power distribution which can be achieved by the use of chemical shim depends on the specific reactor design and on the degree of design refinement which the designer is willing to invest in for the sake of a good power distribution. These considerations apply whether the reactor is controlled by chemical shim or by some competing reactivity-control method. As an example of the improvement achievable with chemical shim, Ref. 7 compares a rod-controlled case with an otherwise identical case in which chemical shim is used. The rod-controlled core is reported to have a maximum/average power-density ratio of 2.5, which is said to be 50 higher than the ratio for the chemical-shim case. This implies a maximum/average ratio of 1.67 for the latter. Even the ratio for the rod-controlled case is considerably lower than the design ratios attained in current practice. Apparently the ratios quoted are not intended to be the worst that might occur over the core lifetime but are simply comparative values for cases in which there are no partially inserted control rods—hence the quite low axial maximum/average ratios. The low ratios are also due partly to a radially zoned fuel loading, with fuel of three different enrichments, and apparently also to the assumption of fueled followers on the control rods which virtually eliminate the local power peaking in fuel elements adjacent to control-rod channels. Fueled followers for cruciform rods are not used in current design practice, but presumably they can be developed.

Pending the adoption of fueled control-rod followers or other methods of dealing with the power peaking introduced by water channels, it is interesting to see whether the chemical shim itself will reduce this local peaking effect because of the additional neutron absorption that it introduces in the water. It is indicated in Ref. 10 that there is a significant, but not large, improvement. Theoretical and experimental investigations of power peaking in fuel elements adjacent to representative water channels are reported in terms of a relative power-peaking factor.[10] This factor is the ratio of the local power density near a perturbation of the core composition (such as a water channel) to the power density that would exist at the same position if the composition were locally uniform. Typically, the relative peaking factor with 970 ppm of natural boron in the water was 97 to 98% of the factor when no boron was present (e.g., a peaking factor of 1.24 was reduced to 1.20 by the boron). Also investigated in the analysis was the effect of increased water temperature on the peaking factor. In the no-boron case, the peaking factors at 543°F ranged from 94 to 96% of those at room temperature.

As previously mentioned, control rods are to be used in conjunction with chemical-shim control, and part of this complement of control rods will remain in the core during normal operation. If the rods are partially inserted from one end of the core, they will produce a significant distortion of the axial power distribution, even though the total inserted worth may be relatively small. Figure IX-11, from Ref. 11, is a very instructive diagram that illustrates the effects of partially inserted control-rod banks in large water-moderated cores, regardless of whether chemical shim is employed in addition to the control rods. When a control rod, or a control-rod bank, is partially inserted from one end of the core, it skews the axial power distribution, causing the position of maximum power density to shift from the center plane of the core to a position farther from the end at which the rods enter. This skewing affects the axial maximum/average ratio, and its severity is, of course, dependent on the reactivity worth of the partially inserted control-rod bank. The solid curves in Fig. IX-11 show the calculated axial maximum/average ratio as a function of the degree of withdrawal of the control-rod bank for rod banks of different total worths. Also shown are lines of constant inserted worth. These lines define the depth of insertion that must be used with the various control-rod banks to compensate for a specified amount of reactivity. The figure also shows lines of constant differential worth, i.e., the amount of reactivity change represented by a 1-in. change in rod-bank withdrawal. For a particular installation, the requirements of the control system may set lower limits on both the inserted worth and the differential worth of the partially inserted rod bank when it is at the position corresponding to normal reactor operation. Figure IX-11 would indicate that, if the differential worth requirement is the more important one, a more favorable power distribution can be obtained by employing a rod bank of relatively high total worth, whereas, if the inserted-worth requirement is the more important one, a more favorable power distribution may be obtained by use of a bank of relatively low total worth. It is understood, of course, that the designer has a good deal of flexibility in the selection of the worth of the partially inserted rod bank, regardless of the total worth of the complete control-rod installation; i.e., he can divide the total complement of control rods into a number of banks and withdraw one bank at a time in sequence. When this is done, the radial power distribution will also be affected if any one or more of the banks of rods is fully inserted under the condition of interest.

A further significant point brought out in Ref. 11 is that a very substantial difference may exist, in a large pressurized-water reactor, between the axial power distributions at full power and zero power. The major source of this difference is the Doppler effect in the oxide fuel, which causes a larger reactivity loss in the hotter fuel, i.e., in the fuel with the higher power density, and therefore tends to flatten the power distribution. Additional, but smaller, effects are present because of the slight variation in equilibrium xenon poisoning with power density and possibly because of the effect of the water temperature rise in traversing the coolant channels (the latter effect is not mentioned in Ref. 11). Shown in Fig. IX-12 are the calculated axial power distributions for the zero-power case and the full-power case. Because of the relatively long thermal time constant of the fuel elements, the changes in power distribution do not immediately follow the changes in fission power level.[11]

Control Requirements and Characteristics

The various requirements for control rods in a chemical-shim reactor, in which the adjustment of dissolved absorber is done relatively slowly, are discussed in Ref. 8. The estimated ranges for various requirements are given in Table IX-11, as well as the requirements for a "reference" core. This reference core, which was mentioned in a previous paragraph, has a rod installation that provides 4.4% reactivity worth plus a stuck-rod margin. The various items listed in Table IX-11 are defined below.

Hot-to-Power Reactivity Swing. This reactivity component is often referred to as the power defect of reactivity and is the amount of reactivity that must be added to raise the reactor power from the hot zero-power condition to full operating power. It is assumed that the power increase takes place over a period of time that is long relative to the thermal time constant of the fuel, but short relative to the xenon half-life. In the reactors considered here, the power defect is due almost entirely to the Doppler effect.

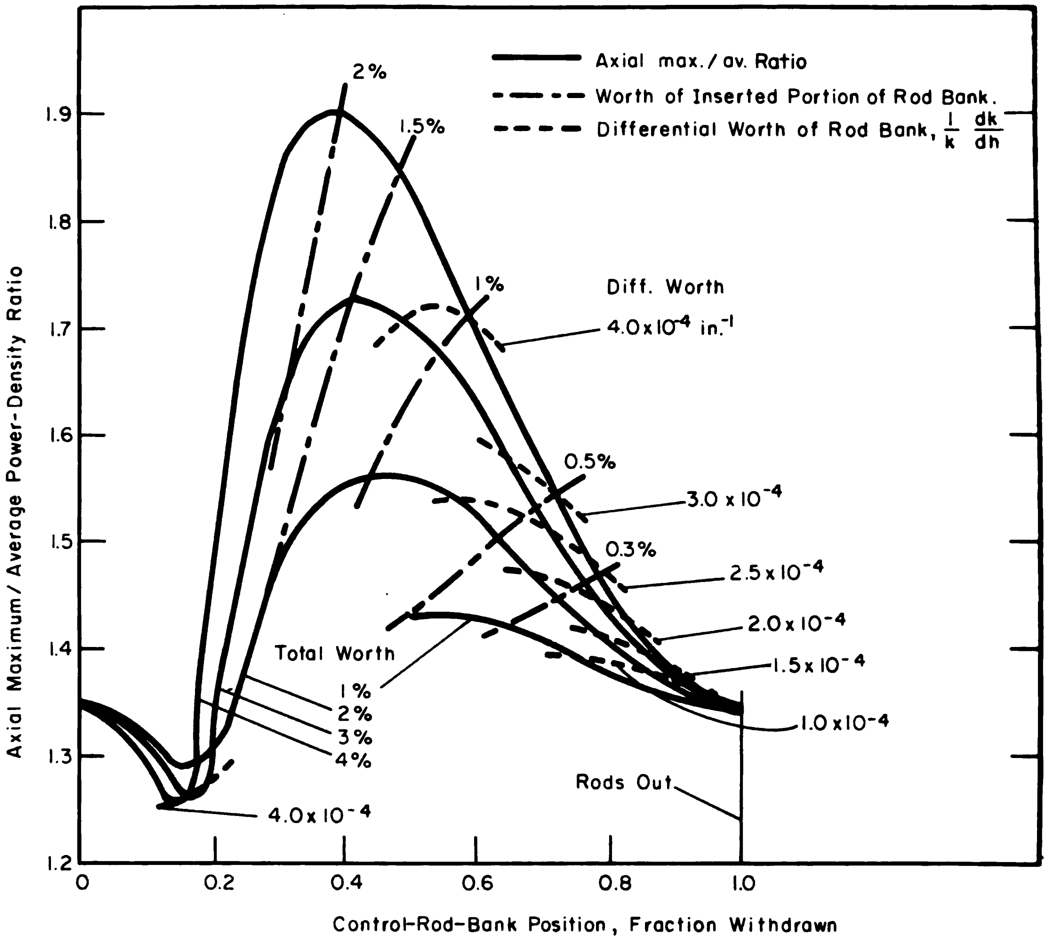

Fig. IX-11 Effect of reactivity worth and depth of insertion of control bank on axial maximum/average power-density ratio.[11] Four different rod banks are considered separately, each composed of unspecified numbers of control rods but worth 1, 2, 3, and 4% k_{eff}, respectively. Each solid curve shows the variation of the axial maximum/average ratio as one of the banks is withdrawn progressively from the core. When the bank is either fully inserted or fully withdrawn, it has a negligible effect on the ratio, which then has the value 1.35 for the particular reactor considered. When a bank is withdrawn only slightly, it decreases the maximum/average ratio slightly, for the beneficial effect of increasing the relative reactivity near one end of the core is more important than the accompanying adverse asymmetry effect. For larger degrees of withdrawal the asymmetry effect becomes large, and there is a strong concentration of power in the unrodded end of the core and a large increase in the maximum/average ratio. The effect increases greatly as the reactivity work of the partially inserted rod bank is increased.

The broken lines on the plot are loci of equal reactivity worth of the inserted portions of the partially inserted rod banks. The dashed lines are loci of equal differential worths of the partially inserted rod banks. The differential worth is the reactivity change produced by a 1-in. change in the position of the partially inserted bank.

The curves shown are qualitatively representative for any large reactor. The quantitative relations will vary greatly with individual core characteristics and especially with the length of the core as measured in neutron-migration lengths; the effects of partially inserted rods on peaking factors will increase as the core becomes longer.

The above curves were computed for a pressurized-water reactor with stainless-steel-clad UO_2 fuel rods, under full-power operation at a temperature of 543°F. The enrichment was 3.25 wt.% ^{235}U, the ratio of water to equivalent uranium metal was 3.4 at room temperature, and the active core length was 104.6 in. The thick axial reflectors were of water containing some structural material. The average power density corresponds to a total power of 825 Mw(t) from a core of about 8.1 ft diameter.

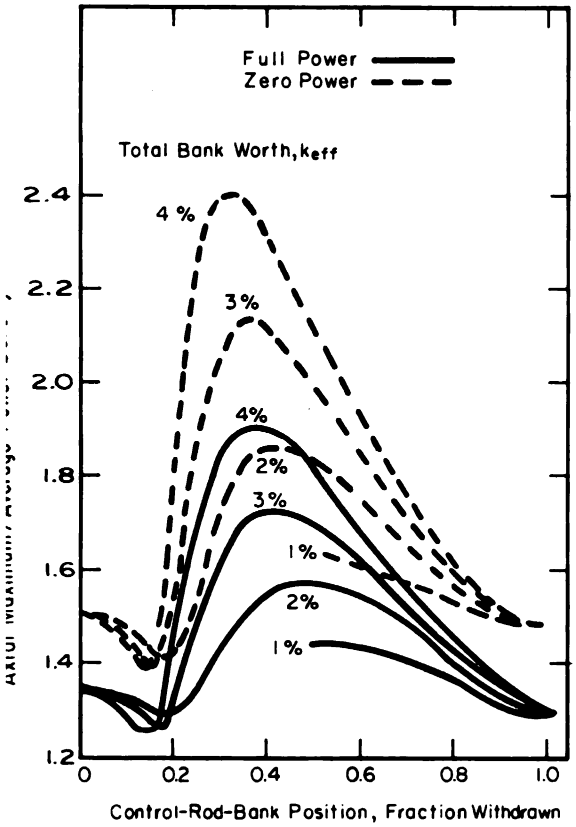

ig. IX-12 Axial maximum/average power-density atios as functions of partial rod-bank insertion, at ıll power and zero power.[11] The reactor considered s the same as that of Fig. IX-11, and the solid curves re the same as in Fig. IX-11. The dashed curves how the maximum/average ratios for the same eactor at zero power, with all other conditions the ame.

Control-Rod "Bite." As illustrated in Fig. IX-11, he differential worth of a control rod or a control-od bank is small unless the bank is inserted to some ubstantial depth in the reactor core. The control-rod ite refers to the amount of reactivity that must be ompensated by the partially inserted rod bank in rder that its differential worth may be great enough o cope with the expected rates of change of reactivity.

Control-Rod Dead Band. This item might be called, nore appropriately, the chemical-shim dead band. It s the range of mismatch that is allowed between the ominal reactivity compensation by the chemical-shim system and the actual compensation. A dead and of 0.35% k_{eff}, in the reference reactor, corre-sponds to about 50 ppm of boron or a temperature hange of approximately 15°F.

Void Content. The void content corresponds to a small amount of statistical boiling which might be allowed in the pressurized-water reactors. The reactivity change of 0.05% indicated for the reference core corresponds to about one-third of 1% of void in the core.

Concurrent Reactivity Insertion. This component of control-rod worth is provided to compensate any accidental reactivity insertion or combination of concurrent insertions that may be conceivable. The 0.8% reactivity estimated for this contingency in the reference core is considered to be made up of 0.4% due to the sudden opening of a loop containing an inadequate amount of boron, plus 0.4% due to the release of plated-out boron from the core.

Power Shaping. This adjustable reactivity component would be used for any shimming of the power distribution which might be done by means of control rods.

Variable Temperature Control. This adjustable reactivity component would be needed if it were desirable to increase the average coolant temperature as power level is increased.

Equilibrium Xenon. Unless the reactor is used strictly as a base-load plant, it is questionable whether it would be desirable to control the changes in xenon poisoning by chemical shim. If this were not done, control rods would have to be provided to control all or part of the equilibrium xenon and possibly some transient xenon.

Shutdown Margin. The shutdown margin considered in Table IX-11 includes only that amount of reactivity reduction which is required to reduce the power level at a sufficiently high rate in the event of scram—the stuck-rod margin is considered as a separate item, outside the scope of the table. In Ref. 8 it is pointed out that a shutdown margin, in addition to the reac-

Table IX-11 REACTIVITY CONTROL REQUIREMENTS FOR A CHEMICAL-SHIM CORE[8]

	Δk, %	
Control requirements	Approximate range	Reference core
Hot-to-power component	1.5 to 2.5	2.0
Control-rod bite	0.4 to 0.6	0.5
Control-rod dead band	0.3 to 0.4	0.35
Void content	0 to 0.1	0.05
Concurrent reactivity insertion	0.4 to 2.6	0.8
Power shaping	0 to 2.0	0
Variable temperature control	0 to 1.5	0
Equilibrium xenon	0 to 3.0	0
Shutdown margin	0 to 2.0	0
Total	2.6 to 14.7	3.7*

*The actual control-rod specification for the "reference" case was arrived at by increasing this value 20%, to a total of 4.4% Δk to account for uncertainties and assumptions in the analysis. These include loss in rod worth because of the change in core spectrum with lifetime, power redistribution during lifetime, depletion of poison material in the control rod, and possible error in rod-worth calculations.

tivity compensation corresponding to the power defect, may not be necessary because of the rather long thermal time constant of the oxide fuel elements. If we visualize the rapid scram, from full-power operation, of a number of control rods corresponding to the power defect, it is clear that momentarily the reactor will be subcritical by an amount nearly equal to the power defect. During the time (a few seconds) required for the fuel elements to cool down enough to make the reactor nearly critical again, the power will have decayed substantially.

In the specific case of the reference core described in Table IX-11, the situation during full-power operation would presumably be as follows. The control rods would normally be partially inserted, as a bank, to a depth such that the inserted worth of the bank is about 0.68% k_{eff}. This would correspond to the control-rod bite plus about half of the dead band. At this point (if the stuck-rod margin is ignored) the remaining worth of the bank, available on full insertion, would amount to about 3.02%, the hot-to-power component plus the components for concurrent reactivity insertion and void content plus about half the dead band. There would be no shutdown margin if the need for shutdown should occur at a time when a rod is stuck and the rods happen to be operating at the high-reactivity end of the dead band and concurrent reactivity insertions have occurred to use up all the 0.8% rod worth provided for that eventuality. From the power-distribution angle, it is important to note that, although a total rod worth of 4.4% is provided, only about 0.7% k_{eff} remains in the core under full-power operation (compare Fig. IX-11).

A study is reported in Ref. 12 on the effectiveness of control-rod scram in a chemical-shim reactor. The accidents considered were initiated by various accidental reactivity insertions by the control rods and by assumed breaks in the secondary steam line which would add reactivity by lowering the temperature of the primary circuit water. The power transients were terminated by the normal scram system, initiated either by overpower or low-pressure signals. The capability of the scram system was assumed to be a reactivity worth of 2.15%, inserted completely in 1.5 sec after initiation of the scram. This worth is stated to represent the conservative limit for the minimum absolute scram worth from full power, to be available at any time during core life. It is not clear from the reference whether the study is intended to be consistent, in detail, with the reference core of Table IX-11; but it would be consistent if the scram were assumed to occur when the control-rod bank is near the outer limit of the dead band.

The very large reduction in the moderator temperature coefficient of reactivity which results from the use of dissolved absorber represents a striking departure from the behavior that has characterized past pressurized-water reactors. In the past the strong temperature coefficient of reactivity, which produces a high degree of automatic load matching in pressurized-water systems, has been utilized to simplify certain features of the overall plant-control system. Some departures from these established practices will no doubt be necessary when chemical shim is used, and, in addition, the situation may be complicated by the rather large change in temperature coefficient that will occur over the core lifetime as the amount of dissolved absorber is changed. Although these considerations may dictate new approaches to plant control, it is unlikely that they will present feasibility problems. Some of these questions are considered in Ref. 12.

Water Chemistry

The work at WAPD has confirmed the choice of boric acid, arrived at earlier in investigations at the Argonne National Laboratory,[13] as the best available soluble absorber for chemical-shim use. References 13 to 19 cover various aspects of the behavior of boric acid solutions in the reactor environment and its effects on such important processes as corrosion and the deposition of corrosion products. These reports cover literature research, laboratory tests, and in-pile loop experiments. Much detailed information is included. Here the discussion will be limited to the most general results and the principles of operation of the chemical-shim system.

Operation with dissolved boric acid poses the following basic problem: to provide a means for varying the boric acid content in a controlled manner from a concentration of practically 0 to 1000 or so ppm and, at the same time, to maintain the rigid standards of pH control and purity (with respect to unwanted contaminants) which are normally sought in pressurized-water-reactor operation.

No report has been noted that gives detailed descriptions of methods for adjusting the concentration of boric acid in a chemical-shim application, but it is clear from Ref. 7 and from implications of the other references that the intention is to use the straightforward method of feed and bleed; i.e., the basic method is to increase the boron content by introducing into the reactor a more concentrated solution and to decrease the boron content by introducing pure water or a solution of lower concentration. Coolant must, of course, be bled from the reactor system to make room for the liquid added. This effluent may be discarded, in which case it adds to the waste-disposal load, or it may be processed by distillation, and the concentrate and/or distillate may be recycled to the reactor as needed for subsequent adjustments of concentration. As pointed out in Ref. 7, the latter method will probably prove more attractive in most cases.

With control of the boron content by the purely mechanical means of feed and bleed, it is feasible to maintain water purity with respect to unwanted contaminants in the normal way, by ion exchange, provided suitable resins are used which will not remove the boron. In this connection it must be noted also that the addition of alkali in the form of LiOH or KOH has been found beneficial for the reduction of corrosion-product deposition. The concentration used is low, of the order 10^{-4} *M* or about 2 ppm for LiOH. However, it is necessary to select ion-exchange resins that will preserve both the boron and alkali contents while removing other impurities.

An experimental program showed the effectiveness of the ion-exchange process in boric acid solutions, both with and without the presence of alkali.[15] For this experiment the alkali used was KOH, rather than LiOH, the favored additive for reactor use. The effectiveness of he ion-exchange process was evaluated for cesium, manganese, cobalt, and iodide ions to show that efficient ion exchange of either cation or halogen anion contaminants may be accomplished in boric acid solutions by the use of a mixed-bed resin in the potassium borate form or in the hydrogen borate form if no alkali s used in the system). The resins used for he tests were Rohm & Haas nuclear grade ^{77}Xe cation-exchanger resin and ^{78}Xe anion-xchanger resin. The anion resin (^{78}Xe) was onverted to the borate form by shaking with boric acid solution until an equilibrium boron oncentration of 1000 ppm was obtained. When the potassium form of the cation resin (^{77}Xe) was desired, the conversion was made by shaking the resin with a solution containing KOH and 1000 ppm of boron. The indications are that the same general principles would be applicable when lithium hydroxide is used and that ion exchange will be effective for the removal of those impurities important in reactor operation.

Aside from the problems of maintaining water purity, *p*H, and boron content, the water chemistry problems that may be visualized in chemical-shim control have to do with corrosion, the behavior of corrosion products, and hideout of the boron. These questions are considered briefly below.

Corrosion. The corrosion tests to date have shown that there are no gross effects of the dissolved boron on corrosion rates and that most materials that are satisfactory in neutral or high-*p*H water at high temperature are also suitable for use in boric acid solution.[7] Out-of-pile tests have been made on core components and have shown no adverse effects. The corrosion problem is, of course, one which can be fully assessed only by observation over long periods of time. Long-term tests are now under way on typical materials of construction in out-of-pile loops, and the results of one such test are described in Ref. 20. The experiment consisted in exposing a number of nuclear reactor structural materials to a partially neutralized 600°F solution of boric acid for a period of nine months. The materials included a number of stainless steels, Inconel, Inconel X, a number of braze materials, Zircaloy-4, and nickel-plated silver-indium-cadmium. The results, in general, indicated that all but three of the materials behaved satisfactorily. Zirconium-beryllium braze on Zircaloy-4, nickel plate on silver-indium-cadmium, and thick layers of Nicrobraz 50 on type 304 stainless steel exhibited excessive corrosion, cracking, and/or pitting. Such long-term tests, and experience with reactor operation, will be necessary to show whether the presence of boric acid produces a significant effect on corrosion, but the evidence to date seems sufficient to eliminate the direct problem of corrosion as a feasibility problem.

Deposition of Corrosion Products. There are two possible adverse effects from the deposition of those corrosion products which do occur in any high-temperature water system. If they are deposited on the fuel elements, they may interfere with heat transfer or coolant flow, and, if they are deposited at points in the coolant system where access is important, they may add greatly to the troublesome radioactivity levels. Tests appear to indicate that the presence of boric acid does increase the deposition of corrosion products, but they have shown also that an increase of *p*H by the addition of alkali is effective in reducing both the release of corrosion products from their point of formation and their deposition at other points. The indication to date is that, with suitable pH control, operation will be acceptable.

Hideout. In its broadest sense the term hideout of boron refers to the possible deposition of boron from solution onto solid surfaces in the coolant system or in deposits of corrosion products that are attached to surfaces. It is conceivable that the boron might subsequently reenter solution at some later time as a result of some change in water chemistry or operating conditions. Such uncontrolled behavior of the boron would, of course, be undesirable in any case since it would throw an uncertainty into the accounting of reactivity, which is important to reactor operation and safety. It would be particularly undesirable if the deposition occurred on the fuel plates or other parts of the reactor core structure, for a subsequent removal of such boron would then cause an increase of reactivity. The term hideout is sometimes used in a restricted sense to apply only to this latter possibility.

Tests and experience to date have indicated that boron does not deposit from solution onto clean surfaces, but there are indications that there may be a certain amount of deposition into corrosion products that may be adhering to surfaces. Out-of-pile investigations of such deposition are reported in Refs. 16 and 17, and both in- and ex-pile results are reported in Ref. 21. In the first investigation,[16] finely divided synthetic corrosion products were agitated in a high-temperature solution of boric acid containing 1000 ppm of boron, and the inclusion of the boron in the settled-corrosion-product sludge was measured. These tests indicated that the inclusion was of the order of 3 mg of boron per gram of synthetic corrosion product. In another portion of the program, the deposition of boron in a stable corrosion-product film was investigated, and in this case the deposition was only about 0.3 mg of boron per gram of corrosion product.

The experiments reported in Ref. 17 were made by a radiotracer technique that allowed the deposition of solute on selected surfaces to be followed continuously during the experiment. In this work it was necessary to utilize sodium as a stand-in for boron since there is no radioactive isotope of boron. The tests indicated that there was no deposition in the absence of boiling, although on fouled surfaces the deposition will occur when there is either subcooled or bulk boiling. However, there appeared to be a minimum thickness of fouling necessary to cause the deposition. This thickness was about 0.3 to 0.4 mil. When such deposition occurred, it appeared to be proportional to the rate of evaporation at the surface.

Reference 21 is a report on a study of the interaction of stainless-steel corrosion products with boric acid solutions at normal and elevated temperatures, utilizing both in- and ex-reactor experiments. The ex-reactor experiments substantiate the results given in Ref. 16, with boron absorptions ranging from about 1.5 to about 4 mg of boron per gram at 600°F, depending on the crud makeup and other experimental details. It is concluded, however, that the borate is not permanently incorporated in the crud, but can be desorbed, with the crud behaving as an amphoteric ion exchanger; i.e., in solutions of high alkalinity, little or no adsorption would occur, whereas, in acidic media, adsorption would occur to an extent determined by the borate-ion concentration and the solution pH. The in-pile capsule tests also indicated that reversible adsorption occurred. These latter tests indicated higher uptakes of boron compared to the ex-pile experiments, but this was believed to be due to boiling in the crud layer at the bottom of the capsule rather than as a specific result of a radiation-induced reaction. The point was not resolved, however, and further complications were noted in that the original magnetite crud had transformed to gamma ferric oxide under irradiation. No instances of rapid release of boron from a surface have been reported. In Ref. 8 the rapid release of boron from fuel plates is considered as a hypothetical means of reactivity insertion in estimating the required strength of the control-rod system for a chemical-shim reactor. In that study it is stated that the maximum amount of reactivity associated with plateout of boron would be limited to 1.2% k_{eff} by continuous evaluation of core reactivity and the initiation of remedial action if the 1.2% level is reached. It is considered inconceivable[8] that more than one-third of the deposited boron could leave the core rapidly.

Although the laboratory type tests may be useful and necessary, they are not as effective as actual reactor operation for establishing the feasibility and practicability of chemical-shim control with boric acid. For this reason, the results of operation of the Saxton reactor with chemical-shim control are of particular interest. This type of operation was begun in May 1963 and was scheduled to continue through August 1964. Mention is made in Ref. 1 that the reactor has been operating for several months with a boron content of approximately 1000 ppm, both with and without nucleate boiling in the core. A test[23] of the predictability of the chemical-shim effect is shown in Fig. IX-13. The crucial factor in the test is the degree to which the theoretical predictions of control-rod position agree with those actually observed. As may be seen from the figure, the agreement is good, even after a reasonably long period of operation that involved a shutdown and a subsequent rise in power level to the point where a substantial fraction of the core area was involved in nucleate boiling. The difference between the predicted and observed control-rod position amounts, on the average, to 0.15% k.

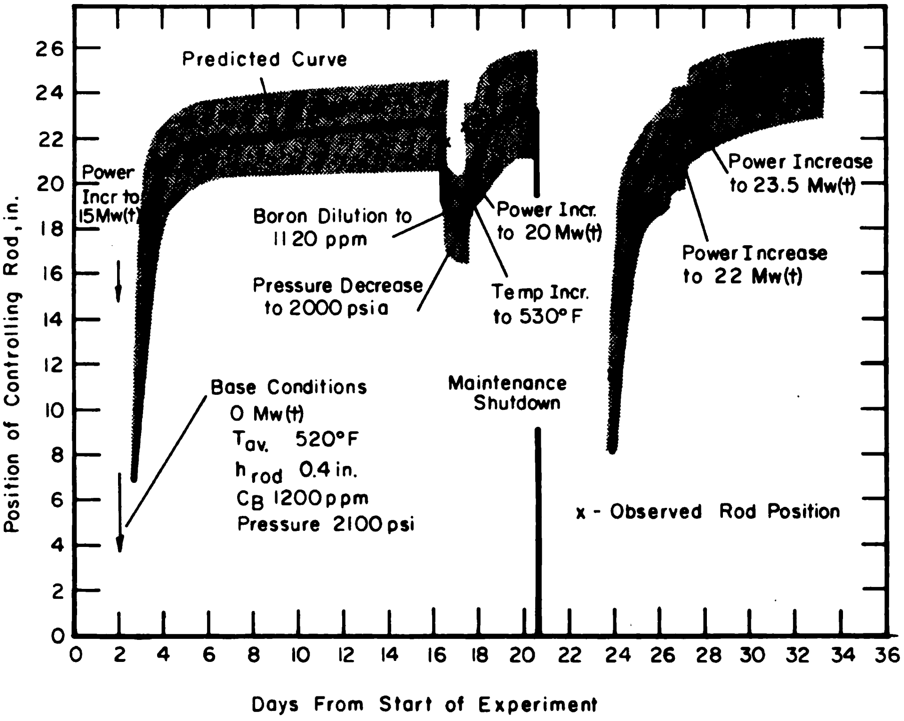

Fig. IX-13 Predicted and observed control-rod positions of the Saxton boron experiment.[23]

and is within the band of uncertainty of the calculations.

Pressurized-Water Reactors: Natural-Circulation Startup

As nuclear power becomes of age, it may be expected that refinements will be made to help reduce the capital cost of the reactor plant components. One possible refinement is discussed in Ref. 24. Although the main purpose of the reference is to describe a computer code for analyzing natural-circulation operation of a pressurized-water reactor, the reason behind the study is of more general interest and will be discussed briefly.

The startup of a power reactor usually requires operation of the primary coolant pumps, both to ensure flow through the reactor core and to help elevate the system temperature. If the pumps are of the constant-speed variety, both the coolant mass flow rate through the pumps and the pump power consumption are considerably higher at the cold, startup condition than at the high-temperature condition of normal reactor operation. One way to provide for this increased flow is to install pumps based on the capacity required during reactor startup. Unfortunately, if the primary coolant pump specified is a canned-motor pump, this solution is likely to be an expensive one for a large plant. The proposed Ravenswood Nuclear Generating Unit, for example, called for five canned-motor pumps with a design capacity of about 60,000 gal/min.[25] According to the estimates of the *Cost Evaluation Handbook*, each pump would have cost[26] approximately $500,000, and, since the cost of canned-motor pumps varies almost directly with capacity (see Fig. 321-1 of Ref. 26), the designer would be reluctant to base his pump specifications on the startup condition. Reference 24 suggests the following operating technique to avoid this penalty:

> ... A method has been proposed that permits optimum design for normal steady state operating conditions and prevents the overheating of the circulating pumps during initial cold conditions. In this method, pump operation is required only for the period of time necessary to bring the reactor power level to a heat production rate consistent with the safe plant heat-up rate. This rate is determined by the thermal stress limitations of the components within the reactor coolant system. The

> power level is of the order of two percent of the reactor full power rating. Power to the pumps is then shut off and the plant heat-up is continued. As the pumps coast down, the forced circulation ceases and an adequate coolant flow is maintained by natural circulation. The operation of the pumps will be resumed when coolant temperatures (hence coolant densities) are such that continuous operation of the pumps is permissible.

The objective of the study, which required the development of the computer code, was to predict the system behavior during the proposed procedure. The code is presented in Ref. 24 and is applied to the startup problem of a large pressurized-water reactor. The particular problem studied gave results indicating the establishment of adequate coolant flow during plant heatup with natural circulation. This method of startup requires a spring-loaded check valve to ensure that the valve remains at least partially open when low flow exists in order to reduce flow resistance during natural-circulation cooling.

Pressurized-Water Reactors: The Large Power-Reactor Program

The objective of the Large Power Reactor (LPR) Program is to determine the potential of a seed-blanket reactor for application in a large central-station power plant [about 500 Mw(e)]. The research, engineering, and design work that is being conducted under the program has been described in a set of interim reports.[27–29] An earlier report on the economic potential of the seed-blanket reactor[30] gives a useful discussion of the general relation in the neutron-physics design of seed-blanket reactors. This report was reviewed in *Power Reactor Technology*, 4(3): 38-41.

Conceptual designs of large reactors utilizing several different fuel cycles have been developed,[27,28] all having the following major design features:

1. All use rod type oxide fuel elements, jacketed in Zircaloy-4 and of full core length.
2. The core is composed of a number of identical modules, each comprising a central seed, a surrounding blanket, and means for reactivity control.
3. Control of reactivity during operation is accomplished by relative motions of portions of the seeds, which vary the neutron leakage from the seeds.
4. The cores have small length/diameter ratios (ranging from 0.53 to 0.62) and are installed in spherical pressure vessels that are welded in the field. Core reloading does not require removal of the vessel head but is done through nozzles in the head. The nozzles also serve as entries for the control mechanisms.

The significance of the seed-blanket program has been summarized as follows:*

> During the earlier phases of the LPR program, seed-blanket reactors using natural uranium in the blanket were studied. Nuclear calculations confirmed by critical experiments indicate that a uranium converter-burner core can be designed to produce over 65% of the total core energy from its natural uranium blanket. While the fuel cycle cost for such a core is about 10% higher than that for slightly enriched cores, its fuel utilization is about 20 to 40% better, as indicated in Table [IX-13].
>
> While these results were promising, it became clear as the work progressed that large seed-blanket reactors using thorium fuel have high potential for (1) low power generation cost in a long-lived, thorium converter-burner design and (2) high fuel utilization in a converter-recycle design. For application in the near future, when the technology of thorium fuel reprocessing and remote fabrication of radioactive fuel has yet to be developed on a practical basis, the thorium seed-blanket converter-burner design is more attractive. This core provides a competitive power generation cost and better fuel utilization when compared to other water cooled reactors. Further, when the problems associated with recycling of irradiated fuel are solved on a practical basis, the thorium converter-recycle design appears capable of breeding.
>
> Accordingly, a core design has been developed consisting of a thorium seed-blanket converter-burner core with a central region of breeder type fuel assemblies. Such a core would have about the same low fuel cycle cost as the converter-burner core, yet would be capable of demonstrating the breeding potential of the thorium converter-recycle design. This would make it possible to demonstrate breeding at an early date without having the power generation cost significantly dependent on the practicality of chemical reprocessing and remote fabrication of radioactive fuel elements.

---

*We are grateful to the Naval Reactors Branch of AEC's Division of Reactor Development for this summary.

Successful operation of a thorium seed-blanket reactor containing a central breeder region will constitute a major advance in reactor technology through the demonstration of breeding in the central region of the core. The thorium seed-blanket concept is the only known approach for extending fuel utilization of light-water reactors significantly beyond today's value of 1 to 2% of the potential energy in the mined ore. The thorium seed-blanket concept is expected to provide a means for ultimately making available for power production about half the energy in the fertile thorium fuel reserves.

A diagram of a core cross section for the uranium converter-burner design is shown in Fig. IX-14. Each of the 37 modules consists of a seed with stationary and moving parts for reactivity control, an annular blanket, and three outer blanket assemblies of chevron-shaped cross section. Each module contains also, on its axis, a round absorbing control rod for shutdown. In the pressure-vessel head, a port provided above each module is of sufficient diameter to pass the seed and annular blanket. The assembly, consisting of the seed, the shutdown rod, and the drive mechanism for the shutdown rod and the movable seed portions, is hung from a shoulder near the top of the fuel port and can be lifted out as a unit for refueling. The annular blanket is also hung from the port and can be lifted out separately. The chevron blanket sections are supported by the fixed bottom plate of the core. They can be removed individually through the fuel port after the removal of the annular blanket section. The arrangement of the core in the pressure vessel is indicated in Fig. IX-15.

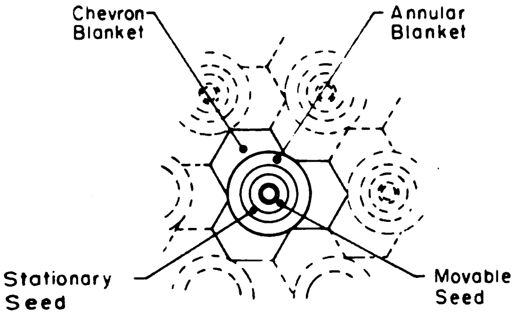

Fuel-Region Details

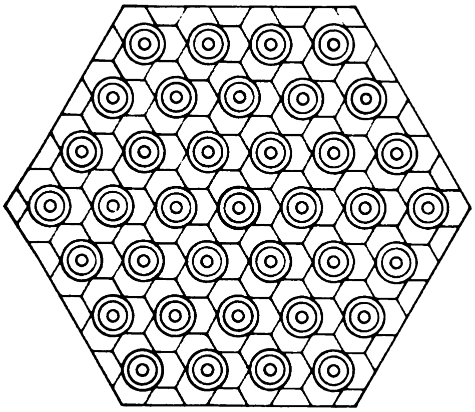

Core Cross Section

Fig. IX-14 Uranium converter-burner reactor concept.[28] Equivalent diameter = 15 ft.

The control of reactivity by "seed leakage" is to be accomplished by dividing the (nominal) seed into two coaxial parts, the inner of which is movable axially, and dividing each of the coaxial parts lengthwise into seed and blanket regions, as shown in Fig. IX-16. When the inner section is moved so that its seed portions are adjacent to the seed portions of the outer, fixed section, the fission neutrons produced in seed fuel will have the maximum probability of being absorbed in other seed fuel, i.e., the neutron leakage from the seed will be minimized, and the reactivity will be maximized. When the seed portions of the two blanket sections are mutually adjacent to blanket portions, the reactivity will be minimized. The range of reactivity adjustment available from seed movement is expected to be at least enough to compensate for fuel burnup, and hence it is expected that the parasitic loss of neutrons to absorbing control rods can be avoided.

Rod type fuel elements of full core length (8 ft) are contemplated for both the seed and blanket regions. The axial seed-blanket segmentation is to be obtained by appropriately segmented pellet loadings of the seed elements. The fuel-rod design is based on self-standing Zircaloy-4 cladding. The fuel rods are supported mechanically by a bottom grid assembly and by spring collars located at intervals along the rod length. The spring-collar design, illustrated in Fig. IX-17, is such that rubbing contact occurs only between the collars. The design of the collars is similar in principle (but different in detail) to that used successfully on a special assembly of blanket-rod elements (SABRE) which was tested in the Shippingport core. In the test assembly, the fuel rods were arranged in a square lattice to suit the basically square Shippingport geometry rather than in the tri-

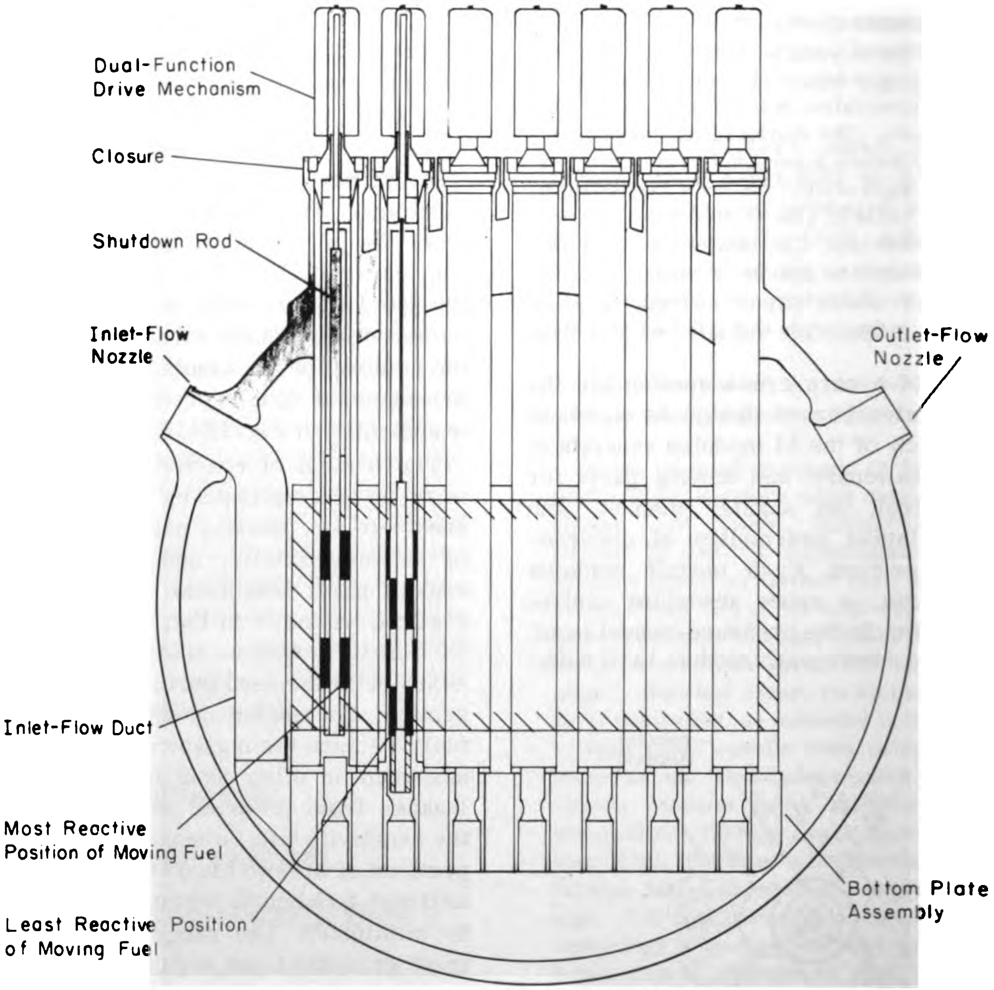
Dual-Function Drive Mechanism
Closure
Shutdown Rod
Inlet-Flow Nozzle
Outlet-Flow Nozzle
Inlet-Flow Duct
Most Reactive Position of Moving Fuel
Least Reactive Position of Moving Fuel
Bottom Plate Assembly

Fig. IX-15 Uranium converter-burner reactor concept (core and vessel elevation).[28]

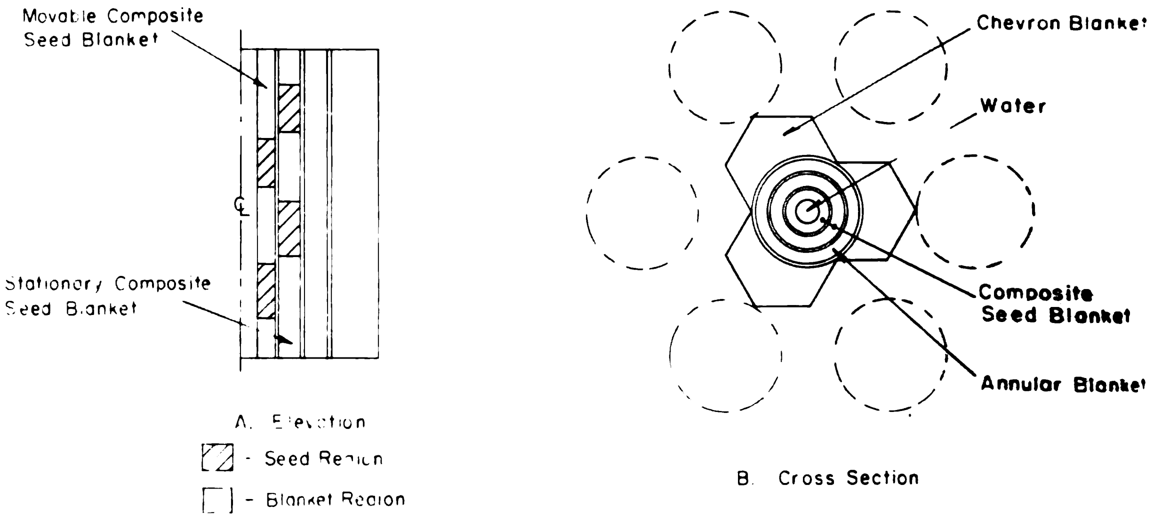

A. Elevation

B. Cross Section

Fig. IX-16 Schematic of the uranium converter-burner unit cell.[28]

angular lattice that is contemplated for the large power reactor. The collar material is Inconel X. The seed rods in this particular LPR uranium converter-burner design are 0.25 in. in diameter. They are spaced 0.085 in. apart and are supported laterally at intervals of 12 to 20 in. The blanket rods are 0.50 in. in diameter. They are spaced 0.175 in. apart and are supported laterally at 24- to 36-in. intervals in the annular region and at 48-in. intervals in the chevron regions. The blanket fuel is natural UO_2, whereas the seed fuel is highly enriched UO_2 combined with a diluent, probably ZrO_2.

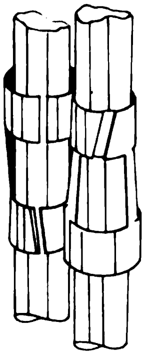

Fig. IX-17 Spring-collar fuel-rod spacers.[28]

A three-pass coolant flow is used: the coolant flows upward through the seed region, downward through the annular blanket, and finally upward through the chevron blanket sections. The flow boundaries are provided by the walls of the several regions in each individual fuel module.

It is proposed that the 24-ft-ID reactor pressure vessel be welded up in the field from the prefabricated sections illustrated in Fig. IX-18. The bottom section and the barrel-stave side sections are visualized as hot pressings, whereas the top section would be a forging or a welded assembly of smaller forgings. The inlet and outlet nozzles, which are designed with reinforcements both inside and outside the

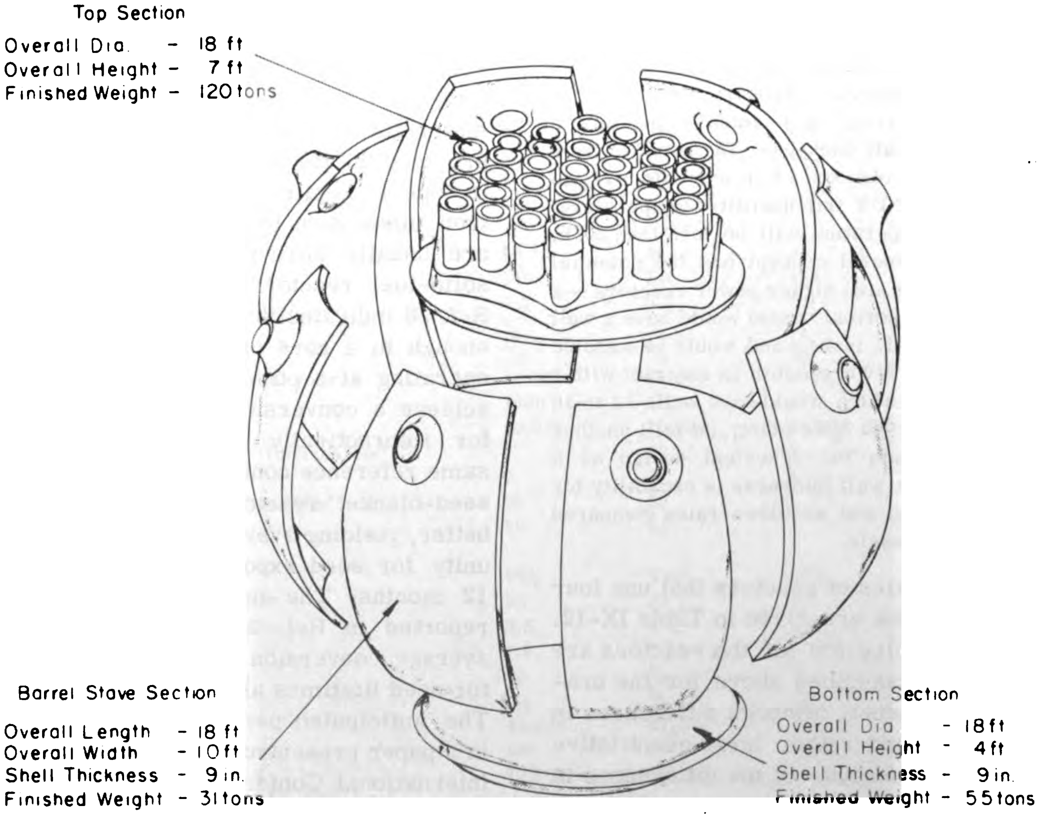

Fig. IX-18 LPR reactor vessel concept.[28] Prefabricated sections are suitable for field erection. The finished vessel is 24 ft in inside diameter, overall height is 28 ft 4 in., and weight is 425 tons without internals and mounting skirt.

shell, would be forgings strength welded into the barrel-stave sections. It is expected that type A-302B steel would be used for the plate sections and type SA-306 for the forgings; the internal cladding would be weld-deposited stainless steel. Stress relieving in the field is visualized by the use of strip heaters or by utilizing a part of the reactor containment structure, lined temporarily with firebrick, as a furnace.

The pressure vessel is a rather impressive structure. The thinking behind this development has been summarized as follows:*

> Pressure vessels for large capacity reactors (greater than about 300 MWe) probably cannot be shipped by rail (regardless of whether spherical or cylindrical in shape) since the minimum clearance dimensions will likely exceed minimum railroad clearances (about 15 feet) even along selected routes. The LPR vessel has therefore been designed for field erection, so as to remove any restrictions on site location posed by pressure vessel shipment limitations. Further, recognizing the operational limitations that would be imposed on a cylindrical pressure vessel by neutron irradiation over a 30 year plant lifetime, the spherical shape was adopted to introduce a thick water shield (about four feet at core midplane) which reduces the lifetime fast neutron exposure to an nvt of 1.5×10^{17} neutrons/cm^2 and actually permits a decreased vessel wall thickness. The benefits from such a design are obvious. For example, (1) the resultant shift in NDT (nil ductility temperature) over 30 years of operation will be less than 50°F; (2) the spherical vessel concept has the potential for accommodating still higher power reactors—a 30 foot diameter spherical vessel would have a wall thickness of about 11 inches and would be suitable for a 1000 to 1500 MWe reactor in contrast with a cylindrical vessel which would have walls 14 to 16 inches thick for a 1000 MWe plant; (3) still another benefit derived from the spherical design as a result of minimum wall thickness is capability for rapid vessel heatup and cooldown rates compared with cylindrical vessels.

The characteristics of reactors that use four different fuel cycles are given in Table IX-12. The design principles for all the reactors are similar to those described above for the uranium converter-burner, although differences in qualitative detail and rather large quantitative differences enter because of the differences in fuel programming and blanket material. When thorium is used as the blanket fuel, the seed must initially produce nearly all the reactor power. Hence the ratio of seed volume to blanket volume must be much larger than when the blanket is composed of natural uranium. This characteristic is illustrated in Fig. IX-19, which is a diagram of the core cross section for the thorium converter-burner (compare Fig. IX-14).

The last two columns of Table IX-12 apply to recycle reactors that use very "dry" blankets. In these designs most of the bred fertile isotope remains at the end of blanket life (rather than being burned in place) and is extracted and recycled to the seed. The Bettis reports indicate that the use of the low hydrogen/fuel ratio in the blanket, coupled with the variable-geometry control method that does not introduce parasitic neutron-absorbing poisons into the core, favors very high conversion ratios.

Considerable attention has been given in the studies[27,28] to the analysis of the ^{233}U-thorium recycle case, and the conclusion is that breeding may be feasible on that cycle with the seed-blanket approach. In the past generalized analyses[31] have indicated that breeding is theoretically possible in the ^{233}U-thorium-H_2O system, provided the neutron losses to structural materials and fission products are kept low and provided the thermal-neutron flux on the fertile isotope is kept relatively low to minimize neutron absorption by ^{233}Pa. These requirements are usually difficult to satisfy in a practical solid-fuel reactor. The analysis reported in Ref. 28 indicates that they are not satisfied well enough in a core of uniform fuel composition, operating at a power density of 60 kw/liter, to achieve a conversion ratio above unity except for impractically short fuel exposures. The same reference contains analyses that show the seed-blanket reactor to perform considerably better, yielding average conversion ratios above unity for seed exposure lifetimes up to about 12 months. The more extensive investigation reported in Ref. 29 finds cases in which the average conversion ratio remains above unity for seed lifetimes as long as about 30,000 EFPH. The anticipated performance is characterized in a paper presented at the Third United Nations International Conference on The Peaceful Uses of Atomic Energy as follows:[32]

> ...The most meaningful way of describing breeder performance appears to be by the fissile inventory ratio, i.e., the ratio of total fissile fuel

---

*Quoted from a summary by the Naval Reactors Branch of AEC's Division of Reactor Development.

> in the core at any time to that at start of life. In a typical case with 2100 kg of ^{233}U in the seed the calculated core endurance is about 15,000 EFPH and the end-of-life value of the fuel inventory ratio exceeds 1.01. If reprocessing losses are about ½ to 1%, this core would then be self-sustaining. As the seed fuel inventory is increased, the values of the fuel inventory ratio decreases slowly but endurance increases rapidly...

Some of the reasons for the higher conversion performance of the seed-blanket reactor are readily apparent. Thus, if the blanket is reprocessed at a relatively low value of fission depletion, high fission-product concentrations will occur only in the seed, where the fissile isotope is in a high enough concentration to compete favorably with them for neutrons. Moreover, the thermal-neutron flux may be kept low in the blanket, and the fast-fission effect may be accentuated, by employing a low coolant/fuel ratio there, since the power density in the blanket is low in any case. These observations imply some of the limitations that are imposed on other performance characteristics when very high conversion ratio is sought. The most important of these appears to be a low ratio of blanket power density to seed power density.

The preceding quotation is consistent with the concept of a "hold-its-own" or self-sustaining reactor—one which does not diminish the resource of fissile isotope, but which does not expand the resource significantly either. In an

Table IX-12 CORE CHARACTERISTICS FOR FOUR 500-Mw(e) SEED-BLANKET CONCEPTS[28]

	Uranium converter-burner	Thorium converter-burner	Uranium converter-recycle	Thorium converter-recycle
Reactor power, Mw(t)	1650	1720	1730	1750
Pressure, psia	2000	2000	2000	2000
Reactor inlet temperature, °F	537	515	515	515
Pressure at turbine throttle, psig	700	600	600	600
Pumping power, % of gross	3.3	4.4	5.3	6.2
Coolant flow rate, 10^6 lb/hr	70	120	95	120
Core				
Pressure drop, psi	80	50	135	100
Diameter, ft	15	15	13.7	13
Active height, ft	8	8	8	8
Average power density, kw/liter	42	42	50	56
Seed				
Volume % of core	10	30	24	40
Power density, kw/liter*	170	140	160	140
Moderator/water ratio	0.7	0.7	0.7	0.7
Fuel-rod diameter, in.	¼	¼	¼	¼
Fuel-rod spacing, in.	3/32	3/32	3/32	3/32
Equivalent full-length fuel rods	16,600	50,000	37,000	55,000
Fuel loading, kg of ^{235}U	1000	4500		
Seed lifetime, EFPH	10,000	70,000	10,000	7000
Average depletion, 10^{20} fissions/cm^3	7	22	7	4
No. of seeds/blanket	7	1	6	3
Peak depletion, 10^{20} fissions/cm^3	20	30		
Wt.% UO_2 in seed fuel	32	35		
Blanket				
Blanket fuel	UO_2	ThO_2	UO_2	ThO_2
Power density, kw/liter*	33	33	27	23
Hydrogen/fuel atom ratio	3.5	4.5	0.8	0.6 to 0.7
Water/UO_2 or ThO_2	1.5	1.75	0.35	0.25
Fuel-rod diameter, in.	½	⅝	¾	¾
Fuel-rod spacing, in.	3/16	5/16	1/32	1/32
Total No. of fuel rods	42,000	21,400	26,000	20,000
Fuel loading, metric tons	100	68	138	100
Blanket lifetime, EFPH	70,000	70,000	60,000	21,000
Average fuel depletion, Mwd/metric ton of fuel	30,000	36,500	10,000	2000
Average blanket power fraction (over blanket life), %	65	50	32	13

*At maximum power fraction.

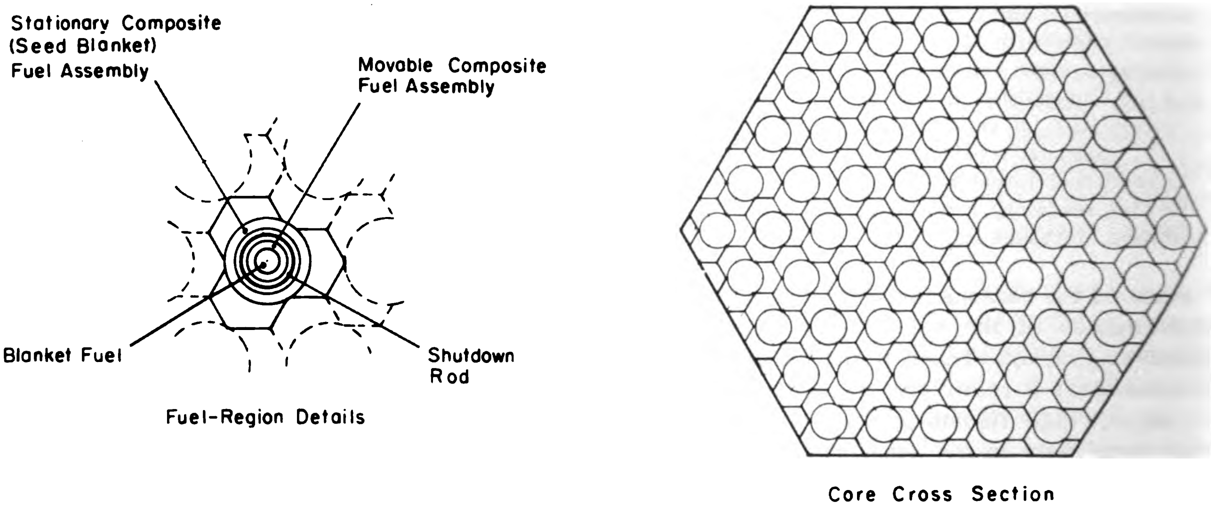

Fuel-Region Details

Core Cross Section

Fig. IX-19 Thorium converter-burner reactor concept.[28]

Table IX-13 COMPARATIVE PERFORMANCE OF WATER-COOLED CONVERTER-BURNER REACTORS[27]

	Potential energy from nuclear fuel mined,* %	^{235}U destroyed,† g/Mwd(t)	Fissionable Pu or ^{233}U remaining, g/Mwd(t)	Fissionable material‡ consumed, g/Mwd(t)	Uranium reprocessed to recover bred fuel, g/Mwd(t)	Natural-uranium input to diffusion plant, g/Mwd(t)	Fuel cost,§ mills/kw-hr
Uranium converter-burner cores							
Seed-blanket	1.4	0.59	0.15	0.44	21	100	2.3
Slightly enriched spectral shift	1.2	0.82	0.37	0.45	39	180	2.1
Slightly enriched poison control	0.9	0.88	0.28	0.60	40	200	2.1
Thorium converter-burner cores							
Seed-blanket	1.4	0.63	0.24	0.39	12	160	1.8

*Includes plutonium or ^{233}U credit.

†Grams per thermal megawatt-day of energy produced by reactor.

‡Assumes ^{235}U in tailings can be utilized; otherwise comparison would indicate the uranium seed-blanket core to be still more favorable.

§The costs given in this table are solely for the purpose of comparing the various reactor concepts on a consistent basis and should not be construed as actual fuel costs.

expanding nuclear power industry, the problem of supplying the inventory of fissile isotope for the increasing number of power reactors is an inherent part of the fuel-supply problem, the importance of which has been recognized in the general breeder-development effort by a strong emphasis on breeding gain and the attainment of short doubling times. Although a reactor which breeds even by a small margin is obviously better than a reactor with a low conversion ratio, opinion varies as to the unique significance of a hold-its-own reactor (of infinite or very long doubling time) in relation to the nuclear fuel supply problem. The question is too complex to be treated here, but some aspects of it have been explored in a previous review of nuclear fuel utilization in *Power Reactor Technology* [6(4): 1-39 (Fall 1963)].

The fuel-utilization characteristics of the nonrecycle seed-blanket reactors are also emphasized.[27,28] Table IX-13, from Ref. 27, gives a comparison with other pressurized-water types.

All entries in the table are self-explanatory except, perhaps, the first column. The number given is the amount of energy derived from unit quantity of virgin natural uranium, expressed as a percentage of the energy that would be available if all the uranium were consumed via conversion of ^{238}U to plutonium and subsequent fission. The total potentially available energy is taken as 915,000 Mwd/metric ton of natural uranium. In arriving at the numbers in the first column, credit is given for the fissile isotope discharged from the nonrecycle reactors by assuming it to be equivalent to ^{235}U.

In the case of the uranium converter-burner, the seed-blanket core shows a higher percentage energy extraction than the spectral-shift core (1.4% vs. 1.2%). Almost all the difference appears to be due to the smaller losses in the diffusion-plant tailings in the seed-blanket case (because much of the energy is produced in the natural-uranium blanket), since the specific net consumption of fissile isotope (fourth column of Table IX-13) is nearly the same in the two cases. In comparison to the conventional poison-control core, the seed-blanket core shows a considerable increase in the percentage energy extraction. This is due partly to the lower tails losses and partly to a lower specific net consumption of fissile isotope.

In a previous issue of *Power Reactor Technology*, the efficiency of fuel utilization has been considered in terms of the specific utilization, Υ, defined as the energy produced per net gram of fissile isotope made unavailable. This quantity may be derived for the several reactor types from Table IX-14, from Ref. 28. Not all

Table IX-14 CHARACTERISTICS OF VARIOUS WATER-COOLED REACTORS USED AS BASIS FOR FUEL-COST CALCULATIONS[28]

	Seed-blanket thorium burner	Seed-blanket uranium burner	Spectral-shift-controlled uranium burner	Poison-controlled uranium burner	Spectral-shift-controlled thorium converter
Nuclear design data obtained from	Bettis calculations	Bettis calculations	AEEW-R-174*	AEEW-R-174*	BAW-1241†
Nuclear constants calculated by	MUFT-KATE codes	MUFT-KATE codes	Adaptation of MUFT-KATE codes	Adaptation of MUFT-KATE codes	BPG code
Type of core cycle	Batch	Batch	Fuel shuffling	Fuel shuffling	Batch
Water/UO_2 volume ratio		1.5 (blanket)	2.0	2.0	
Cladding material	Zircaloy	Zircaloy	Zircaloy	Zircaloy	Zircaloy
Average fuel burnup, Mwd/metric ton of fuel	40,000 (blanket)	30,000 (blanket)	25,000	24,000	21,500
Initial enrichment, % ^{235}U in fuel	93/0	93/0.7	3.5	3.5	3.3
Final enrichment, % ^{235}U in fuel	78.9/0	90/0.7	1.51	1.43	1.61
Grams of ^{235}U consumed/Mwd	0.66	0.61	0.82	0.88	0.92
Grams of ^{239}Pu + ^{241}Pu or ^{233}U discharged/Mwd	0.24	0.14	0.37	0.28	0.65
Net grams of fissionable material destroyed/Mwd	0.42	0.47	0.45	0.60	0.27
Fuel-rod diameter, in.	0.250/0.625	0.250/0.500	0.400	0.400	0.436
Maximum linear heat rating, kw/ft	15.0	15.0	15.0	15.0	10.5
Overall power-peaking factor	3.7/2.4	3.7/4.2	1.9‡	3.0	1.57‡
Fuel residence time, days at 80% load factor	3650/3650	521/3650	883	1339	843
Total feet of fuel rod for 500-Mw(e) core	400,000 (seed) 171,000 (blanket)	133,000 (seed) 356,000 (blanket)	215,000	340,000	305,000
Kw-hr/core × 10^{10}	3.5	3.5	0.848	1.285	0.810

*D. Hicks, Light Water Lattice Calculations in the U.K., British Report AEEW-R-174, April 1962.

†Based on design and compositions of first core for potential plant given in the report by D. Mars, Spectral Shift Control Reactor Design and Economic Study, USAEC Report BAW-1241, Babcock & Wilcox Co., December 1961.

‡Assumes extensive fuel zoning (USAEC Report BAW-1241).

the reactors listed are identical to those represented in Table IX-13. The values of Υ and Υ_r (the specific utilization in the reactor, without regard to diffusion-plant losses) derived from Table IX-14 are given in Table IX-15.

It has been pointed out before [*Power Reactor Technology*, 6(4): 1-37] that in an expanding nuclear power industry the inventory requirements of the nuclear plants may be as important as the actual consumption of nuclear fuel. Estimating from the characteristics quoted in Refs. 27 and 28, and allowing for an ex-reactor inventory equal to 1.5 years of throughput, we can conclude that the seed-blanket uranium converter will require about 0.4 metric ton of natural uranium to supply the inventory for each thermal megawatt of installed capacity. This is about the same as the specific inventory requirement of conventional slightly enriched pressurized-water reactors. The requirement of the seed-blanket thorium converter-burner is considerably higher, amounting to about 0.66 metric ton of natural uranium per thermal megawatt. The very long seed life (10 years) of this reactor is purchased partly at the expense of a large loading of ^{235}U, which accounts for the rather high inventory requirement. The inventory component of the fuel cost (i.e., the use charge) has been computed for this reactor in Ref. 28 as 0.56 mill/kw-hr on the basis of the 4.75% per year "government-ownership" use-charge rate.

Although Refs. 27 and 28 are not intended to give a complete evaluation of the seed-blanket concept, they do indicate its areas of strength and weakness. In the areas of strength, there is the possibility of superior neutron-physics performance in comparison to other pressurized-water types and the possibility of greater operating convenience and higher plant availability. This is due to the very long life of the blanket, the relatively long life of the seed, and the ease of seed refueling. On the other hand, the concept results in a relatively low average power density in the core, apparently an inherent result of the necessity for producing a substantial fraction of the power in a small fraction of the core volume (i.e., in the seeds).

The use of highly enriched fuel in the seed is characteristic of the seed-blanket concept. Except for the fuel cost estimates reported in the references cited, it is difficult to evaluate the long-range economic implications of this feature, for it has not previously been used in

Table IX-15 SPECIFIC FUEL UTILIZATIONS COMPUTED FROM DATA OF TABLE IX-14

	Seed-blanket thorium burner	Seed-blanket uranium burner	Spectral-shift-controlled uranium burner	Poison-controlled uranium burner	Spectral-shift-controlled thorium converter
Grams of ^{235}U consumed/Mwd (total)	0.66	0.61	0.82	0.88	**0.92**
Grams of ^{235}U consumed/Mwd (from enriched fuel	0.66	0.44*	0.82	0.88	**0.92**
Grams of ^{235}U discarded/Mwd in diffusion plant tails† = $B[0.25/(0.72 - 0.25)]$	0.35	0.23	0.44	0.47	**0.49**
Grams of ^{239}Pu + ^{241}Pu or ^{233}U discharged/Mwd	0.24	0.14	0.37	0.28	**0.65**
Net grams of fissile isotope destroyed/Mwd = $A - D$	0.42	0.47	0.45	0.60	**0.27**
Specific utilization of fissile isotope in reactor, Υ_r, Mwd/net grams of fissile isotope destroyed (= $1/E$)	2.38	2.13	2.22	1.67	**3.71**
Net grams of fissile isotope made unavailable/Mwd (= $A + C - D$)	0.77	0.70‡	0.89	1.07	**0.76**
Specific utilization of fissile isotope in fuel cycle, Υ, Mwd/net grams of fissile isotope made unavailable (= $1/G$)	1.30	1.43‡	1.12	0.94	**1.32**

*Assuming an average of 65% of the energy produced in the blanket. The consumption of about 1.26 g of ^{235}U (by fission and neutron capture) yields 1.0 Mwd of energy. If 35% of the power is generated in the seed, the specific consumption of ^{235}U in the seed is $0.35 \times 1.26 = 0.44$ g/Mwd of total core power.

†Assuming tails enrichment of 0.25% ^{235}U.

‡Neglecting the discard of any ^{235}U that may be left in the discharged blanket.

commercial reactors, and consequently there is no generally available body of cost information.

At this stage of development, the recognition of these advantages and limitations of the concept cannot serve as an evaluation, but only as an indication of the probable directions of further development.

References

1. R. G. McGrath (Ed.), Carolinas Virginia Tube Reactor. Large Plant Study, USAEC Report CVNA-184, Westinghouse Electric Corp., Atomic Power Division, June 1963.
2. Combustion Engineering, Inc., Nuclear Division, Organic Cooled, Heavy Water Moderated Reactor Power Plant Conceptual Design and Evaluation, Volume I, Evaluation of the Concept, and Volume II, Reference Plant Design, USAEC Report CEND-175, Vols. I and II of two, March 1963.
3. R. J. Rickert, Fuel Cycle Economics of Large D_2O Moderated, Organic Cooled Power Reactors, *Combustion*, 35(10): 20 (April 1964).
4. D. F. Babcock, R. R. Hood, and D. S. St. John (Comps.), Thorium-Fueled D_2O-Moderated Power Reactors, USAEC Report DP-864, Savannah River Laboratory, December 1963.
5. S. G. Sharma, Plutonium-Fueled Thermal Reactors with High Conversion Ratios (thesis), USAEC Report BNL-7355, Brookhaven National Laboratory, March 1963.
6. D. F. Babcock, R. R. Hood, L. Isakoff, J. C. Jensen, D. S. St. John, and J. W. Wade, An Evaluation of Heavy-Water-Moderated Power Reactors, Status Report as of March 1963, USAEC Report DP-830, Savannah River Laboratory, June 1963.
7. P. Cohen and H. W. Graves, Jr., Chemical Shim Control for Power Reactors, *Nucleonics*, 22(5): 75-82 (May 1964).
8. D. L. Miller, Control Rod Requirements in a Chemical Shim Core, USAEC Report WCAP-3727, Westinghouse Electric Corp., Atomic Power Division, August 1963.
9. P. G. Lacey, Reactivity Dependence upon Moderator Temperature and Boron Concentration in Large PWR Cores Controlled by Chemical Shim, USAEC Report WCAP-3720, Westinghouse Electric Corp., Atomic Power Division, November 1962.
10. P. G. Lacey, Fine Structure Power Peaking in a Critical Experiment Mockup of a Chemical Shim Core, USAEC Report WCAP-3723, Westinghouse Electric Corp., Atomic Power Division, March 1963.
11. H. Aisu, R. F. Barry, and P. G. Lacey, Load Variation Restrictions in a Chemically Poisoned Large PWR Core, USAEC Report WCAP-3724, Westinghouse Electric Corp., Atomic Power Division, March 1963.
12. J. S. Moore and B. H. Axelson, Reactor Control and Protection System Study for Chemical Shim Operation of a Large Closed Cycle Water Reactor, USAEC Report WCAP-3714, Westinghouse Electric Corp., Atomic Power Division, October 1962.
13. D. E. Byrnes and W. E. Foster, Literature Values for Selected Chemical/Physical Properties of Aqueous Boric Acid Solutions, USAEC Report WCAP-1570, Westinghouse Electric Corp., Atomic Power Division, January 1961.
14. D. E. Byrnes, Some Physicochemical Studies of Boric Acid Solutions at High Temperatures, USAEC Report WCAP-3713, Westinghouse Electric Corp., Atomic Power Division, September 1962.
15. W. D. Fletcher, Ion Exchange in Boric Acid Solutions with Radioactive Decay, USAEC Report WCAP-3716, Westinghouse Electric Corp., Atomic Power Division, November 1962.
16. W. D. Fletcher, A. Krieg, and P. Cohen, The Behavior of Austenitic Stainless Steel Corrosion Products in High Temperature Boric Acid Solutions, USAEC Report WCAP-1689, Westinghouse Electric Corp., Atomic Power Division, December 1960, Revised May 1961.
17. L. F. Picone, D. D. Whyte, and G. R. Taylor, Radiotracer Studies of Hideout at High Temperature and Pressure, USAEC Report WCAP-3731(Rev.), Westinghouse Electric Corp., Atomic Power Division, June 1963.
18. L. F. Picone, The In-Pile Test of Chemical Shim, USAEC Report WCAP-3729, Westinghouse Electric Corp., Atomic Power Division, June 1963.
19. C. R. Breden and A. Abers, Corrosion and Stability Tests on Chemical Poisons in High-Temperature Water, USAEC Report ANL-5147 (Rev.), Argonne National Laboratory, Sept. 1, 1953.
20. D. D. Whyte, A Long Term Corrosion Test of Reactor Structural Materials in a Chemical Shim Solution, USAEC Report WCAP-3737, Westinghouse Electric Corp., Atomic Power Division, March 1964.
21. W. D. Fletcher, Interactions Between Stainless Steel Corrosion Products and Boric Acid Solutions, USAEC Report WCAP-3730, Westinghouse Electric Corp., Atomic Power Division, March 1964.
22. D. R. Rees and E. U. Powell, Saxton Tests Lead Toward Better Water Reactors, *Nucl. Eng.*, 21(11): 72-77 (November 1963).
23. S. Bartnoff, J. Weisman, A. J. Impink, W. H. Layman, and D. E. Hetrick, The Saxton Experiment on Chemical Shim Control, *Trans. Am. Nucl. Soc.*, 6(2): 305-306 (November 1963).
24. A. N. Nahavandi, B. H. Axelson, G. B. Killinger, and A. H. Killinger, A Digital Computer Analysis of Closed Cycle Water Nuclear Power Plant Start-Up Using Natural Circulation (THERMO-

SYPHON Code), Vols. I and II, USAEC Report WCAP-3722, Westinghouse Electric Corp., Atomic Power Division, February 1962.

25. Westinghouse Electric Corp. and Stone & Webster Engineering Corp., Consolidated Edison Company of New York, Inc. Ravenswood Nuclear Generating Unit A, Preliminary Hazards Summary Report, Vol. I, USAEC Docket No. 50-204, Exhibit A.
26. U.S. Atomic Energy Commission, *Nuclear Power Plants Cost Evaluation Handbook*, Vol. 3, Mar. 15, 1962.
27. Westinghouse Electric Corp., Large Power Reactor Program Interim Report, USAEC Report WAPD-LPR-141, Bettis Atomic Power Laboratory, July 1963.
28. Westinghouse Electric Corp., Large Power Reactor Program Interim Report Supplement, The Design of Seed-Blanket Cores, USAEC Report WAPD-LPR-154, Bettis Atomic Power Laboratory, July 1963.
29. Westinghouse Electric Corp., Report on Large Power Reactor (LPR) Program, USAEC Report WAPD-LPR-181, Bettis Atomic Power Laboratory, December 1963.
30. F. Schwoerer, Economic Potential of the Seed-Blanket Reactor, USAEC Report WAPD-237, Westinghouse Electric Corp., Bettis Atomic Power Laboratory, December 1960.
31. J. Chernick and S. O. Moore, Breeding Potential of Thermal Reactors, *Nucl. Sci. Eng.*, 6(6): 537 (December 1959).
32. A. Radkowsky, G. W. Harding, and R. G. Luce, Seed and Blanket Reactors, Paper A/Conf 28/P-208, presented at the Third United Nations International Conference on the Peaceful Uses of Atomic Energy, Geneva, September 1964.

Index

Power Reactor Technology

Volume 7

Note: The page range for each of the four issues of Vol. 7 is as follows: No. 1, pages 1 to 106; No. 2, pages 107 to 200; No. 3, pages 201 to 327; and No. 4, pages 329 to 432.

A

- Absorbers, iodine removal by, 58
- Accidents, fission-product release, environmental hazards, 370-1
  - maximum credible, for New Production Reactor, 267
- Algae, control in fuel-transfer canal at Consolidated Edison Thorium Reactor, 313
- Aluminum, reactivity effects in ZPR-III assembly, 11
- Aluminum alloys (Al-Pu), spike enrichment element for Plutonium Recycle Test Reactor, 169, 181
- Aluminum oxide systems (Al_2O_3-B_4C), irradiation testing, 367
- Aluminum systems (Al-Al_2O_3)
  - *See* Sintered aluminum powder
- Ammonia, synthesis using reactor heat, economics, 1-3
- Annealing, postirradiation, of boron-containing stainless steels, 366-7
- Atmosphere, fission-product dispersal after accidental release, 370
- Autocorrelation function, reactor noise analysis studies, 249-50

B

- Baffles, stagnant heavy-water design for thermal insulators, 401
- Barium-140, deposition from gas stream onto surfaces, temperature effects, 371
  - emission from irradiated uranium dioxide, 361
  - release during uranium fire, 370-1
- Belleville-spring washers
  - *See* Washers
- BEPO reactor
  - *See* Reactors (BEPO)
- Beryllium, reactivity effects in ZPR-III assembly, 11
- Beryllium oxide, reactivity effects in ZPR-III assembly, 11
  - subcritical assemblies of, hafnium control studies, 10-11
- Bibliographies, neutron thermalization, 331
- Big Rock Point Power Reactor
  - *See* Reactors (Big Rock Point Power)
- Bismuth alloys (Bi-Pb) (liquid), expansion, reactivity effects in fast reactors, 122
- Bismuth alloys (Bi-Pu), preparation and testing, 182
- Blankets
  - *See* Breeding blankets
- Boiling burnout, correlations, comparison of Russian and U. S. data, 223-35
  - limits for reactors, 14-26
  - in multirod geometries, 154-65
  - in steam-water mixtures, 335-52
- Boiling Nuclear Superheater Reactor
  - *See* Reactors (BONUS)
- Boiling-water reactors
  - *See* Reactors (boiling-water)
- Bonding, gas-pressure, tubular fuel elements, 237-8
  - uranium dioxide-fueled rods, 238-41
- BONUS Reactor
  - *See* Reactors (BONUS)
- BORAX-II Reactor
  - *See* Reactors (BORAX-II)
- BORAX-III Reactor
  - *See* Reactors (BORAX-III)
- BORAX-V Reactor
  - *See* Reactors (BORAX-V)
- Boric acid, chemical-shim use in pressurized-water reactors, 411-21
  - shielding-solution use in ML-1 Reactor, 219
- Boron, burnable-poison use, in experimental fuel assemblies, 34-5
  - in fuel elements, 356-8
  - control-rod use, 365-8
  - cross-section change with burnup in reactors, 216-18
  - dissolution in coolant for control of pressurized-water reactors, 411-21
- Boron carbide, burnable-poison use in fuel elements, 358
  - control-rod use, 367-8
    - in Experimental Gas-Cooled Reactor, 376-7, 378
  - corrosion, 367-8
- Boron carbide (Zircaloy-2-clad), irradiation testing, 368
- Boron carbide systems (Al_2O_3-B_4C), irradiation testing, 367
- Boron carbide systems (B_4C-Cu), corrosion testing, 367
- Boron carbide systems (B_4C-SiC), corrosion, 367-8
- Boron carbide systems (B_4C-SiC) (Zircaloy-2-clad), irradiation testing, 368
- Boron carbide systems (B_4C – stainless steel), corrosion testing, 367
- Boron carbide systems (B_4C – steel), corrosion testing, 367
- Boron carbide systems (B_4C – Zircaloy-2), irradiation testing, 367
- Brazing, heat exchanger for Molten-Salt Reactor Experiment, 374-5
- Breeder reactors
  - *See* Reactors (breeder)
- Breeding blankets, lifetime estimation for Shippingport core 2, 200
  - management, 128
  - power contributions during operation of Shippingport core 1, 195
  - Shippingport core 2 design, 197-8
- Breeding potential, fissile isotopes in various reactors, 113
- Breeding ratios, effects of structural materials in fast reactors, 131-3
  - fast reactors with metal, oxide, and carbide cores, 114-17
  - plutonium-uranium heavy-water systems, 411
- British Experimental Pile O
  - *See* Reactors (BEPO)
- Bromine, release during uranium fire, 370-1
- Buckling, determination for heavy-water lattices, 212-14
  - measurement in substitution critical experiments, 4-5
- Buildings, Big Rock Point comparison with Humboldt Bay plant, 78-9
  - BONUS Reactor containment, 308
  - containment at low pressures, 54-5
  - New Production Reactor, 267
  - Pathfinder Reactor containment, 290
  - reinforced concrete, stress analysis, 54-5
- Burnout, comparison of Russian with U. S. data, 223-35
  - DNB-2 curve significance, 335-43
  - limits for boiling-water reactors, 14-26
  - multirod geometry studies, 154-65
  - in nonuniformly heated channels, 343-52
  - rod-bundle geometry studies, 226-7
  - test device, 15
  - tubular geometry studies, 227-34
- Burnup
  - *See also* Core life
  - fuel assemblies, in Fuel-Cycle Program, 28, 31
    - in High-Power-Density Development Project, 38-39, 42, 44
  - fuel-element studies for Shippingport core 2, 197, 199-200
- Butterfly valves
  - *See* Valves

C

- Cadmium, cross-section change with burnup in reactors, 216-18
- Cadmium alloys (Ag-Cd-In), cross-section change with burnup in reactors, 216-18

Cadmium alloys (Cd-Eu), burnable-poison use studies, 217
Canada, comparison with United States in heavy-water reactor development, 87-95
Canals
    See Fuel-transfer canals
CANDU Reactor (Canada)
    See Reactors (CANDU) (Canada)
Carolinas-Virginia Tube Reactor
    See Reactors (Carolinas-Virginia Tube)
Cerium-141, deposition from gas stream onto surfaces, temperature effects, 371
Cerium-144, emission from irradiated uranium dioxide, 361
  release during uranium fire, 370-1
Cerium alloys (Ce-Co-Pu) (liquid), properties, 182-3
Cermets, plutonium-containing, fabrication and testing, 183
Cesium-137, evolution from irradiated uranium dioxide, 360-2
  release during uranium fire, 370-1
Circuits (electric)
    See Electric circuits
Chromium, neutron-physics effects in fast reactors, 128-33
Cladding
    See also specific cladding materials, e.g., Stainless steels (304) and Zircaloy-2
  boron incorporation for burnable-poison use, 357-8
  failure, effects of uranium dioxide core melting, 46-8
  fuel assemblies, testing in VBWR, 27-34
  sintered aluminum powder use, for fuel elements, 242
    in organic-cooled heavy-water-moderated reactor design, 95, 405
    in WR-1 reactor, 324-5
  stainless steel, failure on fuel elements in Vallecitos Boiling-Water Reactor tests, 354-5
  Zircaloy-2 system with stainless-steel inner lining, 356
  Zircaloy-2 use for boron carbide systems, 368
  Zircaloy-4 use for Shippingport core 2 fuel elements, 197
Coal, gasification by reactor heat, economics, 1-3
Cobalt alloys (Ce-Co-Pu) (liquid), properties, 182-3
Cobalt alloys (Co-Pu), preparation and testing, 182
Cobalt alloys (Co-Pu) (liquid), properties, 182-3
Coke, iodine removal by, 58
Compaction, explosive, of tubular fuel elements, 237-8
  vibratory, annular multitube fuel elements, 241-2
    uranium dioxide fuel rods, 238-41
Components, 60-9, 269-75, 372-5
    See also specific components, e.g., Pumps, Steam generators, and Valves
  of fuel assemblies, functional description, 38, 43
  fuel-handling equipment, 68
  of transducers, limitations on use in reactors, 52-3
Computer programs, AIM-5, graphite-moderated critical assembly studies, 9
  BICEP, graphite-moderated critical assembly studies, 9
  BPG, diffusion-equation coefficient studies for Spectral Shift Control Reactor, 212
  CINDER, time-dependent fission-product concentration studies, 215-16
  fission-product deposition from gas streams, 371
  FORM, graphite-moderated critical-assembly studies, 9
  GAM-I, critical configurations studies, 6
  MUFT-KATE, nuclear constant calculations for seed-blanket reactors, 429
  PDQ-4, perturbation analysis for Spectral Shift Control Reactor, 212
  period-meter output studies during reactor startup transients, 51
  radiation-effects studies of transducer materials, 53
  reactor noise analysis, 248
  REPAD, Doppler effects on neutron absorption resonance, 329-30
  STEWPOT, graphite-moderated critical assembly studies, 10
  TEMPEST, critical configurations studies, 6, 9
  THERMO-SYPHON, pressurized-water reactor natural-circulation studies, 421-2
  THERMOS, heavy-water lattice studies, 7
  TKO, perturbation analysis for Spectral Shift Control Reactor, 212
  TYCHE, fission-neutron age studies, 331
Condensers, BONUS Reactor, 307
  comparison of Big Rock Point with Humboldt Bay plant, 79-81
  Pathfinder Reactor, 289-90
Conferences, fuel management, 201
  Tripartite Organic-Cooled Heavy-Water Reactor Meeting, 324
Construction practices, 70-84, 276-312
Containers, stainless-steel, criticality measurements of uranium and plutonium solutions, 5-6
Containment, 265-7, 370-1
  BONUS Reactor, 307-9
  comparison of Big Rock Point with Humboldt Bay plant, 79
  large heavy-water pressure-tube reactor, 404
  leak studies with concrete buildings, 54-5
  New Production Reactor, vented-containment concept, 265-7
  Pathfinder Reactor, 290-1
Contamination, environmental, from uranium fire, 370-1
  fossil-fired superheaters, 314
  turbines in superheater reactors, 310
Control-rod drives, 272-5
  Big Rock Point Reactor, 82
  electrical switch problems in Consolidated Edison Thorium Reactor, 314
  Heavy-Water Components Test Reactor, problems of, 316-17
  Pathfinder Power Reactor, 274-5
Control rods, BONUS Reactor, 301-3, 306
  boron use, review of, 365-8
  Experimental Gas-Cooled Reactor, design, 376-7, 378
  flexibility for travel in bowed channels, 376-7, 378
  hafnium, studies in BeO subcritical assemblies, 10-11
  hydraulic actuator, 271-4
  materials for, cross-section vs. burnup data, 216-18
  Pathfinder Reactor, 282-4, 288
  pressure-balanced type for Experimental Organic-Cooled Reactor, 274
  requirements in reactors using chemical shim in primary coolant, 415-18
  shim assemblies for Plutonium Recycle Test Reactor, 390
  Shippingport Reactor, neutron-exposure effects, 195-6
  Sodium Reactor Experiment, drop-time studies, 377, 379
  withdrawal program for large multiregion reactor, 331-2
Control systems, 51-3, 248-63
  augmentation in boiling-water reactors by boron steel poison slabs, 207
  chemical shim in primary coolant of pressurized-water reactors, 411-21
  comparison of Big Rock Point with Humboldt Bay plant, 81-3
  Consolidated Edison Thorium Reactor operating experience, 314
  moderator-level control, 385-99
  noise-analysis studies, 248-63
Converter reactors
    See Reactors (converter)
Coolants
    See also specific coolants, e.g., Sodium (liquid) and Water
  expansion, reactivity effects in fast reactors, 118-22
  flow-rate measurement in Plutonium Recycle Test Reactor, 383
  quality control, in reactors using dissolved chemical shim, 418-21
    in Shippingport plant, 196
Cooling systems, comparison of Big Rock Point with Humboldt Bay design, 70-3, 76-9
  Consolidated Edison Thorium Reactor, purification problems, 314
  design variables, effects on burnout in boiling-water reactors, 15
  organic-cooled heavy-water-moderated reactor, 96
  pressure control in Pathfinder Reactor, 288
  recirculation-piping design for Pathfinder Reactor, 384
Copper, mesh, iodine removal by, 58
Copper systems (B_4C-Cu), corrosion testing, 367
Core design, BONUS Reactor, 303-6
  comparison of Big Rock Point with Humboldt Bay plant, 73-6
  evaluation of Zircaloy use in N. S. *Savannah* Reactor, 322-4
  fast-breeder reactor for water desalinization, 138-9
  NPD Reactor, 391
  Pathfinder Reactor, 284-8
  Plutonium Recycle Test Reactor, 387
  seed-blanket reactor, 423-4, 427-8
  thermionic water-cooled reactor, 103
Core life
    See also Burnup
  extension in boiling-water reactors by control augmentation techniques, 207
  plutonium-uranium mixtures in water-moderated reactors, 203-5
Corrosion, alumina–boron carbide pellets, 367
  boron carbide, 368
  boron carbide–copper couples, 367
  boron carbide–stainless-steel couples, 367
  boron carbide–steel couples, 367
  control in reactors using boric acid shim in primary coolant, 419-20
  fuel assemblies tested in VBWR, 29-30, 38, 40, 354-5
  stainless-steel fuel-element cladding in VBWR tests, 354-5
  welds on Shippingport control-rod assemblies, 196
Corrosion products, buildup in coolant pumps of Plutonium Recycle Test Reactor, 315-16
  deposition in reactors using chemical shim in primary coolant, 419-20
Cracking, fuel assemblies tested in VBWR, 38, 40
  spot welds in boron-containing stainless steels, 366
  stainless-steel fuel-element cladding in VBWR tests, 354-5
Critical assemblies, beryllium oxide-moderated types, 10-11
  fast-neutron types, 11-12, 211-12
  graphite-moderated type, 8-10, 209-10
  heavy-water type, 7-8, 209, 213-14

Critical assemblies (Continued)
  light-water-moderated types, effects of variation of ^{240}Pu concentration, 207-8
  noise analysis, 252
  solution type, 5-6
  zirconium hydride types, 211
Critical assemblies (Peach Bottom), thorium resonance-capture studies, 10
Critical assemblies (ZPR-III), comparison of experimental parameters with calculations, 211-12
  reactivity-worth determination for various materials, 11
Critical assemblies (ZPR-VII), uniform lattice experiments, 7-8
Critical experiments, 4-13
  BORAX-V reactor, 206
Critical mass, fast reactors, 114-16, 131-3
Criticality, plutonium-solution studies, 5-6
  ^{235}U aqueous solutions, 6
  uranyl fluoride solutions, 6
Croloy alloy, evaluation for gas-heated steam-generator construction, 65
Cross sections, data for zirconium, 331
  fission products, calculations of change with time, 215-16
  neutron, Doppler effects in reactors, 329-30
  neutron absorption, for gold, 10
    for thorium, 10
  neutron capture, in fast reactors, 111-12
    for materials in fast reactors, 128-33
    for reactor poison materials, 216-18
  neutron fission, in fast reactors, 111-12
  ^{16}O(n,p)^{16}N reaction, measurement, 220

D

D-ring seals, for helium retention in Plutonium Recycle Test Reactor, 381-3
Damping oils, radiation effects on use in reactor instruments, 52-3
Demineralizers, comparison of Big Rock Point with Humboldt Bay plant, 79-81
Density, plutonium carbide–uranium carbide fuel materials, 180
  uranium dioxide, changes during melting, 362-3
  uranium dioxide fuel elements, effects on exposure lifetime in Shippingport core 2, 199
Departure from nucleate boiling
  See also Burnout
  burnout-limit studies, 18-26
  DNB-2 curve significance, 335-43
Desalinization, economic aspects, 138-44
  heavy-water reactor cost studies, 87
Design practices, 70-84, 276-312, 376-84
Dielectrics, radiation effects on use in reactor instruments, 52-3
Diffusion coefficients, fission products in uranium dioxide plates, 362
Diffusion length, thermal neutrons in water, 146-8
Diffusion parameters, thermal neutrons, in graphite, 151-2
    in heavy water, 151
    in water, 148-50
DNB
  See Departure from nucleate boiling
Dome seals
  See Seals
Doppler effect, effect on neutron-absorption resonance in SPERT reactor, 329
  reactivity effects in fast reactors, 122-4
Dose (radiation)
  See Radiation dose
Douglas Point Station
  See Reactors (CANDU)
Dounreay Fast-Breeder Reactor
  See Reactors (Dounreay Fast-Breeder)
Drive mechanisms
  See Control-rod drives
Dry wells, Humboldt Bay Reactor containment-system design, 79
Dual-purpose plants, electricity generation and water desalinization, 87, 142-4
Ductility, boron-containing stainless steel, 365-6
  Shippingport pressure vessel, fast-neutron effects, 193
Dump valves
  See Valves
Dysprosium, cross-section change with burnup in reactors, 216-18

E

Economics, 1-3, 138-44
  CANDU Reactor, fuel management, 202-4
  canned-motor pump costs, 421
  dual-purpose electric power and water desalinization plants, 142-4
  electrical revenue effects on cost of water desalinization by reactors, 144
  fuel cycles for heavy-water–thorium breeder reactors, 410
  heavy-water reactors, review of recent developments, 86-7, 89, 96
    large heavy-water pressure-tube reactor, 403
    large organic-cooled heavy-water-moderated reactor, 405, 408
  Lithium-Cooled Reactor Experiment auxiliary systems, 384
  organic-cooled heavy-water-moderated reactor, 408
  pressurized-water reactors with natural circulation, 421-2
  seed-blanket reactor designs, 429
  SENN Reactor, effects of partial reloading scheme, 202
  solid-fuel gasification, 1-3
  water desalinization, 138-44
  Zircaloy use in core structure of N.S. *Savannah* Reactor, 322-4
Eggs, expected contamination from released fission products, 370-1
Electric circuits, period meters, 51-2
  servomechanisms, 53
  switches, problems in control-rod drive of Consolidated Edison Thorium Reactor, 314
Electrical insulation
  See Insulation (electrical)
Electromagnetic pumps
  See Pumps
Electron-beam welding, fuel-element components, 358-9
Enrico Fermi Fast-Breeder Reactor
  See Reactors (Enrico Fermi Fast-Breeder)
Equipment, for fuel handling, 68
Erbium, cross-section change with burnup in reactors, 216-18
Erbium systems (Er-Eu), burnable-poison use studies, 217
Erbium systems (Er-Gd), burnable-poison use studies, 217
Europium, cross-section change with burnup in reactors, 216-18
Europium systems (Cd-Eu), burnable-poison use studies, 217
Europium systems (Er-Eu), burnable-poison use studies, 217
Europium systems (Eu-Gd), burnable-poison use studies, 217
Experimental Breeder Reactor II
  See Reactors (Experimental Breeder, II)
Experimental Organic-Cooled Reactor
  See Reactors (Experimental Organic-Cooled)
Explosive compaction, tubular fuel elements, 237-8
Exponential experiments, 4-13
Extrusion, tandem, stainless-steel-to-Zircaloy transition-joint preparation, 368-9

F

Fabrication
  See also specific processes, e.g., Bonding, Extrusion, and Swaging
  fuel assemblies for boiling-water reactors, 27-42
  novel methods for fuel elements, 237-46
Feedwater systems, BONUS Reactor, 307
  comparison of Big Rock Point with Humboldt Bay plant, 79-81
  Pathfinder Reactor, 289-90
Fermi Fast-Breeder Reactor
  See Reactors (Enrico Fermi Fast-Breeder)
Ferrule seals, for helium retention in Plutonium Recycle Test Reactor, 381-3
Filters, 55, 58
  for fuel-transfer canal at Consolidated Edison Thorium Reactor, 313
Fires, uranium, fission-product dispersal, 370-1
Fission gases
  See also specific isotopes, e.g., Iodine-131 and Xenon-133
  pressure determination in uranium dioxide-filled fuel rods, 43-5
  release, by irradiated plutonium carbide–uranium carbide fuel materials, 181
    by irradiated plutonium oxide–uranium oxide systems, 178
Fission products
  See also specific isotopes, e.g., Cesium-137 and Strontium-90
  containment in New Production Reactor accident, 266-7
  deposition from gas stream onto surfaces, temperature effects, 371
    effects on breeding ratio in fast reactors, 116
    environmental hazards, 370
    evolution from irradiated uranium dioxide, 359-62
    time-dependent concentration calculations, 215-16
    turbine contamination problems in superheater reactors, 310
Flowmeters, damped signals for, using surge suppressors in Plutonium Recycle Test Reactor, 383
Fluid flow, 14-26, 154-65, 335-52
  axial- vs. cross-flow in steam generator design, 65
  rate measurement in flow channels of Plutonium Recycle Test Reactor, 383
Fluoride ion, effects on Zircaloy-2 corrosion, 356
Foils, ^{197}Au, resonance capture studies, 10
  cadmium-covered gold, flux-traverse measurements in heavy-water lattices, 7
  ^{55}Mn, resonance-capture measurements, 10
  ^{232}Th, resonance-capture measurements, 10
  vanadium, resonance-capture measurements, 10
Food, expected contamination from released fission products, 370-1
French reactors
  See Reactors (Rapsodie) (France)
Fretting corrosion, Zircaloy-clad fuel rods in VBWR tests, 29-30
Fuel assemblies, Big Rock Point Power Reactor, variations of basic design, 37
  BONUS Reactor boiler, 296-8
  BONUS Reactor superheater, 298-301
  comparison of Big Rock Point with Humboldt Bay design, 73-6

- Fuel assemblies (Continued)
  - components, functional description of, 38, 43
  - design for boiling-water reactors, 27-38
  - fabrication for testing in VBWR, 27-38
  - geometric effects on burnout, 23-6, 154-65
  - irradiation testing in VBWR, 27-38
  - large heavy-water pressure-tube reactor, 401-2
  - Pathfinder Reactor boiler, 279-80
  - Pathfinder Reactor superheater, 279, 281-2
  - uranium dioxide-fueled, fabrication and testing, 27-50
- Fuel-Cycle Program, 27-34
  - fuel-element cladding tests in VBWR, 354-5
  - fuel-element fabrication for irradiation testing in VBWR, 356, 357
- Fuel cycles, 201-5
  - CANDU Reactor, 202-4
  - costs, for Canadian and U. S. heavy-water reactors, 89, 97
    - for heavy-water–thorium breeder system, 410
  - fast reactors, 124-6
  - plutonium, review of developments, 167-83
  - plutonium-uranium mixture in water-moderated reactors, 203-5
  - seed-blanket reactor designs, 429
  - SENN Reactor, 202
- Fuel elements, 27-50, 167-83, 237-46, 354-63
  - *See also* Fuel assemblies
  - aluminum-plutonium, plutonium-content determination from reactivity coefficients, 208
  - annular multitube type, novel fabrication techniques, 241-2
  - boron-containing types, 356-8
  - containers, evaluation of Zircaloy use in N.S. *Savannah* Reactor, 322-4
  - design problems for superheater reactors, 310
  - Experimental Boiling-Water Reactor, plutonium-bearing type, 172
  - fabrication by novel methods, 237-46
  - handling equipment, 68
  - internal pressure, contributions of fission-product helium, 455-6
  - organic-cooled heavy-water-moderated reactor, 408
  - Pathfinder Reactor, end-closure fabrication, 245-6
  - plutonium-bearing, review of development, 167-83
  - Plutonium Recycle Test Reactor, 167-73
  - Rapsodie Reactor, 167-9
  - rejuvenation without reprocessing, 172-3
  - rods, design for heavy-water reactors, 93
  - rods fueled with uranium dioxide, novel fabrication techniques, 238-41
  - Shippingport core 2 design, 197-8
  - stainless-steel-cladding failure in Vallecitos Boiling-Water Reactor irradiations, 354-5
  - thermionic water-cooled reactor, 102, 103-4
  - tubular, design for heavy-water reactors, 94
  - tubular, novel consolidation and bonding methods, 237-8
  - uranium dioxide, core-melting effects on cladding failure, 46-8
  - Zircaloy-2-clad, stainless-steel-lined types, 356
- Fuel-transfer canals, Consolidated Edison Thorium Reactor, water clarity and leakage problems, 313
- Fuels
  - *See also* specific fuel materials, e.g., Plutonium oxide (PuO_2) and Uranium oxide (UO_2)
  - cost bases used in CANDU Reactor design, 202
  - costs for seed-blanket reactor designs, 429
  - expansion, reactivity effects in fast reactors, 118
  - management studies, 201-5
  - plutonium-bearing, review of developments, 167-83

G

- Gadolinium, cross-section change with burnup in reactors, 216-18
- Gadolinium systems (Er-Gd), burnable-poison use studies, 217
- Gadolinium systems (Eu-Gd), burnable-poison use studies, 217
- Gas, pipeline, economics of synthesis using reactor heat, 1-3
- Gasification, solid fuels by reactor heat, economics, 1-3
- General Electric Test Reactor
  - *See* Reactors (General Electric Test)
- Geometrical configurations, effects on burnout in multirod fuel assemblies, 23-6, 154-65
  - rod-bundle burnout correlations, 226-7
  - shielding studies, 220
  - tubular burnout correlations, 227-34
- Gold, absorption cross section, 10
  - foils, use in flux-traverse measurements in heavy-water lattices, 7
- Gold-197, foils, resonance-capture studies, 10
- Gold alloys (Au-Ni), brazing alloy use in heat exchanger for Molten-Salt Reactor Experiment, 375
- Graphite, neutron-diffusion parameters in, 151-2

H

- Hafnium, control-rod studies in BeO subcritical assemblies, 10-11
  - cross-section change with burnup in reactors, 216-18
- Halden Boiling-Water Reactor
  - *See* Reactors (Halden Boiling-Water)
- Hazards
  - *See* Safety
- Heat exchangers, Molten-Salt Reactor Experiment, design and fabrication, 374-5
  - U-tube type, for heavy-water reactors, 90-92
- Heat transfer, 14-26, 154-65, 223-35, 335-52
  - burnout, in multirod geometries, 154-65
    - in steam-water mixtures, 335-52
  - burnout correlations, comparison of Russian and U. S. data, 223-35
  - burnout limits for boiling-water reactors, 14-26
  - comparison of Big Rock Point with Humboldt Bay plant, 76
  - data for large heavy-water pressure-tube reactor, 402
  - fuel assemblies for boiling-water reactors, 31, 36, 39-40, 42, 44
  - nonuniformity in heated channels, effects on burnout, 343-52
- Heavy water
  - *See* Water (D_2O)
- Heavy-Water Components Test Reactor
  - *See* Reactors (Heavy-Water Components Test)
- Heavy-Water Lattice Project, 7
- Heavy-water reactors
  - *See* Reactors (heavy-water)
- Helium, content in fuel-element voids from ternary fission of ^{235}U, 455-6
  - seals for, in Plutonium Recycle Test Reactor, 381-3
- Helium system, NPD Reactor, 392
- "Hideout," boron in chemical-shim control of pressurized-water reactors, 420
- High-Performance UO_2 Program, 38-50
- High-Power-Density Development Project, 34-44
  - fabrication-process studies, 243-4
- High-Temperature Gas-Cooled Reactor Experiment
  - *See* Reactors (ZENITH)
- Holmium, cross-section change with burnup in reactors, 216-18
- HPD
  - *See* High-Power-Density Development Project
- HPP
  - *See* High-Performance UO_2 Program
- Humboldt Bay Power Reactor
  - *See* Reactors (Humboldt Bay Power)
- Humidity, effects on control-rod-drive switch in Consolidated Edison Thorium Reactor, 314
- Hydrostatic pressing, tubular fuel elements, 237-8

I

- Impact strength
  - *See* Ductility
- Implosive consolidation, tubular fuel elements, 237-8
- Indium, cross-section change with burnup in reactors, 216-18
- Indium alloys (Ag-Cd-In), cross-section change with burnup in reactors, 216-18
- In-pile loops, uranium dioxide fuel-assembly testing, 45-8
- Instrumentation, BONUS Reactor, 306
  - comparison of Big Rock Point with Humboldt Bay plant, 81-3
  - Pathfinder Reactor, 288
  - period meters, time-constant studies, 51-2
  - reactor control, 51-3
- Insulation (electrical), radiation effects on use in reactor instruments, 52-3
- Insulation (thermal), "MinK" compressed-silica material, 326
  - pressure tubes, 326
- Iodine, behavior in large containers, 58
  - deposition on laboratory surfaces, 57-8
  - removal from BEPO cooling system, 56
- Iodine-131, deposition from gas stream onto surfaces, temperature effects, 371
  - evolution from irradiated uranium dioxide, 360-2
  - release during uranium fire, 370-1
- Iodine-132, release during uranium fire, 370-1
- Iodine-133, release during uranium fire, 370-1
- Iodine-134, release during uranium fire, 370-1
- Iodine-135, release during uranium fire, 370-1
- Ion exchange, pH control in Shippingport reactor, 196
- Iron, neutron physics effects in fast reactors, 128-33
- Iron alloys (Fe-Pu), preparation and testing, 182
- Iron alloys (Fe-Pu) (liquid), properties, 182-3
- Iron oxides, reactivity effects in ZPR-III assembly, 11
- Iron systems (Fe-PuC-UC), fabrication and testing, 183
- Irradiation testing, alumina–boron carbide pellets, 367
  - boron carbide–Zircaloy-2 systems, 367
  - boron-containing stainless steel, 365-6
  - fuel assemblies for boiling water reactors 27-42, 44
  - fuel elements in Fuel-Cycle Program, 354-
  - plutonium alloys, 180-2
  - plutonium carbide–uranium carbide systems 176-80
  - plutonium oxide–uranium oxide systems, 169-78
  - transition joints of Zircaloy to stainless steel, 368
  - type 347 stainless steel, by fast neutrons 187-91
  - uranium dioxide, 359-63

- Irradiation testing (Continued)
  - Zircaloy-2-clad boron carbide systems, 368
  - Zircaloy-2–zirconium boride systems, 367

J

- Joints
  - *See also* Welds
  - stainless-steel-to-Zircaloy, 401
  - stainless-steel-to-Zircaloy, preparation by tandem extrusion, 368-9

K

- Krypton, release during uranium fire, 370-1

L

- Laboratories, iodine deposition on surfaces, 57-8
- Large Power Reactor Program, 197
  - seed-blanket reactor studies, 411, 422-31
- LCRE
  - *See* Reactors (Lithium-Cooled, Experiment)
- Lead alloys (Bi-Pb) (liquid), expansion, reactivity effects in fast reactors, 122
- Lead telluride, thermoelectric power unit use, 106
- Leak testing, dome-seal tube closures, 380-1
- Linings, stainless-steel, use under Zircaloy-2 cladding, 356
- Liquid metals
  - *See* Metals (liquid) and specific metals, e.g., Bismuth alloys (Bi-Pb) (liquid) and Sodium (liquid)
- Lithium, cross-section change with burnup in reactors, 216-18
- Lithium (liquid), expansion, reactivity effects in fast reactors, 118-22
  - LP-1 pump for, 269-72
- Lithium-Cooled Reactor Experiment
  - *See* Reactors (Lithium-Cooled, Experiment)
- Los Alamos Molten-Plutonium Reactor Experiment I
  - *See* Reactors (Los Alamos Molten-Plutonium, Experiment I)
- LP-1 pump, design, for liquid metals, 269-71
- Lubricants, radiation effects on use in reactor instruments, 52-3
- Lutetium, cross-section change with burnup in reactors, 216-18

M

- Magneform Mark I, swaging of fuel-element cladding to core, 242-3
- Magnesite, iodine removal by, 58
- Magnesium oxide systems (MgO-PuO_2), fuel-use studies, 169-71
- Magnetic-pulse forming machine
  - *See* Magneform Mark I
- Manganese-55, foils, resonance-capture measurements, 10
- Manipulators, for fuel handling, 68
- Mass flow, burnout studies of nonuniformly heated channels, 343-52
- Materials, 187-91, 365-9
  - *See also* specific materials
  - structural, effects on neutron physics of fast reactors, 128-33
- Mathematics, analysis of Doppler effects on neutron-absorption resonance, 329
  - control-rod withdrawal program for large multiregion reactor, 331-2
  - reactor noise analysis, 248-63
  - time-dependent fission-product concentration studies, 215-16
- Mechanical properties, boron-containing stainless steel, 365-6
  - cladding materials, 42
  - fuel assemblies for boiling-water reactors, 39
  - hafnium control rods in Shippingport, neutron-exposure effects, 195-6
  - transition joints of Zircaloy to stainless steel, 368
  - type 347 stainless steel, fast-neutron effects, 188-91
- Melting, uranium dioxide in fuel elements, effects on cladding failure, 46-8
- Melting point, uranium dioxide, 362-3
- Metals (liquid), pump designs, 372-4
  - pumps for, 269-71
- Methanol, synthesis using reactor heat, economics, 1-3
- Milk, expected contamination from released fission products, 370-1
- "MinK"
  - *See* Insulation (thermal)
- ML-1 Reactor
  - *See* Reactors (ML-1)
- Moderator-level control, 385-99
- Moisture separators, 55
- Molybdenum, neutron physics effects in fast reactors, 128-33
- Molybdenum alloys (Mo-Pd-Pu-Rh-Ru-U-Zr), irradiation testing for use in Experimental Breeder Reactor II, 180-2
- Molybdenum alloys (Mo-Pu-U), swelling during irradiation, 181
- Molybdenum systems (Mo-PuO_2), preparation, 183
  - properties, 183

N

- Neutron economy, heavy-water reactors, 85-6
- Neutrons, age measurements in water, 331
  - cross sections, Doppler effects in reactors, 329-30
  - effects, on ductility of Shippingport pressure vessel, 193
    - on tensile properties of hafnium control rods in Shippingport, 195-6
  - energy spectra for fast reactors, 108-10
  - fast, effects on type 347 stainless steel, 187-91
  - number produced by fission of various elements by 1.5-Mev neutrons, 112
  - physics, considerations in large fast reactors, 107-34
  - pulsed-source, criticality studies on plutonium solutions, 5-6
  - thermal, diffusion parameters, 145-52
  - thermalization, 331
- New Production Reactor
  - *See* Reactors (New Production)
- Nickel, neutron physics effects in fast reactors, 128-33
  - reactivity effects in ZPR-III assembly, 11
- Nickel alloys (Au-Ni), brazing-alloy use in heat exchanger for Molten-Salt Reactor Experiment, 375
- Nickel alloys (Ni-Pu) (liquid), properties, 182-3
- Nickel oxides, reactivity effects in ZPR-III assembly, 11
- Niobium, neutron-physics effects in fast reactors, 128-33
- Niobium systems (Nb-PuC-Zr), properties, 183
- Niobium systems (Nb-PuO_2-Zr), properties, 183
- Noise, reactor, analysis of, 248-63
- NPD Reactor
  - *See* Reactors (NPD)
- Nuclear Power Demonstration Reactor
  - *See* Reactors (NPD)
- Nuclear reactions, $^{16}O(n,p)^{16}N$, cross-section measurements, 220

O

- O-ring seals, for helium retention in Plutonium Recycle Test Reactor, 381-3
- Oils, damping, radiation effects on use in reactor instruments, 52-3
- Operating experience, 193-6, 276-312, 385-99
  - Consolidated Edison Thorium Reactor, 313-15
  - Experimental Boiling-Water Reactor, 317-20
  - Heavy-Water Components Test Reactor, 316-17
  - NPD Reactor, 391-3, 398-9
  - Plutonium Recycle Test Reactor, 315-16, 386-91, 393-8
  - Shippingport Pressurized-Water Reactor, 193-6
- Organic compounds, radiation effects on use in reactor instruments, 52-3
- Organic coolants, effects on zirconium alloys, 324-5
- ORGEL Program, 97

P

- Palladium alloys (Mo-Pd-Pu-Rh-Ru-U-Zr), irradiation testing for use in Experimental Breeder Reactor II, 180-2
- Pathfinder Power Reactor
  - *See* Reactors (Pathfinder Power)
- Pawling Lattice Test Rig
  - *See* Reactors (Pawling Lattice Test Rig)
- Period meters, time-constant studies, 51-2
- *p*H, control in reactors using boric acid shim in primary coolant, 418-19
  - control system for Shippingport coolant water, 196
- Physical Constants Testing Reactor
  - *See* Reactors (Physical Constants Testing)
- Physical properties, uranium dioxide, 360, 362-3
  - uranium dioxide–zirconium dioxide plates, 362
- Physics, 4-13, 145-52, 206-20, 329-32
  - neutron, considerations in large fast reactors, 107-34
- Plutonium, recycling in breeder reactors, equilibrium composition of fuel, 127
  - recycling study for water-moderated reactors, 203-5
  - thermal breeder reactor studies, 409-11
- Plutonium-239, breeding potential in various reactors, 113
  - critical concentrations of aqueous solutions, 6
  - fission products, time-dependent concentration studies, 215-16
  - fission-rate measurements in graphite, 10
  - fission ratio to ^{235}U in graphite systems, 10
  - fission-ratio measurements in ZPR-III, 11
  - neutron capture-to-fission ratio, 111
  - neutron fission cross sections, 111
  - neutron production in fission by 1.5-Mev neutrons, 112
- Plutonium-239 systems (^{239}Pu-Th), fuel cycle for breeder reactors, 124-6
- Plutonium-239 systems (^{239}Pu-^{238}U), critical mass, fast reactor studies, 115
  - fuel cycle for breeder reactors, 124-6
- Plutonium-240, concentration effects on criticality of light-water assemblies, 207-8
  - fast-fission bonus to breeding in various reactors, 113
  - fission-ratio measurements in ZPR-III assembly, 11
  - neutron fission cross sections, 111
  - neutron production in fission by 1.5-Mev neutrons, 112
- Plutonium-241, breeding potential in various reactors, 113
  - neutron cross sections, Doppler-broadening, 330

Plutonium-241 (Continued)
  neutron production in fission by 1.5-Mev neutrons, 112
Plutonium-242, fast-fission bonus to breeding in various reactors, 113
Plutonium alloys, testing, 181-3
Plutonium alloys (Al-Pu), spike enrichment element for Plutonium Recycle Test Reactor, 169, 181
Plutonium alloys (Bi-Pu), preparation and testing, 182
Plutonium alloys (Ce-Co-Pu) (liquid), properties, 182-3
Plutonium alloys (Co-Pu), preparation and testing, 182
Plutonium alloys (Co-Pu) (liquid), properties, 182-3
Plutonium alloys (Fe-Pu), preparation and testing, 182
Plutonium alloys (Fe-Pu) (liquid), properties, 182-3
Plutonium alloys (Mo-Pd-Pu-Rh-Ru-U-Zr), irradiation testing for use in Experimental Breeder Reactor II, 180-2
Plutonium alloys (Mo-Pu-U), swelling during irradiation, 181
Plutonium alloys (Ni-Pu) (liquid), properties, 182-3
Plutonium alloys (Pu-Th), preparation and testing, 182
Plutonium alloys (Pu-U), fuel-cycle studies for water-moderated reactors, 203-5
  preparation and testing, 182
Plutonium alloys (Pu-Zr), irradiation testing, 182
Plutonium carbide systems (Fe-PuC-UC), fabrication and testing, 183
Plutonium carbide systems (Nb-PuC-Zr), properties, 183
Plutonium carbide systems (PuC-UC), fabrication, 175-80
  properties, 180
Plutonium nitrates, criticality measurements on solutions, 5-6
Plutonium nitride systems (Pu-PuN), properties, 183
Plutonium nitride systems (PuN-W), properties, 183
Plutonium oxide (PuO_2), preparation, 167-9, 174
Plutonium oxide systems ($MgO-PuO_2$), fuel use studies, 169-71
Plutonium oxide systems ($Mo-PuO_2$), preparation, 183
  properties, 183
Plutonium oxide systems ($Nb-PuO_2-Zr$), properties, 183
Plutonium oxide systems (PuO_2–stainless steel), preparation, 183
Plutonium oxide systems (PuO_2-UO_2), fuel-element development, 167-75
  irradiation testing, 173-5
Plutonium oxide systems (PuO_2-UO_2–stainless steel), fabrication and testing, 183
Plutonium oxide systems (PuO_2-W), properties, 183
Plutonium oxide systems (PuO_2-Zr), properties, 183
Plutonium Recycle Test Reactor
    See Reactors (Plutonium Recycle Test)
Plutonium systems (Pu-PuN), properties, 183
Poisons (reactor), BORAX-V critical experiments, 206
  boron, incorporation into fuel elements, 356-8
    use in experimental fuel assemblies, 34-5
  cross-section change with burnup, 216-18
  flat-region critical experiment studies, 4-5
  reactor control augmentation by, 207
  shim elements, for BONUS Reactor, 301-3
    for Pathfinder Power Reactor, 282-4
  soluble chemical-shim use in primary coolant of pressurized-water reactors, 411-21
Portable power plants
    See also Reactors (ML-1)
  thermionic type, design, 99-105
Power spectral density, reactor noise-analysis studies, 250-51, 254-55
Pressing, hydrostatic, tubular fuel elements, 237-8
Pressure, control in Pathfinder Reactor, 288
  effects on gas-heated steam-generator design, 65
  fission gases in uranium dioxide-filled fuel rods, 43-5
Pressure tubes, design for large reactor plant, 402
  dome-seal tube-closure design, 379-81
  insulation, 326
Pressure vessels, BONUS Reactor, 294-6, 303-6
  comparison of Big Rock Point with Humboldt Bay design, 72, 79
  Experimental Boiling-Water Reactor, modification for 100-Mw(t) operation, 318
  Pathfinder Reactor, 284-8
  seed-blanket reactor design, 425-6
  Shippingport, neutron-induced embrittlement, 193
  thermionic water-cooled reactor, 101, 103
Process Development Pile
    See Reactors (Process Development Pile)
Process-heat reactors
    See Reactors (process-heat)
Pumps, canned-motor type, costs for pressurized-water reactors, 421
  canned type for high-temperature organic liquids, 67-8
  electromagnetic, helical-rotor design, 65-8
  for liquid metals, 269-71
    diaphragm type, 372-3
    two-stage centrifugal-displacement type, 372-4
  primary coolant, problems in Plutonium Recycle Test Reactor, 315-16
PWL loop, uranium dioxide fuel-assembly testing, 45-8

R

Radiation control, 54-9, 265-7, 370-1
Radiation dose, environmental, from fission product release, 370-1
Radiation effects
    See also Irradiation testing
  transducer components, 52-3
Radiation protection standards, emergency exposure to released fission products, 371
  ML-1 reactor, 218-19
Rapsodie Reactor (France)
    See Reactors (Rapsodie) (France)
Reactivity, changes with burnup of poison materials, 216-18
  control, in BORAX-V by poison rods, 206
    by chemical shim in primary coolant of pressurized-water reactors, 411-21
  control in Pathfinder Reactor, 288
  effects of Doppler broadening of neutron-absorption resonance, 329
  long-term effects in fast reactors, 116-17
  Plutonium Recycle Test Reactor, moderator-level effects, 394-6
  shutdown, determination by reactor noise analysis, 254-6
Reactivity coefficients, Consolidated Edison Thorium Reactor, 314-15
  fast-reactor safety studies, 118-24
  NPD Reactor, design vs. measured values, 398
Reactivity lifetime, plutonium-uranium mixtures in water-moderated reactors, 203-5
Reactivity parameters, fertile materials, 112
  fissile materials, 112
Reactor control
    See Control-rod drives, Control rods, and Control systems
Reactors
    See also Critical assemblies
  noise analysis, 248-63
Reactors (BEPO), iodine removal from cooling system, 56
Reactors (Big Rock Point Power), design comparison with Humboldt Bay Power Reactor, 70-84
  High-Power-Density Development Project, 34-44
Reactors (boiling-superheater)
    See also Reactors (BONUS) and Reactors (Pathfinder Power)
  annular multitube fuel-element development, 241-2
Reactors (boiling water)
    See also Reactors (BONUS), Reactors (BORAX), Reactors (Experimental Boiling-Water), Reactors (Halden Boiling-Water), Reactors (Humboldt Bay Power), Reactors (Pathfinder Power), Reactors SENN), and Reactors (Vallecitos Boiling-Water)
  burnout limits, 14-26
  comparison of Big Rock Point with Humboldt Bay design, 70-84
  critical experiments, 206-7
  fuel-assembly fabrication and testing, 27-44
  uranium oxide fuel-life studies, 27-34
  void-content measurements, 7
Reactors (BONUS), construction, 292-309
  critical experiments, 5
  design, 292-309
  design comparison with Pathfinder Reactor, 310-12
Reactors (BORAX-II), chemical-shim use in primary coolant, 411
Reactors (BORAX-III), chemical-shim use in primary coolant, 411
Reactors (BORAX-V), critical experiments, 206
  exponential experiment, void-distribution studies, 7
Reactors (breeder)
    See also Reactors (converter), Reactors (Dounreay Fast-Breeder), Reactors (Enrico Fermi Fast-Breeder), Reactors (Experimental Breeder, II), and Reactors (seed-blanket)
  breeding potential of various fissile isotopes, 113
  fuel cycle, 124-6
  fuel recycling, 127
  heavy-water thorium-^{233}U system, 406-11
  heavy-water uranium-plutonium system, 406-11
  water desalinization by, 38-9, 141
Reactors (CANDU) (Canada), design, 89-92
  dome-seal tube-closure design, 379-81
  fuel cycle, 202-4
  iodine removal in, 58
  moderator-level control, 399
Reactors (Carolinas-Virginia Tube), power cost estimates, 86-7, 89
  pressure-tube design, 326
  prototype of large-reactor plant, 401-5
Reactors (Consolidated Edison Thorium), operating experience, 313-15
Reactors (converter), seed-blanket design studies, 197-8, 422-31
Reactors (Dounreay Fast-Breeder), noise analysis, 260-1
Reactors (Enrico Fermi Fast-Breeder), breeding potential of various fissile isotopes, 113
  core B mockup studies in ZPR-III assembly, 11

- Reactors (Experimental Boiling-Water), chemical-shim use in primary coolant, 411
  - operating experience at 100 Mw(t), 317-20
  - plutonium-bearing core fabrication, 172
- Reactors (Experimental Breeder, II), breeding potential of various fissile isotopes, 113
- Reactors (Experimental Gas-Cooled), control-rod design, 376-7, 378
  - lattice studies using Physical Constants Testing Reactor, 210
- Reactors (Experimental Organic-Cooled), canned-pump development, 67-8
  - pressure-balanced control rod, 274
- Reactors (fast)
  - *See also* Reactors (Dounreay Fast-Breeder), Reactors (Enrico Fermi Fast-Breeder), Reactors (Experimental Breeder, II), and Reactors (Los Alamos Molten-Plutonium, Experiment I)
  - breeding potential of various fissile isotopes, 113
  - critical mass, 114-16
  - neutron-balance studies, 113
  - neutron physics, 107-34
  - safety characteristics, 117-24
  - water desalinization by, 138-9, 141
- Reactors (gas-cooled)
  - *See* Reactors (Experimental Gas-Cooled), Reactors (ML-1), and Reactors (ZENITH)
- Reactors (General Electric Test), plutonium oxide—uranium oxide fuel irradiations, 173-5
  - uranium dioxide fuel-assembly testing, 45-8
- Reactors (Halden Boiling-Water), noise measurements, 260
- Reactors (heavy-water)
  - *See also* Reactors (CANDU), Reactors (Carolinas-Virginia Tube), Reactors (Heavy-Water Components Test), Reactors (NPD), Reactors (organic-cooled heavy-water-moderated), Reactors (Plutonium Recycle Test), Reactors (Process Development Pile), Reactors (Spectral Shift Control), Reactors (Whiteshell, No. 1)(WR-1), and Reactors (Zero Energy Experimental Pile)
  - large-plant designs, 401-11
  - review of recent developments, 85-97
  - Tripartite Organic-Cooled Heavy-Water Reactor Meeting, 324
  - water desalinization by, 87, 139-41
- Reactors (Heavy-Water Components Test), drive problems for control and safety rods, 316-17
- Reactors (heavy-water-moderated organic-cooled)
  - *See* Reactors (organic-cooled heavy-water water-moderated)
- Reactors (High-Temperature Gas-Cooled Reactor Experiment)
  - *See* Reactors (ZENITH)
- Reactors (Humboldt Bay Power), design comparison with Big Rock Point Power Reactor, 70-84
- Reactors (liquid-metal-fuel), fuel-alloy studies, 182-3
- Reactors (Lithium-Cooled, Experiment), auxiliary systems design, 384
- Reactors (Los Alamos Molten-Plutonium, Experiment I), fuel-alloy studies, 182-3
- Reactors (ML-1), shield design, 218-20
- Reactors (Molten-Salt, Experiment), heat exchanger, design and fabrication, 374-5
- Reactors (New Production), maximum credible accident, 267
  - vented-containment concept, 265-7
- Reactors (NPD), moderator-level control, 391-3
  - operating experience with moderator-level control, 398-9
  - power cost estimates, 86-7, 89
- Reactors (N.S. *Savannah*), evaluation of a Zircaloy core structure, 322-4
- Reactors (organic-cooled)
  - *See also* Reactors (Whiteshell, No. 1) (WR-1)
  - Tripartite Organic-Cooled Heavy-Water Reactor Meeting, 324
- Reactors (organic-cooled heavy-water-moderated)
  - *See also* Reactors (Whiteshell, No. 1) (WR-1)
  - design, 95-7
  - large-plant design, 405-6, 407, 408
- Reactor (Pathfinder Power), boron control-rod design, 365-7
  - construction, 276-92
  - control-rod-drive design, 274-5
  - design, 276-92
  - design comparison with BONUS Reactor, 310-12
  - fuel-rod end-closure development, 245-6
  - lattice experiments for second-generation core, 6-7
  - recirculation-piping design, 384
- Reactors (Pawling Lattice Test Rig), heavy-water lattice measurements, 213
- Reactors (Physical Constants Testing), critical experiments, 4-5, 6
  - heavy-water lattice measurements, 213
  - lattice studies of Experimental Gas-Cooled Reactor, 210
- Reactors (Plutonium Recycle Test), coolant flow-rate determination, 383
  - dome type nozzle seals, 379
  - fuel elements, 167-73
  - moderator-level control, 385-91
  - operating experience with moderator-level control, 393-8
  - primary coolant pump problems, 315-16
- Reactors (pressure-tube)
  - *See also* Reactors (CANDU), Reactors (Carolinas-Virginia Tube), Reactors (New Production), Reactors (Plutonium Recycle Test), and Reactors (Whiteshell, No. 1) (WR-1)
  - component design, 379-83
  - large-plant design, 401-5
- Reactors (pressurized-water)
  - *See also* Reactors (N.S. *Savannah*), Reactors (Saxton Power), Reactors (Shippingport Pressurized-Water), Reactors (Spectral Shift Control), Reactors (SPERT), and Reactors (Yankee Power)
  - chemical-shim use in coolant system, 411-21
  - Large Power Reactor Program, 422-31
  - natural-circulation startup studies, 421-2
- Reactors (Process Development Pile), buckling-measurement studies of heavy-water lattices, 212-13
- Reactors (process-heat), costs of heavy-water type, 87
  - solid-fuel gasification, economics, 1-3
- Reactors (Rapsodie)(France), fuel-element development, 167-9, 181
- Reactors (Saxton Power), operation with boric acid shim in primary coolant system, 420-1
- Reactors (seed-blanket), economic comparison with other water-cooled reactors, 429-30
  - Large Power Reactor Program, design studies, 422-31
- Reactors (SENN) (Italy), partial-reloading scheme, 201-2
- Reactors (Shippingport Pressurized-Water), core 2 design, 197-200
  - operating experience over past five years, 193-6
- Reactors (sodium-cooled), throttle-valve design, 271
- Reactors (Sodium, Experiment), safety rod drop-time experiments, 377, 379
- Reactors (Spectral Shift Control), critical experiments, 8
  - economic comparison with other water-cooled reactors, 429-30
  - lattice measurements, 212
- Reactors (SPERT), Doppler broadening of neutron-absorption resonance, 329
- Reactors (superheater)
  - *See also* Reactors (boiling-superheater), Reactors (BONUS), Reactors (Consolidated Edison Thorium), and Reactors (Pathfinder Power)
  - design problems, 310-12
- Reactors (thermionic, water-cooled), design, 99-105
- Reactors (University of Florida Training), noise-analysis studies, 253-4
- Reactors (Vallecitos Boiling-Water), fuel-assembly testing, 27-38
  - Fuel-Cycle Program for fuel-element irradiation testing, 354-5, 356
- Reactors (water-cooled, thermionic)
  - *See* Reactors (thermionic, water-cooled)
- Reactors (Whiteshell, No. 1)(WR-1), 97
  - design, 324-5
  - pressure-tube design, 326
- Reactors (Yankee Power), chemical-shim use in primary coolant, 411
- Reactors (ZENITH), reactivity, temperature coefficient studies, 9
- Reactors (Zero Energy Experimental Pile), heavy-water lattice measurements, 213
- Recirculation system, BONUS Reactor, 306-7
  - Pathfinder Reactor, 288-9, 384
- Recycling, plutonium, equilibrium composition of fuel, 127
- Refueling, bidirectional method for CANDU Reactor, 202-4
  - large heavy-water pressure-tube reactor, 401-2
  - partial-reloading scheme for SENN reactor, 201-2
- Resonance integral, fertile isotopes, 214-15
- Rhenium alloys (Mo-Pd-Pu-Rh-Ru-U-Zr), irradiation testing for use in Experimental Breeder Reactor II, 180-2
- Rejuvenation, fuel elements without reprocessing, 172-3
- Reliability, servomechanisms, 53
- Ruthenium-106, deposition from gas stream onto surfaces, temperature effects, 371
  - emission from irradiated uranium dioxide, 361
  - release during uranium fire, 370-1
- Ruthenium alloys (Mo-Pd-Pu-Rh-Ru-U-Zr), irradiation testing for use in Experimental Breeder Reactor II, 180-2

S

- Safety
  - *See also* Containment and Control systems
  - comparison of Big Rock Point with Humboldt Bay plant, 79, 81-4
  - fast reactors, 117-24
  - Shippingport shutdown record over past five years, 195
- Safety rods, Sodium Reactor Experiment, drop-time measurements, 377, 379
- Saline water
  - *See* Water (saline)
- Samarium, cross-section change with burnup in reactors, 216-18
- Santowax, pump development for, 67-8
- SAP
  - *See* Sintered aluminum powder
- Savannah River Plant, ventilation-filtering systems, 55
- Scrubbers, iodine removal by, 57-8

Seals, distortion in coolant pumps of Plutonium Recycle Test Reactor, 315-16
  dome type for pressure-tube closure, 379-81
  for helium retention in Plutonium Recycle Test Reactor, 381-3
  for liquid-metal pumps, 269-70
Seed-blanket reactors
  See Reactors (seed-blanket)
Seed-blankets, Shippingport core 2 design, 197-8
SEF
  See Steam-energy flow
SENN Reactor (Italy)
  See Reactors (SENN) (Italy)
Servomechanisms, reliability studies, 53
Shielding, geometrical attenuation factors, 220
  ML-1 Reactor, 218-20
  ^{16}N activity studies, 220
Shutdown reactivity, determination by reactor noise analysis, 254-6
Shutdowns, effects of Doppler broadening of neutron-absorption resonance, 329
  six-month operating history of Consolidated Edison Thorium Reactor, 313
Silica, thermal-insulation use for pressure tubes, 326
Silicon carbide systems (B_4C-SiC), corrosion, 367-8
Silicon carbide systems (B_4C-SiC)(Zircaloy-2-clad), irradiation testing, 368
Silver, cross-section change with burnup in reactors, 216-18
Silver alloys (Ag-Cd-In), cross-section change with burnup in reactors, 216-18
Sintered aluminum powder, cladding use in organic-cooled heavy-water-moderated reactor design, 405
  compatibility with organic coolants, 95
  fuel-element cladding, 242
  in WR-1 reactor, 324-5
Siting, 265-7, 370-1
Skin, radiation dose from released fission products, 370-1
Sodium, reactivity effects in ZPR-III assembly, 11
Sodium (liquid), expansion, reactivity effects in fast reactors, 118-22
  throttle valves for, 271
Sodium void coefficient, effects of structural materials in fast reactors, 131-3
  reactivity effects in fast reactors, 118-22
Space power units, design of thermoelectric type, 106
Special Power Excursion Reactor Test
  See Reactors (SPERT)
Spectral Shift Control Reactor
  See Reactors (Spectral Shift Control)
SPERT Reactor
  See Reactors (SPERT)
Sprays, water, iodine removal from air by, 56-7
Stack disposal, BONUS Reactor, 309
  Pathfinder Reactor, 292
Stainless-steel systems (B_4C–stainless steel), corrosion testing, 367
Stainless-steel systems (PuO_2–stainless steel), preparation, 183
Stainless-steel systems (PuO_2-UO_2–stainless steel), fabrication and testing, 183
Stainless steels, joining to Zircaloy, 401
  by tandem extrusion, 368-9
  uranium and plutonium solutions, 5-6
  reactivity effects in ZPR-III assembly, 11
Stainless steels (304), cladding of fuel assemblies for boiling-water reactors, 27-34
  cladding of fuel elements, failure by cracking in Vallecitos Boiling-Water Reactor tests, 354-5
  ultrasonic inspection of tubing, 246
Stainless steels (304L), boron-containing, control rod use in Pathfinder Power Reactor, 365-6
  boron-containing, mechanical properties after irradiation, 366-7
  lining of Zircaloy-2-clad fuel elements for corrosion protection, 356
  ultrasonic inspection tubing, 246
Stainless steels (316), ultrasonic inspection of tubing, 246
Stainless steels (347), fast-neutron irradiation effects, 187-91
Statistics, reactor noise analysis, 248-63
Steam, separation from water in superheater reactors, 310
Steam-energy flow, burnout-limit studies, 18-26
  burnout studies of nonuniformly heated channels, 343-52
  comparison of Russian and U. S. data, 225-35
  DNB-2 curve significance, 335-43
  multirod test-section data, 156-65
Steam generators, comparison of Big Rock Point with Humboldt Bay plant, 79-81
  gas-heated types, 64-5
  sodium-heated types, 60-4
Steam systems (steam-water), burnout studies, 335-52
Steel systems (B_4C-steel), corrosion testing, 367
Stress analysis, reinforced-concrete buildings, 54-5
Strontium-89, emission from irradiated uranium dioxide, 361
  release during uranium fire, 370-1
Strontium-90, release during uranium fire, 470-1
Structural materials
  See Materials and specific materials, e.g., Stainless steels
Superheater reactors
  See Reactors (superheater)
Surfaces, laboratory, iodine-deposition studies, 57-8
Surge suppressors, for flowmeter sensing lines in Plutonium Recycle Test Reactor, 383
Swaging, fuel-element fabrication, 243-5
  magnetic technique for fuel-element cladding-to-core bonding, 242-3
Swelling, boron-containing stainless steels during irradiation, 366-7
  cladding materials, effects of uranium dioxide core melting, 46-8
Switches (electrical), problems of control-rod drive, in Consolidated Edison Thorium Reactor, 314

T

Tandem extrusions, stainless-steel-to-Zircaloy transition-joint preparation, 368-9
Tantalum, neutron-physics effects in fast reactors, 128-33
Tellurium-132, deposition from gas stream onto surfaces, temperature effects, 371
  evolution from irradiated uranium dioxide, 360-2
  release during uranium fire, 370-1
Temperature, effects on fission-product deposition onto surfaces, 371
  effects on gas-heated steam-generator design, 65
  thermionic emitters, effects on conversion efficiency, 105
  uranium dioxide fuel-elements effects on exposure lifetime in Shippingport core 2, 199
Tensile strength, boron-containing stainless steel, 365-6
  hafnium control rods in Shippingport, neutron-exposure effects, 195-6
  type 347 stainless steel, fast-neutron effects, 188-91
Thermal conductivity, plutonium carbide–uranium carbide fuel materials, 180-1
  uranium dioxide, temperature effects, 4
Thermal insulation
  See Insulation (thermal)
Thermionic conversion, 99-106
  See also Reactors (thermionic, water-cooled)
  efficiency, effects of emitter temperature, 105
Thermoelectric power units, design for space application, 106
Thorium, absorption cross section, 10
  cadmium ratio, ZPR-VII experiments, 8
  converter-reactor studies, 422-31
  fast-fission bonus to breeding in various reactors, 113
  neutron production in fission by 1.5-Mev neutrons, 112
  resonance-capture measurements in Peach Bottom Critical Assembly, 10
  thermal breeder reactor studies, 406-10
Thorium-232, foils, resonance-capture measurements, 10
  neutron fission cross sections, 111
  resonance integral, 214-15
Thorium alloys (Pu-Th), preparation and testing, 182
Thorium-232 oxide, resonance integral, 214-15
Thorium Systems (^{239}Pu-Th), fuel cycle for breeder reactors, 124-6
Thorium systems (Th-^{233}U), critical mass, fast reactor studies, 115
  fuel cycle for breeder reactors, 124-6
Thorium systems (Th-^{235}U), critical mass, fast reactor studies, 115
  fuel cycle for breeder reactors, 124-6
Throttle valves, for sodium-cooled reactors, 271
Thulium, cross-section change with burnup in reactors, 216-18
Titanium, neutron-physics effects in fast reactors, 128-33
Trail Cable facility, uranium dioxide fuel-rod testing, 46-8
Transducers, fission-gas pressure determination in fuel rods, 43-5
  limitations in nuclear reactor applications, 52-3
Transfer functions, reactor noise-analysis studies, 251-2
Tungsten systems (PuN-W), properties, 183
Tungsten systems (PuO_2-W), properties, 183
Turbines, BONUS Reactor, 307
  comparison of Big Rock Point with Humboldt Bay plant, 79-81
  Pathfinder Reactor, 289-90
  radioactive contamination problems in superheater reactors, 310
Tubing, stainless-steel, ultrasonic inspection, 246

U

Ultrasonic testing, stainless-steel tubing, 246
United States of America, comparison with Canada in heavy-water reactor development, 87-95
University of Florida Training Reactor
  See Reactors (University of Florida Training)
Uranium, converter-reactor studies, 422-31
  emission from irradiated uranium dioxide, 301
Uranium-233, breeding potential in various reactors, 113
  fission-rate measurements in graphite, 10
  fission ratio to ^{235}U in graphite systems, 10
  fission-ratio measurements in ZPR-III assembly, 11

- Uranium-233 (Continued)
  - neutron capture-to-fission ratio, 111
  - neutron fission cross sections, 111
  - neutron production in fission by 1.5-Mev neutrons, 112
  - thermoelectric power supply studies, 106
- Uranium-233 systems (Th-^{233}U), critical mass, fast reactor studies, 115
  - fuel cycle for breeder reactors, 124-6
- Uranium-233 systems (^{233}U-^{238}U), fuel cycle for breeder reactors, 124-6
- Uranium-234, fission-ratio measurements in ZPR-III assembly, 11
- Uranium-235, breeding potential in various reactors, 113
  - cadmium ratio, ZPR-VII experiments, 8
  - critical concentrations of aqueous solutions, 6
  - fission products, time-dependent concentration studies, 215-16
  - fission-rate measurements in graphite, 10
  - fission ratio, to ^{239}Pu in graphite systems, 10
    - to ^{233}U in graphite systems, 10
    - to ^{238}U in heavy-water systems, 7
  - neutron capture-to-fission ratio, 111
  - neutron fission cross sections, 111
  - neutron production in fission by 1.5-Mev neutrons, 112
- Uranium-235 systems (Th-^{235}U), critical mass, fast reactor studies, 115
  - fuel cycle for breeder reactors, 124-6
- Uranium-235 systems (^{235}U-^{238}U), critical mass, fast reactor studies, 115
  - fuel cycle for breeder reactors, 124-6
- Uranium-236, fission-ratio measurements in ZPR-III, 11
- Uranium-238, cadmium ratio in heavy-water systems, 7
  - fast-fission bonus to breeding in various reactors, 113
  - fission ratio to ^{235}U in heavy-water systems, 7
  - fission-ratio measurements in ZPR-III assembly, 11
  - neutron capture cross sections, 111-12
  - neutron fission cross sections, 111
  - neutron production in fission by 1.5-Mev neutrons, 112
  - resonance integral, 214-15
- Uranium-238 systems (Pu-^{238}U), fuel cycle for breeder reactors, 124-6
- Uranium-238 systems (^{239}Pu-^{238}U), critical mass, fast reactor studies, 115
- Uranium-238 systems (^{233}U-^{238}U), fuel cycle for breeder reactors, 124-6
- Uranium-238 systems (^{235}U-^{238}U), critical mass, fast reactor studies, 115
  - fuel cycle for breeder reactors, 124-6
- Uranium alloys (Mo-Pd-Pu-Rh-Ru-U-Zr), irradiation testing for use in Experimental Breeder Reactor II, 180-2
- Uranium alloys (Mo-Pu-U), swelling during irradiation, 181
- Uranium alloys (Pu-U), fuel-cycle studies for water-moderated reactors, 203-5
  - preparation and testing, 182
- Uranium carbide systems (Fe-PuC-UC), fabrication and testing, 183
- Uranium carbide systems (PuC-UC), fabrication, 175-80
  - properties, 180
- Uranium oxide, irradiation testing, 359-63
- Uranium oxide (UO_2), blanket fuel-element use in Shippingport core 2, 197-8
  - boron incorporation for burnable poison use, 357-8
  - expansion during melting, effects on swelling of cladding, 46-8
  - fuel-element development programs, 27-50
  - physical properties, 360, 362-3
  - plates, fission-product diffusion coefficients, 362
  - preparation, 167-9, 174
  - resonance integral for ^{238}U oxide, 214-15
  - thermal conductivity, temperature effects, 48
  - vibratory compaction in fuel-element fabrication, 237-42
- Uranium oxide systems (PuO_2-UO_2), fuel-element development, 167-75
  - irradiation testing, 173-5
- Uranium oxide systems (PuO_2-UO_2—stainless steel), fabrication and testing, 183
- Uranium oxide systems (UO_2-ZrO_2), physical properties of plates, 362
  - plates, fission-product diffusion coefficients, 362
  - seed fuel-element use in Shippingport core 2, 197-8
- Uranyl fluorides, critical concentrations of solutions, 6

V

- Vallecitos Boiling-Water Reactor
  - *See* Reactors (Vallecitos Boiling-Water)
- Valves, dump type, for moderator in Plutonium Recycle Test Reactor, 389
  - butterfly type, cavitation tests, 68
  - throttle, for sodium-cooled reactors, 271
  - for venting pressure from New Production Reactor containment building, 265-7
- Vanadium, foils, resonance-capture measurements, 10
  - neutron-physics effects in fast reactors, 128-33
  - subtraction technique for resonance-capture measurements, 10
- Vibration, coolant pumps of Plutonium Recycle Test Reactor, 315-16
- Vibratory compaction, annular multitube fuel elements, 241-2
  - uranium dioxide fuel rods, 238-41

W

- Washers, Belleville-spring type, use in dome-seal tube closures, 380-1
- Waste handling and disposal
  - *See also* Stack disposal
  - BONUS Reactor, 309
  - comparison of Big Rock Point with Humboldt Bay Plant, 83-4
  - Pathfinder Reactor, 292
- Water, corrosive effects on boron carbide systems, 367-8
  - iodine removal from air by sprays, 56-7
  - neutron-diffusion parameters in, 146-50
  - quality control in reactors using chemical shim in primary coolant, 418-21
  - separation from steam in superheater reactors, 310
  - Shippingport reactor, *p*H and quality control, 196
- Water (D_2O), criticality studies on slightly enriched fuel rods, 7
  - inventory charges for large-reactor designs, 405
  - neutron-diffusion parameters in, 151
- Water (saline), distillation, heavy-water reactor cost studies, 87
  - by reactors, economic studies, 138-44
- Water systems (D_2O-H_2O), criticality studies on slightly enriched fuel rods, 7
- Water systems (steam-water), burnout studies, 335-52
- Welding, electron-beam technique for fuel-element components, 358-9
  - heat exchanger for Molten-Salt Reactor Experiment, 374-5
- Welds, corrosion of Shippingport control-rod assemblies, 196
- Whiteshell Reactor No. 1
  - *See* Reactors (Whiteshell, No. 1)(WR-1)
- Windscale accident, fission-product dispersal, 370-1
- Wood, shielding use during ML-1 Reactor operation, 219-20
- WR-1 Test Reactor
  - *See* Reactors (Whiteshell, No. 1)(WR-1)

X

- Xenon, release during uranium fire, 370-1
- Xenon-133, evolution from irradiated uranium dioxide, 359-62

Y

- Yield strength, boron-containing stainless steel, 365-6
  - cladding materials, 42
  - fuel assemblies for boiling-water reactors, 39
  - hafnium control rods in Shippingport, neutron-exposure effects, 195-6
  - type 347 stainless steel, fast-neutron effects, 188-91
- Ytterbium, cross-section change with burnup in reactors, 216-18

Z

- ZENITH Reactor
  - *See* Reactors (ZENITH)
- Zircaloy, evaluation for core structure of N.S. *Savannah* Reactor, 322-4
  - joining to stainless steel, 401
    - by tandem extrusion, 368-9
- Zircaloy-2, cladding of fuel assemblies for boiling-water reactors, 27-34
  - cladding use for boron carbide systems, 368
  - corrosion due to fluoride ion, 356
  - electron-beam welding, 359
- Zircaloy-2 systems (B_4C-Zircaloy-2), irradiation testing, 367
- Zircaloy-2 systems (Zircaloy-2-ZrB_2), irradiation testing, 367
- Zircaloy-4, cladding of fuel assemblies for boiling-water reactors, 27-34
  - cladding use for Shippingport core 2 fuel elements, 197
  - compatibility with organic coolants, 95
  - neutron-physics effects in fast reactors, 128-33
  - nuclear data, 331
- Zirconium-95, deposition from gas stream onto surfaces, temperature effects, 371
- Zirconium alloys, organic-coolant effects, 324-5
- Zirconium alloys (Mo-Pd-Pu-Rh-Ru-U-Zr), irradiation testing for use in Experimental Breeder Reactor II, 180-2
- Zirconium alloys (Pu-Zr), irradiation testing, 182
- Zirconium boride systems (Zircaloy-2—ZrB_2), irradiation testing, 367
- Zirconium hydride, moderator for critical assemblies, 212
- Zirconium oxide systems (UO_2-ZrO_2), physical properties of plates, 362
  - plates, fission-product diffusion coefficients, 362
  - seed fuel-element use in Shippingport core 2, 197-8
- Zirconium systems (Nb-PuC-Zr), properties, 183
- Zirconium systems (Nb-PuO_2-Zr), properties, 183
- Zirconium systems (PuO_2-Zr), properties, 183
- ZPR-III Critical Assembly
  - *See* Critical assemblies (ZPR-III)
- ZPR-VII Critical Assembly
  - *See* Critical assemblies (ZPR-VII)

LEGAL NOTICE

This journal was prepared under the sponsorship of the U. S. Atomic Energy Commission. Neither the United States, nor the Commission, nor any person acting on behalf of the Commission:

A. Makes any warranty or representation, expressed or implied, with respect to the accuracy, completeness, or usefulness of the information contained in this journal, or that the use of any information, apparatus, method, or process disclosed in this journal may not infringe privately owned rights; or

B. Assumes any liabilities with respect to the use of, or for damages resulting from the use of any information, apparatus, method, or process disclosed in this journal.

As used in the above, "person acting on behalf of the Commission" includes any employee or contractor of the Commission, or employee of such contractor, to the extent that such employee or contractor of the Commission, or employee of such contractor prepares, disseminates, or provides access to, any information pursuant to his employment or contract with the Commission, or his employment with such contractor.

NUCLEAR SCIENCE ABSTRACTS

The U. S. Atomic Energy Commission, Division of Technical Information, publishes *Nuclear Science Abstracts (NSA)*, a semimonthly journal containing abstracts of the literature of nuclear science and engineering.

NSA covers (1) research reports of the U. S. Atomic Energy Commission and its contractors; (2) research reports of government agencies, universities, and industrial research organizations on a world-wide basis; and (3) translations, patents, books, and articles appearing in technical and scientific journals.

Complete indexes covering subject, author, source, and report number are included in each issue. These are cumulated quarterly, semiannually, and annually providing a detailed and convenient key to the literature.

Availability of NSA

SALE *NSA* is available on subscription from the Superintendent of Documents, U. S. Government Printing Office, Washington, D. C., 20402, at $30.00 per year for the semimonthly abstract issues and $22.00 per year for the four cumulated-index issues. Subscriptions are postpaid within the United States, Canada, Mexico, and all Central and South American countries, except Argentina, Brazil, British and French Guiana, Surinam, and British Honduras. Subscribers in these Central and South American countries, and in all other countries throughout the world, should remit $37.00 per year for subscriptions to semimonthly abstract issues and $25.00 per year for the four cumulated-index issues.

EXCHANGE *NSA* is also available on an exchange basis to universities, research institutions, industrial firms, and publishers of scientific information. Inquiries should be directed to the Division of Technical Information Extension, U. S. Atomic Energy Commission, P. O. Box 62, Oak Ridge, Tennessee, 37831.

TECHNICAL PROGRESS REVIEWS may be purchased from Superintendent of Documents, U. S. Government Printing Office, Washington, D. C., 20402. *Isotopes and Radiation Technology* at $2.00 per year for each subscription or $0.55 per issue; the other four journals at $2.50 per year and $0.70 per issue. The use of the coupon below will facilitate the handling of your order.

POSTAGE AND REMITTANCE: Postpaid within the United States, Canada, Mexico, and all Central and South American countries except as hereinafter noted. Add $0.50 per year, or $0.15 per single issue for *Isotopes and Radiation Technology* journal and $0.75 per year or $0.20 per single issue for the other journals for postage to all other countries, including Argentina, Brazil, British and French Guiana, nam, and British Honduras. Payment should be by check, money order, or document coupons, and ST accompany order. Remittances from foreign countries should be made by international money der, or draft on an American bank, payable to the Superintendent of Documents, or by UNESCO book pons.

order form

SUPERINTENDENT OF DOCUMENTS
U. S. GOVERNMENT PRINTING OFFICE
WASHINGTON, D. C., 20402

closed:
document coupons ☐ check ☐ money order ☐

Charge to Superintendent of Documents No.__________

Please send a one-year subscription to

☐ NUCLEAR SAFETY
☐ POWER REACTOR TECHNOLOGY
☐ REACTOR FUEL PROCESSING
☐ REACTOR MATERIALS

(Each subscription $2.50 per year; $0.70 per issue.)

☐ ISOTOPES AND RADIATION TECHNOLOGY

(Each subscription $2.00 a year; $0.55 per issue.)

SUPERINTENDENT OF DOCUMENTS
U. S. GOVERNMENT PRINTING OFFICE
WASHINGTON, D. C., 20402

(Print clearly)

Name ______________________________

Street ______________________________

City __________________ Zone ____ State _______

THE UNIVERSITY
OF MICHIGAN
APR 7 1965
PHOENIX
LIBRARY

Phve

POWER REACTOR TECHNOLOGY

[illegible]

[illegible]

Prepared for DIVISION OF TECHNICAL INFORMATION, USAEC, by
W. H. ZINN and J. R. DIETRICH, GENERAL NUCLEAR ENGINEERING CORPORATION

Winter 1964-1965

Progress on Specific Reactor Types:
A Review of Third Geneva Conference Papers

● VOLUME 8
● NUMBER 1

TECHNICAL PROGRESS REVIEWS

To meet the needs of industry for concise summaries of current atomic developments, the Atomic Energy Commission is publishing this series, Technical Progress Reviews. Issued quarterly, each of the reviews digests and evaluates the latest findings in a specific area of nuclear technology and science.

The five journals published in this series are:

Isotopes and Radiation Technology, P. S. Baker, A. F. Rupp, and associates, Oak Ridge National Laboratory

Nuclear Safety, Wm. B. Cottrell, W. H. Jordan, and associates, Oak Ridge National Laboratory

Power Reactor Technology, W. H. Zinn and J. R. Dietrich, Combustion Engineering, Inc., Nuclear Division

Reactor Fuel Processing, Stephen Lawroski and associates, Chemical Engineering Division, Argonne National Laboratory

Reactor Materials, R. W. Dayton, E. M. Simons, and associates, Battelle Memorial Institute

Each journal may be purchased from the Superintendent of Documents, U. S. Government Printing Office, Washington, D. C., 20402. *Isotopes and Radiation Technology* at $2.00 per year for subscription or $0.55 for individual issues; the other four journals at $2.50 per year and $0.70 per issue. See back cover for remittance instructions and foreign postage requirements.

The views expressed in this publication do not necessarily represent those of the United States Atomic Energy Commission, its divisions or offices, or of any Commission advisory committee or contractor.

Availability of Reports Cited in This Review

Unclassified AEC reports are available for inspection at AEC depository libraries and are sold by the Clearinghouse for Federal Scientific and Technical Information, National Bureau of Standards, U. S. Department of Commerce, 5285 Port Royal Road, Springfield, Va., 22151. Some of the reports cited are not available owing to their preliminary nature; however, the information contained in them will eventually be made available in formal progress or topical reports.

Unclassified reports issued by other Government agencies or private organizations should be requested from the originator.

Unclassified British and Canadian reports may be inspected at AEC depository libraries. British reports are sold by the British Information Service, 45 Rockefeller Plaza, New York, N. Y.; Canadian reports (AECL series) are sold by the Scientific Document Distribution Office, Atomic Energy of Canada, Ltd., Chalk River, Ontario, Canada.

Classified U. S. and foreign reports identified in this journal as Classified may be purchased by properly cleared Access Permit Holders from the Division of Technical Information Extension, U. S. Atomic Energy Commission, P. O. Box 1001, Oak Ridge, Tenn., 37831. Such reports may be inspected at classified AEC depository libraries.

DEPOSITED BY THE
UNITED STATES OF AMERICA

POWER REACTOR TECHNOLOGY

A REVIEW OF RECENT DEVELOPMENTS

Prepared for DIVISION OF TECHNICAL INFORMATION, USAEC,
by W. H. ZINN and J. R. DIETRICH,
COMBUSTION ENGINEERING, INC., NUCLEAR DIVISION

WINTER 1964–1965

VOLUME 8

NUMBER 1

Foreword

This quarterly review of reactor development has been prepared at the request of the Division of Technical Information of the U. S. Atomic Energy Commission. Its purpose is to assist interested organizations in the task of keeping abreast of new results in reactor technology for civilian application.

Power Reactor Technology contains reviews of selected recently published reports that are judged noteworthy in the fields of power-reactor research and development, power-reactor applications, design practice, and operating experience. It is not meant to be a comprehensive abstract of all material published during the quarter, nor is it meant to be a treatise on any part of the subject. However, related reports from different sources are often treated together to yield reviews having some breadth of scope, and background material may be added to place recent developments in perspective. Occasionally the reviews are written by guest authors. Reviews having unusual breadth or significance are placed at the front of the issue as Feature Articles.

The intention is to cover the various areas of reactor development from the general viewpoint of the reactor designer rather than from the more detailed points of view of specialists in the individual areas. To whatever extent the coverage of *Power Reactor Technology* may occasionally overlap the fields of the other Technical Progress Reviews, the overlaps will be motivated by this objective of viewing current progress through the eyes of the reactor designer.

A degree of critical appraisal and some interpretation of results are often necessary to define the significance of reported work. Any such appraisal or interpretation represents only the opinion of the reviewer and (in the usual case, when the review is written by Combustion Engineering, Inc., Nuclear Division staff) the Editor. When the review is predominantly interpretive the reviewer is named; unless identified as a guest author, he is a member of the Combustion Engineering, Inc., Nuclear Division staff. Readers are urged to consult the original references to obtain all the background of the work reported and to obtain the interpretation of the results given by the original authors.

For timely coverage, *Power Reactor Technology* must often review fragmentary material. The fixed subject headings listed below have been adopted in the hope of maintaining some continuity and order in the material from one issue to another: all reviews except Feature Articles will be arranged under these headings. A particular issue will not necessarily contain all the headings but only those under which material is reviewed.

Economics, Applications, Programs
Resources and Fuel Cycles
Physics
Fluid and Thermal Technology
Fuel Elements
Materials
Control and Dynamics
Containment, Radiation Control, and Siting
Systems Technology
Components
Design and Construction Practice
Operating Experience
Specific Reactor Types
Specific Applications
Unconventional Approaches

W. H. Zinn, Vice-President
J. R. Dietrich, Editor
Combustion Engineering, Inc.

DEPOSITED BY THE
UNITED STATES OF AMERICA

Contents

Progress on Specific Reactor Types

A Review of Papers Presented at the Third Geneva Conference

I Introduction 1
References 2

II Boiling and Pressurized Light-Water Reactors 3
Operating Experience 3
Significant Developments 3
Directions of Future Developments . . . 17
References 20

III Vessel Type Superheating Reactors . 22
Status and Design Features 22
Directions of Future Developments . . . 26
References 27

IV Graphite-Moderated Superheating Reactors 28
References 34

V Heavy-Water-Moderated Pressure-Tube Reactors 35
Operating Experience 35
Significant Features 37
Directions of Future Developments . . . 45
References 45

VI Heavy-Water-Moderated Pressure-Vessel Reactors 47
General Status 47
Operating Experience 50
Significant Developments 51
Directions of Future Developments . . . 54
Czechoslovak Nuclear Power Station . . . 56
References 56

VII Gas-Cooled Clad-Fuel Reactors . . . 58
General Status 58
Fuel Elements 61
Pressure Vessels 66
Refueling Machines 68
Control and Instrumentation 68
Advanced Concepts and Future Directions 69
References 71

VIII Gas-Cooled Unclad-Fuel Reactors . . 72
References 74

IX Sodium-Cooled Reactors 75
Technology of Sodium Systems 75
Sodium Graphite Reactors 80
Fast-Breeder Reactors 84
References 95

X Maritime Reactors 97
References 101

XI Other Reactors 103
Portable Power Plants 103
Direct-Conversion Power Plants 105
Advanced Concepts 106
References 106

Issued quarterly by the U. S. Atomic Energy Commission. Use of funds for printing this publication approved by the Director of the Bureau of the Budget on October 14, 1963.

Availability of Third Geneva Conference Papers

1. Copies of all papers may be purchased from the European Office of the United Nations for two Swiss francs (46 cents) per paper plus postage. Address: European Office of the United Nations, Palais des Nations, Geneva, Switzerland, Attention: R. Furstenberg, Chief, Distribution Service Documents Division. When UN stocks are exhausted, reproduced copies of all papers may be purchased from the IAEA in Vienna at a price of $1.50 per paper. Address: International Atomic Energy Agency, Kaerntnerring 11, Vienna I, Austria.

2. Reproduced copies of all U. S. papers (no foreign) may be purchased at a price of $1.00 per paper from the Clearinghouse for Federal Scientific and Technical Information (formerly OTS). Address: National Bureau of Standards, U. S. Department of Commerce, 5285 Port Royal Road, Springfield, Va. 22151.

3. The American Nuclear Society will provide Xerox copies of all papers at 25 cents per page. Address: American Nuclear Society, 244 East Ogden Ave., Hinsdale, Ill. 60521.

4. The U. S. Atomic Energy Commission, Division of Technical Information Extension, Oak Ridge, Tenn. 37831, has produced micronegatives of all Geneva papers. Complete sets of duplicate negatives were distributed to the AEC, other government agencies, and their contractors; sets of U. S. papers only were distributed to AEC depository libraries.

(All U. S. papers were abstracted and indexed in Vol. 18, No. 18, of *Nuclear Science Abstracts*. All foreign papers will be similarly abstracted and indexed in Vol. 18, No. 21.)

Section
I
Power Reactor Technology

Introduction

Of the massive information collection produced by the Third United Nations International Conference on the Peaceful Uses of Atomic Energy, an important fraction deals with specific power-reactor types, with the progress made in their development, and with the experience gained in building and operating individual reactors of the various types. This entire issue of *Power Reactor Technology* is devoted to a review of that information.* More general reviews of the conference have been published elsewhere, notably in *Nucleonics*[1] and *Nuclear News*.[2]

Because of the special nature of this issue, the usual section headings as given in the Foreword do not appear. Instead, each of the following sections is on a particular reactor type.

Of the reactor types under serious development, two can be said to have achieved commercial acceptance: the "water" reactors (pressurized and boiling H_2O) and the "Magnox" gas-cooled reactors. The heaviest building commitments have been made in the latter type, amounting, through 1968, to over 5000 Mw(e) in the United Kingdom and some 1300 Mw(e) in France. The application of the prestressed concrete pressure vessel to this reactor type has done much to improve its potentialities, with respect to both size and operating pressure. Nevertheless, it appears that other types will replace it in future building plans, at least in the United Kingdom. Whether the replacement type will be its direct descendant, the advanced gas-cooled reactor, is not clear at this time.

The water reactors are still in a state of vigorous development, and it appears that, in the economic climate of the United States, it will be difficult for another reactor type to replace them so long as the basic costs of partially enriched nuclear fuels do not rise much above current levels. In the economic competition between the boiling- and pressurized-water types, it is difficult to detect a clear basic advantage of one over the other at the moment, although the rapid trend to plants of very high output may favor the pressurized-water type in the long run.

Another group of reactor types, each of which is represented by one or two bona fide power-generating plants, mostly in the lower capacity ranges, might be said to be in the "demonstration" stage. The most advanced of these are the Russian graphite-moderated superheat reactor (Beloyarsk) and the pressure-tube D_2O reactor [for each of which commitments have been made for a follow-on reactor in the 200-Mw(e) range] and the sodium-graphite reactor. The advanced gas-cooled reactor and the organic-moderated reactor also fall in this group. However, in regard to the latter, indications are that the future of organic liquids in central-station reactors lies in their use as coolants for D_2O-moderated reactors. The interesting variation on the organic-moderated concept represented by the Russian ARBUS reactor appears to be directed specifically to remote-station applications.

The remaining rather large group of reactor types under serious development cannot be said to be "demonstrated" in terms of prototypes of commercial versions. Some are very close to that stage, however. The integral nuclear superheat concept awaits only the full-scale operation of the BONUS and Pathfinder plants to enter the "demonstration" stage: both of these plants are currently in the process of startup. The heavy-water reactor of the pressure-vessel type is represented by two operating plants: the Halden Boiling Water Reactor that produces process steam, and the Agesta plant, a pressurized heavy-water plant that produces 10 Mw of electricity along with hot water for space heating. It would be stretching a point, however, to call these demonstration plants in the sense of the word used here; for the proposed characteristics of the commercial version, as exemplified by the Marviken plant, involve substantial extrapolations in several areas. The high-temperature gas-cooled type has been critical (the Dragon reactor), and the Peach Bottom plant is under construction; the latter is intended as a prototype. At least three versions of D_2O-moderated pressure-tube reactors utilizing coolants other than D_2O are under serious development; the coolants used are H_2O (boiling liquid, fog, or steam), organic, and gas. Experimental reactors having the latter two coolants are being built.

---

*The Conference papers are to be published in bound form. Meanwhile, the papers are available and can be obtained from the sources listed on the preceding page.

The position of the fast-breeder reactor is a little hard to classify, but it can hardly be said to have reached the demonstration stage despite the facts that it was first used to produce electric power in 1951, that a plant of moderately large output (Dounreay) has been in operation for some time, and that a large commercial plant (the EFFBR) is in process of startup. This is primarily because a fuel acceptable for commercial operation has not yet been demonstrated. Nevertheless, of all the reactor types, the fast breeder is probably the one of most universal interest, and continuing strong development efforts are foreseen for the future.

In the following sections the preceding rather brief remarks are expanded, and the status of each of the reactor types is reviewed on the basis of the information presented at Geneva.

References

1. *Nucleonics*, 22(10): (October 1964).
2. *Nucl. News*, 7(10): (October 1964).

Section

II

Boiling and Pressurized Light-Water Reactors

By John S. Wiley

The nonmilitary land-based boiling and pressurized light-water-moderated reactors of the world, other than the purely experimental ones, are listed in Table II-1. The table includes the more important reactors under construction as well as the reactors in operation. These reactor types are the ones of most interest, and the best known, in the United States; indeed, with the exception of the Russian reactor at Voronezh, all the reactors in Table II-1 were designed either by U. S. firms or with their assistance. Because these types have been covered most thoroughly by *Power Reactor Technology* in the past, this review of the many Geneva papers on light-water reactors is abbreviated in favor of greater coverage for the reactor types less well known in the United States. The major past reviews in *Power Reactor Technology*, of design and operating experience for specific water-moderated reactors, may be located by means of Table II-2.

Operating Experience

The operating experience with Yankee, the CETR, Saxton, and Shippingport is detailed in Ref. 1, and Ref. 2 covers operating experience with the Dresden, Big Rock Point, and Humboldt Bay reactors. References 3 and 4 discuss preliminary operating experience with the Russian pressurized-water reactor, WWER. Operating experience with Shippingport, Yankee, the CETR, and Dresden has been reviewed in past issues of *Power Reactor Technology*, as indicated in Table II-2. Much of the information contained in Refs. 1 and 2 on Shippingport, Yankee, Dresden, and the CETR has been covered in these reviews, but Ref. 2 also contains significant information on the Big Rock Point and Humboldt Bay reactors. Both of these reactors went into commercial operation in late 1963 and have had availability factors of about 95% through the end of the year, a period which did not involve refueling. Both reactors experienced leakage past the inner O-ring seal of the pressure-vessel head. In the case of the Big Rock Point reactor, this was attributed to a number of thermal cycles plus the use of three different operating pressures, and the leakage was stopped by replacement of the O-ring. The vessel-head flange-sealing surface of the Humboldt Bay reactor was modified by grinding to prevent further leakage.

An interesting repair technique was employed on the Big Rock Point reactor. Flow-induced vibration was found to be responsible for the loosening of a cap screw from one of the Zircaloy fuel channels; this vibration was caused by direct impingement of the recirculating flow on a portion of the core support, and the core-support plate had to be removed for installation of a new flow distributor. This work was performed inside the water-filled reactor vessel by four divers with a significantly low resultant radiation exposure.

References 3 and 4 discuss physics studies and preliminary experience with the Russian WWER. As of the date of the references (May 1964), the WWER had not produced nuclear electricity, although the turbines had been rolled on steam from auxiliary boilers. Critical experiments had been done, and the primary coolant system had been debugged.

Significant Developments

Fuel Elements, Fuel Materials, and Cladding

As indicated in Table II-1, the water-moderated reactors typically employ fuel in the oxide form (UO_2, or a UO_2-ThO_2 mixture as in the CETR and the ERR), usually as pressed and

Table II-1 BOILING- AND PRESSURIZED-WATER REACTOR-DESIGN DATA

Installation	Power, Mw(e)	Startup	Reactor pressure, psi	Steam conditions, psia/°F	Fuel/cladding	Reactor control	Remarks
			Boiling-Water Reactors				
Dresden Nuclear Power Station, Morris, Ill.	200	1959	1015	Primary: 975/452 Secondary: 500/467	UO$_2$/S.S./Zircaloy-2	Control rods	
Rheinisch-Westfalisches Elektrizitatswerk (RWE), Kahl, West Germany	15.6	1960	1000	750/550	UO$_2$/Zr	Rods and solid shims	
Elk River Reactor (ERR), Elk River, Minn.	20.0	1962	937	865/900	UO$_2$ThO$_2$/S.S.	Rods and fixed (solid) shims	Indirect cycle
Big Rock Point Nuclear Plant, Charlevoix, Mich.	47.8	1962	1050	Direct cycle	UO$_2$/S.S.	Rods and fixed (solid) shims	Steam drum
Humboldt Bay Power Plant, Unit No. 3, Humboldt Bay, Calif.	50	1963	1035	Direct cycle	UO$_2$/S.S.	Rods and poison curtains	Pressure suppression
Japan Atomic Energy Research Institute Reactor (JPDR), Tokai-Mura, Japan	11.7	1963	905	495/530	UO$_2$/Zr	Rods and poison curtains	
Società Elettronucleare Nazionale Reactor (SENN), Punta Fiume, Italy	150	1963	1000	1000/(sat.)	UO$_2$/S.S. and Zr	Control rods and solid shims	Dual cycle, steam drum
La Crosse Boiling Water Reactor (LACBWR), La Crosse, Wis.	50	1965	1300	1300/577	UO$_2$/S.S.		
Kernkraftwerk-RWE-Bayernwerk Reactor (KRB), Gundremmingen, West Germany	237	1966	1015	500/467	UO$_2$/S.S.		
Indian Department of Atomic Energy BWR, Tarapur, India	380 (two reactors)	1968	1015	1015 primary/(sat.) 500 secondary/ (sat.)	UO$_2$/Zircaloy-2	Control rods	Dual cycle forced circulation, internal steam separation, pressure suppression
Oyster Creek Nuclear Electric Generating Station, Oyster Creek, N. J.	540	1967	1000	Direct cycle	UO$_2$/Zr		
Pacific Gas & Electric Bodega Bay Reactor, Bodega Bay, Calif.	313	1968	1075	Direct cycle	UO$_2$/S.S.		Pressure suppression
Nine Mile Point Nuclear Power Station, N. Y.	525	1968	1000	Direct cycle	UO$_2$/Zr	Rods and recirculation pumps	Pressure suppression
N. V. Samenwerkende, Electriciteits Productiebedrijven (SEP), Netherlands	50	1968					

			Pressurized-Water Reactors				
Shippingport PWR, Shippingport, Pa.	60	1957	2000	600/486	U-Zr plates and UO_2/Zircaloy-2 rods	Rods and burnable poison	
Centre d'Études de l'Énergie Nucléaire Reactor (BR-3), Mol, Belgium	10.7	1962	2000	520/471	UO_2/S.S.	Rods and chemical shim	
Yankee Atomic Electric Co. Reactor, Rowe, Mass.	160	1960	2300 (max.)	465/460	UO_2/S.S.	Rods and solid shims	
Consolidated Edison Thorium Reactor (CETR), Indian Point, N. Y.	255	1962	1500	370/1000	UO_2/ThO_2/S.S.	Control rods and solid shims	Oil-fired superheater
Novo-Voronezh Atomic Power Station (WWER), Russia	210	1964	1422	455/(sat.)	UO_2/Zr-Nb	Movable fuel and flux trap, safety rods	
Saxton Nuclear Experimental Corporation Reactor, Saxton, Pa.	5	1962	2000	475/462	UO_2/S.S.	Rods and chemical shim	
Società Elettronucleare Italiana (SELNI), Trino, Italy	240	1964	2015	500/467	UO_2/S.S.		
Southern California Edison Co. San Onofre Reactor, Camp Pendleton, Calif.	375	1966	2065	650/495	UO_2/S.S.		
Connecticut Yankee Atomic Power Co. Reactor, Haddam Neck, Conn.	463	1967	2065	690/502	UO_2/S.S.		
Malibu Nuclear Power Station (Malibu-1), Corral Beach, Calif.	462	1968	2065	690/410	UO_2/S.S. or Zr		
Société d'Energie Nucléaire Franco-Belge des Ardennes (SENA), Chooz, France	242	1966	2100	465/460	UO_2/S.S.	Control rods and chemical shim	Underground containment, in-core instrumentation
Kernkraft Baden-Wurttemberg Planungegesellschaft mbH. (KBWP), Obrigheim on the Neckar, West Germany	283	1968	2062	711/(sat.)	UO_2/Zr	Control rods and chemical shim	Double containment
Union Electrica Madrilena Reactor, Zorita de los Canes, Spain	140	1968					

Table II-2 LOCATIONS OF PREVIOUS REVIEWS OF DESIGN AND OPERATING EXPERIENCE FOR WATER-MODERATED REACTORS IN *POWER REACTOR TECHNOLOGY*

Reactor	Item	Vol.	Issue	Pages
Shippingport	First refueling	4	2	52-58
	Power-generation history, fuel-element examination, experience with major equipment, radiation control, second core	5	4	61-72
	Instrumentation, second refueling	6	2	64-67
	FEDAL system, loss-of-flow experiments, radiation, hydraulics experiments, fuel failure	6	3	49-55
	Operating history, pressure-vessel irradiation, fuel examinations	7	2	193-196
Yankee	Design	4	3	47-55
	Head closure, containment experience, turbine vibration	4	4	69-70
	Control-rod examination	6	3	55-56
	In-core instrumentation, radioactivity problems, reactivity characteristics	6	4	82-91
Dresden	Design	4	4	56-68
	Control rods, grid-plate cracks, load following	5	2	56-59
	Water chemistry, load schedules, transient experiments	6	2	60-64
CETR	Design	6	3	28-40
	Fuel pool experience, control-system operation, performance	7	3	313-315
Elk River	Design	5	2	33-47
Humboldt Bay and Big Rock Point	Design	7	1	70-84

sintered cylindrical pellets in jackets of Zircaloy or stainless steel. An early exception was the Experimental Boiling Water Reactor, which used plates of uranium metal alloyed with small percentages of zirconium and niobium, clad with Zircaloy. The Shippingport reactor used Zircaloy-clad plates of uranium–zirconium alloy for the seed loadings installed in core 1; since the seed fuel is highly enriched, this alloy was rich in zirconium.

In Ref. 5 the results of the U. S. program on oxide fuels are summarized as follows:

> During the past five years in the United States there has been a systematic approach to design formulation, fabrication development, and performance testing of uranium oxide type fuels. Sufficient data are available to allow a quantitative evaluation of oxide fuels for use in economic central-station power applications. The extensive scope of this program includes:
>
> a. Over 130,000 Zircaloy and stainless steel clad UO_2 fuel rods have been irradiated in operating water and steam cooled (260°-316°C) power reactors. Maximum exposure attained is about 28,000 MWD/TU; maximum heat fluxes are about 350,000 Btu/hr-ft^2 for Zircaloy clad fuel and 450,000 for stainless clad fuel. . . .
>
> b. Over 4000 developmental fuel rods representing 37 different fabrication processes have been irradiated in water and steam cooled test reactors and loops. Maximum exposure attained was 16,000 MWD/TU and 1,435,000 Btu/hr-ft^2 peak heat flux. Plate UO_2 fuel has been irradiated in test loops to 127,000 MWD/TU exposure.
>
> c. More recently, oxide fuel elements have been irradiated to 3600 MWD/TU maximum at 445,000 Btu/hr-ft^2 heat flux in superheat steam (510°C) test reactor loops.

The reference continues with a discussion of fuel-fabrication techniques and the behavior of fuel elements clad in zirconium alloys and stainless-steel alloys. Table II-3 gives additional details on oxide cores clad with Zircaloy-2 and stainless steel, which reflect U. S. design practice.

In general, the in-reactor behavior of the Zircaloy-clad elements has been "outstanding,"[5] with but few failures. Purposely defected elements have operated relatively successfully, with little loss of UO_2 to the coolant and little reaction between the fuel and the available oxygen in the water; washout from powder-filled fuel elements has been slight. Hydrogen pickup by the zirconium-base alloys has generally proved acceptable, with in-pile pickup well correlated with autoclave corrosion data (Fig. II-1).

The outstanding example of in-pile experience with stainless-steel-clad fuel elements is

Table II-3 DETAILS OF POWER-REACTOR CORES FABRICATED WITH ZIRCALOY-2 AND STAINLESS STEEL[5]

	Power, Mw(e)	No. of rods	Rod outside diameter, in.	Cladding thickness, in.	Peak heat flux × 10^{-6}, Btu/(hr)(sq ft)	Average exposure,[*] Mwd/ton of U
Zircaloy-Clad Fuel Elements						
Boiling-water reactors						
Dresden	220	15,500	0.570	0.030	3.46	9,000
Dresden[†]		192	0.470	0.025	3.46	7,000
Japan	12	3,460	0.564	0.033	2.96	1,000
Kahl	16	3,200	0.571	0.033	3.38	4,500
SENN	150	17,000				
Pressurized-water reactors						
Shippingport core[‡]	68	16,400	0.411	0.023	3.43	10,000
Shippingport core[§]	150	Flat plates	Flat plate, 0.100 in. thick	0.020	6.50	
Carolinas-Virginia[¶]	17	1,230	0.490	0.022	4.69	1,000
Stainless-Steel-Clad Fuel Elements						
Boiling-water reactors						
Dresden	220	4,900	0.440	0.019 (304 S.S.)	2.76	4,000
Elk River	20		0.452	0.020 (304 S.S.)	3.13	500
Humboldt Bay	65	8,428	0.463	0.019 (304 S.S.)	3.65	3,000
Big Rock Point	50	7,392	0.388	0.019 (304 S.S.)	3.50	3,000
Pressurized-water reactors						
Yankee	185	23,142	0.340	0.021 (348 S.S.)	4.46	8,000
Saxton	20 (thermal)	1,512	0.391	0.015 (304 S.S.)	4.44	3,000
Indian Point[**]	151	23,400	0.304	0.021 (304 S.S.)	5.40	3,000
N.S. *Savannah*	70 (thermal)	5,248	0.500	0.035 (304 S.S.)	2.77	1,500
SELNI	270	24,960	0.385	0.015 (304 S.S.)		Under construction

[*] Editor's Note: This is the exposure attained as of the writing of Ref. 5 and is not necessarily the maximum attainable.

[†] Straight-through 9-ft-long rods.

[‡] Rod fuel only in blanket region.

[§] Flat plates in entire core. Seed is 0.040-in.-thick plates with ZrO_2-UO_2.

[¶] Zircaloy-4 cladding; this reactor is cooled and moderated by D_2O.

[**] Net power is 255 Mw(e), of which 104 Mw(e) is from fossil superheaters.

probably the Yankee reactor. The second core of this power reactor contained two assemblies from the first core, and these two assemblies operated satisfactorily to a maximum burnup of 27,000 Mwd per ton of uranium. Detailed examination of the first core showed that the cladding exhibited no microstructural changes, an increase in burst strength, "limited" amount of crud, and no significant structural changes.[5] Thin-walled cladding, relying on the fuel for support, has been tested in Dresden and in the Vallecitos Boiling Water Reactor (VBWR) with less success; the VBWR results were reviewed in detail in the Winter 1963–1964 issue of *Power Reactor Technology*, 7(1): 27-50, and are summarized in Fig. II-2.

Pertinent conclusions from Ref. 5 are as follows:

> Zircaloy-2 clad rod fuel has been operated satisfactorily to maximum burnup of 16,000 MWD/TU at peak heat fluxes of 510,000 Btu/hr-ft^2, and tests are continuing.
>
> Heavy walled "free standing" fully annealed stainless steel rods have operated satisfactorily to 27,000 MWD/TU maximum and peak heat fluxes of 446,000 Btu/hr-ft^2.
>
> Thin clad "nonfree standing" stainless has shown inter-granular stress induced corrosion at average burnups less than 10,000 MWD/TU and high heat fluxes. Exact cause of the failure mechanism is still under investigation.

It should be noted, however, that more than one variable was changed between the freestanding- and nonfreestanding-cladding experiments. For example, the heavy-walled freestanding fuel elements were irradiated in a pressurized-water-reactor (PWR) environment and were fabricated of type 348 stainless steel. The thin nonfreestanding claddings were irradiated in Dresden and VBWR in a boiling-water-reactor (BWR) environment and were fabricated of type 304 stainless steel.

The irradiation behavior of ceramic fuels is discussed in Ref. 6. The paper presents engineering type information on a number of fuel

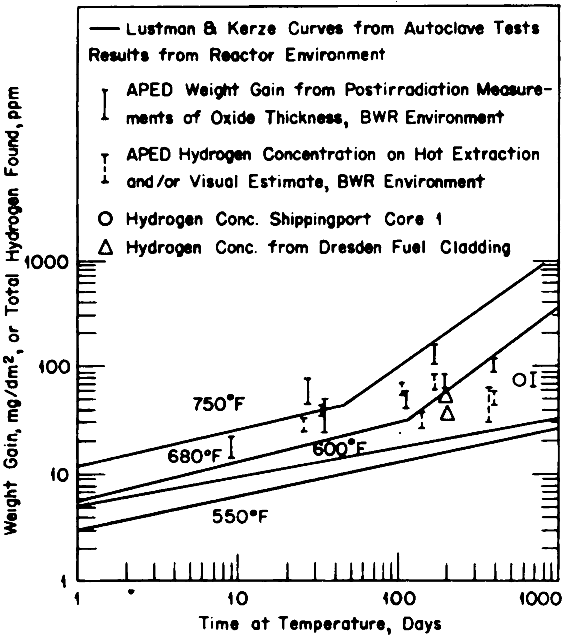

Fig. II-1 Corrosion behavior and hydrogen pickup of Zircaloy-2. Comparison of autoclave and reactor exposures.[5]

materials, including UO_2, ThO_2-UO_2, PuO_2-UO_2, ZrO_2 base–UO_2, UO_2-BeO, UO_2-Al_2O_3, MgO-PuO_2, ZrO_2-PuO_2, UC, PuC, UC-PuC, UN, US, and U_3Si. Of these materials the oxides are of primary importance to water reactors and, naturally, have been investigated most extensively. For example, the thermal conductivity of UO_2, illustrated in Fig. II-3, appears to be reasonably well determined. Increases in k_{UO_2} at high temperatures, where it has been postulated that radiative-energy-transport mechanisms become important, have not been observed in polycrystalline UO_2 even after columnar grain growth. Fission-gas release, although not well understood, is amenable to engineering calculations, at least to the accuracy required for the practical design of fuel elements for the H_2O reactors.* Structural changes in UO_2 have been quantitatively related to fuel operating temperature, temperature gradient, exposure, density, and irradiation history. Reference 6 suggests that future reactor designs may employ lower density UO_2 to encourage fission-gas release and reduce swelling during irradiation. This may be of importance in the design of oxide fuels for long-term irradiation in fast reactors or for those reactors where the provision of a fission-gas plenum results in an unacceptable performance penalty. Reference 7 reports preliminary results for fabrication and irradiation of UO_2-PuO_2 fuel elements in the BR-3 reactor.

References 8 and 9 report on various experiments designed to study the corrosion resistance of zirconium alloys. Reference 8, which is primarily of interest to the specialist, is on metallurgical techniques in which radioactive tracers are used for the study of zirconium alloy corrosion; it also presents some results. Reference 9 is devoted to the zirco-

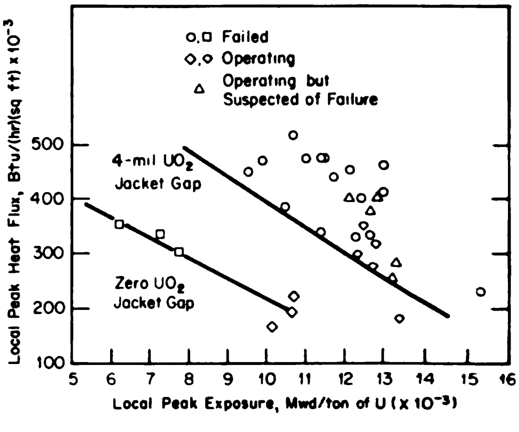

Fig. II-2 Local peak heat flux (within 500 to 1000 hr of failure) vs. local peak exposure for 304 stainless-steel-clad UO_2 fuel.[5]

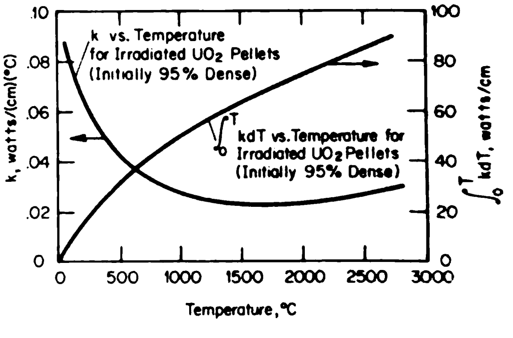

Fig. II-3 UO_2 thermal conductivity and $\int_0^T kdT$ vs. temperature.[6]

---

*An extensive discussion of the engineering and performance of UO_2 fuel assemblies was presented by the Canadians in Refs. 30 to 32. Their special interest in fission-gas release presumably comes from the fact that they cannot design NPD type fuel rods with large fission-gas spaces to allow for imperfections in gas-release calculations without introducing additional difficulties related to end-cap peaking, fuel shuffling, etc.

nium-niobium alloy hydriding problem in water-cooled reactors. This class of alloys is an interesting one since the Russians have traditionally used the zirconium-niobium alloys in their water-cooled power reactors, whereas the Zircaloys have been used almost exclusively in the United States. The reference discusses the effect of stress upon the distribution, or arrangement, of the zirconium hydride corrosion product. The hydride is in the form of platelets, and, if these are oriented parallel to the axis of the tube, their effect on tensile properties is minimized. On the other hand, if the platelets are radially oriented, serious reductions in tensile strength occur. According to Ref. 9:

> ...formation of radially oriented hydrides is a function of values of the tensile stress and does not depend upon the methods of hydriding. Even at the hydrogen content of 0.01% with radially oriented hydrides the pipe properties are sharply impaired; that proves the paramount importance of the values of tensile stress when using zirconium alloys in water-moderated water-cooled power reactors. On all other conditions being equal, preference should be given to the zirconium alloys possessing high yield point as in this case the value of the allowable hydriding stress will be higher and reliability of operation will correspondingly increase.
>
> The allowable hydriding stress of the alloy is the maximum tensile stress at which radial orientation of the hydrides under the specified service conditions does not yet occur. Evidently, it is to be taken into account along with other parameters in designing zirconium alloy claddings for fuel elements or zirconium alloy pipes for service under pressure.

Values of the allowable hydriding stress for two of the zirconium-niobium alloys are given in the reference. For zirconium–1 wt.% niobium, radial orientation of the hydrides occurred at 4.4 kg/mm^2; and, for zirconium–2 wt.% niobium, radially oriented hydrides were formed at a stress of 8.8 kg/mm^2 and over. These values are about half of the yield strength of each alloy at the test temperature of 400°C. Although the stronger zirconium-niobium alloys have not excited much interest in the United States as cladding materials, their use in pressure-tube type reactors and for in-core structural components of pressure-vessel type reactors may increase.

Reference 10 summarizes a considerable amount of U. S. experience on corrosion in aqueous systems. The generally successful use of Zircaloy and stainless steel in power reactors is confirmed, and the superiority of beta-quenched Zircaloy-4 over Zircaloy-2 in high-temperature water is discussed. With regard to stainless steel, the authors note that "...highly stressed thin wall cladding, representing advanced fuel concepts, has failed in VBWR after exposures considerably shorter than required for economic performance... ."[10] Although this is true, failures have also been noted in VBWR irradiation of types H and I elements in the Fuel-Cycle Program; these elements were designed to be freestanding [see reviews in *Power Reactor Technology*, 7(1): 27-50 and 7(4): 354-355].

In summary, there is little doubt that metal-jacketed oxide fuel elements can be made to have attractively long service lifetimes in water-cooled reactors. The quantitative principles of optimum design are not completely understood, however, and caution is in order in making substantial departures from the designs which have been proved out by reactor experience. It follows also that, in quoting and using the experience obtained to date, one must be particular and comprehensive in considering the conditions under which the experience was obtained. Some departure from this principle was evident in the informal discussion in the Geneva sessions, where the Shippingport experience with exposure lifetime of the blanket elements appeared to be regarded as typical for oxide fuel elements, even though the thermal demands on the oxide in these elements are relatively quite mild [see the review of Shippingport Operating Experience in *Power Reactor Technology*, 7(2): 193].

Water Chemistry: Use of Mild Steels in Aqueous Systems

The use of mild steels in portions of power-reactor primary circuit piping has been common practice for some time; Dresden, for example, uses low-alloy and carbon steels for the primary and secondary steam piping and the feedwater system. A full-flow condensate demineralizer is provided, however. In Ref. 10 the use of boiler steel is considered for unclad pressure vessels, and the conclusion reached is that the question is "unresolved." The problem is of more than academic interest, however, since at least one power reactor under construction (the second unit of the WWER) is said[29] to utilize an unclad pressure vessel. Accordingly, the discussion presented in Ref.

11 serves to illuminate some of the problems associated with the use of mild steel in power-reactor primary circuits.

The water and steam of a typical boiling-water reactor will contain about 0.1 and 20 ppm oxygen, respectively.[11] Experiments done at the Kjeller Research Establishment in Norway, and summarized in Ref. 11, indicate that the initial corrosion-product release rate under these conditions is "high" but, under continued high-temperature operation, decreases to a release rate as low as 2 mg/(dm^2)(month). This is comparable to values for stainless steel. The situation has additional complications in the case of reactor operation since the system may from time to time be kept at lower temperatures for relatively long periods (as during refueling); rather high corrosion rates have been reported in neutral water at low temperatures. The paper[11] suggests that during shutdown the oxygen content of the water should be monitored and reduced to the point that harmful corrosion will be prevented. Under low-oxygen conditions the corrosion film formed at high temperatures is apparently stable, although for long periods of downtime it may be necessary to scavenge the oxygen.

As a further consequence of the corrosion in neutral water at low temperature, low-temperature portions of the primary system may present difficulties in the absence of condensate cleanup systems. The corrosion products introduced into the reactor may precipitate on fuel elements, and Ref. 11 mentions that "rust generators" are to be installed in the Halden Boiling Water Reactor (HBWR) to study the problem.

Control: Soluble and Burnable Poisons

The use of soluble poisons to control reactivity in pressurized-water reactors was reviewed in detail in Sec. IX of *Power Reactor Technology*, 7(4). References 12 to 14 are on aspects of soluble-poison control, and the information reviewed here will be supplementary to the material presented in the 7(4) issue.

The dynamic performance of a chemical-shim system is the subject in Ref. 12. The reactor that was used as a neutron source was a swimming-pool type, and the boric acid was contained in a pipe introduced within the core. The control system (feed and bleed) and associated piping and electronics probably are representative of what could be used for power-reactor control, but the range of dynamic variables was much greater than that encompassed by the chemical-shim application currently considered in power reactors. The response of the control system to various reactivity steps and ramps was investigated with the following results:[12]

> ...the control system examined here seems t have satisfactory dynamic characteristics as regards the fine control of the neutron flux level. There are no particular operation and maintenance problems. The whole system appears to be quite reliable, rugged and easy to handle.

The flow diagram of the poison loop is shown in Fig. II-4.

Operation of the Belgian BR-3 plant with boron in the coolant is described in Ref. 13. The steps performed to prepare the system for operation with the chemical shim, and subsequent transient tests, are detailed in Table II-4. The physical, chemical, and radiochemical characteristics of the reactor coolant were monitored during the course of operations in the chemical-shim experiment, which lasted about a month. In general, the results of the experiment were good. Small, unexplained, reactivity variations occurred (Fig. II-5), but they happened over relatively long times and, in fact, were noticed in normal operations without boron. Water chemistry showed no unusual or unexpected trends, and the reactor coolant activity remained below design limits, although the demineralizer has been bypassed for more than six weeks.

Reference 13 concludes with an interesting discussion of the application of chemical shim to a large [250 Mw(e)] reactor. Depending upon the operational program, from 2 to 10 tons of boric acid per year will have to be disposed of. If the core has contained failed fuel elements, this material will be contaminated by fission products to a varying degree, depending on the number of failed fuel rods. Distillation, electrodialysis, and ion exchange are considered as concentration processes, but no specific recommendations are given. It may be that the success of the soluble-poison concept relies on keeping the number of routinely failed fuel elements within some limit, and the value 1% is mentioned. Fortunately, the experience with the reactor type has illustrated that this limit is probably not an unrealistically difficult con

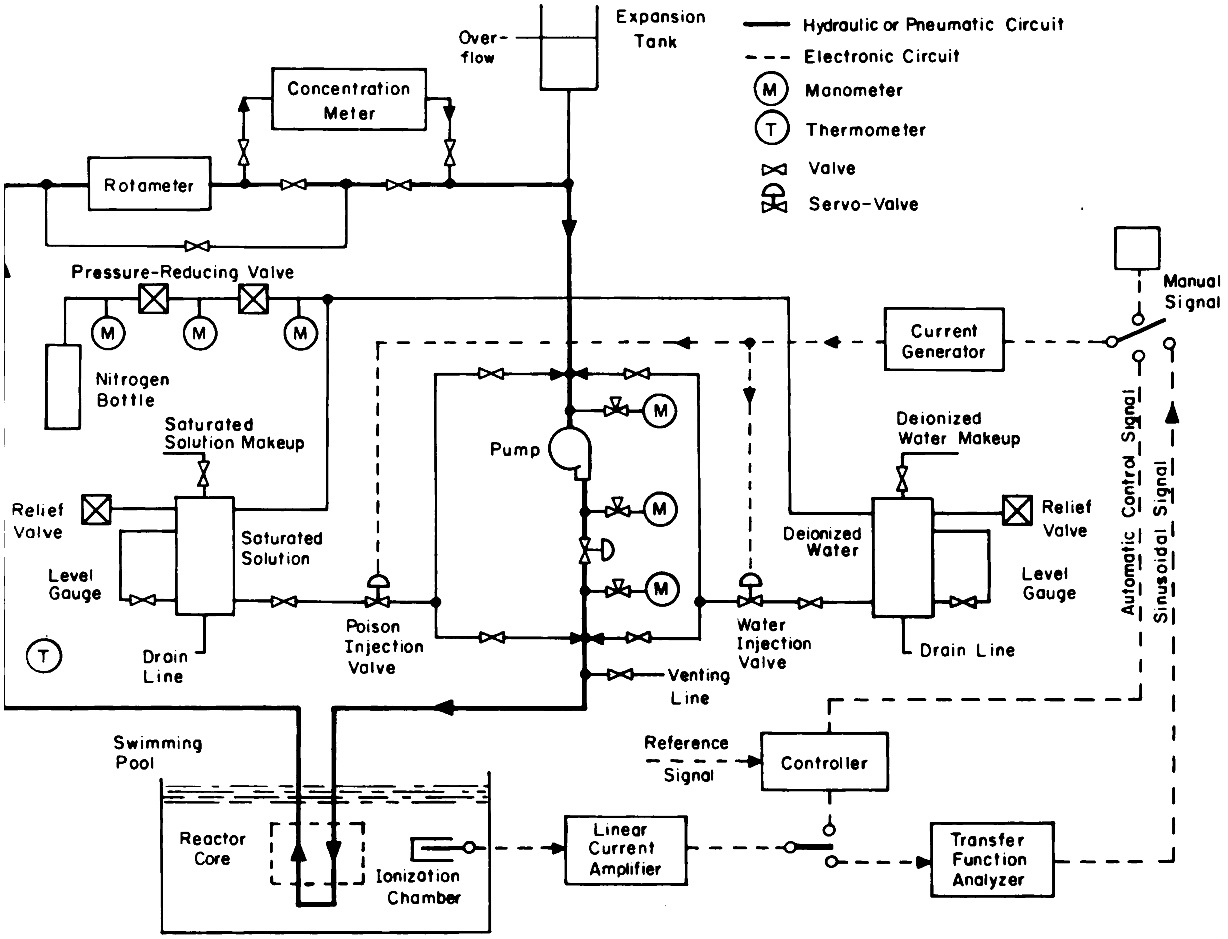

Fig. II-4 Simplified flow diagram of soluble-poison control system.[12]

Table II-4 OPERATIONS WITH THE BR-3 REACTOR: CHEMICAL-SHIM EXPERIMENT[13]

1. Preliminary operation at normal power level, without the mixed-bed demineralizer; the ion beds are not saturated in BO_3^{3-} ions and therefore cannot be used during the boron test.
2. Preliminary operation at normal power level, without demineralizer, the *p*H being reduced from 9.5 to approximately 7.

During these two preliminary tests, the increase of the reactor coolant activity (very predictable) was, however, far from the permissible limits.* Also the air contamination remained, everywhere, far under the maximum permissible concentrations.

3. Power operation with 125 ppm boron present in the primary coolant. This first step in the study of chemical control made it possible to determine the overall effect of bypassing the demineralizer and of the presence of boron in the reactor coolant. It gave information (*a*) on the evolution of chemical characteristics of the water, the boron concentration, and the core reactivity and (*b*) on the possibility of compensating the xenon poisoning.
4. Power operation with a higher boron concentration in the reactor coolant water (350 ppm). This last step, performed after a core shuffling, made possible a more extensive study:

—Startup of the plant, and load pickup with boron present
—Overall compensation of the xenon effect by reduction of the boron concentration
—Power operation with all rods extracted from the core, except two rods for fine control
—Compensation of samarium poisoning and fuel burnup by boron removal. Furthermore, various load rejections and fast load pickups made it possible to test the dynamic behavior of the reactor.

---

*The activity of the primary coolant increased about a factor of 3 when the resin-bed purification system was not operational. The new value[13] was about 0.24 μc/ml.

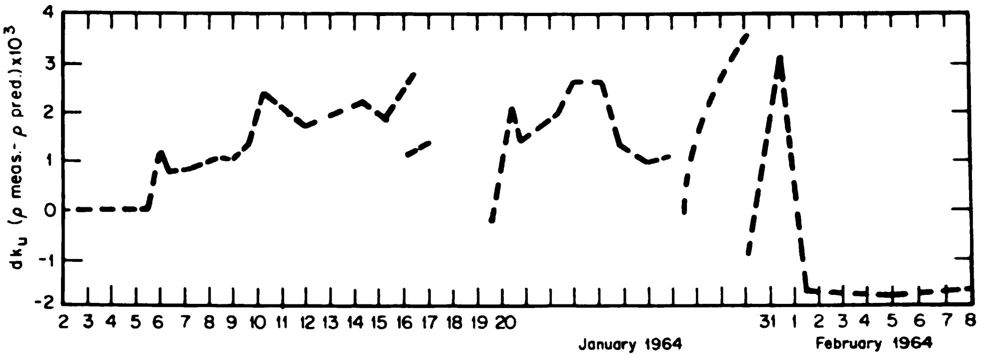

Fig. II-5 Unaccounted reactivity disappearance, dk_u, vs. time. Results of power operation of the BR-3 reactor in the presence of 400 ppm boron.[13]

Operational experience with Yankee, Saxton, and the BR-3 is briefly discussed in Ref. 14. An interesting result of the experiments with Yankee and Saxton has been the discovery of the "*p*H effect"—an increase in reactivity has been observed with increase of the coolant *p*H. The effect has been observed both with and without significant boron levels in the coolant and has not been correlated with the poison content or corrosion-product concentration in the coolant. The increase in reactivity is only a few tenths of a percent, but, as of the time of writing of Ref. 14, no satisfactory explanation had been offered. Hot-laboratory examination of core components of Saxton after nine months of operation with dissolved poison showed "trivial quantities of residual poison on the core."[14]

Reference 14 also discusses recent advances in burnable-poison control. Some of the discussion centers around core 2 of the Shippingport PWR, which utilizes boron–stainless-steel strips as a burnable poison (Fig. II-6). This type of reactor appears to be particularly suited to burnable-poison control since (1) the burnable poison need be incorporated only in the seed elements, (2) only a relatively few burnable-poison sites need be employed, and (3) there is no complication due to the shuffling of fuel assemblies. Also, in the seed-blanket reactor, the control rods are placed in the seed, and hence the burnable poison can be located so as to reduce local peaking due to rod channels. This approach is evident in Fig. II-6.

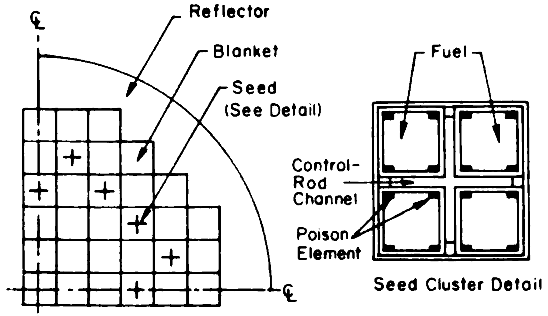

Fig. II-6 Schematic arrangement of burnable poison in the Shippingport core geometry.[14]

Although most of the burnable-poison applications have specified boron as the poison, a number of other materials offer possibilities for use. These are members of the rare-earth family (samarium, dysprosium, erbium, and gadolinium), and each may offer an advantage relative to boron in a particular situation.

Pressure Vessels

Three papers on reactor pressure-vessel design and fabrication[15–17] are from three different countries and present dissimilar views on many aspects of pressure-vessel technology. For example, the "standard" material used for large pressure vessels in the United States is SA-302 grade B steel, the material used for the SEP and SENA pressure vessels is a steel designated "1,2 MD07," and the material of the WWER vessel is a high-strength Cr-Mo-V steel. The exact composition of the latter was not specified, but the compositions of the other two are given in Table II-5. The selection of a pressure-vessel material usually involves a pressure-vessel code, and Ref. 15 contains a discussion of the effects of pressure-vessel codes of various countries.

Table II-5 COMPOSITIONS OF VARIOUS PRESSURE-VESSEL STEELS

Country	Designation	Nominal composition, wt.%
United States	SA-302 grade B	<0.25 C, 1.15–1.50 Mn, 0.45–0.60 Mo
Netherlands	1,2 MD07	<0.18 C, 1.0–1.5 Mn, <0.2 Cr, 0.3–0.7 Ni, 0.35–0.55 Mo

In the fabrication of the Russian- and Netherlands-built pressure vessels for the WWER, SENN, SENA, and the KRB reactors, forged rings were used to form the pressure-vessel bodies.[15,17] In contrast, the cylindrical portions of vessels fabricated in the United States are usually rolled, and, if the vessel wall is thin enough, the cladding is roll bonded. The advantages of the forged-ring fabrication technique are discussed in Ref. 15, although, as pointed out in that paper, the resulting vessel is higher in price than a similar one built of sheet material.

Pressure-vessel design and fabrication in the United States are discussed in Ref. 16. The reference opens with a discussion of the recent amendments to the *ASME Pressure Vessel Code* which have resulted in the approval of Sec. III of the *ASME Power Boiler and Unfired Pressure Vessel Codes*, "Rule for Construction of Nuclear Vessels." Older vessels were fabricated in conformity with either Sec. I or Sec. VIII. Although much of the discussion is primarily of interest to the pressure-vessel specialist, Fig. II-7, which illustrates typical BWR and PWR pressure vessels fabricated by either of the ASME codes, Sec. III or Sec. VIII, is a graphic summary of some important effects of the changes. In the particular cases shown, the design by Sec. III results in significant changes in wall thicknesses for the cylindrical sections of the vessel; Table II-6 gives an estimate of the effect on fabrication time for BWR and PWR vessels of various sizes. At first consideration it is surprising that the fabrication times for vessels for both PWR and BWR ap-

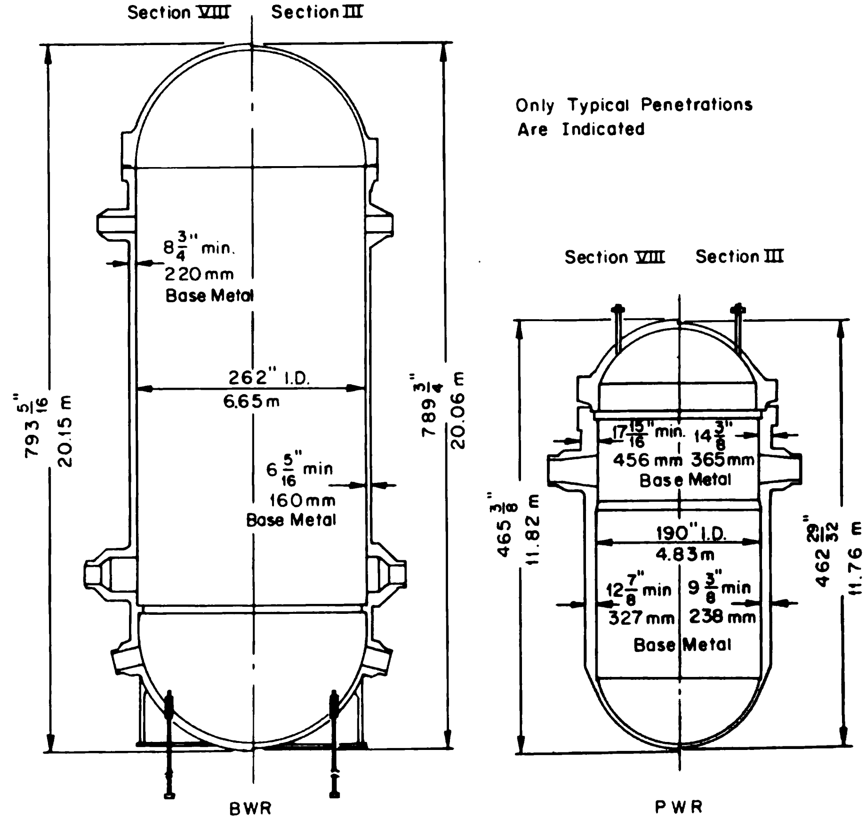

Fig. II-7 Reactor vessel designs for 1000-Mw(e)-capacity plants comparing ASME Code Secs. III and VIII.[16]

Table II-6 FABRICATION TIME FOR REACTOR VESSELS OF VARIOUS SIZES[16]

Plant capacity, Mw(e) net	Fabrication time, weeks	
	Sec. III design	Sec. VIII design
250	95	100
500	120	125
750	145	155
1000	165	175
1500	205	220

plication are approximately equal. The reference explains that this is true because the combination of vessel-diameter and vessel-design-pressure requirements offset each other. This, of course, may not always be the case. The relative size difference between BWR and PWR vessels, as indicated in Fig. II-7, is striking. Figure II-8, from the same paper, presents the data in slightly different form. The vessel-size requirements are, of course, determined by reactor design, rather than by vessel-design considerations. Yet the plotted points, although they are not identified in the paper, presumably represent vessels specified for actual plant designs. Hence the lower section of the curve, at least, has authority as a representation of the current state of the art for BWR and PWR design.

The WWER pressure vessel described in Ref. 17 is an unusual one and, for purposes of description, is divided into lower, middle, and upper zones (Fig. II-9). The lower zone consists of three ring portions, each forged as a single piece. The middle zone contains 24 nozzles, which are welded in place as shown in Fig. II-9. The upper zone consists of a one-piece forged flange and a strengthening ring, fitted by means of a shrink-fit technique. The vessel cover is a forged flat plate with 55 penetrations. The internal surface of the vessel is covered with weld-deposited austenitic stainless steel having a thickness of about 20 mm—quite thick in terms of practice in the United States. The vessel-to-cover seal is accomplished by a wedge-shaped nickel gasket compressed between the cover and vessel by means of a thrust ring held in place by studs. The reference describes an alternative seal involving the welding of a flexible collar to both the vessel and the head.

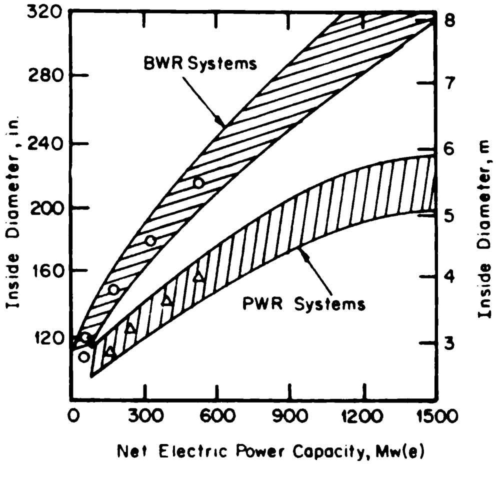

Fig. II-8 Reactor vessel diameter vs. plant power rating.[16]

Thermal and Hydraulic Design

The relatively large number of papers devoted to thermal and hydraulic considerations of water-cooled reactors were all concerned with boiling phenomena and could be grouped into three categories:

—Basic studies of bubble dynamics, velocity profiles, etc.

—Interpretations of experimental data

—Survey papers

The basic studies[18–20] of boiling phenomena were concerned primarily with bubble dynamics, active sites, nucleation, and other variables of interest in two-phase flow. The authors initiated their discussion with a consideration of pool boiling, and, although the detailed results are of primary interest to the specialist, they do indicate that continued progress is being made in gaining an understanding of two-phase behavior.

Of the papers concerned with experimental and analytical results, two presented information on the critical heat flux during unstable burnout in two-phase flow,[21,22] and two were concerned with predicting ϕ_{BO} during stable burnout.[23,24] The test loops used in the experiments reported in Refs. 21 and 22 both employed natural circulation and were instrumented to measure appropriate pressures, powers, flow rates, etc. Typical flow-power curves are illustrated in Fig. II-10. As shown, the flow initially increased, reached a maximum, and then decreased. As power was increased

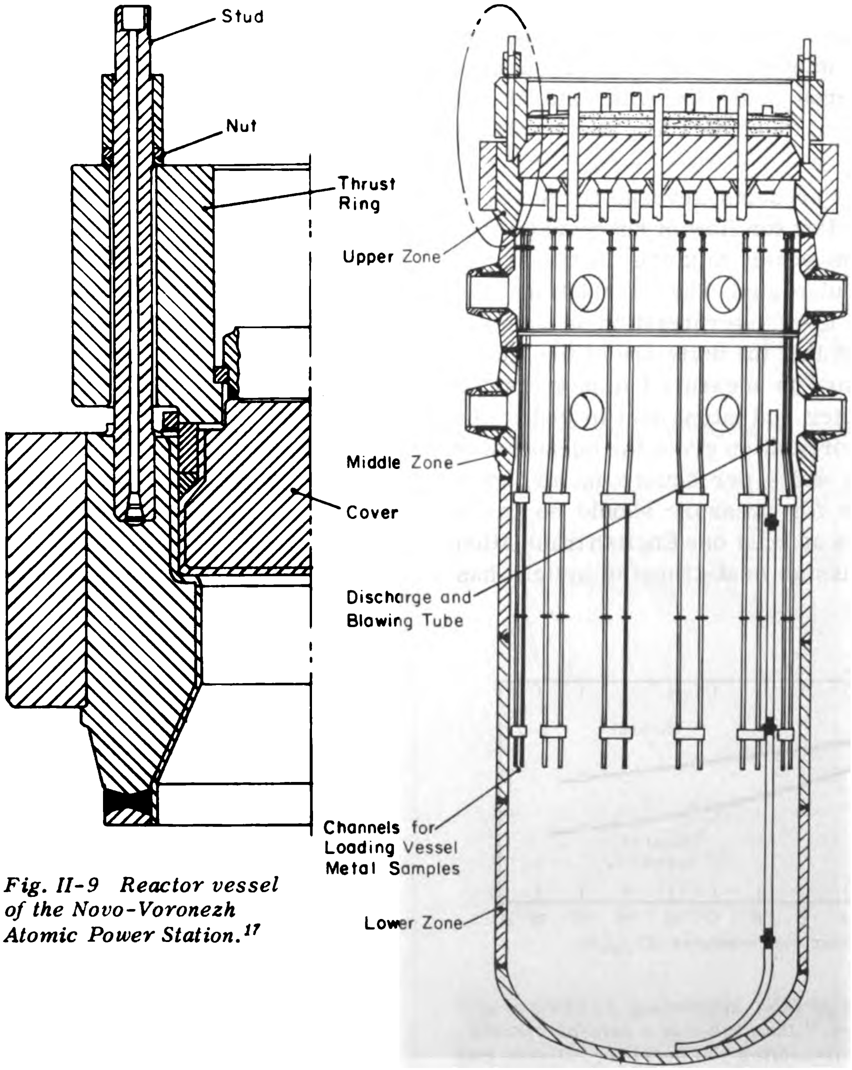
Stud
Nut
Thrust Ring
Cover
Upper Zone
Middle Zone
Discharge and Blowing Tube
Channels for Loading Vessel Metal Samples
Lower Zone

Fig. II-9 Reactor vessel of the Novo-Voronezh Atomic Power Station.[17]

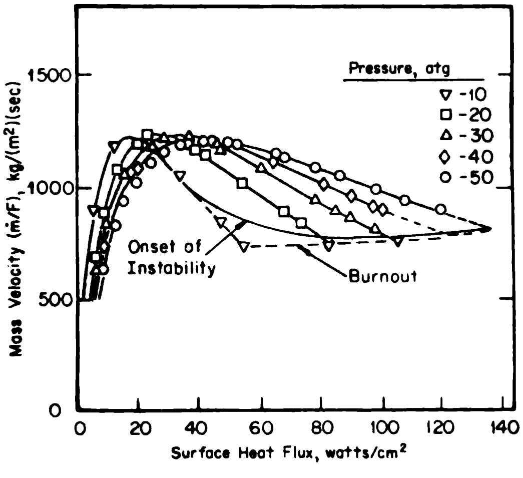

Fig. II-10 Effect of pressure on mass velocity for varying heat flux. Data taken in a natural-circulation loop with test-section diameter of 36 mm and length of 4890 mm. Inlet subcooling, ΔT_{sub}, = 8 ± 0.3°C.

in steps, oscillation usually commenced; three cases are reported:

- —Diverging oscillations causing burnout
- —Stable oscillations
- —Burnout without oscillations

The experimental results were compared against predictions of a theoretical flow model. The predictions were obtained by numerically solving equations of continuity, energy, and momentum; the stability limit was analytically determined as the power input where the oscillations in inlet velocity became divergent upon a step increase of 1% in channel power. Although no general stability criteria are given in the reference, it would appear that the method is generally applicable for specific cases of uniformly heated test sections of simple geometry. Reference 21 also discusses the effects of inlet subcooling and inlet throttling on burnout heat flux and compares operation with natural and forced convection; these data are shown in Figs. II-11 to II-13.

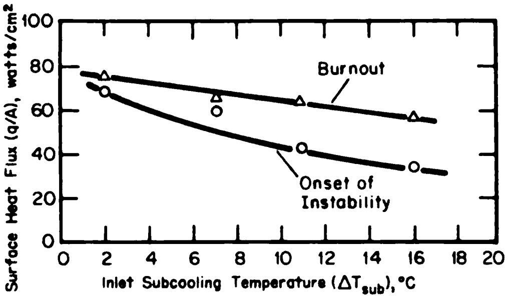

Fig. II-11 Effect of inlet subcooling on critical and burnout heat fluxes.[21] *Data taken in a natural-circulation loop with test-section diameter of 20 mm and length of 4890 mm. Pressure = 50 atg.*

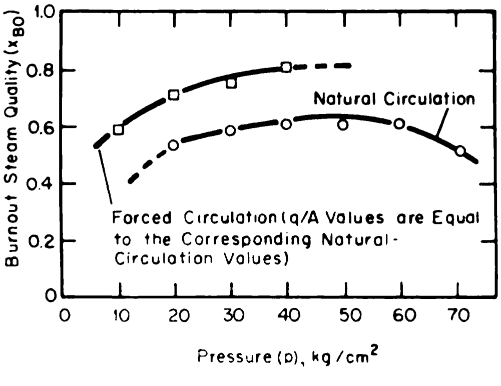

Fig. II-12 Comparison between natural- and forced-circulation burnout data.[21] *Test-section diameter, 20 mm; length, 4890 mm. Forced-circulation data were taken with "heavy" inlet throttling.*

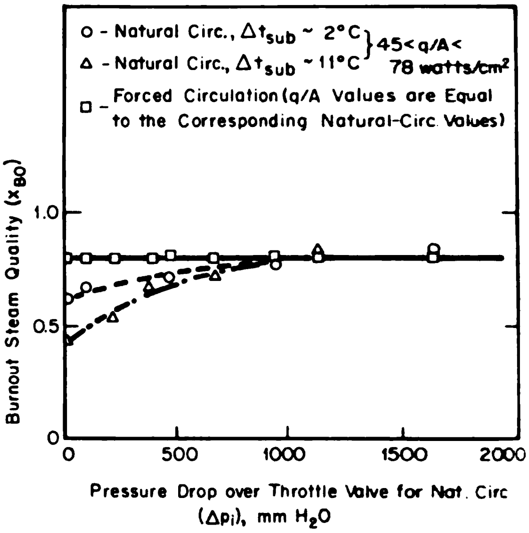

Fig. II-13 Effect of inlet throttling on burnout.[21] *Test-section diameter, 20 mm; length, 4890 mm. Pressure = 50 atg.*

Reference 23 presents several correlations of burnout heat flux for flow of subcooled water in tubes, steam-water mixture in tubes, and flow in an annular gap. The correlations are empirical, and their interpretation is complicated by the fact that the units are of the "mks" system. Pressure is measured in newtons per square centimeter and latent heat in joules per kilogram; the correlation gives the burnout heat flux in units of watts per square meter, however. The units for pressure should be carefully noted since at least one English translation of a recent Russian heat-transfer article has translated pressure in newtons per square centimeter as "neuts/cm²." The correlation for ϕ_{BO} for steam-water mixture in tubes is as follows:

$$\phi_{BO} = \left[1.46 \times 10^{-4}\, r^{1.72}(1-x)^{m} - 0.116\, W_g\right] \frac{2.71}{d_{in}\,0.48} \qquad (1$$

where ϕ_{BO} = burnout heat flux, watts/m²
r = latent heat, joules/kg
x = quality
W_g = mass flow rate, kg/(hr)(m²)
d_{in} = internal tube diameter, mm
m = $3.48-0.54\,(r/4.18 \times 10^6)$

The range of applicability of Eq. 1 is stated to be as follows:

Pressure:	392–981 newtons/cm² (568 to 1422 psi
Mass flow:	2–18 × 10⁶ kg/(hr)(m²)
Quality:	0–0.40
d_{in}:	4–12 mm
Length:	≥200 mm

Equation 1 is plotted in Fig. II-14 for a pipe diameter of 0.18 in., a pressure of 1000 psia, and two different values of W_g. This figure compares the correlation with data appearing in Fig. III-12 of *Power Reactor Technology* 7(1). The correlation does not predict the experimentally determined "best-fit" curve very well, although the range of experimental data falls within the range of applicability of Eq. 1.

Reference 23 also presents the results of burnout experiments utilizing nonuniformly heated test sections, and these are given in Fig. II-15. The ordinate on the curves is believed by the reviewer to be the weighted mean heat flux, and the heat-flux nonuniformity is believed to be a radial one, although the reference is not particularly clear in these two quite important aspects. The experiments were carried out "... with round tubes of $d_{\text{in}} = 10$ mm, tube length is 400 mm and with the eccentricity between external surfaces and internal ones (three values)... ."[23] These three values are probably the ones corresponding to curves 2, 3, and 4 in Fig. II-15.

Reference 24 presents burnout data taken at General Electric—San Jose, Hanford, and Columbia. Since the results of many of these programs have been reviewed in previous issues of *Power Reactor Technology*, additional details will not be discussed here.

References 25 and 26 are in themselves reviews. Reference 25 reviews highlights of two-phase-flow research relative to boiling reactors in the United States, and Ref. 26 describes the experimental work on heat transfer and hydrodynamics with steam-water and two-component mixtures done at the Centro Informazioni Studi Esperienze (CISE), Milan, Italy.

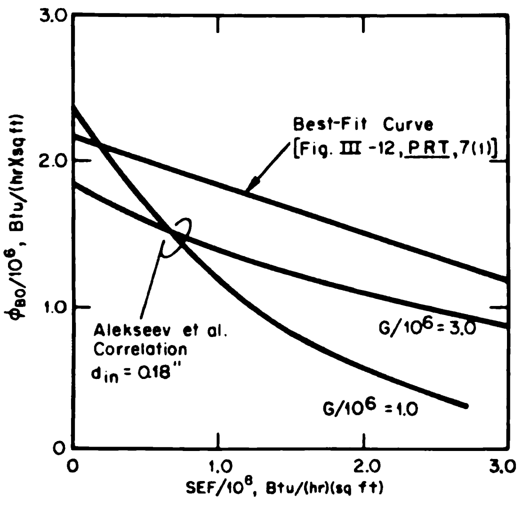

Fig. II-14 Comparison of burnout correlation of Alekseev et al.[23] *with burnout data previously published in* Power Reactor Technology. *Pressure = 1000 psia.*

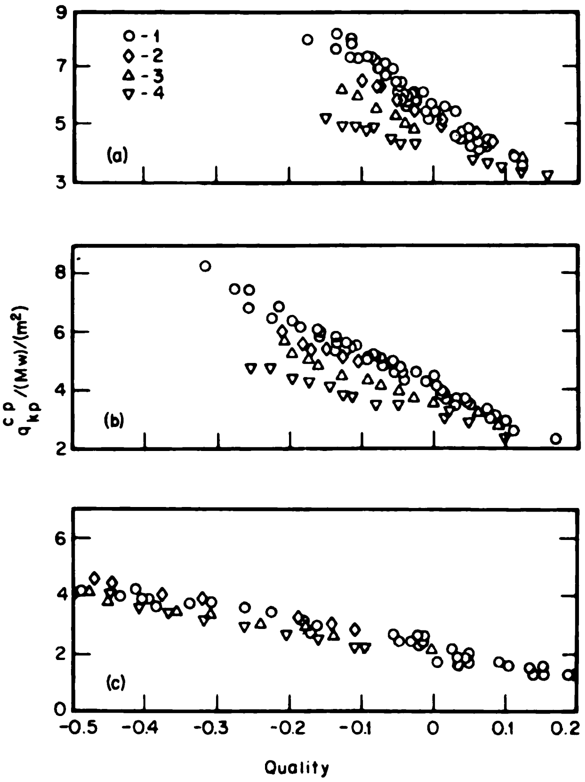

Fig. II-15 Heat-flux concentration nonuniformity influence on q_{BO} in round tubes. Curves 1, 2, 3, and 4 correspond to values $q_{BO}^{max.}/q_{BO}^{av.}$ of 1, 1.12, 1.28, and 1.50. Parts a, b, and c correspond to pressures[23] *of 588, 981, and 1765.8 neutrons/cm^2.*

Directions of Future Developments

To some extent the future developments in water-reactor technology are tied into the design features of the advanced plants of each type; these are listed last under the appropriate headings in Table II-1. References 27 and 28 present views of two water-reactor manufacturers on developments of their particular type, and Ref. 29 discusses advanced Russian water reactors.

The boiling-water reactors designed by the General Electric Company are tied quite closely to the concept of pressure suppression. On the other hand, the recent Westinghouse-designed reactors utilize a variety of containments from an unshielded steel containment vessel to the double-barrier concept, employing a sandwich of porous concrete between two layers of steel and reinforced concrete. Both the pressure-suppression and double-barrier concepts, however, require that the capability be present in the plant to process potentially contaminated air from within the containment or reactor building during routine operation before release from a plant stack.

Early designs of both the BWR and the PWR stations, as exemplified by Dresden and Yankee, used canned pumps in the primary circuit. This practice seems to be declining, however, since the Big Rock Point BWR uses pumps of the shaft-seal type and the San Onofre PWR is scheduled to use them. This change has come about for several reasons. Possibly in the pressurized-water reactors the most important was the desire to utilize pumps of capacities in excess of 50,000 gal/min. In the boiling-water reactors, the change is probably due primarily to confidence that has been built up in the handling of radioactivity: since the direct-cycle boiling-water reactors must, in any case, provide for the handling of radioactive off-gases, there is less incentive to reduce the leakage of primary water to a bare minimum. Reference 27, in addition, mentions that work is being done to develop a jet pump for use inside the reactor vessel of the boiling-water reactor to "substantially" reduce the flow external to the vessel. For other primary system components, Ref. 28 states that PWR plants currently under design and construction do not provide for primary-coolant-loop stop valves and check valves, since safety and operational studies indicated these valves were not needed.

Fuel-element experience has been relatively good for both the pressurized-water and boiling-water reactors, with the exception of the failures of the stainless-steel-clad elements in the VBWR mentioned previously. As a result, Ref. 27 states that Zircaloy is the "favored" cladding material for current boiling-water reactors, with Incoloy and Inconel slated for testing. On the other hand, the pressurized-water reactors have shown no difficulties when utilizing either stainless-steel cladding or Zircaloy, although large-scale experience with rod elements of the UO_2-Zircaloy type has been limited to the rather mild conditions in the Shippingport blanket. Until the VBWR failures can be tied to a cause not connected with the reactor type, the PWR designer may have additional freedom in the choice of cladding materials because of the ability of the pressurized-water reactor to operate with close control of coolant chemistry. Both references mention that spring type spacers will be considered for present and future fuel-assembly fabrication techniques. This eliminates welding and brazing operations on fuel-cladding surfaces and allows cold-worked cladding to be utilized, if desired.

Control and refueling are two areas of interest for future developments. The chemical-shim control of the pressurized-water reactor has been mentioned previously. In addition, Ref. 28 mentions a so-called "rod-cluster-control" scheme for advanced pressurized-water reactors, to be used in conjunction with chemical shim. This utilizes hollow tubes that replace some of the fuel rods within a fuel assembly; inside each hollow tube is a cylindrical, unfollowed, absorber rod. The several rods within the confines of a single fuel assembly are mechanically connected and are operated, as a cluster, by a single drive unit. No cruciform type control rods are employed. The application of soluble-poison control to the boiling-water reactor is less straightforward and has not been proposed in any commercial design. The use of bottom-entering control rods to assist in axial power flattening will no doubt be continued, and further flattening and reactivity compensation may be obtained with fixed shims of boron stainless steel. Both Refs. 27 and 28 mention "scatter loading," in which exposed fuel assemblies and new assemblies are distributed more or less uniformly over the core volume rather than in zones. Upon refueling, the most highly exposed assemblies are replaced by new assemblies, but there is no shuffling of the remaining assemblies.

The refueling of both reactor types is complicated by above-core structure and mechanism. The boiling-water reactor of the future most likely will have internal steam separators, and these will probably have to be removed before refueling. The pressurized-water reactor, on the other hand, while not requiring steam-separation equipment within the pressure vessel, may have control-rod-drive guide structures above the core which must be moved. This structure becomes more complex when "cluster" rods are used. The efficient removal of the above-core components will probably continue to be an important consideration for both reactor types in order to minimize downtime for refueling purposes. In-core instrumentation, mentioned in both references, will probably continue to follow the control-rod-drive position, being inserted into the BWR core from the bottom and into the PWR core from the top. Thus the BWR in-core instrumentation need not be removed during fuel handling, whereas Ref. 28 mentions that the PWR in-core instrumentation probably will be removed as a unit, being attached to a common support plate presumably located above the core. One of the criticisms of the water reactors, heard rather frequently in the informal discussions at Geneva, was the long shutdown time required for refueling. No doubt this problem will receive increasing emphasis in coming years.

Table II-7 COMPARISON OF WWER-1 AND WWER-2

Parameter	WWER-1	WWER-2
Power, Mw(e)	210	365
Status	Operating	Under construction
No. of stationary fuel assemblies	312	276
Length, m	2.5	2.5
Shape, cross sectional	Hexagonal	Hexagonal
Distance across flats, mm	144	144
Pitch	147	
Fuel-pin geometry	Rods	Rods
Cladding material	Zr-Nb	Zr-Nb or S.S.
Cladding outside diameter, mm	10.2	8.8
No. of pins/assembly	90	127
Fuel material	UO_2 pellets	UO_2 pellets
Fuel-pellet outside diameter, mm	8.7	7.7
No. of movable fuel assemblies		
Compensating	31	60
Safety	6	13
Coolant purification	Evaporation	Ion exchange
No. of primary loops	6	8
Pressurizer type	Gas	Electric
Coolant pressure, atm abs.	100	120
No. of turbines	3	5

Reference 29 is interesting partly because the Voronezh reactors (WWER) are quite different in design from the pressurized-water reactors constructed in the United States. The reference discusses the changes between the first unit of the plant (WWER-1) and the second (WWER-2). A comparison of the two reactors is given in Table II-7. Both reactors employ hexagonal fuel assemblies, but there is a difference in the number of fuel pins per assembly. The movable fuel assemblies of the "compensating" type are for slow changes in reactivity. These consist of a flux-trap type of control rod, hexagonal in shape, mounted on top of a movable fuel assembly very similar in design to the stationary assemblies. The safety assembly consists of a guide tube mounted permanently in the core; its shape is hexahedral outside and cylindrical inside. The safety rod is fabricated of a cylindrical absorber 125 mm in diameter, which is followed by a zirconium alloy scatterer without fuel in the WWER-1 and by a fueled follower in the WWER-2.

Some of the differences between the two reactors — for example, the change to electric pressurization and the adoption of ion-exchange water treatment — involve changing to design techniques that have been used in the United States for a number of years. Other features of the WWER-2, notably the elimination of the cladding in the pressure vessel,[29] represent departures from practice in the United States.

The reference concludes with a discussion of future improvements in the reactor type not specifically tied to the WWER plant. One of the most significant areas for improvement is the method of refueling. Although WWER-1 had not been refueled at the time of the writing of Ref. 29, the authors were aware that, in general, refueling operations "...require a lot of time... ." A number of possible solutions are discussed, and the most attractive one is a reactor design employing soluble poison since this application allows the removal of most, if not all, of the control-rod-drive structure from above the core. The resulting reactor is shown in Fig. II-16. The "honeycomb" core design is not well explained in the reference, but the interesting application to refueling is the provision for storage of fuel elements within the pressure vessel. The fuel-element handling would be done after the reactor had been shut down but not depressurized. The centrally located reloading machine would handle the fuel elements, taking new elements from their racks within the vessel and replacing spent elements. After the fuel movement into and out of the core had been accomplished, the reactor would be brought to power, and the spent elements would be transferred through a vessel lock. The latter step need not be done rapidly since reactor operation would not be affected.

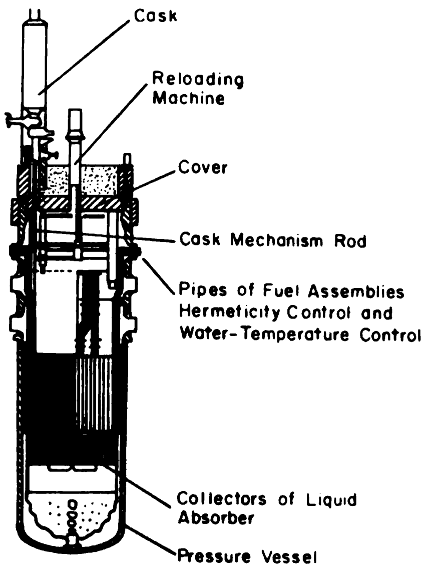
Cask
Reloading Machine
Cover
Cask Mechanism Rod
Pipes of Fuel Assemblies Hermeticity Control and Water-Temperature Control
Collectors of Liquid Absorber
Pressure Vessel

Fig. II-16 Reactor scheme with honeycomb core and with the change of liquid-absorber concentration in the channel system.[29]

Several of the recommendations for advancement in the WWER technology are peculiar to the reactor as designed. In the WWER-1 the clearance between adjacent fuel bundles is only a few millimeters, and the requirement for the movement of the relatively large flux-trap control rods to a position above the core apparently makes the design of the upper grid plate somewhat difficult. If the fuel assemblies are locked in place at their lower end, the lack of open space within the core makes it difficult to get at the locking devices with fuel-handling tools. Accordingly, Ref. 29 suggests that the fuel elements be hydraulically locked in place by a piston located at the bottom of the bundle but connected to the space above the core. The control rods would be bottom driven to facilitate refueling, and the reference illustrates a possible hydraulic-drive mechanism. The upward direction of the flow in the WWER reactor gives rise to what appear to be formidable hydraulics problems, other than the one of merely holding the fuel elements in place. The large fueled followers move against the coolant flow when they move in the direction of reducing reactivity, and they must be adequately cooled during any movement. Downflow is discussed in Ref. 29, but the designers appear reluctant to take the step due to problems connected with flow reversal during main pump coastdown.

References

These references are papers presented at the Third United Nations International Conference on the Peaceful Uses of Atomic Energy, Geneva, September 1964.

1. R. J. Coe and W. C. Beattie, Operational Experience with Pressurized Water Systems, A/Conf. 28/P/202.
2. V. L. Stone, Operating Experience with Boiling Water Reactors, A/Conf.28/P/204.
3. L. V. Komissarov, G. L. L. Lunin, A. N. Novikov, V. A. Sidorenko, and V. D. Sidorenko, Physical Studies of Novo-Voronezh Atomic Power Station Reactor (WWER), A/Conf.28/P/585.
4. G. L. Dunin, V. A. Sidorenko, S. A. Skvortsov, M. A. Borisev, F. Y. Ovchinnikov, V. P. Denisov, V. V. Stekelnikov, A. A. Khokhlachov, and B. S. Yasvenko, Start-Up and Adjustment of Reactor WNER of Novo-Voronezh Atomic Power Station, A/Conf.28/P/305.
5. S. Naymark and C. N. Spalaris, Oxide Fuel Fabrication and Performance, A/Conf.28/P/233.
6. T. J. Pashos, D. R. deHalas, D. L. Keller, and L. A. Neimark, Irradiation Behavior of Ceramic Fuels, A/Conf.28/P/240.
7. J. M. Leblanc, Irradiation of Plutonium Enriched Ceramic Fuel Rods in the BR-3 Power Reactor, A/Conf.28/P/443.
8. V. S. Emelyanov, A. I. Evstyukhin, G. B. Fedorov, G. G. Ryabove, N. V. Borkov, I. I. Korobkov, and P. L. Gruzin, Corrosion Resistance of Zirconium and Its Alloys in Water and Steam at High Temperatures, A/Conf.28/P/341.
9. A. D. Amaev, R. S. Ambartsumyan, A. A. Kiselev, S. T. Konobeevskiy, I. A. Anisimova, A. M. Glukhov, L. M. Lebedev, V. A. Myshkin, V. V. Goncharov, E. G. Ivanov, M. S. Orlov, P. F. Pravdyuk, E. P. Ryazantsev, and V. V. Skvortsov, Influence of Some Factors Upon Hydriding and Variation of Properties of Zirconium Alloy with

1% Nb Used for Fuel Element Cladding in Water-Moderated Water-Cooled Power Reactors, A/Conf.28/P/342.

10. J. E. Draley, J. A. Ayres, W. E. Berry, E. Hillner, and S. P. Rideout, Corrosion in Aqueous Systems, A/Conf.28/P/243.
11. K. Videm, Mild Steel in Primary Circuits of Water Cooled Power Reactors, A/Conf.28/P/592.
12. G. C. Ambrosini, T. Bozzoni, G. Cipollina, E. Colussi, and R. Garroni, Stability Analysis and Dynamic Performance of a Chemical System Operated for the Automatic Fine Control of a Nuclear Reactor, A/Conf.28/P/629.
13. M. Plumier, P. Stacquez, P. Dozinel, R. Muyllie, M. Preat, G. Beuken, M. Gueben, and L. Maesen, Practical Results and Prospects of the Use of Soluble Poison in the Pressurized Water Reactors, A/Conf.28/P/518.
14. A. Radkowsky and R. J. Creagan, Poison Control of Thermal Reactors, A/Conf.28/P/274.
15. K. J. de Jong, C. de Peter, and M. C. van Veen, Experiences on the Design, Calculation and the Manufacture for Power Reactor Components, A/Conf.28/P/728.
16. A. L. Gaines and L. Porse, Problems in the Design and Construction of Large Reactor Vessels, A/Conf.28/P/227.
17. V. V. Stekolnikov, A. A. Khokhlatchev, V. P. Denisov, J. V. Vikhorev, N. I. Prigorovskiy, N. A. Lugov, B. I. Kovalenko, and V. B. Dobronravov, High Pressure Vessels of Light-Water Cooled and -Moderated Power Reactors, A/Conf.28/P/331.
18. C. J. Rallis and H. H. Jawurek, The Mechanism of Nuclear Boiling, A/Conf.28/P/600.
19. K. Torikai, M. Nori, M. Akiyama, T. Kobori, and H. Adachi, Boiling Heat Transfer and Burnout Mechanism in Boiling-Water Cooled Reactor, A/Conf.28/P/580.
20. H. Mondin, P. Lavigne, and R. Semeria, Some Fundamental Aspects of Boiling in Nuclear Reactors, A/Conf.28/P/55.
21. K. M. Becker, S. Jahnberg, I. Haga, P. T. Hansson, and R. P. Mathisen, Hydrodynamic Instability and Dynamic Burnout in Natural Circulation Two-Phase Flow. An Experimental and Theoretical Study, A/Conf.28/P/607.
22. M. Bogaardt, C. L. Spigt, F. J. M. Dijkman, and N. Madsen, Heat Transfer and Hydraulic Stability in Boiling Water Reactors, A/Conf.28/P/589.
23. G. V. Alekseev, B. A. Zenkevitch, O. L. Peskov, N. D. Sergeev, and V. I. Subbotin, Burn-Out Heat Fluxes Under Forced Water Flow, A/Conf.28/P/327a.
24. S. Levy, J. Batch, and J. Casterline, Critical Heat Flux Considerations in the Thermal and Hydraulic Design of Water-Cooled Nuclear Reactors, A/Conf.28/P/224.
25. P. A. Lottes, W. H. Cook, K. F. Neusen, R. W. Wright, S. M. Zivi, and N. Zuber, Fluid Dynamics, Stability, and Vapor-Liquid Slip in Boiling Reactor Systems, A/Conf.28/P/230.
26. N. Adorni, S. Bertoletti, I. Casagrande, L. Cravarolo, G. P. Gaspari, A. Hassid, C. Lombardi, E. Pedrocchi, and G. Peterlongo, Basic Heat Transfer and Hydrodynamics Studies in Two-Phase Flow, A/Conf.28/P/867.
27. G. White, Developments in Boiling Water Reactors, A/Conf.28/P/205.
28. J. C. Rengel and W. E. Johnson, Developments in Pressurized Water Reactors, A/Conf.28/P/203.
29. A. Y. Kramerov, Y. V. Markov, S. A. Skvortsov, V. A. Sidorenko, B. P. Denisov, E. V. Kulikov, Y. P. Sorokin, V. V. Stekolnikov, A. A. Hoblachev, and V. P. Tatarnikov, Some Ways of Water-Water Power Reactor Development, A/Conf.28/P/304.
30. W. B. Lewis, J. R. MacEwan, W. H. Stevens, and R. G. Hart, Fission-Gas Behaviour in UO_2 Fuel, A/Conf.28/P/19.
31. R. D. Page, D. G. Hardy, A. J. Mooradian, J. Howieson, G. R. Fanjoy, and D. B. Nazzer, Engineering and Performance of UO_2 Fuel Assemblies, A/Conf.28/P/18.
32. J. A. L. Robertson, A. S. Bain, J. R. MacEwan, and M. J. F. Notley, UO_2 Performance—The Importance of Temperature Distribution, A/Conf.28/P/17.

Section

III

Power Reactor Technology

Vessel Type Superheating Reactors

Status and Design Features

The status of the various nuclear superheat projects in the United States has been covered in several previous issues of *Power Reactor Technology*. In particular, Vol. 7, No. 3, presented the designs of the BONUS and Pathfinder integral boiling-superheating power reactors. Both these reactors are currently in the process of startup. Two experimental superheating reactors, BORAX-V and EVESR, have had some operating experience. The present state of the art of the U. S. superheat program is summarized in Ref. 1.

Table III-1 lists pertinent data for three integral boiling-superheating plants. The EVESR (Fig. III-1) is a separate superheat reactor in that it superheats steam from an outside source rather than evaporating and superheating within the same vessel. At present the saturated steam is being supplied by a fossil-fired boiler. The fuel is of annular geometry, as shown in Fig. III-2. Steam flows down the annular flow passage to the bottom plenum of the element, reverses flow direction, and flows up the central hole. Other details of the reactor are given in Table III-2.

Superheating reactors are being studied not only in the United States but also in Germany[2] and the Soviet Union.[3] Reference 2 is a description of a prototype integral superheat reactor that was scheduled to be started in Germany in late 1964. The plant is to be 100 Mw(t) and is to produce steam with a temperature of 500°C at a pressure of 60 ata. The plant site is at Kahl, and the prototype reactor will power an existing turbine-generator set. The reactor core is composed of 45 fuel assemblies, arranged in a 7 by 7 lattice with the corners missing (Fig. III-3). Each assembly is composed of 64 fuel elements of a hollow, annular design (Fig. III-4). The interesting coolant-flow path within the vessel starts with the liquid water undergoing heating and boiling on the exterior of the annular fuel elements, under natural-circulation flow. The saturated steam flows to the upper portion of the pressure vessel and enters the superheating passages of the center 25 fuel assemblies via appropriate piping. Each fuel assembly is two-pass in design, with steam flowing down the center hole of the outer 32 fuel elements and up the center hole of the remaining 32 elements. The partially superheated steam then flows to the outer 20 assemblies, shown shaded in Fig. III-3. The same two-pass flow within the assemblies takes place, producing steam of the final desired temperature. The entire reactor is thus essentially a four-pass superheater.

The combination boiling-superheating fuel element is an advanced concept and must be designed carefully with respect to thermal stresses. In the fuel element shown in Fig. III-4, a rather large temperature difference will exist between the walls in contact with the superheated steam and those in contact with the boiling water. In addition, the superheater wall temperature in the second-pass elements will be greater than the corresponding wall temperature in the first-pass elements. The latter problem is to be solved by bellows, and the other thermal stress is to be taken up by the use of proper material combinations to withstand the stresses. Elements of this general type have been constructed and irradiated in the United States; this program was reviewed in the March 1963 issue of *Power Reactor Technology*, 6(2): 75-80. Superheat tests have also been run in the Kahl boiling-water reactor and are briefly reviewed in Ref. 2. The

Kahl facility apparently is an in-pile loop capable of testing fuel elements, but not necessarily elements of full length. In February 1964, two fuel tubes were removed from the loop after a burnup of about 1150 Mwd/ton. These combination elements were clad with Inconel X and Hastelloy C, and both were "undamaged"; the maximum cladding temperature reached was relatively low — about 770°F. These tubes were fabricated from UO_2 pellets of annular geometry, although vibratory compaction is also being studied as a fabrication method.

Details of the Russian superheating reactor are given in Ref. 3. This plant is currently being completed in the Ulyanovsk region of the Soviet Union and will be an extremely flexible test facility. Two cores are presently contemplated for the facility — a small core (for initial use) that will produce saturated steam at a pressure of 100 atm and a large core that will generate 90 atm of superheated steam at a temperature of about 500°C. The reactor as a whole is being designed to generate steam at pressures between 30 and 100 atm. Figure III-5 shows the plant flow diagram. The turbine is designed to operate with saturated steam at a pressure of 29 atm, and the high-pressure steam separator shown in Fig. III-5 provides for throttling of the steam, which will be generated at higher pressures. Superheated steam, when produced, can be delivered to a separate turbine or to a special cooler. The plant also provides for dual-cycle operation by the inclusion of steam generators in which 30 atm of saturated steam can be generated. Data on the reactor are given in Table III-3. Figure III-6 is a view of the reactor as arranged for super-

Table III-1 BOILING-WATER REACTOR PLANTS WITH INTEGRAL SUPERHEAT DESIGN DATA[1]

	BONUS		BORAX-V		Pathfinder	
Site	Puerto Rico		NRTS, Idaho		Sioux Falls, S. Dak.	
Owner*	USAEC		USAEC		NSP	
Reactor designer*	GNEC		ANL		A-C	
Operating contractor*	PRWRA		ANL		NSP	
Electric power, Mw(e) gross	17.5		3.5		66	
Electric power, Mw(t) net	16.5		3.5		62.5	
Thermal output, Mw(t)	50		20		200	
Plant steam cycle	Direct		Direct		Direct	
Position of superheater region	Peripheral		Central or peripheral		Central	
Nominal operating pressure, psig	975		600		600	
Turbine throttle steam pressure, psig	850		350 (587 available)		535	
Saturated steam temp., °F	543		489		489	
Superheated steam temp., °F	900		850		825	
Thermal power to boiling, Mw	37		16.6		157	
Thermal power to superheating, Mw	13		3.4		43	
Gross cycle efficiency, %	35				33	
Net cycle efficiency, %	33				31	
Maximum superheat fuel-cladding temp., °F	1175		1110		1250	
	Boiling	Superheater	Boiling	Superheater	Boiling	Superheater
Effective outside core dia., ft	3.34	4.83	3.25	1.0	5.75	2.5
Core height, ft	4.55	4.55	2.0	2.0	6.0	6.0
Structural material (core)	Zircaloy-2	S.S. 348	Al(X8001)	S.S.	Zircaloy-2	S.S.
Fuel type	Rod	Rod	Rod	Plate	Rod	Double tubular
Fuel material	UO_2	UO_2	UO_2	UO_2–S.S. cermet	UO_2	UO_2–S.S. cermet
Fuel enrichment, %	2.40	3.25	4.95	93	2.2	93
Cladding material	Zircaloy-2	Inconel	S.S. 304	S.S. 304L	Zircaloy-2	S.S. 316L
Control-rod shape	Cruciform	Slab	Cruciform and "T"	Cruciform and "T"	Cruciform	Round rod
Control-rod material	1.0 wt.% B^{10} in S.S.	1.0 wt.% B^{10} in S.S.	Boral	Boral	2 wt.% boron in S.S.	2 wt.% boron in S.S.
No. of steam passes		4		2		1
Average power density, kw(t)/liter	33.6	11.5	42.5	40.5	45.2	46.5

*GNEC = General Nuclear Engineering Corporation.
PRWRA = Puerto Rico Water Resources Authority.
ANL = Argonne National Laboratory.
NSP = Northern States Power.
A-C = Allis-Chalmers.

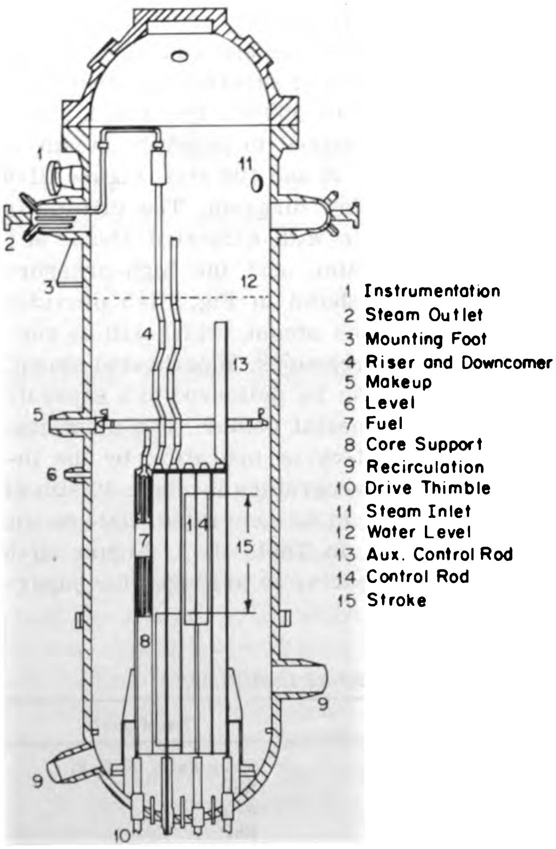

Fig. III-1 EVESR reactor.[1]

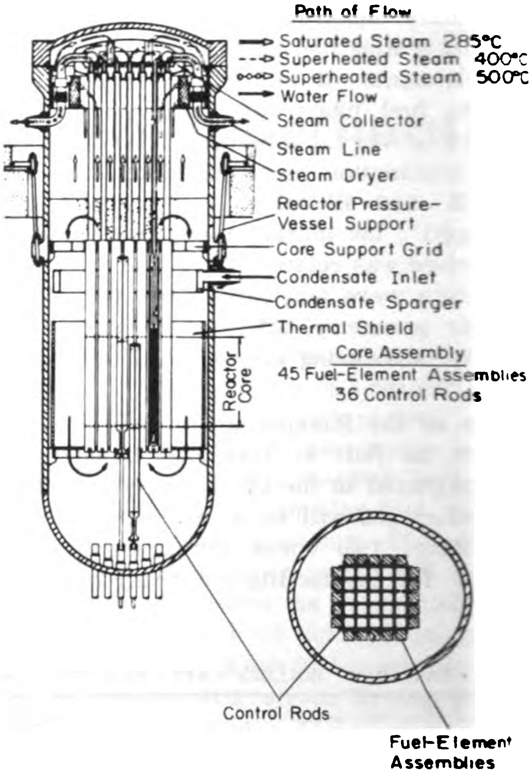

Fig. III-3 Schematic of the Kahl superheating reactor.[2]

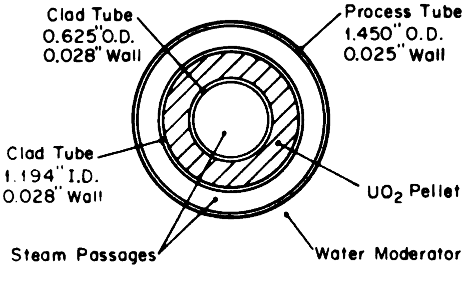
Clad Tube 0.625" O.D. 0.028" Wall
Process Tube 1.450" O.D. 0.025" Wall
Clad Tube 1.194" I.D. 0.028" Wall
UO2 Pellet
Steam Passages
Water Moderator

Fig. III-2 EVESR fuel-element cross section.

Table III-2 DESIGN PARAMETERS OF THE EVESR REACTOR

Type	Heterogeneous, light-water-moderated, thermal-neutron, steam-cooled
Power, Mw(t)	12.5 (initial)
No. of fuel elements	32
Process tubes/fuel element	9 (3 by 3 array)
Cladding	Incoloy, Inconel, S.S. 304 (commercial), S.S. 304VM, S.S. 310VM
Maximum cladding-surface temp., °F	1250

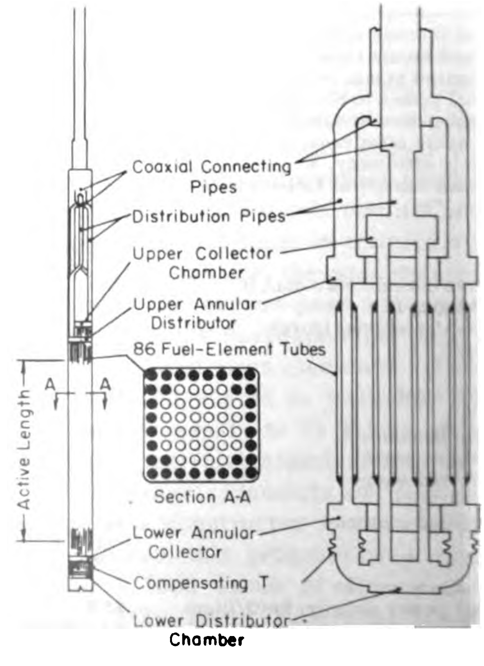

Fig. III-4 Schematic of the Kahl superheating-reactor fuel element.[2] ○, *up pass.* ●, *down pas*

heating, and Fig. III-7 shows the cross section of the "large" core. The reactor is controlled by 31 movable assemblies for reactivity compensation and 6 safety assemblies. These appear to be similar in design and operation to those employed in the WWER, and their positions are illustrated in Fig. III-7. The follower employed in the safety assemblies is a zirconium scatterer, however, and is not fueled.

Table III-3 CHARACTERISTICS OF THE RUSSIAN INTEGRAL SUPERHEATING REACTOR

Pressure-vessel size	
Outside diameter, m	3.8
Height, m	11.0
Boiler fuel-assembly details	
Fuel	UO$_2$
Cladding	Zr alloy
Cladding outside diameter, mm	10.2
Cladding thickness, mm	0.6
Fuel-element geometry	Hexagonal
Distance across flats, mm	176
No. of fuel pins/assembly	127
Fuel-pin pitch, mm	15.1
Superheater fuel-assembly details	
Fuel	UO$_2$
Cladding	S.S.
Cladding outside diameter, mm	~10.2
Cladding thickness, mm	0.5
Fuel-element geometry	Hexagonal
Distance across flats, mm	176
No. of fuel pins/assembly	61
Steam-flow-channel width, mm	1
Insulating material	Stagnant steam

	Large core	Small core
Power, Mw(t)	250	150
Core dimensions		
Diameter, m	2.6	1.8
Height, m	2.0	2.0
No. of fuel assemblies in the core	181	85
Boiling zone	109	
Superheater zone	72	
UO$_2$ loading in the core, tons	19.3	11.4
Boiling zone	14.6	
Superheater zone	4.7	
Water-to-uranium ratio		2.0
Boiling zone	1.5 to 2.0	
Superheater zone	3.0 to 3.5	
Balance of reactivity, % k_{eff}		
Temperature effect (to 309°C)	2.4	3.5
Steam generation (for average steam fraction)	2.0	Up to 3.5
Doppler effect	1.6	2.0
Xenon and samarium poisoning (in equilibrium state)	4.2	4.7
Fuel burnup	5.7	5.3
Structural elements	1.0	2.5
Total reactivity excess in a cold clean reactor	17.0	21.5
Worth of control devices in a cold reactor, % k_{eff} including:		
Absorbers with mechanical drives	19.0	24.0
Liquid poison	20.0	20.0
Maximum fuel-element heat flux, kcal/(m^2)(hr)	1.2×10^6	1.2×10^6

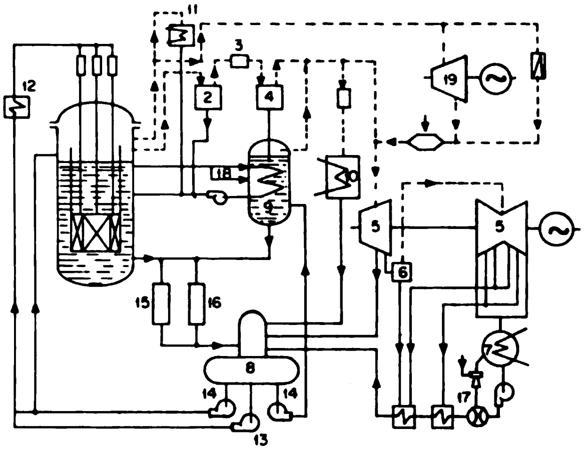

1 Reactor
2 High-Pressure Separator
3 Throttle Valve
4 Mean Pressure Separator
5 Saturated-Steam Turbine
6 Moisture Separator
7 Turbine Condenser
8 Deaerator
9 Steam Generator
10 Auxiliary Condenser
11 Shutdown Cooling Condenser
12 Heat Exchanger
13 Plunger Pump
14 Feedwater Pumps
15 Water-Purifier Evaporating Unit
16 Ion-Exchange Filter
17 Turbine Jet
18 Steam-Generator Feed Line with Step Evaporation
19 Superheated-Steam Turbine

Fig. III-5 Principal flow diagram of the Ulyanovsk plant.[3]

The two-pass superheating fuel element is illustrated in Ref. 3, but the print is of poor quality, at least in the copy seen by this reviewer. Figure III-8 approximates the fuel-pin design, however. The reactor is designed to utilize natural circulation. Construction apparently was well under way when downcomer entrainment was discovered to be a serious design consideration for boiling-water reactors, and according to Ref. 3 the downcomer entrainment will be 10 to 20%.

Consideration of Fig. III-6 indicates that the high downcomer velocity comes about primarily because of the placement of the reactor chimney around the entire core. The BONUS reactor, which is similar in a number of respects to the Russian design, has the core cage around the boiling zone only, and the downcomer velocities are low in the zone of steam-water separation.

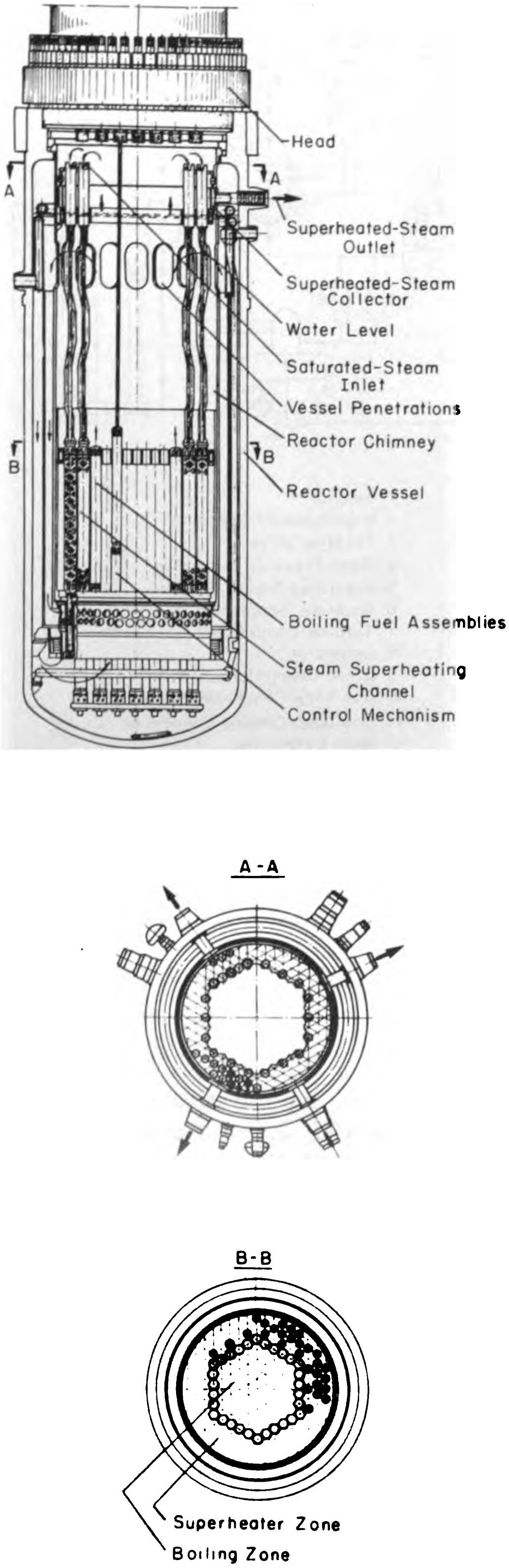

Fig. III-6 General view of the Ulyanovsk steam superheating reactor.[3]

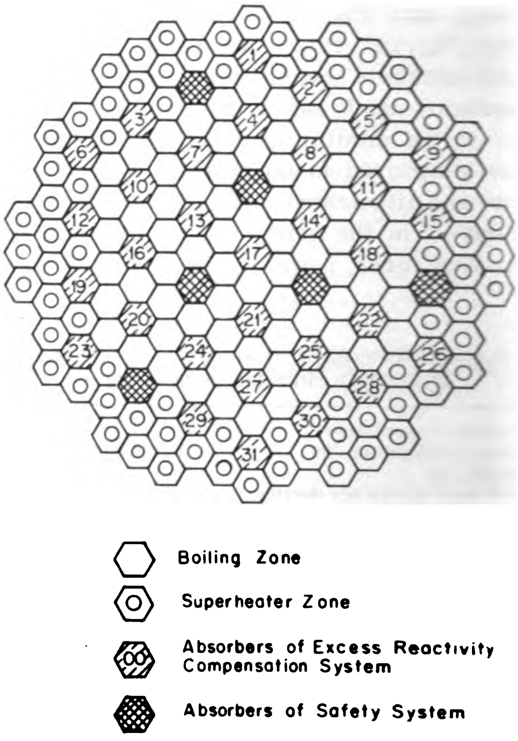

Fig. III-7 Fuel-assembly arrangement in the core of the Ulyanovsk superheating reactor.[3]

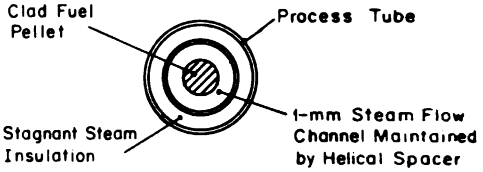
Clad Fuel Pellet
Process Tube
Stagnant Steam Insulation
1-mm Steam Flow Channel Maintained by Helical Spacer

Fig. III-8 Cross section of superheater fuel element in the Ulyanovsk reactor.

Directions of Future Developments

Since no extensive operating experience has yet been gained with a pressure-vessel superheating reactor, it is difficult to comment on the performance of the concept as a whole, much less to predict future trends. In the United States a very considerable effort has been committed to the development of the reactor type, and both integral and separate designs have been constructed. The attention of the reader is directed to the superhea write-up in the Summer 1964 issue of *Power Reactor Technology*, 7(3): 310-312, for a discussion of some of the pertinent problems pertaining to nuclear superheat with integral reactors. With the exception of the nuclear coupling of the boiling-superheating portions of the core, the separate superheat concept exhibits qualitatively the same problems as the integral designs, although the steam-water separation problem may be somewhat different, and presumably more control can be exercised over the conditions of the steam fed to the superheating elements.

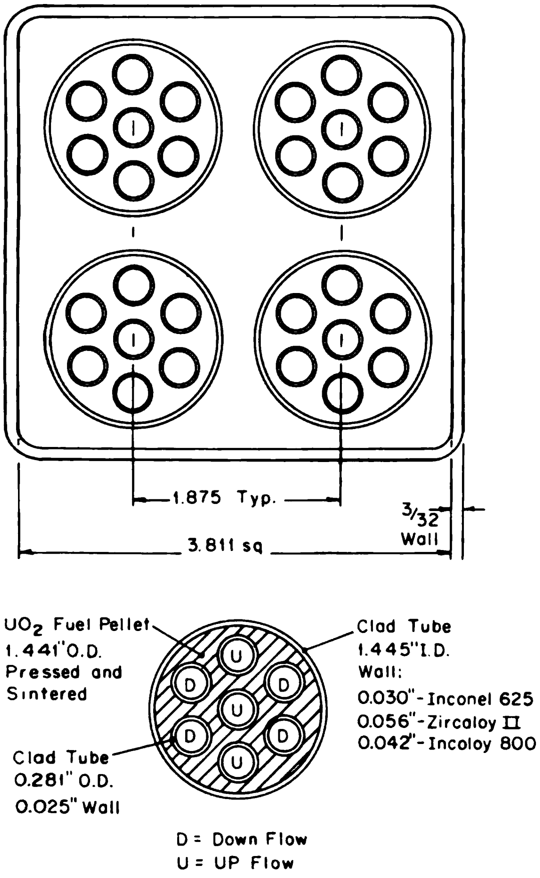

Fig. III-9 Typical fuel-assembly cross section for pelletized fuel in the second core of the BONUS reactor.[4]

The combination boiling-superheating fuel used by the German designers has been discussed previously. A similar principle is being used for the second core of the BONUS reactor,[4] and a typical fuel element is shown in Fig. III-9. The figure shows a design utilizing pelletized fuel, but vibratory compaction is also being considered.

References

The references that contain A/Conf. numbers are papers that were presented at the Third United Nations International Conference on the Peaceful Uses of Atomic Energy, Geneva, September 1964.

1. M. Novick, R.E. Rice, C.B. Graham, D.H. Imhoff, and J. M. West, Developments in Nuclear Superheat, A/Conf.28/P/215.
2. H. Kornbichler, Superheat Reactor Development in the Federal Republic of Germany, A/Conf.28/P/535.
3. I. N. Sokolov, V. I. Gritskov, P. N. Bogdanovich, E. V. Kulikov, S. A. Skvortsov, V. P. Spasskov, V. I. Plutinsky, I. A. Philateyev, and A. A. Hohlachev, Experimental Pressure Vessel Reactor for Studies in Boiling and Steam Superheating, A/Conf.28/P/306.
4. J. F. Gibbons, Objectives and Mechanical Design Features of the Advanced BONUS Fuel, in Proceedings of the Ninth Nuclear Superheat Meeting, April 21, 22, and 23, 1964, San Jose, California, USAEC Report SAN-8003, San Francisco Operations Office, June 30, 1964.

Section
IV
Power Reactor Technology

Graphite-Moderated Superheating Reactors

The existing reactor of the graphite-moderated superheating type is located at the Beloyarsk power station of the USSR. The reactor (called hereafter Bel-1) has been in operation since May 1964, generating electricity at reduced power. A second reactor of this type (called Bel-2) is currently being built at the same site. For the future outlook and the status of the graphite-moderated reactor to be understood, it is necessary to examine the early history of the Bel-1 plant.

The basic design of the Bel-1 type fuel element was established with the First Atomic Power Station (FAPS).[1] The fuel element for the FAPS reactor is shown in Fig. IV-1. In FAPS the coolant was pressurized water, although this same type of element was also operated under boiling conditions and was used in a test loop to superheat steam.[2] The FAPS element was fueled with 5% enriched uranium alloy. The center tube was unfueled, and the uranium was canned as shown. All the tubes in the fuel channel were made of the Russian steel "1X18H9T," which is similar to the AISI 321 stainless steel.[3] Dimensions of the various tubes are given in Table IV-1. The tubular spirals at the upper end of the FAPS element allow for relative movement between the central tube and the assembly of peripheral tubes. This would be particularly important if the element were used for superheating since the central tube wall would run at a temperature somewhat above saturation and the peripheral tube would operate at a temperature approximating the superheated-steam outlet temperature. The peripheral tubes, the fuel, and the outer cladding can operate as a unit; i.e., when the peripheral tubes expand, the fuel and the outer tube can move relative to the graphite surrounding the fuel tubes.

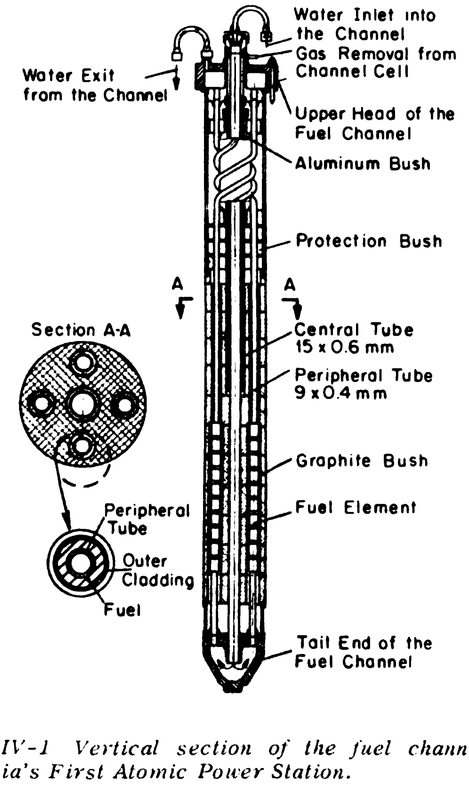
Water Inlet into the Channel
Gas Removal from Channel Cell
Water Exit from the Channel
Upper Head of the Fuel Channel
Aluminum Bush
Protection Bush
A
A
Section A-A
Central Tube 15 x 0.6 mm
Peripheral Tube 9 x 0.4 mm
Graphite Bush
Peripheral Tube
Fuel Element
Outer Cladding
Fuel
Tail End of the Fuel Channel

Fig. IV-1 Vertical section of the fuel channel in Russia's First Atomic Power Station.

Table IV-1 DIMENSIONS OF THE FAPS FUEL-ELEMENT COMPONENTS

Item	Diameter, mm	Thickness, mm
Central tube	15	0.6
Peripheral tube	9	0.4
Outer cladding	14	0.2

The fuel element used in Bel-1 is similar to the FAPS design (Fig. IV-1) except that the temperature-compensating coils are located at the bottom of the element.[4,5] Reference 4 is the Second Geneva Conference paper on the design of Bel-1, and Ref. 5 is the Third Geneva Conerence paper on the development of both Bel-1 nd Bel-2. In addition, the peripheral steam ube in Bel-1 was changed in size with respect o FAPS, so that it had a diameter of 9.4 mm nd a thickness of 0.6 mm with an outer cladding diameter of 20 mm. The change in location f the expansion coils is not explained, and, in act, they are placed back at the top of the element in the Bel-2 fuel-element design. The el-2 design will be discussed shortly. Instead f four peripherally located fuel elements, the el-1 fuel has six, all fed by a central tube. he same size and type of element is used for oth boiling and superheating in Bel-1, but he materials may be different in the two pplications.

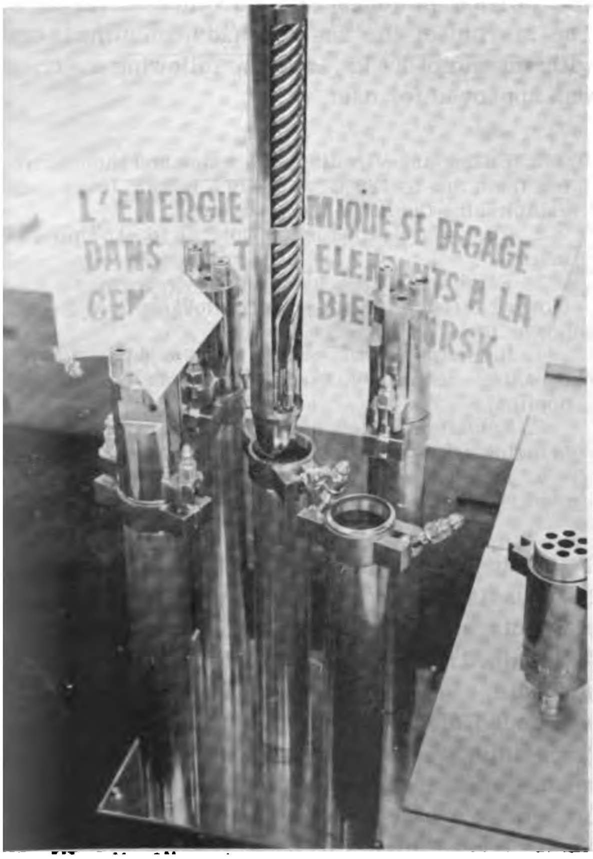

Fig. IV-2a The Bel-1 fuel element on display at the Russian Geneva exhibit. The photograph shows the lower end of a fuel element positioned over a process tube. The mockup shows adjacent process tubes, although for some reason they do not match, positionwise, the holes in the graphite logs. The light-colored blocks shown surrounding the assembly probably simulate the loading face of the reactor, although in the actual plant they are positioned above the location shown in the photograph.

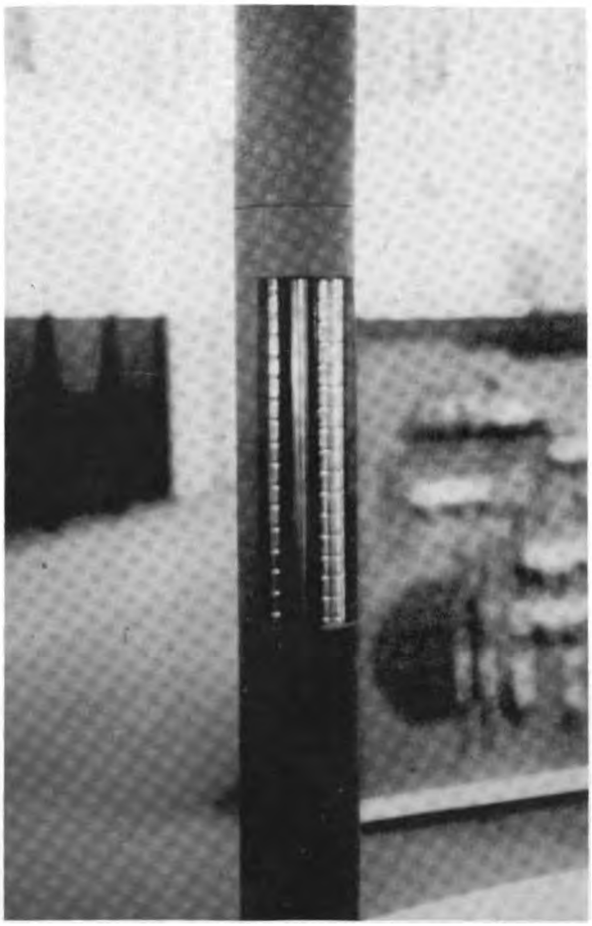

Fig. IV-2b The Bel-1 fuel element showing the upper portion of the compensating coils. The horizontal spacer shown is the same one located at the top of Fig. IV-2a.

Figures IV-2*a*, IV-2*b*, and IV-3 are photographs, taken by the reviewer, of the Bel-1 fuel element on display at the Russian exhibit in Geneva. The compensating coils are shown in Fig. IV-2*b*, and Fig. IV-3 is a cutaway of the fuel element in the uranium-bearing region. Figure IV-3 shows that the outer cladding is dimpled with circular indentations. Although the reasons for these indentations are not given in the references, it is presumed that they assist in giving axial support to the fuel and also act as bellows. There is a thermal-stress design problem arising from a difference in temperature between the inner and outer cladding tubes of the fuel annulus, which are welded together at their ends to contain fission gas. The inner cladding tube is steam cooled, whereas the outer cladding presumably is not. The

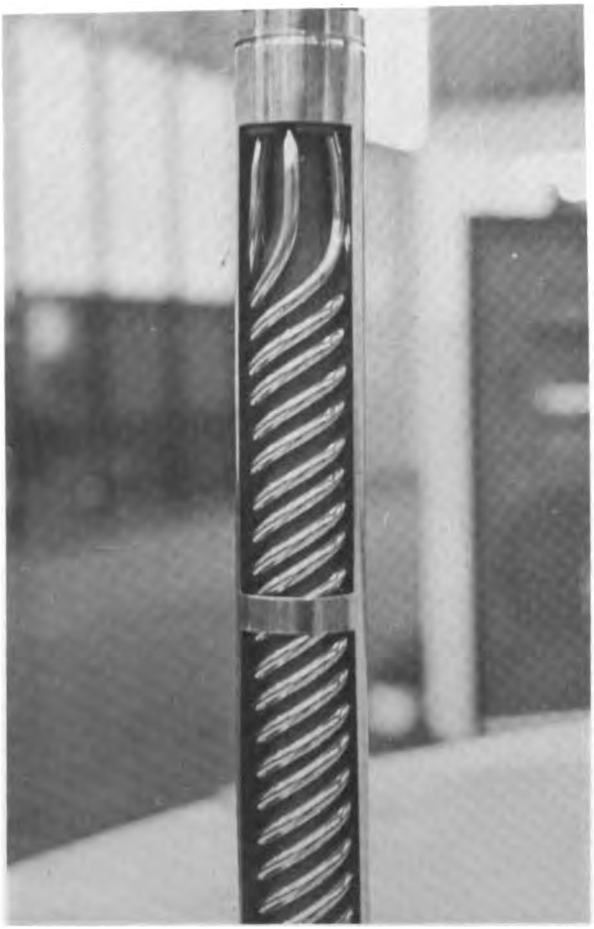

Fig. IV-3 The Bel-1 fuel element illustrating a cutaway view of the fueled region. Three peripheral superheating subelements are shown with the center one being sectioned to illustrate the fuel (dark, vertical portions) and internal cladding surface (shiny, vertical portion). The tubes at the left and right show circumferential indentations, probably for expansion.

fuel is a dispersion of uranium-molybdenum alloy in a magnesium matrix. The evaporating-channel characteristics for Bel-1 and FAPS are listed in Table IV-2, and Table IV-3 lists the superheating-channel characteristics.

An interesting feature of Bel-1 is that the steam to be superheated is not generated directly in the reactor but in a separate steam generator using the indirect-cycle principle. Details are shown in Fig. IV-4.

The permanent structure of the reactor consists of a graphite stack that has a diameter of 9.6 m and a height of 9.0 m. The basic building block is a 200- by 200-mm graphite log penetrated by an axial hole. The core contains 730 boiling assemblies, 268 superheating assemblies, 78 compensating control rods, 16 safety rods, 6 automatic control rods, 2 counting-chamber assemblies, 4 starting-chamber assemblies, and 30 ionization-chamber assemblies, for a total of 1134 core positions. Coolant conditions are given in Table IV-4.

Bel-1 achieved criticality in September 1963, and initial loadings were with boiler-only fuel, both flooded and voided. A full core was loaded for critical experiments. This consisted of 500 evaporating elements enriched to 2%, 230 evaporating elements enriched to 1.5%, and 268 superheating elements enriched to 1.5%. According to Ref. 6, only 64 boron-steel compensating rods were used, however. A number of physics experiments were conducted with Bel-1, and these included power distributions, rod worths, power split, and void coefficients. The startup of the reactor had been simulated with the aid of FAPS,[2] and the following method was approved for use:

1. Filling the circuits with water and then heating them up to 180°C at 5–10% power level and establishing the level in the bubbler.
2. The plant heating up to 230°C at 10–15% power level.
3. Establishing the level in the evaporators and blowing through the superheating channels at 2-[illegible] power level.
4. Raising reactor power level to 20% and increasing secondary circuit pressure up to [illegible] nominal.
5. Establishing the level in separators, i.e. bringing primary coolant to boiling.
6. Feeding steam to the turbine and further power rising.

To study this process with the Bel-1 reactor, the Russians removed all but two superheater elements and the startup procedure previously determined with FAPS was checked and found adequate. Voiding the superheating elements was found to take about 6 min and to proceed "smoothly." A total of 192 superheating elements were loaded, and the reactor was then brought to power to study voiding of this relatively large number. These results are indicated in Fig. IV-5. The "scavenging" operation mentioned in the figure apparently refers to the injection of a solution of hydrazine hydrate into the secondary circuit to control oxygen concentration. On Apr. 26, 1964, steam was fed to the turbine, but, since less than the normal number of superheating elements were still being used (192), the superheat temperature reached only 390°C (734°F). Future [illegible] called

Table IV-2 EVAPORATING-CHANNEL CHARACTERISTICS[5]

	FAPS reactor	Bel-1 reactor	Bel-2 reactor Zone I	Zone II	Zone III	Zone IV	Zone V
Channel power, kw	300	405	771	634	617	545	517
Coolant flow rate through the channel, kg/hr	2500	2400	5500	4700	4150	3550	3250
Steam void at channel outlet, %		33.6	27.6	29.3	30.5	32.1	34.2
Pressure at channel inlet, atm	100	155			155		
Pressure at channel outlet, atm	98	150			145		
Coolant temperature at channel inlet, °C	200	300			300		
Coolant temperature at channel outlet, °C	290	335			338		
Maximum thermal load, kcal/(m²)(hr) (× 10^{-6})	1.8	0.5	0.8	0.7	0.6	0.5	0.5
Circulation rate, m/sec	4	3.5	4.6	4.0	3.5	3.0	2.7
Maximum temperature, °C							
Tube inner wall	324	355			365		
Fuel	382	400			415		
Ratio of burnout heat flux to maximum heat flux		2	1.85	1.9	1.9	2.0	1.95

Table IV-3 SUPERHEATING-CHANNEL CHARACTERISTICS[5]

	Bel-1 reactor	Bel-2 reactor	
Maximum channel power, kw	368	767	
Minimum channel power, kw	202	548	
Steam flow rate through maximum power channel, kg/hr	1900	3600	
Steam flow rate through minimum power channel, kg/hr	1040	2,570	
		Bel-2 downstream fuel elements*	Bel-2 upstream fuel elements*
Channel inlet pressure, atm	110	132	124
Channel outlet pressure, atm	100	125	110
Channel inlet steam temperature, °C	316	328	397
Channel outlet steam temperature, °C	510	399	508
Maximum thermal load, kcal/(m²)(hr) (× 10^{-6})	0.48	0.83	0.68
Maximum steam velocity, m/sec	57	76	112
Maximum temperature, °C			
Tube inner wall	530	426	531
Fuel	550	482	565
Graphite	725	735	

*The terms "downstream" and "upstream" apparently should have been translated "downflow" and "upflow," respectively. Obviously the downstream element is the first-pass element, and the upstream element is the second-pass element.

or the addition of more superheat elements to ncrease the steam temperature to about 500°C.

The future plans for the reactor type introduce the reader to the second Beloyarsk reactor, Bel-2. The graphite stack for this reactor is similar to Bel-1 with respect to size and number of channels, but the second reactor should produce 200 Mw(e). This factor of 2 increase in power is startling at first consideration, but its explanation is reasonably straightforward. The coolant cycle has been changed from indirect boiling to direct boiling, as shown in Fig. IV-6. Two possible arrangements are being considered and are shown as parts *a* and *b* in the figure. The difference between the two cycles is the presence (see part *a* of Fig. IV-6) of a bypass line that allows some of the feedwater to be injected into the steam sepa-

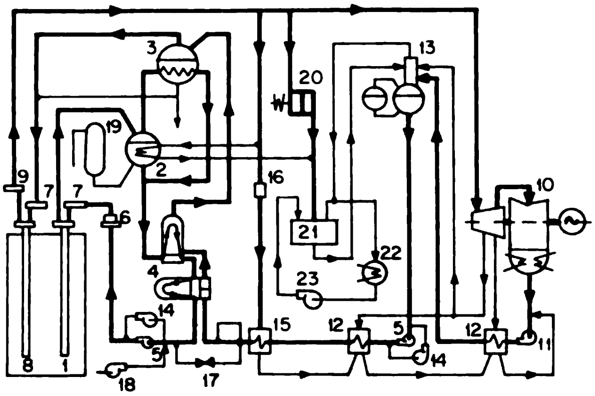

1 Evaporating Channel
2 Steam Drum
3 Evaporator
4 Preheaters
5 Circulating and Feed Pumps
6 Distributing Collector
7 Group Collectors
8 Steam Superheating Channel
9 Superheated-Steam Collector
10 Turbogenerator
11 Condensate Pump
12 Regenerative Preheaters
13 Deaerator
14 Emergency Circ. and Feed Pumps
15 SH Steam Temperature Regulator
16 Fast Oper. Reducing-Cooling Plant
17 Feed Valve
18 Makeup Pump
19 Pressure Compensator
20 Unit of Reducing and Safety Valves
21 Bubbler
22 Process Condenser
23 Process Condenser Pump

Fig. IV-4 Flow sheet of the first unit of the Beloyarsk Nuclear Power Station.[6]

rator after it has passed through the regenerative heater designated as the "steam-generator heater." This is said to be used for "steam washing," but its significance is not readily apparent. Besides the cycle change between Bel-1 and Bel-2, the elements of the latter are to be constructed with slightly larger coolant channels. These details are shown in Table IV-5.

Probably the most significant change between the two reactors is the superheater fuel for Bel-2. Just how the UO_2 is to be used in the Bel-2 superheater elements is not clear; the single mention of UO_2 in Ref. 5 is an offhand one, as follows:

> Upstream superheating elements design and dioxide uranium-based fuel ensure steam superheating up to 500°C; this is confirmed by loop-tests on the first power plant reactor.

On the basis of Table IV-3, we assume that the intent is to substitute UO_2 for the uranium-molybdenum alloy in the dispersion type element, for the maximum fuel temperature listed is far lower than that which would characterize a solid oxide fuel body. It is disappointing that the information on the details of the Beloyarsk elements is so limited, for it is this aspect of the reactor which is probably of greatest interest to designers outside the USSR.

The mechanical design of the Bel-2 superheater elements has also been changed from that of Bel-1. The central, unfueled tube feeding steam to the peripheral channels in the Bel-1 element has been removed and the element converted to two-pass design. These details are shown in Fig. IV-7. As a result the steam velocity is greatly increased, from 57 to 112 m/sec (Table IV-3), and the improved heat-transfer coefficient allows an increase in power. In place of the central tube, an absorber pin is included in the Bel-2 element. These absorbers, which probably are manually manipulated, make possible a reduction of the radial power-peaking factor for the core to 1.3, compared to a value of 1.4 in Bel-1 (see Ref. 5). The evaporating elements for Bel-2 retain the center tube for coolant flow. The increase in power from the boiling portion of the core appears to be the result of rather careful zoning

Table IV-4 MAIN CHARACTERISTICS OF THE REACTOR COOLANT IN THE BELOYARSK NUCLEAR POWER STATION

Characteristics		
Reactor thermal output, Mw	286	
Electrical output, Mw	100	
Ratio of superheating- to evaporating-channel output, %	30.0	
	First circuit	Second circuit
Coolant flow rate, tons/hr	1200	405
Coolant pressure, atm		
At reactor inlet	155	110
At reactor outlet	150	95
Before the turbine	150	90
Coolant temperature, °C		
At reactor inlet	300	316
At reactor outlet	340	510
Before the turbine	340	500
Average steam quality at channel outlet, wt.%	33.6	

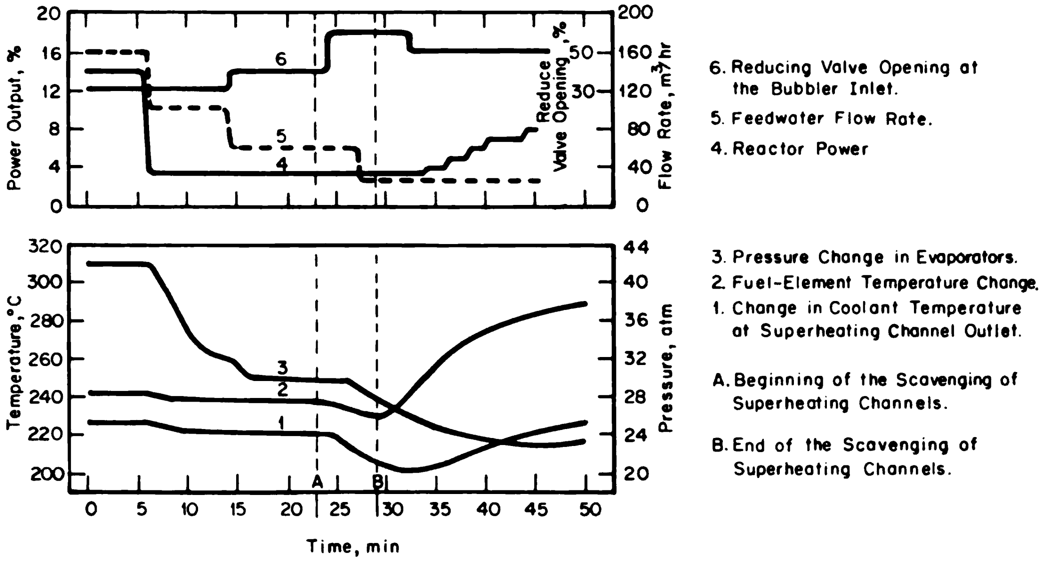

Fig. IV-5 Curves of changes in the main parameters of the plant during transition to steam superheating conditions.[6]

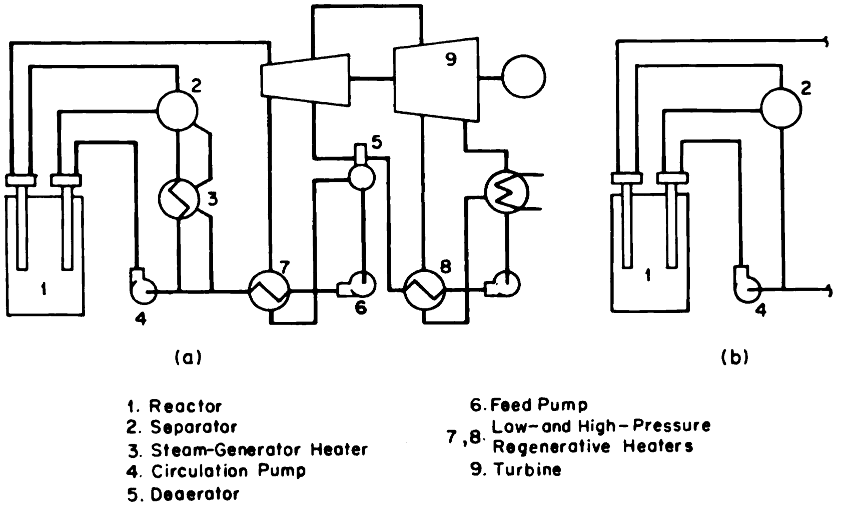

Fig. IV-6 Possible flow sheets for uranium-graphite tube type nuclear superheat reactors.[5]

Table IV-5 COMPARISON OF BEL-1 AND BEL-2 BOILING AND SUPERHEATING FUEL ELEMENTS

	Bel-1	Bel-2
Boiler and superheater fuel-element peripheral-tube diameter/thickness, mm	9.4/0.6	12/0.6
Fuel material		
Boiler element	U-Mo-Mg	U-Mo-Mg
Superheater element	U-Mo-Mg	UO_2

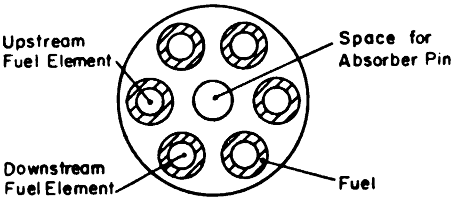

Fig. IV-7 U-shaped superheating channel cross section.[5]

of the reactor to match flow and power of the boiling assemblies. The results are indicated in Table IV-2.

The step beyond Bel-2 is stated to be supercritical operation. The tube type Beloyarsk reactors are suited to this type of operation because the pressure-bearing portions of the reactor are of small diameter. Even so, the cladding begins to get quite thick for supercritical-pressure operation, with attendant thermal-stress problems during transients. It is estimated in Ref. 5 that the Bel-1 and Bel-2 reactor size could be made to produce 800 to 1000 Mw(e) if a supercritical, once-through design were possible. It is also suggested that an advanced reactor be operated with partially unclad fuel to remove fission gas and reduce the amount of steel in the core. This would be accomplished by removing the outer cladding tube, although relative movement of the coolant tube with respect to the graphite would have to be provided for.

References

The references that contain A/Conf. numbers are papers that were presented at the Third United Nations International Conference on the Peaceful Uses of Atomic Energy, Geneva, September 1964.

1. N. A. Dollezhal, A. I. Krasin, N. A. Nikolayev, A. N. Grigoryants, and G. N. Ushakov, Operating Experience with the First Atomic Power Station i USSR and Its Use Under Boiling Conditions, *Pr ceedings of the Second United Nations Internati Conference on the Peaceful Uses of Atomic Ener Geneva, 1958,* Vol. 8, pp. 86-99, United Natio Geneva, 1958.
2. G. N. Ushakov, L. A. Kochetkov, V. G. Konoch V. S. Severjanov, V. Y. Kozlov, O. A. Sudnits N. T. Belinskaja, P. N. Slusarev, and V. A. Ivan Operational Experience of the First Atomic Po Station As An Experimental Set-Up, A/Conf.28 314.
3. General Electric Company, Hanford Works, Ste Cooled Power Reactor Evaluation—Beloyar (URAL) Reactor, USAEC Report HW-67573, A 1961.
4. N. A. Dollezhal, A. K. Krasin, P. I. Aleshchen A. N. Galanin, A. N. Grigoryants, I. Ya. Emelyan N. M. Kugushev, M. E. Minashin, U. I. Mitya B. V. Florinsky, and B. N. Sharapov, Uraniu Graphite Reactor with Superheated High Pressur Steam, *Proceedings of the Second United Natio International Conference on the Peaceful Uses Atomic Energy, Geneva, 1958,* Vol. 8, pp. 398-41 United Nations, Geneva, 1958.
5. N. A. Dollezhal, I. Ya. Emelyanov, P. I. Aleshch kov, A. D. Zhirnov, G. A. Zvereva, N. G. Morgun U. I. Mityaev, G. D. Knywseva, K. A. Kryukov, V. Smolin, L. I. Lunina, V. I. Kononov, and V. Petrov, Development of Superheating Power Re tors of Beloyarsk Nuclear Power Station Typ A/Conf.28/P/309.
6. A. N. Grigoryants, V. P. Nevskii, L. A. Kochetk B. G. Ivanov, P. I. Aleshchenkov, A. G. Phylipp B. G. Dubovskii, M. E. Minashin, M. A. Altshuller and L. V. Konstantinov, Start-Up and Pilot Operation of the First Unit of the Beloyarsk Nucle Power Station After I. V. Kurchatov, A/Conf.28 P 308.

Section

V

Power Reactor Technology

Heavy-Water-Moderated Pressure-Tube Reactors

The effort on heavy-water-moderated pressure-tube reactors throughout the world is indicated in Table V-1. The Canadian effort is by far the largest and the farthest advanced. The two Canadian power reactors, NPD and CANDU, are both cooled and moderated by D_2O, are fueled with natural UO_2 clad with Zircaloy-2, and employ calandria tanks to contain the moderator. The calandria tubes of NPD are aluminum, whereas those of CANDU are nickel-free Zircaloy-2. Design features of NPD are given in Ref. 1, and those of CANDU, in Refs. 2 and 3.

Until the recent announcement[4] of a program directed toward the development of a 300-Mw(e) organic-cooled plant, there had been no definite plans for a large-scale heavy-water reactor in the United States. Nevertheless, the U. S. effort has been considerable and has resulted in the construction of a 17-Mw(e) prototype (the Carolinas-Virginia plant, CVTR), as well as a reactor that operates at comparable temperatures and thermal-power levels for plutonium-recycle development (the Plutonium Recycle Test Reactor) and a reactor for developing fuel elements for D_2O power reactors (the Heavy Water Components Test Reactor). All these reactors are cooled and moderated by heavy water. The Carolinas-Virginia reactor was described in *Power Reactor Technology,* 6(4): 63-81; the most recent general review of heavy-water reactors was in 7(1): 85-98.

Interest in heavy-water-moderated reactors is also high in other countries, but there is considerable diversity in the choice of coolant. The Steam Generating Heavy Water Reactor (SGHWR)[5–8] utilizes boiling light water, the DON reactor uses organic coolant,[9–11] whereas EL-4 (Refs. 12 to 15) and the Lucens reactors[16–18] are cooled with CO_2. Of the reactors under study or development, the DOR,[19,20] the R-1 and R-2, (Ref. 21), and the U. S. project[22] are all designed to be organic cooled. The German reactor study involved gas cooling.[23] In addition to these power reactors, at least two test reactors are being constructed to study the problems arising from organic cooling. These are the Canadian WR-1, reviewed in the Summer 1964 issue of *Power Reactor Technology,* 7(3): 324-327, and the ESSOR.[24]

Operating Experience

Extensive operational experience has been reported[25,26] for the NPD reactor. Reference 25 contains information on reactor physics aspects of the startup. Various reactivity coefficients were determined, including the moderator-level coefficient of reactivity, reflector reactivity worths, and temperature coefficients of reactivity. The reactivity balances at two different points in the lifetime are shown in Table V-2.

As is indicated in Table V-2, the sources of reactivity adjustment, other than fuel management, are quite limited, consisting only of changes in moderator level and moderator temperature. The normal NPD fueling operation consists of inserting a bundle in one end of a pressure tube, thereby shifting all the bundles within the tube by one bundle length and expelling the last bundle. This bundle may then be either discharged or recycled in a channel fueled in the opposite direction. This operation was studied by means of a computer code simulating the reactor, STOKE, which calculated the burnup of all fuel bundles by increments, taking fuel shifts into account. The code was designed to select the best shift for the current state of the reactor, consistent with the particular refueling scheme being studied. The original NPD loading consisted of natural and depleted UO_2. The fuel-management principle consisted of shifting fuel in the channel containing the bundle with the highest burnup and recycling an expelled bundle

Table V-1 D_2O-MODERATED PRESSURE-TUBE REACTORS

Reactor	Country	Status*	Mw(e)	Coolant	Fuel and geometry	Cladding	Core type	Pressure tube	Core orientation	No. of refueling machines	Refueling method	Pressure-tube joints
NPD	Canada	Operational	19.5	D_2O (*l*)	UO_2, rod cluster	Zircaloy-2	Calandria	Zircaloy-2	Horizontal	2	On-power	Expanded
CANDU	Canada	Being built (1965)	203	D_2O (*l*)	UO_2, rod cluster	Zircaloy-2	Calandria	Zircaloy-2	Horizontal	2	On-power	Expanded
CVTR	U. S.	Operational	17	D_2O (*l*)	UO_2, rod cluster	Zircaloy-4	Cold U tubes	Zircaloy-4	Vertical	1	Shutdown, depressurized	Conoseal gasket
SGHWR	England	Being built (1967)	100.0	H_2O (boil)	UO_2 rod cluster	Zircaloy-2 (boiler), S.S. (superheater)	Calandria	Zircaloy-2	Vertical	1	On-power	Expanded
EL-4	France	Being built (1967)	70	CO_2	UO_2	S.S. or Be	Cold tube	Zircaloy-2	Horizontal	2	On-power	Threaded and brazed
DON	Spain	Planned	30	Organic	UC, rod cluster	Finned SAP	Calandria	SAP	Vertical	1		Hot rolled and/or diffusion bonded
Lucens	Switzerland	Being built (1966)	13	CO_2	U–1% Cr	Mg–0.5% Zr	Calandria	Zircaloy-2	Vertical	1 plus a locking machine	Shutdown, depressurized	
DOR	Denmark	Study	235	Organic	UO_2 or UC	SAP	Calandria	SAP	Vertical	1		
R-1	Russia	Study	500	Organic	Beta-U	Mg-Be	Calandria	SAP	Vertical	Probably 1		
R-2	Russia	Study	500	Organic	UO_2		Calandria	SAP	Vertical	Probably 1		
OCHWMPR	U. S.	Study	512	Organic	UO_2	SAP	Cold tube	SAP-lined Zircaloy-2	Vertical	1		
AKB	Germany	Study	100	CO_2	UO_2 or UC	Steel, Zr or Be alloys	Cold tube	Zr-Cu-Mo-lined	Vertical	1		

*The year in parentheses is the probable completion date.

Table V-2 CHANGES IN REACTIVITY BALANCE WITH IRRADIATION[25]

	Reactivity effect in unirradiated core, m*k*	Reactivity effect in irradiated core (230 full-power days), m*k*
Leakage at full tank	−71	−69
Control margin*	−2.8	−0.3
Depleted fuel†	−23	0.0
H_2O in D_2O (relative to 100% D_2O)	−10	−27.0
Xenon	−23.9	−24.1
Samarium	0.0	−8.1
Moderator temp. (21–60°C)	−2.8	+0.4
Coolant temp. (21–254°C)	−7.4	−2.6
Power (fuel temp.)	−3.1	−1.4
Total reactivity load	144	132
Fuel burnup		12

*Operating moderator level is below full tank by amounts shown.

†Depleted fuel removed prematurely.

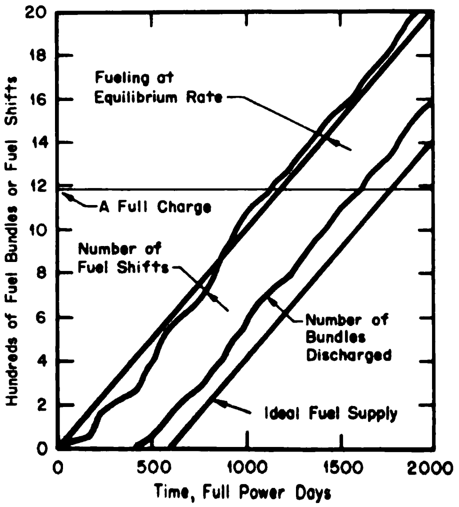

Fig. V-1 Simulation of NPD fueling, assuming that the fuel is recycled if the exit burnup is less than half the equilibrium burnup.[25]

it contained natural uranium and had a burn- less than a specified fraction of the burnup the discharged fuel at equilibrium. The mulation of the NPD fueling, assuming re- cle if the exit burnup was less than half the quilibrium burnup, resulted in the data shown Fig. V-1. This figure predicts the number fuel shifts and number of bundles discharged nd fed), assuming the NPD starts from its itial arrangement of partially depleted fuel. practice, however, the NPD ran with de- leted uranium fuel from its initial criticality April 1962 to December. At that time the oderator and coolant became contaminated ith light water, as will shortly be discussed, nd the depleted fuel was removed to compensate r the resulting reactivity loss.

The degrading of the D_2O was caused by a ajor leak at the seal between the fueling achine and the pressure tube the first time n-power fueling was attempted. The spilled eavy water was downgraded from 99.7 to 9.1% D_2O and was contaminated by oil and rout. An upgrading program was initiated, and e purity was about 99.6% as of the writing f Ref. 26. The reference also states that loss nd downgrading of the moderator have been egligible and that practically all D_2O losses nd downgrading have come from the heat-ransport system. The following quotation sum-narizes the D_2O loss experience on NPD:[26]

> (a) Low escape rates depend a great deal on quality of the original design and construction.
> (b) Quite high chronic escape rates are acceptable if recovery is efficient i.e. if the "dry-room principle" is followed.
> (c) At a large station, it is not economical to sacrifice capacity factor in order to repair leaks. Consequently, if leaks are bad, recovery is essential.
> (d) There is no valid experience to show that escape rates can be held to extremely low values over long periods of time, without serious loss of capacity factor.
> (e) With efficient recovery, loss rates are virtually independent of escape rates, and can be very low.
> (f) NPD experience has shown that use of vapour-recovery equipment is both feasible and sensible.
> (g) With efficient recovery, the loss rate can be virtually unaffected by station size.
> (h) The "dry-room principle" not only is valuable for the everyday situation, but would have reduced the cost of the acute escape on 3 Dec. 1962 by an order of magnitude.
> (i) D_2O losses can be maintained acceptably low in any station whose design is based on NPD experience, and D_2O escape rates can be significantly reduced.

Fuel and pressure-tube performance have been good. Other than the major failure that occurred during the first refueling attempt—the refueling machines have been subsequently modified to prevent a future occurrence—the fueling-machine experience has been "highly successful."

Significant Features

Fuel and Cladding Materials

In support of NPD, CANDU, and various heavy-water-moderated power-reactor studies, the Canadians presented several important papers on the behavior of fuel and cladding materials.[27–30] Some of the details pertain explicitly to NPD and CANDU type reactors, but others are of general interest to reactor designers. A rather interesting conclusion[27] was that high UO_2 density may not be an important goal for operating fuel elements, since low-density material (less than 10.3 g/cm^3) provides for the retrapping of escaped fission gas. The elimination of the need for a plenum or other space within a fuel element to accommodate fission gases may be an important design consideration for certain fuel elements—particularly for the typical short Canadian elements, since plenums at the ends of the elements tend to cause power peaks in the fuel adjacent to the plenums. Reference 28 details the performance of the NPD and CANDU fuel elements and contains some interesting cost data. On the basis of production experience with the NPD and CANDU fuel elements, it is estimated[28] that the average cost of fuel for a 1000-Mw(e) CANDU type reactor would be $50 per kilogram of uranium ±10%. This results in a fuel cost of about 0.8 mill/kw-hr if the fuel is discarded without reprocessing.

Reference 30 discusses in-pile results for test fuel elements cooled by organics. Test elements were manufactured with sintered-aluminum-product (SAP) cladding containing 7 and 10% oxide (SAP 930 and 895, respectively) and a material apparently from another producer also containing 7% oxide, M 257 or M 583. The rods were designed to be freestanding under coolant pressure (300 psi) and with sufficient diametral fuel-jacket clearance to theoretically produce no diametral sheath strain at operating conditions. This was done because of the inability of SAP to deform plastically. The results of the irradiations are given in Table V-3.

Table V-3 RESULTS OF IRRADIATIONS IN TERPHENYL MIXTURE IN NRX TEST LOOP[30]

	Test 704-I	Test 704-II	Test 709-I	Test 709-II	Test 712	Test 713	Test 714-I	Test 714-II	Test 719	Test 720
Sheath material	M 583	M 583	M 583	M 583	M 257	M 257	SAP 930	SAP 930	Zircaloy-2, Zr – 2½% Nb	SAP 895
Element length, cm	30.5	30.5	61	61	122	122	244	244	50	22
Diametral clearance, cm	0.009 to 0.019	0.019	0.013	0.013	0.015 to 0.018	0.015	0.016	0.016	0.008 and 0.015	0.0025, 0.0050, 0.0075, and 0.0125
Irradiation, full-power days	<1	31.5	63.7	<1	59.3	29	44.6	45.6	82	4
Maximum $\int k\, d\theta$, watts/cm	~38	45.5	37.8	45	36.5	36.5	37.5*	39.9	39	40
Average $\int k\, d\theta$ at flux center, watts/cm		39	35		33.4	34	33.9	38.5	35	40
Average sheath temp., °C	420†	~430†	450	420	470	440	470	470	475	462
Maximum sheath temp., °C	†	†	465	470	496	484	497	525	500‡	462‡
Maximum diameter change, %	§	§	0.3	0.8	0.4	¶	1.5	0.5	1.2	0
Average diameter change, %	§	§	~0	0.3	<0.2	¶	0.5	~0	0.7	0
Average length change, %	§	§	0.03	0.05	0.04	0.04	¶	~0	0.3	0
Burnup at flux center, Mwd/metric ton		1100	2400		2100	1000	1500	1500	2600	130
Fuel-sheath heat-transfer coefficient, watts/(cm)(°C)	¶	¶	~0.4	¶	~0.4	¶	~0.6	¶	¶	¶
Fission-gas release, %	¶	¶	~3	¶	~9	¶	¶	¶	¶	¶
Fouling-film thickness, μm	10 to 500	10 to 1400	40 to 80	<5	<1	¶	<1	<1	<1	<1
Ridge height, μm	**	**	**	**	**	**	40 max.	40 max.	30 av., 60 max.	0
Performance	Failed††	Good	Good	Failed‡‡	Good	Good	Failed§§	Failed§§	Good	Good¶¶

*A transient peak in excess of 40 watts/cm may have existed at the time of failure.

†No sheath thermocouples; temperatures listed are from calculation.

‡Estimated.

§Elements were stored under water and corroded before measurements were made.

¶Not measured.

**Circumferential ridges were observed but not measured in these tests.

††Failure was due to burnout. One element did not have ribs or wire wrap and bowed out and touched the pressure tube. This error was corrected in 704-II.

‡‡709-II contained poor-quality sheathing rejected for use in 709-I. This and the gross overpower are suspected to have led to failure.

§§Failure appeared as stress cracks at the axial center of the elements. The cause of these stress cracks is unknown.

¶¶Diametral-clearance experiment.

Although the causes of the stress cracks (tests 714-I and 714-II) were unknown, the reference notes that sheath strain probably did exist, due to migration of cracks within the fuel until the diametral clearance was eventually transferred to a central void. Evidence of a reaction between UO_2 and SAP was observed, and this was also noted in Ref. 31. The good performance of the zirconium-niobium clad UO_2, illustrated in Table V-3, shows promise for the material, but further experiments were planned to test the hydriding behavior.

References 32 through 34 are concerned with metallurgical problems of other cladding materials. The FeAl40, which is an iron-aluminum alloy containing 40 at.% aluminum, is a possible cladding for EL-4, the French gas-cooled reactor. The material offers possibilities as a substitute for beryllium, although it apparently has low ductility.[32] The reference gives mechanical-property data and discusses welding and corrosion resistance. The magnesium-beryllium alloy described in Ref. 33 probably is the alloy mentioned for the Russian organic-cooled reactor R-1 (Ref. 21), although in Ref. 33 it is presented as a possible cladding for a gas-cooled reactor. Several alloys were considered (Table V-4), in composition ranges similar to the British Magnox alloys.

Table V-4 COMPOSITION OF MAGNESIUM-BASED ALLOYS SUITABLE FOR CLADDING OF GAS-COOLED REACTORS[33]

Type of alloy	Composition of alloys, wt.% (balance Mg)										
	Be	Si	Al	Th	Fe	Mn	Ni	Cu	MgO	Ca	Zr
PMB	From 0.5 to 32		0.01		0.04		0.001	0.005	0.2		
MB-3	0.04	0.5			0.01	0.001	0.001	0.005			
MB-4	0.08 to 0.15	0.7			0.01	0.001	0.001	0.005			
Mg-Al-Be	0.04		0.5		0.01	0.001	0.001	0.005			
Mg-Th-Be	0.04			3	0.01	0.001	0.001	0.005			
Mg-Ca-Zr-Be	0.04				0.01	0.001	0.001	0.005		0.5	0.5

Water Chemistry—Experience with D_2O

A key consideration in the heavy-water-moderated reactor is the technology of the moderator itself, and three papers were devoted to this subject.[35–37] Figure V-2 summarizes French experience with a number of low-temperature D_2O-moderated reactors with respect to moderator degradation. The figure apparently pertains to the situation in which no on-stream upgrading was attempted, with the exception of that shown for EL-3. Soluble poisons dissolved in the D_2O were studied, namely boric acid and the sulfates of cadmium, lithium, and gadolinium. Although the concept appeared feasible, the use of a so-called "gaseous" control rod, composed of ^{3}He, is discussed for application to EL-4.

Canadian experience with the decomposition of D_2O in various reactors is summarized in Table V-5. The NRU and NPD results shown in the table illustrate that increasing acidity and temperature both decrease the equilibrium concentrations of dissolved radiolytic gas. The problem of maintaining a nonexplosive atmosphere in spaces adjacent to the moderator water is not a trivial one and must be considered during reactor design. The NPD reactor moderator chemistry is also complicated by irradiation-formation of nitric acid from nitrogen introduced in air leakage.

Canadian experience in upgrading D_2O is contained in Ref. 37. The various Canadian reactors contain about 200 metric tons of D_2O altogether, and a number of incidents over the years have resulted in the reprocessing of many metric tons of degraded D_2O. The various methods discussed include electrolysis and distillation; distillation is the favored method for on-stream upgrading of reactor moderator because of its flexibility. A significant hazard in handling irradiated heavy water is tritium, the product of neutron capture by deuterium. In the NPD reactor the tritium concentration has reached 1.7 curies/liter and is expected to reach at least 10 curies/liter within a few years. Although the problem can be controlled by design and administrative procedures, it is one which is peculiar to the reactor type. A review of the economics of heavy-water production in the United States is given in Ref. 38.

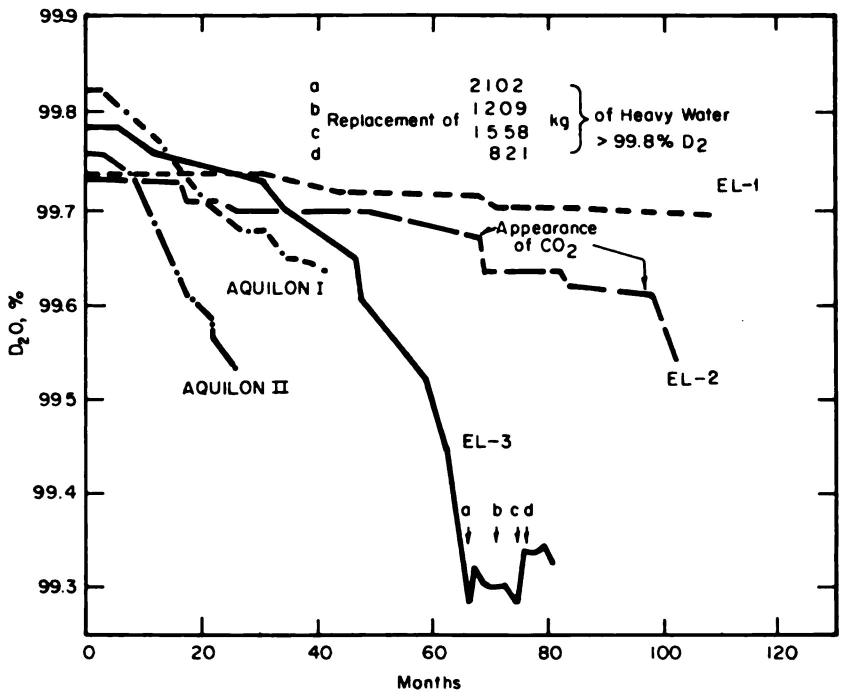

Fig. V-2 Evolution of the isotope content of heavy water in the C.E.A. reactors.[35]

Table V-5 RADIOLYTIC DECOMPOSITION OF HEAVY-WATER MODERATORS[36]

Reactor	Moderator temp., °C	*p*D*	D_2 content of D_2O in core, cm^3/kg	Total gas to recombiner, liters (STP)/min	Water decomposition: Liters of D_2 (STP)/min	Water decomposition: Grams of D_2O/Mw-hr†
NRX	45	~7	1.6	370	0.15	0.2
NRU						
1960-61	50	~7	5	230	6	1.6
1962-63	50	~7	2	230	3	0.8
1963	50	5.7	1	200	1.6	0.4
NPD	80	~6	1.2	280	8.5	5.1
	40	5.5	3.3	700	27	16

*In NRX and NRU *p*D of 7 corresponds to a conductivity of 0.2 megohm/cm (25°C); acidic conditions were due to DNO_3 added to NRU for a two-month experiment and formed in NPD from air in the helium.

†Megawatt-hours of total reactor thermal power; average power densities are 2.6, 5.0, and 1.7 watts/g for NRX, NRU, and NPD, respectively.

Pressure Tubes

Most of the reactors listed in Table V-1 utilize Zircaloy-2 as the pressure-tube material. Two papers were presented dealing with Zircaloy-2 as applied to pressure-tube construction,[39,40] and two papers were concerned with the zirconium-niobium alloy.[41,42]

The pressure tubes in NPD are seamless Zircaloy-2 tubing, fabricated by hot extrusion and cold drawing.[39] Dimensional gauging and borescope examinations were performed on one of the tubes after a year's service in the reactor, and no significant changes were noted. The NPD design stress was chosen as 9.5 kg/mm^2 at 280°C, whereas the CANDU design stress was selected as 11.2 kg/mm^2 at 300°C. Tensile tests on portions of the NPD pressure-tube materials have given the results shown in Table V-6. In the reactor, however, the tubes are biaxially stressed by the combination of transverse and longitudinal loads produced by the pressurized coolant, with the result that the burst strength of the tube is considerably higher than would be predicted from simple tensile-test data; this is an important design consideration.

Table V-6 TENSILE-TEST RESULTS—NPD PRESSURE-TUBE MATERIAL[39]

(Temperature = 280°C)

	Longitudinal properties	Transverse properties
Ultimate strength, kg/mm^2	37.3	35
0.2% yield strength, kg/mm^2	31.6	33
Elongation, %	22.5	21
Reduction in area, %	45	60

The effects of hydrogen pickup by Zircaloy are complicated; they are also important, since the operating lifetime of a pressure tube is expected to be determined by the amount of hydrogen pickup experienced during corrosion. Hydrogen concentrations up to 250 ppm had little effect on mechanical properties of irradiated and unirradiated Zircaloy-2 so long as the hydrides were randomly arranged. These data are shown in Table V-7. It was established that prior strain, fabrication history, and stress were important in determining hydride orientation:[39]

> ... It was found that hydrides precipitated while Zircaloy was under stress, aligned themselves perpendicular to tensile stresses and parallel to compressive stresses and that directional hydrides significantly decreased the mechanical properties of Zircaloy-2 ...

The use of zirconium-niobium alloys as pressure tubes is receiving study in both Canada[41] and the United Kingdom.[42] The advantage of the niobium alloy is in increased strength; properly heat-treated zirconium–2.5 wt.% niobium attains a strength about 50% higher than Zircaloy-2. These data are illustrated in Fig. V-3. The corrosion and hydriding resistance of zirconium-niobium alloys and Zircaloy-2 are similar, as indicated in Fig. V-4, although the impact strength of the niobium-bearing alloy is higher than that of Zircaloy-2. It appears that the zirconium-niobium alloy may become the preferred material for pressure tubes in cases where zirconium-base alloys are applicable.

The ternary alloy zirconium–2.5 wt.% niobium–0.5 wt.% curium is being developed because of its good corrosion resistance in moist CO_2 and is used in CANDU as a pressure-tube spacer. This spacer maintains clearance between the pressure tube and the calandria, and in CANDU this space is filled with the moist CO_2.

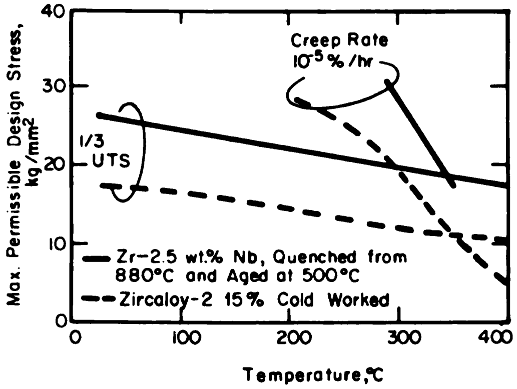

Fig. V-3 Design stresses for zirconium alloys.[41]

Table V-7 EFFECT OF NEUTRON IRRADIATION AND HYDROGEN CONCENTRATION ON THE PROPERTIES OF ZIRCALOY-2 (REF. 39)

(Each Result Is An Average for Three Specimens)

		0.2% proof stress		Ultimate tensile strength		Elongation	
Testing temperature	Hydrogen content, ppm	Unirradiated, kg/mm^2	Irradiated, kg/mm^2	Unirradiated, kg/mm^2	Irradiated, kg/mm^2	Unirradiated, %	Irradiated, %
Room temperature	0	56.6	77.3	66.1	78.7	12.4	5.3
	20	62.0	85.8	70.0	85.8	18.5	6.8
	100	61.8	83.4	70.3	83.7	15.2	7.3
	250	60.5	84.4	70.7	84.4	14.1	6.2
300°C	0	29.7	45.0	33.5	45.0	12.8	5.8
	20	30.1	47.1	33.1	47.1	17.9	7.4
	100	29.7	45.7	33.60	45.7	21.8	8.5
	250	32.2	46.4	36.34	46.4	19.0	8.8
400°C	0	27.5	37.3	29.0	37.3	11.1	6.8
	20	26.5	37.3	28.1	37.3	8.7	10.5
	100	25.9	36.6	27.5	36.6	18.0	9.9
	250	27.2	36.6	28.4	36.6	17.4	10.7

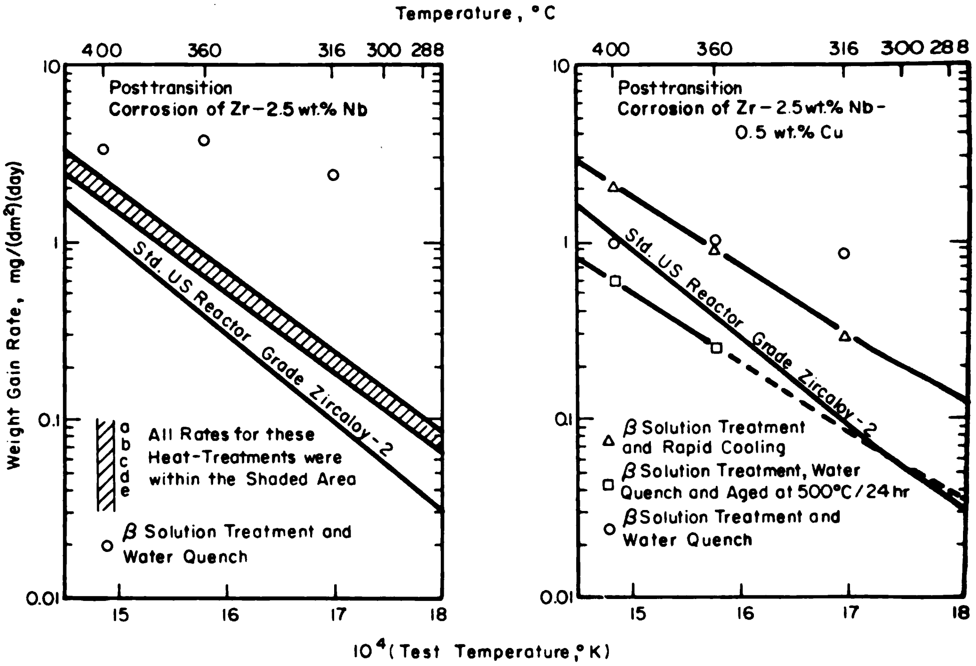

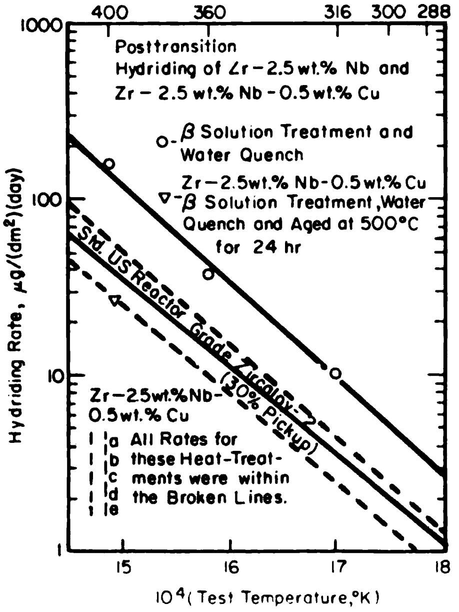

Heat-Treatments Received by Zr-2.5 wt.% Nb:

a Slow Cooled after 2 hr at 650°C

b Air Cooled after 6 hr at 700°C

c Air Cooled after 1/2 hr at 800°C

d Rapidly Cooled after 10 min at 960°C

e Quenched from Temperatures in the Range 880-960°C and Aged 24 hr at 500°C

Fig. V-4 The effect of heat-treatment on corrosion and hydriding of zirconium-niobium alloys in pure water and steam.[41]

Thermal and Hydraulic Studies

The performance of fuel elements cooled with a steam-water mixture is discussed in Ref. 43. Experiments were conducted in an in-pile loop in the NRX reactor and also in an ex-pile loop, termed FLARE. The in-pile tests were done primarily to provide corrosion and hydriding data for Zircaloy-2 and zirconium-2.5 wt.% niobium clad fuel elements operating under various conditions typical of the fog-cool reactor; results are quoted as follows:[43]

> ... corrosion and hydrogen pick-up rates in bo Zircaloy-2 and Zr-2½% Nb fuel sheaths are ac- ceptably low when cooled by fog at the condition interest for fog-cooled or once-through reacto for periods up to 1600 h, provided the sheath su face remains wet ...

Operation of FLARE yielded interesting dat on the "dry-out" heat flux. Dry-out is th

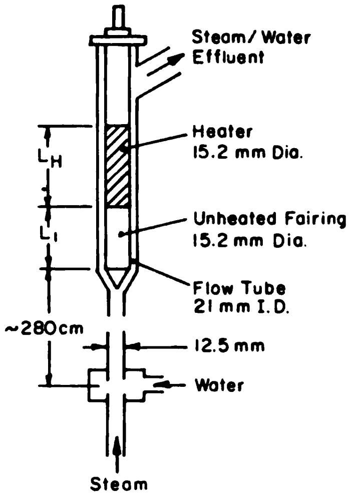

Fig. V-5 Test section.[43]

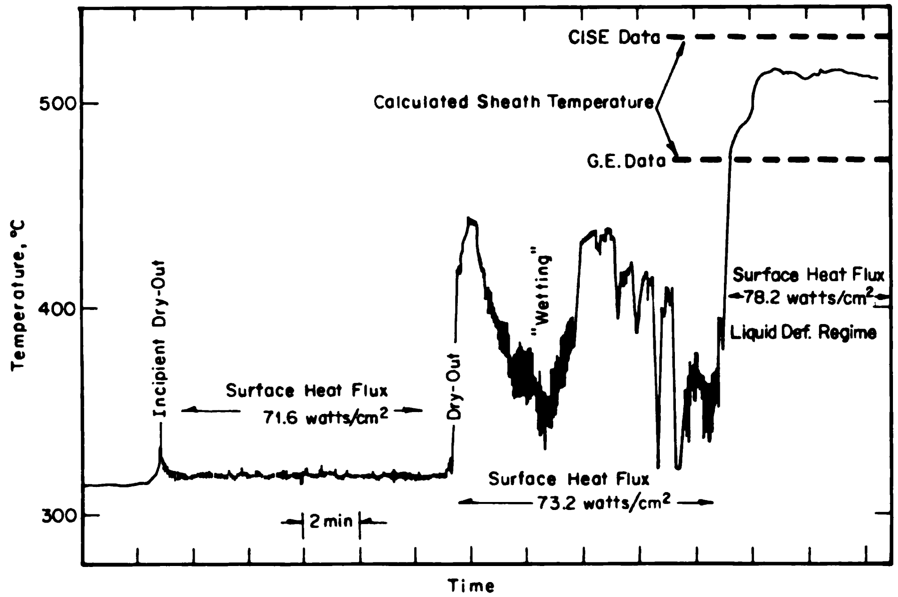

Fig. V-6 Typical sheath-temperature plot obtained from FLARE in dry-out test.[43]

designation of the phenomena that result after the complete evaporation of the protective water film on the heat-transfer surface.[43] Figure V-5 illustrates the test section used in FLARE. Determination of the dry-out heat flux was made for a variety of conditions, and Fig. V-6 illustrates typical wall temperatures for one of the tests. This test was described as follows:

> . . . At the start the test-element power (and heat flux) is being increased until indications of dry-out are noted (incipient dry-out). The power is then adjusted to allow a small temperature oscillation (~5 deg C) and a set of readings taken. At the end of this period a slight increase in the test-element power (~2%) resulted in a sharp increase in surface temperature (~100 deg C)—the dry-out point. Continued operation here gave very large temperature oscillations, despite no recorded changes in the steady-state value of the heat flux, quality or flow. It would appear that there is an alternate wetting and drying out of the surface. A further increase in power (~7%) gives a further rise in surface temperature (up to 512°C). However, in this case there are no oscillations and the surface now appears to be "dry." . . .

Figure V-7 illustrates the effect of the unheated fairing length, L_1 (see Fig. V-5), on $\phi_{\text{dry-out}}$.

References 44 through 48 pertain to organic-coolant technology and originated in a number of different countries. Reference 44 is particularly interesting in that it traces the evolution in thinking on the use of zirconium alloys in organic-cooled systems. In the late 1950's, preliminary experience had indicated that zirconium alloys were unacceptable for use in organic-cooled reactors due to hydriding. This led to increased study of sintered aluminum (SAP), and the work with zirconium was deemphasized. More recent information, however, has indicated that zirconium alloys may be usable in organic systems provided the

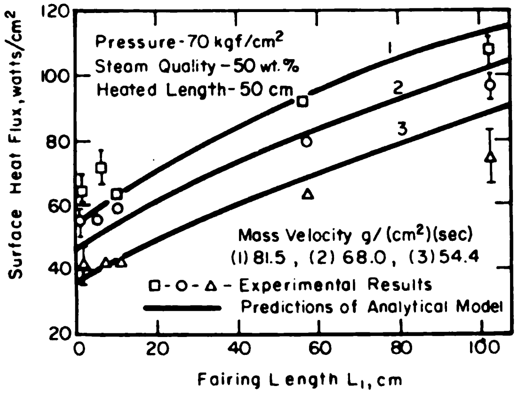

Fig. V-7 The effect of unheated length on the dry-out heat flux.[43]

coolant impurities are carefully controlled. According to the reference:[44]

> The work to date in Canada has shown very clearly that the control of coolant purity is absolutely essential for an organic-cooled reactor. It has been shown further that coolant purity must never be allowed to get out of control since otherwise the subsequent clean-up will be long and difficult. Several years of operating in-reactor and out-reactor loops has proved that the control of coolant purity is no more difficult than in a water-cooled reactor. Provided the proper conditions are observed fouling will not be a problem, at least up to surface temperatures of 500°C, and zirconium alloys such as Zr–2.5% Nb show real promise for fuel sheathing and pressure tubes.

The important variables seem to be water, hydrogen, and chlorine. Water dissolved in the organic seems to have a beneficial effect in reducing hydriding in certain concentration ranges, as may be seen in Table V-8. Increased hydrogen concentrations increase the rate of hydriding at water concentrations less than 40 ppm, but, at "higher" water concentrations, the effect of hydrogen is said to be negligible.[44] Chlorine is thought to be the most important promoter of zirconium hydriding, and Tab V-9 illustrates the effect. Surface preparati has been shown to be important, and the effe of temperature appears minor in the tempera-ture range 365 to 425°C.

Table V-9 EFFECT OF CHLORINE ON HYDRIDING OF ZIRCALOY-2 (REF. 44)

	No chlorine added	50 ppm C_2H added initiall
Temp., °C	375	370
Chloride in coolant at 370°C, ppm		
At start	0.8	8.2
At end (after 67 hr)	0.5	1.6
Hydrogen absorbed, μg/(cm²)(hr)		
Pickled surface	0.39	9.4
Oxidized surface	0.01	2.1

The same importance of coolant purificatio was noted in the French studies.[46] These experimenters studied the effect of various impurities on fouling in terphenyl mixtures. A heated, stainless-steel test section was utilized, but portions of the loop were fabricated of mild steel. The study was directed toward the elimination, or control, of fouling and concluded that fouling could be avoided if the terphenyl used contained "few impurities and no oxygen."[4 Heat-transfer coefficients were determined during some of the experiments, and a correlation is given in the reference. At wall temperatures in excess of 500°C, a decrease in the heat-transfer coefficient was observed, and this was attributed to localized pyrolysis of the coolant at the surface.

References 47 and 48 discuss burnout heat fluxes for organic coolants. The former is on terphenyl mixtures, terphenyl-benzene, and terphenyl-diphenyl mixtures, whereas the latter is on a biphenyl-diphenyl methane eutectic, a biphenyl-diphenylozid mixture, and Dowtherm A.

Table V-8 EFFECT OF WATER ON HYDRIDING IN AUTOCLAVES[44]

(400°C; Dissolved H_2, 100 ml/kg)

Water content of organic, ppm	Hydriding rate, μg/(cm²)(hr)					
	Zircaloy-2		Ni-free Zircaloy-2		Zr–2.5% Nb	
	As pickled	Preoxidized	As pickled	Preoxidized	As pickled	Preoxidized
40	0.5	0.032 ±0.007	0.5	0.010 ±0.005	1.0	0.12 ±0.012
40 to 60	0.4 ±0.1	0.011 ±0.002	0.280 ±0.020	0.001 ±0.001		0.001 ±0.001
60 to 1000	0.045 ±0.02	0.010 ±0.01	0.025 ±0.015	0.002 ±0.002	0.025 ±0.005	0.001 ±0.001

oth referencs employ correlations of the form $_{BO} = a + bG^c + d\ \Delta T G^e$ for their results, where $_{BO}$ is the burnout heat flux, G is the mass flow ate, and ΔT is the subcooling. The remaining ymbols are constants for a particular fluid.

irections of Future evelopments

The direction of development of the heavy-water-moderated power-reactor program in Canada is covered in Refs. 49 to 51. The near-uture plans envision the construction of a 000-Mw(e) station composed of two 500-Mw(e) plants of the CANDU type. This reactor would evolve from CANDU by means of the following mprovements:[50]

—Use of cold-worked zirconium–2½% niobium pressure tubes

—Increase of outlet temperature from 294 to 301.7°C

—Increase of fuel rating from a conductivity integral of 40 to 48 watts/cm

Other changes involve an increase in the pressure-tube diameter, a corresponding decrease in the number of pressure tubes, and, possibly, venting the containment pressure-relief system to a separate gas holder and heat absorber. Interestingly, the large reactor will be controlled by absorbers composed of liquid or gas arranged in vertical through tubes distributed throughout the reactor core, and by soluble poison dissolved in the moderator. The vertical through tubes will be subdivided into a number of separate chambers for flexibility. It thus appears that moderator-level control will not be used for the large reactors, probably for the reasons discussed in Sec. VIII of *Power Reactor Technology*, 7(3).

The longer term direction of the Canadian program is summarized as follows:[51]

> For the water-cooled line itself, the following evolution appears reasonable:
>
> Step 1—(Present Stage)—Pressurized D_2O with CANDU Type UO_2 Fuel Bundles Operating at a Rating of $\int k\,d\theta = 40$ W/cm.
> For the same reactor, a cheaper fuel can be developed by using larger fuel elements operating at $\int k\,d\theta = 48$ W/cm.
>
> Step 2—Boiling D_2O—Indirect Cycle—UO_2 Fuel. From 10% to 20% outlet quality, little change is expected in fuel geometry. From 15% to 30% quality, fuel and/or pressure tube geometry may have to change to keep coolant distribution optimum.
>
> Step 3—Boiling H_2O—Direct Cycle—UO_2 Fuel. When outlet qualities between 20% and 30% are shown to be practical, this reactor will be a strong contender.

Elsewhere, as in Canada, the key question in the future development of the heavy-water pressure-tube reactor is which coolant to use. Although the D_2O-cooled version of the reactor has been developed in Canada, its disadvantages with respect to steam-temperature limits, D_2O leakage, and D_2O inventory considerations are appreciated there, as is attested by the Canadian work on the H_2O-cooled and organic-cooled versions. Considering the work throughout the world, one concludes that the three alternate coolants, gas (CO_2), organic liquids, and H_2O in some form, will receive serious developmental tryouts. Of the coolant systems that have been considered seriously in the past, only sodium and direct-cycle boiling D_2O appear to have been eliminated.

References

The references that contain A/Conf. numbers are papers that were presented at the Third United Nations International Conference on the Peaceful Uses of Atomic Energy, Geneva, September 1964.

1. Nuclear Power Demonstration Reactor, reprinted from *Nucl. Eng.*, 7(77): 398 (October 1962).
2. CANDU Douglas Point Nuclear Power Station, reprinted from *Nucl. Eng.*, 9(99): 289 (August 1964).
3. L. J. Ingolfsrud, P. H. G. Spray, and J. H. Jackson, Manufacturing and Construction for the Douglas Point Nuclear Power Project, A/Conf.28/P/7.
4. AEC Announces Plans for Advanced Converter Reactor Development, AEC Press Release, Sept. 24, 1964.
5. S. Fawcett, A. Firth, and J. E. R. Holmes, General Design of the Steam Generating Heavy Water Reactor, A/Conf.28/P/129.
6. N. Bradley, P. J. Cameron, and N. G. Worley, Some Engineering Problems of the S.G.H.W. 100 MW(e) Prototype Reactor, A/Conf.28/P/143.
7. F. Accinni, R. Bonalumi, C. Bruschi, F. Palazzi, S. Rubbia, and G. B. Zorzoli, The Physics of a Steam-Water Mixture Cooled Heavy Water Power Reactor, A/Conf.28/P/625.
8. C. G. Campbell, D. Hicks, I. Johnstone, and D. C. Leslie, Reactor Physics Studies for Steam Generating Heavy Water Reactors, A/Conf.28/P/174.
9. F. Pascual, L. Palacios, and M. K. Sanders, The DON Project, A/Conf.28/P/601.
10. A. Alonso and B. L. Hoffman, Safety Features of the DON Reactor Concept, A/Conf.28/P/495.
11. E. R. Mayquez, J. L. De Francisco, and F. J. Olarte, Experimental Studies of Uranium Carbide–Heavy Water Lattices, A/Conf.28/P/743.

12. R. Carle, P. Schulhoff, P. Sevin, and J. Buttin, EL4 Features and Construction Problems, A/Conf.29/P/40.
13. B. B. Du Bois, J. L. Bernard, R. Naudet, and R. Roche, Heavy-Water-Moderated Gas-Cooled Reactors, A/Conf.28/P/39.
14. Y. Girard, P. Lourme, and R. Naudet, Heavy Water Reactor Physics, A/Conf.28/P/76.
15. J. L. Bernard, H. Foulquier, and P. Thome, Core Structures of the Heavy Water–Gas Reactor EL4, A/Conf.28/P/69.
16. P. Krafft, The Lucens Experimental Nuclear Power Station, A/Conf.28/P/692.
17. E. Binggeli, P. Verstraete, and A. Sutter, The Underground Containment of the Lucens Experimental Nuclear Power Plant, A/Conf.28/P/459.
18. H. R. Lutz, R. W. Meier, and J. P. Schneeberger, Natural and Slightly Enriched Uranium Lattice Studies of Voided Metal Rod Clusters in D_2O, A/Conf.28/P/691.
19. M. Moller-Madsen, F. List, and J. Elming, Design Problems in the D_2O-Moderated, Organic-Cooled Reactor Concept DOR, A/Conf.28/P/777.
20. C. F. Hojerup, O. Kalnaes, H. Neltrup, and P. L. Olgaard, Heavy-Water-Moderated, Organic-Cooled Lattices Investigations. Experimental Results and Comparison with Theory, A/Conf.28/P/711.
21. A. I. Alichanov, P. P. Blagovolin, B. I. Ilyiechev, G. N. Karavaev, N. N. Kondaritzky, B. A. Medzibovsky, D. M. Mukhamedov, N. N. Nikolaev, V. V. Stekolnikov, V. F. Titov, B. Z. Torlin, and A. A. Khokhlachev, Natural Uranium Heavy-Water Moderated Organic-Cooled Power Converter Reactor, A/Conf.28/P/877.
22. W. H. Zinn and C. A. Trilling, Heavy Water Power Reactors and Organic Cooled Power Reactors, A/Conf.28/P/209.
23. W. Keller, Potentialities of Heavy-Water Moderated Gas Cooled Pressure Tube Reactors, A/Conf.28/P/778.
24. J. C. Leny, A. Ertaud, C. D'Ayguesvives, J. P. Crette, and J. Panossian, ESSOR, Specific Test Reactor for Heavy Water Reactor Concepts Developed by Euratom, A/Conf.28/P/78.
25. J. W. Hilborn, W. M. Barss, M. F. Duret, J. R. Dickinson, A. C. Whittier, and E. Horton, NPD Start-Up, Reactivity Balance and Fuel Management, A/Conf.28/P/9.
26. L. W. Woodhead and W. M. Brown, Performance and Problems of NPD, A/Conf.28/P/8.
27. W. B. Lewis, J. R. MacEwan, W. H. Stevens, and R. G. Hart, Fission-Gas Behaviour in UO_2 Fuel, A/Conf.28/P/19.
28. R. D. Page, D. G. Hardy, A. J. Mooradian, J. Howieson, G. R. Fanjoy, and D. B. Nazzer, Engineering and Performance of UO_2 Fuel Assemblies, A/Conf.28/P/18.
29. J. A. L. Robertson, A. S. Bain, J. R. MacEwan, and J. F. Notley, UO_2 Performance—The Importance of Temperature Distribution, A/Conf.28/P/17.
30. D. G. Boxall, W. M. Brown, D. B. Nazzer, J. T. Rogers, R. G. Hart, and K. L. Smith, Development of Fuel and Coolant Tubes for a Reactor Cooled by Organic Liquid, A/Conf.28/P/23.
31. N. Hansen, P. Knudsen, A. C. Winther, and E. Adolph, Sintered Aluminum Products for Organic-Reactor Applications, A/Conf.28/P/421.
32. G. Sainfort, G. Cabane, and M. Salesse, FeAl - A New Canning Material for Reactors, A/Conf. P/71.
33. V. E. Ivanov, V. F. Zelensky, S. I. Feifer, L. Petelguxov, and V. K. Khorenko, Developmen Heat-Resistant Mg-Be Alloys As a Cladding terial for Fuel Elements, A/Conf.28/P/340.
34. V. Kraus, Diffusion Bonding of Uranium Magnesium by Means of Intermediate Layers. Conf.28/P/526.
35. L. Dolle, D. Conan, and G. Dirian, Behavio Water and Heavy Water in Nuclear Reactors Problems of Power Regulation by Physico-Chem-ical Methods, A/Conf.28/P/70.
36. H. K. Rae, G. M. Allison, A. R. Bancroft, W. Mackintosh, J. F. Palmer, E. E. Winter, J. LeSurf, and S. R. Hatcher, Experience with Chemistry of Water in Moderator and Co Systems, A/Conf.28/P/20.
37. J. A. Morrison, M. H. Thomas, L. C. Watson, L. W. Woodhead, The Management of Heavy Wat for Research and Power Reactors, A/Conf.2 29.
38. W. P. Beddington, J. F. Proctor, W. C. Scott and V. R. Thayer, Production of Heavy Water the U.S.A., A/Conf.28/P/290.
39. W. R. Thomas, S. B. Dalgaard, W. Evans, Fidleris, G. W. Parry, and P. A. Ross-Ross, Ir-radiation Experience with Zircaloy-2, A/Conf. P/21.
40. F. Barbesino, E. Brutto, R. Di Pietro, G. Masin G. Perona, and R. Sesini, Zircaloy-2 Press Tubes Corrosion, A/Conf.28/P/574.
41. C. E. Ells, S. B. Dalgaard, W. Evans, and W. R. Thomas, Development of Zirconium-Niobium A-loys, A/Conf.28/P/22.
42. J. K. Dawson, R. C. Asher, J. Boulton, B. Watkins and J. N. Wanklyn, The Properties of Zirconiu Alloys for Use in Water-Cooled Reactors, A Conf.28/P/158.
43. A. D. Lane and J. G. Collier, Thermal and Ir-radiation Performance of Experimental Fuels Operating in Steam-Water Mixtures, A/Conf.2 P/16.
44. W. M. Campbell, A. W. Boyd, D. H. Charleswort R. F. S. Robertson, and A. Sawatzky, Development of Organic-Liquid Coolants, A/Conf.2 P/15.
45. P. Leveque, F. Franzetti, P. Van der Veene, and M. Giulani, Technological Studies on Organic Cooling Fluids, A/Conf.28/P/53.
46. F. Lanza, R. Ricque, and J. Villeneuve, Heat Transfer by Organic Liquids, A/Conf.28/P/93.
47. D. A. van Meel, Burn-Out in Subcooled Force Convection Boiling of Polyphenyls, A/Conf.2 P/590.
48. I. Kiss and F. Szabo, Radiolytical and Heat Transfer Properties of Some Organic Coolant-Moderators, A/Conf.28/P/449.
49. I. L. Wilson, C. E. Beynon, W. G. Morrison, and N. L. Williams, Studies of CANDU-Type Reactors in the 500-MW(e) Range, A/Conf.28/P/6.
50. G. A. Pon, W. B. Lewis, L. R. Haywood, D. B. Primeau, G. J. Phillips, and E. E. Merlo, Prospective D_2O-Moderated Power Reactors, A Conf.28/P/10.
51. A. J. Mooradian, Future Targets for Canadian Power Reactors, *Can. Nucl. Technol.*, 3(3): 49-53 (Summer 1964).

Section VI

Heavy-Water-Moderated Pressure-Vessel Reactors

General Status

The heavy-water-moderated pressure-vessel reactors have had their most extensive development in Sweden, where the Agesta reactor was built, and in Norway, where the Halden Boiling Heavy Water Reactor (HBWR) is located. The Agesta Nuclear Power Plant (R3/Adam) was started in 1958, completed in 1962, and reached full power in March 1964. The HBWR has been operating since 1959. Further characteristics of both of these reactors are given in Table VI-1.

Heavy-water systems and fuel-handling equipment for the Agesta reactor are discussed in Refs. 1 and 2. Many of the details exemplify straightforward engineering practice, although some are peculiar to the reactor type. Among the latter is the careful preservation of cleanliness of the primary system:

> Before the final assembly of the components at the production workshops, a very comprehensive and stringent cleaning ... was carried out, for the most part in specially arranged clean rooms where the personnel worked under special clean conditions. Cleaning was mostly effected by washing ... in alkaline water and by washing or wiping with acetone.
>
> Pipes and components of carbon-steel were also used, to a limited extent in the heavy-water systems. After cleaning, these parts were rust-protected by a final rinsing in a bath of VPI dissolved in methanol.
>
> After the final assembly, pipe connections and other access openings were carefully sealed with, for example, plastic covers. Large carbon-steel tanks were not rust-protected by means of VPI but kept filled with a controlled over-pressure of dry nitrogen.

A number of basic designs for components in the Agesta heavy-water system are shown in Fig. VI-1. The centrifugal pumps were all canned pumps, whereas the D_2O piston type, feedback pumps were constructed with double seals around the piston shaft with provision for intermediate drainage. The latter principle, of double seals with D_2O recovery through leak-off pipes, is used generally for the nonhermetic closures.

A unique design feature of the Agesta fuel-handling equipment is the provision for transfer of fuel elements from the reactor D_2O to the storage pool, which contains H_2O. Under normal operation the transferred fuel element is gas cooled after its removal from the reactor and prior to its placement in the storage pool. Clean nitrogen is used as a coolant, and the evaporated D_2O is condensed by means of a Freon refrigeration system. In the event of failure of the gas cooling system, a backup spray of either D_2O or H_2O is provided. This spray system also provides cooling when the gas system is not being utilized. A simplified scheme of the cooling and drying circuit is shown in Fig. VI-2.

The second Swedish heavy-water reactor, the Marviken[3] plant, is also of the pressure-vessel type but is cooled by boiling D_2O in natural circulation. The plant is now under construction near Stockholm and should be operational in 1968. Details of the design are given in Table VI-2. The flow path of the primary coolant,

Table VI-1 CHARACTERISTICS OF THE AGESTA AND THE HBWR

Reactor	Power	Coolant	Coolant pressure, psi	Fuel/cladding (first core)
Agesta	10 Mw(e); 55 Mw, space heating	Pressurized D_2O	500	UO_2/Zircaloy-2
HBWR	10 Mw, process steam	Boiling D_2O	400	Uranium/aluminum

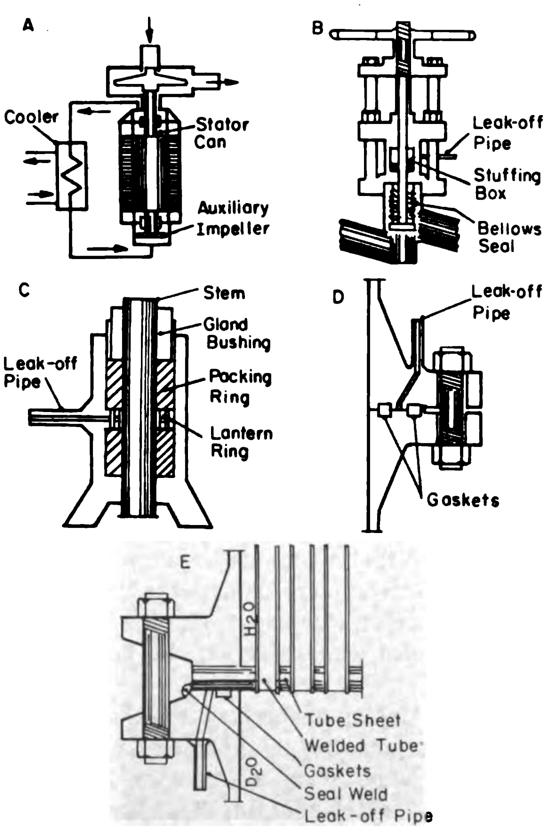

A, Glandless Centrifugal Pump
B, Globe Valve with Bellows Seal
C, Stem with Double Gaskets and Leak-off Pipe
D, Flange Connection with Double Gaskets and Leak-off Pipe.
E, Heat Exchanger D_2O / H_2O

Fig. VI-1 Basic designs for components in the Agesta heavy-water system.[1]

Table VI-2 DESIGN DATA FOR THE MARVIKEN BHWR[4]

Reactor type	
General	BHWR
Cycle	Direct
Circulation	Natural
Superheating	Internal, when provided
Fuel	UO_2
Fuel changing	Onload, continuous
Data	
Net electrical output, Mw(e)	200
Net thermal efficiency, %	34.0
Mean moderator temperature, °C	163
Core volume	
Unreflected, m^3	64.1
Reflected, m^3	94.6
Inner diameter of pressure vessel, m	5.22
Design pressure, bar	57.5
Working pressure, bar	49.5
Pressure-vessel steel	Low alloy (A-302B)
Wall thickness (excluding S.S. lining), mm	76
Outlet steam temp., °C	470
Average enrichment, %	~1.35
Average burnup, Mwd/ton of U	13,000
Fuel for boiling channels	
No. of channels	147
No. of rods per cluster	31
Rod diameter (UO_2), mm	12.5
Can material	Zircaloy-2
Can thickness, mm	0.55
Superheater elements* (2nd charge)	
No. of channels	32
No. of rods per cluster	48
Rod diameter (UO_2), mm	~11.5
Currently assumed can material	20 Cr−35 Ni
Currently assumed wall thickness, mm	0.4−0.25†
Approx. fin height, mm	0.1
Max. surface temp. (hot spot), °C	524

*Current assumption.
†Future changes.

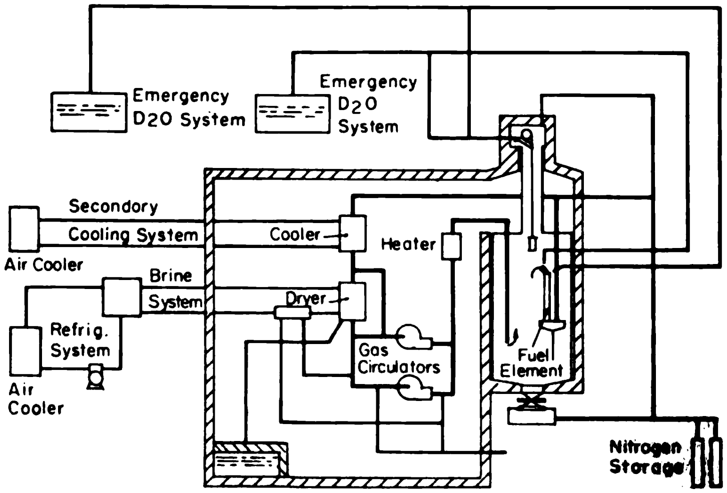

Fig. VI-2 Simplified scheme of the Agesta cooling and drying circuit.[2]

which is quite unusual, is shown in Fig. VI-3. Water from the feedwater heaters is pumped into the moderator space at a temperature of about 250°F. The core is constructed of 179 Zircaloy-2 shroud tubes hydraulically isolating the moderator region of the core from the fuel elements. The moderator water therefore flows to the top of the moderator space and exits at a temperature of about 430°F. At the top of the core, the moderator mixes with the liquid portion of the two-phase mixture that cools the fuel elements, and the resulting coolant flows to the downcomer and thence to the fuel elements. The initial operation of Marviken will be with saturated steam.[3] Thirty-two of the shroud tubes will be left empty to serve as flow channels for the saturated steam; the remainder will contain fuel elements. The turbine contains an inlet blading system suitable for saturated-steam operation and interstage moisture separation, but the inlet blading can be modified for operation with superheated steam. When operating on the saturated-steam cycle, Marviken generates 140 Mw(e). The rated power of 200 Mw(e) is attained only through incorporating superheating fuel elements in the 32 empty shroud tubes.

Operation with the relatively cool moderator is done to improve burnup for a given enrichment.[3] High-pressure tests in a mockup of the reactor was 0.5% for steam carry-under and negligible carry-over of water. Figure VI-4 shows an overall arrangement of the reactor plant. The containment is based on the pressure-suppression principle.

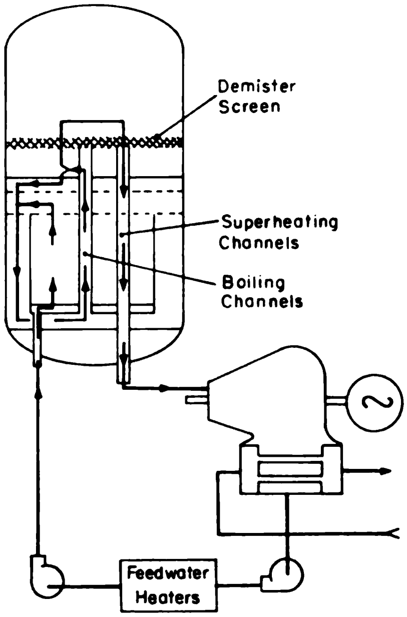

Fig. VI-3 Flow schematic for the Marviken reactor.[4]

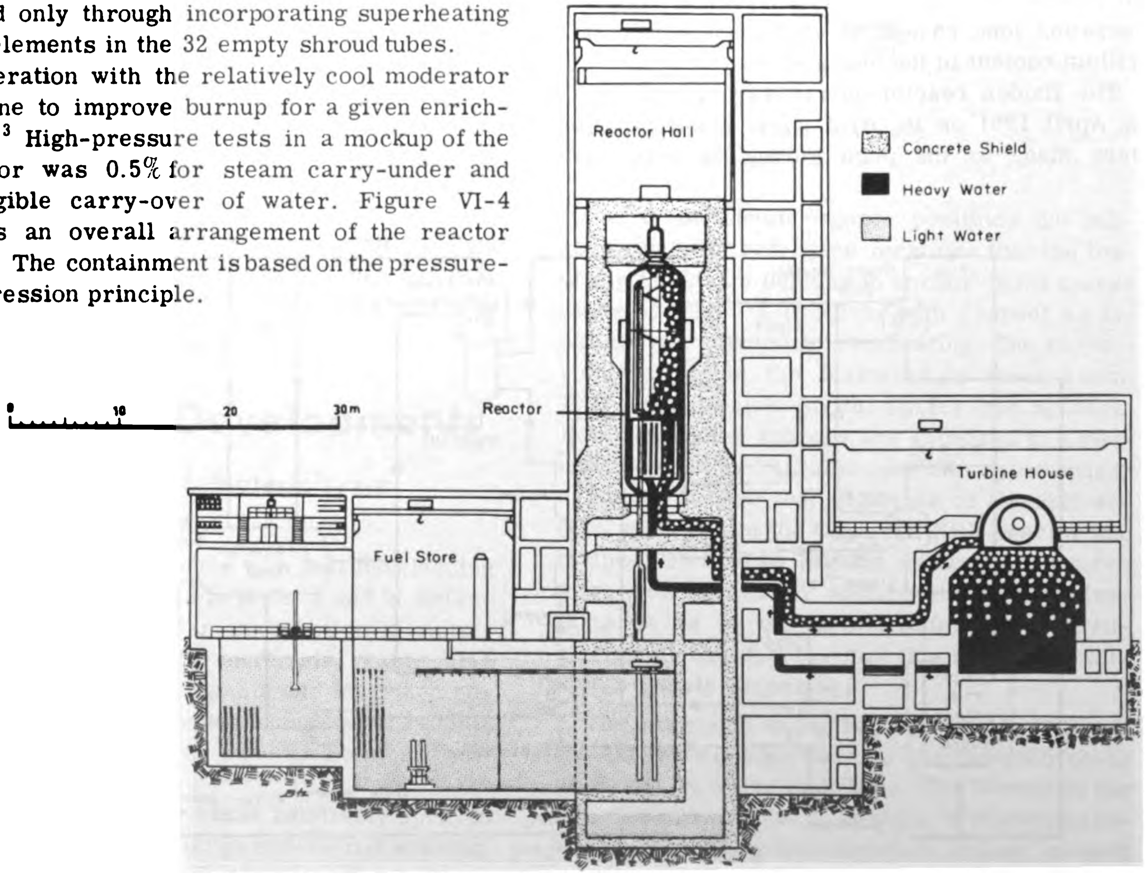

Fig. VI-4 Schematic of the Marviken reactor.

Operating Experience

Some operating experience, partly of a preliminary nature, has been reported for the Agesta reactor.[5,6] Reference 6 was issued in May 1964, and the turbine was commissioned in late April 1964. Space heating occurred a month earlier in the town of Farsta. Only one shutdown at power had been experienced, and this was due to a disturbance in the instrumentation power-supply system. The primary circuit was rinsed with light water prior to filling with D_2O. The light water was then drained, and the system was vacuum dried after a nitrogen flush. A second vacuum drying resulted in a pressure decrease to 1.2 mm Hg, and at that point nitrogen was admitted to the system followed by a few liters of D_2O. The vapor-nitrogen mixture was circulated through the system with the fans in the blanket-gas drying circuit, and the liquid was then condensed. Analyses of the condensate indicated that only a few hundred grams of H_2O were present in the system. The system was then filled with D_2O. The plant has not been in operation long enough to produce a significant tritium content in the heavy water.

The Halden reactor operated from June 1959 to April 1961 on its first core. Modifications were made to the plant during the refueling shutdown, and the second core was loaded i March 1962. The second core utilizes 100 fu assemblies with UO_2 as fuel and Zircaloy-2 as cladding. Each assembly consists of seven fuele pins having a length of 1600 mm (5.25 ft). Although the HBWR is not a power reactor in the usual sense, it does operate at high pressure and temperature, and much of the operating experience is pertinent to power-reactor operation. For example, Ref. 7 contains much information on loss and degradation of D_2O.

Table VI-3 SUMMARY OF HBWR FLANGE AND SEAL STATISTICS

No. of 8-in. flanges	**10**
No. of smaller flanges	**50**
No. of reactor-lid mechanical seals	**335**
Integrated "gasket-length" high-pressure system, m	**100**

The HBWR flow diagram is shown in Fig. VI-5. The system contains a number of flanges and seals that are not backed up with seal welding or leakage collection, and these are summarized in Table VI-3. The D_2O leakage was studied by various means, but the most useful method was found to be monitoring of the outgoing air for tritium. The tritium content of the reactor heavy water was known. The leakage rate could be calculated by measuring the ven-

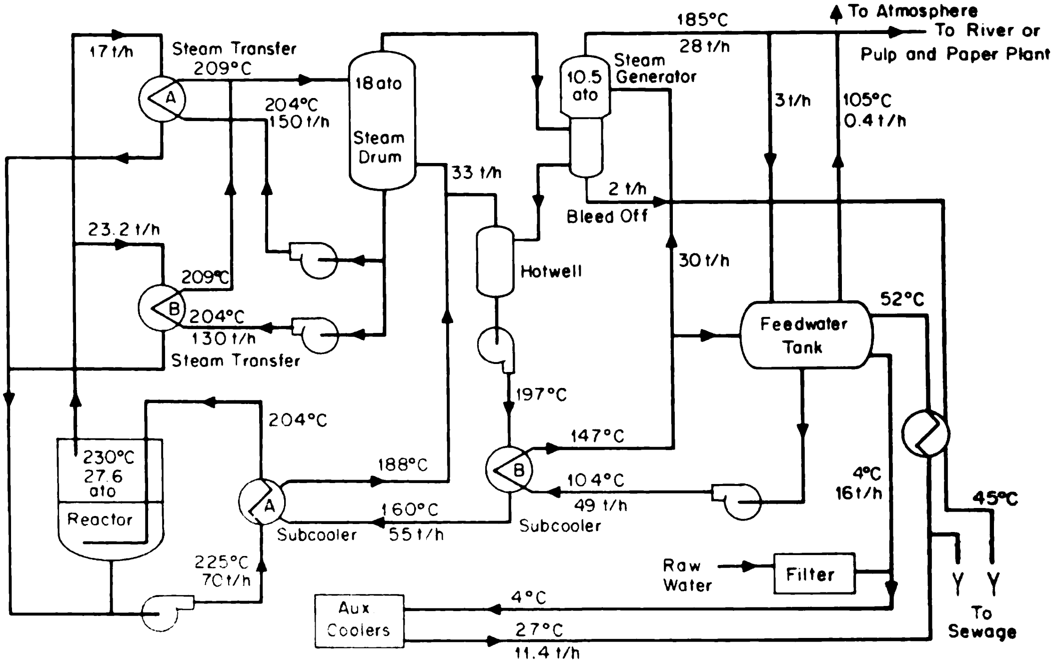

Fig. VI-5 The HBWR simplified flow sheet and 20-Mw operating data.[7]

ilation air flow rate and absolute humidity. Inventory measurements were also made, and hey corresponded "reasonably well" with the racer results. The loss of heavy water and the reactor pressure history for the HBWR are shown in Fig. VI-6. The heavy-water inventory for this reactor is 14.5 tons.[7] The loss of 2500 kg of D_2O over a 20-month period (Fig. VI-6) represents a leakage rate of about 10% per year.

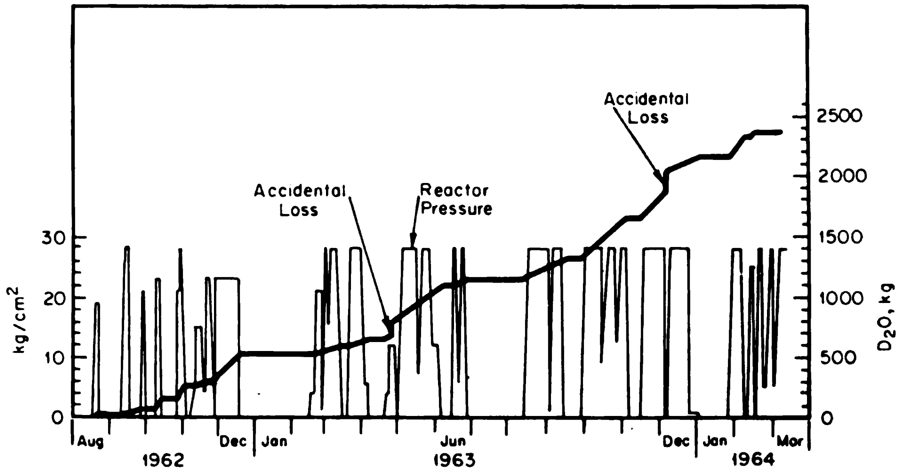

Fig. VI-6 Loss of heavy water in the HBWR and reactor pressure history.[7]

At the start of operation with the second core, the isotopic purity of the D_2O was 99.75%. By the end of 1963 it had fallen to 99.68%. This represents an inleakage of about 10 kg of H_2O to the system.

Significant Developments

Fuel Elements, Fuel Materials, and Cladding

The Swedish experience with fuel and cladding materials is contained in Refs. 8 and 9. Reference 10 is a Norwegian contribution on aluminum alloys as cladding materials. Table VI-4 gives fuel data for the Agesta and Marviken reactors and the pressurized heavy-water reactor (PHWR). The PHWR is a design study and will be discussed shortly.

The Agesta fuel bundle is relatively open, in the sense of having a large rod-to-rod spacing. This is to ensure adequate coolant velocity in natural circulation and also to provide a slightly negative void coefficient. It is said[8] that the helical wire wrap is not applicable to this type of design because of the 3- to 5-mm spacing between rods. The Agesta design provides for spacing and intermediate support points by subdividing the 3-m fuel rod into four subelements and using spring-loaded flexible plate spacers located at the fuel-element junctions.

The Marviken boiling fuel elements are composed of rods built up of two half-length subrods. A midbundle spacer positions the subrods, and the reference mentions that the tendency for steam bubbles to anchor on the spacer grids has been a problem with respect to localized corrosion and overheating. The rod-to-rod spacing in the Marviken is about 9 mm. This is maintained by the spring type spacers. For rigidity the spacers are anchored to a central, supporting Zircaloy tube that apparently is unfueled. In-pile test elements of Swedish design were run in the Canadian NRX reactor and in the VBWR. The highest oxide temperatures were determined by postirradiation examinations to be in the pellet immediately downstream of the spacer, and this is attributed to steam-bubble anchoring.[8]

The corrosion and hydriding results of Swedish experiments on Zircaloy are typical of those observed in other countries. The shroud in the Marviken reactor is a fixed piece of core hardware; thus the requirement of a long in-core lifetime does exist, although the consequences of a failure are not as serious as the failure of a pressure tube in a pressure-tube reactor.

Table VI-4 FUEL DATA FOR SWEDISH POWER-REACTOR FUEL ELEMENTS[8]

	Agesta, 55 Mw(t) + 10 Mw(e)	PHWR, 360 Mw(e)	Marviken	
			Boiling element, 140 Mw(e)	Super-heating element, 200 Mw(e)
Total heat release in fuel, Mw	60	1134	471	122
Reactor pressure, bars	33.3	74	49.5	49.5
Fuel form	UO_2 (sint.)	UO_2 (sint.)	UO_2 (sint.)	UO_2 (sint.)
Enrichment, %	Natural	1.5	1.3	1.6
Active fuel-element height, mm	3047	4455	4420	4220
Free space in rod, mm	10	65	100	150
Fuel rods per assembly	4 × 19	2 × 49	2 × 30	2 × 48
No. of assemblies	140	177	147	32
Total UO_2 weight, tons	18.5	33.7	25.6	7.0
Can	Zircaloy-2	Zircaloy-2	Zircaloy-2	S.S.
Canning-tube inside diameter, nominal, mm	17.2	10.5	12.6	11.6
Can wall thickness, mm	0.7	0.51	0.6	0.4
UO_2 pellet diameter, nominal, mm	17.0	10.4	12.5	11.5
Mean heat loading, watts/cm	78.5	300	227	180.6
Hot-channel factor (including transient)	4	2	2.99	2.72
Max. transient heat loading, watts/cm	314	600	680	491
Max. heat flux on can surface, watts/cm	54	164	156	126
Mean temperature of the fuel, °C	500	900	800	1200
Max. center temperature (including transient), °C	1325	2450	2760	2670
Coolant/UO_2 area ratio	1.13	16.4	3.52	1.92
Coolant inlet temperature, °C	205	254	255	263
Coolant outlet temperature, °C	220	274	263	470
Mean burnup, Mwd/ton	3600	16,000	13,000	13,000

The use of aluminum as a cladding is being studied primarily as an in-pile experiment.[10] Prototype elements were scheduled to be irradiated in the HBWR in late 1964.

Water Chemistry

Reference 11 is a report on the water-chemistry research at the HBWR. The report covers reactor experiments that were designed to study conditions under which corrosion can be reduced to the point where operation is possible without full-flow condensate purification. This involves a search for conditions under which steam will be produced with a low oxygen content and the alkalinity of the recirculating water will be preserved. Reducing the in-core dissociation of D_2O should also reduce the recombiner load. However, this particular point was not mentioned in the reference.

Figure VI-7 shows the oxygen concentration in the HBWR steam as a function of power, with no additions to the coolant. The D_2 was found in stoichiometric amounts. When D_2 was added to the subcooled feedwater, the net decomposition of D_2O was considerably lessened, as is shown in Fig. VI-8. This figure shows the effect of D_2 addition at various pressures, various locations, and several different powers. Ammonia (as ND_3) was added to the coolant, and it was shown that the radiolysis of ammonia into nitric acid could be prevented by maintaining the D_2 concentrations at or above 0.3 to 0.4 ml per kilogram of heavy water. The radiolysis of ammonia into nitrogen and deuterium did increase the ^{16}N content of the steam, however.

Control and Instrumentation

The Agesta reactor is equipped with top-mounted, hydraulically actuated control-rod drives.[12] A stepping action is accomplished by

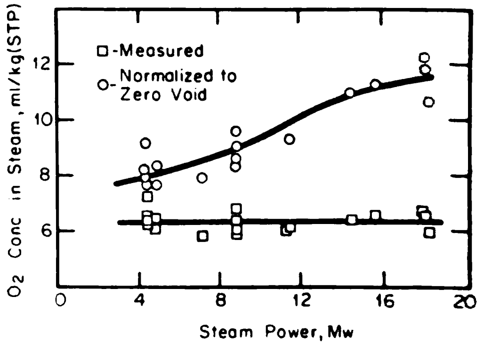

Fig. VI-7 Oxygen concentration in steam vs. stea power at 28 ata.[11]

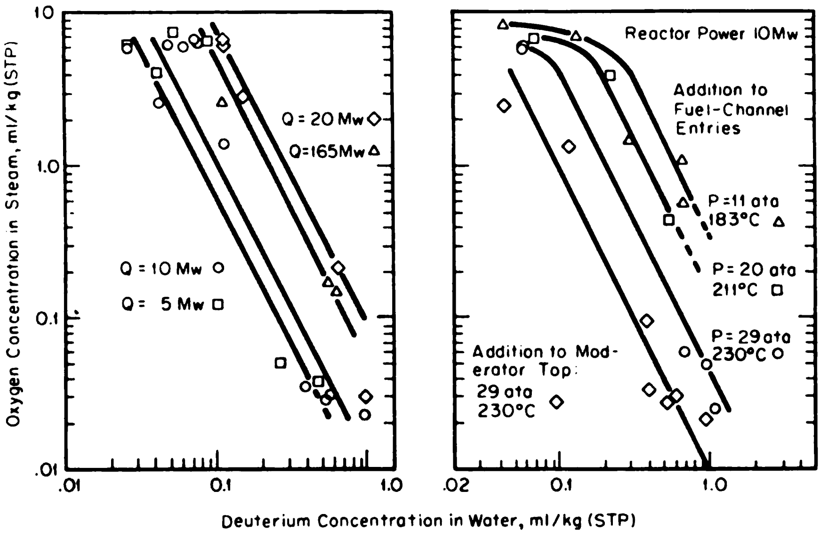

Fig. VI-8 Oxygen concentration in steam vs. deuterium concentration in water entering the fuel channels.[11]

means of two chucks. One chuck normally holds the rod in a given position, and the other grasps the control rod and moves a small distance up or down (10 mm) in response to hydraulic pressure. The Agesta control rods are of silver-indium-cadmium alloy clad with type 304L stainless steel and are tubular in shape.

The Marviken reactor will be equipped with rather unusual control-rod drives. The reactor (Fig. VI-4) is designed for on-power refueling. The entire control-rod drive is to be located within the pressure vessel, immediately above the core, and will be hydraulically actuated. The drive will be positioned by means of the fuel-handling machine and held in place only by the weight of the drive itself. The water, which serves as the hydraulic fluid, is fed through pipes penetrating the pressure-vessel wall and is introduced into the drive by means of piston-ring type seals. The drives are located in the steam atmosphere above the core, but the drive mechanism will be filled with water to control the drop speed upon scram. The position-indicating system is based on ultrasonic location of a reflector plate at the lower end of a control rod. A transducer, at the bottom of the control-rod channel, emits ultrasonic pulses, and the time interval between their transmission, reflection, and absorption back at the transducer gives the location of the control rod.

The in-core instrumentation for the HBWR is detailed in Ref. 13. Most of the information has been presented in *Nucleonics*[14] and will not be repeated here.

Pressure Vessels

The design and fabrication of the Agesta and Marviken pressure vessels are discussed in Ref. 15. The design details of these vessels, and that of a larger reactor to be discussed shortly (BASHFUL-600), are given in Table VI-5. The Agesta vessel has a cylindrical shape with an ellipsoidal bottom dome and a flat lid. The cylindrical portion is roll clad with stainless steel and has an upper flange fabricated of forged parts welded together and clad with weld-deposited stainless steel. The Marviken vessel is quite different from that of the Agesta and is shown in outline form in Fig. VI-4. The

Table VI-5 SURVEY OF REACTOR VESSEL DATA[15]

	Agesta PHWR	Marviken BHWR	BASHFUL-600
Design pressure, bars	40	57.5	80
Design temperature, °C	251	272	293
Vessel inside diameter, m	4.5	5.22	6.6
Cylindrical wall thickness, m	65	76	120
Bottom dome-wall thickness, mm	65	70	175
Vessel steel type	C-Mn	C-Mn-Mo	9% Ni steel
Vessel height, m	9.5	23.96	26.75

bottom dome, which is hemispherical in shape, is penetrated by 87 nozzles, as follows:

- 32 superheater nozzles
- 34 nozzles that indicate the positions of control rods by ultrasonics
- 12 nozzles for neutron detectors
- 8 nozzles for startup heating and coolant inlet
- 1 nozzle that is a transport channel for control rods and fuel elements

The entire internal shell surface is clad with stainless steel by overlay welding, and the shell is penetrated by nozzles for feedwater, control-rod-drive piping, pressure-relief valves, emergency cooling piping, and canning leak-detection piping. The hemispherical upper head is penetrated by three nozzles for television cameras and the large central nozzle supporting the charging machine. The vessel closure system is unique and is illustrated schematically in Fig. VI-9. The design is such that all forces acting in the fixed flange rings pass through one point, thus giving no moment in the ring.

The pressure vessel for the 600-Mw(e) BASHFUL reactor, which is an advanced design of a boiling heavy-water-moderated reactor, has an inside diameter of 6680 mm and a total height of 24,750 mm. The vessel would be shipped to the site in at least two pieces. After installation of the internals at the site, the parts of the vessel would be joined by welding and locally heat-treated. At the present time no welding electrode has been developed that is fully satisfactory with the 9% nickel steel proposed for the vessel, but the reference states that such electrodes are expected to be developed in the near future.

Directions of Future Developments

The direction of development of the pressure-vessel heavy-water-moderated power reactor appears to be largely dependent on the future program in Sweden, as well as on the Norwegian work, although there apparently is also some activity on the reactor type in Germany.[17] Sweden, probably because it is relatively well endowed with water power, anticipates a slow buildup of nuclear capacity in the near future but a rapidly accelerating one later. Reference 18 assumes that Sweden will have an installed nuclear capacity of 200 Mw in 1970, 1000 Mw in 1975, and 4000 Mw in 1980. The figures seem to indicate that, when nuclear energy is finally

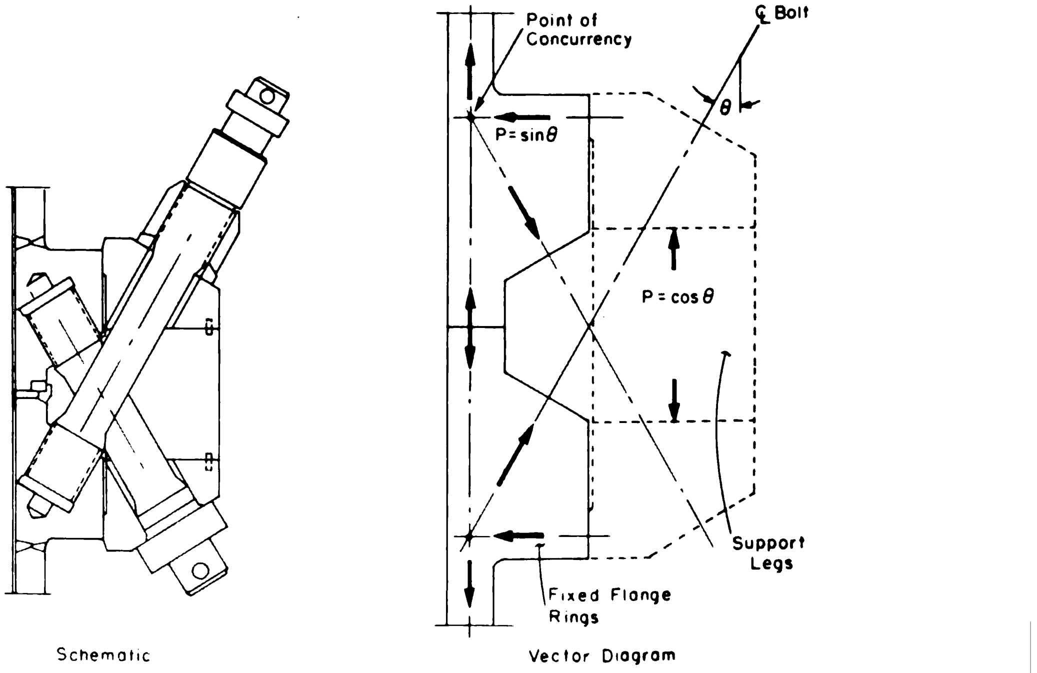

Schematic

Vector Diagram

Fig. VI-9 Details of Marviken vessel-closure flange.[15]

Table VI-6 PARAMETERS CHARACTERIZING ADVANCED SWEDISH REACTORS[18]

	Marviken	BHWR*		PHWR	BASHFUL†
		Natural U	Enriched U		
Thermal efficiency	0.287	0.314	0.314	0.283	0.371
Specific power, kw/kg of U	18.0	18.0	27.0	35.6	24.0/41.2
Enrichment, wt.% ^{235}U					
Initial	1.00	0.71	1.17	1.50	1.05/2.17
Final	0.25	0.25	0.25	0.40	0.2/0.92
Rod diameter, mm	12.5	14.0	11.5	10.4	11.5/8.5
Plutonium, g/kg of U	5.6	4.7	6.6	6.0	6.3/6.9

*The BHWR is a 300- to 500-Mw(e) reactor producing saturated steam.

†BASHFUL is a reactor similar to Marviken in the 400- to 1000-Mw(e) power range. The numerator of the fractional entries pertains to the parameters of the boiling region, and the denominator pertains to the superheating region.

needed, it will be badly needed. This is substantiated in the reference, which states that domestic sources of fossil fuels in Sweden are lacking.

The Marviken reactor represents the 1970 commitment approximately. Beyond this date the reactor type to be built is open; pressurized heavy-water reactors (PHWR),[19] saturated boiling heavy-water reactors (BHWR), and boiling and superheating reactors of the Marviken type (BASHFUL)[18] are all under study. Reference 18 is a discussion of the economics of these various types, and some of the proposed design parameters are given in Table VI-6. Fuel costs are given in Table VI-7. Table VI-7 illustrates the importance of on-power refueling, since this is said to be responsible for the difference in cost between the PHWR and the remaining reactors. The PHWR costs were arrived at by assuming multizone, batch loading, whereas the remaining plants were assumed to be continuously refueled. The penalty can be seen in the enrichment values given for the PHWR, as contrasted to the remaining plants. The processing of fuel appears to be of marginal value, as Table VI-7 shows that the cost of processing about equals the plutonium value.

The Swedish fuel-cycle philosophy is now characterized as follows:[18]

> Use of slightly enriched uranium for normal operation but possibility of optional operation with natural uranium.
>
> Once-through uranium cycle without reprocessing of spent fuel but with possibility of future recycling of plutonium in a self sustained cycle.

The option for use of natural uranium is somewhat peculiar to Sweden but is of general interest. If 4000 Mw(e) is in fact the installed capacity in 1980 and if the annual increase is 800 Mw(e), the net import requirements for natural uranium would amount to $8 million per year, compared to $13 million for enriched uranium. If the nuclear electricity were being generated with conventional BWR's, the corresponding figures, as given in Ref. 18, would be $40 million per year for Zircaloy-clad fuel and $63 million

Table VI-7 FUEL COSTS* FOR DIFFERENT REACTOR TYPES[18]

	Marviken	BHWR		PHWR	BASHFUL
		Natural U	Enriched U		
Cost item, mills/kw-hr					
Fuel consumption	0.51	0.39	0.63	1.04	0.67
Manufacturing	0.88	1.23	0.89	1.10	0.79
Fixed	0.20	0.13	0.13	0.14	0.13
Processing	0.29	0.44	0.26	0.30	0.23
Credit on uranium	0	0	0	−0.04	−0.09
Credit on plutonium	−0.43	−0.55	−0.46	−0.47	−0.38
Once-through (items 1 to 3)	1.59	1.75	1.65	2.28	1.59
Net credit (items 4 to 6)	−0.14	−0.11	−0.20	−0.21	−0.24
Total cost	1.43	1.64	1.45	2.07	1.35

*Basic assumptions: burnups, 15 Mwd per kilogram of uranium, except for natural uranium, which is 9 Mwd per kilogram of uranium; feed cost, $8 per pound; separative work, $30 per kilogram of uranium; interest rate, 7%; fixed costs at 6000 h/g and 60% of initial core; processing, $30 per kilogram of uranium; plutonium credit, $8/g total.

for stainless-clad fuel. These numbers might be important in considerations involving trade balance or emergency situations, but the reference assigns them a "minor importance." Nevertheless, the requirement that the reactor be capable of operation with natural uranium is allowed to compromise the optimization of the reactor fueled with enriched uranium, and this is noted in the reference.[18]

Czechoslovak Nuclear Power Station

The remaining heavy-water power reactor of the pressure-vessel type is the gas-cooled reactor of the Czechoslovakian nuclear power station. Few design details were presented at the conference, but coverage had been reasonably thorough at the Second Geneva Conference. Reference 20 reports on some design and construction problems of the reactor and discusses the charge-discharge machine, control-rod tests, top biological shield design, steam-generator tests, main blower tests, and steam-turbine design. The plant has been scheduled[21] to be critical in 1965. No other dates are given to suggest that this time schedule will not be met, although it is mentioned in Ref. 20 that the construction time has been "elongated."

The pressure vessel for the Czechoslovakian nuclear power station is discussed in Ref. 16 and is shown in Fig. VI-10. The figure does not illustrate the upper head details, but there are approximately 200 nozzles through the head for control and refueling. The reactor is D_2O moderated, and the CO_2 coolant is piped through 12 inlet and 12 exit nozzles. The reference contains much information on stress analysis, material properties, and test results that would be of interest to the specialist. The pressure-vessel steel is designated "CSN 13030," and is composed of <0.20% carbon, 1.10 to 1.14% manganese, <0.10% cobalt with titanium and aluminum added "... for increasing of structural stability and finegrainedness ..."[16] The reference describes the manufacture of a shortened version of the pressure vessel. The vessel is the same as the one shown in Fig. VI-10 but does not include some of the ring sections.

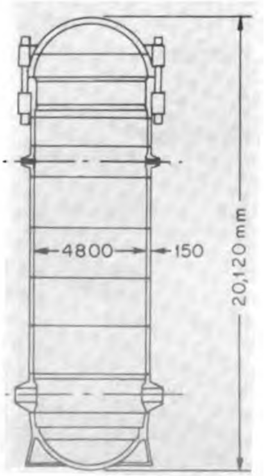

Fig. VI-10 Pressure vessel for the first Czechoslovakian power station.[16]

References

The references that contain A/Conf. numbers are papers that were presented at the Third United Nations International Conference on the Peaceful Uses of Atomic Energy, Geneva, September 1964.

1. P. I. Nylander, P. Hjertberg, and B. Larson, Manufacturing and Installation Experience of the Heavy-Water Systems of the Agesta Nuclear Power Plant, A/Conf.28/P/602.
2. G. Granelli, G. Fagerlund, S-O Brunzell, and G. Fröman, Fuel-Handling Equipment for the Agesta D_2O-Moderated Pressure Vessel Reactor, A/Conf.28/P/808.
3. P. H. Margen, L. Leine, and R. Nilson, The Design of the Marviken Boiling Heavy Water Reactor with Nuclear Superheat, A/Conf.28/P/603.
4. P. H. Margen, The Development Work Leading up to the Marviken Nuclear Power Station, Lecture to the Swiss Nuclear Society, June 22, 1963, Reprint from *New Techniques*, 5(12): 699-714 (1963).
5. G. Apelqvist, P. E. Blomberg, O. Nylund, and R. Persson, Reactor Physics Studies and Comparisons Between Reactor Physics Data from Calculations and Mock-up Studies and from Measurements in the Agesta Nuclear Power Plant, A/Conf.28/P/682.
6. N. Rydell, P. Blomberg, and E. Ericsson, Experience from the Commissioning, the Criticality Experiments and the Power Operation of the Agesta Nuclear Power Plant, A/Conf.28/P/679.
7. E. Jamne, J. A. Firing, M. Øvreeide, and T. Wullum, Operational Experience on the 2nd Charge for the Halden Boiling Heavy Water Reactor, A/Conf.28/P/594.
8. H. Mogard, S. Djurle, I. Multer, H. P. Myers, B. Nelson, and U. Runfors, Fuel Development for Swedish Heavy Water Reactors, A/Conf.28/P/6
9. G. Oestberg and H. P. Myers, Aspects of Swedish Studies of Cladding Materials for Water-Cooled Reactors, A/Conf.28/P/419.
10. S. Aas and K. Videm, Improved Aluminum Alloys as Fuel Cladding Material in Water-Cooled Power Reactors, A/Conf.28/P/591.

11. L. Hammar, R. Rose, and G. M. Allison, Water Chemistry Research at HBWR, A/Conf.28/P/595.
12. S. Ericsson and B. Ahlnaes, Design, Development and Manufacture of Control Rod Drives for Heavy Water Power Reactors, A/Conf.28/P/809.
13. B. Aarset, H. P. Olson, R. D. Smith, and O. Vapaavuori, In-Core Instrument Development in the HBWR Programme, A/Conf.28/P/859.
14. H. Ager-Hanssen and R. D. Smith, Advanced In-Core Instrumentation from Halden, *Nucleonics*, 22(4): 49-56 (April 1964).
15. O. Hellstroem, Design and Manufacture of the Reactor Pressure Vessels for the Agesta and Marviken Power Stations and Some Future Developments, A/Conf.28/P/810.
16. J. Hauer, St. Havel, J. Nemec, and St. Stěpánek, Pressure Vessel for the First Czechoslovak Nuclear Power Station, A/Conf.28/P/522.
17. A. Ziegler, Objectives in the Development of D_2O Pressure Vessel Reactors, A/Conf.28/P/779.
18. L. Zettergren and B. Pershagen, Fuel Cycle Physics and Economics for Heavy Water Reactors, A/Conf.28/P/417.
19. A. Jonsson and B. McHugh, A Large Swedish Nuclear Power Station with a Pressurized Heavy Water Reactor with an Open Uniform Lattice Core, A/Conf.28/P/605.
20. J. Hůlovec, J. Jůza, A. Komárek, J. Kořenek, V. Křížek, J. Tomčík, and K. Wagner, Development and Construction Problems of the First Czechoslovak Nuclear Power Station, A/Conf.28/P/523.
21. *Directory of Nuclear Reactors, Vol. IV: Power Reactors*, International Atomic Energy Agency, Vienna, 1962.

Section
VII

Power Reactor Technology

Gas-Cooled Clad-Fuel Reactors

By Walter Mitchell III

General Status

The Geneva information on gas-cooled reactors that employ metallic fuel jackets deals almost exclusively with reactors developed in the United Kingdom and France. Consequently, this article reviews the status, the significant developments, and the indicated directions of future development in terms of the British and French programs.

Some basic information on specific reactors of the type is presented in Table VII-1. The reactors, all of which are CO_2 cooled and graphite moderated, are classified as "British designed" or "French designed," but the reactors in the former category are not all located in the British Isles. Although the majority of the stations listed are multiple-reactor installations, as indicated in the first column of Table VII-1, the net electric outputs listed pertain to single reactors. The date of power operation for a particular station gives the year in which the first reactor in a multiple-reactor installation began or will begin operation.

The large number of British reactors of the CO_2-cooled graphite-moderated type built or being built and the steady progression in reactor output are striking results of the British program, which has up to now concentrated heavily on this reactor type. The improvements in the type, as indicated by the parameters listed in Table VII-1, illustrate rather vividly the technological advances that occur as a re-

Table VII-1 GENERAL INFORMATION ON GAS-COOLED CLAD-FUEL REACTORS$^{1-16}$

Station (number of reactors in parentheses)	Date of first reactor on power	Net electric output per reactor, Mw	Net efficiency, %	Primary coolant nominal pressure, psia	Primary coolant temperature at reactor outlet, °F	Fuel rating, Mw(e)/metric ton of U	Capital cost, $/kw
British-designed reactors							
Calder Hall (4)	1956	54	23.5	100	652		
Chapelcross (4)	1959	54	23.5	100	652		
Berkeley (2)	1962	138	24.4	140	653	0.59	521
Bradwell (2)	1962	150	28.2	147	739	0.63	492
Latina (1)	1963	200+	28.4	197	739		
Hinkley Point (2)	1964	250	26.4	195	705	0.72	420
Hunterston (2)	1964	150	28.3	161	744	0.60	
Trawsfynydd (2)	1964	250	29.4	246	735	0.85	384
Dungeness (2)	1965	275	32.9	284	770	0.92	319
Tokai (1)	1965	149	26.8	223	739		
Sizewell (2)	1965	290	30.5	282	770	0.91	300
Oldbury (2)	1966	300	33.6	365	770	1.02	302
Wylfa (2)	1968	590	31.5	400	770	1.00	280
AGR (1)	1962	27.3	27.3	285	977		
French-designed reactors							
G2 (1)	1959	40	16.0	215	644		
G3 (1)	1960	40	16.0	215	644		
EDF-1 (1)	1963	70	23.3	406	670		
EDF-2 (1)	1964	200	23.6	385	716	0.80	
EDF-3 (1)	1966	480	30.8	435	770	1.14	240
EDF-4 (1)	1968	480	29.1	435	752	1.08	

sult of the research engendered by a large building program and the experience gained through reactor operations. The French program, although considerably smaller than the British effort, has resulted in rather remarkable advances also. Indeed, the predicted performances of the French reactors presently under construction are fully as impressive as those of the British. For example, a comparison of the data in Table VII-1 for the Sizewell and EDF-3 plants, which are scheduled for on-power operation in 1965 and 1966, respectively, shows that the bulk outlet gas temperatures from the reactors are the same. Pressure and fuel rating in EDF-3 exceed the comparable values in Sizewell by a large margin. Comparisons of cost estimates from different countries can be misleading, but, if the estimates for Sizewell and EDF-3 are comparable, they indicate a considerable advantage for the French design, perhaps because of the larger reactor output.

That the British are proceeding with such a vigorous construction program is not surprising in view of the fact that, even under conservative assumptions, nuclear power in that country is expected to command a place in the generating system on solely economic grounds in the period 1970 to 1975. An indication of the relative costs of nuclear and conventional power in Great Britain is given in Ref. 9 by the statement that the replacement generation cost per day for Bradwell was $75,500 in January 1963 and $36,400 in July 1963. (The replacement cost is the incremental fuel cost per day of the next available stations in the order of merit needed to replace Bradwell's 300 Mw.) Although one would expect the January figure to be high, since this is a peak-load time of the year and the conventional plants available for service are the old and expensive plants, the July figure represents a period of low load during which time it appears reasonable that some fairly good conventional plants would be available for use. The January 1963 replacement generation cost is equivalent to a fuel cost of over 10 mills/kw-hr. It is interesting to note that even the very large conventional power stations that will be commissioned in Great Britain during the period 1965 to 1970 are estimated to have fuel costs[13] of between 4.1 and 5.8 mills/kw-hr.

An interesting trend has developed in the use of the prestressed-concrete pressure vessel for this reactor type. In the British program, all reactors down through Sizewell use metal pressure vessels, whereas Oldbury and Wylfa use prestressed concrete in conjunction with the "integral-plant" arrangement described later in this article. The French, despite (or perhaps because of) previous experience with concrete vessels in the G2 and G3 reactors, reverted to metal enclosures for the EDF-1 and EDF-2 reactors. Then, for EDF-3, they changed again—to a concrete version of the conventional pressure vessel, i.e., a vessel that encloses only the reactor proper. Finally, in the EDF-4 plant, the concrete-vessel integral-plant concept is used. Thus it appears that the evolution of the reactor type in the United Kingdom and France, after having proceeded along somewhat dissimilar paths, has now reached a point in time at which the gross features of the plants under construction are comparable. In the course of this evolution, it seems that the British may have displaced the French as the boldest exponents of the concrete pressure vessel, since they expect to put the integral concept into service in 1966 in the Oldbury plant, two years before EDF-4.

The large gas-cooled reactors have proved their reliability through the years. For some time now, utilization factors of 90% and greater have been common for long periods in the operating history of the Calder Hall reactors, and, as shown in Table VII-2, even the relatively young Berkeley and Bradwell plants are exhibiting a satisfactory degree of reliability. The "utilization factor" is defined as

$$\frac{\text{Units sent out} \times 100}{\text{Design sent-out capacity} \times \text{time}} \ \%$$

The performance of Berkeley and Bradwell during the period from startup to February 1964 is presented in Table VII-3 in terms of the utilization factor.

The reactors listed in Table VII-1, with the exception of the Advanced Gas Cooled Reactor (AGR), are fueled with natural-uranium metal clad in a relatively low-temperature alloy. The fuel elements are massive, to the extent that the entire cross section of a process channel contains only a single fuel element, and the specific power and power density are consequently low. These characteristics result from the use of metallic uranium, since the massive elements not only promote the attainment of the

Table VII-2 PERFORMANCE OF BERKELEY AND BRADWELL STATIONS DURING PEAK LOADING OF U. K. CENTRAL ELECTRICITY GENERATING BOARD SYSTEM[9]

	Berkeley		Bradwell	
	Nov. 1962 to Feb. 1963	Nov. 1963 to Feb. 1964	Nov. 1962 to Feb. 1963	Nov. 1963 to Feb. 1964
Design sent-out capacity, Mw	275	275	300	300
Maximum sent-out capacity achieved, Mw	231	241	278	311
Units sent out, kw-hr × 10^{-6}	528	557	552	807
Utilization factor, %	67	70	64	93
On-power dates	Reactor 1, June 1962 Reactor 2, Oct. 1962		Reactor 1, June 1962 Reactor 2, Nov. 1962	

Table VII-3 ANALYSIS OF PERFORMANCE FROM STARTUP TO FEBRUARY 1964, BERKELEY AND BRADWELL STATIONS[9]

	Berkeley, %		Bradwell, %	
Utilization factor		52		60
Utilization losses				
Output restrictions				
Nuclear fuel temperature		4.8		5.8
Nonnuclear pressure drop in superheaters		8.0		0
Plant nonavailability				
Nuclear				
Reactor trips	0.4		0.4	
Spurious reactor trips	1.1		0.6	
Flux scan tube failure	0		1.8	
Absorber, fuel, etc., movements off load	2.6		2.1	
Fuel failures	0.7	4.8	0.4	5.3
Nonnuclear				
Modification of superheaters	9.6			
Turbines, boilers, etc.	6.3	15.9	7.0	7.0
Planned maintenance		3.6		9.0
External causes		0.2		0.3
All other causes (load changing, startup, fuel integrity tests, etc.)		10.7		12.6
		100		100

necessary reactivity but also keep the fabrication component of the fuel cost at a reasonable level, despite the short exposure lifetime. The logical development of the reactor type, as embodied in the AGR, is a reactor capable of developing considerably higher gas temperatures and much higher power density, along with much extended fuel life. This is accomplished principally through the use of different fuel and cladding materials but requires the use of enriched fuel. Details of the AGR, in which the fuel consists of slightly enriched-uranium dioxide pellets encased in thin stainless-steel cans, assembled in clusters, are in Ref. 17. Fuel loading of the AGR commenced[8] in August 1962, and since February 1963 the reactor has operated at or above its designed power. The designed gross electrical generation of 33 Mw was achieved at startup, and within weeks the output was increased to 37 Mw, the limit of the installed generating plant. The experimental nature of the AGR has required the reactor to be shut down on several occasions, but, despite these periods of shutdown, the plant load factor (utilization factor) for the first year of operation has been a very satisfactory 74.1%. The plant availability factor, defined as the proportion of time for which the reactor was operating at full power, or for which the plant was fully available but was shut down or operated at reduced power for experimental purposes, has been 86.6%. These values, as well as the reasons for losses of equivalent full-power time, are shown in Table VII-4.

In summarizing the current status of the gas-cooled graphite-moderated reactor, one can really state only the obvious things: that a large number of the reactors have been built; that the reactors which have been built have operated satisfactorily and have proved that

Table VII-4 CAUSES OF REACTOR OUTAGE OF THE AGR[8] (FEBRUARY 1963 TO FEBRUARY 1964)

(Losses As Percent of Equivalent Time at Full Power)

Planned annual maintenance and inspection, %	4.5
Unplanned maintenance, %	
Control-rod sleeve faults	4.6
Electrical/mechanical faults	2.8
Instrument faults	0.03
Human errors	1.5
Total operational losses, %	13.4
Operational availability, %	86.6
Off load or reduced power handling of irradiation experiments, %	11.7
Power reduction for physics experiments, %	0.8
Total experimental losses, %	12.5
Plant load factor, %	74.1

the type is reliable; that, typically, original performance capacities are exceeded by technological improvements which are incorporated in the existing plants; that the advanced reactors represented by the British AGR appear to have a sound basis for future development; and, finally, that the development of the technology has proceeded as might have been expected. Thus the very considerable gains that can be made by choosing a reactor type and building and developing it intensively have been demonstrated. If the type still appears to be less than economically competitive in countries like the United States, it is not because of any failure to equal or exceed the early expectations but because of inherent characteristics of the type.

Fuel Elements

The Magnox reactor, which is defined as a graphite-moderated gas-cooled reactor fueled with metallic uranium in Magnox cans, is the "standard" reactor discussed here. The cost reductions that have been achieved in the development of this reactor type are discussed in a paper by Smith et al.[7] which, although written to apply to those reactors developed in the United Kingdom, serves as an excellent guide to the directions of development and remaining areas of exploitability of the general reactor type. The comments that follow are taken largely from Ref. 7.

The primary factors in the cost reductions which have been achieved are increases in unit output, improvements in layout and detailed design, and increases in fuel rating. Since the fuel electrical rating (electrical megawatts per metric ton of uranium) determines the total weight of fuel in a plant of given capacity, it is a significant parameter in the cost of the first fuel charge and also influences strongly the reactor dimensions, which, in turn, are reflected in the cost of the reactor and its associated equipment. The fuel electrical ratings can be increased by increasing fuel heat ratings, by increasing reactor coolant temperatures and steam-cycle efficiencies, or by lowering blower power. The achievement of a net gain by any of the above three means while keeping materials constant requires improvement of the fuel-element heat-transfer performance and/or the coolant heat-transport performance; in the gas-cooled reactor, the most straightforward approach to such a gain is an increase in the coolant pressure. The trend toward higher pressures is illustrated in Fig. VII-1 for a majority of the Magnox reactors designed and built to date. The prestressed-concrete pressure vessels developed for the very large Magnox reactors have enabled the designer to select coolant pressure on the basis of economic optimization. All the high-output plants shown in Fig. VII-1 (Oldbury, Wylfa, EDF-3, and EDF-4) utilize the concrete vessel, and the attendant increase in fuel electrical rating is evident.

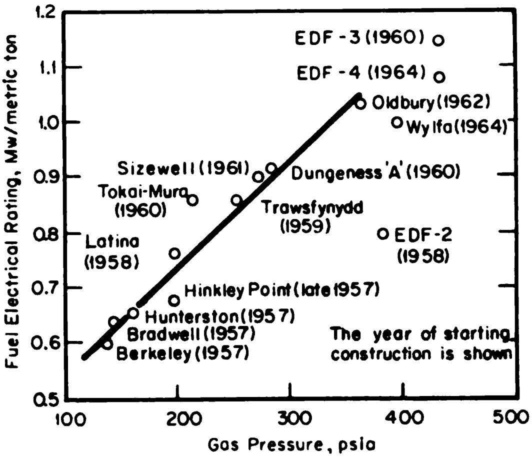

Fig. VII-1 Fuel ratings and gas pressures of various reactor designs.[3,7]

As stated in Ref. 7: "The scope for increasing thermal efficiency of Magnox stations is probably fully exploited, so attention is now focused on increasing the fuel heat rate." Much of the effort on fuel and fuel-element development has been directed toward finding designs that can yield the higher heat ratings simultaneously with a fuel-element life expectancy that is at least as long as the reactivity lifetime afforded by natural uranium.

Fuel Materials

Certainly one of the most significant developments in the Magnox-reactor fuel program has been the production of "adjusted" uranium by the British. In the earlier days of the Magnox reactor, core life was considered to be determined by the swelling in the natural-uranium metal fuel. It is now considered that the behavior of the uranium is not a limitation in the operation of the Magnox fuel elements and that the lifetime limit will be determined by the available reactivity. Basically, adjusted uranium is uranium containing 400 to 1200 ppm aluminum and about 300 ppm iron and 600 ppm carbon. These additions of material produce the greatest individual effect in reducing swelling, but, in order to obtain the effect, it is necessary to quench the uranium from the beta phase and subsequently anneal it in the alpha phase. In uranium produced by this method, the fractional volume increases are remarkably small and are unaffected by fission rate (for a given total burnup). British data[18] indicate that the adjusted uranium is superior to uranium-molybdenum alloy in its swelling behavior and does not have the high-neutron-absorption penalty of the molybdenum alloy. Additionally, the molybdenum content of the uranium-molybdenum alloy presents a considerable problem in the chemical processing stage of the fuel cycle. Figure VII-2 illustrates the relation between the volume increases in uranium and uranium alloys. The adjusted uranium has been tested in thermal-cycling conditions of the amplitude and frequency expected in the Magnox reactors, and its swelling appears to be unaffected by such cycling.

Reference 18 contains an interesting dissertation on uranium swelling which, for the purposes of this discussion, can be said to be dependent largely on the size and distribution of fission-gas bubbles in the metal. In a rather crude sense, it can be said that the swelling of uranium can be held to a minimum by preventing the coalescence of fission-gas bubbles: in other words, although fission-gas generation is a function of irradiation, the effects of such generation can be minimized by preventing the migration and coalescence of the gas bubbles. In even simpler terms the desired condition within the fuel is one in which the number of gas bubbles is kept to a maximum and, consequently, the sizes of the individual bubbles are kept at a minimum. During the production of adjusted uranium, when the material is held in the beta phase, most of the particles of the intermetallic compound UAl_2 and all the particles of U_6Fe precipitated during casting are redissolved. When the material is quenched, the aluminum and iron are retained in solution and, during the subsequent alpha annealing, are reprecipitated as fine particles at the grain boundaries and within the grains of the material. The quenching and annealing apparently produce a fine intragranular and intergranular dispersion of UAl_2 particles with possibly some iron in solid solution. The reason for the excellent performance of the adjusted uranium is thought to be that this dispersion essentially "anchors" the fission-gas bubbles within the material so that migration and coalescence cannot take place.

Although the adjusted uranium has become the standard material used at the Springfields Works (the fuel-element production facility of the UKAEA),[19] and although the British consider[19] that other alloys now undergoing irradiation are unlikely to show an overall advantage as a fuel material when compared to the adjusted uranium, it is evident that the French

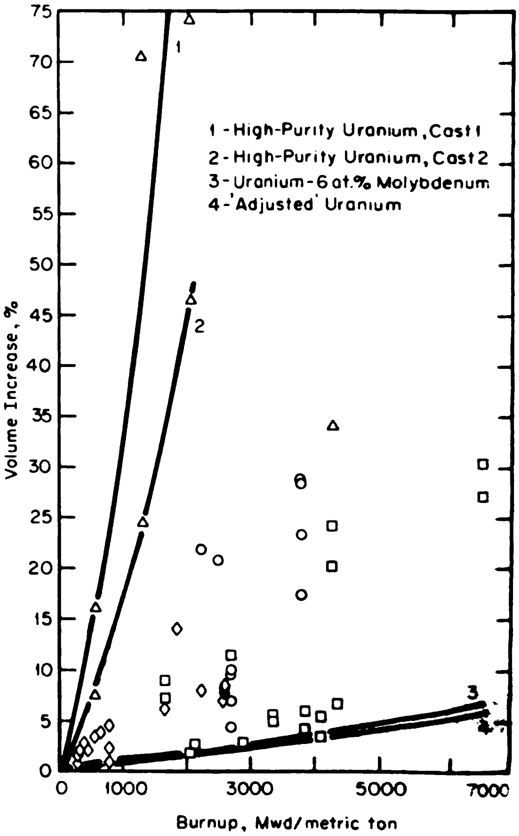

Fig. VII-2 Volume increases in uranium with no added aluminium, irradiated at 500 to 650°C. Curves for high-purity uranium, uranium—6 at.% molybdenum, and "adjusted" uranium are superimposed. ◇, *U. S. results, direct irradiation.* ○, *U. S. results, postirradiation annealing.* ▽, *AERE results, direct irradiation, 30 to 90 ppm carbon.* □, *AERE results, direct irradiation, 300 to 1000 ppm carbon.*

consider other alloys as the preferred Magnox-reactor fuel materials. The French flatly contradict the British proposition that the bubble-migration phenomenon is the dominant factor in the growth of uranium fuel elements and state[20] that no French experiments have ever shown evidence of such a phenomenon. In the later French reactors, the fuel is typically uranium-molybdenum alloy, with the molybdenum content ranging from 0.5 to 1.0%. These fuel elements are hollow-rod type elements with external cooling only. For their advanced fuel element, which has an annular cross section of uranium cooled internally and externally, the French propose a fuel made of uranium of "low alloy contents" in order to avoid the relatively high neutron absorption of the molybdenum alloys, since the mechanical strength of the molybdenum alloy is not required in the internally cooled annular elements. Perhaps the French philosophy on fuel-material development is that the uranium-molybdenum alloys possess a high mechanical strength at elevated temperatures and that this property makes them particularly suitable for use in the hollow-rod elements subjected to high external pressures. Furthermore, growth becomes negligible at temperatures around 525°C and appears to be independent of the type of alloy considered, although no inconvenient swelling has been observed in the uranium-molybdenum alloy during fuel-element tests.[6] Although the French are devoting a substantial effort to the development of the annular fuel element that utilizes less absorptive fuel than their typical uranium-molybdenum alloy, they clearly state[21] that the more conventional closed-tube elements such as those employed in the EDF-2, -3, and -4 reactors will not be abandoned.

Although development of fuel elements for the AGR in Great Britain is continuing, nothing very unusual has been reported concerning the fuel portion of these elements. High-density UO_2 is still the preferred fuel material, and research on this material is proceeding along fairly routine lines. The major emphasis in the development of these fuel elements is in the configuration and cladding materials, which will be discussed in following sections.

Fuel-Element Cladding and Structure

The policy adopted by the British for the development of critical items such as cladding alloy and structural alloy for fuel elements has been one of parallel development with alternative solutions. It appeared likely that the material used for cladding alloy since 1956 in the Calder Hall reactors would have a limited life because of failure by linkage of grain-boundary cavities at temperatures up to 300°C. This material, a coarse-grained magnesium–0.8% aluminum alloy called Magnox AL80, could be replaced by a fine-grained Magnox AL80 that exhibited a greater ductility and could be expected to have a longer life, but the fine-grained structure could be attained only by the controlled application of cold work which might be expected to be a hindrance to bulk manufacturing operations.[19] The principal alternative to the fine-grained Magnox AL80 alloy was an inherently fine-grained two-phase alloy containing 0.55% zirconium and called Magnox ZR55. Cladding made of bulk materials was produced for the Civil Reactor Program in Great Britain, and large-scale proving trials in the UKAEA reactors were begun. Meanwhile, the manufacture of the fine-grained AL80 cladding material was developed until the process was suitable for large-scale production of cans, and this development turned out to be a fortunate one for the program. Because of the diffusion of plutonium through the Magnox ZR55 cladding at irradiations above 1000 Mwd/ton, the operation of the burst-cartridge detection gear in the Magnox reactors was impaired. Consequently, the fine-grained Magnox AL80 has been adopted as the "standard" cladding material for use in the British reactors.

The requirements of some of the structural components of fuel elements are different than those of the cladding since the loadings are different. For instance, the end caps and associated fittings which support the axial loads acting on stacked elements require a high resistance to creep but demand less ductility than is required of the cladding alloys. To date, a 0.7% manganese alloy, Magnox MN70, has been the one most widely used for end caps and fittings,[22] and the most popular material for spreaders and braces has been heat-treated Magnox ZR55 (Ref. 19).

The French presented relatively little information at Geneva concerning the development of cladding and structural materials for the fuel elements of their gas-cooled reactors. Although they are aware of the fine-grained Magnox AL80 used by the British, the French appear to prefer[23] a magnesium-zirconium alloy similar, presumably, to the Magnox ZR55 considered by the British. Although the typical French fuel element does differ[21] from the British elements (in that, since EDF-2, the French have fitted their elements with a graphite sleeve), the plutonium diffusion problem must still remain. Little information was given concerning burst-cartridge detection in the French reactors, but the problem has apparently been reconciled with the operation of the reactors. Apparently the magnesium-zirconium alloy is used for the welded end caps[23] of the fuel elements as well as for the cladding material.

The development of cladding materials for higher temperature gas-cooled reactors (such as the AGR and the French gas-cooled heavy-water-moderated reactor EL-4) indicates that, at least for the fairly near future, reactors of this sort will utilize fuel that is clad with very thin stainless steel. Apparently, the British are not considering very seriously any material other than stainless steel for this high-temperature application, although some years ago beryllium had been considered for use in the AGR. The French, however, although resigned to the use of stainless steel at present, continue studies directed toward the development of beryllium as a cladding material and are investigating, in parallel efforts, other materials such as iron-aluminum alloys. Reference 24 contains descriptions of some of the recent work in France on the development of beryllium and indicates that some progress is being made on the problem of improving the ductility of beryllium in the direction perpendicular to the direction of extrusion.

Fuel-Element Configurations

The fuel-element configuration that has been used or specified most frequently in Great Britain is the solid rod in a polyzonal can, whereas the French ordinarily use the hollow rod in a polyzonal can, housed in a graphite sleeve. The British-designed Tokai reactor, however, has[25] a hollow-rod element and a graphite sleeve, and the Hunterston reactor also has the graphite sleeve.[25] Some of the fuel geometries that have been considered by the British are shown in Fig. VII-3. The arrangement of flat bars in a fuel element is one in which bars with different widths are held parallel to each other to "fill" approximately the circular-cross-section fuel channel. The investigation of these geometries has been prompted by the trend to higher heat ratings. A departure from the solid fuel geometry is required if the desired increases in rating are to be achieved. The British have apparently concluded that the flat-bar and tubular elements offer substantial savings in power-generation cost relative to the current solid-rod designs in very large reactors.[7] Of the two configurations the flat-bar approach is preferred because it appears to have fewer technical uncertainties and slightly better economic potential than the tube.[7] Of the solid-rod type elements used or specified to date, two types appear to have been used in the largest numbers. These are the polyzonal element with helical fins and the polyzonal element with herringbone fins. Drawings of the external appearance of elements of these types are shown in Fig. VII-4. As is indicated by the drawing, the herringbone element is considerably simpler mechanically than the helical type identified as a Dungeness Mark I element. Although the British have been quite cautious and have stated that the herringbone element has yet to demonstrate its stability in such mechanical form,[26] they do plan large-scale irradiation trials and state that the merits of the design[27] have re-

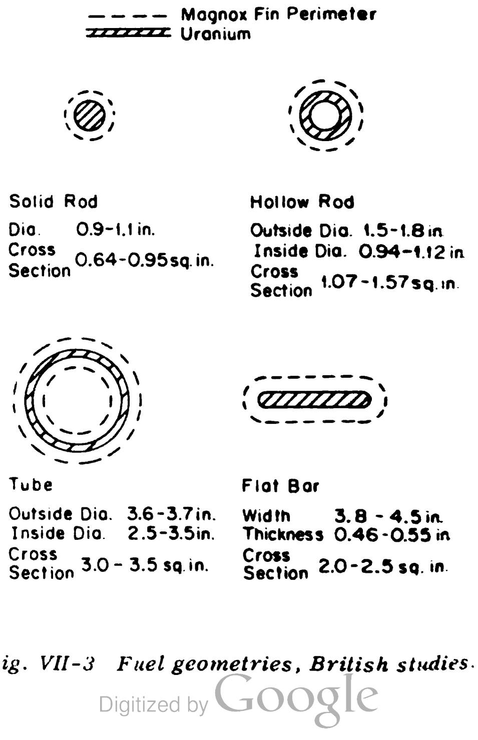

Fig. VII-3 Fuel geometries, British studies.[7]

ulted in its adoption for the second reactor at izewell.

The characteristics of French fuel elements r Magnox reactors are shown in Table VII-5, hich indicates that the reactors in the EDF eries all use hollow rods, that from EDF-2 nward graphite sleeves have been used, and that for the external surfaces of round elements the herringbone finning arrangement is preferred.

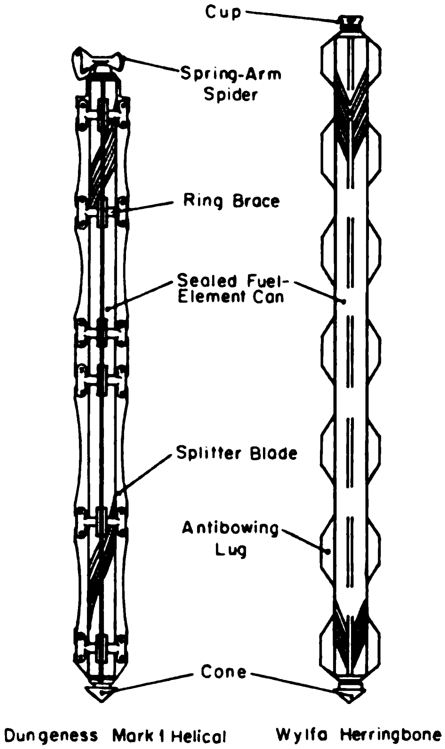

Fig. VII-4 British fuel elements.[26]

The "advanced" French fuel element that corresponds to the flat-plate type envisioned by the British is the annular element listed in Table VII-5 and shown in Fig. VII-5. As indicated in the drawing, this is a very large element, the distance across the span of the centering device being about 7 in. Its cross-sectional area of fuel and its inside and outside diameters correspond roughly to those studied by the British in their search for an advanced fuel element (Fig. VII-3). It is interesting to compare the maximum specific powers shown in Table VII-5 for the French fuel elements with the data presented in Fig. VII-6, which is based on information generated by the British and presented in Ref. 7. The comparative generation costs shown in the figure are based on optimized reactors of 500-Mw(e) output for each of four fuel geometries. Although it is stated that the fuel prices for the flat bar and the tube are nearly the same for their optimum designs,[7] the blowing power requirement at a given coolant pressure is lower for the flat-bar design than for the tube, and this more than offsets the costs associated with the requirement for a somewhat larger core when the flat-bar design is used.

With regard to the French fuel-element program, an interesting comparison of the relative costs of the various operations in preparing fuel elements for the reactors for G2 to EDF-3 is shown in Table VII-6. Since the "new uranium" cost should be the same for each ele-

Table VII-5 CHARACTERISTICS OF FRENCH FUEL ELEMENTS[21]

	EDF-1	EDF-2	EDF-3 and EDF-4	Annular element (INCA)
CO_2 pressure, psia	406	385	435	656
Fuel				
Alloy	U-Mo, 0.5%	U-Mo, 1%	U-Mo, 1%	Slightly alloyed U
Diameter, in.	0.55 × 1.38	0.71 × 1.57	0.90 × 1.69	3.03 × 3.74
Cross section, sq in.	1.24	1.55	1.55	3.88
Maximum specific power, Mw/ton	4.4	5.8	6	11
Can				
Type of fins	Longitudinal	Helical herringbone	Flat-sided herringbone	External, herringbone; internal, longitudinal or corrugated
Maximum heat flux, Btu/(hr)(sq ft)	178,000	260,000	257,000	External, 333,000; internal, 222,000
Element				
Individual support	None	Graphite sleeve	Graphite sleeve	Graphite sleeve
Length, in.	23.6	23.6	23.6	23.6
Number per channel	15	12	15	15

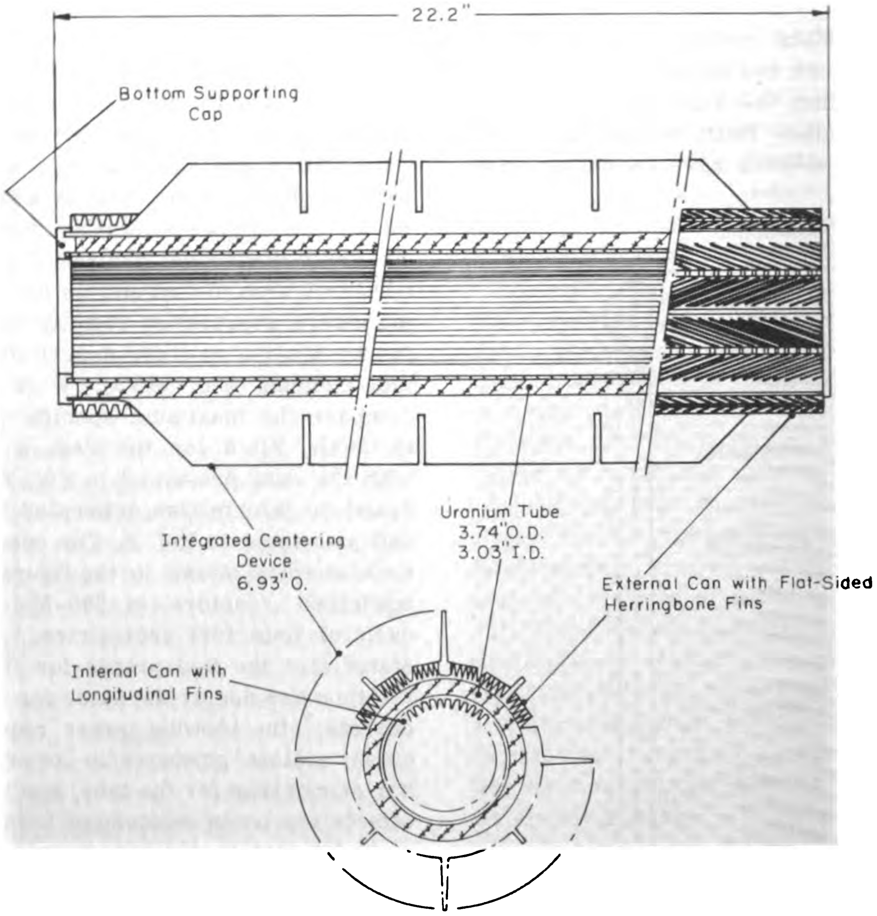
22.2"
Bottom Supporting Cap
Uranium Tube 3.74" O.D. 3.03" I.D.
Integrated Centering Device 6.93" O.
External Can with Flat-Sided Herringbone Fins
Internal Can with Longitudinal Fins

Fig. VII-5 The French annular element (INCA).[21]

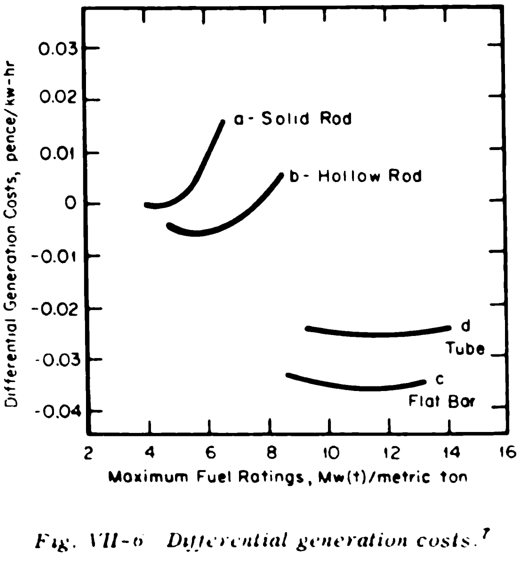

Fig. VII-6 Differential generation costs.[7]

ment type, the relative costs for the complete elements are easily derived.

It appears that no radical changes are forthcoming in the selection of fuel-element configurations for advanced gas-cooled reactors such as the AGR, and the continued use of multirod bundles of small-diameter fuel tubes may be expected.[28]

Pressure Vessels

The British reactor stations up to Sizewell have utilized steel pressure vessels. The full electrical rating has been increased significantly through this series of plants, as indicated in Fig. VII-1, and much of this increase has come about through increases in coolant

Table VII-6 BREAKDOWN OF FUEL CARTRIDGE COST IN FRANCE[23]

	Percent of fuel cartridge cost			
	G2 and G3 solid rod (dia., 1.22 in.)	EDF-1 hollow rod (dia., 0.55 to 1.38 in.)	EDF-2 hollow rod (dia., 0.71 to 1.57 in.)	EDF-3 hollow rod (dia., 0.90 to 1.69 in.)
New uranium (ingots)	72	58	56	54
Solid-rod and hollow-rod manufacture	6	7	6	7
Cans and plugs	4	7	4	5
Alumine pellets		1		
Centering grids			2	
Graphite sleeves			8	8
Manufacture and testing	18	27	24	28

pressure. But increases in design pressure have been limited by the difficulties met in procurement and in on-site welding and inspection of thick steel plate.[7] At the same time the trend in reactor capacity has been to high-capacity units that make possible significant reductions in capital cost, and the influence of this trend has been to increase reactor size despite the higher power density that has been achieved. Consequently the problem of increasing the pressure in order to increase the fuel rating, while at the same time larger and larger plants are achieved, has resulted in the conflicting requirements of higher pressures in larger vessels. An example of this is evident in the designs of the Bradwell and Dungeness reactors. For Bradwell, 3-in.-thick plate was specified at a working pressure of 147 psia. For Dungeness, about three years later, when 4-in.-thick plate was available, coolant pressure was limited to a value somewhat less than 300 psia, and pressure-vessel dimensions were at a maximum of approximately 60 ft in diameter. The use of prestressed-concrete pressure vessels has permitted the economic optimization of coolant pressure and vessel diameter, and it is obvious from inspection of Fig. VII-1 that the desired pressure of the larger and newer power plants is substantially greater than that which had been possible in the units up through Dungeness-A.

The impressive sizes of the concrete pressure vessels which have been specified for planned plants are illustrated by the data presented in Table VII-7. For example, the Wylfa pressure vessel has an internal diameter about half again as great as that of the largest steel vessels, and the nominal pressure of its primary coolant is more than a third again as great as that of the steel-vessel plants. The proponents of the concrete vessel claim that it has other advantages also. A fair body of opin-

Table VII-7 GAS-COOLED CLAD-FUEL REACTORS USING CONCRETE VESSELS[4,10]

Reactor	Date of first reactor on power	Thermal power, Mw	Primary coolant nominal pressure, psia	Primary coolant temperature at reactor outlet, °F	Pressure vessel: Shape of internal cavity	Pressure vessel: Dimensions of internal cavity, ft	Pressure vessel: Approximate minimum wall thickness, ft
G2	1959	250	215	644	Horizontal-axis cylinder	Diameter, 45.9; length, 51.5	9.8
G3	1960	250	215	644	Horizontal-axis cylinder	Diameter, 45.9; length, 51.5	9.8
EDF-3	1966	1560	435	770	Vertical-axis cylinder with truncated cone sections at top and bottom	Diameter, 62.3; height, 69.1	13.9
Oldbury	1966	890	365	770	Vertical-axis cylinder	Diameter, 77.0; height, 60.0	15.0
EDF-4	1968	1650	435	752	Vertical-axis cylinder with upper truncated cone section	Diameter, 62.3; height, 119.0	16.4
Wylfa	1968	1870	400	770	Sphere	Diameter, 96.0	11.0

ion among the British and French designers is that the steel pressure vessels used in the United States are, in fact, susceptible to sudden failure. In the opinion of these people, the maximum credible accident should logically be considered to be the sudden brittle fracture of the reactor pressure vessel; the mode of ultimate failure of concrete pressure vessels, however, is progressive and without sudden rupture.[29] Obviously this theory is not widely popular among the proponents of steel vessels.

Refueling Machines

The performance of refueling equipment in both the British and French reactors has been acceptable, and the development of refueling machines has been characterized by steady improvements based on operating experience gained with the machines used in the relatively early reactors. In the G2 and G3 reactors, the original machinery has been improved principally for increasing operational safety, but the improvements have also permitted increases in the refueling rates so that it is now possible to discharge nearly 27 fuel channels in 24 hr, or about three times the initial design rate of the machines.[1] The EDF-2 reactor is equipped with two refueling machines, the main machine and an auxiliary machine, whereas in EDF-3 the French have reverted to a single all-purpose device. Among the difficulties encountered by the designers of the equipment for these reactors is the problem of lifting of the last few elements in a particular channel when that channel is being unloaded under power. Important design features of the machines[30] are the baffling arrangements that are used to avoid levitation of the final elements by preventing a very high loss of head at the top end of the channel being refueled. The performance of the French refueling equipment will be interesting to observe in view of the fact that studies and tests are said to account for about 35% of the cost of the machines.

A British paper[31] relates the experience obtained with the Bradwell and Latina on-load fuel-handling equipment and discusses the influence of this experience on the design of later machines for the Dungeness and Oldbury reactors. It is sufficient here to point out two of the major conclusions of the paper. The first is that the time required for the machine to perform a certain number of reloading or charging operations is considerably longer in practice than is indicated by design calculations. These differences in time are illustrated by the data in Table VII-8 which show that the actual time is some 2½ times as great as the design time. It is felt that the required time may be reduced to a value of about twice the design time. The other conclusion drawn by the British is given in the following quotation from Ref. 31: "Massive rather than elegant devices give by far the best service."

Table VII-8 BRADWELL CHARGE-MACHINE OPERATING-CYCLE TIMES[31]

Operation	Actual time, hr	Design time hr
Inspect three channels of fuel and load magazine	1½	
Load three channels of fuel into machine	2	1
Travel machine to gas supply and connect	½	¼
Pressurize machine	¾	
Reinstate previous standpipe and prepare new one	3	
Connect machine to standpipe	½	½
Discharge and reload three channels	8	3¾
Disconnect machine and travel to vent point	½	¼
Depressurize machine	½	2
Connect to discharge hole and unload three channels	2	
Travel to vent point and purge machine	½	
Travel to loading point and connect	½	¼
Total times	20¼	8

Control and Instrumentation

The development of larger and more complex reactor plants has had a number of effects on plant operating philosophy. There are trends (1) toward centralized control,[32] (2) toward a better understanding of, and consequently a closer approach to, the temperature limits of the various core materials,[33] and (3), because of the very large reactors currently under construction and operation, toward concentrating on the control and stability problems inherent in very large cores, particularly with regard to spatial variations.[34] The experience gained rough the years, while revealing some probms that had not been anticipated in the early signs, has served as both a firm foundation d an experimental basis for the future operaon of power reactors.[35]

At the time the burst-cartridge detection gear as designed for the Calder Hall reactors, no erating experience existed to indicate the pes of fuel-element failure which might occur. onsequently the systems supplied for the early eactors were designed to meet a few fundaental requirements for burst-cartridge deection and were not particularly suited to deecting properly the types of actual bursts that ould be encountered during operation. As a onsequence of reactor operation and the deermination of the most likely modes of fuel-lement failure, system specifications have een more clearly defined. The fast burst, a uel-element failure that gives virtually instantaneous release of a significant quantity of fission products, has been identified as a particular failure type, and this type of burst nakes important the quick-detection-and-location capability that has led to an increase in the frequency of group scanning at some expense to sensitivity. Since experience with the early reactors became available, the burst-cartridge detection systems for the British reactors have used a combination of the fast scan at low sensitivity with a single-channel scan of long cycle time. Some of the features of systems designed for later British reactors are given in Table VII-9.

The French G2 reactor was initially equipped with a burst-cartridge detection installation similar to that used in the Calder Hall reactors.[1] On the strength of experience acquired with the G1 reactor, modifications to the G2 system and development of the G3 system have been based on a capability which the French feel is important: measuring the time rate of the signal as well as an instantaneous absolute value. The G3 reactor installation has performed satisfactorily and has served as the basis for the burst-cartridge detection systems that will be employed in the EDF reactors.

Advanced Concepts and Future Directions

The concepts that are classified here as "advanced" include the advanced gas-cooled reactor, typified by the Windscale AGR, and the integrated plant designs that utilize concrete pressure vessels to enclose the entire primary system.

The AGR has been described rather thoroughly in the literature, and here it will suffice to say that the reactor was commissioned essentially on schedule and that its operation since commissioning has been entirely satisfactory.

Table VII-9 DETAILS OF RECENT BRITISH BURST-CARTRIDGE DETECTION SYSTEMS[36]

	Dungeness	Sizewell	Oldbury	Wylfa
Reactor No. 1 on load	1964	1965	1966	1968
Channels in reactor	3932	3784	3308	6156
Channels per group sample	32	32	8	32
Period of group scan, min	6.7	Continuous	11	Continuous
Cycle time per sample, sec	25	60	25	60
Single-channel scan period, hr	3.7	4.25	4.0	7.1
Total precipitator units per reactor	20	18*	27	29*
Group sample flow rate at precipitator, lb/sec	0.115	0.037	0.115	0.031
Single sample flow rate at precipitator, lb/sec	0.042	0.017	0.042	0.026
Total circuit mass flow, lb/sec	1.6	5.2	2.4	7.3
Circuit pressure drop, psi	40–45	40	42–47	55
Transit time, channel to precipitator, sec	6	5.9	11	6.7
Sensitivity (M.D.A.)†				
Group, mm^2	10.0	3.5	2.5	3.8
Single, mm^2	0.57	0.11	0.57	0.13

*Eight chambers per precipitator unit.

†Minimum detectable area as determined by an alarm set 25% above background for a scanned system and 15% above background for a continuous system.

As mentioned briefly before, the AGR type fuel elements have undergone no major evolution in the past few years: the reactor type is apparently destined to use the multirod bundle type element. Since an element of this type involves relatively high fabrication costs per unit weight of uranium, favorable economic performance requires a rather long fuel life in the reactor. This requirement poses a difficult task for the designer if it is also imperative to design for the minimum possible fuel enrichment; for, in the absence of a good low-cross-section material for the fuel jacket, he must design for the minimum-thickness jacket of stainless steel. A fairly recent development in the AGR fuel program is the consideration of the use of plutonium[37] as the enriched component of the fuel, since it is felt in Great Britain that the stockpile of plutonium is growing at a rate which will ensure a more than adequate supply of the material when fast-breeder reactors become commercial. Consequently the British philosophy appears to be that the thermal reactors will be permitted to utilize this "extra" plutonium if it appears feasible.

The integrated plants, which are EDF-4, Oldbury, and Wylfa, are typified by their compact arrangements (if such a description can be applied to these huge reactors). Although all three reactor vessels contain all the principal components of the primary circuit, their shapes and arrangements are quite different, as indicated in Table VII-7. EDF-4, for example, utilizes a rather tall, thin configuration in which the steam generator is located below the reactor core. A disadvantage of this scheme is the lack of natural-circulation cooling in the event all CO_2 circulators are lost. With the over-and-under arrangement of the major components of the primary loop, it follows that the EDF-4 pressure-vessel internal space is relatively small in diameter and quite high, as indicated in Table VII-7. The basic arrangements in Oldbury and Wylfa resemble one another in that the steam generators are located peripherally around the reactor core and at about the same elevation as the core. The shapes of the internal cavities of the pressure vessels are different, however, with the Wylfa station retaining the traditional spherical shape of the earlier British stations and with Oldbury using a vertical-axis cylinder.

The directions of future development of the planned stations in both Great Britain and France are rather clearly shown by the information presented in Table VII-1 and by the increases in primary coolant pressure and in electrical rating shown in Fig. VII-1. What is not so clearly shown is the type reactor that will be employed for the "next generation" plants in these two countries.

At the time of its conception, the AGR was felt to be the logical successor to the Magnox stations in Great Britain. Although the AGR has performed as expected, there is still the problem of minimizing absorption in the fuel cladding in order to obtain long fuel lifetimes at low values of enrichment. When one makes the jump to enriched fuel, a variety of reactors enters the picture. Furthermore, although the AGR fuel has behaved well to date, the operation reported has carried the exposure only to the neighborhood of 4000 Mwd per metric ton of uranium, a long way from the economic optimum average burnup of around 20,000 Mwd per metric ton of uranium, or even the average value of 12,000 Mwd per metric ton of uranium which is stated[28] to be the target for the first charge of an early commercial station. Effort is being directed toward the further development of the AGR fuel element along such lines as thinner cladding material, basic studies in oxide fuels, and the development of plutonium enrichment for thermal-reactor fuel. At this time the preferred future concept for construction in Great Britain is not clear, although there have been some indications that the Magnox reactor has about reached the end of the line. Whether the AGR type plant will be built in large numbers as a second-generation gas-cooled-reactor type is uncertain. The selection of a preferred concept for the future will be based largely on economic considerations, but surely there will be a strong tendency toward the gas-cooled type because of the large amount of experience accumulated and the advances expected of the very large integrated plants utilizing concrete pressure vessels.

In France the directions of future development are clearer: the French like Magnox reactors, and, after some apparent early uncertainty, they have committed their gas-cooled program to the concrete pressure vessel. They are developing the integral plant concept with the EDF-4, and they will apparently adopt no other new concept in the very near future, although the performance of EL-4 will affect later plans. In France, then, it appears that the Magnox reactor can look forward to a relatively bright future.

References

The references that contain A/Conf. numbers are papers that were presented at the Third United Nations International Conference on the Peaceful Uses of Atomic Energy, Geneva, September 1964.

1. R. Boussard, F. Conte, and J. Stoltz, Operating Experience with the G2–G3 Reactors at Marcoule and Starting Test Results for the Chinon EDF I Reactor, A/Conf.28/P/35.
2. J. Bourgeois and B. Saitcevsky. The Development of Natural Uranium Graphite Reactors, A/Conf. 28/P/36.
3. C. Bienvenu, P. Passerieux, and P. Bacher, Nuclear Power Stations E.D.F.2–E.D.F.3 and E.D.F. 4, A/Conf.28/P/38.
4. G. Lamiral, L. Laurent, R. Bonnelle, N. Beaujoint, and P. Faurot, The Prestressed Concrete Pressure-Vessels for French Natural Uranium-Graphite-CO_2 Gas Type Reactors, A/Conf.28/P/52.
5. R. Fays, L. Laurent, F. DeVathaire, J. Plisson, and J. Bussi, Safety of Natural Uranium-Graphite-Gas Type Reactors, A/Conf.28/P/81.
6. M. Englander et al., The Effect of Neutron Irradiation on Certain Fuels Used in Gas-Graphite Type Reactors, A/Conf.28/P/97.
7. D. R. Smith, P. D. Murphy, R. Rutherford, C. S. Lowthian, and J. M. Yellowlees, The Trend to Higher Ratings in the Magnox Reactor, A/Conf. 28/P/124.
8. K. Saddington, T. N. Marsham, and J. Moore, The Contribution of the Windscale Advanced Gas Cooled Reactor to the Development of a Commercial Power System, A/Conf.28/P/125.
9. D. R. R. Fair and R. L. Rutter, Early Operation of the C.E.G.B. Nuclear Power Stations, A/Conf. 28/P/128.
10. A. H. Brown, J. D. Hay, R. B. Hyde, and T. W. Spruce, The Design and Construction of Prestressed Concrete Pressure Vessels with Particular Reference to Oldbury Nuclear Power Station, A/Conf.28/P/140.
11. P. R. J. French, D. J. Millard, M. J. Cartmell, and B. K. Casterton, Experience in Relating the Observed Thermal Performance of Civil Magnox-Uranium Power Reactors to Design Predictions and Operating Criteria, A/Conf.28/P/171.
12. W. Penney, Nuclear Power in the United Kingdom, A/Conf.28/P/559.
13. P. W. Cash and F. Faux, Planning for Nuclear Power in the Central Electricity Generating Board's System, A/Conf.28/P/561.
14. A. Bertini, G. Gualtieri, G. Lesnoni, B. Zaffiro, M. Calcagno, and R. Negrini, Latina Nuclear Power Station: Commissioning and First Operational Experience, A/Conf.28/P/865.
15. J. Gaussens, A Few Present Economic Aspects of Nuclear Energy in France (Charge des Etudes Economiques Generales at the C.E.A.).
16. Power Reactors the World Around, *Nucleonics*, 21(2): 112-115 (August 1963).
17. *J. Brit. Nucl. Energy Soc.*, 2(2): (April 1963).
18. R. S. Barnes, R. G. Bellamy, B. R. Butcher, and P. G. Mardon, The Irradiation Behaviour of Uranium and Uranium Alloy Fuels, A/Conf.28/P/145.
19. J. C. C. Stewart, V. W. Eldred, T. J. Heal, D. O. Pickman, and H. Rogan, Review of Progress of Development, Manufacture, and Performance of Magnox Fuel Elements in the United Kingdom, A/Conf.28/P/560.
20. Y. Adda, J. Mustelier, and Y. Quere, Behaviour of Uranium Under Irradiation, A/Conf.28/P/62.
21. M. Salesse, J. Stohr, and G. Jeanpierre, Recent Developments Concerning French Fuel Elements for Natural Uranium-Graphite-CO_2 Reactors, A/Conf.28/P/60.
22. P. Greenfield, R. G. Coffin, G. C. E. Olds, B. Pickles, and T. C. Wells, Development of Magnesium Alloys for Fuel Elements in the United Kingdom, A/Conf.28/P/146.
23. R. Boussard, B. Boudouresques, and J. Nadal, The Manufacture of Fuel Elements in France, A/Conf.28/P/57.
24. J. M. Mallen-Herrero, Effect of Impurities of the High-Temperature Brittleness of Commercial Grade Beryllium, French Report CEA-R-2445, 1964.
25. R. Sagane, T. Yoshioka, N. L. Franklin, B. E. Eltham, P. T. Fletcher, and B. C. Woodfine, The Design and Development of the Tokai Hollow Rod Fuel Element, A/Conf.28/P/426.
26. J. W. Hughes, G. H. Inglis, C. H. Jones, and J. Price, The Development and Evaluation of Uranium Magnox Fuel Elements, A/Conf.28/P/147.
27. C. Cunningham, B. E. Boyce, T. Davis, and B. N. Furber, Heat Transfer and Pressure Drop Performance of Herringbone and Helical Fin Fuel Elements for Uranium/Magnox Reactors, A/Conf. 28/P/135.
28. G. B. Greenough, J. S. Nairn, and J. D. Thorn, Progress Towards the Design of A.G.R. Fuel Elements for Power Reactors, A/Conf.28/P/149.
29. R. S. Taylor and A. J. Williams, The Design of Prestressed Concrete Pressure Vessels, with Particular Reference to Wylfa, A/Conf.28/P/141.
30. B. Saitcevsky and D. Gaussot, Refueling Equipment in Natural Uranium-Graphite-Gas Reactors, A/Conf.28/P/54.
31. J. O. Joss, W. H. Shipley, G. H. Branch, and J. E. Taylor, Experience with Bradwell and Latina On-Load Fuel Handling Equipment and Its Influence on Future Designs, A/Conf.28/P/139.
32. D. S. Hiorns, T. O. Jeffries, D. Moore, H. Moores, and A. H. Weaving, Recent Developments in the Instrumentation and Control of Large Gas-Cooled Reactors, A/Conf.28/P/126.
33. H. A. Hughes, D. S. Briggs, R. Dodds, and R. M. Horsley, Temperature Limits and the Optimisation of Power Output in Calder and Chapelcross Reactors, A/Conf.28/P/178.
34. P. B. Branson, R. L. Carstairs, and A. J. Spurgin, Design of Control Rod Systems for Gas-Cooled Reactors, A/Conf.28/P/180.
35. H. A. Hughes, D. A. L. Clinch, R. M. Horsley, D. J. Millard, and R. Razzell, Experimental Basis of Power Reactor Operation, A/Conf.28/P/170.
36. B. Holmes and A. D. Boothroyd, The Development of Burst Cartridge Detection Systems with Particular Reference to Sizewell Nuclear Power Station, A/Conf.28/P/142.
37. B. Cutts, A Study of Fuel Cycles and Fuel Cycle Problems for Advanced Gas Cooled Graphite Moderated Reactors, A/Conf.28/P/177.

Section VIII

Power Reactor Technology

Gas-Cooled Unclad-Fuel Reactors

The gas-cooled unclad-fuel reactors are characterized by high coolant temperatures and all-ceramic fuels. The two reactors of this type which are under construction, the Dragon experiment in England[1] and the Peach Bottom prototype in the United States,[2] have not changed markedly since their designs were described in past issues of *Power Reactor Technology*. Dragon was described in the December 1962 issue, 6(1): 74, and the Peach Bottom description appeared in the June 1962 issue, 5(3): 61. The Dragon reactor[3] achieved initial criticality on Aug. 23, 1964, and initial operation of the Peach Bottom plant[4] is expected in 1965.

The designation of Dragon as an "experiment" and of Peach Bottom as a "prototype" is explained by the difference in components provided for the two plants. The Dragon installation is not equipped with power-generating equipment—its heat is simply dumped to a heat sink—whereas the Peach Bottom plant is provided with the usual electric-power-generating components of a power plant. A comparison of the characteristics of the two reactors is given in Table VIII-1, which contains information taken largely from Refs. 4 and 5.

As seen in Table VIII-1, the coolant outlet temperatures for two reactors are identical. From an overall point of view, this is perhaps the most significant comparison that can be made between the two reactors since both use the same coolant gas and both have the attainment of high coolant temperature as a major design objective.

As indicated in Table VIII-1, the Dragon core will be loaded with two types of fuel elements. Since the core is quite small, its neutron leakage is very high, and it does not, as a whole, represent a core typical of larger power reactors. It uses a two-zone loading[6] to overcome this disadvantage and generate information applicable to larger cores. The seven center

Table VIII-1 CHARACTERISTICS OF DRAGON AND PEACH BOTTOM

Plant characteristics	Dragon	Peach Bottom
Reactor thermal power, Mw	20	115
Net electric power, Mw	None	40
Coolant gas	Helium	Helium
Pressure, psia	294	350
Inlet temperature, °F	662	652
Outlet temperature, °F	1382	1382
Reactor core	Vertical cylinder	Vertical cylinder
Height, ft	5.25	7.5
Diameter, ft	3.5	9.1
Average power density, kw/liter	14.0	8.3
Fuel elements	Seven-rod clusters	Individual tubes
Number	37	804
Fuel material	Uranium in driver elements; uranium and thorium in test elements	Uranium and thorium
Cladding material	Graphite	Graphite
Control elements	Rods	Rods
Number	24	36
Location	Radial reflector	Core
Poison material	B_4C	B_4C
Drive location	Top	Bottom
Refueling	At shutdown	At shutdown

lements of the core will be representative of those which would be used in a large power reactor and will be fueled with a uranium-thorium mixture. The remaining 30 elements, which surround the seven center elements, will contain no thorium and will serve as driver elements that must be replaced at relatively frequent intervals. By this means the center elements can be irradiated for several years and will effectively "see" conditions that would be typical of a large power-reactor core.

Materials developments for the reactor type in the United States and the United Kingdom have proceeded along quite similar paths. Graphites with helium permeabilities as low as about 10^{-3} cm^2/sec have been developed in both countries, and fuel-particle development has been directed principally toward the design of coated particles.[7,8] Particle-coating investigations are concerned with single, double, and triple coatings utilizing pyrolytic carbon and silicon carbide. In addition to the work on pyrolytic carbon and silicon carbide, work continues in both countries on the development of alumina and beryllia.

The well-known advantages of helium as a reactor coolant are restated in the following quotation from Ref. 2:

> Helium gas is used as the HTGR system's coolant because its chemical inertness and other properties contribute to reliable, easily maintainable, high temperature plant operation. Helium does not react with or corrode any structural material; it does not react with steam, water or air. It does not undergo a change in phase at operating temperatures, nor does it solidify at ambient temperature. Helium does not parasitically absorb in the reactor core, and cannot affect the physics of the reactor; it does not become radioactive . . . .

There are, however, disadvantages to the use of helium, and these center about the fact that it is a relatively high-priced gas. The pressure of the system must be relatively high in order to achieve good heat transfer and heat transport with reasonable pumping powers. High pressure, unfortunately, tends to aggravate the leakage problem that exists with helium. Leakage must be minimized because of cost considerations and, in reactors of the unclad-fuel type, because of the relatively high radioactivity of the primary coolant. Consequently, the ability to fabricate primary coolant systems with a very high standard of overall leaktightness has been of major importance in the Dragon and Peach Bottom plants. Recent tests of the Dragon facility[9] have been very encouraging in this respect since the actual leakage rates encountered were within the specified rate of 0.1% per day of the gas contained in the circuit.

Although technologies developed for Dragon and Peach Bottom have been extended to conceptual designs of large nuclear power plants, the actual directions of future development of plants of this type are not uniquely defined at this time. The developers of Peach Bottom consider a plant in which a fuel-element purge system is employed and fission-product release is encouraged in order to obtain conversion ratios greater than unity.[2] Actually, this is the approach that was used by the Dragon designers[5] in the early stages of the project—they envisaged a fuel element that emitted as many fission products as possible to the fission-product trapping system, thereby obtaining the maximum reactivity benefit through the removal of neutron poisons from the fuel. However, further work showed that some of the more important fission products tended to remain in the fuel, although enough did leave to require the use of a complicated purification system to limit primary coolant activity. Consequently, the Dragon project does have the purge and purification system, but the hoped-for reactivity benefits from the removal of neutron poisons have not materialized. Recent studies, which must be regarded as preliminary, indicate that there could be some cost benefit associated with the development of a fuel element which could be directly cooled by the main helium stream and which would not be supplied with the elaborate purging and purification systems currently employed in Dragon and Peach Bottom.

The pebble-bed reactor[10] represents a different version of the high-temperature gas-cooled concept. It also uses the fuel in completely ceramic form—probably in balls containing UC_2-ThC_2 particles coated with pyrolytic graphite, with a graphite shell surrounding each ball—but no attempt is made to draw off fission products. The reactor is fueled more or less continuously during power operation by adding balls to the top of the assemblage, which constitutes the active portion of the core, and draining off balls from the bottom. Of the balls removed, the most highly exposed and those which may be damaged are discarded, and the good balls of low exposure are recycled to the reactor. One of the developmental problems is to find a means of handling and sorting the balls.

The concept is being developed primarily in Germany, and an experimental power station of 15 Mw(e) (the AVR Reactor), built for a group of utility companies with financial support from the federal government, is reported to be near completion in the Federal Republic of Germany.[10] Development is also proceeding toward a large reactor of the type.

It would appear that the development of the high-temperature gas-cooled reactor, utilizing unclad fuel, must depend heavily on the experimental information and the operating experience gained from the plants now under construction or startup. Until this experience has been gained, speculation as to the future development of these already sophisticated designs should be considered as just that.

References

The references that contain A/Conf. numbers are papers that were presented at the Third United Nations International Conference on the Peaceful Uses of Atomic Energy, Geneva, September 1964.

1. Organisation for Economic Co-operation and Development, European Nuclear Energy Agency, O.E.C.D. High Temperature Reactor Proj Dragon, Fifth Annual Report, April 1, 19 - March 31, 1964.
2. General Atomic Division, General Dynami HTGR, The High Temperature Gas-Cooled Pow Reactor, United States Technical Exhibit, Thi United Nations International Conference on th Peaceful Uses of Atomic Energy, Geneva, Augu 31–September 9, 1964.
3. C. L. Rickard, G. Melese, and P. Fortescue, Ga-Cooled-Reactor Technology, *Nucl. News*. 7(1 73-75 (October 1964).
4. F. de Hoffman and C. L. Rickard, High-Temperature Gas-Cooled Reactors, A/Conf.28/P/213.
5. C. A. Rennie, G. E. Lockett, and R. E. Reynol The Dragon Project, A/Conf.28/P/121.
6. L. R. Shepherd, H. de Bruijn, R. A. U. Huddl, and K. O. Hintermann, Review of Research an Development Work for the Dragon Project, A Conf.28/P/122.
7. F. S. Martin, F. J. P. Clarke, R. W. M. D'Ey, and D. T. Livey, Preliminary Development Dispersed Fuels in the U.K.A.E.A., A/Conf.2 P/152.
8. R. W. Dayton, W. V. Goeddel, and W. O. Harm, Ceramic-Coated-Particle Nuclear Fuels, A Conf.28/P/235.
9. G. Franco, S. B. Hosegood, H. W. Muller, an L. H. Prytz, Review of Engineering Work for th Dragon Project, A/Conf.28/P/549.
10. C. B. von der Decken, J. D. Luders, O. Machnig, H. W. Schmidt, and R. Schulten, Developme Project of a Pebble Bed Power Reactor, A/Con 28/P/536.

Section

IX

Power Reactor Technology

Sodium-Cooled Reactors

By J. R. Dietrich

Technology of Sodium Systems

The two currently important types of sodium-cooled reactors are the sodium graphite reactor and the fast breeder. They differ markedly from each other in some characteristics, and, moreover, there has been increasing interest during the past two or three years in fast breeders using other coolants. Nevertheless, the technology of sodium cooling is important enough to both types to justify discussing them together and in terms of the developments in sodium systems.

The Conference produced reviews of heat transfer[1,2] and corrosion[3,4] in liquid-metal systems, by both U. S. and Russian authors, of value to the designer of sodium-cooled reactors. The heat-transfer papers, which include such practical considerations as burnout, and heat transfer in rod bundles, will be particularly useful. The discussion here, however, will be confined to those aspects of sodium technology which affect the direction of reactor development in more obvious, qualitative ways.

Fission Products in Sodium

One of the important areas of new information is in the behavior of fission products in sodium. Investigations by Atomics International[5,6] have shown that liquid sodium will trap radioiodine quantitatively, and this characteristic is expected to be of considerable significance in determining siting criteria for sodium-cooled reactors. The Dounreay Fast Reactor (DFR) has utilized vented fuel elements, of a uranium–20 at.% molybdenum alloy, which purposely allow the escape of fission products into the sodium coolant.[7] Russian experience with the BR-5 reactor[8] has given other information on the behavior of fission products in the primary coolant system which is worthy of note. A brief summary follows.

The BR-5 reactor, which was fueled with plutonium oxide elements in stainless-steel jackets, began operation in 1959 and reached the design value of fuel burnup (2%) the following year. After a burnup of 2.4% it was noted that the residual activity of the sodium, after the decay of ^{24}Na (half-life, 15 hr), began to increase with fuel exposure. Previously the residual activity had all been attributable to the small amount of ^{22}Na (half-life, 2.6 years) formed by the $(n,2n)$ reaction on ^{23}Na. Most of the new activity was due to ^{137}Cs. Table IX-1 shows the growth of this activity, relative to the ^{22}Na activity, with fuel burnup, and this growth is plotted in Fig. IX-1 in terms of the total residual activity. During the period after the ^{137}Cs became apparent, ^{133}Xe was detected in the argon-gas blanket over the sodium. By the time the fuel burnup had reached 5%, alpha activity due to plutonium was found in the sodium (Table IX-1).

After 5% burnup the reactor was shut down because of trouble with a circulation pump, and all the fuel was removed. Of the total of 81 fuel assemblies, 18 were found to contain fuel elements showing gross leakage of fission products. After decay of ^{24}Na the sodium was drained from the primary system, but the drainage caused no substantial reduction in the activity of the primary system, indicating that the fission products were deposited on pipe walls and other surfaces in the system. The primary system was decontaminated by first washing with steam and then with solutions of 0.5% $KMnO_4$, 5% nitric acid plus 1% oxalic acid, and finally with distilled water. This treatment reduced the gamma background in the primary system cells from several thousand micro-

Table IX-1 GROWTH OF ^{137}Cs ACTIVITY IN BR-5 PRIMARY COOLANT,[8] RELATIVE TO THAT OF ^{22}Na

Fuel burnup, %	Residual activity induced by ^{22}Na, %	Residual activity induced by ^{137}Cs, %	Alpha activity (dis/min per gram of Na), %
2.00	100		
3.20	80	20	
3.90	60	40	
4.55	30	70	
5.00	5	95	50

roentgens per second to about 10 μr/sec. The major activities in the decontamination solutions were ^{137}Cs, ^{95}Zr, and ^{95}Nb. The reactor was reloaded with 63 of the original plutonium oxide fuel assemblies (some of which apparently contained leaky elements) and 50 new assemblies containing UO_2 elements. A bypass circuit was installed in the primary line which could be valved off at will to allow decay of ^{24}Na in the bypass line without interrupting operation of the reactor. A program of experiments on the behavior of fission products produced the following results:

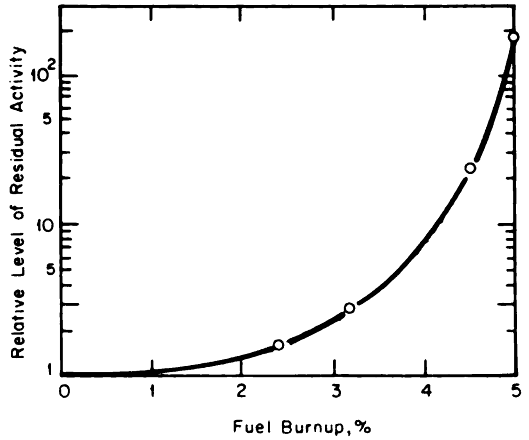

Fig. IX-1 Growth of the residual activity of the primary circuit of BR-5.[8]

1. With the reactor operating at 100 kw with a sodium outlet temperature of 350°C, 90% of the residual gamma activity in the coolant was due to ^{137}Cs, 5% to ^{22}Na, and the remainder to ^{140}Ba, ^{95}Zr, ^{95}Nb, and ^{140}La. The cesium activity level was 4 × 10^5 dis/min per gram of sodium. Draining of sodium from the bypass line decreased the activity of the line by only 10 to 20%.

2. Changes in sodium temperature in the primary circuit and in sodium flow rate through the bypass section did not produce a noticeable effect on the concentration of cesium on the inner walls of the circuit.

3. Heating of the walls of the bypass section while the coolant was circulating, decreased the concentration of ^{137}Cs on the inner walls by several times.

4. With the reactor shut down, after the decay of ^{24}Na, and with the oxide cold traps shut down, heating of the walls of the entire primary circuit caused the ^{137}Cs concentration in the coolant to increase by several times. After the cold traps were put into operation, the ^{137}Cs concentration quickly diminished to the initial level. In the steady state the cesium content of the coolant depends on the cold-trap operating conditions; an increase of cold-trap temperature from 110 to 185°C caused the ^{137}Cs activity in the coolant to increase by a factor of 3.

5. Items of equipment, such as pumps and level gauges, which had some parts submerged in the coolant and some parts in the cover gas, were found to be contaminated by ^{137}Cs in both regions. The contamination was a maximum in the region of the interface between sodium and cover gas.

6. The argon cover gas was found to contain the following radioactive isotopes in addition to ^{41}Ar: ^{133}Xe, ^{129m}Xe, ^{135}Xe, ^{135}Cs, ^{85}Kr, ^{85}Rb, and ^{88}Rb. The important contributors to the activity are ^{133}Xe and ^{135}Xe. The major components of the activity from a sampling during reactor operation at 1000 kw were as follows:

^{133}Xe	4.3 μC/cm³
^{135}Xe	0.95 μC/cm³
^{133m}Xe	0.05 μC/cm³
^{85}Kr	0.017 μC/cm³

The reference calls attention to the fact that no fission products with half-lives less than 2.5 hr were found in the cover gas, although the equipment was capable of detecting half-lives as short as 5 min.

Sodium Handling and Cleanup

The experience in the general handling, cleanup, and maintenance of quality of sodium has been much greater than the amount of reactor operation would indicate, and this phase of sodium technology appears now to be well understood. This was not the case, however,

hen the DFR was first commissioned: con-
derable trouble was experienced in the initial
.eanup of the system.[33] References 5 and 9
escribe the filling and cleanup of the systems
r the Hallam Nuclear Power Facility (HNPF),
ie Experimental Breeder Reactor (EBR-II),
nd the Enrico Fermi Fast Breeder Reactor
EFFBR). The Russian experience in reloading
he fuel elements of BR-5 after examination is
orth noting.[8] The residual sodium and sodium
xide were not removed from the fuel assem-
lies. The assemblies were reloaded, a few at
time, into the reactor sodium system, and
he oxide was cleaned up by the normal system
old traps. The cleanup of carbon from the
sodium of the Sodium Reactor Experiment (SRE)
after it had been contaminated by the inleakage
of Tetralin, as described in Ref. 5, is also of
interest.

Despite the routine solution of sodium clean-up problems, it is still true that the protection of sodium systems from the intrusion of oxygen and other contaminants is a consideration of primary importance. The removal or replacement of components in sodium systems is always done with great care to preserve the cleanliness of the sodium system, and, even when the sodium is drained, care is taken to maintain the inert atmosphere of the cover gas throughout the system. Thus, when it was necessary to perform fairly extensive repairs to the hold-down mechanism of the EFFBR, these repairs were made by workmen who entered the drained reactor vessel through an air lock and worked in gastight suits. The scheme that has been used for removing a primary sodium pump from the EBR-II reactor, without contaminating the cover gas, is illustrated in Fig. IX-2. A system similar in principle has been used on the EFFBR for the removal and replacement of components.

Manipulations Under Sodium

Experience has continued to affirm that the manipulation of components under sodium—and particularly the handling of fuel elements in fast reactors, where rather high precision is required of the mechanisms—is one of the more difficult aspects of sodium technology. It has been pointed out frequently that the opacity of the sodium, and the resulting necessity of carrying out blind operations, adds considerably to this problem. Experience with the EFFBR[9] has shown that relatively minor malfunctions may lead to more serious results because of the difficulty of detecting them. Thus the offset handling mechanism was bent in the course of the preoperational test program when an attempt was made to move it laterally with a partially raised dummy subassembly still in the gripper. Damage also occurred to the hold-down mechanism during this program and appears to have been increased by the continued use of the mechanism after initial slight (and undetected) damage caused by the sticking of a dummy subassembly to one of the fingers of the mecha-

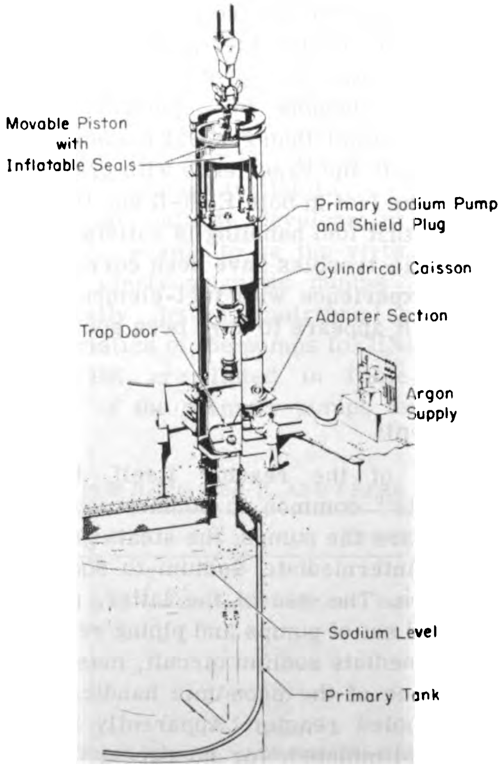

Fig. IX-2 Apparatus used to remove the EBR-II sodium pump.[9] The adapter section, which includes the gastight trap door, was installed, with a gastight seal, around the shield plug of the pump. The cylindrical steel caisson was sealed to the top of the adapter, was purged and filled with argon. The shield plug, with the pump attached, was then lifted slowly by the crane, while the caisson was kept gastight by the movable piston and argon was admitted to hold the pressure constant. After the pump cleared the trap door, the door was closed, resealing the reactor cover-gas system, and it was no longer necessary to maintain the argon atmosphere in the caisson. The operation was carried out with the reactor sodium temperature at 260°F. After the pump had been withdrawn and cooled to room temperature, it was transported to the cleaning and repair area inside the caisson.

nism. A "sweep arm" has been installed to prevent the recurrence of the latter difficulty. This sweep arm can be swept in a horizontal arc to determine that no core component is attached to the hold-down mechanism before lateral motion of the mechanism is initiated.

Preoperational tests of the fuel-handling equipment of EBR-II indicated the desirability of incorporating means of manual operation of the fuel-transfer arm to permit the operator to feel any interference that might be present.[9] This was accomplished by a system of counterweights to balance the weight of the rather heavy mechanism.

Although problems have been encountered with the fast reactor fuel-handling systems, it appears that they are problems of arriving at satisfactory designs for specific pieces of equipment rather than general feasibility problems. Indeed, the experience with practice handling of the fuel in both EBR-II and the EFFBR indicates that fuel handling is satisfactory once the specific troubles have been corrected. The British experience with fuel-element handling in the DFR appears to have been good from the beginning.[7]

Components

Outside of the reactor itself, the major components[10] common to sodium-cooled power reactors are the pumps, the steam generators, and the intermediate sodium-to-sodium heat exchangers. The use of the latter, along with the second set of pumps and piping required for the intermediate sodium circuit, must be reckoned as one of the economic handicaps of the sodium-cooled reactor. Apparently it will not soon be eliminated, for no recent design has appeared without the intermediate sodium system to isolate the radioactive primary sodium from the water in the steam generator. Technically, no serious problems have been found in the design of the intermediate heat exchanger, although the units built to date do not approach the capacities that will be required for plants of economic size and do not reach the temperatures that are ultimately hoped for. The three exchangers for the EFFBR plant, of 143 Mw(t) capacity each, are the largest so far. They operate with primary inlet and outlet temperatures of 900 and 600°F, respectively, and secondary inlet and outlet temperatures of 520 and 820°F.

The steam generators designed to date s great variety of concept. The HNPF and EBR- units are natural-circulation boilers that double-wall tubes. In the former the sodium on the tube side, whereas in the latter it is the shell side. The EFFBR unit is a once-through generator with the water in single-w tubes and sodium on the shell side. The thr HNPF generators, each of which has a capac of 69 Mw(t) in the evaporator and 16 Mw(t) the superheater to produce steam at 895 ps and 875°F, are the only ones that have operat at power. No difficulties have been experienc other than the necessity of controlling the wat level very precisely (within ±1 in.) to giv satisfactory operation without excessive carry-over of water. The design, which utilizes re-entrant tubes to circumvent thermal-expansi problems, has been described previously *Power Reactor Technology*, 5(3): 44–47.

The once-through design of the three EFFB steam generators is shown in Fig. IX-3. Before operation the tubes of one of these unit were found to be cracked at the bends as result of stress corrosion. The corrosion was attributed to residual cleaning solution containing sodium hydroxide and sodium nitrate. During isothermal operation, after about two weeks test with maximum sodium flow, several tube

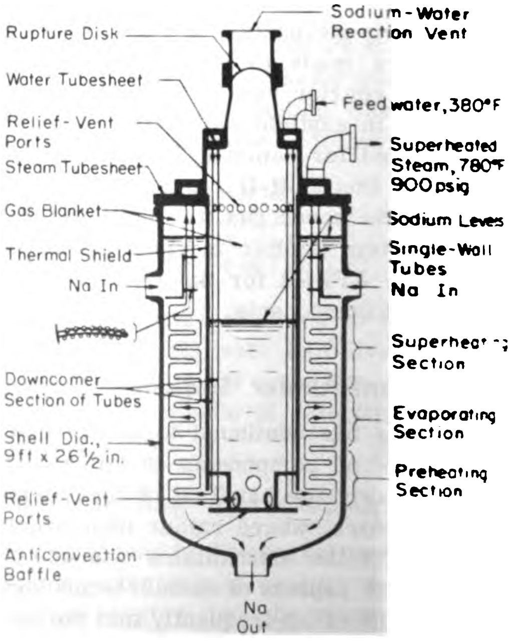

Fig. IX-3 Diagram of the EFFBR steam genera [143 Mw(t)].[19]

ailed in another of the units. The resulting odium-water reaction generated enough hydrogen to break the rupture disk (see Fig. IX-3), which was set at 60 psi. All systems designed o accommodate such a reaction functioned satisfactorily, and the separator collected all he sodium expelled from the unit. This inadvertent demonstration of the ability to accommodate a large sodium-water reaction is considered an important contribution to steam-generator development.[10] The tube failure was attributed to flow-induced vibration of the tubes opposite the sodium inlets. Baffles and tube clips have been installed to correct the trouble.

It is stated[11] in the description of the proposed BN-350 fast-breeder reactor in the USSR that the steam generator will be of the natural-circulation type, with a single separating wall between sodium and water. The choice of single-wall construction is said to have been substantiated by a number of experiments on wall ruptures, and sodium-water and sodium-steam interactions, in models of steam generators.

In the studies of large advanced sodium graphite plants,[5] there has evolved the concept of steam-generator systems made up of many low-capacity modules. Separate modules are proposed for the evaporator, superheater, and reheater functions, each with a capacity of 12 to 15 Mw(t). The superheat and reheat modules would be of stainless steel, and the evaporators would be of chrome-molybdenum steel. All modules are of vertical, once-through design, with single-wall tubes and with the sodium on the shell side. The problems of caustic and chloride stress corrosion are minimized by avoiding crevices and by the use of ferritic steels for the evaporator modules. The justification for the use of single-wall tubes is the choice of shell thickness adequate to contain full steam pressure for short periods of time, plus the provision of rupturable membranes, spaced axially along the shell length, to rupture below full steam pressure and direct any reaction products resulting from a tube break to a relief tank. The modular array is expected to allow the isolation and removal from service of any unit that may give trouble, with a minimum effect on plant availability.

The most definite development in sodium components seems to be the virtual abandonment of electromagnetic pumps in favor of mechanically driven centrifugal pumps. The characteristics of the pumps for HNPF, EBR-II, and EFFBR are listed in Table IX-2, and drawings of the primary pumps for the three

Table IX-2 DESIGN CHARACTERISTICS OF SODIUM PUMPS FOR HNPF, EBR-II, AND EFFBR

	HNPF	EBR-II	EFFBR
Primary system pumps			
Type	Mechanical free surface	Mechanical free surface	Mechanical free surface
No. of units	3	2	3
Capacity, gal/min	7200	5500	11,800
Dynamic head, ft	160	200	310
Design temperature, °F	1000	800	1000
Motor speed, rpm	900	1075	900
Motor power, hp	350	350	1060
Sealing arrangement	Mechanical shaft seal	Totally enclosed drive motor	Mechanical shaft seal
Material	304 S.S.	304 S.S.	304 S.S.
Type of speed control	Eddy-current coupling	Variable frequency and voltage	Wound rotor motor with liquid rheostat
Manufacturer	Byron-Jackson	Byron-Jackson	Byron-Jackson
Secondary system pumps			
Type	Mechanical free surface	A-c linear induction	Mechanical free surface
No. of units	3	1	3
Capacity, gal/min	7200	6500	13,000
Dynamic head, ft	170	142	100
Design temperature, °F	1000	700	1000
Motor speed, rpm	900	1180 (motor-generator set)	900
Motor power, hp	350	500 (motor-generator set)	350
Sealing arrangement	Mechanical shaft seal	Total metal enclosure	Mechanical shaft seal
Material	304 S.S.	304 S.S.	2¼ Cr–1 Mo
Type of speed control	Eddy-current coupling	Variable voltage (motor-generator set)	Eddy-current coupling
Manufacturer	Byron-Jackson	General Electric	Byron-Jackson

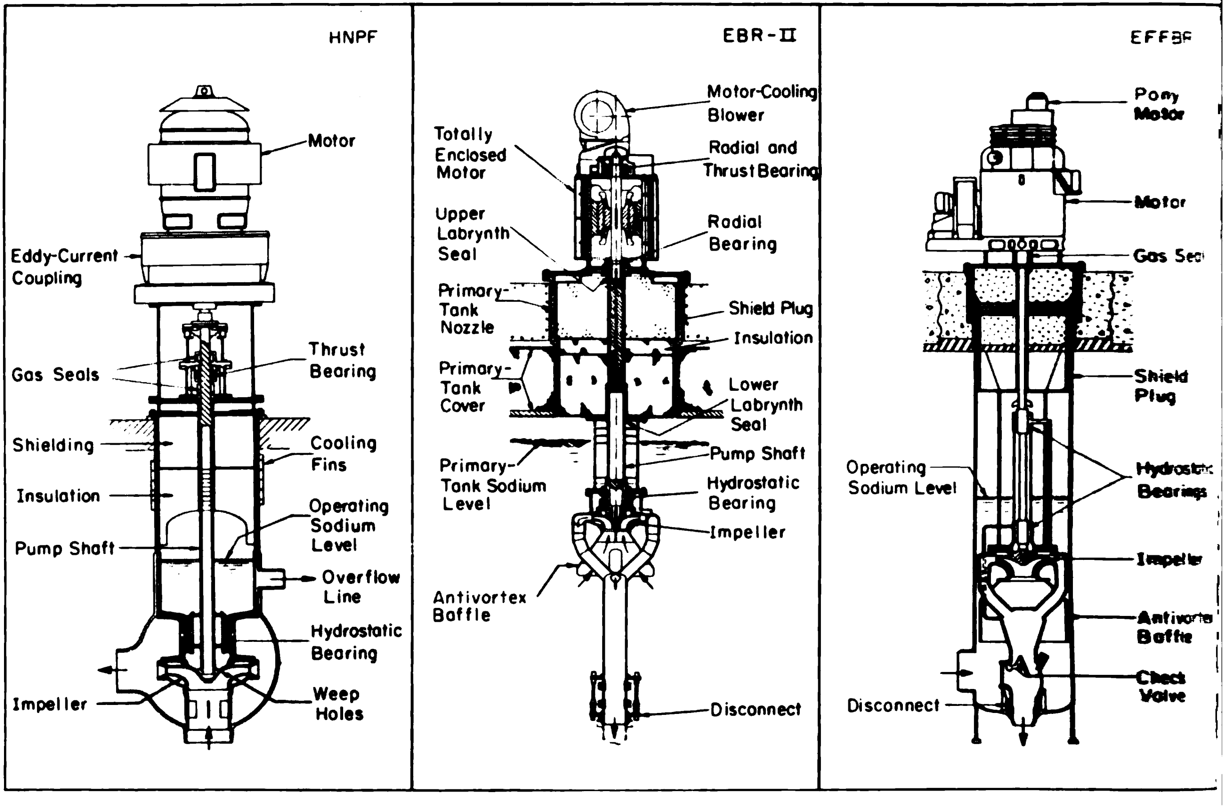

Fig. IX-4 Primary system sodium pumps for HNPF, EBR-II, and EFFBR.[10]

reactors are shown in Fig. IX-4. The EFFBR pumps have been operated for more than 7000 hr without difficulties. Some troubles with binding have been experienced with both the HNPF and EBR-II pumps, and, in both cases, insufficient clearances and misalignment (possibly due to uneven temperature distribution in the pump casing in HNPF and to warpage of the three-piece welded shaft in EBR-II) are judged to be at least partially responsible. The difficulties are believed to be incidental rather than basic, and extrapolation of centrifugal pump designs to large sizes is considered feasible.[10]

Sodium Graphite Reactors

Status and Operating Experience

The development of the sodium graphite reactor has centered around the SRE, a 20-Mw(t) experimental plant, and the HNPF, a 75-Mw(e) generating plant operated by the Consumers Public Power District of Nebraska for the Atomic Energy Commission. The SRE began operation in 1957, and most of the nonroutine items of operating experience have been reviewed in past issues of *Power Reactor Technology*. The major problems were those resulting from the leakage of Tetralin into the primary coolant system [*Power Reactor Technology*, 3(2): 60-64 (March 1960); 5(1): 84-87 (December 1961)] and the unexpected power coefficient of reactivity due to the bowing of fuel elements [*Power Reactor Technology*, 6(1): 57-61 (December 1962)]. Both of these problems were incidental rather than fundamental and have been corrected. The first core, of unalloyed uranium metal, was run to a maximum exposure of 1200 Mwd/ton, and the fuel exhibited volume changes of 8 to 9%. Exposures of about 5000 Mwd/ton have been attained with the second core, of metallic thorium-uranium fuel, with little dimensional change. The SRE is now being modified to raise the power level om 20 to 30 Mw(t) and the sodium outlet tem-erature from 950 to 1200°F; the new fuel ading will consist of uranium carbide ele-ents designed to operate at central tempera-res in the range from 1700 to 2000°F.

The design of the HNPF was reviewed in *ower Reactor Technology*, 5(3): 39-51 (June 962). The plant first attained the design power evel in July 1963. The fuel elements, of ura-ium — 10% molybdenum, have accumulated peak xposures of more than 1200 Mwd/ton. The ain problems encountered in operation were he following:

1. Helium was entrained in the main sec-ndary sodium loops from the cover gas in a ank that was provided to accommodate sodium xpansion and to provide a low-velocity free surface for degasification. The entrainment occurred because of the formation of a vortex at the exit of the tank. The trouble was corrected by bypassing over 90% of the sodium flow past the tank. This does not negate the effectiveness of the tank for its intended function.

2. Leaks developed in one of the intermediate heat exchangers because of flow-induced vibration of the peripheral tubes. The trouble was corrected by installing support shims in all of the six heat-exchanger units.

3. Some of the Zircaloy-2 control-rod thimbles failed because of hydriding and resulting embrittlement. The hydrogen apparently came from titanium hydride shields placed in the thimbles to counter neutron streaming. The trouble was corrected by replacing the Zircaloy-2 thimbles with stainless-steel thimbles; the resulting reactivity loss was about 0.7%. A circulating-gas and hydrogen-removal system was also added to the control-rod-thimble gas-purge system.

The first of these difficulties, the entrainment of gas in the coolant, appears to be a potential problem to be aware of in the design of sodium systems. Both the DFR[33] and the BR-5 fast reactor[8] experienced troubles with cover-gas entrainment in the coolant of the primary loop.

Development of Uranium Carbide Fuel

Although uranium carbide fuel[12] may be attractive in other applications, its development has received the greatest impetus from the sodium graphite reactor program, and forecasts of future developments of the sodium graphite reactor are based on the use of the carbide fuel. The carbide is compatible with sodium and has the advantage, in comparison with uranium metal, of good stability under irradiation. Compared with uranium oxide, the carbide has the advantages of higher density (13.0 g/cm^3) and much higher thermal conductivity [about 0.23 watt/(cm)(°C)]. The latter advantages are particularly important in the sodium graphite reactor, where it is better to use rather massive fuel elements in order to minimize neutron losses to cladding and coolant, without sacrificing the high heat fluxes that the cooling properties of sodium make possible.

Ordinarily, uranium monocarbide (UC, 4.80 wt.% carbon) is used, but acceptable performance does not appear to depend upon the attainment of the exact stoichiometric composition. Most experience with the carbide elements has been accumulated with the slightly uranium-rich composition (hypostoichiometric) in arc-cast slugs with sodium-bonded stainless-steel jackets. The results of capsule irradiations are summarized in Table IX-3.

Reactor experience with full-size carbide elements began in June 1963 when two full-length elements were placed in the second core of the SRE. In September 1963, 10 full-size carbide elements began operation in the HNPF reactor. Experience to date with both groups of elements is described as entirely satisfactory.[12] The second full-core loading for the HNPF reactor will consist of 171 carbide elements, essentially the same in design as the 10 elements currently installed. The fuel-element design data for the HNPF carbide elements, and for two projected designs of large sodium graphite reactors (LSGR) are given in Table IX-4. The anticipated performance is believed to be compatible with test experience to date.[12] The design criteria that led to the data given in Table IX-4 are discussed in Ref. 5.

Higher specific powers than those shown in Table IX-4 are thought to be possible — linear power ratings up to 50 kw/ft, corresponding to central temperatures of about 2400°F — but close control of the carbide composition to the stoichiometric value would probably be necessary to yield high-burnup capability in this temperature range.[12]

Table IX-3 RESULTS OF CAPSULE IRRADIATION TESTS[12] OF URANIUM CARBIDE FUEL SAMPLES*†

Capsule	Cladding	Fuel comp., % C	Annulus width, in.	Bond	Fuel diameter, in.	Actual peak temperature, °C		Average fuel temperature, °C		Burnup (isotopic and/or radiochemical), 10^3 Mwd/metric ton of U	Increase in		Fission-gas release, % ^{85}Kr	Cladding carbon content, wt.%	
						Center	Surface	Center	Surface		Dia., %	Length, %		Preirrad. (nom.)	Postirrad. (max.)
BMI-23-2	304 S.S.		Wire basket	NaK	0.375 gnd‡									0.072	Not analyzed
T§		5.3				1000	580	750	490	5.6	0.9				
B¶		5.1				800	490	570	370	7.8	0.9				
BMI-23-3-B¶	304 S.S.	5.0	Wire basket	NaK	0.375 gnd	890	380	590	330	12.8	0.8			0.072	Not analyzed
BMI-23-5	304 S.S.		Wire basket	NaK	0.375 gnd									0.072	Not analyzed
T		4.6				720	535	720	470	8.6	0.8				
B		4.55				780	455	670	460	6.4	1.2				
BMI-23-6	304 S.S.		Wire basket	NaK	0.375 gnd										
T		4.8					560	780	435	7.0	0.5				
B		4.55					430	510	315	7.0	0.5				
AI-3-1	304 S.S.	4.4 to 4.7	0.015	Na	0.5 ac**	1340	870	980	675	6.5	2 to 6	2.5 to 3	2.3	0.072	0.16
AI-3-4	Ni	4.8 to 5.0	0.050††	Na	0.5 ac	1150	680	1010	535	15.0	1 to 4		0.18	0.10	0.07
AI-3-5	304 S.S.	4.2 to 4.4	0.015	Na	0.5 ac	1530	920	1150	730	13.0	3.8 to 7.6		21.6	0.072	0.32
AI-5-1	304 S.S.	4.8 to 5.0	0.005	NaK	0.5 ac	970	540				0.8	0.4	0.06	0.072	0.51
NAA-48-1	304 S.S.	4.8 to 5.0	0.005	NaK	0.5 ac	1260	780	940 1180	570 690	9.1	1.4		Gas lost	0.072	1.26
NAA-48-2	304 S.S.	4.8 to 5.0	0.005	NaK	0.5 ac	1090	670	480 830	295 500	23.9	0.6 to 5.0		1.3	0.072	0.84
NAA-48-3	304 S.S.	4.8 to 5.0	0.015	NaK	0.5 ac	1110	650	830	490	19.0	3 to 7		7.0	0.072	0.96
NAA-48-6	304 S.S.	4.8 to 5.0	0.015	NaK	0.5 ac	1290	755	950	575	6.4	3.2 to 4.4	0.6	0.74	0.072	1.39
NAA-81-3	304 S.S.	4.4 to 4.8	0.025	Na	0.5 ac	1040	600	980	570		1.0		0.26		
UNC 1-1	Nb–1 Zr	4.45	0.020	Na	0.375 ac	1150	735	1120	715	39.9	10.0		31	Nb–1 Zr cladding	
		4.70				1165	800	1020	700	34.8	8.9		5		
		5.20				1160	790	980	660	36.0	5.7				
UNC 1-2	Nb–1 Zr	4.45	0.020	Na	0.375 ac					22.9	11.0		30		
		4.70								22.9			7		
		5.20				1250	790	1120	720	22.9			4		
SU-20	304 S.S.	4.4 to 4.7	0.020	Na	0.5 ac	870	540	Data not reduced		Not examined					
SU-28	304 S.S.	4.4 to 4.7	0.020	Na	0.8 ac	940	690	Data not reduced		Not examined					

---

*Fuel enrichment was 10% in all capsules.

†Range of heat fluxes calculated at fuel surfaces: 9.15 to 13 × 10^5 Btu/(hr)(sq ft) (288 to 410 watts/cm²).

‡gnd, the fuel surface ground after casting.

§T, the capsule top.

¶B, the capsule bottom.

**ac, the as-cast fuel-surface condition.

††Three 0.050-in.-diameter spacer wires in fuel-cladding annulus.

Table IX-4 DESIGN DATA FOR CARBIDE FUEL ELEMENTS FOR SODIUM GRAPHITE REACTORS[12]

	81-Mw(e) HNPF core I (operating)	200- to 250-Mw(e) LSGR prototype (projected)	1000-Mw(e) LSGR (projected)
Materials			
Fuel (all hypothetically UC)	4.4 to 4.8 wt.% C	4.5 to 4.8 wt.% C	4.6 to 4.8 wt.% C
Cladding	304 S.S.	304 S.S.	304 S.S.
Bond	Sodium	Sodium	Sodium
Enrichment, wt.% ^{235}U	3.7 and 4.9	3.8	3.6
Element			
No. of rods	8	18	18
U content, kg/element	146	124	124
Peak specific power, kw/kg of U	18	52	72
Fuel-slug diameter, in.	0.872 (2.22 cm)	0.500 (1.27 cm)	0.500 (1.27 cm)
Active fuel length, ft	13 (3.96 m)	14 (4.26 m)	14 (4.26 m)
Total fuel-rod length, ft	15 (4.57 m)	18 (5.49 m)	18 (5.49 m)
Cladding thickness, in.	0.010 (0.25 mm)	0.010 (0.25 mm)	0.010 (0.25 mm)
Sodium annulus thickness, in.	0.030 (0.76 mm)	0.025 (0.63 mm)	0.025 (0.63 mm)
Design criteria			
Fission-gas release, % of total produced	3	3	3
Maximum cladding strain, %	0.5	0.5	0.5
Peak cladding temperature, °F	1005 (542°C)	1250 (676°C)	
Peak fuel temperature, °F	1600 (870°C)	1750 (955°C)	2000 (1095°C)
Average burnup, Mwd/metric ton of U	15,000	25,000	25,000
Maximum fuel-volume increase, %	17	17	17
Fuel-diameter increase, %	7	5.3 (average)	5.3 (average)
Maximum rod linear power, kw/ft	28 (920 watts/cm)	24 (788 watts/cm)	35 (1150 watts/cm)
Maximum heat flux, Btu/(hr)(sq ft)	207,000 (128 watts/cm^2)	549,000 (173 watts/cm^2)	
Mixed mean temperature, coolant outlet, °F	945 (508°C)	1150 (620°C)	1150 (620°C)

Directions of Future Development

Studies by Atomics International on large sodium graphite reactors are the sources for projections of the direction of development for he reactor type. With regard to performance, he main effort is in the direction of higher specific power (Table IX-4) and higher temperaure. Conversion ratios above about 0.5 are not predicted for the reactor type.[5] Reference 5 states that supercritical steam pressures can be justified economically for plants above 400 Mw(e) capacity, whereas subcritical pressures, from 1800 to 2400 psig, would be used for smaller plants. Table IX-5 shows projected conditions for reactors in the two size ranges. In either case the projection calls for an increase in the primary sodium outlet temperature to 1150°F, from the 945°F used in HNPF. As mentioned above, the modified SRE is to operate with a sodium outlet temperature of 1200°F.

Perhaps the most annoying problem of the sodium graphite reactor is that of separating the sodium from the graphite moderator. In the SRE and HNPF, the approach is to can the moderator in sizable units in zirconium or steel cans. The advanced design studies for large reactors use a calandria design, with the sodium flowing through the calandria tubes. This approach is expected to permit higher sodium temperatures and higher power density while the parasitic loss of neutrons is being reduced.

Standardization and modular construction are features of the advanced designs which are expected to reduce costs. A common height of

Table IX-5 TYPICAL PROCESS CONDITIONS FOR SMALL AND LARGE FUTURE SODIUM GRAPHITE PLANTS[5]

	200 to 400 Mw(e)	400 to 1000 Mw(e)
Steam conditions, psig/°F/°F (kg/cm^2/°C/°C)	2400/1000/1000 (168.5/538/538)	3500/1000/1000 (246/538/538)
Final feedwater temperature, °F (°C)	473 (245)	512 (267)
Reactor sodium outlet temperature, °F (°C)	1150 (621)	1150 (621)
Intermediate heat-exchanger log mean temperature difference, °F (°C)	75 (24)	90 (31)
Reactor sodium inlet temperature, °F (°C)	750 (400)	750 (400)
Net efficiency, %	41.8	43.6

14 ft is projected for reactors ranging in capacity from 200 to 1000 Mw(e), and a fuel-slug diameter of $\frac{1}{2}$ in. is thought to be near the optimum. A basic loop of 250 Mw(e) capacity is considered to be a practical module for the primary coolant system. The modules for the steam generators are of much lower capacity, 12 to 15 Mw(t), as described in the preceding general discussion of sodium-system components.

Fast-Breeder Reactors

There is general agreement that the fast breeder will be needed in the long term, although opinion varies as to how soon the need will be serious. Most of the countries with major nuclear power programs are pursuing development programs aimed at achieving large, economically competitive, fast-breeder power plants in the next 10 to 15 years. In England and France, where the current nuclear power generation is based on natural uranium, the intention is to start the fast breeders on plutonium from the thermal reactors; and, indeed, some of the incentive for fast-breeder development seems to be the desire to do something with the accumulating plutonium. In the United Kingdom, at least, the plutonium stocks are expected to become large several years before enough fast breeders are in commercial use to absorb them.[13] In France the accumulation of plutonium is expected to be something over 4 tons by 1975. This amount is considered to correspond approximately to the supply for a first large breeder plant.[14]

In the United States and the USSR, where enriched uranium is the fuel for practically all single-purpose power reactors, no great emphasis has been placed on coordinating the development of fast breeders with the growth of the plutonium stockpile. In the United States a considerable analytical effort is devoted to determining the dollar value of plutonium for thermal-reactor fuel, in addition to substantial development efforts aimed at utilizing the plutonium in the thermal-reactor application. In the USSR the economic potential of the fast breeder seems to be regarded more highly than elsewhere, and the forecasts appear to predict its economic superiority even when fissile isotope is not in short supply.

The more favorable Russian estimates may be due, in part, to the different approach used in economic analyses. Instead of trying to evaluate a reactor type by fitting it into an existing complex of mining, transportation, fabrication, processing, and power transmission facilities, the Russians apparently try to evaluate the effort involved in setting up the entire complex for the reactor type in question. This type of approach is also used in evaluating nuclear power vs. coal power. Apparently much of the attractiveness of the fast breeder stems from the expectation that doubling times may be achieved which are short enough to provide for the expansion of nuclear plant capacity without requiring any large expansion of mining operations or enrichment facilities, as indicated by the quotation from Ref. 15:

> Most profitable and at the same time providing for the most effective use of nuclear fuel is a development of nuclear power with the priority given to fast 500 to 1000 MWe reactors with a mixed uranium and plutonium fuel cycle and the increase of the proportion of plutonium breeder reactors.
>
> Such a trend would require small scale industries for production and chemical reprocessing of core fuel elements and moderate capacities for production and chemical reprocessing of blanket fuel elements as well as for reenrichment of the core fuel with the plutonium produced in the reactor, enriched fuel being required only to provide the initial load of every new reactor and one or two of its refuelings.
>
> No constant expansion of uranium mining or enrichment industries will be required; nor practically will the power industry be dependent on these, because two or three sets of fuel cores are a sufficient "trigger pulse" for further operation of reactors that would be self sustaining and at the same time provide a certain plutonium excess for new capacities at the rate of eight to ten per cent of annual power increase. This rate can be considerably increased through the use of fissionable materials formerly intended for defense purposes. Such possibilities are opened up in the Statement made by N. S. Krushchev, Chairman, USSR Council of Ministers on the 21st April 1964.

The relatively low estimate of investment in fuel-cycle installations for the fast breeder (includes mining, ore processing, and transportation investment, as well as investment for chemical processing and fuel fabrication) is indicated in Table IX-6, which summarizes some of the results of a Russian study of future nuclear power possibilities.[15] Surprisingly enough, the unit investment in the power station itself is also estimated to be somewhat lower for the fast breeder than for the water-moderated reactor.

Table IX-6 ESTIMATES FOR THE FUTURE* OF REQUIRED UNIT INVESTMENTS AND POWER PRODUCTION COSTS FOR SEVERAL NUCLEAR PLANT TYPES IN THE USSR[15]

	Gas-cooled graphite natural-uranium reactors	Heavy-water organic natural-uranium reactors	Water-cooled graphite slightly enriched-uranium reactors with steam superheating in the core	Water-cooled water-moderated slightly enriched-uranium reactors	Fast sodium reactors
Mean unit investment, roubles/kw(e)					
Investments in nuclear power stations	179 (75%)	186 (80%)	114 (66%)	135 (66%)	127 (79%)
Investments in fuel-cycle installations	60 (25%)	46 (20%)	59 (34%)	70 (34%)	34 (21%)
Total investment	239	232	173	205	161
Mean power production cost, kopeks/kw-hr	0.40	0.42	0.43	0.48	0.33

*These estimates are from a study covering the period up to 1980. They are based on plants in the 500- to 1000-Mw(e) range.

Problem of the Large Reactor

Although there has been considerable development in fast breeders since the 1958 Geneva Conference, the significance of an important part of the development has been more in the revealing of basic difficulties than in the solution of them. Specifically, the developments in fast reactor physics and safety analysis, and their application in large-reactor design studies, have shown that there is a fundamental problem in extending the design of sodium-cooled fast breeders from small units to large ones: the problem of preserving an inherently negative power coefficient of reactivity under all credible circumstances.

In small fast reactors it was clear that, once the fear of a substantial positive Doppler coefficient of reactivity due to the fission resonances was allayed, the power coefficient of reactivity could always be made inherently negative, at least so long as the mechanical structure of the core remained intact. The major components of the power coefficient were due to: the linear expansion of fuel elements, which increases neutron leakage by reducing the average density of fuel in the core; the Doppler coefficient, either very small (if there was little fertile isotope in the core) or negative; and the reduction of sodium density by thermal expansion or boiling. The latter was a negative component because its major effect was to increase neutron leakage, and this effect was considerably larger than other, positive effects, such as the effect of neutron absorption by sodium. Experience with EBR-I had, of course, shown that the thermal bowing of fuel rods could lead to positive contributions [see *Power Reactor Technology*, 5(2): 24-29], but with suitable mechanical design this possibility could be eliminated. The designer could count on a negative power coefficient that, if large and fast acting, could be a substantial help in countering the effects of accidental power excursions or, if small or slow, would at least not compound the effect of such an excursion.

As much larger reactors were investigated, with relatively high ratios of fertile-to-fissile isotope in the core, it became clear that it was very difficult, if not impossible, to preserve the negative character of the sodium-voiding component of the power coefficient. Also, this component could be so large as to override all negative components and increase the reactivity by the order of dollars in some cases of substantial sodium loss from the core. This is partly because the neutron-leakage effect becomes smaller as the core size is increased. However, in the relatively "soft" neutron-energy spectrum that exists in the large dilute core, the "hardening" of the spectrum due to a decrease in moderation by sodium also results in a reactivity increase. The reactor physics aspects of the sodium coefficient and other reactivity coefficients were discussed at length in *Power Reactor Technology*, 7(2).

Once it is clear that a real threat of a net positive coefficient exists, the problems of evaluating it and its significance become very complex. It soon becomes evident, for example, that the overall sodium-void coefficient for the core is not the only consideration. The designer and the safety analyst must consider the local value of the coefficient at the point in the core where boiling would start first in the event of a power excursion or a cooling interruption. Usually the coefficient is found to be more highly positive in these higher power regions of the core. The process of optimizing the power coefficient through the proper adjustment of design variables is a complex one because all components of the coefficient respond to changes in these variables, and the designer is apt to find, for example, that a design change which reduces the positive nature of the sodium-void coefficient will also reduce the magnitude of the desirable, negative Doppler coefficient. Finally, the evaluation of the coefficients by neutron physics analysis is a very complex problem that still involves large uncertainties.

Although fast reactor theory is, in many respects, the most sophisticated branch of neutron physics, its inadequacies become apparent when it is applied to the evaluation of complex reactivity coefficients. These inadequacies are not due to any deficiencies of fundamental understanding but to the sheer range and detail of data that must be handled (and must be available from experimental measurement). It is still possible that further developments in neutron physics may ease the problem of the power coefficient. For example, the French results summarized in Table IX-7 indicate that calculations which take into account the self-shielding of resonances predict a much more favorable sodium-void coefficient.

It should be made clear that the reactivity-coefficient problem does not appear to be a problem of normal reactor operation, but one that affects the prognosis for the course of a hypothetical accident. The seriousness with which the problem is viewed varies widely from group to group and from country to country and reactions vary from a rather casual recognition of the problem to the initiation [illegible] searches for alternate fast reactor coolants.

In the United States there does not appear to be any widespread inclination to doubt sodium as the optimum coolant for fast breeders, but the problem of the sodium coefficient of reactivity is taken quite seriously. It appears unlikely that any easy solution of general applicability will be found. However, individual solutions for specific designs will be found through detailed and exhaustive safety analyses. This implies that fast reactor physics, safety experiments, and methods of safety analysis will continue to get much attention in the United States and probably abroad. The current emphasis on these fields is attested by the papers at the Conference, listed as Refs. 16 to 25. The papers are too detailed for review here, but they contain much pertinent and useful information.

Fast Reactor Fuels

Although most of the general considerations involved in the selection and development of fuels for thermal reactors apply also to fast breeders, their relative importance is different. In addition, in fast reactors the effects of the fuel on reactivity coefficients and on reactor behavior in hypothetical accidents must be considered carefully.

Even the largest fast breeders must use fuel of relatively high enrichment. For a given method of fuel processing, high enrichment leads to high processing costs (per unit of fuel comprising fissile-plus-fertile isotope) because

Table IX-7 INFLUENCE OF RESONANCE SELF-SHIELDING ON SODIUM-VOID COEFFICIENT AND BREEDING RATIO[14]

(Spherical, 2886-Liter Core with Oxide Fuel; Fuel Volume Is 35% of Core Volume; Fissile Isotope Is ^{239}Pu; and Fertile Isotope Is ^{238}U)

	^{238}U/^{239}Pu	Sodium-void coefficient,* 10^{-5} $(\delta k/k)$/°C				Internal breeding ratio	Total breeding ratio
		Diffusion	Absorption	Degradation	Total		
Without self-shielding	6.25	−0.736	+0.072	+1.361	+0.697	0.916	1.455
With self-shielding	6.86	−0.775	+0.080	+0.597	−0.098	0.874	1.408

*The calculation breaks the sodium-void coefficient down to the components of neutron diffusion (leakage), absorption by sodium, and the effect of sodium in degrading the neutron-energy spectrum. The calculations show a big reduction in the latter (positive) effect when resonance self-shielding is taken into account. The sodium-void coefficient is expressed in terms of a sodium-temperature coefficient, via the volumetric coefficient of expansion of sodium.

the criticality problems and the high cost of el losses. Moreover, the high enrichment ecessitates high specific power if fuel-inven- ry costs are to be kept within reasonable ounds. This in turn requires a highly sub- ivided fuel structure that usually involves high brication costs. Further increases in pro- essing and fabrication costs (relative to ther- al reactors) tend to result from the necessity r recycling plutonium (or ^{233}U) and possibly rom the necessity of processing blanket fuel s well as core fuel. The attainment of low fuel ost in the fast reactor therefore appears to equire either that inherently cheaper methods f processing and fabrication be found, relative o those used for thermal-reactor fuel, or that he exposure lifetime of the fuel be increased reatly beyond that which is acceptable for thermal reactors. The relative insensitivity of the neutron economy of the fast reactor to the presence of some materials that would absorb neutrons strongly in a thermal reactor assists in both these directions. It permits the use of fuel jackets that are rather thick relative to the fuel element. It also makes the neutron economy rather insensitive to the fission-product burden of the reactor, so that long exposures do not degrade the neutron-physics performance importantly; and it removes the neutron-physics requirement for complete fission-product removal during processing.

It appears to be the result of cost studies that if oxide fuel elements are used in fast breeders, the attainment of acceptable fuel costs requires average fuel exposures of about 100,000 Mwd/ton. Documentation of the conclusion is not easy to find, but it is implied by the frequent use of this exposure in economic studies of fast breeders. Processing and fabrication estimates for oxide elements should be more reliable than estimates for other types, because of the more extensive experience with oxide in the United States. Irradiation tests have indicated that exposure lifetimes of 100,000 Mwd/ton are indeed possible for mixed uranium-plutonium oxide elements of types acceptable for fast breeders.[26] Consequently it is tempting to conclude that oxide fuel elements are essentially proved as practical elements for the fast breeder. Certainly it appears that the oxide, although it may not ultimately prove to be best, offers the most straightforward approach to a feasible fast-breeder fuel element. But more extensive irradiation experience is required, and the gap in experience, between processing and fabrication of uranium oxide elements for thermal reactors and comparable experience with the uranium-plutonium oxide elements for fast breeders, must not be overlooked.

Design characteristics of fuel rods proposed for the Fast Ceramic Reactor (Table IX-8) are considered typical for oxide elements.[26] Preliminary estimates of the fabrication cost, for a production rate corresponding to 3000 Mw(e) of generating capacity, yield $211 per kilogram of uranium and plutonium in the core. This corresponds to a fuel-fabrication contribution to the power cost of 0.29 mill/kw-hr for an average exposure level of 100,000 Mwd/ton.

Table IX-8 PROPOSED DESIGN CHARACTERISTICS OF FUEL ELEMENTS FOR THE FAST CERAMIC REACTOR[26]

Form of element	Rod
Fuel composition	80 wt.% UO_2–20 wt.% PuO_2, solid solution
Form of fuel	0.220-in.-diameter pellets, pressed and sintered
Fuel density, % of theoretical density	95
Jacket	AISI 347 S.S. tubing
Jacket outside diameter, in.	0.250
Jacket thickness, in.	0.015
Fuel length, ft	2 to 4, depending on reactor design

British work on the irradiation of oxide fuels is summarized in Ref. 27. It calls attention to erratic behavior with respect to fission-gas release, and another British paper[28] cites oxide fuel-element designs for fast reactors in which plenum volumes are left in the element, for the accommodation of fission gases, of volume equal approximately to the volume of fuel.

With respect to reactivity coefficients, the Doppler component of the power coefficient is usually strongly negative in oxide fuels containing high proportions of fissile isotopes. This characteristic, which results from the strong dependence of the average fuel temperature on the power level, is of course desirable. It is usually assumed that no important negative component of the power coefficient due to axial expansion of the fuel can be counted on in oxide cores because of the uncertainty as to how an element composed of cracked oxide will expand thermally. The British irradiations have shown much less cracking of PuO_2-UO_2 samples than of pure UO_2 samples.[27] However, it is questionable whether this difference will be significant from the point of view of the thermal-expansion behavior of the fuel element.

Metallic fuel elements have been used in the fast reactors EBR-I, EBR-II, EFFBR, and DFR. They have many attractive features for the fast-breeder application, but it seems questionable whether satisfactory resistance to radiation damage can be achieved, at least with plutonium-uranium elements.

In the United States the use of metal fuel has been coupled with the concept of pyrometallurgical processing of the fuel, and the EBR-II plant includes facilities for such processing and on-site remote fabrication by casting techniques. Although there are still large uncertainties in the costs of these processes for a large-scale plant—as indeed there are also uncertainties in the costs of processing and fabrication of oxide fuels for the fast breeder—the current U. S. paper on fast-breeder fuel economics[29] does not forecast substantial cost advantages for them. Consequently it appears that the exposure goals for the metal fuels must lie at least as high as 40,000 to 60,000 Mwd/ton, or, roughly, 4 to 6 at.% burnup.

The uranium-fissium* alloys show at least some encouraging performance under irradiation: at 600°C, for example, uranium-5 wt.% fissium alloy shows a swelling rate of about 8% volume increase per atomic percent burnup.[30] However, uranium-plutonium-iron alloys swell badly even at relatively low temperatures. The alloy uranium-20 wt.% plutonium-10 wt.% fissium, for example, increases about 20% in volume per atomic percent burnup at an irradiation temperature of 400°C (Ref. 30). It has been found possible, however, to restrain the swelling by the use of sufficiently strong jackets on the metallic fuel. Once the fuel swells to the point that it begins to press against the jacket, the internal pressure generated within the fuel by fission gases must be resisted, essentially by the strength of the jacket alone. The exposure lifetime then depends on the tensile strength of the jacket material, the diameter and thickness of the jacket, and the fractional void volume built into the element as an allowance for radial swelling. In its simplest form such an element is c ceived as a rod of the fuel material insi tube of the cladding material, with a sodiu filled annular space (initially) between fuel a jacket. Figure IX-5 shows the calculated effe of cladding-wall thickness and radial cleara (given in terms of the inner diameter of t jacket for a constant fuel diameter) on t achievable burnup for uranium-plutonium-ir elements.

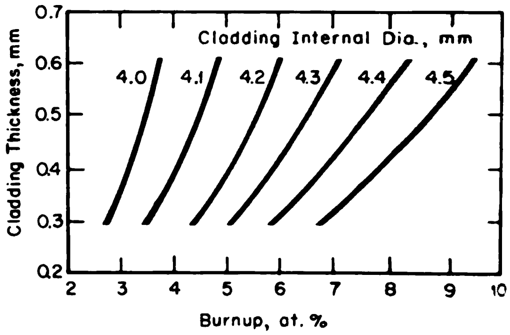

Fig. IX-5 Calculated effect of cladding thickness a internal diameter on the achievable burnup in 3. mm diameter uranium-plutonium-fissium alloy ro under EBR-II temperature conditions. A maxim allowable cladding stress of 30 kg/mm² was assumed.[30]

Thorium-rich thorium-uranium alloys show relatively good resistance to radiation-induced swelling, even at temperatures up to 750°C. Although irradiation results are not available at high temperatures for thorium-plutonium alloys, the few results that have been obtained at 450°C are promising.[30]

Although stainless steel was used as the fuel-jacket material in EBR-I, it has the undesirable property of forming a eutectic alloy with uranium, of relatively low melting point. As jacket materials for uranium metal, the nickel-base alloys have the same drawback. Of the refractory metals that do not present this problem, only vanadium appears completely satisfactory as an alloy base with respect to corrosion resistance and nuclear properties. Currently, an alloy of vanadium-20% titanium appears very promising. Its fabrication into high-quality thin-walled tubing is difficult, however.

In the DFR, metallic fuel elements have been used in a number of design variations, but basically the elements consist of annuli of ranium alloy with strong inner and outer ckets of niobium, originally designed to restrain swelling. The outer diameter of the anular element is approximately 0.75 in. The hicknesses of the fuel annuli have been varied uring the development of the elements. The lements currently in the reactor use uranium—0 at.% molybdenum as the fuel alloy, with nnuli 0.10 in. thick for the central region of he reactor core and 0.13 in. thick for the peripheral core regions. The elements are ented to allow those fission gases which may be released by the fuel to escape to the coolant. rradiation tests have shown that the temperaure of this fuel should be limited to 650°C if rapid swelling is to be avoided. Furthermore, it has been found that there is a lower temperature range, from 480 to 580°C, where rapid swelling of uranium-molybdenum alloys can occur during irradiation because of a transformation of the metastable gamma phase to alpha-plus-delta phases. If the fission density is high enough, however[30,31] [above 8×10^{13} fissions/(cm^3)(sec)], the formation is suppressed and irradiation stability does not suffer. One of the design goals therefore was to hold the fuel temperature below 480°C so long as the fission density is below 8×10^{13} fissions/(cm^3)(sec). The DFR experience has shown that these elements will operate satisfactorily up to a burnup of 1.2%, the maximum yet experienced, and probably considerably higher. These results are for a peak specific power of 205 watts/g. The niobium jacket material has shown some incompatibility with the sodium coolant. It has absorbed hydrogen from the coolant with resulting severe embrittlement when the jacket temperature is reduced to a low value. There is, however, a brittle-ductile transformation at 150 to 200°C, and therefore the properties are not impaired at operating conditions.[31] There is some corrosion of the niobium which is attributed to oxygen. The oxygen level in the DFR coolant has been about 10 ppm. A jacket temperature limit of 480°C is currently imposed on the elements to avoid this corrosion.

---

*The term "fissium" is used to designate the mixture of fission products, comprising molybdenum, ruthenium, technetium, palladium, zirconium, rhodium, and niobium, left in the exposed fuel after pyrometallurgical processing.

If metallic fuel bodies could be counted on to retain their structural integrity, they would offer the favorable property of a substantial negative component of the power coefficient of reactivity due to axial thermal expansion. Although this is probably the case early in fuel lifetime, it is questionable whether the property is retained after long exposure. In particular, if the jacket is relied upon to restrain fuel swelling, it seems improbable that the fuel would expand axially in proportion to its temperature and its normal temperature coefficient of expansion. Rather, it might be expected that the axial expansion would be governed by the jacket temperature, which is relatively insensitive to changes in power level. Compared to the ceramic fuels, the metallic fuels are unlikely to provide a large reactivity sink due to the Doppler effect before the fuel temperature rises to the point of fuel-element failure. This is particularly the case if the jacket material can form a low-melting eutectic alloy with the fuel.

The carbide fuels have been discussed briefly in the preceding paragraphs, primarily in connection with sodium-cooled thermal reactors. When these fuels are considered for fast reactors, interest is concentrated on the mixed uranium-plutonium carbides and on performance at very high levels of burnup. To date the irradiation results on uranium-plutonium carbides appear to be relatively few and to be limited to exposure levels of 30,000 Mwd/ton or lower.[12,28] However, the results have been encouraging and suggest that, at any given temperature, the rate of fission-gas release from carbide fuel is similar to or less than that from oxide.[28] If the temperature limits of the carbide are indeed comparable to those of the oxide, the carbide should allow the use of much more massive fuel-element designs, because of the high thermal conductivity of the carbide.

It appears that, for the fast reactor application, there may be considerably more emphasis on attaining the nominally stoichiometric composition of the monocarbides. It is pointed out in Ref. 28 that a more appropriate description of the desired composition is that of a single-phase alloy, since there may be small quantities of oxygen and nitrogen present as well as carbon. The desired composition is one in which the sum of the concentrations of oxygen, nitrogen, and carbon is close to 50 at.%. The hypostoichiometric (uranium-rich) compositions are to be avoided because it is believed that the accumulation of fission gas in any free metal that may be present will determine the swelling rate of the fuel body. The hyperstoichiometric compositions show poor compatibility with the common jacket materials because of the transfer of carbon from the fuel body to the jacket.

The good conductivity of the carbide makes it worthwhile to consider elimination of the thermal resistance of the fuel-jacket gap through the use of some kind of thermal bonding. Sodium bonding may be used, but it accentuates the transfer of carbon from hyperstoichiometric carbides to the jacket. In the United Kingdom some development is being carried out on the metallurgical bonding of carbide fuel to the jacket.[28] There has been some success with copper- and nickel-based brazing alloys as the bonding material between uranium carbide and steel jackets, but there is some problem of cracking of the carbide under thermal cycling in the bonded elements.

Another approach to the fast reactor fuel problem is through the use of cermets. These are dispersions of fuel materials (fissile or fissile plus fertile) in ceramic form in a metallic matrix. The ceramic is usually the oxide of the fuel material. The basic concept is to take advantage of the irradiation stability of the ceramic while approximating the thermal conductivity and mechanical properties of a metal. It is desirable that the size of the ceramic particles in the dispersion be sufficiently large that only a small fraction of the fission gas can escape from the particles by fission recoil.

One of the main disadvantages of the cermets is that the ceramic component cannot usually be made to constitute the major fraction of the total material. Therefore, if both the fissile and fertile components of the fuel mixture are incorporated in the ceramic form, the amount of fertile material that can be incorporated is severely limited. This means that the internal breeding ratio of the reactor will be low, that the reactor will tend to lose reactivity rapidly with burnup, and that this reactivity loss must be taken care of either by strong control elements or by frequent partial refueling. The possibility of avoiding this difficulty by using the fertile element as the metal matrix and incorporating only the fissile element in the ceramic form is referred to in Ref. 26. This appears to be an attractive possibility from the point of view of nuclear performance, but restriction of the choice of the metal matrix to uranium, and possibly thorium, is a severe metallurgical limitation. Apparently there has been no extensive work on this concept.

The British have under way a program cermet fuels[32] which is directed primarily toward the development of a fast reactor element and which has concentrated on the use of oxides in a steel matrix. The fissile and fertile materials are mixed in the oxide form, and the problem of achieving an acceptably high fertile content is attacked simply by attempting to use the highest possible oxide content in the cermet. The practical limit of oxide content appears to be about 50 vol.%.

The British experience has shown that, although the cermets can be formed by pressing and sintering the metal-oxide mixture, the densities attainable by this process alone are no higher than about 85% theoretical and that mechanical working is necessary to attain higher densities. Both hot rolling and hot swaging have been used for densification. Pin type elements are produced by mixing the oxide and steel particles, cold pressing into pellets and sintering at 1100 to 1300°C, sealing the pellets into a steel tube, and swaging at a temperature between 1000 and 1300°C (Ref. 32). Conceptually the objective in fabrication of the cermet is to produce an assemblage of oxide granules, each surrounded by a small, steel pressure vessel, and the whole bonded together as a structure. It is fairly obvious that this objective will be promoted if the oxide granules are spherical in shape, and the process does include the use of such granules. The spherical particles are produced by first pressing the oxide into green compacts about 1 cm in diameter with aluminum sterate binder. The green pellets are broken down to granules and sized, and the granules are spheroidized by abrasion in a gyrating dish coated with silicon carbide powder. The spherical particles are sintered at a peak temperature of 1600°C in an atmosphere of cracked ammonia. A further improvement in the cermet has been made by coating the sintered oxide spheroids with an organic binder that makes them sufficiently sticky to cause a layer of stainless-steel powder to adhere to each particle before the cermet is pressed. The material preferred for the metal matrix is type 316L (low carbon) stainless steel.

Plate type dispersion elements have been made by processes analogous to those used for the pins but with hot rolling substituted for the swaging process. Cermets have been made with both uranium oxide and plutonium-uranium oxide ixtures and have been irradiation tested. The esults with the plutonium fuels have not been s good as those with uranium, but the irradiaon program has necessarily lagged behind the abrication development, and the latest imrovements have not yet been thoroughly tested. esults[32] to date suggest that the fabrication echnology is capable of producing cermet lates and pins with 30 to 50 vol.% ceramic that ill achieve a burnup of at least 10% heavy toms without failure when the surface temerature is about 625°C.

urrent Status and Future Directions

The fast reactors currently in operation or definitely planned are listed in Table IX-9. Since the Second Geneva Conference, reactors that have contributed new operating experience at substantial power levels are the British DFR[7] and the Russian BR-5.[8] In the United States the EBR-I continued in operation, and its latter-day operation was directed primarily to the rather specialized, but necessary, investigation of dynamic characteristics. These EBR-I results have been covered rather thoroughly in *Power Reactor Technology* in the past.

The escalation of power of the DFR to the design value of 60 Mw(t) was a long, troublesome process, which covered the time period from early 1960 to July 1963. It yielded, however, much useful information on sodium technology and metallic fuels.[33] The early problems had mainly to do with the entrainment of gas in the coolant and with the removal of gross impurities from the primary coolant system. The latter problem was finally solved by the use of hot-dumping operations in addition to the more usual cold-trapping processes. A "hot dump" consisted of heating the primary coolant to 250 to 300°C, transferring it to the dump tanks, cooling it to 80°C, and then returning it to the primary system through a filter. Twelve of these dump sequences were used after the fuel had been removed from the reactor.

A more fundamental obstacle to power escalation was the fuel performance, and full power was attained only after the original fuel elements had been replaced by redesigned elements. The original concept for the annular elements had been to accept a fuel alloy of relatively poor swelling resistance, to restrain the radial swelling by the walls of the element, and to accommodate the volumetric swelling by allowing the fuel material to extrude axially within the confines of the element walls. Early experience showed, however, that the axial extrusion was opposed by frictional forces great enough to exceed the creep strength of the jacket. Redesign of the element involved the substitution of a fuel alloy of higher swelling resistance (uranium–20 at.% molybdenum), reduction of the thickness of the fuel annulus to limit the maximum alloy temperature to 650°C, and the provision of a larger fuel-jacket clearance to allow for more radial swelling. The limit on the alloy temperature and a 480°C limit imposed on the jacket temperature to avoid corrosion have prevented attainment of the design value of coolant outlet temperature. It is suspected that the corrosion of the niobium jacket is accelerated by some impurity in the coolant, possibly carbon, which may be eliminated with time.

Although a number of problems had to be overcome to attain full power, all of them were recognized long before they resulted in operating difficulties, and operation has been smooth and without untoward incident within the recognized limits of the plant. The reactor is continuing operation and is being used extensively for the irradiation of improved fuel elements.

The BR-5 reactor, although much smaller than the DFR, has given valuable results on the behavior of plutonium oxide fuel elements, as well as information (discussed earlier) on the behavior of fission products in sodium systems.

The steel-jacketed, oxide fuel elements of BR-5 are described in Table IX-10. The reactor core operates at an average power density of about 300 kw/liter. The initial fuel loading of plutonium oxide elements operated to an average burnup of 2.4% of the plutonium before any evidence of fission-product leakage was detected. Thereafter the reactor operation was continued, with increasing evidence of fission products in the primary coolant and finally with plutonium alpha activity in the coolant, but without operating difficulty, to a maximum burnup of 5% (see Table IX-1). During this period the primary coolant outlet temperature had been raised from the initial 400 to 450°C level to 500°C. Thereafter the fuel assemblies containing gross failures were replaced by new assemblies of UO_2, and operation was continued at lower temperatures (outlet temperatures of

Table IX-9 FAST REACTORS IN OPERATION, OR UNDER CONSTRUCTION, OR DEFINITELY PLANNED*

Reactor	Country	Power, Mw(t)/Mw(e)	Status	Fuel	Remarks	Reference
Rapsodie	France (with Euratom)	20/none	Being built; full power expected before end of 1967	PuO_2-UO_2 pressed and sintered pellets, 5.7 mm in diameter, in 316L S.S. cans with 0.45-mm wall	The French program is directed toward 1000-Mw(e) fast breeders. It is expected that an intermediate size plant of 80 Mw(e) will be needed between Rapsodie and the large plants.[14] A large critical experiment (Masurca) and a source-calibration pile (Harmonie) are also under construction at Cadarache	34 34
DFR	U. K.	60/14	Operating at full power since July 1963	U−20 at.% Mo alloy in Nb jacket	The reactor is being used primarily to investigate the behavior of various Pu-based fuels and canning materials. The construction of a prototype large enough to demonstrate the core and fuel characteristics for a 1000-Mw(e) commercial plant is planned by the U. K.; this should be on power soon after 1970.[13] Two large critical assemblies are used in the U. K. program, Vera and Zebra [19]	7 33
BR-5	USSR	5/none	Operating at full power since July 1959	PuO_2 in S.S. jackets (See Table IX-10)	The previously announced BN-50 reactor has been eliminated from the USSR program, but plans have been announced to construct the BOR reactor, a 50- to 60-Mw(t) experimental fast reactor. Critical experiments for large dilute reactors are carried out at the "BFS"-stand [21]	8
BN-350	USSR	1000/350	Definitely planned but schedule not announced	PuO_2 in S.S. jackets (See Table IX-11)		11
EBR-II	U. S.	65/20	Critical November 1963. Power escalation under way	0.144-in. U-Fs alloy rods in type 304 S.S. jackets, Na bonded	Although the U. S. has a large program directed to the development of large fast breeders, no commitment has yet been made for the construction of a prototype. The program includes critical experiments on two facilities (ZPR-III and ZPR-VI)[20] and fuel-meltdown studies with the TREAT reactor.[25] Two experimental reactors are under development: FARET, primarily for the test of fuel systems at high temperature, and SEFOR, a 20-Mw(t) developmental reactor using PuO_2-UO_2 fuel[35] (the latter project has participation also by Gesellschaft für Kernforschung mbH and Euratom)	9
EFFBR	U. S.	300/100	Critical August 1963. Power escalation under way	0.158-in. U−10% Mo rods clad with metallurgically bonded Zr cladding		

*This table lists only the reactors that were discussed at the Conference. It does not include some of the older reactors, such as EBR-I.

Table IX-10 CHARACTERISTICS[36] OF FUEL ELEMENTS AND ASSEMBLIES IN THE FIRST LOADING OF BR-5

Fuel element	
Type	Rod
Fuel	Sintered plutonium oxide pellets
Jacket material	Stainless steel, type IX18H9T
Jacket outside diameter/ thickness, mm	5/0.4
Fueled length, mm	280
Thermal expansion space (at top of fueled section), mm high	2 to 3
Filling gas	Helium at atmospheric pressure
Fuel assembly	
Type	Hexahedral stainless-steel tube
Dimensions, mm	26, between parallel sides; 0.5, wall thickness
No. fuel elements per assembly	19
Method of supporting elements in assembly	Top and bottom grids

300 to 430°C) and various power levels to study the effects of fission-product contamination of the primary circuit. By Mar. 1, 1964, the maximum burnup in the original plutonium oxide elements that were still in the core was 5.8%.

At the time of fuel-assembly replacement, all assemblies were tested by pumping gas from them and checking it for radioactivity. Some showed activities thousands of times greater than the average. These were discarded (18 out of a total of 81) and replaced by the new UO_2 assemblies. The following quotation from Ref. 8 describes the condition of elements from the "discarded" and "undiscarded" assemblies:

> ...Two of the discarded subassemblies with a 4.9% burnup (one was processed with steam) and one subassembly with a 5% burnup out of the undiscarded were examined in the hot laboratory. Longitudinal cracks 8–10 cm long and up to 1.0 mm wide were detected on the surface of some elements of these subassemblies. The cracks, as a rule, continued in the plutonium dioxide. Mostly radial cracks were observed on the surface of cross sections of the disintegrated elements. No central cavities were found in any of the disintegrated elements. In the third subassembly examined all the elements turned out to be tight, the element canning was in good condition: the element surface was light-colored and bright and there were no visible defects.

In late 1964 and early 1965 it is planned to load the BR-5 with uranium monocarbide fuel.

It is stated in Ref. 8 that the operation of the BR-5 reactor has already confirmed the practical feasibility of the reactor type for industrial installations. The announced decision[11] to bypass the previously planned 50-Mw(e) commercial plant BN-50 in favor of pushing on directly to the large 350-Mw(e) plant (BN-350) appears to be in harmony with this point of view. However, Ref. 11 also announces a project to construct a "fast pilot reactor," designated BOR, for general development work leading to large fast breeders. This reactor, of thermal capacity 40 to 60 Mw, will test advanced concepts and operating conditions: power densities up to 1500 kw/liter, sodium outlet temperatures to 630 to 650°C, and fuel burnup to 10% with thin-walled fuel elements that allow fission-gas leakage to the coolant. This suggests that the elimination of the "commercial" BN-50 may have been the result of a decision that the effort could be spent more effectively on a reactor of more experimental nature.

With the beginning of operation of EBR-II and the EFFBR, fast reactor progress in the United States should accelerate. Neither of these plants can be considered the prototype of an economic commercial fast breeder. Although the EFFBR will operate as a utility station, its fuel is far from satisfactory even on a nonrecycle basis. The shortcomings of the fuel have restricted the operating power level, in a manner reminiscent of the early DFR experience. The situation is summarized in the following quotation from Ref. 9:

> The present core was de-rated from 300 to 200 MW(t) because of an increase in the estimated pressure drop across the core resulting from a change in the fuel element support arrangement (see Fig. 6, P/2427). Experimental data obtained subsequent to this decision show that the pressure drop will be only 40 psi at 200 MW(t) whereas the subassembly and internals are capable of operating at 65 psi. A higher power level, therefore, is possible but cannot be justified economically because of the burnup limitation on the U–10 w/o Mo fuel alloy. As described in another paper, this alloy has not proven to have the irradiation damage resistance which early results suggested. It has been found that the allowable burnup decreases with increasing fuel temperature. Therefore, after demonstration of 200 MW(t) operation, it is planned to operate at an inlet sodium temperature of 450°F and at a power level of 110 MW(t) which is estimated to double the allowable burnup. Although these conditions are uneconomical for electric power generation, it will extend the fuel life of the two core loadings now on hand and permit use of

the reactor as a test bed for irradiation of experimental fast reactor fuels. Plans are proceeding to utilize the reactor initially for this purpose.

Although the British hope to have a prototype of a commercial fast reactor on power soon after 1970, the date is contingent on the development of a satisfactory fuel and decisions as to the main reactor design features.[13] Apparently only the USSR is committed far enough to a prototype (BN-350) at this time to announce its general features. These are summarized in Table IX-11. However, the construction schedule for the plant appears to be somewhat flexible, and it is not clear whether the current concept has lasting significance.

Table IX-11 CHARACTERISTICS OF THE BN-350 REACTOR[11]

Thermal power, Mw	1000
Core volume, approx., liters	2000
Average power density, kw/liter	500
Sodium volume in reactor vessel, m^3	165
Primary sodium temperature inlet/outlet, approximate, °C	300/500
Maximum sodium velocity in core, m/sec	10
No. of core fuel assemblies	211
No. of blanket assemblies	500
Axial and radial blanket thickness, cm	60
Core diameter/height, m	1.5/1.06
Sodium volume fraction in core, %	39
Fuel	Plutonium and uranium dioxide mixture (19% Pu)*
Critical mass, kg of Pu	780 (or 950 kg ^{235}U)
Fuel element	Rod type; oxide pellets in stainless-steel tube, as in BR-5†
Diameter/thickness of jacket tube, mm	5/0.4
Fuel assemblies	96 mm hexagons with wall thickness of 2 mm
No. of fuel elements per assembly	217
Method of spacing elements in assembly	Top and bottom grids plus ribs on element jackets
Breeding ratio, total/internal	1.5/0.62
Rate of reactivity loss, % k_{eff}/month	0.62 (one month gives about 0.5% burnup)
Control rods	Assemblies similar to fuel assemblies with enriched B_4C in place of fuel

*The first loading may employ enriched UO_2 (23% ^{235}U).

†It is stated that the average oxide density will be lower than in BR-5 to accommodate fission gases.

The key question in predicting the course of fast-breeder development is the selection of fuel type. Although the early experience has been predominantly with metal fuel, that experience has not been highly encouraging even for uranium metal, and the prospects for plutonium appear considerably less favorable. On the basis of current knowledge, the oxides appear to be the surest bet as potentially acceptable fast reactor fuels. The carbides, however, have inherent advantages in thermal conductivity and density, and it is primarily the lack of experience with them that puts them in a less favored position. It is, of course, conceivable that a number of acceptable fast breeders might be developed utilizing different basic fuel types. But for the moment it would be encouraging to be able to verify the completely satisfactory performance — in relation to breeding ratio, reactivity coefficients, and reactivity lifetime, as well as to the more obvious criteria such as fuel lifetime and fabrication cost — of any one fuel. Because of the growing interest in oxide fuels, the commercial operation of Rapsodie in France[34,37] and of the Southwest Experimental Fast Oxide Reactor (SEFOR) in the United States[35] will be awaited with interest.

In whatever direction the fuel development goes, considerations of reactivity coefficients are expected to have an important influence on the design of large fast breeders. In particular, there will be efforts to attain a negative value for the sodium-void coefficient of reactivity or minimize its positive value and to provide as large a sink of reactivity in Doppler effect as possible. The effects of these considerations on reactor design are discussed in Ref. 24 and were reviewed at length in *Power Reactor Technology*, 7(2): 107-144.

Partly because of the difficulty with the sodium coefficient of reactivity and partly to circumvent problems and difficulties in sodium technology, some groups have investigated other coolants for fast reactors. The Karlsruhe proj-t is investigating cooling by helium and dry eam as well as by sodium,[38] and papers on s cooling[39] and steam cooling[40] were also esented at the Conference by Swiss and elgian groups, respectively. The latter is a rect-cycle system that utilizes dry steam as e reactor coolant. Part of the superheated eam from the reactor exit goes to the turbine, nd another appropriate fraction is directed to Loeffler boiler where it is quenched in the oiler water and produces dry saturated steam feed the reactor inlet.

One of the problems with less efficient oolants is to design for the characteristic high pecific power of the fast reactor. This may e not so much a problem of normal cooling as f emergency shutdown cooling, particularly pon loss of coolant pressure. In the gas-ooled concept[39] it is proposed to use water njection as a last-ditch emergency measure. Criticality can be avoided under these conditions by incorporating resonance absorbers in the reactor core. This would be relatively ineffective in the normal "fast" neutron spectrum but would absorb strongly if the spectrum were degraded by water injection. The problem sounds like a difficult one.

References

The references that contain A/Conf. numbers are papers that were presented at the Third United Nations International Conference on the Peaceful Uses of Atomic Energy, Geneva, September 1964.

1. O. E. Dwyer and R. N. Lyon, Liquid-Metal Heat Transfer, A/Conf.28/P/225.
2. V. I. Subbotin, P. A. Ushakov, P. L. Kirillov, M. K. Ibragimov, M. N. Ivanovsky, E. V. Nomophilov, D. M. Ovechkin, D. N. Sorokin, and V. P. Sorokin, Heat Removal from the Reactor Fuel Elements Cooled by Liquid Metals, A/Conf.28/P/328.
3. B. A. Nevsorov, V. V. Zotov, G. P. Fedortsev-Lutikov, D. M. Skorov, N. M. Beskorovagynii, Ju. S. Belomytsev, M. D. Abramovitch, E. V. Umnyashkin, V. A. Ivanov, V. E. Andreev, S. M. Golubenkova, V. K. Ivanov, E. I. Yakovlev, S. A. Iodkovskii, and N. M. Samarina, Corrosion Resistance of Constructional Materials in Alkali Metals, A/Conf.28/P/343.
4. D. H. Gurinsky, J. R. Weeks, C. J. Klamut, L. Rosenblum, and D. H. DeVan, Corrosion in Liquid Metal Systems, A/Conf.28/P/244.
5. C. Starr and S. Siegel, Sodium Cooled Thermal Reactors, A/Conf.28/P/206.
6. W. P. Kunkel, D. M. Elliott, and A. S. Gibson, In-Pile Experiments on Retention of Fission Products in 500°F Sodium, USAEC Report NAA-SR-9163, Atomics International, January 1964.
7. R. R. Matthews, J. L. Phillips, K. J. Henry, R. H. Allardice, D. M. Donaldson, and H. E. Tilbe, Performance and Operation of the Dounreay Fast Reactor, A/Conf.28/P/130.
8. A. I. Leipunskii, O. D. Kazachkovskii, M. S. Pinkhasik, N. N. Aristarkhov, M. S. Poido, A. V. Karpov, Y. P. Larin, I. A. Efimov, N. V. Krasnoyarov, B. S. Tymosh, M. P. Nikulin, D. I. Zhestkov, Y. A. Uralets, and V. I. Galkov, 5-Year Operation Experience on Reactor BR-5, A/Conf.28/P/312.
9. L. J. Koch, F. S. Kirn, G. W. Wensch, C. E. Branyan, and E. L. Alexanderson, Sodium Cooled Fast Breeder Reactors, A/Conf.28/P/207.
10. H. O. Monson, F. A. Smith, W. J. Hellett, and J. J. Morabito, Components for Sodium Reactors, A/Conf.28/P/228.
11. A. I. Leipunskii, O. D. Kazachkovskii, I. I. Afrikantov, M. S. Pinkhasik, N. V. Krasnoyarov, and M. S. Poydo, Sodium Cooled Fast Reactors, A/Conf.28/P/311.
12. H. Pearlman and R. F. Dickerson, Carbide Fuel Fabrication and Performance, A/Conf.28/P/234.
13. W. Penney, Nuclear Power in the United Kingdom, A/Conf.28/P/559.
14. G. Vendyres, The Fast Neutron Reactor Series in France, A/Conf.28/P/41.
15. N. M. Sinev, B. B. Baturov, and V. M. Shmelev, Trends of Nuclear Power Development in the USSR, A/Conf.28/P/294.
16. R. Avery, H. H. Hummel, R. N. Hwang, D. Meneghetti, P. A. Moldauer, A. B. Smith, P. Greebler, and J. B. Nims, Physics of Fast Reactors, A/Conf.28/P/259.
17. A. I. Leipunskii, O. D. Kazatchkovskii, M. V. Troyanov, N. V. Krasnoyarov, M. G. Kulakovskii, V. B. Lytkin, V. I. Matveev, V. M. Murogov, A. I. Novozhilov, L. M. Usatchev, N. M. Shagalin, and S. B. Shikhov, Some Physics Calculations on the Performance of Fast Power Reactors, A/Conf.28/P/369.
18. D. C. G. Smith, K. W. Brindley, D. Tait, and R. C. Wheeler, The Physics of the Dounreay Fast Reactor at Power, A/Conf.28/P/173.
19. R. D. Smith, A. R. Baker, E. P. Hicks, J. E. Mann, J. L. Rowlands, D. C. Smith, and J. Weale, Fast Reactor Physics, Including Results from U.K. Zero Power Reactors, A/Conf.28/P/166.
20. F. W. Thalgott, J. K. Long, W. G. Davey, W. Y. Kato, S. G. Carpenter, H. A. Morewitz, and G. H. Best, Fast Critical Experiments and Their Analysis, A/Conf.28/P/265.
21. A. I. Leipunskii, I. I. Bondarenko, O. D. Kazachkovskii, L. P. Abagyan, Yu. S. Aborin, N. O. Bazazyants, G. A. Batirbekov, V. V. Bondarenko, A. I. Voropaev, V. I. Golubev, E. F. Efimov, Yu. S. Zamyatkin, A. V. Zvonarev, V. P. Zinovyev, M. N. Zyzyn, V. V. Ivanov, N. V. Krasnoyarov, N. N. Krot, M. Ya. Kulakovskii, V. G. Liforov, V. F. Mamontov, B. K. Maslennikov, V. I. Matveev, V. N. Morozov, M. N. Nikolaev, M. Yu. Orlov, V. A. Parfyonov, V. V. Penenko, V. E. Ridkii, V. A. Semyonov, G. N. Smirenkin, A. P. Smirnov-Averin, V. P. Sokolov, M. F. Troyanov, O. P. Uznadze, F. I. Ukraintsev, L. N. Usachev, and N. N. Shagalin, Experimental Studies on Fast-Neutron Reactor Physics, A/Conf.28/P/368.
22. W. Häfele, K. Ott, L. Caldarola, W. Schikarski, K. P. Cohen, B. Wolfe, P. Greebler, and A. B. Reynolds, Static and Dynamic Measurements on

the Doppler Effect in an Experimental Fast Reactor, A/Conf.28/P/644.

23. J. Codd, J. E. Beardwood, D. C. Leslie, and H. M. Sumner, Studies of Resonance Absorption and the Doppler Phenomenon for Fast and Thermal Reactors, A/Conf.28/P/172.
24. D. Okrent, K. P. Cohen, and W. B. Loewenstein, Some Nuclear and Safety Considerations in the Design of Large Fast Power Reactors, A/Conf.28/P/267.
25. W. J. McCarthy, Jr., C. E. Dickerman, A. E. Klickman, and R. B. Nicholson, Fast Reactor Safety Research, A/Conf.28/P/284.
26. R. E. Macherey, H. W. Alter, and A. A. Shoudy, Fabrication of Solid Fuels for Fast Reactors, A/Conf.28/P/238.
27. L. E. J. Roberts, P. Brock, J. R. Findlay, B. R. T. Frost, L. E. Russell, J. B. Sayers, and E. Wait, The Behaviour of UO_2 and of (U, Pu)O_2 Fuel Materials Under Irradiation, A/Conf.28/P/155.
28. L. E. Russell, B. T. Bradbury, H. J. Hedger, N. Parkinson, R. G. Sowden, and M. B. Waldron, Monocarbides as Reactor Fuels, A/Conf.28/P/154.
29. L. E. Link, G. J. Fischer, and E. L. Zebroski, Fuel Cycle Economics of Fast Reactors, A/Conf.28/P/248.
30. J. H. Kittel, T. K. Bierlein, B. R. Hayward, and W. C. Thurber, Irradiation Behavior of Metallic Fuels, A/Conf.28/P/239.
31. S. A. Cottrell, E. Edmonds, P. Higginson, and W. Oldfield, Development and Performance of Dounreay Fast Reactor Metal Fuel, A/Conf.28/P/150.
32. B. R. T. Frost, L. H. Cope, J. B. B. Lambert, H. Lloyd, W. Long, J. E. Manson, and P. G. Mardon, Fabrication and Irradiation Studi
UO_2-Stainless Steel and (U,Pu)O_2-Stainless
Cermets, A/Conf.28/P/153.
33. J. L. Phillips, Achievement of Full Power Op
tion of the DFR, *Nucl. Eng.*, 9(92): 10-16 (Jan
1964).
34. G. Vendryes, Rapsodie, A/Conf.28/P/42.
35. W. Schnurr and J. R. Welsh, The SEFOR Reac
Aspects of International Cooperation, A/Conf
P/533.
36. A. I. Leipunsky, V. G. Gravin, N. N. Aristark
I. I. Bondarenko, O. D. Kazachovsky, O. L.
bimtsev, S. A. Pashkov, M. S. Pinkhasik, K.
Renne, U. Y. Stavissky, F. A. Ukraintsev,
L. N. Usachev, Experimental Fast Reactor
the Soviet Union, in *Proceedings of the S*
United Nations International Conference o
Peaceful Uses of Atomic Energy, Geneva,
Vol. 9, pp. 348-357, United Nations, New Yo
1958.
37. R. Abdon and M. Chaigne, Predicted Dyna
Behaviour of Rapsodie, A/Conf.28/P/79.
38. W. Häfele, K. H. Beckurts, E. Bojarsky,
Engelmann, A. Jansen, K. Kummerer, A. Mül
K. Ott, K. E. Schroeter, D. Smidt, H. H. Vo
and E. Windbühl, The Karlsruhe Fast Bree
Project, A/Conf.28/P/539.
39. P. Fortescue, R. Shanstrom, L. Meyer, W. Sim
and P. Fischer, Gas Cooling for Fast Reacto
A/Conf.28/P/694.
40. G. Tavernier, J. Chermanne, C. Descamps,
Egleme, E. Fossoul, E. Jonckheere, J. Morel
M. Stievenart, L. Tollet, and J. Van Diev
"HERMES" Fast Neutron Superheater Reacto
A/Conf.28/P/516.

Section

X

Power Reactor Technology

Maritime Reactors

Of the two nuclear-powered ships that are in peration, only the icebreaker *Lenin* was formally discussed at the Conference.[1,2] Other Papers concerned the nuclear plant for the German nuclear-powered vessel *Otto Hahn*[3] and design studies of the VULCAIN[4–6] and NERO[7] reactors for marine propulsion.

The icebreaker is powered by three pressurized-water reactors, each capable of producing 90 Mw(t), although the vessel can be operated at design conditions with only two of the three reactors operating. The core of each reactor consists of 219 fuel assemblies arranged as shown in Fig. X-1. Each assembly is composed of 36 fuel pins fabricated of UO_2 pellets clad with zirconium alloy tubing having an outside diameter of 6.1 mm and a thickness of 0.75 mm. The fuel pins are contained in a flow tube that is fabricated of zirconium alloy, bearing ^{10}B as a burnable poison. The amount of poison is varied from tube to tube to reduce the radial power-peaking factor. The reactor is equipped with safety and control rods as well as a so-called "compensation system." Although details of the construction of these control components are not given in Ref. 1, a paper from the Second Geneva Conference[8] may be consulted for additional information.

Each reactor of the *Lenin* is equipped with two coolant loops, each containing a steam generator, two main circulating pumps, an emergency circulating pump, two electrically heated pressurizers, and an ion-exchange filter. Figure X-2, which is a photograph of part of the Russian exhibit, illustrates the reactor compartment of the ship. Although call-outs are not provided, the reader can see the positions of the three reactors in the center of Fig. X-2 as evidenced by their control- and safety-rod "thimbles" protruding above the upper shield structure. The six main coolant pumps and a cutaway showing one of the steam generators can be seen at the left. The loops are designated "bow" or "stern" loops in the reference, the reactor compartment in Fig. X-2 being arranged with the center line of the pumps in a fore-aft orientation. Table X-1 lists additional operating data for the reactors.

In general, the operation of the *Lenin* has been "quite successful." Much of the success perhaps results from the fact that the icebreaker application approximates an "ideal" application of nuclear energy. The vessel became operational in December 1959 and operated on its first fuel for over 11,000 hr, producing about 450,000 Mw(t)-hr. The average burnup reached about 12,000 Mwd per ton of uranium, with peak burnup reaching about 30,000 Mwd per ton of uranium. Refueling was done in the spring of 1963, and in May 1964 the vessel was operating with the second fuel charge. In 1961 the self-regulation of the reactor was demonstrated using the Doppler effect to com-

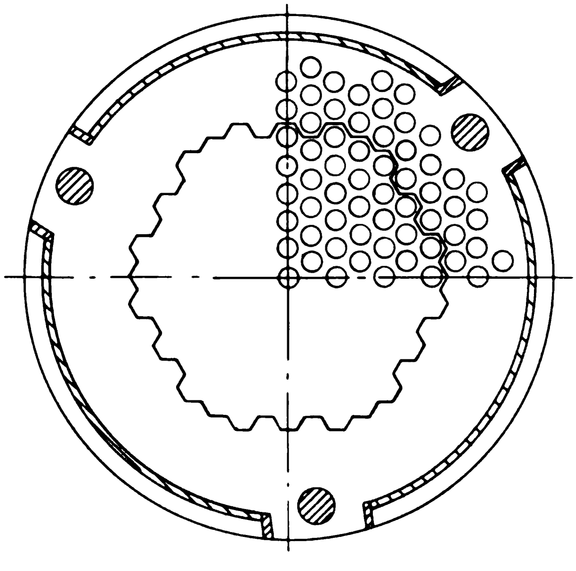

Fig. X-1 Lenin *reactor core cross section.*[2]

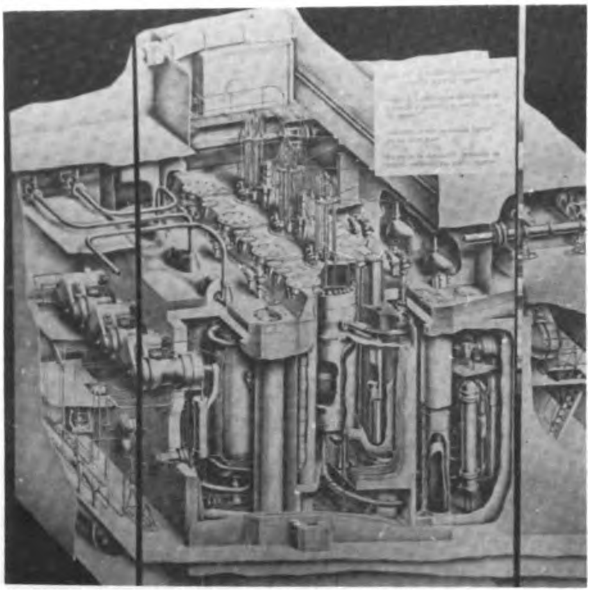

Fig. X-2 Photograph of part of the Russian Geneva exhibit illustrating the reactor compartment of the Lenin.

pensate for load changes. The primary components of the plant operated about 15,000 hr (including the year 1963) at working pressure (180 kg/cm^2). The main circulating pumps have operated up to about 8500 hr without inspection, although some pumps apparently have failed owing to shorting of the stator windings.

The primary circuit components that are permanently or periodically filled with potentially contaminated water are accommodated in the so-called "central compartment" of the plant. In Fig. X-2 this probably consists of the compartments containing the reactors and steam generators, and these compartments are hermetically sealed from the rest of the ship and ventilated separately. Some leakage has been experienced from the primary system. Reference 2 notes that this has come from the packing of various valves in the primary circuit. Contamination from fission gases and long-lived fission products is reported to be low.

Table X-1 OPERATIONAL DATA FOR THE *LENIN* REACTORS[2]

	Designed values for 65 Mw	Operation data for reactors 1, 2, and 3*		
Water flow in primary circuit loops, tons/hr	415	$\frac{435}{430}$	$\frac{458}{467}$	$\frac{435}{453}$
Reactor outlet temperature for loops, °C	317	$\frac{311}{311}$	$\frac{312}{313}$	$\frac{311}{313}$
Reactor inlet temperature for loops, °C	261	260	261	260
Steam output for loops, tons/hr	$\frac{43.3}{43.3}$	$\frac{42}{42}$	$\frac{47}{42}$	$\frac{43}{46}$
Steam pressure, kg/cm^2	29	$\frac{32}{31}$	$\frac{31.5}{30.5}$	$\frac{31}{31}$
Steam temperature, °C	307	$\frac{310}{309}$	$\frac{308}{308}$	$\frac{308}{308}$

*Fraction numerators refer to bow loop and the denominators to stern loop.

Reference 9, although not specifically directed toward the *Lenin* reactors, pertains to a control system that might be uniquely applied to this reactor type. The essence of the system is a reactor in which the coolant is separated from the moderator; the *Lenin* reactors are of this type with their flow-tube design. The principles of the control system are contained in the following quotation:[9]

> Let us consider a reactor core formed by a regular lattice of cylindrical fuel elements placed in a liquid moderator, say in H_2O. Let the top ends of all elements be fastened in some plane thus that any of them can turn independently around the fastening point. Let, further, these elements pass freely through the spacer plate, the holes in it forming a grid similar to that of fastening points. The lattice and the form of the cylindrical reactor do not depend on the distance between the plane of joints (fastening points) and that of the spacer plate. Let the plate be rotated in the horizontal plane around the reactor central axis. Then the core will have the form of a one-sheet hyperboloid of revolution and the fuel element lattice will be deformed thus that the surfaces of the constant spacing will turn out to be, with a greater accuracy, ellipsoids of revolution having one focus with the hyperboloid that forms the side boundary.
>
> The reactivity dependence on the core spacing in a cylindrical reactor is not monotone, it has optimum. When the spacing increases reactivity rises first, and then falls. Therefore to control a reactor by means of the core deformation it is possible to use either the "left" branch of the curve corresponding to the core spacing less than optimum or the "right" one corresponding to the spacing greater than optimum.

The reactivity of a reactor controlled in the above manner was studied both analytically and experimentally, and the reference may be consulted for details.

The power plant for the German research ship *Otto Hahn* is described in Ref. 3. It will be a pressurized-water reactor (PWR) having the characteristics shown in Table X-2. The ship was launched in June 1964, and the time schedule calls for the reactor to be installed in 1966 with power operation to commence in 1967. The normal power of the propulsion plant is 10,000 shp.

Table X-2 MAIN DATA OF REACTOR INSTALLATION FOR THE SHIP *OTTO HAHN*[3]

Core	
Diameter of active zone, mm	1150
Height of active zone, mm	1120
No. of fuel elements	16
No. of control rods	12
Fuel elements (side length), mm	270
No. of fuel rods installed	3128
Fuel-rod diameter, mm	10.9
Fuel-rod cladding thickness, mm	0.33
Total surface, m^2	120
Core entrance temperature, °C	266
Core exit temperature, °C	278
Maximum thermal output, Mw	38
Average reactivity lifetime, Mwd/ton	7200
Maximum reactivity lifetime, Mwd/ton	14,000
UO_2 fuel loading, tons	2.95
Enrichment in four zones, %	~2.5, 2.9, 3.5, and 4.3
Average enrichment, %	~3.6
Surface heat release, kcal/(m^2)(hr)	272,000
Average fuel temperature over lifetime, °C	460–680
Hot-channel load at central fuel melting, %	172
Absorbing material in control rods	Boron carbide in steel
Burnable poison	ZrB_2-ZrO_2 pellets
Excess reactivity (cold, unpoisoned), %	15
Excess reactivity (hot, unpoisoned), %	7
Excess reactivity (hot, poisoned), %	4.5
Shutdown reactivity of control rods, %	25
Pressure vessel	
Operating pressure, ata	63
Inside height, mm	8580
Inside diameter, mm	2360
Wall thickness and plating, mm	50 + 5
Coolant circulation, kg/hr	2.37 × 10^6
Steam generator	
Operating pressure, ata	31
Steam temperature, °C	273
Superheat, °C	36
Tube diameter, mm	19.4
Tube wall thickness, mm	1.2
Material	Inconel
Containment vessel	
Height, m	13.1
Diameter, m	9.5
Wall thickness, mm	30
Design pressure, ata	14.5
Weight including reactor parts, tons	930

The German maritime reactor[3] incorporates some of the advanced techniques described in the review of the Consolidated Nuclear Steam Generator and the Unified Modular plant in the Fall 1963 issue of *Power Reactor Technology*, 6(4): 106-117. These include self-pressurization and location of the primary heat exchangers within the pressure vessel. In addition, the primary pumps are arranged quite close to the core, probably in a manner similar to that shown in Fig. VII-3 of the above-mentioned *Power Reactor Technology* article. The fuel elements are of square geometry with a four-zone-loaded core to achieve power flattening. The pressure vessel will be fabricated by circumferential welding of several forged rings.

The objectives of the VULCAIN program, which is a joint UKAEA–BelgoNucléaire effort, are quoted as follows:

> (i) The basic nuclear physics and engineering design parameters of a compact, highly rated core capable of operating to a peak burn-up of 40/50,000 MWD/TeU.
>
> (ii) The development and manufacture of a VULCAIN core, of 40 MW/thermal output, for loading into the Belgian BR3 reactor later in 1964. The BR3 reactor will then be operated with a mixed D_2O/H_2O moderator and coolant throughout the three years life of the core.
>
> (iii) The engineering design of a compact steam-raising unit of 20,000/25,000 shp suitable either as a single unit for marine propulsion, or as a multi-unit for small land-based power stations.

The physics portion of the work is concentrated in critical experiments in the VENUS zero-energy program and will conclude in 1965. The BR-3–VULCAIN power experiment is concerned with irradiation of a core in the BR-3 reactor. The fuel assembly and a so-called "moderator tube" of the reactor are shown in Fig. X-3, and the core layout is shown in Fig. X-4. The moderator tubes come in two lengths; 14 of them are about 1.4 m long and the remaining four are about 2.4 m. The long tubes house hydraulically operated absorber rods, and 10 of the short tubes house absorber rods actuated by existing BR-3 magnetic-drive mechanisms. The remaining four short tubes are used for instrumentation, sample tubes, and neutron sources (Fig. X-4). Additional core data are given in Table X-3.

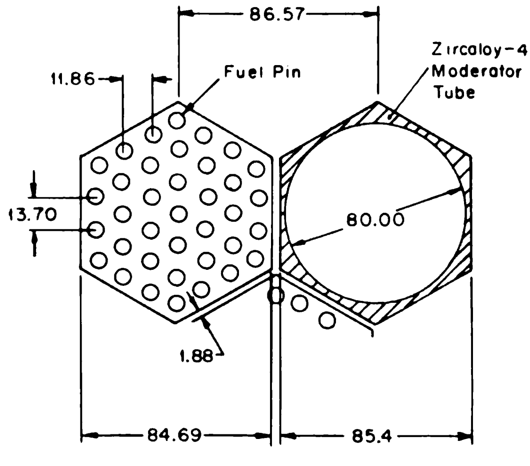

Fig. X-3 VULCAIN fuel assembly and moderator tube.[4] *(Dimensions are in millimeters.)*

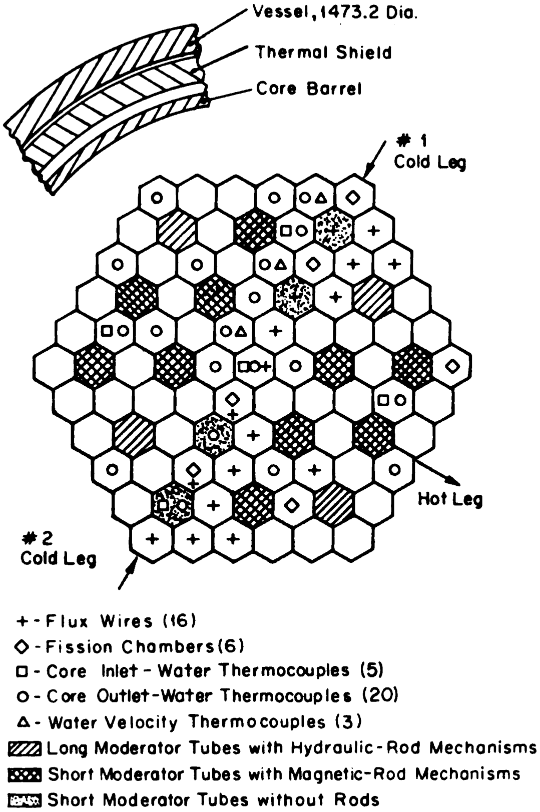
Vessel, 1473.2 Dia.
Thermal Shield
Core Barrel
# 1
Cold Leg
Hot Leg
# 2
Cold Leg
+ - Flux Wires (16)
◇ - Fission Chambers (6)
□ - Core Inlet - Water Thermocouples (5)
○ - Core Outlet - Water Thermocouples (20)
△ - Water Velocity Thermocouples (3)
▨ Long Moderator Tubes with Hydraulic-Rod Mechanisms
▩ Short Moderator Tubes with Magnetic-Rod Mechanisms
▦ Short Moderator Tubes without Rods

Fig. X-4 BR-3—VULCAIN core cross section with in-pile instrumentation.[4]

The reactor normally will be operated without rods in the core and with the coolant containing about 85% D_2O at start of life. The burnup target is an average of about 25,000 Mwd per ton of uranium, and, as burnup proceeds, light water is added until the D_2O concentration is almost zero at end of life. The hydraulically operated absorber rods, described in Ref. 4, are located with their drives entirely within the pressure vessel. The operation is described as follows:

> In this type of hydraulic mechanism, the absorber rod moves up or stays in its top position because of the upwards flow inside the moderator tube created by the pressure differential between the tube inlet and the vessel outlet flow nozzle to which the top end of the tube is connected through a master valve. When the latter connects the tube top end with a higher pressure (vessel inlet flow nozzle), the moderator flow is reversed and the 10 kg rod drops into the core and stays there after being stopped by a dashpot in the bottom of the moderator tube. The H.P. and L.P. connections of the master valve are thus located entirely within the reactor vessel. The servo pressure actuating the spring-loaded master valve is transmitted by a pipe passing through the vessel collar from a pilot valve which is supplied by a high or low pres- to position the master valve for up or down m- ment of the rod, respectively. The system is fail safe, as failure of the servo-pressure, e. due to a pipe rupture, will cause insertion of rod into the core.

The design of the VULCAIN reactor for marine propulsion also incorporates internal pressurization and integral heat exchangers. The design of the reactor is schematically illustrated in Fig. X-5. Provisions are made for gas pressurization, as well as self-pressurization, in order to reduce the in-core voids if desired.

The NERO reactor for ship propulsion was designed by the Reactor Centrum Nederland (RCN) in cooperation with Euratom. The NERO is a pressurized-water reactor having the characteristics shown in Table X-4. The reactor is a conventional PWR design with the exception of the primary flow loop. A system with internal recirculation, somewhat similar to that of a boiling-water reactor, is provided. The external primary flow is pumped to a ring of water ejectors located inside the reactor vessel in the downcomer region, and enough recirculating water is pumped to provide an internal circulation having about 1.5 times the mass flow in the external circuit. The reference states that the reason for this was to reduce the size of the external primary coolant system and still provide sufficient flow of coolant through the core in one pass. This design also provides a path for natural circulation entirely within the pressure vessel to facilitate emergency cooling. The NERO project

Table X-3 CORE DATA FOR THE VULCAIN–BR-3 POWER EXPERIMENT

Parameter	Value
Fuel material, mm	Dished UO_2 pellets
Outside diameter, mm	7.5
Fuel-cladding material	AISI 304 stainless stee
Thickness, mm	0.5
Active length, mm	1000
Total length, mm	1235
No. of pins/fuel element	37
No. of fuel elements/core	73
Absorber rod geometry	Tubular, unfollowed
Material	Unclad 18/16 stainless steel containing 2 wt natural boron
Inside diameter, mm	68
Outside diameter, mm	78
Length, mm	1035
Reactor power, Mw(t)	40.9
Coolant	D_2O–H_2O mixture
Pressure, kg/cm^2	140
Total core flow, m^3/hr	2500

has been under development since late 1961, when a contract was signed between RCN and Euratom. This contract covered critical experiments, irradiation studies of fuel rods, hydraulic experiments, shielding, and other studies. Design of the propulsion reactor also was undertaken, although the data given in Table X-4 are preliminary in nature.

References 10 and 11 pertain to investigations of the dynamic behavior of marine boiling-water reactors. Reference 10 discusses test results with an oscillating, boiling, natural-circulation loop called "Yo-Yo." Although many of the details are of specialized interest, the conclusions are quoted below for the generality:[10]

1) The error introduced by neglecting the direct g-effect upon slip is small. It should therefore be safe to assume that data from stationary rigs may be used with confidence in the design of natural circulation boiling water reactors for marine application.
2) No effects have been found which indicate any sudden transition from one flow regime to another.
3) No carry under has been produced in this geometry where the water velocity in the upper part of the downcomer was 0.2 times the circulation velocity.
4) A stabilizing effect may be achieved by increasing the single phase inertia.

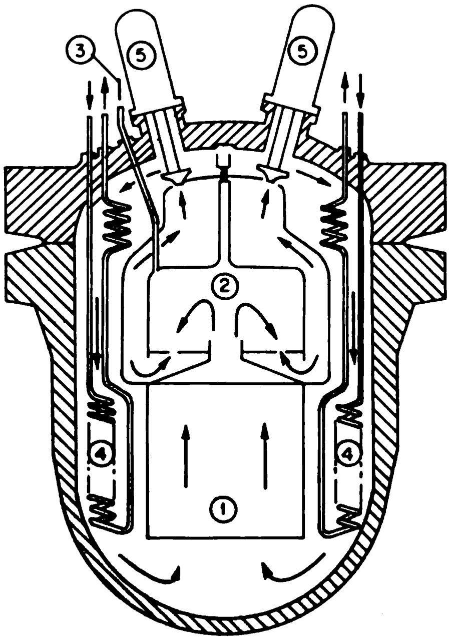

Fig. X-5 Principles of VULCAIN reactor.[5] (1) Core; (2) pressurizer; (3) pressurizing-gas piping; (4) steam generators; (5) pumps.

Table X-4 MAIN PARAMETERS OF NERO DESIGN[7]

General and primary system	
Reactor power, Mw(t)	67
Steam production, metric tons/hr	111.2
Steam pressure, kg/cm^2	40
Temperature, °C	280
Reactor operating pressure, kg/cm^2	151
Nominal reactor inlet temperature, °C	270
Nominal reactor outlet temperature, °C	299
Nominal inlet temperature reactor core, °C	288
Mass flow through reactor core, kg/sec	1155
Mass flow through each of two external circuits, kg/sec	220
Reactor core dimensions	
Core height, mm	1327
Core nominal diameter, mm	1128
No. of full-size fuel elements	30
No. of subsize fuel elements	12
Total No. of fuel rods	4218
Diameter of pellets, mm	10.03 ± 0.01
Total weight of UO_2, kg	4600
Cladding (Zircaloy) inside diameter, mm	10.2
Cladding (Zircaloy) outside diameter, mm	11.9
Pitch of fuel rods, mm	15.0
Core volume fractions	
UO_2	0.3352
H_2O	0.4402
Cladding boxes	0.1725
Control rods	0.0407
Core physics and heat transfer	
Average burnup, Mwd/metric tons of UO_2	16,600
Initial enrichment of central zone	4.4
Initial enrichment of outer zone	4.8
Amount of burnable poison, g of B_4C equivalent	1240
Maximum heat production, watts/cm of rod length	500
General dimensions	
Inside diameter of reactor vessel, m	2.0
Inside height of reactor vessel, m	5.5
Heat-transfer surface of steam generator, m^2 each	200
Heat-transfer surface of superheater, m^2 each	43.8
Inside diameter of containment, m	9.0

The reference also discusses the design of a steam injector-jet pump for use in the downcomer region of a boiling-water reactor. Reference 11 couples the neutronic and hydraulic behavior of a marine boiling-water reactor into a digital-computer code to study transient behavior of the reactor in a rolling and heaving ship. It is shown[11] that the results of the ship's motion produce large neutron-flux variations but affect fuel temperature, heat flux, coolant flow rate, reactor vessel pressure, and rate of steam flow to the turbine only a small amount.

References

The references that contain A/Conf. numbers are papers that were presented at the Third United Nations International Conference on the Peaceful Uses of Atomic Energy, Geneva, September 1964.

1. V. I. Neganov, B. G. Pologikh, and J. V. Sivintsev, Atomic Ships Safety Problems, A/Conf.28/P/378.
2. J. J. Aphrikantov, N. M. Mordvinov, P. D. Novikov, B. G. Pologikh, A. K. Sledzjuk, N. S.

Khlopkin, and N. M. Tsarev, Operating Experience of the Atomic Power Plant on the Icebreaker "Lenin," A/Conf.28/P/313.

3. W. Wiebe, H. Konig, and I. Weisbrodt, The Reactor Plant of the Research Ship of Gesellschaft fur Kernenergieverwertung in Schiffbau and Schiffahrt mbH, A/Conf.28/P/540.
4. J. Storrer and S. Rigg, The Vulcain Core Power Experiment, A/Conf.28/P/515.
5. R. P. Kinsey and P. E. Maldague, Technical Objectives of the Vulcain Reactor Project, A/Conf.28/P/565.
6. J. Smith and F. de Waegh, Physics Problems of Water Reactors Moderated by a Variable H_2O/D_2O Mixture, A/Conf.28/P/176.
7. M. Bogaardt and M. Muysken, The NERO Reactor for Ship Propulsion, A/Conf.28/P/588.
8. A. P. Alexandrov, I. I. Afrikantov, A. I. Brandaus, G. A. Gladkov, B. V. Gnesin, V. I. Neganov, N. S. Khlopkin, The Atomic Icebreaker "L in *Proceedings of the Second United Natio ternational Conference on the Peaceful Us Atomic Energy, Geneva, 1958*, Vol. 8, pp. 2 219, United Nations, New York, 1958.
9. G. A. Bat, G. B. Muhina, D. M. Parfanovich, Klochkov, V. C, Muhortov, H. M. Truhachev, D. I. Sheffer, Compensation of Large Chang Reactivity by Means of Core Lattice Deform A/Conf.28/P/376.
10. E. Kjelland-Fosterud, I. Bencze, B. Kierult, O. R. Kolberg, Two-Phase Flow Investigat for a Marine Boiling Water Reactor, A/Conf. P/801.
11. H. Christensen, K. O. Solberg, and A. O. Wag On the Dynamic Behavior of Boiling Water Reactors, A/Conf.28/P/748.

Section XI

Power Reactor Technology

Other Reactors

A number of reactors discussed at the Conference have not been reviewed in the preceding sections, either because they are intended for special purposes or because their development is still at a stage too early to reveal their ultimate major characteristics. Some of these are discussed briefly in the following paragraphs.

Portable Power Plants

The Army Reactors Program in the United States has resulted in the construction and operation of five nuclear power plants that represent the U. S. effort in the development of portable reactor plants for applications other than space. The first reactor in the series began operation in April 1957. General information on the plants is given in Table XI-1, which is taken from Ref. 1. All the reactors are of the pressurized-water type, with operating pressures from 1200 to 1750 psi, and all use UO_2–stainless-steel cermet fuel.

The truly portable plants in the U. S. series were designed to be transported by a variety of means, such as truck, rail, boat, or aircraft. Consequently shipping modules were limited to a size of 8 by 8 by 30 ft and to a weight of 30,000 lb. About 18 modules of reactor and power-plant equipment, plus about 40 modules of support facilities and buildings, comprise a typical plant. For plant details the reader is referred to Ref. 1, to *Power Reactor Technology*, 6(3): 43, which presents a description of the PM-1 core design, and to Ref. 2, which contains details of all five plants in the portable-power-plant series. The design objectives of the U. S. portable reactor development program, as set forth in Ref. 1, are as follows:

—Minimum size and weight
—Minimum installation effort
—High reliability
—System simplicity
—Self-sufficient plant
—Capability of being relocated

The Russians have developed an interesting portable nuclear power plant, the organic-moderated ARBUS plant, which has been in operation since June 1963. The plant has about half the output of the U. S. plants, as shown in Table XI-2. The coolant used in ARBUS, a hydrostabilized gas-oil, has proved to be satisfactory, probably largely because of the incorporation in the ARBUS plant of a coolant "regeneration" system. Operation of the system is described in the following quotation from Ref. 3:

> . . .The coolant comes from the primary circuit (200–250 liter/hour) to the regeneration system

Table XI-1 U. S. PORTABLE REACTOR POWER PLANTS IN OPERATION[1]

Designation	Location	Startup date	Power	Purpose
SM-1	Fort Belvoir, Va.	1957	10 Mw(t), 1860 kw(e)	Training, experimental
SM-1A	Fort Greely, Alaska	1962	20 Mw(t), 1640 kw(e) + 35 × 10^6 Btu/hr	Power and heat
PM-1	Sundance, Wyo.	1962	9.4 Mw(t), 1000 kw(e) + 7 × 10^6 Btu/hr	Power and heat
PM-2A	Camp Century, Greenland	1960	10 Mw(t), 1600 kw(e) + 1 × 10^6 Btu/hr	Power and heat
PM-3A	McMurdo Station, Antarctica	1962	9.5 Mw(t), 1500 kw(e)	Power

gas oil pump. Then the gas oil at a pressure of 45–60 atm is mixed with an inflow of circulating hydrogen. The latter is obtained by water electrolysis in an electrolyzer from which it is transported to the system by a displacement compressor of the regeneration system. The gas oil and hydrogen mixture is heated in the regenerative heat exchanger, and then it is heated up to the working temperature in an electric furnace. After that the gas oil and hydrogen mixture is fed to the reactor filled with catalyst. The hydrogen and regenerated gas oil mixture coming from the reactor transfers its heat in the heat exchanger, and is finally cooled down to 30–50°C in the cooler. Then the mixture is separated in a gas separator from which the gas oil comes through cermet and felt filters to the primary circuit feed tanks, and hydrogen flows to the circulating compressor. Owing to formation of destruction gas products (methane), small amounts of the circulating gas are continuously rejected to an exhaust stack. Hydrogen total flowrate is found to be 0.45 kg/hr, hydrogen in the amount of 0.36 kg/hr directly takes part in the reaction.

Table XI-2 ARBUS MAIN PARAMETERS[3]

Reactor output, kw	5000
Turbogenerator output, kw	750
Pressure in the primary-circuit pressurizer, psi	88
Coolant temperature	
At reactor inlet, °F	446
At reactor outlet, °F	469
Coolant flow rate of the primary circuit, metric tons/hr	600
Saturated steam temperature in steam generator, °F	433

Inital characteristics of the low-cost gas-oil coolant are given in Table XI-3. It is believed, however, that for the remote-station application of the plant the low melting point of the gas-oil (relative to that of the terphenyls usually used in the nuclear application) is considered at least as important as the low cost. It is believed also that the gas-oil is not being considered for central-station use because of its relatively poor high-temperature capability.

The ARBUS plant consists of separate factory-tested units, similar to the modules of the U. S. plants but apparently of slightly larger size. The plant consists of 19 units, each weighing 20 tons or less, and it is stated[3] that the weights and sizes of the units make possible their transportation to the building site by water or land. Setup of the plant on site requires two or three months,[3] a time that compares with the 77 days required[1] to erect the U. S. plant PM-3A. The ARBUS plant and the U. S. plants differ greatly in design, of course, but a particularly interesting difference is in one of the rather major features of the plants. Early in the design of PM-1, it was recognized that adequate sources of cooling water would not always be available at remote sites. For that reason heat rejection to the air was specified. In the ARBUS plant the condenser is water cooled.

Table XI-3 HYDROSTABILIZED GAS-OIL CHARACTERISTICS[3]

Specific weight at 20°C, g/cm^3	0.8558
Iodine number	Not greater than
Sulfurizing total, wt.%	30
Boiling initiation, °C	212
Boiling termination, °C	300
Carbon content, %	86.89
Hydrogen content, %	13.11
Hydrogen/carbon ratio	1.8
Sodium content, wt.%	2×10^{-5}
Sulfur content, wt.%	3×10^{-3}
Vapor pressure at 350°C, atm	4.85
Chemical compound	
Paraffin, %	30.12
Aromatic, %	30.03
Naphthene, %	39.85

The second Russian portable nuclear power plant,[4] the TES-3, has been in operation since 1961. TES-3, which has a pressurized-water reactor, is more advanced than the other portable plants in one respect: practically all the equipment is arranged in four large packages that are permanently mounted on track type vehicles. When the plant is readied for operation, biological shielding is provided by covering the two vehicles, which carry the reactor and the primary system, with the most convenient locally available shielding material, e.g., earth. The operation of TES-3 has apparently been successful and has confirmed the reliability, the good control characteristics, and the convenience for maintenance of such plants.[4] Principal characteristics of the plant are given in Table XI-4.

Table XI-4 THE MAIN CHARACTERISTICS[4] OF TES-3

Generator power, kw	1500
Reactor power, kw	8800
Pressure in the primary circuit, psi	1910
Temperature at the reactor inlet, °F	527
Temperature at the reactor outlet, °F	572
Parameters of the second circuit	
Pressure in the steam generator, psi	294
Temperature of steam superheat, °F	536
Pressure in the condenser, in. Hg	~3.9
Cooled water flow rate, metric tons/hr	1000
Weight of the plant equipment, metric tons	210
Weight of the transported shield if included, metric tons	28.5
Weight of all power truck-trailers, metric tons	310
Core life, days	250

irect-Conversion ower Plants

The direct-conversion reactors discussed at eneva, although not strictly the type of plant ormally discussed in *Power Reactor Technol-gy*, will be mentioned briefly for whatever earing they may have on civilian power-reac-or development.

A concise history of the SNAP-10A program s given in Ref. 5. The reactor is described, the irect conversion of heat to electricity is disussed, and the integration of the reactor heat ource and a thermoelectric power-conversion ystem into a complete package is discussed. he characteristics of the thermal-neutron NAP reactors are given in the paper, and Tale XI-5 reproduces some of the SNAP-10A data. In mid-1964 the reactor and conversion subsystems had performed satisfactorily in independent tests, and preflight tests of the integrated plant had begun. Flight testing in the actual space environment is scheduled for 1965.

Table XI-5 SNAP-10A DESIGN CHARACTERISTICS[5]

Fuel-moderator elements (U-ZrH)	
Diameter, in.	1.25
Length, in.	13.0
N_H, H atoms/cm^3 × 10^{-22}	6.5
U (fully enriched ^{235}U), wt.%	10
Number of elements	37
Total ^{235}U, kg	4.3
Cladding thickness, in.	0.015
Reactor	
Core-vessel diameter, in.	8.94
Core-vessel height, nominal, in.	15.6
Be reflector thickness, nominal, in.	2
Number of control drums-safety elements	4
Core volume, cu ft	0.3
Weight with reflector control assembly, lb	250
Fuel-element spacing-triangular matrix, in.	1.26
Operating characteristics	
Coolant (NaK) flow, gal/min	13.1
Inlet temperature, °F	900
Outlet temperature, °F	1010
Maximum fuel temperature, °F	1085
Power, kw(t)	34
Power density, average, kw(t)/liter	4.0
Heat flux, average, Btu/(hr)(sq ft)	10,200
Neutron flux, average, neutrons/(cm^2)(sec)	1.7 × 10^{11}

The high-temperature direct-conversion reactor Romashka has operated as a complete system for about 500 hr in the Soviet Union, and the direct-conversion portion of the plant has been tested[6] with electric heat for over 1000 hr. In Romashka, heat generated in the fast reactor core is transferred by conduction radially to a reflector, and then from the lateral surface of the reflector to a semiconductor conversion device mounted coaxially and adjoining the reflector. The cylindrical reactor is built up of horizontal fuel elements, each of which is made of a graphite body and enriched fuel plates of uranium dicarbide. The radial reflector of the reactor is made of graphite and beryllium, and end-face reflectors are fabricated of metallic beryllium. The reactor is controlled by four rods that are inserted in the radial beryllium reflector and by movement of the lower end-face reflector. The cold junctions of the thermoelectric conversion devices are cooled by radiating fins. The average temperature at the bases of the fins is about 550°C. Some basic parameters of the Romashka reactor are given in Table XI-6, which is taken from Ref. 6.

Table XI-6 BASIC PARAMETERS OF THE DIRECT-CONVERSION REACTOR ROMASHKA[6]

Electrical output, kw	0.50 to 0.80*
Total thermal power, kw	40
Maximum temperature of beryllium reflector, °C	1200
Maximum temperature of external surface of beryllium reflector, °C	980
Maximum temperature of uranium dicarbide fuel elements, °C	1900
Charge of ^{235}U, kg	49
Worth of automatic control rod, %	0.2
Worth of manual control rod, %	0.4
Worth of safety rod, %	0.4
Worth of all control rods, %	1.4
Worth of mobile end-face reflector, %	3.5
Total neutron flux in core center, neutrons/(cm^2)(sec)	10^{13}
Total neutron flux at reactor core boundary, neutrons/(cm^2)(sec)	7 × 10^{12}
Neutron leakage from reactor, neutrons/(cm^2)(sec)	3 × 10^{11}

*Depending on temperature conditions.

One result of the Soviet experimental work that may be of interest to the reactor designer is given in Fig. XI-1, which shows the depen-

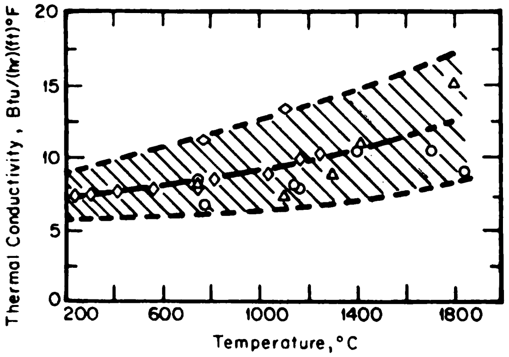

Fig. XI-1 Dependence of thermal conductivity of uranium dicarbide on temperature.[6]

Table XI-7 ADVANCED REACTOR TYPES UNDER CONSTRUCTION IN THE UNITED STATES[11]

	MSRE*	EBOR†	UHTREX‡	FRCTF§
Location	Oak Ridge, Tenn.	NRTS, Idaho	Los Alamos, N. Mex.	Los Alamos, N. Mex.
Contractor or laboratory	ORNL	General Atomic Div. of General Dynamics Corp.	LASL	LASL
Power, Mw(t)	10	10	3	20
Fuel	Molten solution of UF_4 and ZrF_4 in $^7LiF-BeF_2$	62 UO_2−38 BeO	UC_2 coated particles in graphite	Molten Pu-Co-Ce
Fuel enrichment, % ^{235}U	25 to 93	62	93	
Maximum fuel temperature, °F	1225	1900	3000	1200
Cladding or container	INOR-8 (Hastelloy N)	Hastelloy X	None	Ta alloy
Primary coolant	Circulating fuel (LiF, BeF_2-ZrF_4-UF_4)	He	He	Na
Coolant exit temperature, °F	1225	1300	2000 to 2400	1157
Moderator	Graphite	BeO	Graphite	

*MSRE, Molten-Salt Reactor Experiment.
†EBOR, Experimental Beryllium Oxide Reactor Experiment.
‡UHTREX, Ultra-High-Temperature Reactor Experiment.
§FRCTF, Fast Reactor Core Test Facility of the Los Alamos Molten-Plutonium Reactor Project.

dence of the conductivity of uranium dicarbide on temperature.

Other papers concerning direct-conversion devices or techniques are listed as Refs. 7 to 10.

Advanced Concepts

A paper by Sievering[11] describes several advanced reactor concepts currently under development in the United States. The four advanced reactor types listed in Table XI-7 are being built as reactor experiments, and several other concepts are in the stage of laboratory development. The Molten Salt Reactor Experiment is expected to be in operation early in 1965, as is the Experimental Beryllium Oxide Reactor. The Ultra High-Temperature Reactor Experiment is planned to achieve initial criticality late in 1965, and the Fast Reactor Core Test Facility, which will be able to accommodate core-blanket combinations of various designs, is scheduled for initial operation in 1967.

Three papers are on advanced reactor concepts being investigated in the Federal Republic of Germany. One paper is concerned with the pebble-bed power reactor,[12] which has been previously mentioned in Sec. VIII, and the other two describe a sodium-cooled, zirconium hydride-moderated power-reactor experiment[13] and a molten-salt epithermal reactor,[14] respectively.

References

The references that contain A/Conf. numbers are papers that were presented at the Third United Nations International Conference on the Peaceful Uses of Atomic Energy, Geneva, September 1964.

1. M. A. Rosen, J. B. Roll, and R. D. McFarr Portable Reactor Power Plants, A/Conf.28/P/211.
2. *Directory of Nuclear Reactors*, Vol. IV, Power Reactors, International Atomic Energy Agency, Vienna, 1962.
3. K. K. Polushkin, I. Ya. Emelyanov, P. A. Delens, N. V. Zvonov, U. N. Aleksenko, I. I. Grozdov, S. P. Kuznetsov, A. P. Sirotkin, U. I. Tokarev, K. P. Lawrovsky, A. M. Brodsky, A. R. Belov, E. V. Borisyuk, V. M. Gryazev, V. D. Tetyukov, D. N. Popov, U. I. Koryakin, A. G. Filippov, K. V. Petrochuk, V. D. Khoroshavin, N. P. Savinov, M. N. Meshcheryakov, V. I. Pushkarev, V. A. Suroyegin, P. A. Gavrilov, L. N. Podlazov, I. V. Rogozhkin, L. N. Podlazov, and I. N. Rogozhkin, The ARBUS—Organic Cooled and Moderated Nuclear Power Station, A/Conf.28/P/307.
4. N. M. Sinev, A. K. Krasin, I. F. Bichkov, O. I. Blokhin, D. L. Broder, V. N. Gabrussev, Yu. V. Dudnikov, V. A. Zhiltsov, M. A. Koptev, A. Ya. Komarov, A. P. Kotov, M. N. Lantsov, G. A. Lissochkin, G. V. Merzlikin, I. G. Morozov, Yu. I. Orekhov, Yu. A. Sergeev, P. N. Slyusarev, G. N. Ushakov, N. V. Fyodorov, V. Y. Chyornyi, and V. M. Shmelev, Small-Gabarit Atomic Power Plant TES-3, A/Conf.28/P/310.
5. H. M. Dieckamp, R. Balent, and J. R. Wetch, Reactor Direct-Conversion Units, A/Conf.28/P/218.
6. M. D. Millionshchikov, I. G. Gverdtsiteli, A. S. Abramov, L. V. Gorlov, Yu. D. Gubanov, A. A. Efremov, V. F. Zhukov, V. E. Ivanov, E. A. Koptelov, V. G. Kosovskii, N. E. Kukharkin, R. Ya. Kucherov, S. P. Lalykin, V. I. Merkin, Yu. A. Nechaev, B. S. Pozdnyakov, N. N. Ponomarev-Stepnoy, E. N. Samarin, V. Y. Serov, V. A. Usov, V. G. Fadin, V. V. Yakovlev, M. V.

Yakutovich, V. A. Khodakov, and G. V. Kompaniets, High-Temperature Direct Conversion Reactor "ROMASHKA," A/Conf.28/P/873.

7. P. D. Dunn and J. Adam, Fission-Heated Thermionic Diodes, A/Conf.28/P/132.
8. B. C. Lindley, Nuclear Magnetoplasmadynamic Energy Conversion, A/Conf.28/P/133.
9. E. W. Salmi, F. G. Block, G. M. Grover, H. D. Miller, R. W. Pidd, and V. C. Wilson, Thermionic Diodes for Direct Conversion Reactors, A/Conf.28/P/219.
10. I. I. Bondarenko, I. N. Gorelov, Yu. K. Gus'kov, V. M. Dmitriev, I. I. Kasikov, V. P. Karmasin, S. Ya. Lebedev, M. A. Lebedev, V. A. Malikh, S. A. Majev, V. Ya. Pupko, V. G. Petrovskii, V. P. Paschenko, E. E. Sibir, Y. Ya. Stavisskii, I. P. Stakhanov, A. S. Stepanov, and Yu. S. Yur'ev, Theoretical and Experimental Investigations Connected with Development of Thermionic Reactors—Converters, A/Conf.28/P/317.
11. N. F. Sievering, Jr., The U. S. Program for the Development of Advanced Reactor Concepts, A/Conf.28/P/212.
12. C. B. von der Decken, J. D. Lueders, O. Machnig, H. W. Schmidt, and R. Shulten, Development Project of a Pebble-Bed Power Reactor, A/Conf.28/P/536.
13. R. Harde and K. W. Stoehr, A Sodium-Cooled Power Reactor Experiment Employing Zirconium Hydride Moderator, A/Conf.28/P/537.
14. P. R. Kasten, The MOSEL Reactor Concept, A/Conf.28/P/538.

LEGAL NOTICE

This journal was prepared under the sponsorship of the U. S. Atomic Energy Commission. Neither the United States, nor the Commission, nor any person acting on behalf of the Commission:

A. Makes any warranty or representation, expressed or implied, with respect to the accuracy, completeness, or usefulness of the information contained in this journal, or that the use of any information, apparatus, method, or process disclosed in this journal may not infringe privately owned rights; or

B. Assumes any liabilities with respect to the use of, or for damages resulting from the use of any information, apparatus, method, or process disclosed in this journal.

As used in the above, "person acting on behalf of the Commission" includes any employee or contractor of the Commission, or employee of such contractor, to the extent that such employee or contractor of the Commission, or employee of such contractor prepares, disseminates, or provides access to, any information pursuant to his employment or contract with the Commission, or his employment with such contractor.

NUCLEAR SCIENCE ABSTRACTS

The U. S. Atomic Energy Commission, Division of Technical Information, publishes *Nuclear Science Abstracts (NSA),* a semimonthly journal containing abstracts of the literature of nuclear science and engineering.

NSA covers (1) research reports of the U. S. Atomic Energy Commission and its contractors; (2) research reports of government agencies, universities, and industrial research organizations on a world-wide basis; and (3) translations, patents, books, and articles appearing in technical and scientific journals.

Complete indexes covering subject, author, source, and report number are included in each issue. These are cumulated quarterly, semiannually, and annually providing a detailed and convenient key to the literature.

Availability of NSA

SALE *NSA* is available on subscription from the Superintendent of Documents, U. S. Government Printing Office, Washington, D. C., 20402, at $30.00 per year for the semimonthly abstract issues and $22.00 per year for the four cumulated-index issues. Subscriptions are postpaid within the United States, Canada, Mexico, and all Central and South American countries, except Argentina, Brazil, British and French Guiana, Surinam, and British Honduras. Subscribers in these Central and South American countries, and in all other countries throughout the world, should remit $37.00 per year for subscriptions to semimonthly abstract issues and $25.00 per year for the four cumulated-index issues.

EXCHANGE *NSA* is also available on an exchange basis to universities, research institutions, industrial firms, and publishers of scientific information. Inquiries should be directed to the Division of Technical Information Extension, U. S. Atomic Energy Commission, P. O. Box 62, Oak Ridge, Tennessee, 37831.

TECHNICAL PROGRESS REVIEWS

To meet the needs of industry for concise summaries of current atomic developments, the Atomic Energy Commission is publishing this series, Technical Progress Reviews. Issued quarterly, each of the reviews digests and evaluates the latest findings in a specific area of nuclear technology and science.

The five journals published in this series are:

Isotopes and Radiation Technology, P. S. Baker, A. F. Rupp, and associates, Oak Ridge National Laboratory

Nuclear Safety, Wm. B. Cottrell, W. H. Jordan, and associates, Oak Ridge National Laboratory

Power Reactor Technology, W. H. Zinn and J. R. Dietrich, Combustion Engineering, Inc., Nuclear Division

Reactor Fuel Processing, Stephen Lawroski and associates, Chemical Engineering Division, Argonne National Laboratory

Reactor Materials, R. W. Dayton, E. M. Simons, and associates, Battelle Memorial Institute

Each journal may be purchased from the Superintendent of Documents, U. S. Government Printing Office, Washington, D. C., 20402. *Isotopes and Radiation Technology* at $2.00 per year for subscription or $0.55 for individual issues; the other four journals at $2.50 per year and $0.70 per issue. See back cover for remittance instructions and foreign postage requirements.

The views expressed in this publication do not necessarily represent those of the United States Atomic Energy Commission, its divisions or offices, or of any Commission advisory committee or contractor.

Availability of Reports Cited in This Review

Unclassified AEC reports are available for inspection at AEC depository libraries and are sold by the Clearinghouse for Federal Scientific and Technical Information, National Bureau of Standards, U. S. Department of Commerce, 5285 Port Royal Road, Springfield, Va., 22151. Some of the reports cited are not available owing to their preliminary nature; however, the information contained in them will eventually be made available in formal progress or topical reports.

Unclassified reports issued by other Government agencies or private organizations should be requested from the originator.

Unclassified British and Canadian reports may be inspected at AEC depository libraries. British reports are sold by the British Information Service, 45 Rockefeller Plaza, New York, N. Y.; Canadian reports (AECL series) are sold by the Scientific Document Distribution Office, Atomic Energy of Canada, Ltd., Chalk River, Ontario, Canada.

Classified U. S. and foreign reports identified in this journal as Classified may be purchased by properly cleared Access Permit Holders from the Division of Technical Information Extension, U. S. Atomic Energy Commission, P. O. Box 1001, Oak Ridge, Tenn., 37831. Such reports may be inspected at classified AEC depository libraries.

DEPOSITED BY THE
NITED STATES OF AMERICA

POWER REACTOR TECHNOLOGY

A REVIEW OF RECENT DEVELOPMENTS

Prepared for DIVISION OF TECHNICAL INFORMATION, USAEC,
by W. H. ZINN and J. R. DIETRICH,
COMBUSTION ENGINEERING, INC., NUCLEAR DIVISION

SPRING 1965

VOLUME 8

NUMBER 2

Foreword

This quarterly review of reactor development has been prepared at the request of the Division of Technical Information of the U. S. Atomic Energy Commission. Its purpose is to assist interested organizations in the task of keeping abreast of new results in reactor technology for civilian application.

Power Reactor Technology contains reviews of selected recently published reports that are judged noteworthy in the fields of power-reactor research and development, power-reactor applications, design practice, and operating experience. It is not meant to be a comprehensive abstract of all material published during the quarter, nor is it meant to be a treatise on any part of the subject. However, related reports from different sources are often treated together to yield reviews having some breadth of scope, and background material may be added to place recent developments in perspective. Occasionally the reviews are written by guest authors. Reviews having unusual breadth or significance are placed at the front of the issue as Feature Articles.

The intention is to cover the various areas of reactor development from the general viewpoint of the reactor designer rather than from the more detailed points of view of specialists in the individual areas. To whatever extent the coverage of *Power Reactor Technology* may occasionally overlap the fields of the other Technical Progress Reviews, the overlaps will be motivated by this objective of viewing current progress through the eyes of the reactor designer.

A degree of critical appraisal and some interpretation of results are often necessary to define the significance of reported work. Any such appraisal or interpretation represents only the opinion of the reviewer and (in the usual case, when the review is written by Combustion Engineering, Inc., Nuclear Division staff) the Editor. When the review is predominantly interpretive the reviewer is named; unless identified as a guest author, he is a member of the Combustion Engineering, Inc., Nuclear Division staff. Readers are urged to consult the original references to obtain all the background of the work reported and to obtain the interpretation of the results given by the original authors.

For timely coverage, *Power Reactor Technology* must often review fragmentary material. The fixed subject headings listed below have been adopted in the hope of maintaining some continuity and order in the material from one issue to another: all reviews except Feature Articles will be arranged under these headings. A particular issue will not necessarily contain all the headings but only those under which material is reviewed.

Economics, Applications, Programs
Resources and Fuel Cycles
Physics
Fluid and Thermal Technology
Fuel Elements
Materials
Control and Dynamics
Containment, Radiation Control, and Siting
Systems Technology
Components
Design and Construction Practice
Operating Experience
Specific Reactor Types
Specific Applications
Unconventional Approaches

W. H. Zinn, Vice-President
J. R. Dietrich, Editor
Combustion Engineering, Inc.

DEPOSITED BY THE
NITED STATES OF AMERICA

Contents

I Physics 109
Critical and Exponential Experiments . . 109
Age and Diffusion-Length Determinations 113
Cross Sections 115
Neutron Thermalization 115
References 116

II Fluid and Thermal Technology . . . 118
Conduction 118
Gases 121
Pressurized Water 121
Organic Fluids 123
References 124

III Fuel Elements 126
Cermet Fuels for Fast Reactors . . . 126
Fabrication of Various Fuel Assemblies 128
References 131

IV Components 133
EBR-II Control-Drive Mechanisms . . 133
Process Tubes and Fittings for the NPR 134
References 136

V Specific Reactor Types 137
Large Pressurized-Water Reactors . . 137
  EBWR 147
Design Studies of a 1000-Mw(e) Fast Reactor 147
References 155

Issued quarterly by the U. S. Atomic Energy Commission. Use of funds for printing this publication approved by the Director of the Bureau of the Budget on October 14, 1963.

Letter to the Editor

WESTINGHOUSE ATOMIC POWER DIVISION EXPERIENCE WITH STAINLESS-STEEL-CLAD FUEL ELEMENTS

In marked contrast to the VBWR results reported in *Power Reactor Technology*, 7, 4, Westinghouse has not observed failure of stainless steel cladding in a pressurized water reactor environment. Our operating experience to date is summarized in Table I. Stainless steel has clearly performed with distinction under exposures substantially in excess of those at which failures occurred in VBWR, regardless of whether the cladding was annealed or cold worked, freestanding or collapsed. Yankee environment was primary neutral, with periods of high *p*H and boric acid operation; Saxton and Selni are chemical shim systems (boric acid) having added alkali.

Table I IRRADIATION DATA ON STAINLESS-STEEL FUEL ELEMENTS IN WESTINGHOUSE REACTORS

Stainless type	Cladding thickness, in.	Peak exposure Nvt >1 Mev	Peak exposure MWD/MTU	Reactor
Annealed 348	0.021 (freestanding)	7×10^{21}	30,000	Yankee
Cold worked 304	0.016 (freestanding)	3×10^{21}	20,300	Saxton
Cold worked 304	0.010 (collapsed)	1×10^{21}	10,000	Saxton
Cold worked 304	0.015 (freestanding)	1×10^{21}	6,000	Selni

A test assembly irradiated in Yankee Cores I and II is now under test in Core IV and will achieve a peak burnup of 41,000 MWD/MTU (fast flux >1 Mev = 11×10^{21} nvt) by September 1965. Fuel elements in the basic Saxton Core will achieve peak exposures of 25,000 MWD/MTU by June 1965. Selni fuel elements will achieve 16,000 MWD/MTU by July 1966.

Based on an extensive review of experimental data reported by other laboratories, we conclude that in-reactor failures of UO_2 fuel elements clad with commercial stainless steel have occurred only in a boiling water environment. Factors which must be evaluated in explaining the differences between stainless steel behavior in boiling and pressurized water reactors are as follows:

1. *System Pressure*

The higher system pressure in a pressurized water reactor produces a larger compressive stress component on the cladding surface. For example, the circumferential compressive stress contribution from 2,000 psi external pressure will be about 12,000 psi greater than in a boiling water system operating at 1,000 psi, assuming equivalent clad thickness and geometry. The higher system pressure thus prevents or delays the development of tensile stress in the cladding as a result of fission gas accumulation. Crack propagation cannot normally occur in the absence of a tensile stress.

2. *System Chemistry*

Typically, oxygen concentration in pressurized water is less than 0.01 ppm. In direct cyclic boiling systems, however, oxygen in the vapor stage varies from 20–40 ppm; in the liquid, oxygen concentration is typically 0.05 to 0.5 ppm. High oxygen concentrations have been shown in laboratory experiments to accelerate stress corrosion. Differences in corrosion behavior may also arise from differences in the equilibrium distribution of chemical species from radiolytic decomposition.

3. *Corrosion Product Deposition*

Corrosion products deposit on the surfaces of fuel elements irradiated in both boiling and nonboiling water environment (although the examination of the irradiated Yankee elements revealed almost no deposited corrosion product). The corrosion product deposited from a boiling coolant will be highly oxidized; ferric ions are known to be effective crack promoters.

4. *Local Thermal Stresses*

Fundamental heat transfer studies(1,2,3) have shown that rapid thermal fluctuations occur at surfaces where boiling is occurring. These local temperature fluctuations are caused by the growth and detachment of vapor bubbles which temporarily change the local heat transfer rates at the fuel element surface. Amplitude of the observed temperature variations ranges from a few degrees to about 30°F, occurring at somewhat irregular intervals of 3 – 50 milliseconds. The rate at which the temperature decreases during a local thermal fluctuation may be as high as 1500°F/sec. Although the strain resulting from these fluctuations is relatively small, the very high frequencies at which such a strain is cyclically applied may contribute to fuel element failure. Since bubble nucleation occurs preferentially at small surface crevices or pits, thermal cycling is focused on locations which are already sources of potential microcracks. The temperature will fluctuate at any fuel element surface experiencing nucleate boiling (either bulk or local). However, smaller fluctuations occur in a pressurized water system because of the higher pressure and greater forced convection cooling of the surface.

The relative importance of each of these mechanisms has yet to be fully assessed. However, controlled experiments are required to supplement engineering test data and to establish the relevance of these mechanisms to behavior of other cladding materials.

---

(1) F. D. Moore and R. B. Mesler, *A.I.Ch.E. J.*, 7: 4, 620 (1961).

(2) N. Madsen, Memo WWO 26-M31, Technische Hochschule, Eindhoven, 1964.

(3) T. S. Rogers and R. B. Mesler, *A.I.Ch.E. J.*, 10: 5 (September 1964).

R. J. Allio, Manager
Materials and Processes Development
Westinghouse Atomic Power Division

March 19, 1965

Section

I

Power Reactor Technology

Physics

ritical and Exponential xperiments

everal reports of results of critical and expo-ential experiments have been issued since ie last review of the subject in *Power Reac-r Technology* [7(3): 206-212 (Summer 1964)]. hese include some papers from the Third eneva Conference.

Reference 1 describes a series of critical xperiments with a close-packed D_2O-moder-ted lattice in the Special Power Excursion Re-ctor Test II (SPERT-II). These experiments ere directed toward providing information eeded for design of the final operational core id for analysis of power-excursion tests con-icted with that core to investigate the influence f prompt-neutron lifetime on reactor kinetics. i addition to the effects of initial system pres-ire and temperature, planned kinetic experi-ients with the close-packed core configura-on will investigate the dynamic response of ie reactor during forced coolant flow. Fuel ssemblies, spaced on a uniform square pitch f 6.0 in., consisted of 3-in.-square thin-walled luminum cans containing 18 highly enriched, emovable, flat fuel plates separated by heavy-ater channels 0.094 in. thick. The fuel plates ere of a uranium-aluminum alloy meat (0.020 y 2.54 by 24 in.) clad with 0.020 in. of alumi-im. Each plate contained a nominal loading of g of ^{235}U, and therefore each assembly had a tal of approximately 126 g of ^{235}U. The facility as designed to permit operation up to moder-ely elevated temperatures and pressures, g., 400°F and 375 psig, respectively. The ref-rence discusses critical loadings, flux maps, djoint flux maps, and the reactivity coeffi-ients of pressure, temperature, and voids.

Bucklings were measured[2] by substitution chniques in the Process Development Pile for fuel assemblies composed of clusters of 19, 31, and 37 natural UO_2 rods with various rod spacings within the cluster. The UO_2 rods were 0.500-in.-diameter sintered pellets (10.4 g/cm^3) stacked in aluminum tubes having an outside diameter of 0.547 in. and a wall thickness of 0.020 in. The hexagonal rod clusters were placed inside aluminum-housing tubes of circular and hexagonal cross section and were of such dimensions as to limit the coolant-flow area to realistic values. The various coolants investigated were Dowtherm A, polyethylene, H_2O, air, and D_2O. The single-region reference-core loading consisted of 31-rod UO_2 clusters contained in D_2O-filled aluminum-housing tubes; both the reference and test lattices were spaced on a 9.33-in. triangular pitch. Measurements were made by the successive substitution technique wherein effective critical water heights are determined after the substitution of one, three, and finally seven test assemblies. One-group perturbation and two-group flux-matching methods were used in the interpretation of the experimental data.

Reference 3 presents a summary of experimental and theoretical results obtained in the Heavy Water Lattice Project of the Massachusetts Institute of Technology (MIT) during the period October 1962 to September 1963. Experimental methods were developed during previous studies on lattices of 1-in.-diameter natural-uranium rods in the main subcritical (exponential) assembly. These methods were employed in the evaluation of the material buckling, fast-fission effect, and resonance and thermal captures in fuel lattices of 0.25-in.-diameter slightly enriched-uranium-metal fuel rods. The uranium metal was enriched to 1.03% ^{235}U and was clad with aluminum 0.028 in. thick. Values of the material buckling were evaluated for unreflected lattices of the 1.25-in. triangular pitch in both the 3- and 4-ft-diameter tanks and with a 2.50-in. triangular pitch in the 4-ft-diameter tank. Preliminary results on measurements of the ratio of fissions of ^{238}U to fissions of ^{235}U, and on the ratio of epithermal to thermal fission of ^{235}U, are reported for lattice pitches of 1.25, 1.75, and 2.5 in. Results are compared with earlier results obtained in the Miniature Lattice Facility at MIT and with results obtained at Brookhaven National Laboratory with 0.25-in. rods in lattices moderated by H_2O. Measurements of the ^{238}U cadmium ratio, the ratio of ^{238}U capture rate to the ^{235}U fission rate, and intracellular distributions of neutron-capture rates in ^{238}U and copper are described and compared, where possible, to measurements made in the Miniature Lattice Facility. Experimental determinations of intracellular thermal-neutron distributions and comparisons with analytical results are discussed. In particular, the difficulties arising from the cylindrical approximation to the unit cell, mainly with the lattices of 1.25-in. triangular pitch, the use of improved energy-exchange kernels, and modifications of the THERMOS code to include the effects of radial and axial leakage are described. The progress on miniature lattices, two-region or substituted lattices, and pulsed-neutron studies is also discussed.

Experimental data were obtained at both the Savannah River Laboratory (SRL) and the Hanford Laboratories to establish standards for the prevention of accidental criticality in handling, storing, and processing uranium metal enriched to 3 wt.% ^{235}U. In the Hanford experiments the approach-to-critical and exponential methods were used to provide material bucklings and critical masses for H_2O-moderated lattices with fuel-rod diameters of 0.175, 0.300, 0.600, and 0.925 in. The SRL measurements, discussed in Ref. 4, employed subcritical exponential techniques to determine the material buckling for H_2O-moderated lattices containing metal rods of 2- and 3-in. diameters at several lattice pitches. The material buckling for fuel elements of a given diameter and lattice pitch was evaluated from measured values of the neutron relaxation lengths along the axes of assemblies having at least two different effective diameters. The use of assemblies with different effective diameters permitted an evaluation of the radial extrapolation distance without the measurement of transverse flux shapes. Tabulations of the extrapolation distance, transverse buckling, neutron relaxation length, material buckling, and critical mass are given for the configurations investigated at SRL. A summary of both the SRL and Hanford data for the 3 wt.% ^{235}U metal rods is given in Ref. 4.

The ZPR-III facility has been used to study the properties of very large fast power breeder reactors by a two-zone-core technique wherein a small subcritical portion of a large dilute system is positioned in the center of the critical facility matrix and surrounded by a buffer region and an annular driver region. Reference 5 describes the measurements in assembly 42 which were designed to assess the validity of this technique. The central core area of assembly 42 had an effective radius of 9.22 in., a length of 34 in., and a composition identical to that of a previously run dilute simulated uranium carbide reactor (assembly 34). The buffer region consisted of a 0.5-in.-thick depleted uranium filter with a length equal to that of the inner zone. Surrounding the buffer zone radially, and with an axial length equal to that of the two inner regions, was a driver zone of 3.18-in. nominal thickness. This driver zone had a ^{235}U volume fraction approximately twice that of the central core region. A depleted uranium blanket surrounded the entire core assembly in both the axial and radial directions. Reactivity measurements performed in this assembly included determinations of plate-orientation worth, homogeneity corrections, reactor-segment worths, central reactivity coefficients, and radial worth distributions of axial columns of core materials. Spectral-index determinations included central fission ratios, nuclear track emulsion measurements, fission-counter traverses, Rossi-alpha measurements, sodium activation, and natural- and enriched-uranium foil measurements. Comparisons between results obtained for the central core region and assembly 34 are given.

The second two-zone core built in the ZPR-III facility (assembly 43) is described in Ref. 6. In this case the central region with its low-density axial blanket was designed to simulate a projected fast power breeder reactor employing uranium monocarbide with a high proportion of ^{238}U to promote internal breeding. The basic structural and coolant materials were stainless steel and sodium, respectively. The composition of the driver region was so chosen that the complete assembly would be critical within the ZPR-III inventory of enriched uraium. The composition of the buffer region was en chosen, by calculation, to modify the spec- rum of the neutrons diffusing in from the driver a spectrum similar to that in the central one. The low-density axial blanket behind the entral zone was identical in composition to the entral zone except that the enriched uranium as replaced with stainless steel. The remain- ng part of the core was surrounded by a de- leted uranium blanket. In both the central and river zones, experimental determinations were ade for sodium void coefficients and reac- ivity effects resulting from the substitution of nriched and depleted uranium, ^{233}U, ^{239}Pu, simu- ated fission products, and various structural nd control materials. Spectral indices were easured, and reaction-rate traverses and ac- ivation experiments were performed. The re- ctivity change due to the Doppler effect was easured by heating a large depleted uranium xide sample.

In support of the Advanced Sodium Graphite eactor program, a series of critical and ex- onential experiments[7,8] has been performed to etermine values of the material buckling and $_{\text{eff}}$ for graphite assemblies fueled with slightly nriched uranium carbide. These assemblies mployed triangular lattice pitches of 9, 11, nd 12 in. and, in most cases, included control- hannel mockups. The uranium carbide fuel lements each contained 18 fuel rods arranged n two concentric rings about a centrally lo- ated, voided, stainless-steel tube. The inner uel ring consisted of 6 rods evenly spaced on a .47-in.-diameter circle, and the outer ring onsisted of 12 rods evenly spaced on a 2.84- n. circle. Each fuel rod contained a 72-in. stack of 0.500-in.-OD uranium carbide pellets nside a 0.010-in.-thick 0.550-in.-OD stainless-steel tube. The uranium carbide had a density f 13.23 g/cm^3, a carbon weight fraction of 4.9%, nd a ^{235}U enrichment of 3.02%. The region utside the fuel rods and within the 0.025-in.- hick 4.00-in.-ID process tube was filled with sodium to a height of 72 in. The number of uranium carbide fuel elements (24) was much less than the number required for a bare or reflected critical assembly; consequently it was necessary to employ a driver region surrounding the test lattice to achieve a critical configuration. Fuel elements for the graphite-moderated driver region consisted of hollow cylinders (1.026 in. in inside diameter and 1.730 in. in outside diameter) of uranium metal enriched to 2 wt.% ^{235}U and stacked inside a 0.040-in.-thick aluminum tube. Fuel assemblies in the driver region were spaced on a 10.6-in. triangular pitch regardless of the lattice pitch employed in the test region. The critical experiments provided data on source multiplication measurements for the test lattices as well as on the number of driver assemblies required for each lattice to achieve criticality. The former data were used to determine the k_{eff} for each uranium carbide test lattice. Lattice configurations identical to those employed as test regions in the two-region critical assemblies were employed in the exponential measurements. In addition, data were also obtained for the same lattice compositions, but with reduced radial dimensions, to permit an evaluation of the effective radial buckling for a given lattice composition. Material-buckling values inferred from the two-region critical measurements are compared with those obtained from the exponential measurements and with those obtained by multigroup and few-group calculational schemes.

A short description of the critical and exponential facilities at the Institute of Nuclear Research, Swierk, Poland, as well as a brief description of the Institute's research programs, is given in Ref. 9. The critical assembly ANNA is a heterogeneous water-graphite-moderated pile with a graphite reflector. The central region of the graphite pile has 45 cylindrical holes positioned on a square pitch of 14 cm, into which graphite plugs or fuel channels can be inserted. Each fuel element is composed of three aluminum-canned coaxial tubes of 20% enriched UO$_2$. ANNA serves primarily as a mockup facility of the high-flux reactor. The MARYLA reactor is a zero-power (1 kw) flexible pool type facility designed for the study of various light-water systems. The individual fuel assemblies consist of 15 or 16 fuel pins, each of which is 8 mm in diameter by 50 cm long and contains 8 g of ^{235}U. HELENA is a subcritical assembly designed to investigate the parameters of natural-uranium–graphite lattices. The fuel is in the form of aluminum-canned uranium slugs, 30 cm long by 2.5 cm in diameter.

The NPY Project is a joint undertaking in reactor physics between the International Atomic Energy Agency and research laboratories in Norway, Poland, and Yugoslavia. Reference 10 presents a description of the NPY lattices studied, the experimental techniques used in the measurements of neutron-flux distributions, and comparisons between the experimental flux distributions and theoretical predictions. The rod type fuel elements employed in the zero-power facility NORA (Kjeller, Norway) have a fuel radius of 5.64 mm and consist of nonsintered UO_2 powder which has a density of 9.28 g/cm^3 and which is enriched to 3 wt.% ^{235}U. The cladding is type 304 stainless steel with a thickness of 0.71 mm. The lattices reported were moderated by D_2O (99.4 mole %) and employed square pitches of 10, 4.908, and 3.658 cm. The lattices employed in the abovementioned zero-power assembly ANNA (Swierk, Poland) consist of H_2O-cooled annular elements moderated by graphite and positioned at a square pitch of 14 cm. The fuel element is composed of an inner aluminum support tube, three concentric fuel annuli clad with aluminum, and an aluminum tube that separates the outer water annulus from the graphite. Each fuel annulus is 2.3 mm thick and is composed of 38.5 wt.% UO_2 (enriched to 20% ^{235}U) and 61.5 wt.% aluminum. The fuel element employed in the RB zero-power reactor (Vincha, Yugoslavia) consists of a single fuel annulus that is enriched to 2 wt.% ^{235}U, clad with aluminum, and moderated and cooled by D_2O. The D_2O coolant at both surfaces of the fuel annulus is separated from the inner and outer D_2O-moderated regions by thin-walled aluminum tubing. Square lattice pitches of 8 and 17.9 cm were investigated. Experimental data on thermal-flux distributions measured at the three facilities are compared with analytical results obtained by various calculational techniques, e.g., THERMOS, one-group Amouyal-Benoist, and one-velocity P_3.

Reference 11 is a description of the ROSPO critical facility (Comitato Nazionale per l'Energia Nucleare) that was built for the PRO power-reactor project to test organic-moderated cores. This facility was designed to carry out critical experiments in various cores differing in size, geometry, and control-rod type. During operation the moderator temperature can be changed over a range from about 40°C above the melting point to about 20°C below the boiling point, e.g., 190 to 350°C for Santowax OMP. Over this range the moderator temperature can be maintained constant to within ±0.5°C. The moderator level can be varied and controlled to ±1.5 mm. Data to be obtained by means of the ROSPO facility are as follows: critical-mass values vs. core configuration and fuel enrichment; temperature coefficients, control-rod worth, and reactivity effects associated with structural components. In addition to a detailed description of the facility, Ref. 11 gives data on the following for the first core: critical loadings, worth of control rods and peripheral fuel elements, and temperature-coefficient and buckling measurements. The first core is of the plate type and is moderated and cooled by Santowax OMP. The fuel assemblies are square boxes (71 by 71 mm) fabricated from 0.78-mm-thick stainless-steel sheet. The fuel plates are 96.4 cm long by 0.72 mm thick and 70 mm wide. The meat is an enriched (90% ^{235}U UO_2 dispersion in an AISI type 304 stainless-steel matrix; the cladding is AISI type 304L stainless steel.

Reference 12 presents a summary of results obtained by pulsed-neutron techniques on graphite- and H_2O-moderated systems and critical experiments on H_2O-UO_2 systems. The pulsed experiments were made on two reflected, highly subcritical systems: (1) a graphite-moderated and -reflected system in the semihomogeneous critical assembly at the Japan Atomic Energy Research Institute (JAERI) and (2) the light-water-moderated UO_2 subcritical reflected system at the Mitsubishi Atomic Power Industries (MAPI) research laboratories. Reasonable agreement between calculated and measured values of the prompt-neutron decay constant of the fundamental mode was reported. The light-water lattice studies were made by the Ozenji Critical Facility (OCF, Central Research Laboratory, Hitachi, Ltd.) and the Tank-type Critical Assembly (TCA, JAERI). Fuel elements used in the experiments at the OCF facility were of the rod type, containing 10-mm-diameter UO_2 pellets sheathed in 0.8-mm-thick aluminum tubes. The UO_2 enrichments were 1.5 and 2.5 ^{235}U. Rod type fuel elements were also used in the TCA. These elements had an effective diameter of 12.5 mm and contained 2.6% enriched UO_2. The results discussed in Ref. 12 for the various experiments include critical masses, flux distributions, spectral parameters, lattice and water-gap peaking, temperature and void coefficients, and space-dependent reactivity effects of fuel.

Two additional papers (Refs. 13 and 14) presented at the Third Geneva Conference are reviews that cover the work on critical experiments in the United States since the Second Geneva Conference in 1958. The first paper covers in detail the field of fast reactor critical experiments, and the second[14] does the same for the work on D_2O-moderated systems. An extensive list of references is included in each paper.

Age and Diffusion-Length Determinations

Measured and calculated values of the flux age of fission neutrons to the indium resonance energy (1.44 ev) in graphite have been reported in Ref. 15. The measurements were made in 8-ft-high hexagonal graphite assemblies having effective diameters of 5 and 7 ft. The assemblies were centered on a cylindrical graphite thermal column which was 5 ft in diameter and which extended 3½ ft above the core of the 2-kw AE-6 water-boiler reactor. The graphite in the experimental assemblies was of AGOT grade and was cast in the form of 4-ft-long hexagonal logs with a distance across flats of 4 in. The graphite density was 1.697 ± 0.004 g/cm^3 as determined from the total weight and as-built dimensions of the assemblies. Two fission sources were employed; the primary source was 3½ in. in diameter, and the secondary source was 1 in. in diameter. Each was fabricated from 4-mil-thick uranium enriched to 93.2 wt.% ^{235}U and was covered on the top side with a 20-mil-thick cadmium disk that served as a sink for thermal neutrons transmitted through the source from the reactor thermal column. Detector foils were 1 cm square by 5 mils thick and were composed of 40% indium and 60% tin; the cadmium boxes were 40 mils thick.

The various corrections investigated[15] experimentally included source perturbations, detector-foil perturbations, nonisotropic foil activation, and epithermal leakage from the graphite assemblies.

Theoretical values[16] of the spatial moments of the slowing-down density distribution at the indium resonance energy were determined by the TYCHE code, which is an infinite-medium slowing-down Monte Carlo program written in FORTRAN. The effects of both inelastic scattering and anisotropic elastic scattering are included in the calculation. Detailed descriptions of the cross sections employed in the code are given in Ref. 16. Comparison with experimental results requires an evaluation of the flux age, τ^ϕ. The latter quantity is related to the slowing-down age, τ^q, by the method of Goldstein,* which utilizes the Grueling-Goertzel relation to couple flux and slowing-down density.

$$\tau^\phi = \frac{M_2^\phi}{6} = \frac{M_2^q}{6} + \beta$$

where $\beta = \dfrac{\gamma D}{\xi \Sigma_s + \gamma \Sigma_a}$

$$\gamma = 1 - \frac{\alpha(\ln \alpha)^2}{2\xi(1-\alpha)}$$

$$\alpha = \left(\frac{A-1}{A+1}\right)^2$$

and the undefined symbols have the conventional definitions.

Table II-1 presents a comparison between the experimental and theoretical results described above and the previously reported values of the age in graphite. All results are normalized to a graphite density of 1.60 g/cm^3. The experimental values quoted for the present work (Ref. 15) were computed using a parabolic integration procedure over the experimental points as well as an extrapolation of the experimental points. Additional contributions to the uncertainty in the computed flux age including the uncertainties in graphite density, counting statistics, foil positioning, and extrapolated flux distribution. The comments in Table II-1, particularly those relating to the experimental references, give some indication of significant differences between the present and past work.

Measurements of the flux age of fission neutrons to the indium resonance energy in several zirconium-water mixtures are described in Ref. 17. The experimental techniques were similar to those employed in the measurement of the age of fission neutrons in H_2O [reviewed in *Power Reactor Technology*, 7(4): 331 (Fall 1963)]; i.e., the measurements utilized a plane fission source of finite dimension and effectively infinite-plane detectors to give a result equivalent to a measurement using axial detectors and an infinite-plane source. The fission source consisted of an enriched-uranium foil, 28¾ in. in diameter and 4 mils thick, masked down to

---

*H. Goldstein, J. G. Sullivan, Jr., R. R. Coveyou, W. E. Kinney, and R. R. Bate, Calculations of Neutron Age in H_2O and Other Materials, USAEC Report ORNL-2639, Oak Ridge National Laboratory, July 12, 1961.

Table II-1 AGE TO INDIUM RESONANCE ENERGY, FOR FISSION NEUTRONS IN GRAPHITE[15] ($\rho = 1.60$ g/cm^3)

	$\frac{1}{6}M_2$, cm^2	M_4, 10^6 cm^4	M_6, 10^{10} cm^6	Comments
Present work (Ref. 15)				
Experiment	307.8 ± 2.0	6.577	3.843	Foils, 1 by 1 cm; cadmium boxes, 40 mils thick
Theory	307.4 ± 1.0	6.59 ± 0.06	4.01 ± 0.09	Monte Carlo calculation
Experimental reference				
Fermi[*]	317.0			Large point source (293 g), thick (0.102 in.) cadmium boxes
Hill[†]	310.6 ± 3.0	6.89	4.4	Large (4 by 6.35 cm) foils, thick (0.135 in.) cadmium boxes
Davey[‡]	337.9			Source: planar distribution of natural-uranium rods
Hendrie[§]	312.6 ± 0.5	6.87	4.3	Uncertainty based in counting statistics only
Theoretical reference				
Joanou[¶]	305.0			Moments method
Goldstein[**]	304.0 ± 3.0			Monte Carlo calculation

[*] E. Fermi, J. Marshall, and L. Marshall, Slowing Down of Fission Neutrons in Graphite, CP-1084, Nov. 25, 1943.

[†] J. E. Hill, L. D. Roberts, and G. McCammon, Slowing Down of Fission Neutrons in Graphite, ORNL-187, Jan. 19, 1949.

[‡] W. G. Davey, J. C. Field, J. C. Gilbert, and A. L. Pope, An Experimental Study of the Slowing Down of Fission Neutrons and the Diffusion of Thermal Neutrons in Graphite and in Heterogeneous Mixtures of Bismuth and Graphite, AERE-R/R-2501, March 1958.

[§] J. M. Hendrie, et al., Slowing Down and Diffusion Length of Neutrons in Graphite-Bismuth Systems, in *Progress in Nuclear Energy, Physics and Mathematics*, Series 1, Vol. 3, Pergamon Press, Inc., New York, 1959.

[¶] S. D. Joanou et al., Moments Calculations of the Fermi Age in Moderators and Moderator-Metal Mixtures, *Nucl. Sci. Eng.*, 13(2): 171-(1962).

[**] H. Goldstein, J. G. Sullivan, Jr., R. R. Coveyou, W. E. Kinney, and R. R. Bate, Calculations of Neutron Age in H_2O and Other Materials, ORNL-2639, July 12, 1961.

an effective diameter of 12 in. with cadmium. The homogeneous zirconium-water mixtures were simulated by 0.113-in.-thick zirconium plates arranged parallel to the fission source in a tank of water. The detector foils were $\frac{3}{4}$ in. in diameter by 0.005 in. thick and were composed of 40% indium and 60% tin; cadmium covers were 20 mils thick. In a given plane, parallel to the fission plate, the foils were spaced radially from the axis of symmetry of the experimental assembly. The relative infinite-plane activity $\phi(z)$ was obtained by numerical integration of the following equation:

$$\phi(z) = \int_0^\infty r\phi'(r,z)\,dr$$

where $\phi'(r,z)$ is the activity of a foil at a distance r from the axis of symmetry and in a plane at a distance z from the fission source. Detailed descriptions of the methods of data reduction and tabulations of data are given in the reference. For metal-to-water ratios, R, of 0.0, 0.348, 0.565, and 1.20, the measured ages are given by τ (cm^2) $= 26.63 \pm 19.23R$.

Steady-state measurements of the effective thermal-neutron-absorption cross section and diffusion length in graphite, by means of a beryllium-antimony source, are reported in Ref. 18. The effective absorption cross section was evaluated by comparing the volume-integrated thermal-neutron distribution measured in a finite graphite assembly with that measured in an "infinite" water assembly containing the same beryllium-antimony source. Although this method does give a result relative to the absorption cross section of H_2O, it does not require any assumption as to the magnitude of the transport cross section of graphite. The diffusion lengths were also evaluated from the asymptotic flux distributions in both the graphite and water assemblies. The graphite assembly was an 8-ft-high stack of hexagonal AGOT-grade graphite logs forming a decahedron 12 ft across the flats. Since the finite dimensions of the graphite stack allowed thermal leakage in both directions, displaced source measurements were made to facilitate evaluations of leakage effects. A detailed discussion of the experimental procedures, data-reduction techniques, and correction factors, i.e., source absorption, foil depression, and leakage factors, are given in the reference. The average effective absorption cross section $\sigma_a(\hat{v})$, evaluated at the most probable velocity for a Maxwellian distribution at 20°C, was 4.42 ± 0.08 mb and is in good agreement with a value of $\sigma_a(\hat{v}) = 4.38$ mb deterned by the use of the transport mean free :h λ_{tr} (steady state) reported by Campbell.* e graphite cross section can be expressed as = 0.01332 σ_a(H), where σ_a(H) is the absorption ›ss section of hydrogen. The average diffu- ›n length, normalized to a graphite density of ›0 g/cm^3 and measured in the direction paral- to the extrusion axis, was 54.77 ± 0.20 cm, d, in the direction perpendicular to the ex- ısion axis, it was 55.10 ± 0.15 cm. The former lue is in good agreement with the values mea- red by Campbell in graphite assemblies on ; thermal column of the AE-6 water boiler ıctor, namely, 54.7 ± 0.3 cm, corrected to .02 ± 0.20 cm for infinite geometry by a dif- ıion cooling correction. The diffusion length · H_2O was 2.80 ± 0.02 cm.

ross Sections

The fission cross section of ^{241}Pu becomes ›re important for neutron economy and long- :m reactivity changes as fuel elements are veloped to withstand increasing total expo- res and more particularly if plutonium is re- cled. Reference 19 reports measurements ıde with the Materials Testing Reactor fast opper and presents the fission cross section ^{241}Pu from 0.02 to 100 ev. A value of 962 ± 38 rns was measured at 0.0253 ev. Multilevel rameters to 10 ev are given. Reference 20 so reports ^{241}Pu fission cross sections, mea- red with the Rensselaer Polytechnic Institute ıear accelerator. The range of measurement from 2 to 100 ev, with sufficient resolution to rmit multilevel analysis to be carried out for ; neutron energies below 36 ev.

In Ref. 21, measurements of the integral cross ction for the ^{9}Be(n,2n) reaction in the upper d of the fission spectrum (above 2.7 Mev) are ported. The results are based on measure- ›nts of the total amount of helium produced ring irradiation of BeO specimens in the ıttelle Research Reactor. The value reported is 0 ± 60 mb.

The measurement was made as part of an vestigation of the long-term effects of fast- utron irradiation on polycrystalline beryllia. is suspected that helium generated within the ystalline matrix may be the cause of the loss of mechanical strength that has been observed in BeO after high fast-neutron doses at temperatures in the range of 100 to 500°C. The (n,2n) process is perhaps even more troublesome in beryllium metal because the resulting helium is responsible for the swelling of beryllium fuel jackets after substantial exposures at relatively high temperatures. The process is, of course, beneficial to the neutron economy of reactors that contain considerable beryllium in regions where the fast-neutron flux is high. The results reported in Ref. 21 are not inconsistent with the (n,2n) cross sections assumed at the 1959 Conference on the Physics of Breeding (Ref. 22).

Measurements of cross sections for a number of threshold reactions, averaged over the ^{235}U fission spectrum, are reported in Ref. 23. The measurements were made by an activation technique. The target material was irradiated in a fission-flux converter, and a characteristic gamma emission from the product nucleus was counted. Most of the results of the measurements are summarized in Table II-2. The half-lives listed in the table were not measured in the experiments but were taken from other sources for use in reducing the data.

Table II-2 MEASURED AVERAGE CROSS SECTIONS FOR THRESHOLD REACTIONS IN A ^{235}U FISSION SPECTRUM[23]

Reaction	$T_{1/2}$	Gamma rays measured, Mev	Breeding ratio of gamma rays, %	Average cross section measured, mb
^{24}Mg(n,p)^{24}Na	15.05 hr	1.368	100	1.31 ± 0.06
^{27}Al(n,p)^{27}Mg	9.5 min	1.015	98	2.9 ± 0.5
^{27}Al(n,α)^{24}Na	15.05 hr	1.368	100	0.60 ± 0.03
^{31}P(n,p)^{31}Si	2.56 hr			30.5 ± 1.2
^{32}S(n,p)^{32}P	14.3 days			60 ± 1.2
^{47}Ti(n,p)^{47}Sc	3.4 days	0.16	66	22.0 ± 1.5
^{48}Ti(n,p)^{48}Sc	44 hr	1.32	100	0.21 ± 0.016
^{54}Fe(n,p)^{54}Mn	314 days	0.835	100	66 ± 3.5
^{56}Fe(n,p)^{56}Mn	2.58 hr	0.845	99	0.90 ± 0.05
^{58}Ni(n,p)^{58}Co	71.3 days	0.81	100	105 ± 5
^{58}Ni(n,p)^{58m}Co	9.0 hr			30 ± 7
^{64}Zn(n,p)^{64}Cu	12.8 hr	0.51	38	27 ± 1.6
^{67}Zn(n,p)^{67}Cu	61 hr	0.184	45	0.9 ± 0.1
^{92}Mo(n,p)^{92}Nb	10.1 days	0.93	98	6.2 ± 0.4
^{95}Mo(n,p)^{95}Nb	35 days	0.765	99	0.13 ± 0.02

Neutron Thermalization

A general review of neutron thermalization, with attention to reactor applications, is given in Ref. 24. The paper also discusses various computer methods for representing scattering kernels and for determining the thermal-neutron characteristics in reactor lattices.

---

*R. W. Campbell, Diffusion Length in SGR Graph- ·, USAEC Report NAA-SR-Memo-7415, Atomics In- rnational, May 29, 1962.

The "scattering-law" formulation for the handling of differential scattering data was discussed previously at some length in *Power Reactor Technology*, 6(1): 6-14 and 6(4): 46-53. New tabulations of scattering-law data (scattering cross section as a function of energy and momentum transfer) are given in Refs. 25 and 26 for H_2O and D_2O at temperatures of 22 and 150°C. The measurements were made at Chalk River with a neutron spectrometer with selected initial neutron energies ranging from 0.034 to 0.26 ev. A comparison with earlier measurements (Ref. 27) at 24°C shows good agreement; the later compilations (Refs. 25 and 26), however, cover a wider range of variables. Measurements made in the USSR on H_2O at 23 and 90°C, as well as measurements on monoisopropyl-diphenyl ($C_{15}H_{16}$) at 20°C are tabulated in Ref. 28.

References

1. J. A. McClure and R. L. Johnson, Critical Loading and Initial Static Experiments in the SPERT II Reactor with a Closed-Packed D_2O-Moderated Core, USAEC Report IDO-16996, Phillips Petroleum Company, June 1964.
2. F. D. Benton, Measurements of Bucklings and Void Effects in D_2O-Moderated, Organic- or H_2O-Cooled Lattices of UO_2 Rod Clusters, USAEC Report DP-873, E. I. du Pont de Nemours & Co., Inc., June 1964.
3. I. Kaplan, D. D. Lanning, and T. J. Thompson (Eds.), Heavy Water Lattice Project Annual Report, USAEC Report MITNE-46, Massachusetts Institute of Technology, Sept. 30, 1963.
4. W. B. Rogers, Jr., and F. E. Kinard, Material Buckling and Critical Masses of Uranium Rods Containing 3 Wt.% U-235 in H_2O, *Nucl. Sci. Eng.*, 20(3): 266 (November 1964).
5. P. I. Amundson, R. L. McVean, and J. K. Long, A Two-Zone Fast Critical Experiment (ZPR-III Assembly 42), USAEC Report ANL-6733, Argonne National Laboratory, January 1954.
6. J. M. Gasidlo, J. K. Long, and W. P. Keeney, Doppler Effect Measurements, Sodium Void Coefficients, and Critical Studies of a 5000-Liter Fast Power Breeder Reactor by the Two-Zone Method (ZPR-III Assembly 43), USAEC Report ANL-6838, Argonne National Laboratory, May 1964.
7. O. R. Hillig and D. W. Latham, Material Bucklings of Critical and Subcritical Uranium Carbide Fueled Graphite Assemblies, Part I, Experiment, USAEC Report NAA-SR-9771, Atomics International, Dec. 1, 1964.
8. E. R. Specht, Material Bucklings of Critical and Subcritical Uranium Carbide Fueled Graphite Assemblies, Part II, Theoretical Interpretation, USAEC Report NAA-SR-9772, Atomics In tional, Aug. 1, 1964.
9. L. Adamski, Z. Bajbor, W. Dabek, J. Koz W. Suwalski, Critical and Exponential Asse at the Institute of Nuclear Research— presented at the Third United Nations In tional Conference on the Peaceful Uses of A Energy, Geneva, 1964, Paper A/Conf.28/P.
10. L. Adamski et al., Microscopic Neutron Flu tributions in Unit Cells of Critical Assembl the NPY-Project, presented at the Third U Nations International Conference on the Pea Uses of Atomic Energy, Geneva, 1964, Pap Conf.28/P/499.
11. G. Bitelli, G. Gambardella, R. Martinelli, S. osia, F. Orestano, A. Pulacci, E. Santa P. Saya, and R. Zona, ROSPO—Organic M ated Critical Experiments, presented at the T United Nations International Conference o Peaceful Uses of Atomic Energy, Geneva, Paper A/Conf.28/P/871.
12. K. Sumita et al., Subcriticality Measureme Pulsed Method and Critical Experiments on Water System, presented at the Third Uni tions International Conference on the Pea Uses of Atomic Energy, Geneva, 1964, Pap Conf.28/P/846.
13. F. W. Thalgott, J. K. Long, W. G. Davey, Kato, S. G. Carpenter, H. A. Morewitz, and Best, Fast Critical Experiments and Their An sis, presented at the Third United Nations In national Conference on the Peaceful Us Atomic Energy, Geneva, 1964, Paper A/Con P/265.
14. J. L. Crandall, W. L. Brooks, I. Kaplan, F. Langford, Jr., and L. C. Schmid, Lattice St and Critical Experiments in D_2O Moderated tems, presented at the Third United Natio ternational Conference on the Peaceful Us Atomic Energy, Geneva, 1964, Paper A/Con P/268.
15. R. W. Campbell, R. K. Paschall, and V. A. S son, The Age of Fission Neutrons to Indium R nance Energy in Graphite, Part I, Experim USAEC Report NAA-SR-8683, Atomics Inte tional, June 15, 1964; also reported in *Nucl Eng.*, 20(4): 445 (December 1964).
16. H. Alter, The Age of Fission Neutrons to In Resonance Energy in Graphite, Part II, The USAEC Report NAA-SR-8684, Atomics Inte tional, Oct. 9, 1963.
17. R. K. Paschall, The Age of Fission Neutro Indium Resonance Energy in Zirconium-Wa Mixtures, USAEC Report NAA-SR-9503, Ato International, Sept. 15, 1964.
18. J. A. DeJuren, T. E. Stewart, and E. R. Spe Measurements of Thermal Neutron Absorp Cross Section and Diffusion Length of Gra Using an Sb-Be Source, USAEC Report NAA 9803, Atomics International, Aug. 1, 1964.
19. T. Watanabe and O. D. Simpson, Low-En Neutron Fission Cross Section of ^{241}Pu, US Report IDO-16995, Phillips Petroleum Comp June 1964.
20. T. Watanabe, M. S. Moore, O. D. Simpson, Russell, and R. W. Hockenbury, Experim Measurements of the Fission Cross Sect ^{241}Pu, USAEC Report IDO-16976, Phillips P leum Company, Apr. 10, 1964.

1. F. F. Felber, Jr., D. R. Farmelo, and V. C. Van Sickle, The Integral ^{9}Be(n,2n) Cross Section, USAEC Report PWAC-433, Pratt & Whitney Aircraft Division, United Aircraft Corporation, May 19, 1964.

2. Wolf Haefele, The Fast Multiplication Effect Due to the (n,2n) Reaction in Beryllium and Beryllium Oxide, in Proceedings of the Conference on the Physics of Breeding, October 19–21, 1959, USAEC Report ANL-6122, pp.163-176, Argonne National Laboratory.

3. J. W. Boldeman, Fission Spectrum Averaged Cross Sections of Threshold Reactions, *J. Nucl. Energy: Pt. A & B,* 18(8): 417-424 (August 1964).

4. J. R. Beyster, N. Corngold, H. C. Honeck, G. D. Joanou, and D. E. Parks, Neutron Thermalization and Reactor Applications, presented at the Third United Nations International Conference on the Peaceful Uses of Atomic Energy, Geneva, 1964, Paper A/Conf.28/P/258.

25. B. C. Haywood, A Compilation of the Scattering Law for Water at 22°C and 150°C, British Report AERE-R-4484, January 1964.

26. B. C. Haywood, A Compilation of the Scattering Law for Heavy Water at 22°C and 150°C, British Report AERE-R-4582, May 1964.

27. P. A. Egelstaff, Compilation of Early Scattering Law Data, British Report AERE-R-3931, January 1962.

28. V. I. Mostovoy, V. S. Dykarev, D. P. Eremeev, S. P. Ishmaev, I. P. Sadikov, Iu. S. Saltykov, V. A. Taraban'ko, and A. A. Chernyshov, Experimental Studies on Neutron Thermalization, presented at the Third United Nations International Conference on the Peaceful Uses of Atomic Energy, Geneva, 1964, Paper A/Conf.28/P/367.

Section

II

Power Reactor Technology

Fluid and Thermal Technology

Conduction

Reference 1 is a report on an analytical determination of the temperature distribution in long, cylindrical fuel elements cooled internally by several channels. This conduction problem has been treated in the past, and Ref. 2 is a recent article on the subject. The Ref. 2 article describes the derivation of the so-called ROB code for the determination of the steady-state temperature distribution for a heat-generating, circular cylinder cooled by a ring of holes. The ROB code provides for analytically calculating the temperature as a function of radius and azimuthal angle if the heat-generation rate in the cylinder is spatially independent. The particular geometry used in the ROB code is shown in Fig. II-1. The analytical derivation in Ref. 1 is similar to that in Ref. 2 except that a radially distributed heat-generation rate is provided for; Poisson's equation is solved by the method of "sources" and "sinks," with the assumption that the solid is isotropic. The reference presents the equations needed for calculating the temperature distribution for either an arbitrary radial distribution of the heat generation or a radial generation rate developed from neutron-diffusion theory.

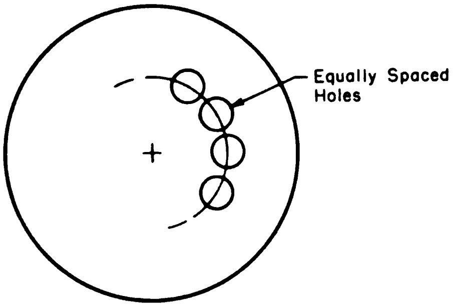

Fig. II-1 Cross section of cylinder illustrating geometry.[2]

Often in real cases the three-dimensional problem is important in elements of this kind until the third dimension is incorporated into the analytical expressions, the designer must handle such problems as best he can. It may well be that the incorporation of a third dimension in the conduction equations would result in a prohibitively complex solution and that entirely numerical techniques will be required in calculation of the temperature distribution in the long, cylindrical fuel elements that are internally cooled.

References 3 and 4 present "large" conduction codes suitable for use on digital computing machines. Reference 3 presents a FORTRAN code suitable for calculation of transient temperatures in a multiregion, axisymmetric, cylindrical configuration. The conduction code (ARGUS) allows up to 25 concentric regions each region consisting of either a stationary or a turbulently flowing material having temperature-dependent properties. The stationary materials can have space- and time-dependent heat-generation rates, and temperatures are calculated at equally spaced nodal points. Material properties of the flowing materials are approximated by second-order polynomials. The thermal properties of the stationary materials must be constant except that, with appropriate heats of transformation, up to nine phase changes are allowed in these materials. Also allowed are 100 nodal points per radial row and up to 16 radial rows.

The IBM-650 code HEAT-1 presented in Ref. 4 is a one-dimensional time-dependent or steady-state heat-conduction code. The program obtains a numerical solution to the oneimensional heat-conduction equation in either lab or cylindrical coordinates by use of the inite-difference approximation to the partial ifferential equations. This program is somehat smaller than the ARGUS code in that it an accommodate 10 regions and a maximum f 51 mesh points. The thermal conductivities nd heat capacities are described by thirdrder polynomials, and a time-dependent and ointwise space-dependent heat source can be ccommodated.

Apparently the thermal designer is accumuating a variety of machine codes that enable im to tackle many formidable conduction probems occurring in reactor design and analysis.

Reference 5 reports on the thermal conducivity of uranium dioxide fuel elements during rradiation. This reference deals with research t the Bettis Atomic Power Laboratory and is n extension of a program originally reported n USAEC Report WAPD-228. That report was eviewed in the March 1961 issue of *Power eactor Technology*, 4(2): 39-43. Briefly the xperiment was designed to measure the effecive thermal conductivity of UO_2 and a zircoium oxide–uranium oxide mixture; the discusion here will be limited to those experiments mploying only UO_2. Table II-1 gives the comosition and density of the fuel materials used n the experiments, and Fig. II-2 illustrates the esign of the capsule used for the in-pile measurements of the thermal conductivity. Table II-2 gives assembly and irradiation data on the several capsules. In Tables II-1 and II-2, the experiments designated "WAPD-22" are reported in WAPD-228, and the experiments designated "BETT" are reported in Ref. 5.

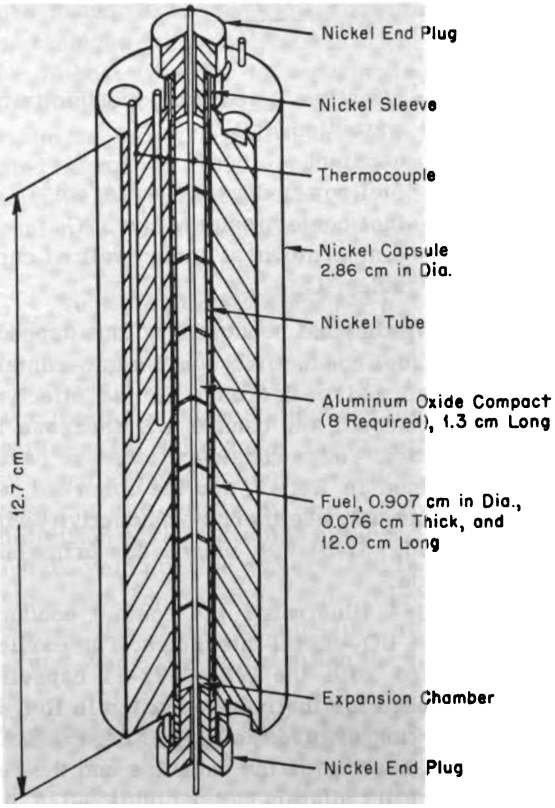
Nickel End Plug
Nickel Sleeve
Thermocouple
Nickel Capsule 2.86 cm in Dia.
Nickel Tube
Aluminum Oxide Compact (8 Required), 1.3 cm Long
12.7 cm
Fuel, 0.907 cm in Dia., 0.076 cm Thick, and 12.0 cm Long
Expansion Chamber
Nickel End Plug

Fig. II-2 Capsule for in-pile measurement of the thermal conductivity of oxide fuels to high fission depletions[5] (BETT-69-4).

Table II-1 COMPOSITION AND DENSITY OF FUEL MATERIALS[5]

Experiment No.	Fuel	Wt.% ^{235}U in total U	^{235}U atoms/cm^3 ($\times10^{-20}$)	Average fuel density	
				G/cm^3	% TD*
WAPD-22-11	UO_2 (natural)	0.7	1.65	10.4	95
BETT-69-1-C1	UO_2	21.0	50.0	10.6	97
BETT-69-4-C1	UO_2	21.4	51.0	10.6	97

*Percent of theoretical density.

The fuel cylinders were pressure bonded between the nickel capsule and a thin inner tube filled with BeO or Al_2O_3 (Fig. II-2). The capsule design was considerably different from the one employed for the WAPD-22 experiments, in which the fuel pellets were shrink fitted into type 304 stainless-steel capsules (Table II-2). The stainless-steel and nickel capsules had radial pairs of thermocouples for the determination of heat flux and a central thermocouple for the determination of the central temperature.

Figure II-3 illustrates BETT-69 capsule results for the effective thermal conductivity. The ordinate of Fig. II-3 shows the effective thermal conductivity, defined as follows:

$$K_{\text{eff}} = \frac{FP_f}{T_c - T_b} \tag{1}$$

where K_{eff} = effective thermal conductivity, watts/(cm)(°C)
F = constant
P_f = fuel power density, watts/cm^3
T_c = fuel center temperature, °C
T_b = temperature at inner wall of capsule, °C

The effective thermal conductivity thus depends on both the fuel conductivity and the gap-contact conductance, and a decrease in the effective conductivity could be caused by decrease in either quantity. These considerations are carefully explained in Ref. 5, and the observed decrease in the effective thermal conductivity with exposure (Fig. II-3) was indeed due primarily to irradiation.

Figure II-4 illustrates the contact conductances of the UO$_2$-metal interfaces. The earlier data obtained with the WAPD-22-11 capsules were reworked for their presentation in Ref. 5. This reworking involved improved estimates of the gamma heating of the capsules and the results of postirradiation determinations of the fuel-to-capsule gaps. Additional conclusions are quoted from Ref. 5 as follows:

> 1. The inpile thermal conductivities of UO$_2$ and UO$_2$ + ZrO$_2$ fuels at practical operating temperatures are essentially the same as their unirradiated conductivities up to fission depletions of about 10^{19} fissions/cc for operating temperatures near 500°C.
>
> . . . .
>
> 3. For operating temperatures near 500°C, the thermal conductivities of UO$_2$, ZrO$_2$ + 34 w/o UO$_2$, and ZrO$_2$ + 46 w/o UO$_2$ decreased approximately 50, 25, and 35 percent, respectively, between 1×10^{19} and 25×10^{20} fissions/cc.
>
> . . . .

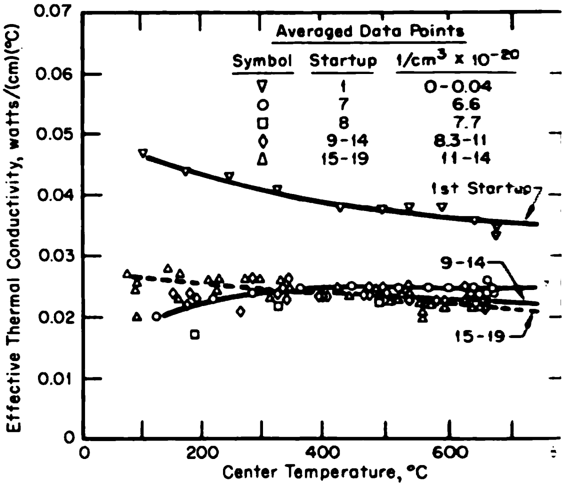

Fig. II-3 BETT-69-4 data for the effective th conductivity of UO$_2$ (Ref. 5).

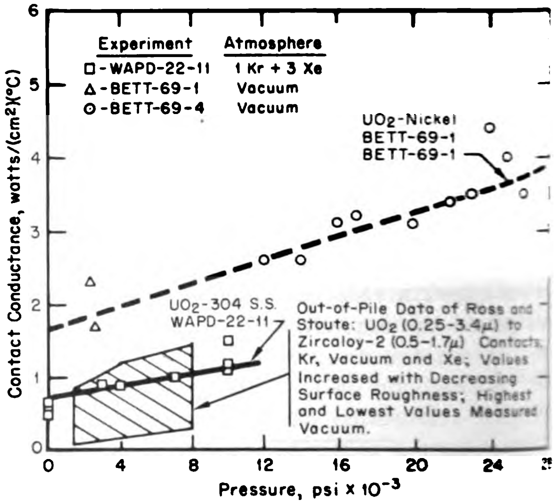

Fig. II-4 Contact conductances of UO$_2$-metal int faces.[5]

Table II-2 ASSEMBLY AND IRRADIATION DATA[5]

Experiment No.	Capsule material	Gas-filling atmosphere	Fuel wall thickness, cm	Estimated total exposure, thermal neutrons/cm^2 ($\times 10^{-20}$)	Total burnup, fissions/cm^3 ($\times 10^{-20}$)	Remarks
WAPD-22-11	Type 304 S.S.	1 Kr + 3 Xe	0.365	4.0	0.35	Shrink-fitted fuel pellets
BETT-69-1-C1	Nickel	1 Kr + 3 Xe	0.365	2.0	5.4	Pressure bonded (thin internal cladding with powdered BeO in bore
BETT-69-4-C1	Nickel	Vacuum	0.076	4.3	28	Pressure bonded (thin cladding supported by Al$_2$O$_3$ pellets shrink fitted after pressure bonding)

5. The initial inpile contact conductances of UO_2 + Zircaloy interfaces, derived from inpile data for UO_2 + nickel and UO_2 + type 304 stainless steel joints, are in good agreement with out-of-pile contact conductances of UO_2 + Zircaloy interfaces measured by Ross and Stoute [Canadian Report CRFD-1075]. Both the inpile data (for first start-ups) and the out-of-pile data indicate that, for interface pressures near 3000 psi, the contact conductance is approximately 1 watt/cm^2-°C for UO_2 + Zircaloy contacts between surfaces having surface roughnesses of less than 1 micron whether the interface is evacuated or filled with krypton and xenon. It is thought that the contact conductance decreases proportionally with the UO_2 conductivity, but additional data are needed to verify such decreases.

The thermal conductivity of uranium dioxide also discussed in Ref. 6. This report pre- nts an improved radial-heat-flow technique r the experimental determination of thermal nductivity, and a large section of the refer- ence is a discussion of the technique and the esults determined for Armco iron. However, e thermal conductivity of polycrystalline ura- um dioxide was measured for the temperature nge −57 to 1100°C. The uranium dioxide was repared in the form of disks of nuclear-grade epleted UO_2 powder, cold pressed and sintered hydrogen at 1850°C for 4 hr. The resulting ellets were 93.4% of the theoretical density .0.97 g/cm^3). The results indicated that the ermal resistivity, which is the reciprocal of e thermal conductivity, is linear between 200 nd 1000°C with a slope of 0.0223 cm/watt. etween 1000 and 1100°C a slight deviation om the linear behavior was noted in the di- ection of increasing thermal conductivity, and e authors of Ref. 6 suggest that this may in- icate a change in the composition of the mate- ial or a change in the basic heat-transport echanism within the solid.

ases

The following thermodynamic properties of elium are discussed in Ref. 7: pressure- olume-temperature and enthalpy relations, pecific heat, viscosity, thermal conductivity, nd Prandtl number. The compilation is an up- ating and expansion of previous work and in- ludes recent information. In general, the roperty data are given for temperatures ap- roaching 2000°F.

References 8 to 10 are British publications ealing with heat-transfer-coefficient calcula- ions for gases at high temperatures. References 9 and 10 are not recent reports but have been included for completeness. The specialized case of heat transfer to superheated steam is presented in Ref. 11. This reference correlates data on the heat-transfer coefficient for superheated steam at 1000 psia flowing in a uniformly heated circular duct. The following expression is recommended for design purposes:

$$\mathrm{Nu}_b = 0.021\ \mathrm{Re}_b^{0.8}\ \mathrm{Pr}_b^{0.6}\left(\frac{T_b}{T_w}\right)^{0.575} \qquad (2)$$

In Eq. 2 the symbols have their usual meanings. The correlation suggests that, as the wall temperature (T_w) increases, the Nusselt number decreases. The functional relation, which is derived by the author of Ref. 11, results from a definition of the Reynolds number in terms of the bulk velocity, the density, and the viscosity at the film temperature. The correlation reproduces the data to within ±10%, although only 18 runs were used to establish the correlation.

Pressurized Water

Fragmentary information on pressurized-water research of general interest was reported by Oak Ridge National Laboratory (Ref. 12) and Hanford Atomic Products Operation (Ref. 13). A dimensionless correlation was developed[12] for predicting the critical-heat-flux value for natural-convection burnout of water in a heated vertical channel closed at the bottom and open at the top to a liquid supply. Data were taken with tubes which were operated at atmospheric pressure and which had inside diameters from 0.086 to 0.25 in. and lengths from 6 to 48 in. This physical situation, although not of interest in reactor operations, might be encountered during the shutdown and depressurization of a power reactor. The correlation given in Ref. 13 is for the pressure drop occurring during local boiling. The experiments were conducted with a 19-rod electrically heated bundle; flow rates varied from 500,000 to 5 × 10^6 lb/(hr)(sq ft) at a pressure of 1200 psia.

References 14 and 15 deal with heat transfer to a fluid flowing in an annulus; Ref. 14 is concerned with water, whereas Ref. 15 deals with an arbitrary coolant. Annular-flow heat transfer was treated in the March 1961 issue of *Power Reactor Technology*, 4(2): 13-15, and the conclusion in that review was that under certain conditions the effect of the diameter ratio on the heat-transfer coefficients of the inner- and outer-wall surfaces was uncertain. In particular, Fig. IV-1 in that issue illustrates that the discrepancies by and large were between results obtained in this country and results obtained by Russian experimenters. After deriving theoretical expressions for heat transfer in an annulus, the author of Ref. 14 presents experimental data on the heat-transfer coefficients of inner- and outer-wall surfaces using average wall temperatures and calculated bulk water temperatures. The important result seems to be that the ratio of film coefficients of the inner- and outer-wall surfaces is dependent on the heat-flux level and the ratio of the inner and outer values of the heat flux. Accordingly the situation is somewhat more complex than was suggested in the earlier review. The author of Ref. 14 states that the theoretical predictions of Maloney, appearing in what is cited as an unpublished work, adequately fit the experimental results.

The analysis given in Ref. 15 extends consideration to heat transfer in an annulus with a variable circumferential heat flux. The treatment is completely analytical, and no experimental data are given. The analysis takes into consideration the resistance to circumferential mixing, with the assumption that in turbulent flow the eddy diffusivity in the circumferential direction is the same as that in the radial direction. Although no experimental support is given, the condition of a circumferentially varying heat flux is the usual one encountered in reactors.

Reference 16 is a report on the transient behavior of a natural-circulation loop operating near the thermodynamic critical point. The particular fluid studied in the report was Freon-114, primarily because it had a low critical temperature (294.2°F) and because thermodynamic data for the material were available. The analytical portion of the study consisted of writing one-dimensional conservation equations for a control volume and stacking the control volumes to obtain the simulated loop. The system of equations thus obtained was solved with the aid of a high-speed digital computer. The computer model, however, failed to represent the system adequately, primarily because of the assumptions used when the model was set up. The flow-stability results, however, are probably of general interest, and the following quotation from Ref. 16 serves to define them

> It has been determined experimentally tha eration of a single-phase, heat-transfer loop i thermodynamic critical region of the fluid o design studied in this experiment will produce sure and flow fluctuations under certain condi The condition determined experimentally fo occurrence of sustained flow and pressure flu tions was that the system fluid be passing th the thermodynamic region in which a maxim the density-enthalpy product as a function of perature, enthalpy, or density occurs. In this re it was found that as little as 1¼ kw of heating necessary to obtain sustained flow oscillations loop would operate stably in the thermodynami gions on either side of this maximum in the den enthalpy product. It was noted experimentally the magnitude and frequency of the pressure flow fluctuations depended on whether the max in the density-enthalpy curve was being trav from the low- or the high-temperature side proach from the low-temperature side resul a dominant frequency of 10 to 20 cps, which wa times the frequency found when traversing the imumum from the high-temperature side.

Reference 17 deals with the critical, or bur out, heat-flux determination in subcooled, b ing water flowing under forced convection. T reference contains a number of arbitrary co relations, mostly derived by manipulatio the Jens-Lottes equation. The existence o number of correlations probably is caused the attempt to correlate data taken from sy tems operating in various subcooled-boi flow regimes. This is recognized by the a thor,[17] and as many as four different regim are postulated. These are the nucleate-boi flow regime, the stratified-bubble flow regi the nonstratified-bubble regime, and froth fl The nucleate-boiling flow regime probably the most straightforward of all. In this cas which occurs only at subcoolings greater th about 50 Btu/lb, the nucleate bubbles a rapidly quenched by the liquid flow strea Occurrence of the regime requires also a sy tem pressure of at least 500 psi, mass veloc in excess of 0.9×10^6 lb/(hr)(sq ft), and equivalent diameter in excess of ⅛ in. T stratified and nonstratified flow regimes a separated by a matter of degree rather th type, the stratified regime changing gradu to a nonstratified flow as the bubbles beco dispersed in the bulk of the coolant. T stratified-bubble flow regime consists of u quenched bubbles which are concentrated c to the heat-transfer surface and which actu inhibit the frictional and heat-transfer eff of the turbulence caused by the nucleate b ng. This "shield" minimizes the effect of the urface condition of the transfer surface, in ontrast to the nucleate-boiling flow regime where a greater dependence of the critical heat lux with respect to the heat-transfer surface ondition is encountered.[17]

Froth flow occurs at low subcoolings, with low channels less than $\frac{1}{8}$ in. in diameter, or at ressures below 500 psi. The regime is characterized by relatively large amounts of unuenched bubbles, and the phase structures are omewhat similar to net vapor generation.

References 18 and 19 present design data pertinent to bundle type fuel assemblies. The particular geometry studied experimentally in Ref. 18 is illustrated in Fig. II-5; it consists of a wire-wrapped seven-rod bundle placed within a flow tube. The spiral wire wrappings are ypical of rod-bundle construction and serve not only to promote mixing between the coolant subchannels but also to help maintain proper spacing between adjacent rods and between the rods and the flow tube. The geometry shown in Fig. II-5 is particularly germane to pressure-tube type reactors. The experiment was conducted by injecting a salt solution into the inner coolant channels of a 70-in.-long seven-rod bundle fitted into the flow tube. Tap water was introduced into the outer coolant channels, and samples were taken of the outer-coolant-channel fluid at several places along the length of the bundle for analysis of salt concentration. The measurements then could be converted into a determination of the amount of coolant mixing that resulted for various wire-wrap configurations. The wire wraps produced considerable interchannel mixing, and the amount of mixing varied with changes in the wire-wrap pitch, although the amount was relatively insensitive to the relative spacing between the wires on adjacent rods.

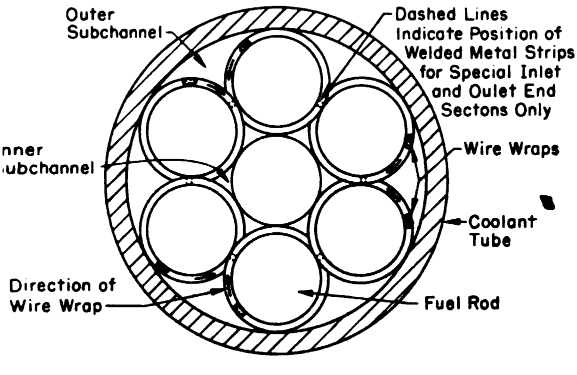
Outer Subchannel
Dashed Lines Indicate Position of Welded Metal Strips for Special Inlet and Oulet End Sectons Only
nner ubchannel
Wire Wraps
Coolant Tube
Direction of Wire Wrap
Fuel Rod

Fig. II-5 Cross section of a wire-wrapped seven-rod bundle in a coolant tube.[18]

Reference 18 presents equations to determine the interchannel coolant-mixing rate and gives two illustrative problems on the use of the equations in a practical reactor design. It is shown, for example, that the use of the wire wraps reduces the temperature inequality between the inner- and outer-coolant-channel streams (for the particular design study) by about a factor of 6. Reference 19 discusses the effect of wire wraps on the pressure drop for axial turbulent flow through rod bundles. The experiments reported in Ref. 19 were done with two basic types of assemblies: one was similar to the bundle shown in Fig. II-5, and the second incorporated a wire wrapped around the entire rod bundle as well as on the individual rods. A 19-rod bundle with wraps on 12 rods plus the overall bundle was also tested. Data were taken with unwrapped rods, and the increase in pressure drop caused by wrapping the rods in the fuel bundle is presented graphically in the reference. It was determined that the ratio of the pressure drop with wrapped rods to the pressure drop for the nonwrapped rods was proportional to the square of the number of wire wraps per unit length of rod. Changing the relative spacing between wires on adjacent rods caused some change in the pressure drop along the rod bundle. The entrance and exit losses across the rod bundle and end fittings are presented in tabular form, and the reference states that the data show only "fair agreement" with generally accepted contraction-expansion loss coefficients.

Organic Fluids

Reference 20 presents data on the heat-transfer properties of organic coolants containing high-boiling (HB) residues. The coolants studied were Santowax R (a mixture of terphenyl isomers), a mixture of Santowax R and HB residues produced by the pyrolytic decomposition of Santowax R, mixtures of Santowax R and HB residue from the Organic Moderated Reactor Experiment (OMRE), and OMRE coolant. Data were taken in the range of Reynolds numbers from 10^4 to 10^5 and were found to correlate within ±8.5% by an equation given in the reference. In addition, several experiments were carried out under subcooled boiling conditions. The coolants used for the experiment were the OMRE coolant and a 55% pyrolytic HB-residue mixture. The authors conclude that subcooled boiling of organic coolants containing HB residues is a complex phenomenon since the multicomponent fluids have a very wide range of boiling points; it is concluded[20] that "the advantages to be gained by operating a reactor in this region may be marginal." This conclusion is based on the fact that as boiling commences the heat-transfer coefficient often decreases and does not return to its nonboiling value until the wall temperature is about 70°C higher than that needed to initiate boiling. Although this conclusion may be peculiar to the experimental conditions and apparatus used in Ref. 20, it is an important one and probably justifies additional study. The investigation wherein the decrease in heat-transfer coefficient with the onset of boiling was observed utilized the 50% pyrolytic HB-residue mixture; when the OMRE coolant was used as the working fluid, small increases in the heat-transfer coefficient were noted at the onset of boiling. In any case the operation of an organic system in the nucleate-boiling regime appears questionable.

References 21 and 22 deal with the determination of heat-transfer and void correlations during the forced-circulation boiling of organic coolants. Reference 21 is primarily a discussion of the test loop used to determine the data, although it contains a correlation of the forced-convection heat transfer of Santowax R and an isopropyldiphenyl mixture. The same coolants were used in the experiments reported in Ref. 22 to determine boiling-heat-transfer behavior, and Santowax R was used as a coolant in the void-fraction measurements. Coolant velocities from 5 to 14 ft/sec were utilized at system pressures from 15 to 35 psia. The boiling-heat-transfer data were compared with correlations of Levy, Rohsenow, and Forster-Greif. Graphical comparisons are given in Ref. 22, and, in general, the equation of Levy represented the data best. The void-fraction data for Santowax R were classified into three regions: region I covering subcooled boiling for coolant subcoolings greater than 8°F, region II covering the transition from subcooled equilibrium bulk boiling, and region III covering equilibrium bulk boiling at qualities greater than 0.00 correlation is developed in Ref. 22 for the su cooled and transitional boiling, and the bu boiling void fraction was correlated with Lockhart-Martinelli curve. The reference c cludes with a discussion of the physical pr erties of isopropyldiphenyl and Santowax R.

References

1. D. E. Amos and F. R. Zaloudek, Temper Distribution in Long Cylindrical Fuel Elem Cooled Internally by Several Channels, USA Report HW-77681, Hanford Atomic Products eration, May 1963.
2. J. C. Rowley and J. B. Payne, Steady-State Te perature Solution for a Heat-Generating Circu lar Cylinder Cooled by a Ring of Holes, *J. Transfer*, 86(4): 531-536 (November 1964).
3. D. F. Schoeberle, J. Heestand, and L. B. Mil A Method of Calculating Transient Temperatu in a Multiregion, Axisymmetric, Cylindrical C figuration. The Argus Program, 1089/RE Written in Fortran II, USAEC Report ANL-6 Argonne National Laboratory, November 196
4. R. J. Wagner, Heat 1 — A One Dimensional T Dependent or Steady State Heat Conduction C for the IBM-650, USAEC Report IDO-16867, Ph lips Petroleum Company, April 1963.
5. R. C. Daniel and I. Cohen, In-Pile Effective Th mal Conductivity of Oxide Fuel Elements to H Fission Depletions, USAEC Report WAPD- Westinghouse Electric Corp., Bettis Ato Power Laboratory, April 1964.
6. T. G. Godfrey, W. Fulkerson, T. G. Kollie, J. Moore, and D. L. McElroy, Thermal Conducti of Uranium Dioxide and Armco Iron by an Im proved Radial Heat Flow Technique, USAEC Re port ORNL-3556, Oak Ridge National Laborato June 1964.
7. D. R. Doman, High-Temperature Thermodyna Properties of Helium, USAEC Report HW-7 Hanford Atomic Products Operation, Decem 1963.
8. A. R. Pickering, Turbulent Heat Transfer Fluids with Variable Physical Properties— Review, British Report AEEW-R-290, Febru 1964.
9. N. Sheriff, P. Grumley, and J. France, He Transfer Characteristics of Roughened Surfac British Report TRG-Report-447, Mar. 7, 196
10. A. C. Rapier, Forced Convection Heat Trans in Passages with Varying Roughness and H Flux Around the Perimeter, British Report TRG Report-519, Mar. 6, 1963.
11. W. A. Sutherland, Heat Transfer to Superhea Steam, USAEC Report GEAP-4528, General El tric Company, Atomic Power Equipment Depar ment, May 1963.
12. Oak Ridge National Laboratory, July 7, 1964. (published)
13. M. M. Hendrickson and J. K. Green (Eds.), R search and Development Programs Executed the Division of Reactor Development, Quarte

Progress Report, July, August, September 1963, USAEC Report HW-79280, Hanford Atomic Products Operation, October 1963.

A. R. Pickering, Forced Convection Heat Transfer to Water in an Annulus, British Report AEEW-R-295, February 1964.

W. A. Sutherland and W. M. Kays, Heat Transfer in an Annulus with Variable Circumferential Heat Flux, USAEC Report GEAP-4571, General Electric Company, Atomic Power Equipment Department, May 1964.

Darrel G. Harden, Transient Behavior of a Natural-Circulation Loop Operating Near the Thermodynamic Critical Point, USAEC Report ANL-6710, Oklahoma State University, Argonne National Laboratory, and Associated Midwest Universities, May 1963.

7. R. J. Weatherhead, Nucleate Boiling Characteristics and the Critical Heat Flux Occurrence in Subcooled Axial-Flow Water Systems, USAEC Report ANL-6675, Argonne National Laboratory, March 1963.

18. E. D. Waters, Fluid Mixing Experiments with a Wire-Wrapped 7-Rod Bundle Fuel Assembly, USAEC Report HW-70178(Rev.), Hanford Atomic Products Operation, November 1963.

19. E. D. Waters, Effect of Wire Wraps on Pressure Drop for Axial Turbulent Flow Through Rod Bundles, USAEC Report HW-65173(Rev.), Hanford Atomic Products Operation, June 1963.

20. A. G. Debbage, M. Driver, and P. R. Waller, Heat Transfer Properties of Organic Coolants Containing High-Boiling Residues, British Report AEEW-R-261, January 1963.

21. F. Bergonzoli (Ed.), Flow-Stability Test Loop, USAEC Report NAA-SR-8610, Atomics International, Mar. 1, 1964.

22. F. Bergonzoli and F. J. Halfen, Heat Transfer and Void Formation During Forced Circulation Boiling of Organic Coolants, USAEC Report NAA-SR-8906, Atomics International, June 15, 1964.

Section

III

Fuel Elements

Cermet Fuels for Fast Reactors

Development at the Oak Ridge National Laboratory (ORNL) of fuel-fabrication processes[1] for core B of the Enrico Fermi reactor has been concentrated[2] on 0.112-in.-thick flat cermet plates containing 35 wt.% UO_2 dispersed in, and clad with, type 347 stainless steel. Spheroidal oxide fuel particles with diameters of 105 to 149 μ (−100 +140 mesh) were used.[2] In the development program different tendencies for fragmentation and stringering were observed for different batches of the spheroidal UO_2 during roll-bonding operations. An attempt[3] was made to establish a specification that would permit the consistent purchase of spheroidal UO_2 with a high degree of reliability to minimize fragmentation and stringering during roll bonding. A number of control tests were devised in an attempt to characterize different batches of powder. The method of evaluation was to compare metallographically the stringering and fragmentation in rolled plates made with material from each batch of UO_2 with that of rolled plates fabricated with fused and ground material. Oxide batches with performances equal to or poorer than the standard were rated as unacceptable, and those with performances superior to the reference were classified in their relative order of quality. Results of the characterization tests reported in Ref. 3 are summarized as follows:

1. Microhardness. Good particles with low porosity and high bulk density cracked severely. No correlation with performance during roll bonding could be established.

2. Attrition. Correlations could not be established.

3. Crushing strength. Results of simple test procedures were capable of differentiating good from poor batches. Differentiation of a large amount of material in the intermediate category could not be made. However, it was felt that more exotic test procedures, requiring larger expenditures of time and effort, might be developed to permit better differentiation of the intermediate batches.

4. Grain size. No correlations could be established.

5. Surface area. The Brunauer-Emmett-Teller (BET) method, using N_2 and krypton, was employed. No correlations could be found. It is interesting to note that differences as great as 40% were observed between BET measurements made at ORNL and fuel vendors, although repetitive measurements at ORNL exhibited reasonably high degrees of reproducibility.

6. Bulk density. Mercury-pycnometer measurements were capable of differentiating between the highest and lowest grades of UO_2 but were not capable of separating acceptable material from intermediate grades of UO_2.

7. Solid embedment. Density determinations on particles embedded in epoxy resin, when combined with empirical density corrections based on metallographic observations, provided the best correlations.

On the basis of the above evaluations, it was concluded that the mercury-pycnometer method would provide gross classification of obviously acceptable and unacceptable batches. A minimum density of 10.1 g/cm^3 was set as a lower limit for grade-A material, and material with a density below 9.8 g/cm^3 was classified as unacceptable. Material having intermediate densities was classified as grades B or C. The solid-embedment technique could then be used to classify batches between these limits.

Uranium dioxide powder that was classified in various grades below the optimum, as a result of the preceding test procedures, was heated in hydrogen for 1 hr at 1750°C. Interorosity decreased, and the quality of all power batches was increased as a result of this reatment.

A rolling temperature of 1200°C was preiously established for the Fermi prototype fuel lements on the bases that the shape of the UO_2 articles was retained and that the condition of e plate surfaces was acceptable. A reevaluaion of rolling temperatures from 900 to 1250°C as made[3] using the standard Fermi prototype olling schedule, the best-rated UO_2 powder atches, and a loading of 33 wt.% UO_2.

Results are summarized as follows:

1. Surface finish. Rolling above 1050°C prouced a mat finish, whereas lower rolling temeratures provided a satin-smooth finish that as free of pits.

2. Fragmentation and sintering. In all cases his was not excessive but increased with dereasing rolling temperature.

3. Density of cermet fuel. In all cases this vas insensitive to the rolling temperature vithin the range evaluated.

4. Core-cladding bond. Bonding occurred at ll temperatures. Grain coarsening became exessive at temperatures greater than 1150°C.

On the basis of the preceding results, it was oncluded that the optimum rolling temperature vas 1150°C. Other investigations[3] indicated that old rolling severely fragmented the cermets nade with either optimum- or poor-quality xide and that fragmentation of the oxide was nhanced if too small an initial reduction was ised in plate rolling. It was demonstrated[4] that he performance of fuel elements containing JO_2–stainless-steel cermets clad with stainess steel is, under thermal-cycling conditions omewhat comparable to those anticipated durng large changes in reactor power levels, a unction of the fabrication method employed. nvestigations centered on stainless-steel-clad ermet fuel plates containing 40 to 50 vol.% JO_2. These studies included evaluation of hot ompacted, as well as cold compacted and sinered, cermet cores and clad plates that were ot rolled at 1100°C to reductions in area from 30 to 90%. The cermet cores in these rolled lates were fabricated either from randomnixed or homogenized-mixed* cermet cores.

The thermal-cycling tests performed[4] on these materials employed a hot-leg temperature of 800°C with the cold leg either at 250°C or at room temperature. Holding times and transfer times were varied in the different tests; however, the most significant results were obtained from tests of up to 1000 cycles at a heating rate of 60 to 70°C/sec and a cooling rate of 250°C/sec.

Examination of the as-rolled plates indicated excessive stringering in the random-mixed cores and a relatively uniform dispersion of the UO_2 in the homogenized-mixed cores. Stringering in the random-mixed cores increased with increasing reductions. In the homogenized-mixed cores, there was no evidence of large agglomerates, stringering, or cracking of the UO_2. Performance of the homogenized-mixed samples during cycling was superior to that for the random-mixed cores. Sigma-phase formation was observed in the type 316L stainless-steel core. The amount of sigma increased with increasing number of cycles and was probably associated with the amount of time at 800°C in each cycle. On the basis of the observed distribution of carbides and sigma phase after cycling, it was concluded that these would not be deleterious to performance.

Although additional details are not given in Ref. 4, it is stated that new fabrication methods had been developed to produce plates of improved quality which would provide better thermal-cycling stability.

It was concluded[4] that stainless-steel-clad cermets containing 40 to 50 vol.% UO_2–stainless steel, prepared by the homogenized-mixed-core process, could withstand 1000 thermal cycles up to 800°C at heating and cooling rates up to 70 and 250°C/sec. The following conditions must be met[4] to provide good resistance to thermal cycling:

1. Elimination of continuous interparticle networks in the core
2. Use of spheroidal UO_2 that is well dispersed in the core
3. Use of spheroids with minimum internal stress and high resistance to fragmentation
4. Good initial bonding between cermet core and picture-frame cladding

The use of Dynapak and a combination of Dynapak plus swaging is under development[5] at Los Alamos for the fabrication of refractory-metal-clad 45 vol.% UO_2–tungsten cermet fuels. The program is aimed at determining the feasibility of coextruding refractory-metal-clad cermet fuel elements. Work has been concentrated on a cermet made from 2-μ tungsten powder and 20-μ UO_2 powder which was hydrostatically pressed into 1¼-in.-diameter cylinders at either 50,000 or 70,000 psi. These compacts were induction sintered at 2200°C for 2 hr. Slow heating (4 hr) and cooling (2½ hr) cycles were required to minimize thermal-stress cracking. After the pellets were sintered, they were machined to dimensions of 1 in. in diameter by 1 in. long; their density was 85% of theoretical. Coextrusion billets were prepared by loading the machined pellets with a light press fit into cans of either molybdenum, 70 wt.% molybdenum–tungsten, or 25 wt.% molybdenum–tungsten and then electron-beam welding the lids. These billets were extruded in air, with glass wool as a lubricant, after they were preheated in H_2 to about 2000°C. Typical conditions included a fire pressure of 750 to 900 psi, velocity at contact from 460 to 540 in./sec, and extrusion ratios of 4 to 9. Typical yields ranged from 75 to 100% for finished lengths and diameters from 4¾ to 7¼ in. and 0.47 to 0.75 in. Although the cermet bond was uneven as a result of the penetration of UO_2 particles into the cladding, core-to-cladding bonding was generally good for all rods, and the bond quality increased with increasing extrusion ratio.

---

*Random-mixed cores are formed from mixtures of UO_2 and stainless-steel particles. Homogenized-mixed cores are formed from mixtures of stainless-steel powder and UO_2 spheres which have been precoated with stainless-steel powder.

One rod clad with 25% molybdenum–tungsten and coextruded to a reduction in area of 89% was further reduced 75% in area by swaging at 1800°C (first third of reduction) and then at 1500°C. The surface appearance and bond quality were good. It was indicated that further reductions were possible.

It was suggested[5] that improvements in both fabrication and performance could be achieved with a 25 wt.% molybdenum–tungsten alloy for the cermet as well as for the cladding. Advantages claimed for this alloy are compatibility with H_2 and UO_2, availability, low relative cost, good high-temperature strength, and a melting point in excess of 3100°C. Furthermore, this alloy is less dense and is simpler to fabricate than tungsten. The success to date with Dynapak extrusions, as well as the potential advantages that can be gained through the use of the 25 wt.% molybdenum–tungsten alloy, have led to suggested programs at Los Alamos involving the extrusion of other shapes, the use of higher UO_2 loadings, and thinner cladding.

Fabrication of Various Fuel Assemblies

As part of the Fuel Cycle Program of U. S. Atomic Energy Commission (AEC), Atomic Power Equipment Department (APED of the General Electric Company initiated program aimed at extending the performa capabilities of UO_2 fuel elements in boili water reactors. Under this program 12 spec assemblies have been fabricated and inserte the Vallecitos Boiling Water Reactor (VBW for irradiation testing. Detailed descriptions the fabrication of 3 of these special assembl are given in Refs. 6, 7, and 10. The APED w under the Fuel Cycle Program has been reviewed previously in *Power Reactor Technol* 7(1): 27-50, and 7(4): 354-355. The repor reviewed here present fabrication details available when the earlier reviews were prepared; some repetition has been allowed f convenience of reading.

The AEC Fuel Cycle Special Assembly containing 16 fuel rods in a 4 by 4 array, aimed[6] at demonstrating the performance of ve thin (0.005 in.) type 304 stainless-steel claddi The selection of the 0.005-in.-thick cladding the program was based upon the realization th this represented the thinnest available stainless-steel tubing capable of performing a claddi function. Of the 16 fuel rods in the 8L assemb 12 contained UO_2 with thin cladding. The corn rods had heavier cladding (0.015 in.) to redu the probability of damage to the fuel assemb during handling. The 12 test rods, about 46 long, contained 4.58% enriched-UO_2 pelle which were 0.370 in. in diameter and wh were clad with ¼-hard stainless-steel tubi A 7-in.-long fission-gas plenum was design to accommodate 100% gas release at twice t target burnup. In an effort to minimize wrinkling of the cladding, the cladding was swa over the pellets, providing a nominal rod diameter of 0.380 in. Target heat flux and burn were 500,000 Btu/(hr)(sq ft) and 10,000 Mw ton, respectively. At this heat flux a differen diametral expansion between the fuel and t cladding of 0.0035 in. was calculated, wh would result in plastic straining of the claddi Cladding-stress calculations, materials spe fications, element design, cladding fabricat and evaluation, fuel-pellet fabrication, fuel-r fabrication, and results of preirradiation tes are discussed and described in detail in Ref. 6. rradiation testing of this special element was begun in November 1961 and was terminated in December 1963 as a result of the final shutdown of the VBWR.

The AEC Fuel Cycle Special Assembly 9L contained UO_2-molybdenum cermet fuel.[7] Molybdenum additions were made in an attempt to ncrease the thermal conductivity of UO_2. Vacuum hot-pressing techniques were used to produce the two types of cermet pellets utilized n this assembly: (1) pellets containing 20 vol.% molybdenum fibers had densities of 94 to 95% of theoretical and (2) pellets fabricated from molybdenum-coated UO_2, containing approximately 16 vol.% molybdenum, had densities of 94 to 96% of theoretical. Radial orientation of the molybdenum fibers in the pellets was achieved by means of unidirectional compaction. Hot pressing of the molybdenum-coated UO_2 particles provided a continuous molybdenum network. The forms of UO_2-molybdenum cermets selected for the program were based on the intent to cover the largest possible range of difference in the mode of metal-phase distribution. Three fuel rods fabricated with each of the two types of uranium-molybdenum cermets were combined with two rods of conventional UO_2 pellet design to form the eight-rod Special Assembly 9L. All fuel cladding was type 304 stainless steel with an outside diameter of 0.515 in., a wall thickness of 0.020 in., and a pellet-to-cladding diametral clearance of 0.003 to 0.004 in. The objective of this test was to compare the performances of the cermet fuels and UO_2 after operation at a surface heat flux of 500,000 Btu/(hr)(sq ft) and a burnup approaching 15,000 Mwd/ton. Irradiation testing was begun in the VBWR in September 1962 and was terminated at the final shutdown of the VBWR in December 1963. The impetus for this series of irradiation tests was based on out-of-pile thermal-conductivity data[8,9] obtained for UO_2-Mo and UO_2-ThO_2-Nb (10 to 30 vol.% metal) which indicated potential improvements of 300%. Calculations of axial and radial temperature profiles anticipated for the cermet rods and the bulk UO_2 rods indicated substantial differences. Relative performance could then be judged by an analysis of microstructure data. Details of these calculations, as well as fuel-element-design characteristics, materials specifications, fabrication procedures, and results of preirradiation evaluations, are given in Ref. 7.

The AEC Fuel Cycle Special Assembly 11L contained[10] sintered UO_2 extrusions prepared independently under two different projects. One project was sponsored by the United States–Euratom Joint Research and Development Program at Compagnie Industrielle des Combustibles Atomiques Frittés (CICAF). The other project was a joint effort of the Allis-Chalmers Mfg. Co. and The Electric Autolite Co. (AC-EA) as part of the AEC Fuel Cycle Program. Fuel densities achieved were 97.6 and 96.2% of the theoretical density for the CICAF and AC-EA sintered extrusions. A 16-rod (4 by 4) assembly was fabricated for testing in the VBWR at a surface heat flux of 400,000 Btu/(hr)(sq ft). It contained 12 rods fabricated with sintered extrusions (6 from each program) and 4 pellet rods for comparison. The cladding was ⅛-hard type 304 weld-drawn stainless steel with an outside diameter of 0.540 in. and a wall thickness of 0.022 in. Extrusion processes, descriptions of extrusions, fabrication and assembly procedures for fuel rods, irradiation design criteria, materials specifications, and results of preirradiation examinations are reported in considerable detail in Ref. 10. Results of some of the VBWR irradiations are summarized in two 1964 Geneva Conference papers (Refs. 11 and 12).

Hanford has published detailed specifications for swage compaction[13] and vibratory compaction (VIPAC)[14] of mixed oxide (UO_2-PuO_2) fuel in Zircaloy cladding for the Mark I-M, 19-rod clusters being irradiated in the Plutonium Recycle Test Reactor (PRTR). Fuel for the swaging process and the VIPAC process is a mixture of UO_2 and PuO_2 formed by a high-energy-rate pneumatic-impaction (NUPAC) method that yields fuel particles with a density greater than 97% of the theoretical density.

Ten full-sized sodium-bonded uranium carbide fuel assemblies of hypostoichiometric composition were fabricated[15] by Atomics International for testing in the Hallam Nuclear Power Facility. The objectives of the program, in addition to the irradiation testing of sodium-bonded fuel elements in the Hallam reactor, included the development of fabrication methods for carbide, the evaluation of storage conditions for cast carbide, and the development of sodium-bonding techniques and nondestructive test methods.

Each clad fuel rod[15] was about 182 in. long and 0.952 in. in diameter and contained a uranium carbide fuel column 0.872 in. in diameter and 156 in. long. The radial sodium annulus between the fuel and the type 304 stainless-steel cladding was 0.030 in.; helium gas at 1 atm occupied the region above the sodium level. Each fuel assembly contained eight fuel rods. Uranium carbide enrichment in eight assemblies was 3.7%, and in the remaining assemblies, 4.9%. One of the eight assemblies with the 3.7% enrichment contained thermocouples located within the fuel and on the cladding surface.

The fabrication and inspection methods used for these sodium-bonded fuel elements are described in detail in Ref. 15. A number of significant observations are summarized below:

1. Uranium dioxide feed was converted to UC melt stock by the carbothermic reaction.
2. Better control of carbon content was attained for melt stock containing less than 500 ppm oxygen. The melt stock of lower oxygen content gave less splatter of the melt on the graphite electrode and thus less erratic carbon pickup.
3. Compensation of carbon pickup from the electrode was made by means of uranium-metal additions.
4. Metallographic determinations of carbon content near stoichiometric (4.6 to 4.8 wt.% carbon), based on comparison with controls, were more accurate than the analytical methods employed.
5. Dry storage was demonstrated to be effective, provided that prescribed fuel-preparation and fuel-storage conditions are followed.
6. Dry cutting methods were developed.
7. Proper fuel cleanliness was a necessary prerequisite for good sodium bonding.

Zircaloy-2-clad tubular fuel elements containing thorium–2.5 wt.% uranium (93.2% enriched)–1 wt.% zirconium fuel alloy were fabricated[16] for irradiation testing in the P-7 high-temperature high-pressure water loop of the Engineering Test Reactor (ETR). Fabrication development, including arc-melting techniques, coextrusion procedures, metallurgical evaluation, and fuel-element-assembly procedures, is described. It was shown that the zirconium addition to the base fuel composition improved the surface quality of arc-cast ingot, improved uranium homogeneity, lowered the fuel-alloy hardness, and was beneficial in consumable-electrode fabrication. Fully bonded tubular fuel, 1.750 in. in outside diameter by 1.050 in. in inside diameter with 0.025- thick Zircaloy cladding on both the outside inside diameters, was produced by coextru at 760°C at a reduction ratio of 17 to 1. elements 8 in. in length were closed by bra Zircaloy-2 end caps with 5 wt.% berylli Zircaloy-2 alloy, followed by electron-b welding of the braze line. Three fuel eleme were charged in the P-7 loop in April 196 were operating at a maximum specific p of 230 kw/ft, a peak heat flux of 1.12 Btu/(hr)(sq ft), and a maximum calculated temperature of 620°C. Interim measureme fuel density will be made throughout the radiation in which the target has a burnu 3 at.%, or approximately 26,000 Mwd/ton.

Information on the potential for plutoni enriched fuel in pressurized-water react will be obtained[17] as a result of the Sax Plutonium Project. Nine fuel assemblies co taining PuO_2-UO_2 are to be irradiated at center of the Saxton core, and 12 stainles steel-clad assemblies containing UO_2 are to irradiated at the core periphery. Two of plutonium fuel assemblies will contain Pu UO_2 fuel that has been vibratorily compac into Zircaloy-4 tubes; the remaining pluton fuel assemblies will contain PuO_2-UO_2 pelle in a Zircaloy-4 cladding. Zircaloy was selecte over stainless steel as the cladding mater for the plutonium-containing elements becau it provides higher initial reactivity and longe lifetime for a given plutonium enrichment. Eq heat ratings are contemplated for both typ of plutonium-containing fuel elements. Descrip-tions of the fuel and fuel rods are summarize in Tables III-1 and III-2. Nuclear Materials Equipment Corp. will supply the pelletiz plutonium-containing fuel elements, and th VIPAC fuel elements will be fabricated[17] b Hanford from feed material prepared by th Dynapak process.

Table III-1 FUEL-ROD DETAILS FOR THE SAXTON PLUTONIUM PROJECT[17]

	Plutonium	Urani
Cladding material	Zircaloy	304 S.S
Cladding thickness, in.	0.023	0.015
Cladding outside diameter, in.	0.391	0.391
Diametral gap, in.	0.005 for pelletized 0.0 for VIPAC	0.00

Table III-2 FUEL DETAILS FOR THE SAXTON PLUTONIUM PROJECT[17]

Material	6 wt.% PuO_2–94 wt.% UO_2	6 wt.% PuO_2–94 wt.% UO_2	UO_2
Type	Pelletized	VIPAC	Pelletized
Diameter, in.	0.340	0.345	0.357
Density, % of theoretical	94	88	93
Enrichment	6 wt.% Pu	6 wt.% Pu	5.7 wt.% ^{235}U

Isotopic content of Pu, %	
^{239}Pu	90.46
^{240}Pu	8.60
^{241}Pu	0.90
^{242}Pu	0.04

Insertion of the plutonium-containing fuel ssemblies in the Saxton reactor is scheduled or July, and plans are that these fuel assem-lies will be irradiated for two years. Post-rradiation examination and analysis are scheduled for the period January 1968 to February 1969. A maximum fuel-rod heat rating of 16 kw/ft has been established[18] for the Zircaloy-4-clad PuO_2-UO_2 fuel rods. The following comments on hydrogen pickup and oxide thickness on the cladding are quoted from Ref. 17:

> The hydrogen pickup by the Zircaloy clad and the thickness of the ZrO_2 coating formed in-pile were calculated for linear rod powers of 16 kw/ft and assuming 40% down time for the reactor. The results showed that the hydrogen level at the end of life, 130 ppm, will be considerably below the level at which hydride problems occur. The ZrO_2 coating thickness and the temperature drop across the coating were found to be negligible.

Also from Ref. 17 a survey of performance of VIPAC fuel in other test programs is summarized as follows:

> 1. Based on technology already developed at the national laboratories, no defects in vibrationally compacted fuel rods are anticipated.
>
> 2. The results of the national laboratory experiments show that no significant fuel washout and no waterlogging results from defects in rods containing loose powder fuel.
>
> 3. The economic incentives for developing vibratory compacted PuO_2-UO_2 fuels and the present state-of-the-art provide strong motivation for carrying out engineering demonstration tests in the Saxton reactor.

References

1. J. E. Cunningham et al., Specifications and Fabrication Procedures for APPR-1 Core II Stationary Fuel Elements, USAEC Report ORNL-2649, Oak Ridge National Laboratory, Feb. 11, 1959.
2. J. H. Cherubini et al., Fabrication Development of UO_2–Stainless Steel Composite Fuel Plates for Core B of the Enrico Fermi Fast Breeder Reactor, USAEC Report ORNL-3077, Oak Ridge National Laboratory, Apr. 18, 1961.
3. A. J. Taylor et al., Characterization of Spheroidal UO_2 Particles and Studies of Fabrication Variables for Core B Fuel Plates of the Enrico Fermi Fast Breeder Reactor, USAEC Report ORNL-3645, Oak Ridge National Laboratory, August 1964.
4. J. M. Davies and C. Steer, Thermal Cycling of UO_2–Stainless Steel Cermets, British Report AERE-M-1253, January 1964.
5. J. M. Dickinson and T. J. Ready, Feasibility Study of the Co-Extrusion of Refractory Metal Clad Reactor Fuel Elements, USAEC Report LAMS-3065, Los Alamos Scientific Laboratory, Apr. 12, 1964.
6. J. P. Hoffman, Design and Fabrication of Pellet Fuel Rods Clad with Thin-Wall Stainless Steel, USAEC Report GEAP-4407, General Electric Company, Atomic Power Equipment Department, February 1964.
7. S. Y. Ogawa, AEC Fuel Cycle Program—Design and Fabrication of Special Assembly 9-L, Irradiation Performance Test of UO_2-Cermet Fuel, USAEC Report GEAP-4435, General Electric Company, Atomic Power Equipment Department, March 1964.
8. S. J. Paprocki et al., Preparation and Properties of UO_2 Cermet Fuels, USAEC Report BMI-1487, Battelle Memorial Institute, Dec. 19, 1960.
9. Y. Baskin et al., Some Physical Properties of Thoria Reinforced by Metal Fibers, *J. Am. Ceram. Soc.*, 43: 489-492 (September 1960).
10. F. H. Megerth, Design and Fabrication of Fuel Rods Containing Sintered UO_2 Extrusions, Assembly 11L, USAEC Report GEAP-4556, General Electric Company, Atomic Power Equipment Department, February 1964.
11. S. Naymark and C. N. Spalaris, Oxide Fuel Fabrication and Performance, presented at the Third United Nations International Conference on the Peaceful Uses of Atomic Energy, Geneva, 1964, Paper A/Conf.28/P/160.
12. W. P. Chernock, R. M. Mayfield, and J. R. Weir, Jr., Cladding Materials for Nuclear Fuels, presented at the Third United Nations International Conference on the Peaceful Uses of Atomic Energy, Geneva, 1964, Paper A/Conf.28/P/255.
13. Hanford Atomic Products Operation, Specifications for Swage-Compacted, Mixed Oxide (UO_2-PuO_2), Fuel Elements for the PRTR (Mark I-M), USAEC Report HW-79290, Oct. 1, 1963.
14. Hanford Atomic Products Operation, Specifications for Vibrationally Compacted, Mixed Oxide

(UO_2-PuO_2), Fuel Elements for the PRTR (Mark I-L), USAEC Report HW-79291, Oct, 1, 1963.

15. W. Draganchuk, UC Fuel Element Design and Fabrication, USAEC Report NAA-SR-9988, Atomics International, Aug. 1, 1964.

16. R. S. Kemper et al., Fabrication of Zircaloy-2 Clad Thorium–Uranium Alloy Fuel Elements, USAEC Report HW-79843, Hanford Atomic Pr ucts Operation, March 1964.

17. N. R. Nelson, Saxton Plutonium Program, Q terly Progress Report for the Period E September 30, 1964, USAEC Report WC 3385-1, Westinghouse Atomic Power Divis October 1964.

Section IV

Components

Power Reactor Technology

:BR-II Control-Drive Aechanisms

'he Experimental Breeder Reactor II (EBR-II)
s controlled by 12 hexagonal-shaped control
ubassemblies, moved vertically by 12 rack-
nd-pinion type electromechanical drive mech-
nisms. These are capable of scramming the
ontrol assemblies with an acceleration of 1.5
, with a pneumatic cylinder providing the as-
ist to attain this acceleration. The design
troke for the mechanism is 14 in. The control
ssembly was described in the EBR-II hazards
ummary report (Ref. 1) that was issued in
Iay 1957. Some of the novel features of the
echanism (shown in Fig. IV-1) are as fol-
ows:

1. The mechanism has internal and external
ellows seals that are fabricated from 0.010-
.-thick stainless-steel sheet to maintain ves-
el integrity.

2. A sensing-device shaft is used to indicate
'hether the control assembly is engaged to the
echanism. This sensing shaft is housed within
e 26-ft-long main shaft.

3. A pneumatic cylinder at the top of the
ain shaft is used to accelerate the control
ssembly during a scram. Normal pressure in
e cylinder is 30 psig.

4. An oil-filled dashpot decelerates the con-
rol assembly during the final 4⅛ in. of scram.

5. All the control-assembly drive mecha-
isms are mounted on a single platform. This
latform can be raised 3 in. to check the con-
rol-assembly grippers to ensure that they are
isengaged and are clear of the adapters of
ther subassemblies in the core. The platform
s lowered ⅞ in. from its normal operating
osition to engage the control assemblies.

6. A labyrinth seal is used to limit the flow
ast the shaft bearing in the vessel cover.

Extensive testing was performed on 2 prototype drive mechanisms and on 1 of the 14

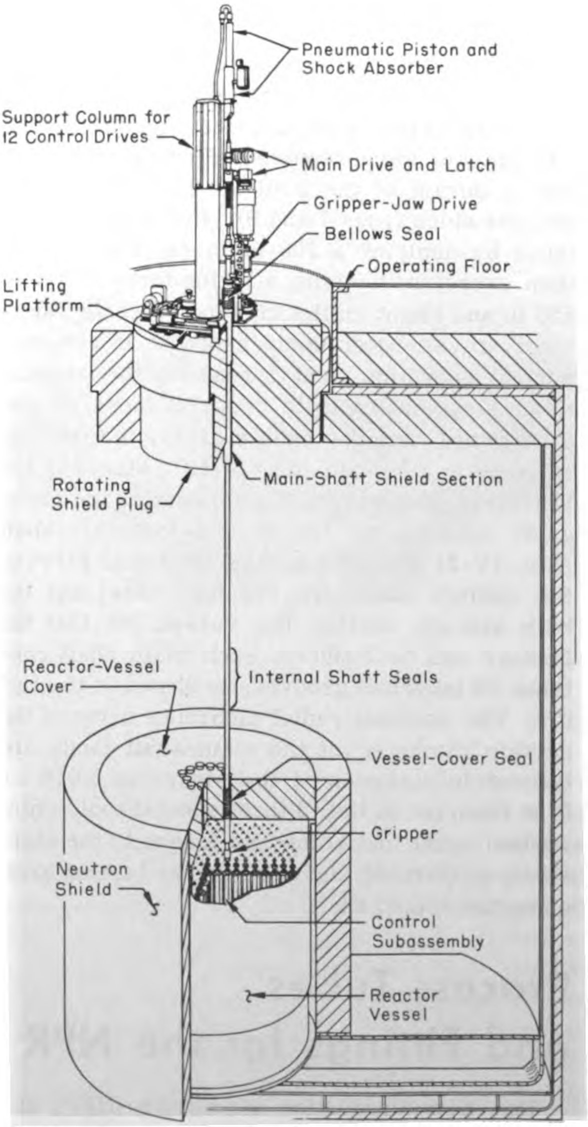

Fig. IV-1 Simplified drawing of components of the EBR-II control-rod drive.[2]

production mechanisms that were fabricated.[2] Table IV-1 summarizes the testing details.

Table IV-1 CONTROL-MECHANISM TESTING[2]

Rod	Environment	Temperature, °F	No. of full-stroke cycles	No. of gripper operations	No. of scrams
P-1	Air	Room	300		
	Sodium	300 to 900	13,200		24
P-2	Air	Room	31,440		
	Sodium	300 to 900	1,680	15	35
F-1	Air	Room	900	20	120
	Air	800	700	6	5
	Sodium	750	1,100	18	80

All these tests were performed with no significant problems. Furthermore, all the production rods were tested in place, and only minor adjustments were required. However, during a recent scram of the EBR-II, 2 of the 12 rods became stuck (rods 7 and 9).[3] Rod 9 was broken loose by applying a 200-lb force. The rod was then exercised by using a lifting force of 350 to 550 lb and slight mallet taps to assist its downward travel. After some exercise it resumed normal operation. Rod 7 required the fabrication of special tools to break it loose. It was determined that the main shaft for the rod was sticking in a 29$\frac{1}{8}$-in.-long Stellite sleeve in the reactor-vessel cover. This sleeve is the lower guide bearing for the control-assembly shaft (Fig. IV-2) and also serves as a seal between the sodium inside the reactor vessel and the bulk storage outside the vessel. So that the leakage can be reduced, each main shaft contains 23 labyrinth grooves, as shown in the figure. The nominal radial clearance between the outside diameter of the main-shaft lands and the inside diameter of the sleeve is 0.015 in. It is reported in Ref. 3 that a special tool, which applied axial and rotational forces to the stuck shaft, performed successfully the task of loosening the seized shaft.

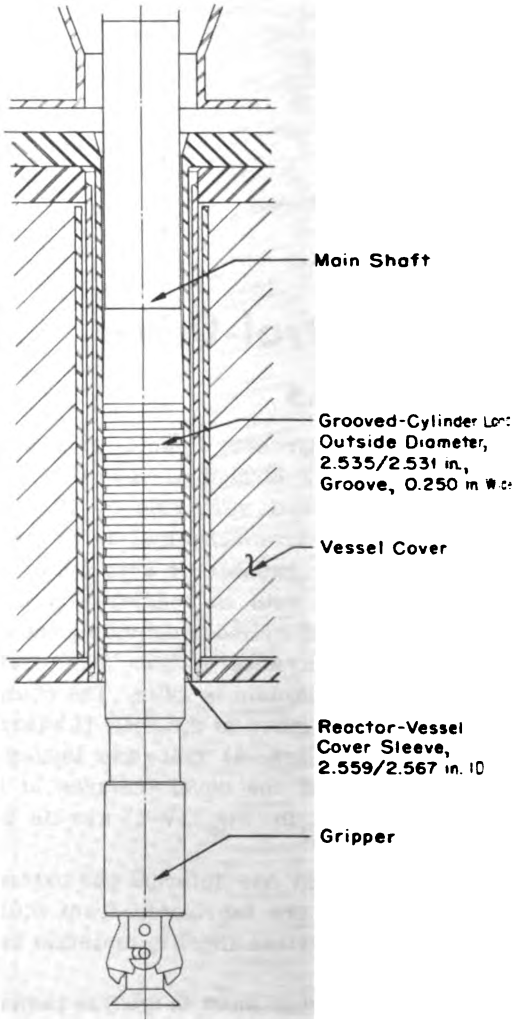

Fig IV-2 Main-shaft seal through the EBR-II reactor-vessel cover.[2]

Process Tubes and Fittings for the NPR

The New Production Reactor (NPR; also called the N Reactor) is a graphite-moderated pressure-tube reactor designed to operate at a coolant pressure of 1600 psi and a temperature of 300°C. The reactor requires 1064 Zircaloy-2 pressure tubes that are 57 ft long, 3.25 in. in diameter, and 0.25 in. in wall thickness, as well as a considerable number of fittings, connectors, and transition joints. Reference 4 is a descriptive summary of a development pilot order and a competitive-bid program for procurement of the pressure tubes. The procedures used for this program were required because of the lack of manufacturing technology and industrial experience with this relatively high-cost material and because of the stringent quality and dimensional requirements specified.

The initial phase of the program consisted of developmental contracts to three vendors on a best-efforts basis. The second, or pilot-order, phase was awarded to the three vendors on a negotiated basis. The final phase was accomplished on the basis of a competitive-bid oduct-guaranteed, fixed-price contract. This ocurement effort developed an industrial cap-ility for producing heavy-walled Zircaloy tub-g to reactor-application specifications[4] and vered the full range of processes from ingot finished product. The effort included the de-lopment of (1) specifications that indicate e level of quality to which such tubing can be oduced and (2) commensurate inspection and ality-control requirements.

Technical problems in the selection, man-acture, installation, and testing of primary-op fittings are discussed in Ref. 5. The fittings cluded the rolled-joint connections between rcaloy and carbon steel, a mechanical "make-d-break" coupling, a venturi assembly, mani-ld piping, and valve-body material. The leak-ght roller joint, shown in Fig. IV-3, was

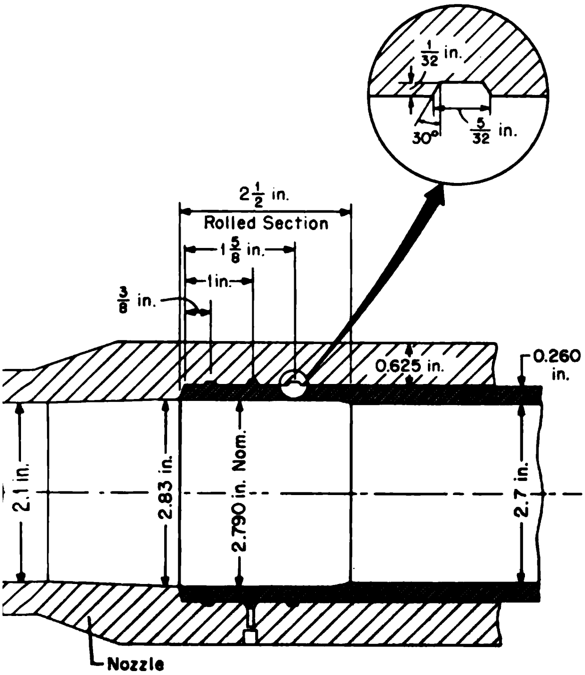

Fig. IV-3 NPR inlet rolled joint.[5]

esigned for 1800 psi at 600°F and to withstand hermal shock from sudden coolant-temperature hanges. This joint was selected over eight ther mechanical type joints on the basis of uperior strength and low-leakage qualities. n this type of connection, the Zircaloy tube is olled into the grooved carbon-steel nozzle by neans of an expander mandrel that provides or a 12% wall-thickness reduction. The rolling process forces Zircaloy into the grooves and provides a joint that is judged to be structurally sound and reliably leakproof.

The quick-connection make-and-break mechanical coupling was required to minimize the maintenance time at the faces of the reactor. Of 15 various candidate assemblies evaluated, the Grayloc type coupling was chosen for this application because of its ruggedness and resistance to leakage under different stress conditions and its clean internal-surface configuration. It features a two-stud split-clamp arrangement that causes axial loading of a tapered metal-seal member within the tapered bores of the coupling flanges. Spherical convex nuts and temporary shims are used during assembly of the coupling to minimize cocking and to maintain parallelism. Figure IV-4 shows the connector-coupling components.

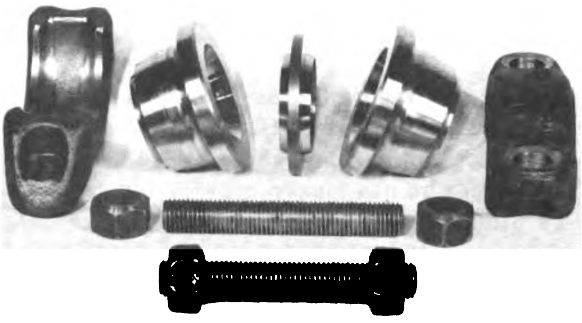

Fig IV-4 NPR connector-coupling components.[5]

The venturi throat assembly is used to monitor continuously the coolant flow in each of the connector pipes. The original design of this component specified a type 316 stainless-steel throat section to be mounted in a carbon-steel body by means of an interference fit. However, subsequent heat-treating operations caused loosening of the throat. The design was modified by substituting Inconel for stainless steel on the throat section, thus minimizing the differential thermal expansion. Extending the tap connection into the throat component corrected the loosening of the throat component.

The manifold piping on the NPR consists of over 100,000 ft of carbon-steel tubing of $2\frac{5}{8}$-in. outside diameter by 0.260-in. wall thickness. The piping connects the individual process tubes to the 18-in. inlet and outlet headers. The connectors did not meet impact-strength requirements after bending. This deficiency was attributed to limitations of the heat-treatment equipment used in the manufacture.[5] It was subsequently corrected by additional heat-treatment, and thereafter the tubing met specified impact-strength requirements. The valve bodies of both forged and cast types failed to meet the impact-strength requirements specified. In some cases an additional grain-refinement treatment at 1550°F completely refined the structure, and notch toughness was raised above minimum values. In other cases detailed analysis of the metallurgical deficiency showed the need for a much more extensive modified heat-treatment procedure, in addition to some pre-heat-treatment machining operations, to bring the product above specified impact- and tensile-strength values.

References

1. L. J. Koch, W. B. Loewenstein, H. O. Mo
D. Okrent, M. Levenson, W. R. Simmons, J.
Humphreys, J. Haugsnes, and V. C. Jankus, Ha
Summary Report, Experimental Breeder Rea
II, USAEC Report ANL-5719, Argonne Na
Laboratory, May 1957.
2. E. Hutter and G. Giorgis, Design and Perform
Characteristics of EBR-II Control Rod D
Mechanisms, USAEC Report ANL-6921, Arg
National Laboratory, August 1964.
3. Argonne Staff, Reactor Development Prog
Progress Report, October 1964, USAEC Rep
ANL-6965, Argonne National Laboratory, Nov.
1964.
4. T. C. Aungst and D. H. Curtiss, Procureme
Zircaloy-2 Process Tubes for N-Reactor, US
Report HW-80566, Hanford Atomic Products Op
ation, March 1964.
5. Staff of the N-Reactor Project, Technical Pr
lems in Fittings for N-Reactor Primary L
USAEC Report HW-79616, Hanford Atomic Pr
ucts Operation, November 1963.

Section

V

Specific Reactor Types

arge Pressurized-Water eactors

he trend toward interconnected power systems
the electric-utility industry has greatly in-
reased the opportunities for reducing unit
ower-generating costs through the use of very
rge plants. This trend has also focused at-
ention on the question of the maximum capacity
vailable from a single reactor in a nuclear
lant. References 1 and 2 present the results
f a study by the Westinghouse Atomic Power
ivision for the U. S. Atomic Energy Commis-
ion (AEC) to evaluate the technical feasibility
nd economic potential of a 1000-Mw(e) all-
uclear power plant incorporating a single
ressurized-water reactor. The work was per-
rmed during the period May 1962 to March
963. The results of the study command par-
icular attention since the work was clearly
ased on the extensive Large Closed Cycle
ater Reactor Research and Development (LRD)
rogram that Westinghouse has been conducting
ince 1960 in association with the San Onofre
uclear Generating Station of the Southern
alifornia Edison Company. It is stated that
he design philosophy adopted for the study
epresents a modest extension of the technology
o be employed in the 375-Mw(e) Southern
alifornia Edison* and the 465-Mw(e) Round
A† plants. The conclusion from the study is
hat the 1000-Mw(e) reactor is technically
easible and economically practical and that
970 is a reasonable date for the commercial
peration of the plant. A $10.5 million research
nd development program is outlined. The prin-
ipal development problems lie in the area of core physics and core development and result from the increased core size.

Except for size the plant is similar to the present generation of pressurized-water reactors under contract, such as those for the San Onofre and Malibu stations. The plant has the following capabilities:

Reactor, Mw(t)	3220
Gross electrical generation, kw	1,058,000
Net electrical generation, kw	1,002,400
Cycle heat rate, Btu/kw-hr	10,377
Full-load net station heat rate, Btu/kw-hr	10,363
Net plant efficiency, %	31.1

Of the principal reactor-plant components, only the reactor vessel represents a measurable extension of present-day fabrication techniques. Although the 615-ton vessel can be shop fabricated and erected at the hypothetical site selected for the study,‡ transportation might be a limitation for less favorable sites. The pressure-vessel-design condition was 2500 psi at 650°F, and the vessel was to be designed, manufactured, inspected, and stamped in accordance with Sec. VIII of the *ASME Boiler and Pressure Vessel Code.* Since this study was completed, Sec. III, Rules for Construction of Nuclear Vessels, was approved and issued by the American Society of Mechanical Engineers. A discussion of the principal difference between the two code sections is presented in Ref. 3. The new Sec. III permits better utilization of the reactor-vessel material, resulting in a lighter weight vessel. For example, a reduction of more than 2 in. in thickness of the 202-in.-ID cylindrical section of the 1000-Mw(e) vessel can be achieved. Reference 3 concludes that the new code permits design of nuclear vessels for water-reactor plants up to 1500 Mw(e).

---

*The Malibu Plant of the City of Los Angeles De-
artment of Water and Power.

†The Connecticut Yankee Atomic Power Company.

‡The "Middletown" site employed in the AEC evaluation studies of utility reactors since 1959.

In the design study presented in Ref. 1, seven primary coolant loops are employed. Each loop contains a vertical U-tube steam generator having 32,726 sq ft of heat-transfer surface and a canned-motor single-speed centrifugal pump with a design flow capacity of 61,000 gal/min against a 280-ft head. The pump volute contains an integral center-guided check valve positioned between the suction nozzle and the impeller. No main coolant block valves are used. In present-day plants the use of the block valves seems to be a customer choice; Connecticut Yankee uses them, but Malibu does not. The main coolant piping is 27-in.-ID rolled and welded carbon steel clad internally with stainless steel. The 3240-cu ft pressurizer vessel is connected to the hot leg of one reactor loop. The steam-generator design data are tabulated in Table V-1.

Table V-1 DESIGN DATA[1] FOR STEAM GENERATOR

Type	Vertical U tube with integral steam drum
Heat-transfer load, Btu/hr	15.729×10^6
Steam flow, lb/hr	2.014×10^6
Design pressure, tube side, psia	2500
Operating pressure, tube side, psia	2050
Tube material	Inconel
Coolant flow in each side, lb/hr	22.86×10^6
Coolant inlet temperature, °F	598
Coolant outlet temperature, °F	546
Shell-side full-load pressure at outlet, psia	700
Full-load steam temperature at outlet, °F	503
Maximum moisture at outlet (full load), %	¼
Shell-side design pressure, psia	1000
Feedwater temperature at full load, °F	442
Logarithmic mean temperature difference, °F	65.5
Heat-transfer surface area, sq ft	32,726
Dry weight, lb	503,800
Flooded weight, lb	738,800

The reactor-plant containment is provided by a reinforced-concrete vertical right-circular cylindrical structure with a flat base and hemispherical dome. The dome has an inside radius of 81 ft, and the total inside height is 211 ft. The structure is lined with a steel membrane ¼ in. thick to make the container vaportight and gastight. The containment is similar in design to the one built at Parr Shoals for the Carolinas-Virginia Nuclear Power Associates, Inc.

The turbine-generator represents a significant extension of current practice. The turbine is of 4-cylinder single-shaft design, operates at 1800 rpm, and turns a single 1,300,000-kw hydrogen-intercooled generator. The throttle pressure condition is 650-psia saturated steam as in current practice. Exhaust from the single double-flow high-pressure cylinder passes through six moisture separators and is reheated with steam at the throttle condition before being expanded in the three double-flow low-pressure cylinders. The entire high-pressure-turbine casing and the last five stages of each low-pressure-turbine casing are lined with stainless steel to minimize moisture corrosion. The low-pressure-turbine rotors are too large to ship completely assembled. The last two stages of each low-pressure turbine are bladed in the field. Similarly, because of size and weight, final assembly of the generator rotor and stator is performed in the field.

The estimated power-generation cost for the plant based on a net generation of 1,002,400 kw is 5.77 mills/kw-hr, made up as follows:

Capital	3.42
Land, working capital, and nuclear insurance	0.27
Fuel	1.83
Operation and maintenance	0.25
	5.77

The estimated total capital cost of the plant is $165,084,000, including land and land rights, interest during construction, and contingency; the resulting unit cost is $165 per kilowatt. The 1.83 mills/kw-hr fuel cost is based on an equilibrium core utilizing zirconium-clad fuel. The first-core fuel-cycle cost for the reference elastically collapsed stainless-steel-clad core is 2.13 mills/kw-hr. The first-core fuel-cycle cost for the alternative freestanding stainless-steel-clad core is 2.23 mills/kw-hr. Fuel cost estimates were based on government ownership of uranium.

The principal improvements and advances over current pressurized-water-reactor technology are in the area of the core and the associated reactor arrangement. Two designs were carried through in the study. The reference design utilized short Zircaloy followers for the control-rod blades and elastically collapsed thin-walled stainless-steel cladding on the fuel. The less-advanced alternate design employed full-length control-rod followers and freestanding stainless-steel cladding. Slightly enriched UO_2 is used as fuel in both designs. The alternate design resulted in an increase of reactor-vessel length of 8 ft. The consequent increase of reactor-coolant-system holdup was 9%, and the increase in plant-container volume was 11%. The estimated capital-cost saving incurred by choice of the reference design is approximately $3 million. Figure V-1 shows the reactor-vessel assembly for both the reference and the alternate designs.

The reference-design core is roughly cylindrical in shape with an active height of 11 ft and an equivalent diameter of 12.8 ft. The individual fuel elements consist of UO_2 pellets, 0.354 in. in diameter by 0.708 in. high, enclosed in stainless-steel tubes of 0.010-in. wall thickness. The cladding operates under an elastically collapsed condition, as described in Ref. 1:

> In order to reduce the amount of steel in the reactor core and improve neutron economy, elastically collapsed 304 stainless steel was selected for the clad material. The normal fuel rod has an inside diameter of 0.358 inches with a wall thickness of 0.010 inches ±0.0005. The collapsed clad is designed to be elastically buckled between 1000 – 1500 psia pressure. At zero power conditions the maximum stress in the clad will be localized at the inner surface of the vertices of the buckled clad and will approach the yield strength of the material. However, it is expected that the clad will be pushed back toward a circular shape by the fuel pellets as the reactor is brought from zero power to full power and that the maximum clad stress will be below the yield strength during normal operations.

The fuel assemblies of the reference core consist of a basic 16-by-16 square array of fuel rods with 20 rods omitted from the periphery of the assembly to provide space for control rods. A cross section of the fuel assembly and control rod is shown in Fig. V-2. The outermost row along the periphery of each

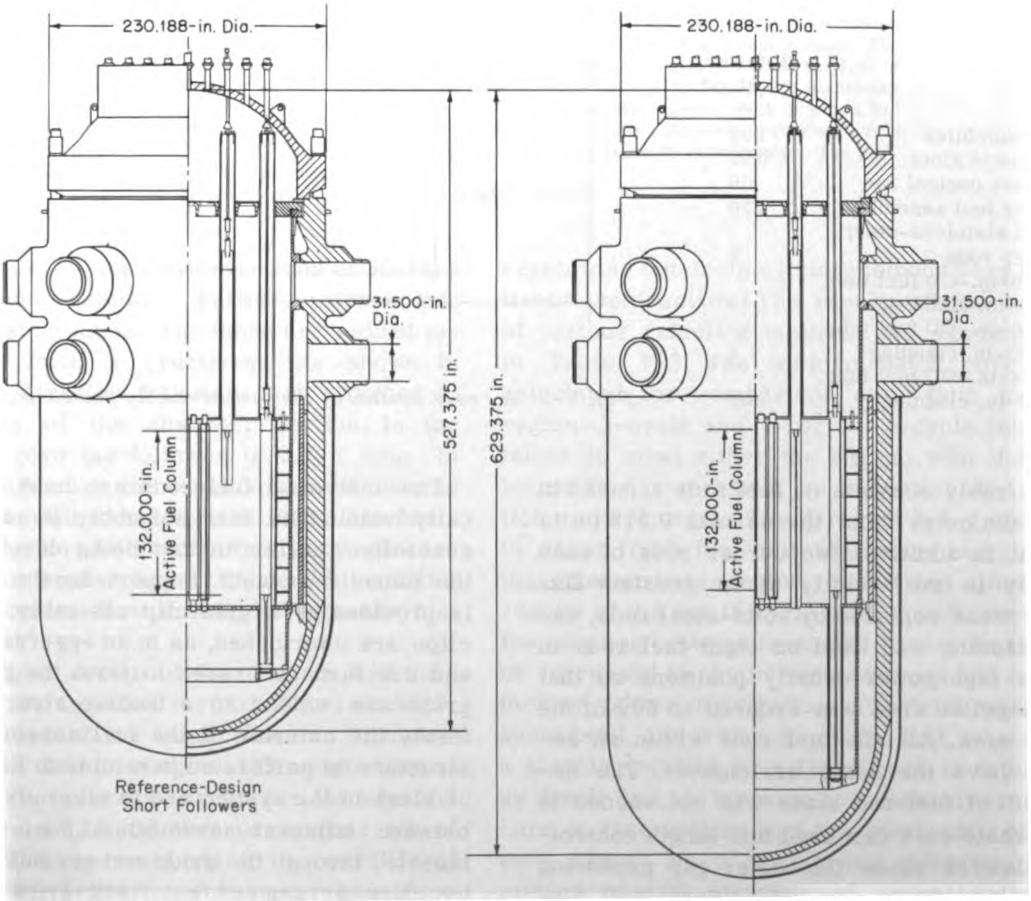

Reference-Design
Short Followers

Alternate-Core-Design
Full-Length Followers

Fig. V-1 Reactor-vessel assembly for both the reference and alternate designs.[1]

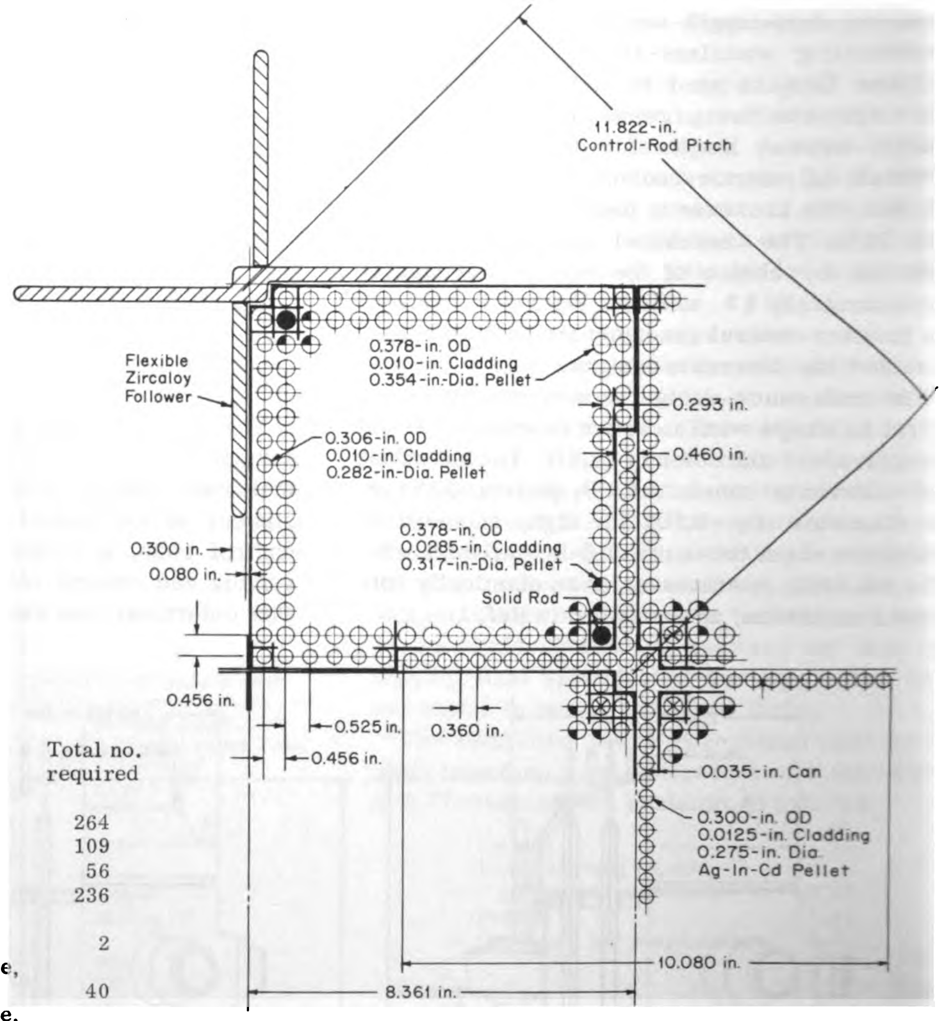

	Total no. required
Fuel assemblies	264
Control-rod slots	109
Tubes per control rod	56
Rods per fuel assembly	236
●, solid stainless-steel corner rods	2
○, 0.306-in.-OD fuel tube, 0.010-in. cladding	40
◐, 0.378-in.-OD fuel tube, 0.0285-in. cladding	8
○, 0.378-in.-OD fuel tube, 0.010-in. cladding	186

Fig. V-2 A cross section of the fuel assembly and control rod.[1]

fuel assembly consists of fuel rods reduced in outside diameter from the normal 0.378 in. to 0.306 in. In addition, two corner rods of each assembly in the vicinity of the greatest flux peaking were replaced by solid-steel rods, and thick cladding was used on eight fuel rods in selected high-power-density positions so that the fuel-pellet area was reduced to 80% of the normal area. All the fuel rods within an assembly have the same enrichment. The assortment of fuel-rod sizes was not needed in the alternate core that used full-length control-rod followers since the water gap producing high peaking factors in the adjacent fuel elements was greatly reduced. The alternate core has the same active fuel length and equivalent diameter as the reference core.

The individual fuel rods are held mechanically within the fuel assembly by a method generally similar to that being developed for the Round 3A plants. Support for the fuel rods is provided by a grid-clip assembly. Rows of clips are interlocked, as in an eggcrate design, and are furnace brazed to form the grid. The grids are welded to a boxlike structure that forms the exterior of the fuel assembly. The structure is perforated to minimize the amount of steel in the system and to allow coolant flow between adjacent assemblies. Fuel rods are inserted through the grids and are held in place by clips or fingers extending from the grid pieces. The clip support is lateral only, and the rods are free to expand axially between the end plates. The end plates and nozzles are welded to the unit after all the fuel rods are inserted to complete the fuel assembly.

Figure V-3 shows the core cross section. The core contains 264 identical fuel assemblies and 109 individually driven cruciform control rods. The rod pattern is such that every internal fuel assembly has a rod centered adjacent to each of two corners on the diagonal of the assembly. The absorber section is fabricated from 0.275-in.-diameter rods of 80-15-5 silver-indium-cadmium alloy inserted into stainless-steel tubes. The tubes are welded together to form a cruciform, as shown in Fig. V-2. Zircaloy followers are attached to the bottom of the absorber section. In the reference core the follower is 3.7 ft long. In the alternate core the length of the follower is equal to the full core length of 11 ft. The function of the short follower in the reference core is to reduce bypass flow in the control-rod slot and to promote flow mixing between the fuel assemblies.

Table V-2 CHARACTERISTICS OF DIFFERENT REFUELING METHODS FOR A 1000-MW(e) PRESSURIZED WATER REACTOR[2]

(Feed Enrichment Is 3.4 Wt.% in All Cases)

Refueling method*	Discharge burnup	Burnup/ batch burnup	Power ratio $P_{\max(\text{radial})}/P_{\text{av.}}$	K_{initial} (no Xe)
Uniform batch	15,250	1.00	1.99	1.229
Out-in				
3 region—3 cycle	20,440	1.34	1.96	1.126
5 region—5 cycle	21,960	1.44	1.92	1.095
3-region 3-1-2	21,740	1.43	2.28	1.158
Roundelay 3-batch	23,290	1.53	1.35†	1.116
Roundelay 5-batch	25,830	1.69	1.22†	1.081

*In the out-in refueling method, fresh fuel is fed to the outermost of several concentric fuel regions and subsequently moved inward at each refueling cycle. Spent fuel is removed from the innermost region. The 3-region 3-1-2 method is a variation in which fresh fuel is loaded into the intermediate region of a 3-region core. The numbering sequence taken in inverse order identifies the region in which the fuel is successively placed, the regions being numbered from out to in. In the Roundelay method the core is divided into a large number of adjacent regions, each of which has a number of fuel batches (usually one assembly is a batch). At every refueling cycle a spent fuel batch is removed and replaced by a fresh batch in each region. The partially spent fuel is never moved.

†These values do not include local "ripple" effects.

The nuclear design of the core is tied intimately to the intended method of fuel management because of the large size and high fuel burnup. The fuel loading is 125 metric tons of uranium. The average burnup for the equilibrium core is 24,000 Mwd per metric ton of uranium. This corresponds to a core life of 22,370 EFPH (effective full-power hours) or about 7,460 hr per refueling cycle and results in a refueling period of 12.7 months on the basis of an 0.80 plant factor.

The Westinghouse workers studied[2] several methods of cycling the fuel assemblies in the core. Their purpose was to determine a suitable means of achieving the lifetime requirements while holding the maximum-to-average radial power-density ratio to the limit of 1.5, which is required before the design thermal output can be reached. As is usually the case for reactors of large size and high burnup, the regionwise out-to-in cycling methods were relatively unattractive. The results of the survey of various refueling methods are summarized in Table V-2. The uniform-batch core was calculated for comparison only. Both the 3-region—3-cycle and 5-region—5-cycle shuffles failed to meet either the burnup with the selected feed enrichment or the power-distribution requirements. The 3-region 3-1-2 shuffle, in which fresh fuel assemblies are inserted in the intermediate region, was tried since the results of the out-in cycle studies indicated that the coupling between fresh and burned fuel must be increased to obtain higher burnup and satisfactory power distribution. The trial was unsuccessful, and it was concluded that, whenever a sizable fraction of a large core is replaced by fresh fuel, a large power peak always occurs in that region, and the remainder of the core serves as a multiplying reflector. The method of fuel management proposed, which avoids regionwise cycling, is designated "Roundelay multibatch." In the equilibrium cycle fresh elements are inserted in a uniform distribution throughout the core at each refueling operation. For example, with Roundelay 3-batch, every third element is replaced, and the other elements are left in place. In Fig. V-3 the fuel assemblies are numbered in the order in which they might be replaced in the reference core; during one refueling all No. 1 fuel assemblies would be replaced, and so on. It was found that the mixing of the fresh and burned fuel assemblies produces strong coupling between them and permits improved power production from the burned elements. The improved burnup is evident in the results shown in Table V-2. The favorable values of maximum-to-average power ratio are illusory, however, since the survey study did not take into consideration the "ripple" on the overall power distribution resulting from significantly different power production from adjacent fuel assemblies with greatly different burnup. As a result the reference core failed to meet the design criteria, although two changes were proposed to permit it to do so, as follows.

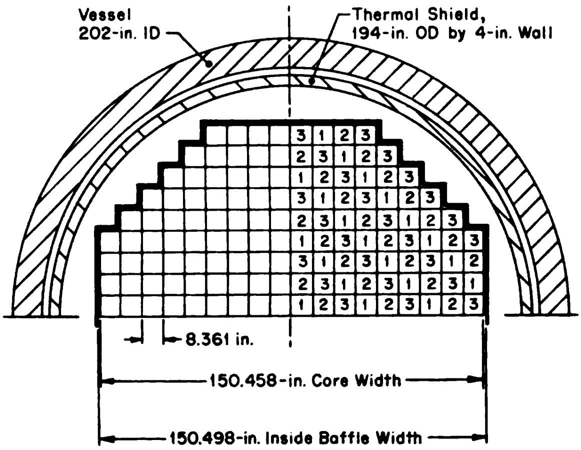

Fig. V-3 Cross section of vessel core.[1]

1. Reduce the local power ripple by increasing the number of fuel assemblies. A 673-fuel-assembly core with a 10-by-10 fuel-rod array showed a much improved power distribution.

2. Select a core array that has a center fuel assembly so that the replacement of the central group of four elements forced by symmetry would be eliminated. A very poor power distribution results from the power spike produced when the four fuel assemblies adjacent to the center are replaced together.

With Roundelay 3-batch refueling, it was that after six refueling steps the core ditions are essentially those of the equilib cycle.

The thermal and hydraulic characteris for both the reference and alternate cores presented in Table V-3. A review of t parameters gives the best insight into methods by which the rather remarkable p density of 80 kw/liter is expected to be achi in these very large cores. No single makes a large contribution to improved p formance, but a substantial improveme expected from a combination of many s items, with careful attention to their det interaction. This attention to detail extends only to the physical arrangements of c components (e.g., the array of different fuel rods within one assembly) and to a m uniform approach to design limitations the core volume (e.g., promoting intercha mixing to reduce enthalpy-rise hot-channel f tors) but also to a reexamination of the limi tions themselves. For example, the design li tation of a DNB (departure from nucle boiling) ratio of 1.25 at 115% of full po represents less margin than is used in curr practice. Evidently the belief is that operatio experience from present-day plants plus a quate in-core instrumentation will permit sat factory operation within these margins.

The composition of F_q, the ratio of maxim heat flux to average heat flux in the core, us for design purposes, is[1]

Subfactor	F_q
Axial	1.60
Radial	1.50
Local power peaking	1.30
Transient hot-channel factor	1.02
Engineering	1.045
Design overall factor	3.33

For $F_{\Delta H}$, the ratio of maximum coolant enthalp rise to average coolant enthalpy rise over th total length of the core, the composition is[1]

Subfactor	$F_{\Delta H}$
Radial	1.5
Transient factor	1.02
Engineering	
Net hot cell	1.07
Uncertainty	1.03
Flow distribution	1.07
Design value total	1.8

Table V-3 THERMAL AND HYDRAULIC CHARACTERISTICS OF THE CORE[1]

	Reference design (short followers)	Alternate design (full-length followers)
tal heat output		
Mw	3220	3220
Btu/hr	10.99×10^9	10.99×10^9
eat generated in fuel, %	97.4	97.4
stem pressure, nominal psia	2050	2050
ot channel factors in steady-state		
Heat flux, F_q	3.33	2.94
Enthalpy rise, $F_{\Delta H}$	1.80	1.80
oolant conditions		
Total flow rate, lb/hr	160.0×10^6	160.0×10^6
Effective flow rate for heat-transfer, lb/hr	144.0×10^6	144.0×10^6
Flow area for heat-transfer flow (unit cells), sq ft	69.77	68.2
Average velocity along fuel rods, ft/sec	12.7	13.0
Average mass velocity along fuel rods, lb/(hr)(sq ft)	2.06×10^6	2.11×10^6
Coolant temperature, °F		
Nominal inlet	546	546
Maximum inlet due to instrumentation error and dead band	550	550
Average rise in vessel	52	52
Average rise in core	57	57
Average in vessel	572	572
Average in core	574.5	574.5
Nominal outlet of hot channel	639	639
Maximum outlet quality of hot channel, wt.%	2.0	2.0
Maximum outlet enthalpy of hot channel, Btu/lb	687	687
Saturation enthalpy at minimum steady-state pressure, Btu/lb	675	675
Average film coefficient, Btu/(hr)(sq ft)(°F)	4850	5040
Average film-temperature difference, °F	34	30
Heat transfer		
"Active" heat-transfer surface, sq ft	65.5×10^3	70.9×10^3
Average heat flux, Btu/(hr)(sq ft)	163.5×10^3	151.0×10^3
Maximum heat flux, Btu/(hr)(sq ft)	544.3×10^3	444.0×10^3
Maximum thermal output, kw/ft	16	13.2
Average fuel temperature in core, °F	1535	1537

	Reference design (short followers)		Alternate design (full-length followers)
Heat transfer (continued)			
Maximum rod-surface temperature at nominal pressure, °F	645		645
DNB ratios*			
Average q''-DNBR at 100% power at 2050 psia	1.51		1.76
Average q''-DNBR at 115% power at 2200 psia	1.39		1.62
H-DNBR at 100% power at 2050 psia	1.49		1.53
H-DNBR at 115% power at 2200 psia	1.23		1.26
	Normal rod	Small rod	
Fuel rod (cold dimensions)			
Outside diameter, in.	0.378	0.320	0.3884
Cladding thickness, in.	0.010†	0.010	0.0152
Diametral gap, in.	0.004	0.004	0.004
Pellet diameter, in.	0.354†	0.296	0.354
Density of UO_2, % of theoretical density	96.5	96.5	96.5
Fuel length (pellets only), in.	132	132	132
Pitch, in.	0.525	0.456	0.523
Rod array in assembly	16 × 16		16 × 16
Rod per assembly	194	40	240
Total number fuel rods in assemblies	51,216	10,560	63,360
Hydraulic equivalent diameter of unit cell, ft	0.0469		0.0424
Additional water gap at edge of assembly, in.	0.0305	0.029	0.0305
Control rod			
Number of slots	109		109
General			
Total core area (inside core baffle), sq ft	128.2		133.9
Equivalent core diameter, ft	12.8		13.1
Maximum diameter of core, in.	166.0		169.3
Core length, between fuel ends, ft	11.0		11.0
Length-to-diameter ratio of core	0.86		0.84
Water-to-uranium ratio, unit cell	3.29		3.12
Fuel weight, lb of UO_2	289.3×10^3		314.8×10^3
Pressure drop, psi			
Across core	36		46
Across vessel, including nozzles	51		57
Core power density			
Kw/liter of core	80.7		77.2
Kw/kg of U	27.8		25.6

*The DNB ratios are based on the correlations presented in Ref. 20 and are minimum ratios, within the core, of the DNB condition to the actual condition. The heat-flux DNB ratio, q''-DNBR, applies to the subcooled regions of the core. The enthalpy-rise DNB ratio, H-DNBR, applies to quality regions of the core.

†Eight rods have a 0.0285-in. cladding thickness and a 0.317-in. pellet diameter.

In both tabulations above the transient factor provides for rod motion required for a 5% step change in load at 95% power level. It is expected that coolant mixing within the core, both between channels and between fuel assemblies, will be required to achieve the $F_{\Delta H}$ design value. Provision has been made in the core to promote mixing. Flow mixing is promoted between fuel assemblies to cool the channels at the assembly edge, where the power peaks, by mixing vanes installed on the grids within the upper 5 ft of the core and by staggering the grids in this region. Bulk boiling at the exit of the hot channel is permitted, to the extent of 2 wt.% quality, to keep the coolant-flow requirements within the capabilities of a seven-loop primary system.

In a study associated with the 1000-Mw(e) pressurized-water-reactor (PWR) design, the effects of core height, enthalpy rise, and burnup on the axial power distribution were investigated. The following quotation from Ref. 2 states the general problem:

> In designing very large reactor cores, it is important to understand the dependence of power distribution on core height, enthalpy rise, and burnup. To illustrate this point, consider the following hypothetical situation. Suppose a reactor with a core height of 10 feet has been designed to produce a given power output. If a new reactor design is required which has a 10% higher output, one might propose an increase in the core height to 11 feet, maintaining the same average power density. However, the axial hot channel factor might be greater in the 11 ft. core; if the increase in hot channel factor is 10%, the power capability is not increased at all in going from a 10 ft. to an 11 ft. core, assuming a burnout heat flux limitation. The power distribution might be expected to become worse as the enthalpy rise is increased since the water density becomes more non-uniform.

The conclusions (Ref. 2) drawn as a result of the study were as follows:

> 1. In the first core, which contains only fresh fuel, the axial peaking increases slightly with core size. At a burnup of a few thousand MWD/MTU, there is little variation in peaking factor with core size. Beyond 3000 MWD/MTU, the larger cores may have slightly less axial peaking than smaller cores.
>
> 2. In a cycle typical of equilibrium, the peaking factor appears to increase substantially with core size; however, burnup effects have reduced the equilibrium peaking factor to a low value in all cases so that the peaking is not serious, even in the larger cores.
>
> 3. All steady state power distributions which were studied had axial peaking factors less than 1.60, which is the design value for the 1000 MWe PWR.

Reactivity control of the reactor is prov by a combination of the mechanically actu neutron-absorbing control rods and a chem neutron poison dissolved in the reactor cool The soluble poison is boron in the form boric acid. Rapid reactivity changes resul from rapid load changes, safety shutdo Doppler, and other rapid transient effects a controlled by the rods. The slower acting reactivity changes due to fuel depletion, samari xenon, and gross temperature effects are accommodated by adjusting the concentration the neutron poison in the primary coolant. Th principal advantages in using a soluble pois are the improved core power distribution resulting from being able to withdraw most of th control rods during operation and the reduce total reactivity compensation required of th control rods since they are no longer require to shut down the reactor to the cold clean condition by themselves. The principal disadvantages are the large volume of primary coola that must be handled when bleed-and-feed dilution is used to reduce the boron concentratio and the influence of the poison in reducing the moderator coefficient of reactivity or eve causing it to change sign. In connection wit the latter point, the criteria for the referenc design permit the moderator coefficient of reactivity to vary from positive to negative during core life. It is proposed that the stability of the reactor be preserved through the combinatio of the Doppler effect and the coolant temperature controller.

The estimated boron concentrations for the first and equilibrium core cycles are[1]

Condition	Boron concentration, ppm	
	1st cycle	Equilibrium
Refueling shutdown; rods in; $k = 0.90$	3880	2930
Cold normal shutdown; rods in; $k = 0.97$	2880	1960
Hot normal shutdown; rods in; $k = 0.97$	2670	1550
Hot full power; no rods; no poison	2780	1810
Hot full power; no rods; Xe poison	2310	1370
Hot full power; no rods; Xe and Sm	2150	1240
End of life	≈ 0	≈ 0

In recent operation the Yankee Atomic Electric Co. reactor at Rowe, Mass., has been successfully employing soluble-poison shim ontrol, and other reactors have run in this anner on an experimental basis. The degree which the soluble poison is employed in the eference large PWR, however, is significantly reater than in systems that have been run to ate.

With the heavy dependence on soluble shim ontrol, it might seem that the reference design mploys an unusually large number of control ods (109). The large number results from uncertainties regarding spatial instabilities in the large core, which might conceivably arise from either sustained xenon oscillations or Doppler oscillations. The possibility of both was studied. It was found that for the conditions normally existing in a PWR, i.e., negative Doppler coefficient, no Doppler oscillations are possible, even for a very large reactor. In regard to xenon oscillation, the conclusions were not as definite and were summarized in Ref. 2 as follows:

> 1. The nominal temperature coefficient is sufficiently negative to prevent sustained Xe oscillations of constant or increasing amplitude, even with pessimistic assumptions for the degree of flux flattening.
> 2. With the minimum temperature coefficient and a pessimistic degree of flux flattening, the calculations predict the 1000 MWe core is near the threshold for sustained oscillations.
> 3. Damped oscillations are predicted in all directions for both the nominal and minimum temperature coefficients. Damped oscillations do not represent a serious operational problem if the degree of damping is sufficient to quickly reduce the amplitude of the oscillation. With the nominal temperature coefficient, the damping is probably sufficient to prevent any serious problem; however, with the minimum coefficient, very little damping is expected and operational problems could occur. These conclusions must be qualified since no definite standards have been established regarding the degree of damping required for satisfactory reactor operation. . . .

It is further stated in Ref. 2 that the possibility of xenon oscillations is not believed to be a feasibility problem of the 1000-Mw(e) PWR since reactors have been operated in the presence of such oscillations.

In-core instrumentation is proposed to detect nuclear flux tilts as well as to monitor reactor-coolant temperatures. Neutron fluxes at selected locations in each of the 66 fuel assemblies in one quadrant of the core and at 3 positions in each of the remaining quadrants would be measured by miniature in-core neutron detectors. Temperatures at the outlets of each of the 66 fuel assemblies in one quadrant of the core and at 34 selected positions in the other three quadrants would be measured by sheathed Chromel-Alumel thermocouples.

A second alternate core design aimed principally at an improvement in control-rod features was proposed, although a complete core design was not developed in the study (Ref. 1). This alternate is based on replacing the separate cruciform control rods by a cluster of poison elements arranged in one or more rings and located within the fuel assembly instead of between the fuel assemblies. The individual poison elements are approximately the size of the fuel tubes and move in thimbles located within the fuel assembly. This "rod-cluster-control" (RCC) concept eliminates the necessity for followers and makes the use of canless fuel assemblies more attractive. A model of the rod-cluster-control assembly is shown in Fig. V-4. The RCC fuel assembly requires no change in the basic fuel lattice, and the spring-clip grids for holding the fuel rods in the lattice are retained. The guide tubes in which the individual control elements move are permanently fixed within the lattice of the fuel assembly. The individual control elements are fastened together above the fuel assembly by means of a spider, as shown in Fig. V-5, and all elements within an assembly move up and down together. The guide tubes within the fuel assembly are perforated over a substantial length to provide for coolant flow. The venting is controlled at the bottom of the tube to serve as a dashpot during scramming of the control element. The rod-cluster control-guide tube is shown in Fig. V-6. Advantages of the rod-cluster control are summarized in Ref. 1:

> 1. Improved power distribution due to (a) separation of interassembly peaking from control slot peaking and (b) breakup of control slot peaking by distributing the control material as individual rods throughout the lattice.
> 2. More control per weight of absorber provided the most favorable geometry can be selected.
> 3. More uniform distribution of control. This will result in better power distribution control in the event of unstable power distribution and better temperature and pressure dead-band control because of the lower worth per rod step.
> 4. Less parasitic absorption if elimination of the stainless steel can is successful which will improve the fuel cycle costs.
> 5. Complete elimination of followers.
> 6. Reduced coolant bypass flow.
> 7. Simplification in mechanical design.

Although rod-cluster control is considered only as an alternative in the 1000-Mw(e) PWR

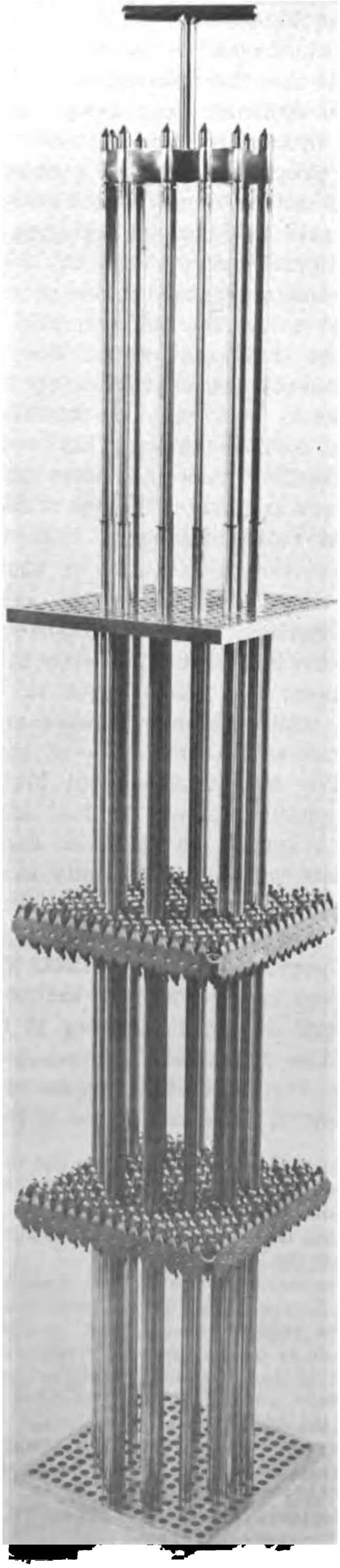

Fig. V-4 Fuel-assembly model for rod-cluster control.[1]

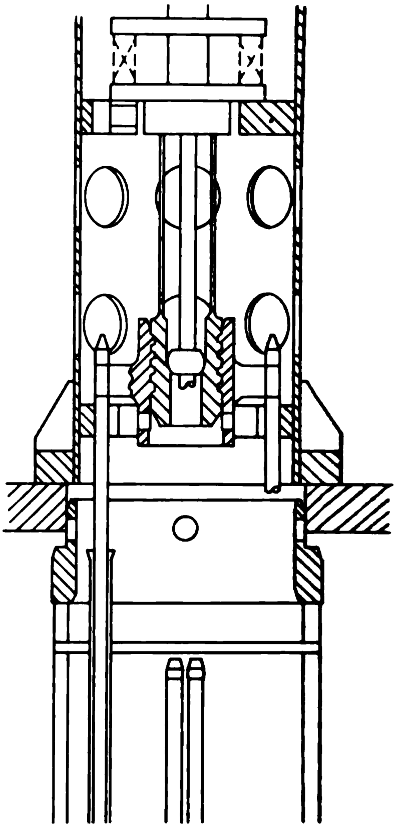

Fig. V-5 Coupling for rod-cluster control.[1]

study, significant development has been devoted to the concept, and it has been incorporated in the design of the San Onofre reactor (Ref. 15). Rod-cluster control could reasonably be expected to be adopted for the Connecticut Yankee and Malibu reactors also.

As mentioned earlier in this review, this 1000-Mw(e) Closed Cycle Water Reactor Study should rest on firmer ground than the usual run of reactor-feasibility studies because it is based on information generated under the massive LRD Program being conducted for the San Onofre reactor. References 4 to 15 are progress reports on this program. Topical reports, Refs. 16 to 39, on the same program treat the reactor subjects covered in the 1000-Mw(e) study (Refs. 1 and 2) in greater depth and are keyed, of course, to the San Onofre reactor. For example, a number of mechanically assembled fuel assemblies have been irradiated in the Saxton reactor, and additional assemblies have been prepared for irradiation. These included two rod-cluster-control assemblies, [illegible] 1-

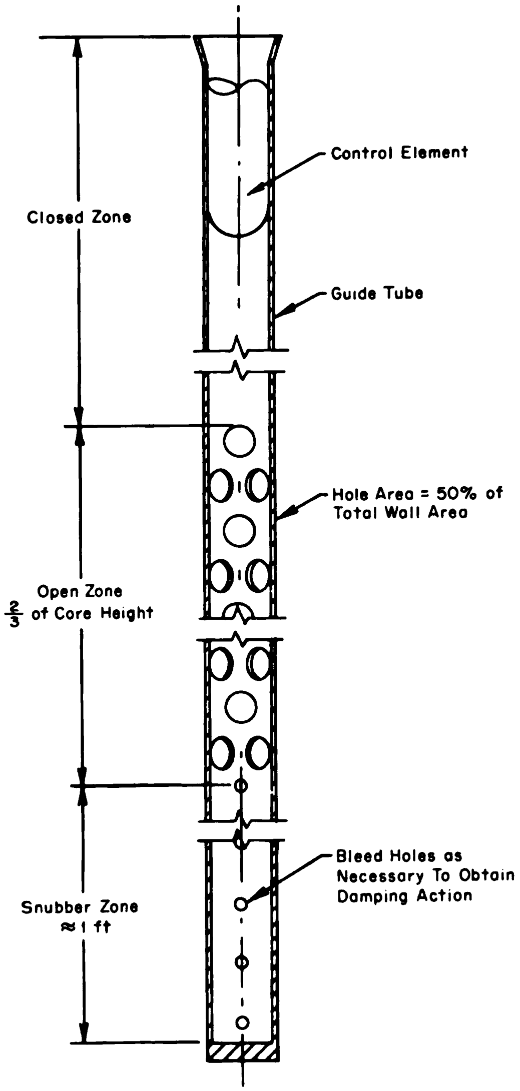
Control Element
Closed Zone
Guide Tube
Hole Area = 50% of Total Wall Area
Open Zone
$\frac{2}{3}$ of Core Height
Bleed Holes as Necessary To Obtain Damping Action
Snubber Zone
≈ 1 ft

Fig. V-6 Guide tube for rod-cluster control.[1]

by-3 and the other a 9-by-9 array. Fuel cladding of these assemblies included both thin-walled stainless steel and Zircaloy.

A general comment appears appropriate on the size of components for large pressurized-water reactors. At the time this 1000-Mw(e) PWR study was conducted, a 1000-Mw(e) power level was believed to be the highest achievable from a single reactor vessel in the relatively near future. Similarly, seven coolant loops were required because of restrictions on the maximum size of steam generators and main coolant pumps. Recent indications are that manufacturers are now capable of providing these key components in higher unit ratings. As previously mentioned, pressure vessels for 1500-Mw(e) units appear to be feasible.[3] Steam generators of almost twice the capacity used in the study are being discussed. If coolant pumps are not restricted to canned-motor units, the remaining restriction would be only the size of volute that can be cast. This would permit pumps of increased capacity.

EBWR

Operation of the Experimental Boiling Water Reactor (EBWR) at power levels up to and including 100 Mw(t) has been previously reviewed in *Power Reactor Technology*, 7(3): 317-320, on the basis of several topical reports. Reference 40 contains a collection of the detailed test reports that cover operation since the modification of the reactor and plant for the higher power up through operation for brief periods at 100 Mw(t). The test reports contain detailed accounts of the loading sequence and initial critical testing. Physics tests included critical control-rod-position determination, rod calibrations, and measurements of temperature and void coefficients and flux distribution. The response of the reactor to step reactivity changes was determined with reactor periods ranging from 15 to 40 sec and peak power levels near 1 Mw(t). Analytical correlation of the peak power and energy production during these transients with the reactor period was obtained using an energy-production-dependent reactivity feedback. Inspection of the control rods irradiated during prior operation of the EBWR is described, including metallurgical and radiochemical examinations. Thermal and hydraulic testing included temperature measurements in the reactor, determination of recirculation rate, measurements of steam-volume fractions in the core and riser, as well as investigation of steam carry-under and moisture carry-over.

Design Studies of a 1000-Mw (e) Fast Reactor

Four independent design studies (Refs. 41 to 44) were made for the AEC on a 1000-Mw(e) ceramic-fueled fast breeder reactor cooled with liquid sodium. In two of the studies the fuel was UO_2-PuO_2, whereas in the other two studies UC-PuC was used. These studies, which were focused on the reactor and primary heat-removal systems, represent the first phase in AEC's program to develop basic fast breeder concepts for large commercial power stations. The objectives in the studies were to develop designs that optimized fuel-cycle costs, obtained attractive fuel-doubling times, and permitted high-temperature steam conditions at the turbine, consistent with safety requirements in fast reactors. The studies thus included core physics and thermal-hydraulic analysis, mechanical design features, fuel-handling concepts, and fuel-cycle economics. The following ground rules were common to all studies:

1. The performance was to be evaluated for equilibrium cores.

2. The fuel cladding was to be a stainless steel.

3. The primary sodium temperature was to be sufficiently high to produce 1000°F steam, taking into account the temperature drop in the intermediate heat exchanger.

4. The breeding ratio was to be greater than 1.2, with a reasonable doubling time.

5. The fuel was to be considered government owned with a 4¾% rental charge.

6. The value of $10 per gram was to be used for ^{239}Pu and ^{241}Pu in the form of the nitrate.

7. The feed material to the plant for the equilibrium core was to be depleted uranium containing 0.3 wt.% ^{235}U.

In a recent feature article by Okrent[45] in *Power Reactor Technology*, various problems were discussed which affect the performance of large sodium-cooled ceramic-fueled fast reactors. In general, the considerations introduced by economics, breeding, and safety give rise to conflicting requirements in optimizing the design of such reactors. A ceramic fuel after exposure in the reactor cannot be considered to provide the reliable axial thermal expansion that, in smaller metal-fueled reactors, is responsible for a significant rapidly acting negative reactivity coefficient. On the other hand, the presence of oxygen or carbon in the ceramic softens the neutron spectrum so that a sizable negative Doppler coefficient of reactivity can be obtained. The change in reactivity upon loss of sodium from the core becomes more positive with increasing reactor size because the positive reactivity effects associated with changes in neutron spectrum become more important relative to the nega neutron-leakage effect. The buildup of and fission products in the equilibrium increases the positive reactivity effects d sodium voiding, as would also the substitu of niobium for steel structures. Any meas that increases the neutron leakage from core also tends to shift the sodium void c ficient in the negative direction for two reas First, the increase makes the effect of sod on the neutron leakage more important. Sec an increase in the concentration of fissile is tope is required; this, therefore, results harder spectrum that is less sensitive changes in sodium density. The higher leak has other, unattractive consequences: if brou about by a thinning of the breeder blanket decreases the total breeding ratio, and brought about by the use of high-leakage c geometry, it decreases the internal bree ratio and increases the rate of reactivity l with fuel burnup. The Doppler reactivity co ficient can be improved by the addition o fixed moderator to the core, such as BeO. soften the neutron spectrum; however, this detrimental to the breeding ratio and doubl time.

Among the other problems that required c sideration in these studies were the limitat of the stainless-steel fuel cladding at the temperature required to obtain the 100 steam temperature specified for high therm dynamic efficiency, the utilization of the fue high burnup and high heat ratings for attract fuel-cycle economics, thermal-stress proble in the reactor vessel and primary system posed by high-velocity sodium operating temperature differences in the range of 20 300°F, and reliable methods of refueling w out excessive reactor downtime.

The four fast reactor design studies we evaluated by the AEC[46] with the assistance the Argonne National Laboratory and the L Alamos Scientific Laboratory. A very br summary description of the four reactor co cepts was presented in a paper by Koch et a A summary of the nuclear and safety cha acteristics of the reactor concepts was com piled by Okrent et al.,[48] and the fuel-cy economics were evaluated by Link et al. paper by Klotz and Miller described the Al Chalmers design.[50]

A brief description is given below of four 1000-Mw(e) concepts. The core arra

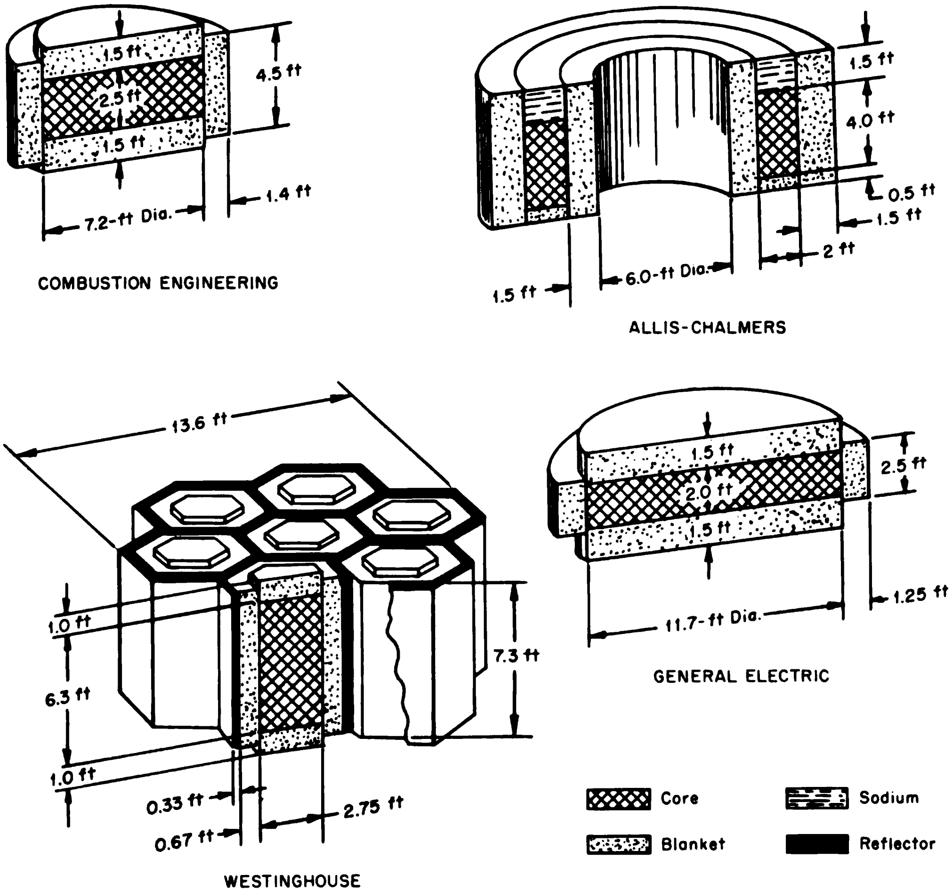

Fig. V-7 Reactor-core arrangements for four 1000-Mw(e) design studies.

ments are shown diagrammatically in Fig. V-7, and the major characteristics of the four concepts are presented in Table V-4.

Allis-Chalmers Reactor Concept

To reduce the sodium void coefficient as much as possible, this concept uses a thin annular core having high neutron leakage. The core annulus is 2 ft thick, 13 ft in outside diameter, and 9 ft in inside diameter, with a volume of 7720 liters. The sodium void coefficient is decreased even further because no breeder blanket is used above the core region; instead a sodium space is provided at the top of the core with a layer of B_4C above the sodium. The fuel pins contain UO_2-PuO_2 pellets that are distributed axially in 3-in. compartments within the pins to minimize reactivity effects from fuel compaction. The fuel pellets have hollow centers to permit a maximum heat rating of 13 kw/ft with a cladding temperature of 1420°F. There are 123 fuel pins in the hexagonal fuel assembly which are held in place by six grids, 12 in. apart, along the length of the assembly, with tie rods at alternate corners of the assembly. The fuel assemblies are held down hydraulically and are individually orificed to obtain a uniform sodium exit temperature. Heat is removed from the 1200°F primary sodium by means of six external loops.

For refueling the fuel elements are located by double rotating and indexing shield plugs. After the reactor is cooled to 350°F and the sodium level is lowered, direct visual observation of the core is possible for grappling the fuel elements. The fuel is removed to an argon-cooled cask, is cleaned with steam to remove the sodium, and is then transferred to an on-site reprocessing plant. The blanket is shuffled in an out-in manner to match the orificed sodium flow with the power generation in the elements. This avoids large changes in exit sodium temperature in the blanket assemblies

Table V-4 CHARACTERISTICS OF THE 1000-Mw(e) CERAMIC-FUELED FAST REACTOR CONCEPT

	Allis-Chalmers[41]	Combustion Engineering[42]	General Electric[43]	Westinghouse[44]
Core and blanket				
Core geometry	Annulus	Flat cylinder	Flat cylinder	7 modules
Core volume, liters	7520	2895	6030	7050
Axial blanket volume, liters	960	3500	9050	2400
Radial blanket volume, liters	17,700	4800	4200	19,850
Fuel form				
Core and axial blanket	Oxide	Carbide	Oxide	Carbide
Radial blanket	Oxide	Carbide	Oxide	Oxide
Active height of core, ft	4	2.5	2.0	6.3
Blanket thickness				
Axial blanket, ft	0.5	1.5	1.5	1.0
Radial blanket, ft	1.5	1.4	1.3	0.7
Composition of core and axial blanket				
Fuel, %	29.4	25.6	34.8*	29.4†
Sodium, %	40	66.5	46.4	55.1
Steel, %	30.6	7.9	18.8	15.5
Composition of radial blanket				
Fuel, %	55	45	50.7	55
Sodium, %	30	43	32.1	25
Steel, %	15	12	17.2	20
Core fissile metal, kg	3690	1155	2304	3686
Blanket fissile metal				
Axial blanket, kg	6	32	58	23
Radial blanket, kg	260	83	80	171
Core load (metal), kg	17,760	8913	12,828	23,420
Blanket loading (metal)				
Axial blanket, kg	2210	10,696	19,242	7800
Radial blanket, kg	84,566	27,886	24,300	56,886
Core load (ceramic), kg	20,200	9400	14,600	25,200
Blanket loading (ceramic)				
Axial blanket, kg	2510	11,250	21,900	8200
Radial blanket, kg	96,100	29,400	27,500	59,800
Power, Mw(t)				
Total	2500	2500	2500	2500
Core	2125‡	1950	2125	2170
Axial blanket		200	300	35
Radial blanket	375	350	75	295
General				
Core irradiation level, Mwd/metric ton of U	100,000	110,000	110,000	100,000
Breeding ratio§	1.32	1.42	1.25	1.57
Doubling time,§ years	19.5	6.2	15.8	11.7
Sodium void worth¶ (100% core voided), %Δk	0.0	1.0	0.4	0.3
Doppler coefficient, $-T(dk)/(dT) \times 10^{+3}$	2.6	5	5	12
Fuel-cycle cost,§ mills/kw-hr	0.69	0.30	0.57	0.28
Size, ft				
Reactor diameter	16.0	10.0	14.2	13.6
Reactor height	6.0	5.5	5.0	8.3
Vessel diameter	20.0	16.5	18.0	18.0
Vessel height	25.0	40.7	33.0	36.0
Thermal parameters				
Specific power, kw/kg				
Core U + Pu ceramic material§	100	198	150	86
Core fissile material¶	640	1680	920	520
Power density in core,§ Kw(t)/liter	282	695	365	308
Temperature, °F				
Core inlet	950	850	800	979
Cladding peak	1330	1400	1332	1400
Fuel peak	4615	2600	4700	2184
Core outlet	1200	1120	1100	1200
Fuel bond	Helium	Sodium	Helium	Sodium
Coolant				
Sodium flow, (lb/hr) × 10^{-6}	114	113.6	95.4	128
Core velocity, ft/sec	10	20	11.1	26.5
Loop pressure drop, psi	90	59.8	40	113

Table V-4 (Continued)

	Allis-Chalmers[41]	Combustion Engineering[42]	General Electric[43]	Westing-house[44]
Fuel				
Fuel-pin-cladding outside diameter, in.				
Core and axial blanket	0.30	0.30	0.25	0.30
Radial blanket	0.607	0.45	0.50	0.464
Cladding thickness, in.				
Core and axial blanket	0.028	0.011	0.015	0.010
Radial blanket	0.015	0.016	0.020	0.020
Sodium-bond gap, in.				
Core and axial blanket		0.010		0.006
Radial blanket		0.011		
Pellet outside diameter, in.				
Core and axial blanket	0.24	0.259	0.22	0.268
Radial blanket	0.574	0.396	0.45	0.420
Pellet, inside diameter, in.	0.10		0.06**	
Active core height, in.	48	30	24	75
Active blanket height, in.				
Axial blanket	6	36	36	24
Radial blanket	72	54	36 and 60	87
Assemblies				
Distance across flats, in.	4.45	6.241	8.75	5.104
Triangular pitch of pins, in.				
Core and axial blanket	0.375	0.468	0.338	0.426
Radial blanket	0.69	0.539	0.565	0.496
No. of pins per assembly				
Core and axial blanket	123	169	470	120
Radial blanket	37	127	208	91
No. of assemblies in region				
Core and axial blanket	498	157	225	252
Radial blanket	858	156	108	357
Total no. of pins in region				
Core and axial blanket	61,254	26,533	105,750	30,240
Radial blanket	31,709	19,812	22,464	19,812
Feed enrichment, average, %				
Core	20.8	13.0††	18.0††	15.7
Blankets	0.3	0.3	0.3	0.3

*Includes BeO.
†Includes cermet.
‡Includes bottom axial blanket.
§Per contractor calculations.
¶Per evaluator calculations.
**Formed during operation.
††Zoned.

with the rapid buildup of plutonium associated with the high radial neutron leakage from the core.

Combustion Engineering Reactor Concept

This concept uses a conventional cylindrical core that has a volume of 2895 liters. The core is 2.5 ft high and is 7.2 ft in diameter, with a length-to-diameter ratio of 0.35. The carbide fuel is sodium bonded to the 11-mil-thick cladding made of type 19-9 DL stainless steel. The sodium bond permits higher heat fluxes for a given maximum temperature limit on the fuel and also accommodates the swelling of the fuel with burnup. The top and bottom axial blankets are integral with the core. A 15-in. gas space is provided on top of the upper axial blanket to accommodate a gas release of 11% over the 100,000 Mwd/ton exposure of the element. The carbide is slightly hyperstoichiometric, i.e., carbon content is greater than 4.8 wt.%, to limit swelling and gas release in fuel operating at a maximum temperature of 2600°F. Several methods are proposed to prevent the carburization of the cladding. The hexagonal fuel assemblies in the core each contain 169 fuel pins that are held together by band wraps. The radial blanket is also carbide fuel, with a residence time three times that of the core. Halfway through its life each blanket element is rotated 180° to equalize its exposure and to increase the coolant flow to accommodate the higher heat generation.

For refueling the fuel elements are located by a single rotating and indexing plug and a manipulator arm and are transferred under sodium to an adjacent decay storage pool of sodium. After three months' decay the elements are removed, steam cleaned to remove sodium, and prepared for shipment off-site in a water-cooled cask.

There are six conventional primary loops outside the reactor vessel. The pump is at the outlet to minimize the pressure of the cover gas in the reactor vessel.

Combustion Engineering also presents an advanced design featuring a voided radial gap between the core and blanket to obtain a negative sodium coefficient for complete voiding of the core coolant. The theoretical basis for the gap was described in a recent paper (Ref. 51).

General Electric Reactor Concept

To obtain high neutron leakage from the core, this concept uses a highly "pancaked" core, 2 ft high and 11.7 ft in diameter, which has a volume of 6000 liters. There are three radial zones of fissile plutonium enrichment for power flattening. The maximum heat rating of 22.7 kw/ft is obtained with oxide fuel that has a hollow cored center, formed during initial reactor operation. The maximum temperatures for the fuel and the type 316 stainless-steel cladding are 4700 and 1330°F, respectively. The fuel pins are fastened to a grid in the fuel box by use of a T slot in the lower end plug and a mating bar in the grid. The pins are positioned along their length by means of slotted spacer tubes that contact the three surrounding fuel pins. There is an upper shield-plug section that is integral with the fuel pins so that the fuel elements are held down by their own weight. The core contains 7 vol.% beryllium oxide to increase the magnitude of the Doppler coefficient by softening the neutron spectrum. The entire primary system, including the reactor core, the six heat exchangers, and the six pumps, is immersed in a large tank of sodium, 52 ft in diameter, so that problems associated with sodium leakage and thermal expansion in the primary piping are minimized.

A shielded inert-gas-filled cell with manual manipulators is provided directly over the reactor for refueling. The vessel head is removed and the fuel is transferred under sodium using hot-cell techniques. After they have decayed in a storage tank, the fuel elements are removed and shipped under sodium without any cleaning.

General Electric also presents an advanced core without beryllium oxide to obtain a higher breeding ratio. The fuel burnup in this design is 200,000 Mwd/ton.

Westinghouse Reactor Concept

The reactor consists of seven hexagonal cylindrical modules, each containing a high-leakage core that is 2.75 ft in diameter and 6.3 ft high, with a total core volume of 700 liters. Each core is surrounded by an 8-in.-thick blanket of UO_2 and a 4-in.-thick layer of graphite that decouple the modules from each other. The fuel consists of pressed and sintered carbide pellets of 90% density; the carbide is hypostoichiometric, carbon content less than 4.8 wt.%, to avoid carburizing the type 316 stainless-steel cladding. The pellets are compartmentalized in the pins to minimize reactivity effects from compaction of the ceramic fuel. The axial blankets containing UC form an integral part of the fuel pins. The maximum temperatures for the fuel and the cladding are 2184°F and 1400°F, respectively. Iron is added to the fuel to combine with the free metallic phase forming $(U\text{-}Pu)Fe_2$. This is to avoid forming in the cladding a plutonium-iron eutectic that has a melting point of only 770°F and also to tie up any free plutonium in the grain boundaries to minimize fuel swelling. The fuel is assembled in what is called a Controlled Fuel-Expansion Assembly to provide a negative reactivity coefficient due to thermal expansion and thus supplement the negative Doppler coefficient. Each ceramic fuel pin is made in two pieces; one piece is attached to the upper assembly plate, and the other is attached to the lower assembly plate. A small gap is left in the center. The size of this gap is controlled by the thermal expansion of seven cermet type fuel pins in each assembly which tie the upper and lower grip plates together. The cermet is 20 vol.% UO_2 in stainless steel with a ^{235}U enrichment of 30%.

The fission-product gases are vented from the fuel pins to the primary sodium coolant to minimize the stresses in the cladding. The fuel assemblies are held down in the reactor by means of a push-pull latching device at the bottom of the assembly.

The reactor vessel is designed with a coaxial arrangement for the inlet-outlet pipes to minimize stresses in the vessel from thermal expansion and to minimize the number of penetrations. As a result of the high neutron leakage into the radial blanket of each module the plutonium content, and therefore the power generation in the blanket elements, increases arkedly with exposure in the reactor. Hence ovision is made for periodic adjustments in e sodium flow to the blanket elements. For fueling the reactor-vessel head is removed, d by hot-cell techniques the fuel is trans- rred visually, using gas cooling, to an anti- ony-lead-filled cask for shipping.

clear and Safety Characteristics

All four reactors have neutron lifetimes in e range from 3 to 6 × 10^{-7} sec, effective layed-neutron fractions of about 0.004, and zable negative Doppler coefficients. The pow- coefficients of reactivity are all negative and the range from -1 to -3×10^{-6} Δk/Mw. elatively flat radial power distributions are tained in the cores with low length-to-di- neter ratios (the Combustion Engineering and eneral Electric cores) by radial zoning of the utonium concentration. The tall thin cores ne Allis-Chalmers annular core and the West- ghouse modules) have favorable radial power stributions without fuel zoning. A brief de- cription is given below of the distinguishing aracteristics of the four concepts, using rameters obtained from the design reports Refs. 41 to 44). Note that the values differ om those listed in Table V-4 for the cases here the table values are taken from the AEC valuation report (Ref. 46) (see Table V-5 for mparison).

The *Allis-Chalmers concept* has a breeding atio of 1.32, giving a doubling time of 20 years r the fuel inventory. The core conversion atio is 0.52; an excess reactivity of 0.06 Δk is equired for the reactivity decrease between artial reloadings of the core when one-third f the fuel is replaced. A major design basis r this concept is minimizing the possibility of rge reactivity insertion should the sodium in e reactor boil, even in the absence of a scram. he voiding of all the sodium in the core gives reactivity increase of 0.002 Δk. If the sodium oiling occurs in such a way that the upper xial sodium gap is also voided, the reactivity ecreases. The Doppler effect will compensate r 0.0017 Δk reactivity before all the oxide uel reaches the melting point. Control in the nnular core requires that several control rods e moved as a coordinated unit because of the mall coupling between different sections of the ore.

In the *Combustion Engineering concept* the reeding ratio is 1.42, and the specific power in the core is 1680 kw per kilogram of fissionable plutonium; the resulting doubling time is seven years. With the core internal conversion ratio of 0.85, the reactivity change with fuel burnup is only 0.0003 Δk per 1000 Mwd/ton. The reactivity increase for complete loss of sodium from the core is 0.024 Δk, whereas the loss of all the sodium from the core and blankets as well gives no reactivity change. It was calculated that the reactor by means of the Doppler effect can safely absorb a step reactivity increase of 1 dollar and 24 cents without any melting of the fuel or boiling of the sodium. The reactor is partially refueled every two and two-thirds months to replace one-eighth of the core elements so that the reactivity to be controlled is only 0.004 Δk or 1 dollar. Also, sources of potential reactivity addition have been similarly limited; the maximum reactivity worth of a control rod is 1 dollar, and the worth of a fuel assembly is 93 cents. In the event of total loss of coolant flow, it is required that the control rods scram to prevent boiling of the core sodium.

A major objective of the *General Electric concept* is the achievement of a large negative Doppler coefficient of reactivity to counteract reactivity increases that would result from voiding the sodium starting at the core center, even for implausible accidents. Enhancement of the Doppler coefficient is even more important for the oxide fuels, which operate at higher temperature than the carbide fuels, since the Doppler coefficient usually decreases with increasing temperature. The beryllium oxide in the core softens the spectrum so that the Doppler coefficient is enhanced; the Doppler effect will compensate for 0.005 Δk reactivity when the fuel is heated from operating temperature to an average temperature of 4700°F. Voiding all the sodium in the core adds 0.008 Δk, with a maximum increase of 0.014 for some configuration of partial voiding.

It has been calculated that a step reactivity increase of 1 dollar and 70 cents will not cause fuel damage or sodium boiling. The blockage of coolant flow in the core at full power will cause boiling to start at the center with a maximum reactivity gain of less than 1 dollar so that the reactor does not become prompt critical. Up to 3 dollars and 50 cents of reactivity can be inserted at a rate postulated for a refueling accident without any sodium boiling in the core. The energy yield on core meltdown, which inserts reactivity at the rate of 50 dollars/sec, is equivalent to 200 lb of TNT.

In this reactor of softer spectrum, the breeding ratio is 1.25, with an internal conversion ratio of 0.69. The doubling time is 16 years. The core is refueled every 6 months, when one-sixth of the fuel is replaced; 0.33 Δk excess is provided for fuel burnup.

In the *Westinghouse concept* the sodium coefficient for complete voiding of the core sodium has been made very small, $-0.001\ \Delta k$, by the use of seven small very loosely coupled core modules, each with its own blanket. A partial voiding of the sodium can increase reactivity by 0.0032 Δk, which is below prompt critical. The controlled-expansion fuel elements provide a reactivity coefficient of $-0.75 \times 10^{-5}/°F$, which supplements the Doppler coefficient of $-0.69 \times 10^{-5}/°F$ at operating temperature. The reactivity sharing between the modules reduces the effect of a reactivity insertion in any one module. The coupling in a clean core is only 0.003 Δk, which increases in the equilibrium core to 0.025 Δk as plutonium builds up in the blanket. The monitoring and control of the modular core may require extensive in-core instrumentation.

The breeding ratio is 1.57, the core conversion ratio is 0.54, and the doubling time is 11 years. The reactor is shut down for refueling every 7 months to replace one-sixth of the core. The reactivity decrease between refuelings, because of fuel burnup, is 0.009 Δk.

Physics and Fuel-Cycle Evaluation

In the course of the AEC's evaluation[46] of the four studies, comparative calculations were performed on breeding ratio, Doppler coefficient, and sodium void coefficient, using consistent cross-section data and calculation methods. The fuel-cycle costs were also recomputed for each concept[49] by applying common procedures for estimating the cost of reprocessing, shipping, and fabrication, taking into account such factors as the diameter, length, and cladding thickness of the fuel pins. A common burnup of 100,000 Mwd/metric ton was used, as well as a load factor of 80%. The plutonium credits, however, reflect the contractors' estimate of breeding ratio rather than the normalized values obtained in the evaluation. A comparison with the contractors' values is presented in Table V-5. Except for inventory charges that depend on specific power and plutonium credits that depend on breeding ratio, the other components of the fuel-cycle costs in mills per kilowatt-hour are nearly the same for all concepts: fuel fabrication, 0.4; core capitalization, 0.1; shipping, 0.1; and reprocessing, 0.1. Inventory charges are in the range from 0.1 to 0.3 mill/kw-hr and plutonium credits, based on the normalized breeding ratios, are in the range from 0.2 to 0.4. The Allis-Chalmers study proposes that the fuel be reprocessed on the reactor site. This would lower the fuel-cycle cost for that reactor in Table V-5 by 0.1 mill/kw-hr.

Table V-5 PHYSICS AND FUEL-CYCLE EVALUATION

	Allis-Chalmers concept	Combustion Engineering concept	General Electric concept	Westinghouse concept
Reactivity change for complete voiding of core sodium, Δk				
Contractor calculation	0.001	0.024	0.008	−0.001
Evaluator calculation	0	0.010	0.004	0.003
Doppler coefficient, $-T(dk/dT) \times 10^3$				
Contractor calculation	2.9	5	10	12
Evaluator calculation	4.3	5.4	5.4	3.3
Breeding ratio				
Contractor calculation	1.32	1.42	1.25	1.57
Evaluator calculation	1.20	1.41	1.21	1.38
Doubling time, years				
Contractor calculation	18.4	6.9	13.5	13
Evaluator calculation	30	7.2	20	19
Fuel-cycle cost, mills/kw-hr				
Contractor calculation	0.78	0.30	0.57	0.28
Evaluator calculation	0.70	0.43	0.54	0.43

The differences between the contractors' values and those calculated by the AEC evaluaors are to some extent indicative of the state of the art in the physics of large fast reactors. Several conclusions are drawn in the AEC evaluation of the four 1000-Mw(e) fast breeder reactors. It is stated in the evaluation that each of the four concepts could be used as the basis of a technically feasible design. A choice cannot yet be made between the mixed-carbide and mixed-oxide fuels because the potential advantages of the carbides depend on information yet to be obtained in development programs. Additional work that should be done prior to committing a 1000-Mw(e) ceramic-fueled fast breeder is outlined in the evaluation. Included are further preliminary designs and optimizations covering the entire plant, safety studies to establish criteria and to predict the course of accidents, physics studies to include cross-section measurements and integral experiments, fuel and materials development, and fuel-handling development.

References

1. Westinghouse Electric Corp., Atomic Power Division, 1000-Mw(e) Closed Cycle Water Reactor Study, Vol. I, USAEC Report WCAP-2385, March 1963.
2. Westinghouse Electric Corp., Atomic Power Division, 1000-Mw(e) Closed Cycle Water Reactor Study, Vol. II, USAEC Report WCAP-2385, March 1963.
3. A. L. Gaines and L. Porse, Problems in the Design and Construction of Large Reactor Vessels, presented at the Third United Nations International Conference on the Peaceful Uses of Atomic Energy, Geneva, 1964, Paper A/Conf.28/P/227.
4. J. C. Rengel, Project Manager, Large Closed-Cycle Water Reactor Research and Development Program, Progress Report for the Period December 1, 1960 to May 31, 1961, USAEC Report WCAP-3703, Westinghouse Electric Corp., Atomic Power Division.
5. J. C. Rengel, Project Manager, Large Closed-Cycle Water Reactor Research and Development Program, Progress Report for the Period June 1, 1961 to August 31, 1961, USAEC Report WCAP-3706, Westinghouse Electric Corp., Atomic Power Division.
6. N. R. Nelson, Project Manager, Large Closed-Cycle Water Reactor Research and Development Program, Progress Report for the Period September 1, 1961 to November 30, 1961, USAEC Report WCAP-3707, Westinghouse Electric Corp., Atomic Power Division.
7. N. R. Nelson, Project Manager, Large Closed-Cycle Water Reactor Research and Development Program, Progress Report for the Period December 1, 1961 to February 28, 1962, USAEC Report WCAP-3708, Westinghouse Electric Corp., Atomic Power Division.
8. N. R. Nelson, Project Manager, Large Closed-Cycle Water Reactor Research and Development Program, March 1, 1962 to June 30, 1962, USAEC Report WCAP-3710, Westinghouse Electric Corp., Atomic Power Division.
9. Westinghouse Electric Corp., Atomic Power Division, 1962. (Unpublished)
10. Westinghouse Electric Corp., Atomic Power Division, 1962. (Unpublished)
11. Westinghouse Electric Corp., Atomic Power Division, 1963. (Unpublished)
12. Westinghouse Electric Corp., Atomic Power Division, 1963. (Unpublished)
13. Westinghouse Electric Corp., Atomic Power Division, 1963. (Unpublished)
14. Westinghouse Electric Corp., Atomic Power Division, 1963. (Unpublished)
15. C. Roderick, Project Manager, Large Closed-Cycle Water Reactor Research and Development Program, Progress Report, January 1, 1964 to March 31, 1964, USAEC Report WCAP-3269-2, Westinghouse Electric Corp., Atomic Power Division.
16. D. E. Byrnes and W. E. Foster, Literature Values for Selected Chemical/Physical Properties of Aqueous Boric Acid Solutions, USAEC Report WCAP-1570, Westinghouse Electric Corp., Atomic Power Division, January 1961.
17. W. D. Fletcher, A. Krieg, and P. Cohen, The Behavior of Austenitic Stainless Steel Corrosion Products in High Temperature Boric Acid Solutions, USAEC Report WCAP-1689 (Rev.), Westinghouse Electric Corp., Atomic Power Division, May 1961.
18. P. Cohen and G. R. Taylor, Ion-Exchange with Equilibrium and Decay, USAEC Report WCAP-1700, Westinghouse Electric Corp., Atomic Power Division, January 1961.
19. A. N. Nahavandi and G. B. Killinger, Primary System Pressure Response Study Due to Power Unbalance (TOPS Code), USAEC Report WCAP-1831, Westinghouse Electric Corp., Atomic Power Division, September 1961.
20. L. S. Tong, H. B. Currin, and A. G. Thorp II, New DNB (Burnout) Correlations, USAEC Report WCAP-1997 (Rev. 2), Westinghouse Electric Corp., Atomic Power Division, May 1963.
21. J. E. Olhoeft, The Doppler Effect for a Non-Uniform Temperature Distribution in Reactor Fuel Elements, USAEC Report WCAP-2048, Westinghouse Electric Corp., Atomic Power Division, July 1962.
22. A. S. Kitzes, Design and Hazards Report, LRD Irradiation Test Number 1, USAEC Report WCAP-3701, Westinghouse Electric Corp., Atomic Power Division, July 15, 1963.
23. W. Zernik, H. B. Currin, E. Elyash, and G. Previti, "THINC," A Thermal Hydrodynamic Interaction Code for a Semi-Open or Closed Channel Core, USAEC Report WCAP-3704, Westinghouse Electric Corp., Atomic Power Division, February 1962.
24. R. A. Dannels and Dermot J. Bredin, Compilation of a Muft Library (Library 567), USAEC Report WCAP-3709, Westinghouse Electric Corp., Atomic Power Division, December 1962.
25. W. J. Eich, H. T. Williams, Jr., and H. Aisu, The Heterogeneous Representation of Control Rods in Light Water Lattices: A Comparison of Analysis and Experiment, USAEC Report WCAP-3711,

Westinghouse Electric Corp., Atomic Power Division.

26. D. E. Byrnes, Some Physicochemical Studies of Boric Acid Solutions at High Temperatures, USAEC Report WCAP-3713, Westinghouse Electric Corp., Atomic Power Division, September 1962.
27. J. S. Moore, and B. H. Axelson, Reactor Control and Protection System Study for Chemical Shim Operation of a Large Closed Cycle Water Reactor, USAEC Report WCAP-3714, Westinghouse Electric Corp., Atomic Power Division, October 1962.
28. W. D. Fletcher, Ion Exchange in Boric Acid Solutions with Radioactive Decay, USAEC Report WCAP-3716, Westinghouse Electric Corp., Atomic Power Division, November 1962.
29. R. E. Wolf and J. F. Noonan, RENEWED: A Program for Nuclear Reactor Fuel Cycle Analysis, USAEC Report WCAP-3717, Westinghouse Electric Corp., Atomic Power Division, November 1962.
30. D. L. Miller, Control Rod Programming in a Large Multiregion Core, USAEC Report WCAP-3719, Westinghouse Electric Corp., Atomic Power Division, October 1962.
31. P. G. Lacey, Reactivity Dependence Upon Moderator Temperature and Boron Concentration in Large PWR Cores Controlled by Chemical Shim, USAEC Report WCAP-3720, Westinghouse Electric Corp., Atomic Power Division, November 1962.
32. A. N. Nahavandi, B. H. Axelson, G. B. Killinger, and A. H. Killinger, A Digital Computer Analysis of Closed Cycle Water Nuclear Power Plant Start-Up Using Natural Circulation (THERMO-SYPHON Code) Vols. I and II, USAEC Report WCAP-3722, Westinghouse Electric Corp., Atomic Power Division, February 1962.
33. P. G. Lacey, Fine Structure Power Peaking in a Critical Experiment Mockup of a Chemical Shim Core, USAEC Report WCAP-3723, Westinghouse Electric Corp., Atomic Power Division, March 1963.
34. H. Aisu, R. F. Barry, and P. G. Lacey, Load Variation Restrictions in a Chemically Poisoned Large PWR Core, USAEC Report WCAP-3724, Westinghouse Electric Corp., Atomic Power Division, March 1963.
35. D. L. Miller, Control Rod Requirements in a Chemical Shim Core, USAEC Report WCAP-3727, Westinghouse Electric Corp., Atomic Power Division, August 1963.
36. L. F. Picone, The In-Pile Test of Chemical Shim, USAEC Report WCAP-3729, Westinghouse Electric Corp., Atomic Power Division, June 1963.
37. L. F. Picone, D. D. Whyte, and G. R. Taylor, Radiotracer Studies of Hideout at High Temperature and Pressure, USAEC Report WCAP-3731, Westinghouse Electric Corp., Atomic Power vision, June 1963.
38. L. E. Strawbridge and R. E. Wolf, Optimiz Study for Large Pressurized Water Reactor Cor USAEC Report WCAP-3733, Westinghouse El tric Corp., Atomic Power Division, Apr. 8, 19
39. R. A. Dean, Coolant Mixing in Open Lattice actor Cores, USAEC Report WCAP-3735, W inghouse Electric Corp., Atomic Power Divis August 1963.
40. EBWR Project Group, EBWR Test Reports MWT Operation), USAEC Report ANL-6703, gonne National Laboratory, January 1964.
41. Allis-Chalmers Mfg. Co., Atomic Power Devel ment Associates, Inc., and The Babcock & Wi Co., Large Fast Reactor Design Study, USA Report ACNP-64503, January 1964.
42. Combustion Engineering, Inc., Liquid Metal F Breeder Reactor Design Study, USAEC Rep CEND-200, Vols. I and II, January 1964.
43. General Electric Company, Atomic Power Eq ment Department, Liquid Metal Fast Breeder R actor Design Study, USAEC Report GEAP- Vols. I and II, January 1964.
44. R. B. Steck (Comp.), Liquid Metal Fast Bree Reactor Design Study, USAEC Report WCAP-3251-1, Westinghouse Electric Corp., Ato Power Division, January 1964.
45. David Okrent, Neutron Physics Considerations Large Fast Reactors, *Power Reactor Techno* 7(2): 107–137 (Spring 1964).
46. Chicago Operations Office, Reactor Engineer Division, An Evaluation of Four Design Studies a 1000-MWe Ceramic-Fueled Fast Breeder Reactor, USAEC Report COO-279, Dec. 1, 1964.
47. L. J. Koch, F. S. Kirn, G. W. Wensch, C. Branyan, and E. L. Alexanderson, Sodium Coo Fast Breeder Reactors, presented at the Thi United Nations International Conference on Peaceful Uses of Atomic Energy, Geneva, 19 Paper A/Conf.28/P/207.
48. David Okrent, K. P. Cohen, and W. B. Loewenstein, Some Nuclear and Safety Considerations the Design of Large Fast Power Reactors, presented at the Third United Nations Internation Conference on the Peaceful Uses of Atomic Energy, Geneva, 1964, Paper A/Conf.28/P/267.
49. Leonard E. Link, George J. Fischer, and Edw L. Zebroski, Fuel Cycle Economics of Fast Reactors, presented at the Third United Nations International Conference on the Peaceful Uses Atomic Energy, Geneva, 1964, Paper A/Conf. P/248.
50. C. E. Klotz and R. S. Miller, The Design of 1000 MWe Fast Breeder Reactor, *Trans. Am. Nucl. Soc.*, 7(1): 196 (June 1964).
51. L. S. Noderer and Sidney Visner, Effect of Voided Gap on Reactivity Coefficient for Voiding Core Sodium in a Fast Reactor, *Trans. Am. Nucl. Soc.*, 7(2): 238 (November 1964).

LEGAL NOTICE

This journal was prepared under the sponsorship of the U. S. Atomic Energy Commission. Neither the United States, nor the Commission, nor any person acting on behalf of the Commission:

A. Makes any warranty or representation, expressed or implied, with respect to the accuracy, completeness, or usefulness of the information contained in this journal, or that the use of any information, apparatus, method, or process disclosed in this journal may not infringe privately owned rights; or

B. Assumes any liabilities with respect to the use of, or for damages resulting from the use of any information, apparatus, method, or process disclosed in this journal.

As used in the above, "person acting on behalf of the Commission" includes any employee or contractor of the Commission, or employee of such contractor, to the extent that such employee or contractor of the Commission, or employee of such contractor prepares, disseminates, or provides access to, any information pursuant to his employment or contract with the Commission, or his employment with such contractor.

NUCLEAR SCIENCE ABSTRACTS

The U. S. Atomic Energy Commission, Division of Technical Information, publishes *Nuclear Science Abstracts (NSA)*, a semimonthly journal containing abstracts of the literature of nuclear science and engineering.

NSA covers (1) research reports of the U. S. Atomic Energy Commission and its contractors; (2) research reports of government agencies, universities, and industrial research organizations on a world-wide basis; and (3) translations, patents, books, and articles appearing in technical and scientific journals.

Complete indexes covering subject, author, source, and report number are included in each issue. These are cumulated quarterly, semiannually, and annually providing a detailed and convenient key to the literature.

Availability of *NSA*

SALE *NSA* is available on subscription from the Superintendent of Documents, U. S. Government Printing Office, Washington, D. C., 20402, at $30.00 per year for the semimonthly abstract issues and $22.00 per year for the four cumulated-index issues. Subscriptions are postpaid within the United States, Canada, Mexico, and all Central and South American countries, except Argentina, Brazil, British and French Guiana, Surinam, and British Honduras. Subscribers in these Central and South American countries, and in all other countries throughout the world, should remit $37.00 per year for subscriptions to semimonthly abstract issues and $25.00 per year for the four cumulated-index issues.

EXCHANGE *NSA* is also available on an exchange basis to universities, research institutions, industrial firms, and publishers of scientific information. Inquiries should be directed to the Division of Technical Information Extension, U. S. Atomic Energy Commission, P. O. Box 62, Oak Ridge, Tennessee, 37831.

TECHNICAL PROGRESS REVIEWS may be purchased from Superintendent of Documents, U. S. Government Printing Office, Washington, D. C., 20402. *Isotopes and Radiation Technology* at $2.00 per year for each subscription or $0.55 per issue; the other four journals at $2.50 per year and $0.70 per issue. The use of the coupon below will facilitate the handling of your order.

POSTAGE AND REMITTANCE: Postpaid within the United States, Canada, Mexico, and all Central and South American countries except as hereinafter noted. Add $0.50 per year, or $0.15 per single issue for the *Isotopes and Radiation Technology* journal and $0.75 per year or $0.20 per single issue for the other four journals for postage to all other countries, including Argentina, Brazil, British and French Guiana Surinam, and British Honduras. Payment should be by check, money order, or document coupons, and MUST accompany order. Remittances from foreign countries should be made by international money order, or draft on an American bank, payable to the Superintendent of Documents, or by UNESCO book coupons.

order form

SUPERINTENDENT OF DOCUMENTS
U. S. GOVERNMENT PRINTING OFFICE
WASHINGTON, D. C., 20402

Enclosed:
document coupons ☐ check ☐ money order ☐

Charge to Superintendent of Documents No. __________

Please send a one-year subscription to

☐ NUCLEAR SAFETY
☐ POWER REACTOR TECHNOLOGY
☐ REACTOR FUEL PROCESSING
☐ REACTOR MATERIALS

(Each subscription $2.50 per year; $0.70 per issue.)

☐ ISOTOPES AND RADIATION TECHNOLOGY

(Each subscription $2.00 a year; $0.55 per issue.)

SUPERINTENDENT OF DOCUMENTS
U. S. GOVERNMENT PRINTING OFFICE
WASHINGTON, D. C., 20402

(Print clearly)

Name ______________________________

Street ______________________________

City ____________________ Zone ____ State _____

Phil

POWER REACTOR TECHNOLOGY

THE UNIVERSITY
OF MICHIGAN
OCT 27 1965
PHOENIX
LIBRARY

A Quarterly Technical Progress Review

Prepared by DIVISION OF TECHNICAL INFORMATION, USAEC,
in cooperation with COMBUSTION ENGINEERING, INC., NUCLEAR DIVISION

Summer 1965

● VOLUME 8

● NUMBER 3

TECHNICAL PROGRESS REVIEWS

To meet the needs of industry for concise summaries of current atomic developments, the Atomic Energy Commission is publishing this series, Technical Progress Reviews. Issued quarterly, each of the reviews digests and evaluates the latest findings in a specific area of nuclear technology and science.

The five journals published in this series are:

Isotopes and Radiation Technology, P. S. Baker, A. F. Rupp, and associates, Oak Ridge National Laboratory

Nuclear Safety, Wm. B. Cottrell, W. H. Jordan, and associates, Oak Ridge National Laboratory

Power Reactor Technology, formerly prepared and edited by W. H. Zinn and J. R. Dietrich, Nuclear Division, Combustion Engineering, Inc. (a new contractor will take over preparation of this journal beginning with Vol. 8, No. 4).

Reactor Fuel Processing, Stephen Lawroski and associates, Chemical Engineering Division, Argonne National Laboratory

Reactor Materials, R. W. Dayton, E. M. Simons, and associates, Battelle Memorial Institute

Each journal may be purchased from the Superintendent of Documents, U. S. Government Printing Office, Washington, D. C., 20402. *Isotopes and Radiation Technology* at $2.00 per year for subscription or $0.55 for individual issues; the other four journals at $2.50 per year and $0.70 per issue. See back cover for remittance instructions and foreign postage requirements.

The views expressed in this publication do not necessarily represent those of the United States Atomic Energy Commission, its divisions or offices, or of any Commission advisory committee or contractor.

Availability of Reports Cited in This Review

Unclassified AEC reports are available for inspection at AEC depository libraries and are sold by the Clearinghouse for Federal Scientific and Technical Information, National Bureau of Standards, U. S. Department of Commerce, 5285 Port Royal Road, Springfield, Va., 22151. Some of the reports cited are not available owing to their preliminary nature; however, the information contained in them will eventually be made available in formal progress or topical reports.

Unclassified reports issued by other Government agencies or private organizations should be requested from the originator.

Unclassified British and Canadian reports may be inspected at AEC depository libraries. British reports are sold by the British Information Service, 45 Rockefeller Plaza, New York, N. Y.; Canadian reports (AECL series) are sold by the Scientific Document Distribution Office, Atomic Energy of Canada, Ltd., Chalk River, Ontario, Canada.

Classified U. S. and foreign reports identified in this journal as Classified may be purchased by properly cleared Access Permit Holders from the Division of Technical Information Extension, U. S. Atomic Energy Commission, P. O. Box [illegible], Oak Ridge, Tenn., 37831. Such reports may be inspected at classified AEC depository libraries.

POWER
REACTOR
TECHNOLOGY

A REVIEW OF RECENT DEVELOPMENTS

Prepared by DIVISION OF TECHNICAL INFORMATION, USAEC,
in cooperation with
COMBUSTION ENGINEERING, INC., NUCLEAR DIVISION

SUMMER 1965

VOLUME 8

NUMBER 3

Foreword

This is an interim quarterly review assembled by the Division of Technical Information, U. S. Atomic Energy Commission, from material supplied by Combustion Engineering, Inc., prior to the termination, at their request, of their contract to prepare the review. A new contractor will assume responsibility for the preparation of *Power Reactor Technology* beginning with the Fall issue, Vol. 8, No. 4.

Power Reactor Technology contains reviews of selected recently published reports that are judged noteworthy in the fields of power-reactor research and development, power-reactor applications, design practice, and operating experience. It is not meant to be a comprehensive abstract of all material published during the quarter, nor is it meant to be a treatise on any part of the subject. However, related reports from different sources are often treated together to yield reviews having some breadth of scope, and background material may be added to place recent developments in perspective. Occasionally the reviews are written by guest authors. Reviews having unusual breadth or significance are placed at the front of the issue as Feature Articles.

The intention is to cover the various areas of reactor development from the general viewpoint of the reactor designer rather than from the more detailed points of view of specialists in the individual areas. To whatever extent the coverage of *Power Reactor Technology* may occasionally overlap the fields of the other Technical Progress Reviews, the overlaps will be motivated by this objective of viewing current progress through the eyes of the reactor designer.

A degree of critical appraisal and some interpretation of results are often necessary to define the significance of reported work. Any such appraisal or interpretation represents only the opinion of the reviewer. Readers are urged to consult the original references to obtain all the background of the work reported and to obtain the interpretation of the results given by the original authors.

For timely coverage, *Power Reactor Technology* must often review fragmentary material. The fixed subject headings listed below have been adopted in the hope of maintaining some continuity and order in the material from one issue to another; all reviews except Feature Articles will be arranged under these headings. A particular issue will not necessarily contain all the headings but only those under which material is reviewed.

Economics, Applications, Programs
Resources and Fuel Cycles
Physics
Fluid and Thermal Technology
Fuel Elements
Materials
Control and Dynamics
Containment, Radiation Control, and Siting
Systems Technology
Components
Design and Construction Practice
Operating Experience
Specific Reactor Types
Specific Applications
Unconventional Approaches

U. S. Atomic Energy Commission
Division of Technical Information

DEPOSITED BY THE
ED STATES OF AMERICA

Contents

I Physics 157
Measurements on Operating Reactors . . 157
Resonance Absorption 159
Heterogeneous Graphite-Moderated Reactors 160
Reduced-Delayed-Neutron-Group Representation 161
References 162

II Fluid and Thermal Technology . . . 163
Liquid Metals 163
Two-Phase Systems 164
References 170

III Fuel Elements 172
Fuel-Performance Evaluations 172
Incoloy 800 Cladding. 174
References 175

IV Components 176
Liquid-Metal-Level Probes 176
Pressure-Tube Fretting Corrosion . . . 177
References 182

V Specific Reactor Types 183
Sodium-Graphite Reactors: Steam Cycles 183
Reference 185

VI Unconventional Approaches . . . 186
Fast Supercritical Water Reactor . . . 186
Hanford Graphite Superheat Reactor . . 193
References 198

NOTE: The Commission regrets to announce that, at the request of Combustion Engineering, Inc., their contract to prepare *Power Reactor Technology* has been terminated. This issue was assembled by the AEC Division of Technical Information from material supplied by Combustion prior to the time the contract expired. A new contractor, Argonne National Laboratory, will assume responsibility for preparation of *Power Reactor Technology* beginning with Vol. 8, No. 4, and the distribution of that issue will be delayed. Please direct any communications regarding this issue to the USAEC Division of Technical Information, Washington, D. C., 20545.

Issued quarterly by the U. S. Atomic Energy Commission. Use of funds for printing this publication approved by the Director of the Bureau of the Budget on October 14, 1963.

Section I

Physics

Power Reactor Technology

Measurements on Operating Reactors

On installation of the second core in the Sodium Reactor Experiment (SRE), a test program was initiated to develop and evaluate techniques for measuring the nuclear parameters of the core and for checking core stability. An objective of this program is to make possible reliable interpretation of measured changes in control-rod positions in terms of reactivity values. A method of monitoring for abnormal behavior would then be available from the comparison of calculated and measured reactivity variations. References 1 and 2 describe some of the work directed toward this purpose.

Reference 1 presents test results that show the feasibility of a technique developed for calibrating shim rods during normal reactor power operation. When compared with other rod-calibration methods that have been used in the past, the new technique is said to have the following advantages: (1) increased plant availability, (2) elimination of operational hazards, (3) use of inexpensive equipment, and (4) elimination of special devices to drive the control rod or elimination of the need for a pile oscillator within the core. The technique utilizes an analog computer that is programmed to simulate the reactor. Six groups of delayed neutrons with a fuel-temperature feedback loop are included in the simulation. For a rod-calibration measurement, the reactor flux is manually cycled by moving the shim rod in equal increments about the critical position. A signal is taken from the shim-rod position indicator and is scaled with a potentiometer to give the shim-rod differential worth, which becomes the reactivity input for the computer. The computer output is the simulated-reactor-flux signal. The differences in actual reactor flux and simulated reactor flux are recorded on a strip chart. The shim-rod differential worth is given by the setting of the shim-rod-worth potentiometer, which results in agreement of the computer-flux response with the actual reactor-flux response. In practice the fuel-temperature feedback constants in the simulation circuit are adjusted until the system indicates the same differential rod worth for all frequencies of rod travel. Results of tests at 12 Mw(t) show that rod worths can be determined within ±5% of the true value. This compares with resolutions of ±2% obtained at zero power with normal period-measurement techniques. Reactor-flux noise was an important limiting factor to the attainment of higher accuracy with the on-line shim-rod-calibration technique.

Reference 2 describes the experiments performed to obtain the reactivity coefficients of core 2 of the SRE. From the results of transfer-function measurements at 10, 15, and 20 Mw(t), it was clearly demonstrated that the positive prompt power coefficient associated with fuel-rod bowing was eliminated when the clusters were constrained to prevent bowing. Through analyses of the reactivity variations introduced by a flow ramp and an inlet temperature ramp, the combined fuel-and-coolant temperature coefficient and the inlet temperature coefficient were determined. The combined coefficient was found to be −0.12 cents/°F, a value that agrees very well with the sum of the calculated Doppler and coolant coefficients. A simple lag model was used in the analysis of the inlet-temperature-ramp data. Although good agreement with calculations was obtained, it is recognized that the simple model used is not entirely adequate because the slow change in inlet temperature used in the experiment results in interactions with the reactivities associated with core temperatures. Other pertinent measurements are described, e.g., shim-rod calibrations, xenon transient, and isothermal core temperature.

Reference 3 presents the results of a number of performance tests conducted at the Plutonium Recycle Test Reactor to investigate the operating characteristics of the plutonium-fueled D_2O-moderated reactor. The test results were obtained during initial operation with a three-zone configuration comprising natural UO_2 elements in the central region surrounded by an annulus of plutonium-aluminum elements and an outer region of UO_2 elements. Reactor refuelings to compensate for burnup were made by charging fresh plutonium-aluminum elements in the intermediate zone. When a steady-state loading was finally achieved, the intermediate plutonium-aluminum zone was somewhat expanded, as compared to the initial loading, at the expense of a reduced central zone of the UO_2 elements. Measurements were made of the change in reactivity with fuel burnup. The rate of loss of reactivity per unit of energy production increased with the inventory of plutonium in the reactor, as expected from the results of diffusion-theory perturbation calculations. As the steady-state loading was approached, the fraction of the total core fissions rate due to the plutonium was about 55%.

Measurements were made of the radial power distribution by computing individual tube power outputs from flow and temperature-rise data; data are presented for exposures of 0, 1000, and 2000 Mwd. As a result of the method of charging the plutonium-aluminum elements in the intermediate zone of the three-zone core (outside-in method), the radial power flattening improved with increasing exposure.

Measurements of the photoneutron flux were observed to decay at a rate determined by a fission-product decay curve derived from the work of Perkins and King;[4] the curve represented a simulation of the decay rate of gamma flux from the emitters giving gammas of energy greater than 2.2 Mev, the threshold energy for the (γ,n) reaction in deuterium. Measurements of the shim-rod worths, using the partial water-height method, showed decreasing total worth as operation of the reactor progressed to the steady-state three-zone fuel loading, i.e., as the plutonium-fission ratio increased. Random-noise techniques were used to measure the reactor transfer function and thus to obtain β/l. The measurements indicated a decrease in β/l as the plutonium inventory in the reactor was increased. The combined fuel-plus-coolant temperature coefficient and the moderator temperature coefficient were observed to become much less negative as the plutonium inventory was increased during the approach to the steady-state configuration. A contributing factor to the decreases in negative temperature coefficients was the gradual degradation of the primary coolant from 99.75% to 95% D_2O during the course of reactor operation. The decreases in negative coefficient values were not considered large enough to affect reactor safety.

References 5 and 6 report on the recent successful operation of the Experimental Breeder Reactor No. 1 (EBR-I) with a plutonium loading (Mark IV). The results of a stability analysis, based essentially on transfer-function and power-coefficient measurements, are presented in Ref. 5, wherein it is noted that there is nothing inherently unsafe or dangerous in the operation of a plutonium-fueled system. The results of breeding-gain measurements, which demonstrate directly the superiority of plutonium as a fuel, are treated in Ref. 6.

Oscillator-rod measurements were conducted on EBR-I, Mark IV, to obtain the zero-power and load-power transfer functions. From the transfer functions a separation was made of the reactivity feedback corresponding to the various reactor power levels and inlet coolant temperatures. Reference 5 describes the reactivity-feedback function by a mathematical model characterized by the following two terms: (1) prompt, small, and associated primarily with power changes in the fuel (axial expansion of fuel, NaK expulsion, radial expansion of the Zircaloy jackets, fuel-slug bowing, and jacket bowing); and (2) relatively delayed, strong, and associated with expansion effects in the coolant, structure, and upper portion of the blanket region. Substitution of the experimental data into the mathematical model results in a set of time constants and power coefficients that adequately describes the experimentally derived reactivity-feedback function for a given set of operating conditions. In all cases the values of the fitted time constants are consistent with values estimated from heat-transfer considerations.

The fitted power-coefficient values for the delayed term greatly exceed the corresponding values established for the prompt fuel

:pansion term. This empirical result is sur-·ising and is attributed to slug-bowing effects at cancel nearly all the usual prompt negative fects. That slug bowing is an important echanism is also indicated by the static mea-ırements of the power coefficient. Insofar as .e stability and safety of the system are con-ərned, it is concluded that the effects of slug)wing are not particularly important. In all ıses studied the overall power coefficient as strongly negative and was still sufficiently ıpid in action to prevent strong reinforce-.ent of input and feedback reactivities. Changes ı coolant inlet temperature were found to :fect strong changes in the feedback, appar-ıtly a consequence of temperature-sensitive learances.

Reference 5 concludes that, in general, a ystem fueled with plutonium would tend to be ıore sensitive to reactivity perturbations than ne fueled with uranium. For a feedback that einforces the input, the neutron kinetics are uch that the system tends to be less stable :elative to ^{235}U fuel). However, for a feedback ıat cancels a portion of the input, the system 'ould tend to be more stable. Hence, if slug-owing and rod-bowing effects could be elimi-ated, it is possible that the kinetic behavior f a plutonium-fueled system would be more table than that of its ^{235}U-fueled counterpart.

The experimental methods used for the reeding-gain measurements on EBR-I, Mark V, are described in detail in Ref. 6. The ıethod is based on integration of the various ission and capture patterns over the system olume. The mapping technique requires ob-ervation of activities generated in thin metallic oils of uranium and plutonium inserted in the ore and blanket regions of the assembly. The :ounting operations for the various types of oils and the operations involved in the organi-:ation of the counting data for integration pur-ıoses are described. Spatial distributions were :stablished for plutonium, ^{235}U, and ^{238}U fis-ıions and captures. It should be noted that ;pecific measurements of captures in plutonium ınd ^{235}U were not carried out on the Mark IV oading. Instead, use was made of the results ıf measurements by Kafalas et al.,[7] who estab-.ished values of α for ^{239}Pu and ^{235}U as a func-:ion of radial distance and elevation in a ^{235}U-:ueled loading in EBR-I.

The breeding ratio is defined as the ratio of ^{239}Pu and ^{241}Pu production to ^{235}U, ^{239}Pu, and ^{241}Pu destruction. The value of breeding ratio arrived at from the measurements is 1.27 ± 0.08. This value demonstrates the importance of ^{239}Pu as a fast reactor fuel since earlier measurements of the conversion ratio of essentially the same system fueled with ^{235}U gave values of the order of unity. The marked increase is directly attributable to a much higher value of ν for ^{239}Pu and a much lower value of α. The results also indicate the beneficial aspects of threshold fissions in ^{238}U and ^{240}Pu. Reference 5 concludes that the results obtained provide tangible proof that a reactor fueled with ^{239}Pu can produce useful power and regenerate substantially more fuel than is consumed.

Resonance Absorption

In the case of isolated rods in the *NR-NR* approximation, collision theory yields

$$RI = \int \left[P_0 \frac{\sigma_p}{\sigma_0} + (1 - P_0)\right] \sigma_a \, dE/E$$

where σ_0, σ_a, and σ_p are the total, absorption, and potential scattering of the fuel, and P_0 is the nonescape probability from the fuel region. If the Wigner rational approximation is used, i.e.,

$$P_0 = \frac{x}{1 + x}$$

where x is the average optical chord length of the rod for a given energy, then the heterogeneous resonance integral is equivalent to the homogeneous resonance integral in which a new potential scattering is defined as

$$\sigma_p' = \sigma_p + \frac{\sigma_0}{x}$$

Reference 8 investigates the use of three better approximations to P_0 that are rational forms in x, namely:

1. From Booth,

$$P_0 = \frac{x(x + c)}{(x + b)^2}$$

2. From Carlvik and Fukai,

$$P_0 = \frac{2x}{x + 2} - \frac{x}{x + 3}$$

3. From Sauer,

$$P_0 = 1 - \frac{1}{x}\left[1 - \left(1 + \frac{x}{n+1}\right)^{-(n+1)}\right]$$

by comparison with the exact escape probabilities.

None of these methods can easily take into account differences in resonance parameters. Reference 9 considers the exact escape probability

$$P_0(x) = 1 - P_0(x) = \left[1 + \frac{x}{A(x)}\right]^{-1}$$

and obtains an average

$$\overline{A} = \frac{1}{I}\int_{-\infty}^{\infty} A\, dI$$

where *I* is the effective resonance integral for a particular resonance. Because the Doppler effect in each resonance is not proportional to its resonance integral, the use of the same relation for P_0 for a series of resonances in ^{238}U, for example, could lead to relatively large errors in temperature coefficients.

A form of the Dancoff factor based on cell calculations with white boundaries—i.e., all neutrons striking the cell boundary are returned with a cosine azimuthal distribution and do not follow the laws of specular reflection—is shown, in Ref. 8, to lead to results in good agreement with Monte Carlo calculations. The paper also justifies the use of the white-boundary condition on theoretical grounds.

Heterogeneous Graphite-Moderated Reactors

A design calculation method for gas-cooled graphite-moderated reactors has been coded in FORTRAN II in the ARGOSY program.[10] The principal approximations are:

1. Spatial effects in fuel and moderator are ignored, and mean fuel and mean moderator effects only are evaluated.

2. The generalized heavy-gas approximation is used to treat neutron thermalization.

3. Resonance integrals are not evaluat the method but are obtained (in the case of from tabular data.

Three energy groups with upper-energy cu of 4 ev, 10 kev, and 10 Mev are used.

Thermal-Group Calculation

A three-region cylindrical cell, with structure within the fuel region reduced simple flux-weighting factors, is used about 100 energy points. An interpolatio tween narrow and wide resonance theor used to compute fluxes through the pluton resonance range. The thermalization in b fuel and moderator is approximated by operator

$$L\phi = \xi\Sigma_s\, d/dx\{f(x)\,[x\phi'(x) + (x-1)\phi(x)]\} \qquad (x = E$$

where *f(x)* is adjusted for crystal-binding fects as a function of plutonium concentrat and moderator temperature. The coupled and moderator equations are integrated us a finite-difference scheme.

Resonance-Group Calculation

Tabular values for the ^{238}U effective res nance integral as a function of fuel temperat and σ_{ex} are utilized.

$$\sigma_{ex} = \frac{\gamma S_{eff}}{4N_{238}\overline{V}_{fuel}}$$

where γ is a factor to correct for inaccura in the normal Wigner rational approxima and S_{eff} is the effective surface of the fuel el ment or cluster. These tables were made uranium oxide and metal by considering each resonance the proper mixture of narr and wide resonance for potential scatter cross sections of uranium and oxygen. F ^{235}U and ^{239}Pu resonances, the infinite res nance integrals are reduced by factors all ing for self-shielding and shielding by other isotopes. These can reduce the dil values by about 20%. The spectrum in group is not calculated, but effects of other sorbers are taken into account.

ast-Group Calculation

A collision-probability approach is used in btaining reaction rates in fuel and moderator or each of three energy subgroups where a patially flat fission source in the fuel is asumed. This yields flux-weighted capture, fision, and removal cross sections. Diffusion oefficients for all groups are modified by treaming factors in the radial and axial irections.

Point core criticality can be achieved through hanges in leakage, absorption, or fission ource. Equivalent control-rod cross sections re evaluated by determining the extrapolation istance from blackness coefficients as a funcion of energy. A simple point burnup calculaion can also be performed. The IBM-7090 ime required for a complete calculation inluding burnup is about 5 min.

Reduced-Delayed-Neutron-Group Representation

In the analysis of the dynamic behavior of a eactor, considerable simplification results rom the use of a reduced number of delayed-eutron groups, often with little sacrifice in ccuracy. The selection of the reduced-group arameters (delayed-neutron yield and decay onstant) generally depends on the type of ransient being investigated. Reference 11 deelops a reduced-group model chosen so that he resulting representation matches the rector transfer function exactly in the limit of oth very-low and very-high frequency. This equirement leads to the so-called "asymptotic" representation, the parameters for which re obtained from the following relations:

$$\sum_{j=1}^{m} \beta_j = \sum_{i=1}^{n} \beta_i \tag{1}$$

$$\sum_{j=1}^{m} \beta_j \lambda_j = \sum_{i=1}^{n} \beta_i \lambda_i \tag{2}$$

$$\sum_{j=1}^{m} \frac{\beta_j}{\lambda_j} = \sum_{i=1}^{n} \frac{\beta_i}{\lambda_i} \tag{3}$$

$$\sum_{j=1}^{m} \frac{\beta_j}{\lambda_j^2} = \sum_{i=1}^{n} \frac{\beta_i}{\lambda_i^2} \tag{4}$$

where β = delayed-neutron yield
λ = decay constant
i = group index of the physical-decay groups
n = number of the physical-decay groups
j = group index of the reduced groups
m = number of the reduced groups

Equations 1 and 2 result from matching the transfer function in the high-frequency limit, and Eqs. 3 and 4 result from matching the low-frequency limit. The equations as given hold for any number of reduced groups, but at least two groups must be used to satisfy all four conditions.

In some cases it is necessary to represent a particular group explicitly, for example, the longest lived group in cases where reactor shutdown is of interest or the shortest lived group for very rapid transients. In such a case the remaining groups are selected to satisfy Eqs. 1 to 4. Reference 12 contains a compilation of reduced-group parameters for various fissile isotopes with one reduced group (Eqs. 1 and 3), two groups (Eqs. 1 to 4), and three groups (Eqs. 1 to 4 with either the longest or shortest lived delay group represented explicitly).

Reference 13 reports a method of obtaining reduced-delay-group parameters by a least-squares fit. The parameters are chosen such that the integral

$$\int_{\omega} \left\{ 1 - \frac{\mathrm{Re}\,[F(j\omega)]}{\mathrm{Re}\,[G(j\omega)]} \right\}^2 d \ln \omega$$

is minimized where $G(j\omega)$ is the transfer function with all six delay groups and $F(j\omega)$ is the transfer function with the reduced groups. Results for two, three, and four reduced groups are tabulated for all fissile isotopes with the least-squares fit over a range of frequencies (ω) of 0.001 to 10 radians/sec. A comparison of the reduced-group parameters obtained from the asymptopic and the least-squares approach as determined in Ref. 13 is given in Table I-1. In addition, Ref. 13 compares calculations of both the reactor transfer function and the reactor response to positive- and negative-

reactivity steps with the reduced-group models and the full six-delay-group model.

Table I-1 COMPARISON OF REDUCED-DELAYED-NEUTRON-GROUP PARAMETERS FOR ^{235}U (THERMAL FISSION)[13]

	Asymptotic	Least squares
Two groups		
λ_1	0.0252	0.0410
λ_2	0.566	0.540
β_1	0.00194	0.00293
β_2	0.00459	0.00360
Three groups (longest lived group isolated)		
λ_1	0.0124	0.0124 (0.0278)*
λ_2	0.0342	0.0512 (0.0231)
λ_3	0.609	0.590 (1.568)
β_1	0.00022	0.00022 (0.00185)
β_2	0.00263	0.00299 (0.00364)
β_3	0.00367	0.00332 (0.00104)

*Three-groups straight least-squares fit.

References

1. E. A. Moore and C. L. Peckinpaugh, On-Line Shim Rod Calibration, USAEC Report NAA-SR-9511, Atomics International, Aug. 1, 1964.
2. M. R. Pellet, Core II Physics Tests on the Sodium Reactor Experiment, USAEC Report NAA-SR-9510, Atomics International, Aug. 1, 1964.
3. V. W. Gustafson, Plutonium Recycle Test Reactor Power Test Results, USAEC Report HW-80253, Hanford Atomic Products Operation, December 1963.
4. J. F. Perkins and R. W. King, Energy R from the Decay of Fission Products, *Nucl.* *Eng.*, 3(6): 726-746 (June 1958).
5. R. R. Smith, R. O. Haroldsen, and F. D. McG Stability Considerations for a Plutonium L in EBR-I, USAEC Report ANL-6863, Ar National Laboratory, May 1964.
6. R. R. Smith, R. O. Haroldsen, R. E. Horne, R. G. Matlock, The Breeding Ratio of a P nium Loading in EBR-I, USAEC Report A 6789, Argonne National Laboratory, Febr 1964.
7. P. Kafalas et al., Determination of the Ra Capture to Fission Cross Sections in EB *Nucl. Sci. Eng.*, 2(5): 657 (September 1957
8. D. C. Leslie, J. G. Hill, and A. Jonsson, I provement to the Theory of Resonance Es in Heterogeneous Fuel. 1. Regular Arrays Fuel Rods, British Report AEEW-R-353, 19
9. J. M. Otter, Escape Probability Approxima in Lumped Resonance Absorbers, USAEC R NAA-SR-9744, Atomics International, Au 1964.
10. J. G. Tyror, A Method of Lattice Calculatio Gas-Cooled Graphite-Moderated Reactors, B ish TRG-Report-754(W), 1964.
11. R. E. Skinner and E. R. Cohen, Reduced Del Neutron Group Representations, *Nucl. Sci. E* 5(5): 291-298 (May 1959).
12. R. W. Albrecht and C. Metelmann, The Us Reduced Delayed Neutron Group Representat in Nuclear Reactor Simulation, USAEC Rep HW-81076, Hanford Atomic Products Operat March 1964.
13. T. E. Springer, Delayed Neutron Reduced Gr by Least Squares, USAEC Report LA-308 Alamos Scientific Laboratory, December 196

Section

II

Power Reactor Technology

Fluid and Thermal Technology

iquid Metals

eferences 1 and 2 are literature reviews of the gineering properties of various liquid metals. ey contain data on properties such as density, ermal conductivity, electrical resistivity, spe-fic heat, surface tension, vapor pressure, and scosity for metals such as mercury, sodium, dium-potassium, potassium, rubidium, and thium. Reference 1 is directed specifically to quid-metal heat transfer by forced convection d presents a comparison of theoretical and perimental results. The report presents “rec-nmended” equations suitable for the engineer-g calculation of heat transfer in fully devel-ed turbulent flow in circular tubes, heat ansfer in fully developed turbulent flow through bes of noncircular cross section, and heat-ansfer-coefficient correlations for flow par-lel to bundles of circular rods and across a aggered tube bank. The discrepancies between perimental and theoretical results are dis-ssed, and several reasons for the discrepan-es are suggested.

Data on forced-convection heat transfer and ressure drop for boiling potassium are given Ref. 3. The particular system considered in e reference is quite specialized in that the xperiments were done to obtain design data r a potassium boiler constructed of serpen-ne tubes. Nevertheless, the reference gives sight into the difficulties of experimentation ith liquid metals and the techniques employed determine heat-transfer coefficients in rather omplex systems. Figure II-1 illustrates the rced-convection local-boiling heat-transfer oefficients for potassium boiling inside ser-entine tubes. The figure shows the “best-fit” orrelation. The data, which show considerable catter, are not reproduced here, but are given in Ref. 3. The range of experimental parameters is shown in Table II-1.

It is interesting to note that the stability of the boiling loop proved to be a continuing problem in the experiments. The loop, which was constructed of Haynes 25 alloy, consisted of a preheater, a test boiler, a superheater, and an air-cooled condenser, coupled with an electromagnetic flowmeter and pump. Much of the instability problem was said to originate in the preheater-preboiler portion of the loop as the result of subcooled nucleate boiling, despite the fact that a rather large pressure drop was established by use of a throttle valve just downstream of the electromagnetic pump. The authors conclude that the stability of two-phase

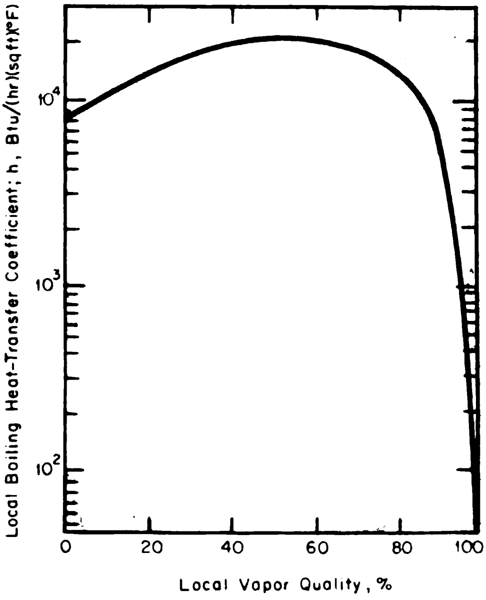

Fig. II-1 Forced-convection local-boiling heat-transfer coefficients for potassium inside a serpentine tube.[3]

Table II-1 RANGE OF EXPERIMENTAL PARAMETERS IN BOILING POTASSIUM EXPERIMENT[3]

Potassium flow rate, lb/hr	17 to 25
Vapor quality, %	0 to 100
Boiling ΔT, °F	2 to 170
Boiling temperature, °F	1625 to 1725
Heat flux in test boiler, Btu/(hr)(sq ft)	17,000 to 52,000
Max. heat flux in preboiler	64,000
Boiling pressure, psia	42 to 62
Max. vapor velocity, ft/sec	330
Test duration, hr	3625
Boiling hours	980

potassium systems cannot be studied by simulation with water or other common fluids. The pressure-drop data taken during the experiments were found to correlate within ±20% by the Lockhart-Martinelli correlation.

Reference 4 presents data on the boiling-heat-transfer coefficients and burnout heat fluxes for pool boiling of sodium. The reference describes in some detail two sodium loops, the larger of which accommodates an instrumented electric heating element on which accurate surface-temperature measurements can be made at heat fluxes up to 10^6 Btu/(hr)(sq ft) in boiling sodium. The test-section portion of this large loop, called the "working loop" in Ref. 4, is fabricated of graphite, electrically insulated with a boron nitride sleeve. The test section, which is heated by the resistance of the graphite, is capable of working to the heat flux of 10^6 Btu/(hr)(sq ft); a second test section heated by electron bombardment is being developed to extend the heat flux limit to 5×10^6 Btu/(hr)(sq ft). The data recorded in Ref. 4 on heat-transfer coefficients and burnout heat flux are of a preliminary nature but nevertheless would be of interest to the specialist.

Reference 5 reports on the determination of void fractions, slip ratios, and flow rates for liquid-vapor metal systems in pipes under critical-flow conditions. The Fauske model is applied to calculate the void fraction, the slip ratio, and the two-phase critical flow rates for mercury, cesium, rubidium, potassium, sodium, and lithium under the postulate that the mechanisms causing critical flow in the liquid-vapor systems are the same as in steam-water systems. Figure II-2 illustrates, for example, the theoretical prediction of the slip ratio for rubidium under critical-flow conditions. According to Ref. 5, no experimental data exist pertinent to the critical flow of liquid metals; it is therefore not possible to compare the theoretical predictions with experimental results.

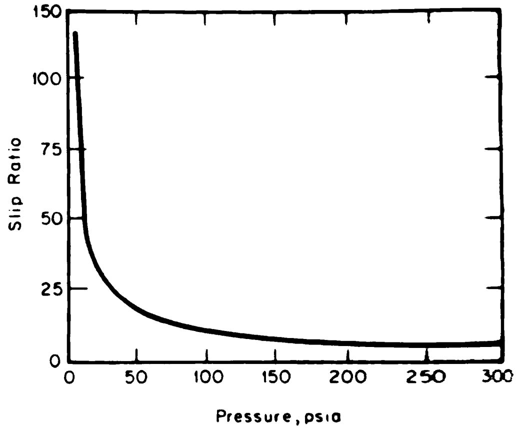

Fig. II-2 Theoretical prediction of slip ratio for rubidium under critical-flow conditions.[5]

Two-Phase Systems

The relatively large volume of literature pertinent to two-phase flow indicates continued interest in the associated phenomena. Reference 6 is an extensive annotated bibliography on the heat transfer and hydraulics of gas-liquid systems. A total of 2843 documents are cited in the bibliography, and the subjects covered represent a wide range of interests. These include such items as the critical heat flux, flow patterns, nozzles, phase and velocity distribution, pressure drops, separation of mixtures, transients and instability, turbulent flow, and visual observations. The references were published between 1950 and 1962 in *Nuclear Science Abstracts, Chemical Abstracts, Science Abstracts — Section A, Engineering Index*, and *Applied Mechanics Reviews*. It is believed that the volume will prove to be a valuable asset to workers in the field of two-phase hydraulics and heat transfer.

References 7 to 12 are somewhat specialized and will not be reviewed in detail. The consideration of the group as a whole, however, indicates the basic lines of attack in attempts to discover basic information on two-phase flow and heat transfer. References 7 and 8 deal with pool boiling. References 9 and 10 are air-water studies pertaining to annular, two-phase flow. References 11 and 12 deal with flow regimes. Reference 12 is particularly interesting in that it reports on an experimental program to determine the transition point between slug- and annular-flow regimes at elevated pressures.

The Armadilla loop at Argonne National Laboratory was used to produce a steam-water mixture at pressures up to 600 psig. Conductivity measurements were made in the riser of the test loop by means of a suitably designed probe. This probe measured the electrical resistance between the center of the pipe and the wall; when the probe was dry, the resistance was very high, and, when wet, the resistance was relatively lower. Figure II-3 is indicative of the results obtained in the study. The figure shows the superficial vapor velocity plotted against the superficial liquid velocity and indicates that the transition between the slug- and annular-flow regimes was not a step change, but that there existed a region designated as "transition" wherein the major mode of liquid transport corresponded to slugs with a large number of bubbles entrained in them. As the superficial vapor velocity was further increased, fully developed annular flow was established. It was found that the transition between the slug- and annular-flow regimes at a given pressure occurred at almost constant quality, independent of flow range, provided that the following relation was satisfied:

$$\frac{V_{gs}^2 \rho_g}{gD \rho_f} \geq 2.0$$

where V_{gs} is the superficial vapor velocity, D is the pipe diameter, and ρ_f and ρ_g are the liquid and vapor densities, respectively. The quality at which the transition occurred ranged from 8.6% at 215 psia to about 18% at 615 psia. The following quotation serves to summarize the results:[12]

> ... Physically, the picture that emerges from these experiments is as follows. When the quality is passed through at which slugs can form, they do. As the annular flow region is approached, these slugs begin to lose liquid to the wall as they rise, ultimately being completely consumed if the pipe is long enough.... If the heat flux were higher, or perhaps if the region in which slug flow could exist were shorter, slug flow might never develop, and one could go right from bubbly to annular flow.
>
> Repeated attempts to obtain bubbly flow in this apparatus always were unsuccessful. Either the heat flux was too low or the pump too small for this condition ever to exist. In the 0.875-in. ID pipe, the maximum inlet liquid velocity was only 10 ft/sec. This is apparently insufficient to give bubbly flow as the fully developed condition. In addition, the water was very pure, which also made it difficult to obtain bubbly flow. It would appear that bubbly flow is an important flow regime only when the pressure and/or the heat flux is very high.

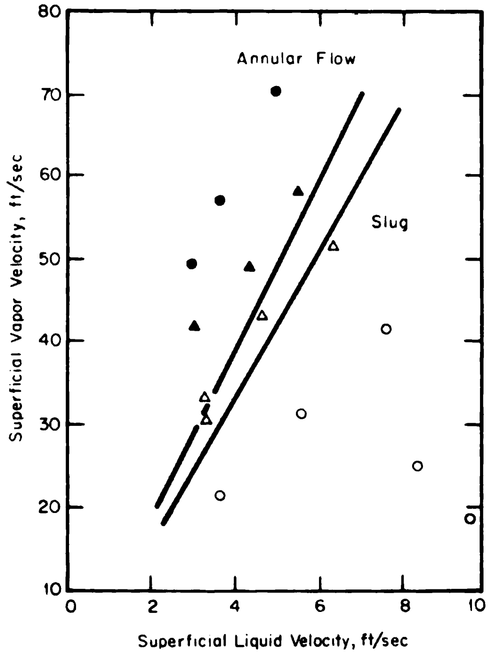

Fig. II-3 Flow-regime map for 0.375-in. pipe.[12] *Pressure is 615 psia. (The open symbols are slug flow, and the solid symbols are annular flow.)*

It is natural that both the analyst and the experimenter would like to "see" what is going on within the test section; indeed, the author of Ref. 12 does present pictures of air-water flow tests at low pressure. References 13 to 15 are devoted to results of photography and X radiography of two-phase flow systems. A perusal of these documents indicates that the problems in optics connected with photographing gas-liquid mixtures probably are as formidable as the problems of analyzing the results obtained from such experiments. The technique discussed in Ref. 14, that of radiography, appears quite promising in that it does allow studies using opaque tubing and high pressures. The discussion in that reference is devoted to a large extent to the mechanics of obtaining the X-ray photographs, although a few results of the experiments are given pictorially. The positive prints of the X-ray plates shown illustrate that it is remarkably easy to tell the positions of the liquid and gas phases (in this case air) within the tube, and the pictures show various flow regimes.

Reference 15 reports on experiments designed to study boiling flow of steam-water mixtures at atmospheric pressures. High-speed motion pictures were made for a variety of flow rates and heat fluxes utilizing a transparent rectangular channel heated by a strip of metal at one side of the flow channel. The reference reproduces a relatively large number of frames of motion pictures which illustrate bubble-, coalescing slug-, and annular-flow regimes. An unusual procedure was developed for measuring the velocities of the various liquid and vapor phases. The reference also contains a quantitative discussion of the important variables affecting the transitions between the different flow regimes.

A relatively large number of publications (Refs. 16 to 23) pertain to the hydrodynamics of two-phase flow. Included are papers on two-phase pressure drop,[16,17] nozzle flow,[18,19] and the prediction of critical flow rates for two-phase mixtures.[20–23] Reference 16 compares a number of analytical methods for the prediction of two-phase pressure drop with experimental results. The analytical techniques were those of Levy, Marchaterre, and Martinelli and Nelson. Experimental pressure drops were measured for circular and annular channels. The results are compared graphically, and no single correlation was found to represent the data adequately. Neither the Martinelli and Nelson nor the Levy correlation provides for the effect of the mass flow on the pressure drop, and this effect appeared to be a relatively large one in the experimental results.

The information in Ref. 17 includes two-phase pressure-drop data as experimentally determined for a variety of piping components such as bends, tees, expansions, contractions, and valves. Most of the data were obtained at 1200 psia (although a few points were run at 800 and 1600 psia) at mass velocities from 1 to 4 million lb/(hr)(sq ft) and at qualities up to 24 wt.%. Pressure-drop ratios were determined for straight-pipe flow and were found to be correlated "favorably" by the Levy model. The effect of flow rate on the pressure-drop ratios was negligible, and the author mentions that this behavior is not consistent with the results of other investigators. The author[17] suggests that this comes about because of the relatively large pipe diameter — 2 in. — used in his measurements. The reference presents a correlation relating the two- to single-phase pressure-drop ratio of bends to the ratio for straight pipes over the pressure range 800 to 1600 psia. Resistance coefficients were obtained for contraction and expansion losses on the assumption of a homogeneous mixture, and the coeffic agreed reasonably well with the data prese in standard engineering textbooks. The ra the two- to single-phase pressure drop for through an orifice at 1200 psia was calcu by the homogeneous model, and the results a peared to agree fairly well with the experim tal data. The pressure losses in flows thr gate and globe valves, however, did not corr late very well with calculations based on homogeneous model.

The expansion of two-phase fluids thr converging-diverging nozzles is discusse Refs. 18 and 19. The emphasis in these papers is not on reactor design, although information they present could be applie mass-flow-rate determination. References to 23 pertain to the predictions of critical of single- and two-phase mixtures. These r erences contain both experimental and anal cal predictions of critical flow rates in a var ety of geometries; the results may be usef the field of nuclear safety, since two-pha critical flow usually would occur in the di charge of coolant from a pipe or pressu vessel break into the reactor containment sy tem. Reference 21, for example, reports experimental determination of the discharg steam-water mixtures from short lengths pipe at upstream pressures approaching psia. The reference[21] presents an equation c relating experimentally determined data.

The subject of boiling burnout is covere Refs. 24 to 27. Reference 24 gives the res of an investigation into forced-convection bur out in Freon and deals with the uniformly hea round tubes utilizing vertical upflow. The use Freon (also called "Acton" in the reference an attempt to gain an insight into the mec nism and important parameters affecting bur out in steam-water systems without encounter ing the many experimental difficulties invol with the actual use of steam and water. Th material (Freon-12) has low vapor pressure a a low latent heat. This combination of physi properties enabled the Freon loop to operate low pressures and temperatures with low pow requirements. The reference reports expe mental data and compares them to results o tained in steam-water experiments, with t following conclusions:[24]

> The qualitative similarity in shapes of fun and detailed effects between the Acton 12 da 155 pounds per square inch and data for wat

1000 pounds per square inch indicates a high probability of success in developing model techniques at least for the study of burn-out in high-pressure water systems.

References 25 to 27 all deal with experimen.l studies of burnout in bundles of heated rods. his subject was previously considered in the ɔring 1964 issue of *Power Reactor Technol-y*, 7(2): 154-165. This previous review conluded that the experimental results for burnout multirod geometry were not well understood. art of the problem was believed to lie in the ifficulty of determining the amount of mixing om one flow subchannel to another within the ultirod bundle. Accordingly the information ppearing in Ref. 25 is of interest in that it eports boiling burnout data taken with two ifferent types of rod spacers, “wires” and warts.” The Hanford tests done with the wirerapped bundle were reviewed in the earlier ssue of *Power Reactor Technology*, and the ata given in Ref. 25 compare results obtained hen the wire wrapping on the rods is replaced y the so-called warts. The warts were made f alumina having a length of $^9/_{16}$ in., a width of .17 in., and a thickness of 0.048 in. and were ositioned on the heated rods by placing them n slots cut in Inconel ferrules soldered to the eated rods. The test section was housed in a orizontal 3.25-in.-ID pressure tube, and presure was controlled to 1200 psig. Results indiated that “there is no discernible difference in e burnout heat fluxes between the test secions with rods spaced with wire wraps and the est sections with rods spaced with warts.”[25] he authors comment[25] that this was somewhat nexpected, in that they believed that the degree f mixing would be increased by the use of the ire-wrapped test section and that this increase ould result in higher burnout heat fluxes. A umber of explanations offered for the lack of ifference in the two sets of data include the ollowing: (1) the amount of mixing between the ubchannels is the same with the wire wrap as ith the warts; (2) a spacing effect predomiates over mixing in determining the burnout onditions; (3) the increased mixing caused by he wires is offset by the tendency of the wires o strip the liquid film from the rods.

Reference 26 reports on burnout experiments mploying a 19-rod bundle as a test section and sing “fog” as a coolant. A cross section of the undle is shown in Fig. III-1 of *Power Reactor echnology*, 7(2): 154. The test section used to take the data in Ref. 26 employed the wart type spacers to ensure that the rod-to-rod spacing (0.074 in.) was maintained. Experiments were conducted at pressures of 1000 and 1200 psia with flow rates from 500,000 to 2 million lb/(hr)(sq ft). One of the test sections had a “flow diverter” present (about 14 in. upstream of the heated length) which was designed to direct the coolant flow to the interior of the bundle at that point; the second test section was similar but was constructed without the presence of the flow diverter. The presence of the flow diverter had little effect on the burnout heat flux when the coolant at the inlet was fog, but the diverter did increase the value of the burnout heat flux some 10 to 20% for subcooled water. Possibly the most important piece of information coming from the tests[26] was the demonstration of the importance of the hydraulic stiffness of the system on the value of the burnout heat flux. Figure II-4 illustrates the burnout heat flux as a function of the outlet enthalpy for a pressure of 1200 psia. The discontinuities in the curves shown in Fig. II-4 were believed to be caused by the presence of a compressible medium, steam, in that portion of the test loop between the steam generator and the test section. The presence of this instability complicates the data and makes their comparison to other results difficult. Of more importance, it indicates extreme care must be taken in applying laboratory data to reactors whose hydraulic characteristics may be different from those of the laboratory apparatus.

In British work[27] on the effect of rod spacing on burnout in a simulated rod bundle, the test section simulated the gap between the rod type

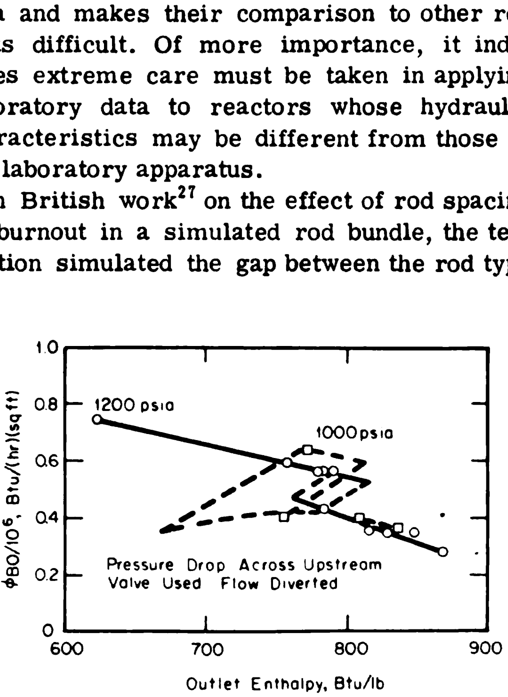

Fig. II-4 Effect of system pressure on boiling burnout for 19-rod bundles at a flow rate[26] of 500,000 lb/(hr)(sq ft).

elements in a multirod bundle by means of a "dumbbell" test section. The cross section of the dumbbell test section is shown in Fig. II-5; the use of such a mock-up permits experiments to be carried out in loops of reduced power capability. The heat generation at the

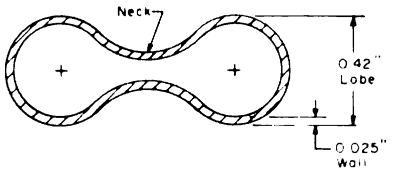

(a) Cross Section of Dumbbell Tube

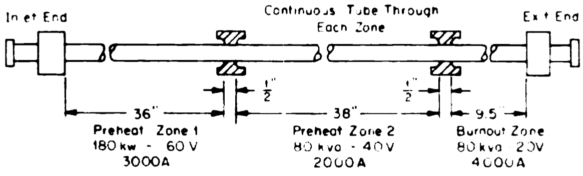

(b) Longitudinal View

Fig. II-5 Details of the dumbbell test section.[27]

neck of the dumbbell test section was increased for some of the runs by fixing a strip of stainless steel to each neck, and tests were run at a pressure of 960 psia, with a mass velocity of 2 million lb/(hr)(sq ft) and vertical upflow of water. Tests were also made with a tubular test section of the same diameter as the lobe of the dumbbell test section. The total length of the test section was about 7 ft, with the first 6 ft being utilized as a preheater and the last 9.5 in. being instrumented to detect burnout. The surfaces of the neck portion of the test section could be forced closer together by insulating blocks, and the gap therein varied from about 0.04 to 0.2 in. The results indicated that for tests with uniform peripheral heat flux the value of the gap was unimportant for gaps ranging within the values just mentioned. Burnout occurred at the exit end of the test section and on the lobe rather than at the neck. Additional tests were done with local increases of heat flux at the neck of the test section, and an arbitrary increase of 40% in heat flux was made by the inclusion of the metal strips. The effect of the gap was again small, although in these runs burnouts did take place in the region of the test-section neck. Correlation of the tubular burnout data[27] with the data from the dumbb illustrated that burnout occurred in the test sections at equivalent values of heat flux.

The remaining group of reports[28–32] de with experimental and analytical studies of dynamics of two-phase systems. Three of reports[28–30] cover analytical studies, and remaining two reports discuss experime results. The analytical approaches are based on the fundamental conservation eq tions dealing with mass, energy, and mom tum plus an equation of state. They are d ferent in the techniques used to solve equations and the models of the system up which the equations are based. The treatm in Ref. 28, for example, uses the simpli model illustrated in Fig. II-6, and the diffe ential equations are solved by the "modifie Euler" integration process combined with a propriate iterative procedures. The author Ref. 29 considers the idealized natural-ci culation system shown in Fig. II-7, and solution of the equations is accompanied perturbation theory. Figure II-8 illustrates system studied in Ref 30, in which pertur tion theory is again used to achieve a solu The treatment in Ref. 28 is quite comple reactivity feedback in the reactor is pro and is coupled into the time-dependent e tions. Separate energy-conservation equat for the fuel, cladding, and the heat exchan are also included, and separated flow is a sumed. The author of Ref. 29 obtains the reactivity feedback by integrating the pro of the perturbed void fraction, both spati

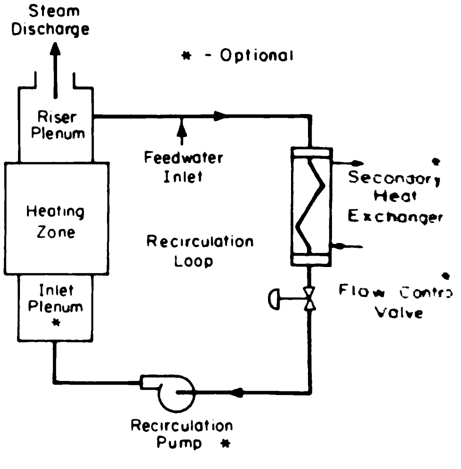

Fig. II-6 Idealized boiling-water system.[28]

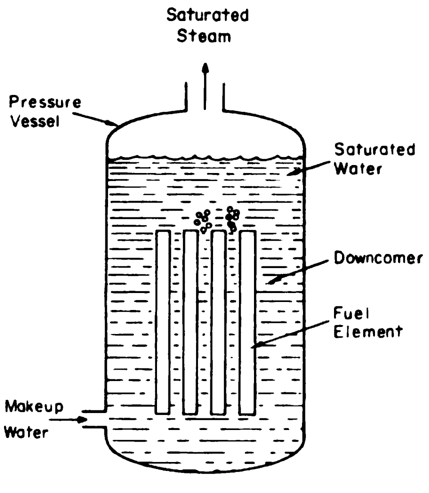

ig. II-7 *Model of a natural-circulation boiling-wa-*
r reactor.[29]

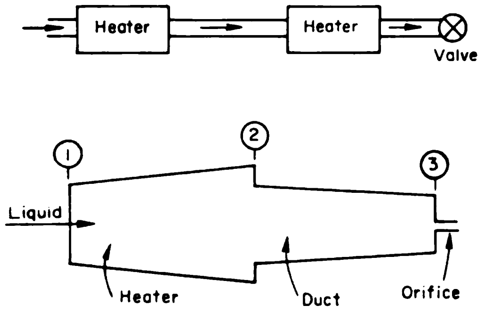

ig. II-8 *Configuration of system studied in Ref. 30.*

nd temporally, and the reactivity worth of the oids. The treatment of power generation in :ef. 30 assumes that the rate of vapor genera- ıon in the heater is constant or is proportional ɔ the system density at point 2 (see Fig. II-8).

It is feasible here only to mention a few of ıe general results of the rather complex dy- amic analyses. The mathematical model de- eloped in Ref. 28 is compared to experimental esults obtained at General Electric Company, ıtomic Power Equipment Department. The au- hors conclude that "the period of oscillations .nd threshold of instability predicted by the ıresent analysis are in good agreement with he test results." The analyses are then applied n studying the response of a "typical" boiling- vater reactor to a variety of perturbations. In Ref. 29 the analytical solutions obtained are applied to several specific problems, namely, the dependence of stability on steady-state conditions, the effect of pressure drops in the downcomer and at the inlet to the channel, and the stability of a parallel-channel system with a common downcomer. The effect of the channel length on the dynamic behavior of the system is also studied.[29] The author of Ref. 30 has specialized his solution to the case of a short heater followed by a long insulated duct and orifice, and also a long heater immediately followed by an orifice with no insulated duct. Briefly the author concludes that, whenever a fluid density ratio greater than about 3 exists across an evaporator, there is a possibility of the development of flow oscillations.

The experiments reported in Ref. 31 are preliminary in nature and were done with two parallel heated channels. Both single-phase liquid (subcooled water) at atmospheric pressure and steam-water mixtures were employed as feed to the test sections. Heating was accomplished by the condensation of steam at pressures ranging from 20 to 50 psi. The results illustrate that a negative slope of the curve of mass flow rate vs. pressure is not a necessary condition for the occurrence of oscillatory instabilities. The authors also conclude that, when there is net quality in the feed to the heated test section, no oscillatory instabilities will occur. This conclusion appears to disagree with the data presented in Ref. 26; in that study the presence of steam in the piping between the steam generator and the test section was believed to have allowed flow oscillations in the test section. The problem is complicated, however, by the fact that the "springiness" of the entire test loop depends on its constructional details; and, although the test loop used to take the data appearing in Ref. 31 did employ two-phase mixtures at the test-section inlet, it may well be that the flow loop nevertheless was "stiff."

The test section utilized in Ref. 32 was an electrically heated stainless-steel tube (0.045 in. in inside diameter and 4.5 in. long). Although the tests were run at 200 psia, a pressure lower than that ordinarily used for water type reactors, the results still are of general interest. The author notes that at low values of subcooling it is possible to obtain high void fractions due to the presence of unquenched bubbles. The bubbles exist because, as the subcooling of zero is approached, the temperature driving force transferring heat from the bubbles to the bulk liquid becomes small, with the result that the bubbles have relatively long lifetimes. The presence of the nonequilibrium situation within the flow channel resulted in a departure from the characteristic burnout pattern in subcooled water. The most noticeable result of this was the reduction of the burnout heat flux to relatively low values. The author suggests that this is due to the initiation of "froth flow" as the unquenched bubbles are entrained in the liquid. The reference presents a table of critical-heat-flux data taken with the apparatus, and each burnout point is accompanied by a description of a hypothesized local flow regime. The local flow regimes were identified by consideration of the behavior of the test-section instrumentation and the past history of a particular run. Some idea of the technique can be obtained by considering Fig. II-9. Figure II-10 illustrates the effect of instabilities on the burnout heat flux for the hypothesized annular flow. T author comments on the figure as follo

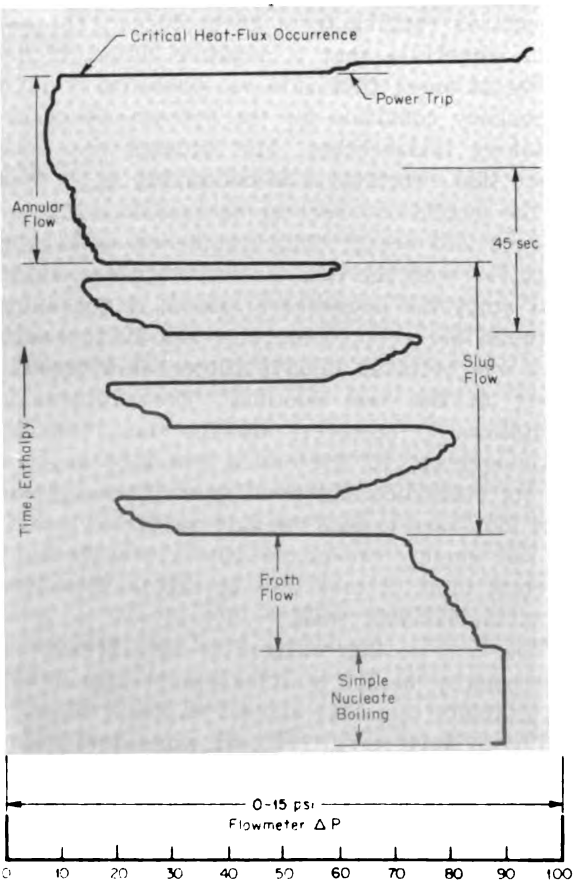

Fig. II-9 Froth flow, periodic vapor slugging, and stable annular flow during net steam generation.[32]

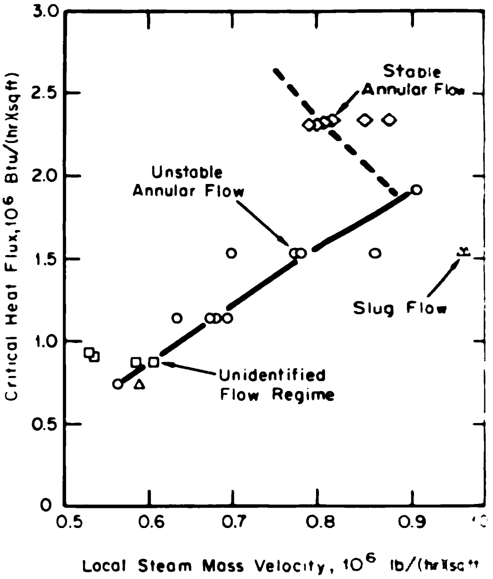

Fig. II-10 Effect of flow regime and degree o drodynamic instability upon critical-heat-flux oc rence during net steam generation[32] *at 200 psia.*

> The positive slope of the critical heat flux-st mass velocity relationship [see Fig. II-10] wh characteristic of unstable annular flow, is dir counter to the negative slope typical for stable Since the slug-flow data follow a similar beha this characteristic may be applied to distin between stable and unstable flow conditions in sy tems using high-damping, slow-response seco flow meters, such as mercury manometers.

This was one of the points made in the revie article in the Fall 1964 issue of *Power Re Technology*, 7(4): 335.

References

1. R. Herrick, Liquid Metal Heat Transfer by Fo Convection, British TRG-Report-546, July 2, 1
2. G. F. Burdi, Snap Technology Handbook, Vo I. Liquid Metals, USAEC Report NAA-SR- (Vol. I), Atomics International, Aug. 1, 1964.
3. E. Bernstein, J. P. Petrek, G. J. Rose, and Horan, Experimental Results of Forced Co tion Boiling Potassium Heat Transfer and P sure Drop Tests, USAEC Report PWAC-429, P & Whitney Aircraft Division, United Airc Corp., July 16, 1964.
4. R. C. Noyes, Boiling Studies for Sodium Re Safety. Part I. Experimental Apparatus and sults of Initial Tests and Analysis, USAEC Re NAA-SR-7909, Atomics International, Aug 1963.

5. Hans K. Fauske, Two-Phase Critical Flow with Application to Liquid-Metal Systems (Mercury, Cesium, Rubidium, Potassium, Sodium, and Lithium), USAEC Report ANL-6779, Argonne National Laboratory and Associated Midwest Universities, October 1963.

6. Robert R. Kepple and Thomas V. Tung, Two-Phase (Gas-Liquid) System: Heat Transfer and Hydraulics, An Annotated Bibliography, USAEC Report ANL-6734, Argonne National Laboratory, July 1963.

7. W. R. Beasant and H. W. Jones, The Critical Heat Flux in Pool Boiling Under Combined Effect of High Acceleration and Pressure, British Report AEEW-R-275, July 1963.

8. W. L. Owens, Jr., An Analytical and Experimental Study of Pool Boiling with Particular Reference to Additives, British Report AEEW-R-180, May 1963.

9. L. E. Gill, G. F. Hewitt, and P. M. C. Lacey, Sampling Probe Studies of the Gas Core in Annular Two-Phase Flow: Part II. Studies of the Effect of Phase Flow Rates on Phase and Velocity Distribution, British Report AERE-R-3955, June 1963.

0. G. F. Hewitt and P. M. C. Lacey, The Breakdown of the Liquid Film in Annular Two-Phase Flow, British Report AERE-R-4303, August 1963.

1. A. A. Kudirka, Two-Phase Heat Transfer with Gas Injection Through a Porous Boundary Surface, USAEC Report ANL-6862, Argonne National Laboratory, March 1964.

2. Peter Griffith, The Slug-Annular Flow Regime Transition at Elevated Pressure, USAEC Report ANL-6796, Argonne National Laboratory, November 1963.

3. K. D. Cooper, G. F. Hewitt, and B. Pinchin, Photography of Two-Phase Flow, British Report AERE-R-4301, May 1963.

4. R. T. P. Derbyshire, G. F. Hewitt, and B. Nicholls, X-Radiography of Two-Phase Gas-Liquid Flow, British Report AERE-M-1321, January 1964.

5. John H. Vohr, A Photographic Study of Boiling Flow, USAEC Report NYO-9650, Columbia University, Oct. 25, 1963.

6. M. Muscettola, Two-Phase Pressure Drop—Comparison of the "Momentum Exchange Model" and Martinelli and Nelson's Correlation with Experimental Measurements, British Report AEEW-R-284, May 1963.

17. D. E. Fitzsimmons, Two-Phase Pressure Drop in Piping Components, USAEC Report HW-80970 (Rev. 1), Hanford Atomic Products Operation, Mar. 20, 1964.

18. E. S. Starkman, V. E. Schrock, K. F. Neusen, and D. J. Maneely, Expansion of a Very Low Quality Two-Phase Fluid Through a Convergent-Divergent Nozzle, *J. Basic Eng.*, 86: 247-256 (June 1964).

19. Joseph A. Vogrin, Jr., An Experimental Investigation of Two-Phase, Two-Component Flow in a Horizontal, Converging-Diverging Nozzle, USAEC Report ANL-6754, Argonne National Laboratory, July 1963.

20. K. Goldmann, R. Hankel, and R. P. Stein, An Equation for the Critical Mass Velocity of Homogeneous Vapor-Liquid Mixtures at Low Pressures, *J. Appl. Mech.*, 31(3): 380-382 (September 1964).

21. F. R. Zaloudek, Steam-Water Critical Flow from High Pressure Systems. Interim Report, USAEC Report HW-80535, Hanford Atomic Products Operation, January 1964.

22. F. R. Zaloudek, The Critical Flow of Hot Water Through Short Tubes, USAEC Report HW-77594, Hanford Atomic Products Operation, May 1963.

23. S. Levy, Prediction of Two-Phase Critical Flow Rate, *J. Heat Transfer,* 87(1): 53-58 (February 1965).

24. G. F. Stevens, D. F. Elliott, and R. W. Wood, An Experimental Investigation into Forced Convection Burn-Out in Freon, with Reference to Burn-Out in Water. Uniformly Heated Round Tubes with Vertical Up-Flow, British Report AEEW-R-321, January 1964.

25. J. M. Batch and G. M. Hesson, Comparison of Boiling Burnout Data for 19-Rod Bundle Fuel Elements Spaced with "Wires" and "Warts," USAEC Report HW-80391 (Rev. 1), Hanford Atomic Products Operation, Jan. 15, 1964.

26. G. M. Hesson, D. E. Fitzsimmons, and J. M. Batch, Boiling Burnout Experiments with Fog-Cooled Nineteen-Rod Bundle Test Sections, USAEC Report HW-80523 (Rev. 1), Hanford Atomic Products Operation, March 1964.

27. D. H. Lee and R. B. Little, U. K. Atomic Energy Authority. (Unpublished)

28. A. N. Nahavandi and R. F. von Hollen, A Space-Dependent Dynamic Analysis of Boiling Water Reactor Systems, *Nucl. Sci. Eng.*, 20(4): 392-413 (December 1964).

29. Chathilingath K. Sanathanan, Dynamic Analysis of Coolant Circulation in Boiling Water Nuclear Reactors, USAEC Report ANL-6847, Argonne National Laboratory, April 1964.

30. A. H. Stenning, Instabilities in the Flow of a Boiling Liquid, *J. Basic Eng.*, 86: 213-217 (June 1964).

31. D. J. Pulling and J. G. Collier, Instabilities in Two-Phase Flow. Preliminary Experiments, British Report AERE-M-1105, July 1963.

32. R. J. Weatherhead, Heat Transfer, Flow Instability, and Critical Heat Flux for Water in a Small Tube at 200 psia, USAEC Report ANL-6715, Argonne National Laboratory, June 1963.

Section III

Power Reactor Technology

Fuel Elements

Fuel-Performance Evaluations

An engineering proof test of seven UO_2 fuel rods, which were 0.412 in. in diameter and which were clad with type 304 stainless steel, was successfully completed[1] in a borated pressurized-water loop in the Westinghouse Testing Reactor (WTR). The loop conditions[1] are summarized below:

Average coolant inlet temperature, °F	560 to 580
Coolant pressure, psi	2000
Flow rate, gal/min	62
Chlorine, ppm	<0.1
Boron (as H_3BO_3), ppm	1500 ± 50
Hydrogen, cm^3 (STP) per kilogram of H_2O	30
Oxygen, ppm	<0.1

The elements were irradiated to a maximum burnup of 4000 Mwd per metric ton of uranium at a maximum heat flux of 340,000 Btu/(hr)(sq ft) for the purposes of demonstrating the feasibility of boron chemical shim and the performance of fuel rods in the large-plant design of the Large Closed Cycle Water Reactor Research and Development (LRD) Program.* The fuel bundle was fabricated as a simulation of a four-rod segment of the fuel assembly in the large plant. The 2.07% enriched UO_2 fuel pellets, of 0.379-in. diameter, were fabricated to 96% of the theoretical density and were clad with 10% cold-worked type 304 stainless steel that was 0.016 in. thick. The fuel-cladding diametral gap of 0.004 in. was filled with air. An attempt to measure in-pile thermal expansion of the UO_2 fuel column by means of markers inside the cladding, to differentiate between the performance of dished and flat pellets, did not succeed. Postirradiation evaluation indicated satisfactory performance, and the results of fission-gas-release measurements and postirradiation microstructure evaluations were consistent with those generally anticipated for UO_2 fuel rods operating under comparable conditions.

The rods that achieved an average burnup of 6.4×10^{20} fissions/cm^3 in the blanket of the Shippingport reactor at the end of the third seed life have been examined.[2] One of these rods operated at an average cladding-surface temperature of 515°F and a lifetime average surface heat flux of 155,000 Btu/(hr)(sq ft). Although the lifetime average heat flux of 139,000 Btu/(hr)(sq ft) noted for the second rod would appear to provide little additional interest, it was found that a heat flux of 428,000 Btu/(hr)(sq ft) had occurred in this rod for about 200 equivalent full-power hours.

Results of postirradiation examinations indicated no cladding failures, no changes in fuel-rod diameters, and fission-gas release less than 1% of that generated. In addition, there was no evidence of structural change in the UO_2 when it was compared with unirradiated microstructures. The range of hydrogen concentration in the cladding of these fuel rods was 51 to 7[illegible] ppm; this represents only a very small increase in the hydrogen content when compared with a nominal content of about 40 ppm in the as-vacuum-annealed unirradiated cladding. All hydrides were in a random orientation. The range of oxide film thickness was 47 to 99 [illegible]

Results of irradiation tests of multicomponent tubular UO_2 fuel elements have been reported.[3] A tube-and-rod assembly was irradiated in a test loop in the Engineering Test Reactor (ETR) at a target maximum surface heat

---

*The LRD Program was discussed in Sec. V of *Power Reactor Technology*, 8(2).

x of 320,000 Btu/(hr)(sq ft). During early ges of the irradiation, a burnout occurred ich was the result of locally reduced coolant w caused by a crossover of two thermo- uples. A nested tubular element (tube-tube- d) fabricated by vibratory compaction of UO_2 o 0.060-in.-thick Zircaloy-2 cladding, to nsities in the range of 83 to 88% of the theo- tical density, was irradiated at 350,000 Btu/ r)(sq ft). After 10 reactor scrams and inad- rtent severe thermal transients, fission-gas akage was noted. Visual examination of the ement failed to indicate defects. During dis- sembly of the components of the test ele- ents, a fibrous material was found lodged tween the rod and the inner tube and adja- nt to a cladding failure. It was concluded that ilure was induced by flow blockage caused by trapped foreign matter. Extensive hydriding as noted at the cladding failure and further bstantiated the postulated cause of failure. he appearance of the microstructure of both e fuel and the cladding in the region of the ilure indicated that failure resulted from in- rference with surface heat transfer rather han from excessive local heat generation. A hird element, containing the tube-tube-rod ar- ay similar to that described immediately bove, was irradiated to its target burnup of 360 Mwd per ton of UO_2 at a maximum sur- ace heat flux of 400,000 Btu/(hr)(sq ft). Post- rradiation evaluations indicated that less than 0% of the fission gases and less than 50% of he sorbed gases were released.

Evaluation[4] of the influence of irradiation on he ductility of Zircaloy tubing by means of nechanical burst, weld-shear, and bend tests as indicated no effective loss in ductility after xposure to an integrated fast flux of 10^{20} neu- trons/cm^2 at less than 100°C. Tubular fuel lements up to 2 ft long, with outside and in- side diameters of about $2\frac{1}{4}$ and $1\frac{1}{2}$ in., were fabricated with Zircaloy-2 or low-nickel Zir- caloy-2 cladding. The fuels used were vibra- tory-compacted and vibratory-compacted-and- swaged UO_2. The following conclusions are quoted from Ref. 4:

> The results of these tests indicate that large diameter tubular elements should not fail by either sheath rupture or weld separation due to irradiation embrittlement. In this event, calculations have shown that the limiting stress should be that stress required to cause sheath collapse. The tests also showed that the irradiation exposures, up to approximately 10^{20} nvt, had no noticeable effect on the sheath ductility, as measured by mechanical burst tests.
>
> These conclusions would be invalid, however, if severe hydriding, such as was previously observed in the . . . test series, were present.

Prototype fuel elements for the first Mobile Low Power Plant No. 1 (ML-1) core loading have been irradiation tested[5] in a gas-cooled General Electric Test Reactor (GETR) loop. The ML-1 core contains 61 fuel elements that are arranged in 61 pressure tubes located in the reactor calandria. Each fuel element contains 19 pins, with 1 unfueled pin in the center surrounded by two concentric rings containing 6 UO_2 and 12 BeO-UO_2 fuel pins. The objectives of these tests, in addition to providing irradiation performance data, included verification of design calculations concerning hot-spot limits and determination of in-pile corrosion resistance of Hastelloy X to the coolant gas. It was also noted[5] that the closed Brayton cycle used in the ML-1 plant was highly sensitive to pressure losses. For example, an increase of 1 psi in the system pressure drop resulted in a loss in net thermodynamic output of 6 kw. Hence another objective of the tests was to evaluate the influence of corrosion-product buildup or changes in fuel-element configuration on pressure drop.

The conditions in the gas loop are summarized below:[5]

Element power, kw	55
Inlet coolant temperatures, °F	800
Outlet coolant temperatures, °F	1200
Mass flow rate, lb/hr	1560
Loop operating pressure, psia	315

Two fuel elements, one of which was instrumented, were irradiated for 6415 hr in a coolant gas that was 99.5 wt.% N_2 and 0.5 wt.% O_2. The irradiation testing of the uninstrumented fuel element was continued in air for an additional 3736 hr.

Results[5] of cladding-temperature measurements indicated good agreement with previous calculations, and it was concluded that the hot-spot limit of 1750°F would not be exceeded at the full element power of 55 kw. Results of pressure-drop measurements during the test indicated no problems with respect to possible reductions in the net thermodynamic output of the cycle. Postirradiation examination of the cladding microstructure indicated the formation of a massive second phase, which was due to an apparent reaction between nitrogen and Hastelloy X in all fuel pins that were instrumented. It was postulated that leaks were present at the brazed joints between the fuel and thermocouples and that the coolant gas permeated the inside of the fuel rods; nitrogen was measured in these rods. It was further postulated that the fuel gettered the O_2, leaving an oxygen-free N_2 atmosphere that reacted with the Hastelloy X to form a second phase which, in some cases, formed a continuous layer on the inside surface of the cladding and extended intergranularly through the thickness. All tubes that contained this second phase were severely embrittled. It was stated[5] that problems of this nature are not anticipated in the operating reactor.

The fuel pins in the 19-rod fuel assembly were spaced by means of spirally wrapped spacer wires on each pin. As a result of a 300°F difference in temperature between the fuel pin and the spacer wire, spiral bending of the fuel pins was observed, after irradiation, on a pitch that was almost the same as that of the wire wrap. It was concluded that the pin bending was a result of unequal expansion of the fuel pins and spacer wires.

An understanding of the performance of sodium-bonded hypostoichiometric UC fuels during transients has been obtained[6] through capsule testing in the Transient Reactor Test Facility (TREAT). Rods resembling the second Hallam fuel loading and containing 0.872-in.-diameter carbide fuel (4.58% carbon) clad with stainless steel of 0.952-in. outside diameter and 0.010-in. wall thickness were subjected to a total of five transients. A summary of results is given in Table III-1.

Evidence of uranium migration was not found even after bursts that provided fuel temperatures in excess of 2700°F. Bursts that increased the temperature to about 4200°F did not produce evidence of melting. However, a decrease in the amount of free uranium was noted, and it is postulated[6] that uranium became redissolved in the UC. Temporary boiling of the sodium, which probably occurred during the final transient, was rapidly quenched by cooler sodium located about the boiling region. The integrity of the fuel rod was such that it was concluded that "power levels of fuel rods of this type can reach values which are 100 times maximum steady-state levels for pulse duration of about 1 second without serious consequence."[6]

Incoloy 800 Cladding

Incoloy 800 is being evaluated[7] as a possible fuel-cladding material for use in nuclear superheat reactors. Procurement, quality control, fabrication, and metallographic evaluation of Incoloy 800 are described in detail in Ref. 7. Prior to 1962 there was little information on the fabrication of this material into thin-walled tubing.

Some of the first tubing received in the welded and drawn condition exhibited unhomogenized weld zones and disturbed surface layers. It was shown that the weld zone was a potentially weaker area than the base metal. It was concluded that the microstructure of all incoming Incoloy 800 tubing should show:[7]

1. No dendritic segregation in the weld zone.
2. Equal grain size in the weld zone and parent metal.
3. Grain size smaller than ASTM Number 5.

Complete recrystallization of the weld zone could be achieved by annealing in the tempera-

Table III-1 RESULTS OF TREAT TESTS* OF SODIUM-BONDED URANIUM CARBIDE FUEL RODS[6]

Transient number	TREAT energy, Mw/sec	Initial reactor period, sec	Peak central fuel temp. (measured), °F	Peak fuel temp.,† °F	Peak bond temp. (measured), °F	Peak pressure increase in fuel section, psi
1	30.7	0.259	1025	1060	845	3
2	63.3	0.157	1380	1520	980	8
3	180.0	0.158	2540	2760	1475	16
4	31.4	0.259	1030	1030	835	2
5	293.0	0.101	3970	4200	1840	20

*Initial temperature about 700°F; initial pressure about 32 psia (fuel section and inner capsule).

†Each value represents the maximum temperature at any position in the fuel since, as a result of flux depression, the peak transient temperature would not be expected to occur in the center of the fuel slug. Values are based on analog calculations and the measured central temperature.

·e range of 1900 to 2100°F, but the dendritic
·ucture could only be eliminated after two
ld reductions of approximately 20 to 30% fol-
ved by annealing at 2000 to 2100°F. The grain
:e could then be reduced by subsequent cold
rking and annealing.

The ductility of Incoloy 800 was reduced after
00 hr at temperatures above 1050°F as a re-
lt of an aging phenomenon associated with the
ecipitation of titanium- and aluminum-con-
.ning intermetallics. As a result of this in-
rmation, the titanium and aluminum content
ιs specified as 0.1% maximum. Cold-worked
coloy 800 was insensitive to annealing tem-
ratures below 1000°F. Softening was initiated
1400°F and was reasonably complete in 10
15 min at 1800°F. Rapid grain growth oc-
ırred at temperatures above 1850°F. Solution
ınealing occurred at 2050 to 2100°F after 1 to
hr. It was necessary to water quench through
e 1100 to 1600°F temperature range in order
prevent carbide precipitation.

Typical chemical and physical properties for
coloy 800 are indicated in Tables III-2 and
I-3.

A monograph on the use of Incoloy 800 for
ıel-element cladding has been prepared[8] which
ıcludes: mechanical properties, physical met-
llurgy, metallography and electron-microscopy
:chniques, radiation damage, strain-cycle fa-
gue, corrosion, and irradiation results of fuel
lements (clad with Incoloy 800) exposed in the
superheat environment. Performance in superheated-steam environments has been superior to that for the austenitic stainless steels, and Incoloy 800 has been selected as the reference cladding in some nuclear superheat applications.

'able III-2 CHEMICAL COMPOSITION[7] OF INCOLOY 800

Constituent	Weight percent
Nickel	30 to 35
Chromium	19 to 23
Iron	Balance
Carbon	0.10 maximum
Manganese	1.50 maximum
Sulfur	0.03 maximum
Silicon	1.00 maximum
Copper	0.75 maximum

Table III-3 MECHANICAL PROPERTIES OF EXTRUDED INCOLOY TUBES[7]

Condition	Tensile strength, 1000 psi	Yield strength (0.2% offset), 1000 psi	Elongation in 2 in., %
As extruded	75-105	25-50	50-30
Annealed	75-100	25-55	50-30

References

1. D. R. McClintock and C. J. Kubit, Fabrication and Irradiation of Stainless Steel Clad UO_2 Fuel Rods (The LRD In-Pile Chemical Shim Loop Experiment), USAEC Report WCAP-3734, Westinghouse Electric Corp., Atomic Power Division, April 1964.
2. L. R. Lynam, Metallurgical Examination of PWR Core 1 Blanket Fuel Rods at the End of the Third Seed Life, USAEC Report WAPD-TM-433, Bettis Atomic Power Laboratory, August 1964.
3. M. K. Millhollen, G. R. Horn, and W. J. Flaherty, Multicomponent Tubular UO_2 Fuel Element Irradiations, USAEC Report HW-80291, Hanford Atomic Products Operation, November 1963.
4. M. R. Louthan, Jr., Destructive Evaluation of Irradiated Zircaloy Sheathing, USAEC Report DP-888, Savannah River Laboratory, May 1964.
5. J. S. Brunhouse et al., Army Gas-Cooled Reactor Systems Program, USAEC Report IDO-28616, Aerojet-General Nucleonics, June 1964.
6. S. J. Stachura, M. Silberberg, and R. N. Cordy, Uranium Carbide Transient Heating Experiments — Phase 1, USAEC Report NAA-SR-9508, Atomics International, Aug. 1, 1964.
7. R. F. Kirby, D. F. Macmillan, and J. R. Punches, Fabrication of Fuel Cladding from Incoloy Alloy 800, An Evaluation of Methods, USAEC Report GEAP-4557, General Electric Company, Atomic Power Equipment Department, April 1964.
8. C. N. Spalaris (Comp.), Incoloy-800 for Nuclear Fuel Sheaths (A Monograph), USAEC Report GEAP-4633, General Electric Company, Atomic Power Equipment Department, July 1964.

Section IV

Power Reactor Technology

Components

Liquid-Metal-Level Probes

Some significant improvements have been made in resistance type probes for determining the level of high-temperature liquid metals in a vessel. Reference 1 reports on an investigation of the various types of probes that can be used for determining the level of liquid metals and concludes that the resistance type is promising. The J probe that was developed utilized a tube with alumina-insulated stainless-steel-clad nickel wires. A straight tube probe, similar in operation and construction to the J probe, but which indicates one discrete level only and is called an I probe, also was studied.

The J probe indicates the level of the liquid metal over the range from the top of the unsupported leg of the J to the bottom of the J. This is accomplished by passing a direct current through one of the insulated internal wires in the tube to the tip of the J as shown in Fig. IV-1. The negative wire from the power supply is connected to the metal vessel. A potential is then impressed between the tip of the J and the vessel and the resistance between these two points is changed as the liquid-metal level around the unsupported leg is changed. The maximum resistance exists when the level is lowest, and the current must pass through the sheath of the J tube. The potential between the tip of the J and the tank is measured by a second insulated internal wire to the tip of the J and a wire to the tank. Unfortunately the resistances of the stainless-steel sheath and the probe wires vary with temperature. In the design shown in Fig. IV-1, compensation is accomplished by maintaining a constant voltage across the entire probe and internal current lead. Figure IV-2 is a refinement of this design wherein the temperature-compensation circuit is connected inside the J tube and the resistance of the current lead is increased. The increased length of the lead is in the same temperature gradient as the probe, and compensation is obtained by maintaining a constant voltage between the tip of the probe and the internal splice.

The I probe, which indicates whether the liquid-metal level is above or below a certain point, is shown in Fig. IV-3. A potential is impressed between the end of the probe and the vessel, and an amplifier connected in parallel to this circuit actuates a relay to signify that the level of the liquid metal is below the probe end. When the liquid metal comes in contact with the end of the probe, a new circuit with less resistance is established and the decrease in voltage causes the amplifier to drop the relay.

In addition to the problem of attaining correct temperature compensation, there is a problem of obtaining thermoelectric voltages

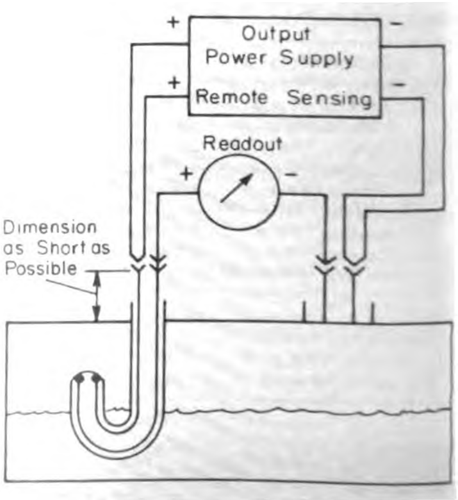

Fig. IV-1 Two-wire J probe with externally connected temperature-compensation circuit.[1]

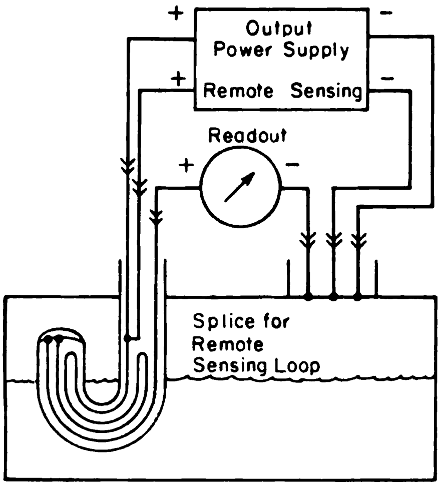

ig. IV-2 J-probe design with internally connected emperature-compensation circuit and increased-esistance remote sensing loop.[1]

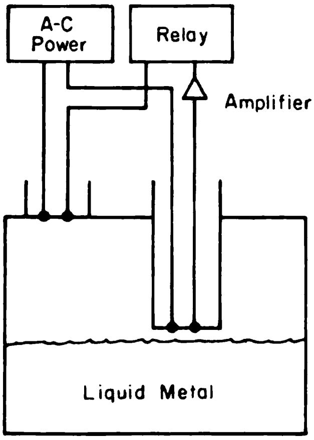

Fig. IV-3 I probe for one-point-level determination.[1]

materials are not carefully selected. Further, complete wetting of the surface of the probe requires careful attention to the preparation of the surface before immersion. Reference 1 indicates that if the probe can be completely wetted, an accuracy within 1% can be achieved.

Pressure-Tube Fretting Corrosion

A continuing surveillance program is being conducted on the Plutonium Recycle Test Reactor (PRTR) to monitor fretting corrosion of the pressure tubes. A summary of results of (1) programs designed to detect and determine the extent of in-reactor fretting attack and (2) associated tests outside the reactor is presented in Ref. 2. The PRTR[3] is a heavy-water-moderated pressurized-heavy-water-cooled reactor that operates at 70 Mw(t). The moderator is contained at low pressure and temperature in an aluminum calandria tank, with 85 calandria tubes arranged vertically. Zircaloy-2 pressure tubes, containing fuel assemblies, are installed in the calandria tubes. The coolant enters the bottom of the pressure tubes at a temperature of 248°C and a pressure of 1090 psig and discharges at the top at 277°C and 1080 psig. The maximum flow rate per pressure tube is 123 gal/min. The Zircaloy-2 pressure tubes are 3.250 in. in inside diameter, with a minimum wall thickness of 0.146 in. The tubes are flanged at the upper end to permit attachment of outlet-nozzle jumper assemblies and are tapered at the bottom for attachment of inlet jumpers. Before installation the pressure tubes were autoclaved to provide a zirconium dioxide surface film.

The fuel assemblies are 19-rod clusters, as shown in Fig. IV-4, and both metallic (aluminum-plutonium) and ceramic (UO_2 and PuO_2-UO_2) Zircaloy-2-clad rods are used. Spacing between rods is maintained with top and bottom brackets and spirally wound spacer wires around the outside of selected fuel rods. The aluminum-plutonium and the PuO_2-UO_2 fuel assemblies are bound with circumferential bands, whereas a wire wrap is used on the UO_2 fuel assembly. A pressure tube containing a fuel assembly is shown in Fig. IV-5. The fuel assembly is attached to an upper hanger that is supported near the outlet nozzle and is free to expand downward. Clearance between the fuel assembly and the pressure tube is a nominal 0.015 in., but it can be as much as 0.050 in. Portions of the fuel assembly that could come in contact with the pressure tube include the following: the three equidistant centering feet on both the top and bottom end brackets; the wire wrap (bundle or individual rods); circumferential bundle bands if the centering feet are sufficiently worn; and the individual fuel rods if the wire wraps and centering feet are sufficiently worn.

A rather comprehensive program[4–6] has been conducted, on a continuing basis, to determine

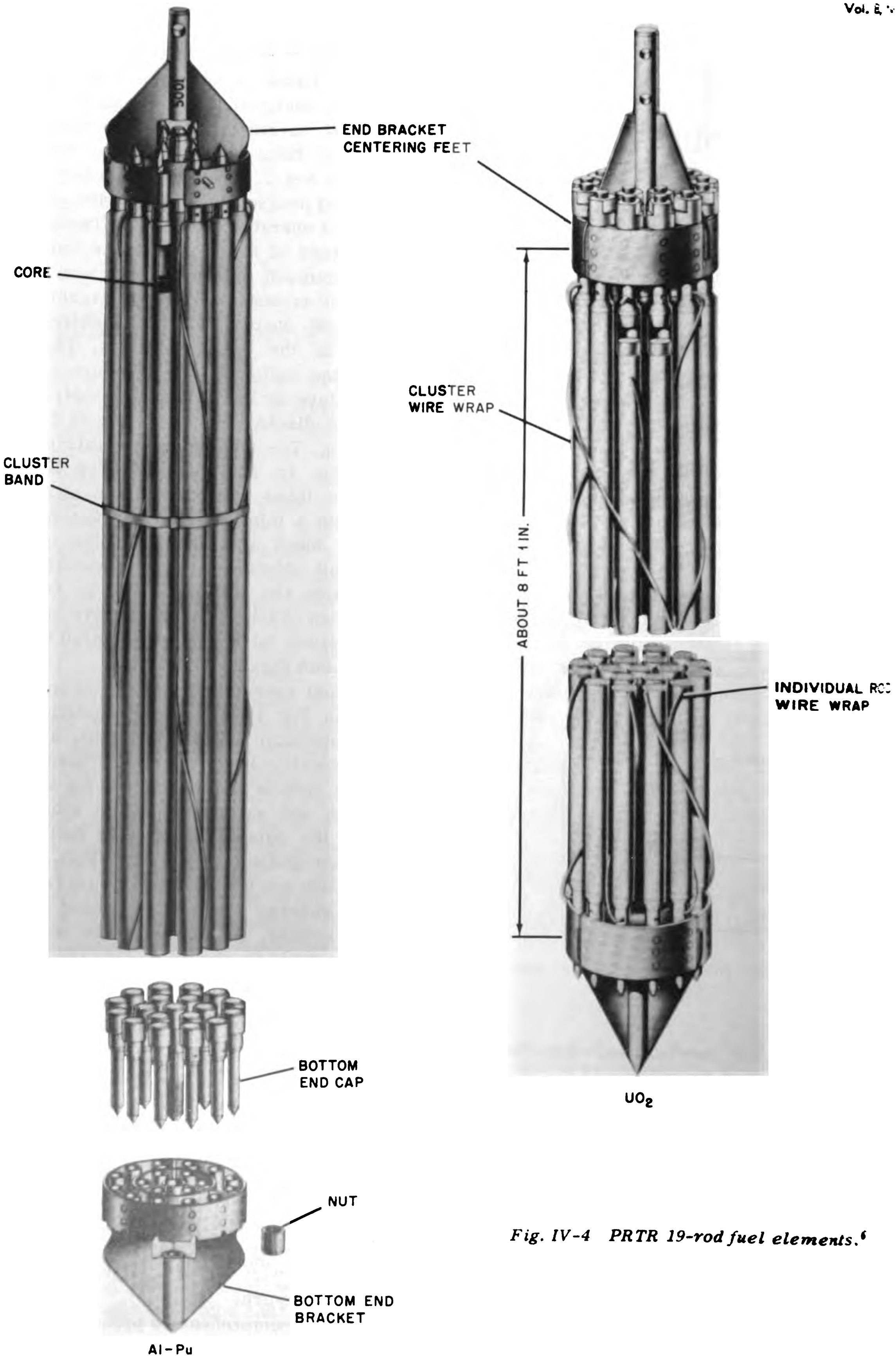

Fig. IV-4 PRTR 19-rod fuel elements.[6]

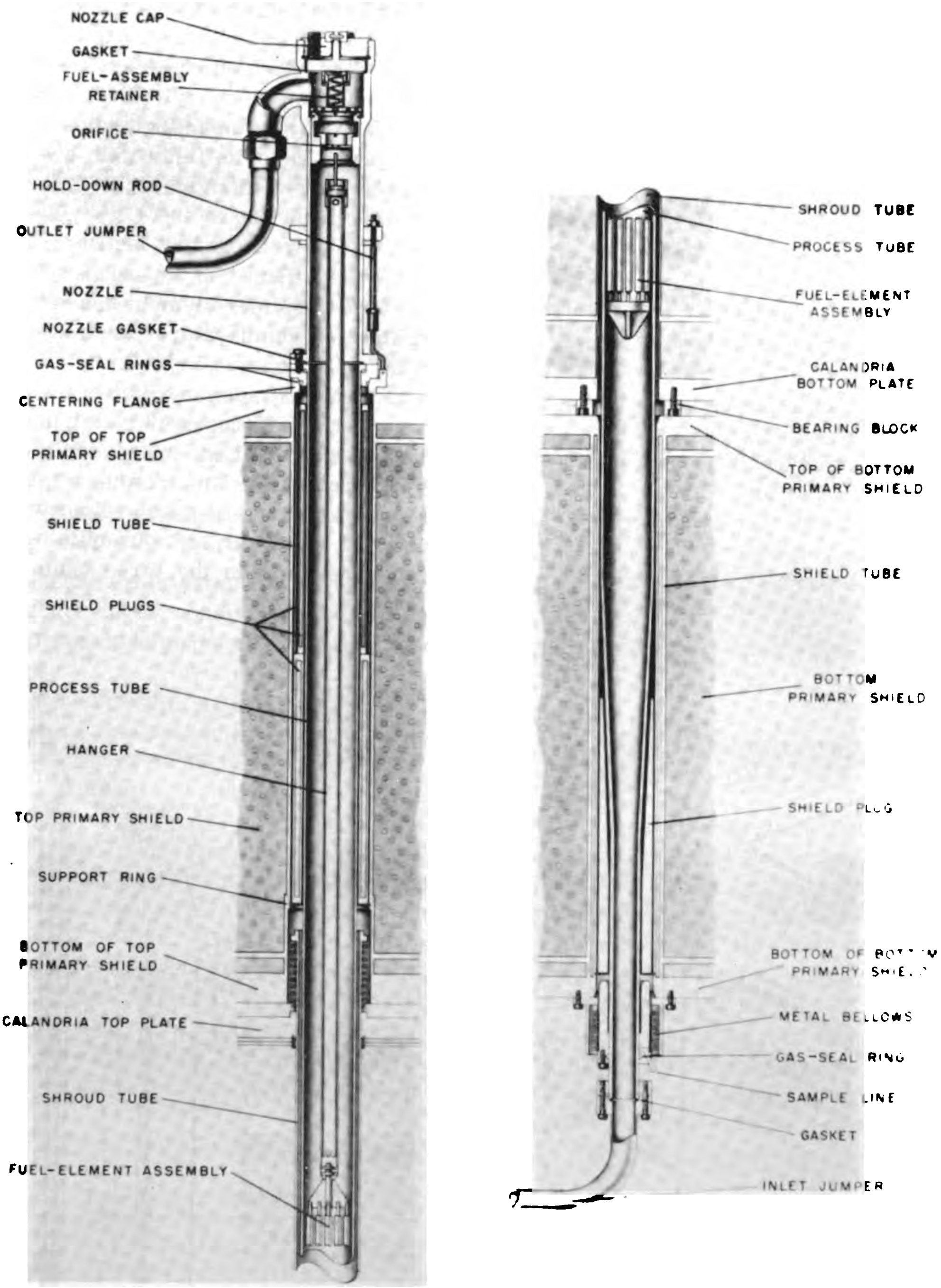

Fig. IV-5 Pressure-tube assembly.[2]

the magnitude of fretting corrosion and to establish methods of minimizing pressure-tube wear. The program consisted of out-of-reactor tests and in-reactor examination. The initial phase of the out-of-reactor program consisted of flow tests in a high-temperature high-pressure facility and autoclave tests. The initial test specimen was a Zircaloy-2 tube with a spirally wound Zircaloy-2 wire. The wire was fastened at one end and was free at the other end. After two weeks of exposure in recirculating water at 300°C and 25 ft/sec, grooves approximately 0.001 to 0.005 in. deep were noted on the tube, and the wire was worn approximately 0.020 in. where the moving wire could contact the stainless-steel housing. This and other similar tests showed that the relative movement induced by flow could result in localized corrosion areas at the point of contact between two surfaces. Sliding- and impact-wear tests were conducted in autoclaves in deionized water at 1500 psi. The sliding-wear test, consisting of a rotating disk in contact with a stationary rod, showed that disk penetration and rod wea
creased with increasing temperature
range from 100 to 400°C. The test also
that the wear increased with contact press
from 5 to 15 psi and also with rotational
of the disk. The impact-wear test consis
a solenoid-activated cylindrical plunger
with Zircaloy-2 impacting against a Zirca
flat plate. Results indicated over twice
plunger wear with an increase in the water
perature from 200 to 400°C.

An out-of-reactor test facility, shown
IV-6, was utilized to test an individual rea
pressure-tube fuel-element assembly at ope
ing flow and temperature. Fretting marks
after facility operation prompted additional
in vertical test sections. Initial tests were
ducted with a Zircaloy-2 collar mounted a
bottom of a steel rod suspended in a tube
with Zircaloy-2. The fretting attack was
to be independent of water velocity in the
from 15 to 30 ft/sec but quite sensitive
clearance between the three centering fe

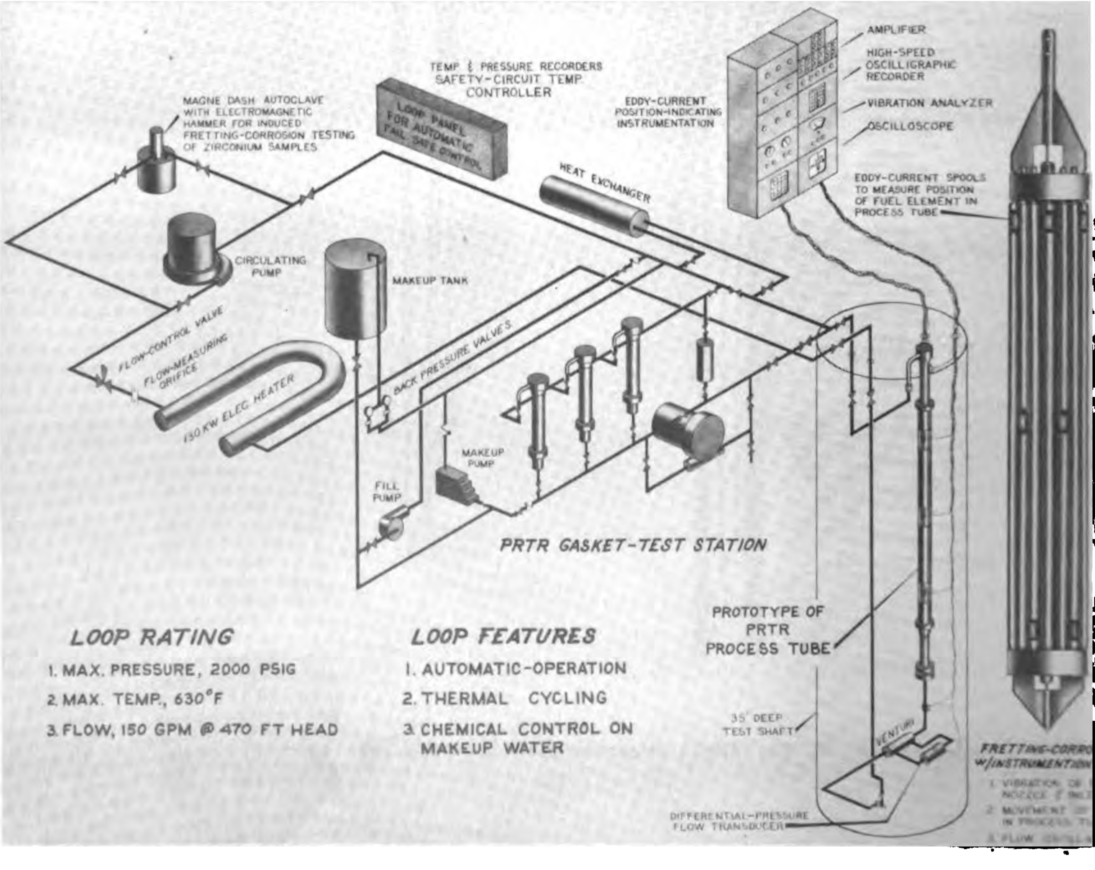
TEMP & PRESSURE RECORDERS
SAFETY-CIRCUIT TEMP CONTROLLER
LOOP PANEL FOR AUTOMATIC FAIL SAFE CONTROL
MAGNE DASH AUTOCLAVE WITH ELECTROMAGNETIC HAMMER FOR INDUCED FRETTING-CORROSION TESTING OF ZIRCONIUM SAMPLES
EDDY-CURRENT POSITION-INDICATING INSTRUMENTATION
AMPLIFIER
HIGH-SPEED OSCILLIGRAPHIC RECORDER
VIBRATION ANALYZER
OSCILLOSCOPE
EDDY-CURRENT SPOOLS TO MEASURE POSITION OF FUEL ELEMENT IN PROCESS TUBE
HEAT EXCHANGER
CIRCULATING PUMP
MAKEUP TANK
FLOW-CONTROL VALVE
FLOW-MEASURING ORIFICE
BACK PRESSURE VALVES
130 KW ELEC. HEATER
MAKEUP PUMP
FILL PUMP
PRTR GASKET-TEST STATION
LOOP RATING
1. MAX. PRESSURE, 2000 PSIG
2. MAX. TEMP., 630°F
3. FLOW, 150 GPM @ 470 FT HEAD
LOOP FEATURES
1. AUTOMATIC-OPERATION
2. THERMAL CYCLING
3. CHEMICAL CONTROL ON MAKEUP WATER
PROTOTYPE OF PRTR PROCESS TUBE
35' DEEP TEST SHAFT
VENTURI
DIFFERENTIAL-PRESSURE FLOW TRANSDUCER
FRETTING-CORRO
W/INSTRUMENTATION
1. VIBRATION OF
NOZZLE
2. MOVEMENT
IN PROCESS
3. FLOW

Fig. IV-6 Out-of-reactor test facility.[2]

collar and the tube. The attack also in- ased with temperature and with a superim- ed external vibrating force. Later tests were ducted in a vertical test assembly consisting he upper 10 ft of a PRTR pressure tube con- ıing a fuel assembly. Water at 300°C was culated upward through the fuel assembly at ı flow rate of 123 gal/min. After two weeks tting marks, approximately 0.005 in. deep, :e noted at the contact points between the ssure tube and the centering feet of the l-assembly end brackets. Continued testing not always increase the depth of penetra- ı, indicating that the process may be inter- :tent. Increasing the contact surface tended lecrease the penetration.

The out-of-reactor tests generally have shown .t fretting attack is increased with increased nperature, vibration, and clearance. The)cess seems to be one of removing the pro- :tive oxide film mechanically and thus per- tting progressive oxidation of the Zircaloy.

The in-reactor examination of the condition the pressure tubes consisted of visual in- ection and measurement of the depth of ob- rved marks.[4–6] A television-camera–bore- ope arrangement was used to examine the ıer surface of the pressure tube and to read dial indicator used to measure the depth of ırks. The number and location of fretting ırks are given in Table IV-1, and an example one of the more severe fretting marks is ıown in Fig. IV-7. This mark was detected :ring an examination of all the pressure tubes May and June of 1962. The diagonal fretting ark is the result of contact with a wire wrap 'ound a fuel assembly and is approximately 025 in. deep. The wire wrap was worn suf- ciently to allow two of the fuel rods to contact e tube wall, and the vertical fretting mark re- ılted.[5]

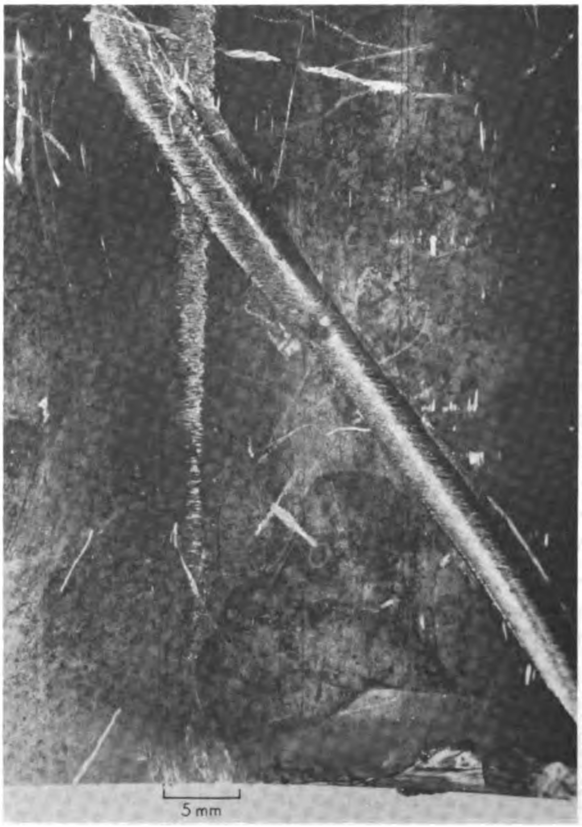

Fig. IV-7 Pressure-tube fretting mark.[2]

The severity of fretting corrosion has decreased as some of the causes have been discovered and corrected. For example, the width of the centering feet on the fuel assemblies has been increased on new fuel, and this has decreased the severity of the fretting.[6] Some of the fretting was attributed to a failed flow-straightening baffle, which has been replaced. Tests are continuing to define more precisely the reasons for fretting attack and to find methods for minimizing or eliminating this

Table IV-1 NUMBER AND LOCATION OF PRESSURE-TUBE FRETTING MARKS[2]

Fuel-element component making mark	9/60 to 6/62*		7/62 to 11/63*		Total*	
	No.	%	No.	%	No.	%
Centering feet, upper end bracket	327	20.0	418	24.2	745	22.1
Centering feet, lower end bracket	484	29.6	524	30.3	1008	30.0
Wire wraps	674	41.2	788	45.5	1462	43.5
Unclassified	150	9.2	1		151	4.4
	1635	100.0	1731	100.0	3366	100.0

*Includes marks found on tubes that have been removed from the reactor.

problem. Techniques are under development for continuous monitoring of PRTR pressure tubes to detect excessive fretting attack — for example, monitoring of the zirconium content of the water shows some promise.[7] Of the analytical methods available (emission spectrographic, radiochemical, and spectrophotometric), emission spectrography is considered most reliable for measuring zirconium contents as low as 0.10 ppb. Work is continuing on the correlation of the results of this technique with fretting attack. Recently a vibration-monitoring program has also been started. Velocity type transducers have been installed on the inlet jumpers of selected pressure tubes; sufficient data have not been obtained as yet to enable a correlation between vibration measurements and zirconium concentration in the coolant water.

References

1. S. J. Fanciullo, Development of Liquid Metal Level Probes, USAEC Report PWAC-423, Connecticut Aircraft Nuclear Engineering Laboratory, 1964
2. W. K. Winegardner, Fretting Corrosion in tonium Recycle Test Reactor, USAEC Repo 80021, Hanford Atomic Products Operation, 1964.
3. N. G. Wittenbrock, P. C. Walkup, and J. K. son, Plutonium Recycle Test Reactor Fi guards Analysis, USAEC Report HW-612 ford Atomic Products Operation, Oct. 1, 19
4. D. R. Doman and P. J. Pankaskie, In-R Monitoring of Zircaloy-2 PRTR Pressure Part I, September 1960–May 1962, USAEC HW-73701(Rev.), Hanford Atomic Products tion, May 1962.
5. D. R. Doman and P. J. Pankaskie, In- Monitoring of Zircaloy-2 PRTR Pressure Part II, May and June 1962, USAEC Repor 74731, Hanford Atomic Products Operati gust 1962.
6. P. J. Pankaskie, In-Reactor Monitoring caloy-2 PRTR Pressure Tubes, Part II, 1963–November 1963, USAEC Report HW- Hanford Atomic Products Operation, De 1963.
7. T. F. Demmitt, Zirconium Concentration Mea ments in the PRTR Primary Coolant: Inter port, December 8, 1962 to June 30, 1963, Report HW-78080, Hanford Atomic Products ation, July 1963.

Section
V

Power Reactor Technology

Specific Reactor Types

odium-Graphite eactors: Steam Cycles

recent steam-cycle optimization study[1] has :en made for sodium-graphite nuclear power ants to determine optimum steam conditions ıd sodium-system parameters for plants in the ›0- to 400-Mw(e) size range. The general re- ılts are summarized as follows:

1. For plant ratings up to approximately 350 w(e), a 2400-psig steam pressure results in e most economical operating condition.
2. For plant ratings above 350 Mw(e), a ›00-psig steam pressure results in the most :onomical operating condition.
3. The highest justifiable initial and reheat eam temperatures are 1000°F each for reheat /cles at a reactor outlet temperature of 50°F.
4. For most economical operation the sodium mperature rise across the reactor should be the range of 350 to 375°F.
5. For the 2400-psig steam cycle, the most :onomical log mean temperature differential of ıe intermediate heat exchanger is 65 to 80°F. For the 3500-psig steam cycle, this range is 85 to 95°F.

The optimum (most economical) cycles for a fuel-cycle cost of \$0.20 per 10^6 Btu and a reactor sodium outlet temperature of 1150°F, in the 400-Mw(e) size, are summarized in Table V-1.

In this study heavy emphasis was given the steam portion of the plant, inasmuch as the costs of the reactor and related sodium systems are relatively insensitive to the steam pressure used, once the outlet sodium temperature for the reactor has been fixed. The major components of the power-generating system considered are shown schematically in Fig. V-1, along with typical sodium and steam temperatures and pressures.

The steam-cycle study was divided into three phases. During phase I studies were made for steam pressures of 1450, 1800, 2400, and 3500 psig for a 350-Mw(e) plant. The basis of comparison was the total evaluated cost, made up of major-equipment costs and capitalized energy costs.

Bases are given in Ref. 1 for costs of such items as heat-exchanger surfaces, feedwater

Table V-1 CHARACTERISTICS OF OPTIMUM STEAM CYCLES FOR 400-Mw(e) PLANTS[1]

	7% capital-charge rate	14% capital-charge rate
Steam throttle pressure, psig	3500	3500
Initial and reheat steam temperatures, °F	1000 each	950 each
Type of steam cycle	Double reheat	Double reheat
Type of steam turbine (last-stage blading size)	Cross compound double flow (30 in.)	Tandem compound four flow (30 in.)
Net station heat rate, Btu/net kw-hr	7665	7870
Fuel-cycle cost at \$0.20 per 10^6 Btu, mills/net kw-hr	1.53	1.57
Reactor sodium ΔT, °F	350	350
Intermediate heat exchanger log mean temperature difference, °F	95	95

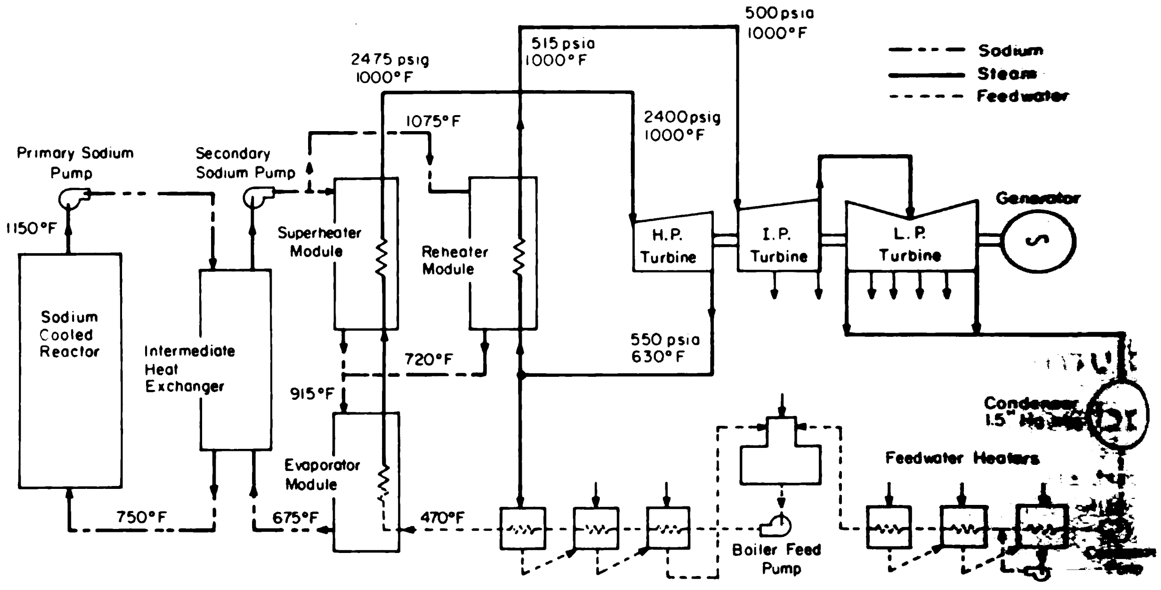

Fig. V-1 Typical schematic of sodium-graphite nuclear power-generating system.

heater-supply and treatment systems, and the steam-condensate systems. Variations in reactor thermal rating due to changes in cycle efficiency were accounted for by use of a reactor cost differential of \$50,000 per 1% change in reactor rating. For the phase I study, all fuel-cycle costs were based on \$0.20 per 10^6 Btu. Other assumptions used for evaluating fuel-cycle costs are also presented.[1]

Phase I results are summarized as follows:

1. The steam-pressure condition with the lowest cost at a 14% capital-charge rate is 2400 psig; the next best pressure is 3500 psig.
2. At a 7% capital-charge rate, the steam-pressure condition with the lowest cost is 3500 psig, followed by the 2400-psig pressure condition.
3. At a 14% capital-charge rate, the best steam-temperature condition is 950°F; at a 7% capital-charge rate, either 950 or 1000°F is recommended.

During phase II a system pressure of 2400 psig was used for a more detailed study of various parameters of a 350-Mw(e) plant.

The following summarizes phase II results:

1. A 350°F sodium-temperature differential across the reactor is optimum.
2. A 65 to 80°F log mean temperature difference for the intermediate heat exchanger is optimum.
3. Although the cross-compound turbine generators with 1800-rpm low-pressure sections are more efficient and provide improved turbine-cycle heat rates over the tandem-compound machines at 3600 rpm, the significant higher cost of the cross-compound unit more than offsets the savings in operating costs for \$0.20 per 10^6 Btu fuel costs.
4. The optimum feedwater temperature is 475°F.
5. As fuel costs increase from \$0.20 to \$0.25 per 10^6 Btu, the trend is toward the more efficient cycle (steam pressure of 2400 psig and initial and reheat steam temperatures of 1000°F).
6. As the plant-capacity factor decreases from 80 to 60%, the trend is to the less efficient cycle (steam pressure of 2400 psig and initial and reheat steam temperatures of 950°F.
7. It is difficult to justify the added capital cost of high-pressure feedwater heaters for feedwater temperatures above 475°F with \$0.20 per 10^6 Btu fuel costs.

In phase III the basic effort was to study in detail the merits of 2400- vs. 3500-psig steam for a 400-Mw(e) plant with 14 and 7% capital-charge rates. For these studies the reactor sodium outlet temperature was held at 1150°F. Areas investigated were generally similar to those in phase II.

esults for the phase III study are summa- ed as follows:

. The 3500-psig double-reheat plant with 0°F steam temperatures and a 7% capital- rge rate provides savings of $1,485,000 over 2400-psig case.

. The 3500-psig plant with 950°F steam peratures and a 14% capital-charge rate ears to provide savings of $292,000 and 44,000 for single and double reheat, respec- ely, over the single-reheat case with 2400- g steam. However, additional analyses would required to verify this trend.

3. A 1050°F steam temperature is not justi- d for any steam-pressure condition studied.

4. The tandem-compound four-flow turbine th a 30-in. last-stage blade is the best selec- n at 14% capital-charge rates: the cross- mpound double-flow unit with a 43-in. last- age blade is the best with the 7% capital- arge rate.

Naturally any generalized study of this kind n be only as valid as the assumptions on which is based, and the author of Ref. 1 has pointed out the need for basing the steam conditions in an actual plant design upon the specific site and ground rules as related to a specific utility company. It is also well to recognize that optimum conditions are strongly affected by the particular designs of some of the components in the sodium system.

The economic results of the study would not apply to other sodium-cooled reactors because the effects of changes in reactor capital costs and fuel costs were not investigated over a wide range. For example, the much lower fuel cost of a sodium-cooled fast reactor plant would tend to justify lower steam-cycle temperature conditions and therefore lower optimum cycle efficiencies than those found for the sodium-graphite case.

Reference

1. G. A. Schneider, Steam Cycle Optimization Study for Large Sodium Graphite Nuclear Power Generating Stations, USAEC Report NAA-SR-9488, Atomics International, Aug. 31, 1964.

Section

VI

Power Reactor Technology

Unconventional Approaches

Fast Supercritical Water Reactor

As a part of the continuing study effort for the U. S. Atomic Energy Commission's Division of Reactor Development, Hanford Atomic Products Operation issued a report by Aase et al.[1] describing the design and economic evaluation of a 300-Mw(e) fast supercritical-pressure water reactor. The fast supercritical-pressure power-reactor (FSPPR) design employed a fast breeder-reactor concept, a plutonium-uranium fuel cycle, and supercritical water as the coolant. Hanford has been involved in the design of supercritical-pressure power reactors for some time, and an earlier design,[2] the supercritical-pressure power reactor (SPPR), was reviewed in *Power Reactor Technology*, 6(3): 73-78 June (1963). The SPPR is quite different in design than the FSPPR in that it is a thermal reactor employing UO_2 as the fuel material. The earlier work was utilized in the preparation of Ref. 1, however, to establish the design of the auxiliary systems for the FSPPR.

The FSPPR was designed for a power of 677 Mw(t) with a net efficiency of 44.3%. The reactor core is fueled with plutonium and uranium oxides with a moderator-segmented-core design and axial and radial blankets. The moderator-segmented-core design was expected to overcome some of the safety considerations that must be dealt with in a fast reactor design and will be discussed shortly. A direct-cycle system provides supercritical-pressure water coolant with turbine-inlet conditions of 3500 psig and 1050°F. Figure VI-1 shows a simplified feedwater-and-steam-system schematic for the FSPPR. It can be seen that two stages of reheat are employed using regenerative heat exchangers and a cross-compound turbine. reactor incorporates three coolant passes temperature control at the inlet to the se and third passes. This coolant-temperatu control system was intended primarily to pensate for the changes in power distrib expected during the life of the core. Sho Fig. VI-2 are one reactor core, a portion o piping, and the containment vault. The tainment vault is designed to contain two re tors in a tandem arrangement. This tan arrangement allows refueling of one core w the other core is in operation, although sim taneous operation of the two cores was intended. It was felt that this type of des should reduce reactor downtime quite sign cantly and thereby increase the product period of the plant. A single FSPPR core w designed for approximately 4.9 full-power yea equivalent to approximately 6.1 calendar yea The volume between the two main reactor va in Fig. VI-2 is a basin to be used in fuel operations. One of the FSPPR cores can b seen in the upper portion of the figure; bel the reactor core is the fuel-transfer pot to used in refueling. A series of headers is plac at the top of the reactor-core assembly deliver and remove the supercritical coola from the various passes of the reactor co Numerous jumper assemblies are utilize few of which are shown in Fig. VI-2, to co nect the toroidal headers to the core assemblies.

The internal composition of the core can seen in Figs. VI-3 and VI-4. The cross sect of the core in Fig. VI-3 shows the two c regions that are refueled with uranium ox and plutonium oxide and separated by an sorber region that contains moderator tank The control rods for the core are locate the moderator tanks, and a radial blanket

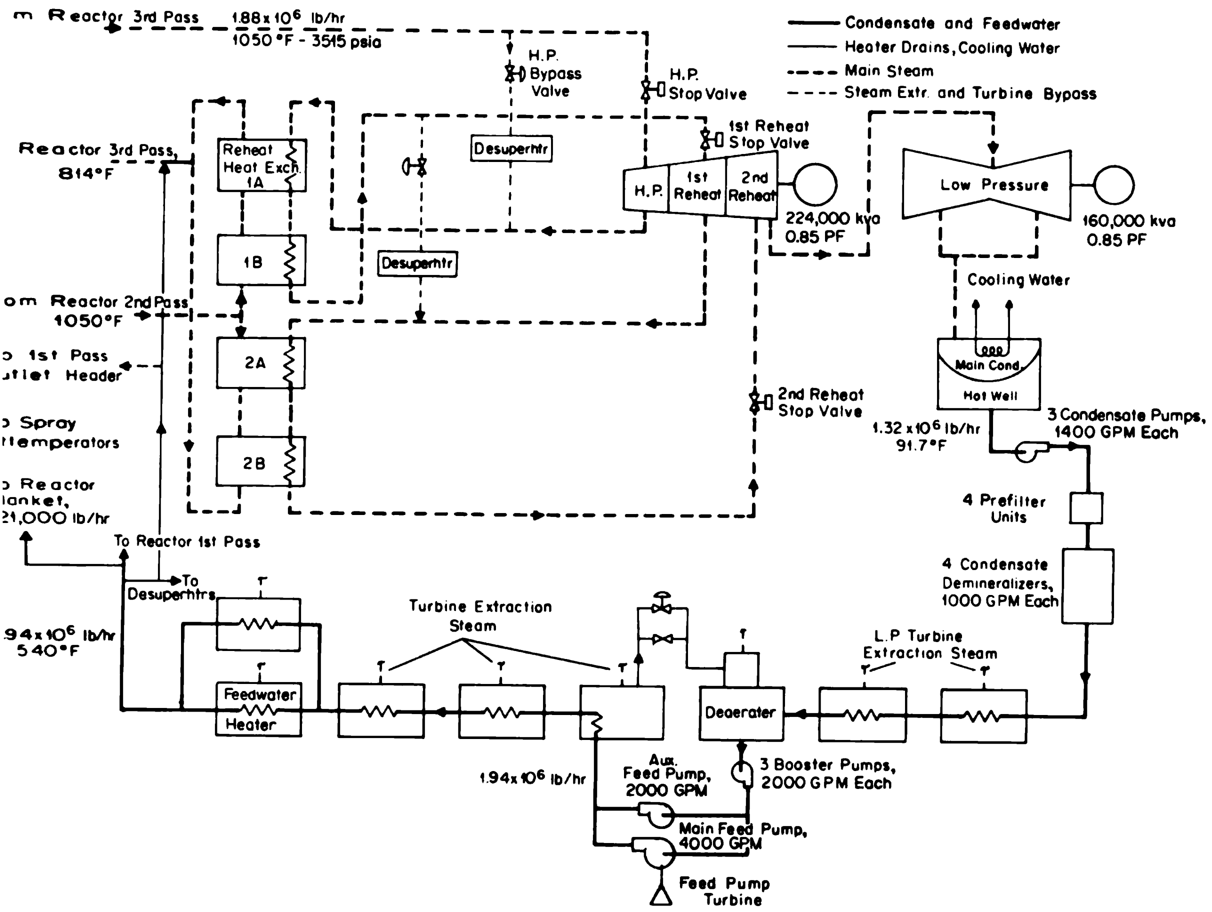

Fig. VI-1 Simplified feedwater and steam system of the FSPPR.

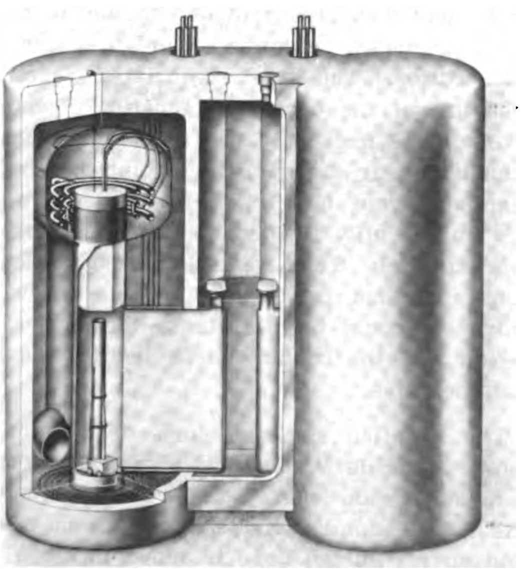

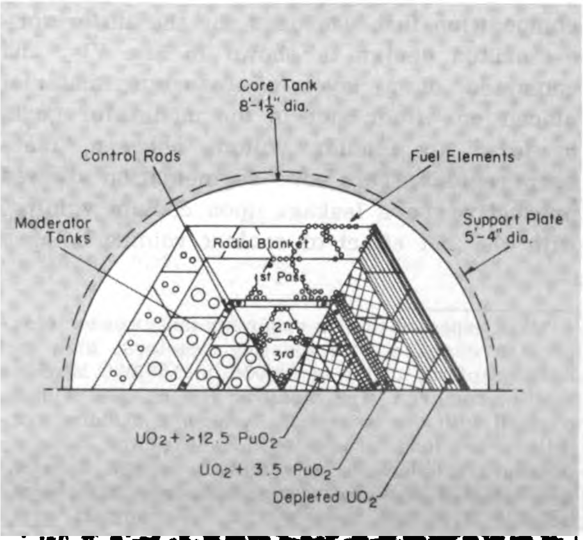

Fig. VI-2 The FSPPR.[1]

Fig. VI-3 Core layout of the FSPPR.[1]

placed around the core assembly. Three coolant passes are provided for the central section of the core, and coolant also is delivered to the radial blanket. The upper and lower axial blankets can be seen in Fig. VI-4. These fuel assemblies are provided either in equilateral triangular shapes or in trapezoidal shapes. Coolant flows to the fuel elements at the outer rows of tubes of the elements, flows down the elements to a mixing chamber at the bottom, and returns up the central portion of the element. The top and bottom of the elements are closed with porous plugs to allow the escape of fission gases.* The fastening plate on the inlet and outlet fuel-element pipes is connected to the top support plate of the reactor, with the fuel elements being suspended from the reactor top support plate. The characteristics of the FSPPR are given in Table VI-1.

The nuclear design of the FSPPR utilized the previously mentioned moderator-segmented-core concept to overcome some of the difficulties associated with the use of a moderating material, water, as the coolant. The amount of water in the reactor core was kept as low as possible to maintain a sufficiently hard neutron spectrum to permit economic operation. The use of a moderator-segmented core reduced the interaction between the coolant and the neutrons by enhancing the internal leakage effect of the core. The coolant flow was arranged such that the lower density flow occurred at the center of the core. The core composition that was used for the moderator-segmented design is shown in Fig. VI-3 and consisted of a layer of absorbing material placed on either side of the moderator tanks to form an annular volume between "fast" core regions. This core segmentation allowed productive core leakage upon coolant voiding, with the net effect of coolant voiding being a reduction of reactivity. A negative floo coefficient was also provided in the desig the appropriate selection of fuel-to-water ume ratios. The total calculated reacti behavior of the core as a function of coo inventory is presented in Fig. VI-5. It ca seen that near the operating point the coo reactivity void coefficient is nearly zero that in the fully flooded condition the cor approximately 9% $\Delta k/k$ subcritical. Calc tions indicated that a considerable amoun hydrogen could be lost from the modera region and the coolant coefficients would main negative.

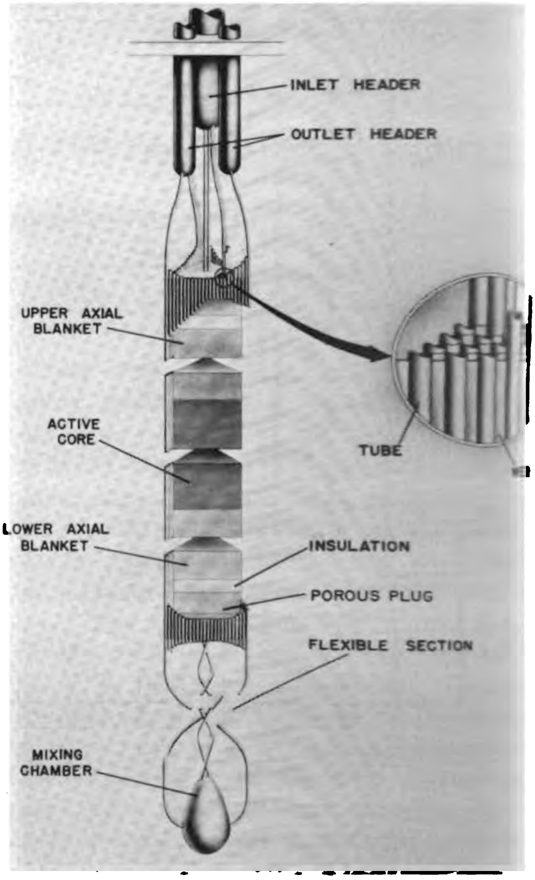

Fig. VI-4 Fuel-element assembly of the FSP

The detailed nuclear core descripti shown in Table VI-2. At the center of the a mean fission energy of 82 kev was cal lated. The radial distribution of the mean sion energy in the core is shown in Fig. V and the calculated initial and end-of-life ra power distributions are shown in Fig. V

---

*It is expected that, in order for fast breeder reactors to compete with existing reactors, high fuel burnups of the order of 80,000 to 100,000 Mwd/ton may be required. The resulting fission-gas release, coupled with the potentially weakened cladding condition after long irradiation, magnifies the internal-pressure problem in fuel-element design. Fission-gas volumes provided to accommodate this release become large and unwieldy for the compact cores envisaged. Faced with these problems some designers are talking of concepts in which "controlled venting" of fuel-element fission gases would be employed. Gases would be collected and separated from the cover gas and processed.

Table VI-1 CHARACTERISTICS OF THE CONCEPTUAL FAST SUPERCRITICAL-PRESSURE POWER-REACTOR (FSPPR) PLANT

General characteristics	
Thermal power, Mw	677
Net electric power, Mw	300
Net efficiency, %	44.3
Gross efficiency, %	47.1
Auxiliary power, Mw	2.83
Equivalent main feed-pump power, Mw	9.93

	General	First pass	Second pass	Third pass	Radial blanket
Reactor dimensions					
Outside dimension of each region, in.		34.8	22.8	13.3	43.5
Core height, in.	60				
Core + axial-blanket height, in.	75¾				
Core volume, liters	3095				
Flux-trap thickness, in.	~8.75				
Reactor fuel inventory					
Depleted uranium, kg	30,895				15,407
Total plutonium, kg	1559				
Fissile plutonium, kg	1059				
Reactor power density, kw/liter of core + blanket	218.7				
Reactor specific power, kw/kg of uranium + plutonium	50				
Fuel-element assembly					
Fuel material	PuO_2 + depleted UO_2				
Initial enrichment, % plutonium		14.5	12.5	12.5	
Fuel density, g/cm^3	9.3				
Flux-trap material	PuO_2 + depleted UO_2				
Enrichment, % plutonium	3.8				
Fuel-element type	Equilateral triangle or trapezoid				
No. of fuel elements	72	18	18	6	30
No. of cooling tubes per fuel element		1216	686	730	43
Fuel-element active length, ft	5				
Fuel-element overall length, ft	15.25				
Cooling-tube material	René 41				
Cooling-tube inside diameter, in.		0.146	0.160	0.204	0.286
Cooling-tube wall thickness, in.		0.013	0.022	0.027	0.030
Cooling-tube spacing, in. (on triangular pitch)		0.291	0.269	0.358	1.20
Weight of fuel per fuel element, lb of oxide		1544	523	906	1132
Fuel-cladding material	René 41				
Cladding thickness, in.		0.090	0.083	0.080	0.090
Heat removal					
Maximum heat flux, Btu/(hr)(sq ft) (× 10^{-5})	8.93	8.73	7.00	6.43	
Average heat flux, Btu/(hr)(sq ft) (× 10^{-5})	2.91	2.98	2.27	4.14	
Average core power density, kw/liter	230				
Maximum fuel temperature, °F	2260	2260	1740	1930	
Maximum pressure-tube temperature, °F	1385	1300	1385	1320	

Table VI-1 (Continued)

	General	First pass	Second pass	Third pass	Radial blanket
Coolant conditions					
Pass inlet temperature, °F		514	804	820	
Pass outlet temperature, °F		804	1050	1050	
Pass inlet pressure, psig		4360	4330	4100	
Turbine throttle pressure, psig	3515				
Coolant flow rate, lb/hr × 10^{-6}	1.88				
Coolant *p*H	8.7 to 9.0				
Nuclear characteristics					
Core life					
Full-power years	4.85				
Calendar years	6.06				
Average fuel irradiation level at discharge, Mwd/metric ton	83,700	69,160	96,840	122,500	
Initial fuel isotopic composition					
^{239}Pu, % of total plutonium	55				
^{240}Pu, % of total plutonium	32				
^{241}Pu, % of total plutonium	13				
Neutron lifetime, sec	8.7×10^{-7}				
Effective neutron fraction	0.0041				
Final fuel isotopic composition					
^{239}Pu, % of total plutonium		63.0	64.0	54.6	
^{240}Pu, % of total plutonium		28.0	25.0	32.1	
^{241}Pu, % of total plutonium		9.0	11.0	13.3	
Initial flux-trap enrichment, % plutonium	3.8				
Final flux-trap enrichment, % plutonium	5.2				
Fuel-temperature effect, m*k*	−20				
Other temperature effects, m*k*	2				
Total safety-rod strength, m*k*	50				
Total control-rod strength, m*k*	25				
Breeding ratio, core + blankets	1.14				
Moderator characteristics					
Moderator material	YH_x or $ZrH_x + H_2O$				
YH_x or ZrH_x, vol.%	70				
Reactor heat in moderator, Mw	1.3				
Control					
No. of control rods	6				
Control-rod material	Stainless steel–1.25% natural boron				
Control-rod diameter, in.	¾				
No. of safety rods	6				
Safety-rod material	Stainless steel–1.10% B^{10}				
Safety-rod diameter, in.	¾				
Coolant	H_2O (same as used for moderator)				
Power-cycle components					
Turbine type	Cross compound				
No. of reheats	2				
High-pressure-stage conditions, °F/psi	1050/3515				
First-reheat conditions, °F/psi	1000/912				
Second-reheat conditions, °F/psi	1000/299				
Exhaust pressure, in. Hg	3.5				
Condenser size, sq ft	110,000				
No. of feedwater stages, including deaerator	7				
No. of feedwater pumps	2				

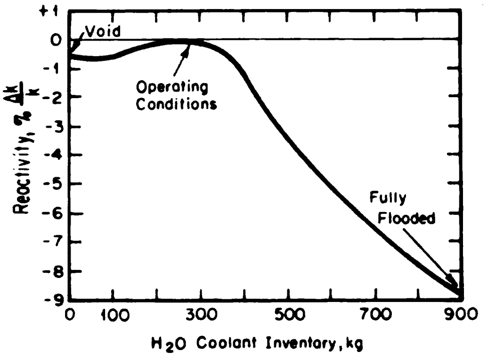

. VI-5 *Reactivity change vs. coolant inventory for FSPPR.*[1]

Table VI-2 NUCLEAR CORE-DESIGN DATA[1]

Region	Radius, cm	Description	Enrichment, % plutonium	Coolant pass	Coolant density, g/cm³	Composition, vol.%				
						Fuel	Coolant	Tube	Wall	Void
1	30.8	Third reactor core	12.5	3	0.108	46.4	30.9	18.4	1.7	2.6
2	44.2	Second reactor core	12.5	2	0.121	46.0	30.7	18.4	1.9	3.0
3	51.2	Absorber region, low plutonium enrichment	3.8	2	0.121	46.0	30.7	18.4	1.9	3.0
4	54.2	Zirconium hydride moderator, water cooled		Low-pressure water		70, ZrH_x	30			
5	61.2	Absorber region, low plutonium enrichment	3.8	1	0.445	63.9	21.3	12.8	0.9	1.1
6	80.4	First reactor core	14.5	1	0.445	63.9	21.3	12.8	0.9	1.1
7	100.4	Depleted uranium	0.0	1	0.445	85.9	5.7	2.2	2.9	3.3

e dimensions and worths of the control and fety rods are presented in Table VI-1. Some dial enrichment zoning was done in the sorber region to reduce power peaking in is region over core lifetime. A fuel-tempera re coefficient of reactivity was computed for e Doppler broadening of the ^{238}U resonances ly as $-2 \times 10^{-5} \Delta k/(k)$(°C). It was recognized at a further positive contribution to the fuel- mperature coefficient would be available from ^{9}Pu and that a negative contribution would be ailable from ^{240}Pu; however, these were not alculated. Fuel- and cladding-expansion ef cts were estimated to be approximately $0^{-6} \Delta k/(k)$(°C). The majority of the static eactor-physics calculations were done utiliz g diffusion-theory codes, and some checking f the validity of diffusion theory for a core of his type with a moderator region located nternally was done using a multigroup trans ort code. The results[1] obtained from the two nethods of calculations "... generally con irmed the data yielded by diffusion theory, although differences in reactivity values indicate that perhaps diffusion theory gave more conservative results."

In calculating the pressure drops of the fuel-element cooling channels, it was determined that a large variation between the minimum and maximum pressure drops within an element existed; however, when the maximum pressure drop was used, the calculated core total pressure drop was 658 psi, and the total pressure drop across the reactor, including turbine reheat exchanges and associated piping, was about 800 psi. The heat-transfer correlations of Chalfant* were used at pressures above 4000 psia. Similarly the correlation of McAdams* was used at pressures from 3500 to 4000 psia. The maximum heat flux in all cases was limited by the pressure-tube wall temperature.

The proposed refueling scheme involves fueling one of the tandem reactors before the other reactor is shut down. The newly loaded reactor then begins operation while the exposed fuel is allowed to decay for a period of two to three months in the reactor core. The fluid jumpers for the individual fuel elements are remotely cut, and the fuel elements are transferred to the fuel storage basin. Plugs are then placed in severed coolant jumpers until the time of refueling, at which time the jumpers are temporarily frozen with liquid nitrogen and the coolant jumpers of the new fuel elements are welded in place. Removal of the frozen coolant

---

*The reader may wish to refer to Refs. 7 and 8 of Ref. 1 for these correlations.

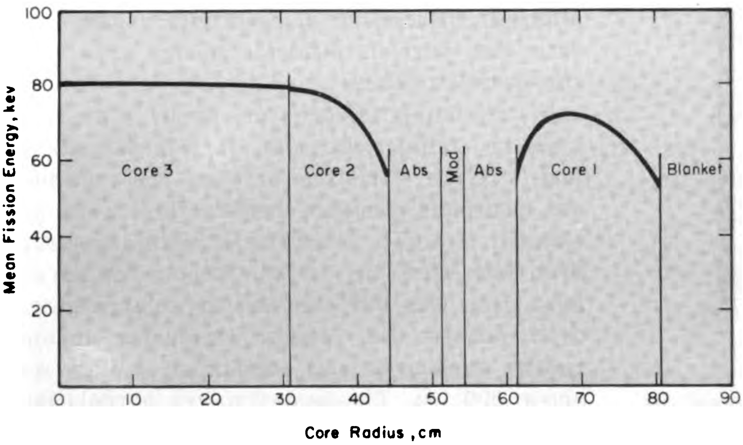

Fig. VI-6 Mean-fission-energ distribution in the FSPPR.[1]

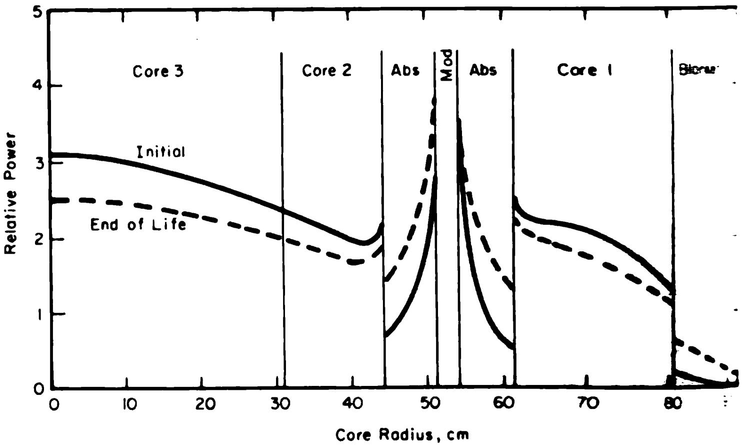

Fig. VI-7 Power distribution in the FSPPR.[1]

then restores the function of the coolant passages.

Startup of the reactor involves first purging the water in the coolant channels with low-density steam to reduce the large shutdown margin. The approach to criticality is made by control-rod withdrawal, and on reaching criticality the design power is approached by simultaneously programmed manipulations of rod position, pressurization, and flow. During normal operation the load changes are accomplished by positioning of the turbine admission valve, and the reactor power level is automatically adjusted, using a banked-control-rod configuration, to hold the coolant outlet temperature constant. Additional control and safety systems are provided to ensure safe operation at power.

The power-generation costs that were computed for the FSPPR are shown in Table VI-3. The cost data given in the "Guide to Nuclear Power Cost Evaluation" handbook were used to arrive at the computed unit cost of po generation of approximately 5.12 mills/kw-

The following required technological devel ments are enumerated:[1]

(1) Analytical and experimental verificatio practical and economical moderator segm core design.

(2) Demonstration of the Doppler effect as a liable prompt negative coefficient in fast cera fueled reactors.

(3) Demonstration of a high endurance (gre than 80,000 Mwt days per tonne) internally c ceramic-fueled element.

(4) Development of high strength alloys and rication techniques for complex pressure tub semblies that are reliable under high expos and fast neutron irradiation.

(5) Development of water treatment cleaning decontamination techniques that avoid fouling carry-over problems in a once through c system.

(6) Demonstration of reliable and economica mote fuel and pressure piping replacement m ods.

Table VI-3 POWER-GENERATION COSTS FOR FSPPR[1]

	Capital cost, $	Rate, %	Annual cost, $	Unit cost,* mills/kw-hr
Fixed charges				
Depreciating capital				
Total capital cost (less land)	51,373,000	14.46	7,429,000	3.534
Nondepreciating capital				
Land and land rights	360,000	13.0	47,000	0.022
Working capital				
Plant operation and maintenance	130,000	13.0	17,000	0.009
Fuel-cycle operations	4,015,000	13.0	522,000	0.248
Nuclear liability insurance			280,000	0.133
Subtotal: fixed charges			8,295,000	3.946
Operating costs				
Operating and maintenance cost			889,000	0.423
Fuel cost			1,572,000	0.748
Subtotal: operating costs			2,461,000	1.171
Total power-generation costs			10,756,000	5.117

*Plant factor is 80%.

anford Graphite uperheat Reactor

The N-Reactor Project Section of the Hanford tomic Products Operation[3] has recently reorted results of a design and evaluation study or a Hanford graphite superheat reactor (HGSR). hese studies involved consideration of two asic reactor sizes, a 300-Mw(e) plant and a 000-Mw(e) plant, both utilizing pressurized rocess tubes, vibratory-compacted uranium ioxide fuel, graphite-moderator blocks, and a nce-through boiling-superheating coolant passage.* Since the 1000-Mw(e) plant design is uite similar to the smaller plant design, a etailed description of the smaller plant will be resented first, followed by some indications f the differences that were encountered in the esign of the larger plant.

The process tubes, fuel elements, and coolant outing are shown in Fig. VI-8, and further escriptive material is presented in Table VI-4. s shown in Fig. VI-8, the process tube would be supported by the top primary shield, and the seal assembly on the fuel element would transmit the load of the fuel to the nozzle. This seal assembly would separate the 400°F water that enters the fuel element and flows down its outer peripheral flow channel from the steam that passes up the central flow channel of the element and exhausts from the nozzle assembly. The tube that separates the water and steam is formed in a 360° helix around the fuel-element supporting rod, thereby eliminating the need to penetrate the steam-tube wall. Subcooled water passes down the outer flow channel, and then the boiling water returns up the two inner annuli where it is further vaporized and superheated. A 10-mil Incoloy cladding is proposed for the fuel that would be uranium dioxide vibratorily compacted to approximately 92% of the theoretical density. The process tubes would be manufactured from Zircaloy (in the active core region) and stainless steel (above the core).

The general arrangement of process tubes, control rods, graphite stack, and coolant-flow zones is shown in Fig. VI-9. Further information is contained in Table VI-4. As shown in Fig. VI-9, the graphite stack is composed of horizontal layers of blocks of graphite with successive layers oriented at right angles to each other. The process tubes and the continuous-chain control rods then pass through the openings provided for them in the graphite stack. The dimensions of the graphite blocks are such that ventilating voids are provided

---

*These designs bear some similarities to the raphite-moderated superheating reactor located at he USSR Beloyarsk Power Station. This reactor was escribed in *Power Reactor Technology*, 8(1): 28-34 (Winter 1964–1965), and the reader may wish to refer to that review for a comparison. Some of the major differences in the two designs involve the general mechanical arrangement of the fuel, the fuel enrichment, and the coolant-flow-passage arrangement.

throughout the graphite stack, which would serve as steam vent volumes in the event of a process-tube rupture. Steam would escape through the core by the lifting of the layer of the stack in which the rupture occurred. Steam would then travel to a plenum located in the reflector which could carry the steam outside the reactor block. The top, bottom, and side reflectors are also composed of graphite, and they maintain the same basic layer formation with the exception that the steam-vent spaces are filled with graphite to increase the reflecting ability. Thermal and biological shields are arranged around the graphite stack. Flow to the process tubes would be controlled in 5 flow-control zones (shown in Fig. VI-9). Each of the 5 zones is divided into two halves that are supplied by headers located on opposite sides of the reactor. Each flow-control zone would theoretically contain tubes of equal power; thus by supplying a control valve on each of 10 supply headers, flow control could be tained to one-half of a zone. Fuel charg discharging would be managed along the zone plan.

The locations of the control-rod blocks also shown in Fig. VI-9. The control-rod incorporates a flexible endless chain, poison sections attached to it, and a b drive that would be supplied power by a draulic motor. This particular flexible design provides for a minimum of s height when the poison is out of the reactor also allows assistance from gravity in h the control material in the reactor. Dimens details and other information on the co rods are in Table VI-4. Cooling water wou supplied to the tubes containing the co rods, and poison could be injected into the coolant passages for backup reactivity con a flow diagram of the poison system is s in Fig. VI-10.

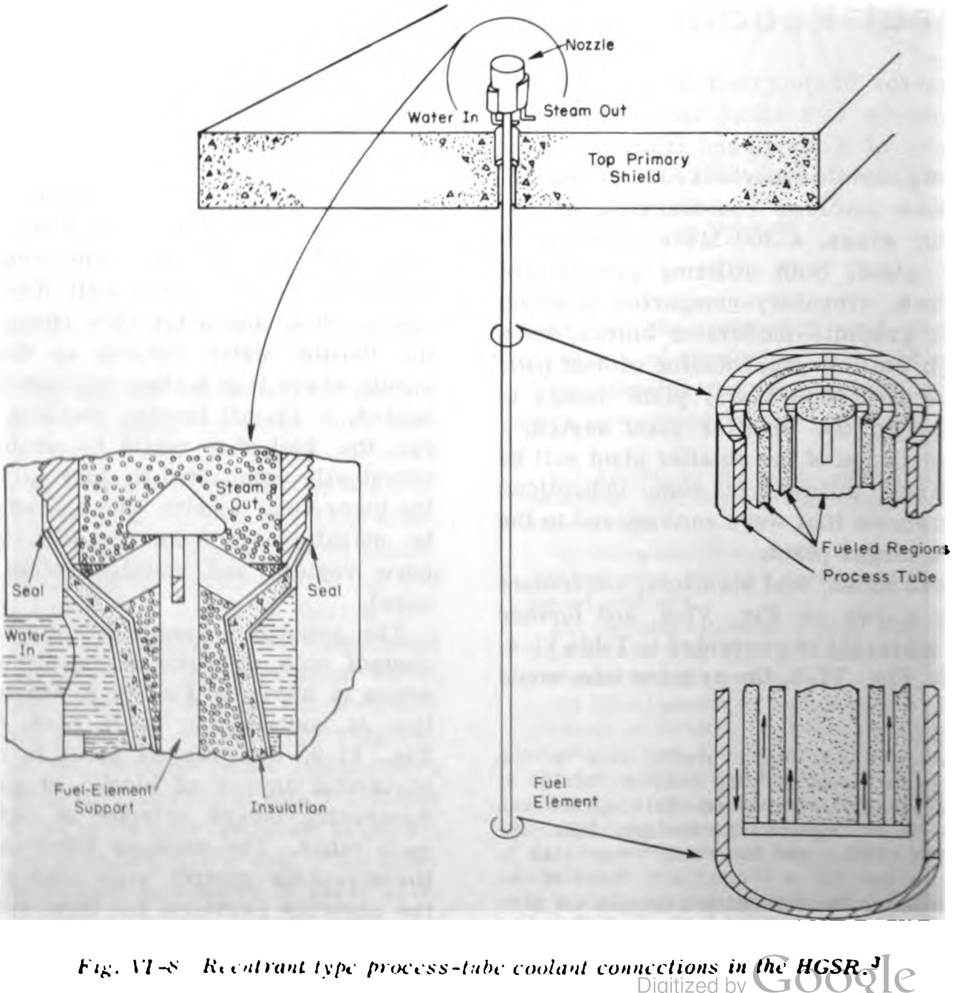

Fig. VI-8 Reentrant type process-tube coolant connections in the HGSR.[3]

Table IV-4 DATA SUMMARY FOR 300- AND 1000-Mw(e) HGSR PLANTS[3]

	300-Mw(e) plant	1000-Mw(e) plant
Gross thermal, Mw(t)	840	2700
Gross electrical, Mw(e)	321	1030
Net electrical, Mw(e)	311	1000
Exit steam condition	1100 psig, 1000°F	Same
Inlet steam condition	1525 psig, 400°F	Same
Steam flow, lb/hr	2.48×10^6	8.10×10^6
Reactor Description		
Reactor core		
Active width, ft	~18	~28
Active length, ft	~18	~26
Lattice spacing, in.	9.25	10.5
Total UO_2 loading, kg	50,600	156,000
Fuel initial enrichment	2.391 wt.%	2.37 wt.%
Reflector material	Graphite	Same
Reflector thickness	2 ft 11½ in.	2 ft 10½ in.
Fuel element		
Fuel material (~92% of theoretical density)	UO_2	Same
Fuel-element dimensions (UO_2), in.		
Outer cylinder	OD, 2.279 ID, 1.690	OD, 2.644 ID, 2.055
Inner cylinder	OD, 1.457 ID, 0.80	OD, 1.603 ID, 0.950
Rod diameter	0.50	0.490
Cladding material (base case)	Incoloy	Incoloy
Cladding thickness, in.	0.010	Same
Process-tube material	Zircaloy-2	Same
Process-tube dimensions, in.	ID, 2.475 Wall, 0.234	ID, 2.907 Wall, 0.275
Reactor-control material	Boron steel	Same
No. of control elements	64	140
Control-rod OD, in.	1.5	Same
Control-rod effective length, ft	18.2	26
Reactor mass velocities (average), lb/(hr)(sq ft)		
Boiler pass	1.22×10^6	1.38×10^6
Superheat pass	1.06×10^6	9.46×10^5
Reactor bulk-coolant inlet temperature, °F	400	Same
Reactor maximum coolant outlet temperature, °F	1115	Same
Steam coolant flow, lb/hr	2.48×10^6	8.10×10^6
Maximum fuel temperature, °F	4100	4700
Maximum cladding temperature, °F	1200	1260
Maximum heat flux, Btu/(hr)(sq ft)(°F)		
Boiler pass	4.70×10^5	4.88×10^5
Transition pass	4.84×10^5	5.21×10^5
Average heat flux, Btu/(hr)(sq ft)(°F)		
Boiler pass	2.09×10^5	2.17×10^5
Transition pass	2.15×10^5	2.32×10^5
Peak-to-average power ratio		
Axial	1.5	Same
Radial	1.5	Same
Relative radial flux distribution in fuel element		
Outer cylinder	1.29	Same
Inner cylinder	1.08	Same
Rod	1.00	Same
Average core velocity, ft/sec		
Inlet	6.5	7.2
Outlet	200	195

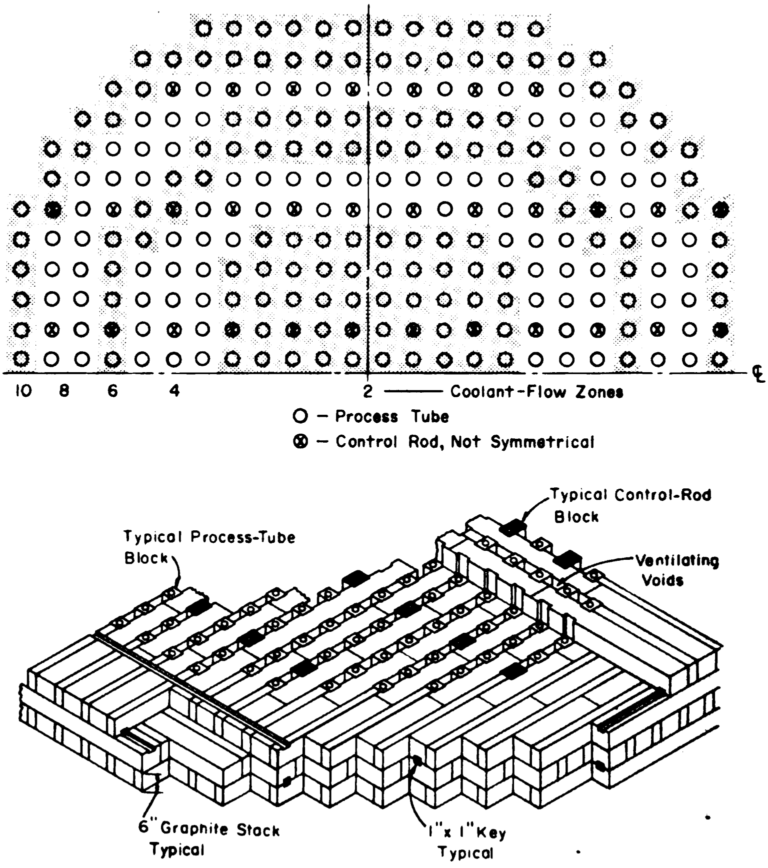

10
8
6
4
2 —— Coolant-Flow Zones
℄
○ – Process Tube
⊗ – Control Rod, Not Symmetrical
Typical Control-Rod Block
Typical Process-Tube Block
Ventilating Voids
6" Graphite Stack Typical
1"x 1" Key Typical

Fig. VI-9 General arrangement of fuel, control rods, graphite stack, and coolant-flow zones in the HGSR.[3]

The IBM-7090 program FLEX-II was used to obtain most of the physics analysis. The computed operational reactivity variations and reactivity coefficients are shown in Table VI-5. Control requirements are minimized because of an assumed staggered discharge scheme wherein about 10% of the fuel would be discharged at a time; a fuel exposure of 22,000 Mwd/ton would be obtained. As reported in Ref. 3: "... If the reactor is loaded with 2.39% enriched material, its reactivity will exceed the capacity of the control system. Therefore, some poison must be charged in the new reactor ..." It is proposed[3] that natural uranium dioxide elements be used as control material to be periodically replaced with the reference enrichment until the equilibrium fuel-management phase is achieved. Computed peak-to-average power ratios are included in Table VI-4.

The flow diagram for the steam- and feedwater-supply system, as well as for some of the auxiliary systems, is shown in Fig. VI-10. helium-gas system is supplied for the HG to provide a chemically stable environment the process tubes and the graphite modera and to provide a means of detecting sm steam or water leaks within the pile. helium would also serve as a carrier of corr sion inhibitors to protect the process tubes fr gas hydriding. Analytical instruments are pr vided in the gas loop to control the carb monoxide and the water-vapor level. During initial 20 sec following scram or shutdow cooling would be provided by the coastdown the feedwater pump; thereafter a shutdow cooling system takes over. The fuel-elem rupture monitoring system consists of a gam spectrometer, which analyzes gas from primary coolant, and a delayed-neutron tector. Location of the particular process tu containing ruptured fuel would be by means traps located in each outlet nozzle. Sup heated steam flows to the 1800-rpm tan

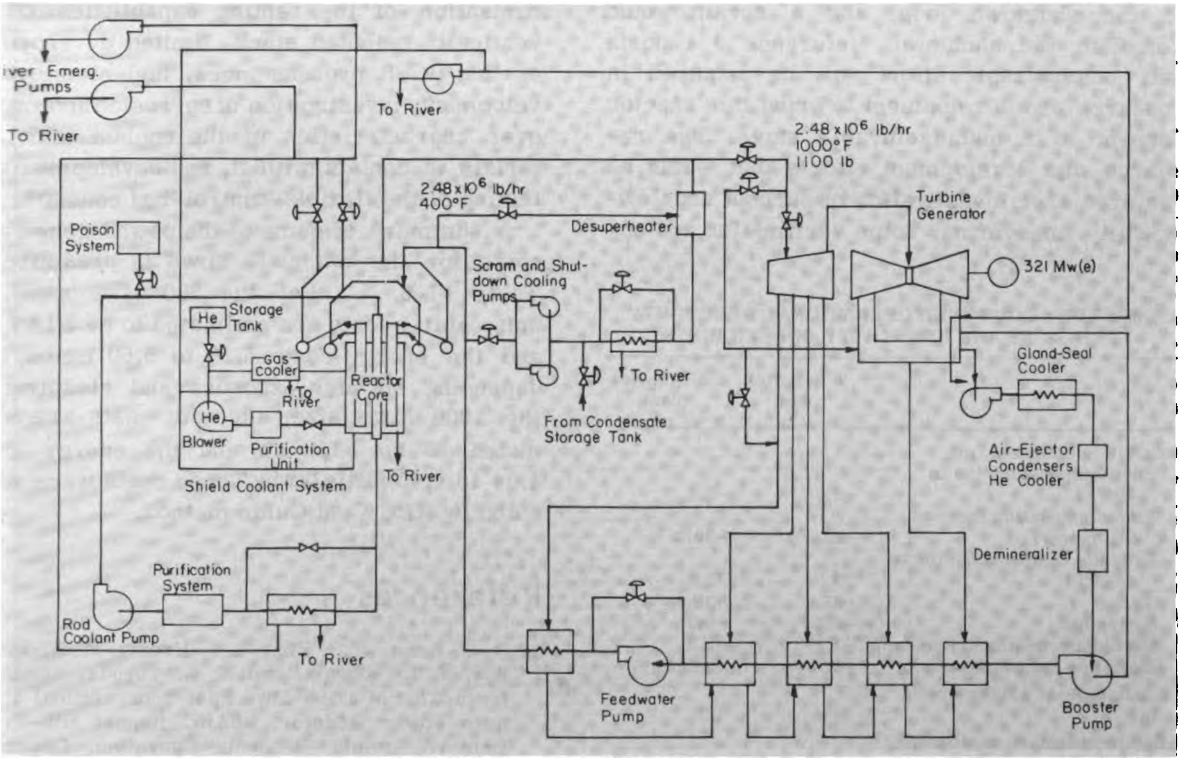

Fig. VI-10 Flow diagram of the 300-Mw(e) HGSR.[3]

mpound turbine with inlet conditions of 1000°F .d 1100 psig.

As previously mentioned, the 1000-Mw(e) sign is quite similar to, and in many in-ances identical to, the smaller design. Only ose differences which are considered sig-ficant will be mentioned here. The flow agram shown in Fig. VI-10 is the same as e schematic for the 1000-Mw(e) plant with propriate changes made in the various ratings. able VI-4 describes some of the parameters at were changed in the 1000-Mw(e) plant. he length of the uranium-bearing section of e fuel elements was increased to slightly ver 26 ft, the active width of the core was creased to approximately 28 ft, additional ntrol rods were added, and the coolant flow as divided into three flow-control zones. omputed operational reactivity variations and eactivity coefficients for the 1000-Mw(e) HGSR re shown in Table VI-5. The larger design equired doubling the capacity of the liquid-oison system, and this was accomplished by stalling two systems identical to the ones sed in the smaller plant. The circulation rate f the helium-gas system was doubled for the larger design; this maintained the same gas velocity through the reactor and the same frequency of gas exchange within the reactor. Steam for the larger unit would be supplied to two turbine-generators at the same inlet-throttle conditions. Nuclear control instrumentation would utilize the same low-level and intermediate-level systems; however, eight power-level channels would be utilized.

The HGSR was designed to operate at approximately a constant load; therefore the reactor operation would be at an approximately constant pressure and temperature. Manual control-rod movement would be used for level-load operations. The procedure that was envisioned for the cold startup involved maintaining the reactor flow rate at its normal operating value during the startup. The startup was estimated to require approximately 4 hr; the hot startup was estimated to require approximately 1 hr. Normal shutdown would be accomplished by gradual power reduction and corresponding flow reduction with steam going through the bypass to the turbine condenser. When the power level was approximately 10% of full power, the cooldown would be transferred to the shutdown loop, and a scram would complete the shutdown. Reference 3 reports that considerable effort will be required in research and development to bring this reactor concept to a manufacturable stage. The research and development efforts that would be required are: investigation of burnout and flow-stability phenomena, some verification and optimization of the venting capabilities o vertically oriented stack, limited develop of the HGSR process tubes, fuel-eleme velopment, investigation of corrosion and over characteristics of the coolant with terials in contact with it, and developme testing of the flexible-control-rod concept.

Table VI-5 COMPUTED OPERATIONAL REACTIVITY VARIATIONS AND REACTIVITY COEFFICIENTS[3]

	300-Mw(e) plant	1000-Mw(e) plant
Reactivity transient, m*k*		
Inlet temperature (68 to 400°F)	−9.5	−9.4
Power escalation (zero to full power)	−22.5	−39.6
Graphite temperature (68 to 1085°F)	29.5	32.5
Xenon	−26.9	−30.4
Samarium	−6.3	−6.3
Neptunium (plutonium holdup)	−3.4	−3.4
Exposure (22,000 Mwd/ton)	−320.0	−280.0
Calculated rod worths (total), m*k*	109	120
Inlet-temperature coefficient,* $\Delta k/(k)(°F)$	-2.85×10^{-5}	-2.82×10^{-5}
Power coefficient,*† $\Delta k/(k)(Mw)$	-2.74×10^{-5}	-1.43×10^{-5}
Graphite coefficient,* $\Delta k/(k)(°F)$	2.90×10^{-5}	3.20×10^{-5}

*These values are at "average" conditions, i.e., in a reactor containing fuel of all exposures from 0 to 22,000 Mwd/ton.

†This includes effects of water density and fuel temperature.

A summary of some of the power-gene costs for the two plant sizes is prese Table VI-6. "... For the 300 Mwe size, unit capital costs are estimated to be $14 and the energy costs 5.13 to 5.60 mills depending on fuel exposure and claddi the 1000 Mwe size, the unit costs are mated to be $112/kw and the energy 4.04 to 4.43 mills/kwh. These costs were puted by AEC Cost Guide method."

References

1. D. T. Aase, J. C. Fox, R. J. Hennig, R. E. son, S. L. Stewart, and K. G. Toyoda, Ec Evaluation of a 300-Mwe Fast Supercritica sure Power Reactor, USAEC Report HW- Hanford Atomic Products Operation, De 1963 (first unrestricted distribution, April
2. H. Harty, J. J. Regimbal, K. G. Toyoda, and Widrig, Economic Evaluation of 300-Mw(e) critical Pressure Power Reactor, USAEC HW-68420(Rev.), Hanford Atomic Products tion, June 1961.
3. Hanford Atomic Products Operation, Graphite Superheat Reactor (HGSR), Design and Evaluation, USAEC Report HW-73130, Ja 1960.

Table VI-6 POWER-GENERATION COSTS FOR 311-Mw(e)* AND 1000-Mw(e) HGSR PLANTS

		311-Mw(e)* plant			1000-Mw(e) plant		
	Rate, %	Capital cost, \$1,000	Annual cost, \$1,000	Unit cost, mills/kw-hr	Capital cost, \$1,000	Annual cost, \$1,000	Unit cost, mills/kw-hr
Fixed charges							
Depreciating capital							
Total capital cost (less land and land rights)	14.5	45,810	6,640	3.04	112,100	16,260	2.32
Nondepreciating capital							
Land and land-rights working capital	13.0	360	47	0.02	360	47	0.01
Plant operating and maintenance	13.0	159	21	0.01	540	70	0.01
Fuel-cycle operation	13.0	2,100	273	0.13	4,490	584	0.08
Nuclear liability insurance			289	0.13		340	0.05
Annual fixed charges, subtotal			7,270	3.33		17,301	2.47
Operating costs							
Operating and maintenance			890	0.41		2,280	0.32
Fuel cost			3,020	1.39		8,760	1.25
Operating costs, subtotal			3,910	1.80		11,040	1.57
Total power-generation costs			11,180	5.13		28,341	4.04

*The exact value of 311 Mw(e) was used in computing these costs instead of the rounded-off "300 Mw(e)" that appears throughout this article.

LEGAL NOTICE

This journal was prepared under the sponsorship of the U. S. Atomic Energy Commission. Neither the United States, nor the Commission, nor any person acting on behalf of the Commission:

A. Makes any warranty or representation, expressed or implied, with respect to the accuracy, completeness, or usefulness of the information contained in this journal, or that the use of any information, apparatus, method, or process disclosed in this journal may not infringe privately owned rights; or

B. Assumes any liabilities with respect to the use of, or for damages resulting from the use of any information, apparatus, method, or process disclosed in this journal.

As used in the above, "person acting on behalf of the Commission" includes any employee or contractor of the Commission, or employee of such contractor, to the extent that such employee or contractor of the Commission, or employee of such contractor prepares, disseminates, or provides access to, any information pursuant to his employment or contract with the Commission, or his employment with such contractor.

NUCLEAR SCIENCE ABSTRACTS

The U. S. Atomic Energy Commission, Division of Technical Information, publishes *Nuclear Science Abstracts (NSA)*, a semimonthly journal containing abstracts of the literature of nuclear science and engineering.

NSA covers (1) research reports of the U. S. Atomic Energy Commission and its contractors; (2) research reports of government agencies, universities, and industrial research organizations on a world-wide basis; and (3) translations, patents, books, and articles appearing in technical and scientific journals.

Complete indexes covering subject, author, source, and report number are included in each issue. These are cumulated quarterly, semiannually, and annually providing a detailed and convenient key to the literature.

Availability of NSA

SALE *NSA* is available on subscription from the Superintendent of Documents, U. S. Government Printing Office, Washington, D. C., 20402, at $30.00 per year for the semimonthly abstract issues and $22.00 per year for the four cumulated-index issues. Subscriptions are postpaid within the United States, Canada, Mexico, and all Central and South American countries, except Argentina, Brazil, British and French Guiana, Surinam, and British Honduras. Subscribers in these Central and South American countries, and in all other countries throughout the world, should remit $37.00 per year for subscriptions to semimonthly abstract issues and $25.00 per year for the four cumulated-index issues.

EXCHANGE *NSA* is also available on an exchange basis to universities, research institutions, industrial firms, and publishers of scientific information. Inquiries should be directed to the Division of Technical Information Extension, U. S. Atomic Energy Commission, P. O. Box 62, Oak Ridge, Tennessee, 37831.

TECHNICAL PROGRESS REVIEWS may be purchased from Superintendent of Documents, U. S. Government Printing Office, Washington, D. C., 20402. *Isotopes and Radiation Technology* at $2.00 per year each subscription or $0.55 per issue; the other four journals at $2.50 per year and $0.70 per issue. The use of the coupon below will facilitate the handling of your order.

POSTAGE AND REMITTANCE: Postpaid within the United States, Canada, Mexico, and all Central and South American countries except as hereinafter noted. Add $0.50 per year, or $0.15 per single issue for the *Isotopes and Radiation Technology* journal and $0.75 per year or $0.20 per single issue for the other four journals for postage to all other countries, including Argentina, Brazil, British and French Guiana, Surinam, and British Honduras. Payment should be by check, money order, or document coupons, and MUST accompany order. Remittances from foreign countries should be made by international money order, or draft on an American bank, payable to the Superintendent of Documents, or by UNESCO book coupons.

order form

SUPERINTENDENT OF DOCUMENTS
U. S. GOVERNMENT PRINTING OFFICE
WASHINGTON , D. C., 20402

Enclosed:

document coupons ☐ check ☐ money order ☐

Charge to Superintendent of Documents No.__________

Please send a one-year subscription to

☐ NUCLEAR SAFETY

☐ POWER REACTOR TECHNOLOGY

☐ REACTOR FUEL PROCESSING

☐ REACTOR MATERIALS

(Each subscription $2.50 per year; $0.70 per issue.)

☐ ISOTOPES AND RADIATION TECHNOLOGY

Each subscription $2.00 a year; $0.55 per issue.)

SUPERINTENDENT OF DOCUMENTS
U. S. GOVERNMENT PRINTING OFFICE
WASHINGTON, D. C., 20402

(Print clearly)

Name ______________________________

Street ______________________________

City __________________ Zone ____ State _____

POWER REACTOR TECHNOLOGY

UNIVERSITY
OF MICHIGAN
JUL 1 1966
PHOENIX
LIBRARY

Phoenix

A Quarterly Technical Progress Review

Prepared for DIVISION OF TECHNICAL INFORMATION, USAEC, by
ARGONNE NATIONAL LABORATORY

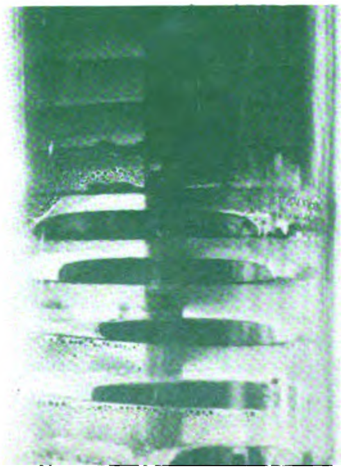

Trapping
liquid-metal
vapor . . .
see page 259

Fall 1965

● VOLUME 8

● NUMBER 4

DEPOSITED BY THE
UNITED STATES

TECHNICAL PROGRESS REVIEWS

To meet the needs of industry for concise summaries of current atomic developments, the Atomic Energy Commission is publishing this series, Technical Progress Reviews. Issued quarterly, each of the reviews digests and evaluates the latest findings in a specific area of nuclear technology and science.

The five journals published in this series are:

Isotopes and Radiation Technology P. S. Baker, A. F. Rupp, and associates
Oak Ridge National Laboratory

Nuclear Safety Wm. B. Cottrell, W. H. Jordan, and associates
Oak Ridge National Laboratory

Power Reactor Technology
Argonne National Laboratory

Reactor Fuel Processing Stephen Lawroski and associates
Chemical Engineering Division, Argonne National Laboratory

Reactor Materials R. W. Dayton, E. M. Simons, and associates
Battelle Memorial Institute

See the back cover for availability information.

The views expressed in this publication do not necessarily represent those of the United States Atomic Energy Commission, its divisions or offices, or of any Commission advisory committee or contractor.

Availability of Reports Cited in This Review

Unclassified AEC reports are available for inspection at AEC depository libraries and are sold by the Clearinghouse for Federal Scientific and Technical Information, National Bureau of Standards, U. S. Department of Commerce, 5285 Port Royal Road, Springfield, Va., 22151. Some of the reports cited are not available owing to their preliminary nature; however, the information contained in them will eventually be made available in formal progress or topical reports.

Unclassified reports issued by other Government agencies or private organizations should be requested from the originator.

Unclassified British and Canadian reports may be inspected at AEC depository libraries. British reports are sold by the British Information Service, 45 Rockefeller Plaza, New York, N. Y.; Canadian reports (AECL series) are sold by the Scientific Document Distribution Office, Atomic Energy of Canada, Ltd., Chalk River, Ontario, Canada.

Classified U. S. and foreign reports identified in this journal as Classified may be purchased by properly cleared Access Permit Holders from the Division of Technical Information Extension, U. S. Atomic Energy Commission, P. O. Box 1001, Oak Ridge, Tenn., 37830. Such reports may be inspected at classified AEC depository libraries.

DEPOSITED BY THE
ITED STATES OF AMERICA

Contents

Power Reactor Technology

Vol. 8, No. 4

UNCONVENTIONAL APPROACHES	Liquid-Metal MHD Topping Cycles	199
PHYSICS	Evaluating Heavy-Atom Cross Sections for Plutonium-Recycle Calculations	210
	Critical and Exponential Experiments with Plutonium	211
	Use of Soluble Poisons in Critical Experiments	214
	Water-Reactor Data Generally Verify Theory	214
	Reactivity Changes with Long Irradiation	215
	Improvements in Resonance-Integral Theory	217
CONTROL and DYNAMICS	Reactor Control Experience	221
FLUID and THERMAL TECHNOLOGY	Heat-Transfer Conference Highlights	228
MATERIALS	Effect of Hydriding on Zircaloy Properties	245
FUEL ELEMENTS		
Letters to the Editor	Stainless-Steel Cladding in Boiling-Water Reactors	252
	Rebuttal	254
	Re-rebuttal	255
COMPONENTS	Vapor Traps Protect Liquid-Metal Systems	259
OPERATING EXPERIENCE	Operational Problems and Solutions	271
	Hallam Operation in Retrospect	279
SYSTEMS TECHNOLOGY	Advancements in Organic Coolants	290
INDEX	Volume 8	297

This issue of *Power Reactor Technology* is behind schedule because of problems attendant to the assumption of editorial and writing responsibility by Argonne National Laboratory and because of scheduling problems at the AEC production facility. It is expected that future issues will soon return to a proper seasonal schedule.

Issued quarterly by the U. S. Atomic Energy Commission. Use of funds for printing this publication approved by the Director of the Bureau of the Budget on October 14, 1963.

Statement by the New Editors

This quarterly review of developments in reactor technology has been prepared at the request of the Division of Technical Information of the U. S. Atomic Energy Commission. It is intended to help designers of power reactors stay abreast of significant progress and experience in their field. Thus its scope includes research and development in the various technical specialties in the field as well as design and construction practices, reactor concepts, applications, economics, and operating experience.

Although they are not meant to be comprehensive abstracts of all information published during the quarter, the articles in each issue will call to the reader's attention various publications that merit study. In addition, some articles will summarize and critically evaluate individual reports. Other articles will review a topic more broadly so that designers can interpret new developments and trends against the perspective of the state of the art. Because any appraisal involves the reviewer's opinion of the significance of the work reported, readers are urged to consult the references for additional information and the judgments of the original authors. If a reader has information that causes his evaluation to reinforce, modify, or contradict the opinions of our reviewers, he is encouraged to write to the Editor.

For reasonably timely coverage, articles often must be based on fragmentary information. Thus continuity will be maintained from one issue to another by use of the following subject headings whenever appropriate:

- Economics, Evaluations, Programs
- Specific Applications
- Unconventional Approaches
- Fuel Resources and Cycles
- Physics
- Control and Dynamics
- Fluid and Thermal Technology
- Containment, Radiation Control, Siting
- Materials
- Fuel Elements
- Design and Construction Practice
- Specific Reactor Types
- Components
- Operating Experience
- Systems Technology

Because reactors are being developed and considered for power applications other than the generation of central-station electricity — and because of the similarity and transferability of the technology — the content of future issues will be broadened to include progress in reactor systems for process heat, desalting, undersea, space and other advanced applications.

This is the first issue prepared by Argonne National Laboratory. The new editors wish to express their appreciation to the previous editors, W. H. Zinn and J. R. Dietrich of Combustion Engineering, Inc., for earning *Power Reactor Technology* its respected stature in the field. Only from the experience of preparing an issue can their accomplishment be truly comprehended.

The Reactor Engineering Division (L. J. Koch, Director) has the principal responsibility for the preparation of *Power Reactor Technology*, with the regular assistance of the Reactor Physics Division (R. A. Avery, Director) and the occasional assistance of other Laboratory divisions (Metallurgy, Chemical Engineering, Chemistry, Reactor Operations, and Idaho). Thus, unless noted otherwise, the reviewers and authors of articles are Laboratory staff members. The editors will welcome interpretive review articles contributed by readers outside the Laboratory.

JAMES J. DUTTON, Editor; DAVID H. LENNOX, Technical Editor;
EDWARD J. CROKE and RAYMOND GOLD, Associate Editors
Argonne National Laboratory

- Section
I

Power Reactor Technology

Unconventional Approaches

quid-Metal MHD opping Cycles

Michael Petrick

r all practical purposes, development of the eam cycle has reached a plateau. Further ins in efficiency by increasing steam pres- re and temperature do not appear very ofitable. Thermodynamically, steam is a poor rking fluid because it absorbs too little heat the maximum cycle temperature. However, other single fluid is superior when all fac- rs are considered. A logical improvement ould be to use a binary system in which a econd working fluid is used in a "topping" cle.

A promising binary concept couples a liquid- etal topping cycle with a conventional steam ottoming cycle. In the topping cycle a liquid- etal magnetohydrodynamic (MHD) generator tied directly to a liquid-metal-cooled reactor at heats the working fluid to 1500°F or pos- ibly to as high as 2000°F.

Recent advances in magnetohydrodynamics how that an MHD device is a feasible way to onvert heat into electricity. Although the lasma MHD cycle has a formidable obstacle to vercome—the attainment of adequate elec- rical conductivity within practical temperature imits—liquid metals have electrical conduc- ivities five orders of magnitude higher than he electrical conductivity of plasma. The power lensity of an MHD generator is directly pro- ortional to the fluid conductivity times the squares of fluid velocity and magnetic flux. Thus, even though the velocities that can be achieved in a liquid-metal generator are about a hundred times lower than with a plasma, liquid-metal MHD systems have a greater potential for compact or low-capital-cost generators than do plasma MHD systems.

The introduction of a topping cycle above 1000°F creates problems that must be resolved, e.g., high-temperature-material limitations affect component fabrication, cost, reliability, and, most important, longevity. The lifetimes of power equipment of various maximum operating temperatures are shown in Fig. I-1, which depicts typical experience with commercial rotating equipment, ducted gases, and reactors, as well as the goals of ambitious programs for space power using thermionics and alkali-metal cycles.[1] It appears that a turboelectric topping cycle would be limited to a range of 900 to 1400°F because of turbine reliability

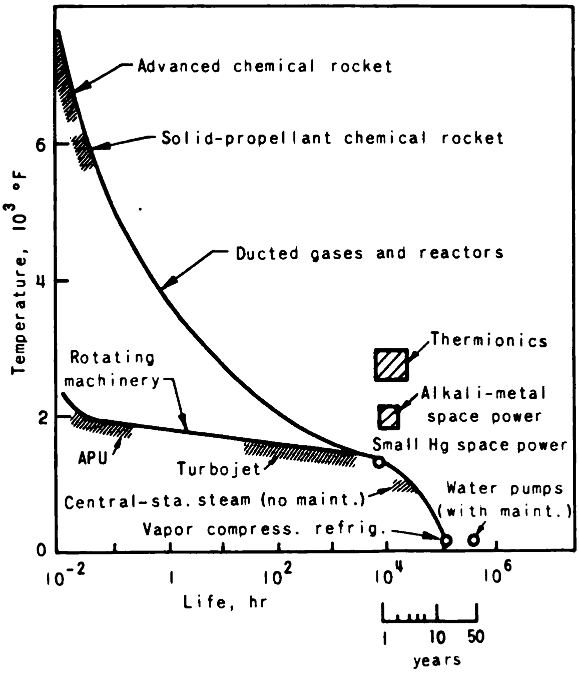

Fig. I-1 Operating temperature affects life of power equipment.[1]

problems. Unlike the conventional turboelectric generator, the MHD generator contains no moving parts that are subject to extreme temperature and dynamic stress and require close machine tolerances. As a result the MHD generator should be able to operate under conditions that conventional energy-conversion devices could not tolerate for prolonged times.

Liquid-Metal MHD Cycles

Five types of cycles have been proposed for liquid-metal MHD power systems. They are similar in that they are based on the conversion of thermal energy into kinetic energy, which then is converted into electric energy by an MHD generator. The cycles differ primarily in the way the thermal energy is converted to kinetic energy.

Two-Loop Two-Fluid Cycle. In the MHD cycle first proposed by Elliott[2] (of the Jet Propulsion Laboratory) as a space power cycle (Fig. I-2), one metal circulates in the vapor loop and another circulates in the liquid loop. The fluid circulating in the vapor loop leaves the condenser as condensate and is pumped (by an electromagnetic pump) to the mixer, where it vaporizes on contact with the liquid; the vapor expands with the liquid through a two-phase nozzle, separates from the liquid in the separator, and recondenses in the condenser. Cycle efficiency is raised by a heat exchanger that cools the vapor while it preheats the condensate. In the liquid loop the liquid is heated in the reactor heat source, is cooled as it vaporizes the condensate in the mixer, is accelerated by the vapor in the nozzle, separates from the vapor in the separator, decelerates by producing electricity in the MHD generator, and returns through the diffuser to the heat source.

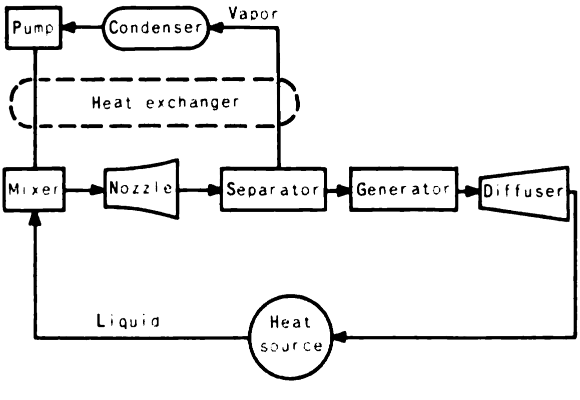

Fig. I-2 In the two-loop two-fluid MHD cycle proposed by Elliott,[2] one metal circulates in the vapor loop and another circulates in the liquid loop. Condensate from the vapor loop vaporizes when it mixes with hot liquid before both expand through a two-phase nozzle.

Two-Loop One- or Two-Fluid Cycle. The cycle proposed by Prem at Atomics International is also bicyclic.[3] It can be operated with either one or two fluids. The single-fluid version (Fig. I-3) is especially suited for large power stations. After the liquid metal in the first loop is partially vaporized by the heat source, the two-phase fluid expands by passing through a supersonic nozzle to transform the thermal energy to kinetic energy. Downstream of the nozzle, considerably cooler atomized liquid from the second loop is injected into the two-phase high-velocity stream. Momentum exchange accelerates the injected stream, and mass and heat transfer between the two streams condenses the vapor component of the two-phase fluid. The resulting high-velocity predominantly liquid stream enters the generator, where most of the fluid kinetic energy is transformed into electric energy. The second loop carries a portion of the liquid metal through a heat exchanger, where cycle waste heat is rejected.

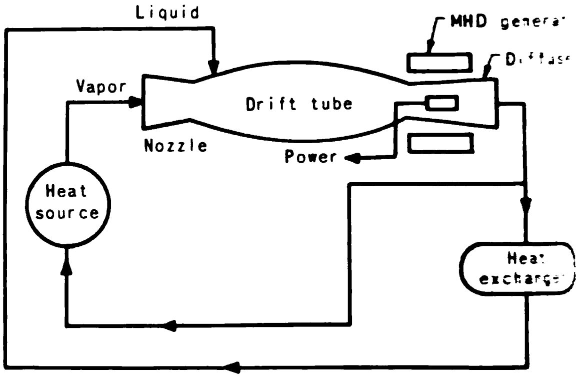

Fig. I-3 In the single-fluid version of the two-loop single- or two-fluid MHD cycle proposed by Prem hot partially vaporized fluid expands through a supersonic nozzle before cooler atomized liquid is injected to form mostly liquid stream.

One-Loop One-Fluid Cycle. A [illegible] single-fluid version (proposed by [illegible] Arnne) of the two-fluid cycle is shown in Fig. 4. After the velocity of a two-phase mixture a saturated vapor from the reactor is in- eased by being passed through the nozzle, e two-phase fluid passes directly through e MHD generator to produce electric energy. ıen the fluid has been condensed, it goes rough a diffuser and back through the reactor. ıis cycle has fewer parts and is more effi- ent than the two-fluid cycle of Fig. I-2 be- use of potentially lower friction losses and imination of the vapor loop. Solubility and trainment problems are also eliminated.

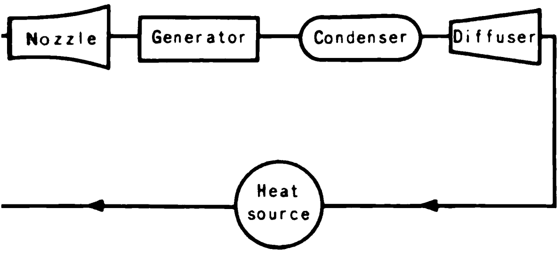

g. I-4 *In a simpler single-loop single-fluid ver- on (proposed by Petrick[4]) of the two-fluid MHD cle, heat converts liquid metal to a two-phase mix- re or a saturated vapor before velocity is raised in e nozzle. There is no separate vapor loop, mixer, separator.*

Two-Loop One-Fluid Condensing-Injector Cy- e. The condensing-injector single-fluid MHD wer cycle proposed by MIT's Jackson and rown[5] (Fig. I-5) consists of a vapor loop eating loop) and a liquid loop (heat-rejection op). The vapor is generated in the reactor at source and passes into the condensing jector, where it condenses in mixing with e liquid emerging from the waste heat exchanger to give a high-velocity liquid that passes through the MHD generator, where the kinetic energy is converted to electric energy. Then the liquid separates into two streams; one returns to the reactor, where it is vaporized, and the other stream goes to the liquid loop, where waste heat is rejected.

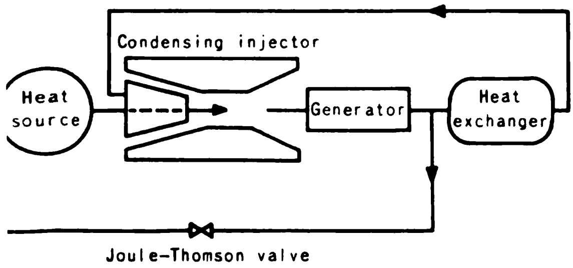

g. I-5 *In the two-loop one-fluid condensing-injec- r MHD cycle proposed by Jackson and Brown,[5] por generated by heat condenses when it mixes with oler liquid in the condensing injector before the ıid passes through the generator.*

Slug-Generator Cycle. This cycle, proposed by Powell and coworkers at Brookhaven,[6] is similar in principle to a conventional steam-engine cycle. In this cycle (Fig. I-6) the vapor expands to accelerate liquid slugs through the generator.

The two modes of operation are either (1) to keep the intake valve open during the expansion stroke and irreversibly exhaust the high-pressure vapor through a Joule–Thomson isoenthalpic expansion to a condenser, or (2) to close the intake valve partway through the cycle and continue an adiabatic isentropic expansion to condenser conditions. The latter is more efficient and is used in conventional steam engines.

Potential Cycle Efficiencies

Calculated efficiencies for the various liquid-metal MHD cycles are reported in Refs. 6 to 9. Although the primary emphasis in this review is on the performance of the MHD cycle as a topping unit on a central-station power plant, the results of these studies also can be applied to compact power systems. Data are presented on the following working fluids: mercury, mercury–potassium alloy (40 mole % potassium), potassium, cesium, and lithium.

Two-Loop Two-Fluid Cycle. The efficiency of the Elliott cycle[9] employing cesium and lithium is shown in Fig. I-7. Assumptions made in the analysis are that: (1) the kinetic energy is converted to electric energy in the generator with 70% efficiency, including the effect of all fluid friction losses between the separator and the generator and between the generator and the diffuser; (2) diffuser efficiency is 85%; (3) the vapor-loop pump is 50% efficient; and (4) the pressure drops across the reactor, radiator, and mixer are each 10 psi.

Figure I-7 shows how cycle efficiency (defined as MHD generator output minus vapor-loop pump input divided by reactor thermal power) varies with sink temperature when the nozzle inlet is at 2000°F. Under the stated assumptions, cycle efficiency reaches a maxi-

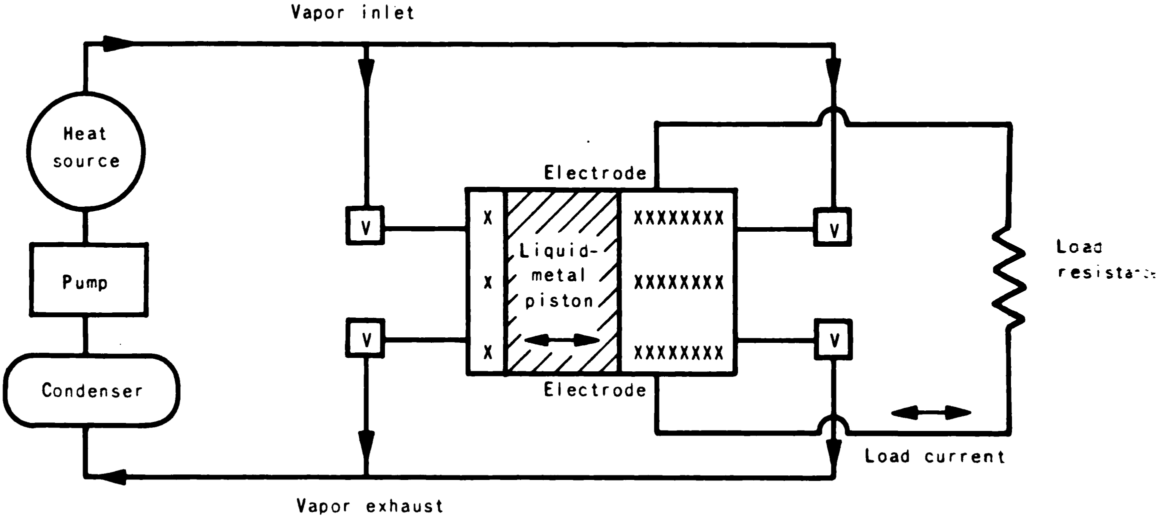

Fig. I-6 In the slug-generator MHD cycle proposed by Powell et al.,[6] liquid-metal vapor expansion pushes liquid slugs through the generator in a manner reminiscent of a conventional steam-engine cycle. V designates valves for liquid metals; X represents transverse magnetic field.

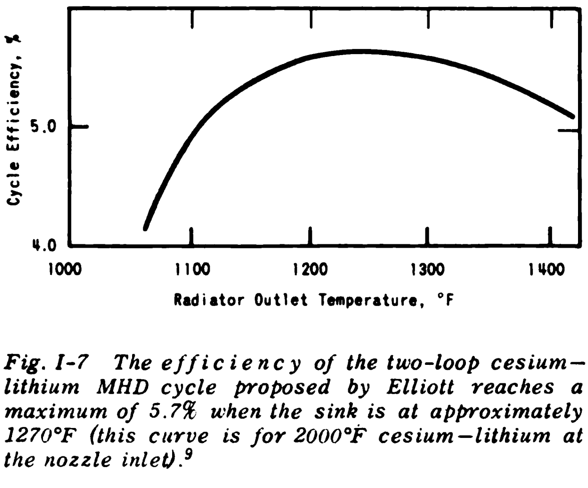

Fig. I-7 The efficiency of the two-loop cesium–lithium MHD cycle proposed by Elliott reaches a maximum of 5.7% when the sink is at approximately 1270°F (this curve is for 2000°F cesium–lithium at the nozzle inlet).[9]

mum of 5.7% when the sink is at approximately 1270°F. [At 30 kw(e) the flow rates are about 19 lb of cesium per second and 120 lb of lithium per second.] The efficiency decreases at higher sink temperatures because the Carnot efficiency decreases; it decreases at lower sink temperatures because the separator area increases and more lithium vapor enters the radiator.

Figure I-8 shows the cesium–lithium cycle efficiency as a function of the liquid and gas flow rates, exit nozzle pressure, and generator efficiency.[8]

It is apparent that this cycle has low efficiency. The maximum pressure of the system, and consequently the inlet pressure to the nozzle, is set by the working fluids used. For a cesium–lithium system, the temperature and pressure before the nozzle were set at 2010°F and 150 psia. Thus the maximum theoretical cycle efficiency is approximately 16 if the nozzle exit pressure is 0.25 psi and the generator is 100% efficient; but the maximum practical cycle efficiency is only approximately 7.5% with a more realistic exit nozzle pressure of 10 psi and an 80%-efficient generator.

Two-Loop One- or Two-Fluid Cycle. Efficiency analyses for both the single- and two-fluid versions of the Prem[7] cycle are shown in Fig. I-9; no attempt was made to optimize the cycle. Optimum cycle efficiency occurs at approximately 10% quality for a single-fluid system and supersonic nozzle inlet conditions of 2000°F and an outlet temperature equal to the vaporization temperature of the fluid at 14.7 psia. The upper three curves represent predicted efficiencies for the two-fluid cycle using an immiscible cesium–lithium mixture. The top curve shows how efficiency improves if the working fluid is expanded to 3 psia instead of 14.7 psia; the lower two curves (both of which are for 14.7-psia nozzle outlet pressures) show the importance of reducing average radiator temperature from 1050 to 780°F.

The predicted cycle efficiencies shown are based on assumed efficiencies of 70% for elec-

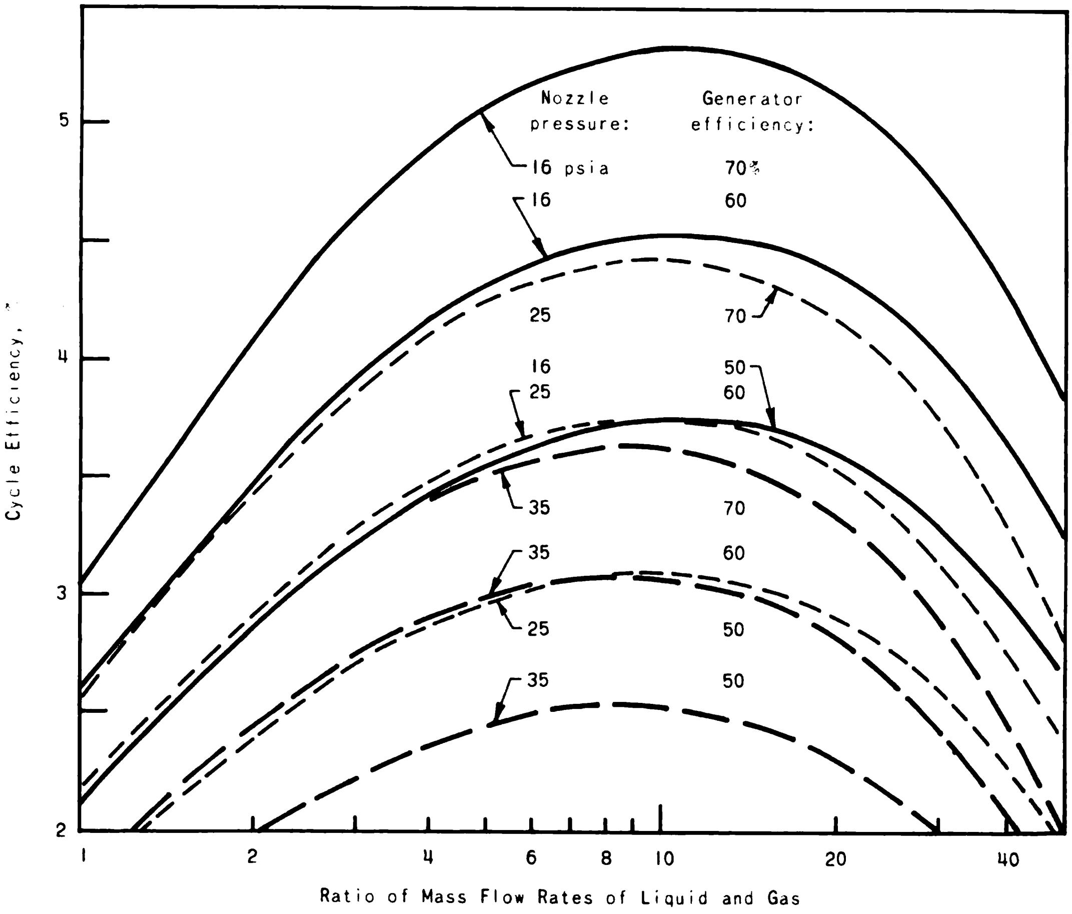

Fig. I-8 How efficiency of two-loop cesium–lithium MHD cycle varies with liquid and gas flow rates, exit nozzle pressure, and generator efficiency.[8]

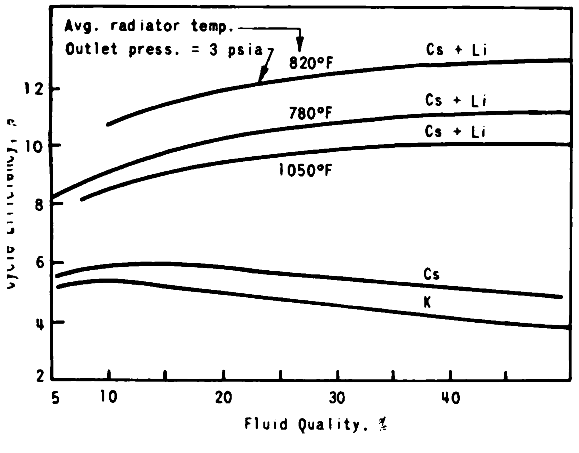

ig. I-9 The efficiency of the two-loop MHD cycle of rem with two fluids (upper three curves) is greater han with single fluids (lower two curves).[7] *Nozzle nlet is at 2000°F; outlet temperature is equal to the aporization temperature at 14.7 psia. except for psia for the top curve.*

trical conversions. The mechanical efficiency allows for losses in the nozzle plus frictional losses throughout the system; the electrical efficiency includes end losses in the generator and the magnetization current for producing the magnetic field.

One-Loop One-Fluid Cycle. Typical predicted cycle efficiencies for mercury, mercury–potassium, and potassium are shown in Figs. I-10 to I-12. The maximum efficiency in the cycle occurs with 100% vapor quality at the nozzle inlet.

Within the boundary conditions specified, mercury gives the highest efficiencies for the one-fluid cycle. The overall cycle efficiency is 22.5% with the source at 1540°F, the sink at 540°F, and the efficiencies of the MHD generator and the nozzle are 75 and 80%, respectively. For the potassium–mercury mixture,

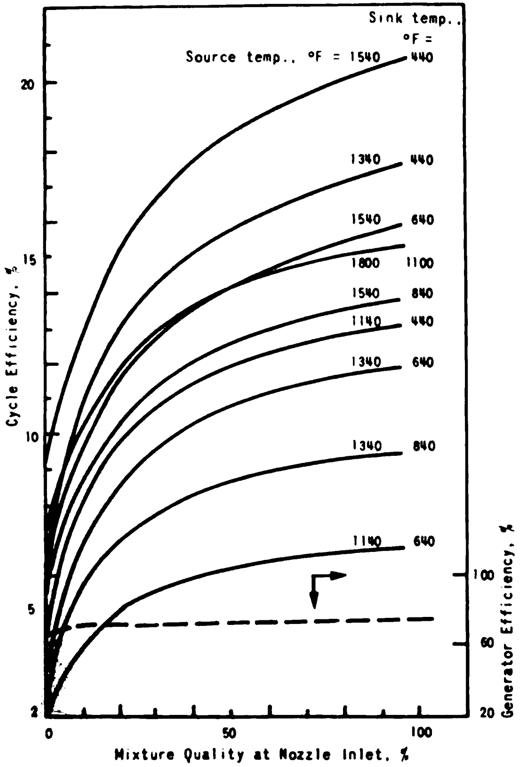

Fig. I-10 Cycle efficiency with mercury as the single fluid in the single-loop MHD cycle by Petrick.[8]

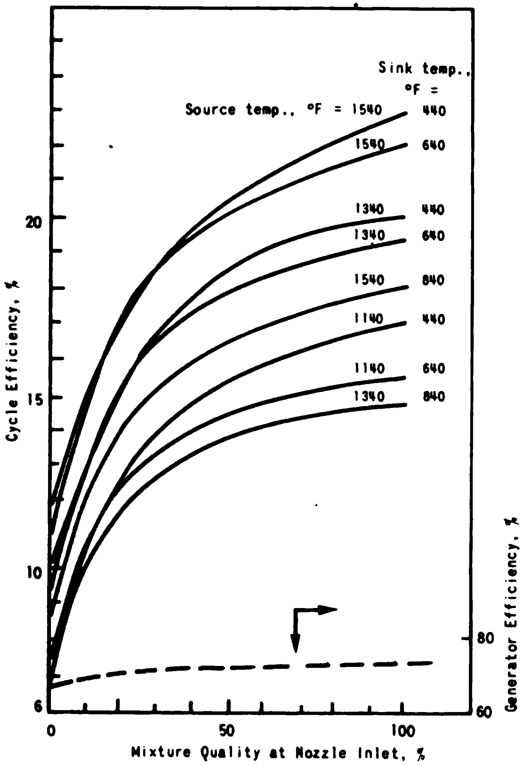

Fig. I-11 Cycle efficiency with a mercury–potassium alloy eutectic as the single fluid in the single-loop MHD cycle by Petrick.[8]

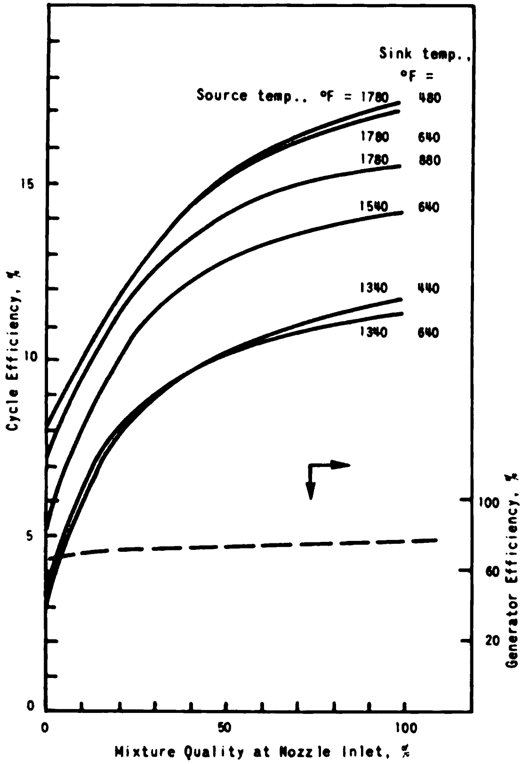

Fig. I-12 Cycle efficiency with potassium as the single fluid in the single-loop MHD cycle by Petrick.[8]

le efficiencies are approximately 10 to
% lower and are much more sensitive to
source and sink temperatures.

n comparison with alkali metals, mercury
d the mercury–potassium eutectic have lower
ling points, which permit operating tem-
ratures nearer present technological limits.
is advantage rapidly diminishes for the pure-
rcury system because the vapor pressure
mercury increases rapidly with temperature;
1540°F its pressure is 1762 psi. At the same
mperature the vapor pressure of the mer-
ry–potassium eutectic is only 198 psi.

Of the alkali metals, the best fluid for the
e-component cycle apparently is potassium,
ose calculated maximum cycle efficiency is
proximately 20% over the range 2240 to
60°F. Although cesium gives essentially the
me efficiency as potassium, its lower elec-
ical conductivity reduces its effectiveness in
e MHD generator. The conductivity of sodium
higher than that of cesium or even potassium,
it sodium as a working fluid yields the lowest
cle efficiencies.

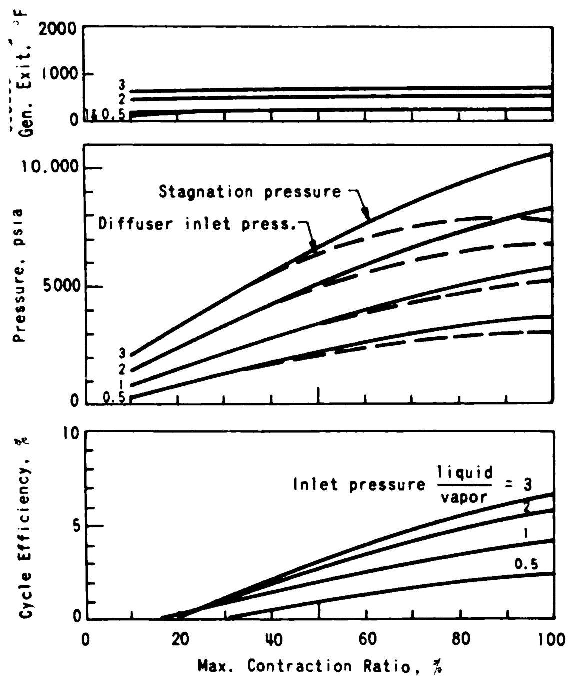

*ig. I-13 Efficiency with mercury in the condensing-
jector MHD cycle when the source is at 1860°F, the
ink is at 860°F, and the liquid-to-vapor mass flow
atio is 5. For inlet liquid-to-vapor pressure ratios
f 0.5, 1, 2, and 3, maximum contraction ratios are
5, 49.2, 69.4, and 84.8, respectively.*[8]

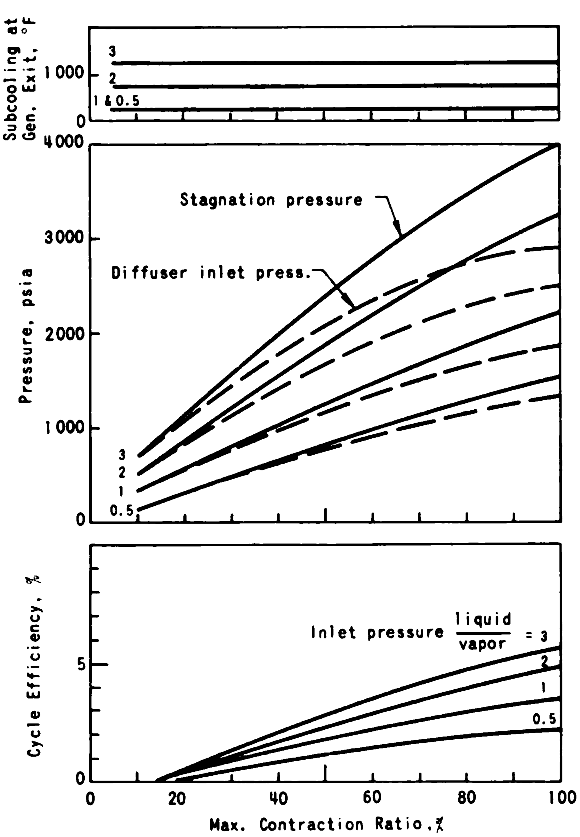

Fig. I-14 Efficiency with potassium in the condensing-injector MHD cycle when the source is at 2700°F, the sink is at 1060°F, and the liquid-to-vapor mass flow ratio is 3. For inlet liquid-to-vapor pressure ratios of 0.5, 1, 2, and 3, maximum contraction ratios are 23.2, 33.0, 46.7, and 57.2, respectively.[8]

Two-Loop One-Fluid Condensing-Injector Cycle. Figures I-13 and I-14 show typical estimated efficiencies of the condensing-injector cycle with mercury and potassium.[8] For these computations it was assumed that the MHD generator is 80% efficient and that the actual pressure rise in the condensing injector is 80% of theoretical. The cycle data show that mercury as a working fluid produces the highest cycle efficiency, 10%, and that it is followed closely by cesium at 8%. Sodium has the lowest performance potential. The ratio of the cycle efficiency to Carnot efficiency is in the range 0.17 to 0.25.

Some noteworthy trends derived from the cycle analysis are that: (1) cycle efficiency increases with injector contraction ratio and inlet stagnation pressure ratio but decreases with mass flow ratio (however, the variation of these parameters is limited by the second law of thermodynamics); (2) cycle efficiency decreases with sink temperature and increases with heat-source temperature; (3) increasing the velocity from the condensing injector so that the total stagnation head is caused mostly by the kinetic head requires the injector geometry to give a contraction ratio greater than 50% of the maximum so that the MHD generator can be of the variable-area type, and thus it and the injector can be designed for much lower pressures.

Slug-Generator Cycle. Figure I-15 shows the calculated maximum ideal cycle efficiency for the slug-generator cycle,[6] assuming no generator losses, for adiabatic and isopressure expansions with potassium vapor. Note that isopressure expansion is about half as efficient as adiabatic expansion. As with all cycles, efficiency increases with vapor temperature.

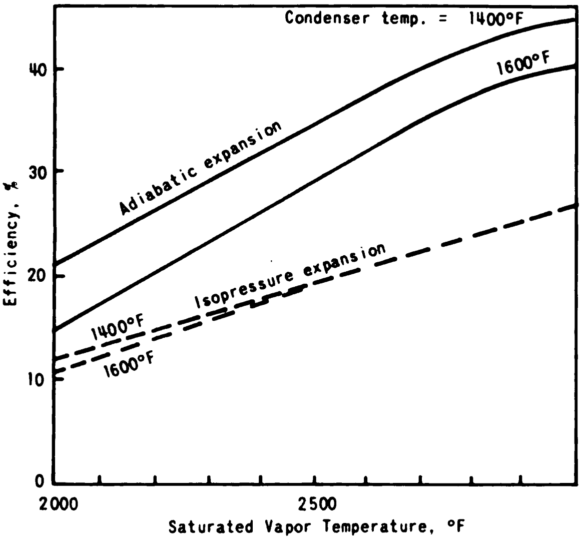

Fig. I-15 Ideal efficiencies for the slug-generator cycle with potassium vapor show that adiabatic expansion is nearly twice as efficient as isopressure expansion.[6]

Overall Plant Efficiency

The overall efficiency of a binary power system that has an MHD topping cycle and a normal steam cycle as the sink or bottoming cycle can be estimated by combining the efficiencies:

$$\epsilon_C = \epsilon_{MHD} + (100-\epsilon_{MHD})\,\epsilon_{SC}$$

where ϵ_C is the binary cycle efficiency, ϵ applies to the topping cycle, and ϵ_{SC} is the e ciency of the steam bottoming cycle.

From this analysis the following conclusi are reached:

1. The potential overall efficiency of a c tral-station nuclear power system employin liquid-metal MHD topping cycle appears to excellent. (A fossil-fired boiler using a liqui metal coolant also could be used as the h source, in which case the boiler could oper at high cycle temperatures with the low vap pressures possible with liquid metals.)

2. With an alkali metal as the working flui the maximum potential overall cycle efficien appears to be 55% and results from either a potassium–steam or a cesium–steam binar cycle. The liquid-metal topping cycle operat between 2240 and 1100°F and produces 33 the total power. The bottoming steam plant the equivalent of a modern supercritical pla such as the Eddystone unit, operating at 40 psi and 1050°F; the efficiency of the steam pla is estimated to be approximately 45% and based on upgrading the published Eddyston efficiency of 40.7% by eliminating boiler an stack losses.

3. The maximum potential efficiency of t mercury–steam binary cycle is approximate 53%, which is slightly lower than the cesium-steam or potassium–steam binary cycle. This efficiency is based on the source being 1540°F and the condenser at 1100°F. If the sin temperature is dropped to 440°F, the overall cycle efficiency drops to approximately 47 even though the efficiency of the topping cycl increases substantially. Although mercury is thermodynamically the superior working flui it has several major drawbacks: (*a*) vapo pressure rises rapidly with temperature, (*b*) the use of additives to improve the wettability an heat transfer tends to increase operational problems considerably, (*c*) limited availability and (*d*) relatively high cost. Thus the feasibility of the high-pressure mercury system is questionable.

4. For the medium-temperature range (110 to 1600°F), mercury–potassium alloy and potassium appear to be the most promising working fluids for the liquid-metal cycle. Overall cycle efficiencies could be as high as 50%; the efficiency of the MHD topping cycle alone coul be as high as 15% at a maximum working pressure below 75 psi.

Economics. Although no detailed economic dies have been reported, a preliminary dy[8] indicates two major areas in which MHD ping cycles could save money: (1) the capac- of the steam bottoming plant could be re- ced in proportion to the power generated in MHD topping cycle, and (2) fuel costs would lower because of the increased efficiency. e money saved in these two areas is avail- e for converting the steam plant to the bi- ry cycle and thus is a measure of the eco- mic incentive for doing so.

For illustrative purposes, Fig. I-16 shows total savings that would result from adding MHD topping cycle to a base steam plant as function of fuel cost and increase in plant iciency. The values shown are for a 1000- v(e) plant operating with a 90% load factor, cost of $30/kw(e) for the steam turbine- nerator plant, and a 14.7% capitalization arge on the annual fuel savings (which trans- rs the annual fuel savings to an equivalent pital expenditure). As an example of the vings from a 20% increase in overall plant iciency on a steam plant whose efficiency s 40%, the break-even point is approximately $25 million for a fuel cost of $0.20/10^6 Btu. The 20% increase in cycle efficiency can be achieved by an MHD topping cycle whose efficiency is 12.5%, which could be obtained with a maximum cycle temperature near 1600°F.

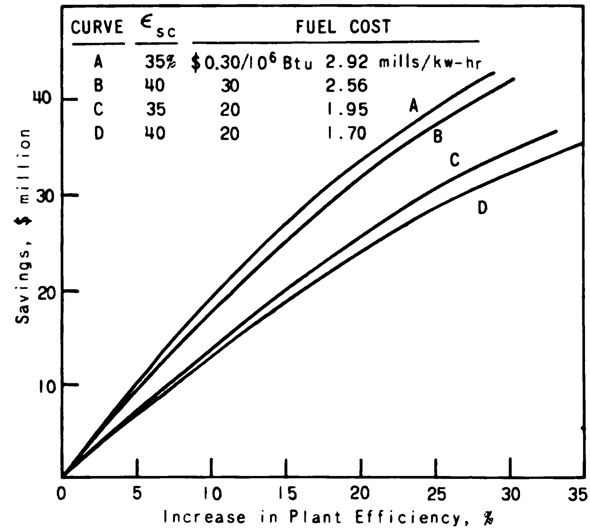

Fig. I-16 Savings from increasing plant efficiency by adding MHD topping cycle to a base steam plant.[8]

quid-Metal MHD: State of the Art

Active experimental programs are under way at t Propulsion Laboratory, Atomics International, rookhaven National Laboratory, Massachusetts In- itute of Technology, and Argonne National Labora- ry to resolve uncertainties concerning the effi- encies of the various liquid-metal MHD cycles d components that have been proposed.

The Jet Propulsion Laboratory program to develop space power source is the most comprehensive fort in liquid-metal MHD research that has been ported. In addition to tests on the MHD generator ith NaK as the working fluid, the nozzle, separator, d diffuser have been tested with water and nitrogen. he nozzle has delivered 90% of isentropic exit ve- city, the separator had about 1% liquid loss and 0% velocity loss, the diffuser was 75% efficient, and e generator operated at approximately 50% effi- iency. Potential lifetime limitations due to erosion d to insulator loss were also investigated in water- ow and lithium-capsule tests; results indicated egligible material loss up to 1000 hr.[9,10]

The Atomics International development program is studying (1) the simultaneous mass heat-transfer and momentum-transfer process, which occurs in their "drift tube"; (2) the electrical resistivity of two-phase mixtures under various pressures, temperatures, void fractions, and impurities; and (3) generator types and performance. (Analyses and research toward the development of an MHD electric generator suitable for utility applications are being sponsored by the Edison Electric Institute.) The only results reported pertain to the acceleration and momentum-transfer process. Studies with sand and air indicate that the acceleration is accomplished very rapidly, reaching 60% of the air velocity at a distance of 30 to 40 cm from the injection point.[11] A potassium test-loop facility has been built to demonstrate the overall power-conversion process.

The Argonne National Laboratory program is studying the performance of liquid-metal generators and evaluating the condensing injector. The generator experiments will provide data on its efficiency with a dispersed two-phase entering fluid for various generator geometries, angles of incidence of the entering fluid, and phase distributions. A second study, with a single-phase fluid, will confirm end losses in variable-area generators and establish maximum generator efficiencies, develop means to minimize end losses, and investigate the fluid mechanics of the generator. These investigations will provide data for defining the actual efficiencies of the condensing injector and two-phase single-fluid cycles.

At Massachusetts Institute of Technology, Jackson and Brown have concentrated on developing the condensing injector and the a-c generator. Brown has shown that a large pressure rise across the condensing injector is possible if a convergent mixing section is used. Jackson and coworkers[12,13] have developed the theory and outlined the performance limitations of the a-c induction generator. Experimental equipment is being fabricated to obtain extensive data on the performance characteristics of the a-c generator.

The Brookhaven National Laboratory program is oriented primarily toward investigating a slug generator.[6] Extensive studies of slug stability were made using high-speed movies of water, methanol, and mercury slugs accelerated through rectangular channels. Measurements of hydrodynamic and hydromagnetic wave growth rates agree approximately with theory. A mercury slug generator has reached an output of 100 watts, and, although its efficiency was only 10%, work is under way on an alkali-metal slug generator whose efficiency is expected to be 90% or greater. Also, work is being done on a reciprocating solid-piston MHD generator.

Others. Although programs are also being conducted at Allgemeine Elektrizitätsgesellschaft in Germany and at Space Technology Laboratories in the United States, they have not been reported in detail.

When these experiments have been completed, it should be possible to make a more thorough appraisal of the merits of the various liquid-metal MHD power cycles. Both efficiencies and needed materials development will be more clearly defined.

Comparison of Liquid-Metal and Plasma MHD Cycles

Because most of the work done in the field of magnetohydrodynamics has been on the plasma MHD cycle, the major problem areas and limitations of this concept have been pinpointed.

Efficiency and Temperature. Gunson et al.[14] have described a detailed study of a binary plasma MHD–steam power plant. Rosa and Kantrowitz[15] have calculated efficiencies for a closed-cycle plasma MHD–steam binary system, as well as for a purely MHD system; Fig. I-17 is based on their study. Both studies involved a helium cycle. Gunson reports a net efficiency of 47.1% for a plasma MHD–steam binary cycle operating with a top temperature of 3000°F.

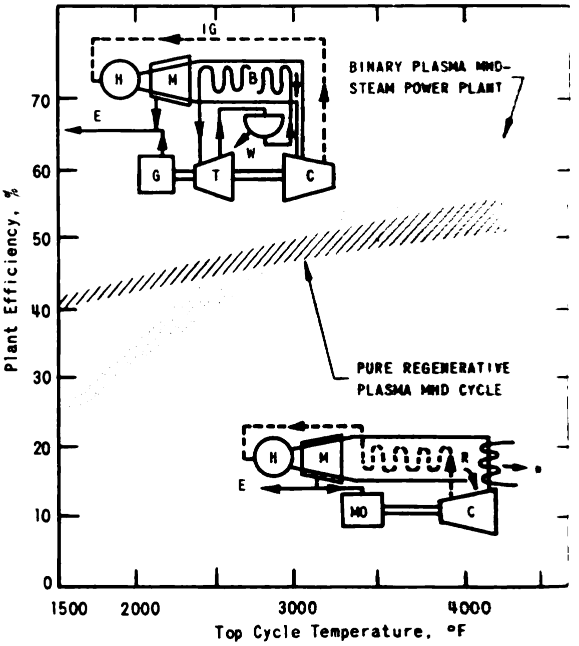

Fig. I-17 Plant efficiency with a closed-cycle pla MHD–steam binary system exceeds that with a p regenerative plasma MHD cycle when the top c temperature exceeds 2500 to 3500°F. Symbols boiler; C, compressor; E, electrical output; G, g erator; H, heat source; IG, inert gas; M, MHD g erator; MO, motor; R, regenerator; T, turbin W, waste heat.[14]

For the same condition, Fig. I-17 indicates a valu approximately 51%. Thus, to better the efficienc a modern steam plant, the temperature of a bi plasma MHD–steam plant must approach 3000° Temperatures must approach 4000°F to achie overall cycle efficiencies of 55%. It also is interest to note that the pure regenerative plasma MHD cy (also shown in Fig. I-17) must approach 4000°F achieve 50% efficiency. In studies of the open-cy combustion-fired plasma MHD cycle, Way and You indicate that the overall efficiency of a binary syst is 43 to 50% for a cycle top temperature of 4500° the highest efficiency would be achieved with a super-critical steam plant as the bottoming cycle. In co parison, liquid-metal MHD–steam binary syst overall efficiencies of 50% appear possible at a proximately 1600°F, and efficiencies of approxima 55% appear possible below 2200°F.

A major factor that tends to reduce the efficie of the plasma MHD cycle is that it is essenti Brayton cycle, and so a large fraction of the po generated is required for the compressors ci lating the gas. For example, in the study ma Gunson et al., about 25% of the total electri generated was used by the compressors. Sec techniques and heat sources greater than 3 probably will be required to achieve an adeq onductivity of the plasma in the plasma closed-cycle system. Although the development of a commercial reactor to operate at 3200°F appears possible, there are many unanswered questions about fuel performance and structural behavior.

Magnet Size and Cost. In addition to efficiency at reasonable temperatures, the liquid-metal MHD cycle offers other potential advantages. The power density achievable in a liquid-metal generator might be an order of magnitude higher than for a plasma generator; consequently smaller and less expensive magnets or coils (superconducting or normal) are easible. Because the magnet or coil is a major cost tem in an MHD plant, these potential savings are mportant.

Direct A-C Generation. Because d-c to a-c converters are expensive, the possibility of direct a-c generation is especially attractive. Jackson and Pierson[12] have shown that the feasibility of an MHD induction generator depends on a high magnetic Reynolds number, which is based on the wavelength of the field structure and the velocity difference between the wave and the fluid. Ionized gas flows in the conductivity range attainable now have very low magnetic Reynolds numbers, approximately 10^{-2}, and therefore direct a-c generation with such gases does not appear to be feasible. On the other hand, a characteristic magnetic Reynolds number of a liquid-metal generator would be approximately 10; thus the probability of producing a-c power directly is much more promising.

References

1. An Evaluation of Systems for Nuclear Auxiliary Power, USAEC Report TID-20079, January 1964.
2. D. G. Elliott, Two-Fluid Magnetohydrodynamic Cycle for Nuclear-Electric Power Conversion, *Am. Rocket Soc. J.* (June 1962).
3. L. L. Prem and W. E. Parkins, A New Method of MHD Power Conversion Employing a Fluid Metal, in *Proceedings of the International Symposium on MHD Electric Power Generation, Paris, France*, European Nuclear Energy Agency, Paper 63, July 1964.
4. M. Petrick and Kung-You Lee, Performance Characteristics of a Liquid Metal MHD Generator, USAEC Report ANL-6870, Argonne National Laboratory, July 1964.
5. W. D. Jackson and G. A. Brown, Liquid Metal Magnetohydrodynamic Power Generator Utilizing the Condensing Ejector, Patent Disclosure, Massachusetts Institute of Technology, October 1962.
6. J. R. Powell et al., Summary of Direct Conversion Work, USAEC Report BNL-8199, Brookhaven National Laboratory, March 1964.
7. L. L. Prem, Atomics International, private communication, September 1964.
8. M. Petrick and Kung-You Lee, Liquid Metal MHD Power Cycle Studies, USAEC Report ANL-6954, Argonne National Laboratory, June 1965.
9. D. G. Elliott, D. J. Cerini, et al., Liquid MHD Power Conversion, Vol. IV, JPL Space Programs Summary No. 37-27, Jet Propulsion Laboratory.
10. D. G. Elliott, D. J. Cerini, and E. Weinberg, Investigation of Liquid MHD Power Conversion, in *AIAA Third Biennial Aerospace Power Systems Conference, September 1–4, 1964*, Paper 64-760.
11. L. L. Prem, Fluid-Metal MHD/Steam Binary Cycle Developed, *Electrical World* (Oct. 19, 1964).
12. W. D. Jackson and E. S. Pierson, Operating Characteristics of the MPD Induction Generator, in *Proceedings of the IEE Magnetoplasmadynamic Electrical Power Generation Conference, New Castle upon Tyne, England, September 6–8, 1962*, Institution of Electrical Engineers Conference Report Series No. 4, pp. 38-42, 1963.
13. W. D. Jackson, E. S. Pierson, and R. P. Porter, Design Considerations of MHD Induction Generators, in *Proceedings of the International Symposium on MHD Electric Power Generation, Paris, France*, European Nuclear Energy Agency, Paper 61, July 1964.
14. W. E. Gunson et al., MHD Power Conversion, *Nucleonics*, 21(7): 43-47 (July 1963).
15. R. Rosa and A. Kantrowitz, MHD Power, *Intern. Sci. Tech.*, pp. 80-92 (September 1964).
16. S. Way and W. E. Young, The Feasibility of Large Scale MHD Power Generation, in *Proceedings of the International Symposium on MHD Electric Power Generation, Paris, France*, European Nuclear Energy Agency, Paper 98, July 1964.

Section II

Power Reactor Technology

Physics

Evaluating Heavy-Atom Cross Sections for Plutonium-Recycle Calculations

By Edwin M. Pennington

Reactivity calculations were made[1] for Yankee critical experiments and for Hanford experiments that involved plutonium fuel. The calculational methods were standard. But significant is the fact that large reactivity differences were obtained by using different cross sections in the same computational model.

Experiments

The Yankee criticals studied consisted of four lattices with H_2O-to-UO_2 volume ratios varying roughly from 1 to 3.5. The UO_2 contained 2.73 at.% ^{235}U and was in 122-cm-high pins of 0.381-cm radius; the pins were clad with stainless steel 0.0407 cm thick.

Hanford criticals had PuO_2-UO_2 in 123-cm-high pins of 0.472-cm radius clad with zirconium 0.0685 cm thick; the isotopic enrichments were 1.366 at.% ^{239}Pu, 0.117 at.% ^{240}Pu, 0.011 at.% ^{241}Pu, 0.219 at.% ^{235}U, and 98.287 at.% ^{238}U. Four lattices were examined with H_2O-to-UO_2 volume ratios varying from 1 to 5.

Subcritical experiments at Hanford used 1.82 wt.% plutonium–aluminum fuel, with the plutonium consisting of 93.97 wt.% ^{239}Pu, 5.58 wt.% ^{240}Pu, and 0.44 wt.% ^{241}Pu. The pins were 111.3 cm high, of 0.635-cm radius, and were clad with zirconium 0.0762 cm thick. Five water-moderated lattices with hydrogen-to-plutonium atom ratios varying from 630 to 1418 were investigated.

Calculations

The calculational model of Ref. 1 involves three fast groups and a thermal group. Fast-group constants were obtained from the GAM-I code[2] using the original library,[3] except that versions of ^{240}Pu and ^{235}U having resonance parameters were used, and the Hanford RBU library[4] values were used for ^{238}U. When ^{239}Pu was involved, self-shielding factors calculated with the RIC code[5] were input to GAM-I. The RIC code computes resonance integrals in a manner similar to the Adler–Heinman–Nordheim method[6] used in GAM-I.

A preliminary SOFOCATE[7] problem using the actual isotopic densities as input provided thermal-group constants. The resulting cross sections were then used in a DSN[8] cell calculation with an extra scattering region to mock-up the isotropic return at the cell boundary. A final SOFOCATE problem using the DSN flux-weighted isotopic densities as input provided the thermal-group cross sections. Thermal-neutron cross sections for ^{235}U, ^{240}Pu, and ^{241}Pu for the SOFOCATE library were taken from Ref. 9. For ^{239}Pu, σ_f values from Ref. 9 were used with values of α^{49} adjusted as described in Ref. 1.

The four-group cross sections obtained as described above were used in one-dimensional diffusion theory (REX) calculations to obtain k_{eff} for the experimental radius. Values of k were within approximately 1% of experimental values for all cases.

Comparisons

For the Yankee critical experiments, calculations were done both with the RBU library version of ^{238}U and the original GAM-I ^{238}U. Figure II-1 shows the calculations and provides a striking example of the reactivity differences

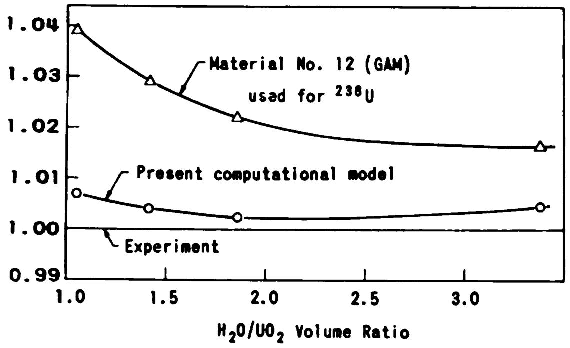

g. II-1 *Comparison of computational model with* *nkee critical experiments.*[1]

at can result from using different cross sec- ons in the same calculational model. Values k_{eff} for the tightest lattice differ by over 3%, hereas it is desirable to calculate with an rror of not more than about 1%. Even larger ifferences result[10] from using various cross ections in the same model for the highly ndermoderated high-conversion critical ex- eriments.[11–13]

For undermoderated light-water lattices, in hich above-thermal processes are of con- iderable importance, uncertainties in cross ections are of more significance than errors roduced by using approximate calculational ethods. There is need for further work to etermine basic cross-section data for use in eactor-physics computations.

ritical and Exponential xperiments with lutonium

y Karl E. Plumlee

Plutonium produced by modern nuclear power lants significantly affects their economy. arious uses are made of recycled plutonium. ome has been used to enrich depleted ura- ium (as will be described). Plutonium also an be used for fuel spikes, driver regions, nd full cores in reactors that require the arger number of neutrons produced per fis- ion in plutonium than in uranium; in compari- on with uranium, this characteristic tends to roduce higher neutron fluxes without increasing the power level, which is an advantage for research and production reactors. On the other hand, if plutonium composition varies spatially, as it does during the operation of many cores, it poses a challenge to the physicist or engineer who is interested in determining the flux and power throughout such a core.

The Need for Data

Recent reports of critical and subcritical experiments indicate growing interest in plutonium-enriched cores and in the use of plutonium recovered from spent fuel.[14–24] Development of more durable fuel elements permits longer fuel exposures and greater plutonium utilization before the spent fuel must be reprocessed. Such highly exposed fuel contains plutonium having sizable concentrations of ^{240}Pu and ^{241}Pu (the ^{240}Pu is formed by nonfission capture of neutrons in ^{239}Pu, and the ^{241}Pu, by capture in ^{240}Pu). Because ^{240}Pu has a large capture resonance for 1-ev neutrons, its reaction rate varies nonlinearly with neutron-energy distribution as well as concentration (because of self-shielding). Thus differences in geometry, and operating variables, such as moderator temperature, affect the ^{240}Pu reaction rate. Designers must know the extent of these effects if plutonium is to be used economically.

Predictions of reactivity, power and temperature coefficients, burnup, and power and flux distributions are quite complicated for plutonium systems—particularly in the often-encountered situation in which both plutonium and uranium are in the core. Consequently experiments are needed to develop and check analytical approximations.

Experiments

Because there are several variables to be considered, measurement of the reactivity effects in plutonium cores requires carefully designed experiments and various fuel samples. But the elaborate procedures and equipment required with plutonium make fuel preparation and critical experimentation difficult. The extreme toxicity of plutonium limits permissible contamination to very low levels; the rapid accumulation of radioactive daughter elements severely limits the exposure time permitted during fuel handling.

In addition to showing the kinds of work being done, a review of the experiments being conducted will indicate rates of progress and the problems encountered, even though some of the work is preliminary.

UO_2-PuO_2, Water Moderated. Critical and subcritical water-moderated experiments, fueled by rods of 1.5 wt.% PuO_2 blended with depleted UO_2 (0.22 wt.% ^{235}U in uranium), have been performed at Hanford.[14] Part of this fuel is being used in the Plutonium Recycle Program in the EBWR (Experimental Boiling Water Reactor), which will involve lengthy operation of the reactor to study reactivity trends, fuel burnup, and operational problems with a plutonium-fueled region. The 4-ft-high fuel rods are clad with Zircaloy-2 tubing 0.37 in. in diameter and 0.03 in. in wall thickness. The oxide-fuel content averages 827 g, of which approximately 86.7 wt.% is uranium and 1.3 wt.% is plutonium; the plutonium isotopic composition is 91.4 wt.% ^{239}Pu, 7.8 wt.% ^{240}Pu, and 0.73 wt.% ^{241}Pu.

The fuel rods were loaded in the subcritical experiment with hexagonal pitches of 0.55, 0.60, 0.71, 0.80, 0.90, and 0.93 in.; as much as 96% of the critical mass was accumulated so that inverse multiplication methods could be used to extrapolate the data to criticality. These extrapolated subcritical-experiment loadings indicated 2 to 5% smaller critical masses than predicted by calculations that were made using computer codes (GAM-I, HRG, TEMPEST, and THERMOS for cross sections, and HFN for criticality). Critical experimentation using the 0.7-in. fuel spacing indicated a somewhat larger critical loading (496 fuel rods) than did the subcritical experiment with the same spacing (484 rods). The change was mainly the result of component modifications, such as substitution of polycarbonate for Lucite plastic grids (or templates) to space the fuel rods.

Uranium and Plutonium Alloys, Graphite Moderated. A series of measurements was made at Winfrith in subcritical plutonium- and uranium-metal-fueled graphite-moderated assemblies that were representative of up to 4000 Mwd/metric ton fuel exposure.[15] The facilities, which were called Scorpio-I and Scorpio-II, were designed for buckling measurements and for fine flux and power-distribution measurements at 20 to 390°C; the experiments were planned to yield data for evaluating methods of calculating reactivity and temperature coefficients in power reactors. Plutonium compositions of ¼ and ½% of the uranium content were employed, with 2.5 to 3.2% ^{240}Pu in the plutonium; composition of ^{235}U was 0.42 to 0.4[illegible] in the uranium rods. In some cases the plutonium was present in plutonium–aluminum alloy strips, whereas in others plutonium-uranium rods were used; fuel-rod diameters were typically 1.1 to 1.2 in., and the length was 18 in. Volume ratios of moderator to fuel were from 17 to 108. Square lattice pitches were 7, 8, 9.9, and 11.3 in. Scorpio-I was the larger assembly with minimum dimensions of 84 by [illegible] by 84 in.; there were a few significantly larger arrays; the largest reported was 98 by 112 by 91 in. Details of the techniques used to measure power distribution in Scorpio-II have been described.[16]

Sample Measurements in Reactors. Related experiments were carried out by introducing a variety of 18-in.-long samples (similar to those described in Ref. 15) into an insulated cell in the uranium–graphite reactor Hector.[17] Because only samples are needed rather than complete uniform lattice loadings, this technique offers the advantage of savings in cost of fuel and in preparation.

Reactivity differences were measured over the range 20 to 450°C. Analysis of the results yielded values of k_∞ agreeing within 0.5% with the values obtained from uniformly loaded lattices. The report indicates that the effects of small perturbations in fuel composition (presence of small amounts of plutonium) can be compared without large corrections being applied in the analysis of results — provided the lattice spacing is large, typically 8.5 in. or larger. A comparison of the experimental results with the Tracer method of lattice calculation shows good agreement for room-temperature reactivities, but the calculation gave k_∞ values 1.5% lower than those measured at 400 to 450°C.

Experiments in France

A list of French CEA-operated critical facilities and typical experiments has been published.[18] Two graphite-moderated facilities are mentioned: Marius, which is operated at room temperature, and Cesar, which is operable at high temperatures. Aquilon is a D_2O facility, and both Alize and Azur are H_2O experiments. Alecto-I and Alecto-II are homogeneous-solution experiments.

Marius is a natural-uranium–graphite reacr that has been used for survey work, includg variation of lattice pitch (19 to 38 cm), ameter of fuel channels (7 to 14 cm), and el-element geometry, including both annular d rod type fuel.[19] Tubular fuel elements were to 10 cm in diameter, and fuel rods were 3 to cm in diameter. The data have been used to velop improved methods of calculation, parcularly in regard to large annular fuel eleents. The development program requires meaurements of relative fission rates in ^{239}Pu and ^{5}U and of their reactivities by oscillation and y substitution methods with plutonium–uraium fuel, irradiated fuel, and enriched and epleted samples. Experimental data and methds of analysis for obtaining reactivities, migraon lengths, and related information have been eported.[19]

Marius and EDF-1. Measurements and analses of flux fine structure and of indexes of eutron-energy spectrum, including some eleated-temperature experiments in the EDF-1 ower reactor, as well as in Marius, have been eported.[20] The first part of the report details nethods of fine-structure measurement and nterpretation using ^{235}U, ^{239}Pu, and ^{115}In bare nd cadmium-covered detectors, as well as omparison with calculated fuel and moderator lux ratios obtained by the Amouyal–Benoist–Hurwitz method. The second part concerns pectral index measurements (including ^{239}Pu, ^{35}U, indium, manganese, europium, and lutetium letectors), details of data treatment, and enironmental conditions.

Marius and Minerve. Systematic experiments using oscillation techniques have been used to letermine the reactivities as functions of sample omposition of ^{235}U (enrichments up to 86%), ^{39}Pu, and boron (up to 12 ppm), for comparison with irradiated fuel samples.[21] The changes in effective cross sections of fuel as functions of neutron-energy spectrum and exposure will be studied by sample irradiation in the EL3 (D_2O) reactor, followed possibly by reactivity measurements in Minerve and by chemical and isotopic analysis. The precision of various techniques used to measure small reactivities, including sinusoidal- and square-wave input of reactivity or source, and also pulsed-source methods, has been studied.[22] Time requirements for equivalent accuracy are estimated for comparable methods. Limitations of the various methods are analyzed and reported, and sensitive areas are pointed out.

Aquilon-II. Bucklings and migration areas with depleted, natural, enriched, and plutonium-alloyed uranium lattices have been measured[23] in the D_2O reactor Aquilon-II. Progressive substitution measurements were made as the reference cores (natural-uranium lattices) were replaced by fuels containing 0.69, 0.71, 0.83, or 0.86% ^{235}U, and natural uranium plus 0.043% plutonium. Uranium pieces were 23.4 cm long and 2.9 cm in diameter; when assembled with aluminum containers, the rods were 240 cm long and 3.2 cm in diameter. The plutonium–uranium assemblies included double aluminum jackets and were also 240 cm long but 3.4 cm in diameter. Lattice pitches were 12, 13, 17, 19, and 21 cm. The analysis indicates consistent results by use of standard treatment. An interesting technique involves using the spontaneous neutron emission rate to measure the uniformity of the plutonium in the plutonium–uranium elements.

Homogeneous Experiments

Critical experiments have been conducted with H_2O solutions of 90% enriched uranyl nitrate and of plutonium nitrate.[24–28] The experiments provide data needed for safely handling fissionable material in solution. Typical geometries were cylinders and annuli. In addition to bare and H_2O-reflected systems, there were thick reflectors of wood and concrete and thin shells of cadmium. Experimental and calculated compositions of solutions involved plutonium in the range 19 to 104 g/liter. Experimental measurements are given for several geometries;[24] values of k_{eff} calculated by two- and four-group diffusion theory are also given for several cores; critical-height measurements are also compared with calculated values. Agreement was within 1% in most of the plain-geometry experiments. Further calculations were by the transport code TDC employing the S-4 approximation and four neutron-energy groups with RZ geometry. Monte Carlo calculations also are reported, and these indicate that 20 to 30 min of computer time is required to obtain a precision of approximately 1.2% in k_{eff} for complicated geometries involving plutonium solutions.

Homogeneous plutonium–hydrogen critical-mass measurements performed at Hanford over the past few years have been summarized.[29] Data are reported for hydrogen-to-plutonium atomic ratios ranging from 15 to 870. The effect of nitrate was studied for concentrations as high as 460 g of NO_3 per liter. Assemblies were made with bare spherical geometry, with cadmium liners, and with reflectors of H_2O, paraffin, or concrete. A number of PuO_2–polystyrene plastic assemblies were reported, particularly for lower hydrogen-to-plutonium ratios. Information helpful in understanding the physics of the plutonium homogeneous systems was developed. Experimental techniques included standard critical-mass measurements, noise measurements, pulsed-source experiments, and spectral-index measurements with foils. Temperature variations also were studied.

Use of Soluble Poisons in Critical Experiments

By Karl E. Plumlee

Boric acid was used to poison the moderator of the Alize-II critical facility.[30] This was done to obtain measurements of temperature coefficients and excess reactivities at various temperatures; boric acid concentrations ranged from 20 to 300 ppm boron. Fuel was aluminum-clad enriched-uranium–aluminum alloy containing 12.8 g of ^{235}U per fuel plate. Plate size was 0.1 by 7.9 by 65 cm. Core composition was varied by assembling aluminum, boron–aluminum, and zirconium components, as well as fuel plates, into boxes. The boxes were inserted into grid positions to form cores. Different grids were available, providing a selection of box spacings. Numerous details are given of the steps taken to control the boron solutions. Measurements of boron deposition rates on aluminum, zirconium, and coated surfaces are reported for various conditions of temperature, concentration, etc. Residual amounts in the core were reported, as well as methods of analysis for less than 1-ppm boron concentration in rinse water. Degassing of the moderator to prevent bubble formation during temperature-coefficient measurements is also described.

Soluble-poison studies also have been conducted with cadmium sulfate solutions.[31] Cadmium solutions, which are alternatives to boron solutions as reactor poisons, were studied in detail to determine the circumstances under which irreversible deposition occurs on reactor components. Quantitative laboratory measurements were made with various surface finishes both aluminum and zirconium components, and with variations of temperature, *p*H, etc., with 13-ppm cadmium solutions.

Water-Reactor Data Generally Verify Theory

By Charles N. Kelber

The growth of low-enrichment light-water-cooled and -moderated power-reactor technology has in large measure been predicated upon a massive amount of experimental and theoretical work in reactor physics. Although some discrepancies remain, a recent summary demonstrates basic agreement between theory and experiment for these systems. Thus reactor theory can be used confidently as the major predictive tool in the design of these systems.

Material Buckling

Material-buckling measurements and calculations are compared and examined for systematic error. Two methods are in common use for measuring material buckling: "flux shape and "variable loading." The flux-shape method, which uses a fit to activation traverses, has a major difficulty in that data from points near the lattice boundary must be rejected and, especially in small systems, the detector response depends on the system size. The variable-loading method involves measuring the axial flux distribution for each of many different-sized loadings of the lattice. A two-parameter least-squares fit to the axial buckling vs lattice radius yields the reflector savings and material buckling. The basic assumption that leads to systematic error is the constancy of the radial-reflector savings. Theory predicts that this is not so, but to remove this assumption requires a three-parameter least-squares fit, with a loss of accuracy, in general.

Similarly, a number of systematic errors were found in theoretical analysis. Three chief sources were (1) use of incorrect thermal-neutron cross sections for ^{235}U, (2) neglect of the effect of cladding on the Dancoff correction nd (3) overestimation of the fast effect. Buckling data were sorted for 96 lattices, and theory was compared with the experiment. For the 11 lattices with the smallest reported error in buckling, the predicted k_{eff} had an average value of 0.9992 ± 0.0016 instead of 1.0. For 55 lattices the average predicted k_{eff} is 0.9988 ± 0.0027. The greatest discrepancy, as expected, is in predicting the properties of closely packed lattices. The authors conclude that the "usual four-group theory" systematically underestimates the worth of the radial reflector.

atio of ^{238}U to ^{235}U Fissions

A quantity directly related to the fast effect is the ratio of fissions in ^{238}U to those in ^{235}U, δ^{28}. The determination of δ^{28} depends on knowledge of a function $P(t',t)$, the ratio of measured activity per fission in ^{235}U to that from ^{238}U; t' is the irradiation time, and t is the time between shutdown and measurement of the activity. Uncertainties in $P(t',t)$ contribute an error of 5% to δ^{28}. For specific fission products such as ^{140}La, the function $P(t',t)$ is a constant, but the relative yields are uncertain.

Fast-effect calculations are fundamentally homogeneous-mixture calculations, but heterogeneity calculations show that the rod advantage factor can yield as much as 1% in k_{eff} and 25% in δ^{28}. These effects can be treated accurately enough by a one-group treatment of neutrons above the fast-fission threshold in ^{238}U. Monte Carlo calculations using the MOCA-2 code[33] agree excellently with experiments. A simple relation can be obtained from a two-region representation of the lattice cell. The fast advantage factor (ratio of average flux in the fuel to that in the moderator) ζ^{28} can be represented by

$$\zeta^{28} = 1 + V_1/V_0\beta\Sigma_1 l_0$$

where V_1 = moderator volume
V_0 = fuel volume
Σ_1 = removal plus absorption cross section of the moderator
l_0 = mean chord length of the fuel
β = a numerical factor that can be related to the chord-length distributions in fuel and moderator
β = 0.67 for a single rod and approximately 0.45 for typical light-water lattices

A second result is that δ^{28} (effects of leakage neglected) is given by

$$\delta^{28} = \delta_{\infty}^{28}\,\bar{l}/(\gamma + \bar{l})$$

where $\bar{l}$ is $l_0 + V_0/\Sigma_1 V_1$, γ is the mean free path in the fuel augmented by fast fission, and δ_{∞}^{28} is the fission ratio in an infinite block of fuel. This representation works best for closely spaced lattices.

Resonance Capture in ^{238}U

Measurement of this quantity or of the related ratio ρ^{28} (epicadmium to subcadmium capture ratio) is too inaccurate to evaluate the various theoretical methods available. Although some progress is being made, the authors feel that "... new and improved experimental methods are necessary to resolve the problems of resonance-neutron capture in light-water lattices."

Thermal-Neutron Distributions

Errors in measurement of thermal-neutron spatial and spectral distribution by means of foil activation stem in part from perturbations of the flux by the foil holder. Another source of error is reduced by careful selection and calibration of foils. Theoretical techniques in common use are the MARC-2B (Ref. 34) and THERMOS[35] codes and the Nelkin scattering kernel.[36] Predicted and measured spectra and distributions are in good agreement, but discrepancies of 1 to 5% in the disadvantage factors remain.

An important source of theoretical error is the treatment of the boundary, especially in closely packed lattices. Use of a condition of isotropic return eliminates most of this source of error.

Reactivity Changes with Long Irradiation

By Bernard I. Spinrad

As plant capital costs go down, reactor fueling costs become a larger fraction of power cost. Therefore the incentive to reduce fuel-cycle costs in reactors becomes greater, and the impact of even small cost reductions becomes more significant. The ability to understand and predict the isotope and reactivity history of the reactor and its fuel is the major physics contribution to fuel economy.

Fuel-Management Methods

There are three general regimes of fuel management, and these depend on the specific power of the reactor. For reactors of low specific power and long fuel residence times (several years), reactivity changes are small over appreciable lengths of time; then, because the problem is to schedule fuel loading and unloading most advantageously, reactivity-change studies emphasize the achievement of criticality under steady-state fuel management. (The same situation holds for higher specific-power reactors if they have rapid fuel-change mechanisms, as do CANDU and the newer British gas-cooled reactors.)

For reactors of somewhat higher specific power, such as most of the higher power water reactors, refueling is not done frequently enough to be used as the major means of reactivity control. Because fuel residence times are from one year to a few years, reactivity changes appreciably during irradiation, requiring the use of control systems for major shimming. The change of flux shape and spectrum under irradiation, coupled with the fact that these changes also depend on the means of control adopted, become important. However, appreciable reactivity is also manageable by zoned or other forms of graded fuel loading, and some relocation of fuel elements at reloading times is possible.

At very high specific power, refueling time becomes a major economic factor; unless on-line fueling is adopted, fuel lifetime is limited by the excess reactivity loaded and the method of controlling this reactivity. One or two, or at most three, running periods exist between load and discharge of an element, and only very limited fuel management can be employed. The physics of control and of isotope—and flux—change as a function of position becomes the overriding problem.

A survey of papers presented at the Geneva Conference provides the opportunity of reviewing this important field. Future issues of this journal may then report further progress.

Prediction and Measurement

Four major papers were presented on the subject—one each from the United States, United Kingdom, Canada, and France.

Light-water reactor physics was emphasized in a bibliographic review of the status of U.S. technology.[37] Light-water power reactors tend to have rather high specific powers and long refueling times. Therefore the emphasis is on calculation of reactor changes over long irradiation, with fuel-management studies being less developed. References are given to the depletion and flux-evolution codes that have been used and are recommended. Because the detailed evaluation of a three-dimensional reactor with control system, as a function of time is an expensive process even with modern computing machinery, there has been a recent trend toward reactivation of few-group diffusion theory and few-region flux synthesis, with very good results reported. These methods are all cited in the paper's bibliography. The authors conclude that calculational methods are, by and large, adequate and that the next improvement in predictive capability will come from isotopic analysis of irradiated fuel and its correlation with improved basic cross-section data.

Gas-cooled-reactor fuel management was studied in the United Kingdom.[38] Because these reactors are capable of virtually continuous refueling, the details of flux-shape evolution are unimportant, and the scheduling of regional fuel relocation is the major problem. No recommendations are made; the antagonistic aims of uniform power (maximum equilibrium reactivity on the reactor fringes) and maximum fuel residence time (maximum reactivity at the center) must be evaluated in detail for any set of reactor economic criteria.

Experimental burnup physics studies were described in a status report on the French program.[39] The report is of value, first, as a bibliography of pertinent French work (mostly CEA reports), and, second, as a good example of the sort of coordinated experimental program required to understand integral properties of irradiated fuels. To calibrate single-sample measurements on irradiated samples, the program features measurement of clean plutonium–uranium fuels as regional lattices in substitution experiments. The fuel enrichments are low, as would be employed in heavy-water reactors.

The D_2O reactors, particularly CANDU, benit from comparisons of theoretical and exerimental isotope—and reactivity—changes D_2O reactors. The Canadian program, which possibly the most integrated one of theory id measurement for a single reactor type, as described in detail.[40] The computational odel used is the standard two-group fourctor formula with, however, each term raonalized for both logical correctness and xperimental verifiability. As irradiation proeeds, effective cross sections and resonance itegrals are varied to account for changes neutron spectrum and isotopic concentraons. Fission-product cross sections have been easured and reported. The effect of radial onuniformity of burnup in a rod has been ivestigated and found to be small owing to anceling effects of plutonium and fission roducts. The conclusion is that reactivity iange in a D_2O reactor can be predicted osely—0.1% or so in reactivity, correspondig to ±10% of a 10,000 Mwd/metric ton lifeme.

perating Experience

The measurement and prediction of reactivity ianges in British gas-cooled reactors were escribed in some detail.[41] By frequent rod ecalibration, both reactivity change and temerature coefficient of reactivity have been llowed up to several hundred megawatt-days er metric ton. Reasonably good theoretical t is obtained with a two-group reactor model, which the neutron temperature is obtained y a thermal-spectrum calculation and selfielding of plutonium resonances is computed detail as a function of local plutonium conentration.

Reactivity experiments after irradiation of atural uranium, ^{235}U, and ^{233}U in the Materials esting Reactor (MTR) were reported.[42] Alough the irradiation spectrum in the MTR is ot very characteristic of a power-reactor istory, the results of the natural-uranium iradiations provide a valuable checkpoint for ieoretical methods since they extend to 15,000 Iwd/metric ton. This work has been reported reviously.[43] The experiments agree well with a tandard depletion code. The ^{235}U and ^{233}U exeriments serve as measures of the effective ross section of stable and long-life fission roducts (after the xenon transients, which they also measured, had decayed). An effective $1/v$ cross section of approximately 50 barns (for each fission caused by 2200 m/sec neutrons, *not* per fission product), in good agreement with theory, is found for several irradiations. A resonance integral between approximately 170 and 210 barns per fission is also reported, which is about 10% lower than theoretically estimated.

Burnup experience with the Novo-Voronezh reactor (WWER) was described without going into details of fuel or control management or of evaluation methods.[44] An initial fuel enrichment of 2% permits operation to a discharge burnup of 12,000 Mwd/metric ton.

Calculations

A method for calculating global flux changes during irradiation was reported without presentation.[45] The method uses two-group theory and a simplified method for solving the Helmholtz equations in a few-region system.

Local reactivity as calculated by standard depletion codes fits remarkably well to a quadratic in flux time.[46] With this simplifying assumption, analytic expressions for reactivity lifetime can be obtained for a variety of fuel-management schemes. Amusingly, this paper cites no Western references, even though the work is similar in spirit to Canadian and U. S. work reported at the 1955 Geneva Conference.

The use of soluble and burnable poison in water reactors was evaluated.[47] No reactivity experience is listed in the paper, which is to be considered rather as a bibliographic source. Soluble- and burnable-poison control-physics calculations are key problems in reactivity calculations for high-specific-power reactors because the errors in predicting control margin are comparable to the normal errors in reactivity-change prediction.

Improvements in Resonance-Integral Theory

By Paul F. Gast

During the slowing-down process, neutrons may be captured by the reactor materials through the action of resonances. Because such captures in ^{238}U or thorium make important contributions to fissionable-material production, they have been studied extensively. Thus neutron-capture rates in ^{238}U and thorium can be computed satisfactorily for simple fuel shapes by semiempirical methods. However, captures in other materials or in more complicated fuel shapes require theoretical treatment, at least in the exploratory conceptual design stages. Work on resonance-integral theory began in the University of Chicago Metallurgical Laboratory days. Some recent developments are reported here.

It is now possible to calculate resonance integrals for isolated resonances to an accuracy limited only by a knowledge of the resonance parameters and by the time and effort appropriate for the case in hand. Monte Carlo methods have been available for some time; recently, numerical analytical techniques have been applied to these problems.

The collision densities and fluxes for homogeneous mixtures of uranium and carbon have been obtained for the 6.7-, 21.0-, and 36.8-ev resonances of ^{238}U by numerical solution of the integral equation.[48] A well-moderated case and one with very little moderation were considered. Although the results are unlikely to find direct application in reactor design, the paper has considerable didactic value because the six cases considered nicely illustrate most of the features of resonance absorption that are neglected in the usual approximations.

A similar solution for a uranium cylinder in a graphite lattice has been worked out for the 6.7-ev resonance only.[49] Details of the method have not been published, but isotropic scattering was assumed, and a polynomial approximation of the transport kernel was used.

In reactor design work such calculations are not usually feasible, so most theoretical attention has been directed toward less laborious methods that give accuracies appropriate for reactor work. The intermediate-resonance method[50] has been extended to the heterogeneous case[51] by the use of equivalence principles. A physical interpretation of the method[52] permits easy computation of the "width parameter" and extension to Doppler-broadened cases.

Equivalence principles rest on two approximations: (1) the assumption of a flat source in computing the escape probabilities from the absorber and (2) the use of a rational appr mation to represent the resulting probabili The errors arising from the flat-source sumption have been examined.[51,53] The ba approach is the same in both papers, but method of Ref. 53 has the advantage of being limited to thin slabs. Table II-1 sh

Table II-1 PERCENT ERRORS FROM FLAT-SOU APPROXIMATION[53]

Slab thickness	Neutron width/resonance width, Γ_n			
	0.2	0.4	0.6	0.8
0.0	1.1	2.7	5.5	11.5
0.3	1.3	2.9	5.7	11.7
0.6	1.6	3.2	6.0	11.9

the results obtained by numerical integratio which depend on the amount of resona scattering and the slab thickness (in pote scattering mean free paths). Presumably, si lar values would apply for other simple co shapes with the same surface-to-volume ra appreciable errors occur when the resonan a strongly scattering one.

Improvements in the rational approxima are the subject of continuing investigation, three recent efforts were described in Summer 1965 issue of *Power Reactor T nology*.[54] An additional formulation has b reported,[55] and its extension to nonblack tub absorbers has been developed.[56]

References

1. D. P. Moon, Consistent Heavy-Atom Cros Section Evaluation for Plutonium Recycle C culations, USAEC Report ANL-6972, Arg National Laboratory, December 1964.
2. G. D. Joanou and J. S. Dudek, GAM-I: A C sistent P_1 Multigroup Code for the Calcula Fast Neutron Spectra and Multigroup Cons USAEC Report GA-1850, General Dynamics C June 28, 1961.
3. G. D. Joanou et al., Nuclear Data for GA Data Tape, USAEC Report GA-2451, Vols. I- II, General Dynamics Corp., Aug. 22, 1961.
4. R. C. Liikala, Updated RBU Basic Lib USAEC Report HW-75716, Vols. 1, 2, 3, Han Atomic Products Operation, 1963.
5. D. A. Klopp and W. E. Zagotta, Reso Integral Determination, ARF Progress Re A-1918-8, Illinois Institute of Technology, Ar Research Foundation, March 1962.
6. F. T. Adler, G. W. Hinman, and L. W. Nord The Quantitative Evaluation of Resonance grals, in *Proceedings of the Second Unite*

tions International Conference on the Peaceful Uses of Atomic Energy, Geneva, 1958, Vol. 16, pp. 155-171, United Nations, New York, 1958.

H. Amster, The Calculation of Thermal Constants Averaged Over a Wigner-Wilkins Flux Spectrum: Description of the SOFOCATE Code, USAEC Report WAPD-TM-39, Westinghouse Electric Corp., Bettis Atomic Power Laboratory, January 1957.

B. Carlson, C. Lee, and J. Worlton, The DSN and TDC Neutron Transport Codes, USAEC Report LAMS-2346, Los Alamos Scientific Laboratory, February 1960.

D. J. Hughes, B. A. Magurno, and M. K. Brussel, Neutron Cross Sections, USAEC Report BNL-325 (2nd ed.) (Suppl. 1), Brookhaven National Laboratory, Jan. 1, 1960.

E. M. Pennington, Argonne National Laboratory, in preparation.

Q. L. Baird and A. R. Boynton, Bucklings, Disadvantage Factors, and δ^{28} Measurements in Some Undermoderated Slightly Enriched Cores, *Trans. Am. Nucl. Soc.*, 6(1): 258 (1963).

Q. L. Baird et al., Initial Conversion Ratio and ρ_c^{28} Measurements in Very Undermoderated Slightly Enriched Oxide Cores, *Trans. Am. Nucl. Soc.*, 7(1): 80 (June 1964).

A. R. Boynton, Experimental Thermal-Disadvantage Factors in Some Very Undermoderated, 3%-Enriched Water-Uranium Oxide Lattices, *Trans. Am. Nucl. Soc.*, 8(1): 249 (June 1965).

L. C. Schmidt, R. C. Liikala, W. P. Stinson, and J. R. Worden, Critical Masses and Bucklings of $PuO_2-UO_2-H_2O$ Systems, *Trans. Am. Nucl. Soc.*, 7(2): 216 (1964); USAEC Report HW-83187, Hanford Atomic Products Operation, July 1964; USAEC Report HW-84608, Hanford Atomic Products Operation, June 15, 1965.

D. H. Carter et al., Buckling and Reaction Rate Experiments in Plutonium/Uranium Metal Fueled, Graphite Moderated Lattices at Temperatures Up to 400°C, Part I. Experimental Techniques and Results, British Report AEEW-R-318, July 1964.

D. H. Carter, B. J. Puckett, and A. E. Richards, Measurements of $Pu^{239}:U^{235}$ Fission Ratio Using Foils at Temperatures Up to 400°C, British Report AEEW-M-447, May 1964.

R. C. Bannerman, H. H. W. Pitcher, and R. Richmond, Analysis of the Results of Reactivity Change Measurements on Plutonium–Uranium Fuel Elements, British Report AEEW-M-441, July 1964.

D. Breton and P. LaFore, Experimental Methods in Thermal Reactor Physics, presented at the Third United Nations International Conference on the Peaceful Uses of Atomic Energy, Geneva, 1964, Paper A/Conf.28/P/102.

F. Congé, Mesures Globales de Reseau a Graphite dans l'Empilement Critique Marius, French Report CEA-R-2478, August 1964.

F. Cogné and J. Journet, Mesures Fines dans les Reseaux Graphite, French Report CEA-R-2479, 1964.

O. Tretiakoff et al., Mesure des Sections Efficaces Effectives d'Echantillons Fissiles par une Methode d'Oscillation dans les Assemblages Critiques, French Report CEA-R-2487, August 1964.

J. Valat and T. E. Stern, Analyse de la Precision de Certaines Methodes de Mesure des Tres Basses Reactitivities, French Report CEA-R-2229, August 1964.

23. R. Naudet et al., Experiences Critiques dans Aquilon Portant sur des Combustibles Legerement Enrichis en U^{235} et en Plutonium, French Report CEA-R-2477, August 1964.

24. M. F. Ithurralde et al., Interpretation des Experiences de Criticite sur des Solutions Homogenes de Plutonium et d'Uranium, French Report CEA-R-2488, August 1964.

25. D. Breton and C. Clouet d'Orval, Etudes de Criticite, presented at the Third United Nations International Conference on the Peaceful Uses of Atomic Energy, Geneva, 1964, Paper A/Conf.28/P/84.

26. J. G. Bruna et al., Alecto, Experiences de Criticalite sur une Solution de Plutonium. Resultats Experimentaux, Cuve No. 1, French Report CEA-2274, 1963.

27. J. G. Bruna et al., Alecto 1—Experience de Criticite sur une Solution de Plutonium et d'Uranium Enrichi a 90%. Resultats Experimentaux et Calculs Concernant la Cuve No. 2, French Report CEA-R-2453, June 1964.

28. E. Deilgat et al., Experiences de Criticite sur des Cylinders Annulaires Contenant des Solutions de Plutonium, French Report CEA-R-2495, June 1964.

29. E. D. Clayton, Progress in Plutonium Critical Mass Physics, USAEC Report HW-83603, Hanford Atomic Products Operation, October 1964.

30. J. Bailly et al., Etude des Reseaux a l'Eau Legere par la Methode d'Empoisonnement Homogene au Bore, French Report CEA-R-2489, August 1964.

31. O. Croix et al., Utilisation du Cadmium en Solution dans le Moderateur du Reacteur EL_4, Fixation Irreversible du Cadmium sur les Surfaces Metalliques, French Report CEA-R-2504, August 1964.

32. Glenn A. Price and R. L. Hellins, Lattice Studies in Light Water Moderated Systems, presented at the Third United Nations International Conference on the Peaceful Uses of Atomic Energy, Geneva, 1964, Paper A/Conf.28/P/264.

33. H. Rief, An IBM 704 Monte Carlo Code To Calculate the Fast Effects in Homogeneous and Heterogeneous Systems, USAEC Report BNL-647, Brookhaven National Laboratory, Jan. 1, 1961.

34. E. M. Gelbard, H. B. Ondis, and J. Spanier, MARC—A Multigroup Monte Carlo Program for the Calculation of Capture Probabilities, USAEC Report WAPD-TM-273, Westinghouse Electric Corp., Bettis Atomic Power Laboratory, May 1962.

35. H. C. Honeck, THERMOS. A Thermalization Transport Theory Code for Reactor Lattice Calculations, USAEC Report BNL-5826, Brookhaven National Laboratory, September 1961.

36. M. Nelkin, Scattering of Slow Neutrons by Water, *Phys. Rev.*, 119(2): 741-746 (July 15, 1960).

37. G. H. Minton and H. W. Graves, Jr., Calculation of Criticality, Power Distribution, and Fuel Burnup in Thermal Power Reactors, presented at the Third United Nations International Conference on the Peaceful Uses of Atomic Energy, Geneva, 1964, Paper A/Conf.28/P/266.

38. B. Cutts, A Study of Fuel Cycles and Fuel Cycle Problems for Advanced Gas Cooled Graphite

Moderated Reactors, presented at the Third United Nations International Conference on the Peaceful Uses of Atomic Energy, Geneva, 1964, Paper A/Conf.28/P/177.

39. O. Tretiakoff, Burn Up Physics, presented at the Third United Nations International Conference on the Peaceful Uses of Atomic Energy, Geneva, 1964, Paper A/Conf.28/P/77.

40. M. F. Duret et al., Fuel Burn-Up and Reactivity Changes, presented at the Third United Nations International Conference on the Peaceful Uses of Atomic Energy, Geneva, 1964, Paper A/Conf.28/P/26.

41. H. A. Hughes, D. A. L. Clinch, R. M. Horsley, D. J. Millard, and R. Razzell, Experimental Basis of Power Reactor Operation, presented at the Third United Nations International Conference on the Peaceful Uses of Atomic Energy, Geneva, 1964, Paper A/Conf.28/P/170.

42. R. G. Nisle, D. R. deBoisblanc, E. Fast, J. C. Connor, and S. B. Gunst, Fission-Product Buildup and Long-Term Reactivity Effects, presented at the Third United Nations International Conference on the Peaceful Uses of Atomic Energy, Geneva, 1964, Paper A/Conf.28/P/269.

43. S. B. Gunst, E. D. McGarry, and J. J. Scoville, The Reactivity of Natural UO_2 Irradiated to 6×10^{21} n/cm^2, *Nucl. Sci. Eng.*, 7: 407-418 (1960).

44. L. V. Kommisarov, G. L. Lunin, A. N. Novikov, V. A. Sidorenko, and V. P. Sidorenko, Physical Studies of Novo-Voronezh Atomic Power Station, presented at the Third United Nations International Conference on the Peaceful Uses of Atomic Energy, Geneva, 1964, Paper A/Conf.28/P/585.

45. F. Accinni, R. Bonalumi, C. Bruschi, F. Palazzi, S. Rubbia, and G. B. Zorzoli, The Physics of a Steam-Water Mixture-Cooled Heavy Water Power Reactor, presented at the Third United Nations International Conference on the Peaceful Uses of Atomic Energy, Geneva, 1964, Paper A/Conf. P/625.

46. V. Bartosek, M. Hron, V. Lelek, and M. Nepras (Prague), On Some Physical Problems of Ura Burnup in Heavy Water Reactors, presented Third United Nations International Conference the Peaceful Uses of Atomic Energy, Gene 1964, Paper A/Conf.28/P/630.

47. A. Radkowsky and R. J. Creagan, Poison Co of Thermal Reactors, presented at the Th United Nations International Conference on Peaceful Uses of Atomic Energy, Geneva, 19 Paper A/Conf.28/P/274.

48. Hans-Jürgen Siegert, Das Neutronenspektru der Umgebung von Resonanzen, *Nukleonik*, 6 307-310 (October 1964).

49. F. T. Adler and E. E. Lewis, Compariso Exact and Approximate Treatments of Resona Effects in Cylindrical Lattices, *Trans. Am. N Soc.*, 7(1): 29 (June 1964).

50. R. Goldstein and E. R. Cohen, *Nucl. Sci. En* 13(2): 132 (June 1962).

51. R. Goldstein and H. Brooks, Intermediate Resonance Absorption in Nonhomogeneous Syste *Nucl. Sci. Eng.*, 20(3): 331-337 (November 19

52. Guido Forti, Evaluation of Resonance Integrals Homogeneous and Heterogeneous Systems— Intermediate Approximation, *Nucl. Sci. E* 19(4): 449-457 (August 1964).

53. J. Berg, The Flat Source Approximation in Resonance Integral Calculations, *Nukleonik*, 6(4): 20 209 (July 1964).

54. *Power Reactor Technol.*, 8(3): 159-160 (Summ 1965).

55. H. Neltrup, An Approximate Collision Probab Formula for Resonance Integrals, *J. Nucl. Energy, Pt. A & B*, 18: 704-708 (December 1964).

56. H. Aisu, Effective Surface of a Tubular Absorbe in the Calculation of Resonance Integrals. N *Sci. Eng.*, 21(2): 250-255 (February 1965).

Section
III

Power Reactor Technology

Control and Dynamics

eactor Control xperience

Joseph M. Harrer

ontrol-system designers sometimes introduce ant features that, although good in principle in laboratory tests, do not always work out ccording to plan when the plant is operated. hus the experience with control equipment and e failure analyses that were aired at the Conrence on Reactor Operating Experience (sponored by the Reactor Operations Division of the merican Nuclear Society) are significant for esigners. One attendee's summary and interretations are given here.

eactor Accident Frequency

The general opinion exists that reactor acidents are unusual occurrences. Over a period f a little more than 20 years, all types of rectors and critical experiments have amassed total of more than 1000 years of operating istory. Despite the fact that many of these evices were of new or experimental configuations, no member of the general public has ver been overly exposed to radiation or sufered inconvenience from a reactor accident.[1] ut during these 20 years there have been about 0 accidents or incidents that resulted in rompt criticality, crew fatalities, or massive amage to the plant. At least half of these acidents would not have occurred if the reactor afety systems had operated correctly.

Components Have Been Reliable. In an effort o prevent reactor excursions, reactors still re being built with equipment that automatially checks safety-system performance as frequently as once per second. The object of these tests is to detect safety-component failure before any reactor excursion occurs. But the actual record of one uncontrolled excursion per million operating hours shows that not one of them resulted from failure of a safety-system component.

The System Must Be Able. Some excursions occurred when the safety system lacked proper input information; several failures resulted from slow response by the safety system. In at least two cases, the safety system was paralyzed by the accident; in another case the accident was intensified by safety action—and in still another case the accident was caused by an attempt to scram the reactor. Thus, rather than being related to component failure or lack of reliability, these performance failures occurred because the safety systems were inherently unable to protect the reactors. Clearly, although it is impossible to anticipate or simulate the exact conditions under which the safety system must perform, much more must be done to make tests uncover more than just component failure. In this way designs and operating procedures can be corrected so as to prevent uncontrolled excursions.

Although the statistical experience of one uncontrolled excursion per million hours was acquired with all sorts of reactors and critical experiments—and thus is not really applicable to the situation in which we are operating proved and stably operated reactors—its importance can be appreciated from the facts that (1) most reactors today have higher powers and greater fission-product inventories and (2) direct extrapolation of these statistics would indicate (improperly, however) that, over a 25-year life, one out of four reactors would suffer an uncontrolled excursion that results in massive damage.

Perhaps a significant question is, "Have we been learning enough from experience?" Simple component testing is not the answer. Operators and designers must devolve tests and corrections that will prevent accidents more effectively.

Rod Problems

The primary safety device has always been control rods. Thus tests that detect impending trouble in control rods are important for preventing accidents. But how dependable is a test that simply assures the time for scram is less than a predetermined value? Not very dependable, according to experience with the UMRR (University of Missouri at Rolla, Reactor), a 10-kw swimming-pool reactor,[2] and with the 61-Mw Heavy Water Components Test Reactor (HWCTR) at Savannah River Laboratory.[3]

UMRR Rod Swelling. Each of the original shim-safety rods consisted of a type 304 stainless-steel shell lined with 30 mils of cadmium and filled with B_4C powder. Because such rods elsewhere have a history of failure, the UMRR rods were checked closely by measuring rod-drop times at six-month intervals. These tests were expected to yield information on the condition of the rods, particularly about swelling, as well as simultaneously checking the scram circuit.

But during one routine startup, control-panel instruments indicated that a control rod would not withdraw beyond 17 in. Inspection showed that the rod was hung at a partially withdrawn position. After the reactor was shut down, rod-drop times were measured and found to be normal for withdrawals of up to 16 in. After the core was dismantled and the suspect control rod was removed, measurement with a micrometer showed an 8.6% increase in rod thickness, which was enough to cause the rod to bind in its channel. Although similar measurements showed that the other two shim-safety rods had swelled 3.2 and 3.0%, rod-drop times gave no indication of this swelling.

A possible failure mechanism is that a shell leak allows water to accumulate in the rod, radiation decomposes the water, the gas pressure seals the hole by forcing damp B_4C powder into it, and subsequent water decomposition raises the pressure, which swells the shell.

The original rods in the UMRR have now been replaced by solid rods consisting of 18-18 stainless steel alloyed with 1.5% boron. As expected, these new rods have a measured worth 80% that of the original B_4C rods. This is more than adequate for the excess reactivity used in the UMRR. And, because of the greater reliability of the new rods, safer operation results.

The UMRR reactor staff concludes that, although rod-drop-time tests provide a good monitor on the total scram circuitry, they are not adequate for monitoring control-rod condition; for this, periodic direct inspection and measurement of rod dimensions are necessary.

HWCTR Rod-Guide-Tube Ruptures. The time measured in rod-drop tests is often judged as satisfactory if it is less than some standard value for a particular rod system. But experience at the HWCTR shows that a simple go–no-go test does not guarantee that failure is not in progress.[3] Safety-rod drop times were measured at HWCTR before each startup, analyzed for unusual results, and compared with previous results to indicate trends. When rod-drop time decreased, loss of snubbing action was the cause; the problem was traced to rupture of the Zircaloy-2 guide tubes for four of the six safety-rod assemblies. The rods had been in service for nearly three years.

The failures consisted of longitudinal splits starting at a transition in size of the guide tube. These tubes are 11.3 ft long, but the inside diameter of the bottom 3.4 ft is 1.310 in. (rather than 1.375 in. as in the upper section) to provide a $\frac{1}{4}$-in.-high transition piece for hydraulic snubbing action when the control rod drops. The splits were attributed to a combination of high residual stress in the necked-down area and cumulative tensile-stress pulses when the rods were snubbed.

The existence of residual stresses might have been expected. The upper and lower sections were of the same thickness, and the design called for absorbing the snubbing forces in tension in the lower section. This in itself leads to the second observation, that tensile pulses contributed to the failure. It is well known that considerable tensile stress can develop under those conditions. The vertical tensile stress could have been eliminated by a bottom support for the guide tube, but the basic stress that initiated the failures would remain. The correction involved lengthening the transition section from $\frac{1}{4}$ to 1 in. and changing the ecifications to assure less residual stress d higher ductility.

Further study of the tubes showed that D_2 ntent of the Zircaloy was 100 to 300 ppm, ich is considered high; generally, the D_2 con- nt at the transition piece was at the higher lue. Other Zircaloy tubes that had endured e same reactor environment — but which were low nickel content — did not display this high pickup and remained much more ductile when sted by completely collapsing the tubes. They d not crack even when fully collapsed. On the sis of these tests, an overall conclusion is at either Zircaloy-4 or low nickel Zircaloy-2 ould be much better for use under the HWCTR nditions, which are 200 to 250°C, *p*D of 10 to (at 25°C), chlorides less than 0.1 ppm, O_2 ss than 0.1 cm^3 per kilogram of D_2O (0.14 m).

ravity-Independent Rods

Gravity rod-insertion systems are as old as actors themselves. But what if you do not ve gravity acting in the proper direction at l times? A gravity-independent system with rings provided one answer.[4] The need arose cause the Aerospace Shield Test Reactor STR) had to be rotatable in two planes and sitionable vertically for various shielding periments. Thus, rather than heavy rods (on hich gravity usually has a beneficial effect), lighter rod had to be found for this reactor. ptimum performance was obtained by select- g a minimum thickness of silver–indium– dmium by means of critical-experiment tests; these tests a 0.200-in.-thick absorber was rst tried in the critical assembly; then the lver–indium–cadmium was machined to 0.18, 15, 0.12, and finally to 0.100 in., at which ickness a sharp drop in effectiveness was ob- rved. With the 0.125-in. thickness selected, ch 24-in.-long rod weighs only 13 lb. Spring rces vary between 30 and 80 lb, with the gher force when the rod is fully withdrawn. hus maximum and minimum forces are 6 and *g*. Even if the reactor and rod are completely verted so that gravity acts against the rod rings, the basic 1 *g* is always present to hold e rods in the shutdown position.

Springs Vs. Pneumatics. Gravity-independent ods are widely used on critical experiments, pecially for fast reactors — where the as- mbly and the rods are operated horizontally (to make it easy to assemble fuel in trays), but in air rather than in water as is the ASTR. Many designers feel that air cylinders provide an adequate and neat stored-energy package and prefer them to springs. Assemblies of springs usually are much more bulky, and some mechanical designers do not consider them more reliable than a well-designed pneumatic system. But the big objection to pneumatic systems is that an oil explosion could suddenly wreck the entire system and rapidly remove the stored energy force. Although oil explosions in air storage systems can be prevented by using pumps that do not need an oil lubricant, self-lubricating pistons (for example, graphite rings) would also be needed in the scram cylinders. The pistons could be lubricated with high-flash-point oil, but this would not be an ideal solution.

The use of springs or pneumatic systems for stored energy in gravity-independent systems remains an open question. Designers and users are well-advised to keep abreast of pertinent experience and observe any failures realistically. It may well be that springs could be far superior when one considers the long-term maintenance problem and the fact that catastrophic failure of a spring is not likely if inspection is adequate.

Control of Critical Assemblies by Moderator Level

Usually the dumping of moderator from a critical assembly is considered a backup for control rods. But experience with moderator control at the Westinghouse Reactor Evaluation Center shows that variation of moderator level can be a useful primary control method.[5] The important principle is to vary the moderator level so that at the operating point the k_{eff} is approximately unity due to the upper reflector. Then the upper portion of the reflector is of decisive importance; lowering it will produce negative reactivity immediately even with the rods partially controlling the reactivity.

Use of the moderator as the basic control device is desirable when the cores being studied have nonhomogeneous fuel enrichments, dimensions, and cladding. Criticality is achieved first by movement of control rods and then by the exchange of reactivity in control rods and moderator until the rods are fully withdrawn.

Advantages. The achievement of uniform lattices requires complicated design and fabrication efforts if rods are used at all. Fueled followers (for control-rod slots) tend to produce core uniformity. But if any fuel protrudes into the lower reflector, nonuniformity is introduced. The coupling of control material to fuel represents a potential source of weakness in the rod structure, and, because a hazard is created, the absorber follower section could fall through the core. This type of problem calls for a meticulous design effort to assure safety. For a reduction in this time-consuming and costly work, and at the same time for an increase in the inherent safety, it is much better to rely on moderator-level control completely.

The most probable and most severe accidents considered in hazard analyses for critical facilities and reactors are presumed to come from rapid (step) movement of control material. Thus, in terms of positive insertion of reactivity, operation by moderator control is a significant step in the direction of safer operations because it eliminates a possible accident-creating component.

The ramp rate one obtains from moderator control is a single continuous variable, whereas the ramp rates of control rods vary with radial location; thus, for a given core, the operator does not have to be concerned with there being different ramps available at his fingertips. There is only one method of adding reactivity, and any mechanical failure in the moderator-fill system (leak, pipe failure, etc.) results in moderator loss and reactivity loss.

It has been argued that, with a high moderator level, the moderator reactivity differential effectiveness is low and then one has no rapid means of inserting negative reactivity. However, this argument tends to be countered by the fact that under such circumstances fast insertion of positive reactivity is not even possible.

The whole problem as discussed in Ref. 5 gives one side of one of the oldest arguments in critical-facility operation. Should one raise water with rods withdrawn ready to stop an uncontrolled reaction, or, knowing that the rods will prevent an uncontrolled reaction, should one leave the rods in place until the water moderator is fully in?

The usual method is a compromise. One or two rods are removed, then the water is raised, and later the other rods are raised to ach a critical assembly. If moderator level alon used, it is argued that first all rods shoul raised and then the raising of the modera should begin. However, in many assemblies cannot be done without violating interlocks.

A strong case can be made for moderat only control, but it is very difficult to pr that by itself it assures safety. If rods present or even possible, it seems safer to them in some way to limit the bulk moder effect and then later achieve a uniform cor changing moderator level and exchanging erator reactivity for rod reactivity as they drawn out of the core.

Subcriticality Measurement

All reactor operators want a simple and s way of measuring subcriticality during s down. Although this is one of the most diff measurements to make in a power reactor can be done relatively well in "clean" crit assemblies and in low-power multiplication e periments. As always, the key factor is inst mentation—but, in theory, the measurem is always possible.

The measurement consists in comparing neutron statistical variation at two or m frequencies. As the ratio of the low-to-h frequency amplitude increases, criticality approached. But in a power reactor, the gamma background makes this measurem difficult if not impossible. As a step towa circumvention of this problem, an experim was performed in which a conventional 12 cou (sec)(nv) BF_3-filled detector was connected 20-Mc wide-band video amplifier by a 75-o impedance transmission line.[6] A pulse widt about 100 μμsec was observed. Although neut counting rates were higher, even with the w band electronics there was no significant provement in gamma tolerance. This led to of a lower-multiplication gas tube.

A boron-lined detector about 9 in. long $^1/_4$ in. in diameter was selected. For gre sensitivity and efficiency, four prototype were operated in parallel. One tube ha boron-coating thickness of 1 mg/cm^2 and wa filled with argon–isobutane at a pressure 250 mm Hg; the other three tubes were fille with argon–carbon dioxide to the same pr sure, but their coating thicknesses were 0. and 1.2 mg/cm^2. The detectors were chec ith a neutron source, and spent fuel elements erved as a gamma source. The typical countate response for various pulse-height settings own in Fig. III-1 indicates only slight deensitization of the detector in a gamma field 19,000 r/hr. Thus the author concludes that tension of the wide-band techniques with iniature boron-lined detectors will permit easurement of the reactivity of shutdown ower reactors by noise-analysis techniques.

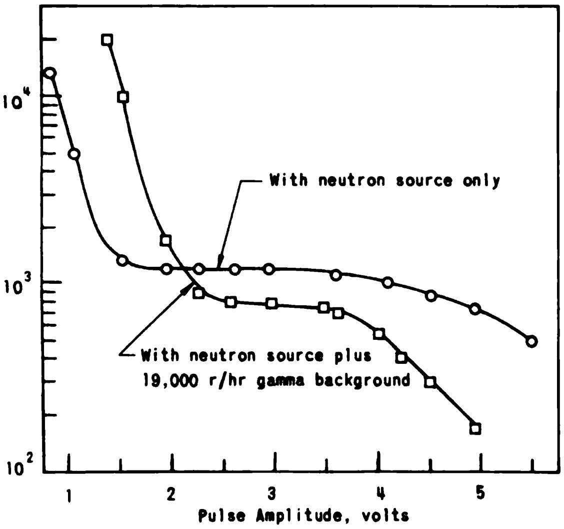

ig. III-1 Count-rate response at various pulseeight settings for four miniature prototype boronoated detectors operating in parallel shows that 19,000 r/hr gamma field desensitizes detector only lightly.[6]

iquid-Poison Injection

Even with good instrumentation, fast safety ircuits, and control rods to prevent and stop any uncontrolled excursion, reactor designers have always tried to install a backup system that could be used if the rods failed to control the reactor. A survey of the methods of backup protection used on reactors is given in *Nuclear Safety*, 7(1): 45-52. This backup often is in the form of a neutron-absorbing liquid poison, such as boric acid, that could be forced into the reactor coolant or moderator. But the design of such a system calls for a special approach. How fast should it operate? Should it be automatic or under procedural control? Is stored high-pressure gas a good force to inject poison into a pressurized reactor system? Experience with liquid-poison injection systems at Savannah River Laboratory can help answer such questions.

In the HWCTR[3] protection comes from injecting poison ($K_2B_4O_7-4H_2O$) into the coolant (D_2O) stream. The operator would actuate this system if the neutron flux fails to decrease after a scram signal. The solution has the same reactivity worth as the control rods, a minimum of 24% $\Delta k/k$. If uniformly distributed in the full 7000 gal of D_2O in the primary system, the poison would keep the reactor subcritical under all conditions.

The system was tested at least once a year during an outage by replacing the poison solution with D_2O and timing an injection; poison injection was never actually required during reactor operation.

As the system was originally designed and built, poison solution was delivered rapidly from a storage tank pressurized by helium from an external source. It was planned to adjust the helium pressure for the proper injection time, depending on whether the reactor was pressurized or unpressurized, and to determine the proper helium pressures experimentally during prestartup tests. These tests showed that this arrangement would not deliver the poison properly under certain combinations of reactor pressure and flow. On several occasions with the reactor unpressurized and when some D_2O was blown out of the tank, the main D_2O circulating pumps became gasbound by large volumes of helium.

These problems were avoided by the following changes: the pressure between the reactor gas space and the storage tank was equalized by connecting the reactor gas space to the poison storage tank, which was elevated about 50 ft above the reactor so that gravity would provide the driving force; an orifice was installed in the injection line to control the injection time. After these changes the remaining variable that affected the injection time was the coolant flow through the reactor. About half the system pressure drop is across the core—and thus between the reactor gas space and the moderator space where the poison is injected. Therefore the coolant flow in the reactor directly affects the driving force for injection.

Injection time must be quite a bit longer than the recirculation time of coolant to assure that enough poison is always in the reactor core. If too-rapid injection were allowed, each coolant-flow cycle could sweep the poison completely out of the core and result in a power excursion. Table III-1 shows the amount of poison injected and compares its injection time to the D_2O circulation time for full flow and shutdown flow. This method was proved by test, and there was no gas binding in the pumps.

Table III-1 HWCTR POISON-INJECTION CHARACTERISTICS

	D_2O full flow	D_2O shutdown flow
D_2O circulation time, min	0.6	2.0
Poison total injection time, min	3.6	3.9
Total poison injected, gal	73	60

Actual injection of another neutron-absorber liquid was tested in a production reactor at Savannah River Laboratory.[7] This system injects $Gd(NO_3)_3-D_2O$ solution directly into the D_2O moderator.

Important mechanical features of the system are that: (1) it operates on self-contained pneumatic power that is independent of other pneumatic or electrical networks, (2) injection is not automatic, but rather is initiated from the reactor control room in accordance with specified procedures, and (3) injection of $Gd(NO_3)_3$ starts not less than 5 sec after initiation of the signal but then is completed within 3 sec after injection is begun.

In a special test in a production reactor operating at power, reactor power began to decrease 3.5 sec after the system was actuated and had decreased to 50% after 6.5 sec. Reactor response to the poison injection is shown in Fig. III-2. (The poison was subsequently removed from the moderator by ion exchange.)

Computer Applications

The work of compiling a large amount of data accurately, quickly, and selectively is obviously the job for a computer. At Savannah River, the application of modern computer technology is helping ease operational problems.

An on-line digital computer[8] at the K production reactor there improves reactor safety and operating efficiency by providing more thorough surveillance and by compiling accurate operating information much faster than could be

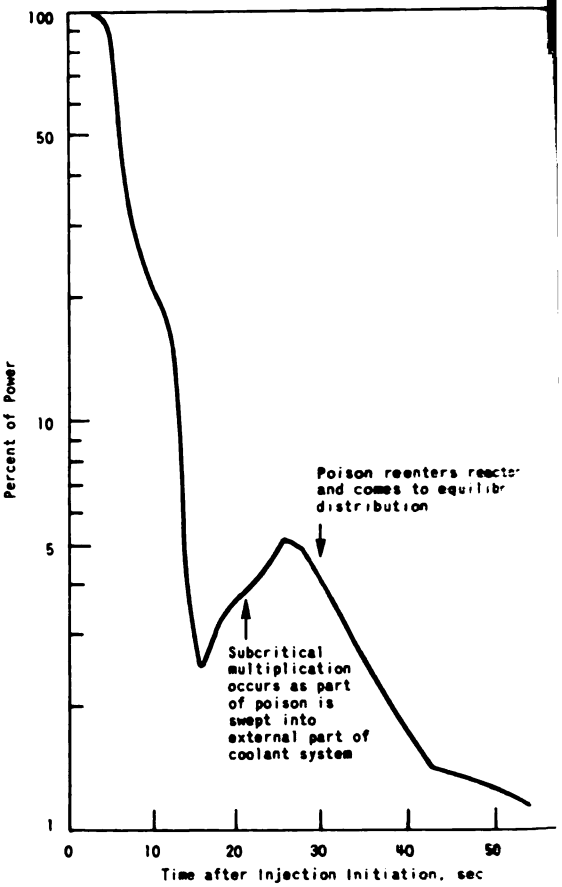

Fig. III-2 Rapid shutdown occurred when
absorbent liquid was injected into reactor mode

obtained otherwise. Signals from about thermocouples, flow and pressure meters, monitors, and other sensors provide infor tion from all regions of the reactor.

Two types of data scans are provided: sequential scan of 2400 temperatures and f in the 600 reactor-lattice positions, and random-access scan for nuclear instrume in-core flux sensors, and miscellaneous se sors in the D_2O primary and H_2O secon (river water) coolant systems.

Surveillance of reactor operating limits an important function of the computer. Sever types of fuel elements can be used in one re tor charge, and each may have distinct hydr lic characteristics and operating limits. Ala programs compare reactor data with the a propriate limits for coolant flow, temperat temperature rise, and bulk moderator (temperature. An alarm is typed in red if operating limit is exceeded. A periodic pr ıt of the margin from the nearest limits is sed by reactor operators to adjust reactor ower level. Complicated limits, such as prox- nity to burnout heat flux, are calculated on emand with axial flux data from in-core sen- ors and fuel-coolant temperature data stored the computer.

An analog system[9] was used to compute the afety margin from burnout in a special high- ux core [$>4.3 \times 10^{15}$ neutrons/(cm^2)(sec)] in ne of the D_2O-cooled and -moderated produc- on reactors at the Savannah River Plant. The ower density of greater than 130 kw per gram ^{235}U was controlled with the aid of a direct- eading analog-computer circuit that displayed ne safety factor against burnout of the fuel urface within an accuracy of 5%. The circuit ompares the operating heat flux [$\sim 2.5 \times 10^6$ tu/(hr)(sq ft)] to the heat flux at burnout as efined by the correlation

$$HF_B = 463{,}000(1 + 0.04V)[1 + 0.0167(T_s - T_b)]$$

here HF_B = heat flux at burnout in British thermal units per hour per square foot

V = coolant velocity in feet per second

T_s = coolant saturation temperature in degrees Fahrenheit

T_b = coolant bulk temperature in degrees Fahrenheit

For the burnout safety factor, the computer ircuit solves the simplified equation

$$(BOSF)_x = \frac{(C_1 - C_2 x)\sum_{i=1}^{5} \Phi_i}{\Phi_x \Delta T} - \frac{C_3 \sum_{i=0}^{x-1} \Phi_i}{\Phi_x} - C_4$$

where Φ_x = relative power intensity measured by gamma-flux monitors at five vertical locations (x) equally spaced along the fuel surface

Φ_i = 0 for convenience of notation

C_1 to C_5 = constants for fuel design, pressure, and velocity

ΔT = coolant temperature rise

For more information on control experience discussed at the same ANS meeting, see the article that begins on page 271.

References

1. E. P. Epler, Safety System Performance Failures, *Trans. Am. Nucl. Soc.*, 8(Suppl.): 49-50 (1965).
2. D. R. Edwards, Experience with Rod Drop Times at the UMRR, *Trans. Am. Nucl. Soc.*, 8(Suppl.): 53 (1965).
3. C. P. Ross, Performance of HWCTR Safety Systems, *Trans. Am. Nucl. Soc.*, 8(Suppl.): 50 (1965).
4. J. T. Pancoast, A Gravity Independent Reactor Control System, *Trans. Am. Nucl. Soc.*, 8(Suppl.): 51-53 (1965).
5. G. N. Hamilton, E. G. Taylor, and D. F. Hanlen, Design Considerations in Safety Analysis of Partial Moderator-Level Controlled Reactors, *Trans. Am. Nucl. Soc.*, 8(Suppl.): 49 (1965).
6. Irwin Bluestein, Neutron Measurements in High Gamma Backgrounds, *Trans. Am. Nucl. Soc.*, 8(Suppl.): 24 (1965).
7. L. A. Heinrich, Gadolinium Nitrate Injection as an Auxiliary Shutdown System for Savannah River Reactors, *Trans. Am. Nucl. Soc.*, 8(Suppl.): 58 (1965)..
8. K. L. Gimmy and F. R. Field, On-line Computer Assists Reactor Operation at Savannah River Plant, *Trans. Am. Nucl. Soc.*, 8(Suppl.) 53-54 (1965).
9. E. S. Occhipinti, P. E. Mix, J. S. Stutheit, and F. R. Field, Analogue Computer Simplifies Operation of Savannah River High Flux Charge, *Trans. Am. Nucl. Soc.*, 8(Suppl.): 54-55 (1965).

Section IV

Power Reactor Technology

Fluid and Thermal Technology

Highlights of the 8th National Heat Transfer Conference

By David Miller

Many papers of fundamental and applied interest for reactor technology were presented and discussed at the 8th National Heat Transfer Conference, Los Angeles, Aug. 9–11, 1965, which was jointly sponsored by the American Institute of Chemical Engineers and the American Society of Mechanical Engineers. Although many of the studies were sponsored by the U. S. Atomic Energy Commission (AEC) and have been published in project reports, most were being reported for the first time.

Topics discussed ranged from applications such as heat exchangers, packed beds, desalinization, and loss-of-coolant accidents in reactors to more fundamental studies of boiling and condensation, two-phase flow and pressure drop, and radiation and thermophysical properties.

Boiling and Two-Phase Flow

Boiling, two-phase flow, and stability received a major share of attention. In particular, studies of critical heat flux are of interest to reactor designers.[1–8]

Pertinent to the design of a greater than 600-psia forced-convection water-reactor system is a study in which the coolant entered cylindrical test sections of 0.1- and 0.2-in. inside diameters as a subcooled liquid and during certain tests left as superheated steam.[2] Emphasis was placed on the region with wall temperature higher than that corresponding to the critical heat flux where the surface temperature oscillations were not large; this region is often called the transition or par film-boiling region. Experiments covered pressure range 2420 to 3120 psia, mass fl of 0.5 to 2.5 × 10^6 lb/(hr)(sq ft), heat fluxe 0.1 to 0.65 × 10^6 Btu/(hr)(sq ft), and exit qua ties of 7 to 100%. These data were combi with other data[9] that extended down to 580 p to obtain the equation

$$\left(\frac{hD}{k}\right)_f = 0.0193\left(\frac{DG}{\mu}\right)_f^{0.80}\left(\frac{C_p\mu}{k}\right)_f^{1.23}\left(\frac{\rho_v}{\rho_b}\right)^{0.68}\left(\frac{\rho_v}{\rho_L}\right)^{0.068}$$

for flows of greater than or equal to 0.8 lb/(hr)(sq ft) over the range 580 to 3190 p for steam qualities as high as 100%. This co relation has a 2σ probability limit of ±1 Density was calculated with a void-fract weighted sum of the gas and liquid densities homogeneous model was used to calculate t void fraction. This study showed that the t phase entrance length and the length-to-diameter ratio have an important effect on heat transfer. Thermodynamic nonequilibrium found low flows [0.5 × 10^6 lb/(hr)(sq ft)] was attributed to unevaporated water droplets pass through the test section; low-flow-rate da were not included in the correlation. The ma mum heat-transfer coefficient after the cri heat flux occurred near or at 100% quality.

For a fog-cooled reactor concept, the "dr out" heat flux (a term used to describe critical or burnout heat flux at high ste qualities) was measured at mass velocities 0.5 to 1.4 × 10^6 lb/(hr)(sq ft) and outlet qualities in the 38 to 78% range.[3] For two-phase in conditions, dry-out behavior of geometries si ulating reactor fuels was investigated w (1) angular misalignment of 0 to 60° betwe an unheated bundle upstream of the 19.25-i long heated bundle, (2) two bundle end geom tries (CANDU-reactor type and flat-end), (3) bundle-mounted stripping rings intended emove the parasitic water film from the uneated flow tube and redistribute it to the eated rods. All experiments were for a 19-rod undle cooled by steam–water fog at 515 psia. ngular misalignment reduced the dry-out heat ux on some surfaces (usually inner elements) y as much as 20% but increased it on others ısually outer elements) by up to 70%. Stripping ings raised the dry-out heat flux by up to 100%.

The effects of upstream compressibility on ubcooled critical heat flux were investigated.[4] loderate upstream volumes of subcooled water ere shown to have sufficient compressibility o promote oscillatory behavior, which greatly educes the subcooled critical heat flux for a ingle channel. This oscillatory instability can e avoided only by operation to the right of the ninimum in the overall pressure drop–flow urve characteristic of the heated section. Jsually a flow restriction at the inlet of the ıeated section is needed to alter the overll characteristic so that stable critical heat luxes can be obtained.

Although inlet-fitting losses make some sysems inherently stable, it usually is necessary o provide another restriction at the heatedection inlet. The necessary throttling at the nlet can be estimated readily from

$$\frac{\partial(\Delta P)_{\mathrm{TS}}}{\partial w} = 0$$

where $(\Delta P)_{\mathrm{TS}}$ is the pressure drop across the est section in pounds per square inch] if the ıeated-section hydraulic characteristics are nown.

The influence of axially nonuniform heat luxes on the departure from nucleate boiling DNB) was studied.[7] Heat-flux distributions studied are shown in Fig. IV-1. For a limited ange of parameters, the results are given in he form of a correction factor

$$F = \frac{C}{q''_{\mathrm{DNB,local}} + 1 - \exp\left(-CL_{\mathrm{DNB}}\right)} \times \int_0^{L_{\mathrm{DNB}}} q''(z) \exp\left[-C(L_{\mathrm{DNB}} - z)_{dz}\right]$$

Here C is a coefficient defined as $h/\rho v s c_p$. Because the components of C are not known well enough to permit analytical evaluation, C was correlated by the equation

$$C = 0.44\ (1 - x_{\mathrm{DNB}})^{7.9}/(10^{-6}\,G)^{1.72}\ \mathrm{in.}^{-1}$$

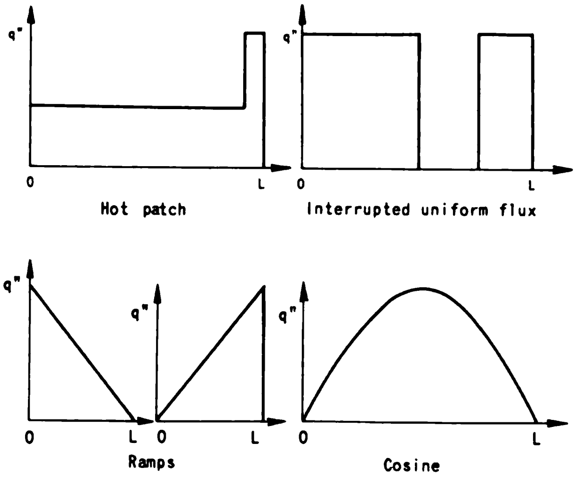

Fig. IV-1 Four shapes of heat-flux distributions were considered in studying how axially nonuniform heat fluxes influence the departure from nucleate boiling.[7]

Pool-boiling critical heat flux was studied by various investigators.[1,5,6,8] Saturated pool boiling on horizontal wire heaters of 0.0025 to 0.254-in. radii was measured[1] over a reduced-pressure (pressure divided by critical pressure) range of 0.0010 to 0.0197. The peak and minimum boiling heat fluxes were correlated with pressure and heater configuration (horizontal and vertical wires and flat horizontal plates) for five fluids: methanol, isopropanol, acetone, benzene, and water. All data can be represented by a single three-dimensional surface that is the product of a function of geometrical scale and a function of pressure. The function of pressure appears to be the same in any configuration. The effect of radius on critical heat flux for small wires at low pressures is significant and complex.

Experimental and analytical investigations of critical heat flux in pool boiling show that the addition of small amounts of calcium sulfate to distilled and deionized water allows increased boiling heat fluxes from stainless-steel heaters.[5] For a $\frac{1}{16}$-in. cylindrical stainless-steel heater coated with calcium sulfate, the critical heat flux was increased by 35%. Pool-boiling tests in water, with a porous graphite heater having air flow through its wall, decreased critical heat flux by 37% over the same heater with no air flow. If it is assumed that departure from nucleate to film boiling occurs when the heater surface becomes nonwetting at a temperature equal to the maximum possible superheat for the liquid, it is possible to postulate a critical-heat-flux equation for the special case of a small-diameter heater. Significant variation in the critical heat flux with heater properties is predicted by this equation, which contains several coefficients that must be determined experimentally.

When the effects of thermal conduction on the critical heat flux and pool boiling were measured,[6] the critical heat flux of propanol that was boiling at atmospheric pressure on heater strips mounted horizontally in a saturated pool was seen to increase by a factor of 2 as the element conductance parameter, *kt* (which is the thermal conductivity times "effective" thickness of heater), increased in the range of 4.5 to 1680 × 10^{-4} watts/°C. A proposed analytical model qualitatively predicts these trends but does not agree quantitatively with the experimental data. The authors conclude that the prime reason that thin heat-transfer elements have lower critical heat fluxes is lower conductance and not lower heat capacity.

Designers concerned with space power units, fast reactor safety, and advanced reactor technology will be interested in studies of the critical heat flux for boiling liquid-metal systems. Eighteen critical-heat-flux experimental data points were presented: two for sodium, eight for rubidium, and eight for water, all taken in the same apparatus. A correlation that represents 60 data points also includes data of other investigators for sodium and potassium; from it results the nondimensional equation

$$\left(\frac{q_c''C_p\sigma}{\lambda^2\rho_v k}\right) = 1.18 \times 10^{-8}\left(\frac{\rho_L}{\rho_v}\right)^{0.71}$$

where all values are at saturation conditions. This expression was modified by introducing the Prandtl number to the 0.71 power to include both metallic and nonmetallic data in a single dimensionless correlation

$$\left(\frac{q_c''C_p\sigma}{\lambda^2\rho_v k}\right)\mathrm{Pr}^{-0.71} = 1.02 \times 10^{-6}\left(\frac{\rho_L-\rho_v}{\rho_v}\right)^{0.65}$$

that is recommended for predicting the critical heat flux over a range of Prandtl numbers from 0.004 to 11; this correlation is shown in Fig. IV-2.

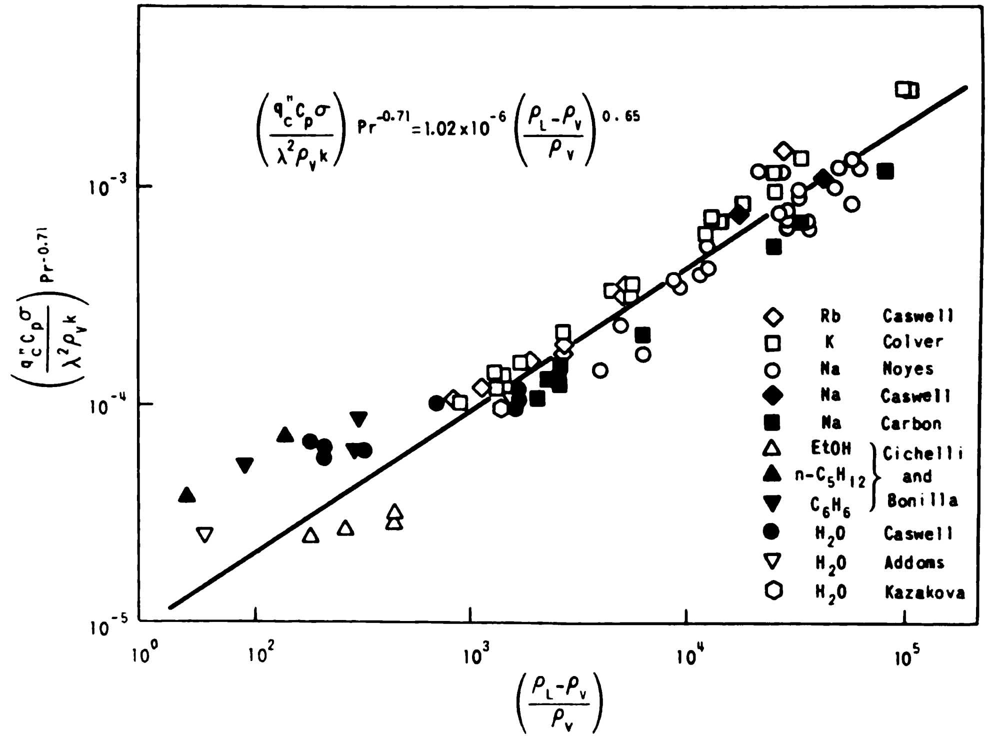

Fig. IV-2 Critical heat flux (q_c'') for various metallic and nonmetallic boiling fluids can be determined by means of a single dimensionless correlation.[8]

The boiling behavior of metallic liquids was lso investigated.[10-12] How boiler surfaces anging from highly polished mirror finishes to oarse, porous coatings affect nucleate pool oiling of sodium was studied.[12] Heat fluxes as igh as 236,000 Btu/(hr)(sq ft) were attained at ressures below 1 atm with sodium at 1200 to 500°F. The qualitative effects of roughness, ging, and hysteresis were determined. For eproducible data to be obtained, it was essenial to employ uniform cleaning and filling rocedures. Incipient nucleate-boiling heat flux s. wall superheat were discussed, as were the ffects of pressure and pool depth on the ucleate-boiling curve. The surface roughness nd past history were found to affect signiantly the incipient boiling, the nucleate-boiling all superheat, and the slope of the boiling urve of sodium. The wall superheat required initiate sodium nucleate boiling is signiantly greater (at least a factor of 5) than that equired to sustain it. Natural convection for a orizontal disk in pool boiling, particularly at ow boiling heat fluxes, may appreciably inuence sodium heat transfer. Clearly, nucleateoiling heat-transfer data cannot be correlated ithout including the effect of surface condions.

In a companion theoretical study of nucleateoiling instability for alkali metals, a simplified eoretical model for bubble nucleation stability as proposed and an approximate stability cririon was developed.[10] This criterion contains oth fluid and surface properties and predicts at nucleation for sodium should be unstable. easurements of the effects of surface mateal and its chemical treatment, heat flux and vity geometry on nucleation stability agreed ith theoretical predictions. The stability cririon developed from an analysis of the bubble cleation and dynamics is unique in that it inudes the thermal properties of the surface, e cavity geometry, and the wetting behavior the fluid. Inertial effects have been omitted. nly double reentrant type cavities appeared to effective in maintaining nucleation stability sodium. Thus an artificial nucleating site uch as a doubly reentrant type cavity, a patch porous plate or porous weld, or a "hot nger") might be used to maintain stability in kali-metal boilers.

A transient-quenching method of determining e critical heat flux and heat-transfer coeffients in film- and nucleate-boiling magnesium was presented.[11] A tungsten sphere, instrumented with thermocouples, was heated to 3100°R and then quenched in a boiling pool. As the sphere cools, its surface temperature and heat flux follow the boiling curve for the liquid metal being studied. Critical heat flux and heat-transfer coefficients in the transition- and nucleate-boiling regimes for subcooled (265°F) pool-boiling magnesium are included. Analytical predictions of the critical heat flux, however, were a factor of 5 to 10 higher. It was hypothesized that the low measured value of critical heat flux of magnesium was caused by the lack of wetting of the tungsten sphere by the magnesium during transition boiling.

Stability of Flow in Heated Channels

The interaction between hydrodynamics and heat transfer was studied analytically[13] and experimentally.[14] A very restrictive set of assumptions was applied in a theoretical calculation of the dynamic stability of flow oscillations in a heated channel.[13] The stability of this channel was investigated by applying the Hurwitz criterion after a perturbation solution of the usual equations. The resulting third-order characteristic equation shows that, under certain operating conditions, there exists both upper and lower stability bounds on the stability map. The analysis was applied to correlate experimental data of other investigators and to study the effects of various system parameters on system stability. The trends predicted agree with the limited range of experimental conditions (five points for two pressures by one investigator) for which the comparison was attempted.

Flow stability in multitube forced-convection vaporizers was investigated with a transparent closed test loop having Freon-113 as the test fluid.[14] Dimensionless simulation criteria were defined on the basis of the significant parameters determined from a literature survey. Conclusions and discussions are based on the measured data and high-speed photographs of two-phase flow in a five-tube boiler whose tubes had twisted-tape inserts. Stable flow was achieved by inserting an orifice at the entrance of each boiler tube to give pressure drops between 20 and 160% of the two-phase pressure drop. The importance of visual observations was stressed.

Theoretical Boiling Studies

Reactor designers will be interested in theoretical studies of boiling phenomena, including film boiling and bubble formation in nucleate boiling.

Film boiling was explored by several investigators.[15–18] The relation between bubble diameter and frequency of removal from a heated sphere during film boiling in saturated liquid nitrogen was studied,[15] as was the Leidenfrost phenomenon of film boiling of drops on a hot surface.[16–18] The vibrations and breakup of such a drop corresponded to those calculated from spherical-shell theory.[16] An analytical model for boiling heat transfer to waterdrops on a flat-plate-covered heat transfer to the waterdrop, heat transfer from the plate, and the heat-transfer coefficient for the special case where radiation can be neglected.[17] The effect of film boiling for large drops was measured experimentally and compared to theoretical analyses.[18] The maximum drop diameter and the minimum temperature difference for stable film boiling were predicted by stability considerations — similar methods have been suggested for nucleate boiling. These studies may be useful to estimate fuel-element cooling time after a reactor accident.

Bubble phenomena relevant to nucleate-boiling heat transfer were discussed.[19–21] The delay time, growth rate, contact diameter, and bubble size and shape at departure are interrelated.[19] A longer delay brings about faster growth, a larger contact diameter, and a bigger bubble at departure. Spherical bubbles have little or no delay time, slow growth, little contact area, and small size at departure; hemispherical bubbles have a long delay time, very fast growth, a large contact area, and a very large bubble volume at departure; oblate bubbles have intermediate values for all these factors.

Bubble shapes apparently can be explained in terms of inertial and surface-tension forces. For spherical bubbles, the surface-tension force is always greater than the inertial force, but for hemispherical bubbles the inertial force is dominant. For oblate bubbles, either can be dominant. Bubble departure diameters, departure velocities, and contact angles were measured by means of high-speed motion pictures of steady-state boiling.[20] A zirconium-ribbon heater insulated at its undersurface and edges was immersed in a pool of the liquid maintained at saturation temperature. Data for various liquids at subatmospheric pressure were represented by

$$D_d = 0.028\beta \left[\frac{g_c \sigma}{g(\rho_L - \rho_v)}\right]^{0.5} \left[1 + 0.0025 \left(\frac{dD}{dt}\right)^{1.}\right.$$

Mixtures are of interest for increasing boiling heat transfer and for determining the relative importance of thermal and diffusional resistances in the growth and formation of a bubble. Bubble growth rates were given for two mixtures.[21]

Condensation

Studies of condensation are of interest for the design of reactor equipment and, additionally, represent a phase change that is the inverse of boiling.

Laminar film condensation in two-phase channel flow was investigated in an analytical study that includes the interaction between the vapor and liquid interfaces and that proposes a dimensionless criterion for neglecting inertia and convection effects in the condensate film.[22] A relation was derived with the use of a universal velocity profile for predicting condensate-film heat-transfer coefficients for various surface-roughness heights.[23] Two regions were found — an upper limit corresponding to fully developed rough flow and a lower limit corresponding to hydraulically smooth flow. Some experimental data on the condensation of water gave results that fall between these two boundaries.

Film condensation of metal vapors has shown consistently lower heat-transfer coefficients than predicted from Nusselt's classical theory[24] or from more recent modifications of that theory. Kinetic-theory calculations to resolve this discrepancy between theory and experiment show that a significant thermal resistance can exist at the liquid–vapor interface of liquid metals.[25] This resistance increases with decreasing vapor pressure and depends on the value of an accommodation coefficient, namely the "condensation coefficient." Experiments to verify this liquid–vapor interfacial-resistance hypothesis used mercury condensing on a vertical nickel surface at low pressures in the bsence of noncondensable gases. Because the ondensation coefficient is a function of the tate of the liquid surface, it is probably inuenced by contamination in the experimental ystem and may vary with vapor pressure and emperature. Calculations for condensing metls at pressures significantly less than 1 atm hould include the condensation coefficient. In ractice, particular attention must also be aid to the presence of noncondensable gases in experiments and in operating equipment.

In certain cryogenic applications, heat exhange between condensing and boiling streams s limited by the condensing-side heat-transfer erformance. This occurs primarily at high heat fluxes because condensing coefficients decrease with increasing heat flux. The Nusselt equation for film type condensation on a horizontal tube suggests that the coefficient ncreases in a multi-*g* acceleration field. More mprovement would be expected if the resisance of the condensate layer to heat flow were reduced by a thin porous coating on the condensing surface. Results of condensation experiments in smooth and porous coated tubes under acceleration agree with the theory.[26] At he highest test acceleration of 325 *g*'s, the condensing coefficient improved by a factor of at least 4.25 over that for 1 *g* with the same emperature driving force. At heat fluxes greater than 10,000 Btu/(hr)(sq ft), experimental coefficients were better than theory predicted; this was attributed to rippling of the condensate film with consequent enhancement of the heat-transfer coefficient. At 325 *g*'s and with a heat flux of 20,000 Btu/(hr)(sq ft), condensation on a porous aluminum surface was 4.5 times better than on a smooth surface. Therefore the combined improvement over a smooth tube at 1 *g* was a factor of 19.1.

Experiments showed that radially grooved rotating disks reduced the condensing film resistance by some 65% but improved the rate of heat transfer through the disks by only 12 to 14%. In these experiments only a relatively small amount of the feed was evaporated, and thus most of the resistance to heat transfer was on the evaporating side.[27]

Dropwise condensation was discussed by Westwater in an invited lecture and in his papers,[28,29] which showed renewed interest in this method of improving condensing heat transfer. Dropwise condensation of water was shown to occur at active nucleation sites (and therefore should be termed nucleate condensation) whose number depends on the surface preparation and its subcooling.[28] The heat flux may be greater than, less than, or equal to that for filmwise condensation at the same temperature difference, depending on the active-site population. Exact calculation of the heat flux requires an involved iterative technique to account for the nucleation, growth, and coalescence of every drop. The functional relation between the temperature difference and active-site population is unknown for any surface. Oleic acid[29] promoted dropwise condensation of ethylene glycol on a copper condenser when the surface was cooler than 290°F. Correlation of data over a wide range of variables was achieved through modification of an Isachenko[30] equation to

$$\mathrm{Nu} = 1.46 \times 10^{-6}\,(\mathrm{Re}^*)^{-1.63}\Pi_k^{1.16}\,\mathrm{Pr}^{0.5}$$

where

$$\mathrm{Re}^* = k_L\,\Delta T/\mu_L\lambda \quad \Pi_k = 2g_c\sigma(d\sigma/dT)\,T_s\,/J\lambda\mu_L^2$$

and

$$\mathrm{Pr} = (C_p\,\mu/k)_L$$

This study also indicates there may be as many as 7 million active nucleation sites per square inch during dropwise condensation. A drop may experience an estimated 400,000 coalescences in reaching its final size. Thus the liquid-film fracture theory of dropwise condensation is rejected.

Two-Phase Pressure Drop

Reactor thermal and safety analyses frequently involved predictions of the properties of two-phase fluids. That interest in this subject continues strong was evidenced by seven papers.[31 – 37] Two-phase frictional pressure drop was correlated on the basis of data for mercury–nitrogen, water–air, and three sets of data for steam.[37] The ratio of two-phase to all-liquid pressure-drop gradient was expressed as

$$\Phi_{L_0}^2 = \frac{(\Delta P/\Delta L)_{\mathrm{TP}}}{(\Delta P/\Delta L)_{L}}$$

where the subscript 0 stands for total mass flow rate. The relation between this two-phase multiplier and the Lockhart–Martinelli[38] correlation

$$\Phi_L^2 = \frac{(\Delta P/\Delta L)_{\mathrm{TP}}}{(\Delta P/\Delta L)_L}$$

is given by

$$\Phi_{L_0}^2 = \Phi_L^2(1-x)^{1.8}$$

where x, the quality, is the ratio of gas (or vapor) mass flow rate to total flow rate, for both single- and two-component flow. The correlation consists in a plot of the two-phase multiplier as a function of the property index, $(\mu_L/\mu_g)^{0.2}/(\rho_L/\rho_g)$, with quality as a parameter for mass velocities from 0.25 to 3 × 10^6 lb/(hr)(sq ft). This correlation was based on 129 experimental points and the mass-flow-rate data of Sher and Green[39] for 2000-psia steam. The latter set of curves shows a rather unusual behavior and cannot be represented by any analytical expression.

Experimental pressure-drop and void-fraction data are compared with this correlation for water–air, kerosene–air, diesel oil–air, NaK–nitrogen, potassium (in a horizontal serpentine and an annulus with a helical tape), and steam. No effort was made to include the effect of changing flow patterns in the correlation. However, because the two-phase multiplier ratio may both increase and decrease at a given mass velocity and quality as the property index increases, this unusual aspect of the correlation may implicitly include the effects of flow-pattern changes. Application of the correlation to data on boiling potassium required the use of a previous correlation[40] to predict liquid fraction.

Bubbling mixtures in turbulent flow within a vertical plexiglass tube were used in an experiment that included analyses and separate measurements of frictional, hydrostatic, and momentum pressure drops.[35] Calculational procedures are suggested. The authors found the simplest correlation for bubbling-flow wall shear stress is obtained when a Reynolds number and friction factor are defined by use of the actual mixture velocity and density along with the liquid viscosity. The resulting friction factors are then approximately 10% above the Moody smooth-pipe friction factor. Momentum fluxes in bubbling flow were found to be not necessarily bounded by the homogeneous and separated flow models. The momentum fluxes were found to be better correlated by the separated model but would always be 5 to 25 larger than predicted by that model.

When the void fraction was less than 25 bubbles formed at the wall diffused only slowly toward the center, giving rise to slip ratios less than 1. This behavior is characterized as "developing flow"; however, the length required for fully developed flow is not known. Photographs helped define a map of the boundary between bubbly flow and unsteady exit flow on the coordinates of superficial liquid velocity vs. superficial gas velocity. For large volumetric flow concentrations, the void fraction approaches the slug-flow limit.

The transition from the slug-annular to two-phase flow was studied with an electrical-conductivity probe.[34] The purpose of this study was to identify the flow pattern for correlations of pressure drop and heat transfer. Simultaneous void measurements indicate that the transition occurs when the void fraction is between 80 and 90%. For superficial liquid velocities greater than about 1 ft/sec, the mass quality at transition is a constant that depends only on pressure. For low superficial liquid velocities, transition occurs at a superficial gas velocity that depends on pipe diameter. When the liquid flow is small, transition is unaffected by a reduction in liquid surface tension or the effects of liquid impurities. The liquid viscosity does not significantly affect the transition line.

During the discussion of this paper, it was mentioned that substantial subcooling eliminates slug flow to give transition directly from bubbly to annular flow. As an alternate to the electrical-conductivity probe, a study of the power spectral density of pressure fluctuations at the wall was suggested for determining the flow regime.

Void fractions in a developing two-phase flow system with flowing and nonflowing liquid phases were investigated for steam–water mixtures flowing vertically in a large unheated duct over a wide range of flow conditions.[36] The scope of the experiment covered superficial liquid velocities of 0 to 20 ft/sec and pressures of 60 to 1500 psig. A gamma attenuation system was used to measure chordal void fractions, which were integrated to give an average. Also, a manometer technique was evaluated for giving the average void fraction.

Void distributions obtained with the variable-ensity model of Bankoff[41] (this reference was ncorrectly cited in the paper) were compared ith those from the film–exponential model. he latter model assumes a thin film of liquid t the wall. The average void fractions were ompared with slip-ratio correlations of Marhaterre and Hoglund[42] and the kinematic-wave model of Zuber and Findlay.[43] In the discussion f this paper, the question of flow development was raised again. For an explanation of the lip ratios of less than 1, it is necessary to ssume that the vapor was near the wall where elocity is least. Experimentally it was found, owever, that there was liquid at the wall. It was also pointed out that equations for two-hase flow should include the dependence beween velocity and void profiles. Fluctuations n velocity and density give rise to terms imilar to the Reynolds stresses in turbulence heory.

The phase velocities in boiling flow systems are given by their relation for minimum voids n terms of phase densities and parameters related to the velocity distribution by use of a otal energy balance.[31] The correlating interval which is a function of the quality and the vapor- and liquid-phase viscosities and densities) was derived from diffusion theory. A simple relaion was obtained between quality, vapor fracion, and power input per unit flow volume in he test section. Qualitative predictions of void variation with heat flux and hydraulic diameter were said to agree with data from the literature. n the discussion of this paper, it was pointed out that application of minimization principles without rigorous justification could lead to serious errors. Kinetic-energy distribution facors dependent on velocity distributions were ntroduced in this model; they varied from 0.5 to 1, and the variation depended on whether the flow was laminar or fully turbulent. If the flow pattern in each of the phases cannot be specified, these constants may only serve to curve-fit the data.

Sudden contraction in two-phase flow in round pipes caused pressure drops that were measured and reported as functions of system pressure, flowing-mixture quality, contraction-area ratio, and mass velocity.[32] No void measurements were made, and water at saturation pressures of 200 to 500 psia was the only fluid studied. Pressure drop caused by the contraction was correlated in terms of a contraction coefficient that was independent of mass velocity over the range of conditions studied. The homogeneous model gave the best correlation of the data, but it was about 20% high, supposedly because of a large amount of mixing in the reexpansion after the vena contracta.

Two-phase heat transfer was simulated by the bubbling of air through the wall of a porous heated tube into water and into ethylene glycol flowing upward at room temperature and atmospheric pressure.[33] A simplified superposition type model based on microconvection, vapor–liquid exchange, and "convection-area-reduction" mechanisms was found to predict the trends of the air bubbling rate on heat transfer. Heat transfer increases over that of pure forced convection at low and moderate bubbling rates compared favorably with those caused by pool nucleate boiling when convective heat-transfer rates were relatively low. Photographs of pool boiling and air bubbling from identical tubes in a tank of Freon-11 showed qualitatively that bubble diameters and flow formations were similar in both processes. The result of this theory suggests that the enhancement in heat transfer and boiling could be considered as hydrodynamic in nature, thus making latent-heat transport unimportant as a heat-transfer mechanism.

Heat Exchangers

A lively commercial and technical interest in heat-exchanger design and operation is indicated by the large number of relevant papers that were presented.

Experimental heat-transfer coefficients were presented[44] for in-line, turbulent flow of NaK along the surface of an unbaffled bundle of nineteen ½-in.-diameter rods arranged on an equilateral triangular pattern with a pitch-to-diameter ratio of 1.75. The shell and all rods in the bundle were heated electrically to provide equal and uniform heat fluxes of 18,000 to 30,000 Btu/(hr)(sq ft) throughout the bundle. Tests covered conditions of fully established velocity and temperature profiles and also conditions where entrance effects were important. These results agreed with theoretical predictions and earlier similar experiments with mercury except at very low flow rates corresponding to Peclet numbers less than 500. It was hypothesized that the low heat-transfer coefficient ($\sim$10% below theory) was caused by gas collection and incomplete wetting at the heated surface.

An analytical study of the wall and fluid temperature field in a counterflow heat exchanger includes the effects of longitudinal conduction in the wall and unbalanced flow.[45] In addition to the general solution, balanced flow and insulated boundary conditions are considered. Longitudinal conduction in the wall separating the fluids distorts the temperature-distribution curves for both streams and produces a larger temperature difference at the ends; the minimum difference is at some point between the ends. With these exact solutions and the temperature-distribution plots, it is possible to determine how thermal performance is affected at low flow rates.

The effectiveness (the ratio of the enthalpy actually transferred to the maximum possible) and temperature difference of the unmixed fluid in "split cross-flow" heat exchangers were determined analytically.[46] Of particular interest is the "split–mixed crisscrossed–unmixed" heat exchanger, which provides the most uniform exit temperature distribution of the unmixed fluid among the simple-configuration cross-flow heat exchangers (Fig. IV-3). Effectiveness and temperature distribution are compared with conventional cross-flow heat exchangers. Heat exchangers with one shell pass and n tube passes, where n is an even number, are often referred to as 1-n exchangers. A generalized equation[47] has been derived for the effectiveness, ϵ, of 1-n exchangers in terms of the capacity-rate ratio, R, and number of transfer units, NTU. Values of ϵ at small intervals of R and NTU are tabulated for the 1-2 exchanger together with correction factors to give ϵ for each 1-n exchanger through $n = 12$. Deviations from 1-2 exchanger effectiveness increase with n and NTU. Thus, in addition to the significant effect that these deviations have on thermal stability and control of exchangers, the correction factor is particularly important in the design and selection of large heat exchangers whose purpose is the economic recovery of heat from a fluid. Because economic evaluations of such exchangers often involve the difference between two large numbers, the accuracy of the deviations and correction factors is an essential factor. The use of analog and digital computers to design plate type

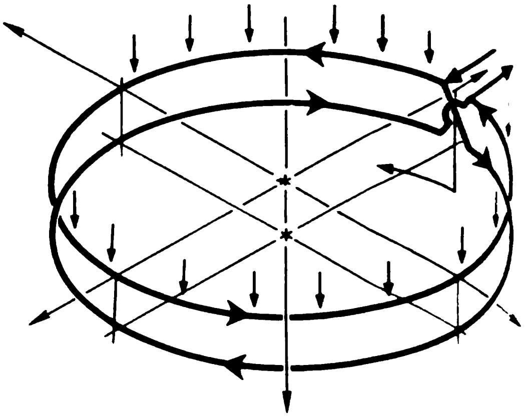

Split-mixed unmixed flow

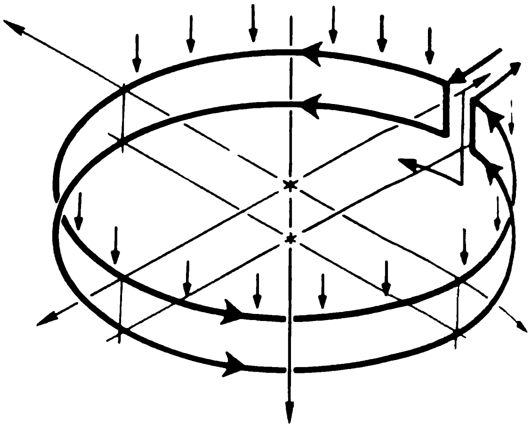

Split-mixed crisscrossed-unmixed flow

Fig. IV-3 Schematic of flows in split cross-flo exchangers within cylindrical envelopes.[46]

exchangers by the ϵ–NTU method was scribed.[48] The techniques were outlined detail, and some results were given.

Finned tube heat-exchanger design data procedures were given in seven papers. Pressure drop of air flowing across triangul pitch banks of finned tubes is correlated in t form of a friction factor as a function of Reynolds number and a pitch-to-diame ratio.[54] Measurements are reported of conve tive heat transfer and flow friction for pin–fin surfaces with square spacing of 3, and 4 times the fin diameter and with spacing of 4, 8, and 12 times the diamete Vibration was found to be important, and tense noise occurred at certain flow velo ties because of vortex shedding, which have been coupled with a natural frequen the heat exchanger. Vibrations increased friction factor but did not significantly af-

heat transfer. Natural frequencies of the
t exchangers may be either acoustical or
chanical. Free-convection heat transfer to
new type of extended surface covered with
vs of finned pins was studied.[51] With an
rage temperature excess of 200°F at the
ots of the pins, the rate of heat transfer from
h an extended surface was 475% higher
n that from the basic surface without the
ned pins.

The problem of optimizing finned geometry
maximize free-convection heat transfer in
at atmospheric pressure, taking into ac-
unt nonuniform fin temperatures, was in-
stigated[49] by introducing the fin effectiveness
o the Elenbaas[56] solution for uniform fin
nperature. This yields an optimum fin spac-
for the nonuniform case, together with
timum values for fin thickness and tube
ameter for a tube with square fins. A theo-
tical analysis of optimization of parabolic-
aped fins considers the combined effect of
nduction, radiation, and solar irradiation.[50]
e governing differential equation is reduced
an equivalent double-integral equation that
elds the relation between the finned geometry
d weight parameters. The resulting geometry
least mass is plotted as a function of the
mensionless irradiation parameter and the
ructure-to-weight ratio (total weight to the
ight of the fins).

A novel lightweight heat-rejection system for
por was reported.[55] It uses cooling fins made
plastic film to condense the vapor coolant
r a portable direct-conversion energy sys-
m. The plastic film can accommodate changes
heat input by changing shape or by partially
llapsing. The durability and long-term per-
rmance of finned tubes under steady-state
d thermal-cycling conditions were evaluated
means of tests on both extruded-fin tubes
d tension-wound-fin tubes (in each specimen
e fin and tube were of different metals).[53]
ngle-tube heat-transfer and strain-gauge tests
ere run both at the original contact pressures
d at the isothermal tube-wall temperatures
which the fin-to-tube contact was lost.

A dynamic analysis was made of a concentric-
be heat exchanger with a time-varying flow
s the forcing function.[57] The mathematical
odel agrees well with experiments for step,
quare wave, and sinusoidal changes in the
be flow rate. Errors introduced by linearization of the equations were investigated to determine the accuracy of the approximation.

Two novel heat-exchange devices were reported.[58,59] The Spiralator uses a rotating twisted tape to scrape the interior wall of tubes containing viscous or fouling liquids.[58] Small-diameter flexible-tube Teflon* heat exchangers offer high corrosion resistance, smooth slippery surface, tube flexibility, and inertness.[59] The favorable nucleation characteristics of Teflon for boiling and condensation and the fact that about 200 sq ft of surface area per cubic foot of shell volume can be built into a small tube exchanger stimulate interest in this new development. The higher thermal resistance of the Teflon wall can be offset by the lack of fouling for crystalline deposits and the versatility of its use.

Packed Beds

Relevant to some advanced reactor concepts are several papers on packed-bed heat transfer and pressure drop. Heat-transfer and pressure-loss characteristics of glass–ceramic matrices for regenerative heat exchangers were measured.[60] The steady-state axial temperature distributions in moving-bed fluid-to-particle heat exchange was determined analytically for a vertical duct of constant area in cocurrent and countercurrent flow.[61] If the regeneration principle is used, the distance over which the gas and solid temperatures are different and heat is transferred can be predicted. The small value of the effective length indicates that such a fluid-to-particle heat exchanger would be very compact. An analysis of unsteady-state heat transfer to a fluid flowing through porous heated solids provides solutions for both solid and fluid temperatures, some of which were verified experimentally.[62] Theory and experiments were reported for the heat-transfer and flow-friction characteristics of air-cooled matrices of high porosity that were heated by radiation which gives an exponential heat source.[63] A transient solution of simultaneous convection and radiation heat-transfer equations, when used with experimental data taken in the steady state, gave volumetric heat-transfer coefficients for convection only in the matrices. Correlations were obtained with

---

*Trademarked name for Du Pont fluorocarbon resin copolymer.

Reynolds numbers, based on a characteristic length obtained by equating pressure drop to the sum of viscous and inertial resistance terms. A related but more theoretical paper reported a study of the time-dependent temperature distribution for incompressible flow past a sphere.[64] A numerical solution of the diffusion equation showed that the temperature gradients at a spherical surface, as well as the time required to approach steady state, depend markedly on the value of the Peclet number.

Desalinization

The possibilities of the desalting of seawater as an auxiliary process while generating power in a dual-purpose nuclear plant have been receiving considerable attention from reactor designers. The interest in such technology is indicated by the six papers presented on this subject.[65-70] The thickness of a laminar liquid film draining from a vertical wall can be found analytically for the case of a constant evaporation rate from the surface of the film.[65] Transient as well as steady-state expressions are found that show the location where the film vanishes, the rate of evaporation, and the total mass evaporated.

The U. S. Department of the Interior's Plant No. 1 at Freeport, Tex., for desalting seawater by the falling-film distillation process was described thoroughly.[70] Reference 70 gives a description of the process, analysis of pilot-plant data and a report on evaporator performance. An alternate method of heat transfer in desalinization involves a multiphase exchanger that uses direct-contact heat transfer from a nonvolatile immiscible liquid to change the phase of a volatile fluid.[69] The initial diameter of pentane droplets evaporating within an immiscible water medium in a 3-phase (pentane, water, and pentane vapor) heat exchanger was found to affect the overall heat-transfer coefficients. The heat-transfer coefficient increased with a decrease in droplet size, and, apparently, surface tension and excess pressure from curvature are relevant parameters. Although scraped or wiped falling-film evaporators have been used industrially for some years, little has been published about their heat-transfer performance. An experimental study of evaporation at a scraped surface found that the Nusselt number was proportional to Reynolds number to the 0.25 power, to a ro Reynolds number to the 0.43 power, to t Prandtl number to the 0.33 power, and to t number of the blades to the 0.33 power.[68]

Deposits formed beneath bubbles during n cleate boiling of radioactive calcium sulf solution were found in detailed studies to related to heat transfer and the problem fouling of surfaces during evaporation of se water.[66] Calcium sulfate is of interest beca of its scale-forming ability. Studies of s deposits show that the bubble behavior is c sistent with the microlayer vaporization h pothesis proposed by Moore and Mesler.[71] T relative distribution of the deposits revea by autoradiographs indicates that there is m evaporation beneath the bubble (as was su gested by Moore and Mesler) than there is evaporation at the triple interfaces (as w proposed by Partridge and White).[72] A sec study of heat transfer and fouling rates dur pool boiling of calcium sulfate solution sh the deposition rate is proportional to the squ of the heat flux and nearly constant in time constant heat flux.[67] It follows that the depos tion rate is proportional to the concentrat driving-potential squared, as proposed by Mi yauchi.[73] Deposition of $CaSO_4$ on a surface nucleate boiling creates additional nuclea boiling sites, which raises the heat-transf coefficient during part of the operating time— although the eventual result of fouling is reduce heat transfer. Thin polyhydrocarb coatings retarded scaling by an order of mag nitude and increased the overall coefficient heat transfer during calcium sulfate deposit Polymerization fouling, which was also stud produces a temperature–time behavior co pletely different from that of crystalline foul and is not well understood. The heated surf temperature remained constant for a time t depended on the heat flux and polymer conc tration. It then increased 350 to 400°F wit 1 to 2 min and began oscillating with an amp tude of 40°F and a period of about 0.1 min.

Radiation

Interest in radiation heat transfer contin to grow because of the increase in design te peratures of reactor systems and because the importance of this mechanism for h sinks for space power plants.

A method was presented for calculation of diative exchange in enclosures whose surface flectance can be approximated by the sum of diffused and a specular component.[74] Heat insfer by simultaneous internal conduction d surface radiation in plates with specular flection was treated in terms of a nonlinear :egro-differential equation that was converted an integral equation and then solved numerilly.[75] Solutions have been obtained for a wide nge of conditions, including those for which :fuse reflection results are available. Reflecon and transmission intensities from gray abs were found by use of the powerful inriant embedding method that was developed r phenomena such as neutron transport.[76] ·oblems of simultaneous convection and raation in a laminar boundary layer on a flat ate were formulated and solved.[77] In these lutions it was assumed that the plate surface black and that the fluid medium is a perfect s for which the mass absorption coefficient r radiation is independent of frequency and mperature. The iterative solution includes e effect of viscous dissipation, secondary ıission and absorption, and incident external diative fluxes.

ıermophysical Properties

A novel use of heat-transfer techniques enıles the measurement of thermophysical propties at extremely high temperatures. The ermal conductivities of noble gases in the nge 1500 to 5000°K were determined by easurement of heat-transfer rates from heated ses to the end wall from a reflected shock ave.[78] Consideration of density variation in e thermal boundary layer was found to be gnificant in evaluation of the data; some preous investigations had neglected this effect. ıe thermal conductivity of hydrogen from)00 to 4700°F and 15 to 150 psia was deterined from the measured effective conductivity porous tungsten specimens filled with presırized hydrogen;[79] thermal conductivity as etermined by subtracting the solid conductivity ontribution compares within a factor of 2 with cisting experimental and theoretical work. eat transfer through porous ceramics in a ermally degraded ablation material was meaıred and tested against different theories.[80] the correct model is assumed, the apparent onductivity is the sum of the separate contributions of solid and gas conduction in radiation. The radiant portion of the conductance is proportional to the product of the mean temperature cubed times the average pore size.

Other Heat-Transfer Studies

Studies important to cryogenic heat transfer were described.[81,82] Heat transfer from laminar boundary layers was considered, with emphasis on large free-stream velocity gradients and highly cooled walls.[83] In experiments on how free convection affects laminar forced-flow heat transfer in a uniformly heated horizontal tube, the free-convection-flow component that caused secondary flow was observed as a decrease in the wall-to-bulk fluid temperature difference required to transfer heat as compared to the pure forced flow.[84] Local as well as average heat-transfer coefficients between an isothermal flat plate and impinging two-dimensional jets were measured for both single jets and arrays of jets.[85] Viscous and thermal boundary-layer behavior on the electrically insulating wall of a rectangular magnetohydrodynamic channel was analyzed theoretically by use of momentum and energy integral approximations.[86] Measurements of the way in which asymmetrical heating in a parallel-plate channel affects fully developed turbulent heat transfer show it to be qualitatively as predicted analytically.[87] An analysis of a thermal flowmeter includes the normally neglected effect of axial conduction along the tube.[88] Transient heat transfer between a thin circular tube and the incompressible fluid moving through it was analyzed for constant inlet fluid temperature;[89] both radial conduction in the wall and the heat loss at the outer surfaces of the cylinder were included. The effect of heat conduction on wall temperature was determined for a well casing passing vertically through a planar heat source of constant temperature.[90]

An approximate calculation was presented for natural-convection melting of an ice-water system.[91] Although an analytical study of transient heat transfer to a Bingham plastic (a material with a finite yield stress and linear stress–strain curve) in laminar flow in a circular tube with energy generated internally was given with a justification of its applicability to slurry reactors, experiments reported in the paper generally agree poorly with the theory, showing wall temperatures 30% lower to 100% higher than predicted plus a different transient response.[92] Equations were given for the temperature of moving solid materials undergoing heating or cooling.[93,94] The determination of the surface heat flux from the measured-temperature history inside a heat-conducting solid is called the inverse heat-conduction problem; this problem becomes nonlinear if the thermal properties depend on temperature and was solved by a finite-difference method.[95] A stable, explicit numerical solution of the conduction equation for multidimensional nonhomogeneous media was presented.[96] This method, which may be called an alternating-direction explicit procedure, takes less computational time than the alternating-direction implicit procedure and appears to combine the computational ease of the explicit methods with the stability of the implicit methods.

Evaporation rates from hot vertical flat plates, which are relevant to reactor safety analyses, were analyzed.[97] It was concluded that a correction factor accounting for the effect of transverse mass flux must be incorporated in the correlation expression for pure heat transfer. Also of potential importance to reactor safety is an experimental study of transient heat transfer to liquids in cylindrical enclosures.[98]

The thermal-control techniques and the thermal-design calculations for the Nimbus satellite were reviewed.[99] Movable insulation panels provide active temperature control of exterior surfaces. The analytical methods described agree with thermal model tests and actual space-flight data.

Loss-of-Coolant Accidents

One facet of heat transfer directly related to reactor safety and containment was discussed by a panel. Most of the discussion concerned the LOFT (Loss-of-Fluid Test) program that is part of the reactor safety program of the AEC. For this program a 50-Mw(t) pressurized-water reactor and test facility are being built in Idaho to learn how a reactor is affected by a sudden loss of coolant and the extent of any resulting radioactivity release. Phillips Petroleum Company is responsible for building and testing the LOFT blowdown facility; Kaiser Engineers, a Division of Henry J. Kaiser Co., is designing the LOFT facility.

R. P. Rose (of Phillips) described the proposed five-phase test program: (1) containment pressure and leak tests, (2) coolant blowdown tests with a dummy core, (3) low-power physics tests and power operation, (4) loss-of-coolant test, and (5) facility cleanup and posttest examination. Rose pointed out that the many unknowns associated with the blowdown program have suggested the need for a scale model to mock up the LOFT geometry before the full-scale tests. He discussed the scaling down of the LOFT physical dimensions for the proposed blowdown test facility, which would preserve the relative dimensions of the piping, vessel, and core rather than the time scale. As a result the metastable fluid behavior during blowdown may be affected because linear three-dimensional scaling involves shortening of the time scale.

J. S. Busch, W. D. Harrington, and S. F (of Kaiser) discussed analyses that gave the system boundary conditions for transient containment as well as for the primary-loop transients resulting from blowdown; generalized digital-computer programs and subsequent parametric analyses were used.

S. Esleak (of The Babcock & Wilcox Co.) discussed some of the more important problems pertaining to a loss-of-coolant accident: (1) two-phase critical flow, (2) two-phase pressure drop, (3) dynamic effect in the core, and (4) coolant expansion and degree of separation in the reactor vessel. The bases of his discussion are available in a recent state-of-the-art report.[100]

Specific phenomena pertaining to the loss-of-coolant accident were discussed by J. A. Redfield, P. J. Moody, and H. Fauske. Redfield (of Bettis Atomic Power Division, Westinghouse Electric Corp.) presented a simplified model for fuel-element heat transfer during a loss-of-coolant accident which has been applied to the Zircaloy-clad oxide-rod fuel elements for LOFT. He concluded that more data are needed for transient heat transfer under conditions of rapidly falling pressure, rapidly rising coolant quality, and highly unsteady flow conditions.

Moody (of General Electric Company) discussed an idealized model for estimating critical flow rates and pressure drops for given vessel conditions and flow break geometries. Although this ideal-nozzle model agreed well with one previous test (for the Humboldt B nuclear power plant), it clearly overpredicted another test (for the Bodega Bay plant). An extension of the energy model to include fr losses yielded fair agreement with the ent data of Fauske.[102]

auske (of Argonne) evaluated existing mod- for calculating maximum escape rates of ctor coolant. On the basis of recent mea- ements of voids at critical flow conditions, concluded that previously formulated models uske,[102] Levy,[103] and Moody[104]) are physi- lly incorrect and that their good predictions sulted from the high values of velocity ratios, ich compensated for metastability effects. new model was suggested, including both the ects of slip and metastability.

menclature

A = area, sq ft
C_p = heat capacity, Btu/(lb)(°F)
D = test-section diameter, ft
D_d = diameter of bubble at departure
g = local acceleration, ft/sec^2
g_c = gravitational conversion factor, 32.16 lb$_{\text{mass}}$-ft/sec^2/lb$_{\text{force}}$
G = mass velocity, lb/(hr)(sq ft)
h = heat-transfer coefficient, Btu/(hr)(sq ft)(°F)
J = mechanical equivalent of heat = 778 ft-lb/Btu
k = thermal conductivity, Btu/(hr)(ft)(°F)
L = length, ft
TU = number of transfer units = $AU_{\text{av.}}/(C_p w)_{\text{min.}}$
P = pressure, psi
q'' = heat flux, Btu/(hr)(sq ft)
q_c'' = critical heat flux, Btu/(hr)(sq ft)
R = capacity-rate ratio = $(C_p w)_{\text{hot fluid}}/(C_p w)_{\text{cold fluid}}$
s = liquid-layer thickness, ft
t = time, sec
t = effective thickness of heater, ft
T = temperature, °F
U = overall heat-transfer coefficient, Btu/(hr)(sq ft)(°F)
v = velocity, ft/sec
w = weight rate of flow, lb/hr
x = vapor weight fraction, lb vapor/lb fluid
z = distance from inception of local boiling, measured in the direction of flow, ft
β = contact angle, deg
ϵ = heat-exchanger effectiveness, heat transferred/maximum possible heat transfer
λ = latent heat, Btu/lb
μ = viscosity, lb/(ft)(hr)
ρ = density, lb/cu ft
σ = surface tension, Btu/sq ft = 778 × lb/ft
Φ = two-phase flow multiplier

ubscripts

$av.$ = average
b = bulk
c = critical
DNB = departure from nucleate boiling
f = film conditions
g = gas
L = liquid
S = saturation
TP = two-phase
v = vapor
max. = maximum
min. = minimum

References

Most of these papers were presented at the 8th National Heat Transfer Conference, Los Angeles, Calif., Aug. 9–11, 1965, sponsored jointly by the American Institute of Chemical Engineers and the American Society of Mechanical Engineers; they are marked with the initials of the appropriate society.

Individual papers are available from the two societies; some of the ASME papers will appear in the ASME Journal of Heat Transfer; but all the AIChE papers will appear in a volume in the Chemical Engineering Progress Symposium Series.

1. J. H. Leinhard and K. Watanabe, On Correlating the Peak and Minimum Boiling Heat Fluxes with Pressure and Heater Configuration. (ASME)
2. A. A. Bishop, R. O. Sandberg, and L. S. Tong, Forced Convection Heat Transfer at High Pressure After the Critical Heat Flux. (ASME)
3. E. O. Moeck, F. Stern, G. A. Wikhammer, and R. T. Dempster, Dryout in a 19-Rod Bundle Cooled by Steam/Water Fog at 515 psia. (ASME)
4. R. S. Daleas and A. E. Bergles, Effects of Upstream Compressibility on Subcooled Critical Heat Flux. (ASME)
5. W. J. Frea, G. S. Dzakowic, J. M. Hamelink, and W. S. Harjala, Some Experimental and Analytical Investigations on the Critical Heat Flux in Pool Boiling. (AIChE)
6. M. Carne and D. H. Charlesworth, Thermal Conduction Effects on the Critical Heat Flux in Pool Boiling. (AIChE)
7. L. S. Tong, H. B. Currin, P. S. Larsen, and O. G. Smith, Influence of Axially Non-Uniform Heat Flux on DNB. (AIChE)
8. B. F. Caswell and R. E. Balzhiser, The Critical Heat Flux for Boiling Liquid Metal Systems. (AIChE)
9. Z. L. Miropol'skii, Heat Transfer in Film Boiling of a Steam–Water Mixture in Steam-Generating Tubes, *Teploenerg.*, 10: 99 (1963) (in Russian). Also available as USAEC Report AEC-tr-6252.
10. P. J. Marto and W. M. Rohsenow, Nucleate Boiling Instability of Alkali Metals. (ASME)
11. J. M. Adams, An Investigation of Heat Transfer to Pool-Boiling Magnesium. (ASME)
12. P. J. Marto and W. M. Rohsenow, Effects of Surface Conditions on Nucleate Pool Boiling of Sodium. (ASME)
13. M. N. Ozisik and T. Cebeci, Dynamic Stability of Flow Oscillations in a Heated Channel. (ASME)
14. P. J. Berenson, An Experimental Investigation of Flow Stability in Multitube Forced-Convection Vaporizers. (ASME)
15. T. H. K. Frederking and D. J. Daniels, The Relation Between Bubble Diameter and Frequency of Removal from a Sphere During Film Boiling. (ASME)
16. G. J. Schoessow and K. J. Baumeister, Liquid Drop Model Vibrations and Simulated Fission. (AIChE)
17. K. J. Baumeister, T. D. Hamill, F. L. Schwartz, and G. J. Schoessow, Film Boiling Heat Transfer to Water Drops on a Flat Plate. (AIChE)
18. B. M. Patel and K. J. Bell, The Leidenfrost Phenomenon for Extended Liquid Masses. (AIChE)

19. M. A. Johnson, J. de la Peña, and R. B. Mesler, Bubble Shapes in Nucleate Boiling. (AIChE)
20. R. Cole and H. L. Shulman, Bubble Departure Diameters at Sub-Atmospheric Pressures. (AIChE)
21. J. M. Yatabe and J. W. Westwater, Bubble Growth Rates for Ethanol-Water and Ethanol-Isopropanol Mixtures. (AIChE)
22. G. J. Hordmann and Kwang-Tzu Yang, Laminar Film Condensation in Two-Phase Channel Flow. (ASME)
23. J. O. Medwell and A. A. Nicol, Surface Roughness Effects on Condensate Films. (ASME)
24. W. Nusselt, Die Oberflaschen Kondensation Des Wasserdampf, *Z. Ver. deut. Ing.*, 60: 541, 569 (1916).
25. S. P. Sukhatme and W. M. Rohsenow, Heat Transfer During Film Condensation of a Liquid Metal Vapor. (ASME)
26. D. W. Weiler, A. M. Czikk, and R. S. Paul, Condensation in Smooth and Porous Coated Tubes Under Multi-G Accelerations. (AIChE)
27. L. A. Bromley, R. F. Humphreys, and W. Murray, Condensation on and Evaporation from Radially Grooved Rotating Disks. (ASME)
28. J. L. McCormick and J. W. Westwater, Drop Dynamics and Heat Transfer During Dropwise Condensation of Water Vapor on a Horizontal Surface. (AIChE)
29. A. C. Peterson and J. W. Westwater, Dropwise Condensation of Ethylene Glycol. (AIChE)
30. V. P. Isachenko, Mechanism and Criteria Equations of Heat Transfer in the Condensation of Steam in Drops, *Teploenerg.*, 9: 81 (1962) (in Russian).
31. E. E. Polomik, Phase Velocities in Boiling Flow Systems by Total Energy and by Diffusion. (ASME)
32. G. E. Geiger and W. M. Rohrer, Sudden Contraction Losses in Two-Phase Flow. (ASME)
33. A. A. Kudirka, R. J. Grosh, and P. W. McFadden, Two Phase Heat Transfer in a Tube with Gas Injection from the Walls. (ASME)
34. R. E. Haberstroh and P. Griffith, The Slug-Annular Two-Phase Flow Regime Transition. (ASME)
35. S. C. Rose, Jr., and P. Griffith, Flow Properties of Bubbly Mixtures. (ASME)
36. K. F. Neusen, Void Fractions in a Developing Two-Phase Flow System with Flowing and Non-flowing Liquid Phase. (ASME)
37. C. J. Baroczy, A Systematic Correlation for Two-Phase Pressure Drop. (AIChE)
38. R. W. Lockhart and R. C. Martinelli, Proposed Correlation of Data for Isothermal Two-Phase, Two-Component Flow in Pipes, HART, *Chem. Eng. Progr.*, 45: 39 (1949).
39. N. C. Sher and S. J. Green, Boiling Pressure Drop in Thin Rectangular Channels, Chemical Engineering Progress Symposium Series, No. 23, p. 61, American Institute of Chemical Engineers, 1959.
40. C. J. Baroczy, Correlation of Liquid Fraction in Two-Phase Flow with Application to Liquid Metals, Chemical Engineering Progress Symposium Series, No. 57, p. 179, American Institute of Chemical Engineers, 1965.
41. S. Bankoff, A Variable Density Single-Fluid Model for Two-Phase Flow with Particular Reference to Steam Water Flow, *J. Heat Tra fer*, 82: 265 (1960).
42. J. F. Marchaterre and B. M. Hoglund, Corr tion for Two-Phase Flow, *Nucleonics*, 20 142 (August 1962).
43. N. Zuber and J. A. Findlay, The Effects Nonuniform Flow and Concentration Distr tions and the Effect of the Local Rela Velocity on the Average Volumetric Concen tion in Two-Phase Flow, USAEC Report GEA 4592 (EURAEC-1096), General Electric C pany, April 1964. [See also *J. Heat Trans* 87: 453 (1965).]
44. S. Kalish and O. E. Dwyer, Heat Transfer NaK Flowing In-Line Through a Bundle Circular Rods. (ASME)
45. C. L. Pan and N. E. Welch, Exact Analyt Wall and Fluid Temperature Field for a Counte flow Heat Exchanger with the Effect of Lo tudinal Heat Conduction. (ASME)
46. H. Kamei, Effectiveness and Temperature D tribution of Split Cross Flow Heat Exchange (ASME)
47. A. D. Kraus and D. Q. Kern, The effective of Heat Exchangers with One Shell Pass Even Numbers of Tube Passes. (ASME)
48. B. W. Jackson and R. A. Troupe, Plate He Exchanger Design by ϵ-NTU Method. (AIChE
49. D. R. Fairbanks and M. Mark, An Optimiza Procedure for Finning in Free Convect (ASME)
50. K. Kotan and O. A. Arnas, On the Optimiz of the Design Parameters of Parabolic Radia Fins. (ASME)
51. S. T. Hsu, B. C. Vatsaraj, and C. Hsieh, Extended Surface with Finned Pins Under Fr Convection Cooling. (ASME)
52. G. Theoclitus, Heat-Transfer and Flow-Frict Characteristics of Nine Pin-Fin Surface (ASME)
53. E. C. Smith, S. P. Victory, and A. Y. Gunte Evaluation of Fin Tube Performance Un Steady State and Thermal Cycling Conditio (ASME)
54. K. K. Robinson and D. E. Briggs, Pressu Drop of Air Flowing Across Triangular Banks of Finned Tubes. (AIChE)
55. W. R. Martini, A Light Weight Vapor-Fin He Rejection System. (AIChE)
56. W. Elenbaas, Heat Dissipation of Parallel Pl by Free Convection, *Physica*, 9: 1 (1942).
57. W. J. Privott and J. K. Ferrell, Dynamic Ana sis of a Flow-Forced, Concentric Tube He Exchanger. (AIChE)
58. W. R. Penney, The Spiralator—Initial Te and Correlations. (AIChE)
59. R. E. Githens, W. R. Minor, and V. J. Tom Small Diameter Flexible Tube Heat Exchange (AIChE)
60. F. J. Bayley and C. Rapley, Heat Transfer Pressure Loss Characteristics of Matrices Regenerative Heat Exchangers. (ASME)
61. L. E. Sissom and T. W. Jackson, Tempera Distribution of Solids and Fluid in Fluid Particle Heat Exchange. (ASME)
62. F. T Hung and R. G. Nevins, Unsteady-S Heat Transfer with a Flowing Fluid Throu Porous Solids. (ASME)
63. J. P. Chiou and M. M. El-Wakil, Heat Trans

and Flow Characteristics of Porous Matrices with Radiation as a Heat Source. (ASME)

64. M. Bentwich, G. Szwarcbaum, and S. Sideman, Time Dependent Temperature Distribution in Flow Past a Sphere. (ASME)
65. J. R. O'Loughlin, Evaporation from a Draining Liquid Film. (ASME)
66. N. B. Hospeti and R. B. Mesler, Deposits Formed Beneath Bubbles During Nucleate Boiling of Radioactive Calcium Sulfate Solutions. (AIChE)
67. J. W. Palen and J. W. Westwater, Heat Transfer and Fouling Rates During Pool Boiling of Calcium Sulphate Solutions. (AIChE)
68. T. R. Bott and M. R. Sheikh, Evaporation at a Scraped Surface. (AIChE)
69. S. Sideman, G. Hirsch, and Y. Gat, Direct Contact Heat Transfer with Change of Phase: Effect of the Initial Drop Size in 3-Phase Heat Exchangers. (AIChE)
70. D. I. Dykstra, Desalination of Sea Water by the Falling-Film Distillation Process. (AIChE)
71. F. D. Moore and R. B. Mesler, The Measurement of Rapid Surface Temperature Fluctuations During Nucleate Boiling of Water, *A.I.Ch.E. J.*, 7: 620 (1961).
72. E. P. Partridge and A. H. White, Mechanism of Scale Formation of Calcium Sulfate Boiler Scale, *Ind. Eng. Chem.*, 21: 835 (1929).
73. T. Miyauchi and T. Moriyama, Rate of Anhydrous $CaSO_4$ Scale Formation in Seawater Evaporators, *Kagaku Kogaku*, 25: 531 (1961) (in Japanese).
74. A. F. Sarofim and H. C. Hottel, Radiative Exchange Among Non-Lambert Surfaces. (ASME)
75. R. G. Hering, Radiative Heat Exchange Between Conducting Plates with Specular Reflection. (ASME)
76. J. O. Mingle, Reflection and Transmission Intensities from Gray Slabs Utilizing Invariant Imbedding Methods. (AIChE)
77. C. C. Oliver and P. W. McFadden, The Interaction of Radiation and Convection in the Laminar Boundary Layer. (ASME)
78. D. J. Collins and W. A. Menard, Measurement of the Thermal Conductivity of Noble Gases in the Temperature Range 1500 to 5000 Deg Kelvin. (ASME)
79. S. L. Israel, T. D. Hawkins, R. T. Salter, and S. C. Hyman, Thermal Conductivity of Hydrogen from 2000 to 4700°F. (AIChE)
80. C. M. Pyron, Jr., and C. D. Pears, The Mechanisms of Heat Transfer Through Porous Materials at Elevated Temperatures. (ASME)
81. R. F. Barron and L. S. Han, Heat and Mass Transfer to a Cryosurface in Free Convection. (ASME)
82. J. C. Burke and A. H. Rawdon, An Experimental Study of Heat Transfer to Two-Phase Film-Boiling Nitrogen. (ASME)
83. L. H. Back and A. B. Witte, Prediction of Heat Transfer from Laminar Boundary Layers, with Emphasis on Large Free-Stream Velocity Gradients and Highly Cooled Walls. (ASME)
84. S. T. McComas and E. R. G. Eckert, Combined Free and Forced Convection in a Horizontal Circular Tube. (ASME)
85. R. Gardon and J. C. Akfirat, Heat Transfer Characteristics of Impinging Two-Dimensional Air Jets. (ASME)
86. W. C. Moffatt, Approximate Solutions for Skin Friction and Heat Transfer in MHD Channel Flows. (ASME)
87. E. M. Sparrow, J. R. Lloyd, and C. W. Hixon, Experiments on Turbulent Heat Transfer in an Asymmetrically Heated Rectangular Duct. (ASME)
88. G. E. Zinsmeister and J. R. Dixon. Thermal Flowmeters: The Effect of Axial Conduction. (ASME)
89. N. Hayasi and K. Inouye, Transient Heat Transfer Through a Thin Circular Pipe Due to Unsteady Flow in the Pipe. (ASME)
90. P. J. Closmann, Effect of a Heat-Conducting Well Wall on Temperature Distribution in an Observation Well. (ASME)
91. Chi Tien and Yin-Chao Yen, An Approximate Solution of a Melting Problem with Natural Convection. (AIChE)
92. C. D. Henning and W. J. Yang, Transient Heat Transfer to Laminar Bingham-Plastic Flow in a Circular Tube with Internal Energy Generation. (AIChE)
93. J. A. Clumpner, Equations for Calculating the Temperature of Moving Solid Plates and Cylinders Undergoing Heating or Cooling. (AIChE)
94. L. E. Erickson, L. T. Fan, and L. C. Cha, The Cooling of a Moving Continuous Flat Sheet. (AIChE)
95. J. V. Beck and H. Wolf, The Nonlinear Inverse Heat Conduction Problem. (ASME)
96. S. R. Allada and D. Quon, A Stable, Explicit Numerical Solution of the Conduction Equation for Multi-Dimensional Non-Homogeneous Media. (AIChE)
97. F. S. Li and W. H. Gauvin, Evaporation from Vertical Flat Plates in High-Temperature Surroundings. (AIChE)
98. L. B. Evans and N. E. Stefany, An Experimental Study of Transient Heat Transfer to Liquids in Cylindrical Enclosures. (AIChE)
99. A. London, Heat Transfer as Applied to the Thermal Design of the Nimbus Control System. (AIChE)
100. C. E. Parks, Blowdown Models Applicable to the Loss-of-Fluid Test Facilities (LOFT), USAEC Report BAW-1195-4, The Babcock & Wilcox Co., June 1965.
101. S. G. Margolis and J. A. Redfield, Heat Transfer Aspects of the Loss of Coolant Accident, USAEC Report WAPD-T-1811 (CONF-650920-1), Westinghouse Electric Corp., Bettis Atomic Power Laboratory, August 1965.
102. H. Fauske, The Discharge of Saturated Water Through Tubes, Chemical Engineering Progress Symposium Series, No. 59, p. 210, American Institute of Chemical Engineers, 1964.
103. S. Levy, Prediction of Two-Phase Critical Flow Rate, *J. Heat Transfer*, 87: 53 (1965).
104. F. J. Moody, Maximum Flow Rate of a Single Component, Two-Phase Mixture, *J. Heat Transfer*, 87: 134 (1965).
105. M. R. El-Saden, Theory of Nonequilibrium Thermodynamics with Application to the Transport Processes in a Solid. (ASME)
106. G. S. Springer and R. Ratonyi, Heat Conduction from Circular Cylinders in Rarefied Gases. (ASME)
107. V. P. Tyagi, Laminar Forced Convection of a Dissipative Fluid in a Channel. (ASME)

108. B. F. Elam, Heat Transfer in Honeycomb-Core Sandwich Panels. (ASME)
109. J. V. Beck and A. M. Dhanak, Simultaneous Determinations of Thermal Conductivity and Specific Heat. (ASME)
110. W. R. Stubstad, Thermal Contact Resistance Between Thin Plates in Vacuum. (ASME)
111. W. R. Wilcox and R. L. Duty, Macroscopic Interface Shape During Solidification. (ASME)
112. K. C. Cheng, Analog Solution of Laminar Heat Transfer in Noncircular Ducts by Moire Method and Point-Matching. (ASME)
113. T W. Jackson and K. R. Purdy, Resonant Pulsating Flow and Convective Heat Transfer. (ASME)
114. J. M. Davies, Input Power Determined from Temperatures in Simulated Skin Protected Against Thermal Radiation. (ASME)
115. B. Koh and J. E. A. John, The Effect of Interfacial Metallic Foils on Thermal Contact Resistance. (ASME)
116. D. H. Elliott, Thermal Conduction Across Aluminum Bolted Joints. (ASME)
117. J. R. Larson and R. J. Schoenhals, Turbulent Free Convection in Near Critical Water. (ASME)
118. H. A. Blum and G. J. Moore, Transient Phenomena in Heat Transfer Across Surfaces in Contact. (ASME)
119. J. H. Van Sant and M. B. Larson, Convective Heat Transfer for Turbulent Flow in Subsonic Diffusers. (ASME)
120. L. Hoogenboom, Electrical Analog Model of Two-Dimensional Transient Heat Conduction. (ASME)
121. E. Talmor, Film Cooling of Small Diameter Throat Tubes. (AIChE)
122. D. Gidaspow and B. S. Baker, Heat Transfer in a Fuel Cell Battery. (AIChE)
123. D. A. Willoughby and T. J. Dwyer, Heat and Mass Transfer with an Exothermic Chemical Reaction in a Tubular, Laminar Flow Reactor. (AIChE)

Section V

Materials

Power Reactor Technology

ffect of Hydriding on Zircaloy Properties

y C. Roger Sutton

irconium-base alloys and austenitic stainless teels have been the preferred materials for he cladding of water-cooled power-reactor uel elements. In choosing between them, rector designers balance the lower cost and impler fabrication of the stainless steels gainst the better neutronic efficiency of the irconium alloys—thus the cladding for each eactor is selected on the basis of economic onsiderations. Today's economic conditions ften favor the use of Zircaloy. With the transiion to private ownership of fuel in the 1970's, here is expected to be a still clearer economic dvantage for zirconium alloys. Zircaloy-2, the eference zirconium-base alloy for the fuel ladding of water-cooled reactors for many ears, has very good corrosion resistance and sually adequate mechanical and physical proprties. Nevertheless, anything that changes the roperties of the cladding material can have a rofound effect on the life and economics of the uel.

Occurrence of Hydride

One factor affecting the life and properties f Zircaloy, and thus the economics of its use, s the formation of zirconium hydride. Investiations of failed Zircaloy-2 cladding on fuel ods has indicated that the presence of oriented irconium hydride caused brittle failure.[1,2] When the hydrides are oriented perpendicularly o the stress axis, both ductility and strength are decreased appreciably.[3] Preferential orintation of the zirconium hydride platelets can be caused by strains during fabrication[4] or by the application of stresses greater than some threshold intensity while the hydrides are precipitating.[3,5]

Sources of Hydride

Zirconium-base alloys usually contain little hydrogen (10 to 25 ppm) of the melting and fabrication procedures as a result. When the alloys are exposed in oxidizing aqueous media, additional hydrogen is generated continuously by the reaction

$$Zr + 2H_2O \rightarrow ZrO_2 + 4H$$

In a system that is not degassed continuously, some of this hydrogen diffuses into the zirconium alloy. Because the solubility[6] of hydrogen in zirconium is very limited (see Fig. V-1), a second phase ($ZrH_{1.53}$) precipitates, usually in the form of platelets. The amount, size, distribution, and orientation of this precipitated

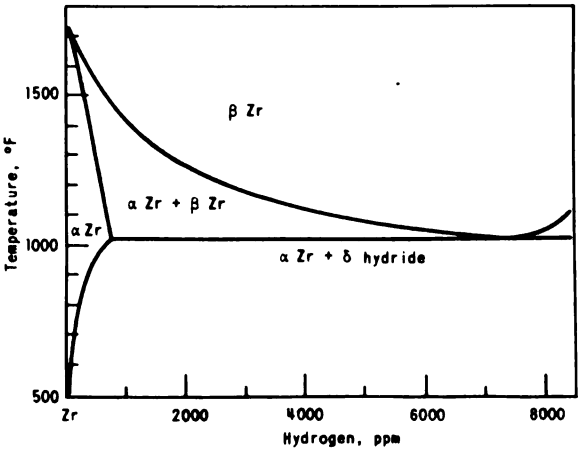

Fig. V-1 Zirconium—hydrogen phase diagram shows that solubility of hydrogen in zirconium increases with temperature up to about 1020°F, above which hydrides will not accumulate.[6]

phase may have a pronounced effect on the mechanical properties of the zirconium alloy.

Factors Affecting Hydrogen Uptake

Kirk[7] predicts that 30 to 50% of the available corrosion-product hydrogen will be absorbed by Zircaloy-2 and Zircaloy-4. Other data[8–10] indicate that 50% is probably the high side of the range and that absorption may be as low as 5%, depending on temperature, pressure, irradiation field, and other factors.

The dominant factors affecting the rate and amount of hydrogen uptake of available corrosion-product hydrogen are: zirconium-alloy composition, temperature, characteristics of the oxide film, radiation field, and coolant chemistry.

Alloy Composition. In discussing Zircaloy-2, nickel-free Zircaloy-2, and Zircaloy-4, Kass[11] states that hydrogen absorption is enhanced by the presence of nickel in the alloy. He reports that nickel-free Zircaloy-2 and Zircaloy-4 are superior to Zircaloy-2 in less than or equal to 680°F water because of their lower hydrogen pickup and decreased sensitivity to hydride failure but that above 750°F Zircaloy-2 has better oxidation resistance; beta quenching permits all three alloys to be used up to 850°F. Klepfer and Douglass[12] demonstrated that zirconium-base alloys containing copper and iron have less long-term hydrogen pickup than Zircaloy-2 (Table V-1). Greenberg and Youngdahl[9] report the combined effect of alloying and heat-treatment on hydrogen uptake (Table V-2); they conclude that hydrogen absorption in a particular alloy is primarily sensitive to exposure temperature and that a zirconium-base alloy containing 1.1% copper and 1.2% iron merits further study. Freer, Silvester, and Wanklyn[10] show the effect of 1% copper on hydrogen uptake at 932°F (Figs. V-2 and V-3). Weinstein and Holtz[13] determined the hydrogen pickup of various alloys in 680°F water and 750°F steam (Tables V-3 and V-4).

Temperature. Greenberg and Youngdahl[9] show (Table V-2) that hydrogen absorption by zirconium alloys after long exposure to steam is relatively insensitive to heat-treatment and composition of the alloys but very sensitive to temperature at least above about 1000°F. The percentage of corrosion-product hydrogen absorbed is much less at 1200°F than at 1000°F.

Table V-1 EFFECT OF TEMPERATURE ON LONG-TERM HYDRIDING OF THREE ZIRCONIUM ALLOYS*[12]

Alloy, at.%	Hydride rate, 10^{-2} mg/(dm^2)(day) At 750°F	At 930°F
Zircaloy-2	1.8	41.6
Zr–1 Nb–1 Cu–0.3 Fe	1.4	4.4
Zr–1.1 Cu–0.3 Fe	0.068	6.1

*In 1000-psi low-velocity flowing steam containing 20 ppm O_2 and 2.5 ppm H_2. Exposure time: rate data taken "posttransition," 1000 to 3000 hr. Specimens were fabricated from sponge by double consumable arc melting, forged and hot rolled at 1450°F, water quenched, 20% cold rolled, and alpha annealed 8 hr at 1050°F.

This result[6] is to be expected since zircon hydride is unstable at temperatures above abo 1020°F (see Fig. V-1).

Oxide Film. Gulbransen and Andrew[14] fo that oxide films may inhibit the gaseous driding of zirconium by factors of 1000 more. Smith[15] showed that the hydrogen pick rate is inversely proportional to the ZrO_2 fil thickness. Freer, Silvester, and Wanklyn[10] stu- ied hydrogen uptake during initial stages corrosion in superheated steam at 930°F. The suggest that reactions at the steam–oxide fil interface, rather than bulk oxide films, contr hydrogen entry into the alloy. Figure V-4 sho typical hydrogen uptakes[10] in steam at 932°F.

Irradiation. Exposure of zirconium allo to irradiation conditions in a reactor can eithe increase or decrease hydrogen pickup. By co- tributing to a slow but steady buildup of ox film on the surface of zirconium alloys means of radiolytically produced oxygen activation of the surface), radiation can reta hydrogen pickup. MacDonald and Parry[16] fo that the ZrO_2 film on alpha-annealed Zircalo fuel sheaths that had been irradiated 13,000 in less than or equal to 480°F pressuri water (the fuel was run at $\int_{T_1}^{T_2} k\, dT \leq 40$ watt cm until a burnup of 10,000 Mwd per metric of uranium was attained) was 2 to 3 μm thick than expected from out-of-reactor tests. Th caused hydrogen pickup to be considerably le (3 to 20%) than the 50% pickup predicted by of-reactor tests.

In general agreement with MacDonald Parry,[16] Burns and Maffei[17] state that a neutron exposure of 0.3 to 8.2×10^{20} neutr cm^2 increases greatly the average corros

Table V-2 HOW COMPOSITION AND HEAT-TREATMENT OF ZIRCONIUM ALLOYS AND THE TIME AND TEMPERATURE OF THEIR EXPOSURE TO SUPERHEATED STEAM AFFECT THEIR ABSORPTION OF CORROSION-PRODUCT HYDROGEN[9]

Alloy, wt.% heat-treatment*	Exposure to 600-psi steam: Temperature, °F	Exposure to 600-psi steam: Time, days	Weight gain, mg/cm²	H_2 concentration, ppm	Hydrogen absorbed, %
Zr−3 Ni−0.5 Fe (initially contained 20 ppm H_2)					
As cast	1000	35	0.8	80	93
As cast	1000	97	1.8	119	56
Zr−3.1 Ni−0.6 Fe (initially contained 22 ppm H_2)					
As hot rolled	1000	1	1.1	166	45
As hot rolled	1000	7	1.9	203	41
H, Q, A	1000	108	5.30	666	55
H, Q, A	1200	88	9.38	348	14
H, Q	1200	88	9.19	330	14
H, C, Q, C	1000	108	6.88	1451	61
H, C, Q, C, A	1000	108	7.51	1320	53
Zr−2.1 Ni−0.6 Fe (initially contained 16 ppm H_2)					
As hot rolled	1000	117	8.63	1208	67
H, Q, A	1000	108	6.58	875	62
H, C	1000	117	9.69	1518	63
H, C, Q, C	1000	108	7.68	868	40
H, C, Q, C, A	1000	108	7.22	940	43
Zr−1.1 Cu−0.7 Fe (initially contained 22 ppm H_2)					
H, Q, A	1000	108	9.81	980	46
H, C, Q, C	1000	108	10.8	1175	41
Zr−0.5 Cu−1.0 Fe (initially contained 18 ppm H_2)					
H, Q, A	1000	108	6.21	641	47
H, C, Q, C	1000	108	4.80	356	25
H, C, Q, A	1000	108	7.25	1080	62
Zr−1.1 Cu−1.2 Fe (initially contained 21 ppm H_2)					
As hot rolled	1000	1	0.60	30	7
As hot rolled	1000	7	1.20	38	8
H, Q, A	1000	108	6.90	716	44
H, Q, A	1200	88	8.53	131	5.5
H, Q	1200	88	8.30	90	3.6
H, C, Q	1000	108	6.71	583	32
H, C, Q, A	1000	108	7.42	932	49

*H = hot rolled; Q = quenched from 1650°F; A = aged for 1 hr at 1290°F, then air cooled in capsule; C = cold rolled with <20% reduction.

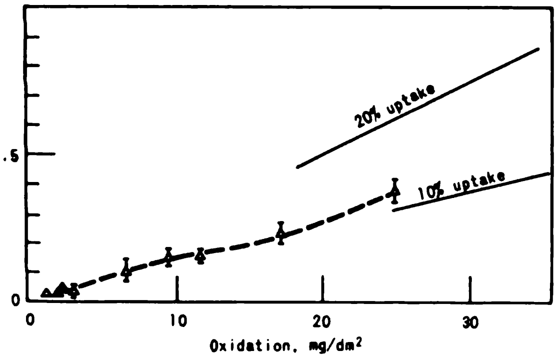

g. V-2 *Hydrogen uptake of crystal-bar zirconium*
932°F steam of atmospheric pressure.[10]

tes of Zircaloy-2 in 540°F water having pH =
, but that the fraction of corrosion–hydrogen
ckup remains in the low part of the range
rmally found in the absence of radiation.

They note that the corrosion proceeds at a nearly uniform rate above an as-yet-undetermined threshold flux rate.

On the other hand, under coolant flow and temperature conditions that erode the oxide film or encourage hydride pickup, the surface activation and hydrogen produced by irradiation can cause more total hydrogen to be picked up. Tobin[18] shows in Fig. V-5 that Zircaloy-2 at 540°F in a reactor loop picks up markedly more hydrogen than it does in an out-of-reactor loop at the same temperature; but he states that percentage uptake in the reactor is on the low side of the out-of-reactor results.

Water dissociates radiolytically. The amount and types of net steady-state dissociation products depend on at least two reactions: (1) a forward reaction that depends primarily on the intensity and type of radiation and (2) a back reaction that depends on temperature, the concentration of decomposition products, the type and intensity of radiation, the type and concentration of impurities in the water, and possibly on catalytic effects of materials in the immediate zone of dissociation.

In high-temperature pressurized-water reactors, the net dissociation is very low. It is probable that the only hydrogen available to react with the zirconium alloy is the small residual amount from reaction of equilibrium oxygen with metallic surfaces.

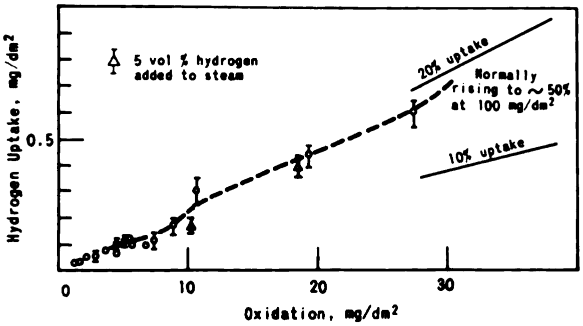

Fig. V-3 Hydrogen uptake of zirconium–1% copper alloy in 932°F steam of atmospheric pressure.[10]

Coolant Chemistry. **Dalgaard**[19] states zirconium–2.5% niobium alloys, with or wit 0.5% copper, are very sensitive to LiO water of *p*H = 10; he also reports that s concentrations of oxygen or oxidizing agents water or steam may depress hydrogen up significantly.

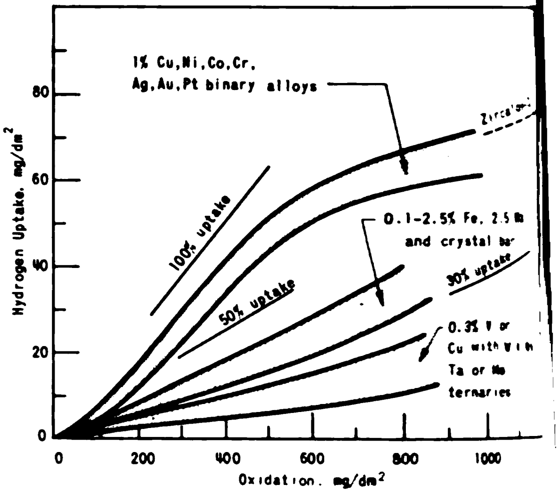

Fig. V-4 Hydrogen-uptake ranges of zirconium loys in 932°F steam.[10]

Table V-3 HYDROGEN PICKUP AND TENSILE STRENGTH OF ZIRCONIUM ALLOYS IN 680°F WATER FOR 200 DAYS[13]

Composition, wt.%	Hydrogen pickup			Ultimate tensile strength (at 680°F), psi
	Weight gain, mg/dm²	Total H_2, ppm	Pickup, %	
Zircaloy-2	68.47	183	46	27,800
Zr–1 Cr–0.25 Te	35.79	54	15	32,800
Zr–1 Sb–0.5 Nb	68.59	63	12	
Zr–1 Sb–0.25 Te	49.66	62	17	30,300
Zr–1 Sb–0.25 Ge	52.85	38	8	32,700
Zr–0.5 Sn–0.25 Ge	36.98	51	18	25,100
Zr–0.5 Sn–0.25 Te	42.84	55	18	30,200
Zr–0.5 Nb–0.25 Te	46.88	65	22	30,700

Table V-4 HYDROGEN PICKUP AND TENSILE STRENGTH OF ZIRCONIUM ALLOYS IN 750°F STEAM FOR 125 DAYS[13]

Composition, wt.%	Hydrogen pickup			Ultimate tensile strength (at 750°F), psi
	Weight gain, mg/dm²	Total H_2, ppm	Pickup, %	
Zircaloy-2	87.96	256	50	26,500
Zr–1 Fe–0.25 Cr	51.81	126	55	24,800
Zr–1 Fe–0.25 Te	68.84	204	71	22,300
Zr–1 Fe–0.5 Nb	88.60	212	58	30,200
Zr–1 V–1 Fe	72.00	163	50	31,800
Zr–3 Cr–1 Fe	65.43	158	50	30,000
Zr–3 Cr–0.25 Te	67.03	141	43	32,700
Zr–0.5 Nb–0.25 Cr	97.47	79	13	27,900
Zr–0.5 Nb–0.25 Te	66.95	94	30	27,200

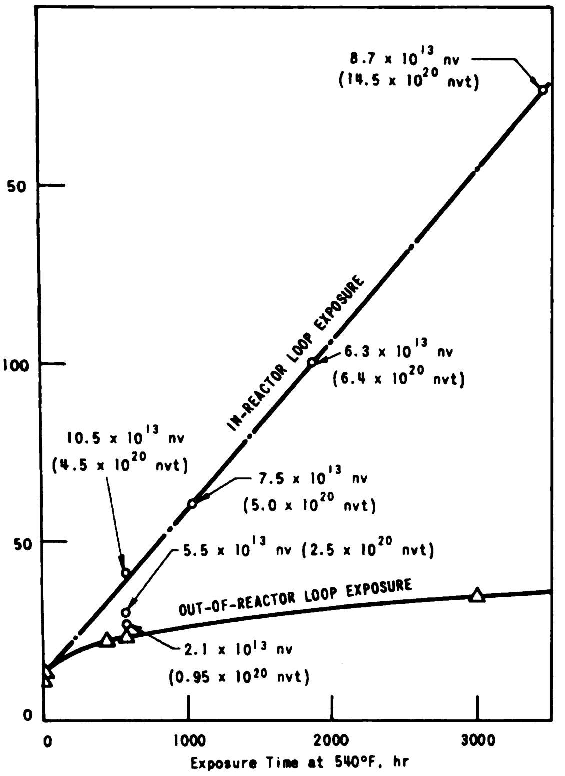

g. V-5 Much more total hydrogen is picked up by rcaloy-2 in a reactor loop with 540°F water than in out-of-reactor loop with same-temperature water.[18]

ow Hydrides Affect Properties

The major effect of adversely oriented hy-
ides is to decrease ductility,[20] but tensile
rength[20] and stress-rupture life[21] also might
reduced. From studies of the effect of irra-
ation on Zircaloy-2 containing 0 to 200 ppm
and zirconium–2.5% niobium containing 0
300 ppm H_2, Sawatzky[22] concludes that hydro-
n has little effect on tensile strength at 77 to
2 °F. He also found that hydrogen decreased
e ductility of both alloys, but the effect was
ss than that of irradiation to 10^{21} neutrons/cm^2
> 500 ev) at 536°F. Sawatzky also noted that
uterium and hydrogen have the same effect
the impact strength of Zircaloy-2 on an
om-for-atom basis.

By means of drop-weight tests on unirradi-
ed pressurized tubes, Farrow and Watkins[23]
und that 20%-cold-worked Zircaloy-2 contain-
g less than 100 ppm H_2 does not support crack
ropagation at room temperature, but that
ibes having 200 ppm H_2 exhibit crack propa-
ation below 250°F. Standard drop-weight tests on the same material indicated a ductile–brittle transition temperature of 230°F; Zircaloy-2 with as much as 800 ppm H_2 has a ductile–brittle transition temperature less than 445°F, which is well below the operating temperatures of power reactors.

Babyak, Bourgeois, and Salvaggio[8] show that increased hydrogen content causes little loss of necking strain in Zircaloy-2 at 500°F. They also note that beta-quenched Zircaloy-2 with uniformly distributed hydrides shows greater necking strain than material to which no hydrogen has been added. At room temperature the necking strain of alpha-annealed Zircaloy-2 containing 500 ppm H_2 is about half the initial (low hydrogen) value, regardless of morphology, but beta-quenched material with uniformly distributed hydrides shows little effect. Samples containing 200 to 300 ppm H_2 in the form of grain-boundary hydrides show a decrease to only 1 to 2% strain.

Causes and Control of Orientation

Data presented by Burton[24] and by Mehan and Wiesinger[25] indicate (1) little if any effect of hydrogen content (up to at least 500 ppm) on the tensile strength of annealed Zircaloy-2 from room temperature to 600°F and (2) no effect on ductility above about 300°F. But if the hydride is situated in the grain boundaries or, particularly, if the hydride platelets are preferentially oriented in a direction perpendicular to the stress direction, brittleness develops.[5]

Marshall and Louthan[3] also report that, like the effect prior strain has on hydride orientation, stress applied during hydride precipitation causes the hydride platelets to orient preferentially—and, when the treatment produces hydrides oriented perpendicularly to the stress axis, both strength and ductility decrease significantly.

Marshall and Louthan[3] also observe that unfavorable orientation can be corrected by applying stress (in a direction perpendicular to the platelets) during hydride precipitation (precipitation occurs when the material is cooled below the hydrogen solubility temperature or during the longer times while the alloy is absorbing more than a soluble amount of hydrogen); the amount of stress needed depends on fabrication history. Although Louthan and Marshall[5] found that for highly susceptible material the minimum transverse stress to change hydride orientation may be as low as 6000 psi, Wootton[20] shows that a stress of 16,000 psi appears to be somewhat below that required. But both investigators agreed that hydrides oriented parallel to the applied stress are unaffected by as much as 16,000 psi. Parry and Evans[4] found that the hydride precipitated parallel to the direction in which grains are deformed and that a minimum strain of 7% is required to produce directionality.

Significance

From the data described it can be concluded that reactor designers can avoid or alleviate the problems of hydride-induced brittleness and loss of strength in Zircaloy: (1) by selecting alloys and the surface films and water conditions that reduce hydrogen absorption, (2) by choosing operating temperatures that prevent hydride formation or accumulation, and (3) by designing components and specifying fabricating methods that cause any hydride platelets that do form to precipitate either in random orientation or parallel to the principal operational stress.

Slow Hydrogen Absorption. Much effort is being exerted to learn techniques to reduce the rate by which corrosion-induced hydrogen is absorbed by zirconium alloys. The fact that many reactor cores of pressurized- and boiling-water reactors have performed satisfactorily with Zircaloy-2 at about 600°F or less is prima facie evidence that either the reaction rate

$$Zr + 2H_2O \rightarrow ZrO_2 + 4H$$

is very slow below this temperature or that the diffusion rate of hydrogen through the existing oxide film is very low, or both. Above 600°F the amount of hydrides formed is, in many instances, sufficient to cause concern. The removal of nickel from Zircaloy-2 and other slight modifications has resulted in an alloy designated as Zircaloy-4. It is slightly less corrosion resistant than Zircaloy-2, but it is substantially less susceptible to hydriding. Although other alloys, notably zirconium–2.5% niobium, have been proposed, they have not yet been specified for a reactor core.

As noted by Burns and Maffei[17] and by MacDonald and Parry,[16] neutron irradiation lowers the percentage uptake of hydrogen, thus tending to offset any increased concentration of hydrogen in the coolant resulting from possible increased in-reactor oxidation rate of the zirconium alloy. Tobin[18] showed higher total hydrogen uptake under irradiation owing to increased corrosion rates but stated that the percentage uptake is on the low side of the out-of-reactor results.

Prevent Hydride Formation. Designers can select alloys and operating temperatures such that the solid solubility limit of hydrogen is not exceeded (so that zirconium hydride will not form and precipitate). In the intermediate-temperature range of interest for reactor application, moderate hydrogen pickup may not be deleterious because the solubility of hydrogen increases with temperature. For example, Fig. V-1 shows that, at 750°F, up to about 250 ppm H_2 can be accommodated without hydride formation; at 1000°F about 800 ppm can be tolerated. The designer can take advantage of this phenomenon if the operational conditions maintain the zirconium alloy above the temperature corresponding to the predicted hydrogen saturation level.

If the zirconium-alloy component operates at a temperature above that at which the zirconium hydride phase becomes unstable (~1020°F; see Fig. V-1), the hydride will accumulate slowly, if at all. This is supported by Greenberg and Youngdahl,[9] who report only a 5.5% uptake of corrosion-product hydrogen at 1200°F in out-of-reactor tests. However, the relief from hydride problems above about 1020°F is usually only of academic comfort because of oxygen embrittlement and loss of strength at such temperatures.

Random or Parallel Orientation. The orientation of the precipitated zirconium hydride phase in either a completely random fashion or in preferred orientations related to the operational stress is the factor that most readily lends itself to control by the designer. Although the presence of hydrogen, per se, in zirconium alloys has little effect on the metal properties, there is a pronounced deleterious effect if zirconium hydride precipitates as platelets either in the grain boundaries or preferentially oriented perpendicular to the principal stress. This behavior corresponds in many ways to the ductile–brittle transition in steel.

In fully alpha-annealed or beta-quenched zirconium alloys, the hydrides present at the

nealing or quenching temperature tend to
ecipitate randomly. However, slow cooling
ɔm these temperatures tends to cause the
dride platelets to accumulate in the grain
undaries, thus resulting in brittleness. If the
etal is free of stress, corrosion-product
drogen will form randomly oriented hydrides.
ɔwever, when the metal is in a stressed con-
tion, the hydrides precipitate preferentially in
orientation perpendicular to tensile stresses
ıd parallel to compressive stresses; in fact,
e preferential orientation can be changed by
versing the stress direction in service.[5]
ence it is important that the designer specify
oduction and fabrication methods that yield
ɔtimum orientation of the hydride platelets.
e also should design Zircaloy reactor in-
rnals in a manner that ensures platelet orien-
tion parallel to the principal stress axis
ıring operation.

eferences

.. A. S. Bain, G. M. Allison, L. M. Howe, and A. Ridal, Failure of Swaged UO_2 and Co-extruded U_3Si Specimens Irradiated in X-2 Loop (Test X-2-q), Canadian Report CRMet-904, Appendix III, 1959.

:. G. R. Caskey, Jr., G. R. Cole, and W. G. Holmes, Failures of UO_2 Fuel Tubes by Internal Hydriding of Zircaloy-2 Sheaths, in Proceedings of the Symposium on Powder Packed Uranium Dioxide Fuel Elements, Windsor, Conn., 1961, USAEC Report CEND-153, Vol. II, pp. 77-101.

ı. R. P. Marshall and M. R. Louthan, Jr., Tensile Properties of Zircaloy with Oriented Hydrides, *Trans. Am. Soc. Metals*, 56: 693 (1963).

ı. G. W. Parry and W. Evans, The Effect of Strain on the Directional Precipitation of Zirconium Hydride in Zircaloy-2, Canadian Report CRGM-1135 (AECL-1707), December 1962.

ɔ. M. R. Louthan, Jr., and R. P. Marshall, Control of Hydride Orientation in Zircaloy, *J. Nucl. Mater.*, 9(2): 170-184 (1963).

ɔ. D. H. Stone, Some High Temperature Mechanical Properties of Zircaloy-2, Type 304 Stainless Steel, and AM-350 Stainless Steel, USAEC Report NAA-SR-11047, Atomics International, June 15, 1965.

7. W. W. Kirk, Corrosion and Hydrogen Pickup of Zircaloy-2 and Zircaloy-4, in Zirconium Highlights, USAEC Report WAPD-ZH-21, pp. 8-14, Bettis Atomic Power Laboratory, Westinghouse Electric Corp., December 1959.

3. W. J. Babyak, W. F. Bourgeois, and G. J. Salvaggio, Effect of Hydride Morphology on the Tensile Properties of Zircaloy-2, in *Corrosion of Zirconium Alloys*, American Society for Testing and Materials, Special Technical Publication No. 368, pp. 76-100, 1964.

9. S. Greenberg and C. A. Youngdahl, Superheated Steam Corrosion of Zirconium Alloys Containing Small Amounts of Iron and Copper or Nickel, *Corrosion*, 21(4): 113-124 (April 1965).

10. D. W. Freer, D. R. Silvester, and J. N. Wanklyn, Hydrogen Uptake of Zirconium and Its Alloys During Early Stages of Corrosion in Steam, *Corrosion*, 21(4): 137-142 (April 1965).

11. Stanley Kass, The Development of the Zircaloys, in *Corrosion of Zirconium Alloys*, American Society for Testing and Materials, Special Technical Publication No. 368, pp. 3-27, 1964.

12. H. H. Klepfer and D. L. Douglass, The Factors Limiting the Utilization of Zirconium Alloys in Superheated Steam, in *Corrosion of Zirconium Alloys*, American Society for Testing and Materials, Special Technical Publication No. 368, pp. 118-142, 1964.

13. D. Weinstein and F. C. Holtz, Development of Improved Zirconium Alloys for Use in Superheated Water and Steam, USAEC Report GEAP-4089, Vol. 1, Paper 6, General Electric Company, Vallecitos Atomic Laboratory, Nov. 30, 1962.

14. E. A. Gulbransen and K. F. Andrew, Diffusion of Hydrogen and Deuterium in High Purity Zirconium, *J. Electrochem. Soc.*, 101: 560-566 (1954).

15. T. Smith, Hydrogen Permeation of Films on Zirconium, USAEC Report NAA-SR-6267, Atomics International, May 15, 1962.

16. R. D. MacDonald and G. W. Parry, Zircaloy-2 Clad UO_2 Fuel Elements Irradiated to a Burnup of 1000 MWd/Tonne U, Canadian Report CRFD-1178 (AECL-1952), January 1964.

17. W. A. Burns and H. P. Maffei, Neutron Irradiation and Cold Work Effects on Zircaloy-2 Corrosion and Hydrogen Pickup, in *Corrosion of Zirconium Alloys*, American Society for Testing and Materials, Special Technical Publication No. 368, pp. 101-117, 1964.

18. J. C. Tobin, Progress on the Irradiation Damage to Reactor Metals Program. A Summary of Hanford Laboratories Achievements in This Program under General Electric Company Management, 1962–1964, USAEC Report HW-83615, p. 28, Hanford Atomic Products Operation, Dec. 15, 1964.

19. S. B. Dalgaard, Factors Affecting Oxidation and Hydriding of Zirconium Alloys, *Trans. Am. Nucl. Soc.*, 6(2): 370 (November 1963).

20. G. C. Wootton, The Effect of Oriented Hydride on the Mechanical Properties of Zircaloy-2 Tubing, Canadian Report AECL-1989, March 1964.

21. R. C. Aungst, Stress Rupture Tests of Zircaloy-2 Pressure Tubes, USAEC Report BNWL-8, Battelle–Northwest, January 1965.

22. A. Sawatzky, The Effect of Neutron Irradiation on the Mechanical Properties of Hydrided Zirconium Alloys, Canadian Report AECL-1986, June 1964.

23. M. Farrow and B. Watkins, The Effect of Hydrogen on the Embrittlement of Zirconium-base Pressure Tubes, British Report TRG-Report-774, Apr. 23, 1964.

24. H. H. Burton, Hydrogen Effects of Zircaloy-2 Tensile Properties, USAEC Report HW-61077, Hanford Atomic Products Operation, July 10, 1959.

25. R. L. Mehan and F. W. Wiesinger, Mechanical Properties of Zircaloy-2, USAEC Report KAPL-2110, Knolls Atomic Power Laboratory, Feb. 1, 1961.

Section

VI

Power Reactor Technology

Fuel Elements

Letters to the Editor

Boiling-Water Environment Not Necessarily Detrimental to Stainless-Steel Cladding

In the letter by R. J. Allio in *Power Reactor Technology*, 8(2), the successful application of stainless-steel cladding in pressurized-water reactors (PWR) is contrasted with the experience with s cladding reported from the Vallecitos Boiling Water Reactor (VBWR).[1] It is the purpose of communication to review the statements in the reference letter concerning the differences between PWR and BWR cladding behavior and, further, to examine in some detail why the VBWR data *not* applicable to BWR's in general.

1. *System Pressure*

"Higher pressure prevents or delays development of tensile stress." The 12,000-psi compressive stress corresponds to an incremental strain of approximately 5 × 10^{-4} in./in., which with fueled rods corresponds to an increase in allowable burnup of about 250 Mwd per metric ton uranium. Since the PWR fuels cited exceeded the VBWR burnups by factors of 2 and 3, clearly increased compression on the cladding due to the higher pressure cannot explain the different behavior.

"Crack propagation cannot normally occur in the absence of a tensile stress." Both tensile and compressive stresses lead to failure via cracking in *cold-worked* austenitic stainless s even in oxygen- and chloride-free water.[2]

2. *System Chemistry*

"High oxygen concentrations have been shown in laboratory experiments to accelerate stress corrosion." This statement is erroneous unless qualified by the statement "in the liquid phase in the presence of chloride ion."[3] The concentration of oxygen in the vapor phase in BWR's is material to this discussion and, depending upon the residence time of the coolant in the core, reactor power density, system pressure, etc., can be an order of magnitude smaller than the 20 to ppm cited. However, oxygen does not always act in a detrimental manner; some metals, including the austenitic stainless steels, form a highly impervious oxide film that provides resistance further attack,[4] and oxygen has been employed to passivate steels in high-temperature water.[5]

3. *Corrosion-Product Deposition*

System chemistry and corrosion-product deposition are inseparable aspects of intermesh phenomena and system design philosophy and criteria. Hence such an arbitrary separation is inappropriate to a technical discussion. The evidence indicates that corrosion-product deposition stainless-steel claddings in both PWR's and BWR's has been negligible[6] and that only after relaxation of water purification specifications did the VBWR exceed negligible deposition.[7] Only Experimental Boiling Water Reactor (EBWR)[8] was scaling of fuel elements appreciable, and was due to aluminum oxide formed in the core from the aluminum–nickel alloy dummy fuel elements.

One could argue that the dynamic action of nucleate-boiling bubble formation, at the fuel-element surface in BWR's, should "scour" the surface free of "crud"; therefore the "crud bursts" and short-term high-coolant impurity levels encountered in PWR's after thermal shocks should occur in a BWR.

4. *Local Thermal Stresses*

The thermal fluctuations cited in the reference letter are based on measurements made under conditions (1) of atmospheric pool boiling, (2) of very low heat flux — to permit the study of individual bubble histories, and (3) of specially prepared poorly nucleating surfaces — again to study the life cycles of individual bubbles. The effect of pressure on boiling superheat (wall temperature minus saturation temperature) results in a decrease in required superheat, at equal heat fluxes, of factors of 3 for subcooled boiling,[9] and of 3.7 for bulk boiling;[10] thus the maximum magnitude of these fluctuations falls from the 30°F claimed to 8 to 10°F at 1000 psia. The effect of increasing heat flux at atmospheric pressure, according to the Eindhoven research,[11] is to decrease the amplitude and increase the frequency of thermal fluctuations; therefore higher heat fluxes cause damping even at low pressure where the driving force is large. Fuel-element surfaces are characteristically "rough" by laboratory standards, providing numerous, randomly spaced and random-sized nucleating sites (the "small surface crevices or pits" of the reference letter as well as grain boundaries, discontinuities in the oxide layer, etc.). With numerous nucleating sites scattered randomly over a surface, the surface temperature in a representative region will be the result of summing the thermal fluctuations from the surrounding bubble generating sites, each of which is randomly producing bubbles at various stages in their life cycles. Thus "real" surfaces tend to damp both the severity (amplitude) and frequency of thermal fluctuations.

In addition to these basic arguments, the measurements cited are inapplicable because they ignore the effect of coolant velocity on the bubbling layer adjacent to the heated surface. The large increase in frictional pressure drop with nucleate boiling is graphic evidence of increased shear in the bubble layer. A recent study[12] confirms that bubbles migrate on the heated surface under the influence of coolant velocity. Therefore, during the life cycle of a bubble, it may not remain at the nucleation site, and that site, therefore, cannot experience the full thermal fluctuation proposed in the reference letter.

VBWR Data Not Applicable to BWR's in General

We have discussed the points raised and have shown that the arguments against BWR's are questionable. It is appropriate, however, to examine why the VBWR fuel elements did fail and to show that the VBWR experience is atypical of BWR practice. The behavior of stainless steels in water-cooled nuclear reactor environments has been extensively studied. The results obtained to date may be conveniently summarized graphically[13] as shown in Fig. VI-1. Two regions may be defined: that below an exposure of approximately 10^{21} neutrons/cm^2 and that beyond this level. In the first region the effects of water chemistry (corrosiveness of coolant), degree of cold-work initially imposed on

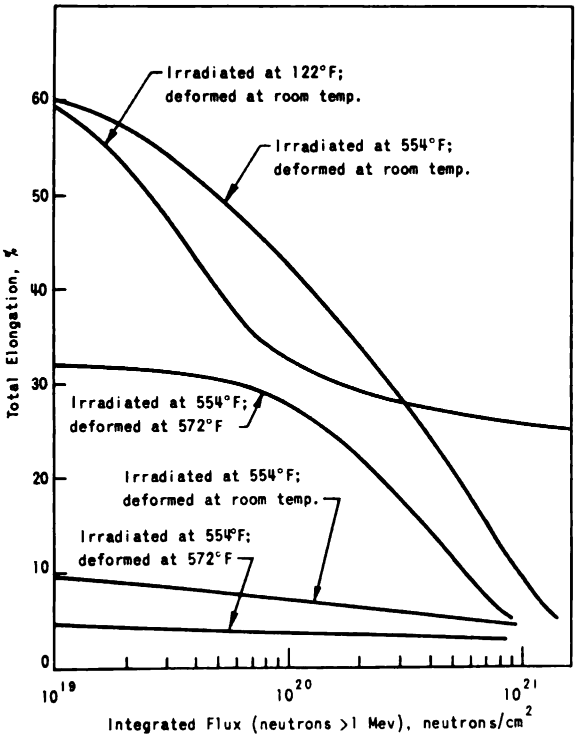

Fig. VI-1 Effects of radiation on ductility of type 348 stainless steel; upper three curves are for annealed samples; lower two curves are for 25% cold-worked samples.[13]

the metal, and stress imposed by the mechanical design all play an important role. This is the region in which all the VBWR failures lie. If a fuel-element design and the environment are both favorable, exposures in excess of 10^{21} neutrons/cm^2 (>1 Mev) may readily be attained, as shown by the PWR experience cited. The history of the J-10 loop (ETR) pressure tube[14] shows that thermal cycling and stress, of themselves, do not cause failure.

Despite the reported low level of chloride ion in the VBWR coolant,[15] coolant chemistry control must have been grossly inadequate, since chemical analysis of the crud deposited on some VBWR elements revealed up to 4000 ppm chloride ion.[16,17] This is not the whole story, however. Three classes of fuel cladding were irradiated in the VBWR: highly cold-worked, commercially annealed, and fully annealed. Although the VBWR personnel refer[18] to the commercially annealed cladding as annealed, they had measured the residual stress level in this tubing at 10,000 to 20,000 psi. Commercial annealing consists of a 10-min exposure to 1800°F; full annealing requires at least an hour at 1800°F for 300-series steels.[19] Both the cold-worked (residual stress of 10,000 to 40,000 psi) and commercially annealed tubing failed in the VBWR tests. However, a series of elements had been prepared by Nuclear Metals, Inc., by coextrusion of the UO_2 and type 304 stainless steel at temperature high enough (>1800°F) to assure full annealing of the cladding; these were irradiated under the same environmental conditions as the other elements, and, although the density of the UO_2 was higher (97 vs. 95% of theoretical) and these elements had no gap between the UO_2 and steel, none failed.[16,17] Thus we have evidence of the value of fully annealed cladding relative to the cold-worked varieties under irradiation, extending the out-of-pile experience previously reported.[20] In addition, the high chloride-ion content of the crud testifies to the hostile coolant environment in the VBWR. The inescapable conclusion is that the VBWR environment embrittled stainless-steel claddings causing intergranular and transgranular cracking.

To show that high-quality coolant ensures satisfactory BWR cladding performance, consider the experience in the Elk River reactor. Although the strength of the cladding has been compromised by incorporation of 600 ppm boron (as burnable poison), exposures have exceeded levels at which similar elements (0.003-in. diametral gap and 95% theoretical density UO_2) had failed in the VBWR without any failures.

Thus the assertion that the boiling-water environment is necessarily detrimental to stainless-steel cladding cannot be substantiated.

L. Bernath and B. W. Colston
Atomics International

Rebuttal: Boiling Water Is Detrimental to Stainless-Steel Cladding

I commend Messrs. Bernath and Colston for their attempts to provide additional insight into the behavior of stainless-steel-clad fuel elements in water-reactor environments. However, the validity of my original position, to wit, that a boiling-water environment is detrimental to stainless-steel cladding, has recently been affirmed by other knowledgeable investigators.[21,22] Nevertheless, the reader may appreciate our identification of several fallacies Bernath and Colston attempt to promulgate.

1. *System Pressure*

Both PWR and BWR stainless-steel-clad fuel elements are normally designed to have a 0.003 to 0.006-in. diametral fuel-cladding gap. In such fuel elements the primary source of stress is fission-gas accumulation. Thus a simple calculation of fission-gas release as a function of burnup shows that an increase in external pressure of 1000 psi may permit even a "factor of 2 and 3" increase in burnup, assuming exposure to be limited by the attainment of a specific tensile stress. The Bernath and Colston calculation of 250 Mwd per metric ton of uranium may refer to a fuel swelling phenomenon, which is not relevant to the fuel elements under discussion.

Crack propagation normally occurs only when the resulting decrease in elastic strain energy is greater than the energy required to create new surface. Bernath and Colston have misinterpreted their Ref. 2, which does not provide evidence for "crack propagation in the absence of a tensile stress." Nor does their Ref. 2 demonstrate that "compressive stresses lead to failure." Explicit interpretation of the experimental results of their Ref. 2 is not possible because of the failure of the authors to define the actual stress state at the surface. Stress state in the specimens tested will be determined by the sum of residual stresses introduced by the heat-treatment and cold-hardening process, local mechanical stress caused by the roller separating the specimens, and the gross bending load. Cracking kinetics will also be determined by strain energy of the specimen. Thus their Ref. 2 appears to demonstrate only that stainless steel can corrode intergranularly in high-temperature water under certain conditions.

2. *System Chemistry*

The presence of chloride was implicit in my observation that high oxygen concentration accelerates stress corrosion, as shown, for example, by the work of Williams and Eckel.[23] Moreover, the suggested qualification of "in the liquid phase" is unnecessary, as shown by the same research.

I cannot possibly disagree with the contention that "oxygen does not always act in a detrimental manner." Unfortunately the examples cited by Bernath and Colston deal with mass corrosion and are not germane to the matter of crack initiation and propagation.

3. *Corrosion-Product Deposition*

It is hardly sporting in a technical discussion to place heavy emphasis on evidence from privy sources, the validity of which cannot be verified by the reader (namely, Bernath and Colston Refs. 6, 15, and 18). Corrosion-product deposition is apparently adjudged to be "negligible"—by what standard, may I ask?

Bernath and Colston may choose to argue that nucleate-boiling bubble formation scours the surface. I prefer to accept the experimental evidence[24] that nucleate boiling in fact promotes crud formation.

4. *Local Thermal Stresses*

The thermal fluctuations measurements cited in my original letter were indeed performed at low heat flux and pressure. Although the magnitude of measured thermal fluctuations will diminish with increasing pressure, the finite mass and dimensions of the thermocouples result in a significant underestimate of the true thermal fluctuations at a point in the cladding surface. Furthermore, the implied generalization that increasing heat flux decreases the amplitude of thermal fluctuation is a gross simplification. In thermal transient phenomena the amplitude of thermal fluctuation is a complex function of not only heat flux but also thermal capacitance, thermal resistance, and source frequency.

The study of the effect of coolant velocities quoted in their Ref. 12 was limited to low pressure, low heat flux, and large bubbles; whereas bubble migration under these conditions cannot be extrapolated directly to behavior under PWR or BWR conditions. In any case, after the sudden growth of a bubble at a heat-transfer surface, liquid inertia will tend to pull the bubble away from the surface. The horizontal shear force associated with high coolant velocity will cut the bubble close to the surface, introducing cooler liquid. Collapse of the remaining bubble will still produce a large thermal fluctuation.

VBWR Data

The relevance of VBWR data to BWR's in general has been confirmed,[1,2] as noted previously.

Figure VI-1, showing decreases in total elongation of stainless steel with increasing neutron exposure (hardly a revelation), surely does not constitute a summary of the "behavior of stainless steels in water cooled nuclear reactor environments." For that matter, total elongation is not even a suitable measure of cladding ductility. I suggest that the relevance of the figure to the Bernath and Colston mechanism for failure is obscure at best.

The addition of boron to stainless steel does not compromise strength.[25] Fuel-element integrity in any event is not a unique function of cladding strength. Moreover, the exposure to date of Elk River fuel elements is insufficient to disprove the generalization that boiling-water environment is detrimental to stainless-steel cladding.

R. J. Allio, *Manager*
Materials and Processes Development
Westinghouse Atomic Power Division

Re-Rebuttal: Readers Can Decide Relevance

We are faced with the onerous task of affirming the factual and rejecting the extraneous and misleading from Allio's rebuttal. The difficulty arises from the fact that Allio's original letter was propaganda and, as such, was a melange of fact and "smoke-screen" against *all* BWR's.

Allio's rebuttal, Refs. 21 and 22, in fact, confirm our position by stressing the importance of the coolant environment. Allio has extracted, out of context, one statement to support his position, namely, "Contrary to initial expectations, Type-304 stainless steel clad fuels have proven unsatisfactory for boiling water reactor service above peak exposures of 15,000 Mwd/tonne." He fails to note, in the same sources, that "Type-304 stainless steel clad was found susceptible to intergranular cracking *in at least some water-reactor environments*," and he omits the table in Ref. 21, which shows that *four* BWR's have been operated to between 7500 and 17,000 Mwd/metric ton exposures and that these are continuing to perform satisfactorily. Allio prefers to cite the VBWR experience as typical, to the possible embarrassment of the GE–San Jose people, who cannot fully defend themselves without admitting to a very cavalier treatment of the pertinent mechanical properties of the cladding as well as of coolant purity requirements. This may have been deliberate on the part of GE—at the initial of the VBWR tests, it was desired to show that no special care was required. It was precisely this situation that prompted us to cite the facts omitted by Allio and to present an objective assessment of the VBWR results.

1. *System Pressure*

Allio cites the existence of a 0.003- to 0.006-in. diametral gap between fuel and cladding to support his contention of the beneficial effects of increased system pressure. What he does not consider is that the cited gap exists only in the cold, as-fabricated condition; simple calculation of the differential expansions of UO_2 and stainless steel, at operating conditions, shows that at zero burnup this gap disappears and that as much as 0.1% strain may be imposed on the cladding. Thus fuel growth or swelling with increasing exposure is most pertinent to the discussion, refuting Allio's opinion that it is not relevant. In fact, Allio's coworkers agree (see page 320 of his Ref. 24) that dimensional stability of UO_2 (which determines the stress condition of the cladding with increasing burnup) is a function of such parameters as "burnup, heat rating, fuel density and grain size, and clad restraint."

As Allio points out, our original Ref. 2 was subject to interpretation. Obviously then, his statements that we have misinterpreted the reference are his opinion and are very much open to question. There is, however, significant merit to his further comments, namely, "Stress state in the specimens tested will be determined by the sum of residual stresses. . ." It was to summarize these effects, plus the effect of water chemistry and irradiation, that we included our figure of "obscure" relevancy.

2. *System Chemistry*

Allio's allegation that "the presence of chloride was implicit in my observation, etc." cannot be accepted, as repeated reading of his original letter fails to substantiate any appreciation of the effects of chloride ion. He glosses over his misconceptions relative to oxygen concentrations in BWR's and implies that vapor-phase stress corrosion is observed under high coolant purity conditions.

3. *Corrosion-Product Deposition*

Allio not only ignores the evidence we cited, but he also distorts the direct findings of his coworkers (his Ref. 24). The experimental evidence he cites is based on five out-of-pile tests at low bulk velocity and relatively low heat flux, in which ferrous hydroxide was injected to simulate in-reactor corrosion; the validity of this simulation is unsubstantiated. The results obtained are highly suspect since calculation of the density of the deposit (page 4.32 of Ref. 24) indicates a value of approximately 0.5 g/cm^3 rather than the customary one of approximately 3 g/cm^3, a factor of 6 that cannot be explained. The results show (page 4.42 of Ref. 24) that when vigorous boiling occurred (the 1000-psi test condition) the pressure drop across the test section decreased, confirming a significant removal of deposited material (scouring action?).

4. *Local Thermal Stresses*

Allio persists in his belief in the existence of large local thermal stresses in boiling. To buttress his case, he equates the "low heat flux and pressure" of the pool boiling data he cited [10,000 to 30,000 Btu/(hr)(sq ft) and atmospheric pressure] with our Ref. 12, channel flow data [~100,000 Btu/(hr)(sq ft) and 200 psi]; the ratio of liquid-to-vapor density in these two cases, which is a paramount factor in bubble dynamics, differs by more than an order of magnitude, 1600 in the former and 124 in the latter. Allio insists on "sudden growth of a bubble at a heat transfer surface" while ignoring the effects of high coolant velocity to keep bubbles small and to move them along the surface during their growth cycle. Collapse of the bubble, which can only occur in subcooled nucleate boiling, may produce a "thermal fluctuation," but such collapse occurs in the bulk of the fluid, not at the surface!

VBWR Data

The relevance of VBWR data to BWR's in general and of our figure showing the total elongation of stainless steel with increasing neutron exposure is discussed in the second paragraph.

We do wish to thank Mr. Allio for his one useful comment. We agree that the addition of boron to stainless steel does not compromise the strength. We inadvertently used the word "strength." instead of "ductility." The pertinence of our comment concerning the Elk River cladding is, however, substantiated in Allio's Ref. 25. It is shown in this reference that irradiated boron stainless steel shows large (70 to 90%) decreases in elongation after irradiation with the degree of deterioration increasing with thermal-neutron exposure and concentration of boron. We are sure that Mr. Allio is also aware of the recent work in this field.[26, 27]

An argument such as this can only deteriorate — my father can lick your father — to the point where even the interpretation of the same results can be disputed with vehemence. We suggest, therefore, that only the individual readers of our comments can decide relevance and that each will utilize the discussion to delve into the referenced material to the extent of his immediate interest.

Again, we thank you for the opportunity, via publication of our letter, to present what we feel is a more objective interpretation of the VBWR results.

L. Bernath and B. W. Colston
Atomics International

Editors' Comment

Inasmuch as the objectives of *Power Reactor Technology* are to call its reactor-designer readers' attention to data of concern to them — and to venture interpretation and evaluation in the form of opinions as to the applicability of the data — we particularly welcome contributions from readers that either offer their original evaluations or interpretations that differ with those expressed in articles or letters in our issues. We believe the usefulness of our pages will be enhanced by expressions of differing opinions, which in turn will encourage our authors to venture and verify their interpretations more vigorously. As more data become available to substantiate or refute evaluations presented in our pages, we hope that readers will call them to our attention. In this light, we thank Messrs. Allio, Bernath, and Colston for their useful exchange and invite other readers to volunteer articles or communications on matters of mutual interest.

References

1. Stainless-Steel-Cladding Failures in VBWR, *Power Reactor Technol.*, 7(4): 354-355 (Fall 1964).
2. P. A. Akol'zin and L. V. Korneeva, Study of Corrosion Under Stress of 1Kh18N9T Steel Depending on the Composition of the Medium and State of the Metal, in Corrosion of Reactor Materials: A Collection of Articles, USAEC Report AEC-tr-5219, pp. 124-145, V. V. Gerasimov (Ed.), translated from a Russian publication of the State Publishing House of Literature in the Field of Atomic Science and Technology, Moscow, 1960.
3. D. J. DePaul (Ed.), Stress Corrosion, in Corrosion and Wear Handbook for Water Cooled Reactors, USAEC Report TID-7006, pp. 187-223, March 1957.
4. F. L. LaQue and H. R. Copson (Eds.), *Corrosion Resistance of Metals and Alloys*, 2nd ed., p. 378, Reinhold Publishing Corporation, New York, 1963.
5. Ya. M. Kolotyrkin, G. M. Florianovich, P. S. Petrov, N. K. Smirnova, and L. M. Vyazankin, Use of Oxygen for Protecting Steel from Corrosion in Water at High Temperatures, in Corrosion of Reactor Materials: A Collection of Articles, USAEC Report AEC-tr-5219, pp. 26-40, V. V. Gerasimov (Ed.), translated from a Russian publication of the State Publishing House of Literature in the Field of Atomic Science and Technology, Moscow, 1960.
6. T. J. Pashos, General Electric Company, Atomic Power Equipment Department, unpublished, September 1963.
7. F. J. Brutschy, H. W. Dreyer, and W. L. Pearl, Vallecitos Boiling Water Reactor, Coolant Technology, *Ind. Eng. Chem.*, 51: 1262-1264 (October 1959).
8. C. R. Breden et al., Water Chemistry and Fuel Element Scale in EBWR, USAEC Report ANL-6136, Argonne National Laboratory, November 1960.
9. W. H. Jens and P. A. Lottes, Analysis of Heat Transfer, Burnout, Pressure Drop and Density Data for High-Pressure Water, USAEC Report ANL-4627, Argonne National Laboratory, May 1, 1951.
10. W. M. Rohsenow, A Method of Correlating Heat Transfer Data for Surface Boiling of Liquids, *Trans. ASME*, 74: 969-976 (1952).
11. University of Eindhoven, Final Report on the Research Programme on Heat Transfer and Stability Studies in Boiling Water Reactors, USAEC–Euratom Report EURAEC-335, p. 22, February 1965.
12. G. J. Kirby et al., A Visual Study of Forced-Convection Boiling, Part I, British Report AEEW-R-281, March 1965.
13. J. E. Irvin et al., The Combined Effects of Temperatures and Irradiation on the Mechanical Properties of Austenitic Stainless Steel, in *Flow and Fracture of Metals and Alloys in Nuclear Environments*, pp. 236-250, American Society for Testing and Materials, Special Technical Publication No. 380, 1964.
14. William E. Murr, Frederic R. Shober, Robert Lieberman, and Ronald F. Dickerson, Effects of Large Neutron Doses and Elevated Temperature on Type 347 Stainless, USAEC Report BMI-1609, Battelle Memorial Institute, Jan. 21, 1963.
15. T. J. Pashos, GE-San Jose, personal communication, Dec. 16, 1963.
16. W. H. Arlt and S. R. Vandenberg, Fuel Failure Examinations and Analyses in the High Power Density Program, USAEC Report GEAP-4360,

General Electric Company, Vallecitos Atomic Laboratory, Sept. 16, 1963.

17. General Electric Company, Atomic Power Equipment Department, Nuclear Superheat Project. Nineteenth Quarterly Report, February–April 1964. USAEC Report GEAP-4619, May 1964.
18. T. J. Pashos, GE–San Jose, personal communication, Dec. 16, 1963.
19. V. V. Gerasimov, A. I. Gromova, and E. T. Shapovalov, Corrosion Cracking of 1Kh18N9T Steel, in Corrosion of Reactor Materials: A Collection of Articles, USAEC Report AEC-tr-5219, pp. 146-151, V. V. Gerasimov (Ed.), translated from a Russian publication of the State Publishing House of Literature in the Field of Atomic Science and Technology, Moscow, 1960.
20. A. V. Stanyukovich and E. E. Levin, Causes of Failure of Steam Superheater Pipes Made from 18 Cr/12 Ni/1 Ti steel, British Report TRG-Inf-Ser-191, 1963, translated from *Energomashinostroenie*, 10: 27-30 (1961).
21. T. J. Pashos, H. E. Williamson, and R. N. Duncan, Fuel Performance in Boiling Water Reactors, *Trans. Am. Nucl. Soc.*, 8(2): (1965).
22. T. J. Pashos (Comp.), Stainless Steel Failure Investigation Program. First Quarterly Progress Report, February 15–June 30, 1965, USAEC-Euratom Report GEAP-4915, General Electric Company, Atomic Power Equipment Department, Aug. 1, 1965.
23. W. Williams and J. Eckel, *J. Am. Soc. Naval Engrs.*, 68(93): (February 1965).
24. C. Roderick, Large Closed-Cycle Water Reactor Research and Development Program. Progress Report, April 1–June 30, 1964, USAEC Report WCAP-3269-3, Westinghouse Electric Corporation, Atomic Power Division, 1964.
25. W. K. Anderson and J. Theilacker, Neutron Absorber Materials for Reactor Control, *Naval Reactors, Division of Reactor Development*, Washington, 1962.
26. W. R. Martin and J. R. Weir, Effects of Elevated Temperature Irradiation on Hastelloy N, *Nucl. Appl.*, p. 160, April 1965.
27. R. S. Barnes, Embrittlement of Stainless Steels and Nickel Based Alloys at High Temperature Induced by Neutron Radiation, *Nature*, p. 1307, June 1965.

Section VII

Components

Vapor Traps Protect Liquid-Metal Systems

y David H. Thompson

nstruments and equipment in liquid-metal systems are damaged if the liquid-metal vapor ntrained in the inert cover gas condenses out n them. Vapor condensation also can plug gas supply, vent, or instrument lines. Traps that will prevent such damage or plugging are installed in the gas circuits of liquid-metal systems to remove the metal vapor.

We will consider here the principles of such traps, early versions, the variety of types and ways they are used in reactors and other dynamic systems, some recent developments, and conclusions and recommendations concerning their use and the need for improved technology for future reactors. Experience with traps for static systems also is discussed briefly in connection with fume traps for spent-reactor-fuel melt-refining furnaces.

Trapping Principles

Among the phenomena that have been studied for vapor traps are stagnation, impingement, condensation, adsorption, chemical reaction, and repulsion. Vapor traps now used in dynamic systems depend on condensation to remove liquid-metal vapor from the flowing inert gas; stagnation and impingement also are involved in trap operation. Table VII-1 summarizes the features of such traps.

Table VII-1 PRINCIPLES OF CONDENSING VAPOR TRAPS

- Type (and temperature)
  - Configuration
    - Maintenance of operation
      - Examples

ACCUMULATING CONDENSER (outlet gas cooler than vapor freezing temperature)

- Impingement–condensing type
  - Cylinder filled with mesh, shot, or liquid NaK; trap is cooled by natural or forced convection
    - Heated to remove accumulated Na when trap plugs—or replace trap internals
      - EBR-I, EBR-II, Fermi, SRE, Hallam, SCTI, FARET, SEFOR, S1G
- Stagnation–condensing type
  - Lengths of relatively large diameter pipe
    - Heated to remove accumulated Na when trap plugs
      - STF, LAMPRE

CONTINUOUSLY REFLUXING CONDENSER (outlet gas slightly hotter than vapor freezing temperature)

- Impingement–condensing type
  - Cylinder filled with mesh, shot, and/or baffles
    - After liquid metal agglomerates on trap surfaces, it runs off and is returned to system
      - FRCTF, Pratt & Whitney research, ANL research

In a condensing vapor trap, natural- or forced-convection cooling reduces the temperature of the inert gas passing through, which results in the metal vapor condensing on surfaces within the trap. The amount of metal vapor that passes through such a vapor trap is a function of the vapor pressure of the liquid metal at the trap outlet temperature—and is extremely small if gas temperatures are kept near the metal freezing point.

In impingement–condensing vapor traps, the extended surfaces formed by the mesh, shot, or baffles force the vapor-laden gas to follow a tortuous path, which promotes both heat transfer from the gas and condensation of the metal vapor.

In stagnation–condensing vapor traps, the relatively large-diameter lengths of pipe lack the extended-surface inner packing or fill of the impingement–condensing vapor traps. They operate most satisfactorily in systems that have slow flows of relatively cool gas.

Early Versions

In early work with sodium and NaK experimental facilities, it was postulated that the relatively large amount of sodium and NaK entrained in the gas was caused by the formation of a stable sodium or NaK aerosol that did not readily condense onto the surfaces over which it passed.[1] Another theory suggested that oxygen present with the inert gas reacted with the sodium vapor to form a stable aerosol of sodium oxide. The conditions required for aerosol production and the nature of the aerosol itself still are not fully understood. However, if aerosol is present in the cover gas of liquid-metal systems, it apparently is not present in concentrations large enough to influence vapor-trap effectiveness.

Some attempts at vapor trapping included experiments with a copper-coil condenser, an electrostatic precipitator, and a NaK bubbler.[1] Gas flow through these devices ranged from 130 to 1560 cu in./hr, and vapor was produced by passing purified argon over a 1500°F sodium pool. The room-temperature NaK bubbler operated effectively over the entire flow range (maximum velocity was ~1 ft/sec), but the condenser (a 16-turn 2-in.-diameter coil of ¼-in. copper tubing maintained at 235°F in an oil bath) allowed vapor to pass at high gas flows. The electrostatic precipitator was the least effective vapor trap for dynamic conditions, but it proved satisfactory under static conditions. In work predating the Sodium Reactor Experiment (SRE), it was shown that the stainless-steel wool- or mesh-filled trap could be ver effective,[2] but these experiments showed the effectiveness depends on gas temperatures and flows.

Gas Systems, Trap Applications

Much of the developmental effort on vapor traps has been directed toward a particular system or systems for individual reactor projects. Thus most of the concepts, design details and experience with them have not been reported in the literature. Because of the increasing need for dependable large fast reactor systems it is worthwhile to describe in some detail the inert-gas blanket systems and vapor-trap installations at a number of liquid-metal-cooled facilities. In this discussion no attempt is made to distinguish between aerosol and vapor or to define the exact nature of the trapping action, whether it be technically termed a filter, trap, or condenser.

EBR-I, EBR-II, FERMI

These first-generation breeder reactors use metallic fuels and have reactor-coolant-outlet temperatures of less than 900°F. All three reactors have argon as the inert cover gas for the primary coolant system, and the gas-supply system of each was constructed with NaK-bubbler type purification units followed by a stainless-steel wool- or mesh-filled vapor trap. However, because the Experimental Breeder Reactor No. 2 (EBR-II) facility is supplied with relatively pure liquid argon, rather than bottled argon as originally proposed, the NaK-bubbler purifier has not been operated. At the Experimental Breeder Reactor No. 1 (EBR-I), the primary-system cover gas was continuously recirculated, whereas, at both EBR-II and the Enrico Fermi Fast Breeder Reactor, the cover-gas systems are operated on a demand type basis and provide for recovery and recirculation of the gas transferred from the primary vessel.

EBR-I. Because EBR-I used NaK, which is liquid at room temperature, as both the primary and secondary coolants, there was only limited need for vapor traps. During operation a continuous downward flow of argon gas through the reactor top plate was maintained to retur upward diffusion and condensation of NaK vapor on the surfaces near the top of the vessel. The NaK vapor was removed from the recirculating argon primary cover gas by a centrifugal separator and strainer near the inlet to the parallel centrifugal blowers.[3] The strainer tank, approximately 2 ft in diameter and 4 ft high, was fitted near the bottom with a perforated plate and was filled with steel wool. In operation the oxides and NaK liquid trapped in the strainer formed a semisolid mass that allowed little liquid to be withdrawn during draining attempts. When flow through the strainer became restricted, rapping the tank with a hammer was sufficient to restore free flow. This strainer fulfilled the EBR-I trapping requirements, without replacement, for the operation of all four cores. In addition to this strainer, a small-diameter stainless-steel-mesh-filled trap was installed ahead of the piston type positive-displacement depressurizing pump in the gas-transfer line.

Fermi. In addition to the purification-unit vapor trap, Fermi has (1) a Dowtherm-cooled vapor trap in the gas-recirculating system, (2) a vapor trap in the line to the fission-product detector, and (3) lengths or coils of pipe used as vapor traps in the gas lines having slow flows, such as instrument lines. The Dowtherm-cooled vapor trap and other components of the recirculating gas system are located in the Fermi inert-gas building; gas is conveyed from the reactor building to the inert-gas building through a resistance-heated gas line in an underground tunnel. In the gas building the gas flows into a 500-cu ft vacuum tank, then to the Dowtherm-cooled vapor trap, which protects the compressors from liquid-metal entrainment.

As shown in Fig. VII-1, this trap consists of a 26-in.-OD inner shell that is surrounded by a 41.5-in.-OD outer shell charged with Dowtherm A as coolant.[4] The contacting surface of the vapor trap is increased by a 6-ft section of stainless-steel wool enclosed between perforated baffle plates. Downstream from the vapor trap is a cyclone separator, followed by three gas compressors in parallel. Although the line downstream from the vapor trap is not equipped with a sampling means to check trap effectiveness, there has been no evidence of sodium reaching the compressor diaphragms, which are changed periodically.

The EBR-II primary-gas system, like that of Fermi, operates on a demand type basis, with the primary-tank argon pressure controlled by a floating-head tank. When gas volume changes because of temperature fluctuations, the floating head in the tank moves to maintain the cover-gas pressure constant.

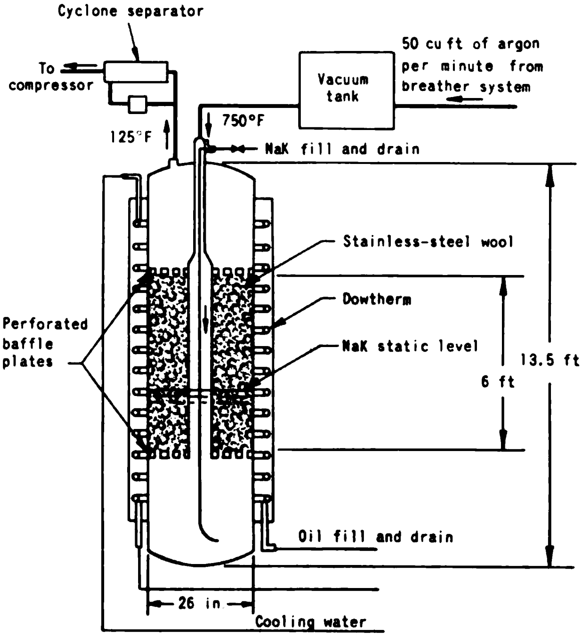

Fig. VII-1 Fermi vapor trap in gas recirculation system bubbles argon through NaK and passes it through stainless-steel wool; water-cooled Dowtherm in annulus cools trap and gas.[4]

Figure VII-2 shows the two stainless-steel-mesh-filled vapor or aerosol traps in the EBR-II argon cover-gas system.[5] These traps are not equipped with heaters, and therefore, if plugging occurs, the gas flow can be rerouted through a bypass line to keep the system operative while the traps or their mesh are replaced. Gas discharged from the primary tank passes up through a cleanout or access flange, then through the small vapor trap, through a silicone-oil-cooled heat exchanger that cools the argon to 150°F; then it passes through the large vapor trap and on to the floating-head tank. If the volume change exceeds the capacity of the floating-head tank, one of the two parallel blowers pumps gas into the argon receiver tank for future use (the second blower is a standby unit).

The traps see little flow except when the system is purged. When the primary tank was purged with the system still at approximately 700°F, the small vapor trap became plugged.

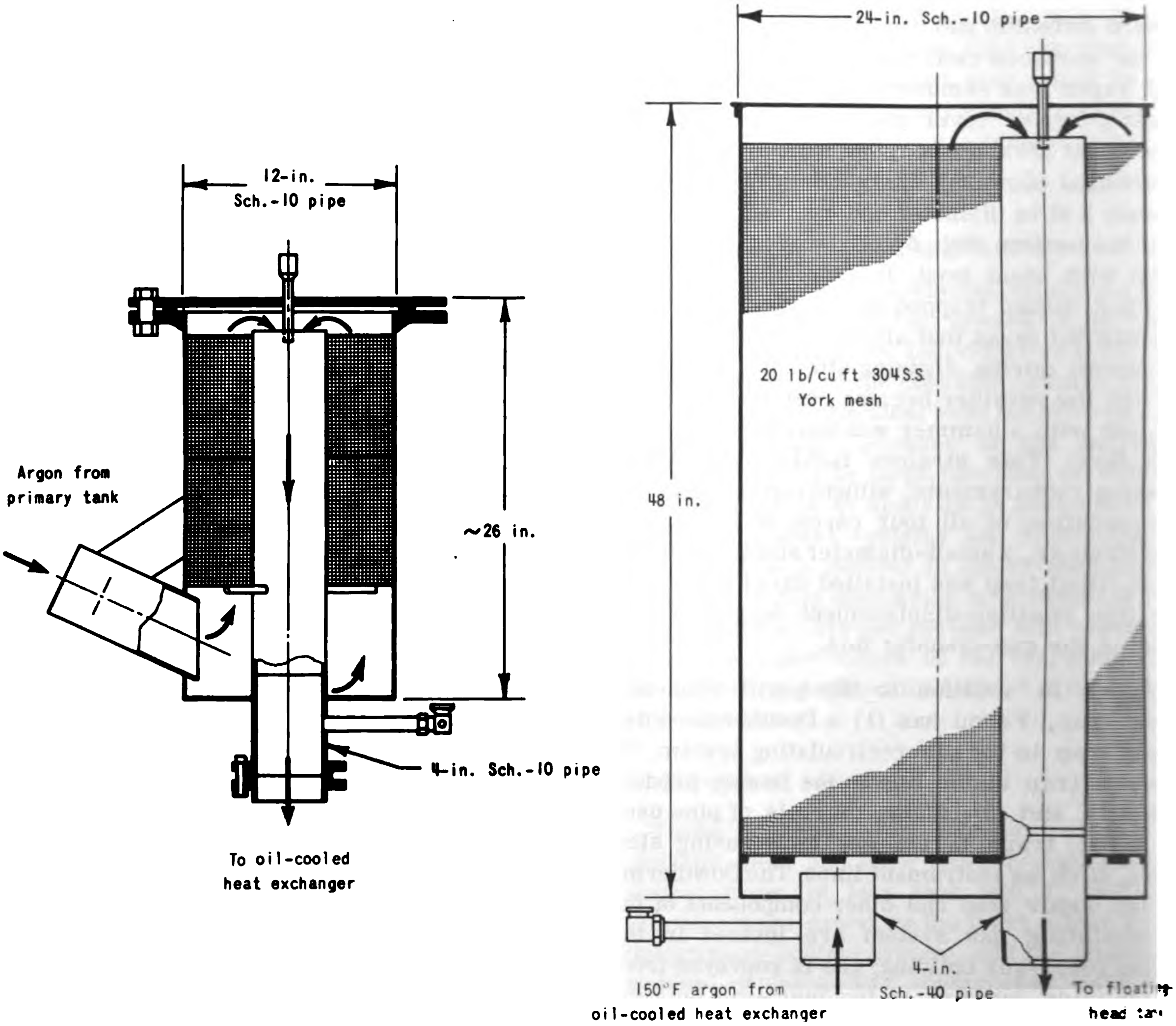

Fig. VII-2 EBR-II vapor or aerosol traps for primary-system argon are packed with stainless-steel mesh; heat exchanger in circuit between the traps cools the gas.[5]

When the operators removed the two-piece mesh packing through the flanged upper end of this vapor trap, they found that the lower section of mesh was plugged for approximately 1 in. from the mesh surface near the inlet nozzle, but the remainder of the mesh packing was relatively free of accumulated sodium. Although the operators removed the plugged-mesh piece and left only the upper piece of mesh in place, the trap has worked satisfactorily since.

The EBR-II fueling machine is cooled by an argon system, most of whose components are in an area depressed beneath the main operating floor. This argon system, which is separate from the reactor cover-gas system, includes two turbine type blowers, a multiple-tu natural-convection argon-to-air heat exchange a stainless-steel-mesh-filled vapor trap, an two molecular sieves in parallel. The vap trap and molecular sieves, which are beds o crystalline sodium aluminosilicate pellets, re-move vapor and fission-product gases from t argon drawn from the reactor vessel into t system piping during fuel-handling operations.

As shown in Fig. VII-3, mounted on t fueling-machine carriage are another lea shielded vapor trap and molecular sieve, sim lar to the units in the argon system, for trea ing argon that is drawn directly into the fuel machine. Subassembly-heated argon (210 450°F) from the fueling machine passes throu

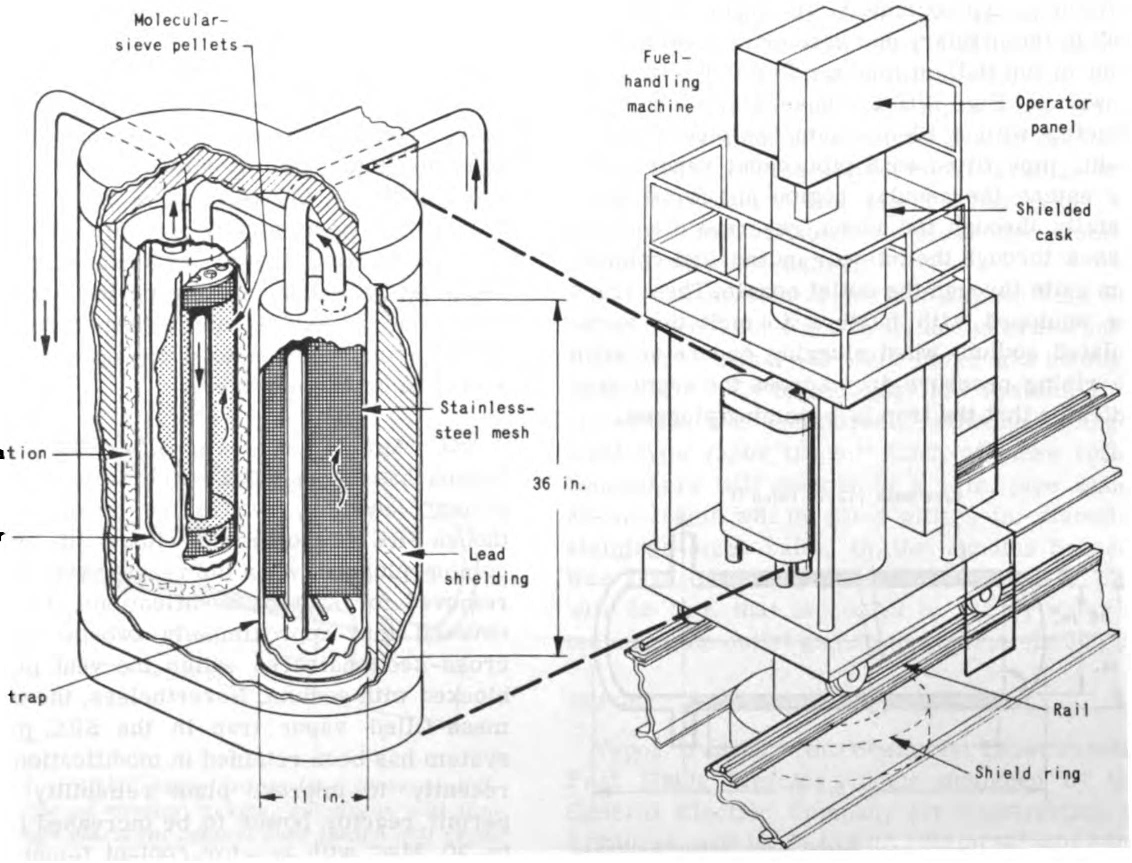

Fig. VII-3 EBR-II fueling machine has shielded vapor trap and molecular sieve to remove vapor and fission-product gases from argon drawn directly into machine.[5]

200-in.-long flexible hose to the heat exhanger, is cooled to approximately 100°F, and hen enters the main turbine type blower (the maller blower serves as a standby unit).

The vapor trap on the fueling machine has artially plugged once. Inspection revealed that e stainless-steel mesh had not plugged, but e lower opening of the gas-inlet tube had beome blocked by sodium that had condensed nto the trap cold internal surfaces beneath the esh.

The vapor trap in the depressed area also as plugged once. Operation was restored by emoving the flanged outlet end of this horizonally installed trap and replacing the stainless-teel-mesh packing. When one of the turbine ype blowers was disassembled recently to corect a manufacturing error, a fine white powder was seen in the piping and blower. This substance has not been analyzed, but its talcum-powder texture indicates that it is probably powder from the pellets in the molecular sieves and not sodium oxide.

Fission-Gas Monitor. When difficulty was experienced in obtaining vapor- and aerosol-free gas samples for the EBR-II fission-gas monitor that detects fuel-cladding failures, an 8-in.-diameter vapor trap containing a 4-in. thickness of stainless-steel mesh was installed in the gas line to the monitor and has operated satisfactorily. Argon enters this trap at 230°F and leaves at ambient temperature; gas flow is less than 200 cm^3/sec.

SRE, HALLAM, FARET, SCTI

These facilities can operate at temperatures up to 1200°F, where the vapor pressure is approximately 20 times greater than at 900°F. This is reflected in a wider use of vapor traps at these facilities than at EBR-I, EBR-II, or Fermi.

Hallam. Approximately 10 vapor traps are used in the primary and secondary sodium systems of the Hallam Nuclear Power Facility. As shown in Fig. VII-4, these traps are constructed with a 10-in.-diameter pipe within a 12-in. pipe fitted with pipe caps; vapor-laden gas enters the annular region and flows horizontally through the mesh, reverses direction, passes through the interior cylindrical volume, then exits through the outlet nozzle. These traps are equipped with heaters to melt the accumulated sodium when plugging occurs or when the rising pressure drop across the vapor trap indicates that the trap is becoming plugged.

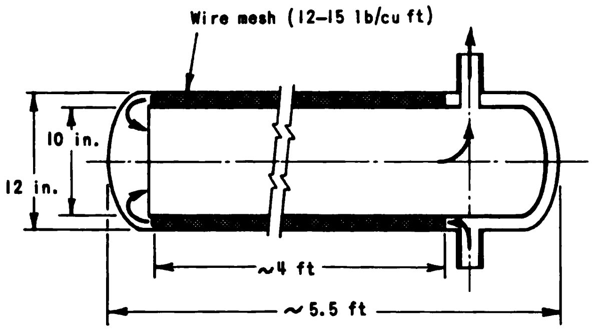

Fig. VII-4 Hallam vapor traps pass vapor horizontally through stainless-steel mesh in annular region, then through interior cylindrical volume; cooling is by natural convection. Heaters melt sodium when plugging occurs.[6,7]

The criterion for designing the Hallam vapor traps was to provide sufficient heat capacity and heat-transfer surface in the trap that the heat from the gas passing through the trap could be absorbed and dissipated rapidly enough to cool the gas below the melting point of sodium. Summary evaluation of the Hallam traps[6] indicates that "Operation of the vapor traps, installed in the system to prevent sodium vapor from entering and clogging the helium lines, has been satisfactory except at high reactor venting rates, such as when control-rod thimble leaks developed. Trap design and efficiency should provide many years of satisfactory maintenance-free service, but consideration should be given to the installation of more heaters."

The vapor trap in the reactor vent line plugged about four times during Hallam operation.[7] To unplug the trap, personnel entered the primary-system pipe gallery to insulate the plugged trap, which then was heated until sufficient sodium melted and drained to restore proper operation. The melted sodium drained directly into the liquid-metal system through the trap inlet nozzle. Although the plugging occurred during changes in reactor-operating conditions, no reactor shutdowns were caused specifically by the plugging of a vapor trap. If it had been necessary to shut down the reactor specifically to unplug the vent-line trap, an approximately 10-day waiting period would have been required for the radioactivity of the sodium in the primary pipes to decay enough for personnel to enter the gallery.

SRE. Atomic International's SRE at Santa Susana has mesh-filled vapor traps (one in the primary system, two in the secondary). Although SRE has operated without the trap becoming plugged, when the reactor vent line was removed for system modifications, it was discovered that approximately two-thirds of the cross-sectional area within the vent pipe was blocked with sodium. Nevertheless, the original mesh-filled vapor trap in the SRE primary system has been retained in modifications made recently to improve plant reliability and to permit reactor power to be increased from 20 to 30 Mw, with reactor-coolant temperature raised from 960 to 1200°F.

SCTI. The vapor traps for the Sodium Components Test Installation (SCTI) at Atomic International's Santa Susana site differ from those at Hallam because of uncertainty concerning the flow rates through the SCTI gas system. The cylindrical SCTI vapor traps are 6 in. in diameter and 3 to 4 ft high. Installed vertically, they are filled with $^1/_8$-in.-diameter steel shot to increase the heat capacity.

FARET. Vapor traps in the Argonne's Fast Reactor Test Facility will be of the annular design, similar to the Hallam traps, but the gas flow will be reversed so as to use the quiescent central volume of the trap as a refluxing condenser before the vapor-laden gas passes through the annular mesh. The design objective is to cool the outlet gas below 200°F regardless of whether the gas system has a slow flow of hot gas (to satisfy normal "breathing" requirements) or a fast flow of cool gas (such as during purging). As shown in Fig. VII-5, these traps will be installed with the longitudinal axis inclined 10° from the horizontal to facilitaraining; they will be covered with 1-in.-thick nsulation.

FARET vapor traps will be located in the rgon supply and vent lines for the main sec- ndary sodium system, auxiliary secondary odium system, wet-fuel-storage tank, NaK rain tank, wet-fuel cooling system, and reac- or-annulus drain tank—as well as on the rgon supply line for the main primary sodium ystem and on the vent of the drain tank in the rimary sodium system.

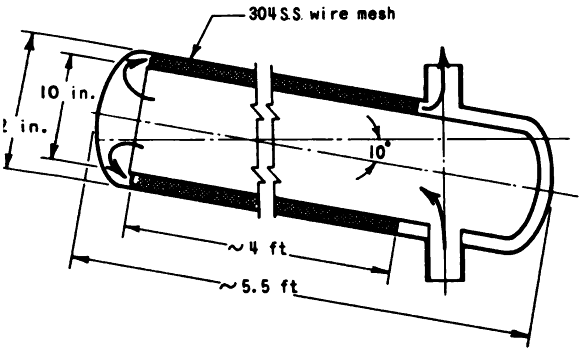

ig. VII-5 FARET vapor traps, like those at Hal- am, will be of annular design, but argon will flow irst through quiescent central zone (which will serve s a refluxing condenser) before passing through esh-filled annulus; 10° inclination will facilitate raining sodium.[10]

The coolant-gas-system equipment for the ARET fuel-handling machine, including the ompressors, filters, vapor trap, heat ex- hangers, and argon supply tank, will be lo- ated in the transfer tunnel beneath the oper- ting floor of the primary-containment cell and ill be connected to the carriage of the fuel- andling machine by flexible metal hoses ap- roximately 50 ft long.[10] For this system the nctions of vapor trap and heat exchanger will e combined in a single unit that has an am- onia evaporative coil immersed in NaK main- ained at 40°F; it is designed for gas flows of p to 60 cfm.

TF, LAMPRE, FRCTF

Los Alamos Scientific Laboratory has had otable success using stagnation type vapor raps on its 2-Mw Sodium Test Facility and the os Alamos Molten Plutonium Reactor Ex- eriment.[11] These facilities are relatively mall, tight systems that do not require high gas flows and in which the gas is drawn from system locations where the sodium temperatures are relatively low. In general, the stagnation type vapor traps are pipes 4 to 5 ft long and greater than or equal to 3 in. in diameter that connect the liquid-metal system with smaller diameter gas piping. The traps are equipped with heaters to clear accumulated sodium when necessary.

The gas system of the Los Alamos Fast Reactor Core Test Facility is designed to recirculate the primary-system cover gas continuously. For this higher gas-flow system, it is planned to use continuously refluxing impingement type vapor traps.[12] Each of these reflux condensers will consist of a 1-in. pipe whose 30-in. length will be filled with $\frac{1}{8}$-in.-diameter stainless-steel balls. In the annulus between this 1-in. central pipe and an outer 2-in. pipe will be NaK that is cooled by air or water to maintain the outlet gas at approximately 300°F.

SEFOR

Vapor traps for the Southwest Experimental Fast Oxide Reactor, being designed by the General Electric Company for construction in Arkansas, will be 2- to 8-in.-diameter pipe sections that are packed with stainless-steel mesh for lengths[13] of approximately 18 in. These configurations, which were chosen as the result of General Electric experience with sodium loops and with the prototype power plant for the nuclear submarine *Seawolf*, are sized to maintain gas velocity less than 1 ft/sec. Although the larger traps will be equipped with heaters, sufficient heat is expected to be transferred through the short lengths of pipe between the vapor sources and the smaller vapor traps that heaters will not be required on these units.

LARGE TREAT SODIUM LOOP

The large sodium loop in the Transient Reactor Test Facility, located at the National Reactor Testing Station in Idaho, will be used to test unirradiated and preirradiated fast reactor fuels to failure under variable coolant temperature and flow conditions.

Possible contamination will be localized during fuel tests by operation of the loop on a once-through mode—sodium coolant will flow from a storage vessel through the test section and then to a dump vessel. A vapor-trapping demister, molecular sieve, and liquid-nitrogen-cooled charcoal trap in the gas system remove gaseous fission products and entrained sodium or sodium vapor from the helium cover gas transferred between vessels during the once-through flow. The demister is constructed of a 12-in. length of 4-in.-diameter pipe fitted with knitted stainless-steel wire mesh having a bulk density of 20 lb/cu ft; the molecular sieve is a 9-in.-deep bed of $\frac{1}{8}$-in.-diameter sodium aluminosilicate (Linde 4A) pellets in an 8.5-in.-diameter container. Neither the demister nor the molecular sieve has heating or cooling provisions but are valved and flanged for replacement when necessary. Gas transfer through the system may reach 20 cfm at temperatures up to 900°F but will be sustained for a duration of only several minutes.

MELT-REFINING FURNACES

In conjunction with the development of the melt-refining process for purifying discharged EBR-II fuel, screening tests were conducted to determine the capability of various materials to trap alkali-metal vapors[14] as hot as 1470°F. Although the application was to statically trap sodium vapors and other condensible volatiles released by the melt-refining process, the materials were tested in a dynamic system. Argon gas was bubbled through a vaporizer containing a shallow pool of alkali metal and then through the bed material until breakthrough occurred; breakthrough was detected by white oxide fumes formed when the untrapped metal vapor reacted with oxygen at the end of the bed. The tests indicated that simple condensation alone is ineffective for retaining vaporized sodium but that nearly all surface-active materials, such as molecular sieves, activated carbon, and activated alumina, were effective.

Although molecular-sieve beds initially were used as fume traps for the EBR-II fuel melt-refining furnaces, their maintenance in a remotely operated plant would require additional handling equipment. Thus a simpler disposable fume trap was sought. Tests of an absorber type trap consisting of a molded, porous Fiberfrax (aluminum silicate ceramic fiber) cup showed it to retain sodium vapors quite effectively.[15,16] This trap works on the principle of absorption and chemical reaction of the sodium with the trap surface; the reacted layer can be seen in Fig. VII-6.

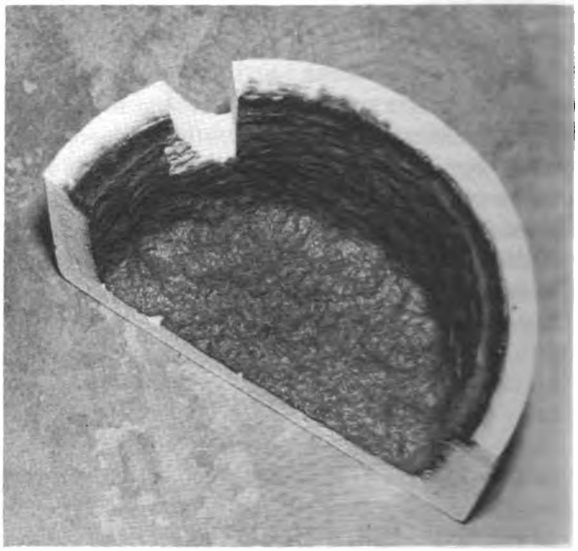

Fig. VII-6 Melt-refining-process development for reprocessing spent EBR-II fuel showed t porous Fiberfrax molded cup effectively traps so vapor by absorption and chemical reaction.[15]

Recent Developments

Recent research on vapor traps has be reported by Pratt & Whitney (CANEL) and t Argonne National Laboratory (ANL), with bo efforts directed toward developing continuousl refluxing vapor traps.

P&W. The lack of suitable design criter can be seen in recent developmental work vapor traps that was being conducted for t Lithium Cooled Reactor Experiment (LCRE). Gas-system tolerances were to be defined as result of long-term system testing, but, unfortunately, this work ceased when the LC project was terminated.

Four separate operating regimes had be defined for the LCRE vapor-trap tests: 1000°F lithium vapor in 60 to 100 cu ft of helium per hour, (2) 120 to 1000°F lithium va in approximately static helium, (3) 700 1000°F NaK vapor in 30 to 50 cu ft of heli per hour, and (4) 100 to 300°F NaK vapor approximately static helium. Air- or nitroge cooled traps were being developed to preve more than an arbitrarily chosen 2-ppm weight) vapor carry-over; screening tests we made on a number of vapor-trap designs, cluding shell-and-tube heat exchanger, baff continuous-refluxing bubbler, mesh-packed, helical-fin types. Most promising of these e continuous-helical-fin type vapor trap. Thus ve helical-fin vapor traps were fabricated for sts to determine how helix pitch ($^{1}/_{4}$ to $^{3}/_{4}$ in.) ıd fin-surface slope affect trap performance; g. VII-7 describes their geometries. These thium tests showed the trap with $^{1}/_{4}$-in. pitch be the most efficient: approximately 80% for 00°F lithium and approximately 99% for 00°F NaK; Fig. VII-8 shows this trap. Figures I-9 and VII-10 show the transparent housing r visually observing condensation in the lical-fin vapor traps and the tendency of the ndensed liquid metal to agglomerate before aining back to the vapor source.

Stringent gas-purity requirements for the CRE were to be met by the use of various ettling, impingement, and filter devices downream and in series with the $^{1}/_{4}$-in.-pitch lical-fin trap. Mesh-filled settling chambers were tested with the helical-fin traps for about 400 hr, but the LCRE termination prevented completing these evaluation tests.

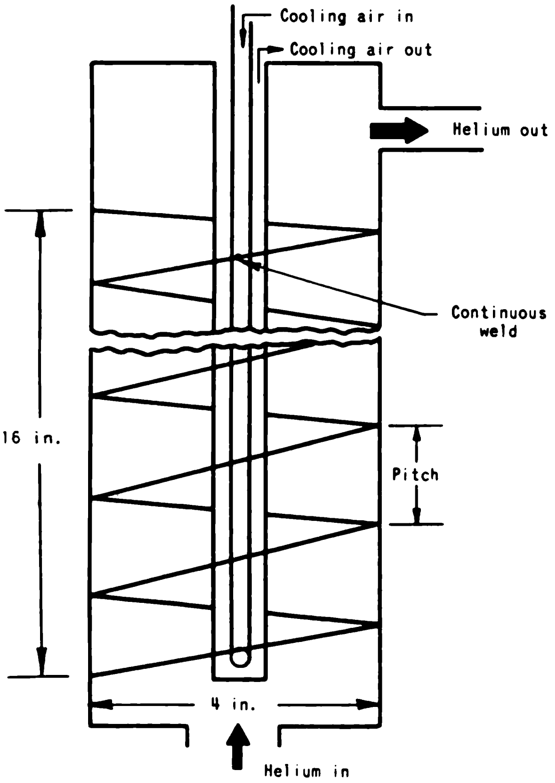

'ig. VII-7 When LCRE vapor-trap screening tests ıdicated that continuous-helical-fin type refluxing rap promises best efficiency, five such traps were uilt to test effect of helix pitch and fin slope. Fins f one trap were conical and on $^{1}/_{2}$-in. uniform pitch. 'lat fins on each of other three were uniform $^{1}/_{4}$, $^{1}/_{2}$, nd $^{3}/_{4}$ in.; Fig. VII-9 shows the fifth trap, whose flat ins had nonuniform pitch.[18]

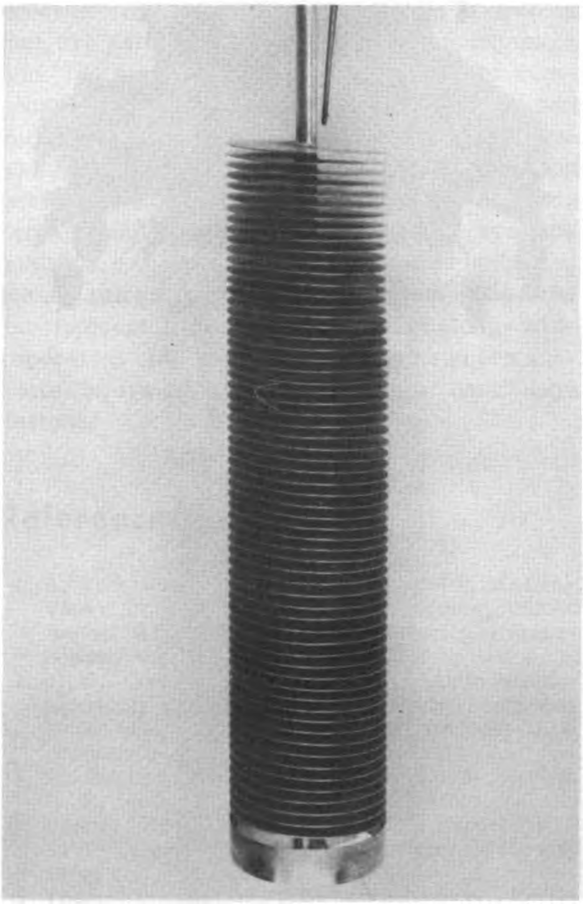

Fig. VII-8 Most efficient of the vapor traps tested by Pratt & Whitney for LCRE lithium vapor in helium was helical-flat-fin type trap having $^{1}/_{4}$-in. uniform pitch.[18]

ANL. Recent work on the development of a 1200°F sodium vapor trap at ANL has been reported.[19] Two experimental vapor traps were constructed. Figure VII-11 shows the second, mechanically improved vapor trap. It was tested with gas flows up to 40 cu ft/hr from a sodium tank maintained at 1200°F; vapor-removal efficiency was as high as 99.8%. Sodium condensation rates were determined by radiography of a calibrated U-tube beneath the vapor-trap inlet. At a gas flow of 20 cu ft/hr, the condensation rate was 13.6 cm^3/hr; it increased to 86 cm^3/hr when gas flow was 40 cu ft/hr.

These test results indicate that vapor-trap configuration and temperature can be adjusted

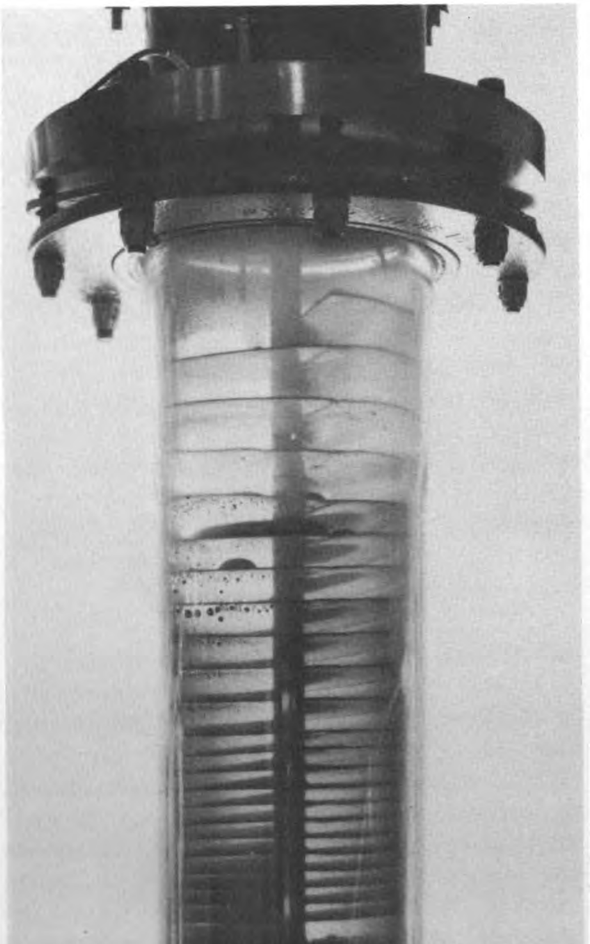

Fig. VII-9 Pyrex transparent shell permits observation of nonuniform pitch of this helical-flat-fin trap: $^{1}/_{4}$ in. for middle 3 in. of helix, $^{1}/_{2}$ in. for next 3.5 in. upper and lower, and $^{3}/_{4}$ in. for top and bottom ends.[18]

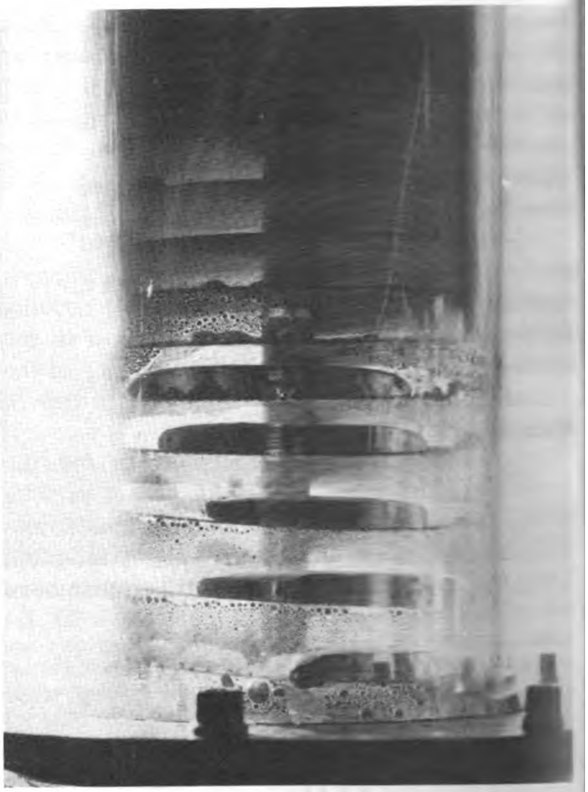

Fig. VII-10 Condensed liquid metal in helical-flat-fin trap tends to agglomerate on fins before draining back to vapor source, which in this case and in Fig. VII-9 was 1000°F NaK; photographs were taken after trap operated 5 hr.

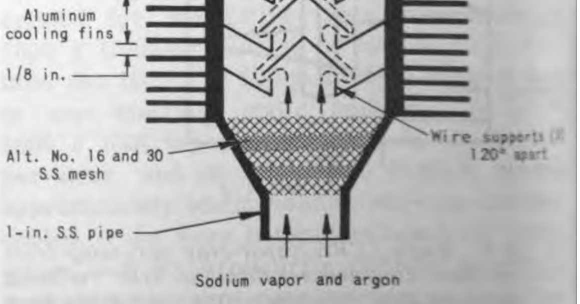

Fig. VII-11 Refluxing type impingement-condensing trap being developed at Argonne for 1200°F sodium vapor has cooling fins and internal baffles as well as mesh.[19]

provide continuous refluxing of sodium vapor. addition to avoiding trap plugging, this would ermit reducing trap size and cost. But this ap would not operate satisfactorily if the gas ontained an oxide aerosol because oxide accumulation on the limited condensing surface ould plug the trap.

A larger trap with a 2-in. inlet is being tested ow. It has operated for about 650 hr at 570°F nd 800 hr at 1020°F. The major operating roblem has not been with the vapor trap, but ith maintenance of the tank heaters.

ecommendations for System Design

Vapor traps should be located near the vapor ources to minimize sodium plugging or obtruction of gas lines. However, because traps or handling appreciable gas volumes are rather ulky, and space within containment cells is ften at a premium, traps cannot always be ositioned next to sodium-containing vessels. hus system designers must ensure that the as piping has enough heat capacity to overcome iquid-metal accumulation and plugging and that he entrapped liquid metal can be drained from he piping.

Trap Design. Field experience with replaceable mesh-filled vapor traps indicates that lugging occurs in a small volume of the mesh ear the gas inlet and that most of the mesh olume in a plugged trap remains relatively ree of liquid-metal accumulation. This experience suggests that trapping capacity might e improved by the use of graduated-density r zoned-density packings. Another improvement on current practice might be to increase he frontal-area-to-volume ratio of the mesh acking, such as by arranging the mesh packing n a relatively thin annulus through which the as would pass radially.

Conclusions: Development Needed

The mesh-filled vapor trap has found almost universal application in liquid-metal-reactor systems where large volumes of gas are transferred. The operation of these traps can be described as tolerable or even acceptable, but in few installations have they proven to be completely satisfactory.

There has not been a significant change in vapor-trap technology during the past decade. The early experimental work with vapor traps covered almost the entire spectrum of devices that are being used now. The first impingement type units were purposely oversized to compensate for lack of adequate design criteria and uncertainties surrounding the nature of the sodium vapor or aerosol, and this approach persists today. However, the vapor-trapping requirements of liquid-metal-cooled systems continue to rise as system size and operating temperatures increase. Thus a comprehensive developmental program is needed to provide vapor-trap and reactor-system designers adequate information upon which to base their designs.

References

1. A. J. Erickson, C. L. Gregory, and P. M. Lang, Vapor Traps for Handling Liquid Sodium, USAEC Report AECU-3200, MIT Engineering Practice School, Aug. 25, 1951.
2. J. C. Cochran (Ed.), Sodium Graphite Reactor Quarterly Progress Report, July–September 1955, Section B, USAEC Report NAA-SR-1513, Atomics International, Mar. 15, 1956.
3. R. O. Haroldsen, F. D. McGinnis, M. Novick, R. R. Smith, and F. W. Thalgott, Safety Analysis Report, EBR-I, Mark IV, USAEC Report ANL-6411, Argonne National Laboratory, February 1963.
4. Power Reactor Development Company, Enrico Fermi Atomic Power Plant Revised License Application. Part B, Technical Information and Hazards Summary Report, Report NP-10458, Vol. 1, pp. 107.7–107.12, July 1961.
5. L. J. Koch, W. B. Loewenstein, and H. O. Monson, Addendum to Hazard Summary Report Experimental Breeder Reactor-II (EBR-II), USAEC Report ANL-5719(Add.), Argonne National Laboratory, Jan. 7, 1964.
6. J. E. Price, Final Evaluation Report — Hallam Nuclear Power Facility, USAEC Report NAA-SR-9777, Atomics International, 1964.
7. G. L. Ballew, Hallam Nuclear Power Facility, personal communication, Aug. 31, 1965.
8. W. J. Freede and J. K. Roberts (Eds.), Sodium Reactor Experiment. Power Expansion Program — Heat Transfer Systems Modifications, USAEC Report NAA-SR-10379, Atomics International, Oct. 9, 1964.
9. R. Cygan, Atomics International, personal communication, Sept. 22, 1965.
10. W. R. Simmons et al., Argonne National Laboratory, unpublished, 1965.
11. L. A. Whinery, Los Alamos Scientific Laboratory, personal communication, Aug. 12, 1965.
12. B. J. Melton, Los Alamos Scientific Laboratory, personal communication, Sept. 22, 1965.
13. H. N. Bass, Atomic Power Equipment Department, General Electric Company, personal communication, Aug. 31, 1965.
14. J. Wolkoff and A. A. Chilenskas, The Melt Refining of Irradiated Uranium. Application to EBR-

II Fast Reactor Fuel. IX. Sorption and Retention of Sodium and Cesium Vapor on Stationary Beds at Elevated Temperature, *Nucl. Sci. Eng.*, 9(1): 71-77 (January 1961).

15. S. Lawroski, W. A. Rodger, R. C. Vogel, and V. H. Munnecke, in Chemical Engineering Division Summary Report for January, February, March 1960, USAEC Report ANL-6145, p. 32, Argonne National Laboratory, 1960.
16. J. C. Hesson, M. J. Feldman, and L. Burris, Description and Proposed Operation of the Fuel Cycle Facility for the Second Experimental Breeder Reactor (EBR-II), USAEC Report AN 6605, Argonne National Laboratory, April 196
17. H. J. Banach, LCRE Auxiliary Systems Term tion Report, USAEC Report PWAC-416, Pr Whitney Aircraft, Mar. 9, 1964.
18. E. H. Donnelly, Final Report on the Design Development of Lithium and NaK Vapor Tr Report PWAC-400, Pratt & Whitney Airc Mar. 3, 1964. (Classified)
19. E. L. Kimont, Engineering Development Practical 1200°F Sodium-Vapor Trap, *Trans.* A *Nucl. Soc.*, 8(1): 147 (1965).

Section VIII

Operating Experience

)perational Problems ınd Solutions

Rolf C. Skaardal

eactor designers should be interested to learn at reactor operators have found out about eir products. Some reactor operational diffilties traced to design, fabrication, and inection were reported at the Conference on eactor Operating Experience sponsored by the eactor Operations Division of the American uclear Society (ANS). Some of the "nuts-and-lts" type problems are reported here. Most these involved hydraulically induced vibraons, corrosion, leaks in components, and ntrol-system peculiarities. Repair methods, ntrol of oxygen in heavy water, and changes research-reactor experimental facilities also e of interest to operators and designers and erefore are taken into account in this review.

ontrol Systems

Difficulties have occurred with neutron-aborber rods and control circuitry at various ower reactors.

Control Rods. During a routine license test ith the Indian Point reactor shut down, one ontrol rod stuck when it was being inserted.[1] fter borating the water, cooling the system, d removing the vessel head, the operators und that a tapered stainless-steel pin ($1\frac{3}{4}$ in. ng by $\frac{5}{32}$ to $\frac{9}{32}$ in.) had wedged between the oper grid plate and a blade of the cruciform ontrol rod. They removed the pin, of unknown rigin, with a 19-ft-long slender wrench when e control rod was jacked from below.

Also at Indian Point, when it was time to emove the 12 boron–stainless-steel fixed shim rods that had been installed in the first core to limit reactivity during the early part of core life, several blades were found to be stuck.[1] The rods were freed by partially removing, as a unit, all four fuel elements around each rod. The sticking was caused by considerable buckling of the rods, which apparently occurred because of radiation-induced growth of the shim blades relative to their rigidly attached nonborated stainless-steel tips. These shim rods had been in the reactor for only 189 effective full-power days.

Specimens of Elk River reactor control rods of a similar material (2% boron–stainless steel) also suffered radiation damage, in this case, ductility loss.[2] About a year after the plant reached full power, the control rod was replaced because tests on a specimen of the rod material indicated that it might no longer meet the technical-specification requirement of 3.4% elongation. However, visual inspection of the removed rod showed no apparent mechanical damage. Studies are under way to determine (1) how much rod embrittlement is tolerable and (2) whether periodically changing the core location of the rods to expose all rods uniformly would be a more practical program than replacing each rod as it reaches its limiting ductility.

When the nickel plating on the silver–indium–cadmium control rods of the Yankee reactor failed to protect the silver from corrosion, radioactive silver corrosion products circulated and deposited throughout the primary system.[3] This caused maintenance problems, particularly during the first refueling. After the reactor pit was flooded (to provide shielding for the refueling crew) and the vessel lid was removed, the radioactive silver in the reactor water got into the pit water and plated out on the stainless-steel liner. To avoid the problem thereafter, the operators replaced the original rods with hafnium rods. For two years they also have successfully used two experimental silver–indium–cadmium rods that are clad with Inconel and now have installed two new silver–indium–cadmium rods clad with stainless steel.

Chemical Shim. Yankee, like Indian Point, was designed to use boric acid solution in the coolant–moderator to reduce reactivity during cold shutdown. As an extension of this, during operation with the second core, the Yankee operators experimented with boric acid injection as a chemical shim method.[3] Although the experiments were successful, for some unexplained reason the boric acid in the operating reactor system was accompanied by higher crud concentrations and appeared to cause oxygen generation in the pressurizer. While the causes are being investigated, the solution at Yankee has been to arrange for degassing from the top of the pressurizer and recombination by reinjecting into the main coolant system with 25 cm^3 of hydrogen per liter in the coolant.

Temperature Sensor. The Elk River reactor experienced several spurious scrams caused by a malfunctioning temperature bulb and pressure switch.[2] After tests indicated this equipment was sensitive to radiation, it was replaced by a thermocouple system.

Level Control. When a water-level indicator in the Special Power Excursion Reactor Test No. 3 (SPERT-III) 2500-psi 650°F pressurizer reported that the water was more than 2 ft higher than it actually was, the electric heaters became partly uncovered and superheated the steam to 1000°F. This caused the pressurizer-vessel material to fail in creep and ruptured its seam weld.[4] The error illustrates the mutual dependence of instrumentation and mechanical-hardware designs. The signal from a differential-pressure cell was used to sense the water level. Compensation for the effect of density changes on the water-level indication was provided through a temperature signal received by the automatic controller from a single sensor near the top of the normal water level. Unfortunately this signal did not recognize the water-temperature stratification that occurred when certain operating conditions led to diminished internal circulation of the pressurizer water.

Reliable water-level control in the new pr
surizer is to be obtained by (1) electric hea
staged to operate at different elevations s
to circulate the water by convection (hea
response is delayed only slightly) and (2) t
for the differential-pressure cell located s
that the normal operating water level is 25
the differential range above the bottom
Although this increases the safety mar
temperature–density compensation is still ne-
essary for water levels other than normal.

Electrical Circuit. Routine checks of
SPERT-III scram circuit five years after in-
stallation revealed abnormal operation and re-
lay chatter.[5] After wiring checks did not f
the cause, a complete evaluation of the syste
disclosed that electrical leakage to gro
through faulty insulation could actuate rel
that should be deenergized (such as the r
withdrawal circuit). This failure by leakage
ground occurred on leg *a* of the "floati
ground" power-distribution system (Fig. VIII-1

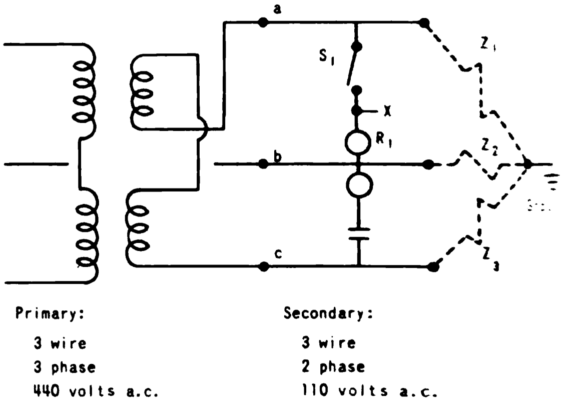

*Fig. VIII-1 Original power-distribution schem
SPERT-III proved "fail-unsafe" when the wire
lation deteriorated, permitting a short circuit
wiring to override the control-rod switch by e
tively shorting it closed.*[5]

where the insulation on the wiring in t
control-rod drives was particularly suscep
to deterioration because of exposure to vibration, heat, and moisture.

Because the leakage impedance *Z* on any
the three lines shown in Fig. VIII-1 was ma
up of both the resistance path through de-
teriorated insulation and the strong inhere
capacitance built into the a-c control syste
by its long wiring runs to ground, an accide

uld result (because the switch S_1 is effectively orted by impedance Z_1, the relay R_1 cannot deenergized) if a failure to ground occurs ar point X in Fig. VIII-1. Although R_1 is a 0-volt relay, 60 volts will energize it, and will remain energized down to 45 volts. ɜspite the intention to design a fail-safe sys- m, the discovery that ground failures might ıt deenergize certain relays meant that the ʼstem was not, in fact, fail-safe.

Because of the hazard, the control-system ›wer-distribution circuit was modified as ıown in Fig. VIII-2 so that wiring deteriora- ɔn can be detected before serious conse- ıences result. The transformer neutral line

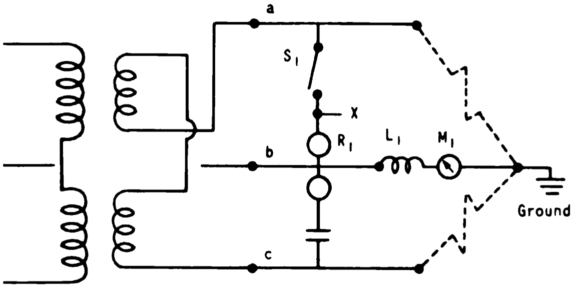

ig. VIII-2 *Modified circuit for SPERT-III alarms ˈdeteriorated insulation permits leakage to ground. ʼhus insulation can be repaired before a short cir- uit occurs and overrides the switch.*[5]

was grounded through a current-limiting amp L_1 in series with an ammeter M_1. Any eakage to ground from either of the high- ʼoltage legs *a* or *c* then completes the circuit ınd causes current to flow through the lamp ınd meter. Although this system cannot prevent aults, it does keep the reactor operator in- ʼormed as to the condition of the system and ›rovides an alarm if an abnormality occurs.

This ground-loop problem at SPERT-III taught several lessons applicable to any electrical system. For instance, operators must bear in mind that the usual insulation checks are d-c measurements that will not detect capacitance paths, which are serious for a-c systems. Designers must consider the operating characteristics of components, such as relays, and the likelihood of large capacitance in their leads. Because of the impossibility of designing a completely failproof system and the chance of practical problems such as insulation deterioration, systems must be designed so that failures will not have serious consequences.

For more information on control experience discussed at the same ANS meeting, see page 221.

Flow Oscillations

The Elk River reactor[2] has exhibited flow pulsations ever since the initial power-escalation runs in 1963. The oscillations, which are well defined and repeatable, apparently are caused by surges in the feedwater flow at around 50% of rated power. These flow oscillations cause the reactor power to vary less than 2.5%. Although the conditions are adjudged to present no operational hazard to the reactor, studies are continuing to permit better understanding of the phenomenon.

Flow-Induced Vibrations

Flow of the coolant at high speeds through a reactor can buffet components and cause them to vibrate and wear. Failures resulting from this at the Big Rock Point, Yankee, General Electric Test Reactor (GETR), and SPERT-III reactors emphasize the need for designers to assess potential vibration sources, components that are susceptible to such damage, and ways to keep broken items out of the pumps and the core.

Excessive vibration loosened, and in some cases dislodged, bolts connecting fuel channels to channel support tubes in the high-power-density forced-circulation reactor in the Big Rock Point Nuclear Power Plant.[6] Investigations using accelerometers and strain gauges showed that the vibration was caused by inadequate distribution of the water coolant as it entered the reactor vessel. The manner in which the problem was solved by adding a baffle and by modifying the core support plate and 72 fuel channels will be described in an article on reactor-modification methods in the next issue of *Power Reactor Technology*. That article also will discuss modifications to the thermal-shield support in the Big Rock Point reactor.[7] These were required when several studs fractured by thread-root fatigue after fretting had enlarged clearances. The fretting occurred when small pressure fluctuations across the large surface of the thermal shield caused significant wear forces between line-contact sliding surfaces.

Hydraulically induced fretting corrosion was found when the Yankee power reactor was first refueled.[3] Zircaloy to stainless-steel joints on the fuel elements had corroded to a depth of more than 0.1 in. Later, stainless-steel tubes of the in-core instrumentation package were found to have been damaged by fretting corrosion to a depth of 0.040 in. Evidence also has been found that the Yankee control rods had fluttered, causing notches to be worn into the stainless-steel rubbing straps.

Steps to prevent such hydraulic problems at Yankee have included substitution of stainless steel for Zircaloy in parts that might rub, replacement of the 24 guide tubes, and installation of impact sleeves to act as cushions or vibration absorbers, and at the same time to give larger (100-fold in some cases) surfaces for dissipating impact.

The problem caused by hydraulic flow at Yankee has been the failure of 10 holders for irradiation coupons. Four were recovered in 1963, but the other six holders and basket parts remained lodged in uncertain positions in the reactor vessel until they were recovered during the 1965 refueling.

In the GETR,[8] hydraulically induced vibrations of control-rod guide tubes caused excessive wear of aluminum core-component spacer pads (see Fig. VIII-3). The pads provide lateral support for the upper ends of the fuel elements and beryllium filler pieces; there is no upper grid plate. The ½-in. 8-cps vibration of the guide tubes affected the reactor log-N period instrument, causing large-period recorder oscillations as the spacer pads ablated. When the reactor was operating at a steady 30 Mw, the recorder showed periods as short as ±30 sec, which caused repeated alarms.

Reactor modifications to stop the vibration consisted in bolting the free upper ends of the control-rod guide tubes to the coolant-flow distributor, replacing the guide-tube aluminum spacer pads with stainless-steel bands (fitted into slots milled circumferentially around each aluminum guide tube in the pad region), and installing complete stainless-steel top ends on the beryllium pieces.

No significant log-N period oscillations have been observed since; at a steady 30 Mw, recorder oscillations indicate periods of ±400 sec (for reference, the period indication is ±1000 sec with the reactor shut down). No pad wear could be detected after operation for one year.

In the SPERT-III reactor primary syste vibrations broke loose a thermowell.[5] For nately this failure occurred downstream of pumps, and the 8-in.-long piece of ½-in. p was caught below the core. This occurre together with earlier fatigue failures of in-co instrumentation (due to vibration of small par exposed to the turbulent coolant stream), caus concern about the 17 remaining thermowells the primary system. Investigation revealed t none of these conformed with vendor's dra- ings. Strain-gauge tests showed that 9- 6-in. wells were excited at their natural fre-

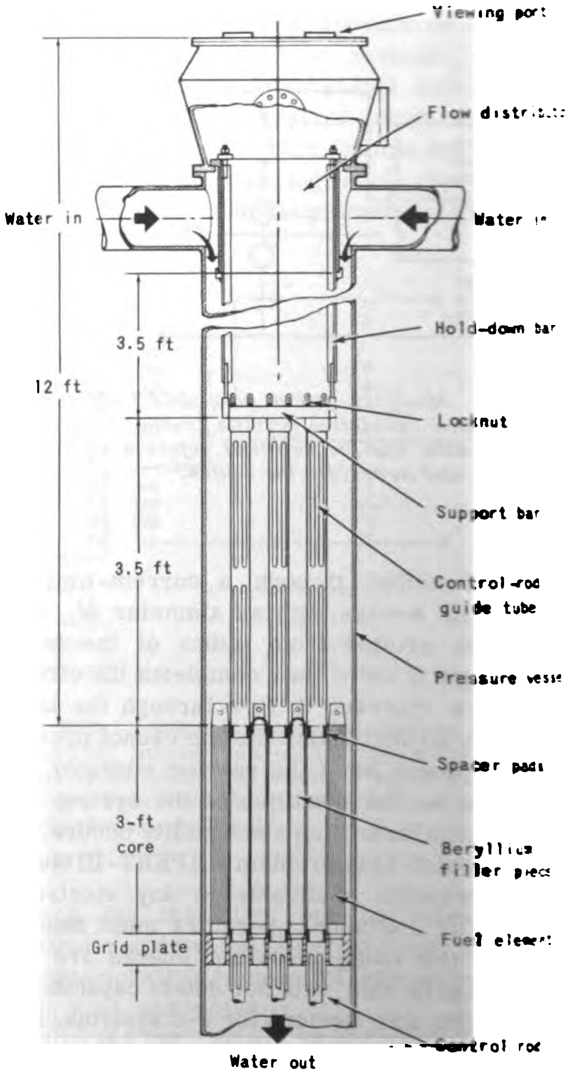

Fig. VIII-3 The GETR, which does not have an grid plate, employed aluminum spacer pads for eral support of the upper ends of the core co nents.[8]

encies, but 5-in. wells showed essentially no citation. Thus 5-in. wells have been installed, d no further thermowell problems have been countered.

orrosion Problems

A mysterious form of corrosion of Inconel s been discovered at the Ågesta Nuclear ower Plant in Sweden.[9] The Ågesta reactor, pressurized D_2O-cooled and -moderated re- tor, has a flat hollow lid that is filled with ght water for cooling the lid and for radiation ielding. This lid is penetrated by 188 Inconel pes for heavy water; 11 of these pipes, used r charging irradiation specimens, are located t the periphery and barely pass through the side of the lid (Fig. VIII-4). Leakage of heavy ater into the lid was discovered and found to e caused by corrosion of three of these eripheral tubes.

Examination revealed intercrystalline stress-orrosion cracking on the tube surface, originating from the light-water side. The lid-water hemistry had been harmless—*p*H was maintained between 9.5 and 10.5 by addition of LiOH. Chloride-ion concentration was ≤0.5 ppm, and stresses were less than 20% of yield stress. Thus this stress-corrosion phenomenon is not fully understood; the damaged tubes are being examined metallurgically. In this reviewer's opinion the cause for this "abnormal" stress corrosion might be traced to the Inconel-tube manufacturing process itself.

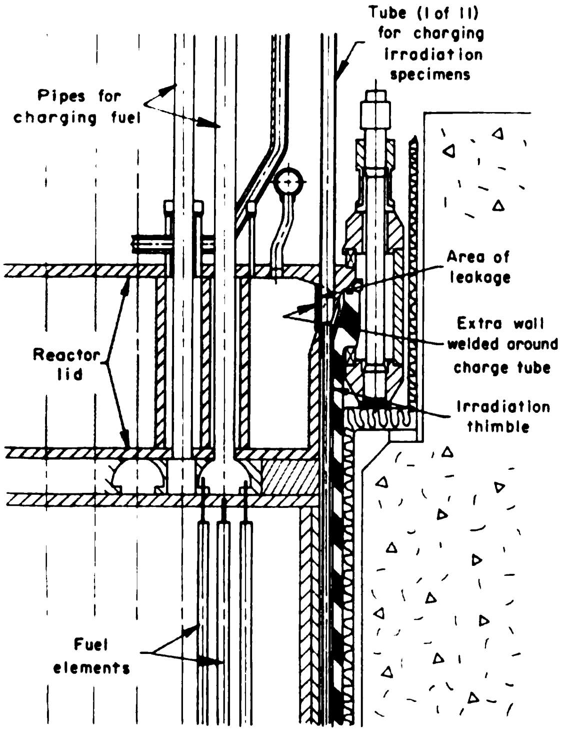
Tube (1 of 11) for charging irradiation specimens
Pipes for charging fuel
Area of leakage
Extra wall welded around charge tube
Irradiation thimble
Reactor lid
Fuel elements

ig. VIII-4 Extra wall section was welded around ach of 11 Inconel specimen-charging tubes in the hield lid of the Ågesta reactor after three tubes racked due to stress corrosion.[9]

Leaks in Mechanical Components

The Yankee and SPERT-III pressurized-water-reactor systems have experienced a variety of difficulties with leaks in mechanical components and resulting troubles.

At Yankee, early problems were encountered with leaks from canned-motor-pump flanges and from stem-leakoff type valves.[3] The flange leakage, which was caused by differential thermal expansion, is prevented by the use of the thermal expansion itself for final tightening of the closure; the operators do not pressurize the primary system when fluid temperature is low. For any cold hydraulic test of the system, the operators must adjust the pump flange by tightening the bolts. When the inner packing on the leakoff type valves could not control the leakage to desirable levels, it was necessary to remodel the valves to provide deeper inner packings. Leakage from the refueling water cavity and the ion-exchange pit at Yankee presented vexing problems. Also, one 2-in. stainless-steel pipe in the charging line failed by cracking due to suspected vibration and fatigue, and eight socket welds and seal welds have leaked. As the plant has become "broken in," such problems have tapered off—Yankee has now logged two complete one-year cycles without a primary-system cooldown or depressurization.

The SPERT-III reactor has experienced leaks from valves, gaskets, and piping.[5] The desirability of waterproofing all control-system electrical connections was demonstrated by the failure of a single tube fitting in the primary-coolant system. Extensive damage from short circuits resulted from the complete drenching of control-system wiring.

An unusual kind of leakage was experienced with one of the four canned-motor pumps in the SPERT-III primary system. During a plant cooldown in November 1964, a pump circuit breaker dropped out. Inspection showed that water had leaked through the seals of the stator-winding terminal posts and short-circuited the windings. The rotor can, stator liner, and stator were damaged, and the motor section had to be completely rebuilt. Although no cause for the leak has been ascertained, it is believed that the pump had operated for some time with a damaged rotor can. Thus the initial damage might have been caused either by a foreign particle entering the motor from the primary system or by a piece corroded from the nitrided surface of the thrust disk. This latter is considered more likely because some corrosion has been observed on the thrust disks of all four pumps. The operators are considering replacing the nitrided 17-4 PH material on the thrust-bearing disks by Stellite 19, which better resists pitting corrosion.

All gaskets in the SPERT-III system, except the heat-exchanger head gaskets (which are solid stainless steel), are of the spiral-wound asbestos-filled stainless-steel type (Flexitallic); diameters range from 1 to 53 in. Although experience with this type of gasket has been generally satisfactory, some flanged connections leak slightly during the cooldown portion of about the first three cycles after gasket installation. Thus retightening during each cycle is necessary until the gasket firmly seats. Also, if this type of gasket is installed without an inside-diameter retaining surface, water flow tends to unwind the gasket and pieces break off. This adds tramp metal to the system as well as weakening the gasketed joints.

The SPERT-III experience with metal gaskets has not been satisfactory. The heat-exchanger stainless-steel gaskets leak slightly and erratically at operating temperature. Although the primary control valves originally were fitted with solid-metal gaskets and welded canopy seals, frequent leaks and repair difficulties have prompted their replacement by Flexitallic type gaskets.

Stem galling and leakage through valve seats also occurred at SPERT-III. The motor-operated temperature-control valves were furnished with chrome-plated type 304 stainless-steel valve stems and Stellite 6 bonnet bushings and lantern rings. After about a year of service, a valve stem seized and the motor force, in addition to the 2500-psi internal pressure, broke the packing-gland bolts, necessitating an emergency shutdown. After the valve stems were overlaid with Colmonoy 6 and new bushings of bearing bronze were fitted with greater clearance, there were no further troubles of this kind.

Repair Procedures

At Indian Point, two maintenance jobs involved welding in high-radiation areas.[1] One job was the modification of the nuclear boilers secondary-side blowdown piping (the original design did not provide for differential thermal expansion relative to the boiler shell). To protect the welder from the 1.5 to 3 r/hr radiation field, a special lead shield on four wheels was made of 3- by 3-ft 0.25-in.-thick lead plates stacked as many as eight thick; the shield was just high enough for the welder to position himself under it and "turtle" along while doing the work, which required two to three weeks to complete. The other task involved rewelding of an inspection cover on a control-rod guide tube in the upper grid-plate assembly. This plate is located 4 ft below the reactor-vessel flange. The radiation field was 10 r/hr with the water level lowered to just below the plate. A 3- by 4- by 4-ft lead box, with its top open and a small round hole in the bottom was made from 0.25-in. lead sheets. The welder did his work through this hole. He spent an uninterrupted 30 min and received only a very low radiation dose.

At the Ågesta Nuclear Power Plant, an unusual repair job was accomplished in connection with the peculiar stress-corrosion cracking of Inconel-600 tubes in the shield lid.[9] These tubes, which are part of the D_2O circuit, penetrate the periphery of the H_2O-filled lid over the reactor vessel; they serve as charging pipes for irradiation specimens. Only 3 of the 11 peripheral tubes were cracked by the intercrystalline corrosion, which originated on the H_2O side, but it was decided to protect all 11 tubes from further attack by enclosing each within an extra wall section that would be welded to the inside of the lid (Fig. VIII-4). This repair work was extremely difficult because the work area was severely restricted by the heavy-water piping on the lid. Further, the lid structure permitted holes of only approximately 6 in. in diameter to be made for access to the welding area. Thus it was necessary to use mirrors and bent electrodes. The repairs took four months, including demonstration of an efficient repair method and recommissioning of the [illegible]

The radiation levels in the work area were oderate, 1 to 5 mr/hr, and were chiefly from ud deposits in the heavy-water piping atop e lid. The fuel contributed to the background ly slightly and, therefore, was not discharged om the core during the repair. No worker eceived more than 0.7 rem.

ontrol of Oxygen in D_2O

Operators of the Plutonium Recycle Test eactor (PRTR) reported difficulties in reducng the oxygen content of the helium-blanketed eavy-water systems.[10] The oxygen came from adiolysis of the D_2O and air leaks. The exess oxygen quickly disperses through all the $_2O$ systems because of the common surge tank, or the helium, which is the pressurizing nedium for the reactor coolant, provides an nert atmosphere over the moderator and relector, as well as serving as blanket gas etween the calandria and shields.

The usual method for reducing the excess xygen involved recombination by adding "shots" of hydrogen gas directly into the D_2O coolant. Although chromatographic analyses of the helium showed that these injections partially reduced the oxygen, they also unexplainably decreased the indicated content of hydrogen in the gas. Investigations employing mass-spectrometric analyses showed that the chromatograph was inaccurate (at equilibrium before H_2 was injected, no H_2 was present and only 12 to 17% as much D_2 as the chromatograph had indicated total H_2 plus D_2) and that the oxygen in the gas preferred to combine with the H_2 injected into the water rather than with the D_2 already present in the gas.

When it became clear that injecting hydrogen gas into the coolant still did not sufficiently reduce the oxygen content of the D_2O, tests were made to learn the effectiveness of a uniform concentration of excess hydrogen in the helium supply. Although calculations indicated that an initial concentration of 0.3% H_2 would be enough to combine with the oxygen from radiolytic dissociation and air inleakage, it only very slowly reduced the O_2 concentration in the D_2O. Increasing the H_2 concentration to 0.6% produced faster results, but only after reactor systems reached equilibrium temperature after startup. Since a 1% H_2 concentration in the helium was selected for routine operation, there has been very little problem with excess oxygen.

Research-Reactor Modifications

Designers of reactor experiments will be interested in considering the modifications made to irradiation facilities at two pool type research reactors to increase their usefulness for certain types of experiments.

Rabbit Facility. An interesting pneumatic irradiation system has been operated in the thermal column of the Industrial Reactor Laboratories (IRL) 5-Mw pool type research reactor.[11] It permits samples to be inserted and removed from the 10^{11} neutrons/(cm^2)(sec) flux in the column during full-power operation. The unique feature of this rabbit facility is that the track and 1- by ½-in. vent line were machined from graphite and assembled to form two 4- by 4- by 51-in. standard graphite pieces (Fig. VIII-5) which, when connected end-to-end, fully penetrate the thermal column. The 1⅜-in.-diameter track has an S shape to prevent radiation streaming. The low-friction graphite track is ideal for rabbit travel; no liner is needed that might perturb the flux or cause contamination problems in the column.

A maximum rabbit-surface contamination of 0.05 μc/cm^2, due mainly to the 12.9-hr ^{64}Cu and 2.58-hr ^{56}Mn from impurities in the AGOT graphite, has presented no serious handling problems.

Figure VIII-6 shows the pneumatic system used in inserting and returning the rabbit.

D_2O Reflector. A vented rectangular aluminum tank[12] containing 45 gal of heavy water has been installed along one full face of the core of the University of Michigan reactor (Fig. VIII-7). When the core size was reduced, installation of the tank converted two radial beam ports into tangential ports, increased the thermal-neutron flux at the beam-port source planes by 80%, and improved the signal-to-background ratio by factors of 2.8 and 4.7. Figure VIII-8 shows how the installation of the heavy-water reflector influenced the ionization-chamber readings.

When tests showed that the D_2O-filled-tank reactivity worth (compared to H_2O) was only half the +0.04 $\Delta k/k$ prediction calculated, the operators increased the core operating mass by 12% so as to provide enough excess reactivity for routine operation at 2 Mw.

The maximum credible accident is postulated to involve the release into the reactor pool of tritium produced in the D_2O tank. Thus the

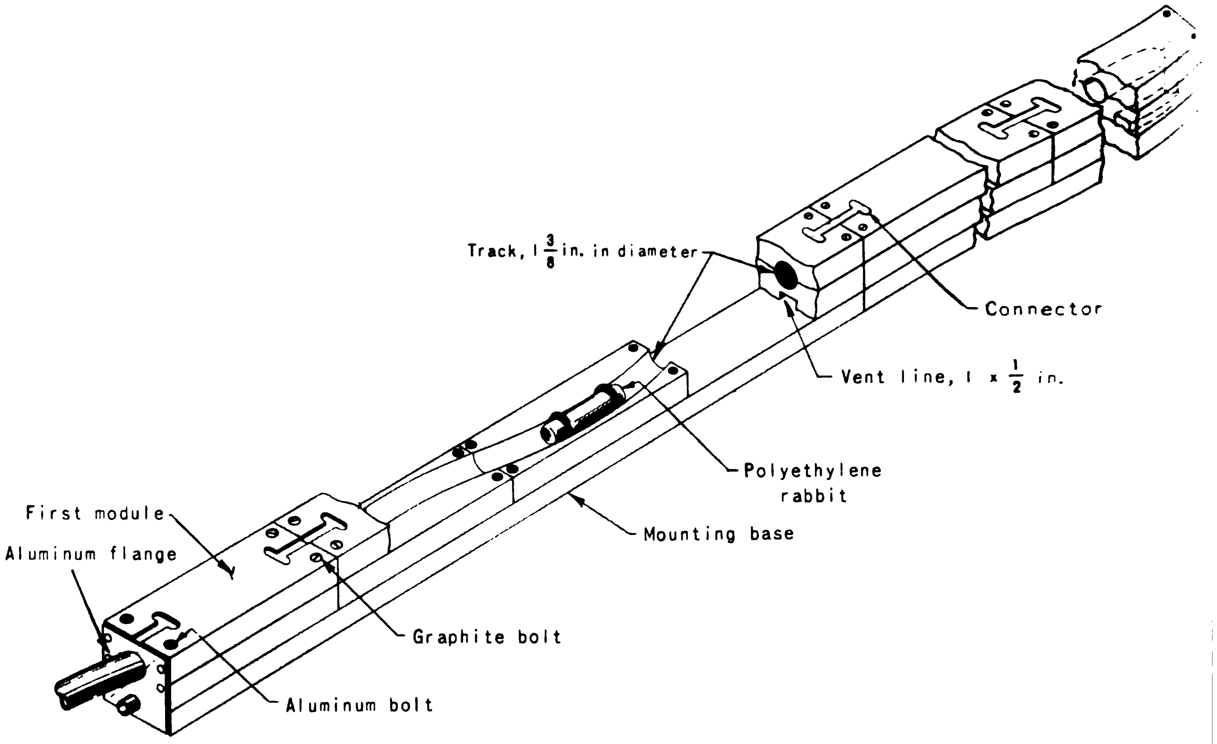

Fig. VIII-5 Assembly of graphite modules for rabbit-travel guide in IRL reactor thermal column. Graphite modules, each 12¾ in. long, are mounted on two 1- by 4- by 51-in. graphite pieces placed end-to-end.[11]

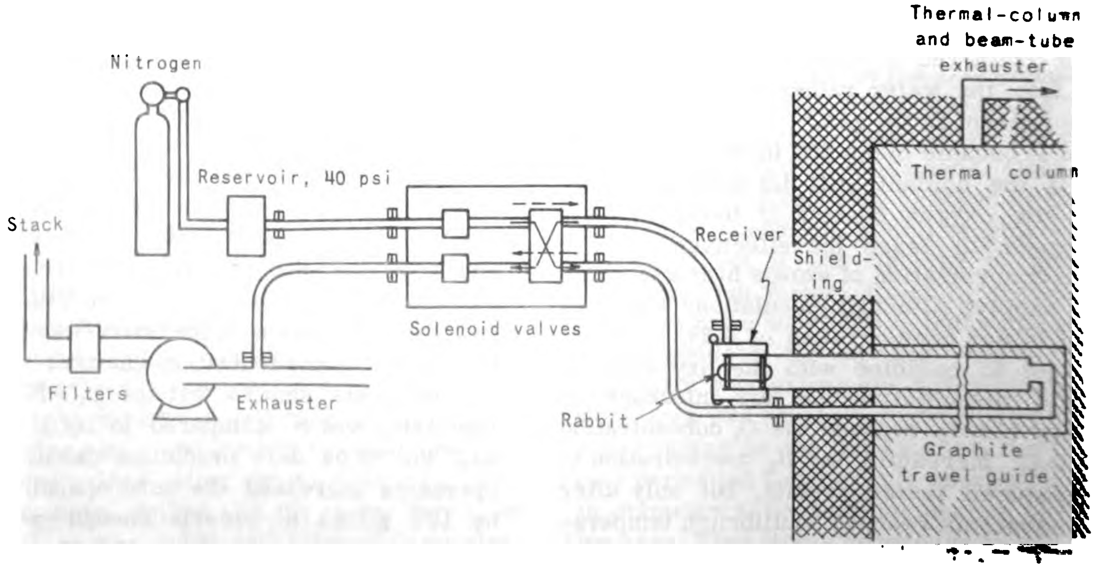

Fig. VIII-6 Pneumatic system controlled by solenoid valves supplies 40-psi nitrogen pulse for insertion and return of rabbit.[11]

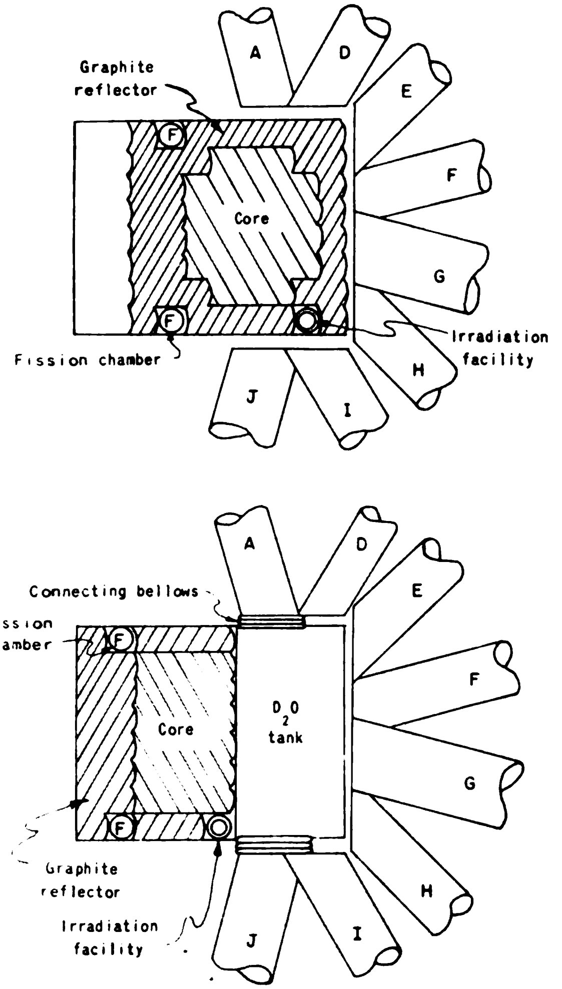

g. VIII-7 *Arrangement of core, graphite reflec-r, and beam tubes of the University of Michigan actor was modified from standard configuration ›p) by adding D_2O reflector next to north face of re (bottom).*[12]

tritium content in the tank will be checked every 800 Mw-hr to ensure that it does not exceed 50 curies; production-rate measurements predict that the D_2O will not need reprocessing or replacement until the reactor has operated 15,800 Mw-hr. Calculations had predicted a neutron-flux peak in the tank of twice the core flux, but preliminary measurements in the tank show that no peak occurs. No evidence of D_2O radiolysis has been detected.

Hallam Operation in Retrospect

By Fred A. Smith

The future operation of the Hallam Nuclear Power Facility has been under serious consideration since the reactor was shut down in September 1964, after failure of seven moderator elements,[13,14] and August 1965, when the U. S. Atomic Energy Commission announced termination of its operating contract with the Consumers Public Power District of Nebraska. Nevertheless, the operating experience gained in starting up and operating the 250-Mw(t) sodium-cooled graphite-moderated reactor is well worth reviewing because of its applicability to other reactors, particularly those cooled by sodium.[15–22]

On the basis of a review of the information on Hallam testing, startup, operation, problems encountered, corrective steps, and recommendations for improving plant performance and reliability, I have summarized highlights and

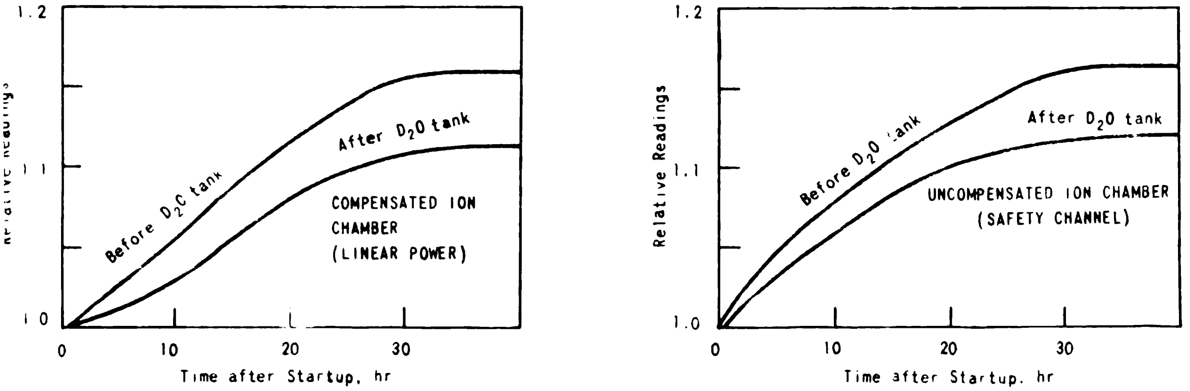

Fig. VIII-8 Effect of D_2O reflector on reactor ionization-chamber readings (average data from 10 runs before and after tank installation).[12]

have attempted to evaluate the significance of this experience. For convenience, I have considered the experience in three categories: normal operation, difficult component problems, and unresolved problems.

Summary

In general, the 80-Mw(e) plant performed well until the moderator elements failed.[14,23–25] Figure VIII-9 summarizes the plant operating history. The measured core-physics parameters agreed well with predictions. Although the sodium-heated steam generators operated safely, they were not in service long enough to appraise realistically their operating and maintenance costs. The numerous difficulties encountered in operating with sodium components, and some caused by sodium chemistry, emphasize the need for progress in these technologies.

Normal Operating Experience

As with the startup and early operation of most power plants, many Hallam activities and components gave no trouble, and others caused minor difficulties that required modifications involving only modest cost and time to make.

Plant Preoperational Tests. These tests, which involved 57 systems or functions,[20] began after "beneficial occupancy" of the facility in August 1961. Dry criticality was achieved in January 1962. Then seven months of system checkout were required before wet criticality was attained on Aug. 25, 1962. Rise-to-power tests followed; electricity was generated May 29, 1963, and full power was reached in July 1963. Thus the total time to take this plant from postconstruction occupancy to full power spanned 23 months. This accomplishment must be classed as a successful, normal operating experience much like that which should be expected for any nuclear plant of this size and complexity. Although some of the systems tested contained components whose operation later proved to be difficult or presented unresolved problems, the plant test program represents a successful joint venture between Atomics International, Consumers Public Power District, and the U. S. Atomic Energy Commission.

Initial Sodium Fill. The primary and secondary systems were initially filled with 741,500 lb of sodium in a problem-free operation similar to the large-scale transfers sodium at Fermi and Experimental Breeder Reactor No. 2 (EBR-II). An electrically heated oil-circulation system liquified the sodium which was pumped electromagnetically from railroad tank cars. Plant cold traps reduced the oxide content of the sodium enough that the sodium plugging temperature was brought below 250°F after only approximately 24-hr operation in the secondary system and approximately 36 hr in the primary system.

Nuclear Tests. In general, calculated and measured nuclear reactivity values agreed excellently. In criticality tests[26,27] sodium worth at 350°F in a 53-element core was measured as −6.1% $\Delta k/k$; the value calculated was −5.5 $\Delta k/k$. For the 140-element cold, clean core, k_{eff} was measured as 1.109 (9.8% $\Delta k/k$); the predicted value was 1.069 (6.5% $\Delta k/k$). Measurements of zero-power temperature coefficients of reactivity[28] showed the isothermal coefficient of reactivity to be +0.123 cent/°F at 400°F and +0.088 cent/°F at 500°F. With 20% sodium flow in the primary system, the "prompt" power coefficient is −0.4 cent/Mw and is −0.05 cent/Mw(t) at 240 Mw(t) with 96% sodium flow.

The peak of ^{135}Xe buildup[29] occurs approximately 4.5 hr after a scram from full power and is worth −263 cents · of reactivity. Samarium-149 has a peak buildup of 160 full-power days and an equilibrium worth of −122 cents.

For power operation, investigations of control-rod patterns[30] indicate that the axial power distribution has a range of peak-to-average ratios of 1.40 to 2.62.

Plant Control System. A number of minor problems were experienced. These related to faulty components, fabrication errors, and design shortcomings.

Of 13 interrelated subsystems of the plant control system, 7 demonstrated satisfactory operation without any corrective action. The satisfactory systems were the (1) plant power control, (2) nuclear power control, (3) fuel-temperature and coolant-flow ("convection power") control, (4) outlet steam ("attemporator") control, (5) steam-generator pressure-relief control, (6) primary block-valve control, and (7) secondary-flow control. Minor modifications were required to the division-of-load

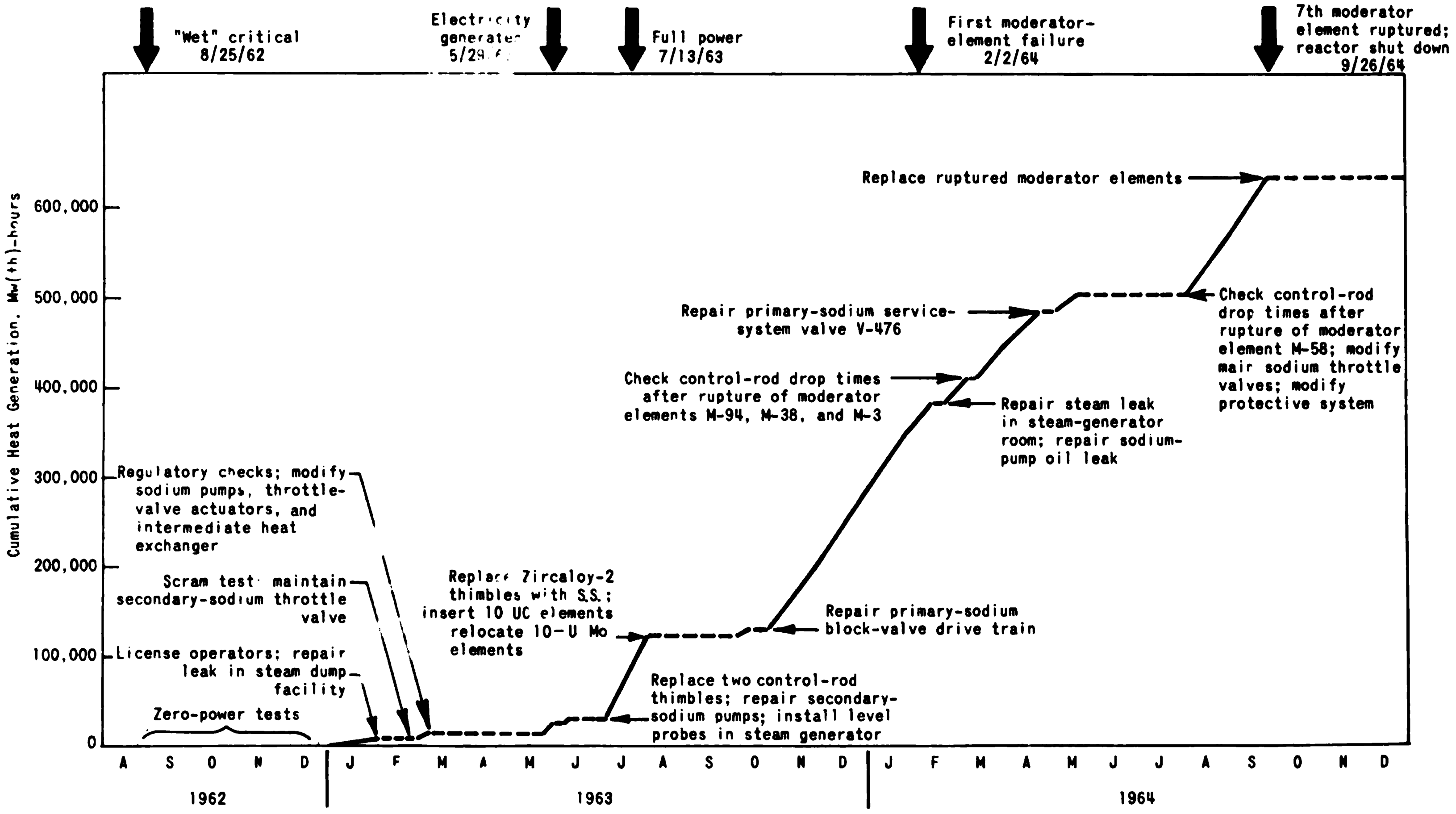

Fig. VIII-9 Summary of Hallam reactor operating performance shows cumulative thermal power generated vs. time and reasons for various outages. Before the last shutdown, moderator-element failures during 1964 seriously affected operations; a 1668-hr outage followed failure of moderator element M-58. Two other 1964 outages lasted 230 and 253 hr; 12 others lasted less than 100 hr each.[59]

computer, moderator–coolant control, and steam-dump control systems. Although the primary-sodium flow control system has operated satisfactorily, the need for the existing recorder–controllers for this system should be evaluated more completely for actual plant load-following conditions.

The neutron-flux control system encountered difficulties because of below-average reliability of components. However, after more reliable plug-in components were installed, the neutron-flux control system operated uninterruptedly longer and was easier to maintain. Feedwater-level control posed a difficult problem; because level control was limited by the lack of vertical head in the horizontal steam generator, it was really a problem of steam-generator design rather than of instrument control.

In general, the overall control system has responded excellently to intentional transients.[31] On one occasion the operator manually overrode the instruments, which resulted in a reactor scram. Subsequent investigation revealed that the automatic control-rod response had been legitimate.

On another occasion, when both the conventional and nuclear plants were operating simultaneously and the conventional boiler suddenly dropped off the line, nuclear response was immediate. As designed, the reactor picked up the full turbine load faster than approximately 20%/min.

Control-Rod Operation. The control-rod design speeds were verified by preoperational tests in air.[32] No change in drive speed and no malfunctions were found when the control rods were tested again during the plant rise to power.[33] There were small differences in design-vs.-actual rod drop times for the 9-ft free fall and full drop-to-snubber closure, but they were well within specifications.

Faulty magnets, shorted coils, and improper limit switches caused spurious scrams of the control rods. After the causes of these problems were corrected, the control rods worked perfectly. Although the difficulties with the rod drives involved normal installation adjustments, the original control-rod-drive thimbles, which were to keep the control rods in a dry helium atmosphere, failed; they are discussed further under the subsection Unresolved Problems.

Reactor Heat-Transfer Systems. Overall performance of the heat-transfer system has been equal to or better than design. Total heat losses were independent of load and remained at approximately 1.5 Mw(t), which is less than a 1% loss at full load. High-temperature, high-flow, and low-pressure operation has been effected satisfactorily for prolonged periods. Reactor operation as a load-following plant has been very successful.

Sodium Mechanical Pumps. Both during preoperational testing and after plant power operations, the six vertically mounted overhung mechanical type pumps had to be removed for maintenance.[19] Subsequently, these centrifugal and free-surface pumps (the primary and secondary systems each have three) were modified to: (1) loosen the diametral running clearances of the impeller upper and lower wear rings, (2) make more uniform the temperature distribution of the exterior casings of the pumps so as to prevent impeller binding, (3) provide greater area for sodium flow from the bearings to the pump suction, and (4) install sintered metallic filters to prevent foreign material (beads from the welding rods that had been used in fabricating the steam generators) from entering the secondary-system pumps. Since these corrections, overall performance of the pumps has been satisfactory. Fortunately, like the EBR-II and Fermi mechanical pumps, the Hallam pumps were designed so that that the impeller and shaft can be removed relatively easily from the volute casing, making field maintenance possible.[19] It is easier to remove, maintain, and replace a sodium pump than a deep-well pump, a boiler feedwater pump, or a similar major pump.[34]

Leakage Through Sodium Valve Seats. For plant safety the sodium in the reactor drain and fill lines must be kept molten by heating the lines. However, seepage of radioactive sodium across the drain-line valves limited personnel access to the sodium service cell (where the cold and hot traps are located) during reactor operation. To avoid the problem, a bypass line has been installed in the primary-sodium service system to connect each main coolant loop to the drain tanks without passing through the sodium service cells.

Bellows-Seal Valves. The bellows in about 11% of the 2-in. (or less) sodium valves in the cold-trap and drain circuits have failed. Most of the leaks occurred on valves that were

rtially open for throttling service—none of
e bellows valves that normally are either
lly open or closed failed. The bellows-seal
lves that have not leaked were operated
bsequently as stop valves. The failed valves
ve been replaced with freeze-seal valves or
ced orifices, both of which are recommended
r future installations. It also has been recom-
ended[35] that the number of throttle valves
ould be minimized in future sodium plants
d that any bellows-seal valves be tested
oroughly at various openings and with sodium
rbulence to be certain that any bellows will
ot oscillate.

Plugging Meters. These units, which indi-
ate the oxide concentration in sodium, have
perated well in each of the primary and sec-
ndary systems. However, to eliminate poor
ushing of the plugged area when the oxide
aturation temperature approaches the bulk so-
ium temperature, a minor modification would
e desirable—a heater should be added to
aise the temperature of the sodium flowing
hrough the meter above the bulk sodium tem-
erature.[36]

Handling of Core Components. These han-
ling operations have involved the movement of
uel elements and control-rod thimbles and,
nore recently, the removal of moderator ele-
nents. Facilities for cleaning and inspecting
ore components have operated as designed.[37,38]
he fuel-handling machine and its gantry and
rolley assembly were tested with a core
nockup vessel before delivery to the site.[39]
hus the system has operated well with only
ninor changes required since installation. This
uccess indicates the desirability of pretesting
ull-size components. Hallam experience with
andling damaged core components points up
he desirability of handling-equipment designers
iving thought to being able to dislodge and re-
nove damaged core components expeditiously.

Difficult Component Problems

The operation of some components and systems revealed considerable or sustained difficulties that involved substantial cost and time to correct.

Nuclear Instruments. Electrical noise interference, high instrument temperatures, and difficulty in achieving rapid response have been problems. Power-range instruments required only minor modifications. But the intermediate-range log-N instruments encountered difficulties caused by poor design and poor quality control. Because the average signal-to-noise ratio was only 5 : 1, the startup-range channels initially provided readings with fluctuations of far greater magnitude than normally associated with nuclear statistics.

These instrument problems were greater than should be expected. An evaluation[40] report recommends more stringent performance specifications for future plants to eliminate extensive testing, repair, and modification of nuclear instrumentation.

Plant Protective Instruments. The main functions of this system,[41] which is separate from the plant regular control systems, are to prevent inadvertent hazardous operation and to detect off-normal conditions and then act automatically to prevent damage to the reactor system or heat-transfer-system components.

Tests and use of the plant protective system[42] led to numerous improvements that eliminated (1) noise caused by poorly regulated a-c power, (2) noise caused by the grounding pattern, (3) drift related to insufficient cooling, (4) short lifetime of mechanical "choppers" in the amplifier, and (5) interaction between protective-system components. With these modifications the system proved to offer adequate protection against potentially hazardous conditions. For future designs of such systems, it has been recommended that electric power be regulated at the point of end use rather than at the source with a common regulator.[43] Future designs also should be studied closely for clear definitions of the purpose and function of protective-system components.

Control-Rod Thimbles. The control-rod thimbles were intended to isolate the rods from the reactor sodium by containing them in a pressurized helium atmosphere.[41] The reason for the selection of a dry control-rod system was the state of development of mechanisms in sodium at the time the design was fixed. However, the Zircaloy-2 walls of 3 of the 19 thimbles cracked early in the prestartup tests of the primary sodium system. Study indicated[44] that a possible cause of the failure was hydrogen embrittlement due to the diffusion into the Zircaloy-2 of hydrogen from the titanium hydride used as a shielding material in the control-rod-drive housing. (For more information on hydrogen embrittlement of Zircaloy, see page 245.) It is interesting to note that earlier engineering proof tests of the control-rod-drive mechanism and thimbles in sodium were conducted without the titanium hydride shielding installed. The problem was solved when all 19 Zircaloy-2 thimbles in the reactor were replaced with thimbles of type 304 stainless steel.

Throttle Valves. The Hallam primary-system throttle valves are freeze-seal ball valves actuated by a double jackscrew driven by an air motor.[45] Difficulties were encountered with the valve actuator, shafts, torque limiter, and jackscrews. Although the various modifications eventually resulted in satisfactory operation, the problems were bothersome and both they and the corrective measures involved an extended period of time.

Intermediate Heat Exchangers. Vibration caused a tube to fail in one of the three intermediate heat exchangers—which convey heat from the radioactive primary-system sodium to the nonradioactive sodium in the secondary system—in November 1962, which was before the reactor was used to produce power. Analysis indicated that failure was caused by flow-induced vibration in the shell (secondary) side near the sodium inlet baffles.[46] The natural frequency of vibration was changed when shims were installed between tube rows in the 12 to 15 ft/sec sodium inlet area. Subsequent tests and operations indicate that the vibration ceased. Nevertheless this internal modification was difficult to make.

More favorable was the fact that the heat transferred by the intermediate exchangers was within 12% of the value predicted,[26] and it did not vary significantly over the plant history. Pressure drops were greater than predicted—6 vs. 1.2 psi on the primary side and 14 vs. 6.8 psi on the secondary side. These greater than predicted drops are of little concern because the pump head is sufficient to achieve the flows required.

Steam Generators. These units, of which there are three, are described in Refs. 19, 20, 41, 47, and 48. When plant auxiliary steam was used to preheat the steam generators to 300°F before they were filled initially with sodium, the steam did not distribute the heat evenly over the entire steam generator. This relatively minor problem was corrected by maintaining a partial vacuum on the steam generator w admitting the preheat steam; this proce distributed the heat so that temperatures w within ±25°F.

A more difficult problem arose during t tests for the initial rise to power. The thr steam generators had 0.60 to 0.70% liq water in the steam leaving the separator, wh exceeded the maximum acceptable moistu carry-over of 0.25%. After numerous tests,[4 it was found that the water level was droppi enough that some of the horizontal sodiu heated tubes did not have water over the Water level was varying as much as 5 in. at f power. Thus carry-over was limited by t installation of more precise control equipme to hold the water level in the evaporator se tion within ±0.7 in. at full power. With thes conditions the steam separators have li capacity above their steam rated capacities 251,000 lb/hr.

Although it is significant that the overa heat-transfer coefficients for steam generat have remained essentially constant (wh means no fouling has occurred) and that t steam generators have not leaked sodium t air or to water (which testifies to the safety the design bases and the fabrication quali control), the need for the numerous tests a modifications to solve the moisture carry-ove problem makes it necessary to consider t experience with Hallam steam generators a having been difficult.

Gas Entrainment in Sodium Expansion Ta Originally, all sodium in the three seconda system parallel loops flowed through an expansion tank in each loop. During preoperational tests, it was discovered that heliu cover gas in the expansion tanks became entrained by the sodium and circulated throu the system. Although this problem was eliminated by modifications that caused 96% of t sodium flow to bypass the expansion tanks this type of design deficiency cannot be co- sidered normal; the modifications requir approximately three months to complete. O of these expansion tanks cracked during la operation; because this problem has not bee rectified, it is discussed in the next subsecti

Unresolved Problems

Operating experience uncovered some pro lems that either have no positive means rrection or whose resulting difficulties have t yet been corrected.

Crack in Sodium Expansion Tank. The shell one of the three expansion tanks in the secdary systems cracked near a nozzle.[52] The ack was caused by weld-rod coating entrapent at an internal baffle plate (the lesson arned from this is that internal welds require ecifications similar to external sodium-coninment welds). Analysis of the nature of this dium-leakage failure indicates the desirality of replacing all three tanks if the plant to resume operation.[53] Such a change would a relatively minor task.

Cold Traps for Oxide. Although the initial ficiency of the cold traps, estimated as nearly 0%, shows their ability to keep the oxide conent of the sodium low, the operator must either eriodically replace the 10 to 12 plugged cold aps or install larger traps. The original aps plugged relatively rapidly because of the xide that formed in the sodium during the reairs and modifications to the secondary system nd the intermediate heat exchanger.

Because of mechanical interference, mainenance men must enter the cell to remove the rimary-system cold traps.[54] This is no probem now, but, if a fuel cladding fails and leaks ission products into the sodium, remote methds might have to be devised to replace the raps.

Hot Traps for Carbon. To monitor the carbon ontent of the primary-system sodium, operaors placed type 304 stainless-steel tabs at the odium inlet of a carbon trap. After being held t 1200°F in the 30 to 40 gal/min sodium flow or 100 hr, the tabs were removed and analyzed hemically and metallurgically. These tabs showed no evidence of carburization.[55] In contrast, when fresh type 304 stainless-steel tabs were exposed statically at 1200°F for 100 hr to a sodium sample withdrawn from the carbon trap, the tabs invariably carburized to a range of 4 to 147 ppm. Obviously, the problem of understanding and measuring the chemical effects of various forms of carbon in sodium is still unsolved.

Freeze Traps for Sodium Vapor. Condensation or freeze traps are installed at high points in the reactor auxiliary sodium systems to remove sodium vapor from the cover gas that is vented or purged when the sodium system is being drained or filled.[56] Each of these traps contains a sodium-level float valve that controls the leakage of cover gas to the vent; the valve opens the gas path to the vent when the rising sodium level raises the float, which engages a cam that operates a shaft running through a sodium "freeze seal." However, the shaft packing that contains and backs up the freeze seal has leaked helium and permitted some liquid sodium to leak through the shaft annulus into the vent, which plugged it. Also, because of the variable resistance of the freeze seal, excessive manual pressure has been applied to this shaft, which broke on several occasions.

Although these problems have not been so severe as to warrant redesign of the Hallam system, a better system for venting and filling inert gas is needed for future sodium plants. (For more information on inert-gas systems and vapor traps, see page 259.)

Fuel-Channel Orifices. Adjusting the coolant flow by means of variable orifices in each fuel channel in the core allowed the operators to hold coolant exit temperature from each channel to within 15°F of the average.[41,57] Flow through the orifice could be adjusted 30 to 100% by moving the orifice plug its full 4-in. stroke; at 100% flow, 4-in. travel changes sodium temperature at the channel exit 90 to 150°F. However, the inability to move some of the plugs, due primarily to sodium oxide, has limited the use of these devices. Twelve orifices became either fully closed (but there is also a bypass), stuck, or broken. In other cases, when the drive cable would remain in tension after turning was difficult, the orifice plug would "creep" so that further adjustment would be necessary.

Although these fuel-channel variable orifices could be improved by replacing the flexible shaft with a rod or by installing a bellows, it was not practical to make changes on the initial core.

Moderator-Element Failure. Leakage of the type 304 stainless-steel cladding on the graphite moderator elements[41,58] was a significant event of major proportion in that it necessitated shutting down the plant for core repairs. By the end of September 1964, the cladding on seven moderator elements had failed and had flooded the elements with sodium; Fig. VIII-10 shows the core locations of the failed and suspect moderator elements.[34] This flooding reduced core reactivity, tilted the flux, and depressed the power, by which means the failures were detected and the suspect failed elements were identified[59] (see Table VIII-1); these tests indicated that 8 and possibly 9 moderator elements had failed, but subsequent examination with boroscopes and electromagnetic probes showed that only 7 elements had failed. However, this leakage also permitted the sodium to react with the graphite, which swelled the elements and caused 19 fuel elements to become stuck in place (none of the thimble-enclosed control rods stuck.)

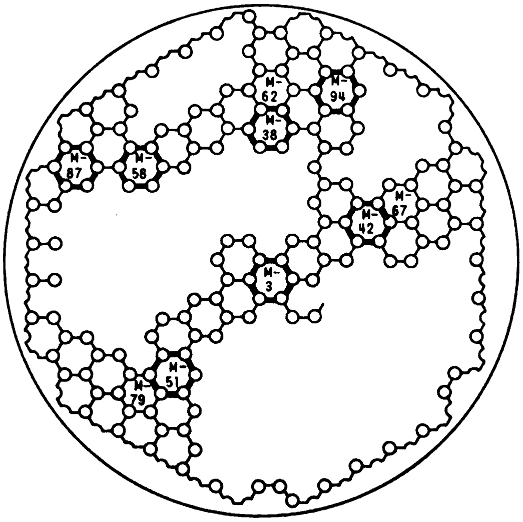

Fig. VIII-10 Locations in the core of the failed and suspect moderator elements.[34] The seven cans that actually failed are shown with heavy borders. Element M-87 was not suspected initially. On the basis of flux patterns, M-62 and M-67 were suspected, and M-79 was regarded as a possible failure, but examination showed that all three were intact.

Subsequent core-repair work removed the 19 stuck fuel elements; the 7 failed moderator elements, together with 3 others that suffered damage in the handling operations, were replaced with 10 new moderator elements on July 12, 1965.

A review of the moderator-element design, material specifications, and inspection and fabrication methods that was made before the failed elements were removed uncovered no obvious reasons for the failures, although it cast suspicion on rewelds that were made in initially defective welds.[60] Although the final report on the detailed examination and analysis of the cans was not available as of this writing, Fig. VIII-11 shows a typical crack, which occurred approximately 3 in. from the top of the element in core position M-42. Six element cans cracked in similar locations; metallographic study of the type 304 stainless steel near the cracks revealed little or no

Table VIII-1 REACTIVITY REDUCTIONS WHEN MODERATOR-ELEMENT CANS CRACKED AND SODIUM ENTERED ELEMENTS[34]

			Reactivity reduction, cents					
Moderator-element location	Date ruptured	Date of additional disturbance	Actually observed		Corrected for rod-calibration error		Predicted worth*	
M-94	2/2/64		3		4		4	
M-38 and M-62	2/2/64 and 2/20/64–2/22/64		9	25	10.5	29	20 (M-38) 11 (M-62)	31
		3/6/64–3/12/64	9		10.5			
		3/29/64–4/5/64	7		8			
M-3	3/4/64		18		21		21	
M-58	5/15/64		16		19		18	
M-51	9/9/64		23		23		20	
M-42 and M-67	9/26/64		25	43	25	43	23 (M-42) 20 (M-67)	43
		9/27/64–9/30/64	18		18			
Total			128		139		137	

*Predicted worth is determined by flux weighting to corrected-observed worth of M-3 as base.

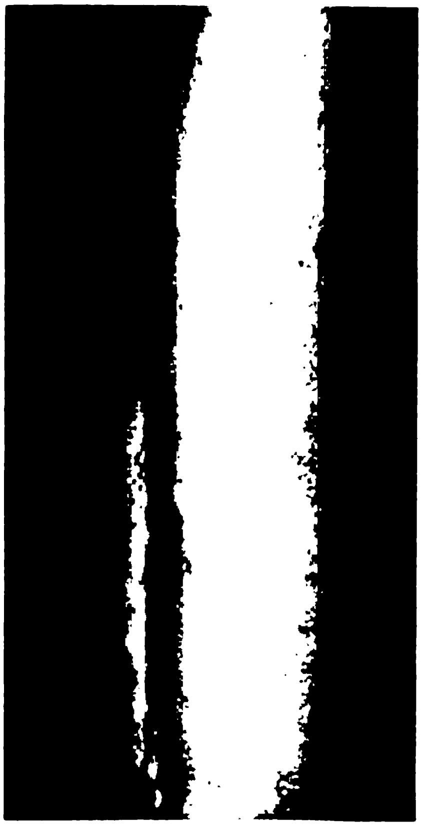

g. VIII-11 *Crack that occurred near the top of the n on moderator element in core position M-42 is pical of the cracks in six of the seven failed cans.*[34]

inning or grain distortion[62] but found inter-ranular separation of the type that occurs om long-term stress in the range of creep eformation (below the yield stress). In this rea near the top of the cans, which contain a acuum, the thin type 304 stainless steel is not pported by the graphite. Although a series of ingers" is intended to support the cladding all, in six of the failed cans some of the ngers did not give support.[63] (The seventh lement failed rapidly when the swelling of the her elements damaged a process tube, which uged the seventh can.)

The plant designers believe the problem can e solved by eliminating the vacuum in the 41 moderator cans.[63] This could be done within out six months by installing on each mod-rator element an 11-ft snorkel tube that would nt it to the inert cover gas above the sodium rface in the reactor vessel.

From studies made of the design of the failed oderator elements,[64] it is now clear that the Hallam design does not represent an engineering extrapolation of the moderator elements used in the Sodium Reactor Experiment.[65] Future liquid-metal-cooled reactor designs must be considered carefully to determine precisely which features are truly represented by previous experience and to identify design features that involve advancements in the state of the art and therefore constitute a performance risk.

References

1. J. A. Prestele, Operating Experience at Indian Point, *Trans. Am. Nucl. Soc.*, 8(Suppl.): 30-31 (1965).
2. Robert Campbell and Joseph A. Signorelli, Elk River Reactor Operations, *Trans. Am. Nucl. Soc.*, 8(Suppl.): 31 (1965).
3. Glen A. Reed, Major Operating and Refueling Problems at the Yankee Atomic Electric Company Rowe Power Plant, *Trans. Am. Nucl. Soc.*, 8(Suppl.): 28 (1965).
4. R. E. Heffner, Failure of SPERT III Pressurizer Vessel, *Trans. Am. Nucl. Soc.*, 5(1): (1962); also USAEC Report IDO-16743, Phillips Petroleum Company, January 1962.
5. R. E. Heffner, Six-Years Operating Experience with PWR Plant Components, *Trans. Am. Nucl. Soc.*, 8(Suppl.): 29-30 (1965).
6. J. I. Riesland and E. A. Gustafson, Work Performed on Fuel Channels and the Core Support Plate at Big Rock Point Nuclear Power Plant, *Trans. Am. Nucl. Soc.*, 8(Suppl.): 5-9 (1965).
7. L. M. Hausler, R. L. Haueter, and R. C. Christianson, In-Vessel Modification of Irradiated Reactor Internals at Big Rock Point, *Trans. Am. Nucl. Soc.*, 8(Suppl.): 3-5 (1965).
8. C. Arthur Dalke, Elimination of Hydraulically Induced Core Vibrations in the General Electric Test Reactor, *Trans. Am. Nucl. Soc.*, 8(Suppl.): 2 (1965).
9. Nils Rydell, Some Aspects of Operating Experience at Ågesta Nuclear Power Plant, *Trans. Am. Nucl. Soc.*, 8(Suppl.): 31-32 (1965).
10. R. V. Dulin, Control of Oxygen in PRTR Helium Systems, *Trans. Am. Nucl. Soc.*, 8(Suppl.): 46-47 (1965).
11. Arthur de Saint Maurice and Richard Canfield, Thermal-Column Pneumatic Facility, *Trans. Am. Nucl. Soc.*, 8(Suppl.): 1 (1965).
12. Robert D. Martin, Operating Experience with a Heavy-Water-Reflector Tank, *Trans. Am. Nucl. Soc.*, 8(Suppl.): 46 (1965).
13. Consumers Public Power District, HNPF Monthly Operating Report No. 36, p. 1, July 1965.
14. R. H. Davidson, Moderator Element Failures in the HNPF, *Trans. Am. Nucl. Soc.*, 8(Suppl.): 35 (1965).
15. Consumers Public Power District, HNPF Monthly Operating Reports, A Series, Nos. 1–37.
16. Atomics International–AEC Chicago Operations Office, HNPF Reactor Operating Analysis Reports, USAEC Reports, A Series, Nos. 1–28.
17. R. C. Gerber, Hallam Nuclear Power Facility, in Symposium Proceedings on Sodium Reactors

Technology, Lincoln, Nebraska, May 24–25, 1961, USAEC Report TID-7623, pp. 73-88.

18. W. P. Venable, Integration of Hallam Nuclear Power Facility into Consumers Public Power District of Nebraska System, in Symposium Proceedings on Sodium Reactors Technology, Lincoln, Nebraska, May 24–25, 1961, USAEC Report TID-7623, pp. 89-96.
19. H. O. Monson et al., Components for Sodium Reactors, presented at the Third United Nations International Conference on the Peaceful Uses of Atomic Energy, Geneva, 1964, Paper A/Conf.28/P/228.
20. Atomics International, Final Evaluation Report, Hallam Nuclear Power Facility, USAEC Report NAA-SR-9777(Vols. I–VI), 1964.
21. L. E. Keller and R. H. Davidson, Hallam Operating Experience, *Nucl. Safety*, 7(2): 236-242 (Winter 1965–1966).
22. K. K. Brown, Operating Hallam, *Nucleonics*, 22(9): 41-46 (September 1964).
23. J. D. Cochran, Operating Experience at Hallam Nuclear Power Facility, in *American Power Conference, Chicago, Illinois, March 26–28, 1963*, Vol. XXV, pp. 204-212.
24. J. D. Cochran and J. E. Owens, Initial Operation of the Sodium Graphite Reactor at the HNPF, in *26th Annual American Power Conference, Chicago, Illinois, April 14–16, 1964*, Vol. XXVI, p. 201.
25. Emerson Jones and J. D. Cochran, HNPF Operating Experience and Testing to 250 Mw(t) to November 1, 1963, USAEC Report TID-20396, November 1963.
26. J. E. Price (Comp. and Ed.), Final Evaluation Report, Hallam Nuclear Power Facility, USAEC Report NAA-SR-9777(Vol. I), p. 34, Atomics International, Sept. 29, 1964.
27. J. E. Price and J. W. Rocke (Eds.), Final Evaluation Report, Hallam Nuclear Power Facility, Wet Excess Fuel Loading, AI-PC-710, USAEC Report NAA-SR-9777(Vol. VI), Atomics International, June 12, 1964.
28. *Ibid.*, Zero Power Coefficients of Reactivity, AI-PC-760.
29. *Ibid.*, Xenon Poisoning, AI-PC-840.
30. *Ibid.*, Power Coefficient, AI-PC-770.
31. P. F. Shaw, HNPF Control System Response During Transient Conditions, USAEC Report NAA-SR-9584, Atomics International, June 15, 1964.
32. J. E. Price and J. W. Rocke (Eds.), Final Evaluation Report, Hallam Nuclear Power Facility, Control Rod Drive and Actuator Assemblies, AI-P-1145, USAEC Report NAA-SR-9777(Vol. III), Atomics International, June 12, 1964.
33. J. E. Price and J. W. Rocke (Eds.), Hallam Nuclear Power Facility, Master Schedule Including Rise-to-Power, AI-PC-830, USAEC Report NAA-SR-9777(Vol. VI), Atomics International, June 12, 1964.
34. Ivan O. Sunderman, Consumers Public Power District, personal communication, Sept. 17, 1965.
35. J. E. Price (Comp. and Ed.), Final Evaluation Report, Hallam Nuclear Power Facility, USAEC Report NAA-SR-9777(Vol. I), p. 17, Atomics International, Sept. 29, 1964.
36. *Ibid.*, Sodium Service System, AI-P-1104.
37. J. E. Price and J. W. Rocke (Eds.), Final Evaluation Report, Hallam Nuclear Power Facility, Wash Cells, AI-P-1133, USAEC Report N SR-9777(Vol. III), June 12, 1964.
38. *Ibid.*, Maintenance Cell., AI-P-1139.
39. W. A. Kaspic, Experimental Testing of C Component Handling Equipment and Handl Techniques for Hallam Nuclear Power Fac USAEC Report NAA-SR-7785, Atomics Inter tional, Sept. 15, 1964.
40. J. E. Price (Comp. and Ed.), Final Evalu Report, Hallam Nuclear Power Facility, US Report NAA-SR-9777(Vol. I), p. 69, Atomics ternational, Sept. 29, 1964.
41. Atomics International, Final Summary Sa guards Report for the Hallam Nuclear Po Facility, USAEC Report NAA-SR-5700, pp. 2 269, Apr. 15, 1961.
42. J. E. Price (Comp. and Ed.), Final Evalu Report, Hallam Nuclear Power Facility, US Report NAA-SR-9777(Vol. I), p. 60, Atomics ternational, Sept. 29, 1964.
43. *Ibid.*, p. 63.
44. R. K. Wagner and S. L. Essglebert, Results HNPF Control Rod Thimble Examinatio USAEC Report NAA-SR-TDR-9142, Atomics ternational, October 1963.
45. J. E. Price (Comp. and Ed.), Final Evalu Report, Hallam Nuclear Power Facility, US Report NAA-SR-9777(Vol. I), pp. 13-17, Atom International, Sept. 29, 1964.
46. R. E. Durand, Operating Experience with Intermediate Heat Exchangers at HNPF, USAEC Report NAA-SR-9718, Atomics Internation June 15, 1964.
47. Robert W. Dickinson and John B. Willia Trends in Sodium Equipment, *Nucleonics*, 19 65-70 (January 1961).
48. Frank Boni and Philip S. Otten, Fermi and Hal Steam Generators, *Nucleonics*, 19(6): 58-61 (J 1961).
49. Consumers Public Power District, HNPF O erating Report for December 1963.
50. Atomics International, HNPF Reactor Operat Analysis Program, Semiannual Progress Rep No. 2, March 1–August 31, 1963, USAEC Rep NAA-SR-9265, pp. 105-111, Mar. 1, 1964.
51. J. E. Price (Comp. and Ed.), Final Evalu Report, Hallam Nuclear Power Facility, M Heat Transfer System, AI-P-1103, pp. 12- USAEC Report NAA-SR-9777(Vol. I), Atom International, Sept. 29, 1964.
52. Consumers Public Power District, HNPF Mon Operating Report No. 26, October 1964.
53. Consumers Public Power District, HNPF Mon Operating Report No. 28, December 1964.
54. J. E. Price (Comp. and Ed.), Final Evalu Report, Hallam Nuclear Power Facility, US Report NAA-SR-9777(Vol. I), p. 52, Atomics ternational, Sept. 29, 1964.
55. Atomics International, HNPF Reactor Operat Analysis Program, Semiannual Progress Report No. 1, September 1, 1962, to February 1963, USAEC Report NAA-SR-8401, July 1, 19
56. J. E. Price (Comp. and Ed.), Final Evalu Report, Hallam Nuclear Power Facility, US Report NAA-SR-9777(Vol. I), p. 54, Atomics ternational, Sept. 29, 1964.
57. J. E. Price and J. W. Rocke (Eds.), Final Eval tion Report, Hallam Nuclear Power Fac Radial Power Distribution and Fuel Cha

Orifice Adjustment, AI-PC-800, USAEC Report NAA-SR-9777(Vol. VI), Atomics International, June 12, 1964.

. *Power Reactor Technol.*, 5(3): 39-51 (June 1962).

. Atomics International, HNPF Reactor Operations Analysis Program, Semiannual Progress Report No. 4, February 29–September 30, 1964, USAEC Report NAA-SR-10743, May 15, 1965.

. *Ibid.*, pp. 61-69.

. Consumers Public Power District, HNPF Monthly Operating Report No. 35, June 1965.

62. John J. Purcell, AEC Chicago Operations Office, Sodium Components Development Program, Project Coordination Report, Hallam Nuclear Power Facility, p. 12, August 1965.

63. *Nucl. Ind.*, 12(9): 11 (September 1965).

64. *Reactor Handbook*, 2nd ed., Vol. IV, Engineering, p. 677, edited by Stuart McLain and J. H. Martens, John Wiley & Sons, Inc., New York, 1964.

65. *Reactor Handbook*, 2nd ed., Vol. IV, Engineering, p. 665, edited by Stuart McLain and J. H. Martens, John Wiley & Sons, Inc., New York, 1964.

Section IX

Power Reactor Technology

Systems Technology

Advancements in Organic Coolants

By J. E. Sawyers, Combustion Engineering, Inc.

The investigations in organic-coolant technology have involved seven general aspects: (1) decomposition by radiolysis and pyrolysis, (2) additives to improve resistance to decomposition, (3) reclamation methods for used coolant, (4) fouling-film formation, (5) corrosion properties, (6) heat-transfer properties, and (7) possible new coolant materials. Although biphenyl and other organics have been studied, the major work has concentrated on the terphenyls, especially Santowaxes OMP and R. Much of the work summarized here is discussed[1] in detail in a comprehensive analysis of the status of organic-coolant technology through mid-1964.

Decomposition

Experiments on pyrolysis of biphenyl, orthoterphenyl, and metaterphenyl included limited investigations of gamma radiolysis.[2]

The pyrolytic exposures involved various durations at 750 to 825°F in an autoclave controlled within 5°F. After pyrolysis products were analyzed and molecular-weight distributions were measured, rate constants and heats of reaction were calculated. Orthoterphenyl pyrolyzes about five times faster than biphenyl and metaterphenyl. The data indicate that pyrolysis is a first-order reaction. Rate constants for all three materials increase with temperature and fit reasonably well to an Arrhenius plot. Calculated heats of reaction are 93 kcal/mole for biphenyl, 89 kcal/mole for orthoterphenyl, and 83 kcal/mole for metaterphenyl.

Probable mechanisms are discussed on the basis of reaction-product analyses. Calculations of entropies of activation (at 800°F) suggest formation of a high-entropy complex that subsequently reacts or decomposes to give the products observed.

The radiolysis experiments were conducted by surrounding the autoclave with spent reactor fuel elements. Low-temperature (below 500°F experiments, where pyrolysis is not significant, indicate that radiolysis depends on temperature—but there were insufficient data to determine this effect quantitatively. In a 775°F radiolysis experiment, exposure to 2.5 Mr/hr for 840 hr (2.1×10^9 r total dose) decomposed approximately twice as much organic as did pyrolysis alone in a control sample. Analysis of the radiolytic decomposition products suggests that the reaction mechanisms change as temperature increases. Gases produced by gamma irradiation in the absence of air include acetylene, ethylene, propylene, and propane. The observations that radiolysis rate and reaction mechanisms depend on temperature agree with work summarized earlier.[3]

The dose-rate effect on the radiolysis of paraterphenyl was investigated by exposing samples at approximately 660°F to electrons from a Van de Graaff generator.[4] Values of $G_{polymer}$, defined as the number of molecules of paraterphenyl converted to less-volatile material per 100 ev absorbed, were 0.17 to 0.2[illegible] G_{gas} values, defined analogously for conversion to gaseous products, were 0.017 to 0.037. Dose rates between 0.24 and 10 watts/g did not affect either $G_{polymer}$ or G_{gas}.

Reactor irradiations of Santowax OMP at 600°F in a loop in the MIT reactor have been reported.[5] After initial buildup of high boilers, unirradiated organic was added to maintain eir content at approximately 33 wt.%. Total radiation time was approximately seven onths (equivalent energy dose to the cool- t was not reported); specimens were taken roughout this time. Coolant viscosity, density, d average molecular weight remained essen- lly constant because of the coolant replace- ent. The Santowax OMP degraded to higher iler at the rate of 0.15 molecule per 100 ev sorbed.

Seventeen organic compounds, including 12 ndensed-ring polyaromatics, biphenyl, ortho- rphenyl, metaterphenyl, and paraterphenyl, d bibenzyl, were studied in pyrolytic and diolytic experiments.[6] The objectives were determine their general decomposition be- vior and parameters that correlate with it. l experiments were performed in vacuum and the range 375 to 840°F. A ^{60}Co gamma fa- lity and the Brookhaven Graphite Research eactor (BGRR) were used for the irradiations. amma-irradiated samples were exposed to $\times 10^8$ rads over 7 days; reactor-irradiated mples were exposed to 2.1×10^9 rads over days.

Gas production increases with temperature gamma radiolysis and in pyrolysis (no pro- sion was made for measuring gas from the GRR samples). For many compounds, pyroly- s and gamma radiolysis produced markedly ifferent concentrations of hydrogen and meth- ne. In general, the most common gases pro- uced were ethylene and propane, with less con- istent or smaller amounts of ethane, acetylene, nd about eight other gases.

The decomposition rate usually increases ith temperature, and the amount of decompo- ition in the radiolytic experiment always ex- eeded that from the control samples, in which nly pyrolysis occurred. Data for decomposi- on rate as a function of temperature reveal e same general relation for all compounds— ere is a temperature "breakpoint," below hich the increase in decomposition rate with emperature is not very substantial and above hich the increase becomes very marked. For given compound this apparent breakpoint oc- urs at about the same temperature during ra- iolysis as in pyrolysis, but it occurred at ower temperatures for the reactor-radiolyzed amples than for the gamma-radiolyzed sam- les. This difference is attributed to the three- old difference in irradiation times.

Experiments showed that, in general, aromatic carbon–carbon bonds are more stable against both radiolysis and pyrolysis than are aliphatic carbon–carbon bonds. The control pyrolysis experiments show that pyrolytic decomposition rate increases with time, that is, pyrolysis products form increasingly quickly as pyrolysis products build up. Thus the investigators concluded that the results of short-term pyrolysis studies cannot be extrapolated meaningfully to long exposures. On the basis of breakpoint observations, they recommend that the maximum operating temperature for these organic materials be in the neighborhood of 750°F to avoid extensive decomposition.

Several attempts were made to obtain a correlation between radiolytic stability and other compound parameters. Two of these parameters, singlet–triplet excitation energy and electron affinity, were reported to indicate some reasonable degree of correlation with radiolytic decomposition rate.

Six-Mev electrons have been used[7] to irradiate biphenyl, the three terphenyl isomers, and Santowax OMP at approximately 600°F to decompositions of approximately 40%. Five specific conclusions are reported: (1) second-order kinetics best describe the radiolysis reaction; (2) paraterphenyl is more stable than metaterphenyl, which is more stable than orthoterphenyl; (3) rate constants increase for successive steps in biphenyl radiolysis reactions; (4) concentration of molecular-weight multiples of the starting material (biphenyl or terphenyl) rises rapidly in the radiolysis-product fraction; and (5) there is a linear relation between total dose and molecular weight (up to $\sim 1.5 \times 10^{10}$ rads). Nuclear magnetic-resonance measurements were interpreted to suggest that part of the hydrogen generated during radiolysis might react with the polymeric products.

Additives

Irradiations with 6-Mev electrons were performed to determine the effects of selected additives on the radiolytic stability of terphenyl.[7] Total dose was 0.5 to 1.0×10^{10} rads at approximately 650°F. Additives that contribute substantial stability against electron radiolysis can be broadly described in three general groups: (1) elemental sulfur and compounds containing divalent or tetravalent sulfur; (2) fused-ring compounds structurally related to anthracene, in which either none of the rings, the end rings only, or the center ring only is hydrogenated and in which 9 and 10 positions of the center ring are occupied by sulfur, nitrogen, and carbon (or, in a few cases, oxygen) atoms; and (3) hydrogenated or partially hydrogenated fused-ring compounds not necessarily related to anthracene. They reduce electron radiolysis by approximately 10 to 25% when added to terphenyls in concentrations of 3 mole % or less. Compounds of the second group depend only slightly on concentration, but those of the first and third groups depend greatly on concentration — elemental sulfur is most effective at 0.7 mole %. Effectiveness of none of the better additives appears to depend much on temperature.

Electron and reactor irradiations have been used to measure how various additives affect the decomposition of biphenyl, Santowax R, and paraterphenyl.[8] The addition of small (10 to 20%) portions of paraquaterphenyl to biphenyl slows the decrease in biphenyl degradation by electrons slightly (≤20%) but does not significantly affect the reactor-irradiation results. In reactor irradiation of paraterphenyl, gas and high-boiler formation was slowed 10 to 20% by the addition of approximately 0.5% of any of various additives, including ferrocene, phthalocyanine, iron, copper, and cobalt phthalocyanines.

Coolant Reclamation

Catalytic hydrocracking has been studied as a means to reclaim used organic coolant.[9–11] In catalyst-screening experiments, cobalt molybdate, nickel oxide, platinum, and cobalt oxide plus vanadia (all on low-surface alumina, 50 to 80 m^2/g) proved to be efficient catalysts for terphenyls at 600 to 900°F and 500 to 1000 psig. Catalytic efficiency increased with phenyl chain length; nickel oxide on alumina was the most selective to chain length. Further experiments were performed with the cobalt molybdate and nickel oxide using coolant from core 2 of the Organic Moderated Reactor Experiment (OMRE) and several other synthetic terphenyl mixtures. Continuous-flow hydrocracking of OMRE core 2 coolant (23% high boilers) at 900°F and 1000 psig removed 90 to 100% of the high boilers and recovered 85 to 95 wt.%. of the feed as usable product (some material was lost as light ends and some deposited on the catalyst). The average molecular weight of the product was 205 to 225, compared to 270 for uncracked core 2 coolant.

Radiolytic stability of the cracking products was investigated by use of a linear accelerator for irradiations of 0.48 to 1.3 × 10^{10} rads at 650°F. The selectively hydrocracked material was slightly more stable than Santowax OMP. Although the hydrocracked material released up to four times as much gas as did Santowax OMP, the gas amounted to only approximately 0.3 wt.% of the sample, and total radiolytic decomposition was significantly less for the hydrocracked material. Pyrolytic stability of the reclaimed coolant also was studied in 48-hr experiments. No thermal high boiler was measured up to 650°F; results are interpreted to suggest a "threshold" for pyrolysis at 750 to 825°F.

Cost estimates were performed for a 1000-Mw [300 Mw(e)] organic-moderated and -cooled reactor that produces high boilers at either 25,000 or 50,000 lb/day. On the basis of equipment amortization within seven years, total cost for manufacturing hydrocracked usable coolant would be $0.083/lb (later revised to $0.07/lb) for the 25,000 lb/day case and $0.053/lb for the 50,000 lb/day case, compared to fresh terphenyl coolant costing $0.17/lb. Advantages of the hydrocracking reclamation process would be (1) reductions in coolant-makeup and waste-disposal requirements and (2) removal of film-forming material that would foul the fuel elements; these improvements would reduce overall operating costs. A disadvantage would be the possible net buildup in the coolant of biphenyl, whose high vapor pressure might cause reactor operating difficulties.

Economics estimates have been performed for catalytic hydrocracking processes to reclaim damaged coolants from the 11.4-Mw(e) Piqua Nuclear Power Facility.[12] Three hydrocracker feed schemes were considered: feed supplied from the bottoms of a flash tank, from the bottoms of the presently installed distillation column, and directly from the main coolant stream. Selective hydrocracking of either concentrated high boilers or total coolant would be efficient and economical, but flash-tank feed is recommended as the most economical. The plant for the flash-tank-fed hydrocracker recommended for Piqua would cost $300,000. It could maintain high-boiler concentration in the coolant below 10% and ash concentration at om. Without interest or taxes, payout time ould be approximately 4.6 years, with a sub-equent power-cost saving of 1.08 mills/kw-hr efore taxes (0.52 mill/kw-hr after taxes), as-uming full-power reactor operation 60% of the me.

Also studied briefly were the economics of a lash-tank-fed hydrocracker for a 500-Mw(e) rganic-cooled D_2O-moderated reactor that op-rates at full power 60% of the time. If a hydro-racker is used instead of a distillation system o maintain coolant quality, the estimated saving s $205,400/year, and the payout time is 1.0 ear if there are no taxes on the saving (or 1.9 ears with taxes) and if the unit is amortized over 7.5 years.

The study also evaluated whether hydrogen ould be recovered from radiolytic gases to educe hydrocracker operating costs. Although echnically feasible, such a process would be economically advantageous only with plants larger than Piqua.

Film Formation

Pyrolytic capsules were used for fouling tests performed to evaluate the film-forming tendencies of OMRE core 2 coolant.[13–14] These tests consisted essentially of maintaining coolant samples at 600°F for 24 hr under a nitrogen blanket while a stainless-steel tube held at 1050°F was immersed in the coolant, after which the amount of film deposited on the tube was measured. Results indicated that some coking did take place on the heaters and that ^{60}Co and ^{54}Mn concentrated on the heater surface to approximately 500 times their concentration in the coolant. Preliminary screening of adsorbents that might be useful in removing ^{35}S and ^{32}P from organic coolants indicated that metals and reduced oxides might be useful, and, in particular, a reduced nickel oxide hydrogenation catalyst showed good removal efficiencies for the concentrations used.

Engineering-scale equipment and static capsules were used for fouling studies and iron and water solubility studies.[6] In the static-capsule fouling tests, no fouling-film deposits nor detectable traces of alpha iron were found on the type 304 stainless-steel heater test specimens exposed to individual terphenyl isomers at 500 to 800°F. No correlation was apparent between the test conditions and the presence or absence of small amounts of alpha iron. Terphenyl generally absorbed or reacted with 1 vol.% oxygen placed in the cover gas. In the iron and water solubility studies, purified orthoterphenyl and paraterphenyl were covered with argon containing up to 6.5 vol.% water. No iron was found in the coolant. Water added to the coolant to a maximum concentration of 68 ppm did not noticeably affect iron solubility. Although water was slightly soluble in orthoterphenyl, no water was found in paraterphenyl.

Mechanisms of fouling-film formation were studied by testing Santowax OMP and coolant fluid from core 2 of the OMRE in pyrolytic capsules or in a circulating loop in which the organic was irradiated with 6-Mev electrons.[7] Also studied were the effects of temperature, flow, pressure, cover gas, and various preventive additives.

In regard to mechanisms, the study indicated that film formation on hot surfaces comes from (1) mass transfer of iron from the container and pipes and (2) deposition of a composite material that forms when high-molecular-weight polymers adhere to either soluble or insoluble iron in the coolant—and that "to a limited degree, certain higher molecular weight high boilers were more effective in fouling."

The pyrolytic capsule tests showed that film formation increases exponentially with surface temperature, but bulk temperature is also important and is greatly speeded by temperature "spikes" of less than 1-min duration.

In the electron-irradiation loop, film formation was (1) not affected greatly by blanket-gas pressures over the range 400 to 700 psig, (2) inversely proportional to coolant velocity, (3) enhanced by surface roughness or projections into the coolant stream, and (4) affected by the radiation intensity. When the blanket over the fluid was hydrogen, rather than nitrogen, the film was heavier and had greater thermal conductivity.

Corrosion Properties

Out-of-pile tests in a tilting-furnace apparatus were used to test the corrosion properties of type 304 stainless steel, A-285C mild steel, 1100 aluminum, Al-288, and SAP M-257 in 500 to 800°F paraterphenyl and 500 to 710°F orthoterphenyl.[6] On the basis of rather sketchy data, it was concluded that these materials are highly resistant to corrosive and mass-transfer attack by the terphenyls.

The combined effects of exposure to both an organic moderator–coolant and reactor radiation were measured on specimens of various materials that had been placed in the core of the OMRE for 26 months.[15] Specimens included SAE 1020 carbon steel, SAE 4130 low-alloy steel, types 410 and 304 stainless steels, aluminum, and magnesium. High-boiling-point impurities in the organic were allowed to rise to nearly 30%, at which level they were held during most of the last half of the exposure. The SAE 1020 and 4130 steels corroded at the rate of approximately 0.0001 in./year. Aluminum and types 410 and 304 stainless steels were quite resistant to corrosion. Magnesium was the only metal that corroded appreciably; these measurements seemed to confirm that magnesium, whether anodized or not, is unsuitable for organic-reactor service. It was concluded that measurements of corrosion rates in an out-of-pile laboratory can predict in-pile corrosion rates with sufficient accuracy for design purposes.

Corrosion of iron by terphenyl was investigated with a variety of organic mixtures and reagent-quality iron wire.[7] Clean terphenyl, either irradiated (by 6-Mev electrons) or unirradiated, does not corrode iron, but it becomes corrosive upon oxidation by air. Two commercial automotive motor-oil detergents were tested for preventive effects, but first indications were unfavorable.

Autoclave and loop tests have been used to determine the corrosion rates of structural materials exposed to commercially available terphenyls (Santowax mixtures); potential corrosion inhibitors also were evaluated.[16] Santowax R was used in agitated autoclave tests, and Santowax OMP was used in the loop tests. Corrosion rates usually decrease with exposure and depend on fluid velocity and temperature. Although the corrosion rates of the various alloys seem relatively insensitive to water additions, water did seem to promote a more adherent oxide scale in the autoclave tests.

Steel corrosion rates were insensitive to water content up to 2000 ppm, which contrasts to the OMRE experience in which particulate-formation rates depended directly on water or air contamination. Corrosion rates that can be expected for carbon or SAE 4130 steels as a function of organic bulk temperature are reported as 0.05 to 0.06 mg/(cm^2)(month) at 600°F, 0.10 mg/(cm^2)(month) at 650°F, and 0.2 to 0.25 mg/(cm^2)(month) at 750°F. Of the three steels tested, annealed, or sensitized, type 3 stainless steel is the most corrosion resistant (it shows negligible corrosion in both the autoclaves and the loop), and carbon steel is less resistant than ferritic type 410 stainless steel. Limited tests with type 406 stainless steel (13 chromium–4% aluminum) indicate a corrosion rate as low as that for type 304 stainless steel. One advantage of type 406 stainless steel is that it absorbs approximately 25% fewer thermal neutrons than type 304.

Aluminum and specimens made from sintered aluminum powder (called SAP or APM) were almost inert to terphenyls with normal water content. Type 1100 aluminum oxidized only when water content exceeded 1000 ppm. Although the tests indicated that magnesium and its alloys might be attractive as water-removal agents, they are unsuitable for use in organic reactors because they are readily corroded by organic coolants.

Protective coatings were evaluated in autoclave tests. None of a wide variety of coatings on zirconium alloys was able to prevent hydriding of the zirconium. Copper and brass corrodes faster than carbon steel, but beryllium appears to be quite inert. Although niobium apparently corrodes more than carbon steel, it might be an effective diffusion barrier between aluminum cladding and metallic-uranium fuel.

Contaminants. The results of these tests and other considerations show that, in general, the presence of water, hydrogen, air (oxygen), or sulfur in terphenyl enhances corrosion and film formation. Although the effects of minor air contamination were negligible in the laboratory experiments, experience at the OMRE indicates that air contamination of irradiated coolant tends to increase fouling. The fouling tendency of coolants can be reduced if (1) the water or oxygen content is minimized, (2) the access of air and water to the coolant system is strictly controlled, and (3) larger and more effective particulate-removal systems are used.

Sampling. For these experiments the workers developed a significantly improved technique for sampling Santowax to determine its water content. The difficulty had been caused by the ability of water to flash off from the Santowax at 750°F when the pressure was reduced. A mpler that simulated a flow sample from the toclave was developed to avoid this problem.

at-Transfer Properties

Forced-circulation heat transfer in organic stems has been studied extensively.[17] Boiling at transfer with forced-circulation Santowax and isopropyl diphenyl has been measured in out-of-pile test loop having an electrically ated vertical test section;[18] Table IX-1 shows e range of variables investigated. Data for ntowax R heat transfer correlated best with evy's equation;[19] Rohsenow[20] and Forster–reif[21] equations were less successful. The rrelation was insensitive to flow direction. ata for isopropyl diphenyl correlated within % using Levy's equation; the Rohsenow and orster–Greif relations were not tried because uncertainty concerning the surface tension of opropyl diphenyl.

Table IX-1 CONDITIONS IN BOILING HEAT-TRANSFER EXPERIMENTS[18]

Conditions	Isopropyl diphenyl	Santowax R
eat flux, Btu/(hr)(sq ft)	40,000–100,000	27,000–110,000
ass velocity, lb (sec)(sq ft)	325–630	280–750
stem pressure, psia	21–33	15–28
ow direction	Up only	Up and down
bcooling, °F	0–17	0–57

Void fraction was measured in the Santowax experiments by an X-ray transmission tech-que. With greater than 8°F subcooling, these ta were correlated using a modified form of aurer's equation.[22] An expression was de-loped and used with moderate success to rrelate void-fraction data near equilibrium lk boiling. For equilibrium boiling the ex-erimental results were consistent with pre-ictions from a modified Martinelli model.[23]

ossible New Coolants

Attempts have been made to find an inexpen-ive organic coolant with properties similar to e terphenyls.[7,24] A large group of high-boiling istillates from the petroleum industry which ere studied included recycled oils from some atalytic-cracking operations, highly aromatic ractions used as feed for producing carbon lack in furnaces, and coal-tar distillates. Irradiation with 6-Mev electrons usually liberated more gas from these oils than from Santowax OMP. Radiation resistance of these oils ranged from somewhat lower to somewhat greater than Santowax OMP. In general, their thermal stabilities were unsatisfactory above 650°F.

When these petroleum-base stocks had been hydrodealkylated and the coal-tar stocks hydrodesulfurized, they had pyrolytic thresholds approximately 50°F less than terphenyl. Radiolysis of coolants prepared in this manner formed polymer only 50 to 75% as fast as did terphenyl but liberated gases several times faster than terphenyl. Viscosities, vapor pressures, densities, and hydrogen densities were very similar to terphenyl. The film-forming tendency of these materials has not been tested, but no coking was observed up to 750°F. Although estimates based on these data indicate that these coolants could be produced cheaply enough that inventory and makeup costs would be somewhat less than for terphenyl in a conventional steam plant where bulk temperatures do not exceed 700°F, these experiments did not include in-pile or neutron irradiations. Thus the results are only indicative.

Acknowledgments

The author gratefully acknowledges the assistance of reviewers at Atomics International for their help with, and further organization of, this article.

References

1. R. F. Makens (Ed.), Organic Coolant Summary Report, USAEC Report IDO-11401, Idaho Operations Office, December 1964.
2. D. G. Kuper, Organic Coolant Degradation Studies, USAEC Report IDO-16851, Phillips Petroleum Company, Mar. 25, 1963.
3. *Power Reactor Technol.*, 6(3): 71 (June 1963).
4. A. W. Boyd, The Radiation and Thermal Stability of Some Potential Organic Moderator-Coolants, Part VII. The Effect of Radiation Intensity on the Decomposition of Paraterphenyl by Fast Electrons, British Report AERE-R-4048, August 1963.
5. E. A. Mason and C. D. Sawyer, Irradiation Loop Studies of Organic Reactor Coolants, Progress Report, January 1–September 30, 1962, USAEC Report MITNE-29(IDO-11106), Massachusetts Institute of Technology, Feb. 15, 1963.
6. H. Susskind et al., Organic Reactor Coolant Studies, USAEC Report BNL-7650, Brookhaven National Laboratory, June 30, 1963.
7. J. C. Hillyer, Organic Coolant Research Summary

Report, July 1, 1960–March 31, 1963, USAEC Report IDO-16911, Phillips Petroleum Company, Oct. 1, 1963.

8. W. G. Burns, C. R. V. Reed, and J. A. Winter, The Radiation and Thermal Stability of Some Potential Organic Moderator-Coolants. Part VIII. Pile and Electron Irradiation of Various Polyphenyl Mixtures and Work with Additives, British Report AERE-R-4072, November 1963.
9. L. E. Gardner, Reclamation of Damaged Nuclear Reactor Coolant by Catalytic Hydrocracking, USAEC Report IDO-16853, Phillips Petroleum Company, Mar. 29, 1963.
10. L. E. Gardner, Evaluation of Catalysts for Selective Hydrocracking of Polyphenyls, USAEC Report IDO-16858, Phillips Petroleum Company, Apr. 25, 1963.
11. L. E. Gardner, Catalytic Hydrocracking of High Boiler in Nuclear Reactor Coolant, USAEC Report IDO-16877, Phillips Petroleum Company, May 20, 1963.
12. J. L. Griffith and G. J. Russell, Economics of Hydrocracking Damaged Coolant from Organic Reactors, USAEC Report IDO-11400, Idaho Operations Office, November 1963.
13. J. F. Black, M. E. Conn, and P. R. Geissler, First Semi-Annual Progress Report on Organic Coolant Technology During May Through October 1962, USAEC Report IDO-11221, Esso Research and Engineering Company, Dec. 14, 1962.
14. P. R. Benson, Development of the Pyrolytic Fouling Test for Organic Reactor Coolants, USAEC Report NAA-SR-7362, Atomics International, Nov. 30, 1962.
15. R. S. Neymark, Performance of Structural Materials Exposed to the Coolant in the OMRE,
USAEC Report NAA-SR-9796, Atomics Inter-
tional, Aug. 1, 1964.
16. R. S. Neymark, Corrosion of Structural M-
rials in Impure Santowax, USAEC Report N-
SR-7755, Atomics International, May 15, 1963.
17. Atomics International, Organic Reactor H
Transfer Manual, USAEC Report NAA-SR-Me-
7343, Dec. 1, 1962.
18. F. Bergonzoli and F. J. Halfen, Heat Trans
and Void Formation During Forced Circul
Boiling of Organic Coolants, USAEC Report NA-
SR-8906, Atomics International, June 15, 1964.
19. S. Levy, Generalized Correlation of Boiling H
Transfer, ASME Paper 58-HT-8, *J. Heat Tra-
fer*, 81: 37-42 (1959).
20. W. M. Rohsenow, A Method of Correlating H
Transfer Data for Surface Boiling Liquids, *Tra
Am. Soc. Mech. Engrs.*, 74: 969-976 (1952).
21. H. K. Forster and R. Greif, Heat Transfer
Boiling Liquid: Mechanism and Correlat
ASME Paper 58-HT-11, *J. Heat Transfer*
43-53 (1959).
22. G. W. Maurer, A Method of Predicting Stea-
State Boiling Vapor Fraction in Reactor Co
Channels, in Bettis Technical Review—Reac
Technology, USAEC Report WAPD-BT-19, Wes-
tinghouse Electric Corp., Bettis Atomic Pow
Laboratory, June 1960.
23. R. W. Lockhart and R. C. Martinelli, Propose
Correlation of Data for Isothermal Two-Ph
Two-Component Flow in Pipes, *Chem. E
Progr.*, 45(1): 39-48 (January 1949).
24. L. E. Gardner, W. M. Hutchinson, and J. C. H-
yer, Low Cost Organic Moderator-Coolants
Nuclear Reactors, USAEC Report IDO-169
Phillips Petroleum Company, Dec. 23, 1963.

Index

Power Reactor Technology

Volume 8

Note: The page range for each of the four issues of Vol. 8 is as follows: No. 1, pages 1 to 108; No. 2, pages 109 to 156; No. 3, pages 157 to 198; and No. 4, pages 199 to 296.

A

Accidents
  frequency, 221-22
  loss-of-coolant, 240-41
Aerosols
  formation in NaK systems, 260
  traps for, 259-70
Air
  effects on corrosion by polyphenyls, 294
  reactivity effects, 109
Air-water systems
  flow, techniques for observing, 165
Aluminum
  corrosion by polyphenyls, 293-94
Aluminum alloys
    (see also SAP)
Aluminum alloys (Al-Pu)
  criticality, 210, 212
Aluminum oxide systems (Al_2O_3-UO_2)
  radiation effects, 8
Analog computers
  use for reactor control, 227
Annuli
  heat transfer in, 121-22
Argonne National Laboratory
  liquid-metal magnetohydrodynamic research, 207-8
ARGOSY code
  for graphite-moderated reactor core design, 160-61
ARGUS code
  thermal conductivity calculations, 118
Atomics International
  liquid-metal magnetohydrodynamic system research, 207

B

Bellows
  failures in Hallam Power Reactor, 282-83
Beryllium
  corrosion by polyphenyls, 294
Beryllium-9
  integral cross section, 115
Beryllium oxide systems (BeO-UO_2)
  radiation effects, 8
Beryllium oxide systems (BeO-UO_2)
    (Hastelloy-X-clad)
  fuel elements, evaluation, 173
Bibliographies
  two-phase flow, 164
Biphényl
  heat transfer properties, 295
  pyrolysis, 290
  radiolysis, 290-92
Boiling, 14-17
  bubble growth and control, 256
  burnout in Freon, 166
  burnout in Na, 164
  burnout in steam-water systems, 166-70
  heat transfer, 235
  heat transfer from K, 163-64
  phase velocity in two-phase flow, 235
  stability in two-phase flow, 228
  subcooled, burnout heat flux in, 122-23
Boiling (film)
  heat transfer coefficients, 231
  theoretical studies, 232
Boiling (nucleate)
  bubble phenomena, 232
  convection effects, 235
  effects on frictional pressure drop, 253
  heat flux effects on, 229
  heat transfer in brines, 238
  liquid metal instability, 231
Boiling (pool)
  effects of heat flux, 229-30
  heat transfer, 253
Boric acid
  use as chemical shim, 272
  use as soluble poison, 214
  use of solution for reactor shutdown, 225
Boron
  use as soluble poison, 10-12
Brass
  corrosion by polyphenyls, 294
Breeding blankets
  design for large fast breeder reactors, 147-52
Brines
  deposit formation in boiling, 238
Brookhaven National Laboratory
  liquid-metal magnetohydrodynamic system research, 208
Bubbles
  effects on heat transfer, 253
  effects on thermal stresses, 255
  formation and control in boiling, 256
  formation rate during boiling, 235
  phenomena in nucleate boiling, 232
  in turbulent flow, 234-35
Buckling
  experiments, 109-10
  fuel elements, UC, 111
  materials, in light-water reactors, 214-15
Burnable poisons
    (see Poisons)
Burnout, 14-17
  in boiling Na, 164
  in fog-cooled reactors, 228-29
  in Freon, 166
  safety margin computation, 227
  in steam-water systems, 166-70
  in water, 121-23
Burnup
  fuel elements, Magnox-clad, 62
  measurements, 216-17

C

Cadmium sulfates
  solution, use as poison, 214
Calcium sulfates
  deposits in boiling solutions, 238
Catalytic hydrocracking
  reclaiming of organic coolants, 292
Ceramics
    (see Fuel elements (ceramic))
Cermets
    (see Fuel elements (cermet))
Cesium (liquid)
  thermal, thermodynamic, and flow properties, 164
Channels
  burnout of water in vertical, 121
  fluid flow stability in heated, 231
Chloride ions
  corrosive effects on stainless steels, 254
Coatings
  corrosion by polyphenyls, 294
Cold traps
  for oxides in Hallam Power Reactor, 285
Components
  reliability, 221
Computer codes
  ARGOSY, 160-1
  ARGUS, 118
  GAM-I, 210, 212
  HEAT-1, 118
  HFN, 212
  HRG, 212
  MARC-2B, 215
  MOCA-2, 215
  REX, 210
  ROB, 118
  SOFOCATE, 210
  STOKE, for heavy water reactor simula-

  - tion, 35
  - TEMPEST, 212
  - THERMOS, 212, 215
  - TYCHE, 113
- Computers
  - use for reactor control, 226-27
- Condensation
  - dropwise, of ethylene glycol, 233
  - dropwise, of water, 233
  - of laminar films, 232
  - of liquid metals, 232-33
  - vapor traps utilizing, 259-60
- Conductivity
  - (see Thermal conductivity)
- Control, 221-27
  - calibration for EBR-I, with Pu core, 158
  - calibration for SRE, second core, 157
  - computer use for, 226-27
  - critical assemblies using moderator level, 223-24
  - gas-cooled reactors, 68-69
  - poisons, 10-12, 214, 217, 225-26
- Control rods
  - drive mechanisms for EBR-II, 133-34
  - gravity independent, 223
  - operation in Hallam Power Reactor, 282
  - radiation effects, 271
  - reliability, 221-22
  - thimble failure in Hallam Power Reactor, 283-84
- Control systems, 272-75
  - ASTR, 223
  - development, 18
  - Elk River Power Reactor, 271-72
  - Hallam Power Reactor, 280, 282
  - Indian Point Power Reactor, 271
  - large pressurized-water reactors, 144-46
  - Yankee Power Reactor, 271-72
- Convection (forced)
  - in boiling K, 163-64
  - burnout heat flux in subcooled boiling water, 122
  - effects in boiling, 235
  - fluid flow stability, 231-32
  - two-phase flow, 228
- Convection (free)
  - burnout of water in vertical channel, 121
  - coolant loop transient behavior, 122
  - effects on film condensation, 232
  - heat transfer coefficients for ice-water systems, 239-40
  - heat transfer at cryogenic temperatures, 239
  - heat transfer to finned tubes, 236-37
  - liquid metal boiling in, 231
- Coolant loops
  - fluid flow stability, 122
  - transient behavior under free convection, 122
- Coolants
  - (see also Potassium alloys (K-Na) (liquid))
  - contamination in Dounreay Fast Reactor, 75
  - flow oscillations in Elk River Power Reactor, 273
  - loss accidents, 240-41
  - Na, 75-96
- Coolants (organic)
  - corrosive effects, 293-94
  - film formation by, 293-94
  - heat transfer properties, 123-24, 295
  - pyrolysis, 290-91
  - radiolysis, 290-94
  - reactivity effects of Dowtherm A, 109
  - reclamation, 292-93
- Cooling systems
  - Hallam Power Reactor, 282
- Copper
  - corrosion by polyphenyls, 294
- Cores
  - radiation effects on lifetime, 216
- Cores (graphite moderated)
  - physics calculations, 160-61
- Corrosion
  - by nitrogen, 173-74
  - by organic coolants, 44-45, 293-94
  - in Agesta Reactor, 275
  - of ceramic fuel elements (Zircaloy-2-clad), 177-82
  - of Hastelloys, 23, 173-74
  - of Incoloy-X, 23
  - of Nb alloys, 42-45
  - of stainless steels, 254-55, 293-94
  - of steels, 9-10, 293-94
  - of Yankee Power Reactor control rods, 271-72
- Corrosion products
  - deposition in reactors, 252, 256
- Cracks
  - propagation in boiling water reactor fuel elements, 254
- Critical assemblies
  - control by moderator level, 223-24
  - perturbations in graphite-moderated, 115
- Critical assemblies (Anna)
  - design, 111-12
- Critical assemblies (Helena)
  - design, 111
- Critical assemblies (OCF)
  - pulsed neutrons in, 112
- Critical assemblies (ROSPO)
  - design, 112
- Critical assemblies (Scorpio I)
  - criticality measurements in, 212
- Critical assemblies (Scorpio II)
  - criticality measurements in, 212
- Critical assemblies (TCA)
  - pulsed neutrons in, 112
- Critical experiments, 109-13, 210-14
- Critical facilities (Alize-II)
  - use of soluble poisons in, 214
- Cross sections, 114-15
  - absorption, thermal neutrons in graphite, 114-15
  - calculations, 210, 212
  - fission, of ^{241}Pu, 115
  - fission spectrum, of ^{235}U, 115
  - integral, of ^{9}Be, 115
  - neutron capture, of Pu isotopes, 211
- Crud
  - analysis from VBWR, 254, 256
- Cryogenics
  - heat transfer, 232-33

D

- Decontamination
  - sodium reactor coolants, 75-77
- Delayed neutrons
  - calculations, 161-62
- Departure from nucleate boiling
  - effects of nonuniform heat flux on, 229
- Desalination
  - deposits during boiling and heat transfer through films, 238
- Diffusion length
  - thermal neutrons in graphite, 114-15
- Digital computers
  - use for reactor control, 226
- Diphenyl
  - (see Biphenyl)
- Direct power conversion
  - plants, 105-6
- "Dowtherm A" coolant
  - reactivity effects, 109

E

- Economics
  - of catalytic hydrocrackers for organic coolant reclamation, 292-93
  - fast breeder reactors, 85
  - radiation effects on core lifetime, 216
  - sodium graphite reactors, 185
- Electrical circuits
  - SPERT-3, failure, 272-73
- Electrons
  - radiation effects on polyphenyls, 291-92
- Electrostatic precipitations
  - use with NaK vapors, 260
- Energy conversion (direct)
  - plants, 105-6
- Ethylene glycol
  - condensation, dropwise, 233
- Excursions, 221-22
- Exponential experiments, 109-13, 211-14

F

- Fission parameters
  - calculations, 161-62
- Fission products
  - contamination at Dounreay Fast Reactor coolant, 75
  - gases, monitor for, 263
- Fluid flow, 14-17, 118-25, 163-71, 228-44
  - effects on boiling, 253
  - large pressurized water reactors, 142-44
  - oscillations in Elk River Power Reactor, 273
- Fluid flow (annular)
  - transition to two-phase, 234
- Fluid flow (froth)
  - occurrence and characterization, 123
- Fluid flow (turbulent)
  - bubble studies, 234-35
  - heat transfer in annuli, 122
- Flowsheets
  - Halden Reactor, 50
  - soluble poison control systems, 11
- Forced convection
  - (see Convection (forced))
- Free convection
  - (see Convection (free))
- Freeze traps
  - for Na in Hallam Power Reactor, 285
- Freon systems
  - boiling burnout in, 166
- Froth flow
  - (see Fluid flow (froth))
- Fuel assemblies
  - design for large pressurized-water reactors, 139-41
- Fuel cycles
  - evaluation for large fast breeder react 154-55
- Fuel elements
  - Agesta Reactor, 51-52
  - burnout of rods, 167
  - criticality of pins, 210
  - design, 3, 6-9
  - design for AGR Reactor, 62
  - design for Anna Critical Assembly, 112
  - design for BONUS Reactor, 27
  - design for NORA Reactor, 112
  - design for RB Reactor, 112
  - development for fast breeder reactors 86-91
  - development of SAP, 37, 39
  - fabrication, 126-31
  - failures in boiling water reactors, 254-

  failure due to internal pressure, 252
  failure in VBWR, 252-54, 256
  Marviken Reactor, 51-52
  radiation effects, 7-8, 62, 82, 255-56
  thermal conductivity, 118-21, 129
'uel elements (Al-Pu)
  criticality in graphite lattices, 212
'uel elements (BeO-UO_2)(Hastelloy-X-clad)
  evaluation, 173
'uel elements (ceramic)
  design, 3, 6-9, 147-52
  evaluation, 172-74
'uel elements (ceramic)(Zircaloy-2-clad)
  fretting corrosion, 177-82
'uel element (cermet)
  development, 89, 126-28
  fabrication, 129
  thermal conductivity, 129
'uel elements (enriched U)
  criticality in D_2O lattices, 213
'uel elements (Incoloy-800-clad)
  evaluation for superheating reactors, 174-75
'uel elements (Magnox-clad)
  burnup, 62
  design, 63-66
  radiation effects, 62
'uel elements (Mo-UO_2 cermet)
  fabrication and thermal conductivity, 129
'uel elements (Mo-W-UO_2 cermet)
  development, 128
'uel elements (Nb-ThO_2-UO_2 cermet)
  thermal conductivity, 129
'uel elements (Pu)
  criticality in graphite lattices, 212
'uel elements (Pu-U)
  criticality in graphite lattices, 212-13
'uel elements (PuC-UC)
  design for large fast breeder reactors, 147-49, 151-52
'uel elements (PuO_2-UO_2)
  criticality in water, 212
  design for large fast breeder reactors, 149-52
  specifications, 129
'uel elements (PuO_2-UO_2)(Zircaloy-2-clad)
  fretting corrosion, 177-82
'uel elements (PuO_2-UO_2)(Zr-clad)
  criticality, 210
  fretting corrosion, 177-82
'uel elements (stainless steel-clad)
  design, 3, 6-9
'uel elements (stainless steel-UO_2 cermet)
  development, 126-27
'uel elements (Th-U)
  development for fast breeder reactors, 89
'uel elements (Th-U-Zr)(Zircaloy-2-clad)
  fabrication, 130
uel elements (ThO_2-UO_2)
  design, 3, 6-9
'uel elements (W-UO_2 cermet)
  development, 127-28
'uel elements (U)
  criticality in graphite lattices, 212-13
'uel elements (UC)
  buckling studies, 111
  development for sodium graphite reactors, 81-83
  radiation effects, 82
'uel elements (UC)(stainless steel-clad)
  evaluation, 174
  fabrication of Na-bonded, 129-30
'uel elements (UO_2)
  design, 3, 6-9
  fabrication, 129
  thermal conductivity, 119-21
'uel elements (UO_2)(enriched)
  pulsed neutron studies, 112
Fuel elements (UO_2)(stainless steel-clad)
  evaluation, 172
  fabrication, 128-29
Fuel elements (UO_2)(Zircaloy-2-clad)
  evaluation, 172-74
  fretting corrosion, 177-82
Fuel elements (Zircaloy-clad)
  design, 3, 6-9
  evaluation, 18
Fueling machines
  Bradwell Reactor, operation, 68
  EBR-2, vapor traps for, 262-63
  design, 68, 141-42

G

Gadolinium nitrates
  use of solutions for reactor shutdown, 226
GAM-I code
  criticality and cross section calculations, 210, 212
Gases
  entrainment in Hallam Power Reactor, 284
  fission product monitoring, 263
  thermodynamic properties, 121, 239
Graphite
  criticality of Pu alloys in lattices of, 212-13
  moderator, pulsed neutron studies in, 112-13
  thermal neutron absorption cross section and diffusion length in, 114-15
Gravity
  control rod independence from, 223

H

Hastelloy-C alloy
  corrosion in superheating reactors, 23
Hastelloy-X alloy
  corrosion by N_2, 173-74
HEAT-1 code
  thermal conductivity calculations, 118
Heat exchangers
  concentric tube, dynamic analysis of, 237
  design, 236-37
  efficiency, 236
  failures in Hallam Power Reactor, 284
  finned tube, 236-37
  heat transfer coefficients for NaK, 235-36
Heat transfer, 14-17, 118-25, 163-71, 228-44, 253
  large pressurized-water reactors, 142-44
  organic coolants, 123-24, 295
Heavy water
  chemistry of, 39-40
  control of oxygen in, 277
  criticality studies in lattices of, 213
  moderator, pulsed neutron studies in, 113
  reactivity effects, 109
  reflector, in University of Michigan Reactor, 277, 279
Heavy Water Lattice Project
  buckling experiments, 109-10
Helium
  thermodynamic properties, 121
HFN code
  cross section calculations, 212
Hot traps
  for carbon in Hallam Power Reactor, 285
HRG code
  cross section calculations, 212
Hydriding
  Zr alloys, 9, 246-51
Hydrogen
  effects on corrosion by polyphenyls, 294
  reactions with Zircaloys, 245-46
  thermal conductivity at high temperatures, 239

I

Ice-water systems
  free convection melting, heat transfer calculations, 239-40
Impingement
  vapor traps utilizing, 260
Incoloy-800 alloy
  testing for fuel element cladding, 174-75
Inconel-X alloy
  corrosion in superheating reactors, 23
Indium resonance energy
  flux age, 113-14
  TYCHE code, determination by, 113
Instrumentation
  gas-cooled reactors, 68-69
  Hallam Power Reactor, 283, 285
  large pressurized water reactors, 145-47
  level controllers, failure, 272
  liquid metal level indicators, 176-77
  neutron detectors, 224-25
  pressure switches, failure, 272
  temperature sensors, failure, 272
Integral cross sections
  ^{9}Be, 115
Iron
  corrosion by polyphenyls, 294

J

Jet Propulsion Laboratory
  liquid-metal magnetohydrodynamic system research, 207

L

Leaks
  Hallam Power Reactor, 282
  pressure vessels, 3
  SPERT-3, 275-76
  Yankee Power Reactor, 275-76
Level controllers
  SPERT-3, failure, 272
Level indicators
  for liquid metals, 176-77
Light water
  (see Water)
Liquid metals
  (see Metals (liquid))
Lithium (liquid)
  thermal, thermodynamic, and flow properties, 163-64
Loss-of-coolant
  accident analysis, 240-41

M

Magnesium
  corrosion by polyphenyls, 294
Magnesium alloys
  corrosion by polyphenyls, 294
Magnesium oxide systems (MgO-PuO_2)
  radiation effects, 8

Magnetohydrodynamic systems, 199-209
Maintenance
  handling of Hallam Power Reactor core components, 283
MARC-2B code
  thermal neutron distribution calculation, 215
Massachusetts Institute of Technology
  liquid-metal magnetohydrodynamic system research, 208
Melt Refining Process
  vapor traps, 266
Mercury
  condensation in Ni surfaces, 232-33
  thermal, thermodynamic, and flow properties, 163-64
Metals (gaseous)
  film condensation, 232-33
Metals (liquid)
  boiling behavior, 231
  level indicators, 176-77
  pumps for, 282
  thermal, thermodynamic, and flow properties, 163-64
  use in magnetohydrodynamic systems, 199 209
  vapor traps for use with, 259-70
Meters
  plugging in Hallam Power Reactor, 283
MHD system
  (see Magnetohydrodynamic systems)
MOCA-2 code
  criticality calculation, 215
Moderators
  criticality control with, 223-24
  element failure in Hallam Power Reactor, 285-87
Molybdenum systems (Mo-W-UO_2 cermets)
  development for fuel elements, 128
Molybdenum systems (Mo-UO_2 cermets)
  fabrication into fuel elements and thermal conductivity, 129
Multiplication factors
  for EBR-I, with Pu core, 158-59

N

NaK
  (see Potassium alloys (K-Na)(liquid))
Natural convection
  (see Convection (free))
Neutrons
  age determination, 113-15
  delayed, 161-62
  detector design, 224-25
  flux measurements, 157-58
  pulsed, 112-13
  scattering, 116
  thermal, 114-15, 215
  thermalization, 115-16
Nimbus Satellite
  thermal design calculations, 240
Niobium
  corrosion by polyphenyls, 294
Niobium alloys (Nb-Zr)
  corrosion, 42-45
  hydriding stress allowance, 9
  use in pressure tubes, 41
Niobium systems (Nb-ThO_2-UO_2 cermets)
  thermal conductivity, 129
Nitrogen
  corrosive effects, 173-74
Noble gases
  thermal conductivity at high temperature, 239
NPY Project, 111-12

O

Organic coolants
  (see Coolants (organic))
Orifices
  operating problems in Hallam Power Reactor, 288
Oxide films
  effects on hydriding of Zr alloys, 246-48
Oxygen
  control of concentration in D_2O, 277
  effects on corrosion by polyphenyls, 294

P

Packed beds
  heat transfer, 237-38
Petroleum distillates
  development for reactor use, 295
Physics, 109-17, 154-55, 157-62, 210-20
Plates
  evaporation rates from hot, 240
  heat transfer from at cryogenic temperatures, 239
Plutonium
  critical experiments, 211-14
  neutron capture cross sections, 211
Plutonium-239
  neutron capture cross sections, 211
Plutonium-240
  neutron capture cross sections, 211
Plutonium-241
  fission cross sections, 115
  neutron capture cross sections, 211
Plutonium alloys
  criticality in D_2O lattices, 213
Plutonium alloys (Al-Pu)
  criticality, 210, 212
Plutonium alloys (Pu-U)
  criticality in lattices, 212-13
Plutonium carbide systems (PuC-UC)
  design of fuel elements for large fast breeder reactors, 147-49, 151-52
  radiation effects, 8
Plutonium carbides (PuC)
  radiation effects, 8
Plutonium nitrates
  criticality of solution, 213-14
Plutonium oxide systems
  critical experiments in water lattices, 210
Plutonium oxide systems (MgO-PuO_2)
  radiation effects, 8
Plutonium oxide systems (PuO_2-UO_2)
  critical experiments in water lattices, 210, 212
  design of fuel elements for large fast breeder reactors, 149-52
  fuel elements, fretting corrosion of Zircaloy-2 cladding, 177-82
  fuel elements, specifications, 129
  radiation effects, 8
Plutonium oxide systems (PuO_2-ZrO_2)
  radiation effects, 8
Plutonium oxides
  criticality in polystyrene, 214
Pneumatic systems
  use in control systems, 223
Poisons, 10-12
  boric acid, 214, 225
  $CdSO_4$ solution use, 214
  $Gd(NO_3)_3$, 226
  use in water-moderated reactors, 217
Polyethylene
  reactivity effects, 109
Polyphenyls, 123-24, 290-95
Polystyrene
  moderating effects on PuO_2, 214
Potassium (liquid)
  thermal, thermodynamic, and flow properties, 163-64
Potassium alloys (K-Na)(liquid)
  aerosol formation in, 260
  heat transfer coefficients, 235-36
  thermal, thermodynamic, and flow properties, 163
Power conversion (direct)
  plants, 105-6
Pressure
  effects on boiling superheat, 253
Pressure drop
  of air in finned-tube heat exchangers, 236-37
  turbulent flow through wire-wrapped, seven-rod fuel assemblies, 123
  two-phase, 166, 233-35
Pressure switches
  Elk River Power Reactor, failure, 272
Pressure tubes
  design, 40-41
  fretting corrosion, 177-82
Pressure vessels, 12-14
  design for large pressurized water reactors, 138-39
  design for Magnox reactors, 66-68
  KRB Reactor, 12-13
  leaks, 3
  SENA Reactor, 12-13
SENN Reactor, 12-13
  SEP Reactor, 12
  WWER-1 Reactor, 9-10, 12-14
Pressurized water
  burnout calculations, 121-23
Pumps
  development for reactors, 18
  liquid metal, for Hallam Power Reactor, 282
  Hallam Power Reactor, 282
Pyrolysis
  organic coolants, 290-91

R

Rabbit facility
  design and fabrication, 277
Radiation (thermal)
  heat transfer calculations, 238-39
Radiation effects
  biphenyl, 290
  control rods, 271
  core lifetime, 216
  fuel elements, 7-8, 62, 82, 255-56
  hydriding of Zr alloys, 246-48
  polyphenyls, 290-91, 293-94
  reactivity, 217
  SAP, 38
  Zircaloy-2, 38, 41
Radiolysis
  organic coolants, 290-94
Reactivity
  calculations, 217
  changes with irradiation, 216
  effects on, 109-10
  measurements in reactors, 157-59
Reactors
  (see also Critical...)
  corrosion product deposition in, 252
  future development, 17-20
  reactivity, 216-17
  subcriticality measurement during shut-down, 224-25
Reactors (Advanced Gas Cooled)(AGR)
  design, 58
  fuel element design, 62
  operation, 60
Reactors (Advanced Sodium Graphite)
  buckling studies, 111

Reactors (Aerospace Shield Test)(ASTR)
  control system, 223
Reactors (Agesta)
  corrosion in, 275
  design, 47-48, 52-53
  repair procedures, 276
Reactors (AKB)
  design, 36
Reactors (Aquilon-II)
  criticality measurements in, 213
Reactors (ARBUS)
  design and operation, 103-4
Reactors (AVR)
  design, 73-74
Reactors (Bashful-600)
  design, 53, 55-56
Reactors (Beloyarsk-1)
  design, 28-34
Reactors (Beloyarsk-2)
  design, 28-34
Reactors (Big Rock Point Power), 6
  design, 4, 7
  flow-induced vibrations, failures from, 273
  operating experience, 3
  pumps, 18
Reactors (BN-350)
  design, 94
  status, 92
Reactors (Bodega Bay Power)
  design, 4
Reactors (Boiling, Experiments-5) (BORAX-5)
  design, 23
Reactors (Boiling heavy-water)
  design, 55
Reactors (boiling-water), 3-29
  corrosion product deposition in, 256
  fuel element failure, 254-56
  radiation effects on fuel elements, 255
  water quality control, 254
Reactors (BONUS)
  design, 23, 25, 27
Reactors (BR-3)
  design, 5
  use of soluble poison control, 10, 12
Reactors (BR-5)
  coolant contamination, 75-76
  status, 95
Reactors (Berkeley)
  design, 58
  performance, 60
Reactors (Bradwell)
  design, 58
  performance, 60
  refueling machine operation, 68
Reactors (Calder Hall)
  design, 58
Reactors (CANDU), 37-44
  physics, 217
Reactors (Chapelcross)
  design, 58
Reactors (Connecticut Yankee Power)
  design, 5
Reactors (Czechoslovakian Heavy Water)
  design, 56
Reactors (DON)
  design, 36
Reactors (DOR)
  design, 36
Reactors (Dounreay Fast)
  fission product contamination of coolant, 75
  status, 92
Reactors (Dragon)
  design, 72-73
Reactors (Dresden Power), 6
  design, 4, 7
  operating experience, 3
  pumps, 18
Reactors (Dungeness)
  design, 58
Reactors (EDF-1)
  criticality studies in, 213
  design, 58
Reactors (EDF-2)
  design, 58
Reactors (EDF-3)
  design, 58
  pressure vessel, 67
Reactors (EDF-4)
  design, 58
  pressure vessel, 67
Reactors (EL-4)
  design, 36
Reactor (Elk River Power)
  control system, 271-72
  coolant flow oscillations, 273
  design, 4
  instrument failure, 272
Reactors (Enrico Fermi Fast Breeder)
  auxiliary systems, 77-78
  coolant decontamination, 77
  design, 78-80
  operation, 78
  status, 92
  vapor traps, 261
Reactors (Experimental Beryllium Oxide) (EBOR)
  development, 106
Reactors (Experimental Boiling Water) (EBWR)
  operation, 147
  scaling, 252
Reactors (Experimental Breeder-I) (EBR-I)
  nuclear parameters for Pu core, 158-9
  vapor traps, 260-61
Reactors (Experimental Breeder-2) (EBR-2)
  control rod drive mechanisms, 133-34
  design, 78-80
  coolant decontamination, 77
  status, 92
  vapor traps, 261-63
Reactors (fast breeder), 84-95
  criticality studies, 110
  design of large, 147-55
  gas coolant, 95
Reactors (Fast Supercritical Pressure Power)(FSPPR)
  design, 186-93
Reactors (Fast, Test)(FARET)
  vapor traps, 264-65
Reactors (First Atomic Power Station)
  design, 28-29
Reactors (fog-cooled)
  heat transfer, 228-29
Reactors (G2)
  design, 58
  pressure vessel, 67
Reactors (G3)
  design, 58
  pressure vessel, 67
Reactors (gas-cooled), 56, 58-74
  design of fast breeders, 95
  operating experience, 216
  physics, 216
Reactors (General Electric Test)(GETR)
  flow-induced vibrations, failures from, 273-74
Reactors (graphite-moderated), 28-34
  core physics calculations, 160-61
Reactors (Halden)
  flowsheets, 50
  operation, 50-51
  water chemistry, 52
Reactors (Hallam Power)
  coolant decontamination, 77
  design, 78-80
  operation, 81, 279-80, 282-88
  vapor traps, 264
Reactors (Hanford Graphite Superheat) (HGSR)
  design, 193-98
Reactors (heavy-water), 35-37
  oxygen concentration control in coolant, 277
  physics, 217
Reactors (Heavy Water Components Test) (HWCTR)
  control rod-guide-tube rupture, 222-23
  shutdown with boric acid, 225
Reactors (Hector)
  criticality measurements in, 212
Reactors (Hinkley Point)
  design, 58
Reactors (Humboldt Bay Power), 6
  design, 4, 7
  operating experience, 3
Reactors (Hunterston)
  design, 58
Reactors (Indian Point Power) (CETR), 6
  control system, 271
  operating experience, 3
  repair procedures, 276-77
Reactors (Industrial Reactor Laboratories)
  rabbit facility design and fabrication, 277
Reactors (JPDR)
  design, 4
Reactors (Kahl Superheating)
  design, 22, 24
Reactors (KBWP)
  design, 5
Reactors (KRB)
  design, 4
  pressure vessel, 12-13
Reactors (La Crosse Boiling Water) (LACBWR)
  design, 4
Reactors (Large Closed Cycle Water)
  fuel element evaluation, 172
Reactors (Latina)
  design, 58
Reactors (Lenin)
  design and operation, 97-98
Reactors (liquid metal-cooled), 75-96
Reactors (Lithium Cooled, Experiment) (LCRE)
  vapor traps, 266-67
Reactors (Los Alamos Fast, Core Test Facility)(FRCTF)
  vapor traps, 265
Reactors (Los Alamos Molten Plutonium. Experiments)(LAMPRE)
  vapor traps, 265
Reactors (Loss-of-Flow Test)(LOFT)
  program analysis, 240-41
Reactors (Lucens)
  design, 36
Reactors (Magnox), 58-71
Reactors (Malibu-1 Power)
  design, 5
Reactors (marine), 97-102
Reactors (Marius)
  criticality measurements in, 213
Reactors (Maryla)
  design, 111
Reactors (Marviken)
  design, 47, 49, 52-55
Reactors (Minerve)
  criticality measurements in, 213
Reactors (ML-1)
  fuel element evaluation, 173-74
Reactors (Molten Salt, Experiment) (MSRE)

development, 106
Reactors (NERO)
design, 100-1
Reactors (New Production)(NPR)
tubes and fittings, 134-36
Reactors (Nine Mile Point Power)
design, 4
Reactors (NORA)
fuel element design, 112
Reactors (Novo-Veronezh)(WWER)
burnup, 217
Reactors (NPD), 35-44
Reactors (NRX)
testing of reactor materials in, 38
Reactors (Oldbury)
design, 58
pressure vessel, 67
Reactors (Organic Cooled, Heavy Water
Moderated Power)
design, 36
Reactors (Otto Hahn)
design, 98-99
Reactors (Oyster Creek Power)
design, 4
Reactors (Parr Shoals Power)
design, 36
Reactors (Pathfinder Power)
design, 23
Reactors (Peachbottom Power)
design, 72-73
Reactors (pebble bed)
design, 73-74
Reactors (Plutonium Recycle Test)
(PRTR)
control of oxygen in D_2O system, 277
nuclear parameters, 158
pressure-tube fretting corrosion,
177-82
Reactors (PM-1)
status, 103
Reactors (PM-2A)
status, 103
Reactors (PM-3A)
status, 103
Reactors (portable power), 103-4
Reactors (pressure-tube), 35-45
Reactors (Pressurized Heavy Water)
design, 51-53, 55
Reactors (pressurized-water), 3-29
development and design of large, 137-47
use of soluble poisons for control, 10-12
Reactors (Puerto Rico Power)(BONUS)
design, 23, 25, 27
Reactors (R-1)
design, 36
Reactors (R-2)
design, 36
Reactors (R3/Adam)
(see Reactors (Agesta))
Reactors (Rapsodie)
status, 92
Reactors (RB)
fuel element design, 112
Reactors (Romaska)
design, 105-6
Reactors (RWE)
design, 4
Reactors (San Onofre Power)
design, 5
pumps, 18
Reactors (Savannah River)
burnout computation, 227
Reactors (Saxton Power)
design, 5, 7
operating experience, 3
use of soluble poison control, 12
Reactors (SELNI)
design, 5
Reactors (SENA)
design, 5
pressure vessel, 12-13
Reactors (SENN)
design, 4
pressure vessel, 12-13
Reactors (SEP)
design, 4
pressure vessel, 12
Reactors (Shippingport Pressurized Water)
(PWR), 6
design, 5
fuel element performance, 172, 252
operating experience, 3
use of burnable poison, 12
Reactors (Sizewell)
design, 58
Reactors (SM-1)
status, 103
Reactors (SM-1A)
status, 103
Reactors (SNAP-10A)
design, 105
Reactor (Sodium, Experiment)(SRE)
nuclear parameters of second core,
157-58
operation, 80-81
vapor traps, 264
Reactors (sodium graphite), 80-84
steam cycles, 183-85
Reactors (Southwest Experimental Fast
Oxide)(SEFOR)
vapor traps, 265
Reactors (Special Excursion, Tests-2)
(SPERT-2)
critical experiments with, 109
Reactors (Special Power Excursion, Tests-3)
(SPERT-3)
electrical circuits, failure, 272-73
flow-induced vibrations, failures from,
273-75
leaks, 275-76
level controller failure, 272
Reactors (Steam Generating Heavy Water)
design, 36
Reactors (superheating), 22-34
design of HGSR, 193-98
fuel element development, 174-75
Reactors (Tarapur)
design, 4
Reactors (TES-3)
operation, 104
Reactors (Tokai Mura)
design, 58
Reactors (Transient, Test Facility)
(TREAT)
vapor traps, 265-66
Reactors (Trawsfynydd)
design, 58
Reactors (UEM)
design, 5
Reactors (Ultra High Temperature, Experi-
ment) (UHTREX)
development, 106
Reactors (Ulyanovsk)
design, 25-26
Reactors (University of Michigan)
D_2O reflectors, 277, 279
Reactors (University of Missouri at Rolla)
(UMRR)
control rod swelling, 222
Reactors (Vallecitos Boiling Water)
(VBWR)
fuel element failure in, 252-54, 256
Reactors (Vallecitos Superheat)
design, 22, 24
Reactors (VULCAIN)
design, 99-101
Reactors (water-cooled), 3-29
material buckling in, 214-15
physics, 216
Reactors (water-moderated), 3-29
material buckling in, 214-15
physics, 216
use of poisons in, 217
Reactors (WWER)
design, 5
operating experience, 3
Reactors (WWER-1)
design, 19-20
pressure vessel, 9-10, 12-14
Reactors (WWER-2)
design, 19-20
Reactors (Wylfa)
design, 58
pressure vessel, 67
Reactors (Yankee Power), 6
control system, 271-72
critical experiments, 210
design, 5
flow-induced vibrations, failures from,
273-74
leaks, 275-76
operating experience, 3
pumps, 18
use of soluble poison control, 12
Reactors (ZPR-3)
core design, 110-11
Reflectors
D_2O in University of Michigan Reactor,
277, 279
Resonance absorption
mathematical analysis, 159-60
Resonance capture
in U-238, 215
Resonance Integral Theory
calculations, 218
REX code
criticality calculations, 210
ROB code
thermal conductivity calculations, 11
Rubidium (liquid)
thermal, thermodynamic, and flow prop
ties, 163-64

S

Safety
accident frequency, 221-22
burnout computation in Savannah River
Reactors, 227
coolant flow oscillations in Elk River
Power Reactor, 273
fast breeder reactors, 85-86, 153-54
Hallam Power Reactor, 280
instrument failures, 272-73
leaks, 275-76, 282
loss-of-coolant accidents, 240-41
shutdown, emergency, 225-26
University of Michigan Reactor, 279
University of Missouri at Rolla Reac
222
vibrations, flow-induced, 273-75
Salt solutions
heat transfer to, from wire-wrapped
seven-rod fuel element bundles, 1
Santowax
sampling techniques, 294-95
Santowax OMP
corrosive effects, 294
film formation by, 293-94
radiolysis, 290-91
use in ROSPO Critical Assembly, 11
Santowax-R
corrosive effects, 294
heat transfer properties, 123-24, 295
radiolysis, 291-92
SAP

  corrosion by polyphenyls, 293-94
  development for reactor fuels, 37, 39
  radiation effects, 38
atellites (man-made)
  Nimbus, thermal design calculations, 240
eals
  pressure vessel, leaks, 3
  use of freeze, in Hallam Power Reactor, 283
hims (chemical), 10-11
  Yankee Power Reactor, 272
hutdown (emergency)
  use of boric acid, 225
  use of gadolinium nitrate, 226
intered aluminum products
  (see SAP)
odium (gaseous)
  freeze traps for, 285
odium (liquid)
  heat transfer from boiling, 164
  reactor cooling, 75-96
  thermal, thermodynamic, and flow properties, 163-64
odium alloys (K-Na)(liquid)
  aerosol formation in, 260
  heat transfer coefficients, 235-36
  thermal, thermodynamic, and flow properties, 163
odium Components Test Installation
  vapor traps, 264
odium Test Facility
  vapor traps, 265
OFOCATE code
  criticality calculations, 210
ecifications
  fuel elements, PuO_2-UO_2, 129
  pressure vessels, 13-14
piralator
  heat exchanger, design, 237
prings
  use in control system, 223
agnation
  vapor traps utilizing, 260
ainless steel systems (stainless steel-UO_2 cermets)
  development for fuel elements, 126-27
ainless steels
  cladding for fuel elements, 3, 6-9
  corrosion of, 254, 293-94
  effects of boiling water on, 255
  performance in water-cooled reactors, 254, 256
eam
  effects on hydriding of Zr alloys, 246
eam (superheated)
  heat transfer, 40, 121
eam generators
  design for large pressurized water reactors, 138
  operating problems in Hallam Power Reactor, 284
eam-water systems
  boiling burnout in, 166-67
  flow and heat transfer, 165, 166-70
eels
  corrosion, 9-10, 293-94
TOKE code, 35
  for heavy water reactor simulation, 35
ress corrosion
  effects of oxygen concentration, 255
resses
  (see also Thermal stresses)
  effects on cracking, 252, 255
bcriticality
  measurement, 224-25
lfur
  effects on corrosion by polyphenyls, 294
perheated steam
  (see Steam (superheated))
Superheating
  pressure effects on boiling, 253
Surfaces
  effects on boiling, 231, 253

T

Tanks
  failure of Na expansion, in Hallam Power Reactor, 285
Teflon
  flexible tube heat exchangers, 237
Temperature sensors
  failure in Elk River Power Reactor, 272
TEMPEST code
  cross section calculations, 212
Terphenyl
  heat transfer properties of irradiated, 123-24
Thermal conductivity
  effects on pool boiling, 230
  fuel elements, 118-21, 129
  heat transfer calculations, 239
  hydrogen at high temperatures, 239
  noble gases at high temperature, 239
Thermal neutrons
  absorption cross section and diffusion length in graphite, 114-15
  distribution in light-water reactors, 215
Thermal radiation
  heat transfer calculations, 238-39
Thermal stresses
  in fuel elements, 253, 255
Thermometers
  failure in Elk River Power Reactor, 272
THERMOS code
  cross section calculations, 212
  thermal neutron distribution calculations, 215
Thorium alloys (Th-U)
  fuel element development for fast breeder reactors, 89
Thorium alloys (Th-U-Zr)(Zircaloy-2-clad)
  fabrication of fuel elements, 130
Thorium oxide systems (Nb-ThO_2-UO_2 cermets)
  thermal conductivity, 129
Thorium oxide systems (ThO_2-UO_2)
  fuel element design, 3, 6-9
  radiation effects, 8
Traps
  for aerosols, 359-70
  for carbon, oxides, and Na in Hallam Power Reactor, 285
  for liquid metal systems, 259-70
Tubes
  (see also Pressure tubes)
  burnout, 16-17
  burnout of water in, 121
  heat transfer from, at cryogenic temperatures, 239-40
Tubes (finned)
  use in heat exchangers, 236-37
Tungsten systems (Mo-W-UO_2 cermets)
  development for fuel elements, 128
Tungsten systems (W-UO_2 cermets)
  development for fuel elements, 127-28
Turbulent flow
  (see Fluid flow (turbulent))
Two-phase flow
  (see Fluid flow)

U

Uranium
  criticality in D_2O lattices, 213
  criticality in graphite lattices, 212-13
  radiation effects on reactivity, 217
Uranium-233
  radiation effects on reactivity, 217
Uranium-235
  fission ratio to U-238, 110
  fission spectrum cross section, 115
  radiation effects on reactivity, 217
Uranium-238
  fission ratio to U-235, 110
  resonance capture, 215
Uranium (enriched)
  criticality in D_2O lattices, 213
Uranium alloys (Pu-U)
  criticality in lattices, 212-13
Uranium alloys (Th-U)
  fuel element development for fast breeder reactors, 89
Uranium alloys (Th-U-Zr)(Zircaloy-2-clad)
  fabrication of fuel elements, 130
Uranium carbide systems (PuC-UC)
  design of fuel elements for large fast breeder reactors, 147-49, 151-52
  radiation effects, 8
Uranium carbides (UC)
  buckling studies, 111
  development for fuel elements for sodium graphite reactors, 81-83
  evaluation for fuel elements, 174
  fabrication of Na-bonded fuel elements, 129-30
  radiation effects, 8, 82
Uranium nitrides (UN)
  radiation effects, 8
Uranium oxide systems
  critical experiments in water lattices, 210
Uranium oxide systems (Al_2O_3-UO_2)
  radiation effects, 8
Uranium oxide systems (BeO-UO_2)
  radiation effects, 8
Uranium oxide systems (BeO-UO_2) (Hastelloy-X-clad)
  fuel elements, evaluation, 173
Uranium oxide systems (Mo-UO_2 cermets)
  fabrication into fuel elements and thermal conductivity, 129
Uranium oxide systems (Mo-W-UO cermets)
  development for fuel elements, 128
Uranium oxide systems (Nb-ThO_2-UO_2 cermets)
  thermal conductivity, 129
Uranium oxide systems (PuO_2-UO_2)
  critical experiments in water lattices, 210, 212
  design of fuel elements for large fast breeder reactors, 149-52
  fuel elements, fretting corrosion of Zircaloy-2 cladding, 177-82
  fuel elements, specifications, 129
  radiation effects, 8
Uranium oxide system (stainless steel-UO_2 cermets)
  development for fuel elements, 126-27
Uranium oxide systems (ThO_2-UO_2)
  fuel element design, 3, 6-9
  radiation effects, 8
Uranium oxide systems (W-UO_2 cermets)
  development for fuel elements, 127-28
Uranium oxide systems (UO_2-ZrO_2)
  radiation effects, 8
Uranium oxides (UO_2)
  evaluation, 172-74
  fretting corrosion, 177-82
  fuel elements, design, 3, 6-9
  fuel elements, evaluation, 172-74
  fuel elements, fabrication, 128-29
  fuel elements, thermal conductivity,

119-21
  pulsed neutron studies, 112
  radiation effects, 8
Uranium silicides (U_3Si)
  radiation effects, 8
Uranium sulfides (US)
  radiation effects, 8
Uranium systems
  criticality in water lattices, 210-11
Uranyl nitrate
  criticality of solutions, 213

V

Valves
  performance in Hallam Power Reactor, 282-84
Vapor traps
  for liquid metal systems, 259-70
Vaporizers
  flow stability in forced convection, 231-32
Vena contracta
  mixing during reexpansion, 235
Vertical channels
  (see Channels)
Vibrations
  flow-induced, failures from, 273-75

W

Water
  burnout heat flux under forced convection, 122
  condensation, 233
  corrosion of steel, 9-10
  criticality studies in lattices of, 210-212
  dissociation, effects on hydriding of Zr alloys, 248
  effects on corrosion by polyphenyls, 294
  moderator, pulsed neutron studies in, 113
  quality control, 254
  reactivity effects, 109-10
Water (pressurized)
  burnout calculations, 121-23
Water-air systems
  flow, techniques for observing, 165
Water-ice systems
  free convection melting, heat transfer calculations, 239-40
Water-steam systems
  boiling burnout in, 166-67
  flow and heat transfer, 165, 166-70

Z

Zircaloy alloy
  cladding for fuel elements, 3, 6-9
  effects of hydriding on properties, 245
Zircaloy-2 alloy
  corrosion, 42-45
  effects of hydriding on properties, 245, 248-49
  hydriding, control of, 249-50
  hydrogen absorption, 246
  radiation effects, 38, 41
  use in pressure tubes, 41
Zircaloy-2 alloy (Ni-tree)
  hydrogen absorption, 246
Zircaloy-4 alloy
  hydriding, control of, 250
  hydrogen absorption, 246
Zirconium alloys
  hydriding, 246-51
Zirconium alloys (coated)
  corrosion by polyphenyls, 294
Zirconium alloys (Nb-Zr)
  corrosion, 42-45
  hydriding stress allowance, 9
  use in pressure tubes, 41
Zirconium alloys (Th-U-Zr)(Zircaloy-2-clad)
  fabrication of fuel elements, 130
Zirconium hydride
  formation in Zircaloys, 245-46
  orientation, 250-51
Zirconium oxide systems (PuO_2-ZrO_2)
  radiation effects, 8
Zirconium oxide systems (UO_2-ZrO_2)
  radiation effects, 8

LEGAL NOTICE

This journal was prepared under the sponsorship of the U. S. Atomic Energy Commission. Neither the United States, nor the Commission, nor any person acting on behalf of the Commission:

A. Makes any warranty or representation, expressed or implied, with respect to the accuracy, completeness, or usefulness of the information contained in this journal, or that the use of any information, apparatus, method, or process disclosed in this journal may not infringe privately owned rights; or

B. Assumes any liabilities with respect to the use of, or for damages resulting from the use of any information, apparatus, method, or process disclosed in this journal.

As used in the above, "person acting on behalf of the Commission" includes any employee or contractor of the Commission, or employee of such contractor, to the extent that such employee or contractor of the Commission, or employee of such contractor prepares, disseminates, or provides access to, any information pursuant to his employment or contract with the Commission, or his employment with such contractor.

NUCLEAR SCIENCE ABSTRACTS

The U. S. Atomic Energy Commission, Division of Technical Information, publishes *Nuclear Science Abstracts* (*NSA*), a semimonthly journal containing abstracts of the literature of nuclear science and engineering.

NSA covers (1) research reports of the U. S. Atomic Energy Commission and its contractors; (2) research reports of government agencies, universities, and industrial research organizations on a worldwide basis; and (3) translations, patents, books, and articles appearing in technical and scientific journals.

Complete indexes covering subject, author, source, and report number are included in each issue. These are cumulated quarterly, semiannually, and annually providing a detailed and convenient key to the literature.

Availability of NSA

SALE *NSA* is available on subscription from the Superintendent of Documents, U. S. Government Printing Office, Washington, D. C., 20402, at $30.00 per year for the semimonthly abstract issues and $22.00 per year for the four cumulated-index issues. Subscriptions are postpaid within the United States, Canada, Mexico, and all Central and South American countries, except Argentina, Brazil, British and French Guiana, Surinam, and British Honduras. Subscribers in these Central and South American countries, and in all other countries throughout the world, should remit $37.00 per year for subscriptions to semimonthly abstract issues and $25.00 per year for the four cumulated-index issues.

EXCHANGE *NSA* is also available on an exchange basis to universities, research institutions, industrial firms, and publishers of scientific information. Inquiries should be directed to the Division of Technical Information Extension, U. S. Atomic Energy Commission, P. O. Box 62, Oak Ridge, Tennessee, 37830.

TECHNICAL PROGRESS REVIEWS may be purchased from Superintendent of Documents, U. S. Government Printing Office, Washington, D. C., 20402, at $2.50 per year for each journal or $0.70 per issue. The use of the coupon below will facilitate the handling of your order.

POSTAGE AND REMITTANCE: Postpaid within the United States, Canada, Mexico, and all Central an South American countries except Argentina, Brazil, British and French Guiana, Surinam, and British Honduras. For these Central and South American countries and all other countries, add $0.75 for ea annual subscription or $0.20 for a single issue. Payment should be by check, money order, or documen coupons, and MUST accompany order. Remittances from foreign countries should be made by international money order or draft on an American bank payable to the Superintendent of Documents or UNESCO book coupons.

order form

SUPERINTENDENT OF DOCUMENTS
U. S. GOVERNMENT PRINTING OFFICE
WASHINGTON, D. C., 20402

Enclosed:
document coupons ☐ check ☐ money order ☐

Charge to Superintendent of Documents No. ____________

Please send a one-year subscription to

- ☐ NUCLEAR SAFETY
- ☐ POWER REACTOR TECHNOLOGY
- ☐ REACTOR FUEL PROCESSING
- ☐ REACTOR MATERIALS
- ☐ ISOTOPES AND RADIATION TECHNOLOGY

(Each subscription $2.50 per year; $0.70 per issue.)

SUPERINTENDENT OF DOCUMENTS
U. S. GOVERNMENT PRINTING OFFICE
WASHINGTON, D. C., 20402

(Print clearly)

____
Name

____
Street

____
City, State, ZIP Code